AGSO BULLETIN 242

Petrology and platinum-group-element geochemistry of Archaean layered mafic-ultramafic intrusions, west Pilbara Block, Western Australia

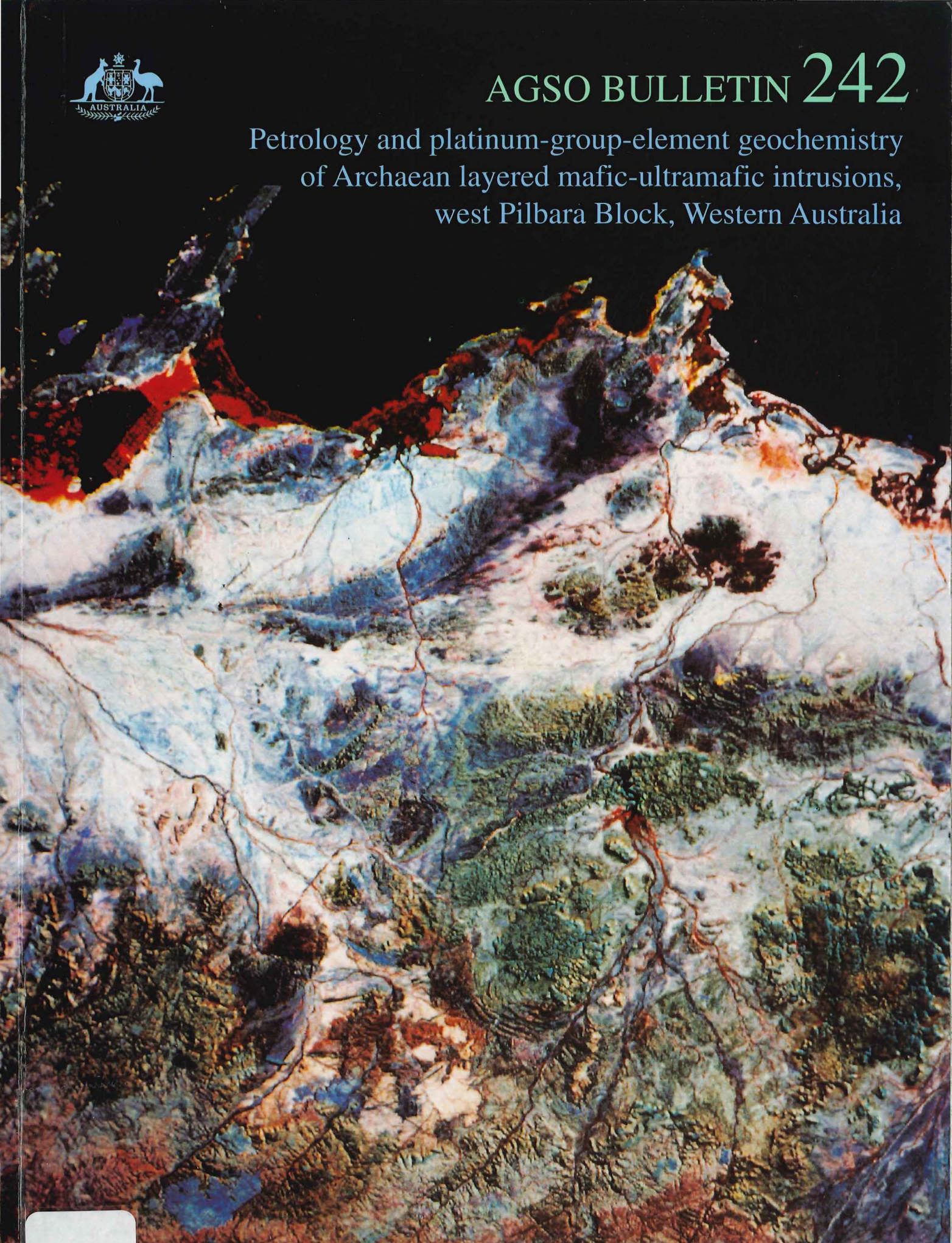

D.M. Hoatson, D.A. Wallace, S-S. Sun,
L.F. Macias, C.J. Simpson, & R.R. Keays

S55(94)
BUL.45
C. 8

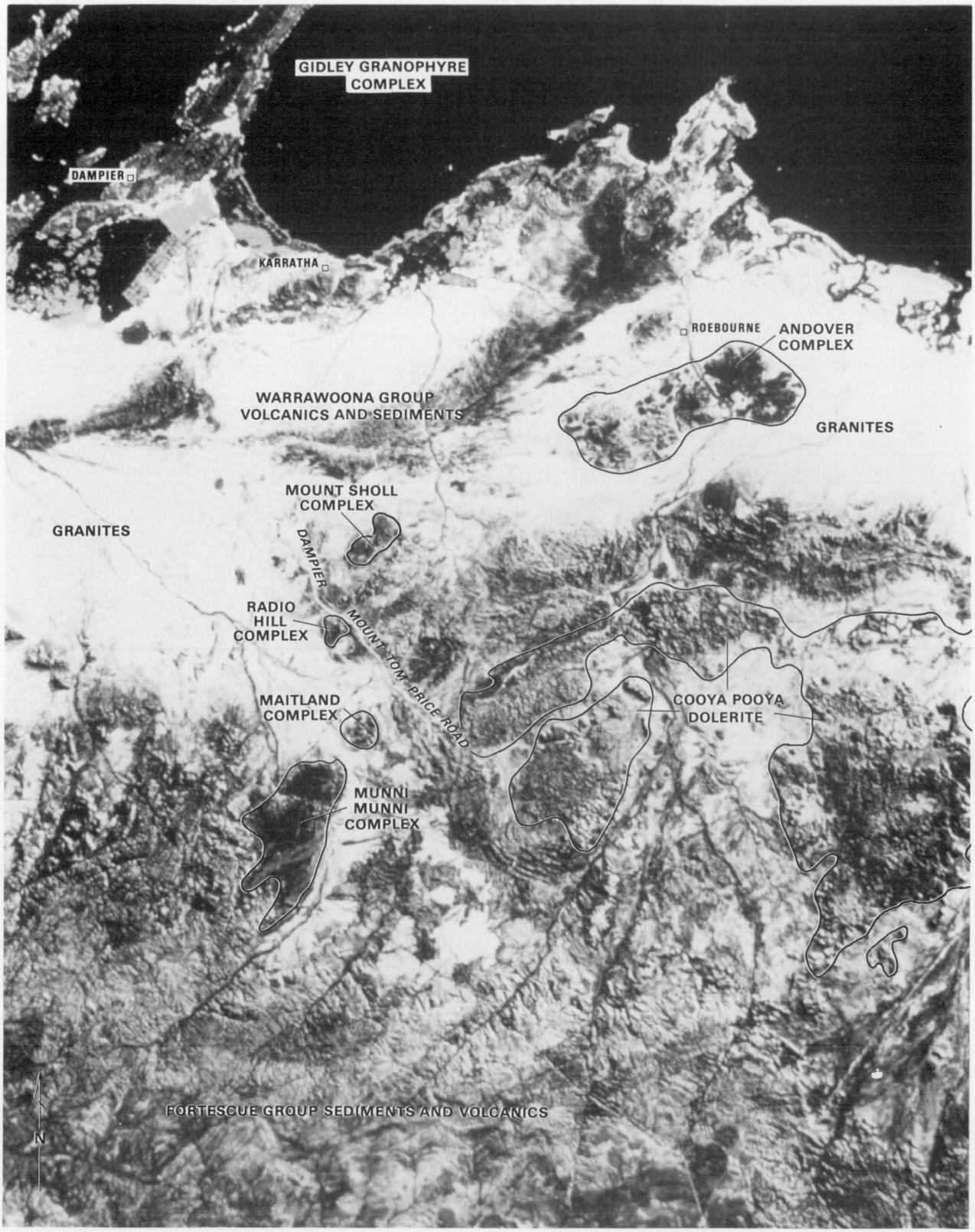
GIDLEY GRANOPHYRE COMPLEX
DAMPIER
KARRATHA
ROEBOURNE
ANDOVER COMPLEX
WARRAWOONA GROUP VOLCANICS AND SEDIMENTS
GRANITES
MOUNT SHOLL COMPLEX
GRANITES
DAMPIER
RADIO HILL COMPLEX
MOUNT TOM PRICE ROAD
MAITLAND COMPLEX
COOYA POOYA DOLERITE
MUNNI MUNNI COMPLEX
FORTESCUE GROUP SEDIMENTS AND VOLCANICS
N

DEPARTMENT OF PRIMARY INDUSTRIES & ENERGY
AUSTRALIAN GEOLOGICAL SURVEY ORGANISATION
(formerly Bureau of Mineral Resources, Geology & Geophysics)

Bulletin 242

Petrology and platinum-group-element geochemistry of Archaean layered mafic-ultramafic intrusions, west Pilbara Block, Western Australia

*D. M. Hoatson, D. A. Wallace, S-S. Sun, L. F. Macias, C. J. Simpson, & R. R. Keays**
(Minerals & Land Use Program)

*School of Earth Sciences, University of Melbourne

AUSTRALIAN GOVERNMENT PUBLISHING SERVICE, CANBERRA

© Commonwealth of Australia 1992

This work is copyright. Apart from any use as permitted under the *Copyright Act 1968*, no part may be reproduced by any process without written permission from the Director, Publishing & Marketing, AGPS. Inquiries should be directed to the Manager, AGPS Press, Australian Government Publishing Service, GPO Box 84, Canberra ACT 2601.

ISSN 1039-2645

National Library of Australia Cataloguing-in-Publication entry:

Petrology and platinum-group-element geochemistry of Archaean layered mafic-ultramafic intrusions, west Pilbara Block, Western Australia.

Bibliography.
ISBN 0 644 24907 2.

1. Petrology—Western Australia—Pilbara Block. 2. Platinum group. 3. Geochemistry—Western Australia—Pilbara Block. 4. Intrusions (Geology)—Western Australia—Pilbara Block. I. Hoatson, D. M. (Dean M.). II. Australian Geological Survey Organisation. (Series: Bulletin (Australian Geological Survey Organisation); 242).

553.422099413

Recommended bibliographic citation:

Bulletin as a whole:

Hoatson, D. M., Wallace, D. A., Sun, S-S., Macias, L. F., Simpson, C. J., & Keays, R. R., 1992—Petrology and platinum-group-element geochemistry of Archaean layered mafic-ultramafic intrusions, west Pilbara Block, Western Australia. *Australian Geological Survey Organisation, Bulletin* 242.

Individual chapters:

Hoatson, D. M., Sun, S-S., & Keays, R. R., 1992—Petrogenesis of the west Pilbara layered mafic-ultramafic intrusions. *In* Hoatson, D. M., & others—Petrology and platinum-group-element geochemistry of Archaean layered mafic-ultramafic intrusions, west Pilbara Block, Western Australia. *Australian Geological Survey Organisation, Bulletin* 242, 150–166.

Cover: Landsat 5 Thematic Mapper composite image (recorded on 17 September 1986) of part of the west Pilbara Block using bands 4, 5, and 7 displayed as red, green, and blue, respectively. This combination of bands helps to discriminate felsic, mafic, and ultramafic rock units. The prominent red colour near the coast is due to salt evaporation pans near Dampier and saline coastal flats. Landsat data received by the Australian Centre for Remote Sensing, Canberra and provided by Geoimage Pty Ltd, Queensland and processed by L. F. Macias. Scale approximately 1 cm = 4 km.

Frontispiece: Regional setting of Archaean layered mafic-ultramafic intrusions described in this Bulletin.

Editing: Sandy Paine (28 Jansz Crescent, Griffith, ACT), Dean Hoatson

Cover design: Leanne McMahon

Typeset in Australia by AGPS

Printed for AGPS by J.S. McMillan Printing Group

CONTENTS

(authorship in brackets)

	Page
ABSTRACT	xi
SUMMARY	xiii
INTRODUCTION (*DMH*)	1
Status of research into the genesis of layered mafic-ultramafic intrusions	1
Platinum-group-element mineralisation in Australia	4
Purpose, scope, and methods of the study, and nomenclature used	6
Previous investigations and history of exploration	7
Acknowledgements	9
REGIONAL GEOLOGY, METALLOGENESIS, AND TECTONIC EVOLUTION OF THE WEST PILBARA BLOCK (*DMH*)	11
Introduction	11
Archaean sedimentary-volcanic units of the Pilbara Supergroup	11
Archaean sedimentary-volcanic units of the basal Fortescue Group	11
Archaean granitoid intrusions	15
Archaean layered mafic-ultramafic intrusions and metallogenesis	15
Synopsis	15
Layered intrusions not covered in this study	17
Balla Balla Complex	17
Dingo Complex	17
Gidley Granophyre Complex	17
Sherlock Bay Complex	17
Tectonic evolution of the west Pilbara Block	18
FIELD RELATIONSHIPS, PETROGRAPHY, MINERALOGY, AND GEOCHEMISTRY OF THE MUNNI MUNNI COMPLEX (*DMH*)	19
Introduction	19
Size and age	19
Distribution of rock types	19
Ultramafic zone	19
Gabbroic zone	27
Distribution of sulphides and chromite	27
Sulphides	27
Chromite	28
Stratigraphic relationships	28
Contact relationships with country rocks	30
Dykes	32
Layering	34
Ultramafic zone	34
Gabbroic zone	34
Structure	34
Petrography	35
Introduction	35
Altered marginal rocks (cpx ± opx ± ol)	37
Dunite, lherzolite, wehrlite (ol ± cpx)	41
Websterite, olivine websterite (cpx + ol)	42
Clinopyroxenite, olivine clinopyroxenite (cpx ± ol)	44
Plagioclase websterite, gabbronorite (cpx ± opx ± ol)	44
Orthopyroxenite, olivine orthopyroxenite (opx ± ol ± spinel)	45
Chromitite (chrom ± ol ± opx)	45
Megacrystalline orthopyroxenite (cpx)	45
Mixed norite-orthopyroxenite rock (plag + opx: norite; opx: orthopyroxenite)	46
Inverted-pigeonite-bearing gabbronorite (plag + inv. pig + cpx ± mt-ilm)	46
Anorthositic gabbronorite, anorthositic gabbro, 'anorthosite' (plag)	49
Other rock types of the gabbroic zone	49
Mineralogy	49
Introduction	49
Stratigraphic variations in mineral chemistry	50
Olivine	50
Clinopyroxene	53
Orthopyroxene	55
Inverted pigeonite	56
Plagioclase	56
Alkali feldspar	58
Biotite	58
Chromium-bearing spinel	58
Magnetite-ilmenite	61
Sulphides	62
Variations in mineral chemistry across cycles in the ultramafic zone	62
Compositional trends of clinopyroxene across the ultramafic/gabbroic zone contact	64
Evolution of pyroxene in the Munni Munni Complex	67
Platinum-group-element mineralogy	69
Whole-rock geochemistry	71
Introduction	71
Major elements	72
Trace elements	74
Platinum-group-element and incompatible-trace-element geochemistry	76
Introduction	76
Sulphur	77
Copper, nickel	79
Platinum, palladium, gold, iridium	79
Copper, nickel, platinum, palladium, gold, iridium across the ultramafic/gabbroic zone contact	85
Osmium, ruthenium, rhodium across the ultramafic/gabbroic zone contact	86
Incompatible trace elements selenium, cesium, rubidium, strontium, zirconium	87
Ratios, correlation coefficients, and chondrite-normalised trends of precious metals and trace elements	88
FIELD RELATIONSHIPS, PETROGRAPHY, MINERALOGY, AND GEOCHEMISTRY OF THE MOUNT SHOLL INTRUSION (*DMH*)	92
Introduction	92
Size and age	92
Distribution of rock types and stratigraphic relationships	92
Structure	95
Mineralisation	96
Petrography and mineralogy	96
Metaperidotite (ol + cpx)	97
Metagabbro (cpx + opx ± plag; cpx + plag ± mt-ilm)	97
Geochemistry and orientation of the Mount Sholl Complex	97
Major and trace elements	98
Platinum, palladium, iridium, gold	98

	Page
FIELD RELATIONSHIPS, PETROGRAPHY, MINERALOGY, AND GEOCHEMISTRY OF THE RADIO HILL COMPLEX (*DMH*)	101
Introduction	101
Size and age	101
Distribution of rock types and stratigraphic relationships	101
Ultramafic zone	101
Gabbroic zone	101
Structure	104
Mineralisation	104
Petrography and mineralogy	105
Sulphide-bearing microgabbro, gabbronorite, plagioclase websterite (cpx ± opx)	105
Dunite, lherzolite, wehrlite, olivine websterite, plagioclase olivine websterite (ol + cpx ± opx)	106
Plagioclase websterite, websterite, plagioclase clinopyroxenite, clinopyroxenite (cpx + opx ± ol)	106
Gabbro, gabbronorite, olivine gabbro, olivine gabbronorite (cpx ± ol ± opx)	106
Quartz gabbro, quartz gabbronorite (plag + cpx ± opx)	106
Geochemistry	107
Major elements	107
Trace elements	108
Platinum, palladium, iridium, ruthenium, gold, silver	109
Discussion and origin of sulphide mineralisation	111
FIELD RELATIONSHIPS, PETROGRAPHY, AND GEOCHEMISTRY OF THE MAITLAND COMPLEX (*DMH*)	117
Introduction	117
Size and age	117
Distribution of rock types and stratigraphic relationships	117
Structure	120
Petrography	120
Melagabbro, melagabbronorite, leucogabbro, leucogabbronorite (plag ± cpx)	120
Anorthosite, anorthositic gabbro (plag)	120
Norite (plag + opx ± cpx)	121
Olivine gabbronorite (opx + ol)	121
Peridotite (ol ± cpx ± opx ± chrom)	121
Geochemistry	121
Major elements	122
Trace elements	123
Platinum, palladium, iridium, ruthenium, gold	123
Discussion	124
FIELD RELATIONSHIPS, PETROGRAPHY, MINERALOGY, AND GEOCHEMISTRY OF THE ANDOVER COMPLEX (*DAW*)	126
Introduction	126
Mining	126
Regional setting	127
Structure	128
Country rocks	128
Stratigraphy	128
Petrography	130
Peridotite (ol ± opx)	130
Pyroxenite (opx ± ol ± cpx; cpx)	131
Gabbro, anorthositic gabbro, and anorthosite (plag ± opx ± cpx)	131
Alteration	131
Mineralogy	132
Geochemistry	132
Major elements	134
Trace elements	135
Discussion of results	136
Distribution of platinum, palladium, iridium, ruthenium, gold	137
Role of sulphur	137
Platinum-group-element potential	139
Acknowledgements	140
CHEMICAL AND ISOTOPIC CHARACTERISTICS OF PARENT MAGMAS OF THE WEST PILBARA LAYERED INTRUSIONS: IMPLICATIONS FOR PETROGENESIS, MAGMA MIXING, AND PGE MINERALISATION IN LAYERED INTRUSIONS (*S-SS & DMH*)	141
Introduction	141
Methods of approach	141
Neodymium and Sr isotope analytical methods	141
Age of the Munni Munni Complex	141
Chemical and isotopic characteristics of parent magmas	142
Proposed petrogenetic model for the SHMB parent magma	144
Variations in Nd and Sr isotope compositions and Zr/Nd ratios in the Munni Munni Complex: implications for magma-chamber processes	146
Neodymium isotope data for the Andover Complex: a comparison with the Munni Munni Complex	147
Genetic connection between M and G magma types: implications for different magma types of layered complexes and PGE mineralisation	148
Conclusions	148
PETROGENESIS OF THE WEST PILBARA LAYERED MAFIC-ULTRAMAFIC INTRUSIONS (*DMH, S-SS, & RRK*)	150
Introduction	150
Munni Munni Complex	150
Evidence for magma mixing at the ultramafic/gabbroic zone contact	150
Composition of the parent magma for the ultramafic zone	151
Role of sulphur saturation during magma evolution	154
Formation of the basal-contact sulphide zone	157
Genesis of PGE mineralistaion in the porphyritic websterite layer	158
Conditions of crystallisation	159
Temperature, oxygen fugacity, and P_{H_2O}	159
Pressure	161
Sulphur isotope geochemistry of the west Pilbara layered intrusions	161
Comparison with well-known, PGE-bearing layered mafic-ultramafic intrusions outside Australia	163
Implications for exploring layered mafic-ultramafic intrusions	165
GEOLOGICAL REMOTE SENSING OF THE MUNNI MUNNI AND ANDOVER COMPLEXES (*LFM & CJS*)	167
Introduction	167
General geology	167
Munni Munni Complex	167
Andover Complex	168
Scanner data characteristics	168

Page

Spectral reflectance 169
Digital data processing 171
Munni Munni Complex 171
NS001 scanner data 171
Additional implications for NS001 data interpretation 172
TIMS data 174
Landsat TM data 174
Andover Complex 174
Landsat TM data 174
Discussion 174
Availability of spectral instrumentation 177
Airborne multispectral scanners 177
Airborne imaging spectrometers 177
Field spectrometers 177
Acknowledgements 177

REFERENCES 178

APPENDIXES 188
1. Analytical procedures 188
1.1. Radiochemical neutron-activation analysis (RNAA) 188
1.2. X-ray fluorescence spectrometry (XRFS) and atomic-absorption spectrophotometry (AAS) 188
1.3. Leco titration for sulphur analysis 191
1.4. Sulphur-isotope analysis 192
1.5. Electron-microprobe and scanning-electron-microscope analysis 192
2. Mineral chemistry of the Munni Munni and Andover intrusions 193
Minerals analysed from the Munni Munni Complex 193
Minerals analysed from the Andover Complex 193
Explanation of attribute data and atomic ratios used in the mineral tables 193
Mineral tables 195
Mineral analyses from the Munni Munni Complex 195
Regional traverse: olivine (UZ) 195
clinopyroxene (UZ, GZ) 200
orthopyroxene (UZ) 207
inverted pigeonite (GZ) 210
plagioclase (UZ, GZ) 220
alkali feldspar (UZ) 224
biotite (UZ, GZ) 225
spinels (UZ, Eastern Munni Munni Dyke) 227
magnetite and ilmenite (GZ) 229
sulphides (UZ) 232
Detailed traverse across cycles 1–5 in subzones C and D (UZ):
olivine 234
clinopyroxene 240
orthopyroxene 247
Detailed traverse across ultramafic/gabbroic zone contact (UZ, GZ):
clinopyroxene 251
clinopyroxene cores and rims 261
plagioclase 265
Pyroxene analyses from the Andover Complex 271

Page

3. Whole-rock (major, trace, PGEs) geochemistry of the Munni Munni, Mount Sholl, Maitland, Radio Hill, and Andover intrusions 273
Munni Munni Complex 274
Mount Sholl Complex 288
Maitland Complex 293
Radio Hill Complex 299
Andover Complex 310

APPENDED MAP SHEET
Layered Archaean mafic-ultramafic intrusions of the west Pilbara Block, Western Australia (1 : 20 000 scale maps)

FIGURES

Introduction
1. Distribution of Australian platinum-group-element mineralisation styles with geological time 4
2. Frequency of Australian platinum-group-element styles with geological time 5

Regional setting of the west Pilbara Block
3. Geology of the Pilbara Block 10
4. Distribution of Archaean layered mafic-ultramafic intrusions in the west Pilbara Block 14
5. Landsat multispectral-scanner, standard false-colour, composite image of the west Pilbara Block 16

Munni Munni Complex
6. Aerial photograph of complex 20
7. Geology 21
8. Aeromagnetics, Munni Munni Complex region 22
9. Gravity, Munni Munni Complex region 23
10. Generalised stratigraphy of the ultramafic zone 25
11. Distribution and relative abundances of sulphides and spinels 28
12. Detailed geology of the ultramafic/gabbroic zone contact 29
13. A—weathered porphyritic plagioclase websterite orthocumulate; B—porphyritic plagioclase websterite block detached by invading gabbroic magma; C—weakly porphyritic websterite layer hosted by gabbronorite; D—mixed orthopyroxenite and norite rock 30
14. Aerial views: A—northern basal contact of ultramafic zone; B—contact between ultramafic and gabbroic zones; C—northeastern contact of ultramafic zone; and D—Pinderi Hills Dyke 31
15. A—low-angle cross-bedding in clinopyroxene-olivine adcumulate; B—microrhythmic or 'inch-scale' layering; C—rhythmically layered olivine-clinopyroxene and clinopyroxene-olivine cumulates; D—rhythmic layering in accidental orthopyroxenite block; E—complexly layered peridotite sequence; F—compositional layering and lamination in basal gabbronorite 33

Page

16. Equal-area projection of poles to layering in ultramafic and gabbroic zones 35
17. Interpretive block diagram 36
18. Rose diagram of strike-trends of faults in ultramafic and gabbroic zones 37
19. Distribution of cumulus and intercumulus minerals 40
20. Ternary modal variation diagrams of rock types 41
21. Modal distributions of major minerals in the gabbroic zone 42
22. Photomicrographs: A—lherzolite adcumulate; B—lherzolite orthocumulate; C & D—porphyritic plagioclase websterite orthocumulate; E & F—sulphide mineralisation in porphyritic plagioclase websterite 43
23. Photomicrographs: A—olivine orthopyroxenite adcumulate; B—orthopyroxenite-spinel adcumulate; C—chromite-olivine cumulate 45
24. Photomicrographs: A & B—laminated gabbronorite from base of gabbroic subzone A; C & D—intergranular magnetite-ilmenite gabbronorite from middle part of gabbroic subzone A 47
25. Summary of electron microprobe data for major silicate minerals 51
26. Variations in mg, MgO, Total FeO, and NiO in olivine 52
27. Variations in NiO and MnO in olivine with mg 52
28. Classification of clinopyroxene 53
29. Variations in mg of pyroxene versus mg of coexisting olivine 54
30. Variations in mg, MgO, Total FeO, CaO, Cr_2O_3, MnO, TiO_2, and Al_2O_3 in clinopyroxene 55
31. Variations in mg, MgO, Total FeO, and Cr_2O_3 in orthopyroxene 56
32. Variations in An, CaO, Na_2O, K_2O, and Al_2O_3 in plagioclase 57
33. Variations in An, CaO, Na_2O, Al_2O_3, SrO, K_2O, and BaO in plagioclase 57
34. Compositions of Cr-bearing spinels in the oxidised spinel prism 59
35. Variations in Cr-Al-Fe^{3+} in Cr-bearing spinel from various layered intrusions 60
36. Variations in Cr/(Cr + Al) with Mg/(Mg + Fe^{2+}) in spinel from various intrusions 61
37. Variations in mg, MgO, Total FeO, and NiO in olivine across cyclic units 62
38. Variations in mg, MgO, Total FeO, and Cr_2O_3 in clinopyroxene across cyclic units 63
39. Variations in mg, MgO, Total FeO, and Cr_2O_3 in orthopyroxene across cyclic units 64
40. Variations in mg, MgO, Total FeO, CaO, Cr_2O_3, MnO, NiO, and TiO_2 in clinopyroxene 64
41. Variation in mg in clinopyroxene for the stratigraphic interval 1750–2000 m 64
42. Variations in Cr_2O_3, NiO, MnO, and TiO_2 in clinopyroxene with mg 65
43. Variations in clinopyroxene core and rim compositions across the UZ/GZ contact 65
44. A—Summary of pyroxene fractionation trends. B—Pyroxene fractionation trends from various layered intrusions 66
45. Scanning-electron-microscope images of platinum-group minerals 68

Page

46. Scanning-electron-microscope images of platinum-group minerals 70
47. Whole-rock major-element compositions plotted against stratigraphic height 72
48. Whole-rock major-element compositions for the stratigraphic interval 1810-1900 m 73
49. Ternary plots of whole-rock major-element compositions 74
50. Whole-rock trace-element compositions plotted against stratigraphic height 75
51. Whole-rock trace-element compositions plotted against stratigraphic height 76
52. Variation diagrams of trace-element compositions plotted against mg 77
53. Variation diagrams of major- and trace-element compositions plotted against Zr 77
54. Profiles of Pt, Pd, Ir, Au, S, Se, Cu, and Ni through the ultramafic and gabbroic zones 78
55. Ternary plots of precious-metal contents for ultramafic and gabbroic zone rocks 82
56. Profiles of Pt, Pd, Cu, and Ni across the mineralised porphyritic websterite layer 83
57. Diamond-drillhole profile across the mineralised porphyritic websterite layer 86
58. Profiles of Cs, Rb, Zr, and Sr through the ultramafic and gabbroic zones 87
59. Profiles of S, Cu, Sr, and Zr trends normalised to 100% melt 88
60. Profiles of various PGE and trace-element ratios through the ultramafic and gabbroic zones 89
61. Chondrite-normalised Pt, Pd, Ir, and Au patterns for various rock types 91

Mount Sholl Complex

62. Geology 93
63. A—aerial view east across the complex; B—B_2 mineralised trend; C—pillowed ?Talga Talga Subgroup metabasalt; D—gabbroic vein intruding metavolcanics; E—rhythmic layering in gabbro 94
64. Whole-rock geochemical variations along traverse A 98
65. Whole-rock geochemical variations along traverse B 98

Radio Hill Complex

66. Geology 102
67. A—aerial view northeast across the complex; B—aerial view of Radio Hill; C—wispy plagioclase layering in melagabbro; D—commingling of mafic magmas 103
68. Drillhole profile through the mineralised basal contact 105
69. Whole-rock major-element compositions plotted against stratigraphic height 107
70. Ternary plots of whole-rock major-element compositions 108
71. Whole-rock trace-element compositions plotted against stratigraphic height 109
72. Whole-rock trace-element compositions plotted against stratigraphic height 110
73. Variation diagrams of major- and trace-element compositions plotted against Zr 111
74. Variation diagrams of Pt, Pd, Ir, Ru, Au, Pt/Pd, Pd/S, and S against stratigraphic height 111
75. Variation diagrams of precious metals plotted against S and Ni 113

Page

76. Precious-metal geochemistry of the mineralised basal contact 114

Maitland Complex

77. Geology 118
78. A—modal layering in leucogabbro unit; B—pegmatoidal melagabbro unit; C—mottled anorthosite; and D—sharp contact between dolerite dyke and gabbro 119
79. Whole-rock major-element compositions plotted against stratigraphic height 121
80. Whole-rock trace-element compositions plotted against stratigraphic height 122
81. Whole-rock trace-element compositions plotted against stratigraphic height 123
82. Variation diagrams of Pt, Pd, Ir, Ru, Au, Pd/S, Pt/Pd, and (Pt + Pd)/Ir against stratigraphic height 123
83. Ternary plots of whole-rock precious-metal compositions 124

Andover Complex

84. Major structural units of the Roebourne–Karratha region 126
85. Geology 127
86. A—aerial view southeast across the centre of the complex; B—shallow-dipping peridotite and anorthosite cycles; C—modal layering in gabbroic unit; D—dolerite dykes 129
87. Hydration and oxidation status of rocks 131
88. A—summary of pyroxene fractionation trends. B—variations in mg of coexisting pyroxenes plotted against stratigraphic height 132
89. Whole-rock variations of Cr, Ni, and mg plotted against stratigraphic height 132
90. Histograms of MgO contents for different rock types 133
91. A—ternary plot of whole-rock MgO, Al_2O_3, and CaO compositions. B—whole-rock variations of MgO versus Al_2O_3 from the Andover and Munni Munni complexes 133
92. Whole-rock major- and trace-element variations with stratigraphic height 134
93. Whole-rock variations of major- and trace-element geochemistry 135
94. Variations of Cr, Ni, and mg plotted against stratigraphic height for peridotites 136
95. Normative quartz plotted against Cr contents for peridotites from subzones A to G 136
96. Whole-rock variations of precious-metal abundances and ratios plotted against stratigraphic height 138
97. Whole-rock variations of Zr against S for the Andover and Munni Munni complexes 139

Isotope studies

98. Locations of samples used for isotope analysis from the Munni Munni Complex 143
99. Primitive mantle-normalised trace-element diagrams for late Archaean SHMB 144
100. Locations of samples used for isotope analysis and initial Nd values from the Andover Complex 147

Petrogenesis

101. Geochemical plots of boninites, siliceous high-Mg basalts, and U-type chill rocks 153
102. Plots of Pt against Pd, Cu against Ni, Pt + Pd against Cu, and Pt + Pd against S 155

Page

103. Plots of Pt against Pd, Cu against Ni, Pt + Pd against Cu, and Pt + Pd against Ni 156
104. Schematic diagram showing suggested evolution of the Munni Munni Complex 157
105. Plot of $\log f_{O_2}$ against temperature for coexisting magnetite and ilmenite 160
106. Comparative thickness of major layered mafic-ultramafic intrusions 163
107. Chondrite-normalised PGE and Au patterns for mineralised units in various intrusions 165

Remote sensing studies

108. Alteration of ultramafic rocks, Andover and Munni Munni complexes 168
109. Spectra of representative mafic and ultramafic rocks, Andover and Munni Munni complexes 169
110. Reflectance versus wavelength area diagram for 0–74 μm particle size range samples 169
111. Modified geological map of the Munni Munni Complex as interpreted from scanner data 170
112. NS001 composite image of the Munni Munni Complex 171
113. NS001 composite image of the Munni Munni Complex 172
114. TIMS composite image of the Munni Munni Complex 173
115. TM composite image of the Munni Munni Complex 175
116. TM composite image of the Munni Munni Complex 175
117. Geological map of the Andover Complex 176
118. TM composite image of the Andover Complex 176

Appendix 1

119. RNAA flow chart for nickel-sulphide-button technique 189
120. RNAA flow chart for whole-rock-powder technique 190

TABLES

Introduction

1. Colour aerial photography used in mapping the west Pilbara intrusions 6
2. Investigations of the west Pilbara layered intrusions 8

Regional setting of the west Pilbara Block

3. Precambrian stratigraphy of the Pilbara Block 12
4. Summary of isotopic ages 13
5. Statistics of major Archaean layered mafic-ultramafic intrusions 17

Munni Munni Complex

6. Stratigraphy 24
7. Summary of mineral associations and alteration relationships 38
8. Salient geochemical features of minerals 50
9. Composition of inverted pigeonite from the gabbroic zone 56
10. Composition of Cr-bearing spinel in the Munni Munni Complex region 58
11. Platinum-group minerals 69
12. Platinum-group-element and trace-element geochemistry 80

Page

13. Statistical summary of precious-metal data for the major rock groups 81
14. Precious-metal and trace-element geochemistry of the platiniferous horizon in DDH MMD 1 84
15. Pearson correlation coefficients for mineralised drill core 85
16. Pearson correlation coefficients for rock types from the ultramafic and gabbroic zones 90
17. Major geochemical subgroups with similar Pearson correlation coefficients 91

Mount Sholl Complex

18. Geochemical features of nickel-copper sulphide mineralisation 99

Radio Hill Complex

19. Generalised stratigraphy 104
20. Precious-metal and trace-element geochemistry 112
21. Precious-metal and trace-element geochemistry of the basal Ni-Cu sulphide mineralisation 115
22. Precious-metal and trace-element geochemistry of the basal Cu-Ni sulphide mineralisation 115

Maitland Complex

23. Precious-metal and trace-element geochemistry 122

Andover Complex

24. Stratigraphy 130
25. Precious-metal and trace-element geochemistry 139

Isotope studies

26. Neodymium isotope compositions of minerals and whole-rock samples from the Munni Munni Complex 142
27. Samarium and Nd whole-rock data for samples from the Munni Munni and Andover complexes 145

Page

28. Rubidium, Sr, and Nd data for minerals from the Munni Munni Complex and granite country rock 145

Petrogenesis

29. Estimated composition of the parent magma to the ultramafic zone of the Munni Munni Complex 151
30. Comparison of chilled rocks having siliceous high-magnesium komatiitic affinities 152
31. Calculated equilibration temperatures for coexisting clinopyroxene and orthopyroxene pairs 159
32. Calculated equilibration temperatures and oxygen fugacities for coexisting magnetite and ilmenite pairs 160
33. Pressure estimates based on the Ca Tschermak's molecule in clinopyroxene 161
34. Summary of sulphur-isotope compositions of west Pilbara layered intrusions 162
35. Sequences of cumulus minerals from various mafic-ultramafic geological settings 163
36. Compositions of parent magmas proposed for different layered intrusions 164

Remote sensing studies

37. Wavelengths recorded by Landsat-5 TM and NS001 scanners 169
38. Wavelengths recorded by TIMS scanner 169
39. Daedalus 1268 band combinations 177

Appendix 1

40. Nuclear parameters of isotopes and detection limits for RNAA data 188
41. Detection limits of XRFS and AAS major and trace elements 191
42. Accuracy of XRFS and AAS data 191

Appendix 2

43. Locations of samples from the Andover Complex 194

ABSTRACT

In a group of Archaean, layered, mafic-ultramafic intrusions in the west Pilbara Block, Western Australia, the Munni Munni Complex (2925 Ma) contains a substantial resource of PGEs (20--30 Mt @ 2.9 ppm Pt + Pd + Au) and other intrusions contain subeconomic resources of Ni and Cu. Contrasting PGE distribution patterns within the group indicate that the timing and mechanism of S-saturation were critical for the formation of PGE-enriched sulphide units. Generally, overlying mafic units are thicker than the rhythmically layered ultramafic components. Olivine and clinopyroxene were usually the first minerals to crystallise and cumulus orthopyroxene is restricted to the upper parts of the ultramafic zones. Chromium partitioned into early crystallising clinopyroxene, thus downgrading the potential for PGE-chromite associations. The parent magmas were probably siliceous, high-Mg basalts of Al-depleted komatiitic affinity. In this study, the variations of PGEs and incompatible trace elements were documented up the entire stratigraphic successions. In the Munni Munni Complex (the intrusion studied in most detail) the PGE-sulphide mineralisation is directly below the ultramafic/gabbroic contact and is thought to have resulted from crystal fractionation and mixing of S-undersaturated and S-saturated magmas; as in the Great Dyke of Zimbabwe, it does not occur at or near the base of clearly defined cyclic units. The other (smaller, mainly sheet-like) intrusions studied typically contain basal segregations of PGE-poor Ni-Cu sulphides; the magmas were generally S-saturated early in their evolution and there was no PGE enrichment at higher levels. In exploration, variations in the ratios of precious metals and the trends of the incompatible lithophile and chalcophile elements should be used in association with field and mineralogical evidence to indicate potential PGE-enrichment processes, such as S-saturation, crustal contamination, crystal fractionation, magma mixing, and/or hydrothermal remobilisation.

SUMMARY

In recent years, considerable exploration interest has been generated by the platinum-group-element (PGE) and Ni-Cu potential of Archaean layered mafic-ultramafic intrusions in the west Pilbara Block, Western Australia. The Munni Munni Complex contains the largest resource of PGEs (20–30 Mt of 2.9 ppm Pt + Pd + Au) associated with a layered intrusion in Australia. The Munni Munni (Sm/Nd mineral isochron age 2927 ± 13 Ma), Mount Sholl, Radio Hill, Maitland, and Andover complexes lie in a northeast-trending 25 x 80 km belt, in a granite-greenstone terrane. They share common field relationships and mineralogical, geochemical, and isotopic features, but their contrasting PGE distribution patterns show that the timing and the mechanism of the S-saturation event were critical for the development of PGE-enriched sulphide units.

The differentiated intrusions are thick (> 5.5 km) 'dyke'-like and relatively thin (1–2 km) sheet-like bodies that were emplaced at different levels and along major lithological discontinuities in the upper crust. Remote sensing (Thermal Infrared Multispectral Scanner and Thematic Mapper Simulator NS001) is useful in discriminating mafic and ultramafic rock units and structures in the layered intrusions. Generally, the rhythmically layered ultramafic components are thinner and occur along the northern side of the overlying more massive mafic components. The ultramafic zones consist of rhythmically layered dunite, lherzolite, wehrlite, olivine websterite, clinopyroxenite, and websterite; poorly-layered olivine gabbronorite, gabbronorite, gabbro, anorthositic gabbro, and anorthosite comprise the mafic sequences. Harzburgite, orthopyroxenite, and anorthosite are also major rock types in the ultramafic zone of the Andover Complex.

Olivine and clinopyroxene were generally the first minerals to crystallise, although, in the Andover Complex, orthopyroxene preceded clinopyroxene, which may reflect greater contamination of the parent magma by felsic crustal material. With the exception of the Andover Complex, the crystallisation of chromite was inhibited in the ultramafic zones by the high partitioning of Cr into the early crystallising clinopyroxene; this downgrades the potential of the west Pilbara intrusions for a PGE-chromite association. The parent magmas are believed to have been siliceous high-Mg basalts of Al-depleted (Barberton-type) komatiitic affinity with 9–12% MgO, 15–25 ppm Sc, 12–18 ppm Y, low Al_2O_3/TiO_2 (~ 11, or half chondrite ratios), and light-rare-earth enrichment (chondrite-normalised La/Sm = 2.7, La/Lu = 9.0).

The emphasis of the study has been to document the variations of PGEs and incompatible trace elements up the entire stratigraphic successions rather than focusing solely on the mineralised horizons. The PGE mineralisation in the Munni Munni Complex occurs in the upper levels of a porphyritic plagioclase websterite orthocumulate layer. The mineralisation is directly below the ultramafic/gabbroic zone contact (at the 1850 m level above the base of the intrusion) and is believed to have resulted from crystal fractionation and magma mixing. In the ultramafic zone, cyclic variations of olivine (mg_{83-71}) and clinopyroxene (mg_{89-58}) compositions and trends of incompatible-element concentrations normalised to 100% melt indicate that the lower and middle parts of the zone formed from regular new pulses of S-undersaturated primitive magma (containing ~ 600 ppm S), whereas above 1400 m magma input was more limited and closed-system fractionation generally prevailed. Owing to their incompatible behaviour, Pt, Pd, Au, Cu, S, Se, Cs, Rb, and Zr increased in the residual melt in the upper part of the zone, but Ir and Ni partitioned with early crystallising olivine and decreased in concentration with increasing fractionation. Mixing of the PGE-enriched fractionated components of the resident magma with a S-saturated gabbroic magma (~ 1700–2600 ppm S) by fountaining triggered S-saturation and established a moderately-high R factor (silicate/sulphide mass ratio) in the hybrid magma. The platinum-group minerals, comprising arsenides, sulpharsenides, tellurides, native metals, and Hg-bearing phases, form small (< 10 μm) grains enclosed in silicates or are associated with chalcopyrite-pentlandite-pyrrhotite blebs.

In geometry, stratigraphy, and mineralisation the Munni Munni Complex strongly resembles the Great Dyke of Zimbabwe, and together they appear to comprise a distinctive class of mineralised layered intrusion. Unlike the Bushveld, Stillwater, and Penikat (Finland) intrusions, PGE enrichment in these 'dyke-like bodies' occurred before the crystallisation of cumulus plagioclase and has no spatial or genetic relationships with cyclic units.

In contrast to the Munni Munni Complex, the magmas that formed the Mount Sholl, Radio Hill, Maitland, and Andover intrusions were saturated in S before they were emplaced into the magma chambers. These smaller, sheet-like intrusions typically contain basal segregations of PGE-poor (5–400 ppb Pt + Pd + Au, 1–45 ppb Ir) massive and disseminated pyrrhotite-chalcopyrite-pentlandite, although localised chalcopyrite-rich zones at Radio Hill contain enhanced Pd and Pt contents of up to 3330 and 1125 ppb, respectively. Ultramafic and mafic cumulates overlying the basal sulphides are low in PGEs (< 200 ppb Pt + Pd + Au), indicating that, because the magmas were S-saturated, there was no PGE enrichment by magmatic processes at higher stratigraphic levels.

Variations in the ratios of the precious metals and the trends of the incompatible lithophile and chalcophile elements are important in understanding the S evolution and PGE potential of layered intrusions in the west Pilbara Block and other Precambrian terranes. When used in association with field and mineralogical evidence, these chemical parameters may indicate the importance of potential PGE-enrichment processes, such as S-saturation, crustal contamination, crystal fractionation, magma mixing, and/or hydrothermal remobilisation.

INTRODUCTION (*DMH*)

Status of research into the genesis of layered mafic-ultramafic intrusions

During the past twenty years there have been important advances in the understanding of the magmatic and mineralising processes that operate in layered intrusions. Classical works by Wager & others (1960), Hess (1960), Jackson (1961, 1967, 1970), and Wager & Brown (1968) provided the foundation for this expanding research by introducing cumulus terminology for the classification of the rocks in layered intrusions. The basis of this genetic classification was the concept of gravitational settling, where dense early-crystallising minerals nucleate in the overlying primitive magma and settle through a less dense melt medium to the floor of the magma chamber. The accumulated crystals were referred to as 'cumulus crystals' and the melt component trapped among the crystals was called 'intercumulus liquid'. Irvine's (1965) study of the Duke Island ultramafic complex, Alaska, reinforced the ideas of gravitational settling by highlighting the analogy of sedimentary structures, *sensu stricto*, with magmatic structures, such as size-graded cumulus layers, preferred orientation of cumulus grains, cross-bedding, and slump features, that are observed in stratified cumulus sequences.

However, complications relating to the cumulus theory have been highlighted by various investigators and consequently different models and processes have been proposed that modify or supersede the cumulus theory. Campbell (1978) noted that for some intrusions:

- rhythmic layering involving plagioclase and pyroxene may be inverted, with the light plagioclase-rich cumulates at the base of the layer and heavy pyroxene-rich cumulates at the top;
- plagioclase cannot sink in Fe-rich tholeiitic liquids;
- igneous layering, cross-bedding, and graded-bedding are common in layered sequences with near-vertical primary dips; and
- the relative disposition of adcumulate rocks (containing up to 7 volume % intercumulus minerals) with orthocumulate rocks (25–50% intercumulus minerals) was also inconsistent with the results predicted by the cumulus theory.

Results from investigations of the crystallisation and layering features of the Skaergaard intrusion by McBirney & Noyes (1979) questioned the concept of crystal settling, and suggested that the controlling mechanism for layering was the relative rates of chemical and thermal diffusion during cooling. They proposed that fine rhythmic layering (millimetre to centimetre scale) could be achieved by periodic oscillatory nucleation and diffusion-controlled growth of different minerals. Another aspect of the *in situ* crystallisation concept was proposed by Maaløe (1978). He believed (1) that rhythmic layering was due to variations in nucleation rates of the primocrysts, i.e. where crystallisation occurs under supercooled conditions, and (2) that the crystallisation of one phase may change the composition of the magma, to influence the nucleation rates of other phases. Similarily, Morse's (1979) fractionation studies of the Kiglapait intrusion, Labrador, suggested rhythmic layering could be formed at the floor of the chamber by oscillations through a cotectic boundary; i.e., as a phase grows after attaining supersaturation, the surrounding melt becomes supersaturated in another phase, which subsequently nucleates and grows. Various further origins other than crystal settling have been postulated for the formation of rhythmic layering. These include multiple intrusion (Irvine, 1974b), intermittent currents (Hess, 1960; Wager & Brown, 1968; Irvine, 1983; Maaløe, 1987), rhythmic or oscillatory nucleation events in the magma (Hawkes, 1967; Goode, 1976; McBirney & Noyes, 1979; Parsons, 1979; Maaløe, 1987), density currents (Irvine, 1980d, 1987a), and solidification contraction (Petersen, 1987). Irvine (1982, 1987b) reviewed the nomenclature used for layered intrusions, with an emphasis on redefining the name 'cumulate', so that crystal settling was a possible but not essential process in the origin of rocks to which it is applied.

Mathison (1989) noted that the type of cumulate (adcumulate, mesocumulate, or orthocumulate) would be governed by various genetic factors, such as cooling and diffusion rates, the density of the residual magma at the crystallisation site (relative to the parent magma), and the extent of crystal settling, if any; and that the degree of cumulate compaction and consequent loss of intercumulus liquid would influence the efficiency of crystal-liquid separation.

In recent years a greater understanding of layered intrusions has been achieved by the application of low-temperature experimental studies which simulate the fluid dynamical and fractional crystallisation mechanisms that are believed to occur in magma chambers. Scaled-tank experiments involving aqueous solutions at various temperatures and containing salts and sugars of various densities (Chen & Turner, 1980; Irvine, 1980a; Huppert & Sparks, 1980; Huppert & Turner, 1981a, b; Sparks & others, 1984; Campbell & Turner, 1986a, b; Sparks & Huppert, 1987; Huppert & others, 1987; Tait & Kerr, 1987) have attempted to simulate various magmatic processes, such as convection, overturning, mixing, and crystallisation. Findings from these experiments have led to the concept of double-diffusive convection and its application to layered intrusions (Turner & Gustafson, 1978; Irvine 1980b; Irvine & others, 1983; Huppert & Sparks, 1984; Campbell & Turner, 1986b). Irvine & others (1983) believed double diffusion involved the formation of igneous layering where gently inclined layers were not deposited sequentially, but rather were formed concurrently by downdip accretion, with individual rock layers crystallising from a corresponding liquid layer. Irvine (1980c) noted that double-diffusive convection was important for heat and mass transfer between liquid layers, and that magmatic liquids can become stratified through density variations related to small differences in composition. This stratification can be a dominant control for convection, crystallisation, and mineralising processes. However, Sparks & Huppert (1987) have pointed out that results of McBirney (1985) and Spera & others (1986) have raised some doubt about the occurrence of double-diffusive layering in magmatic systems. In particular, it has not been ascertained under what circumstances this process can form in magma chambers, and it has become clear that some of the mechanisms observed in the tank experiments could prove to be unimportant in magma evolution.

Based on scaled-tank modelling studies and field evidence from the Skaergaard and Duke Island intrusions, Irvine (1980d, e, 1987a) suggested that density currents may be an important mechanism for the movement of

cumulates from the upper levels of the chamber to the floor, and for the development of rhythmically repeated modally graded layers. In this model, plagioclase crystals can be transported down via the walls of the magma chamber and spread across the cumulate floor, thus negating the problem of the buoyancy of plagioclase in tholeiitic melts. Irvine (1980d) has interpreted various layering structures, such as the distribution of xenoliths and unconformities—and the local erosion and redeposition of layered cumulates in response to impact of xenolithic blocks at low angles of incidence—to support the idea of current deposition. Bhattacharji & Smith (1964), Bhattacharji (1967), and Komar (1972a, b) postulated that flowage-differentiation is an important mechanism in causing magmas to separate into diverse rock types, and may produce chemical or cryptic zoning of the cumulates, such as that seen in the zoned feeder dyke of the Muskox intrusion, Canada, and the picritic dykes of Skye. However, Barriere (1976) argued that because of the 'Bagnold Effect' (grain dispersive pressure due to the shear of the suspension), magmatic differentiation related to flowage is not an applicable mechanism for intrusions with a width or diameter over 100 m.

In summary, there has been a greater acceptance of the concept of *in situ* crystallisation in recent years, but it is apparent that in some intrusions or parts of intrusions, gravitational (vertical movement), density-current, and flowage-differentiation mechanisms are also significant.

The improved understanding of magmatic processes operating in layered intrusions has also led to the development of various mineralisation models. Some broad generalisations about the geological setting of layered intrusions hosting significant platinum-group-element (PGE) deposits can be made. For example, they are generally Archaean or Early Proterozoic, are emplaced into stable tectonic terranes, and have stratigraphic thicknesses exceeding 5 km. But in detail there is considerable variation in style, stratigraphic level, and tenor of mineralisation that cannot be explained by a particular genetic model. This variation is highlighted by the Bushveld Complex where within one intrusion, PGE enrichment is related to magmatic, hydrothermal, and contamination processes, e.g: (1) narrow stratabound sulphide-bearing pegmatoidal layers 400–500 m above the appearance of cumulus plagioclase and in the vicinity of cumulus augite joining cumulus orthopyroxene (e.g. Merensky Reef); (2) chromitite layers (UG 2 and UG 3 chromitites); (3) discordant dunite pipes (Onverwacht and Driekop pipes); and (4) contaminated floor rocks (Platreef). Variations in mineralisation styles may reflect the relative importance of such factors as the chemical heterogeneity of the mantle source (e.g. source enriched in PGEs?), magma type and magma generation processes (e.g. boninite-type, second-stage melting of refractory mantle, timing of S saturation), magma chamber processes (crystal fractionation, crystallisation sequences, crustal contamination, magma mixing), and post-emplacement mechanisms (adcumulus growth, late magmatic fluids, hydrothermal remobilisation).

Various hypotheses relating to magmatic and hydrothermal mineralising processes in layered intrusions have been proposed. Some of the more important processes include: (1) liquid immiscibility; (2) filter pressing and ascending fluids; (3) crustal contamination; (4) crystal fractionation and the timing of S saturation; (5) magma mixing; (6) constitutional zone refining; and (7) hydrothermal processes.

(1) *Liquid immiscibility.* McDonald (1965) indicated that liquid immiscibility was an important process for the formation of Lower Critical Zone chromitite layers in the Bushveld Complex, and Vermaak (1976) suggested that sulphide immiscibility in the Merensky Reef was related to the increase in S fugacity following the depletion of iron in the magma due to the settling of chromite.

(2) *Filter pressing.* Vermaak (1976) and von Gruenewaldt (1979) argued that the PGE tenor of the Merensky Reef sulphides was upgraded by ascending, PGE-enriched, late-magmatic intercumulus fluids which had been expelled during the compaction of the underlying cumulus pile. Similarily, Boudreau & McCallum (1986) in their study of the Picket Pin deposit in the Stillwater Complex, noted the presence of transgressive sulphide zones and the Cu-rich nature of the sulphide assemblage and suggested that ascending hydrothermal fluids became trapped below impermeable anorthositic zones and were responsible for the PGE enrichment of the ores. Gain (1985) used the filter-pressing model to explain the PGE-enrichment of the UG 2 chromitite layer by the upward-migration of highly fractionated intercumulus fluids under highly reducing conditions.

(3) *Crustal contamination.* Contamination mechanisms that have been proposed for the driving of mafic magmas towards S saturation include the direct addition of S by the assimilation of sulphides, or H_2S, or SO_2-bearing material from the basement rocks, and the increase in fO_2 by addition of oxygen or water. Sulphide precipitation and crustal contamination along the basal contact of the Bushveld Complex have been discussed by Liebenberg (1970), de Waal (1977), von Gruenewaldt (1979), Grunshaw (1983), Buchanan & Rouse (1984), Cawthorn & others (1985a,b), and Barton & others (1986).

(4) *Crystal fractionation.* The incompatibility of Pt, Pd, and Rh during crystal fractionation of S-undersaturated magmas, and the importance of late S-saturation in these magmas for the development of PGE-enriched layers, has been highlighted by McCarthy & others (1984), Barnes & others (1985), Hamlyn & others (1985), Lee & Tredoux (1986), Hoatson & Keays (1987, 1989), and Wilson & Tredoux (1990).

(5) *Magma mixing.* There is now considerable evidence (Irvine, 1977; Sharpe, 1981; Irvine & others, 1983; Campbell & others, 1983; Campbell & Turner, 1986b; Irvine & Sharpe, 1986a,b; Naldrett & others, 1986, 1990; Hatton & von Gruenewaldt, 1987; Naldrett & others, 1987; Wilson & others, 1989; Hoatson & Keays, 1989; Prendergast & Keays, 1989; Eales & others, 1990a,b; Wilson & Tredoux, 1990) to indicate that magma mixing is an important mechanism which can induce saturation of sulphides and chromite in layered intrusions. Laterally extensive mineralised layers, such as the Merensky and J-M Reefs, are believed to have formed from the complex interactions between a fractionated, density-stratified resident magma and a hot new pulse of primitive magma that may be injected into the chamber as a plume or fountain. The formation of a plume or fountain depends largely on the relative densities of the two liquids and the velocity and volume of the new magma. Campbell & Naldrett (1979), Campbell & others (1983), and Naldrett (1989) have emphasised the importance of the R factor (i.e. the silicate/sulphide mass ratio) during turbulent magma mixing and the formation of a PGE-enriched layer. The most favourable condition for producing a high R factor is when a new, hot, buoyant pulse is injected into a density-stratified magma chamber. The pulse convects

turbulently, as it rises to find its own density level, where it spreads out laterally like a plume to form a hybrid layer. During the early crystallisation of plagioclase, the density of the magma increases, and the density stratification within the hybrid layer may destabilise, resulting in turbulent mixing with the resident magma and permitting equilibration of any immiscible sulphides with large volumes of silicate melt. Because of the large volume of melt, and the high partition coefficients of the PGEs for sulphides (in the range 10^4 to 10^5: Campbell & others, 1983; Campbell & Barnes, 1984; Barnes & Naldrett, 1985; Peach & others, 1989; Stone & others, 1990), the PGE tenor of the sulphides will be maximised. This proposed large-scale magma mixing accounts for the very high concentrations of PGEs in the mineralised layer (around 10 ppm Pt compared to 10 ppb Pt in the unmineralised cumulates) and can explain why the mineralised layer occurs about 500 m above the stratigraphic level where plagioclase first becomes a cumulus mineral. In an extension of this model, Naldrett & others (1986) suggested that the Merensky Reef formed from downspouts of a dense mixture of crystals, sulphides, and entrained liquid that spread out across the crystal-pile floor after having originated from the mixing of anorthositic and ultramafic magmas at higher levels in the chamber. Irvine & others (1983) and Campbell & others (1983) have described the fluid dynamics of various mixing models that involved magmas of different relative temperatures and compositions, and their effect on the R factor in plume, jet, and double-diffusive magma mixing systems.

Various isotopic systems (reviewed by Lambert & others, 1985), such as rhenium-osmium and osmium-osmium (Hart & Kinloch, 1989; Lambert & others, 1989, 1990; Richardson & others, 1989; Hattori & others, 1991), samarium-neodymium (Lambert & others, 1988, 1989, 1990; Martin, 1989), oxygen (Schiffries & Rye, 1989, 1990), lead (Auret & others, 1989; Wooden & others, 1991), sulphur (Godlevskii & Grinenko, 1963; Mainwaring & Naldrett, 1977; Ripley 1981, 1983; Zientek & Ripley, 1990), and strontium-rubidium and strontium-neodymium (Kruger & Marsh, 1982; DePaolo, 1985; Sharpe, 1985; Palacz & Tait, 1985; Kruger, 1989; Lee & others, 1989; Stewart & DePaolo, 1990; Eales & others, 1990a,b; Cawthorn & others, 1991) have been used (1) to provide geochronological data, and information about the magma source(s) and crustal contamination, and (2) to identify isotopically distinct magma types. Isotopic studies and geochemical studies of feeder-dykes and marginal rocks (Sharpe, 1981; Sharpe & Hulbert, 1985; Davies & Tredoux, 1985) have supported the hypothesis that the Merensky Reef formed from large-scale mixing of magmas of different composition, namely anorthositic (A-type) and ultramafic (U-type). The A-type magmas were largely tholeiitic, with low incompatible-element concentrations (von Gruenewaldt & others, 1985) whereas the U-type magmas had higher MgO and SiO_2 contents and were enriched in LIL elements and PGEs relative to the A-type magma. Mixing of different magma types has been proposed for the Stillwater Complex (Todd & others, 1982; Barnes & Naldrett, 1986; Lambert & Simmons, 1987, 1988), although the U-type magma is more evolved and the A-type magma is silica-undersaturated with respect to the equivalent magmas in the Bushveld Complex.

(6) *Constitutional zone refining.* The distribution of breccia, pegmatite, plagioclase-rich gabbro segregations, and extremely fractionated PGE proportions in the Lac des Iles Complex, Ontario (Brugmann & others, 1989) is believed to have resulted from volatile-induced partial melting of cumulates and subsequent S-saturation of the melt, a process that McBirney (1987) has referred to as 'constitutional zone refining'. Mineralisation is irregular and non-stratabound and is believed to have formed from the interaction of water with hot cumulates, and the subsequnet volatile-induced partial remelting of the overlying cumulates and the scavenging of the PGEs by an upward advancing melt. This style of remobilised PGE mineralisation is not believed to be of hydrothermal origin in the Lac des Iles intrusion, since typical vein-related hydrothermal alteration is absent and sulphides are not associated with veins, but are concentrated in specific rock types (Brugmann & others, 1989).

(7) *Hydrothermal processes.* In recent years there has been considerable debate about the relative importance of magmatic processes, *sensu stricto*, versus fluid-volatile processes in the formation of PGE deposits. It is generally recognised by most researchers that the primary mineralising mechanism for laterally-extensive stratabound deposits, such as the Merensky Reef and chromitite layers of the Bushveld Complex, and the J-M Reef of the Stillwater Complex, is largely magmatic. However, this is not the case for all deposit types and there appears to be a spectrum of enrichment mechanisms, ranging from dominant magmatic processes, through magmatic deposits which have various degrees of hydrothermal overprinting, to deposits which are largely hydrothermal-metasomatic in origin. Fluids transporting PGEs encompass a wide range of compositions and temperatures ranging from C-O-H-S-Cl volatile-fluids at 600°C in pegmatoidal pyroxenite horizons in layered intrusions, to chlorine brines around 300°C, down to temperatures of 4°C in sea water (Stumpfl, 1986).

Elliot & others (1982), Schiffries (1982), Boudreau & others (1986), Stumpfl (1986), Ballhaus & Stumpfl (1986), Stumpfl & Ballhaus (1986), Schiffries & Skinner (1987), Boudreau (1990a, b), Beaudoin & others (1990), and Stumpfl (1990) have used the occurrence of pegmatoidal bodies, discordant dunite pipes, potholes, veins, and the distribution of Cl-rich hydrous phases (notably apatite), intergrowth of sulphides with intercumulus hydrous phases, graphite, and fluid inclusions to highlight the importance of fluid-volatile systems in the transport and concentration of PGEs during the cooling history of a layered intrusion. In these models, Cl-rich fluids, which were generated by vapour exsolution from the intercumulus melt, are liberated and transport PGEs upwards from the trapped liquid in the underlying cumulus pile, to interact with S in the reefs to produce PGE-rich sulphides. Barnes & Campbell (1988), however, argue that these hydrothermal-type features are the result of postcumulus processes superimposed on layers whose extensive, uniform PGE concentrations were formed by magmatic cumulus processes. In defence of a magmatic origin, Barnes & Campbell (1988) noted the: (1) close association of PGEs with the bases of cyclic units and with chromitite layers, indicating a genetic relation to new magma influxes; (2) the lateral persistence of grade of the Merensky Reef and UG 2 chromitite; and (3) the systematic stratigraphic controls on PGE contents of sulphides within the UG 2 chromitite. In addition, they claim the ascending-hydrothermal-fluid models do not account for the paucity of mineralisation in horizons stratigraphically below the Merensky Reef, such as the Pseudoreef and various chromitite horizons, and they

also note that the highest grades often occur in the margins of some intrusions, e.g. Great Dyke, which do not overlie great thicknesses of ultramafic cumulates. Naldrett & others (1987) believe that the extreme stratiform nature and constant composition of mineralised layers, such as the Merensky Reef, and the difficulties inherent with the derivation of the PGEs from below, indicate that the PGE-bearing sulphides accumulated at the same time as the rocks enclosing them, from a homogeneous layer of magma.

Platinum-group-element mineralisation in Australia

Although minor, subeconomic PGE mineralisation is widespread in the Precambrian and Palaeozoic terranes of Australia, the only currently mined PGE resources are in the komatiitic Ni-Cu sulphide mineralisation of the Eastern Goldfields Province of the Yilgarn Block, WA, where significant PGE abundances are associated with other metals (Hoatson & Glaser, 1989). However,

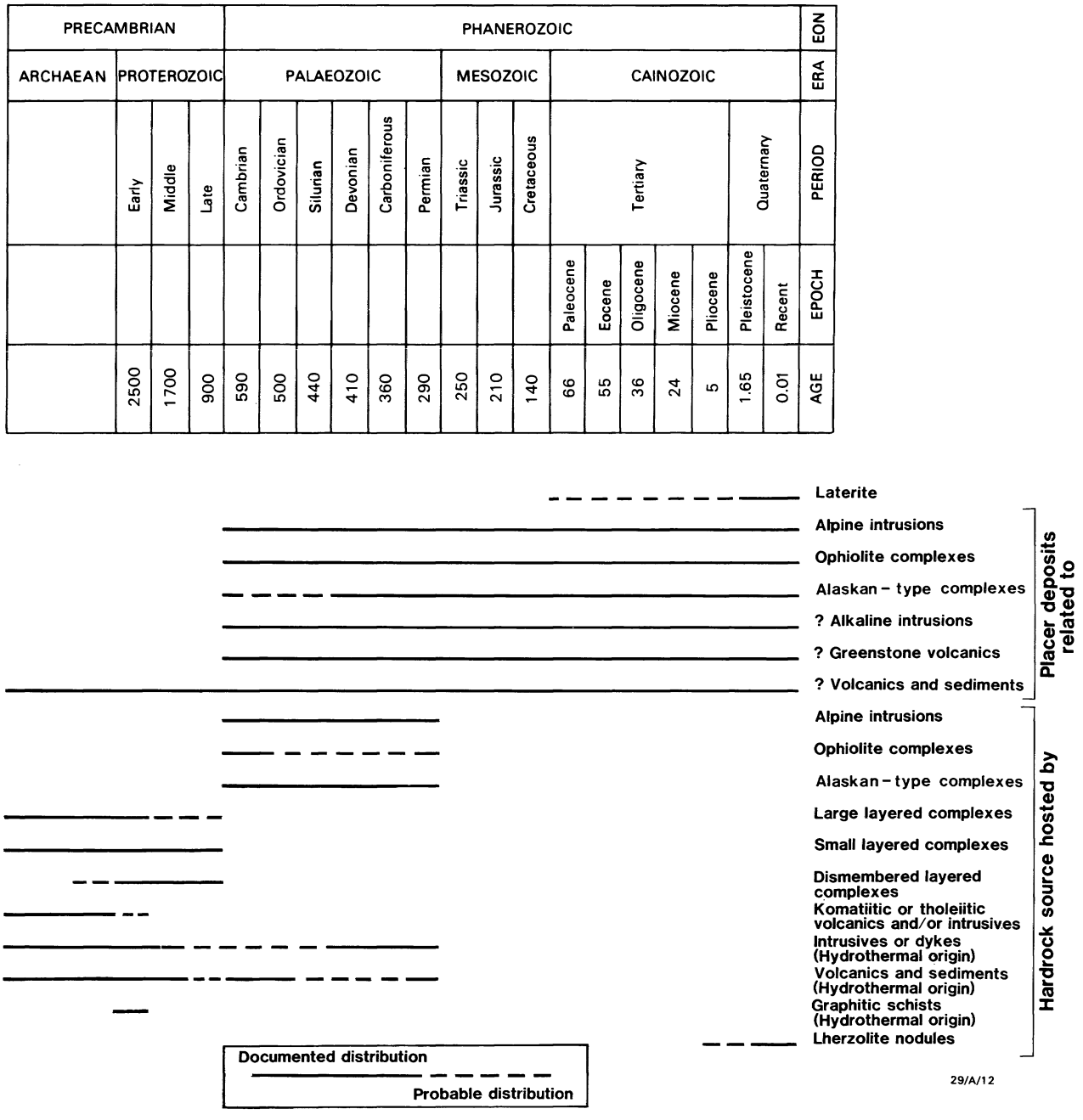

Fig. 1. Distribution of Australian platinum-group-element mineralisation styles with geological time. The ages of the placer deposits are not well constrained, but the source rocks for most of these deposits are generally Palaeozoic. Many of the placer deposits have had a complex history of reworking (erosion and burial) since the Palaeozoic.

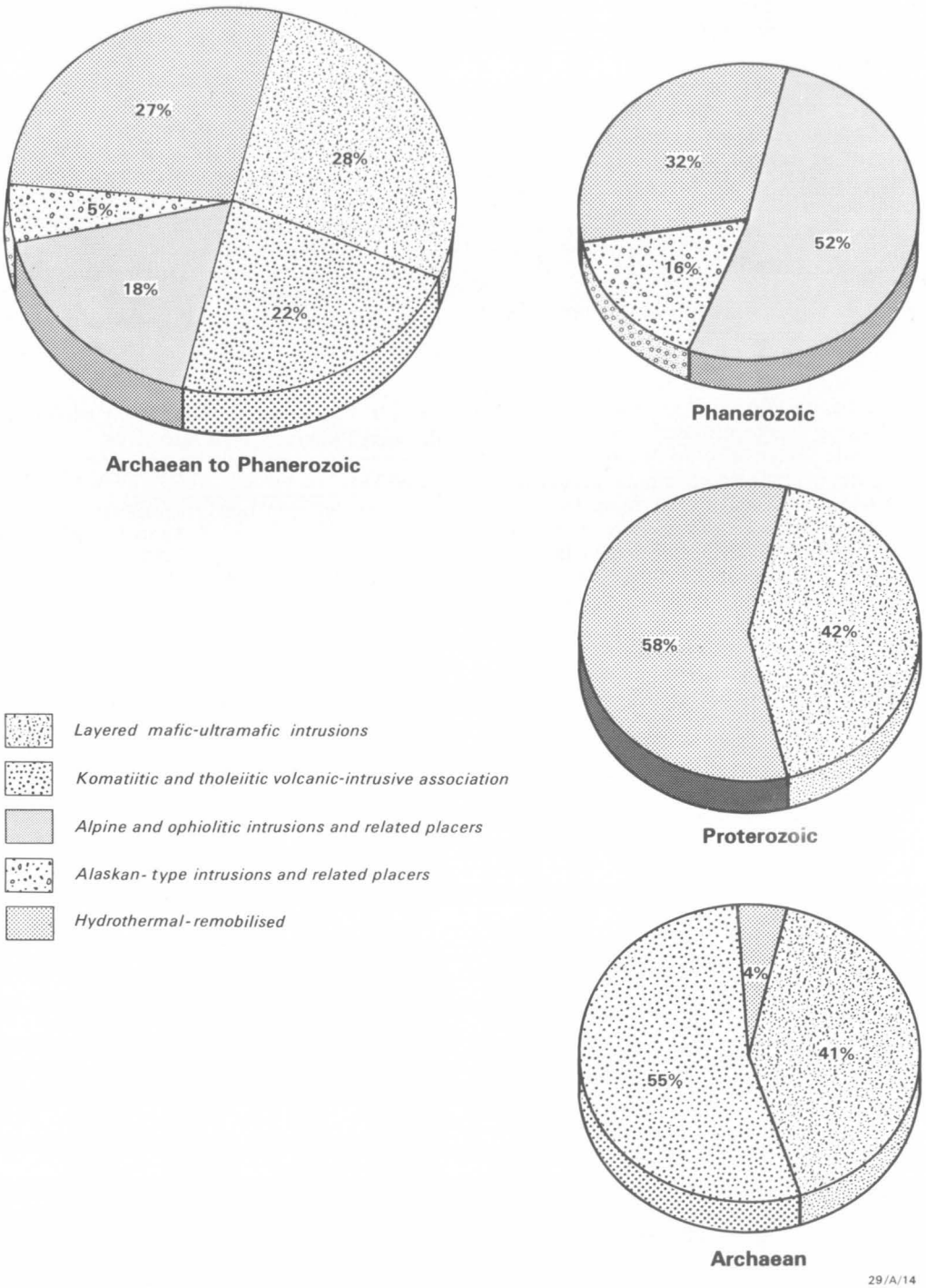

Fig. 2. Frequency of Australian platinum-group-element mineralisation styles with geological time, based on the number of platinum-group-element occurrences.

several prospects, such as Munni Munni, WA (sulphide-bearing layer in an Archaean layered mafic-ultramafic intrusion), Panton Sill, WA (sulphide-bearing chromitites in a tectonised Early Proterozoic mafic-ultramafic intrusion), Fifield, NSW (possible Alaskan-type intrusions), Coronation Hill, NT (remobilised Au-PGEs), and Yarawindah Brook, WA (laterite) have highlighted the geological potential of Australia for different styles of PGE mineralisation at economic levels (Hoatson, 1990a, b). In addition to these deposits there are many minor hard-rock occurrences of diverse geological setting and varying economic significance. When based on age of host rock and tectonic environment they can be subdivided into six hard-rock subclasses, with placer deposits forming another subclass. These occurrences encompass the three broader classes of Macdonald's (1987) petrogenetic classification of PGE deposits worldwide, namely orthomagmatic, hydrothermal, and alluvial.

Most Australian PGE occurrences can be related to the following geological settings:

— Layered mafic-ultramafic intrusions
— Fe-Cu-Ni sulphide deposits associated with komatiitic volcanics and intrusives
— Alpine and ophiolitic intrusions
— Alaskan-type intrusions
— Occurrences related to remobilisation, including hydrothermal activity
— Other settings, such as laterite, and carbonaceous sediments
— Placer deposits

Australian PGE occurrences appear to show associations with time and space (Hoatson & Glaser, 1989). These include: (1) sulphide-bearing 'layers' in large Archaean layered intrusions, or in komatiitic volcanic-intrusive sequences, in Western Australia; (2) sulphide-bearing chromitite cycles in dismembered intrusions in Proterozoic mobile zones, also in Western Australia; and (3) chromite in Palaeozoic alpine peridotite or ophiolite and related placers in eastern Australia. This distribution reflects the secular variation of the PGEs associated with S and Cr from the Archaean to the Proterozoic to the Phanerozoic. Platinum-group-element mineralisation related to Palaeozoic Alaskan-type intrusions does not appear to show any clear affinity with sulphides or chromite. However, PGEs in remobilised-hydrothermal settings are generally associated with Cu and Ni in the Archaean, Au and U in the Proterozoic, and Au, Ag, Cu, Ni, Pb, and As in Phanerozoic terranes.

The layered mafic-ultramafic-PGE association is most prominent in the Archaean Yilgarn and Pilbara blocks, and Proterozoic Halls Creek and Albany–Fraser mobile zones, whereas the komatiitic-hosted deposits are largely restricted to the eastern parts of the Yilgarn Block. Hard-rock occurrences related to small tectonised intrusions having alpine-ophiolite affinities and Alaskan-type intrusions are of Cambrian to Permian and Devonian age, respectively, and are confined to meridional belts in the Tasman Fold Belt System of eastern Australia. Remobilised (hydrothermal) PGE mineralisation is not restricted to any time period or tectonic setting. The age and frequency distribution of Australia's PGE occurrences are summarised in Figures 1 and 2, respectively.

Purpose, scope, and methods of the study, and nomenclature used

The main objectives of the study were to assess the geological setting and PGE potential of the major Archaean layered mafic-ultramafic intrusions of the west Pilbara Block. The study examined the field relationships, petrology, whole-rock major- and trace-element chemistry, mineral chemistry, Sm-Nd and Rb-Sr isotopic systematics, geophysical, and remote sensing features of the Munni Munni, Mount Sholl, Radio Hill, Maitland, and Andover complexes. The well-exposed Munni Munni Complex contains the largest resource of PGEs associated with a layered intrusion in Australia and forms the focus of the study. In contrast to PGE studies of layered intrusions overseas, which have generally been confined to the mineralised layer or the cyclic units that contain the mineralisation, the approach of this study has been to document the distribution of the PGEs, incompatible lithophile and chalcophile elements, and mineral chemistry throughout the entire intrusion. In addition, this information has been integrated with more detailed studies across cyclic units and in mineralised environments to provide a geochemical framework that can be readily used to assess the PGE potential of Proterozoic and Archaean layered intrusions.

An important aspect in the mapping of layered intrusions is the selection of a suitable scale that allows detailed documentation of structural and petrological features, such as the nature of layering and cumulus crystallisation trends. Details of the aerial photography used during the mapping are summarised in Table 1. The results of the field mapping and sampling of the Munni Munni, Mount Sholl, Radio Hill, and Maitland intrusions are shown on the appended 1 : 20 000 geological sheet, and the geology of the Andover Complex is shown in Figure 85.

Table 1. Colour aerial photography used in mapping the west Pilbara layered intrusions

Intrusion	*Scale*	*Description of aerial survey*
Munni Munni	1 : 11 000	Cherratta, Runs 1-6, flown by Aerial Surveys Australia, 2 May 1984
Mount Sholl	1 : 12 000	Mt Sholl, Runs 1-4, flown by Aerial Photographs & Surveys Pty Ltd, 30 October 1969
Radio Hill	1 : 17 000	Radio Hill, Run 2, flown by Associated Surveys International Pty Ltd, 9 July 1986
Maitland	1 : 13 500	Munni Munni, Runs 1-2, flown by Aerial Photographs & Surveys Pty Ltd, 27 February 1971
Andover	1 : 20 000	Roebourne/Andover Complex, Runs 1-3, flown by Australian Survey Office, 9 April 1986
Regional–west Pilbara Block	1 : 50 000	Karratha Joint Venture, Runs 1-5, flown by Aerial Surveys Australia, 28 October 1987

To complement the regional sampling coverage, detailed sampling at Munni Munni was carried out: (1) on a traverse across the entire intrusion at ~ 40 m spacing in the ultramafic zone and ~ 125 m spacing in the gabbroic zone (see appended map sheet); (2) at 10 m spacing over five cyclic units in subzones C and D of the ultramafic zone; and (3) at 0.25 to 10 m spacing across the mineralised contact between the ultramafic and gabbroic zones in the central part of the intrusion. This latter traverse incorporated diamond-drill core supplied by Hunter Resources Ltd. Sampling in the Mount Sholl Complex was undertaken along two regional traverses at right angles (see appended map sheet) to help establish geochemically the geometry of the intrusion. Basal sulphide mineralisation in drill core supplied by Whim Creek Consolidated was studied from the western (B_2 mineralised area), northern (B_1 mineralised area), and northeastern margins (A_1 mineralised area) of the Mount Sholl Complex to note if the mineralised settings have distinctive geochemical signatures and to document any lateral variations in PGE concentrations. Sampling was carried out along regional traverses in the Maitland, Andover, and Radio Hill intrusions, and drill core supplied by Agip Australia Pty Ltd was also used in the Radio Hill study. Samples for PGE analysis were selected on the basis of petrographic evaluation and trace-element geochemical criteria (e.g. using immobile incompatible-element trends, such as Zr, and various element ratios, such as Cu/Ni and S/Se). Sample preparation and analytical procedures are described in Appendix 1.

A combination of cumulus and traditional rock classifications has been employed in this study. The cumulus terminology has involved a hierarchical listing of cumulus minerals and a descriptive classification based on the abundance of intercumulus minerals, e.g. adcumulates have up to 7 volume % intercumulus minerals, mesocumulates 7–25%, and orthocumulates 25–50%. For other features relating to cumulates and their components, and layering elements of intrusions, the terminology proposed by Irvine (1982) is used. Complementing the cumulus terminology is the traditional classification of plutonic rocks based on the modal mineral content as recommended by the IUGS Subcommission on the Systematics of Igneous Rocks (Streckeisen, 1973, 1976).

Previous investigations and history of exploration

The Pilbara Block (Fig. 3) has experienced an intermittent history of explorative expeditions since 1861 when F. T. Gregory noted shallow-dipping sandstone capping granite and numerous 'trap dykes' during his investigation of the geography and pastoral potential of the northwest region of Western Australia (Gregory, 1861). In 1890, the Western Australian Government Geologist H. P. Woodward documented mineral occurrences in the Roebourne region, diorite at nearby Cossack, hornblende rock east of the Harding River, and black dolerite hills near Sherlock River (Woodward, 1890). Four years later Woodward (1894) produced a geological map of the Pilbara which differentiated metamorphic rocks (greenstones and granite) and Palaeozoic rocks (now recognised as Proterozoic rocks). Investigations during the turn of the century were stimulated by the establishment of the Geological Survey of Western Australia in 1896, and the search for minerals. The new Government Geologist, A. G. Maitland, was instrumental in this resurgence and published three Bulletins describing the geology of the Pilbara. Important geological maps featuring mafic-ultramafic rocks in the west Pilbara were compiled by Maitland (1909) and Woodward (1911).

The period between 1915 and 1960 witnessed only minor prospecting activity in the west Pilbara. In his assessment of the iron ore deposits of Western Australia, Connolly (1959) noted that the Andover Complex magnetite deposits were of low grade and had a high titanium content. Kriewaldt (1964) and Ryan (1966) published the Dampier–Barrow Island and Roebourne 1 : 250 000 geological sheets that encompass the Mount Sholl–Radio Hill and Andover complexes, respectively.

Ryan (1965) appears to have been the first investigator to describe a 'large basic igneous complex', which was later to be called the Munni Munni Complex by Williams (1968). Munni Munni is Aboriginal for 'striped rock' and refers to the striped appearance (due to preferential spinifex growth) on the sides of the Zebra Hill Dyke that traverses the southeastern margin of the Munni Munni Complex. Williams (1968) noted that the complex was folded (this study indicates this is unlikely), contained chrysotile, and magnetics showed it extended underneath the Proterozoic cover rocks (since also shown to be Archaean). Donaldson's (1974) petrographic study described the Munni Munni Complex as having layering and structural features similar to other major layered intrusions, and being derived from a tholeiitic basaltic magma that differentiated by *in situ* fractional crystallisation due to the removal of early-formed crystals by settling.

Some of the earliest workings in the Munni Munni Complex are shallow pits located in chrysotile-rich portions of sheared serpentinised dunite of the ultramafic zone (subzone B: see appended map sheet). The small scale of the diggings indicates that only minor amounts of asbestos were mined. Since the late 1960s, considerable company interest has developed in the Ni-Cu sulphide potential of the Archaean volcano-sedimentary successions (e.g. Ruth Well) and layered mafic-ultramafic intrusions (Mount Sholl, Radio Hill, and Munni Munni). Much of the impetus for this early exploration was generated by the discovery of the komatiitic-hosted Ni-Cu deposits of the eastern Yilgarn Block, WA, e.g. Kambalda and Mount Windarra. Consequently, exploration philosophies in the west Pilbara often paralleled the exploration strategies implemented in the Yilgarn, and were directed towards stratabound sulphide mineralisation near the basal contacts of the mafic-ultramafic successions. Aeromagnetics were initially used to facilitate the demarcation of poorly-exposed mafic-ultramafic rocks for follow-up reconnaissance mapping and gossan-search programs. Stream-sediment and soil sampling, ground magnetic, induced polarisation, electromagnetic and Sirotem geophysical surveys proved useful in the detection of sulphide-bearing mineralisation (de Angelis & others, 1987, 1988).

One of the first intrusions to be extensively explored in the west Pilbara was the Mount Sholl Complex. Diamond and percussion drilling along the western basal contact (B_2 region) defined disseminated and massive Ni-Cu mineralisation. The mineralisation is blind, and thus magnetic and electrical geophysical techniques were useful tools during the early phases of exploration. Intermittent exploration was carried out during 1960–1974, and culminated in the late 1970s, when Whim Creek Consolidated NL delineated a subeconomic resource of 4.04 million tonnes of sulphide ore grading 0.5% Ni and 0.6% Cu (0.5% Ni + Cu cutoff) (Marston, 1979; Mathison & Marshall, 1981). In the mid 1980s, Agip Australia Pty Ltd located extensions of the B_2 mineralisation to the southwest with similar subeconomic grades of around 1% Ni + Cu.

The potential for PGE mineralisation in the west Pilbara intrusions was not fully realised during the early phases of Ni-Cu exploration. Limited PGE analyses were carried out on Ni-rich intervals from near the basal contacts, and little consideration was given to possible PGE enrichment at higher stratigraphic levels, or in different settings, such as structurally controlled hydrothermal types of mineralisation.

The AGSO began a study of the Munni Munni Complex in 1983, as part of a regional evaluation of the PGE potential of layered intrusions in the Pilbara Block. Of particular interest was the Archaean age and large size of the intrusion and the presence of a porphyritic pyroxenite unit reported by Donaldson (1974) at the interface between the ultramafic and gabbroic zones. By analogy with large overseas intrusions where PGE mineralisation is commonly hosted by coarse-grained sulphide-bearing layers close to where plagioclase becomes an early-crystallising phase, it was believed by the present author (Hoatson, 1984, p. 45) that the Munni Munni Complex was prospective for PGE mineralisation at the base of cyclic units in the ultramafic zone, and/or in the porphyritic pyroxenite layer at the interface between the ultramafic and gabbroic zones, i.e. in the vicinity of the first appearance of cumulus plagioclase at the expense of cumulus olivine. Follow-

Table 2. Investigations of the west Pilbara layered intrusions

Year/s	*Intrusion/s*	*Company/Organisation*	*Program*
1968	Various	US Steel	Aeromagnetics Reconnaissance mapping, geochemistry
1969	Munni Munni	US Steel	Drilling (Ni, Cu)
1969–72	Munni Munni	Whim Creek, Westfield Minerals	Mapping, gossan search, stream and soil geochemistry, ground magnetics, Turam electromagnetics, drilling (Ni, Cu)
1969–78	Mount Sholl Radio Hill	Whim Creek, Westfield Minerals	Mapping, gossan search, stream and soil geochemistry, ground magnetics, induced polarisation, Turam, crone pulse electromagnetics, drilling (Ni, Cu), metallurgical tests
1981–82	Radio Hill	Teck Explorations	Aeromagnetics, Sirotem, mapping
1983	Munni Munni Mount Sholl Andover Gidley Dingo Cooya Pooya Ruth Well	AGSO	Reconnaissance mapping, rock geochemistry
1984–	Munni Munni Mount Sholl Radio Hill Maitland Andover	AGSO	Mapping, rock geochemistry, mineral chemistry, isotope analysis, remote-sensing studies
1984	Munni Munni	Hunter Resources	Mapping; soil, stream, rock geochemistry
1984–	Radio Hill Mount Sholl	Agip Australia	Mapping, soil and stream geochemistry, ground magnetics, electromagnetics, applied potential, Sirotem, gravity, drilling (Ni, Cu), metallurgical testing
1984–	Munni Munni	Agip Australia	Mapping, soil and trench geochemistry, ground magnetics, Sirotem, gradient-array induced polarisation
1985–	Munni Munni	Hunter Resources	Mapping, aeromagnetics, drilling (PGEs), metallurgical testing
1986–89	Andover	Greater Pacific Investments	Aeromagnetics, mapping, rock and trench geochemistry, diamond drilling (PGEs, Au)
1987–	Munni Munni North	Agip Australia	Drilling (Ag, Cu, Pb, Pd)

Whim Creek Consolidated NL and Agip Australia Pty Ltd information from de Angelis & others (1988).

up field sampling by AGSO in 1983 located sulphide-bearing porphyritic plagioclase websterite containing anomalous PGE concentrations near the ultramafic/gabbroic interface.

Hunter Resources Ltd in 1984 carried out a 400 m line-spaced soil geochemical survey and confirmed that the ultramafic/gabbroic contact zone region had potential for stratabound-type PGE mineralisation. Subtle geochemical signatures occurred on eight of the 11 soil traverses at the same stratigraphic position. Maximum soil geochemical results were 93 ppb Pt and 430 ppb Pd. Trenching intersected significant PGE anomalies in nine of the 15 trenches, and included a best intersection of 2 m averaging 2.3 ppm Pt and 1.7 ppm Pd in the porphyritic plagioclase websterite layer. To 1992, 66 diamond drillholes have been completed along a 7.5 km strike-length section of the mineralised layer, 63 of which have intersected the mineralised zone at the same stratigraphic level. The best intersection to date has been DDH MMD 34, which was drilled in the central part of the complex and obtained 5.5 m (543.0--548.5 m) @ 1.4 ppm Pt, 2.8 ppm Pd, 0.5 ppm Au, 0.7% Cu, and 0.3% Ni. A potential resource of 20 to 30 million tonnes of approximately 2.9 ppm Pt + Pd + Au, 0.3% Cu and 0.2% Ni has been delineated to a depth of 500 m. Rhodium and Au average 42 and 300 ppb, respectively, while Ru, Os, and Ir are present in minor amounts. The PGE mineralisation has been described by Hoatson & England (1986), Hoatson & Keays (1987, 1989), Williams & others (1990), Hoatson (1991), Sun & others (1991), and Barnes & others (1990, 1991, 1992).

Anomalous PGE grades of around 1 ppm have been defined by Hunter Resources Ltd in altered pyroxenite and gabbroic rocks along the southeastern contact of the Munni Munni Complex, near the Zebra Hill Dyke. These rocks are believed to be the southern extension of the mineralised porphyritic plagioclase websterite layer. In 1987, Agip Australia Pty Ltd investigated major lineaments at Munni Munni as potential loci for hydrothermal mineralisation. Spectacular secondarily-enriched Ag contents were reported, with an unusual polymetallic association on the Munni Munni Fault, near the basal contact of the ultramafic zone with the granite country rock. Percussion hole PH MM9 contained 6 m @ 3478 ppm Ag, including a peak of 2 m @ 6800 ppm Ag. Maximum values of 6450 ppm Cu, 3130 ppm Ti, 2180 ppm Ni, 1550 ppm Pb, and 494 ppm Mo were also present in the hole. Hole PH MM12 contained 9 m @ 0.21 ppm Au and 0.59 ppm Pd. The localised mineralisation consists of primary and supergene silver, chalcopyrite, chalcocite, bornite, pyrrhotite, linarite, pyrite, and marcasite (de Angelis & others, 1988).

Various geophysical (Peters & de Angelis, 1987) and diamond-drilling programs (de Angelis & others, 1987, 1988) during the 1980s defined a small Ni-Cu-PGE sulphide resource (1.1 Mt @ 2.5% Ni, 1.8% Cu) near the basal contact of the Radio Hill Complex. Underground mining operations began in 1991, but were soon terminated and the mine was placed on care-and-maintenance. In view of the encouraging exploration results at the Munni Munni Complex, Greater Pacific Investments Ltd in 1986–89 carried out a geophysical-geochemical program for precious metals at the Andover Complex. The program focused on contacts between mafic and ultramafic units, but results were disappointing. Table 2 summarises the exploration history of the west Pilbara layered intrusions.

Important contributions that review the metallogenesis of mafic-ultramafic rock associations in the west Pilbara Block include Baxter (1978), Marston (1979, 1984), Hickman (1983), Hoatson & Glaser (1989), Western Australia Geological Survey (1990), and Sun & others (1991).

Acknowledgements

This detailed study of the west Pilbara layered intrusions would not have been possible without the initial support of the then Chief of the Division of Petrology & Geochemistry at AGSO, Dr John Ferguson. The manuscript was improved by the constructive criticisms of John Sheraton, Lynton Jaques, John Creasey, Stewart Needham, Gladys Warren, Andrew Glikson (all AGSO), Gerhard von Grunewaldt (University of Pretoria, Pretoria), and David Lambert (Department of Earth Sciences, Monash University, Melbourne). Sandy Paine (consultant) is thanked for the editing of the Bulletin. We are indebted to Craig Williams of Hunter Resources Ltd, Peter Alexander of Whim Creek Consolidated NL, Charter Mathison of the University of Western Australia, and Marcello de Angelis of Agip Australia Pty Ltd for providing drill core and data from the Munni Munni, Mount Sholl, and Radio Hill complexes. Agip Australia Pty Ltd is thanked for the use of aerial photographs for the Radio Hill and Maitland complexes. The study benefited from discussions with many AGSO colleagues, and a number of non-AGSO geoscientists, including David Andrews, Steve Barnes, Ian Campbell, Dick England, Paul Hamlyn, Maurie Hoyle, Jenny Parks, and Frans Voermans.

Nick Ware (Research School of Earth Sciences, Australian National University, Canberra), and Dave Sewell and Pat Kelly (School of Earth Sciences, University of Melbourne) are gratefully acknowledged for their assistance with the electron microprobe work. Dean Hoatson thanks the RNAA and XRFS laboratory staff at the School of Earth Sciences, University of Melbourne. Bruce Cruikshank, John Pyke, Bill Pappas, and Julie Haldane carried out the XRFS-AAS analyses, and Julie Kamprad and Robert Drew (all AGSO) the XRD analyses and S isotope determinations, respectively. Shen-Su Sun thanks Malcolm McCulloch for the use of isotope analytical facilities at the Australian National University. Shane Reeves (School of Earth Sciences, University of Melbourne) carried out the RNAA data from the Radio Hill, Maitland, and Andover intrusions.

Heike Apps, Vera Ashby, Jill Clarke, Neale Jeffrey, Joe Mifsud, Neville Montgomerie, and Karen Somerville drafted the line figures, and the professional cartographic skills of Terry Brown and Geoff Butterworth are evident in the appended 1 : 20 000 geological map sheet of the west Pilbara layered intrusions.

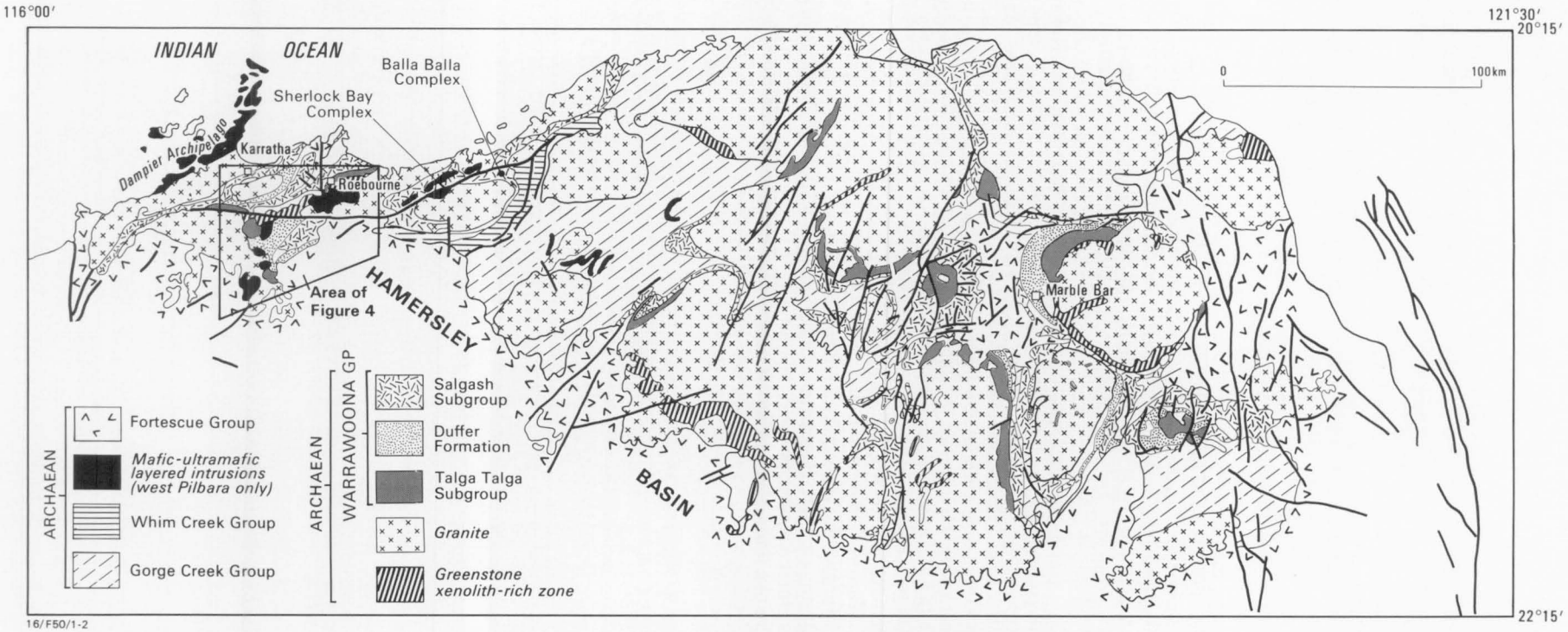

Fig. 3. Geology of the Pilbara Block (modified after Hickman, 1983).

REGIONAL GEOLOGY, METALLOGENESIS, AND TECTONIC EVOLUTION OF THE WEST PILBARA BLOCK *(DMH)*

Introduction

The Pilbara Block (Fig. 3) is an elongate east–west trending Archaean (~ 3600–2850 Ma) granite-greenstone terrane covering about 60 000 km^2. It is unconformably overlain by sediments and volcanics of the late Archaean to Early Proterozoic (about 2765 to < 2500 Ma) Mount Bruce Supergroup (Table 3) to the south and east, and Phanerozoic sediments to the north. The Pilbara Block is the best exposed granite-greenstone terrane in Australia, consisting of domal granitic batholiths separated by synclinal belts of greenschist- to lower-amphibolite-facies metasedimentary and metavolcanic rocks, collectively called the Pilbara Supergroup (Hickman, 1981). In contrast to the central and eastern parts of the Pilbara Block, the west Pilbara (Figs. 4, 5) is characterised by a number of large, differentiated, Archaean layered mafic-ultramafic intrusions (e.g. Munni Munni, Andover, and Mount Sholl) and mafic sills (Cooya Pooya Dolerite). The most comprehensive geological summaries of the Pilbara Block are given by Hickman (1981, 1983) and Griffin (1990).

The Pilbara Block had a prolonged evolutionary history in the early part of the Precambrian. Table 4 is a summary of isotopic ages that have been documented for the Mount Bruce and Pilbara Supergroups, and various intrusions in the western Pilbara Block. It is apparent that certain isotopic systems have been reset by younger geological events, such as metamorphism and regional hydrothermal alteration (e.g. some of the younger Rb-Sr ages for the Pilbara granitoids in Table 4), or were susceptible to crustal contamination (e.g. the Sm-Nd ages of entries 23 to 25 in Table 4 are probably at least 200 Ma too old).

Archaean sedimentary-volcanic units of the Pilbara Supergroup

The volcanic-dominated Warrawoona Group is the oldest supracrustal sequence in the Pilbara Supergroup (Table 3). The 3600 to 3300 Ma old group is composed of komatiitic and tholeiitic basalts, interlayered with cherty sediments and calc-alkaline volcanics which are commonly preserved in synclinal belts around ovoid to elongated granitoid batholiths (Barley, 1984). The total thickness of the group is about 15 km. In the west Pilbara, volcanic sequences near Mount Sholl and Munni Munni have been tentatively correlated with Hickman's (1983) Talga Talga Subgroup and Duffer Formation of the lower Warrawoona Group (Table 3). However, Horwitz (1988) questioned the validity of the Warrawoona Group stratigraphy used by Hickman (1983) in the Mount Sholl region. He suggested the stratigraphy was more consistent with the younger Whim Creek Group (~ 2900 to 3100 Ma) located further east. Further detailed stratigraphic studies supported by unambiguous geochronological data are required to resolve this problem. In this study, 'Warrawoona Group' is used rather than 'Whim Creek Group' for the metavolcanic successions near the Mount Sholl, Radio Hill, Maitland, and Munni Munni intrusions.

Volcanic sequences surrounding the Mount Sholl intrusion (see appended map sheet) have been subdivided into three associations: (1) metabasalt, chert, and metadolerite sills (?Talga Talga Subgroup); (2) meta-andesite and pyroclastics (?Duffer Formation); and (3) metarhyolite, metarhyodacite, chert, and pyroclastics (?Duffer Formation). The intermediate and felsic volcanics of associations (2) and (3) are the dominant rock types, exposed along the margins of the Mount Sholl intrusion, whereas the Talga Talga metabasalts are prominent in the B_2 mineralised zone and in alluvium-covered valleys along the eastern side of the intrusion (see appended map sheet). A feature of the volcanic successions is the lateral variation of rock types along their northeastern strike. This is particularly evident in the B_2 region where pillowed and aphanitic metabasalts intercalated with meta-andesite, metarhyolite, chert, and metadolerite sills show rapid facies changes. The sills are distinguished from younger (?Early Proterozoic) dolerite dykes by their conformable relationship to the enclosing metavolcanics and their microporphyritic spotted textures. The pyroclastics are a minor component of the Duffer Formation, and consist of thin ash tuff, crystal tuff, ignimbrite, and rare agglomerate units. Epidotisation and silicification are pervasive in most mafic volcanic units.

The oldest rocks around the Munni Munni Complex occur near the northeastern margin of the intrusion, where areas of intercalated phyllite, schist, psammite, calc-silicate, and gneiss in granite are correlated with the Talga Talga Subgroup (?McPhee Formation and North Star Basalt). The fissile and gneissic character of these rocks may be related, in part, to shearing during the early development of the Munni Munni magma chamber.

Archaean sedimentary-volcanic units of the basal Fortescue Group

The Fortescue Group (Table 3) is the lowest group of the Mount Bruce Supergroup and rests unconformably on the southern margin of the Pilbara Block. It consists of a complex succession of shallow-dipping subaerial and subaqueous tholeiitic basalt, basaltic andesite, high-Mg basalt, komatiite, mafic tuff, felsic tuff, felsic pyroclastic breccia, epiclastic volcanic rocks, minor carbonate sedimentary rocks, and terrigenous clastic sedimentary rocks (Blake, 1990).

The base of the Fortescue Group is estimated to have a minimum age of about 2765 Ma (Arndt & others, 1991). It covers about 40 000 km^2 and varies in thickness from over 6 km in the south to about 0.5 km at the extreme southeast limit of its outcrop (Arndt & others, 1991). The earliest formations of the group filled the basins of the Pilbara palaeo-surface, and later formations progressively encroached onto granitic topographic highs. The present outcrop of the Fortescue Group does not reflect the size and shape of original depositional systems, but rather has been determined by syn- and post-Fortescue Group folding, faulting and erosion (Blake, 1990). During the late Archaean, the group covered the entire Pilbara craton, but erosion has since removed most of the platform sequence from the craton (Hickman, 1983). Arndt & others (1991) have estimated that the deposition rate for the whole Fortescue Group was in the range of 40 to 120 m per Ma, although during the period of initial volcanism at 2765 Ma local depositional rates may have been as high as 1000 m per Ma. Blake (1984) believes that deposition of the Fortescue Group resulted from the superimposition of a regional tensional regime on a

Table 3. Precambrian stratigraphy of the Pilbara Block (after Hickman, 1983)

		Formation	Major lithologies	General thickness (km)
MOUNT BRUCE SUPERGROUP — Archaean to Early Proterozoic	FORTESCUE GROUP	Jeerinah Formation	Shale, sandstone, chert	0.3
		Maddina Basalt	Basalt	0.2
		Kuruna Siltstone	Siltstone	0.1
		Nymerina Basalt	Basalt	0.3
		Tumbiana Formation	Tuff, limestone	< 0.1
		Kylena Basalt	Basalt, sandstone	0.3
		Hardey Sandstone	Sandstone, conglomerate, shale	1.0
		Mount Roe Basalt	Basalt, agglomerate	0.2
PILBARA SUPERGROUP — Archaean		Negri Volcanics	Basalt, andesite	0.2
		Louden Formation	Basalt, ultramafics	1.0
		WHIM CREEK GROUP	Volcanics, minor sediments	0.9
		GORGE CREEK GROUP	Sediments, minor volcanics	12.5
	WARRAWOONA GROUP	Wyman Formation	Rhyolite, tuff	1.0
	Salgash Subgroup	Euro Basalt	Basalt, dolerite	2.0
		Panorama Formation	Felsic volcanics, sediments	1.0
		Apex Basalt	Basalt and high-Mg basalt	2.0
		Towers Formation	Chert, basalt	0.5
		Duffer Formation	Felsic volcanics	5.0
	Talga Talga Subgroup	Mount Ada Basalt	Basalt	2.0
		McPhee Formation	Carbonate, schist, chert	0.1
		North Star Basalt	Basalt, dolerite	2.0

Table 4. Summary of isotopic ages for the west Pilbara Block

Stratigraphic unit	*Age (Ma)*	*Dating method*	*Reference*
Mount Bruce Supergroup			
Fortescue Group			
(1) Various basalts	2100–2300	Rb-Sr (whole rock/ mineral isochron)	de Laeter & Trendall, *in* Trendall (1983)
(2) Jeerinah Formation	2684 ± 6	U-Pb (zircon)	Arndt & others (1991)
(3) Jeerinah Formation	2690 ± 16	U-Pb (zircon)	Arndt & others (1991)
(4) Pillingini Tuff	2715 ± 6 2936 ± 6 3200–3350	U-Pb (zircon)	Arndt & others (1991)
(5) Kylena Basalt	2760 ± 20	Pb (model)	Richards & others (1981)
(6) Kylena Basalt	2760 ± 30	Pb (model)	Richards & Blockley (1984)
(7) Lyre Creek Formation	2900–3250	U-Pb (zircon)	Arndt & others (1991)
(8) Cliff Springs Sandstone	2878	Rb-Sr (model)	Compston & Arriens (1968)
(9) Hardey Sandstone	2707 ± 151	Rb-Sr (whole rock/ mineral isochron)	Hickman & de Laeter (1977)
(10) Mount Roe Basalt	2028 ± 168	Rb-Sr (whole rock/ mineral isochron)	de Laeter & others, *in* Trendall (1983)
(11) Mount Roe Basalt	2545 ± 292	Pb-Pb (whole rock/ mineral isochron)	University of Western Australia (unpublished data)
(12) Mount Roe Basalt	2375 ± 200	Pb-Pb (whole rock/ mineral isochron)	University of Western Australia (unpublished data)
(13) Mount Roe Basalt	2775 ± 10	U-Pb (zircon)	Arndt & others (1991)
(14) Mount Roe Basalt	2763 ± 13	U-Pb (zircon)	Arndt & others (1991)
(15) Basal lavas	2770 ± 10	Pb (model)	Richards (1981)
(16) Base of Fortescue Group	2765	U-Pb (zircon)	Arndt & others (1991)
Pilbara Supergroup			
Warrawoona Group			
(17) Duffer Formation	3400	Sm-Nd (model)	Collerson & McCulloch (1983)
(18) Duffer Formation	3430	Sm-Nd (model)	Collerson & McCulloch (1983)
(19) Duffer Formation	3452 ± 16	U-Pb (zircon)	Pidgeon (1978)
(20) Duffer Formation	3470 ± 10	Pb (model)	Richards & others (1981)
(21) Duffer Formation	3506 ± 62	Rb-Sr (whole rock/ mineral isochron)	Cooper & others (1982)
(22) North Star Basalt	3560 ± 32	Sm-Nd (isochron)	Hamilton & others (1981)
(23) Mount Ada and North Star Basalts	3695 ± 47	Sm-Nd (isochron)	Glikson (1986)
(24) Talga Talga Subgroup	<3712 ± 98	Sm-Nd (whole rock)	Gruau & others (1987)
(25) Talga Talga Subgroup	3517 ± 80	Sm-Nd (whole rock)	Gruau & others (1987)
Minor intrusions into Fortescue Group			
(26) Black Range Dolerite	2280 ± 89	Rb-Sr (whole rock/ mineral isochron)	Lewis & others (1975)
(27) Spinaway Porphyry	2610 ± 20	Pb (model)	University of Western Australia (unpublished data)
(28) Spinaway Porphyry	2768 ± 16	U-Pb (zircon)	Pidgeon (1984)
(29) Vein in intrusive dolerite	2720 ± 20	Pb (model)	Richards & others (1981)
Mafic-ultramafic intrusions			
(30) Gidley Granophyre	2150 ± 26	Rb-Sr (whole rock/ mineral isochron)	de Laeter & Trendall (1971)
(31) Gidley Granophyre	2557 ± 56	Rb-Sr (whole rock/ mineral isochron)	de Laeter & Trendall (1971)
(32) Munni Munni Complex	2925 ± 16	U-Pb (zircon)	Arndt & others (1991)
(33) Munni Munni Complex	2927 ± 13	Sm-Nd (mineral isochron)	Sun & Hoatson (this Bulletin)
(34) Millindinna Complex*	2830 ± 20	Sm-Nd (whole rock/ mineral isochron)	Korsch & Gulson (1986)
(35) Millindinna Complex*	2960 ± 20	Pb-Pb (whole rock)	Korsch & Gulson (1986)
Granitoid intrusions			
(36) Harding Granite	1800 ± 30	Pb (model)	Richards & others (1981)
(37) Harding Granite	1990 ± 40	Pb (model)	Richards & others (1981)
(38) Satirist Granite	2242	Rb-Sr (whole rock/ mineral isochron)	Leggo & others (1965)
(39) Satirist Granite	2976	Rb-Sr (model)	Leggo & others (1965)
(40) Mons Cupri Granite	2366 ± 60	Rb-Sr (whole rock/ mineral isochron)	Sylvester & de Laeter (1987)
(41) Mons Cupri Granite	2471 ± 172	Rb-Sr (whole rock/ mineral isochron)	Sylvester & de Laeter (1978, unpublished data)
(42) Mons Cupri Porphyry	2610 ± 80	Rb-Sr (whole rock)	Sylvester & de Laeter (1987)
(43) Caines Well Granite	2713 ± 53	Rb-Sr (whole rock/ mineral isochron)	Sylvester & de Laeter (1987)

Table 4 (continued). Summary of isotopic ages for the west Pilbara Block

Stratigraphic unit	*Age (Ma)*	*Dating method*	*Reference*
(44) Caines Well Granite	2975 ± 107	Rb-Sr (whole rock/ mineral isochron)	Sylvester & de Laeter (1978, unpublished data)
(45) Caines Well Granite	ca 3000	Rb-Sr (model)	Sylvester & de Laeter (1987)
(46) Munni Munni granite	3000	Sm-Nd (model)	Sun (1985, unpublished data)

* Refers to a number of intrusions in the west Pilbara Block. Samples came from the Andover Complex and mafic-ultramafic intrusions at the southwestern margin of the Caines Well Granite, near Little Sherlock and George rivers.

Data in this table partly from Blake & McNaughton (1984) and Barley & McNaughton (1988).

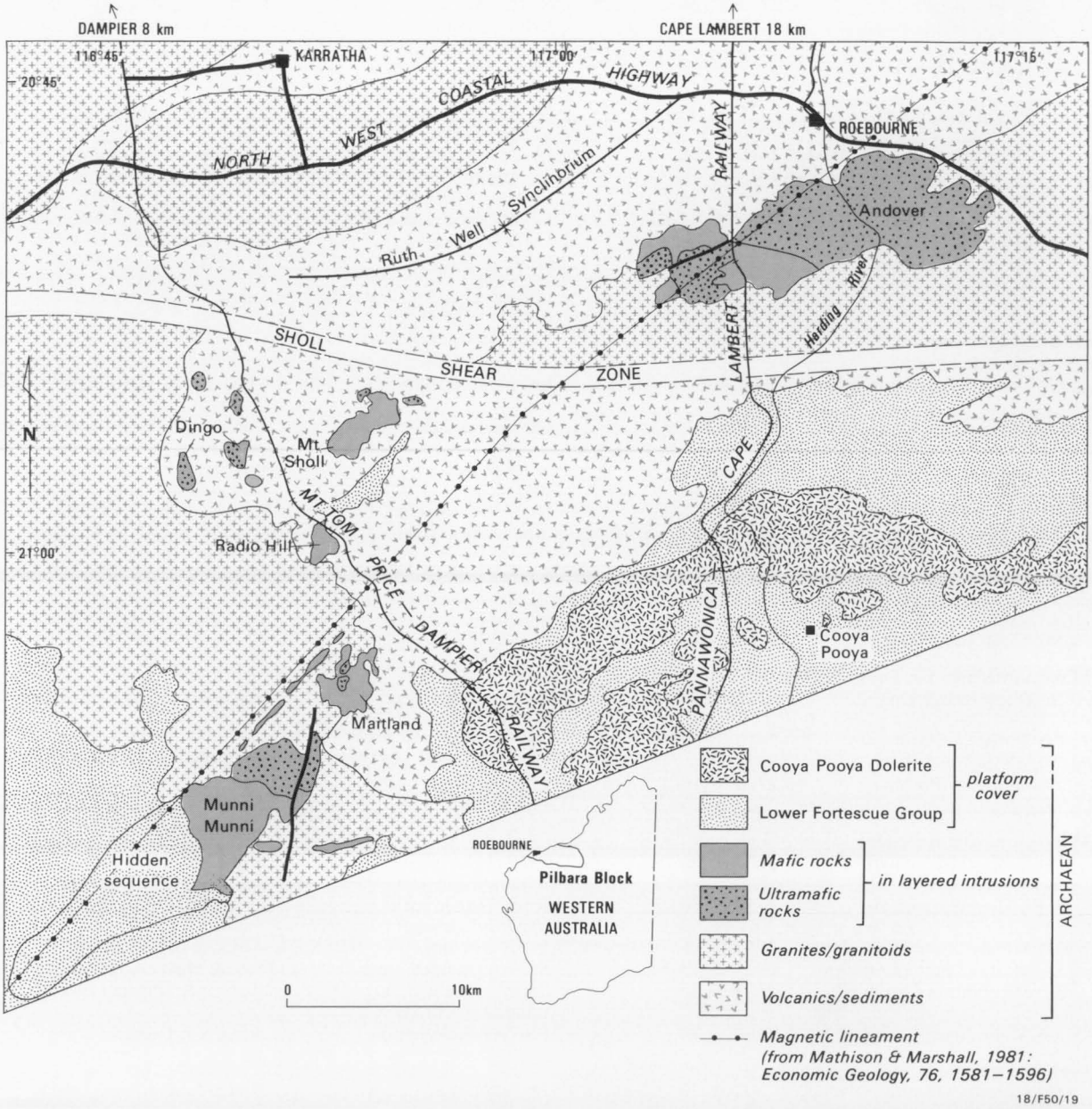

Fig. 4. Distribution of outcropping Archaean layered mafic-ultramafic intrusions in the west Pilbara Block. Distribution of Lower Fortescue Group, Cooya Pooya Dolerite, volcanics and sediments from Hickman (1983).

stabilised Archaean craton, although minor diapiric movements resulted in some local internal mobility. Significant lithospheric thickening and associated stabilisation occurred during the 130 to 160 million years between the last Archaean plutonism and the commencement of the Fortescue Group deposition. These events marked a major change in the tectonic evolution of the Pilbara Block.

Blake (1990) noted that the volcanic rocks of the Fortescue Group showed similarities in total thickness, areal extent, proportions of mafic to felsic rocks, basalt flow morphologies, associated dykes and sills, and geo-

chemistry to Phanerozoic flood basalt terranes. The thick clastic sedimentary sequences were deposited in discrete extensional basins within a craton-wide tensional stress field. He stated that such an association of volcanics and extensional structures was consistent with major continental rifting.

The lowest two Archaean formations of the Fortescue Group, the Mount Roe Basalt and the Hardey Sandstone (Table 3), were briefly investigated in this study. Flanking the southeast side of the Mount Sholl intrusion is a southwest-trending upthrown block which contains shallow-dipping Mount Roe Basalt unconformably overlying steeply-dipping Duffer Formation metavolcanics (see appended map sheet). The Mount Roe Basalt sequence consists of amygdaloidal and massive basalt, andesite, epidotised chert, ferruginous siltstone, sandstone, and tuff.

The Hardey Sandstone conformably overlies the Mount Roe Basalt, or in places unconformably overlies the Archaean craton. A shallow-dipping ($< 30°$) platform sequence of arenaceous, argillaceous, and pyroclastic sediments covering the southwestern extension of the Munni Munni Complex is here correlated with the Hardey Sandstone. Rock types include siltstone, chloritic shale, greywacke, sandstone, tuff, agglomerate, and minor felsic lavas. At the southwestern corner of the Munni Munni Complex, argillaceous sediments of the Hardey Sandstone become increasingly ferruginous towards a well defined sub-horizontal unconformity with the underlying basement granites.

Archaean granitoid intrusions

Granitic rocks constitute about 60% of the Pilbara Block and range in composition from alkali-feldspar granite to tonalite (Hickman, 1983). Blake & McNaughton (1984) have recognised two major age groups for the granitoids and gneisses, namely 3500–3300 Ma and 3050–2850 Ma. Major batholiths in the west Pilbara include the Balla Balla Granite, Caines Well Granite, Cherratta Batholith, Harding Granite, Karratha Batholith, Portree Granite, and Satirist Granite. The granite batholiths are generally poorly exposed and have not been studied in detail. Dominant rock types include foliated monzogranite, granodiorite, microcline granite, adamellite, and migmatite.

Granitic rocks abutting the Munni Munni Complex have been subdivided into (1) northern and eastern granites, and (2) western granites, based on subtle differences in accessory mineral assemblages and textures. Ferromagnesian minerals rarely exceed 3 vol. % in both the northeastern and western granites.

(1) The northern and eastern granites crop out along the northeastern and southeastern margins of the intrusion and comprise gneiss, gneissic granite, equigranular leucocratic microcline granite, and granodiorite. Granites along the northeastern margin are strongly foliated: gneiss and gneissic granite predominate over more homogeneously textured varieties. The gneissic fabric decreases southwards along the eastern contact, with granitic rocks adjacent to the gabbroic zone showing an incipient foliation defined by the alignment of mica. The northern and eastern granites contain similar amounts of quartz, albitised microcline, plagioclase, and accessory biotite, muscovite, zircon, apatite, and magnetite. A weakly-foliated, leucocratic microcline granite near the eastern margin of the Munni Munni intrusion has a T^{Nd}_{CHUR} model age of 3000 Ma (S-S. Sun, personal communication, 1985).

(2) The western granites occur along the northwestern side of the Munni Munni intrusion from near the southern end of the Pinderi Hills Dyke towards the Fortescue Group in the south. They contrast with the northeastern granites through the absence of strongly foliated textures, the presence of microcline and plagioclase phenocrysts, the greater intensity of albitisation of microcline, and the absence of muscovite and zircon.

On the western side of the intrusion and immediately southwest of Munni Munni Creek, some large, isolated, hornblende quartz syenite outcrops are discordant with the southwest extension of the Munni Munni ultramafic stratigraphy. These more mafic granitoids of I-type affinity may be younger than the western granite and the Munni Munni Complex. They comprise albitised microcline, plagioclase, minor quartz, hornblende, and accessory ferrostilpnomelane, chlorite, ferroactinolite, calcite, apatite, magnetite, epidote, and sphene.

Leucocratic biotite-muscovite granite, aplitic granite, and granodiorite crop out along the western and southeastern margins of the Maitland and Radio Hill complexes, respectively, but no such rocks ocur in the vicinity of the Mount Sholl Complex. Leucocratic granite, granodiorite, tonalite, and hybrid granite characterise the southern margin of the Andover Complex.

Archaean layered mafic-ultramafic intrusions and metallogenesis

Synopsis

In addition to the five intrusions documented in this study, a number of smaller layered mafic-ultramafic intrusions occur in the west Pilbara Block (e.g. Balla Balla, Dingo, Gidley Granophyre, and Sherlock Bay complexes). With the exception of the younger Gidley Granophyre Complex (2557 ± 56 Ma: de Laeter & Trendall, 1971) that forms the Dampier Archipelago, the west Pilbara intrusions occur in a northeast-trending belt, 120 km long and 35 km wide, stretching from the Munni Munni Complex in the southwest to the Balla Balla Complex ~ 65 km east of Roebourne (Hoatson & Barnes, 1991). The zone crosses the Sholl Shear Zone (Fig. 4), a major crustal dislocation which extends over 140 km and has a sinistral displacement of 20 to 30 km (Hickman, 1983).

Fitton & others (1975) grouped many of the Pilbara intrusions into one major complex, the 'Millindinna Complex'. They believed that this extensive differentiated complex, covering an area of 40 000 km^2, was emplaced along a regional unconformity between upper and lower Archaean successions. Hickman (1983) argued that since the intrusions occur at many different stratigraphic levels, the concept of a single intrusive sheet occupying one particular stratigraphic horizon should be rejected. Age determinations for the intrusions are few; the Munni Munni and Millindinna complexes falling in the period 2830 to 2960 Ma (Table 4).

The intrusions are generally characterised by a subordinate ultramafic component relative to the mafic component, the largest intrusions (Munni Munni and Andover) having the thickest ultramafic successions. The ratio of ultramafic rocks to mafic rocks is less than 0.5, and for most intrusions it is less than 0.2. Rock types range in composition from peridotite to granophyre, and the ultramafic component is dominated by olivine and clinopyroxene cumulates. The intrusions have experienced low-grade regional metamorphism (generally upper-greenschist facies), and the bodies close to the Sholl Shear Zone (e.g. Andover Complex) are

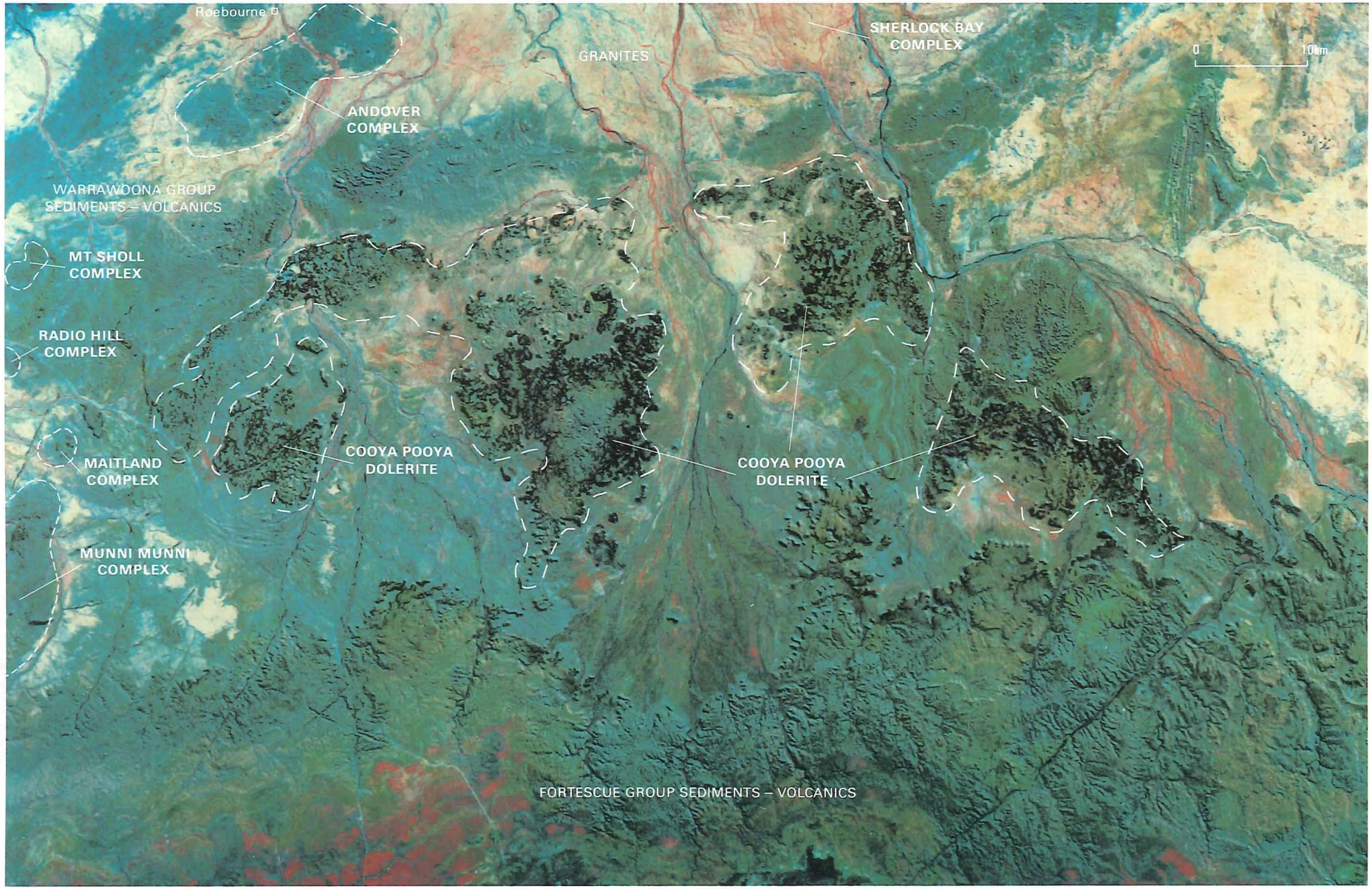

Fig. 5. Landsat 5, multispectral-scanner, standard false-colour, composite image of the west Pilbara Block. Image from path 113 and run 075 and taken on 20/04/84. Scale: 1 cm ~ 4.4 km. Dashed lines show the distribution of outcropping layered mafic-ultramafic intrusions and the Cooya Pooya Dolerite.

Table 5. Major Archaean layered mafic-ultramafic intrusions in the west Pilbara Block

Intrusion	*Extent (km)*	*Thickness (km)*	*Major rock types*	*Mineralisation*	*Outlined resources*	*References*
Andover	7 × 20	2.1	Per, Gab, Px, An	V, Ti	3 Mt @ 0.92% V_2O_5	Hickman (1983) Wallace (this Bulletin)
Balla Balla	15 × ?	1–2	Gab, An, Px	V, Ti	1.94 Mt @ 0.75% V_2O_5	Baxter (1978) Louthean & Seidel (1988)
Dingo	1.5 × 5	< 0.5	Per, Gab, Px	Ni, Cu, PGEs	—	Mathison & Marshall (1981) Hoatson (this Bulletin)
Gidley Granophyre	10 × 50	3	Gran, Gab, Dior	—	—	Hickman (1983)
Maitland	3.5 × 4	2	An, Gab, Per	—	—	Hoatson (this Bulletin)
Mount Sholl	3 × 6	1–2	Gab, Per, Px	Ni, Cu, PGEs	4 Mt @ 0.5% Ni, 0.6% Cu	Mathison & Marshall (1981) Hoatson (1991; this Bulletin)
Munni Munni	9 × 25	> 5.5	Gab, Px, Per	PGEs, Cu, Ni	20–30 Mt @ 2.9 ppm Pt + Pd + Au, 0.3% Cu, 0.2% Ni	Donaldson (1974) Hoatson & Keays (1987; 1989) Barnes & others (1990; 1991; 1992) Hoatson (1991; this Bulletin)
Radio Hill	1.8 × 2	> 1.2	Gab, Per, Px	Ni, Cu, PGEs	1.1 Mt @ 2.5% Ni, 1.8% Cu	Richardson (1976) de Angelis & others (1987; 1988) Hoatson (this Bulletin)
Sherlock Bay	0.5 × 2.5	< 0.5	Gab, Per, Gran	Ni, Cu	18 Mt @ 0.75% Ni, 0.1% Cu	Miller & Smith (1975) Marston (1984)

Per—Peridotite; Px—Pyroxenite; Gab—Gabbro; An—Anorthosite; Dior—Diorite; Gran—Granophyre.
Rock types in order of decreasing abundance.

strongly serpentinised and sheared. Country rocks to the intrusions include metasedimentary and metavolcanic sequences (Warrawoona Group), microcline granites, biotite granodiorites, tonalites, and contaminated hybrid granitic rocks.

Layered intrusions not covered in this study

The following section and Table 5 briefly summarise the main features of the layered intrusions not covered in this study.

Balla Balla Complex (Baxter, 1978; Louthean & Seidel, 1988). The Balla Balla Complex (Fig. 3) is a poorly outcropping mafic intrusion 12 km north of the Whim Creek Cu-Zn mine and 65 km east of Roebourne. It was emplaced between the Caines Well Granite and overlying older Archaean felsic and mafic-ultramafic schists. Titaniferous magnetite layers divide a saussuritised metagabbroic sequence into an upper unit of granophyre and leucogabbro, and a lower unit of anorthositic gabbro, anorthosite, norite, and minor pyroxenite. Twelve vanadium-bearing magnetite layers up to 0.5 m thick, separated by chloritic rocks, have been delineated. A resource of 1.94 Mt @ 0.75% V_2O_5 has been estimated (Baxter, 1978). Weak Cu-Ni-PGE-Au anomalies have been delineated in soil overlying a favourable horizon in the lower mafic unit.

Dingo Complex (Mathison & Marshall, 1981; Marston, 1984). The Dingo Complex (Fig. 4) is a group of small isolated ultramafic-mafic bodies 6 km west of the Mount Sholl Complex. Alluvium separates the low outcrops, which cover an area of 1.5 by 5 km. Peridotite, pyroxenite, gabbro, and hybridised gabbroic units are interlayered with felsic and mafic metavolcanics. The intrusive bodies have variable dips, are poorly layered, and the mafic rocks are extensively uralitised to fine-grained assemblages of tremolite-actinolite. Hunter Resources Ltd have described one of these areas (Toorare Pool) as a block-faulted shallow-dipping body that contains minor weakly PGE-enriched disseminated sulphides in irregular gabbroic units. Interpretations for the origin of the Dingo intrusions range from rafts in underlying granite gneiss to a sequence of sills, possibly related (? slowly cooled lateral equivalents) to the extrusive komatiites in the Ruth Well Synclinorium, 8 km to the north. This major east- to northeast-trending structure, which is truncated to the south by the Sholl Shear Zone, contains a mineralised bimodal spinifex-textured komatiite and komatiitic basalt suite and associated mafic-ultramafic intrusives, chert, and banded-iron formation (Nisbet & Chinner, 1981). At Ruth Well, subeconomic concentrations of disseminated and minor massive and matrix Ni-Cu sulphides, together with massive magnetite layers, occur in peridotite which has been altered to antigorite, tremolite, chlorite, talc, and carbonate.

Gidley Granophyre Complex (Hickman, 1983). The Gidley Granophyre Complex forms the Dampier Archipelago (Fig. 3) and is areally (~ 500 km^2) the largest layered intrusion in the Pilbara Block. Relative to the other west Pilbara intrusions, it is younger and more fractionated, and has no exposed ultramafic component. A ~ 3 km thick succession of basal, coarse gabbro, grading up into feldspathic diorite, quartz diorite, and granophyre intrudes the basal unconformity of the Fortescue Group. The granophyre ranges from massive to weakly layered, even-grained to porphyritic, and spectacular coarse-grained spherulitic to granophyric textures are locally prominent (e.g. Hearson Cove). Arkosic sandstones of the Mount Roe Basalt have been metasomatised by the granophyre and intruded by granophyric dykes, and Archaean granites have been assimilated along the basal contact of the gabbros.

Sherlock Bay Complex (Miller & Smith, 1975; Marston, 1984). Several elongated mafic-ultramafic bodies, including the Sherlock Bay Complex, lie near the periphery of the Caines Well Granite, 42 km east of Roebourne (Fig. 3). The northern margin of the granite is characterised by a steeply-dipping, lenticular Archaean volcanic belt, about 12 km long and 1 km wide, which contains basalt, andesite, rhyolite, greywacke, together with lithic and crystal tuffs. Metadolerite, metagabbro, serpentinised peridotite, and talc-chlorite-calcite schist are generally restricted to the southern margin of the belt. Metamorphism attained transitional greenschist-amphibolite facies.

The Sherlock Bay Ni-Cu deposit is hosted by a banded quartz-magnetite-amphibole schist, which in outcrop resembles a sheared iron-formation. Mineralisation is

confined to a 2 km long zone that extends to a depth of 1 km. Pyrrhotite is the major sulphide, with lesser pyrite, pentlandite, and chalcopyrite. The Ni/Cu ratio is 5 : 1. Reserves, based on a 0.6% Ni cut-off and to a depth of 900 m, are 18 Mt @ 0.75% Ni (Marston, 1984). The mineralisation is interpreted as fracture-controlled vein-filling with the Ni and Cu derived from the nearby altered peridotite and talc-chlorite-calcite schist. Anomalous PGE-Au concentrations are associated with gossans near the base of the intrusion. Keays & others (1982) reported variable, but generally low, Pd, Ir, and Au contents (Pd $<$ 335 ppb, Ir $<$ 0.29 ppb, Au $<$ 55 ppb) in the sulphide mineralisation.

Tectonic evolution of the west Pilbara Block

No comprehensive tectonic model for the west Pilbara Block has been proposed, but several important contributions have been made. Miller (1975) introduced the rather controversial concept of a eugeosyncline to account for the distribution of volcanic and sedimentary rocks, and base-metal deposits. The northeasterly-trending eugeosyncline, which extends 240 km from the Munni Munni Complex area towards Port Hedland, comprises both volcanic-arc and sedimentary-trench components. Using stratigraphic, geochemical, and structural evidence, Hickman (1981, 1983) argued that none of the evolutionary models proposed for other granite-greenstone terranes are entirely applicable to the Pilbara Block. These models include oceanic, geosynclinal, rift-zone, plate-tectonic, and extraterrestrial. Rather than invoke a new model, Hickman (1981, 1983) presented a stage-by-stage evolutionary scheme, which will not be reproduced here. Other investigators, including Bettenay & others (1981), Barley & others (1984), Bickel & others (1980, 1985), Barley (1987), Krapez & Barley (1987), and Krapez & others (1990) have discussed the tectonics of specific areas within the Pilbara Block.

Structural studies of the Whim Creek Belt by Barley (1987) and Krapez & Barley (1987) emphasised that the tectonic pattern of the Pilbara was not simply a consequence of gravity-driven diapiric uprise of granitic batholiths into overlying supracrustal sequences (Hickman, 1983). These studies affirmed the importance of subhorizontal deformation, in particular strike-slip faulting, during the tectonic evolution of ensialic basins in the Archaean crust. Krapez & others (1990) believe that deep-seated and long-lived crustal lineaments formed an integral part of the Pilbara craton from the late Archaean onwards. They controlled the location, size, and shape of sedimentary basins and focused igneous and tectonic activity in both the granite-greenstone basement and overlying units of the Mount Bruce Supergroup.

Horwitz (1990a) has noted a correlation between tectonic provinces and metal associations in the Pilbara Block. Nickel sulphides are restricted to mafic units of the Gorge Creek and Whim Creek groups, whereas Cu and Zn sulphides occur in the Sholl and Whim Creek back-arc environment. Osmiridium (Hudson & Horwitz, 1985) may have been derived from oceanic crust, and all known Sn is restricted to the proto-craton area.

Modelling of seismic data by Drummond (1981, 1982, 1988) has shown the thickness of the crust in the Pilbara craton is 28 km in the north and 30–33 km in the south, and the boundary between the crust and the upper mantle dips south at less than 1°. The observed upper-crustal velocities are consistent with the bulk mineralogy of the upper crust being near that of granite. A seismic boundary at 10 to 15 km depth could be explained by a transition from granite or granodiorite above the boundary to felsic granulite below. The more usual classification of a continental crust into an upper granitic layer and a lower basaltic layer does not appear to be the case in the Pilbara Craton. The Pilbara crust differs from that of the northern Yilgarn Block, in that the crust in the northern Yilgarn Block is much thicker ($>$ 50 km) and has a thick basal zone of garnet granulite; this appears to be absent in the Pilbara.

FIELD RELATIONSHIPS, PETROGRAPHY, MINERALOGY, AND GEOCHEMISTRY OF THE MUNNI MUNNI COMPLEX *(DMH)*

Introduction

The Munni Munni Complex is 42 km south of Karratha, at latitude 21°07′S and longitude 116°51′E, on the Pinderi Hills 1 : 100 000 Topographic Sheet 2255 and Yarraloola 1 : 250 000 Geological Sheet SF/50-6. It is one of Australia's largest and most prospective layered Archaean mafic-ultramafic intrusions, and contains significant amounts of platinum and palladium, and relatively minor amounts of rhodium, ruthenium, copper, nickel, and gold.

Size and age

Covering an exposed area of about 4 by 9 km, the Munni Munni Complex is composed of a lower 1850 m-thick ultramafic zone and an overlying 3630+ m-thick gabbroic zone (Figs 6 & 7). The highest stratigraphic levels of the gabbroic zone are obscured by the Fortescue Group platform cover, but aeromagnetic (Fig. 8) and gravity (Fig. 9) data show near-coincident magnetic (1700+ nT) and gravity (150 μms^{-2}) highs which indicate that the complex extends to the southwest for 16 km beneath the cover rocks. Hence, the overall dimensions of the intrusion are 9 by 25 km. The elongate shape of the complex is similar to that of the Great Dyke of Zimbabwe, although the Munni Munni Complex has a considerably smaller length-to-width ratio. The excellent preservation of the complex compared to other intrusions in the Pilbara Block is attributed to its large size and to the covering effect of the Fortescue Group.

Along the western side of the intrusion is a curvilinear magnetic low (Fig. 8) that persists for over 80 km southwards through the featureless magnetic terrain of the Fortescue Group platform sequences. Parts of this basement feature coincide with the pyroxenite Cadgerina Dyke which is believed to be a feeder dyke to the Munni Munni Complex (Barnes & others, 1990). With an areal extent of about 225 km^2 and a stratigraphic thickness of at least 5480 m, the Munni Munni Complex is one of Australia's largest mafic-ultramafic intrusions. Other Archaean to Proterozoic intrusions of comparable thickness in Australia include the Windimurra Complex (Yilgarn Block, 10 to 13 km thick: Mathison & Booth, 1990; Mathison & others, 1991), Narndee Complex (Yilgarn Block, 6 to 10 km: C. Williams, personal communication, 1988), McIntosh Intrusion (Halls Creek Mobile Zone, around 6 km: Mathison & Hamlyn, 1987), and various intrusions of the Giles Complex (Musgrave Block, around 5 to 7 km: Nesbitt & others, 1970; Glikson & Ballhaus, 1989).

The age of the Munni Munni Complex is constrained by: a relative age determined from the overlying Fortescue Group sequence; U-Pb zircon and Sm-Nd mineral separate ages for the emplacement of the intrusion; and a T^{Nd}_{CHUR} model age of granite from the eastern margin of the intrusion. A minimum age for the Munni Munni Complex is indicated by the age of the Fortescue Group, which unconformably overlies the southern two-thirds of the intrusion. The age of the basal Fortescue Group is constrained by: (1) the average age of 2765 Ma from six U-Pb zircon ages of various basal Fortescue Group volcanic and sedimentary units (Arndt & others, 1991); (2) U-Pb zircon age of 2768 ± 16 Ma from the Spinaway Porphyry which intrudes the Hardey Sandstone (Pidgeon, 1984); and (3) Pb model age of 2760 ± 30 Ma for the Kylena Basalt (Richards & Blockley, 1984). Therefore the best estimate for the age of the base of the Fortescue Group is about 2765 Ma, which provides a minimum age for the Munni Munni Complex.

The Archaean age of the complex is confirmed by a U-Pb zircon age of 2925 ± 16 Ma for a ferrogabbro pegmatite immediately below the ultramafic/gabbroic zone contact (Arndt & others, 1991). The pegmatite is believed to have been derived from late-crystallising intercumulus liquid, and therefore the age is believed to be a reliable estimate for the crystallisation age of the intrusion and not an inherited age from xenocrystic zircon. Sun (see Sun & Hoatson, this Bulletin, p. 142) has obtained a Sm-Nd mineral isochron age of 2927 ± 13 Ma for the intrusion. Leucocratic granite from the eastern contact of the intrusion, adjacent to the top of the ultramafic zone, has a T^{Nd}_{CHUR} model age of 3000 Ma (S-S. Sun, personal communication, 1985).

Distribution of rock types

Ultramafic zone

The ultramafic zone consists of a 1850 m-thick macrorhythmic sequence of dunite, lherzolite, wehrlite, olivine websterite, clinopyroxenite, and websterite, with olivine orthopyroxenite, orthopyroxenite, norite, spinel-bearing orthopyroxenite, chromitite, and mixed norite-orthopyroxenite rock occurring immediately below the interface with the gabbroic zone (see appended map sheet). It has been subdivided into 10 subzones (Table 6), designated A′ (at the base of the intrusion), A, B, C, D, E, F, G, H, and I (highest subzone), based on the different relative proportions of olivine-, clinopyroxene-, and orthopyroxene-rich cumulates in each subzone. The more traditional method of zonal subdivision by cyclic units was not used since complete units are poorly developed.

There is a broad, even distribution of olivine- and clinopyroxene-dominant cumulates throughout the Munni Munni ultramafic zone. This is shown by the parallel cumulative trends of the olivine- and clinopyroxene-dominant cumulates in the generalised stratigraphy depicted in Figure 10. Orthopyroxene-dominant cumulates have a restricted distribution, occurring mainly at the top of subzone I, but also as thin lenses in the lower parts of the zone.

Subzone A′ (stratigraphic interval 0–205 m, thickness 205 m) extends along the northern, northeastern, and southeastern margins of the intrusion. A feature of this subzone is the variability of rock types. Along the northern part of the contact, gabbro, gabbronorite, olivine gabbronorite, plagioclase websterite, plagioclase olivine websterite, and olivine websterite are the major rock types. Variably altered quartz gabbronorite, gabbronorite, plagioclase websterite, and websterite characterise the northeastern and southeastern margins. This variability also occurs towards the centre of the intrusion, with more fractionated rocks near the complex/granite contact grading into more melanocratic variants towards the centre of the intrusion. Hybridisation textures are dominant over chilling features along the northeastern and southeastern contacts. These rocks have been subdivided according to the intensity of silicic-hydrous-alkali alteration related to the partial

Fig. 6. Aerial photograph of the Munni Munni Complex.

melting of the granitic country rocks. Rock types denoted "A'" on the appended map sheet are more intensely altered relative to rocks marked "a".

Subzone A (205–295 m, thickness 90 m) is transitional from subzone A′, as reflected in the steadily increasing olivine-to-plagioclase ratio for the pyroxenites with increasing stratigraphic height. Gabbroic rocks are absent, and lherzolite and olivine websterite appear as minor components of the pyroxenite-dominated stratigraphy. A distinctive porphyritic websterite lens occurs near the upper levels of the subzone and texturally resembles the mineralised porphyritic websterites of

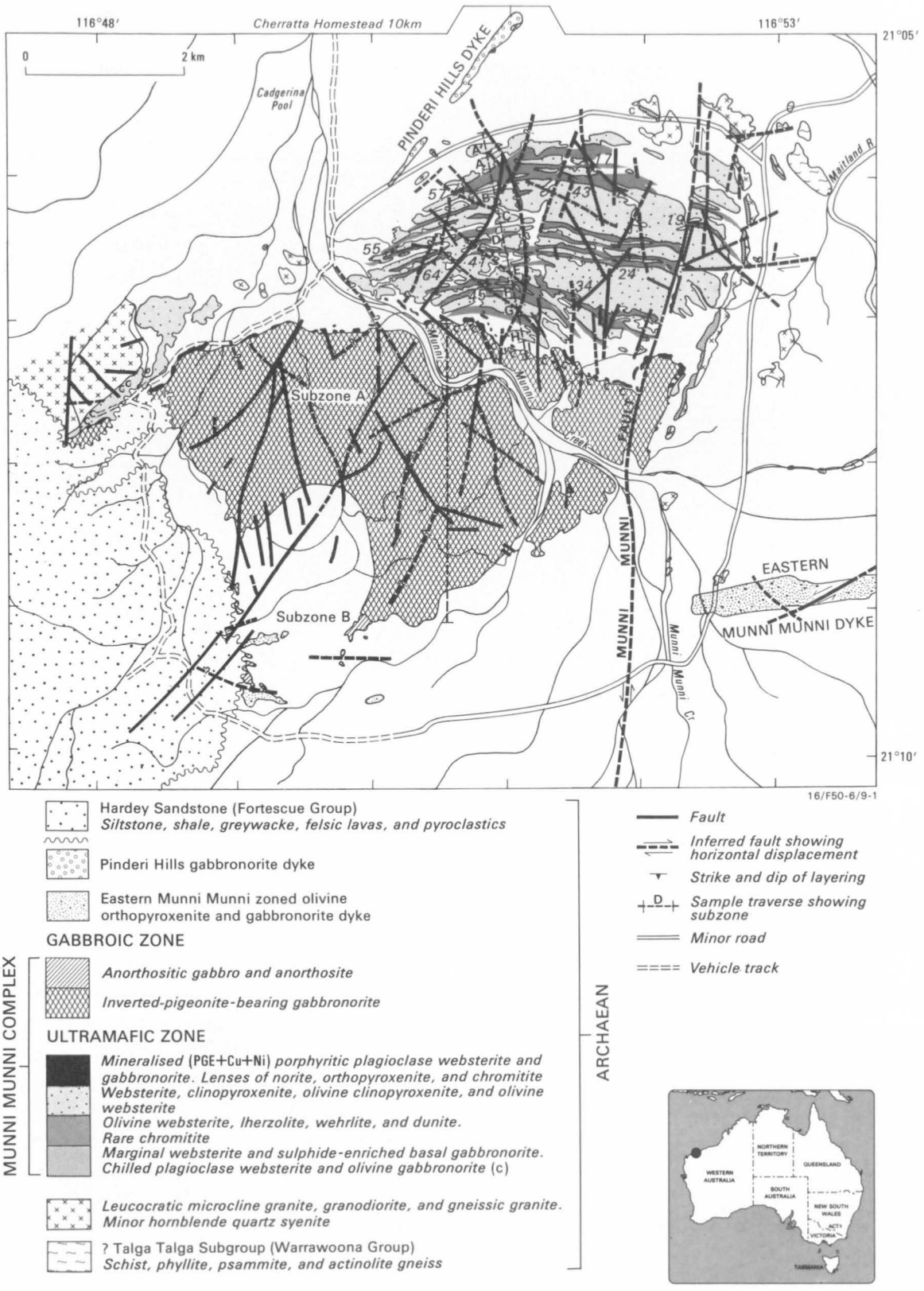

Fig. 7. Geology of the Munni Munni Complex (simplified from appended map sheet).

subzone I. The porphyritic wesbsterites occur throughout the lower parts of the ultramafic zone as thin conformable lenses up to 200 m long.

Subzone B (295–425 m, thickness 130 m) has the greatest proportion of peridotites in the ultramafic zone. Interlayered lherzolite, serpentinised dunite, and ser-

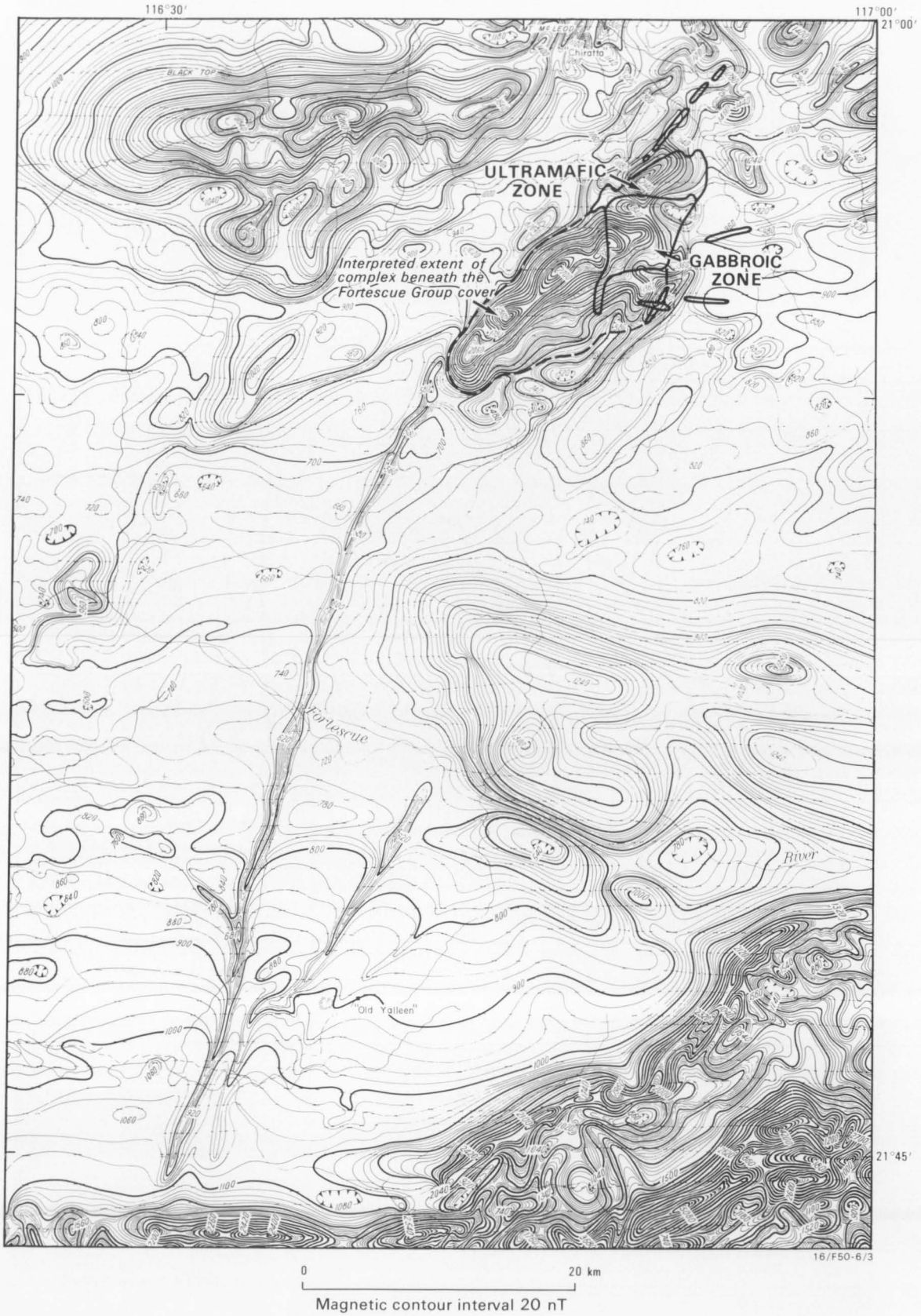

Fig. 8. Aeromagnetic image of the Munni Munni Complex region. The featureless area south of the complex correlates with platform volcanic and sedimentary sequences of the Fortescue Group, and the intensely disturbed area in the south correlates with the Marra Mamba and Brockman iron formations of the Hamersley Basin. Yarraloola 1 :250 000 AGSO Total Magnetic Intensity & Radioactivity Sheet F50/B1-7, 1963.

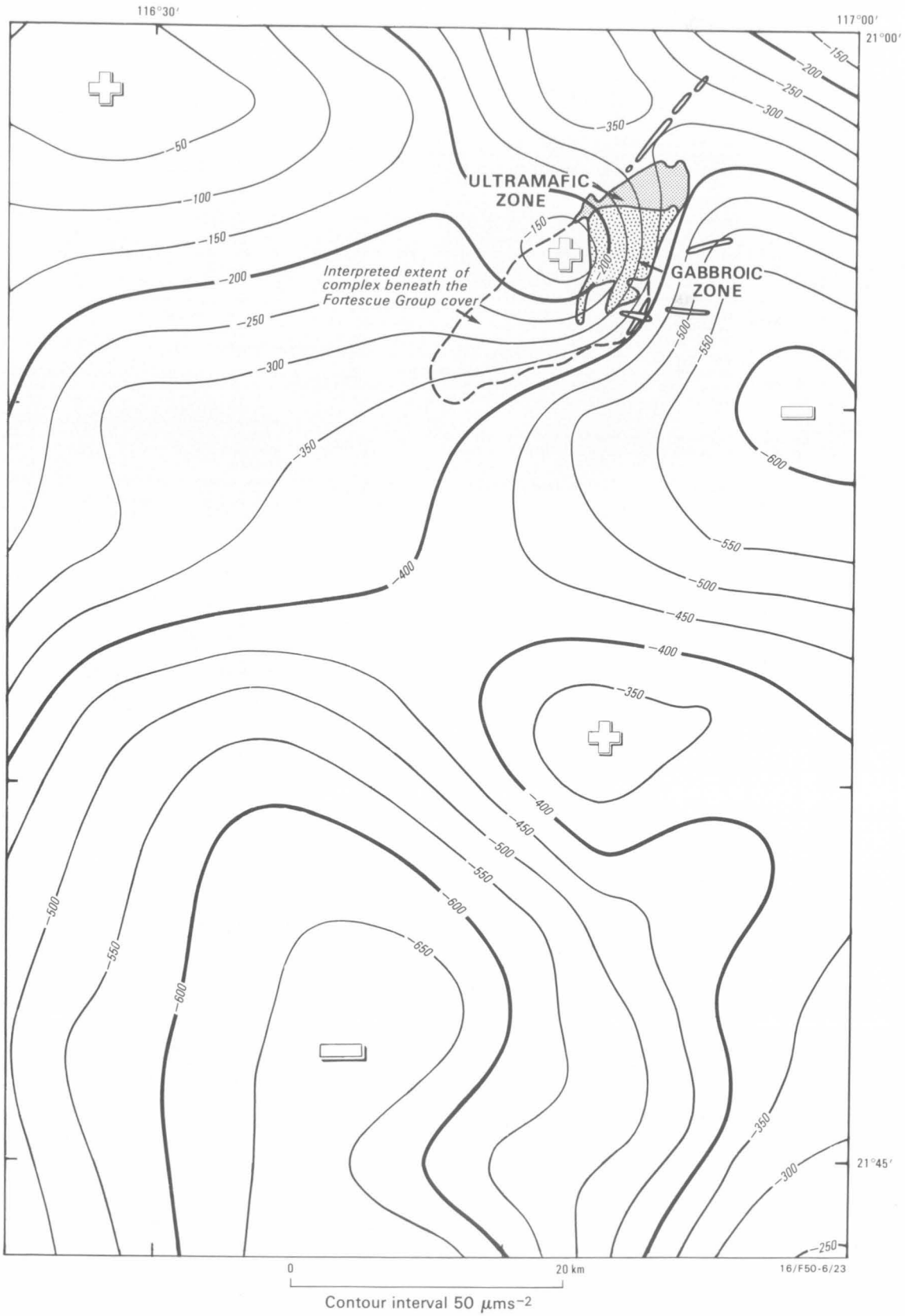

Fig. 9. Gravity image of the Munni Munni Complex region. Yarraloola 1 : 250 000 AGSO Bouguer Anomalies Sheet 21-1/F50-6, 1979.

pentinite dominate, whereas olivine websterite and websterite constitute less than 20%. Contacts of the massive serpentinised dunite and serpentinite layers with the underlying and overlying pyroxenitic subzones are sharp. The peridotites are extensively faulted, and chrysotile and magnesite-rich layers, which have been

				Thickness (m)
MUNNI MUNNI COMPLEX	GABBROIC ZONE	Subzone B	*Medium to coarse-grained anorthosites and anorthositic gabbros. Minor granophyric gabbro, quartz monzonite, and quartz syenite occur near the top of the subzone and abutting the Fortescue Group platform cover*	>1160
		Subzone A	*Homogeneous, medium to coarse-grained, inverted pigeonite-bearing gabbronorite, leucogabbronorite, and magnetite-ilmenite gabbronorite. Medium-grained laminated inverted pigeonite-bearing gabbronorite with recrystallised banded microgabbro xenolith blocks along the base of the subzone*	2470 6-32 3
	ULTRAMAFIC ZONE		*Discordant fine-grained dunite and olivine orthopyroxenite? pipe intrusion*	30 (diameter)
		Subzone I (105 m)	*Minor interlayered serpentinised lherzolite, dunite, and weakly porphyritic websterite, grading into strongly porphyritic plagioclase websterite and gabbronorite towards the gabbroic zone contact. Disseminated (up to 2% vol total sulphides) chalcopyrite, pyrrhotite pentlandite, pyrite, and platinum-group-element mineralisation in upper levels of porphyritic plagioclase websterite and gabbronorite. In the central region of the complex, the porphyritic plagioclase websterite merges laterally into lenses of banded mixed rock (norite containing irregular orthopyroxenite layers), orthopyroxenite, olivine orthopyroxenite, and dunite. The orthopyroxenites are accidental blocks that locally contain numerous aluminous-spinel cycles*	*Porphyritic plagioclase websterite, lherzolite, orthopyroxenite, norite, and aluminous spinel-bearing orthopyroxenite*	105
		Subzone H (154 m)	*Interlayered serpentinised lherzolite and websterite. Websterite becomes porphyritic towards* subzone I	*Websterite* *Lherzolite* *Websterite* *Lherzolite*	95 15 12 32
		Subzone G (130 m)	*Massive olivine websterite and minor websterite*	*Olivine websterite, websterite,*	130
		Subzone F (182 m)	*Interlayered serpentinised lherzolite, olivine websterite, and websterite. Rare thin chromitites in serpentinised dunite*	*Lherzolite, dunite, chromitite* *Olivine websterite, websterite* *Lherzolite, olivine websterite* *Websterite* *Lherzolite, olivine websterite* *Websterite* *Lherzolite, olivine websterite*	32 25 20 20 25 40 20
		Subzone E (192 m)	*Massive clinopyroxenite, minor lherzolite, and websterite*	*Clinopyroxenite, websterite* *Lherzolite lens* *Clinopyroxenite*	115 5 32
		Subzone D (262 m)	*Interlayered serpentinised lherzolite, wehrlite with olivine clinopyroxenite, olivine websterite, and websterite*	*Lherzolite* *Websterite* *Wehrlite* *Websterite, olivine clinopyroxenite* *Lherzolite, olivine websterite* *Websterite* *Porphyritic websterite* *Lherzolite, olivine websterite* *Websterite* *Lherzolite*	15 25 15 60 25 25 5 15 65 12
		Subzone C (400 m)	*Massive and weakly layered olivine websterite with thin serpentinised lherzolite layers, and a distinctive coarse-grained basal orthopyroxenite lens*	*Websterite* *Lherzolite* *Olivine websterite* *Lherzolite* *Olivine websterite* *Porphyritic websterite lens* *Olivine websterite* *Lherzolite* *Olivine websterite* *Lherzolite* *Olivine websterite* *Megacrystalline orthopyroxenite lens*	65 4 100 20 32 5 45 5 60 12 40 12
		Subzone B (130 m)	*Complexly interlayered recessive lherzolite, serpentinite, containing olivine websterite, and minor websterite, porphyritic websterite lenses with rare dunites containing chrysotile zones*	*Lherzolite, serpentinite* *Olivine websterite, websterite* *Dunite, chrysotile*	130
		Subzone A (90 m)	*Olivine websterite, websterite, with thin lherzolite and porphyritic websterite lenses*	*Websterite* *Porphyritic websterite lens* *Olivine websterite* *Lherzolite* *Olivine websterite* *Lherzolite lens*	20 5 12 5 45 3
		Subzone A′,a (205 m)	*Variably altered, contaminated eastern marginal plagioclase olivine websterite and plagioclase websterite. Intensity of alteration: A′>a.* *Western and northern contact rocks dominantly gabbronorite and olivine microgabbro with basal disseminated (up to 6% vol total sulphides) pyrrhotite, chalcopyrite, and pentlandite mineralisation. Chilled plagioclase websterite and gabbronorite abut coarse-grained* western granite *at the southwestern end of complex*		205
		Agm	Western granite. *Leucocratic microcline granite with ? younger hornblende quartz syenite to the southwest of Munni Munni Creek*		
		Ag	Northern and eastern granite. *Leucocratic, two-mica microcline granite and granodiorite to the east and gneissic granite and gneiss to the north of* MUNNI MUNNI COMPLEX		
		At	? TALGA TALGA SUBGROUP (WARRAWOONA GROUP). *Intercalated schist phyllite psammite and calc-silicate with coarse-grained spotted ? actinolite gneiss*		

Table 6. Stratigraphy of the Munni Munni Complex

16/F50-6/20-1

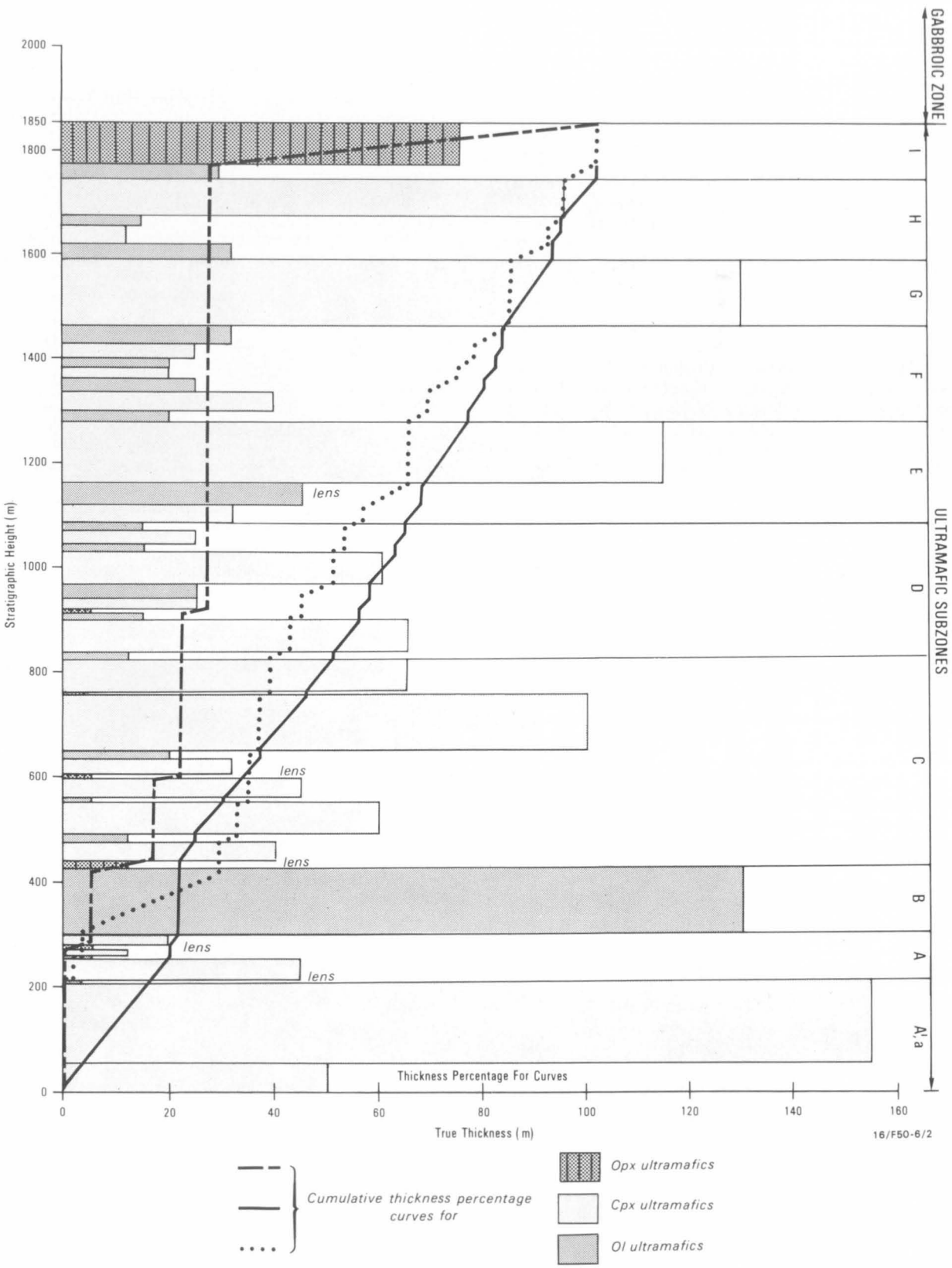

Fig. 10. Generalised stratigraphy of the ultramafic zone of the Munni Munni Complex, based on orthopyroxene(Opx)-, clinopyroxene(Cpx)-, and olivine(Ol)-dominant cumulates. The horizontal scale shows the true thickness (below the line) and cumulative percentages (above the line) for the three cumulate-dominant rocks. The cumulative curve trends illustrate the fairly even distribution of clinopyroxene- and olivine-dominant cumulates throughout the ultramafic zone and the preferential distribution of orthopyroxene-dominant cumulates to the upper part of the zone.

mined, are prominent in the upper levels of the subzone. The main peridotite unit of the subzone splits into three peridotite and two pyroxenite sub-units towards the east. These sub-units persist laterally until masked by alluvium near the Munni Munni Fault.

Subzone C (425–825 m, thickness 400 m) is the thickest subzone of the ultramafic zone, consisting of weakly layered lherzolite, olivine websterite, and websterite. An interlayered peridotite-pyroxenite sequence in the western parts of the intrusion passes along strike into a more pyroxenitic-dominated sequence to the east. A distinctive 'megacrystalline orthopyroxenite' lens about 100 m long marks the base of subzone C. This unusual 'cumulate' is characterised by large (up to 10 cm) interlocking poikilitic orthopyroxene grains, and forms a 12 m thick conformable lens between peridotites of subzone B and overlying websterite and olivine websterite.

Subzone D (825–1087 m, thickness 262 m) consists of an interlayered sequence of serpentinised lherzolite, wehrlite, olivine websterite, olivine clinopyroxenite, and websterite. The peridotites have a recessive relief and are commonly bounded by strike ridges of pyroxenite. The olivine-rich units are indicated by low, rubble-strewn pavements of carbonate (mainly magnesite) and serpentine alteration products. Subzone D cyclic units show great lateral continuity and extend almost 5 km across the ultramafic zone.

Subzone E (1087–1279 m, thickness 192 m) is largely composed of clinopyroxenite, with lesser websterite and serpentinised lherzolite. The clinopyroxenite adcumulates are generally massive and are the best-exposed rock type in the intrusion. Despite the common usage of 'clinopyroxenite' by previous workers, clinopyroxenites, *sensu stricto*, are rare in the ultramafic zone.

Subzone F (1279–1461 m, thickness 182 m) consists of interlayered serpentinised lherzolite, olivine websterite, websterite, and minor dunite. The peridotites are of similar abundance to the pyroxenites, with the latter rocks more prominent towards the east. A 5 cm thick poorly-exposed chromitite lens is hosted by serpentinised dunite near the top of the subzone. This is the first appearance of cumulus chromite in the ultramafic stratigraphy, but it has no economic significance. In contrast to the underlying subzones, the regional strike of subzones F, G, and H is markedly arcuate. At its eastern and western ends, subzone F is terminated by the porphyritic websterite layer of subzone I and by the gabbroic zone.

Subzone G (1461–1591 m, thickness 130 m) is pyroxenite-dominated and consists of olivine websterite and minor websterite. Rare peridotite lenses are restricted to the eastern part of the subzone.

Subzone H (1591–1745 m, thickness 154 m) is distinguished from subzone G by a greater abundance of peridotites. Serpentinised lherzolite and websterite are interlayered throughout this subzone, with lherzolite comprising about 30% of the stratigraphy. The websterite is equigranular at low stratigraphic levels, but becomes increasingly porphyritic up the subzone owing to an increase in the grainsize of bronzite. This feature persists into subzone I, where the websterites become strongly porphyritic and orthopyroxene changes from intercumulus to cumulus. Paralleling these textural changes is the appearance of traces of sulphide.

Subzone I (1745–1850 m, thickness 105 m) is the highest subzone of the ultramafic zone and can be referred to as the critical subzone, since it contains apparent 'chromitites' (probe analyses show these to be Cr-poor, Al-rich spinels) and the main PGE-enriched layer of the intrusion. It is characterised by a variety of rock types which show marked mineralogical and textural differences from the cumulates in the lower subzones. These differences include: the disappearance of cumulus olivine at high levels; introduction of cumulus orthopyroxene; the first major occurrence of spinel; increased abundances of intercumulus plagioclase, biotite, and sulphides; and the transition from adcumulates and mesocumulates to orthocumulates.

The dominant rock types of subzone I are strongly porphyritic websterite and plagioclase websterite, followed by equigranular and weakly porphyritic websterite, lherzolite, dunite, olivine orthopyroxenite, orthopyroxenite, norite, mixed orthopyroxenite-norite rock, and spinel-bearing orthopyroxenite. There is a consistent increase in the porphyritic character of the pyroxenites upwards, from weakly to moderately porphyritic websterite to strongly porphyritic plagioclase websterite directly below the ultramafic/gabbroic zone contact.

The PGE-mineralised strongly porphyritic plagioclase websterite layer has an average thickness of 30 to 50 m (maximum 80 m) and crops out along the base of the gabbroic zone for at least 12 km. Its southwestern extent on the northwestern side of the intrusion is masked by the Fortescue Group platform sequence, whereas along the southeastern side of the intrusion it is partly covered by alluvium. Textural and geochemical evidence indicates that the porphyritic plagioclase websterite layer merges into the southeastern marginal rocks and extends beyond the Zebra Hill Dyke, a total strike extent of at least 22 km. The porphyritic websterite typically forms large (up to 5 m high), sub-rounded, dark-coloured outcrops directly below the contact with the gabbroic zone. Equigranular to weakly porphyritic websterite, interlayered with minor thin serpentinised peridotite, forms the footwall rocks to the porphyritic websterite layer, and gabbronorite, minor norite, and anorthosite of the gabbroic zone constitute the hanging-wall units. Layering is weakly developed in the porphyritic websterite layer, the most prominent feature being large subhedral to euhedral cumulus orthopyroxene grains (up to 3 by 4 cm). In some places, plagioclase forms large poikilitic grains and attains 18 vol. %; thus the rock becomes a melagabbronorite. Disseminated sulphide blebs consistently increase from trace amounts near the lower stratigraphic levels of the porphyritic websterite to 2–3 vol. % for the more leucocratic variants near the gabbroic zone interface.

A feature of subzone I is the lateral variation of rock types associated with the porphyritic websterite in the central areas of the complex (see section Y on the inset of the Munni Munni Complex geological map on the appended map sheet). These rocks include conformable lenses and irregular blocks of orthopyroxenite, olivine orthopyroxenite, spinel-bearing orthopyroxenite, mixed norite-orthopyroxenite rock, and various small xenoliths of gabbroic affinity. The orthopyroxenites and spinel-bearing units are believed to be accidental blocks forming a slumped-sedimentary feature near the base of the gabbroic zone. The mixed norite-orthopyroxenite is a distinctive banded rock which occurs within 20 m of the ultramafic/gabbroic zone contact. It consists of a fine-grained norite host containing irregular medium-grained orthopyroxenite layers. Further to the west (see section X on the inset of the Munni Munni geological map on the appended map sheet) the orthopyroxene-rich rocks are absent and the upper levels of subzone I consist of an interlayered sequence of porphyritic websterite and serpentinised lherzolite. In this area, olivine

occurs closer to the ultramafic/gabbroic zone contact than in the central part of the complex.

Gabbroic zone

The gabbroic zone constitutes about two-thirds of the exposed Munni Munni Complex. The base of the gabbroic zone is defined by the first appearance of cumulus plagioclase in the intrusion. The zone has been subdivided into a lower subzone (A) of inverted-pigeonite-bearing gabbronorite grading into inverted-pigeonite-magnetite-ilmenite-bearing gabbronorite, and an upper subzone (B) of anorthositic gabbro, with minor anorthosite and norite. Granophyric gabbro, quartz monzonite, and quartz syenite, which crop out at the top of the subzone against the Fortescue Group, may represent the most fractionated rocks of the complex (Williams & others, 1990).

Subzone A (stratigraphic interval 1850–4320 m, thickness 2470 m) largely consists of a monotonous sequence of inverted-pigeonite- and inverted-pigeonite-magnetite-ilmenite-bearing gabbronorite that displays little textural or mineralogical variation with stratigraphic height. However, within the lower 40 m of this subzone there are a number of minor rock types of different origins. The dominant rock along the basal contact is a laminated sericitised medium-grained gabbronorite. Aligned plagioclase laths and prismatic pyroxene define a lamination that parallels the trend of the basal contact. Within 30 m of the basal contact these textural features grade into the more massive intergranular textures typical of the overlying gabbronorite. The laminated gabbronorite also locally contains thin layers of leucogabbro, anorthosite, pegmatoidal gabbro, and fine-grained banded enclaves of gabbronorite, gabbro, and quartz gabbro. The enclaves display granoblastic textures and tight irregular folding of plagioclase-rich bands, indicating a complex deformational history.

Most of subzone A consists of a massive, medium-to-coarse inverted-pigeonite-bearing gabbronorite, which gradually grades into inverted-pigeonite-magnetite-ilmenite-bearing gabbronorite above the 2800 m stratigraphic level. At these higher levels the magnetite-ilmenite content of the gabbronorites reaches 10 vol. % and the rocks are strongly magnetic. In the middle and upper parts of subzone A most of the drainage systems contain thick concentrations of alluvial Fe-Ti oxides. As these rocks generally have no structure, determination of stratigraphic level is based on the assumption that the rocks have a similar dip to the basal laminated gabbronorites and ultramafic-zone rocks, i.e. about 40° to the southwest, south, and southeast. Mineralogical and whole-rock-chemical trends confirm that the gabbroic zone youngs towards the south.

Subzone B (4320–5480 m, thickness 1160 m) comprises a poorly-outcropping medium-to-coarse anorthositic gabbro and anorthosite sequence which is apparently truncated by gabbroic rocks of the Eastern Munni Munni Dyke. The spatial relationship of the two units is hard to establish because of poor outcrop and intense carbonate-chlorite alteration in the subzone B units.

From above the 5480 m stratigraphic level, a gently undulating peneplain is covered by ferruginous skeletal *in situ* soils which mantle gabbroic rocks at shallow depth. Granophyric gabbro, quartz monzonite, and quartz syenite (see appended map sheet), which abut the Fortescue Group, may be related to the Munni Munni Complex. They are the most fractionated and highest-level rocks exposed in the intrusion. Assuming an average dip of about 40° to the south for the gabbroic-zone rocks, the total true thickness of the exposed part of the intrusion is approximately 6770 m.

Distribution of sulphides and chromite

Sulphides

Sulphide mineralisation occurs in two major settings in the Munni Munni intrusion: along the basal (northern and northeastern) contact of the ultramafic zone (subzone A′); and within the porphyritic websterite layer immediately below the ultramafic/gabbroic zone contact (subzone I). In both regions there are strong lithological and stratigraphic controls for the mineralisation.

Gabbronorite, gabbro, and plagioclase websterite host disseminated pyrrhotite, chalcopyrite and minor pentlandite along the northern basal contact of the ultramafic zone. The sulphide content is patchy along strike, with relatively sulphide-rich gabbroic rocks (up to 6.0 vol. % total sulphides) interspersed with sulphide-poor rocks. The basal segregations of sulphide appear to be a lateral extension of the mineralisation that persisits along the northeastern margin of the ultramafic zone. The northern zone of sulphide enrichment is 1–3 m thick and is situated a couple of metres above, and concordant with, the basal contact of the complex. The sulphide content decreases rapidly upwards, with trace sulphides visible up to the 270 m stratigraphic level of the ultramafic zone. Thin (5–15 cm), steeply-dipping, silicified shears containing traces of remobilised sulphide and small limonitic gossans also define the sulphide-rich layer along the base of the intrusion.

Sulphides are absent from the stratigraphic interval 270–1400 m. At the 1400 m level (subzone F), rare very small (< 0.3 mm) pentlandite grains appear to be associated with the serpentinisation of olivine (release of Ni from olivine?). Chalcopyrite is a rare subordinate component at 1400 m, but becomes slightly more prominent from the 1600 m level (subzone H), and above 1695 m exceeds the modal pentlandite content. Paralleling the increasing intercumulus plagioclase content and porphyritic character of the websterites upward through subzone I, is a consistent increase in the sulphide content to a maximum of 2–3 vol. % at approximately the 1840 m stratigraphic level. The disseminated sulphides comprise chalcopyrite with lesser pyrrhotite and pentlandite. They form irregular, 0.2–4 mm-sized grains interstitial to the pyroxene cumulates. Locally, in the more sulphide-rich units, chalcopyrite is subordinate to pyrrhotite. Sulphides are rare in outcrop, but their distribution in the porphyritic websterite layer is indicated by limonitic staining on weathered surfaces or by gossanous shear zones that traverse the mineralised layer. Outcrop and drill core material indicate that the sulphide distribution is very patchy, with sulphide-bearing websterite grading into websterite barren of sulphides within a few metres. This variation, which is also evident on a thin-section scale, is largely primary but some minor remobilisation has been caused by alteration.

Traces (< 0.5 vol. %) of disseminated sulphide occur throughout subzone A of the gabbroic zone. Chalcopyrite, pyrite, and lesser pyrrhotite and pentlandite are the main sulphides in the lower and middle parts of the subzone, but above 4000 m, pyrite becomes dominant relative to chalcopyrite. Much of the chalcopyrite has been remobilised: it is often associated with chlorite veinlets and zones of altered silicates. The intense carbonate and chlorite alteration in subzone B of the gabbroic zone has remobilised any sulphides which

may have been present. The relative increase in pyrite abundance up-section in the gabbroic zone is also a feature of the layered sills of the Deer Lake Complex, Minnesota (Ripley, 1979); the pyrite generation is thought to be related to the reaction between Fe^{2+}-bearing minerals and a residual fluid enriched in S-bearing volatile phases. A similar mechanism could also have applied in the formation of pyrite in the Munni Munni gabbroic rocks, with prominent Fe^{2+}-bearing minerals biotite and magnetite-ilmenite having crystallised from a S-saturated melt in the upper parts of the zone.

Chromite

Chromium-bearing spinels have a restricted distribution in the Munni Munni Complex. This is largely attributed to the dominance of clinopyroxene in the ultramafic stratigraphy, since Cr partitions strongly into clinopyroxene (partition coefficient of $\sim$ 3) relative to orthopyroxene (partition coefficient $\leq$ 1; see references in Sheraton & Simons, 1988). This preferential partitioning reduces the Cr content of the melt and inhibits the formation of chromitite layers. Minor 'chromitites' are associated with dunite and orthopyroxenite in the upper parts of the ultramafic zone, but neither association has any economic significance for chromite or PGEs.

The first occurrence of chromite in the intrusion is associated with olivine cumulates at the top of subzone F (see appended map sheet). The dunite-hosted chromitite lens occurs in a structurally complex region at the intersection of several major faults. Detailed rock relationships are masked by intense talc and carbonate alteration. The 5 cm thick chromitite has a strike extent of only 2 m and is characterised by pinch and swell features.

Multiple, thin spinel-bearing cycles are hosted by an orthopyroxene adcumulate in the upper part of the porphyritic websterite layer (see inset of the geological map of the Munni Munni Complex on the appended map sheet). The western end of the orthopyroxenite unit (50 m long by 40 m wide) has been truncated by a high-angle fault that has a sinistral dispacement of 40 m. There is a progression from olivine orthopyroxenite at the base to orthopyroxenite near the top of the spinel-bearing unit. A zone of magnesite-talc alteration separates the olivine orthopyroxenite which contains the thickest spinel-bearing cycles (1–5 cm) from the orthopyroxenite. The extensively-jointed sequence dips at $\sim$ 65° and youngs to the north, since the more mafic olivine orthopyroxenite component with the greatest abundance of spinel cycles is closer to the gabbroic-zone contact. The spinel-bearing cycles display colloform structures with delicate antiformal bulges and synformal troughs, and bifurcate along strike. Microprobe analyses show the spinels are unusually aluminous and Cr-poor and the orthopyroxenes have compositions anomalously primitive for their stratigraphic level (see Mineralogy section, pp. 58–61). These anomalous compositions and the northerly-dipping attitude of the unit support the interpretation that much of the orthopyroxenite in subzone I occurs as slumped accidental blocks derived from higher stratigraphic levels in the magma chamber.

Figure 11 summarises the regional distribution and relative abundances of the sulphides and spinels in the Munni Munni Complex.

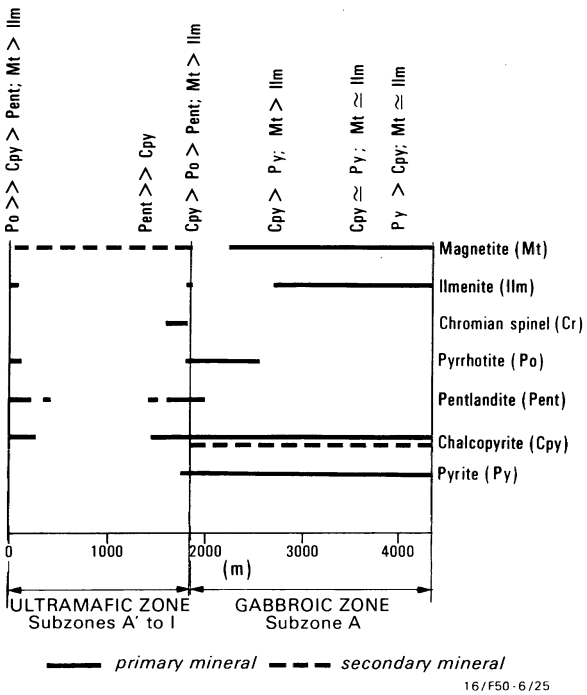

Fig. 11. Munni Munni Complex: distribution and relative abundances of sulphides and spinels in the ultramafic zone and subzone A of the gabbroic zone.

Stratigraphic relationships

The layered sequences of the ultramafic zone have different spatial relationships with the margins of the intrusion. The layered rocks along the northern parts of the zone are generally conformable with the basal contact of the intrusion, whereas the northwestern contact is characterised by an upward deflection (towards the southwest) and apparent thinning of the layered units along the side of the intrusion (see appended map sheet). The relationship on the southeastern side of the intrusion is partly obscured by alluvium, but regional trends indicate that the layering is generally at a high angle to the margin.

The apparent discordance of the layering to the southeastern margin of the complex is similar to that documented for the Skaergaard Intrusion, between the Marginal Border Group (in particular the Tranquil Division) and the Layered Series (Wager & Brown, 1968: p. 106–130). The fairly massive character of the marginal Munni Munni pyroxenites is also consistent with the poorly-layered fabrics of the Tranquil Division contact rocks.

A feature of subzones A to H is the lateral continuity of the cyclic units across the total width of the the intrusion. The cycles are conformable with each other and their contacts vary from sharp to transitional. Exceptions to this regional uniformity of stratigraphy include the bifurcation of peridotite cycles in subzone B and the occurrence of small porphyritic websterite and peridotite lenses in the lower parts of the zone.

The porphyritic plagioclase websterite layer of subzone I parallels the basal contact of the gabbroic zone (Fig. 12), and its base is discordant to the regional arcuate layering trends of subzones F, G, and H in the centre of the intrusion. In these respects, the websterite layer has closer affinities to the gabbroic zone than the ultramafic zone, but chemical and mineralogical data indicate it is transitional in character between the two

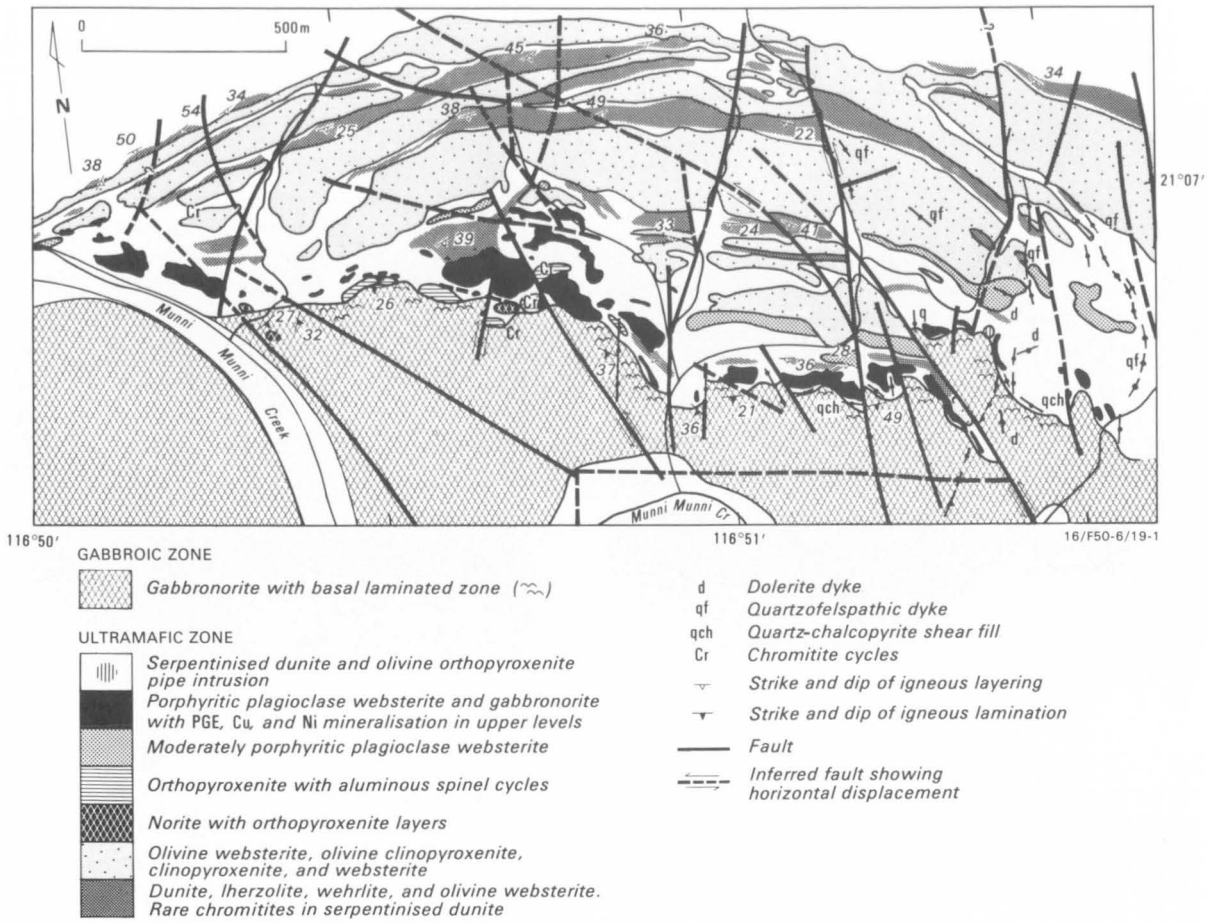

Fig. 12. Munni Munni Complex: detailed outcrop-distribution map along the ultramafic/gabbroic contact region in the central part of the complex, showing relationships of norite, orthopyroxenite, chromitite, dunite ?pipe, and the porphyritic plagioclase websterite layer. The unornamented area along the contact is alluvium.

zones. The implications of these features are discussed in the Petrogenesis chapter, p. 150.

Minor rock types, including orthopyroxenite, olivine orthopyroxenite, and spinel-bearing orthopyroxenite, form blocks and conformable lenses up to 200 m along strike and 40 m thick in the upper parts of subzone I (Fig. 12). The lenses thicken and thin along strike and have sharp contacts with the enclosing rocks. As discussed above, they are interpreted as accidental blocks derived from higher levels in the chamber.

A distinctive homogeneous outcrop of altered olivine orthopyroxenite and minor ?dunite traverses the ultramafic/gabbroic contact in the central part of the intrusion (right central area of Fig. 12). The talc- and serpentine-dominated rocks form a conical outcrop 5 m high and 30 m across. This feature is discordant to the structural elements of the area and is interpreted as a steeply dipping pipe that post-dates the gabbroic zone.

The different spatial and structural relationships of the blocks and the pipe to the enclosing rocks indicates they were emplaced by contrasting mechanisms. The confining of the large blocks and lenses to the synformal axis of the intrusion, and their absence on the flanks, indicates that gravitational processes were responsible for their emplacement. In contrast, the pipe appears to have been a late intrusion possibly emplaced upwards along a structural weakness at the contact between the ultramafic and gabbroic zones.

The relationship between the ultramafic and gabbroic zones varies considerably along the exposed 12 km extent of the contact. Along the northwestern side of the complex, the contact between the porphyritic websterite (Fig. 13A) and the laminated gabbronorite of the gabbroic zone is sharp and dips moderately towards the centre of the intrusion. In the central part of the complex, rock relationships indicate magma mixing. Such features include: the injection of gabbroic magma that has detached and partially assimilated subangular blocks of websterite (Fig. 13B); a stacked sequence of thin discontinuous websterite layers in gabbronorite host that have a cuspate lower surface and a planar upper surface (Fig. 13C); and mixed rock containing irregular contorted orthopyroxenite layers in norite (Fig. 13D).

The mixed rock (Fig. 13D) is texturally distinctive and forms small lenses and pods close to the contact. The medium-grained orthopyroxenite component has mineralogical and chemical affinities with the ultramafic zone. It comprises 20 to 40% of the mixed rock; irregular discontinuous layers and smaller finger-like apophyses branch off at various angles from the main orthopyroxenite layers. The norite host is of gabbroic-zone affinity; locally it contains size-graded cumulus plagioclase grains. There is a large outcrop of mixed rock 30 m west of the altered orthopyroxenite pipe described above.

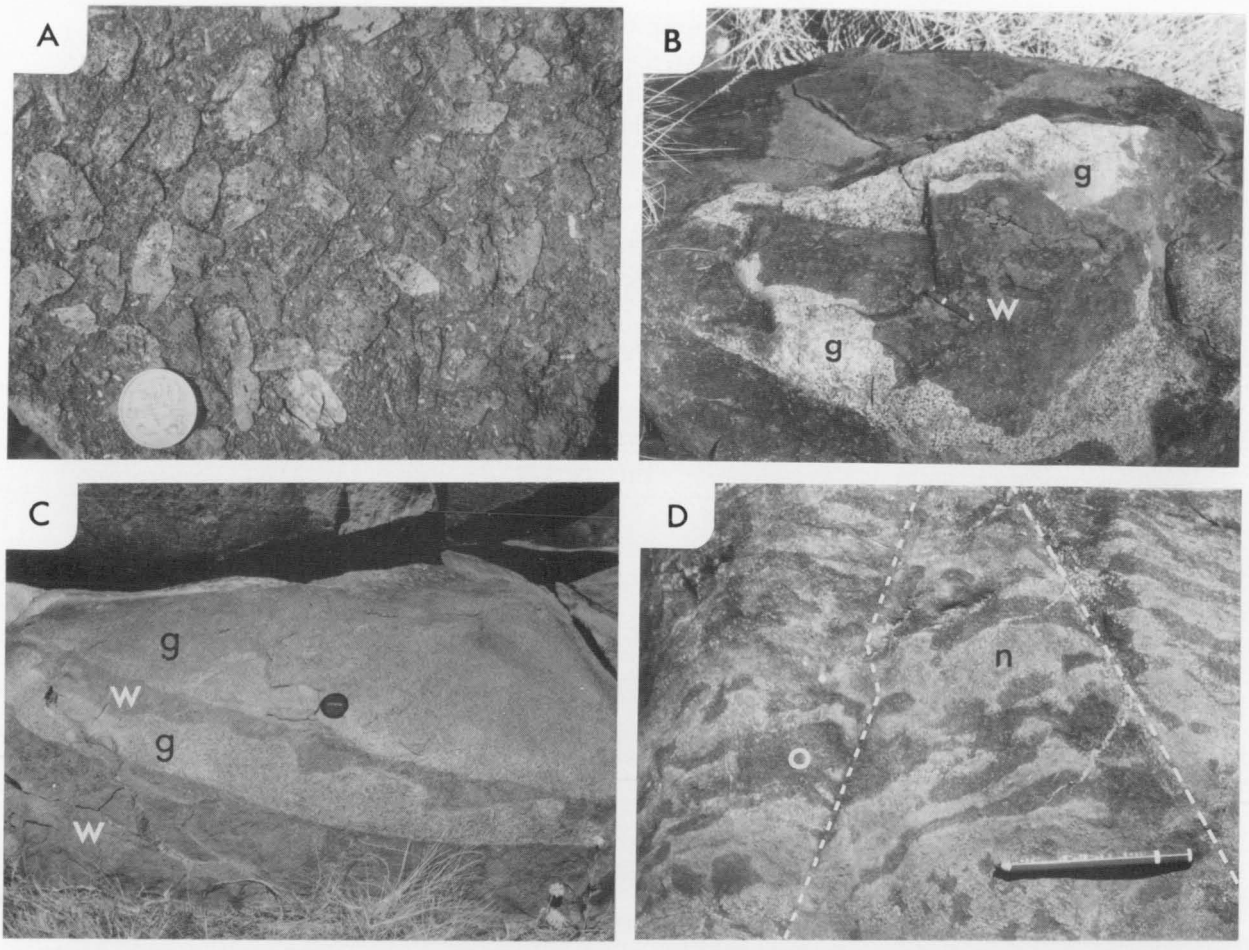

Fig. 13A–D. Munni Munni Complex: rocks from the contact between the ultramafic and gabbroic zones. A—Weathered outcrop of porphyritic plagioclase websterite orthocumulate from subzone I of the ultramafic zone, showing large euhedral cumulus bronzite-hypersthene grains. Diameter of coin 2.8 cm. B—Detached porphyritic plagioclase websterite block(w) partly assimilated by invading gabbroic magma(g) in the central part of the complex. C—Weakly porphyritic websterite layer(w) with cuspate lower surface (reflecting small-scale convection-mixing processes?) and planar upper surface, hosted by gabbronorite(g), east of the Munni Munni Fault. In this region, contact relationships range from a single thin websterite layer to more complex systems involving stacked sequences of up to 12 discontinuous websterite layers. D—Mixed orthopyroxenite(o) and norite(n) rock. The orthopyroxenite layers have been disrupted along two faults (indicated by dashed lines) that outline a wedge-shaped block.

Contact relationships with country rocks

The ultramafic zone of the Munni Munni Complex represents a nearly complete cross-section through the lower levels of a layered intrusion. Megascopic cyclic units (Figs. 14A & B) generally extend across the total width of the zone, and the contact relationships of these units with the granites are generally well exposed along the northern and southeastern sides of the intrusion. In contrast, the contact between the gabbroic zone rocks and granites is masked by alluvium (see appended map sheet).

The marginal contact rocks of the ultramafic zone are varied and, based on textural, mineralisation, and alteration features, can be subdivided into:

— The northern sulphide-bearing basal contact
— The northeastern and southeastern hybridised contact
— The northwestern chilled contact

The northern sulphide-bearing basal contact region of the ultramafic zone (i.e. basal contact immediately west of Munni Munni Fault) contains a complex group of rocks which have been variably deformed by syn- and post-intrusive faulting. On a regional scale, the basal contact follows an arcuate trend symmetrically around the northeast-trending longitudinal axis of the intrusion. In detail however, these marginal rock types have a stepped disposition relative to each other owing to strike-slip faulting in the basal parts of the ultramafic zone and basement fractures in the granites. Displacements across the basal contact are generally of the order of 100 to 200 m, but this increases to 600 m for the Munni Munni Fault. It is apparent that the northern basal region has been more dislocated and deformed than the southeastern and northwestern margins of the intrusion. This may be attributed to the reactivation of deep-seated faults that were related to the development of the lower parts of the magma chamber.

Rock types along most of the northern contact of the ultramafic zone display a transition, inwards towards the centre of the complex, from gabbro and gabbronorite, to plagioclase websterite, plagioclase olivine websterite and olivine websterite, reflecting an increasing ratio of olivine to plagioclase. Plagioclase in the websterite generally disappears within 200 m of the contact, whereas olivine forms a rare component of the basal

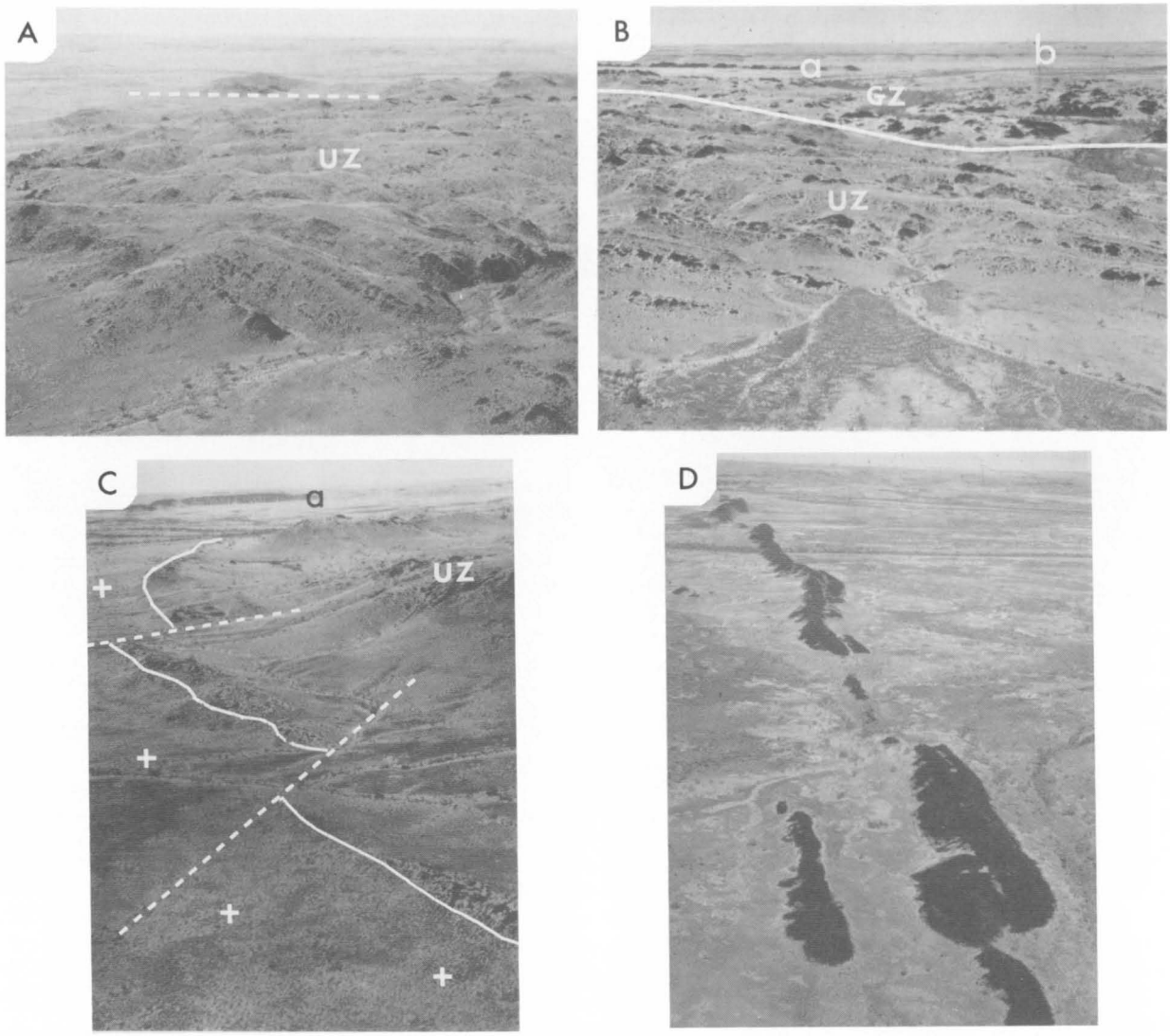

Fig. 14A–D. Munni Munni Complex and Pinderi Hills Dyke: aerial views. A—Looking east across the northern arcuate basal contact of the ultramafic zone (UZ). Strike ridges of pyroxenite cycles and more recessive peridotite cycles define the macrorhythmic layering. The northern part of the Munni Munni Fault is indicated by the dashed line. B—Looking southeast across the contact between the ultramafic zone (UZ) and gabbroic zone (GZ). Macrorhythmic layering in the ultramafic zone is defined by alternating pyroxenite cycles containing olivine websterite, websterite and clinopyroxenite and more recessive serpentinised peridotite cycles of dunite, lherzolite, wehrlite, and olivine websterite. The full line is the approximate position of the mineralised porphyritic plagioclase websterite layer directly below the contact between the two zones; a = zoned Eastern Munni Munni Dyke; b = shallow-dipping Fortescue Group sedimentary and volcanic platform cover overlying the gabbroic zone. The major drainage system shown is Munni Munni Creek. C—Looking southeast along the northeastern contact (full line) and marginal rim of the ultramafic zone; + = granites, a = Zebra Hill Dyke. High-angle faults are indicated by the dashed lines. D – Looking southwest along the Pinderi Hills Dyke.

gabbro and gabbronorite. The latter rocks locally contain up to 6.0 vol. % disseminated pyrrhotite with subordinate chalcopyrite and pentlandite. Spatially associated with the mineralised gabbronorite are rare small chilled 'tongues' of olivine microgabbro and olivine gabbronorite that abut the granitic country rocks.

A diversity of country rocks is present next to the northern basal region of the ultramafic zone. The dominant rocks are variably deformed leucocratic microcline granite and minor granodiorite, with fabrics ranging from gneiss through gneissic granite to weakly foliated granite. The gneissic textures in these rocks form a 'halo' around the northern part of the complex. Spatially associated with the gneissic granites immediately to the northeast of the complex are small inliers of intercalated metasediments and metavolcanics that are correlated with the Talga Talga Subgroup of the Warrawoona Group (see appended map sheet). They consist of fissile actinolite-biotite schist, coarse-grained spotted actinolite-plagioclase gneiss, phyllite, psammite, epidosite, and calc-silicate gneiss.

The northeastern and southeastern hybridised contact region of the ultramafic zone (east of the Munni Munni Fault) consists of an outer rim that rises 10 m above the eastern granite pavements and an alluvium-filled depression, which separates the rim from the rest of he complex (Fig. 14C). The rim extends for over 4 km and contains altered pyroxenitic rocks that directly overlie

leucocratic granite. The contact between the pyroxenites and granite dips at 20 to 40° towards the centre of the complex. The pyroxenites have varying intensities of silicic-hydrous-alkali alteration along the contact, but have retained their medium-grained character and show little textural evidence of chilling or recrystallisation. A porphyritic character (orthopyroxene) is locally developed in the marginal pyroxenites 1.5 km north of Munni Munni Creek. This coincides with where the porphyritic plagioclase websterite layer (subzone I) of the ultramafic zone comes in close contact, and appears to merge, with the marginal pyroxenites.

Granitic material is incorporated in the altered marginal rocks along most of the northeastern and southeastern contact, and takes the form of:

— intergrowths of quartz and feldspar interstitial to pyroxene grains;
— thin irregular net-veined and veinlet complexes enclosing altered pyroxenite fragments; and
— apophyses up to 2 m wide containing blocks of laminated ?basement rocks.

It is believed the net-vein textures and the granitic component in the marginal pyroxenites resulted from the commingling of two magmas during the emplacement of the Munni Munni Complex into an older granite terrane, i.e. the Munni Munni Complex partly remelted the granitic rocks, causing mixing of the two magmas. It is believed the magma that formed the ultramafic zone had liquidus temperatures of about 1250°C (see Petrogenesis chapter, p. 160). A large body of this magma would have the ability to partly remelt granitic rocks that it came into contact with. These partial granitic melts may back-intrude or become assimilated into the partly consolidated mafic magma. Conversely, a granitic magma with crystallisation temperatures of 750–950°C (Sparks & others, 1977) would not be able to remobilise or assimilate a significant amount of an older mafic component (R. N. England, personal communication, 1985). Net-veined complexes resulting from the injection of mafic magma into felsic magma or partly remelted felsic rocks have been described by Blake (1981) in a number of high-level Palaeozoic and Precambrian intrusions of eastern and central Australia. It is possible that the felsic components in many net-veined complexes may have been incorrectly interpreted as the younger phase.

Traces of disseminated pyrrhotite, chalcopyrite, and pentlandite or their secondary alteration products occur locally in the marginal altered pyroxenites along the northeastern and southeastern contact and increase in tenor towards the northern basal contact. Small outcrops of massive, laminated, and colloform limonitic gossan are the surface expression of the mineralisation. Transgressing the southeastern margin, about 600 m north-northeast of Munni Munni Creek (see appended map sheet), is a series of 5 to 20 cm-thick limonitic quartz-carbonate veins with minor galena (2%), chalcopyrite (0.5%), and traces of pyrite, malachite, azurite, and ?cuprite. Lead mineralisation also occurs in granite immediately to the west of the Munni Munni Complex (D. Crook, personal communication, 1984), and at the Andover Mine on the southern margin of the Andover Complex, near Roebourne. The strong spatial association of the base-metal mineralisation with the margins of the layered intrusions suggests the latter may have provided a heat source for remobilising base metals from the granites or older basement rocks.

The northwestern chilled contact occurs along the northwestern margin of a southwesterly-trending tongue of weakly porphyritic websterite (subzone I) and equigranular websterite (subzone H) that flanks the western extremity of the gabbroic zone (see 'c' symbol on the appended map sheet). This pyroxenite tongue is unconformably overlain by shallow-dipping Fortescue Group sediments and volcanics to the southwest and represents part of the Cadgerina feeder dyke. For a distance of 1 km along its northwestern linear contact, a fine-grained chilled phase of the pyroxenite abuts medium-grained microcline granite. The chilled pyroxenite (grainsize 0.5 mm) grades into a medium-grained (1.5–2.0 mm) equigranular websterite within 1 m of the granite contact. In contrast to the northeastern and southeastern contacts of the complex, these chill rocks have incorporated no significant granite component by assimilation of remelted granite material.

Dykes

Dykes range in composition from quartz, aplite, granite, and dolerite, through to anorthosite, gabbronorite, and olivine orthopyroxenite. They can be broadly subdivided into three major groups: a comagmatic suite; a suite derived from the partial melting of the country rocks; and a post-magmatic suite which has no genetic relationship with the complex.

Dykes comagmatic with the Munni Munni Complex are believed to have formed from the migration of late-crystallising liquids during the compaction of the cumulus pile. Examples include thin pegmatoidal gabbro and anorthosite dykes near the contact of the ultramafic and gabbroic zones, and gabbroic dykes at higher stratigraphic levels. The 'Southern Munni Munni Dyke' (see appended map sheet) is not a true dyke, but a linear body that represents the southeastern margin of the complex. It consists of altered websterite, plagioclase websterite, and quartz-bearing gabbro. The Cadgerina Dyke is a 2.5 km long northeast-to-north-trending pyroxenite dyke lying west of Cadgerina Pool (see appended map sheet). It intrudes granites and may be a possible feeder dyke to the complex.

The second suite of dykes encompasses a group of felsic bodies concentrated in a 1 km wide zone along the southeastern margin of the ultramafic zone. The spatial distribution of the quartz, aplite, aplitic granite, granite, and hybrid granite dykes suggests that they were probably derived by the partial melting of the basement granitic country rocks by the complex; the partial melts then back-intruded the marginal rocks of the complex.

The final suite includes post-magmatic dykes ranging from thin ?Early Proterozoic dolerite dykes to large topographically prominent dykes, such as the Eastern Munni Munni, Pinderi Hills, and Zebra Hill. Aphanitic and fine-grained, subophitic, tholeiitic dolerite dykes are ubiquitous throughout the complex and surrounding rocks. They have apparent strike lengths of < 10 m in the complex, but may reach 3 km in the granites. In the granites, the dykes have a constant width and strike direction, but deflect and rapidly wedge out when they intrude the complex. An unusual dolerite dyke containing abundant, partly assimilated xenocrystic quartz fragments intrudes the upper levels of the gabbroic subzone A (see appended map sheet). Similar doleritic and granophyric dykes traverse the Mount Sholl and Gidley Granophyre intrusions.

The large zoned Eastern Munni Munni Dyke on the southeastern side of the intrusion (Fig. 14B) contains a 300 m-wide core of plagioclase harzburgite and plagio-

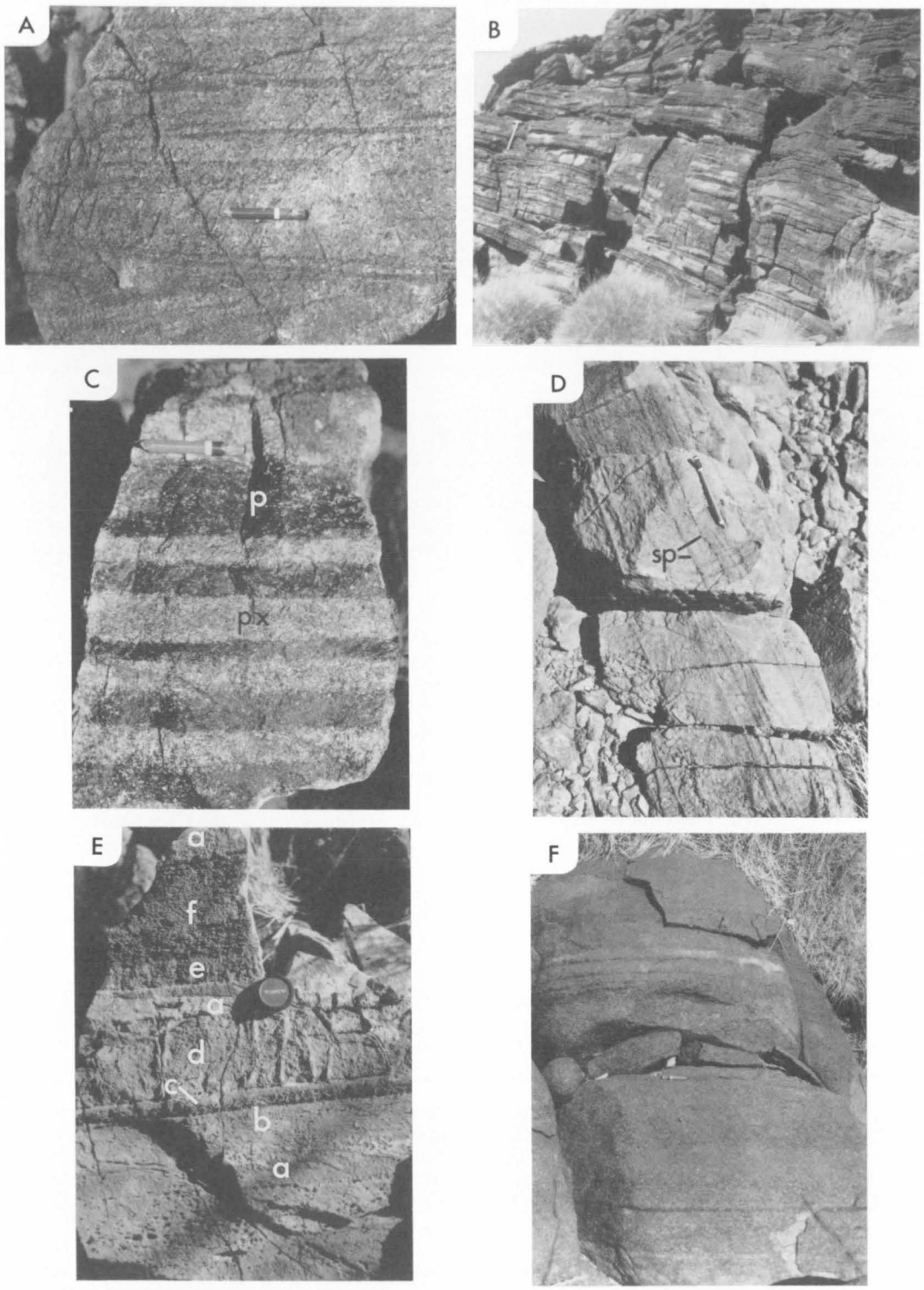

Fig. 15A–F. Munni Munni Complex: types of layering. A—Low-angle cross-bedding of wispy serpentinised olivine-rich laminae(black) in a clinopyroxene-olivine adcumulate. B – Moderately dipping microrhythmic or 'inch-scale' layering consisting of alternating olivine-clinopyroxene and clinopyroxene-olivine cumulates. C—Rhythmically layered sequence consisting of olivine-clinopyroxene(p) and clinopyroxene-olivine(px) cumulates. D—Fine-scale rhythmic layering: aluminous-spinel cycles in accidental orthopyroxenite block hosted by porphyritic websterite layer. E—Complexly layered sequence comprising massive, uniformly-graded and isomodal-laminated components. In ascending order, the sequence consists of a massive 30 cm serpentinite layer(a), a 2 cm isomodal lamination of serpentinised olivine cumulate(b), a 2 cm serpentinite lamination(c), a 15 cm uniformly-graded clinopyroxene-olivine cumulate with irregular fracturing(d), a 5 cm massive serpentinite layer(a), a strongly laminated 15 cm layer comprising a lower clinopyroxene-rich part(e) overlain by an alternating olivine- and clinopyroxene-rich laminated part(f), and an upper layer of massive serpentinite(a). F—Compositional layering and lamination in sericitised gabbronorite along the basal contact of subzone A of the gabbroic zone. The fine-scale layering consists of various thicknesses of diffuse melanocratic and leucocratic layers containing varying proportions of cumulus plagioclase and clinopyroxene. The melanocratic layers are clinopyroxene-rich, whereas minor clinopyroxene characterises the leucocratic layers. A platy lamination (parallel to pencil) defined by the alignment of plagioclase laths parallels the layering.

clase olivine orthopyroxenite, and a 50 m-wide outer zone of gabbronorite. Minor disseminated chromite is associated with the olivine- and orthopyroxene-bearing units, but not with the more fractionated marginal gabbroic rocks. The large Zebra Hill (Fig. 14C) and Pinderi Hills (Fig. 14D) dykes are unzoned and are more fractionated than the Eastern Munni Munni Dyke, and are more contaminated by partly assimilated granitic material. The Pinderi Hills Dyke crops out over 10 km (Fig. 14D) and its 035° strike direction is the dominant orientation for dykes and faults in the Pilbara Block. It is a homogeneous body of medium-grained intergranular gabbronorite that contains large blocks of granite.

Layering

Ultramafic zone

The gross layering in the ultramafic zone of the Munni Munni Complex takes the form of megascopic cyclic units which extend across the total width of the zone. These large units consist of smaller cycles that in turn contain various outcrop-scale layering components. These include:

— **Isomodal lamination**
— **Microrhythmic or 'inch-scale' layering**
— **Rhythmic layering**
— **Modally graded layers**
— **Complex composite layering**

Isomodal lamination. Alternating 1 mm (i.e. grain-size) to 1 cm-thick olivine-rich and clinopyroxene-rich laminae are a feature of olivine-clinopyroxene cumulates. These delicate isomodal laminations have sharp contacts and constant thicknesses along strike, although the olivine-rich laminae often disappear and reappear along the same layer. Clinopyroxene grains commonly have a weak preferred orientation parallel to the layering. The olivine-rich laminae weather recessively relative to the clinopyroxene-rich laminae, imparting a regular fluted appearance to weathered surfaces. Low-angle cross-bedding (Fig. 15A) and scour and fill structures are locally present.

Microrhythmic or 'inch-scale' layering. Microrhythmic or 'inch-scale' layering (Fig. 15B) is most prominent in clinopyroxene-olivine cumulates in the upper stratigraphic levels of the ultramafic zone. It is characterised by a stacked sequence of 2 to 6 cm-thick layers which show remarkable uniformity of thickness and no obvious internal modal variation. A lamination defined by alternating thin clinopyroxene-dominant and olivine-dominant laminae may be developed within the 'inch-scale' layers.

Rhythmic layering. The most common form of layering in the ultramafic zone is rhythmic layering consisting of alternating isomodal layers of olivine-clinopyroxene and clinopyroxene-olivine (or clinopyroxene) cumulates (Fig. 15C). Individual layers vary from 1 cm up to several metres thick, and for some rhythmic units there is an overall upward increase in the proportion of clinopyroxene- to olivine-rich cumulates. The lower contacts of the olivine-rich layers are generally sharp, whereas the upper contacts of these layers are often more diffuse. Thickening and thinning are common along strike, and some layers pinch out and show evidence of warping and truncation by adjacent layers. Fine-scale rhythmic layering (Fig. 15D) comprising alternating spinel-orthopyroxene versus orthopyroxene layers are also displayed in the orthopyroxenite blocks of subzone I.

Modally graded layers. Rare cyclic units which are both modally and texturally graded are restricted to the upper parts of the ultramafic zone. The units range from a few centimetres to a couple of metres in thickness and modal variations throughout the units reflect the general cumulus paragenesis of the ultramafic zone. They consist of a basal serpentinised olivine cumulate grading upwards into olivine-clinopyroxene and clinopyroxene-olivine cumulates, which contain increasing amounts of oikocrystic orthopyroxene, and the top of the unit is often a massive clinopyroxene cumulate. Alternating thin olivine- and clinopyroxene-rich laminae may occur in the upper parts of the layered unit. In addition to this modal grading, the antipathetic distributions of olivine and orthopyroxene impart a textural grading, with equigranular fabrics passing upwards into coarser poikilitic textures. The upper contacts of the graded cycles define a phase contact, with the reappearance of abundant cumulus olivine abutting the pyroxene-rich part of the lower cycle.

Complex composite layering. Peridotites in the lower part of the zone locally display complexly layered sequences comprising isomodal laminations, microrhythmic and rhythmic layers, and massive layers (Fig. 15E). There is no systematic order of occurrence for the different types of layering and the individual layers vary in thickness and internal fabric.

Gabbroic zone

Laminated textures are a feature of gabbronorites in the basal 30 m of the gabbroic zone. Above this stratigraphic level, homogeneous, intergranular textures generally predominate. The platy lamination is defined by the preferred alignment of euhedral plagioclase laths (Fig. 15F). Locally associated with the lamination is a compositional layering defined by alternating diffuse layers of melanocratic and leucocratic gabbronorite. The melanocratic layers are clinopyroxene-rich and plagioclase-poor, whereas minor clinopyroxene characterises the leucocratic layers. Modal grading is present in some of the thicker layers.

Structure

The Munni Munni Complex is interpreted as a slightly asymmetric boat-like structure, plunging moderately to the south, with the cyclic units thickening along the axis of the intrusion and thinning out as they deflect upwards along the walls of the magma chamber. The complex has similar geometrical features to the Jimberlana Dyke of the Yilgarn Block (Keays & Campbell, 1981), the Muskox Intrusion of Canada (Smith & Kapp, 1963), and in particular, with the Great Dyke of Zimbabwe (Wilson & Prendergast, 1989).

Layering in the central part of the ultramafic zone has a predominant east–west strike, which swings to the southwest along the northwestern contact of the zone. Along the southeastern side of the ultramafic zone, the layering is almost perpendicular to the contact. Complementing these deviations in strike direction are increases in dip angles across the intrusion. Dips of 15 to 35° towards the south are typical for the southeastern and central parts of the zone, but the dips increase to 42 to 64° towards the southeast for the northwestern side of the zone. This change in dip partly accounts for the apparent thickening of some cyclic units in the central part of the intrusion. The different relationships between the layering and the contacts of the intrusion may be due to an asymmetrically shaped

magma chamber, and/or some differential tilting of the intrusion to the southeast. This asymmetry is also reflected in the regional discordance of the dominant east–west layering trends of the ultramafic zone and the northeast alignment of the intrusion.

The higher subzones of the ultramafic zone (e.g. F, G, and H) contain arcuate trends (Fig. 12), which Williams (1968) suggested was due to folding. The symmetrical relationship of the curved cyclic units to the axis of the intrusion and the 'straight' strike trends for the lower cycles indicate that folding was not responsible for these features. The arcuate trends are believed to be due to the sagging of the upper parts of the cumulus pile along the central axis of a boat-shaped body, rather than to deformation.

The lamination within the lower part of the gabbroic zone generally parallels the basal contact of this zone. Dips of the lamination range from 29 to 49° in the centre of the complex, and from 31 to 36° along the northwestern side of the gabbroic zone. Dip directions are mainly towards the south and southeast, similar to the layering in the ultramafic zone. Figure 16 shows the distribution of poles to layering for the ultramafic zone and poles to lamination in the gabbroic zone. The two sets of data plot in similar fields, although in detail the lamination is discordant to the regional arcuate layering trends that characterise the upper subzones of the ultramafic zone. The parallelism of the lamination with the basal contact of the gabbroic zone suggests that the lamination may have formed during the emplacement of the gabbroic magma, e.g. by shearing, flowage differentiation, and/or magma mixing.

The upward deflection of both the cyclic units and the ultramafic/gabbroic contact near the margins of the intrusion, and the presence of chilled and hybridised rocks along the margins, indicate that the Munni Munni Complex is a near-complete intrusion and not a fault-bounded block. An interpretation of the subsurface geometry of the intrusion is shown in Figure 17.

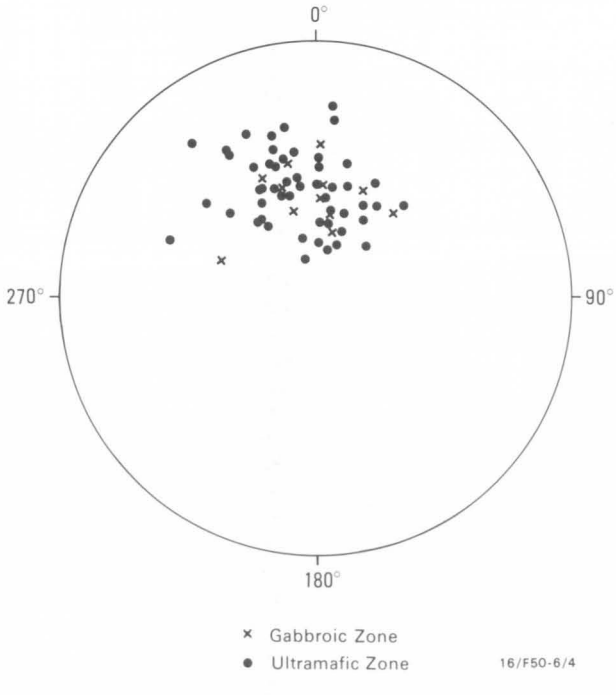

Fig. 16. Munni Munni Complex: equal-area projection of poles to igneous layering in the ultramafic zone (53 poles) and lamination in the gabbroic zone (12 poles).

High-angle faulting is prominent throughout both zones of the intrusion. For most faults the dominant movement has been dip-slip, although this has been limited to a few hundreds of metres. An exception is the largest fault in the complex, the Munni Munni Fault, which has a 600 m sinistral dispacement along the eastern side of the complex. It forms a major escarpment through the complex and is part of a regional fault that can be traced along the western margin of the Maitland Complex to the north and past the Zebra Hill Dyke to the south.

Numerous high-angle faults cut the contact between the ultramafic and gabbroic zones. These narrow silica-carbonate-rich zones contain gossanous limonite and traces of chalcopyrite and pyrite remobilised from the mineralised porphyritic websterite layer. Faults in the gabbroic zone typically extend over large distances and are infilled by epidote-quartz-carbonate-amphibole-bearing assemblages. Stockworks of these veins are prominent along the sheared southeastern side of subzone A of the gabbroic zone. Traces of chalcopyrite are locally present in these low-temperature, structurally-controlled vein systems.

The different fault orientations in the ultramafic and gabbroic zones are summarised in Figure 18. The majority of faults in the ultramafic zone have a strike direction between 320 and 020°, whereas in the gabbroic zone they have more variable orientations that largely fall in the 080–100° and 140–180° sectors. The strong north-south clustering of faults in the ultramafic zone appears to be partly governed by the east-west layering of the zone, whereas the weakly layered gabbroic zone has no dominant pervasive grain to influence the fault trends.

Petrography

Introduction

The broad subdivision of the complex into a lower ultramafic zone and an overlying gabbroic zone is on the basis of the distribution of cumulus assemblages (Fig. 19; Table 7). The ultramafic zone is largely characterised by varying proportions of cumulus olivine and clinopyroxene, and intercumulus orthopyroxene, which attains cumulus status in the upper parts of subzone I. Plagioclase as an intercumulus phase is restricted to the marginal rocks (0–170 m level) and the upper 50 m of the ultramafic zone. The base of the gabbroic zone (1850 m level) is defined by the first appearance of cumulus plagioclase, which is associated with cumulus clinopyroxene and cumulus inverted pigeonite. Magnetite and ilmenite are of trace abundance above the 2300 m stratigraphic level, and become a major cumulus component above 2800 m. The ultramafic/gabbroic contact is therefore delineated by the disappearance of cumulus olivine and the appearance of cumulus plagioclase; clinopyroxene is the only mineral which retains its cumulus character across the contact (Fig. 19).

The dominance of clinopyroxene and olivine in the ultramafic zone cumulates is illustrated by the ternary diagram of Figure 20A. Significantly there is a major compositional break to the orthopyroxene-dominant fields of olivine orthopyroxenite and orthopyroxenite. The absence of any transitional orthopyroxene-bearing rocks supports the view that the orthopyroxenites are an anomalous group of rocks relative to the other cumulates of the ultramafic zone. The olivine-poor and plagioclase-rich character of the porphyritic plagioclase

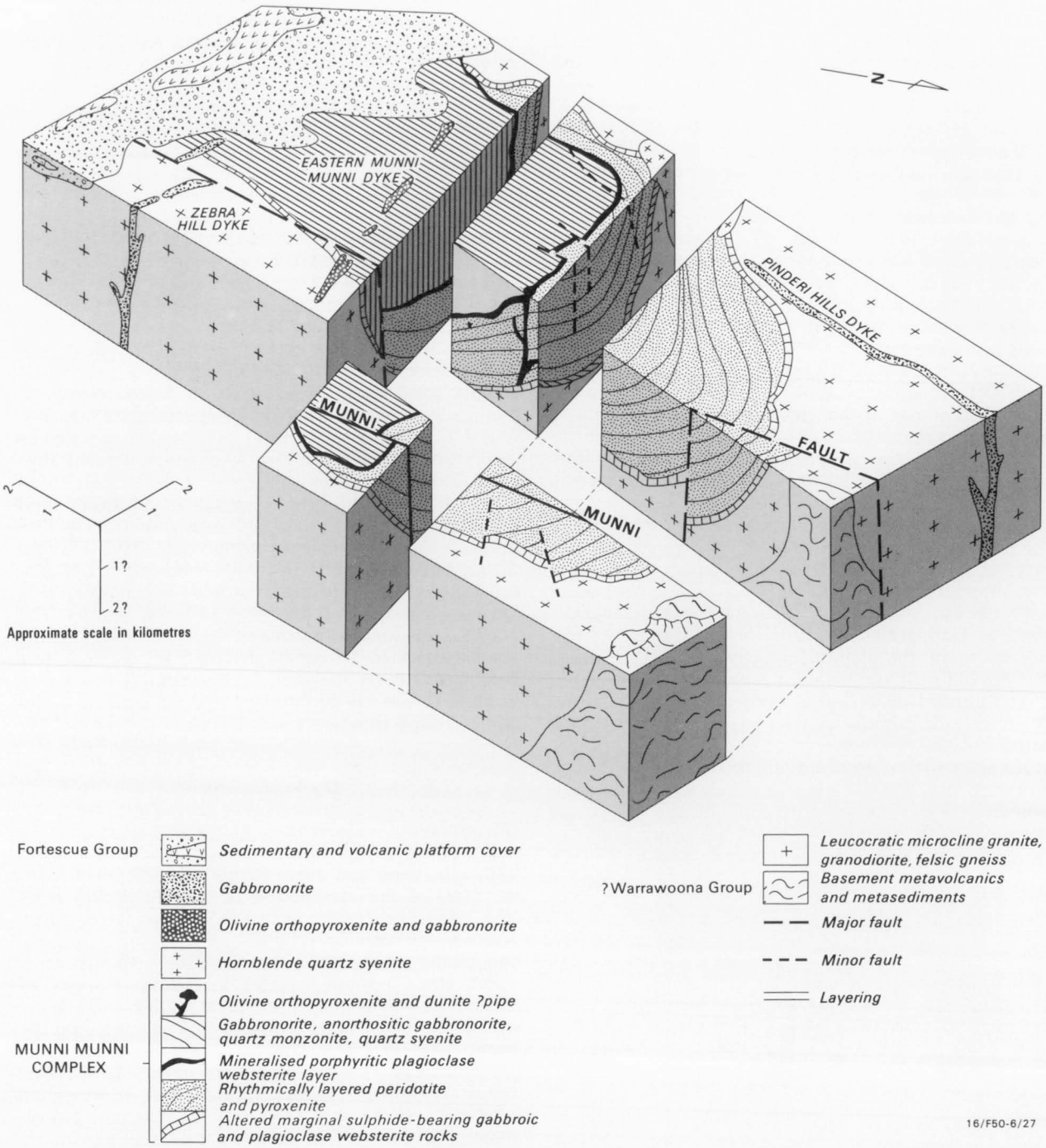

Fig. 17. Interpretive block diagram of the Munni Munni Complex.

websterite of subzone I is shown in Figure 20. In some of these mineralised orthocumulates the plagioclase content attains 18 volume % and thus the rock is strictly a melagabbronorite. Sympathetic with this increase in plagioclase is an increase in orthopyroxene relative to clinopyroxene. The most felsic rocks of the ultramafic zone are the altered marginal rocks along the northern and northeastern contacts.

Subzone A of the gabbroic zone is dominated by a monotonous gabbronorite sequence of plagioclase-clinopyroxene-inverted-pigeonite cumulates that grade into plagioclase-clinopyroxene-inverted-pigeonite-magnetite-ilmenite cumulates in the upper parts of the subzone. Above the 4320 m level, anorthositic gabbro and rare anorthosite characterise subzone B. Quartz monzonite, quartz syenite, and granophyric gabbro (see appended map sheet) crop out along the erosional contact of the Fortescue Group cover rocks and may represent the most fractionated rocks exposed in the intrusion.

The modal distribution trends in subzones A and B of the gabbroic zone are summarised in Figure 21. The uniform modal variation trends and the generally increasing amounts of magnetite-ilmenite and biotite upwards in subzone A are consistent with Fe-Ti enrichment during closed-system fractionation of a parent magma of tholeiitic affinities.

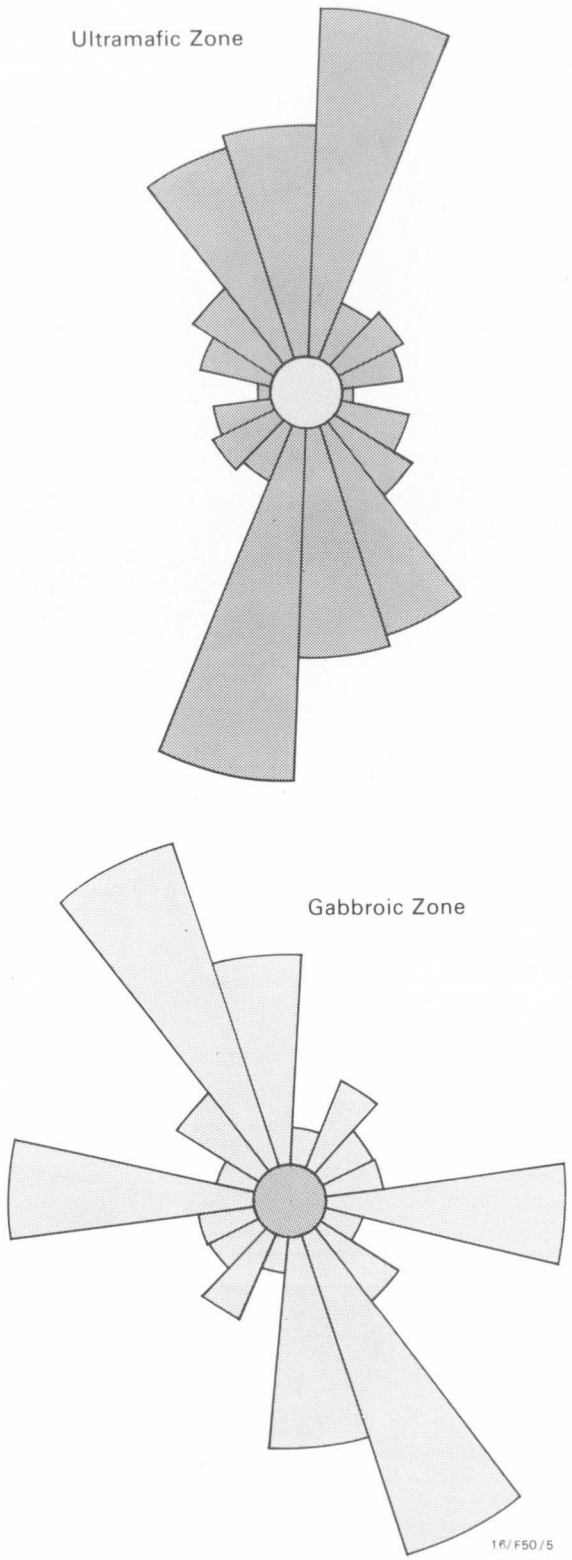

Fig. 18. Munni Munni Complex: rose diagram showing strike-trends of faults in the ultramafic and gabbroic zones. The total number of faults represented in the 20° sectors is 64 for the ultramafic zone and 38 for the gabbroic zone.

The rock types of the ultramafic zone have been subdivided into the following subgroups (cumulus assemblages in brackets):

- **Altered marginal rocks (cpx ± opx ± ol)**
- **Dunite, lherzolite, wehrlite (ol ± cpx)**
- **Websterite, olivine websterite (cpx + ol)**
- **Clinopyroxenite, olivine clinopyroxenite (cpx ± ol)**
- **Plagioclase websterite, gabbronorite (cpx ± opx ± ol)**
- **Orthopyroxenite, olivine orthopyroxenite (opx ± ol ± spinel)**
- **Chromitite (chrom ± ol ± opx)**
- **Megacrystalline orthopyroxenite (cpx)**
- **Mixed norite-orthopyroxenite rock (plag + opx: norite; opx: orthopyroxenite)**

Altered marginal rocks (cpx ± opx ± ol)

The marginal rocks of the ultramafic zone differ markedly in mineralogy, texture, and intensity of alteration and hybridisation from the overlying olivine- and clinopyroxene-rich cumulates. The fractionated compositions of the basal rocks are reflected in the introduction of intercumulus plagioclase, cumulus hypersthene, paucity of cumulus olivine, and the presence of minor inverted pigeonite, quartz, quartz-feldspar intergrowths, and magnetite-ilmenite. The dominant rocks range in composition from websterite, plagioclase websterite, plagioclase olivine websterite, and gabbronorite to (more rarely) olivine gabbronorite. The gabbronorites are dominantly medium-grained mesocumulates and orthocumulates, but locally, where the intercumulus plagioclase component attains 50 vol. % (samples 84770100, 102), they are extreme orthocumulates or more strictly non-cumulates.

Medium-grained gabbronorite (84770100–102) and plagioclase websterite (84770001–003) are the commonest rock types along the northern basal contact. They contain 30–60 vol. % clinopyroxene, 0–50% plagioclase, 0–20% hypersthene, minor olivine, inverted pigeonite, biotite, ilmenite, magnetite, and sulphides. There is an antipathetic relationship between olivine and plagioclase, with the olivine-to-plagioclase ratio increasing away from the contact towards the centre of the intrusion. Olivine rarely exceeds 2 vol. % in the plagioclase-rich rocks. Clinopyroxene (mg_{72-71}; the mg number 'mg' is defined by the atomic ratio 100 x Mg/(Mg + total Fe)) in the marginal gabbronorites forms 1.0 x 1.5 mm subhedral prisms slightly finer-grained than clinopyroxene further into the intrusion. Hypersthene in the basal rocks is the most Fe-rich orthopyroxene in the intrusion (mg_{59}) and its co-crystallisation with inverted pigeonite is consistent with the fractionated compositions of these rocks. The pyroxenes are enclosed in coarse (4 x 8 mm) poikilitic plagioclase laths (An_{41-37}) that interlock at varying angles. The high modal proportions and coarse grainsize of the plagioclase in these rocks contrast with the general plagioclase-poor character of the cumulates higher up in the zone.

Sulphides are heterogeneously disseminated in the marginal rocks of the northern basal contact. They generally average 0.1 to 1.0 vol. %, but some gabbronorites contain up to 6 vol. %. Pyrrhotite (80%), pentlandite (10%), and chalcopyrite (10%) form irregular blebs up to 4 mm interstitial to the cumulus pyroxene grains. Despite their intercumulus habit (due to subsolidus modification), the sulphides are cumulus since they are not associated with intercumulus plagioclase and locally form small (0.1 mm) euhedral inclusions in unaltered clinopyroxene. Coarse pyrrhotite grains contain exsolved spindle and flame-like lamellae of pentlandite or coarse blades of chalcopyrite (0.1 x 0.5 mm) aligned across the pyrrhotite host. Pyrrhotite and chal-

Table 7. Summary of cumulus, intercumulus, and alteration relationships in the Munni Munni Complex

Zone	*Subzone*	*Rock types*	*Cumulus minerals*	*Intercumulus minerals*	*Alteration assemblages*
GABBROIC	B	Anorthositic gabbro and anorthosite	Plagioclase	?Orthopyroxene Magnetite, ilmenite Quartz, ?apatite	Plagioclase—chlorite, sericite, calcite, clinozoisite Orthopyroxene—talc, calcite, chlorite Magnetite—biotite
	A	Gabbronorite (above 2300 m stratigraphic level)	Plagioclase Clinopyroxene ?Inverted pigeonite Magnetite, ilmenite	Clinopyroxene Inverted pigeonite Biotite, quartz Hornblende Orthopyroxene, apatite ?Alkali feldspar	Plagioclase—chlorite, sericite, clays Clinopyroxene—hornblende, ferroactinolite, chlorite Inverted pigeonite—?grunerite, ferroactinolite, talc, chlorite, opaques Magnetite—biotite, hematite, limonite Orthopyroxene—talc, clinoamphibole, limonite Biotite—chlorite
		Gabbronorite (for stratigraphic interval 1850–2300 m)	Plagioclase ?Inverted pigeonite Clinopyroxene	Inverted pigeonite Clinopyroxene Orthopyroxene	Plagioclase—sericite, chlorite, grossular, epidote, calcite, clays Inverted pigeonite—ferroactinolite, talc, chlorite, opaques Clinopyroxene—ferroactinolite, hornblende, chlorite, opaques Orthopyroxene—talc, clinoamphibole
ULTRAMAFIC	I	Norite	Plagioclase Orthopyroxene (hypersthene)	Clinopyroxene Biotite	Plagioclase—sericite, clays Orthopyroxene—talc, clinoamphibole
		Orthopyroxenite and olivine orthopyroxenite	Orthopyroxene (bronzite) Olivine Spinel	Clinopyroxene Plagioclase Biotite/phlogopite	Orthopyroxene—talc, clinoamphibole, calcite, ?antigorite Olivine—antigorite, magnetite, iddingsite Plagioclase—chlorite Spinel—hematite Biotite—chlorite, talc
		Plagioclase websterite and gabbronorite	Clinopyroxene Orthopyroxene (hypersthene) Sulphide ?Inverted pigeonite	Plagioclase Orthopyroxene (hypersthene) Inverted pigeonite Biotite, sulphide Magnetite, ilmenite Alkali feldspar Quartz, apatite	Clinopyroxene—clinoamphibole, hornblende Orthopyroxene—talc, chlorite Plagioclase—chlorite, sericite, clays Biotite—chlorite, talc Sulphide—actinolite, calcite

Table 7 (continued). Summary of cumulus, intercumulus, and alteration relationships in the Munni Munni Complex

Zone	*Subzone*	*Rock types*	*Cumulus minerals*	*Intercumulus minerals*	*Alteration assemblages*
ULTRAMAFIC	E	Clinopyroxenite	Clinopyroxene Olivine	Orthopyroxene (bronzite)	Clinopyroxene—?grunerite, magnetite, calcite, talc, limonite Orthopyroxene—talc, clinoamphibole, calcite, magnetite Olivine—?antigorite, chrysotile, talc, magnetite, calcite, iddingsite
	A to I	Websterite, olivine websterite, olivine clinopyroxenite	Clinopyroxene Olivine	Clinopyroxene Orthopyroxene (bronzite) Plagioclase Biotite/phlogopite Alkali feldspar	Clinopyroxene—?grunerite, magnetite, calcite, talc, limonite Olivine—?antigorite, chrysotile, magnetite, talc, calcite, iddingsite, hematite Orthopyroxene—talc, clinoamphibole, calcite, magnetite Plagioclase—sericite, chlorite, clays Biotite—chlorite, magnetite, limonite
		Wehrlite and lherzolite	Olivine Clinopyroxene	Clinopyroxene Orthopyroxene (bronzite) Phlogopite	Olivine—antigorite, chrysotile, magnetite, talc, calcite, iddingsite, magnesite, chlorite, hematite Clinopyroxene—antigorite, chlorite, talc, magnetite Orthopyroxene—antigorite, talc, calcite, magnetite
		Dunite	Olivine Clinopyroxene Chromite	Clinopyroxene Orthopyroxene (bronzite) Phlogopite	Olivine—antigorite, chrysotile, magnetite, talc, calcite, chlorite, iddingsite, magnesite, hematite Clinopyroxene—antigorite, chlorite, talc, magnetite Orthopyroxene—antigorite, talc, calcite, magnetite Phlogopite—chlorite
	A′	Altered marginal gabbronorite, plagioclase websterite, and olivine plagioclase websterite	Clinopyroxene Olivine Orthopyroxene (hypersthene) Sulphide ?Inverted pigeonite	Clinopyroxene Orthopyroxene Plagioclase Quartz Biotite Magnetite Ilmenite ?Inverted pigeonite	Clinopyroxene—hornblende, chlorite, biotite, actinolite, ?vesuvianite Olivine—serpentine, magnetite, talc, clinoamphibole, chlorite Orthopyroxene—talc, ?grunerite, sericite Plagioclase—sericite, chlorite, calcite Biotite—opaques, chlorite Sulphide—actinolite, calcite, hematite, limonite

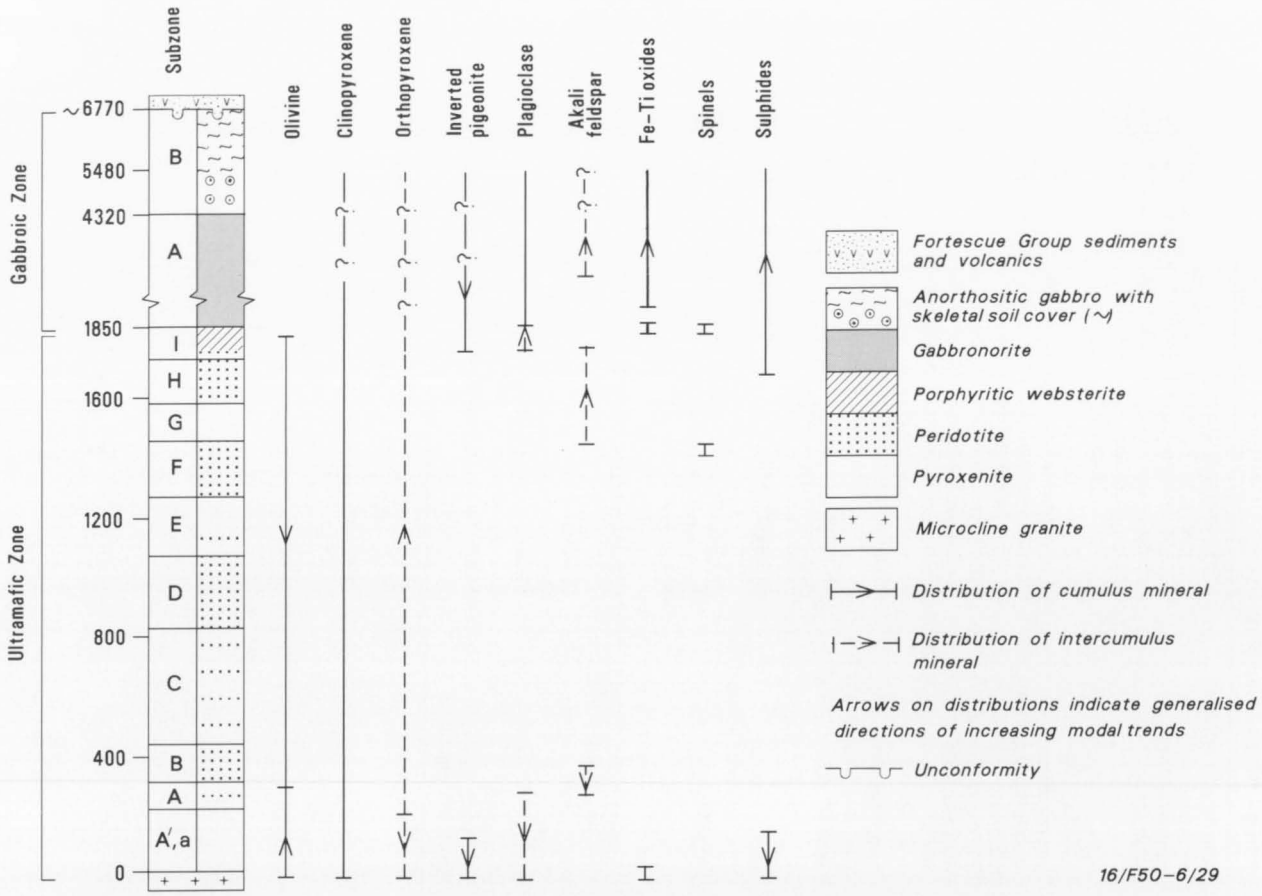

Fig. 19. Distribution of cumulus and intercumulus minerals in the Munni Munni Complex.

copyrite also show zonal arrangements, with pyrrhotite rimming cores of chalcopyrite and also invading cracks in magnetite. These different associations indicate the sulphides have experienced a complex history of unmixing and subsolidus re-equilibration during cooling.

The sulphides are variably replaced by actinolite-tremolite, chlorite, biotite, and calcite. This replacement ranges from incipient overgrowth of clinoamphibole, along sulphide grain boundaries, to disaggregation of coarse pyrrhotite grains to smaller sub-grains by decussate blades of clinoamphibole and interstitial carbonate and biotite. The final stage of replacement is represented by an interlocking mat of coarse decussate amphibole and carbonate anhedra superimposed with fine dustings of sulphide. These textures are a common feature of sulphide-bearing intrusive rocks in the west Pilbara. They are similiar in style to that seen in the mineralised porphyritic plagioclase websterite of subzone I and the basal sulphide assemblages of the Mount Sholl (Mathison & Marshall, 1981) and Radio Hill intrusions (this publication). Mathison & Marshall (1981) attributed the sulphide replacement at Mount Sholl to progressive recrystallisation during metamorphism, although Barnes & Campbell (1988) have noted that the intergrowth of amphibole, biotite, and sulphide is a common postcumulus feature of sulphide-bearing gabbros. They conclude that the solidification of sulphide liquid and crystallisation of amphibole and phlogopite occur over similar temperature ranges. Consequently the sulphide liquid and fractionated parts of the silicate melt are pushed into residual pore space by postcumulus growth of anhydrous silicates and are forced to share this limited pore space during the last stages of solidification. The high melt component of the basal Munni Munni gabbronorites (up to 50 vol. %) indicates that the modified sulphide textures are unlikely to be related to postcumulus growth in limited space but are probably due to metamorphism.

Spatially associated with the northern marginal gabbronorites, and abutting the granites, are chilled olivine gabbronorites (85770179) that are believed to be the best representation of the parent magma for the ultramafic zone. Minor 0.5 mm olivine ?microphenocrysts (mg_{75-71}) and acicular orthopyroxene are sporadically set in a fine-grained (< 0.3 mm) granular groundmass of prismatic clinopyroxene (mg_{72}), interstitial plagioclase (An_{31-28}), biotite, magnetite, ilmenite, and trace sulphide. Olivine shows partial alteration to magnetite, talc, clinoamphibole, chlorite, and minor serpentine, and orthopyroxene is sometimes rimmed by clinopyroxene.

Variably altered medium-grained websterite, plagioclase websterite, gabbronorite, and quartz gabbronorite comprise the southeastern marginal rocks (84770109, 110, 113, 118, 119) of the ultramafic zone. In contrast to the northern basal contact, olivine-bearing gabbroic rocks are rare, alteration is more intense, and there is partial assimilation of granitic material. Subhedral clinopyroxene grains are bounded by intercumulus plagioclase and variably altered to actinolite, hornblende, chlorite, calcite and magnetite. Orthopyroxene consists of large (1.0 x 3.0 mm) subhedral grains that have fine Ca-rich clinopyroxene lamellae parallel to {100} and a strong pale-pink to green pleochroism. Associated min-

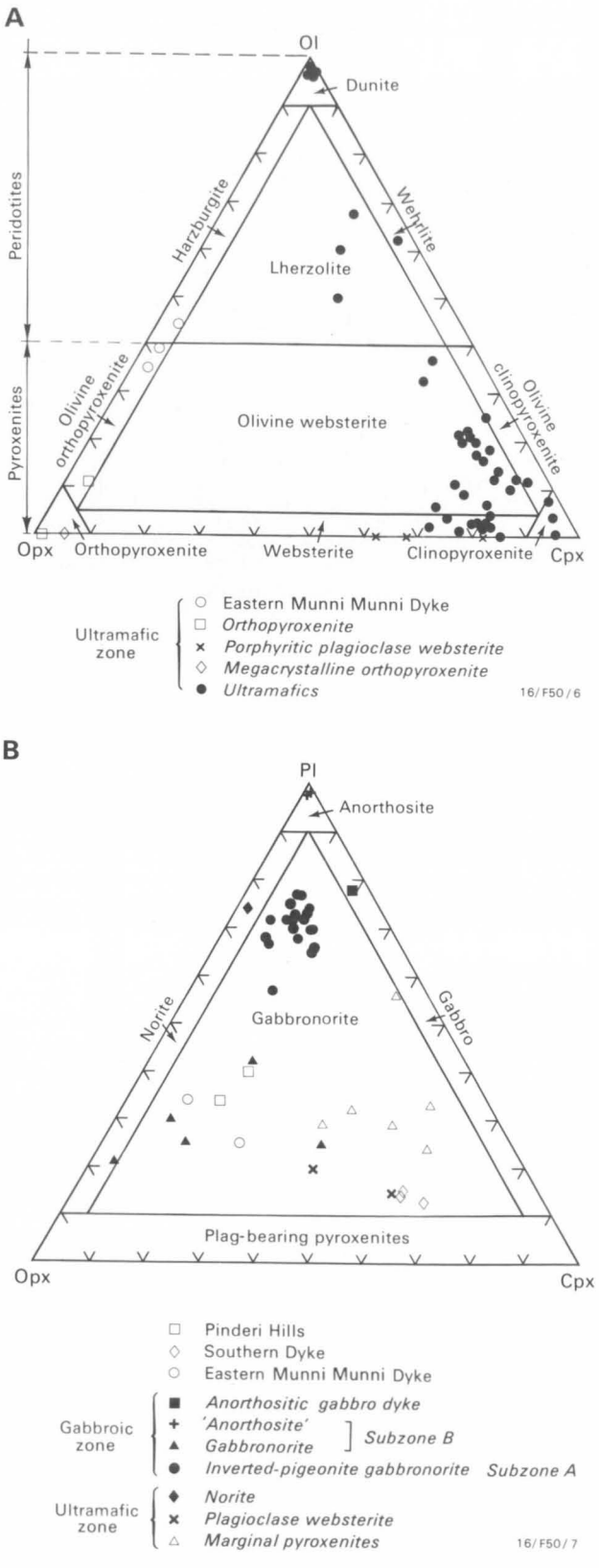

Fig. 20A–B. Ternary plots of modal variations (from point counts) of ultramafic and gabbroic rocks from the regional sample traverse through the Munni Munni Complex (see appended map sheet), and large dykes surrounding the Munni Munni Complex. Ol = olivine, Cpx = clinopyroxene, Opx = orthopyroxene, Pl = plagioclase.

erals include inverted pigeonite, alkali feldspar, quartz, biotite, magnetite, ilmenite, and sulphides (< 1.2 vol. %). A feature of the marginal rocks is the development of micrographic intergrowths of ?orthoclase and quartz surrounding sericitised and chloritised antiperthitic plagioclase and more rarely orthopyroxene. The symplectic textures comprise radiating patterns of alternating quartz and feldspar-rich vermicular zones and also hieroglyphic arrangements of optically continuous, small, euhedral quartz and feldspar.

Chilled gabbronorite, plagioclase websterite, and olivine-plagioclase websterite (85770168 to 174) comprise the northwestern marginal rocks of the Cadgerina Dyke. In contrast with the northeastern contact rocks, they are finer-grained (< 1.0 mm) and less altered, and there is negligible contamination by granitic components. The sulphide content is significantly lower (< 0.2 vol. %), consistent with the regional trend of decreasing sulphide content in the contact rocks up the intrusion. This trend, and the paucity of quartz in these higher-level rocks, indicates that both temperature and SiO_2 content may have been important parameters for sulphide precipitation along the margins of the ultramafic zone.

Dunite, lherzolite, wehrlite (ol ± cpx)

Peridotites in the ultramafic zone contain various amounts of olivine (mg_{83-76}), clinopyroxene (mg_{89-81}), orthopyroxene (mg_{84-79}), minor phlogopite, and rare plagioclase. Adcumulates and mesocumulates dominate, with olivine and orthopyroxene cumulus and intercumulus, respectively, whereas clinopyroxene may be cumulus or intercumulus.

Dunites are generally intensely altered to serpentine and fine dustings of magnetite. However, their adcumulus granular textures are well preserved as a tight interlocking array of subhedral cumulus olivine and minor intercumulus clinopyroxene. Lherzolites (Fig. 22A & B) are characterised by large (up to 2 cm) optically continuous intercumulus bronzite grains that locally attain 20 vol. %. The bronzite oikocrysts have thin exsolved lamellae of calcic pyroxene and contain embayed olivine and clinopyroxene inclusions. The antipathetic modal distributions and close spatial association of the embayed olivine and bronzite indicate that the orthopyroxene was largely derived from the reaction of olivine with a SiO_2-saturated (basaltic) melt.

Olivine-to-olivine, and olivine-to-clinopyroxene grain boundaries in the peridotites are well defined and straight. Clinopyroxene-to-clinopyroxene grain boundaries are often cuspate, irregular, and interlocking, indicating some migration of clinopyroxene boundaries due to adcumulus growth. Sharp contacts between dunite and lherzolite layers are of both phase and textural type. This is shown by the marked increase in clinopyroxene and orthopyroxene contents (phase contact), and the change from intercumulus clinopyroxene to cumulus clinopyroxene (textural contact), from the dunite to lherzolite layers.

The intensity of serpentine alteration in the peridotites is generally proportional to the modal olivine content of the rock. Olivine in dunite is invariably totally altered to antigorite, chrysotile, magnetite, hematite, chlorite, talc, iddingsite, calcite, and/or magnesite, whereas olivine in lherzolite is only partly altered, as a result of the 'shielding effects' of abutting clinopyroxene. The altered olivine grains form a space-filling cellular arrangement of mesh and hourglass structures of antigorite and discontinuous trains and fine dustings of secondary magnetite. Antigorite appears to be the

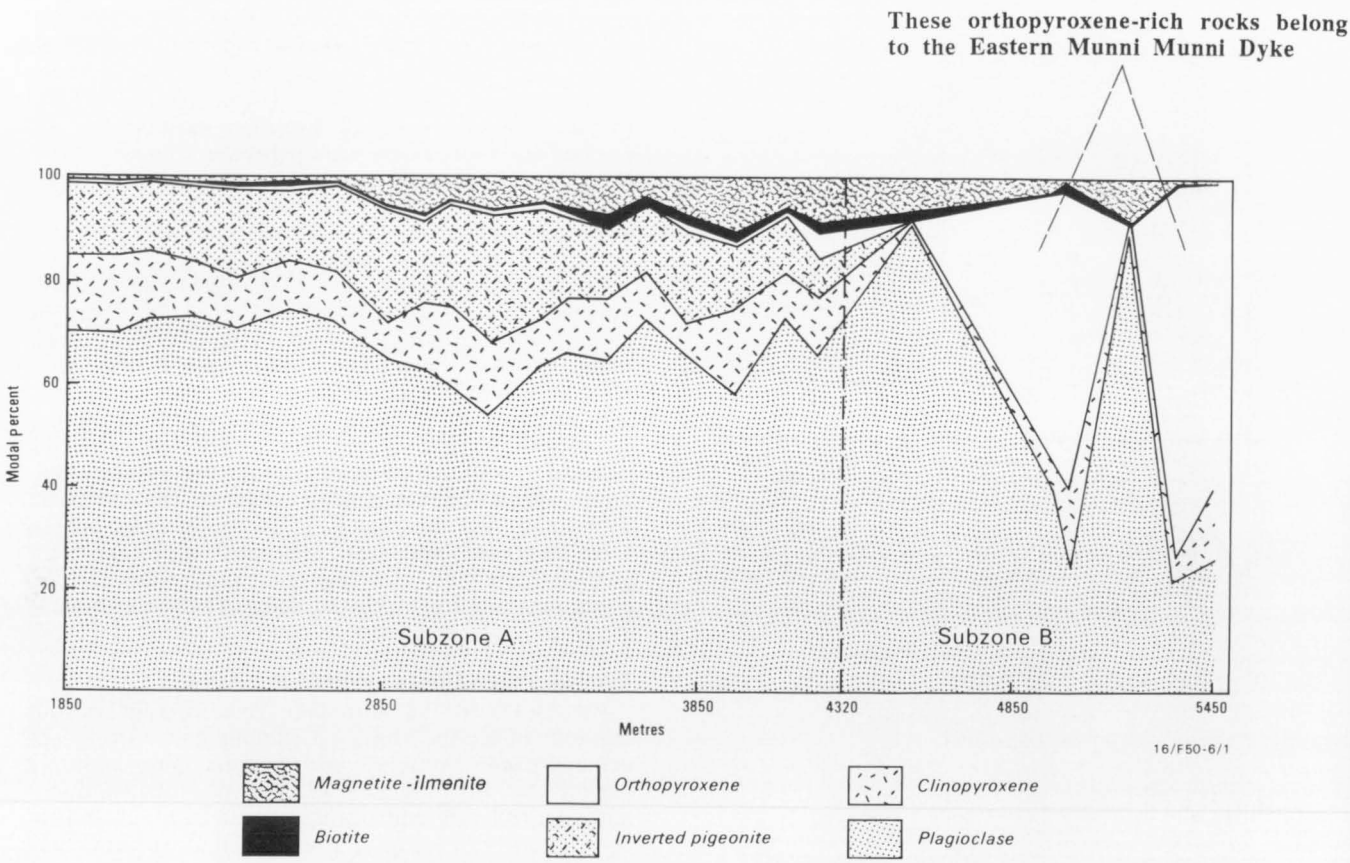

Fig. 21. Munni Munni Complex: modal variations (from point counts) of the major cumulus and intercumulus minerals through the gabbroic zone. The samples are from the type traverse shown on the appended map sheet.

dominant serpentine mineral, although fibrous chrysotile (both minerals confirmed by X-ray diffraction analysis) is also present in sheared dunite. Trace small pentlandite blebs are associated with, and derived from, the serpentinisation of olivine. Clinopyroxenes in dunite are often intensely altered to serpentine, chlorite, and/or talc; they can be readily distinguished from olivine pseudomorphs by amorphous Fe oxides that have replaced exsolved Fe-rich material along {100} cleavage traces.

Websterite, olivine websterite (cpx + ol)

Olivine websterites are a transitional group of rocks often located between the lherzolite and websterite components of cyclic units. Clinopyroxene (mg_{86-81}) and olivine (mg_{82-78}) are cumulus, whereas bronzite (mg_{83-77}), plagioclase, alkali feldspar, and biotite are intercumulus. Websterites are generally massive mesocumulates or orthocumulates, whereas the olivine websterites are generally layered and are more adcumulus in character.

The websterites are dominated by clinopyroxene (50–80 vol. %), with subordinate bronzite (5–25%), olivine (0–20%), and minor plagioclase, alkali feldspar, and biotite. Bronzite averages 5–15 vol. % for most websterites, but there is a steady increase in its content to 25 vol. % at the expense of olivine above the 1500 m level. Intercumulus plagioclase and Ba-bearing alkali feldspar also display a well-defined mutual distribution in websterite throughout the zone. Plagioclase is an intercumulus phase in the marginal websterites of the zone; however, for the interval 260–300 m, alkali feldspar occurs at the expense of plagioclase. Ba-rich alkali feldspar reappears from 1470–1740 m, and, above 1800 m, plagioclase dominates over alkali feldspar. Feldspar is absent from the intervening stratigraphic interval 300–1470 m. Thus, there appears to be a central distribution of alkali feldspar bordered by plagioclase in the more fractionated parts of the ultramafic zone. Alkali feldspar in the ultramafic zone is unusual since it is generally found in the mafic parts of layered intrusions. Biotite is present as a minor intercumulus mineral in olivine websterite below the 300 m level and in websterite and olivine websterite above the 1470 m level.

Textures in the websterites and olivine websterites are largely governed by the relative proportions of cumulus olivine and intercumulus bronzite. Distinctive consertal notched grain boundaries in the websterites consist of fine-grained stepped and serrated patterns at clinopyroxene-clinopyroxene and clinopyroxene-orthopyroxene grain boundaries, whereas curvilinear contacts occur between clinopyroxene and olivine grains. For the clinopyroxene and bronzite boundaries, the extension of adcumulus intergrowth is from the cumulus clinopyroxene into the intercumulus orthopyroxene grain.

Very small ($< 20\ \mu m$) dark-brown to green subhedra are associated with cumulus clinopyroxene grains in the websterites. They form small, isolated clusters within, and between, clinopyroxene grains, or discontinuous trains traversing the orthopyroxene lamellae {100} and twins of the host clinopyroxene grain. Their colour and rare sub-octahedral form indicate they may

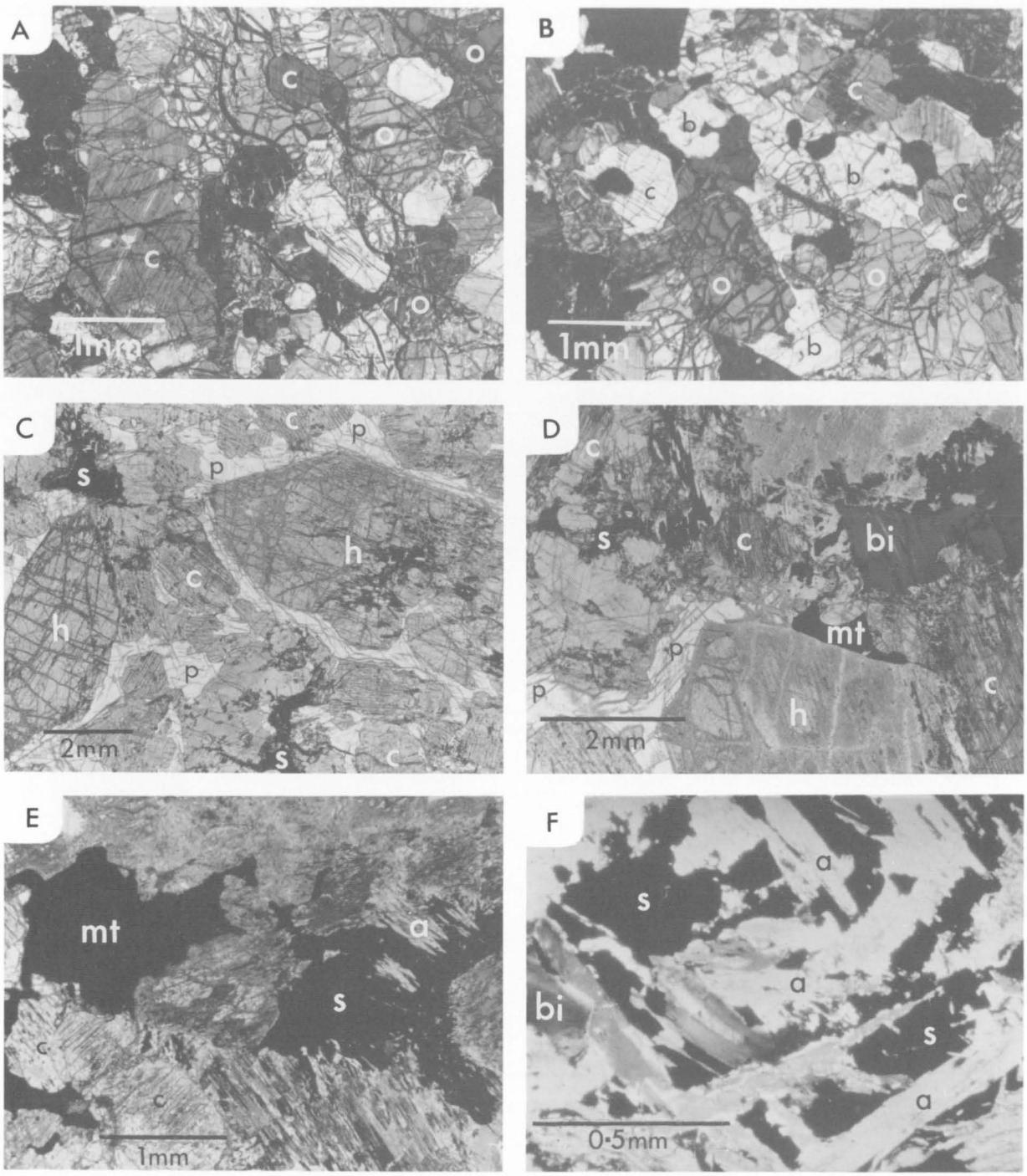

Fig. 22A–F. Munni Munni Complex: textural and mineralisation features of cumulates from the ultramafic zone. A(84770105, from subzone B, crossed nicols): lherzolite adcumulate consisting of subhedral to euhedral cumulus olivine(o) and subhedral cumulus clinopyroxene(c). These low-porosity cumulates are characteristic of most peridotites in the lower to middle parts of the ultramafic zone. B(85770209, from subzone D, crossed nicols): lherzolite orthocumulate consisting of intercumulus bronzite(b) surrounding embayed cumulus olivine(o) and clinopyroxene(c). The bronzite is optically continuous across the total grain and has formed from the reaction of olivine with a siliceous melt. C(84770094, from subzone I, plane-polarised light): the mineralised porphyritic plagioclase websterite from the upper part of subzone I is a distinctive orthocumulate consisting of large cumulus euhedral bronzite-hypersthene(h) and granular clinopyroxene(c) grains mantled by intercumulus plagioclase(p). Chalcopyrite-pyrrhotite-pentlandite comprise the sulphide(s) blebs that have been partly remobilised into fractures and embayments of the silicates. D(84770094, from subzone I, plane-polarised light): porphyritic plagioclase websterite with basal plates of biotite(bi); magnetite(mt) and plagioclase(p) are bordering cumulus bronzite-hypersthene(h). E(84770094, from subzone I, plane-polarised light): marginal overgrowths of small, bladed actinolite-tremolite(a) aggregates result in the suturing of the sulphide(s) boundaries. The sulphides comprise chalcopyrite, pyrrhotite, and minor pentlandite. Clinoamphibole development is most pronounced where the sulphide abuts clinopyroxene(c) and does not affect the magnetite-ilmenite(mt) grains. Relict primary igneous textures are still preserved. F(84770094, from subzone I, crossed nicols): primary igneous texture destroyed by the disaggregation of the sulphide(s) grains into chalcopyrite subgrains by mats of prismatic actinolite-tremolite(a), interstitial carbonates and biotite(bi).

be Cr-poor spinel inclusions that were exsolved from the clinopyroxene host.

Pyroxenes in the websterites are partly altered to clinoamphibole, talc, carbonate, chlorite, and magnetite. Actinolite-tremolite is the most common clinoamphibole, but locally above the 1300 m stratigraphic level, clinopyroxene alters to an Fe-poor ?grunerite which has formed small aggregates along grain boundaries and cleavages. The alteration appears to liberate Ca from clinopyroxene to form calcite anhedra interstitial to the blades of ?grunerite.

Clinopyroxenite, olivine clinopyroxenite (cpx ± ol)

Clinopyroxenites, *sensu stricto*, and olivine clinopyroxenites are massive coarse-grained rocks that have the lowest residual porosity of any cumulate in the ultramafic zone. They consist of interlocking clinopyroxene (mg_{85-82}) grains with up to 5 vol. % each of cumulus olivine (mg_{79-78}) and intercumulus orthopyroxene. Clinopyroxene grain boundaries are of both serrated-intergrowth and curvilinear types. Olivine occurs as partly altered subhedral cumulus grains or as smaller embayed inclusions in clinopyroxene. The coarse and variable grainsize and subhedral to anhedral form of the cumulus clinopyroxene grains, the paucity of intercumulus bronzite and the absence of intercumulus plagioclase and biotite collectively indicate that adcumulus growth strongly modified the clinopyroxenites.

Clinopyroxene grains are masked by fine-grained magnetite, hematite, and limonite. The alteration clouds grain surfaces, follows cleavage traces and grain boundaries, and forms long transgressive veinlets. The Fe-oxide content, which is anomalously high relative to other pyroxenites, may be due to the paucity of other potential Fe-bearing secondary minerals such as chlorite, talc, and antigorite-chrysotile.

Plagioclase websterite, gabbronorite (cpx ± opx ± ol)

Porphyritic plagioclase websterite and gabbronorite form rare, thin (< 5 m thick) lenses associated with peridotites in the lower parts of the zone and, of greater economic significance, as a 30–50 m thick laterally continuous mineralised layer (subzone I) directly below the gabbroic zone. In the latter setting, the mineralogical and textural features of these rocks contrast with those of the underlying rhythmically layered ultramafic cumulates. These features include the disappearance of cumulus olivine, appearance of cumulus bronzite-hypersthene (mg_{75-64}), presence of more Fe-rich clinopyroxene (mg_{79-57}), significant upward increase in intercumulus plagioclase (An_{44-18}) and in minor hydrous phases such as phlogopite-biotite, clinoamphibole, and sulphides. In addition, there is an upward transition from equigranular adcumulates and mesocumulates to porphyritic orthocumulates.

The porphyritic plagioclase websterite is a texturally distinctive rock that contains 40–80 vol. % clinopyroxene and 10–40% bronzite-hypersthene as cumulus phases, and up to 18% intercumulus plagioclase. Accessory minerals include phlogopite-biotite, inverted pigeonite, olivine, ilmenite, magnetite, chalcopyrite, pentlandite, pyrrhotite, alkali feldspar, apatite, and secondary clinoamphibole and carbonate. The cumulus assemblages of the porphyritic websterite are transitional compared to the cumulus assemblages that characterise the rocks in the main part of the ultramafic zone and the gabbroic zone. In the latter zone, plagioclase, clinopyroxene, and inverted pigeonite are cumulus.

The most distinctive textural feature of these poorly-layered rocks is the development of large subhedral to euhedral orthopyroxene grains (Fig. 22C & D) that progressively increase in size from the middle stratigraphic levels of subzone H (see inset of the Munni Munni Complex geological map on the appended map sheet) upwards through subzone I towards the gabbroic zone. Sympathetic with this increasing size trend is an increasing development of intercumulus to cumulus fabrics, and a change from bronzite to bronzite-hypersthene compositions. The porphyritic orthopyroxene grains (0.5 x 1.0, up to 3 x 4 cm near the top of the subzone) are euhedral when mantled by plagioclase, but subhedral when abutting cumulus clinopyroxene grains. They display fine exsolved lamellae of clinopyroxene and a weak pink to pale-green pleochroism. The more fractionated nature of these rocks is reflected by accessory amounts of inverted pigeonite, Ba-bearing alkali feldspar, and apatite. Intercumulus plagioclase (3–18 vol. %) shows a marked range in composition from mid-andesine to mid-oligoclase (An_{43-18}) for websterites near the top of subzone I (see Mineralogy section, p. 57). Plagioclase mantles the large euhedral cumulus orthopyroxene grains (Fig. 22C & D) or, rarely, the smaller granular clinopyroxene grains. In the upper part of the porphyritic websterite layer, plagioclase commonly forms large poikilitic grains that are optically continuous over several centimetres.

Sulphides are heterogeneously distributed throughout the porphyritic plagioclase websterite and gabbronorite. In general, most plagioclase websterites contain traces of sulphides (< 0.5 vol. %), whereas in the gabbronorites sulphides may attain 2 vol. %, comparable with the low sulphide content of the Merensky and J-M reefs. This indicates a correlation between increasing sulphide content and increasing plagioclase content, i.e. increasing porosity. Chalcopyrite, pentlandite and pyrrhotite are the dominant sulphides, in contrast to the Fe-rich sulphide assemblages along the northern basal contact of the ultramafic zone (subzone A′).

The sulphides form small (0.2–3 mm) irregular disseminations near cumulus clinopyroxene or smaller blebs 'squeezed' into interstitial sites between cumulus grains, or into deep embayments, fractures, and cleavages within the cumulus pyroxene grains. The sulphides show various stages of hydrous silicate replacement, ranging from: (1) unaltered remobilised blebs with curved and cuspate grain margins; to (2) partly altered grains with sutured margins due to fine-grained bladed aggregates of actinolite-tremolite that have grown at high angles to the sulphide margins (Fig. 22E); to (3) completely disaggregated irregular subgrains or fine-grained dustings of sulphide in decussate clinoamphibole (Fig. 22F); to (4) complete replacement of the sulphide grain by mats of clinoamphibole, interstitial carbonate, phlogopite-biotite, and minor talc and chlorite. In this final stage of alteration there is no evidence of the original sulphide grain. The final stage of complete replacement constitutes only a small proportion of the total sulphide occurrences. The distribution of the platinum-group minerals (PGMs) in the porphyritic websterite layer is discussed in detail in the Mineralogy section (pp. 69–71).

Alteration of the silicate phases is generally not intense, although orthopyroxene may form isolated 'atolls' that are optically continuous in a fine-grained matrix of talc. Clinopyroxene grains are locally partly altered to olive-green to pale-brown hornblende, or more

commonly to bladed actinolite-tremolite. Plagioclase shows variable chloritisation and sericitisation, and phlogopite-biotite plates are locally invaded by fine-grained sulphides along the cleavages and by chlorite around the margins.

Orthopyroxenite, olivine orthopyroxenite (opx ± ol ± spinel)

Orthopyroxenite and olivine orthopyroxenite adcumulates (Fig. 23A) form accidental blocks and rare pipes in close association with the upper parts of the porphyritic plagioclase websterite layer. They have a simple mineralogy of cumulus bronzite (mg_{87-85}), variable minor amounts of cumulus olivine, and intercumulus clinopyroxene, plagioclase, and phlogopite. Minor cumulus, Cr-poor, Al-rich spinel (mg_{68-65}, where mg number = 100 x Mg/(Mg + Fe^{2+}), and Cr'_{16-13}, where Cr′ number = 100 x Cr/(Cr + Al + Fe^{3+})) is associated with the orthopyroxenite adcumulates.

The orthopyroxenites commonly display fine-scale modal layering defined by alternating laminations of tightly packed bronzite subhedra (0.3–0.5 mm) and discontinuous dark-olive-green to brown aluminous spinel (0.1–0.4 mm) laminations (Fig. 23B). Disseminated spinel subhedra also form small inclusions in bronzite and more rarely in olivine. Spinel abundances attain 3 vol. % in the olivine orthopyroxenites and 0.5 vol. % in the orthopyroxenites. The anhedral habit and large size (up to 2 x 3 mm) of accessory olivine (0–10%) relative to bronzite indicates that it has been strongly modified by postcumulus growth. Associated minerals include small clinopyroxene (0–5%) anhedra interstitial to bronzite, and rare plagioclase subhedra commonly near olivine. This spatial association is at variance with the general antipathetic relationship of olivine and plagioclase in the ultramafic zone.

In the totally altered (talc-?antigorite-chlorite-calcite-clinoamphibole) olivine orthopyroxenite ?pipe, the subhedral to euhedral forms of the disseminated spinels are preserved and there is no evidence of size reduction of the grain due to fragmentation. This is in contrast to the brittle appearance of chromite in a dunite layer in subzone F (discussed below).

Chromitite (chrom ± ol ± opx)

Chromite (mg_{45-43} and Cr'_{65-63}) is associated with cumulus olivine in a small sheared serpentinised dunite lens near the top of subzone F. This is the only known occurrence of chromite, *sensu stricto*, in the intrusion. The chromite forms fragmented cumulus grains of variable size (< 1.2 mm), set within a fine-grained matrix of serpentine, carbonates and talc (Fig. 23C). No relics of unaltered olivine are preserved. The higher Cr and Fe contents of these chromitites relative to the green-brown aluminous spinels in the orthopyroxenites is shown by their opaqueness. The brittle nature of the chromite grains is indicated by the extensive internal fracturing and haloes of smaller subgrains that have broken away from the 'parent' grain. Fine-grained chromites also mantle and fill the interstitial parts between large (1.0–2.5 mm) serpentinised olivine grains, indicating possible gravitational settling of the chromite (Fig. 23C).

Megacrystalline orthopyroxenite (cpx)

An unusual, coarse orthopyroxenite orthocumulate forms a 12 m thick lens at the base of subzone C of the ultramafic zone. It is characterised by extremely large interlocking orthopyroxene oikocrysts (up to 8 x 10 cm) rimmed by thin veneers of plagioclase and con-

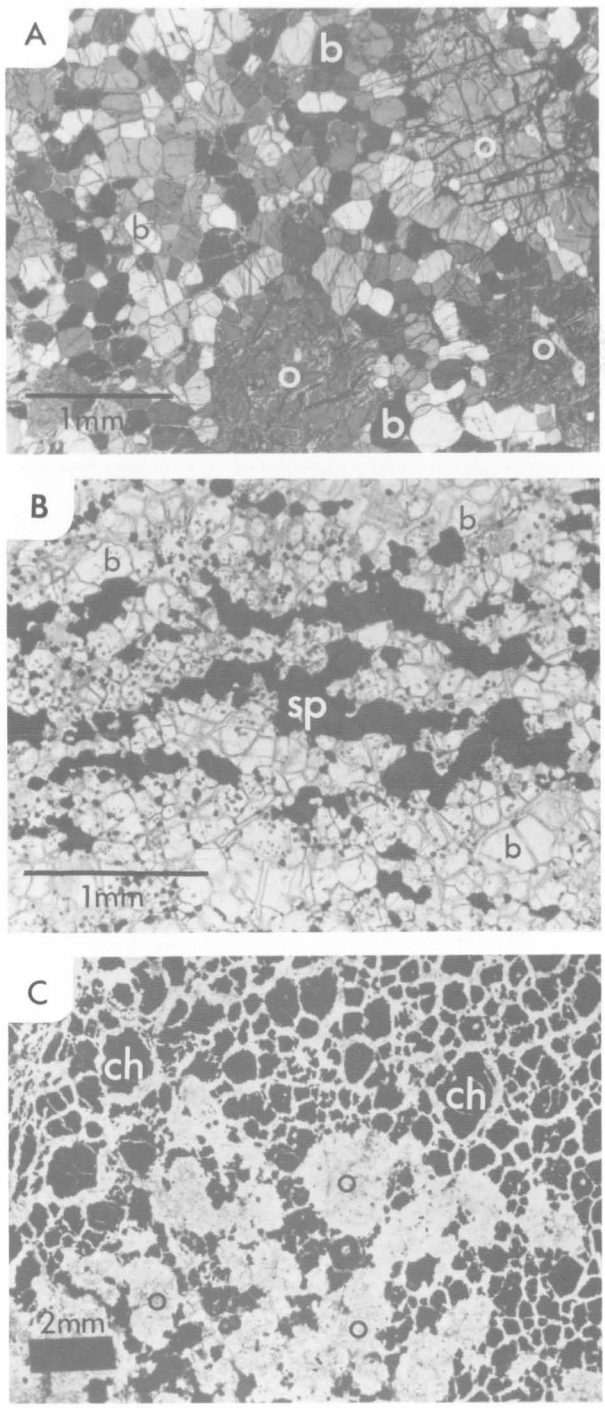

Fig. 23A–C. Munni Munni Complex: rock types from the upper part of the ultramafic zone. A(84770087, from subzone I, crossed nicols): olivine orthopyroxenite adcumulate consisting of large anhedral cumulus olivine(o) strongly modified by adcumulus growth, and a tight-packing polygonal array of cumulus bronzite(b). Intercumulus clinopyroxene, intercumulus plagioclase and cumulus chromite are accessory (not shown here). The olivine orthopyroxenite forms an accidental block in the mineralised porphyritic plagioclase websterite layer. B(85770159, from subzone I, plane-polarised light): orthopyroxenite adcumulate containing numerous irregular and discontinuous segregation trains of dark-olive-green to brown Cr-poor, Al-rich, spinel(sp). Fine-grained spinels also occur as disseminations at bronzite(b) grain boundaries and more rarely as inclusions in cumulus bronzite grains. C(85770156, from subzone F, plane-polarised light): chromite-olivine cumulate consisting of serpentinised cumulus olivine(o) grains mantled by fragmented chromite(ch) grains.

taining numerous embayed inclusions of zoned clinopyroxene and rarer inverted-pigeonite anhedra. The oikocrysts show no preferred crystallographic orientation or systematic variation in size. Quartz and biotite are minor phases and, together with the inverted pigeonite and orthopyroxene, indicate that the orthocumulate was derived from a highly evolved melt. Alteration is incipient in these rocks, which may be due to their near-monomineralic compositions and coarse grainsize.

The megacrystalline orthopyroxenite is an extreme orthocumulate, or, more strictly, a non-cumulate, since its residual porosity appears to exceed 90 vol. %. However, fine exsolved lamellae persist across the width of the unzoned orthopyroxene grains, indicating that despite their apparent intercumulus habit, they may represent slowly cooled phases that have exsolved Ca-rich pyroxene; alternatively they may be of replacement origin.

Various origins have been proposed for similar coarse poikilitic textures. Jackson (1961) has interpreted similar textures in the Stillwater Complex as being due to peritectic replacement of cumulus grains. Other origins include the upward migration of intercumulus melt from lower stratigraphic levels by filter pressing of the cumulus pile and subsequent supercooling of the melt, and possible heteradcumulate nucleation processes which resulted in extremely high residual porosities. Poikilitic grains in heteradcumulate textures are ascribed to their nucleation within the intercumulus liquid, and their growth with constant composition to adcumulus diffusion from the overlying magma (Cox & others, 1984).

Mixed norite-orthopyroxenite rock (plag + opx: norite; opx: orthopyroxenite)

The mixed norite-orthopyroxenite rock (referred to as 'banded norite' on the appended map sheet) has a restricted distribution near the ultramafic/gabbroic zone contact in the central part of the intrusion. It is generally found within 10 m of the contact and is associated with porphyritic plagioclase websterite of subzone I or laminated gabbronorite of the gabbroic zone. The mixed rock is a transitional lithology in the intrusion since it has mineralogical features common to both zones. The high modal proportion of cumulus plagioclase (74 vol. %) in the norite suggests an affinity with gabbroic subzone A, whereas the cumulus orthopyroxene character of the orthopyroxenite layers is more consistent with the mineralogy of the porphyritic websterite layer of subzone I of the ultramafic zone.

The norite is a layered adcumulate consisting of equigranular aggregates of cumulus plagioclase (An_{56-48}) and orthopyroxene (mg_{67}) in uniformly size-graded layers that are cryptically zoned. Plagioclase subhedra in the graded layers consistently decrease in size from 1.5 x 2.0 mm near the base to 0.2 x 0.4 mm near the top of the layer, and orthopyroxene similarly decreases in size from 0.5 x 0.8 mm anhedra to small granular grains less than 0.2 mm. Clinopyroxene is a minor intercumulus phase to the plagioclase and orthopyroxene. The graded norite layers are sharply truncated by remobilised discordant orthopyroxenite layers (described below). The cumulus plagioclase grains form an interlocking polygonal texture with triple-point interfacial angles, similar to that seen in the recrystallised banded mafic xenoliths from the base of the gabbroic zone. Similar triple-point textures have been documented for various cumulates in the Bushveld Complex (Nienaber-Roberts, 1986), and the Rhode Island Complex (Rutherford & Hermes, 1984). Processes such as recrystallisation, or annealing and sintering (Stanton, 1972), have been proposed for the formation of triple junctions. The Munni Munni textures are believed to be due to slow crystal accumulation and adcumulus growth rather than recrystallisation since these features only pertain to plagioclase and not the other minerals. Plagioclase composition also varies with grainsize, with the smaller grains more sodic (An_{48}) than the larger grains (An_{56}). Plagioclase compositions in the norite are similar to those in the adjacent basal gabbronorite of the gabbroic zone.

The orthopyroxenite layers comprise euhedral cumulus orthopyroxene (mg_{67}), minor intercumulus clinopyroxene, and minor to trace intercumulus plagioclase and dark-brown biotite. Plagioclase, which is of similar composition (An_{49-48}) to the finer-grained plagioclase in the norite, shows evidence of subsolidus deformation between the tightly-packed orthopyroxene grains. Spinels are absent in these orthopyroxene-rich adcumulates.

The rock types of the gabbroic zone have been subdivided into the following subgroups (cumulus assemblages in brackets):

- **Inverted-pigeonite-bearing gabbronorite (plag + inv. pig + cpx ± mt-ilm)**
- **Anorthositic gabbronorite, anorthositic gabbro, 'anorthosite' (plag)**
- **Other rock types of the gabbroic zone**

Inverted-pigeonite-bearing gabbronorite (plag + inv. pig + cpx ± mt-ilm)

Gabbronorites in subzone A of the gabbroic zone consist of varying proportions of cumulus plagioclase (An_{54-30}), orthopyroxene that formed by inversion of cumulus pigeonite (inverted pigeonite), clinopyroxene (mg_{77-48}), and titanomagnetite. Plagioclase-inverted-pigeonite-clinopyroxene-bearing cumulates comprise the basal parts of the subzone, which grade upwards into plagioclase-clinopyroxene-inverted-pigeonite-magnetite-ilmenite-bearing cumulates. The spatial arrangement of the plagioclase grains largely determines rock textures: gabbronorites in the lower part of the subzone have a laminated texture due to the preferred crystallographic orientation of plagioclase laths. At higher stratigraphic levels, plagioclase forms glomeroporphyritic clusters, variolitic sprays, and, more commonly, intergranular textures consisting of randomly orientated laths and interstitial cumulus pyroxene.

The basal laminated gabbronorites consist of subparallel euhedral labradorite-andesine (An_{54-47}) laths (average size 1 x 4 mm) that are flanked by smaller inverted-pigeonite (1 x 2 mm) and clinopyroxene (1 x 1 mm) subhedra (Fig. 24A,B). The larger plagioclase laths display lenticular or bent albite twins, bending of grains, radiating microfractures and alteration veinlets at high angles to the lamination, and pervasive dislocations across the grain. Various origins have been proposed for similar deformational textures of plagioclase in the Bushveld Complex. These include post-depositional deformation (von Gruenewaldt, 1971), nucleation in the solid state at stressed positions and by growing into a grain by a spear head of dislocations (Smith, 1974), and the equilibration of cumulus minerals at lower temperatures that would cause shearing stress on the crystal mush (Wager & others, 1960). It is believed that the basal Munni Munni gabbronorite was deformed by lateral shearing and overloading stresses that were imparted during, or soon after, the fairly

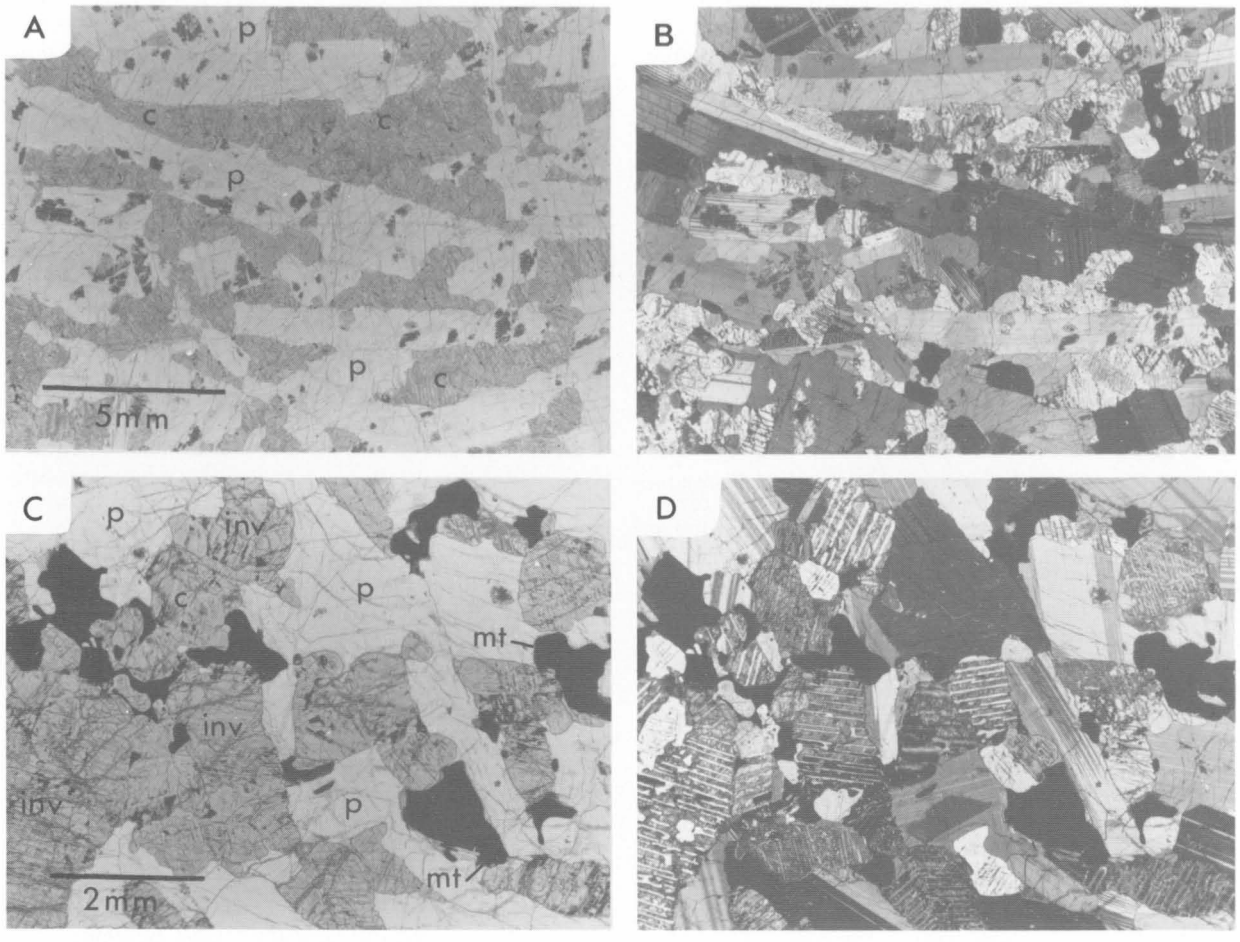

Fig. 24A–D. Munni Munni Complex: cumulates from the gabbroic zone. A(84770052, from subzone A, plane-polarised light): laminated gabbronorite from base of gabbroic subzone A, consisting of large plagioclase(p) laths which have a strong crystallographic orientation, and granular subhedral clinopyroxene(c). Inverted pigeonite is also a minor phase (not shown here), but magnetite-ilmenite is absent in the basal gabbronorites. Elongate pyroxene grains typically occur at the intersections of early-crystallising plagioclase laths. B(84770052, from subzone A, crossed nicols): as for A, except crossed nicols. C(84770058, from subzone A, plane-polarised light): medium-grained intergranular magnetite-ilmenite gabbronorite from middle part of gabbroic subzone A, consisting of randomly orientated cumulus plagioclase(p) laths, inverted-pigeonite(inv) and clinopyroxene(c) anhedra, and magnetite-ilmenite(mt) aggregates. The cumulus plagioclase grains have a seriate texture comprising subhedral to euhedral laths; the high modal proportions of Fe-Ti oxides indicate that these oxides are of cumulus status even though they mantle the silicate phases. D(84770058, from subzone A, crossed nicols): as for C, except crossed nicols.

rapid emplacement of the overlying gabbroic magma. The laminated textures indicate the gabbronorite was in a semi-fluid crystal-mush state at the time of deformation.

Some {001} plagioclase sections display vague oscillatory zoning, but they invariably have a clouded appearance due to sericite, chlorite, grossular garnet, epidote, and calcite alteration. Inverted pigeonite is often intensely altered to ferroactinolite, minor chlorite, talc, and Fe oxides. At higher stratigraphic levels, the ferroactinolite becomes subordinate to a pale-brown 'grunerite' clinoamphibole, reflecting increasing Fe to Ca compositions of the host pyroxene. The presence of partly altered inverted-pigeonite grains (mg_{64-59}) is indicated by relict exsolved rods and irregular flattened blebs of Ca-rich pyroxene (mg_{73-70}) sub-parallel to {001}of the original pigeonite host and a second generation of post-inversion exsolved strings and stringlets parallel to {100}. Clinopyroxene subhedra are variably altered to ferroactinolite, chlorite, Fe oxides, and hornblende. Trace sulphides in the lower parts of the subzone consist of fine-grained chalcopyrite, pyrite, pyrrhotite, and rare pentlandite. The chalcopyrite and pyrite occur as small (< 20 μm) irregular blebs aligned along the cleavages of the pyroxenes or as secondary fine-grained (< 5 μm) dustings associated with chlorite in altered plagioclase or with clinoamphibole after inverted pigeonite.

Gabbronorites in the middle to upper levels of the subzone contain mineral assemblages and textures reflecting fractionation processes that involved greater initial porosities and more hydrous conditions relative to gabbronorites lower in the subzone. The rocks are dominated by medium- to coarse-grained intergranular textures consisting of randomly orientated cumulus oligoclase-andesine laths and clinopyroxene and inverted-pigeonite anhedra and titanomagnetite sub-grains moulded around plagioclase and pyroxene. A greater variety of accessory phases are present relative to the lower gabbronorites, including biotite, orthopyroxene, quartz, hornblende, apatite, alkali feldspar, chalcopyrite, and pyrite.

Cumulus plagioclase has a seriate texture comprising subhedral to euhedral laths ranging in size up to 2 by

6 mm. They show a consistent increase in the Na/Ca ratio up the subzone (see Mineralogy section, p. 58), and attain their most sodic composition of oligoclase-andesine (An_{30}) at the 4222 m level. This represents an increase of 24 molecular percent in the albite component over a stratigraphic interval of about 2370 m. In contrast to the seriate textures of plagioclase, inverted pigeonite and clinopyroxene have more equigranular fabrics consisting of clusters of anhedral grains in interstitial sites formed by the high-angle interlocking plagioclase laths. Contact relationships between plagioclase and pyroxene indicate the latter are mainly cumulus, although in some cumulates, clinopyroxene may be intercumulus.

The inverted-pigeonite grains (Fig. 24C,D) generally display similar exsolution features to those seen in the lower gabbronorites. The host and lamellae components show more fractionated compositions (mg_{57-54} and mg_{68-66}, respectively) relative to the inverted pigeonite lower in the zone. Inverted pigeonite commonly forms large composite grains (some in excess of 1 cm) that comprise numerous smaller irregular grains poikilitically enclosing cumulus plagioclase and clinopyroxene grains. In this respect the inverted pigeonites appear to have formed from a melt, although they are generally believed to be of cumulus origin. The large composite grains are optically continuous across their width and the enclosed plagioclase and clinopyroxene grains have embayed and scalloped margins, indicating some resorption by the surrounding inverted pigeonite. The pre-inversion generation of coarse exsolved rods have random orientations within the composite grain, whereas the later generation of fine wispy lamellae have a well-developed crystallographic orientation parallel to $\{100\}$ of the inverted-pigeonite grain. The trends of the coarse exsolution lamellae indicate the pigeonites were randomly orientated prior to the inversion of the host grain and their preferred crystallographic orientation was obtained during, or soon after, inversion. Similar textures of clusters of inverted-pigeonite grains with the same optical orientation have been documented in the Dufek (Himmelberg & Ford, 1976) and Bushveld (von Gruenewaldt, 1970) intrusions. Von Gruenewaldt (1970) believes the crystallographic orientation was formed during inversion as a result of the directed pressure of the overlying crystal mass. A similar mechanism may be applicable to the Munni Munni Complex, since a large volume of magma would have been involved in the evolution of subzone A, and gabbronorites along the base of the subzone show evidence of deformation, believed to be related to overloading forces.

The distribution of titanomagnetite reflects the increasing Fe-Ti fractionation trends in subzone A. Oxides are absent from the lower 400 m of the subzone, whereas for the 2250–2692 m stratigraphic level, they occur as small (< 1 mm) disseminated anhedra of 0.2 to 1 vol. %. Above 2692 m, they progressively become larger and more abundant, attaining 4 mm and 10% at the top of the subzone. The high modal proportions of titanomagnetite (composite grains of ilmenite and magnetite) in the upper parts of the subzone indicate that despite their intercumulus habits (Fig. 24C,D) they are of cumulus origin. Magnetite is the dominant oxide component in the middle stratigraphic levels, although the ilmenite component becomes more abundant (but still subordinate to magnetite) in the upper part of the subzone. This implies the magma was initially undersaturated with TiO_2 for the temperature and oxygen fugacity of formation. Stratabound layers of cumulus Fe-Ti oxides have not been observed in the intrusion, although they may exist at higher fractionated levels beneath the Fortescue Group if crystallisation conditions remained favourable.

The Fe-Ti oxides typically form composite granular aggregates and at no stratigraphic level does ilmenite form an independent component, i.e. as grains spatially isolated from the magnetite. In addition, ilmenite is generally contained within the magnetite and rarely on the margins of the magnetite. The ilmenite granules are optically homogeneous, whereas the magnetite varies from homogeneous granules, to granules containing irregular coarse blades and granules of ilmenite, to a titaniferous magnetite host containing fine-scale ilmenite lamellae along $\{111\}$ planes. Exsolution features are often enhanced by ?titanomaghemite alteration products. Buddington & Lindsley's (1964) study of magnetite and ilmenite associations has shown that increasing degrees of oxidation and diffusion result in a systematic series of fabrics, from: (1) a single-phase homogeneous spinel; to (2) trellis intergrowths of thin ilmenite lamellae in all sets of $\{111\}$ planes of the host; to (3) sandwich intergrowths of thick ilmenite lamellae predominantly in one set of $\{111\}$ planes; to (4) granules of ilmenite within the magnetite; and to (5) granules or rare lamellae of ilmenite on the boundaries of the magnetite grain, or recrystallised granular aggregates of ilmenite and titaniferous magnetite. Each type may occur alone; types 2 and 3, 3 and 4, or 2, 3, and 4 may occur together in the same grain or in different grains in the same rock.

The ilmenite and magnetite associations in the subzone A gabbronorites dominantly fall into type 4 with lesser amounts of type 2. Buddington & Lindsley (1964) have noted that the conditions that favour large amounts of granule exsolution of ilmenite from titaniferous magnetite, as in type 4, are relatively high diffusion rates which imply high temperatures, slow cooling, the presence of fluid catalysts, and extensive oxidation of the primary titaniferous magnetite. Crystallisation of the primary magnetite at high temperatures and low oxygen fugacity, with a concomitant high Fe_2TiO_4 content in the magnetite, would also favour granule exsolution, in that relatively small decreases in temperature or increases in fO_2 result in extensive oxidation. The coexisting presence of type 2 exsolution features and the absence of pronounced recrystallisation features in the Munni Munni gabbroic rocks indicates the ilmenite granules were not formed during metamorphism, but are believed to be primary exsolution features that reflect high-diffusion rates during protracted periods of slow cooling of the magma. Closed-system fractionation conditions prevailing throughout the evolution of gabbroic subzone A and the large volume of magma involved would engender a long, stable period of slow cooling and oxidation of the fractionating magma. The close spatial association of biotite and hornblende with the oxides may also indicate the importance of fluid catalysts for the formation of the ilmenite granules in the upper parts of the mafic stratigraphy.

Biotite increases in size and modal proportions up the subzone and has parallel distribution trends to that of the Fe-Ti oxides. It shows a strong spatial association with the margins of the oxide aggregates and rarely occurs as isolated grains in the silicates. Biotite forms small stunted aggregates radial to serrated magnetite-ilmenite margins, or sheafs of larger blades parallel to curvilinear margins of the oxide grains. Biotite fringes both magnetite and ilmenite, although it displays a preference for the latter, especially where it abuts plagioclase. The same association and textural relation-

ships of Fe-Ti oxides, biotite, and plagioclase have been documented in gabbro from the Dutchmans Creek intrusion, South Carolina (McSween & Nystrom, 1979) and from gabbronorite in the Potgietersrus area of the Bushveld (Nienaber-Roberts, 1986).

Quartz is a minor (0.1–2 vol. %), late-crystallising interstitial phase locally present above the 2550 m level. It forms small inclusions in plagioclase or more commonly as coarse-grained aggregates filling interstices between interlocking plagioclase laths. The quartz is often strained as a result of volume constraints imposed by the cumulus plagioclase laths.

The sulphide content (0.1–0.5 vol. %) consistently increases upwards in the fractionated gabbronorites, and pyrite becomes the dominant sulphide relative to chalcopyrite. Pyrrhotite is a rare component in the middle and upper parts of the subzone. The pyrite is coarse-grained (up to 0.8 mm) and often forms clusters of grains near, or inclusions in, the Fe-Ti oxides. The inclusions are primary and reflect the S-saturated status of these rocks. Smaller, ragged chalcopyrite anhedra are largely secondary and are invariably associated with fine-grained chlorite in the alteration of inverted pigeonite, clinopyroxene, and plagioclase.

Relative to the basal gabbronorites, clinoamphibole alteration of pyroxene is less intense in the upper levels of the subzone. Clinopyroxene is marginally altered to hornblende, with minor ferroactinolite and chlorite, whereas inverted pigeonite is more altered to pale-brown grunerite with dustings of Fe oxides. Inverted pigeonite at the top of the subzone shows a two-stage sequence of alteration to grunerite, which in turn breaks down to Fe oxides. Plagioclase is invariably traversed by complex networks of chlorite veinlets, but unlike the basal gabbronorites, sericite alteration is less intense.

Anorthositic gabbronorite, anorthositic gabbro, 'anorthosite' (plag)

The most plagioclase-rich rocks (up to 92 vol. %) in the Munni Munni Complex occur as isolated recessive outcrops in subzone B of the gabbroic zone. The anorthositic rocks are characterised by uniform modal proportions and intense pervasive carbonate-chlorite alteration. Cumulus plagioclase of oligoclase-andesine (An_{30}) composition has the same albite component as the plagioclase in gabbronorite near the top of subzone A. This is consistent with the view that these felsic rocks are probably related to the subzone A rocks. The plagioclase forms interlocking laths (1 x 3 mm) that are replaced by pale-green chlorite, sericite, calcite, clinozoisite, and clays. Disseminated between the plagioclase laths are intercumulus magnetite-ilmenite anhedra that are of similar abundance (5.6–7.3 vol. %) to anhedra in the fractionated gabbronorites of subzone A. In most aggregates, the magnetite is outlined by relict exsolved ilmenite lamellae, whereas ilmenite subgrains are largely unaltered. Quartz is a minor interstitial mineral and sulphides are rare. A distinctive feature of these rocks is the intensity of carbonate-chlorite alteration. These minerals have preferentially replaced coarse-grained prismatic ?orthopyroxene that is interstitial to plagioclase.

Other rock types of the gabbroic zone

Small mafic blocks and enclaves are concentrated along the basal contact of the gabbroic zone in the central parts of the intrusion. These accidental rock types have sharp contacts with their gabbronorite hosts and display deformational features. The foliation in the microgabbros and quartz gabbro enclaves is defined by thin, contorted plagioclase-clinopyroxene-rich versus plagioclase-rich laminae. Granoblastic polygonal textures with interlocking margins and triple-point interfacial angles are prominent, and the calcic compositions of the plagioclase (An_{60}) may be attributed to subsolidus re-equilibration. The foliated enclaves may represent partly consolidated material that was detached from the wall rock contacts and deformed during the emplacement of the subzone A gabbroic magma.

Altered quartz monzonite and quartz syenite lying above the subzone B gabbroic rocks and directly below the Fortescue Group cover rocks were not examined in this study. It is not known if these poorly-exposed rocks are highly-fractionated components of the layered mafic stratigraphy, or contaminated roof rocks of the complex, or are unrelated to the Munni Munni Complex. They are unlikely to have formed from assimilation of roof material since aeromagnetics indicates that the intrusion extends for 16 km beneath the Fortescue Group to the south, and these rocks are thus distant from the roof of the intrusion. However, their mineralogy and alteration are generally consistent with their relatively high stratigraphic position in the intrusion, suggesting they may be genetically related to the complex. The following summary of these high-level rocks, is, in part, from the 1986 Hunter Resources Ltd Annual Report on the Munni Munni project.

The fractionated orthocumulates at the top of the exposed gabbroic zone contain significant amounts of granophyric quartz and alkali feldspar, biotite, magnetite, ilmenite, and trace to accessory amounts of pyrite, pyrrhotite, apatite, and hornblende. They have been pervasively and intensely chloritised and carbonated. The altered quartz monzonite is a medium-grained granitic rock containing plagioclase (45–50 vol. %), alkali feldspar-microcline (30%), quartz (6–10%), carbonate-chlorite pseudomorphs after clinopyroxene (0–10%), magnetite and ilmenite (5%), biotite (0–3%), and trace apatite, pyrrhotite and pyrite. The quartz-alkali feldspar locally becomes granophyric, and chlorite, carbonate, and sericite alteration is pervasive. Quartz syenites are believed to be the highest fractionated components that are exposed in the complex. They contain alkali feldspar (70 vol. %), quartz (12%), plagioclase (10%), biotite, altered mafic minerals (7%), and trace apatite and muscovite. The mineralogical trends of increasing quartz, alkali feldspar, apatite, magnetite and ilmenite up-section is believed to be consistent with a fractionating oversaturated tholeiitic parent magma.

The petrography of comagmatic and postmagmatic dykes, and of the granites surrounding the Munni Munni Complex, has been described by Hoatson (1991).

Mineralogy

Introduction

This section summarises the variations in composition of olivine, clinopyroxene, orthopyroxene, inverted pigeonite, plagioclase, alkali feldspar, biotite, Cr-bearing spinel, ilmenite-magnetite, sulphides, and platinum-group minerals throughout the intrusion. In addition, the variations of silicate mineral compositions were documented across five cyclic units in subzones C and D of the ultramafic zone and across the ultramafic/gabbroic zone contact. All mineral data and definitions of atomic ratios used are listed in Appendix 2. Salient geochemical features of silicate and oxide minerals for the Munni Munni Complex are summarised in Table 8 and Figure 25.

Table 8. Salient geochemical features of minerals from the Munni Munni Complex

		Range of mg number				*Range of An*	*Range of mg no.*	*Range of Cr′*
		Olivine	*Clinopyroxene*	*Orthopyroxene*	*Inverted pigeonite*	*Plagioclase*	*Spinel*	*Spinel*
Gabbroic zone		N/P	77–48	N/D	60–56 (bulk)	54–30	N/P	N/P
Subzone	Rock type							
A	Gabbronorite	N/P	77–48	N/D	60–56 (bulk)	54–30	N/P	N/P
Ultramafic zone		83–71	89–58	87–59	N/D	56–18	67–65 44–41	16–13 65–63
Subzone	Rock type							
I	Orthopyroxenite*	N/D	N/D	85	N/P	N/D	67–65	16–13
I	Orthopyroxenite	N/D	N/D	87	N/P	N/D	N/P	N/P
I	Norite–orthopyroxenite	N/P	73	67	N/P	56–48	N/P	N/P
I	Porphyritic websterite	N/D	79–58	75–64	N/D	44–18	N/P	N/P
F	Dunite*	N/D	N/P	N/P	N/P	N/P	44–41	65–63
A–I	Pyroxenite	82–78	86–81	83–77	N/P	N/D	N/P	N/P
A–H	Peridotite	83–76	89–81	84–79	N/P	N/P	N/P	N/P
A′	Plagioclase websterite Olivine websterite	78–75	85–82	80–79	N/P	26–25	N/P	N/P
A′	Gabbronorite	N/P	72–71	59	N/P	41–37	N/P	N/P
A′	Chilled gabbronorite	75–71	72	N/D	N/D	31–28	N/P	N/P

mg number of silicates = atomic 100 × Mg/(Mg + Fe), where Fe = Total Fe; An = atomic 100 × Ca/(Ca + Na + K); mg number of spinels = atomic 100 × Mg/(Mg + Fe^{2+}); Cr′ = atomic 100 × Cr/(Cr + Al + Fe^{3+}); * = spinel-bearing units; N/D = not determined; N/P = not present.

Stratigraphic variations in mineral chemistry

Olivine. Olivine displays no marked gross trend of Fe enrichment upwards in subzones A to H of the ultramafic zone (Fig. 26). The most fractionated olivine compositions, of mg_{75-71}, are associated with the plagioclase-bearing marginal rocks of subzone A′, whereas the peridotites and pyroxenites of the overlying subzones A to H (218–1695 m) contain olivine with mg between 83 and 76. Although there are no overall systematic changes in mg with increasing stratigraphic height in the ultramafic zone, there are more localised compositional trends that indicate that the crystallisation of olivine was sensitive to various magmatic processes. These include:

(1) the tendency for olivine compositions to be more primitive in gabbronorite, plagioclase-bearing websterite, and olivine websterite away from the basal contact of the ultramafic zone, i.e. mg steadily increases from 71 at the base of the intrusion to 81 at the 285 m level. Orthopyroxene and clinopyroxene show similar reverse compositional trends to olivine over the same stratigraphic interval (discussed below). The trend to more fractionated mineral compositions towards the margins of layered intrusions has also been documented in the Bushveld (McDonald, 1967), Great Dyke (Wilson, 1982), Stillwater (Naldrett & von Gruenewaldt, 1989), Sudbury (Naldrett & others, 1970), and Insizwa (Lightfoot & Naldrett, 1984) complexes. In respect to the Munni Munni Complex, it is believed that an increase in supercooling towards the basal contact produced the reverse fractionation trend, and the variable amounts of trapped liquid and subsequent re-equilibration with this trapped liquid were responsible for the variation of olivine compositions.

The relationship of olivine compositions to the cumulus-postcumulus proportions of associated minerals (in most cases plagioclase) has been documented in a number of intrusions, including Duke Island, Muskox, Kiglapait, Stillwater, and Duluth (Irvine 1974a, 1979, 1980b; Morse, 1979; Raedeke & McCallum 1980; Todd & others, 1982; Chalokwu & Grant, 1987). Grant & Molling (1981) suggested that the downward changes in both the abundances of the intercumulus minerals and mineral compositions of the Duluth Complex are the result of downward increases in the amounts of intercumulus liquid. A model for the fractionation sequences in the Stillwater Complex and lunar rocks by Raedeke & McCallum (1980) predicts that mineral compositions will be most modified where the intercumulus liquid/cumulus mineral ratios are highest;

(2) olivine compositions show well-defined small-scale differentiation trends across cyclic units in the ultramafic zone. These trends generally involve a progressive decrease in mg of olivine up the cycle and a return to more primitive compositions in the basal olivine-rich part of the overlying cyclic unit; and

(3) the ultramafic zone can be broadly separated into three sub-domains based on gross chemical trends of olivine. The lowest sub-domain (up to the 300 m level) shows reverse fractionation trends, with the mg steadily increasing with stratigraphic height, as described in (1) above. Sub-domain 2 (300 to about 1400 m) is characterised by relatively abrupt reversals in olivine compositions over short stratigraphic intervals, and sub-domain 3 (1400 to at least 1695 m) shows a consistent decrease in mg with increasing stratigraphic height. The oscillating compositional trends in sub-domain 2 are indicative of open-system crystallisation involving periodic replenishment by new primitive magma pulses that may mix with residual differentiated magma in the chamber (Campbell, 1977; Tait 1985; McGuire & Coleman, 1986). Sub-domain 3 is more typical of closed-system crystal factionation of a single batch of magma in which fractional crystallisation becomes the dominant mechanism and the composition of the magma in the upper parts of the zone becomes progressively more evolved with time. The variation in the mg of cumulus clinopyroxene (Fig. 25) indicates that closed-system fractionation generally extended to the top of the ultramafic zone. The change from open- to closed-system factionation with stratigraphic height is believed to have important implications regarding the formation of the PGE-enriched layer at the ultramafic/gabbroic zone contact.

Naldrett & von Gruenewaldt (1989) have noted that in the early stages of development of most layered

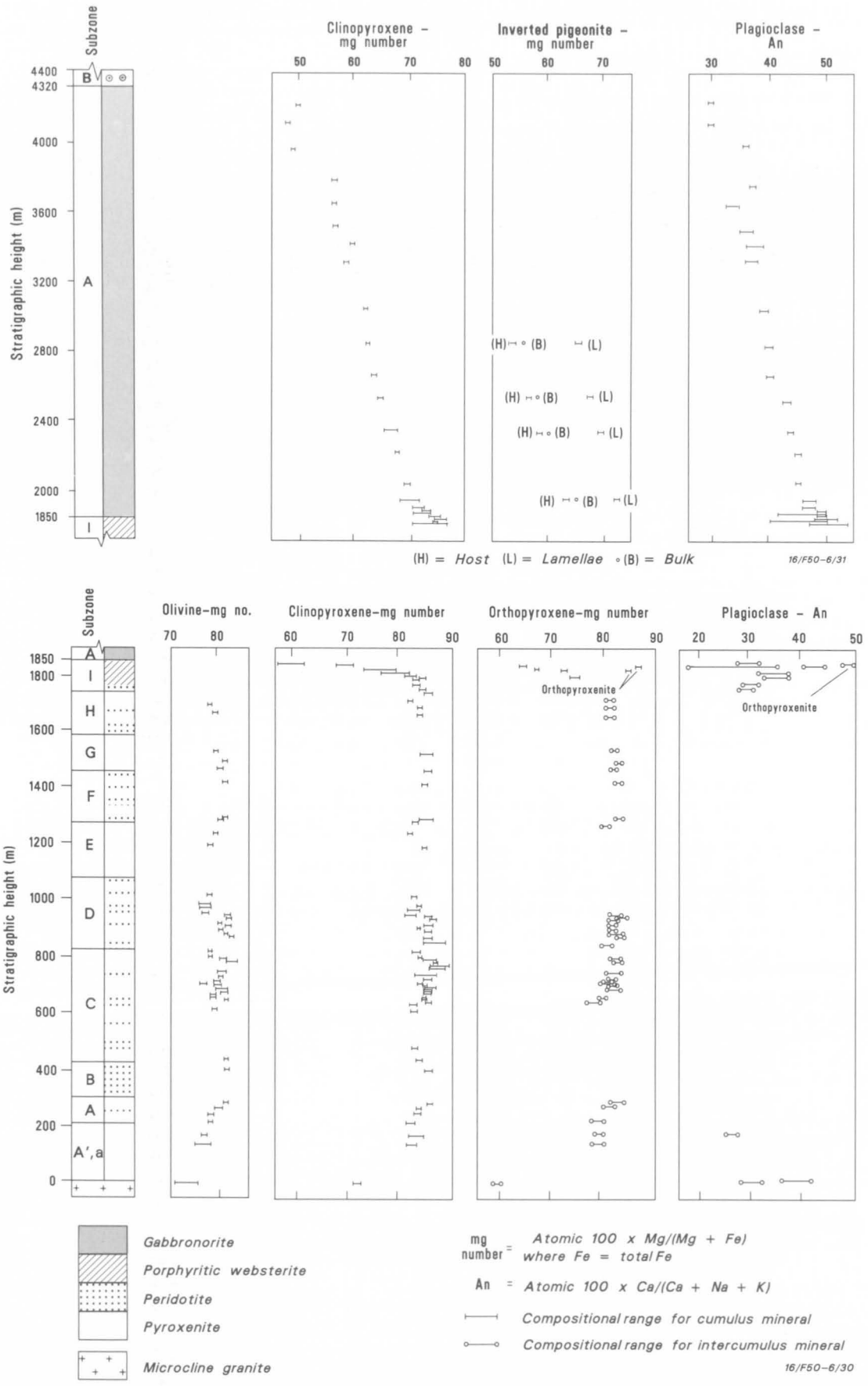

Fig. 25. Summary of electron microprobe data for olivine, clinopyroxene, orthopyroxene, inverted pigeonite, and plagioclase from the ultramafic and gabbroic zones of the Munni Munni Complex.

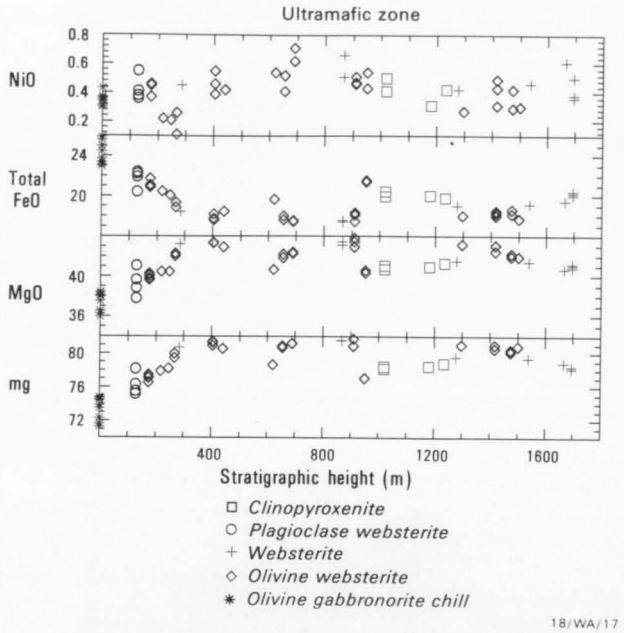

Fig. 26. Munni Munni Complex: variations in mg (mg number), MgO, Total FeO, and NiO (weight %) in olivine with stratigraphic height.

intrusions the initial magma input is relatively fractionated. This is followed by the addition of progressively more primitive magma which overrides the effect of fractional crystallisation and results in the resident magma, and resulting cumulates, becoming progressively more magnesian. Eventually, fractional crystallisation becomes the dominant mechanism and the composition of the magma in the intrusion becomes progressively less primitive. This sequence of events, with the added importance of supercooling near the basal contact, appears to be generally applicable to the evolution of the Munni Munni ultramafic zone.

Nickel contents of olivine range from 0.1% NiO (860 ppm Ni) to 0.7% (5600 ppm Ni), although most olivine has NiO contents between 0.3% (2360 ppm Ni) and 0.5% (3930 ppm Ni). There are no significant gross variations of Ni content with stratigraphic height (Fig. 26), although there are weak positive correlations between Ni and the mg of olivine and possibly between Ni and the type of host rock (Fig. 27). Nickel contents of olivine in plagioclase websterite and gabbronorite near the basal contact are the lowest in the ultramafic zone (except for altered peridotites), with NiO contents between 0.3 and 0.4%. Nickel concentrations steadily increase, from plagioclase websterite, through the olivine-poor pyroxenites (e.g. olivine websterite, clinopyroxenite, and websterite), to a maximum of 0.7% NiO in olivine websterite. In these olivine-rich cumulates, the Ni contents are anomalously high relative to the mg of the olivine, and indeed relative to olivine from other layered intrusions (Simkin & Smith, 1970). The high Ni content of olivine from Munni Munni is believed to reflect the moderately high Ni content of the primary magma (366 ppm Ni at mg_{60}, see Table 29), and the efficient and almost complete partitioning of Ni into the olivine lattice during crystallisation from an extremely S-poor magma, i.e. there was little competition for Ni because of the absence of cumulus sulphide.

In a S-undersaturated environment, Ni will partition between olivine and a silicate melt in a ratio of about 12 : 1, whereas in the presence of sulphides, the partitioning of Ni into the sulphide relative to that of a gabbroic melt increases to about 250 : 1 (Rajamani & Naldrett, 1978). Therefore, it is expected that in a sulphide-bearing system, there will generally be a decline in the Ni content of the coexisting cumulus olivine grains. This has been documented in the sulphide-bearing layers of the Jimberlana intrusion (Keays & Campbell, 1981) and in the Katahdin and Moxie intrusions in Maine (Thompson & Naldrett, 1984). However, as pointed out by Barnes & Naldrett (1985), the depletion of Ni in olivine associated with sulphides is also dependent on the R factor (silicate/sulphide mass ratio) of the system. In their study of the olivines from the J-M Reef they found that there was no depletion of Ni in olivine from the reef relative to olivine in sulphide-free layers; in fact, the reverse was true. They noted that where R is large, in excess of about 2500, separation of sulphides will produce no detectable depletion of Ni in the silicate melt or in the coexisting olivine. At lower R values, such as that derived for the Merensky Reef, some minor depletion of Ni in olivine may be expected.

Basal sulphides at Munni Munni have low Cu, Ni, and PGE contents (see section on whole-rock geochemistry, p. 79), indicating that they formed at very low R values, much lower than in the J-M and Merensky reefs. Thus, according to the observation of Barnes & Naldrett (1985), olivine along the Munni Munni basal contact should be depleted in Ni relative to olivine in the overlying sulphide-poor cumulates. This does not appear to be the case for the olivine gabbronorite chill sample shown in Figure 27, which contains trace amounts of sulphide (871 ppm S). Olivine in most Munni Munni rock types, including the S-poor pyroxenites and peridotites and S-bearing basal rocks, displays a gross trend of decreasing NiO with decreasing mg and there is no preferential decrease in the Ni content of olivine in the S-bearing basal rocks. Therefore, the lower Ni content of olivine in the basal rocks relative to olivine higher up in the sequence appears to be largely a function of their more evolved compositions. The small amount of sulphide present appears to have had a negligible effect in reducing the availability of Ni for the crystallisation of olivine. The absence of any marked Ni depletion may be attributed to the very small amount of sulphide present, or more likely, the partitioning of Ni between the olivine and sulphide

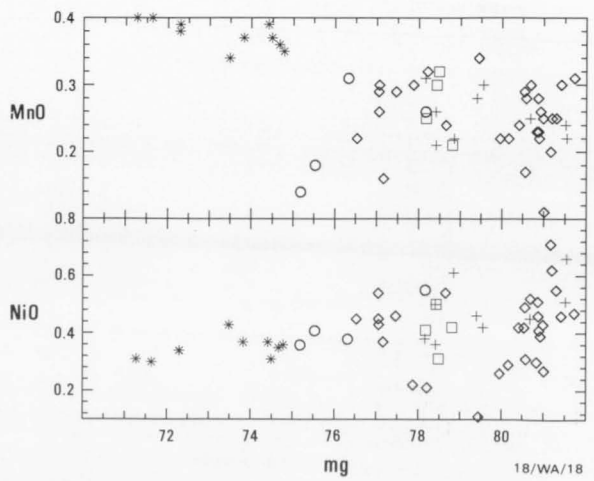

Fig. 27. Munni Munni Complex: variations in NiO and MnO (weight %) in olivine with mg. Symbols as in Figure 26.

occurred under non-equilibrium conditions, e.g. as influenced by a rapid drop in temperature and changes in initial porosity of the magma near the basal contact. Non-equilibrium magmatic conditions at the base of the ultramafic zone are also indicated by the partitioning of Fe and Mg between coexisting olivine and orthopyroxene (discussed in the orthopyroxene sub-section below).

Clinopyroxene. Clinopyroxene displays a wide range of composition, with mg ranging from 89–81 in refractory peridotite, to 86–81 in pyroxenite, to 79–58 in porphyritic websterite of the ultramafic zone. It has a maximum mg of 77 at the base of the gabbroic zone, and decreases continuously to 48 in fractionated gabbronorite near the top of the zone. Thus there is a change in mg of 41 units from the most primitive to the most evolved rocks in the intrusion. Clinopyroxenes in the upper two metres of the porphyritic websterite layer have the most evolved compositions and have the strongest normal compositional zoning of any clinopyroxene in the ultramafic zone.

Clinopyroxenes from the Munni Munni Complex mostly fall near the Ca-Mg side of the atomic Ca-Mg-Fe ternary diagram (Fig. 28). Their compositions from the different rock types define a fairly continuous n-shaped fractionation trend which extends from about $Ca_{37}Mg_{53}Fe_{10}$ for olivine websterite, to more calcic compositions centred around $Ca_{42}Mg_{49}Fe_9$ for clinopyroxenite, websterite and plagioclase websterite. Clinopyroxenes in the porphyritic websterite show the first evidence of Fe enrichment, with compositions of $Ca_{42-44}Mg_{39-44}Fe_{12-19}$. Clinopyroxenes in gabbronorite from the gabbroic zone display a continuous trend of marked Fe enrichment, with compositions extending from $Ca_{42}Mg_{49}Fe_9$ to $Ca_{32}Mg_{33}Fe_{35}$. Using the pyroxene classification scheme of Poldervaart & Hess (1951), Ca-poor augites characterise clinopyroxene in olivine websterite, endiopsides and Fe-poor augites occur in the websterite and clinopyroxenite, and clinopyroxene from the mineralised porphyritic websterite layer and gabbronorite from the gabbroic zone are Ca-rich augites that border on salite compositions. Fractionated clinopyroxene from the highest levels of gabbroic subzone A are ferroaugites.

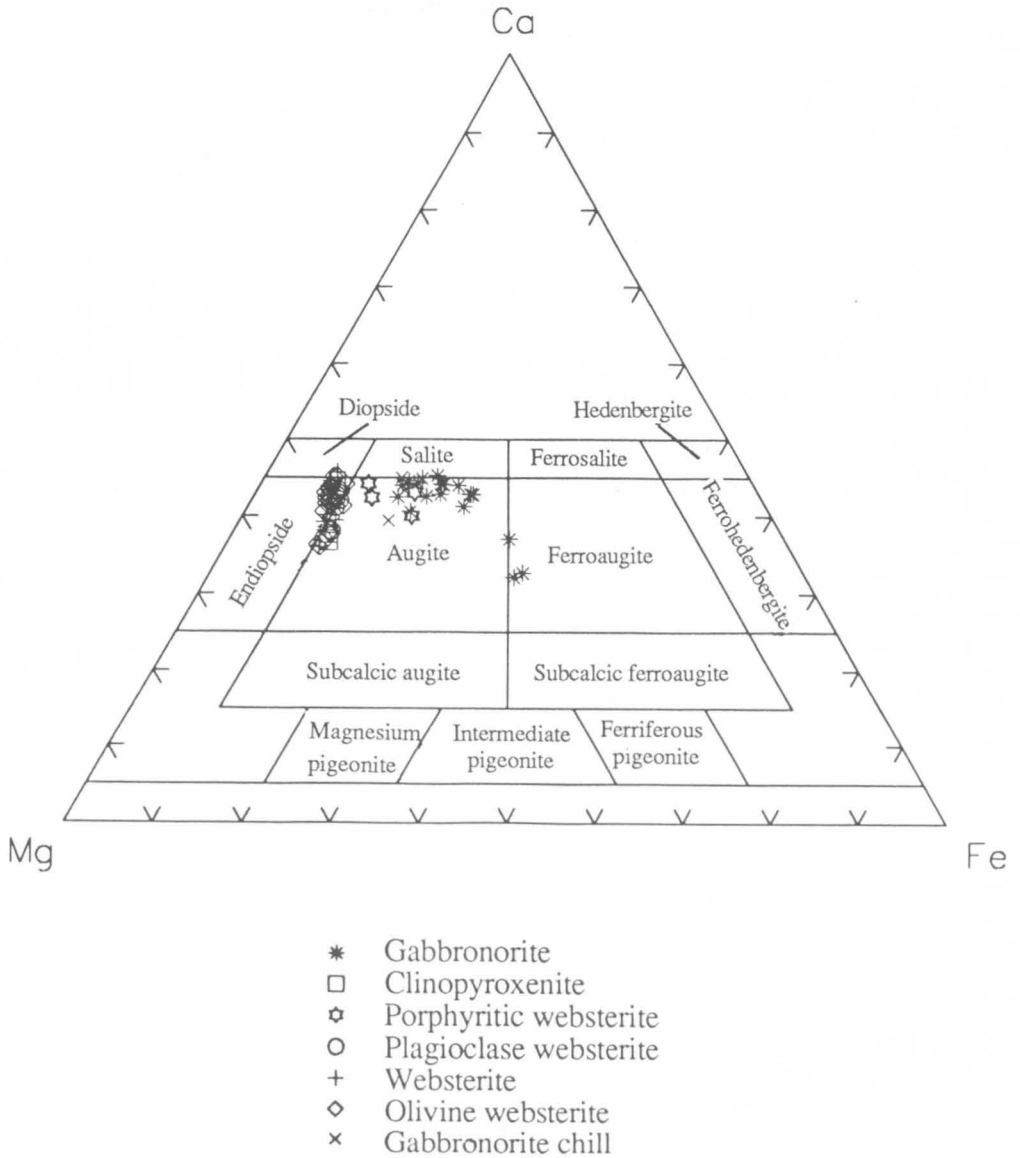

Fig. 28. Classification of clinopyroxene from the Munni Munni Complex. Nomenclature of clinopyroxene in the system CaMgSi$_2$O$_6$-CaFeSi$_2$O$_6$-Mg$_2$Si$_2$O$_6$-Fe$_2$Si$_2$O$_6$ is after Poldervaart & Hess (1951).

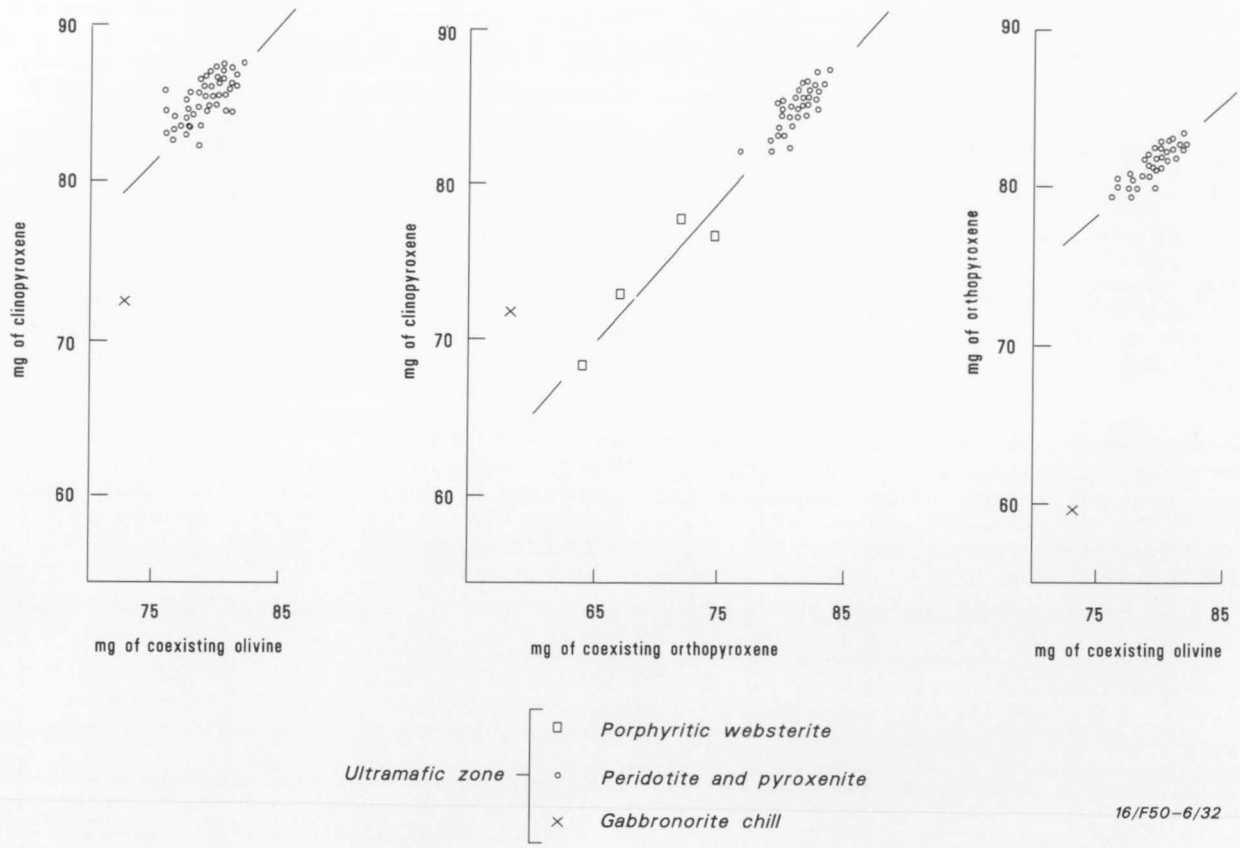

Fig. 29. Munni Munni Complex: variations in mg for coexisting clinopyroxene, olivine, and orthopyroxene, for various rock types in the ultramafic zone.

Clinopyroxene generally shows sympathetic trends in mg with olivine and orthopyroxene throughout the ultramafic zone (Fig. 25), with the mg about 4–6% and 3–5% higher than those of coexisting olivine and orthopyroxene, respectively. These positive correlations are illustrated (Fig. 29) by the general linear variation trends of the mg for coexisting olivine, clinopyroxene, and orthopyroxene in peridotite, pyroxenite, and porphyritic websterite. The consistency of compositions between the mafic minerals shows that the Munni Munni clinopyroxenes have not undergone significant subsolidus re-equilibration. Only in the upper 2 m of the ultramafic zone is there a pronounced zoning of clinopyroxene grains from the same sample.

Compositional trends in clinopyroxene can be used to subdivide the ultramafic zone into the same three sub-domains as for olivine, and an additional fourth sub-domain from above the 1745 m level. Sub-domain 4 was not previously defined because of the paucity of olivine at these high stratigraphic levels. Clinopyroxene in the lowest sub-domain (0–300 m) shows reverse fractionation trends, with mg increasing upwards from 72–71 at the 2 m level, to 83–82 at the 128 m level, to 86–82 at the 300 m level. This is similar to that observed for olivine, but there is no increase in the range of compositions towards the basal contact, indicating that clinopyroxene compositions were less sensitive to changes in initial porosity and temperature gradients near the contact than were olivine compositions. Clinopyroxene in sub-domain 2 (300–1400 m) displays abrupt oscillations in mg over small stratigraphic intervals that are indicative of open-system fractional crystallisation, whereas those in sub-domain 3 (1400–1745 m) display a subtle but progressive upward decrease in mg. The transition from sub-domain 3 to sub-domain 4 is defined by an increase in mg from 82 in websterite at the top of subzone H to 86–85 in dunite at the base of subzone I (1745 m level). In the upper part of sub-domain 4 (1745–1850 m), clinopyroxene displays a continuous and rapid decrease in mg, from 85 at the 1810 m level to a minimum of 58 at the top of the zone. In general, clinopyroxene mg trends in sub-domains 3 and 4 are fairly continuous and tentatively indicate that closed-system crystallisation conditions largely prevailed for the upper 450 m of the ultramafic zone. More probe analyses in sub-domains 3 and 4 are required to confirm this.

Clinopyroxene in the gabbroic subzone A displays a similar closed-system fractionation trend to the upper part of the ultramafic zone, with mg steadily decreasing from around 77–69 at the base of the zone to 50–48 at the 4222 m level. With the exception of the marked discontinuity of compositions in the upper 2 m of the ultramafic zone, changes in clinopyroxene mg across the ultramafic/gabbroic zone contact are continuous and support the concept of a common magma for the formation of the two zones. Moreover, clinopyroxenes from the base of the gabbroic zone display the greatest range of compositions, similar to that observed at the top of the ultramafic zone. Clinopyroxene trends in subzone A of the gabbroic zone constitute sub-domain 5, although in many respects, one could interpret sub-domain 5 as an upward continuation of sub-domain 4.

Figure 30 summarises the variation of major elements for clinopyroxene throughout the intrusion. Total FeO, TiO_2, and Al_2O_3 display the characteristic U-shaped fractionation trend through the ultramafic zone, with high concentrations in the lower and upper parts

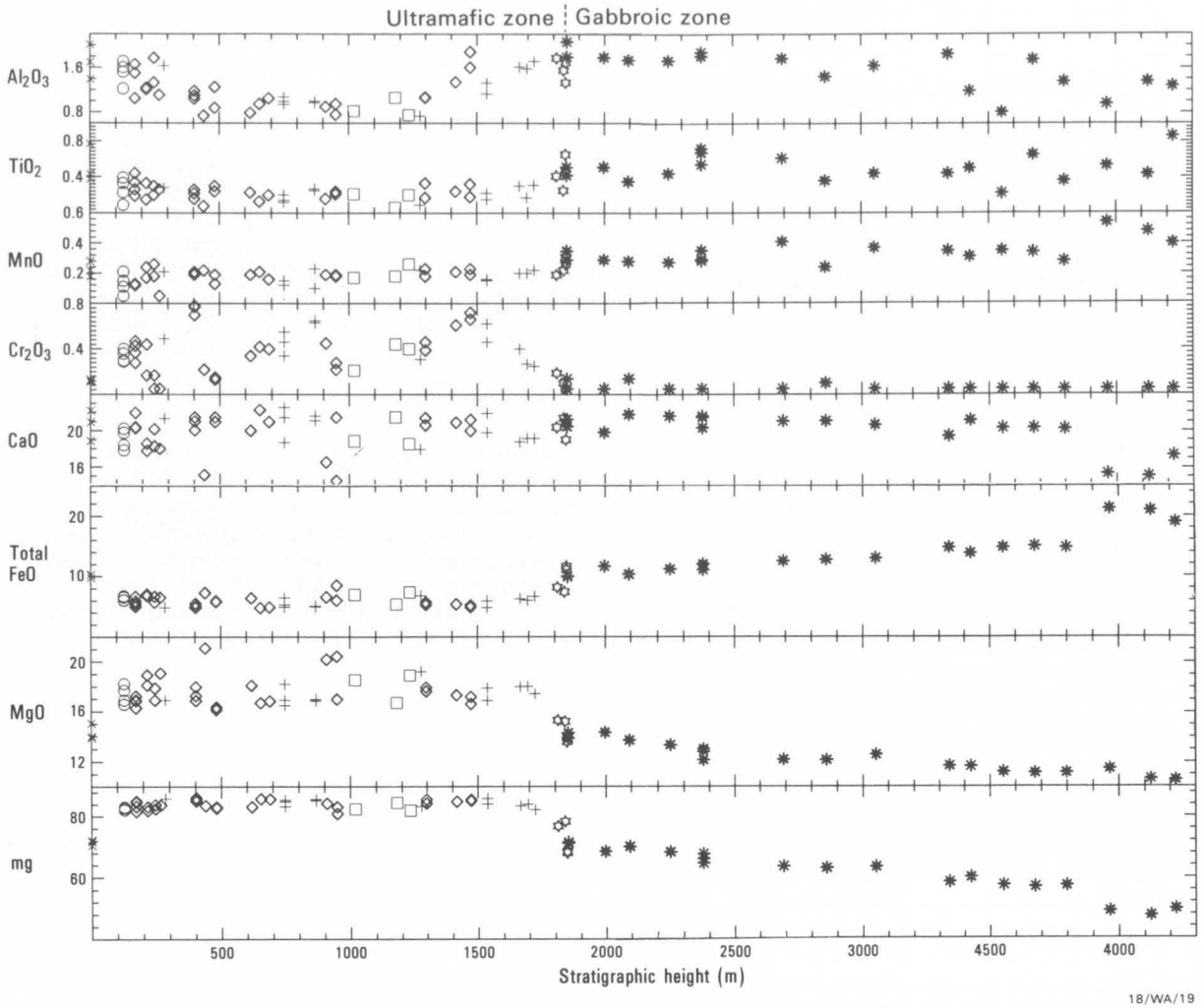

Fig. 30. Munni Munni Complex: variations in mg, MgO, Total FeO, CaO, Cr_2O_3, MnO, TiO_2, and Al_2O_3 (weight %) in clinopyroxene with stratigraphic height. Symbols as in Figure 28.

of the ultramafic zone. Gross trends of Cr_2O_3 and Al_2O_3 also highlight the five sub-domains of the intrusion, as defined by the variation of mg. Although Cr_2O_3 contents of clinopyroxene are variable for most rock groups, there is a positive correlation between Cr_2O_3 and rock type, with clinopyroxene in olivine websterite containing up to 0.8% Cr_2O_3, followed by websterite (0.6%), clinopyroxenite (0.4%), plagioclase websterite (0.4%), porphyritic websterite (0.2%), and gabbronorite chill (0.1%). Clinopyroxenes in gabbronorite of the gabbroic zone are lower in Cr_2O_3 ($\leq$ 0.1%) than those in any of the ultramafic zone cumulates.

The fairly high Cr_2O_3 contents of clinopyroxene in the most primitive rocks (up to 0.8%) of the ultramafic zone may explain why there is a paucity of chromitites in the Munni Munni Complex. Because of the dominance of early-crystallising clinopyroxene over orthopyroxene (cumulus orthopyroxene is restricted to above the $\sim$ 1800 m level) in the ultramafic zone, Cr in the melt strongly partitioned into clinopyroxene during crystal fractionation. This preferential partitioning left the residual melt depleted in Cr and inhibited the formation of chromitite layers in the ultramafic stratigraphy.

Orthopyroxene. Orthopyroxene shows similar compositional trends to those of olivine and clinopyroxene, consistent with the subdivision of the ultramafic zone into four sub-domains. Orthopyroxene compositions are also sensitive indicators of the intercumulus versus cumulus status of orthopyroxene through the zone.

Gabbronorite along the basal contact of the ultramafic zone contains the most evolved orthopyroxene in the ultramafic zone (Fig. 31). The orthopyroxenes form small prismatic hypersthene (mg_{59}) grains of possible cumulus origin that are depleted in Cr_2O_3 ($<$ 0.1%), Al_2O_3 (0.6%), and SiO_2 (52%), and are eriched in MnO (0.5%) relative to orthopyroxene in the overlying ultramafic cumulates. The mg of orthopyroxene steadily increases from 79–80 in plagioclase websterite at the 128 m level to 82–83 in websterite at the 285 m level, indicating an antipathetic relationship between mg and modal plagioclase content. These more primitive compositions correlate with a transition from cumulus hypersthene at the basal contact to intercumulus grains of bronzite affinity at higher stratigraphic levels. Intercumulus bronzite persists up to about the 1800 m level, where large cumulus grains of bronzite and hypersthene replace the intercumulus bronzite. Throughout the middle part of the ultramafic zone, the mg trends of bronzite (irrespective of their intercumulus status and modal proportions) display the open-system crystallisation features typical of sub-domain 2. These features indicate

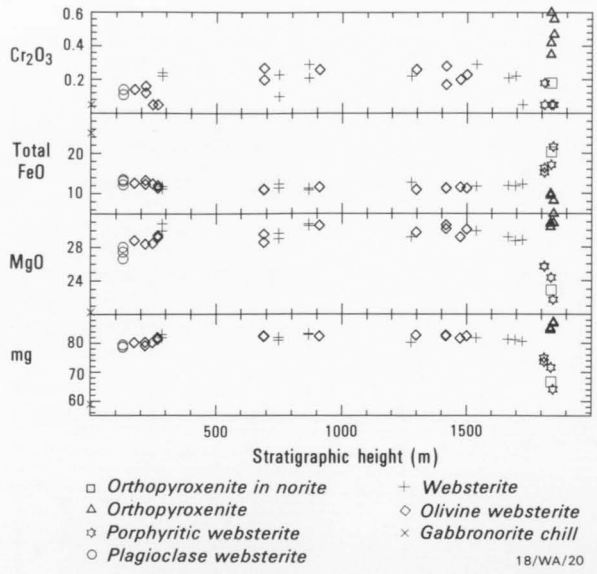

Fig. 31. Munni Munni Complex: variations in mg, MgO, Total FeO, and Cr_2O_3 (weight %) in orthopyroxene with stratigraphic height.

that the melt component was in communication with the changes in composition of the cumulus grains, which implies that the melt did not migrate to any significant distance away from the cumulate pile, e.g. by filter pressing or postcumulus processes. This is also indicated by the close spatial association of bronzite mantling cumulus olivine in the rocks.

Bronzite throughout the main part of the ultramafic zone replaces olivine according to the reaction $2FeSi_{0.5}O_2$ (in olivine) + SiO_2 (in the melt) = $2FeSiO_3$ (in orthopyroxene). Bronzites in the replacement coronas have primitive compositions that appear to be inherited from the parent olivine grain. This is indicated by the striking correlation of mg in olivine and coexisting bronzite throughout the zone (Figs 25 & 29) and the distribution ratio defined by (Fe/Mg)olivine / (Fe/Mg)orthopyroxene between coexisting olivine and orthopyroxene. For olivine and orthopyroxene in chemical equilibrium, the ratio should be about 1.12 (Medaris, 1969). The mean distribution ratio for 21 different olivine-orthopyroxene pairs (for the stratigraphic interval 128–1695 m), is 1.13 ± 0.06; and for three mineral pairs from the basal part of the zone (1–2 m) it is 0.54 ± 0.04. This suggests that in most of the ultramafic zone bronzite was in equilibrium with olivine, whereas due to the effects of temperature gradients and variable initial porosities, non-equilibrium crystallisation conditions prevailed in the basal contact region. Non-equilibrium conditions are also indicated by the position of the gabbronorite chill sample relative to the trend defined by the ultramafic cumulates in Figure 29.

Closed-system crystallisation conditions are reflected in sub-domain 3, where bronzite (mg_{83-81}) shows a slight, but consistent, enrichment in Fe with stratigraphic height. As for clinopyroxene, there is a dramatic change to more evolved compositions for orthopyroxene (mg_{75-64}) in the upper part of sub-domain 4. Compositions near mg_{70} characterise the large cumulus orthopyroxene grains in the porphyritic websterite layer. Cumulus grains from near the top of the zone have high CaO contents (2.9–3.0%), suggesting crystallisation in chemical equilibrium with clinopyroxene, whereas intercumulus bronzite lower down in the zone is relatively low in CaO (0.7–2.1%). Cumulus bronzite-hypersthene is also characterised by lower SiO_2, Cr_2O_3, and NiO, and higher TiO_2 and MnO contents compared to the intercumulus bronzite. There is a positive correlation between Al_2O_3 and mg for both intercumulus and cumulus orthopyroxene throughout the zone.

Othopyroxenes in spinel-bearing orthopyroxenite blocks have the most primitive compositions (mg_{87-85}) in the intrusion and lie away from the main fractionation trend. They also have three times the Cr_2O_3 (0.4–0.6%) and up to 10 times the Al_2O_3 (1.7–5.5%) of that in peridotites and pyroxenites in the ultramafic zone. The contrasting fractionation status of orthopyroxene in the orthopyroxenite blocks and the abutting porphyritic websterite layer (a difference of 23 mg units) indicates that the former rocks have not crystallised *in situ*.

Inverted pigeonite. Inverted pigeonite has a restricted distribution in the ultramafic zone. It is present in minor amounts in the fractionated gabbroic rocks along the basal contact and in the upper part of the porphyritic websterite layer, where it appears to 'anticipate' its more copious crystallisation in the gabbronorites of the overlying gabbroic zone. The distribution of inverted pigeonite in the intrusion is related to the crystallisation of cumulus orthopyroxene in regions where fractionated magmatic conditions prevailed.

Owing to the heterogeneous and coarse nature of the exsolution lamellae in the inverted-pigeonite grains, a method of integrated multiple analysis (the procedure is described in Appendix 1.5) was used to determine the average composition of the lamellae and host components, and an estimate for the bulk composition, of three grains from three different levels of subzone A of the gabbroic zone (Appendix 2). The variation in composition of the lamellae and host components, and bulk analyses (Table 9) for the three grains, are consistent with that expected from increasing fractionation up the mafic stratigraphy.

Table 9. Composition of inverted pigeonite from the gabbroic zone of the Munni Munni Complex

Sample number	*84770052*	*84770053*	*84770055*
Stratigraphic level (m)	*2377*	*2551*	*2859*
mg no. of lamellae	70	68	66
CaMgFe of lamellae	$Ca_{44}Mg_{39}Fe_{17}$	$Ca_{44}Mg_{38}Fe_{18}$	$Ca_{44}Mg_{37}Fe_{19}$
mg no. of host grain	59	57	54
CaMgFe of host grain	$Ca_2Mg_{57}Fe_{41}$	$Ca_2Mg_{56}Fe_{42}$	$Ca_2Mg_{53}Fe_{45}$
mg no. of bulk grain	60	59	56
CaMgFe of bulk grain	$Ca_{12}Mg_{53}Fe_{35}$	$Ca_{13}Mg_{51}Fe_{36}$	$Ca_{11}Mg_{49}Fe_{40}$

There appear to be positive correlations between mg and TiO_2, and mg and Al_2O_3, and a negative correlation between MnO and mg (see Appendix 2). The positive relationship between mg and TiO_2 indicates that Ti is being partitioned into the liquid by the crystallisation of plagioclase and pyroxene, and, with increasing fractionation, intercumulus Fe-Ti oxides will take up the excess amounts of Ti.

Plagioclase. Plagioclase has a similar distribution to inverted pigeonite in the intrusion. It occurs as an intercumulus mineral of variable abundance in gabbronorite and plagioclase websterite at the basal contact and as a minor intercumulus mineral that increases in abundance upwards in the porphyritic websterite layer of subzone I. This increasing modal trend and its tendency to form large Na-rich poikilitic grains enclosing cumulus pyroxene in the upper parts of the porphyritic

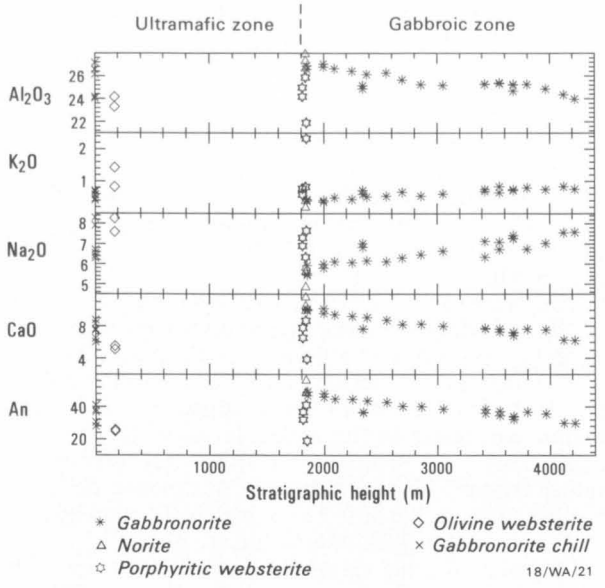

Fig. 32. Munni Munni Complex: variations in An, CaO, Na_2O, K_2O, and Al_2O_3 (weight %) in plagioclase with stratigraphic height.

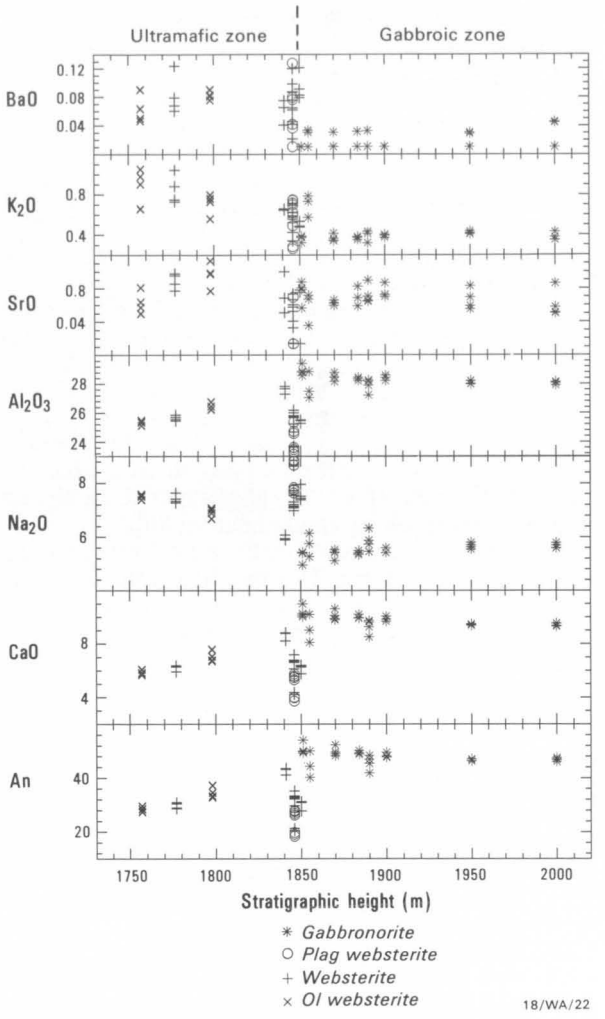

Fig. 33. Munni Munni Complex: variations in An, CaO, Na_2O, Al_2O_3, SrO, K_2O, and BaO (weight %) in plagioclase across the ultramafic/gabbroic zone contact.

websterite layer suggests plagioclase was on the verge of crystallising as a cumulus phase near the top of the ultramafic zone. Plagioclase is of cumulus status throughout the gabbroic zone (the criterion used to define this zone) and of much greater abundance relative to the ultramafic zone cumulates.

In contrast to olivine and pyroxene, the composition of plagioclase in the basal part of the ultramafic zone (Fig. 32) is sympathetically related to its modal proportions rather than to stratigraphic level. Minor amounts of intercumulus oligoclase-andesine (An_{31-28}) characterise the olivine gabbronorite chill at the 1 m level, mid-andesine (An_{41-37}) is a major component of coarse gabbronorite at the 2 m level, and trace amounts of oligoclase (An_{26-25}) in olivine websterite at the 174 m level are the most Na-rich plagioclase in the basal contact region. These features indicate that one of the most important parameters that controlled the composition of plagioclase in the basal rocks was the ratio of intercumulus plagioclase to cumulus clinopyroxene. The intercumulus plagioclase component is significantly lower (< 15 vol. %) and the cumulus clinopyroxene content higher for the gabbronorite chill and olivine websterite than for the more clinopyroxene-poor, plagioclase-rich (up to 50 vol. %) coarse gabbronorite. The higher clinopyroxene-to-plagioclase ratio in the former rocks reduced the Ca available for small amounts of late-crystallising plagioclase and consequently plagioclase is Ca-poor relative to that in the coarse gabbronorite.

Plagioclase compositions in subzone I (Figs 25 & 33) show reverse fractionation features, with a progressive increase in the An component with increasing stratigraphic height. Kruger & Marsh (1985) documented a similar shift to more Ca-rich compositions upwards for plagioclase in the Merensky Cyclic Unit and also the Merensky Footwall Unit of the Bushveld Complex. The increase in An at Munni Munni correlates with the increase in the plagioclase-to-clinopyroxene ratio for the rock types olivine-plagioclase websterite to plagioclase websterite to porphyritic plagioclase websterite to porphyritic gabbronorite. The Ca enrichment of intercumulus plagioclase up-section indicates that CaO and Na_2O activities in the melt were also dependent on the relative modal proportions of plagioclase and clinopyroxene in the cumulates. Cumulates with a high cumulus-clinopyroxene-to-intercumulus-plagioclase ratio generally have sodic plagioclase, whereas cumulates with a low cumulus-clinopyroxene-to-intercumulus-plagioclase ratio have more calcic plagioclase.

Alternatively, the reverse An trend may be due to increased P_{H_2O} in residual liquids up towards the ultramafic/gabbroic zone contact. Johannes's (1978) study of the melting of plagioclase in the Ab-An-H_2O and Qz-Ab-An-H_2O systems at 5 kb water pressure, showed that plagioclase crystallising under high water pressure is more calcic than that crystallising under anhydrous conditions. High activities of silica and water in the upper parts of the porphyritic websterite layer are suggested by the marked increase in modal proportions of orthopyroxene, inverted pigeonite, and biotite relative to cumulates lower in the sequence.

At the 1845.5 m level, plagioclase changes abruptly to more sodic, and a greater range of, compositions (An_{35-18}), whereas directly below the base of the gabbroic zone, at the 1849.75 m level (diamond-drill core), it has a more calcic, and less variable, composition of An_{31-28}. The most evolved plagioclase occurs a couple

of metres below the stratigraphic level of the most evolved clinopyroxene. This decoupled distribution further highlights the antipathetic relationship between these minerals and indicates that homogeneous crystallisation conditions did not occur in the stagnated pockets of magma that were trapped at the top of the ultramafic zone. Kruger & Marsh (1985) and Eales & others (1990b) have also documented the decoupling of plagioclase compositions with respect to the ferromagnesian minerals in the vicinity of the Merensky Reef.

Cores of cumulus plagioclase grains from the basal part of the gabbroic zone have the most variable compositions (An_{54-40}) of any plagioclase in the zone. Compositional variations from grain to grain are greater than variations within grains. Extrapolating the increasingly calcic trend of plagioclase in the 1757–1841 m interval of the ultramafic zone upwards to the base of the gabbroic zone (Fig. 25), plagioclase there should have a composition of approximately An_{50-45}, assuming the gabbroic and ultramafic zones were derived from a common magma. This predicted composition is close to that defined by the regional gabbroic-zone plagioclase trend at the 1850 m stratigraphic level, i.e. about An_{50-48}. This indicates that there is a continuum in plagioclase compositions across the zone contact, which supports the concept of a common magma system for the two zones. Above the 1870 m level, An content consistently decreases to An_{30} with increasing stratigraphic height. With the exception of some minor displacements of the trend to slightly more Ca-rich compositions in the 3800–4000 m stratigraphic interval, the chemical evolution of plagioclase in subzone A of the gabbroic zone is consistent with closed-system fractionation.

Alkali feldspar. A few intercumulus alkali feldspar grains were analysed from olivine websterite and websterite of subzones A, G, and H of the ultramafic zone (see Appendix 2). They have a range of compositions, K_2O varying from 8.2 to 12.7%, Na_2O from 2.0 to 5.3%, CaO from 0.7 to 2.1%, and the Or component from 45 to 74. Above the 1474 m level, the Or component appears to decrease up-section, although further analyses are required to confirm this. Alkali feldspar from the 1723 m level has the unusually high FeO content of 0.7%, which is probably due to Fe-rich impurities along cracks. The most distinctive chemical feature of the alkali feldspars is their high BaO content (0.1–2.3%); the most BaO-rich feldspars (> 2%) are barium feldspars rather than alkali feldspars (Deer & others, 1978). There is a strong positive correlation between BaO and Or, which indicates there is limited substitution by Ba for K; rather, Ba is replacing Na and to a lesser degree Ca. The apparent depletion in BaO contents above the 1474 m level is unexpected since the incompatible Ba would be partitioned into the liquid by olivine and clinopyroxene and the melt should become enriched in this element with increasing fractionation. Intercumulus plagioclase in the porphyritic websterites above 1811 m has similarly low BaO (< 0.04–0.15%); thus the depletion of Ba in the melt fraction at these high stratigraphic levels is not unique to alkali feldspar.

Biotite. Biotite occurs as an accessory phase in the upper parts of the ultramafic zone and in the middle to upper parts of the gabbroic zone, where it is in close spatial association with ilmenite-magnetite. Biotite compositions from the two zones are distinctive: those in the ultramafic zone have higher mg (66–56), TiO_2 (4.6–5.5%), NiO (0.2–0.3%), and lower Al_2O_3 (12.7–12.9%) contents relative to most biotites from the gabbroic zone (mg_{49-32}, 3.0–4.2% TiO_2, 0.03–0.11% NiO, and 12.75–14.35% Al_2O_3). Biotites from 2859 m have anomalously high mg (66 and 56) with respect to other biotite from the gabbroic zone. The high mg is probably due to fine-grained Mg-rich chlorite, which is the commonest alteration product of biotite in the middle parts of the gabbroic zone. Mica in the upper part of the ultramafic zone ranges from biotite (Mg : Fe < 2 : 1) to compositions transitional between biotite and phlogopite (Mg : Fe ~ 2 : 1).

The decreasing mg, TiO_2, and NiO, and increasing Al_2O_3 and MnO of biotite up the ultramafic-mafic stratigraphy are features consistent with those expected during increasing fractionation. To a varying extent, biotite forms fringes around composite magnetite-ilmenite aggregates in the higher levels of the gabbroic zone. This close spatial association may explain the rather erratic TiO_2 trend through this part of the zone: biotite abutting ilmenite has a higher Ti content than biotite next to magnetite or a silicate phase.

Chromium-bearing spinel. In contrast to many other major layered mafic-ultramafic intrusions, in the Munni Munni Complex Cr-bearing spinel is of restricted distribution and there are no known significant chromitite layers. The most likely reason (discussed in the clinopyroxene sub-section, p. 55) for the rarity of chromite is the early crystallisation of cumulus clinopyroxene relative to orthopyroxene and the consequent progressive depletion of Cr from the melt. Compositions of cumulus spinel from the Munni Munni region fall into three geochemical subgroups:

(1) high-Cr, low-Al chromite from a dunite lens in subzone F;
(2) high-Cr, high-Fe^{3+}, low-Al chromite in gabbronorite and orthopyroxenite of the Eastern Munni Munni Dyke; and
(3) high-Al, low-Cr spinel in accidental orthopyroxenite blocks in subzone I.

The major geochemical features of the three subgroups are summarised in Table 10. Subgroup 1 spinels are characterised by their restricted compositions and lower Fe^{2+} and Fe^{3+} contents relative to subgroup 2 spinels. Disseminated chromite from gabbronorites (mg_{44-35}, mg = Mg/(Mg + Fe^{2+})) and orthopyroxenites of the Eastern Munni Munni Dyke (mg_{48-26}) of subgroup 2 have similar compositions. Orthopyroxenite lenses and blocks along the ultramafic/gabbroic zone contact contain aluminous spinels (subgroup 3) which show the greatest deviation in composition from the chromites of subgroups 1 and 2. Zinc shows minor substitution for Mg in subgroup 1 chromite (up to 0.4% ZnO), but spinels from subgroups 2 and 3 generally have less than

Table 10. Composition of Cr-bearing spinel in the Munni Munni Complex region

Subgroup	*1*	*2*	*3*
$Mg/(Mg+Fe^{2+})$	41–44	26–48	65–67
$Cr/(Cr+Al+Fe^{3+})$	63–65	53–71	13–16
$Al/(Cr+Al+Fe^{3+})$	29–31	18–34	78–82
$Fe^{3+}/(Cr+Al+Fe^{3+})$	5–6	7–22	5–6
Cr_2O_3	47.2–48.8%	39.1–53.1%	12.1–15.1%
Al_2O_3	14.1–15.6%	8.2–17.3%	47.0–50.2%
Fe^{2+}	20.7–22.2%	20.1–28.5%	14.4–15.3%
Fe^{3+}	4.2–5.1%	6.0–15.7%	4.9–5.9%

Subgroup 1—high-Cr, low-Al chromite from a dunite lens in subzone F.

Subgroup 2—high-Cr, high-Fe^{3+}, low-Al chromite in gabbronorite and orthopyroxenite from the Eastern Munni Munni Dyke.

Subgroup 3—high-Al, low-Cr spinel in accidental orthopyroxenite blocks in subzone I.

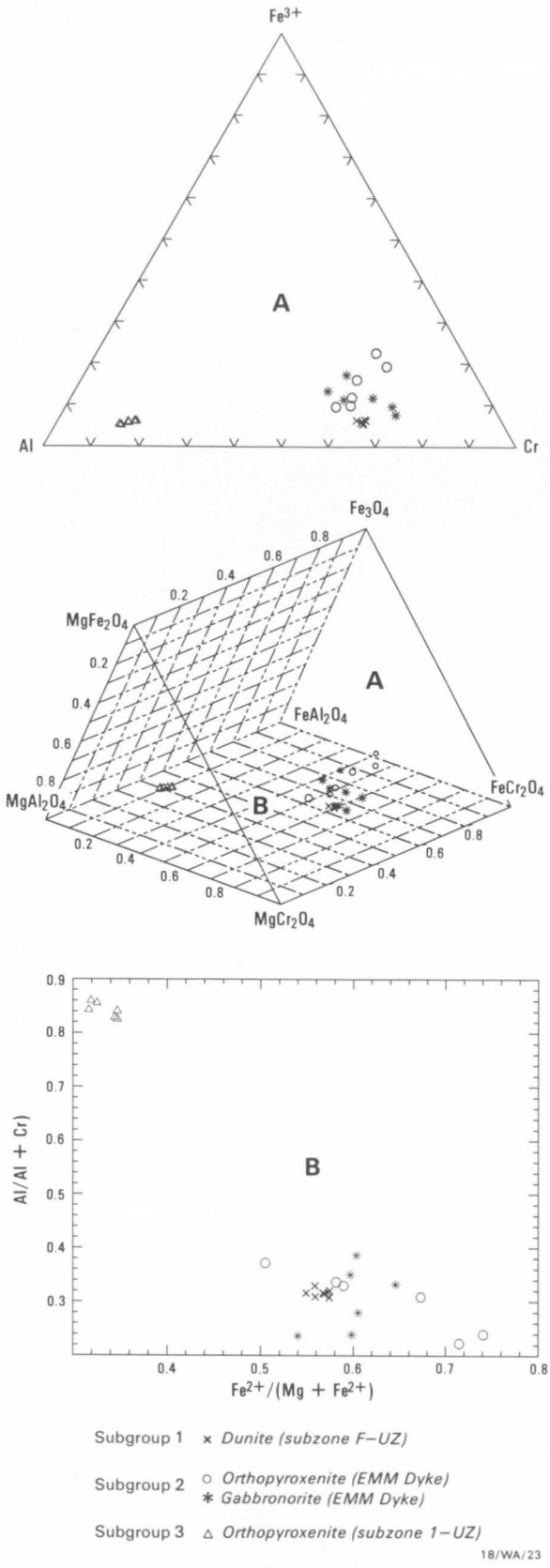

Fig. 34. Compositions of Cr-bearing spinel from the Munni Munni Complex (subgroup 1), Eastern Munni Munni Dyke (subgroup 2), and accidental blocks in the Munni Munni Complex (subgroup 3) in the oxidised-spinel prism (defined by the $MgCr_2O_4$-$FeCr_2O_4$-$FeAl_2O_4$-$MgAl_2O_4$-$MgFe_2O_4$-Fe_3O_4 components), and their projections on faces A (Al-Cr-Fe^{3+}) and B (Al/(Al + Cr)−Fe^{2+}/(Mg + Fe^{2+})).

0.2% ZnO. Subgroup 3 spinels have low TiO_2 contents of 0.1 to 0.2% compared to 0.4 to 3.6% TiO_2 for the chromites of subgroups 1 and 2. Dickey (1975) and Leblanc (1987) noted a relationship between the TiO_2 content of spinel and the geological setting of the intrusion that hosts the spinel. Chromite in stratiform layered intrusions commonly has TiO_2 contents greater than 0.3%, whereas chromite from podiform-type deposits has TiO_2 contents less than 0.3%. Subgroup 3 spinels show no obvious affinity with the various mafic-ultramafic associations (see below).

The compositional features of the three spinel subgroups are illustrated by their contrasting distributions in the oxidised-spinel prism and their projections on faces A and B in Figure 34. For the variation of trivalent cations Cr, Fe^{3+}, and Al (side A), subgroup 1 chromites have a restricted distribution near $Cr_{64}Fe^{3+}{}_7Al_{29}$, subgroup 2 chromites have a wider range of compositions centred near $Cr_{60}Fe^{3+}{}_{15}Al_{25}$, and the subgroup 3 spinels from the orthopyroxenite blocks have distinctively high Al/Cr ratios and plot near the Al apex at $Cr_{15}Fe^{3+}{}_6Al_{79}$. The spinels from subgroups 1 and 2 define a weak trend (side B) of increasing Al/(Al + Cr) with decreasing Fe^{2+}/(Mg + Fe^{2+}).

In comparison to other major mafic-ultramafic intrusions, chromite from the Munni Munni Complex has chemical affinities with chromite from the Bushveld Complex and the Great Dyke (Fig. 35). Subgroup 1 chromites partly overlap the Bushveld chromitite field and are slightly more Fe^{3+} rich relative to the dunite-chromite association of the Great Dyke. Subgroup 2 chromites contain more Fe^{3+} than the subgroup 1 chromites, and fall into the same compositional fields as the silicate-hosted chromite from the Bushveld Complex and the poikilitic harzburgite chromite field of the Great Dyke. The subgroup 2 chromites are weakly enriched in Fe^{3+} and Al, as in the Stillwater and Great Dyke intrusions. The subgroup 3 aluminous spinels (shown in the small ternary diagram of Fig. 35) have no chemical similarities with spinel from the major intrusions shown.

Duke (1988) noted that the mg of chromites in layered intrusions varies over a greater range than their Cr/(Cr + Al) ratio (Fig. 36). Chromites of subgroup 1 show a similar variation in mg-to-Cr/(Cr + Al) ratios to chromites from the Bushveld, Stillwater, and Bird River intrusions, but are significantly poorer in Mg than chromites from the Great Dyke. Subgroup 2 chromite has a much wider distribution within the layered intrusion field, and the subgroup 3 spinels plot near spinels from the Bay of Islands at the Cr-poor part of the field defined for ophiolitic intrusions. This is coincidental and there is no suggestion here that subgroup 3 spinels are of ophiolitic origin.

The origin of the aluminous spinels in the orthopyroxenite blocks is unknown. The fine-grained (< 1 mm) orthopyroxenite host rocks have strong adcumulus textures, and delicate layering, and there is little evidence of pervasive alteration or replacement. Eales & Marsh (1983: fig. 1) have documented the variation of Al-Cr-(Fe^{3+} + 2Ti) for 825 spinels from various geological settings (not shown here). Chromite from Munni Munni subgroups 1 and 2 plot in the field defined by mafic layered intrusions. Aluminous spinels of subgroup 3 fall well outside this field, but overlap in composition with spinels from a number of settings, namely alpine peridotites, alkali basalts, and nodules in kimberlites. A trend towards Al-enriched spinels is apparent in some layered intrusions, such as the Rhum Complex, Scotland (Henderson & Suddaby, 1971; Henderson,

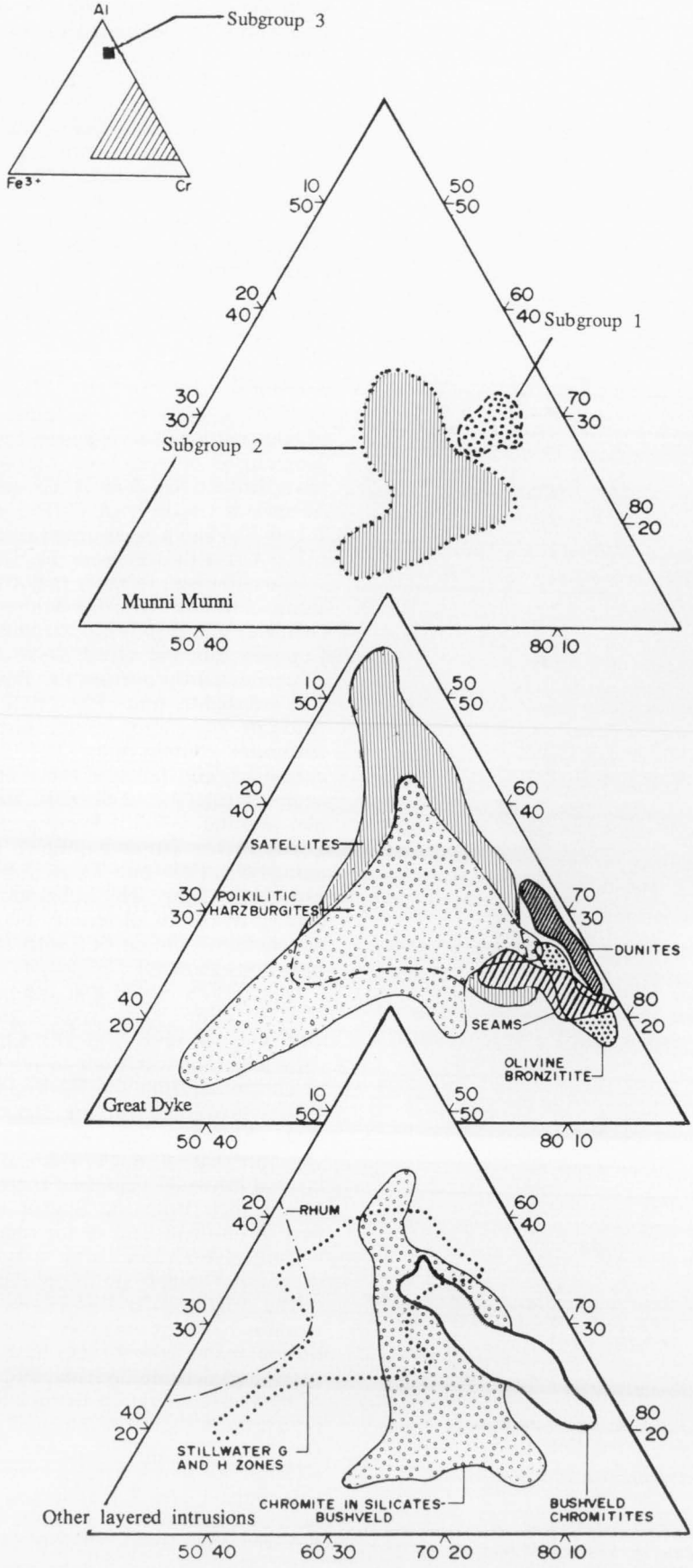

Fig. 35. Variations in Cr-Al-Fe^{3+} in Cr-bearing spinel from the Munni Munni Complex, Eastern Munni Munni Dyke, Great Dyke and other layered intrusions. The position of each ternary plot is represented by the shaded area in the small key Al-Cr-Fe^{3+} diagram. The plots for the Great Dyke and other layered intrusions are modified after Wilson (1982). Spinel subgroups as in Figure 34.

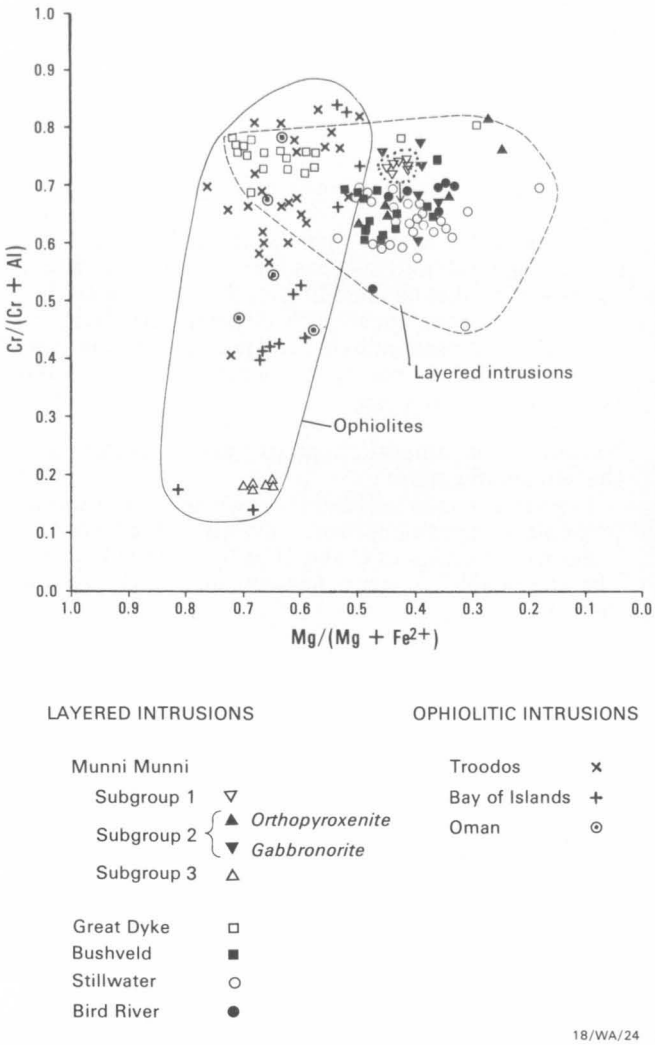

Fig. 36. Variations in Cr/(Cr + Al) with Mg/(Mg + Fe^{2+}) for Cr-bearing spinel from the Munni Munni Complex and Eastern Munni Munni Dyke, and various layered and ophiolitic intrusions. Modified after Duke (1988).

1975), Wingellina Hills Complex, central Australia (Ballhaus & Glikson, 1989), and the Panton Sill, WA (Hamlyn & Keays, 1979). This Al enrichment has been explained by late-stage reactions, or continuous re-equilibration during the magmatic and subsolidus stages, or rapid depletion of Cr and compositional gradients in crystallising magmas. In contrast to some of the Wingellina spinels that have re-equilibrated during granulite-facies metamorphism, the Al/Cr ratios of the aluminous spinels at Munni Munni are significantly higher than those from the Rhum and Panton intrusions.

Two major mechanisms can account for the compositional variation of spinels: (1) variations in the physical or chemical parameters of the parent magma during the early crystallisation (cumulus) stage; and (2) reaction with adjacent silicates or intercumulus liquid, either during the postcumulus stage or the subsolidus stage (Hamlyn & Keays, 1979). Henderson (1975) defined two reaction trends for the Cr-spinels from the Rhum intrusion. He found that spinels in chromite-rich layers or in peridotite adcumulates have compositions that show a reaction trend involving a marked increase in the Al/Cr ratio and little variation in Fe^{3+} (Al trend); whereas chromite in cumulates that contain trapped liquid define a trend involving enrichment of Fe^{3+} and depletion of Al (Fe trend). The Al trend is believed to have resulted from the postcumulus reaction of the spinel with cumulus olivine, and either plagioclase or a liquid rich in the plagioclase component, and the Fe trend was due to postcumulus reaction of the spinel with trapped intercumulus liquid alone. Olivine and plagioclase are rare accessory minerals in the Munni Munni orthopyroxenite adcumulates and there is no textural evidence for the formation of the subgroup 3 spinels by postcumulus reaction involving cumulus and/or intercumulus components. Olivine in the orthopyroxenites shows little evidence of reaction; in fact, its abundance increased due to postcumulus growth, and plagioclase forms rare inclusions, indicating that the small amounts of melt involved in these strongly modified adcumulates were not rich in a plagioclase component. The aluminous character of the spinels is believed to have been inherited during the primary crystallisation stage and was controlled by the composition of a parent magma (i.e. mechanism 1 above) that was distinctly different in composition to the magma that formed the Munni Munni Complex. Other variables, such as fO_2 and temperature, were also probably important in determining the composition of the aluminous spinels. Alternatively, the aluminous-spinel-bearing blocks may have formed from SiO_2-rich contamination products near the roof of the intrusion and may have descended via density flows to the ultramafic/gabbroic contact during a major overturn of the magma chamber.

Magnetite-ilmenite. Cumulus Fe-Ti oxides occur as small disseminated anhedra (< 1 vol. %) in the middle levels of subzone A of the gabbroic zone and as composite coarse grains (up to 10 vol. %) at higher stratigraphic levels. Ilmenite occurs as small-scale and coarse-bladed exsolved lamellae, and more commonly as coarse granules, within the titaniferous magnetite host. The consistent increase in the modal proportions of the oxides and the increase in the ilmenite to magnetite ratio up-section reflect closed-system fractionation processes that involved a progressive enrichment of Ti in the magma. Coexisting titaniferous magnetite and ilmenite grains were analysed from the middle and upper parts of the gabbroic subzone A.

Ilmenite shows no obvious systematic variation in TiO_2 contents up the gabbroic zone, although there is a suggestion that ilmenite from the middle parts of the zone has marginally higher TiO_2 contents (up to 51.6%) relative to ilmenite above the 3425 m level (47.3–49.6%). However, the heterogeneous compositional nature of the exsolved ilmenite granules is indicated by the similar magnitude of variation in composition between grains in the same rock to the variations observed for all grains. Manganese is a significant minor component of ilmenite, particularly at the lower stratigraphic levels, with MnO_2 contents of 4.6–6.1% at 2377 m, decreasing to 1.7–2.3% near the top of subzone A. This is the reverse of the trend documented for ilmenite from the anorthositic Bjerkrem-Sogndal intrusion, Norway (Duchesne, 1972a), and may indicate that Mn preferentially partitioned into pyroxene during fractionation and hence diminished its availability for the crystallisation of the oxide phase in the upper parts of the subzone. Ilmenite is ferrian throughout subzone A, with Fe_2O_3 contents between 2.2 and 12.0%, and has lower Cr_2O_3 (< 0.05%) than the coexisting titaniferous magnetite. Low concentrations of MgO (< 0.05%) and Al_2O_3 (< 0.06%) characterise the ilmenite granules since these oxides also preferentially partition into the early crystallising silicates.

The coexisting titaniferous-magnetite host grains show a wide range in TiO_2 contents from 0.1 to 12.7%, with most grains having between 3.5 and 11.5% TiO_2. This range is similar to that documented for magnetite from gabbroic rocks by Buddington & Lindsley (1964: fig. 7). In the middle part of the subzone there appears to be a positive correlation between the TiO_2 content of the spinel host and the TiO_2 content of the exsolved ilmenite component. However, at higher stratigraphic levels the relationship is obscure. Major and minor element trends of titaniferous magnetite with stratigraphic height are not well defined because of the compositional heterogeneity (due to subsolidus exsolution) of the grains. Minor amounts of Al (0.1–4.0% Al_2O_3), V (0.7–2.5% V_2O_3), and Cr (up to 0.2% Cr_2O_3) have substituted for Fe^{3+}, and minor to trace amounts of Mn (up to 0.8% MnO), Zn (up to 0.3% ZnO), and Ni (up to 0.1% NiO) have substituted for Fe^{2+} in titaniferous magnetite.

Sulphides. Pyrrhotite, pentlandite, and chalcopyrite from basal gabbronorite of subzone A′ (2 m level) and from the porphyritic plagioclase websterite layer of subzone I (1845.4 and 1846 m levels) were analysed to investigate if sulphides from different mineralised settings in the intrusion have distinctive chemical features. Sulphides (0.1–1.0 vol. %) in the subzone A′ rocks are dominated by pyrrhotite, with lesser amounts of pentlandite and chalcopyrite. Sulphides from subzone I (up to 3.0 vol. %) have a higher pentlandite-to-pyrrhotite ratio and are richer in chalcopyrite than the subzone A′ sulphides. The contrasting modal and chemical features of the sulphide assemblages reflect the different cooling rates in the various parts of the intrusion and the incompatible and compatible behaviours of Cu and Ni, respectively, during crystal fractionation.

Pyrrhotite from the basal rocks has a higher Ni content (0.4–0.6%) than pyrrhotite (0.1–0.5% Ni) from near the ultramafic/gabbroic zone contact. The partitioning of Ni into both sulphide and olivine throughout the ultramafic zone is believed to have caused the low Ni contents in pyrrhotite from higher stratigraphic levels. The large range of Ni concentrations in pyrrhotite from subzone I may be due to extremely small exsolved pentlandite components in the slowly cooled pyrrhotite grain rather than a general substitution of Ni for Fe in the pyrrhotite lattice. It is not known what influence the non-equilibrium conditions that prevailed in the basal contact region had on the composition of pyrrhotite, but rapid cooling would probably have inhibited the unmixing of pentlandite from the pyrrhotite host. In contrast to Ni, pyrrhotite from subzone I has a variable, but higher, Cu content (up to 0.2%) compared to pyrrhotite from the basal contact (< 0.04%). The higher Cu/(Cu + Ni) ratios of these pyrrhotites (up to 0.5) relative to the basal pyrrhotites (< 0.09) highlights the more incompatible behaviour of Cu relative to Ni during crystal fractionation. The Munni Munni pyrrhotites have almost identical Fe (59.3 to 61.9%) and Cu (< 0.04 to 0.2%), but higher Ni (0.1 to 0.6%) contents relative to pyrrhotite (59.9 to 61.6% Fe, 0.05 to 0.2% Cu, and 0.05 to 0.2% Ni) from the Dunka Road deposit of the Duluth Complex (Rao & Ripley, 1983). Mathison & Marshall (1981) have shown that pyrrhotite from the nearby Mount Sholl intrusion has high Ni (0.7%).

Chalcopyrite from both mineralised settings displays little minor-element substitution. Trace levels of Zn (~ 0.04%) may be associated with chalcopyrite from subzone I, but further detailed analyses involving longer count times are required to confirm these low contents. Zinc may replace Cu or Fe, or occur as an admixed impurity such as sphalerite in chalcopyrite, or limited amounts of ZnS may be present as a solid solution in $CuFeS_2$ (Deer & others, 1978). Pentlandite from the basal contact is characterised by Co contents that range from 4.4 to 6.4%. There is an antipathetic relationship between Co and Ni, so that Co is probably replacing Ni in the pentlandite structure. Pentlandite grains from subzone I disintegrated when exposed to the microprobe beam (ideally a low-voltage defocused beam analysis should be carried out on these grains). This contrasting behaviour suggests they may be of different composition from pentlandite in the basal sulphides, e.g. a volatile component, such as perhaps Hg, may be present in the pentlandite since Hg is a common constituent of various platinum-group minerals from the same sulphide assemblages.

Variations in mineral chemistry across cycles in the ultramafic zone

The variations in olivine, clinopyroxene, and orthopyroxene compositions were investigated across five cycles within subzones C and D of the ultramafic zone. The stratigraphic interval 664–982 m was chosen for the sampling traverse (at ~ 10 m spacing) since it is equidistant from the basal and upper contacts of the ultramafic zone where various mineralising and magmatic events occurred. The main purpose was to determine whether the compositional trends of the cumulus and intercumulus minerals across the units resulted from open- or closed-system fractionation in the chamber. The cycles are numbered 1 to 5 in ascending order. The complete cycles of 60 to 80 m thickness show normal fractionation trends from lherzolite at the base of a cycle to olivine websterite and, more rarely, to websterite at higher levels. The transition in rock types represents a system involving varying modal proportions of cumulus olivine and cumulus clinopyroxene in the lower parts of the cycles, and increasing amounts of intercumulus orthopyroxene at the expense of olivine towards higher stratigraphic levels. Only the upper part of cycle 1 was sampled and is represented by olivine websterite and websterite. No minerals hosted by websterite were analysed in the upper parts of cycles 2 to 5.

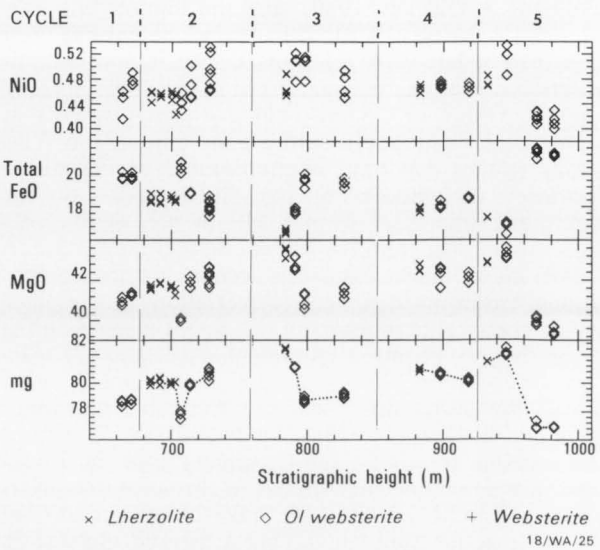

Fig. 37. Munni Munni Complex: variations in mg, MgO, Total FeO, and NiO (weight %) in olivine across cyclic units 1 to 5 of subzones C and D of the ultramafic zone.

Olivine mg trends (Fig. 37) for all cycles are consistent with those expected from open-system fractional crystallisation involving new pulses of hot, primitive magma of similar or identical composition into an evolving magma chamber. Discontinuities in mg trends are coincident with major lithological breaks in the cycles. The basal lherzolite components of cycles 2 to 5 have more primitive olivine compositions than olivines from the pyroxenite components of the underlying cycles. Olivine mg ranges from 83 to 79 in lherzolite and from 81 to 76 in olivine websterite. The trend of decreasing mg with height varies for the different cycles: cycles 2 and 4 show a much flatter gradient than cycles 3 and 5. Reversal trends in mg characterise the upper parts of cycles 2 and 4 and to a lesser extent cycle 3. Extremely fractionated olivine at the 707 m level defines the lower limit of the reversal trend in cycle 2. Nickel contents generally show sympathetic trends with mg in cycles 3 and 5, but for the less differentiated cycles 2 and 4, Ni has flat, or in places weak, reversal trends with stratigraphic height. This is not caused by preferential remobilisation of Ni by serpentinisation in the more olivine-rich rocks, since the Cr content of clinopyroxene and orthopyroxene in cycle 2 shows similar reversal trends. The reversal trends are probably related to primary magmatic processes described below.

The S-undersaturated character of the olivine-rich cumulates in cycles 1 to 5 and the absence of any major Ni-bearing silicate phases allows one to estimate the partitioning of Ni between olivine and a silicate liquid (i.e. Kd_{Ni} = concentration of Ni in olivine/concentration of Ni in liquid). An approximation of Kd_{Ni} can be obtained by comparing the maximum Ni content of olivine in the cycles (4320 ppm) to the amount in the parent magma (366 ppm: Table 29). On this basis, Kd_{Ni} is about 12, which is consistent with the experimental results of about 2 for a komatiitic melt, and 8 to 14 for a basaltic melt (Arndt, 1977). The determined Kd_{Ni} for the Skaergaard intrusion is 12 (Wager & Mitchell, 1951: p. 154), and between 10 and 15 for the Muskox intrusion (Irvine & Smith, 1967: p. 46). Minor amounts of Ni (up to 0.12% NiO) in coexisting cumulus clinopyroxene apparently did not affect the Kd_{Ni} ratios in olivine at Munni Munni.

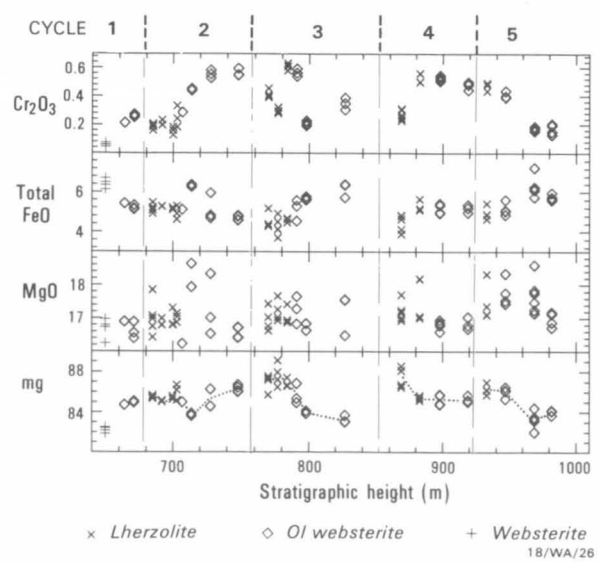

Fig. 38. Munni Munni Complex: variations in mg, MgO, Total FeO, and Cr_2O_3 (weight %) in clinopyroxene across cyclic units 1 to 5 of subzones C and D of the ultramafic zone.

Clinopyroxene (Fig. 38) has trends sympathetic to olivine across the five cycles. The most primitive compositions, of mg_{89}, are associated with the basal lherzolites and these progressively decrease to a minimum of mg_{82} for the overlying olivine websterites. The displacement to more primitive compositions across the upper contacts of the cycles is greater (2–5 mg units) than for olivine (2 mg units). Clinopyroxene mg trends indicate that the upper part of cycle 1 may comprise at least two small-scale cycles. The chemical trends in the upper parts of cycle 2 contrast with the trends of cycles 3 to 5, with mg and Cr contents consistently increasing with height. This is the reverse of that expected during crystal fractionation. This anomalous behaviour occurs marginally later in the sequence than with the mg and Ni content of olivine and mg of orthopyroxene. A possible explanation for the reversals is that the upper part of cycle 2 represents a hybrid zone formed from the mixing of an evolved magma component from cycle 2 with a more primitive magma component from cycle 3. This would have the effect of increasing the primitive character of the magma in the upper part of cycle 2 and decreasing it in the lower part of cycle 3. This latter feature may be reflected by the slightly lower mg of clinopyroxene in lherzolite at the 770 m level relative to that at the 780 m level (Fig. 38). The more abrupt chemical trends at the interface of cycles 3 to 4 and 4 to 5 indicate that magma mixing may have been inhibited in these regions by a hiatus before the emplacement of the new pulse or by a contrast in fluid dynamical properties, such as density and viscosity, between the resident and new magma pulses. Alternatively, the abrupt chemical trends could be due to thermal erosion ('beheading') of the resident cyclic units by new pulses; however, there is no field evidence, such as cross-cutting structures, dimpling of contacts between rock units, and potholing, as seen in other intrusions (Irvine & others, 1983; Campbell, 1986; Eales & others, 1988), to indicate such a process. The coexistence of both abrupt (cycles 3 to 5) and gradual (cycle 2) reversals in cryptic trends indicates that it is unlikely that the gradual reversals resulted from the diffusive mixing of magma components by compositional stratification due to double-diffusive convection (Chen & Turner, 1980; Huppert & Sparks, 1984).

Eales & others (1990a,b) have documented similar oscillatory fluctuations in mineral and whole-rock chemical trends in cyclic units of the Critical Zone of the Bushveld Complex. They noted both (1) smooth reversal trends defined by a gradual increase in primitive character, followed by a gradual decline with height, and (2) more abrupt reversal changes at major rock interfaces at higher stratigraphic levels. The contrasting reversal styles were attributed to declining volumes of fresh mafic magma being injected, and increasing contrasts between the physical properties of resident and newly emplaced liquid at higher levels. Mathison & Hamlyn (1987) also noted gradual reverse cryptic trends over 650 m-thick sections of mafic cumulates in the McIntosh intrusion, in Western Australia. They also invoked magma mixing, and discounted alternative mechanisms, such as the progressive reduction in the degree of supercooling (Campbell, 1978) or postcumulus infiltration metasomatism (Irvine, 1980b), on the basis that the reversals are too great and spread over too large a stratigraphic interval. Prendergast & Keays (1989) proposed that upward reversals of pyroxene mg in the Great Dyke were due to magma replenishment, overturning, and supercooling in a double-diffusive convecting system.

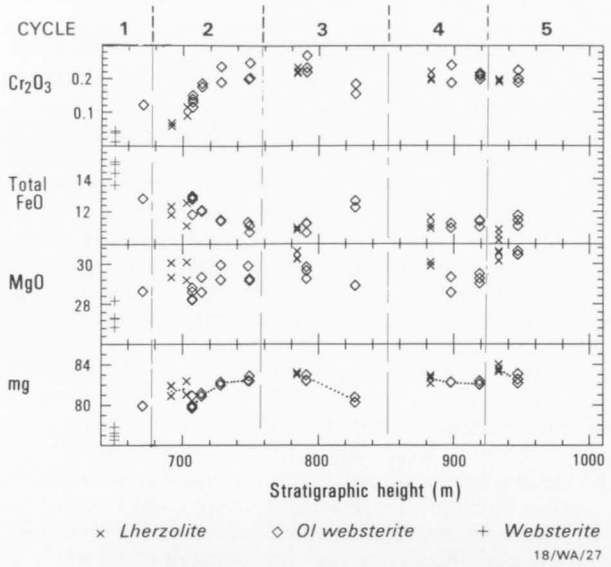

Fig. 39. Munni Munni Complex: variations in mg, MgO, Total FeO, and Cr_2O_3 (weight %) in orthopyroxene across cyclic units 1 to 5 of subzones C and D of the ultramafic zone.

The mg and Cr trends of intercumulus orthopyroxene (Fig. 39) are generally in accordance with that of olivine and clinopyroxene, although the chemical definition of the different cycles is not as pronounced as that displayed by the cumulus minerals. Reverse fractionation trends are typical of cycle 2, whereas normal fractionation profiles occur in cycles 3 to 5. Despite its intercumulus status and the preferential partitioning of Cr into clinopyroxene, the Cr content of orthopyroxene is a sensitive indicator of fractionation through most cyclic units. The mimicking of the composition of orthopyroxene with the cumulus components indicates that the melt was in physical communication, i.e. did not migrate to any significant distance from the cumulus pile during the open-system crystallisation.

Compositional trends of clinopyroxene across the ultramafic/gabbroic zone contact

Clinopyroxene is one of the few minerals that persists across the ultramafic/gabbroic zone contact as a cumulus phase, so its compositional trends may provide important insights into the magmatic processes which occurred in this region and the nature of the magma(s) that formed both zones. Core compositions of clinopyroxene were documented for the stratigraphic interval 1745–2000 m and the relationships between core and rim compositions were investigated for the stratigraphic interval 1757–1870m. This interval encompasses all of subzone I and the lower part of subzone A of the gabbroic zone. The variation of major-element compositions of clinopyroxene cores is summarised in Figures 40–42 and the core-to-rim relationships are shown in Figure 43.

In the lower half of subzone I (1750–1800 m), fractionation trends are weak: the mg of clinopyroxene in peridotite, olivine pyroxenite (equivalent to olivine websterite and olivine clinopyroxenite), and plagioclase websterite decreases from 86 to about 84 (Fig. 40). These values are similar in magnitude to the mg values documented below the 1750 m level (Fig. 30). At the 1808 m level, clinopyroxene shows the first evidence of significant Fe enrichment: the mg decreases to 83–81 in websterite, followed by a further decrease to 79–76

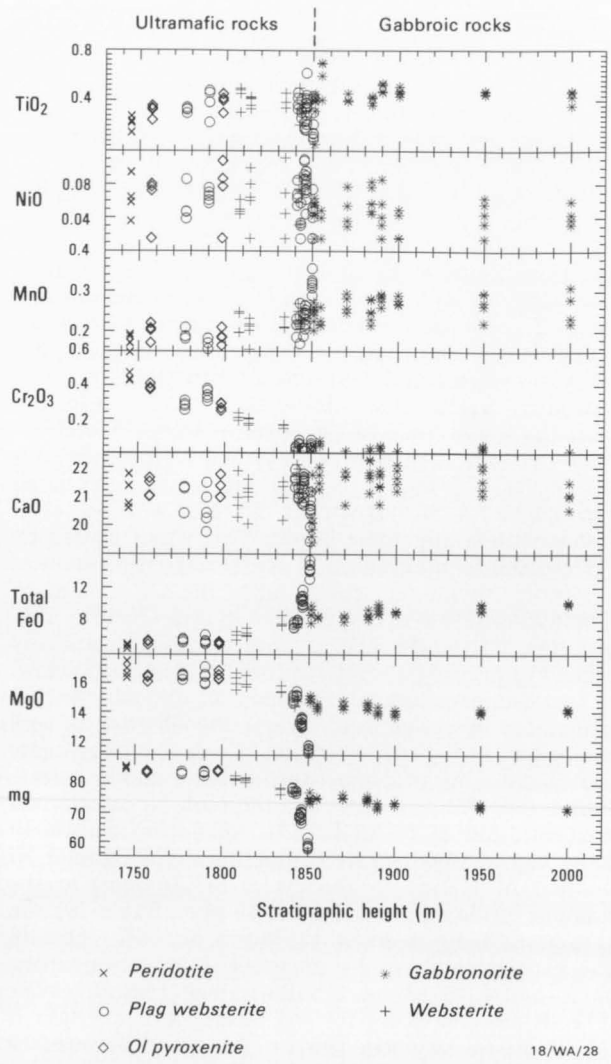

Fig. 40. Munni Munni Complex: variations in mg, MgO, Total FeO, CaO, Cr_2O_3, MnO, NiO, and TiO_2 (weight %) in clinopyroxene across the ultramafic/gabbroic zone contact.

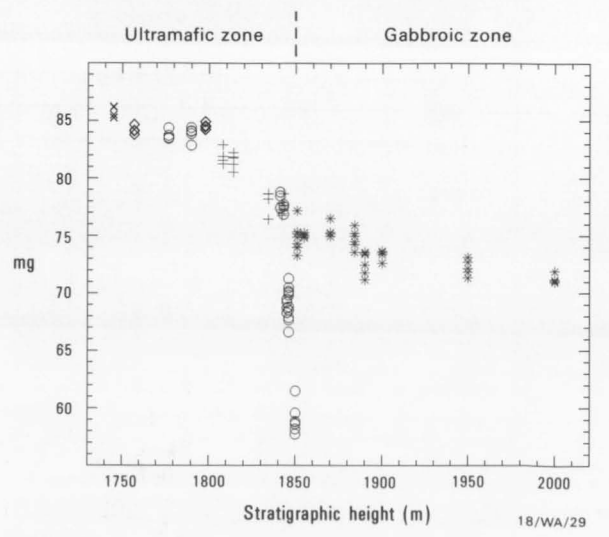

Fig. 41. Munni Munni Complex: variations in mg in clinopyroxene for the stratigraphic interval 1750–2000 m. Symbols as in Figure 40.

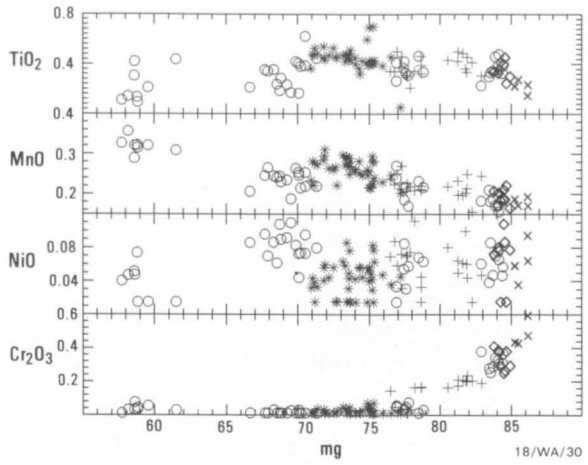

Fig. 42. Munni Munni Complex: variations in Cr_2O_3, NiO, MnO, and TiO_2 (weight %) in clinopyroxene with mg for rocks near the ultramafic/gabbroic zone contact. Symbols as in Figure 40.

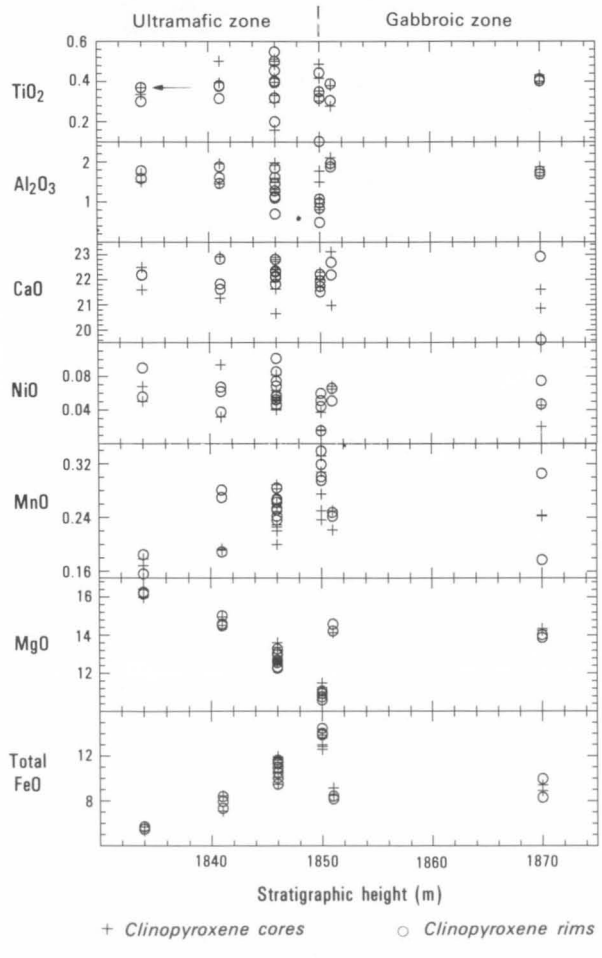

Fig. 43. Munni Munni Complex: variations in core and rim compositions of clinopyroxene across the ultramafic/gabbroic zone contact. The arrowed sample is from the 1757 m stratigraphic level.

in porphyritic plagioclase websterite at 1841 m. This enrichment trend accelerates in the upper 5 m of the ultramafic zone, mg rapidly decreasing from 71–67 at 1845 m to a minimum of 58 directly below the ultramafic/gabbroic zone contact, at 1849.75 m. Such a marked change to more evolved compositions is attributed to closed-system crystallisation of clinopyroxene in a stagnant magma containing large amounts of trapped melt. This is supported by the strongly orthocumulate textures of the rocks, compositional zoning of clinopyroxene, and the associated change to more sodic plagioclase. Clinopyroxene compositions in the basal gabbronorites of the gabbroic zone show a consistent decrease in mg from 77–73 at 1851 m to 72–71 at the 2000 m level.

The consistent mg trends of clinopyroxene across the zone contact is evident from Figure 41. There is no major regional compositional discontinuity between the two zones (excluding the 1845–1850 m interval), or a change in the gradient of decreasing mg for the interval 1800–1900m. The compositional trends reinforce the suggestion that clinopyroxene in the 1808–1845m interval of subzone I crystallised from a hybrid magma that resulted from the mixing of the magma(s) that formed both the ultramafic and gabbroic zones. The mg of clinopyroxene in the hybrid rocks is an approximate average between the primitive compositions of the ultramafic zone cumulates and the more evolved compositions in the gabbroic zone cumulates. Clinopyroxene continued to fractionate in the hybrid magma, as shown by the decreasing gradient in mg trends above the 1808 m level and the abrupt change to more evolved compositions near the top of the zone. The continuity of mg trends above 1808 m supports the concept of a single-magma system. However, since much of this continuity could be attributed to homogenisation processes during magma mixing and protracted fractionation processes after magma mixing, the less appealing option of chemically unrelated magmas cannot be entirely excluded.

Chrome in clinopyroxene generally displays trends sympathetic to those of mg (Fig. 40), although Cr_2O_3 contents appear to 'anticipate' mg trends by starting to decrease as far down as the 1500 m level of the ultramafic zone (Fig. 30). In subzone I, there is a consistent decrease in Cr_2O_3, from 0.60–0.40% at 1745 m, to 0.30–0.25% at 1798 m, to 0.17–0.15% at 1834 m. Above 1841 m, most clinopyroxenes have $\leq$ 0.05% Cr_2O_3. This marked depletion precedes the dramatic drop in mg by about 4 m. Similar low Cr_2O_3 values persist into the basal levels of the gabbroic zone. Figure 42 shows there is a positive correlation between mg and Cr_2O_3 contents for most rock types across the zone contact. The high-mg, high-Cr clinopyroxene in peridotite and pyroxenite fall along the same trend as the low-mg, low-Cr clinopyroxene in gabbronorite of the gabbroic zone. Only clinopyroxenes ($< mg_{71}$) from the evolved plagioclase websterite at the top of the ultramafic zone lie off the trend.

Clinopyroxene from the top of the ultramafic zone has a normal compositional zoning that involves variations in Fe, Mg, Mn, and Al contents (Fig. 43). Clinopyroxene below the 1841 m level is generally unzoned, whereas at the 1846 m level, the rims are slightly enriched in Mn and Al relative to their cores, but show no obvious variation in Fe or Mg. The most prononced zoning is evident at the 1849.75 m level, where rims are enriched by 1.0–2.0% FeO, 0.2–0.9% MnO, and depleted by up to 0.5% MgO and 1.3% Al_2O_3 relative to their cores. The depletion of Al in the rim is unexpected, since, in most of the intrusion, there is a negative correlation between Al and mg for clinopyroxene. No systematic compositional trends between core and

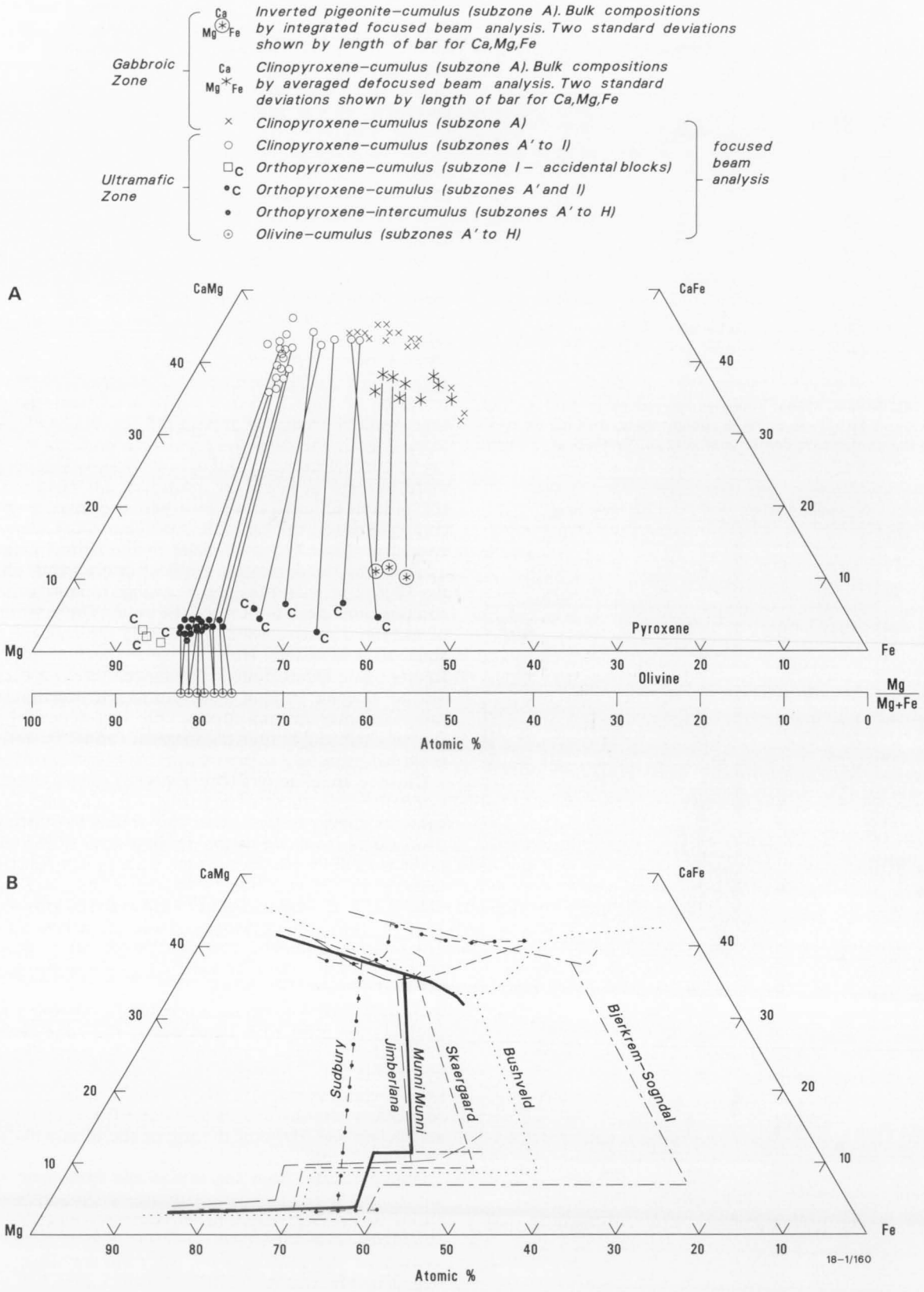

Fig. 44A–B. (A) Summary of Munni Munni Complex pyroxene fractionation trends in the pyroxene quadrilateral (part of the Ca-Mg-Fe pyroxene triangle). Coexisting Ca-rich and Ca-poor pyroxene pairs and coexisting pyroxene-olivine pairs are indicated by tie lines. All the cumulus Ca-poor pyroxenes indicated by a 'c' symbol (and their coexisting Ca-rich pyroxenes) are from subzone I, except the most fractionated Ca-poor pyroxene at $Ca_4Mg_{57}Fe_{39}$, which is from subzone A'. Two standard deviations of the Ca, Mg, and Fe components for estimations of the bulk composition of clinopyroxene and inverted pigeonite are also indicated. Mineral compositions were determined by various electron microprobe techniques listed in the legend and detailed in Appendix 1.5. (B) Comparison of the Munni Munni pyroxene fractionation trend with those from other layered mafic-ultramafic intrusions. The trends shown for the other intrusions are from various sources quoted by Campbell & Nolan (1974).

rim are evident for clinopyroxene from the lower parts of the gabbroic zone.

The postcumulus overgrowths on cumulus clinopyroxene grains in orthocumulates near the top of the ultramafic zone are believed to reflect non-equilibrium crystallisation in a closed system. It is proposed that small residual components of fractionated Fe- and Mn-enriched melt derived from the hybrid magma may have become trapped below early crystallising plagioclase-rich basal cumulates of the gabbroic zone and may have continued to crystallise slowly in a stagnant magma. During this protracted period of closed-system fractionation, the compositions of the clinopyroxene grains were continually readjusting to the changing composition of the melt; thus there was almost unrestricted chemical exchange between the melt and the cumulus grains.

Evolution of pyroxene in the Munni Munni Complex

The compositions of the Munni Munni Ca-rich and coexisting Ca-poor pyroxenes are summarised in Figure 44. For pyroxene in the gabbroic zone (Fig. 44A), bulk compositions by averaged defocused- and focused-beam analysis of clinopyroxene are compared and the estimated bulk compositions of three inverted-pigeonite grains by integrated analysis are shown (see Appendix 1.5 for method). Most of the Ca-poor pyroxenes shown in Figure 44A comprise intercumulus bronzite from subzones A′–H and cumulus bronzite and hypersthene from the upper part of subzone I of the ultramafic zone. Compositions of cumulus orthopyroxene from the spinel-bearing orthopyroxenite blocks and from a basal gabbronorite of subzone A′ (at $Ca_4Mg_{57}Fe_{39}$) are also indicated.

The Munni Munni pyroxenes display fractionation trends generally similar to those of other large differentiated mafic-ultramafic intrusions of tholeiitic affinity (Fig. 44B). The decrease in the Ca component with increasing fractionation for the Ca-rich pyroxenes and the enrichment of Fe for the transition orthopyroxene-to-inverted pigeonite are features common to other major intrusions. Munni Munni Ca-rich pyroxenes show a decrease in Ca with fractionation similar to that of the Skaergaard and Bushveld intrusions, with the replacement of Ca and Mg in almost equal proportions by Fe. Clinopyroxenes that coexist with the cumulus orthopyroxene grains from subzone I and A′ (Fig. 44A) plot above the Ca-rich pyroxene fractionation trend, and their distribution is more consistent with clinopyroxenes from the gabbroic zone that were analysed by a focused-beam technique (cross symbol). As with the latter clinopyroxenes, those of subzones I and A′ are also thought to be non-representative estimates of the bulk composition of the grain since they were also determined by a focused beam.

Most tie-lines between Ca-rich and Ca-poor pyroxene pairs are sub-parallel throughout the pyroxene fractionation trends, indicating they are equilibrium assemblages. Similarly, the Ca-poor-pyroxene-to-olivine tie-lines show no evidence of crossing or abrupt changes in gradient. An exception is the crossing of tie-lines for the most fractionated Ca-poor pyroxene in the ultramafic zone (at composition $Ca_4Mg_{57}Fe_{39}$). This hypersthene from the basal gabbronorites of subzone A′ has an anomalously high Fe content relative to the Fe content of its coexisting Ca-rich pyroxene, and indeed relative to other Ca-poor pyroxenes from both zones. These features support the view that equilibrium conditions were not achieved in the lower parts of the ultramafic zone. Another pyroxene pair at more primitive compositions also has crossed tie-lines. This may indicate disequilibrium, although the crossing of the tie-lines at a sharper angle relative to the other pyroxene pair may indicate analytical inconsistencies only (Nienaber-Roberts, 1986).

The Ca minimum at the limit of the two-pyroxene field has not been defined in this study. The limit of the two-pyroxene field in Figure 44B is tentatively indicated by the compositions of the most evolved coexisting pair of clinopyroxene and inverted-pigeonite grains that were analysed, e.g. at approximately $Ca_{36}Mg_{37}Fe_{27}$ for the Ca-rich pyroxene and $Ca_{11}Mg_{49}Fe_{40}$ for the Ca-poor pyroxene. This is a minimum since some Ca-rich pyroxenes have more evolved compositions and the most fractionated coexisting inverted pigeonite shown in Figure 44B is from the 2859 m level, although crystallisation of inverted pigeonite persists to much higher stratigraphic levels. The bulk composition of these grains was not determined owing to intense alteration, but they are predicted to fall along the extrapolated dashed line of the Ca-poor pyroxene trend shown in Figure 44B. Hence, the limit of the two-pyroxene field for the Munni Munni Complex may fall between those for the Skaergaard and Bushveld intrusions.

It is not known if more fractionated Ca-rich pyroxenes (e.g. from beneath the Fortescue Group) would display a trend to more Ca-rich compositions after the limit of the two-pyroxene field, or whether they would continue to decrease in Ca, as shown by the augite-ferroaugite series in the Dufek intrusion (Himmelberg & Ford, 1976) and the pyroxene series of the Palisades Sill (Walker & others, 1973). However, it is apparent that the most sub-calcic clinopyroxenes from Munni Munni are richer in Fe than the Sudbury, Jimberlana, and Skaergaard clinopyroxenes, and are similar in composition to the sub-calcic Bushveld clinopyroxenes.

The Ca-poor pyroxene trend of the Munni Munni Complex is defined by a continuous evolution with increasing stratigraphic height, from bronzite, to hypersthene, to inverted pigeonite. This compositional continuity and the transition from intercumulus to cumulus status supports the view that Ca-poor pyroxene from both zones is likely to be derived from parent magmas that are genetically related. Cumulus orthopyroxene from the orthopyroxenite blocks in subzone I also lie on the Ca-poor pyroxene fractionation trend, but their distribution at the Mg end of this trend is inconsistent with their high stratigraphic level and highlights their accidental origin. In addition, they are more primitive than the lowermost orthopyroxenes found in large layered intrusions, which are rarely more magnesian than mg_{85} (Wager & Brown, 1968; Atkins, 1969; Campbell & Borley, 1974; Nwe, 1976; Cameron, 1978). Their mg and aluminous spinel compositions are comparable with orthopyroxenes from cumulus ocean-floor peridotite (Hodges & Papike, 1976; Jaques, 1981), but there is no inference here that they are of such an origin.

The change from hypersthene to inverted pigeonite at Munni Munni occurs between $Ca_4Mg_{59}Fe_{37}$ and $Ca_{11}Mg_{53}Fe_{36}$, which is close to the boundary between magnesium pigeonite and intermediate pigeonite (nomenclature of Poldervaart & Hess, 1951). The orthopyroxene-pigeonite transition in the Munni Munni Complex is similar in composition to that in the anorthositic Bjerkrem-Sogndal intrusion of southwest Norway (Duchesne, 1972a, b), but at significantly more Fe-rich compositions than in the other intrusions (Fig. 44B). Atkins (1969: p. 239–240) excluded a Ca-poor

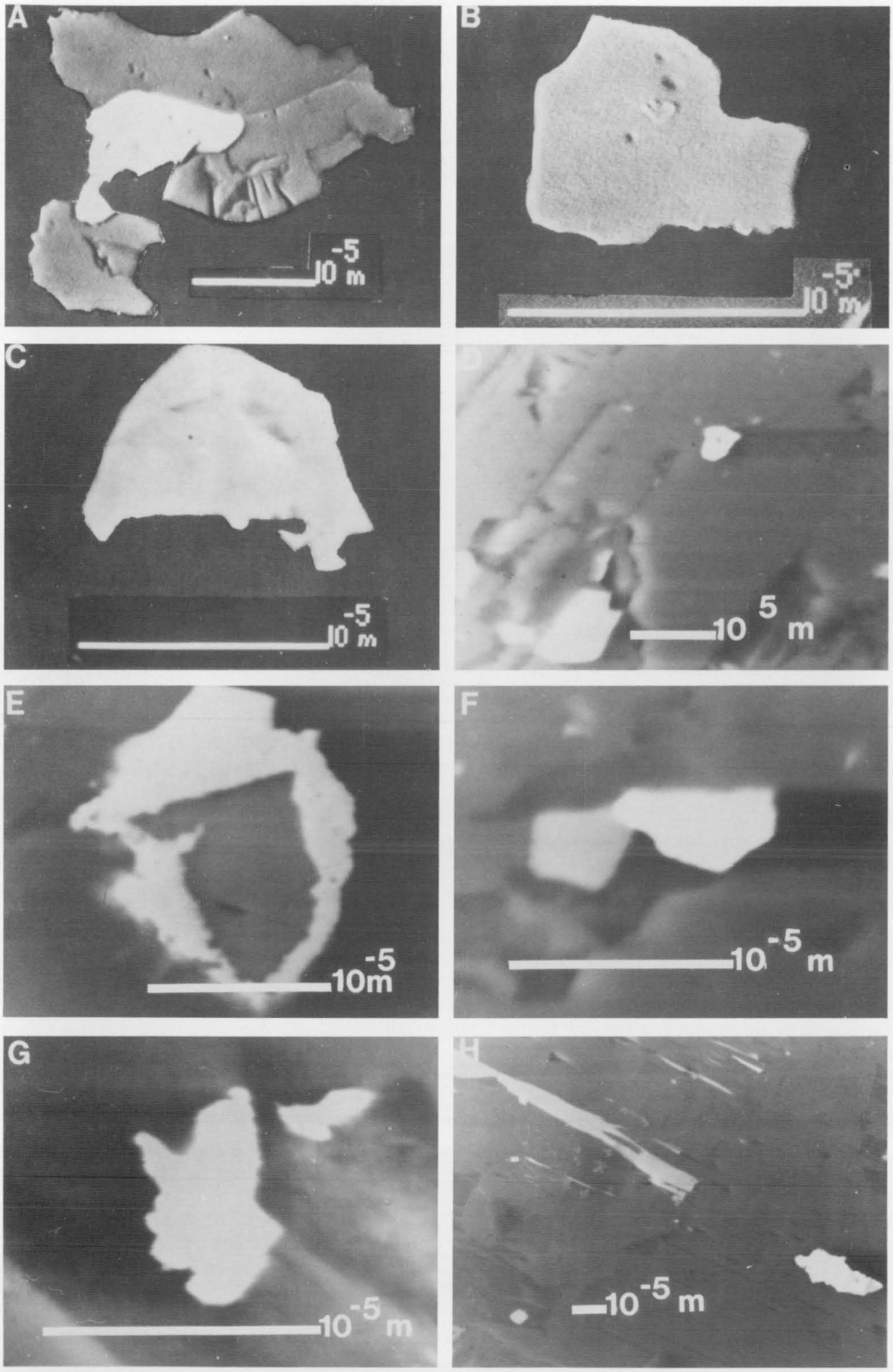

Fig. 45A-H. Munni Munni Complex: scanning-electron-microscope images of platinum-group minerals from the mineralised porphyritic websterite layer (subzone I). Diamond-drill core kindly provided by Hunter Resources Ltd.

A. Subhedral cooperite(PtS) prism associated with chalcopyrite and pentlandite aggregate. Note suturing of cooperite grain where enclosed by silicates (opaque) and subhedral faces where enclosed by base-metal sulphides.
B. Cooperite subhedron enclosed in silicates.
C. Cooperite anhedron enclosed in silicates.
D. Small, highly-reflective native platinum(Pt) subhedron enclosed in silicates and associated with base-metal sulphide grains.
E. Large sperrylite(Pt-As) grain surrounding and ?replacing pentlandite grain.
F. Sperrylite subhedron adjoining chalcopyrite grain.
G. Sperrylite anhedra enclosed in silicates.
H. Small horseshoe-shaped sperrylite anhedron (near top left-hand corner) closely associated with blades of chalcopyrite aligned along the cleavage in cumulus pyroxene grains.

pyroxene (analysis number 8a) for the Bushveld trend shown in Figure 44B that had exsolution features of an inverted pigeonite, but a Ca content too low for pigeonite. If one includes this analysis in the pyroxene trend, the Munni Munni orthopyroxene-pigeonite transition is almost identical to that of the Bushveld Complex. Moreover, Markgraaff (1976) has documented the orthorhombic to monoclinic Ca-poor pyroxene transition in the Upper Gabbro Unit of the western Bushveld Complex at mg_{63}, i.e. very close to the Munni Munni transition. The displacement of the orthopyroxene-pigeonite transition to more Fe-rich compositions at Munni Munni is attributed to the protracted crystallisation of orthopyroxene in stagnated magmatic conditions that involved low solidus temperatures in the upper parts of the porphyritic websterite layer.

Platinum-group-element mineralogy

Semi-quantitative analyses of the platinum-group minerals (PGMs) (SEM study, see Appendix 1.5) were carried out on drill core (provided by Hunter Resources Ltd) from a 3.5 km strike-length section of the mineralised porphyritic websterite layer of subzone I. The mineralogy of the PGMs is currently the subject of a detailed collaborative project between the AGSO and BRGM, France.

Drillholes, and the respective depths of the samples investigated in the SEM study, were: MMD 1 (64.4 and 65.6 m), MMD 3 (78.2 and 78.4 m), MMD 6 (148.6 m), MMD 10 (81.3 m), MMD 11 (114.0 m), and MMD 15 (90.4 m). Platinum and Pd contents for these intervals ranged from 960–2250 ppb Pt, and from 1880–3500 ppb Pd, whereas Cu and Ni showed greater variation from near-background levels of 150 ppm Cu and 200 ppm Ni, to 7600 ppm Cu and 2200 ppm Ni. Sulphide-poor (< 0.5 vol. %) samples are generally dominated by chalcopyrite with lesser pentlandite and pyrrhotite, whereas pyrrhotite and pentlandite are the dominant sulphides in the more sulphide-rich samples (up to 2.0 vol. %). Associated minor minerals identified during the SEM study were ilmenite, magnetite, pyrite, galena, and ?molybdenite.

Platinum- and Pd-bearing minerals were documented in all sections studied (Hoatson & England, 1986); minerals containing Rh and Ru were rare (Table 11, Figs 45 & 46). Iridium and Os-bearing phases were not detected, which is in accord with the extremely low whole-rock Ir and Os concentrations of the mineralised zone, e.g. ≤ 37 ppb Ir and ≤ 9 ppb Os for DDH MMD1. Platinum-dominant minerals (45 grains) are of similar abundance to the Pd-dominant minerals (42); arsenides, sulpharsenides, tellurides, mercury-bearing arsenides and native metals are the most common. *Sperrylite* (ideal formula of $PtAs_2$) is the most common, followed by *telluropalladinite* (Pd_9Te_4), *potarite* (PdHg) or *atheneite* ($(Pd,Hg)_3As$), *moncheite* ($PtTe_2$), *platarsite* (PtAsS), *native Pt* (Pt), and *native Pd* (Pd). Minerals of minor significance include *cooperite* (PtS), *braggite* (Pt,Pd)S, *?vincentite* $(Pd,Pt)_3(As,Sb,Te)$, *michenerite* (PdBiTe) or *kotulskite* (PdTe), *temagamite* (Pd_3HgTe_3), *isoferroplatinum* (Pt_3Fe) and various sulpharsenides of Pd. Platinum and Pd-bearing sulphides (cooperite, braggite, vysotskite, etc) form a subordinate group (10% of all grains) relative to the As-, Te-, Hg-bearing PGMs. Gold occurs as a rare argentiferous phase and as a minor component of Pd-Hg-As minerals.

Platinum-group minerals enclosed by unaltered Fe-Cu-Ni sulphides are commonly subhedral (Figs 45A and 46H). However, boundaries with hydrous silicate minerals are invariably sutured or cuspate (Figs 45A and 46B), indicating localised remobilisation of the PGM associated with replacement of the sulphide. Sperrylite was observed mantling and possibly replacing pentlandite (Fig. 45E) and, in one example, surrounded a core of silicates. Zoned sperrylite (rim) and platarsite (core) anhedra also occur in the talc-carbonate-chlorite matrix of silicified shear zones which traverse the mineralised websterite horizon. The shears contain up to 3.4 ppm Pt and 4.9 ppm Pd (R. N. England, personal communication, 1985), which are some of the highest PGE contents reported from surface material at Munni Munni. These examples perhaps illustrate the greater chemical mobility of the sulpharsenide minerals relative to the other PGMs during

Table 11. Platinum-group minerals in the Munni Munni Complex

Major components	*Number of grains*	*Percentage of grains examined*	*Probable mineral/s*	*Ideal formula*	*Size range (μm)*	*Mean size (μm)*	*Percentage of associations*
Platinum-dominant minerals							
Pt	4	5	Native Pt	Pt	2–6	4	Sil—100
Pt-Fe	2	2	?Isoferroplatinum	Pt_3Fe	2–6	4	Sil—100
Pt-S	2	2	Cooperite	PtS	12–15	14	Sil—50, Pent/Cpy—50
Pt-Pd-S	3	3	Braggite	(Pt, Pd)S	4–8	6	Sil—67, Pent—33
Pt-As	17	19	Sperrylite	$PtAs_2$	2–20	5	Sil—70, Cpy—20, Pent—10
Pt-As-S-Fe	7	8	Platarsite	PtAsS	2–10	5	Sil—100
Pt-As-S-Ru	1	1	?Platarsite	PtAsS	20	20	Cpy—100
Pt-Te	8	9	Moncheite	$PtTe_2$	2–30	8	Sil—100
Pt-Te-As-S	1	1	?Moncheite	$PtTe_2$	4	4	Sil—100
Palladium-dominant minerals							
Pd	4	5	Native Pd	Pd	4–8	6	Sil—100
Pd-Pt-S	2	2	Braggite	(Pd, Pt)S	2–25	12	Sil—100
Pd-Pt-As-Te	2	2	?Vincentite	$(Pd, Pt)_3(As, Sb, Te)$	4–10	7	Sil—100
Pd-S-As-Fe	3	3	Vysotskite	PdS	2	2	Cpy—100
Pd-S-Te-Fe	3	4	?		2	2	Sil—67, Py—33
Pd-Te	13	15	Telluropalladinite	Pd_9Te_4	2–12	5	Sil—80, Sil/Cpy—10, Cpy—10
Pd-Te-Bi	3	4	Michenerite	PdBiTe	2–8	5	Sil/Cpy—100
Pd-Hg-As	10	12	Atheneite Potarite	$(Pd, Hg)_3As$ PdHg	2–5	4	Sil—100
Pd-Hg-Te-Cu	2	2	Temagamite	Pd_3HgTe_3	2	2	Cpy —100
Au-dominant mineral							
Au-Ag	1	1	Argentian gold	(Au, Ag)	8	8	Sil—100

Overall association: Sil—69 occurrences (78% abundance), Cpy—10 (12%), Pent—3 (3%), Py—1 (1%), Sil/Cpy—4 (5%), Pent/Cpy—1 (1%).
Sil—silicates, Cpy—chalcopyrite, Pent—pentlandite, Py—pyrite, Sil/Cpy—along boundaries of silicates and chalcopyrite. Note: in some cases for the smaller (2 μm) minerals described above, the Cu, Ni, and Fe component may be partly attributed to surrounding Cu–Ni sulphide phases and not the platinum-group mineral.

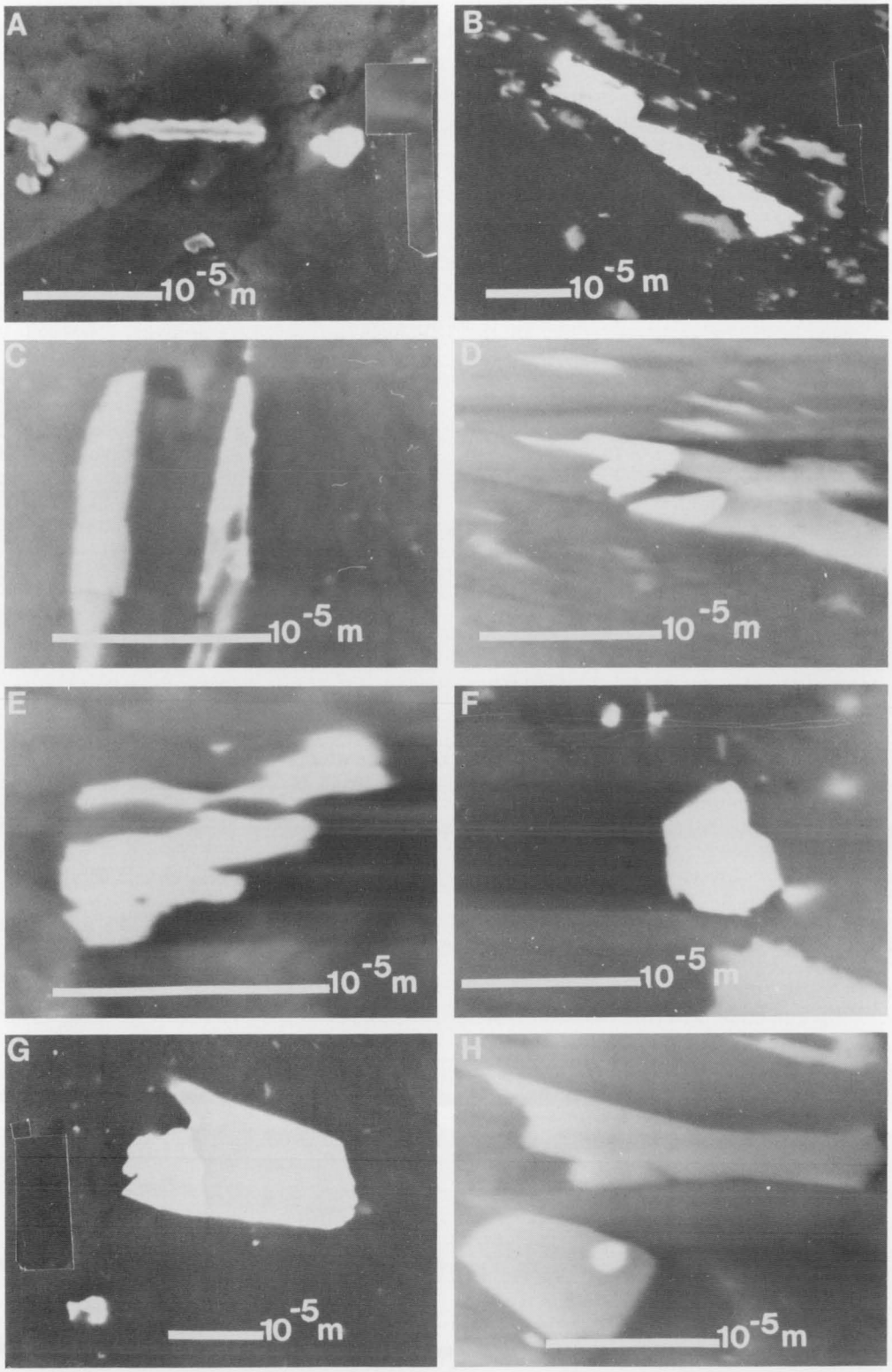

Fig. 46A-H. Munni Munni Complex: scanning-electron-microscope images of platinum-group minerals from the mineralised porphyritic websterite layer (subzone I). Diamond-drill core kindly provided by Hunter Resources Ltd.

A. Cluster of zoned platarsite(Pt-As-S-Fe; core)-sperrylite (rim) anhedra in a carbonate-talc-chlorite-quartz matrix of a shear zone traversing the mineralised porphyritic websterite layer.
B. Large moncheite(Pt-Te) anhedron with sutured margins aligned with small stringers of chalcopyrite.
C. Possible vincentite(Pd-Pt-As-Te) anhedron (centre of image) aligned parallel to bladed pentlandite grain.
D. Sperrylite and telluropalladinite(Pd-Te) anhedra associated with chalcopyrite.
E. Telluropalladinite anhedra enclosed in silicates.
F. Michenerite(Pd-Te-Bi) subhedra enclosed in silicates and near chalcopyrite grains.
G. Large prism of braggite(Pd-Pt-S; right of centre) adjoining smaller, more reflective potarite(Pd-Hg-As) grain.
H. Small hexagonal temagamite(Pd-Hg-Te) euhedron enclosed in chalcopyrite.

hydrothermal redistribution. The mercury-bearing Pd minerals potarite, atheneite and temagamite display the most euhedral forms, commonly occurring as small hexagonal grains in sulphides (Fig. 46H).

Except for the Pt-Pd sulpharsenide minerals, all PGMs are $\leq$ 10 μm in average size. The Pt-dominant minerals are marginally coarser-grained (average grainsize 6.5 μm) than the Pd-bearing phases (5.0 μm). The largest PGMs (maximum size 30 x 5 μm) are enclosed in, or at the boundary of, silicate grains, whereas PGMs in Fe-Cu-Ni sulphides are generally smaller. The low Pt/Pd ratios (0.2–1.0) for the mineralised drill core intervals and the similar abundances of Pt- and Pd-bearing grains may indicate that Pd is also present in solid solution in associated sulphides. Palladium concentrations (at detection limits of up to 500 ppm) in pentlandite have been reported in the Bushveld, Stillwater, Lac des Iles, and Talnakh complexes (Cabri & Laflamme, 1981), but analyses employing extended count times on a limited number of Munni Munni pentlandite grains did not reveal any Pd-enrichment. All PGMs found in the Munni Munni Complex have been documented previously from other major layered intrusions, including the Bushveld, Stillwater, Lac des Iles, Sudbury, New Rambler, and Noril'sk. Potarite is a rarer phase, originally reported from the Potaro River region of Guyana (Cabri & Laflamme, 1981).

Of significance is the strong spatial association of the PGMs with silicate phases. For the 87 grains identified, 78% are either totally enclosed within silicate minerals or along silicate grain boundaries, 12% are within chalcopyrite, 3% within pentlandite, 1% within pyrite, and 6% along grain boundaries between pentlandite-chalcopyrite or silicate-chalcopyrite. Although the PGMs are largely hosted by silicates on a micron scale, most are actually spatially associated with sulphides in either of two ways. Firstly, PGMs are associated with hydrous silicate assemblages (e.g. actinolite-tremolite-biotite) that appear to result from the replacement of Fe-Cu-Ni sulphide blebs. Secondly, PGMs which show no direct relationship to pre-existing sulphides still display an association with sulphides, either by parallel alignment with the sulphide grain (Fig. 46C), or by location near sulphides along cleavage traces (Fig. 45H) or embayments of pyroxenes. Thus, despite the silicate-PGM association at a micron scale, sulphides are the most important factor governing the regional distribution of the PGMs. From an exploration point of view, therefore, it would be important to sample and analyse both sulphide-rich and sulphide-poor intervals of the prospective websterite layer. The large silicate-hosted component of the Munni Munni PGMs is similar to that observed for the Merensky Reef in the western Bushveld between Marikana and Amandelbult. Northeast of Amandelbult and at Atok the sulphide-PGM association becomes more dominant (Kinloch, 1982). Individual PGMs at Munni Munni appear to show affinities for various associations. Native Pt, native Pd, ?isoferroplatinum, Pt-tellurides, ?vincentite, potarite, and atheneite show an exclusive association with silicates, and the remaining arsenide, sulpharsenide and Pd-telluride PGMs are associated with Fe-Cu-Ni sulphides and/or silicates. Cooperite, braggite and ?vysotskite, sperrylite, telluropalladinite, and temagamite display the closest relationship with Fe-Cu-Ni sulphides.

The PGMs appear to be broadly zoned, from the margin to the central region of the Munni Munni intrusion. Platinum minerals near the western margin (DDHs MMD 3 and MMD 15) are dominantly Pt-Pd tellurides, whereas in the central parts of the complex, the characteristic PGMs (MMD 1, MMD 6, MMD 10, and MMD 11) are arsenides, sulphides, mercury-bearing, and minor bismuthinides. The sequence of elements characterising zoning of the PGMs from the margin to the centre of the intrusion is Te → As-S-Hg →Hg-As → Bi. Lateral variations of PGMs along strike have been well documented for the Merensky Reef (Kinloch, 1982; Viljoen & others, 1986) and the J-M Reef (Page & others, 1976; Todd & others, 1982; Volborth & others, 1986), but the processes which govern their varying distributions are not well understood. Adjacent holes MMD 1 and MMD 6 (Fig. 57) provide the only insight into any possible vertical zonation of the PGMs. At the 55 m level from the surface (MMD 1) sulphides and Hg-bearing PGMs predominate, whereas at the 130 m level (MMD 6), the Hg-bearing PGMs persist, but the sulphides become subordinate to arsenides. Further SEM studies of materials from different holes are required to confirm these trends and to investigate whether the distribution of the PGMs is controlled by such variables as sulphide assemblage, e.g. Cu-rich compared to Fe-rich, porosity changes in the cumulates, or volatile/fluid processes.

Whole-rock geochemistry

Introduction

Whole-rock major- and trace-element analyses (see Appendix 3) were obtained for 110 surface samples, of which samples 84770001 to 84770066 were collected in ascending order from the base of the ultramafic zone to subzone B of the gabbroic zone (sample traverse and sample locations are shown on appended map sheet). Other important samples (e.g. 84770094, 100, 102, 125, 85770179), distant from the sample traverse, are also included in the chemical variation diagrams, for completeness of coverage.

This study has concentrated on the incompatible trace element and mineral compositional trends throughout the intrusion since whole-rock major-element compositions of cumulates rarely reflect the compositions of their parent liquids. Various petrogenetic studies (Haskin & Korotev, 1977; Hanson, 1980; Irvine, 1980b; Lambert & Simmons, 1980, 1987) have highlighted that there are a number of complications relating to the modelling of trace-element abundances in cumulate rocks and the minerals that comprise these rocks. These include: (1) processes such as subliquidus re-equilibration, infiltration metasomatism, and subsolidus re-equilibration that may have a significant effect on trace-element distributions; (2) uncertainties in mineral-melt distribution coefficients (e.g. Kd's) for rocks of different compositions; (3) the percent crystallisation of the solid; (4) assumptions involving the intercumulus material (e.g. determining extent of adcumulus growth); and (5) whether or not one magma was involved. These complications can hinder the interpretation of such processes as multiple injections, magma mixing, and magma contamination. In addition, the Munni Munni whole-rock data illustrate the different mobilities and redistribution behaviours of certain elements in response to secondary processes, such as weathering, alteration, and regional metamorphism (Wallace & Hoatson, 1990). Because of their greater mobility, K, Rb, Ba, S, Ce, Sr, Ga, and La have less application as petrogenetic indicators than the more immobile high-field-strength cations, such as Zr, Ti, Al, Y, Se, and Sc. The effects of alteration are most apparent in altered peridotites, where serpentinisation has resulted in Fe_2O_3/FeO ratios as high as 9.5 and loss-on-ignition values of up to 12.90%.

Despite these limitations, major and trace elements can be useful in defining gross fractionation trends and the chemical affinities of parent magmas.

Geochemical data and sample information for the Munni Munni Complex rocks and the large Southern, Zebra Hill, Pinderi Hills, and Eastern Munni Munni dykes are listed in Appendix 3. The mg number for the whole-rock samples is abbreviated to 'mg' in the text and is defined as (100 x MgO/40.32) / (FeO/71.85 + Fe_2O_3/79.85 + MgO/40.32). The analytical techniques, elements analysed, and their detection limits are summarised in Appendix 1.2.

Major elements

The variations in the major oxides largely reflect the gross compositional changes, as defined by the variable proportions of olivine, clinopyroxene, and orthopyroxene in the ultramafic zone, and plagioclase, clinopyroxene, inverted pigeonite, and Fe-Ti oxides in the gabbroic zone. Peridotite has low SiO_2, TiO_2, Al_2O_3, CaO, and Na_2O, and high MgO relative to the other major rock types of the intrusion. Clinopyroxenite and websterite have similar compositions to each other; gabbronorite from the base of the ultramafic zone has similar high FeO, Fe_2O_3, Al_2O_3, Na_2O, K_2O, and TiO_2, and low

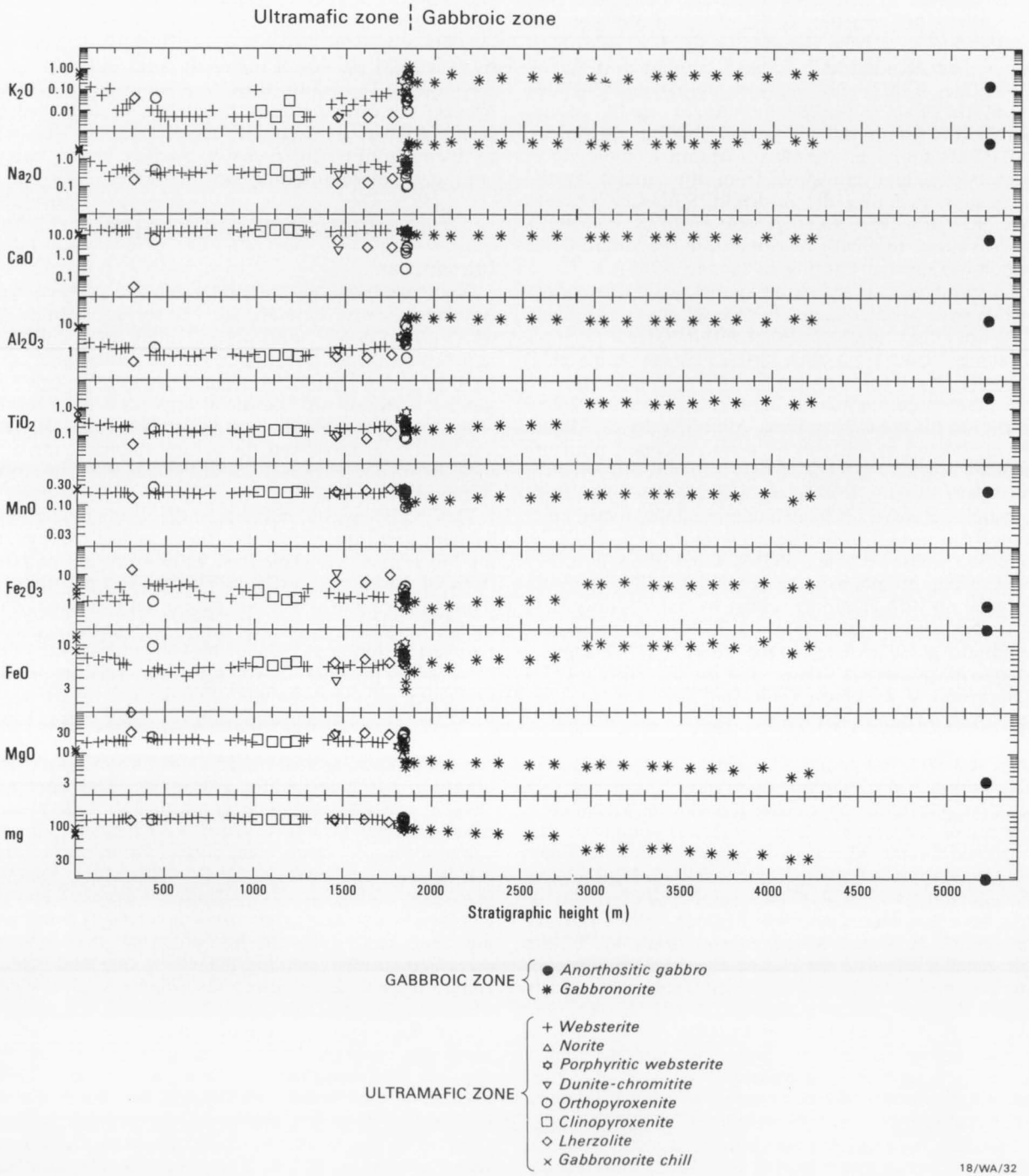

Fig. 47. Munni Munni Complex: variations in whole-rock major-element compositions (weight %) with stratigraphic height. See Figure 48 for detail on zone contact.

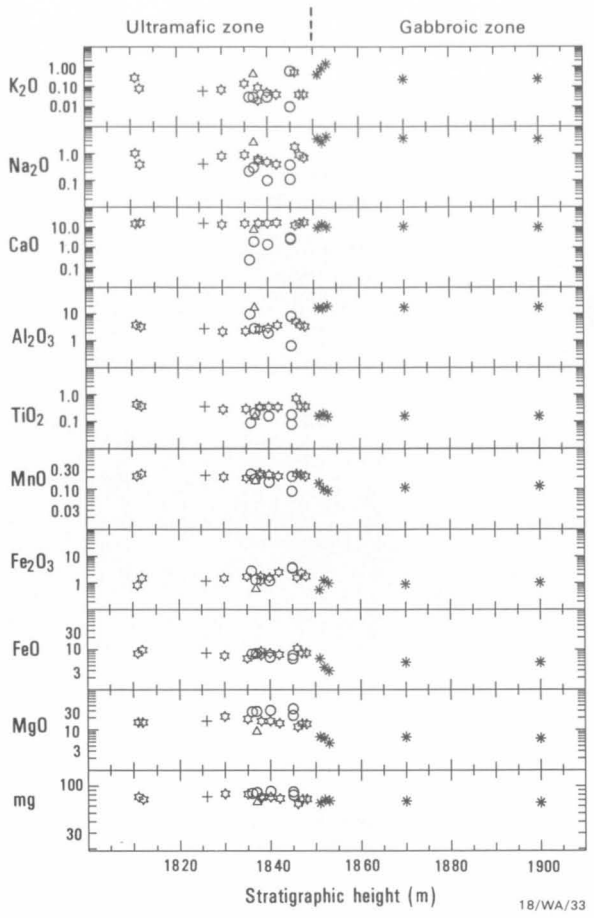

Fig. 48. Munni Munni Complex: variations in whole-rock major-element compositions (weight %) for the stratigraphic interval 1810–1900 m. Symbols as in Figure 47.

MgO contents to gabbronorite from the gabbroic zone. Porphyritic websterite of subzone I is intermediate in composition between the rocks of the ultramafic and gabbroic zones, and the orthopyroxenite blocks associated with the porphyritic websterite have contrasting compositions with all rocks in the Munni Munni Complex.

Major-element variation trends throughout the intrusion are shown in Figure 47, and in more detail across the ultramafic/gabbroic zone contact in Figure 48. The ultramafic and gabbroic zones have contrasting major-element fractionation trends, which largely reflect open- and closed-system fractionation, respectively. Fairly flat trends with localised deviations near the base and top of the zone characterise the ultramafic zone, whereas consistently increasing or decreasing fractionation trends are characteristic of the gabbroic zone. The fractionated character of the basal ultramafic zone rocks is indicated by their higher FeO, Fe_2O_3, MnO, TiO_2, Al_2O_3, Na_2O, and K_2O and lower MgO and mg (55.6–76.4) contents relative to the overlying pyroxenites and peridotites. This reverse fractionation is believed to be due to rapid cooling at the basal contact. Most olivine- and clinopyroxene-rich cumulates of the ultramafic zone vary little in major-element concentrations, mg having a restricted range between 84.5 and 81.0. With the exception of slight increases in Al_2O_3, K_2O, and Na_2O concentrations above 1400 m, which reflect the crystallisation of minor intercumulus feldspar, the regional uniformity of major-element trends in the ultramafic zone indicates the dominance of clinopyroxene and olivine in most cumulates. It is not until the upper parts of subzone I that a transformation to more Fe-rich compositions is observed. An ascending sequence of porphyritic websterite and gabbronorite samples from a trench across the ultramafic/gabbroic zone contact (samples 84770139–84770154) illustrates the transitional nature of this late fractionation trend. The mg and stratigraphic levels of the samples are 82.1 (1830 m), 81.4 (1835 m), 76.9 (1838 m), 75.6 (1840 m), 72.7 (1842 m), 71.3 (1847 m), 71.7 (1848 m), 70.0 (1852 m; start of gabbroic zone), 68.8 (1853 m), 68.0 (1870 m), and 65.5 (1900 m). The whole-rock mg variations generally parallel the Fe-enrichment trends of clinopyroxene in the upper part of subzone I, but they do not reflect the abrupt changes in clinopyroxene and plagioclase compositions above the 1845 m level (see Mineralogy section, p. 49). In fact there is a slight increase in whole-rock mg from 1847–1848 m. This suggests that mineral compositions are more sensitive to changes in temperature and porosity than those of the bulk cumulates. Todd & others (1982) documented a similar trend of more fractionated whole-rock mg and sympathetic olivine compositions directly below the J-M Reef. They attributed these changes to the different effects of trapped Fe-enriched intercumulus liquid in cumulates that contain varying proportions of cumulus and postcumulus mafic minerals. The transitional nature of the compositional trends across the ultramafic/gabbroic zone contact at Munni Munni (Fig. 48) is also indicated by regular variations in Fe_2O_3, MnO, CaO, and TiO_2 contents, although Na_2O, K_2O, and Al_2O_3 show some discontinuity across the contact owing to the contrasting abundance of plagioclase in the two zones.

The megacrystalline orthopyroxenite of subzone C (at 430 m in Fig. 47) has mg, MgO, TiO_2, and Na_2O contents consistent with the degree of fractionation of adjacent cumulates. However, the orthopyroxenites of subzone I have high mg and MgO, and low MnO, TiO_2, CaO, Na_2O, and K_2O with respect to the host porphyritic websterite. This is consistent with the interpretation that the subzone C orthopyroxenite crystallised *in situ*, whereas the subzone I orthopyroxenites are of accidental origin.

Major-element trends are generally consistent throughout the gabbroic zone. There is a change in some major-oxide trends at 2692 m, where an increase in TiO_2 and Fe_2O_3 correlates with the increased abundance of intercumulus Fe-Ti oxides. Increasing P_2O_5 contents from 0.1–0.3% up the gabbroic sequence are consistent with the greater abundance of apatite in the more fractionated rocks. A subzone B anorthositic gabbro (at 5220 m) falls along the extrapolated major-oxide trends of the subzone A gabbronorites, indicating it is likely to be derived from the same magma as the subzone A rocks.

The primitive character and limited fractionation status of the ultramafic-zone rocks are highlighted by their restricted distribution in the ternary plots of Figure 49. Dunite, lherzolite, clinopyroxenite, and websterite have low alkali contents and plot in a cluster on the Fe-Mg side of Figure 49A. Porphyritic websterite shows a trend to more Fe-rich compositions and a very weak enrichment in alkalies. A porphyritic websterite sample and a norite sample from the top of subzone I have compositions intermediate between the main group of porphyritic websterites and the gabbronorites of the gabbroic zone. These two samples also overlap the composition of the gabronorite chill samples of the ultramafic zone, which have a wider range of composi-

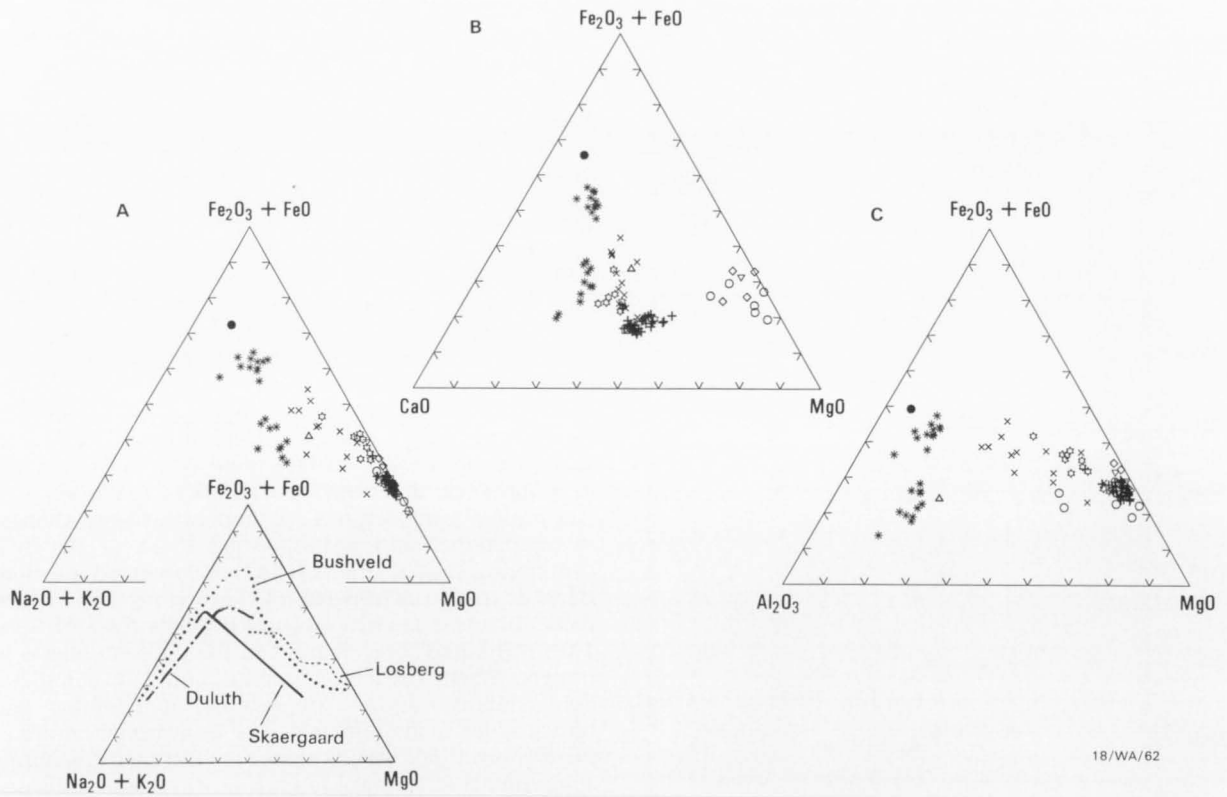

Fig. 49A–C. Ternary plots showing variations in whole-rock major-element compositions (weight %) and fractionation trends in various layered intrusions. Bushveld and Losberg rock trends from Danchin & Ferguson (1970); Duluth rock trend from Taylor (1956); and Skaergaard liquid trend from Wager & Brown (1968). Symbols as in Figure 47.

tions relative to the other cumulates of the ultramafic zone. Gabbronorites of the gabbroic zone show a pronounced enrichment in Fe_2O_3 + FeO at the expense of MgO, over similar concentrations of Na_2O + K_2O. The apparent bimodal distribution of gabbronorites along the Fe-enrichment trend correlates, in part, with the absence and presence of Fe-Ti oxides. The anorthositic gabbro from subzone B is the most fractionated rock analysed from the intrusion. The primitive compositions of the orthopyroxenite blocks, and the fairly continuous fractionation trends between the ultramafic and gabbroic zone cumulates, are indicated in Figure 49B. The different Al_2O_3 trends (Fig. 49C) for the ultramafic and gabbroic cumulates is largely controlled by the different abundances of plagioclase in the two zones.

Major-element variations with stratigraphic height in the Munni Munni Complex are broadly similar to those of other layered intrusions of basaltic affinity. These include an upward increase in FeO, Fe_2O_3, MnO, TiO_2, Al_2O_3, Na_2O, K_2O, and P_2O_5, and a decrease in mg, MgO, and CaO. The MgO–Fe_2O_3 + FeO–Na_2O + K_2O trends of the Bushveld and Losberg intrusions of South Africa (Danchin & Ferguson, 1970), the Duluth complex (Taylor, 1956), and the Skaergaard intrusion (Wager & Brown, 1968) are shown in the inset diagram of Figure 49A. The general fractionation trend of the ultramafic zone cumulates of the Munni Munni Complex is smilar to the initial trend of the Losberg intrusion, whereas cumulates from the gabbroic zone follow a tholeiitic trend and parallel the Fe-fractionation trend of the Bushveld. The change in the fractionation trend to alkali enrichment, which is seen in the overseas intrusions, is not observed in the gabbronorites of subzone A. However, the quartz monzonites and quartz syenites abutting the Fortescue Group platform cover are almost certainly likely to show this feature. Wallace & Hoatson (1990) have also noted the similar MgO-CaO-Al_2O_3 compositional trends of the Munni Munni rocks with similar rock associations (websterite-gabbronorite-anorthositic gabbro) from Archaean complexes of the Barberton Mountain Land (Anhaeusser, 1983).

Trace elements

The dominant control on the distribution of trace elements (Figs 50 & 51) in the Munni Munni Complex is their degree of compatibility with the cumulus phases olivine, pyroxene, and plagioclase, and the intercumulus phases in the whole rock. Copper, S, Rb, Sr, Ba, Zr, Ga, La, Nd, Ce, Zn, and Y display similar U-shaped distribution patterns to that of whole-rock mg in the ultramafic zone. This reflects their incompatible behaviour to varying degrees with the crystallisation of olivine and clinopyroxene (note: Cu, S, Rb, Sr, Zr, Se, Cs, and Ni are discussed in more detail later in this section). Plagioclase-bearing orthocumulates along the basal contact are enriched in these elements relative to the overlying olivine- and clinopyroxene-rich cumulates which comprise much of the zone. The higher trace-element concentrations reflect the more fractionated compositions and higher melt components in these basal rocks. The incompatible trace elements have fairly flat fractionation trends for the stratigraphic interval 64–1400 m, whereas above 1400 m they generally increase to reach a maximum in porphyritic websterite at the top of the zone. The incompatible-trace-element concentrations in subzone I are similar to those in the basal ultramafic zone rocks. The 1400 m level represents a significant stage in the evolution of the Munni

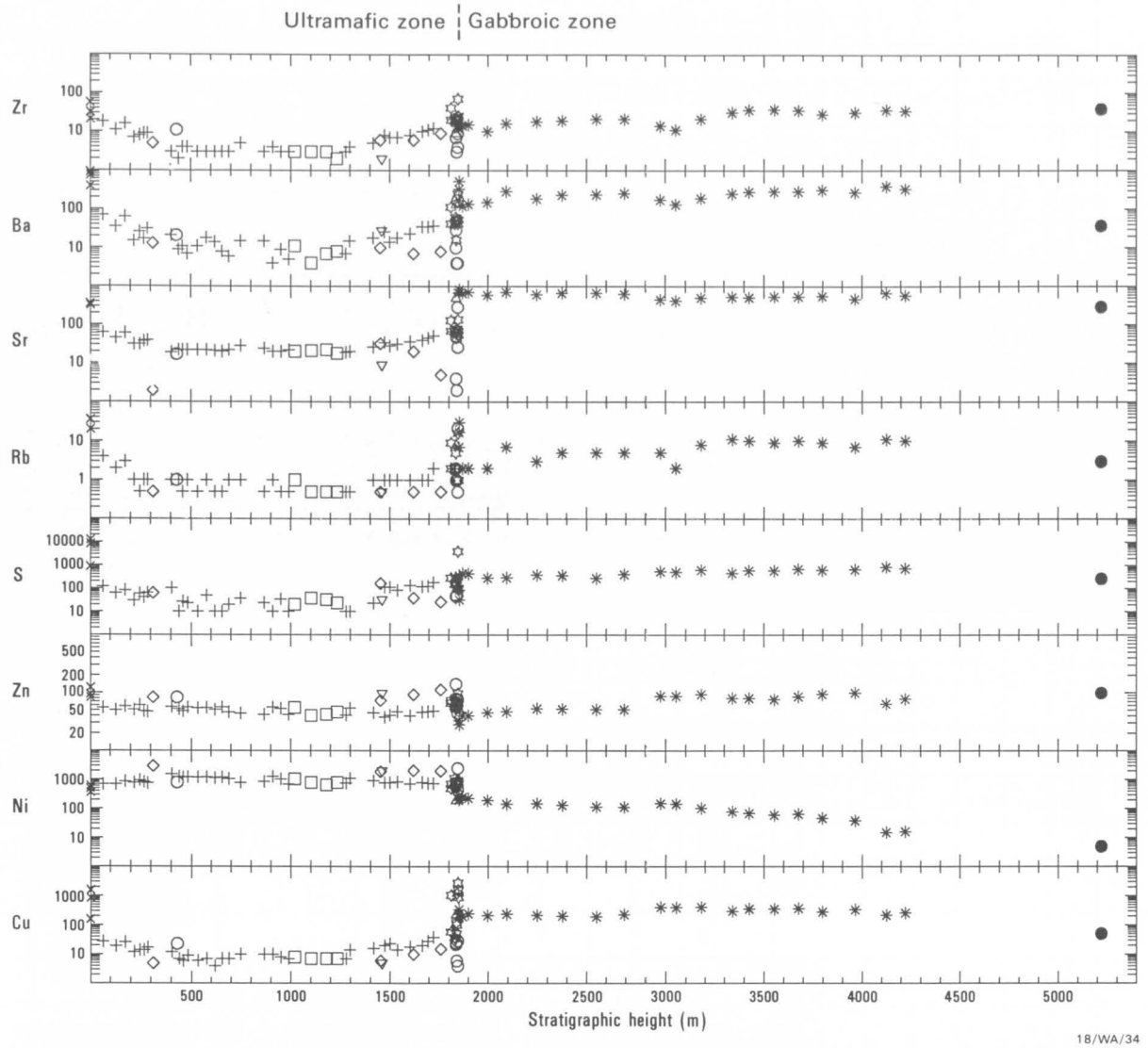

Fig. 50. Munni Munni Complex: variations in whole-rock trace-element compositions (ppm) with stratigraphic height. Symbols as in Figure 47.

Munni Complex, as indicated by the transformation to more evolved mineral compositions and the change in whole-rock compositional trends.

In contrast to the incompatible trace elements, Ni, Cr, Co, and V have n-shaped or flat fractionation patterns, which reflect partitioning into early-crystallising olivine and/or clinopyroxene. Nickel, Cr, and to a lesser degree Co, are depleted in the basal and upper parts of the ultramafic zone and have a sympathetic relationship with olivine-rich cumulates, whereas V shows a stronger affinity with clinopyroxene-bearing cumulates. The orthopyroxenite blocks of subzone I are enriched in Cr, Co, and Ni, but depleted in most incompatible trace elements, relative to the other cumulates of the ultramafic zone.

Gross trace element trends in the gabbroic zone are generally consistent with closed-system fractionation processes. Copper, Zn, S, Rb, Ba, Zr, Co, Ga, La, Nd, Ce, and Y steadily increase in concentration up the mafic sequence, reflecting their incompatible behaviour with respect to plagioclase and pyroxene. Zirconium, Ba, Sr, and Rb are slightly depleted at the 3050 m level, which may be due to subtle changes in cumulate porosity. Nickel and Cr partition into sulphide and clinopyroxene, respectively, and decrease upwards, whereas the slightly decreasing Sr trend upwards indicates Sr partitioning into plagioclase. Vanadium shows complex variation trends which are largely controlled by modal distributions of titaniferous magnetite. Weak enrichment occurs upwards in the basal part of the gabbroic zone, followed by a rapid increase in concentrations from 2700–2975 m, after which V steadily decreases to the 5220 level. The trace-element geochemistry of the anorthositic gabbro sample of subzone B lies along the same trace-element fractionation trends as the subzone A rocks.

The negative correlations of Cu, Zn, S, Ti, V, Zr, and Y with mg (Fig. 52) highlight the incompatible behaviour of these elements during fractional crystallisation. Most variation trends are consistent over the total range of mg, although Cu and V concentrations decrease in the fractionated gabbronorites (mg of < 40) owing to their greater partitioning into sulphides and magnetite, respectively, in higher levels of the gabbroic zone. The compatible behaviour of Ni and Cr with the crystallisation of olivine and pyroxene is shown

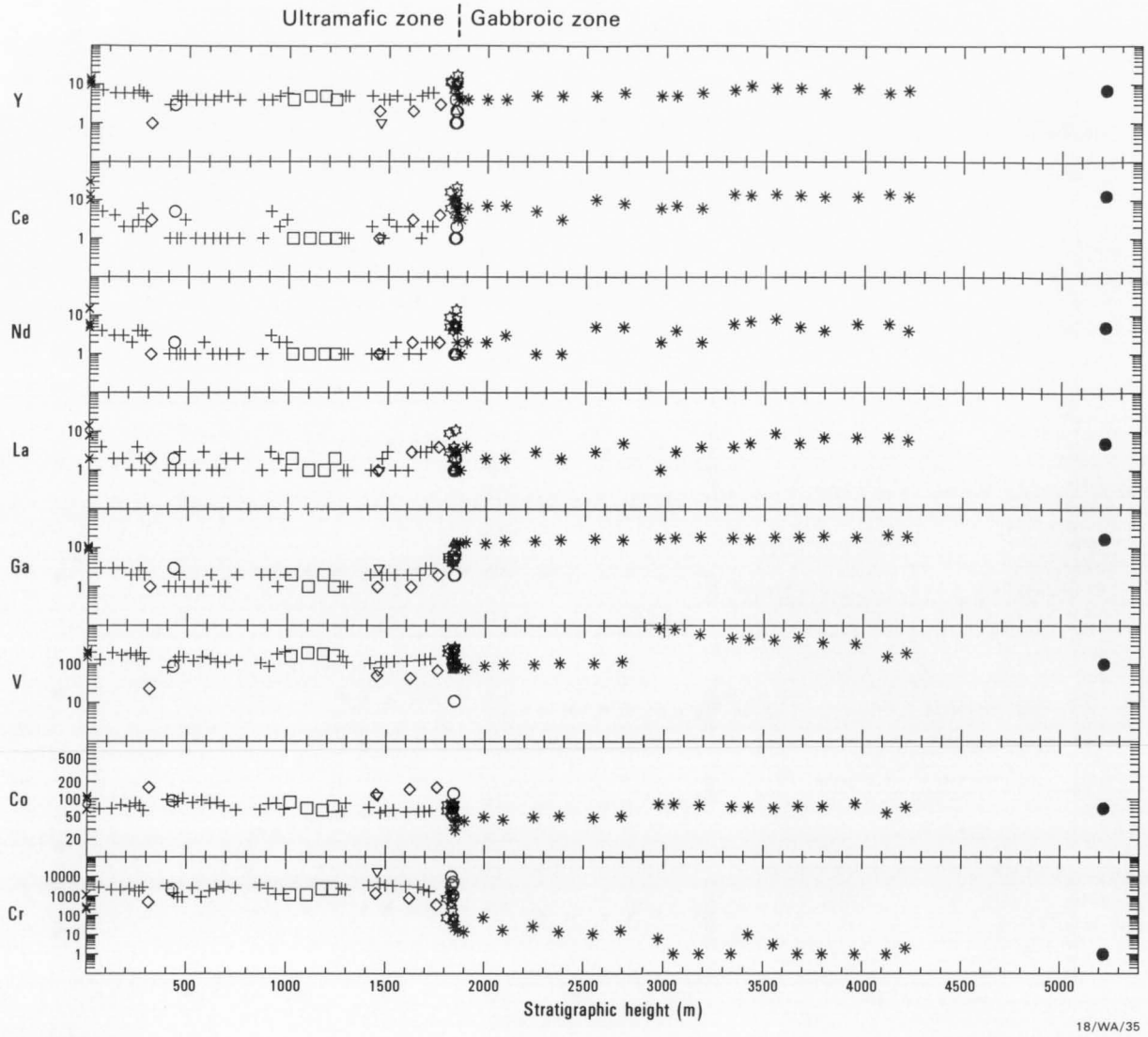

Fig. 51. Munni Munni Complex: variations in whole-rock trace-element compositions (ppm) with stratigraphic height. Symbols as in Figure 47.

by their strong sympathetic relationships with mg, whereas Co has fairly flat trends. The essentially continuous variation trends of Y, Ce, S, and TiO_2 (excluding Ti-rich gabbroic rocks) with Zr between the ultramafic and gabbroic zone rocks (Fig. 53) is in agreement with the view that the two zones are comagmatic. This is supported by the similar Y/Zr, Ce/Zr, S/Zr, and P_2O_5/Zr ratios of the rocks in both zones, whereas their different Sr/Zr, Ba/Zr, and K_2O/Zr ratios largely reflect changing mineral assemblages with fractionation, e.g. crystallisation of abundant cumulus plagioclase in the gabbroic zone.

Platinum-group-element and incompatible-trace-element geochemistry

Introduction. The PGEs exhibit both siderophile and chalcophile characteristics (Cousins, 1973), and because of their extremely high sulphide/silicate partition coefficients (10^4 to 10^5 for Pt and Pd: Campbell & others, 1983; Campbell & Barnes, 1984; Barnes & Naldrett, 1985; Peach & others, 1989; Stone & others, 1990), they are particularly useful in establishing the time of S saturation of a fractionating magma. During crystallisation of mafic-ultramafic magmas, Ir and Os are largely removed, along with early crystallising phases, such as olivine and chromite (Ross & Keays, 1979). In contrast, Pt, Pd, and Au behave incompatibly and become enriched in fractionating magmas as long as such magmas remain S undersaturated, but are rapidly depleted from S-saturated magmas. Hence, cumulates formed from S-undersaturated magmas should have significantly higher Pt/S ratios than cumulates formed from S-saturated magmas. In order to assess the degree of incompatibility of the PGEs during fractionation, it is necessary to compare their behaviour with incompatible lithophile elements that have partition coefficients much less than unity for cumulus olivine and pyroxene. Cesium, Zr, Rb, and Sr have been determined, to obtain a measure of the amount of interstitial melt in cumulates. These incompatible elements are ideal, since Zr, for example, has partition coefficients of 0.01, 0.03, and 0.1 for olivine, orthopyroxene, and clinopyroxene, respectively (Mattey & others, 1981).

The main objective in documenting the PGEs and incompatible lithophile elements across the entire Munni Munni stratigraphy was to determine whether these elements could be used to predict the location of any mineralised layer(s) and to ascertain the behaviour of

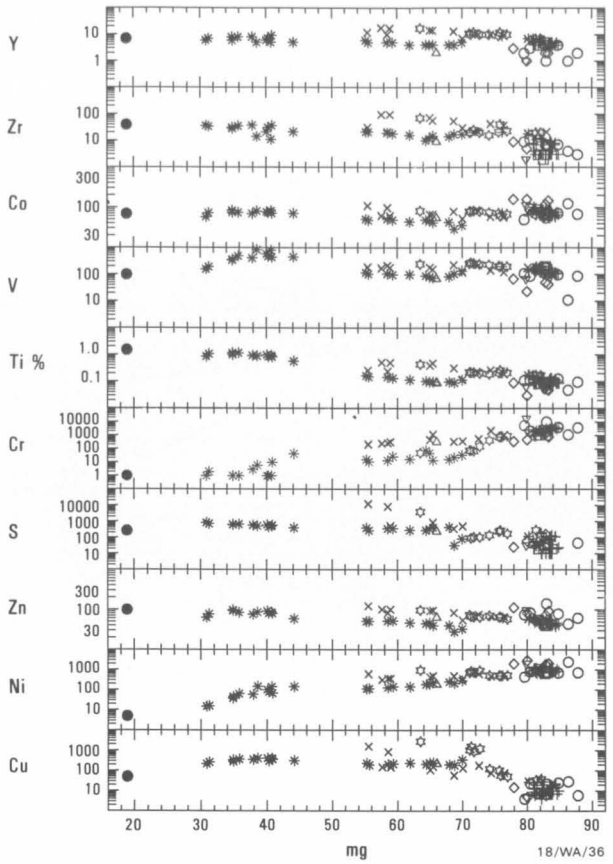

Fig. 52. Munni Munni Complex: variations in trace-element compositions (ppm) with mg number. Anorthositic gabbro and gabbronorite are from the gabbroic zone; all other rock types are from the ultramafic zone. Symbols as in Figure 47.

the PGEs and other elements during the course of fractionation of the magma(s). Most PGE fractionation studies on other layered intrusions have focused on the mineralised layer or the cyclic unit containing the layer, whereas there are few detailed studies describing trends through the complete differentiated sequence of a layered intrusive body. Lee (1983) investigated the trace and PGE geochemistry of the Merensky Unit and McCarthy & others (1984) have studied the variation of incompatible elements through the lower and critical zones of the Bushveld Complex. The PGE fractionation trends in the Lac des Iles Complex, Ontario have been documented by Watkinson & Dunning (1979), Dunning & others (1981), and Talkington & Watkinson (1984). Page & others (1972, 1976) reported on the vertical and lateral variation of PGEs in the Stillwater Complex. Fractionation trends of PGEs in the Bushveld, Stillwater, and Fiskenaesset complexes have been summarised by Page & others (1982), and in the Great Dyke by Prendergast & Keays (1989). Precious-metal fractionation studies in other mafic-ultramafic intrusions include: Koillismaa, Finland (Alapieti & Piirainen, 1984), Fiskenaesset, Greenland (Page & others, 1980), Jimberlana, Western Australia (Keays & Campbell, 1981), the York Haven diabase sheet, Pennsylvania (Gottfried & others, 1990), the Great Lake dolerite, Tasmania (Greenland, 1971), and Heazlewood, Tasmania (Peck & Keays, 1990a, b).

The analytical techniques for the PGEs and incompatible elements are described in Appendixes 1.1 & 1.2.

Sulphur. The distribution of S in the ultramafic zone of the Munni Munni Complex has a pronounced U-shaped configuration (Fig. 54) with enrichment in gabbronorites along the basal contact of the zone (subzone A′) and in the porphyritic plagioclase websterite layer at the top of the zone (subzone I). The S contents are largely independent of the olivine and clinopyroxene cumulates that comprise the bulk of the zone, but there is a strong correlation between S and stratigraphic height.

The basal contact region of the ultramafic zone is enriched in S (up to 12 420 ppm), followed by rapid depletion to 118 ppm at the 64 m stratigraphic level, and then a more gradual depletion to 63 ppm at 313 m. The gabbroic rocks along the basal contact are the most S-rich rocks in the intrusion, with S contents exceeding those of the mineralised porphyritic websterites in subzone I by a factor of about 3. Background contents of $\leq$ 37 ppm are characteristic of websterite and clinopyroxenite through the main central part of the zone (440–1417 m). The consistent S trends through this region indicate that S contents have not been changed by the emplacement of new pulses of magma. The multiple pulses that formed the lower parts of the zone must have contained similar low S contents, although some S appears to have been lost as a result of alteration. Above the 1417 m level, the S contents of lherzolite and websterite increase, most samples having S contents between 80 and 280 ppm. Sulphur contents rapidly increase upwards from about 10–20 m below the ultramafic/gabbroic zone contact and reach a maximum of 3940 ppm in the mineralised porphyritic web-

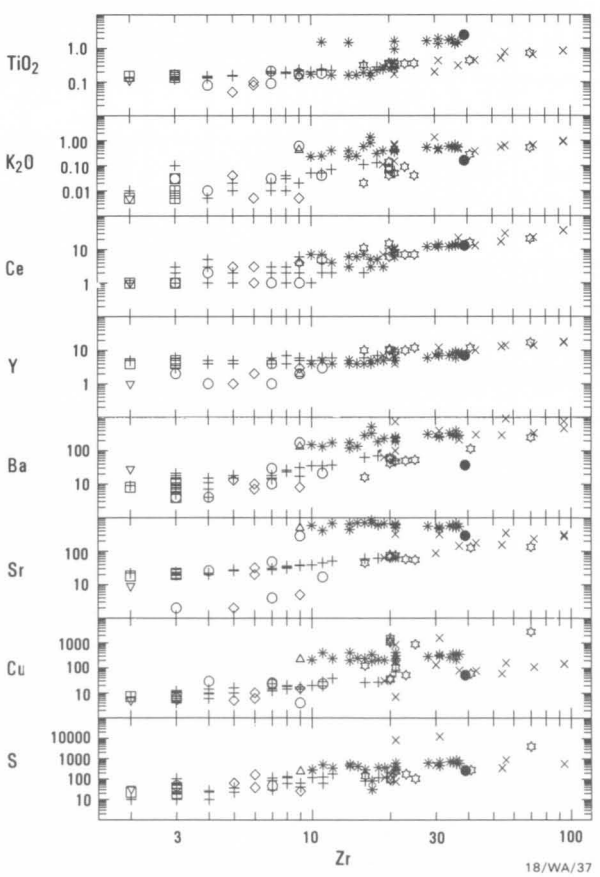

Fig. 53. Munni Munni Complex: variations in major (weight %) and trace (ppm) element compositions with Zr. Symbols as in Figure 47.

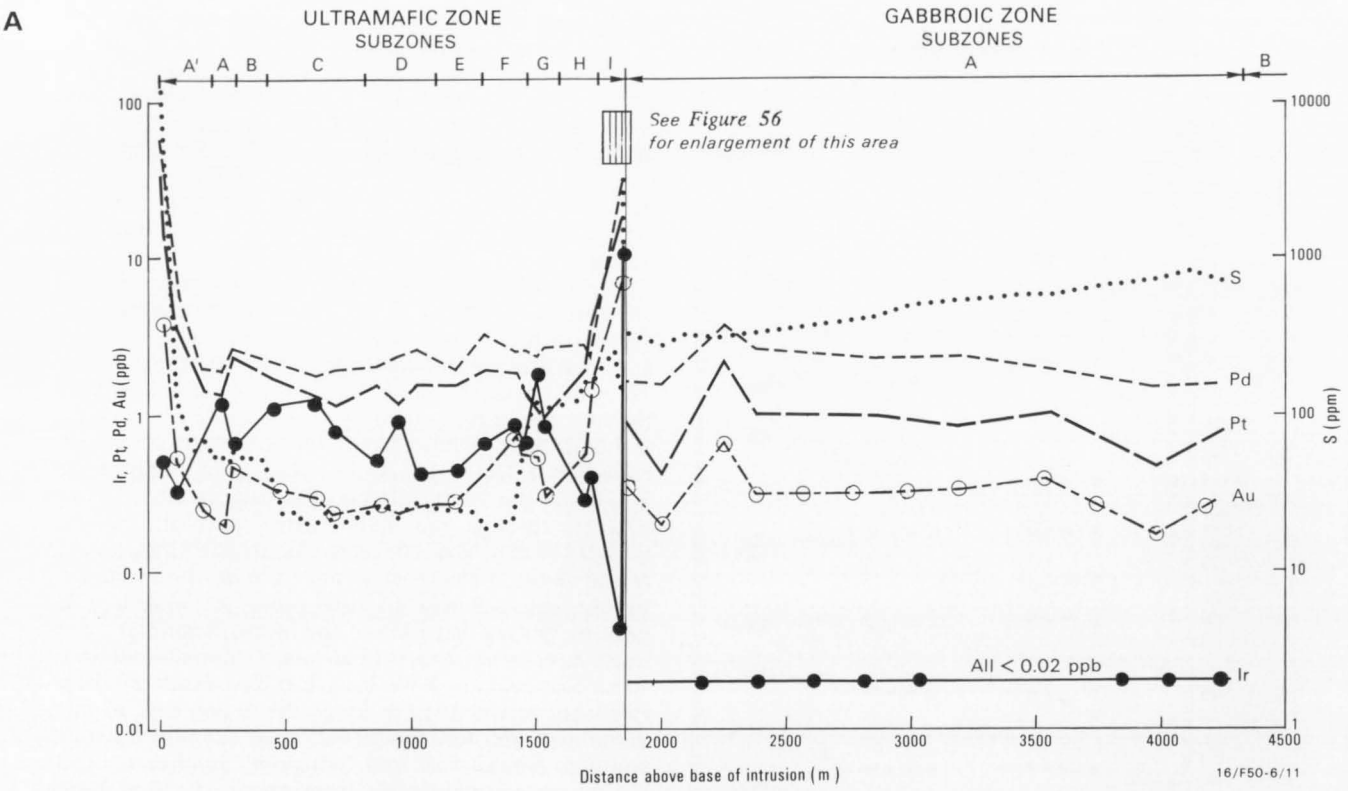

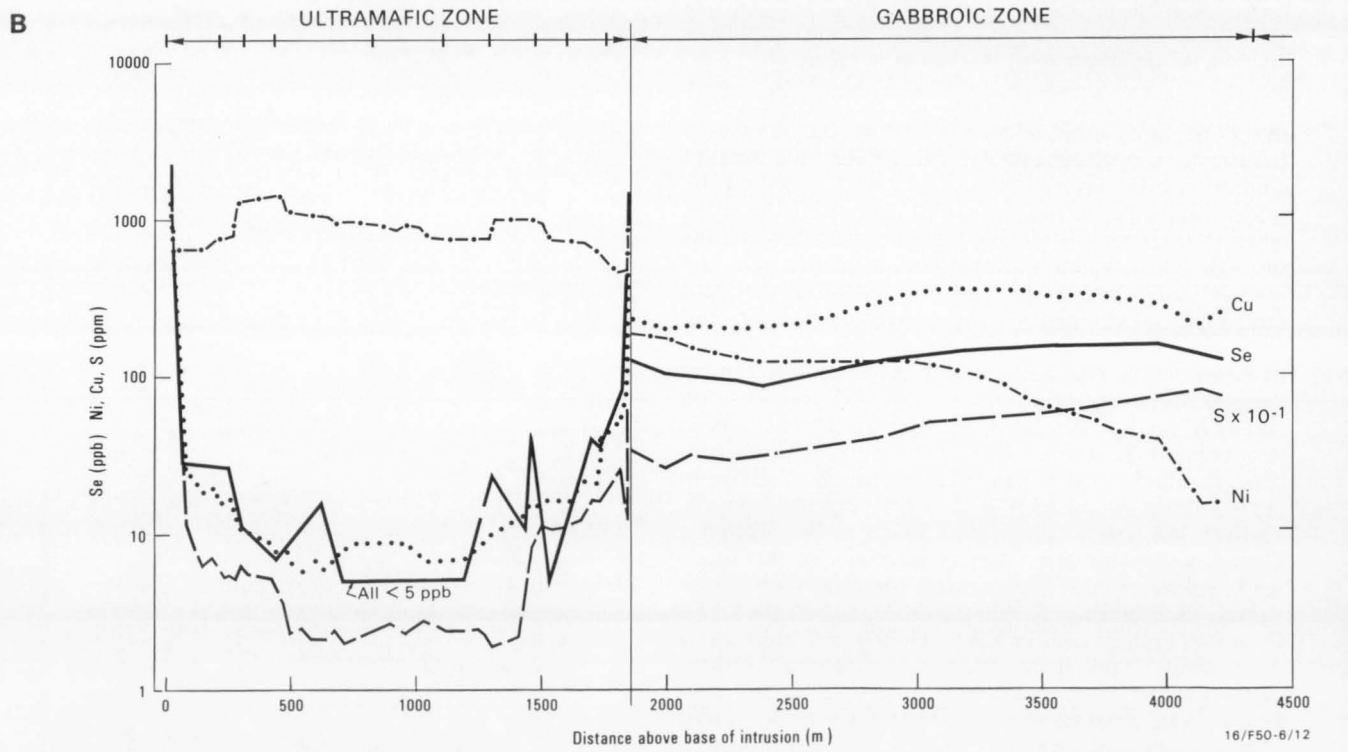

Fig. 54A–B. Munni Munni Complex: profiles of Pt, Pd, Ir, Au, S, Se, Cu, and Ni through the ultramafic and gabbroic zones. A moving average of five sample points was used for the S, Cu, and Ni data.

sterite layer at the 1846 m stratigraphic level. Minor rock types, such as orthopyroxenite (84770046) and spinel-bearing orthopyroxenite (85770159) which form lenses and accidental blocks at the top of subzone I, are S-poor (S < 50 ppm). A dunite-hosted chromitite lens (85770156) in subzone H also has low S (33 ppm),

but this rock is intensely serpentinised so that any original sulphides would presumably have been remobilised. The higher initial S content of the chromitite lens relative to the orthopyroxenites is indicated by its Se content of 122 ppb compared to 6 ppb for the orthopyroxenite. Talc-carbonate-chlorite shear zones (84770088, 85770163), which traverse the mineralised porphyritic websterite layer, are S-rich (S contents up to 5750 ppm).

In contrast to the ultramafic zone, S contents in the gabbroic zone are generally higher and increase regularly upwards through the whole zone. As discussed in the Petrogenesis chapter (p. 156), the magma that formed the gabbroic zone was S saturated, whereas only the base and top of the ultramafic zone are S saturated. Sulphur contents drop dramatically across the ultramafic/gabbroic contact, from a high concentration in the mineralised websterite layer to 350 ppm in basal gabbronorites of the gabbroic zone. The S content continues to decrease, to 280 ppm at the 2000 m level and then consistently increases upwards to a maximum of 835 ppm at the 4125 m level. The gradient of S enrichment from the base of subzone A to the 4125 level is approximately 24 ppm for each 100 m of mafic stratigraphy. The overall consistency of the S trends in subzone A suggests closed-system fractionation of a single magma pulse.

Copper, nickel. Copper and Ni abundances have contrasting trends through the ultramafic and gabbroic zones (Fig. 54B). This is attributed to Cu in S-undersaturated conditions behaving as an incompatible element and increasing in concentration in the intercumulus melt fraction, whereas Ni strongly partitions into olivine (partition coefficient of $\sim$ 13) and to a lesser degree orthopyroxene ($\sim$ 4) and clinopyroxene ($\sim$ 3; partition coefficients from various references cited in Sheraton & Simons, 1988). This contrasting behaviour is strongly modified by the effects of S-saturation, since both elements strongly partition into sulphides (partition coefficients of $\sim$ 250–275: Naldrett, 1989).

The abundance of Cu, owing to its strong chalcophile tendencies and incompatible nature with respect to the silicate phases, closely parallels the trends of S through most of the intrusion. Basal gabbronorites have Cu contents that range from 159–1575 ppm, but these drop rapidly to 27 ppm at the 64 m level. For the interval 64–1695 m, websterite, clinopyroxenite, and lherzolite have near-background Cu contents of less than 28 ppm. Copper abundances steadily increase from 38 ppm at the 1723 m level to a maximum of 2810 ppm in the porphyritic websterite at the 1846 m level. As with S, the Cu content drops sharply across the ultramafic/gabbroic zone contact, to 240 ppm in basal gabbronorite of the gabbroic zone. It then steadily increases upwards through the zone, but plateaus and then begins to decrease above 3000 m. The upper 1200 m of gabbroic subzone A is the only part of the intrusion where Cu has an antipathetic trend to that of S.

Nickel abundances generally decrease with increasing stratigraphic height. Abundances are depleted (362–609 ppm) in the fractionated gabbroic rocks along the basal contact, and after attaining a maximum (excluding mineralised rocks in subzone I) of 2916 ppm for lherzolite of subzone B, Ni abundances steadily decrease upwards through the zone, declining to 527 ppm in plagioclase websterite near the upper parts of subzone I. There is a well-defined positive correlation between Ni content and mg of rock type in the ultramafic zone. The basal gabbronorites (mg_{58-68}) have low Ni contents of 362 to 494 ppm, whereas websterite, olivine websterite, lherzolite (mg_{83-86}), contain about 800 ppm, 1200 ppm, and 2000 ppm Ni, respectively. Nickel contents are significantly lower in the gabbroic zone, and decrease more rapidly upwards (from 195 ppm at the base of subzone A to 16 ppm at the top of the subzone) because of the partitioning of Ni into sulphide and pyroxene. Since orthopyroxene (as inverted pigeonite in the gabbroic zone) and clinopyroxene are present throughout the intrusion, the more significant decrease in Ni content with increasing stratigraphic height in the gabbroic zone (particularly above 3000 m) compared to the ultramafic zone, highlights the higher partitioning of Ni for sulphide than for olivine.

Platinum, palladium, gold, iridium. Platinum, Pd, and Au abundances have broadly sympathetic trends through the ultramafic zone (Fig. 54A). The basal contact and the porphyritic websterite layer are enriched in these elements relative to the rest of the zone. In the gabbroic zone, Pt, Pd, and Au contents generally decrease, or remain constant, with increasing stratigraphic height. Iridium throughout the intrusion shows antipathetic distribution trends to Pt, Pd, Au, and S.

Gabbronorites (85770179, 84770100, 0102) of subzone A′ are enriched in Pt, Pd and Au, but depleted in Ir relative to the olivine and clinopyroxene cumulates that comprise the main part of the ultramafic zone (Table 12). The olivine gabbronorite chill at the 1 m level has approximately 10 times less Pt and Pd (3.76 ppb Pt, 3.40 ppb Pd) relative to the coarse gabbronorites at the 5 m level (15–35.0 ppb Pt, 57.5 ppb Pd). However, the Au content of the chilled gabbronorite (1.57 ppb) is only one-third that of the coarse gabbronorite (4.79– 5.06 ppb). Sulphur in the gabbronorite chill (870 ppm) is about 10 times lower than in the coarse gabbronorite (8310–12 420 ppm), indicating that Pt and Pd are more sensitive than Au to changes in S concentrations in the basal gabbronorites.

The slight depression in Pt, Pd, and Au concentrations at the 200 m level of the ultramafic zone (Fig. 54A) is also seen at a similar relative stratigraphic level above the base of the gabbroic zone (discussed below). These depletion features indicate that the mineralising events at the base of the ultramafic zone and near the ultramafic/gabbroic zone contact were probably in communication with the overlying magma, and subsequently depleted Pt, Pd, and Au from these parts of the magma. Platinum ($<$ 2.0 ppb), Pd ($<$ 3.3 ppb), and Au ($<$ 0.75 ppb) remain at near-background concentrations for most of the ultramafic zone and it is not until the 1695 m level that there is a minor increase in Pt (3.81 ppb) and Au (1.72 ppb). Palladium increases (17.0 ppb) later in the sequence at the 1838 m level. Thus, in the upper parts of the zone there is localised decoupling of Pd relative to Pt and Au. The Pt/Pd ratio remains fairly constant (range of 0.50–0.90) through the differentiated ultramafic sequence. Iridium displays a broad maximum of around 1 ppb in the centre of the ultramafic zone and decreases significantly toward the gabbroic zone contact. Its distribution trends are most consistent with those of Ni and mg, suggesting an affinity with olivine, as discussed later.

The PGE, Au, Cu, and Ni trends near the ultramafic/gabbroic zone contact are also discussed later (p. 85).

Platinum, Pd, Au, and Ir are markedly depleted in subzone A of the gabbroic zone relative to the mineralised layer (Table 12). Iridium has the highest depletion factor (2550), followed by Pt (1900), Pd (1050), and Au (950). As with the basal contact of the ultramafic zone, Pt, Pd, and Au are depleted near the base of the gabbroic zone relative to the rest of the zone.

Table 12. Platinum-group-element and trace-element geochemistry of the Munni Munni Complex

Sample number	Stratigraphic level (m) and subzone	Lithology	mg no.	Pt (ppb)	Pd (ppb)	Ir (ppb)	Au (ppb)	S (ppm)	Se (ppb)	Cs (ppb)	Cu (ppm)	Ni (ppm)	Cr (ppm)	Zr (ppm)	Sr (ppm)	$\frac{Pt}{Pd}$	$\frac{Pt+Pd}{S}\times10^6$	$\frac{Pt+Pd}{Ir}$	$\frac{Pt+Pd}{Zr}\times10^4$	$\frac{Cu}{Cu+Ni}\times10^3$
Ultramafic zone (base of complex at 0 m stratigraphic level)																				
0179	1, A′	Min Ol Gab	0.68	3.76	3.40	0.60	1.57	871	148	5565	159	494	1155	56	350	1.10	8.22	11.93	1.28	243
0100	5, A′	Min GabN	0.61	35.0	57.5	0.38	4.79	8310	1825	5555	843	362	266	21	323	0.61	11.13	243.42	44.05	538
0102	5, A′	Min GabN	0.58	15.0	—	0.51	5.06	12420	2460	—	1575	609	212	31	319	—	—	—	—	563
0001	64, A′	Plag Ol Web	0.82	3.27	5.81	0.31	0.50	118	29	298	27	683	2775	18	62	0.56	76.95	26.71	5.04	38
0003	174, A′	Ol Web	0.83	1.46	1.97	0.81	0.25	82	—	—	26	856	2060	16	60	0.74	41.83	4.23	2.14	29
0005	247, A	Ol Web	0.83	1.34	1.99	1.37	0.20	60	26	104	14	947	1835	8	31	0.67	55.50	2.43	4.16	15
0007	285, A	Web	0.85	2.40	2.67	0.63	0.48	64	12	188	17	759	2745	9	39	0.90	79.22	8.05	5.63	22
0011	440, C	Ol Web	0.84	1.77	2.27	1.14	0.35	<20	7	128	7	1250	1410	2	22	0.78	>202.00	3.54	20.20	6
0016	620, C	Ol Web	0.84	1.38	1.84	1.30	0.30	<20	16	336	4	1130	1840	3	21	0.75	>161.00	2.48	10.73	4
0018	690, C	Ol Web	0.86	1.18	1.96	0.85	0.23	20	<5	223	7	1060	2970	3	22	0.60	157.00	3.69	10.47	7
0020	867, D	Web	0.86	1.55	2.09	0.51	0.27	24	<5	148	10	846	3630	3	24	0.74	151.66	7.14	12.13	12
0022	950, D	Ol Web	0.83	1.20	2.40	0.92	0.24	34	<5	94	8	1045	1240	3	20	0.50	105.88	3.19	12.00	8
0024	1020, D	Ol Cpx	0.83	1.56	2.60	0.42	0.26	20	<5	109	8	1040	1120	3	20	0.60	208.00	9.90	13.67	8
0028	1180, E	Cpx	0.84	1.58	2.01	0.45	0.29	32	<5	117	7	660	2300	3	22	0.79	112.19	7.98	11.97	10
0031	1298, F	Ol Web	0.85	1.99	3.30	0.67	0.42	20	22	207	14	1110	2120	4	20	0.60	264.50	7.90	13.22	12
0032	1417, F	Ol Web	0.85	1.89	2.59	0.88	0.74	23	10	311	16	910	3575	5	26	0.73	194.78	5.09	8.96	17
0034	1453, F	Lherz	0.84	1.53	2.59	0.69	0.57	164	42	124	6	1890	1355	6	32	0.59	25.12	5.97	6.87	3
0036	1500, G	Ol Web	0.86	1.52	2.40	1.90	0.55	113	12	269	23	786	3550	7	28	0.63	34.69	2.06	5.60	28
0037	1538, G	Web	0.85	1.05	2.69	0.86	0.31	83	<5	193	14	829	3290	7	31	0.39	45.06	4.35	5.34	17
0041	1695, H	Web	0.81	1.97	2.82	0.28	0.57	125	42	293	28	735	2145	11	45	0.70	38.32	17.11	4.35	37
0042	1723, H	Web	0.84	3.81	2.23	0.42	1.72	180	34	341	38	727	1715	12	51	1.71	33.55	14.38	5.03	50
0044	1838, I	Plag Web	0.76	2.60	17.0	0.04	0.39	144	90	460	122	527	439	16	45	0.15	136.11	490.00	12.25	188
0143	~1845, I	Min Plag Web	0.75	525.0	1854	12.09	108.57	—	237	—	1235	898	155	20	78	0.28	—	196.77	1189	579
0094	1846	Min Plag Web	0.66	88.0	6.28	0.06	44.79	3940	1630	2060	2810	955	51	70	135	14.00	23.93	1571.3	13.47	746
(See Table 14 for further data on the mineralised horizon at the ultramafic–gabbroic zone contact)																				
Gabbroic zone																				
0048	1851, A	GabN	0.67	0.91	1.66	<0.02	0.36	349	125	533	240	195	47	12	669	0.55	7.36	>128.50	2.14	552
0049	1998, A	GabN	0.67	0.42	1.59	0.02	0.20	280	106	795	210	188	77	10	587	0.26	7.18	100.50	2.01	528
0051	2248, A	GabN	0.62	2.22	3.71	0.008	0.67	374	99	511	215	146	27	18	604	0.60	15.86	770.13	3.29	596
0052	2377, A	GabN	0.61	1.03	2.62	0.007	0.32	357	90	324	204	129	14	19	662	0.39	10.22	553.03	1.92	613
0055	2859, A	GabN	0.47	0.98	2.28	<0.005	0.31	405	132	304	311	144	43	21	597	0.43	8.05	>652.00	1.55	684
0058	3181, A	GabN	0.43	0.84	2.37	0.007	0.33	614	150	2200	410	102	<2	21	499	0.35	5.23	433.78	1.53	801
0061	3553, A	GabN	0.40	1.04	1.97	0.018	0.38	581	158	795	354	59	3	37	54	0.53	5.18	170.06	0.81	857
0064	3965, A	GabN	0.37	0.46	1.48	0.008	0.17	657	161	572	337	38	<2	31	468	0.31	2.95	255.26	0.63	899
0066	4222, A	GabN	0.34	0.74	1.53	0.023	0.28	721	129	655	262	16	2	34	576	0.48	3.15	99.56	0.67	942
0131	4974, B	GabN	0.77	5.78	4.01	0.14	0.67	281	116	1050	58	89	1885	51	285	1.44	34.84	69.93	1.92	69
Other rock types																				
0046	~1836, I	Opx	0.89	0.88	2.88	0.23	0.26	47	6	625	6	729	3730	3	2	0.31	80.00	16.35	12.53	8
0156	~1800, H	Chrom	0.82	<10.0	3.19	1.47	0.32	33	122	—	5	2040	22700	2	9	—	<399.70	<41.22	<65.95	2
0159	~1836, I	Chrom	0.84	<20.0	2.81	0.32	5.88	46	13	—	22	655	9915	7	4	<7.12	<495.87	<71.28	<32.58	32
0088	— —	Shear	0.52	50.00	11.9	0.16	20.33	5750	1655	—	3685	1399	203	47	131	3.47	10.77	387.00	13.17	568
0163	— —	Shear	0.64	<20.00	3.47	<0.02	7.61	1158	725	—	1590	766	97	23	21	<5.76	<20.27	—	<10.20	675

Sample numbers are prefixed by AGSO reference numbers 8477 or 8577. Min Ol Gab = Mineralised olivine gabbro, GabN = Gabbronorite, Plag Ol Web = Plagioclase olivine websterite, Web = Websterite, Ol Web = Olivine websterite, Cpx = Clinopyroxenite, Lherz = Lherzolite, Opx = Orthopyroxenite, Chrom = Chromitite. Shear = Quartz-carbonate-talc from rock shear that traverses the ultramafic/gabbroic zone contact. Pt, Pd, Ir, Au, Se, Cs determined by RNAA; Cr, Zr, Sr by XRF; Cu, Ni by AAS; S by Leco titration. mg no. = atomic Mg/(Mg + 0.9 Fe), where Fe = Total Fe. — = not determined.

Table 13. Statistical summary of precious-metal data for the major rock groups of the Munni Munni Complex. All concentrations in ppb unless otherwise stated.

	Pt	*Pd*	*Ir*	*Au*
Gabbroic zone				
Magnetite-rich gabbronorite				
Range of data	0.46–1.04	1.48–2.37	7.4 ppt–22.8 ppt*	0.17–0.38
Mean ± standard deviation	0.81 ± 0.23	1.93 ± 0.41	12.1 ± 7.7 ppt*	0.29 ± 0.08
Number of samples	5	5	5	5
Magnetite-poor gabbronorite				
Range of data	0.42–2.22	1.59–3.71	6.6 ppt–0.02	0.20–0.67
Mean ± standard deviation	1.14 ± 0.76	2.39 ± 0.99	13.57 ± 7.4 ppt*	0.39 ± 0.20
Number of samples	4	4	4	4
Ultramafic zone				
Shear across UZ-GZ contact				
Range of data	< 20–50	3.47–11.92	< 0.02–0.16	7.61–20.33
Mean ± standard deviation	—	7.69 ± 5.97	—	13.97 ± 8.99
Number of samples	2	2	2	2
Porphyritic websterite				
Range of data	2.60–525	6.28–1855	0.04–12.09	0.39–108.6
Mean ± standard deviation	131 ± 222	385 ± 821	2.46 ± 5.39	33.6 ± 45.4
Number of samples	5	5	5	5
Spinel-bearing orthopyroxenite				
Range of data	0.88–< 20	2.81–2.88	0.23–0.32	0.25–5.88
Mean ± standard deviation	—	2.84 ± 0.05	0.27 ± 0.06	3.06 ± 3.98
Number of samples	2	2	2	2
Chromitite				
Range of data	< 10	3.19	1.47	0.32
Mean ± standard deviation	—	—	—	—
Number of samples	1	1	1	1
Websterite				
Range of data	1.05–3.81	2.09–2.82	0.28–0.86	0.27–1.72
Mean ± standard deviation	2.16 ± 1.05	2.50 ± 0.32	0.54 ± 0.22	0.67 ± 0.60
Number of samples	5	5	5	5
Clinopyroxenite				
Range of data	1.56–1.58	2.01–2.60	0.42–0.45	0.26–0.29
Mean ± standard deviation	1.57 ± 0.01	2.30 ± 0.42	0.43 ± 0.02	0.27 ± 0.02
Number of samples	2	2	2	2
Lherzolite and olivine websterite				
Range of data	1.18–1.99	1.84–3.30	0.67–1.90	0.20–0.74
Mean ± standard deviation	1.53 ± 0.28	2.33 ± 0.44	1.05 ± 0.38	0.38 ± 0.18
Number of samples	10	10	10	10
Basal sulphide-rich gabbronorite				
Range of data	15.00–35.00	57.55	0.38–0.51	4.79–5.06
Mean ± standard deviation	25.00 ± 14.14	—	0.44 ± 0.09	4.92 ± 0.19
Number of samples	2	2	2	2
Basal chilled gabbro				
Range of data	3.76–4.96	3.40–6.39	0.16–0.60	1.48–1.57
Mean ± standard deviation	4.36 ± 0.84	4.90 ± 2.11	0.38 ± 0.31	1.52 ± 0.06
Number of samples	2	2	2	2

* Parts per trillion.

This feature appears to be real, since all three elements and S (and also Cs, Sr, Zr) show similar concentration depressions at the 2000 m level. Above 2250 m, Pt, Pd, and Au concentrations steadily decrease, or remain constant, with increasing stratigraphic height.

The statistical parameters for the precious-metal data of the major rock types in the Munni Munni Complex are shown in Table 13. Salient features include:

— the enrichment of Pt, Pd, and Au, and depletion of Ir in the S-saturated basal gabbronorites;
— the lower Pt, Pd, Ir, and Au contents in the S-saturated gabbroic zone rocks relative to the S-undersaturated ultramafic zone cumulates;
— the incompatible behaviour of Pt, Au, and in particular, Pd, is reflected by their increasing concentrations with fractionation for most of the ultramafic rocks;
— Ir shows highest concentrations in peridotite and chromitite, suggesting an affinity with olivine and chromite;

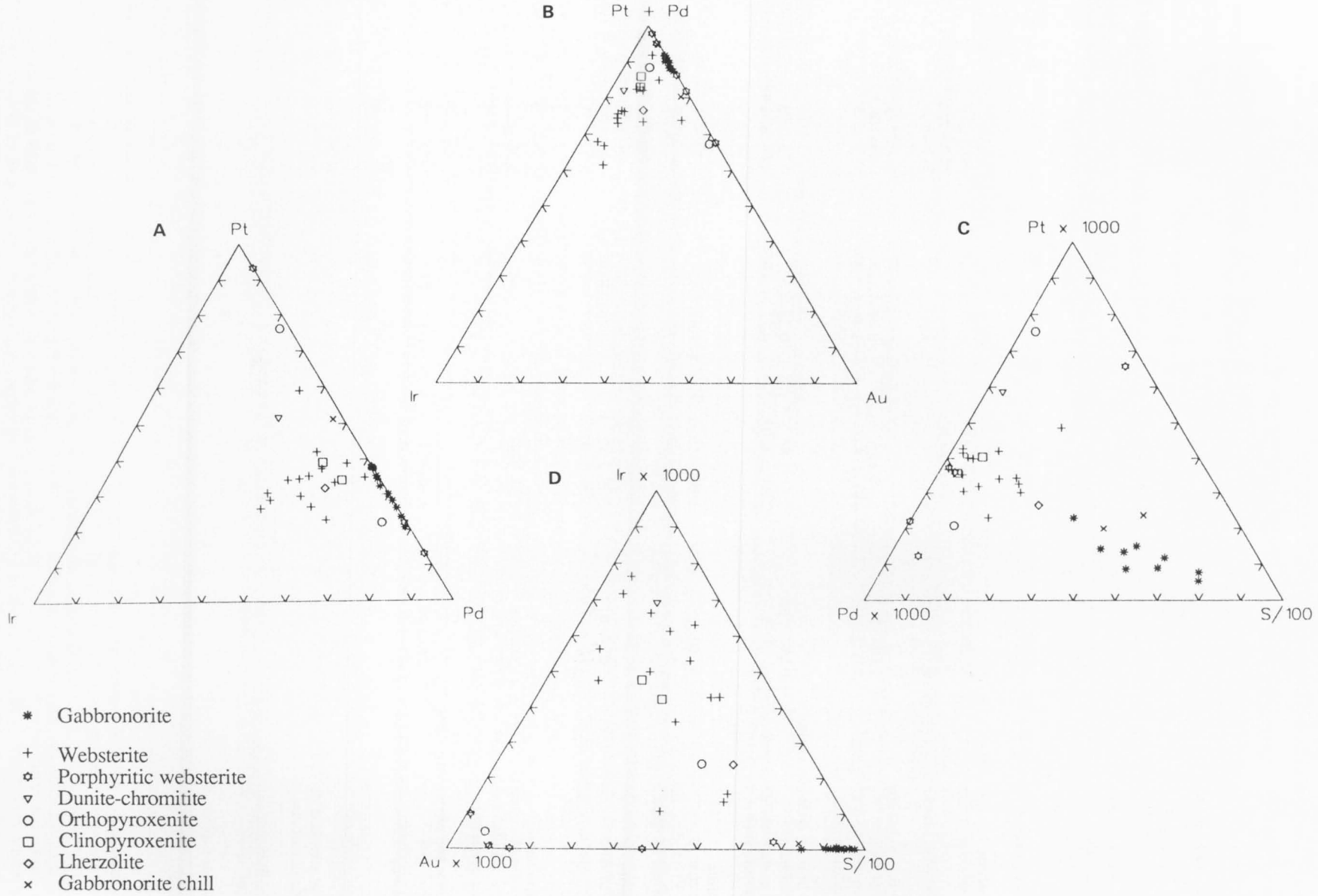

Fig. 55A–D. Munni Munni Complex: ternary plots showing variation in precious-metal contents in ultramafic and gabbroic zone rocks.

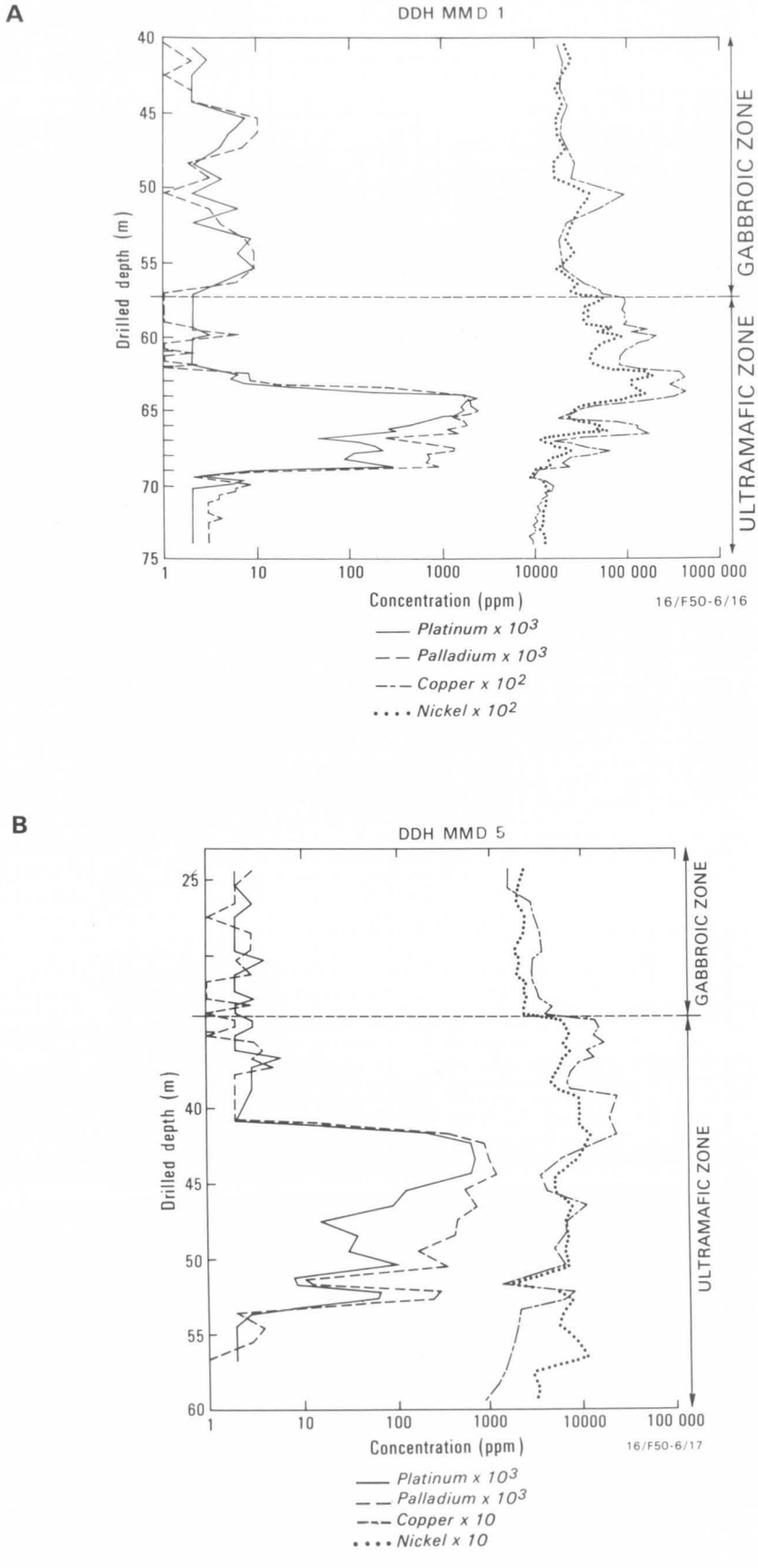

Fig. 56A–B. Munni Munni Complex: (A) profiles of Pt, Pd, Cu, and Ni across the mineralised layer in DDH MMD 1. Rock types for the drillhole section are shown in Table 14. (B) profiles of Pt, Pd, Cu, and Ni across the mineralised layer in DDH MMD 5. DDH MMD 5 was collared 1.5 km along strike from DDH MMD 1, in laminated gabbronorite.

Table 14. Precious-metal and trace-element geochemistry of the Munni Munni Complex platiniferous horizon in DDH MMD 1

Sample no.	*Interval down hole (m)*	*Pt (ppb)*	*Pd (ppb)*	*Ir (ppb)*	*Os (ppb)*	*Ru (ppb)*	*Rh (ppb)*	*Au (ppb)*	*Cu (ppm)*	*Ni (ppm)*	*Pt/Pd*	*(Pt + Pd)/(Ir + Os + Ru)*	*Cu × 10^3/(Cu + Ni)*
Gabbroic zone													
32246	10.00–11.00	<2	5	—	—	—	—	—	249	190	<0.40	—	567
32251	15.00–16.00	8	10	—	—	—	—	—	221	280	0.80	—	441
32256	20.00–21.00	4	3	—	—	—	—	—	330	200	1.33	—	623
32261	25.00–26.00	<2	4	—	—	—	—	—	223	210	<0.50	—	515
32266	30.00–31.00	<2	3	—	—	—	—	—	423	280	<0.66	—	602
32271	35.00–36.00	3	4	—	—	—	—	—	354	210	0.75	—	628
32276	40.00–41.00	<2	1	—	—	—	—	—	186	200	<2.00	—	482
32281	45.00–46.00	7	9	—	—	—	—	—	194	170	0.77	—	533
32286	50.00–51.00	<2	1	—	—	—	—	—	820	890	<2.00	—	480
32291	55.00–56.00	9	9	—	—	—	—	—	200	170	1.00	—	540
Ultramafic zone													
32163	60.00–60.25	3	6	—	—	—	—	—	2160	840	0.50	—	720
32167	61.00–61.25	2	1	—	—	—	—	—	980	440	2.00	—	690
32171	62.00–62.25	2	2	—	—	—	—	—	870	430	1.00	—	669
32175	63.00–63.25	5	8	—	—	—	—	—	2900	1110	0.62	—	723
32176	63.25–63.50	7	12	—	—	—	—	—	2900	1110	0.58	—	723
32177	63.50–63.75	29	265	—	—	—	—	—	3200	1200	0.11	—	727
32178	63.75–64.00	270	670	—	—	—	—	—	4200	1500	0.40	—	737
32179	64.00–64.25	1600	1780	8	<3	<14	42	490	3600	1300	0.90	>135	735
32180	64.25–64.50	2200	1990	13	<3	38	73	220	2600	970	1.10	>78	728
32181	64.50–64.75	1900	2020	—	—	—	—	—	1010	450	0.94	—	692
32182	64.75–65.00	1600	2130	24	9	69	110	94	438	300	0.75	37	593
32183	65.00–65.25	1700	2560	34	9	94	170	60	289	250	0.66	31	536
32184	65.25–65.50	1400	2230	37	9	100	180	39	264	220	0.63	25	545
32185	65.50–65.75	960	1880	31	6	83	150	45	152	200	0.51	24	432
32186	65.75–66.00	700	1820	29	6	130	130	69	650	340	0.38	15	657
32187	66.00–66.25	430	1910	12	<3	66	89	230	1280	540	0.23	>29	703
32188	66.25–66.50	280	1170	5	4	29	42	85	1230	490	0.24	38	715
32189	66.50–66.75	310	1730	—	—	—	—	—	1730	680	0.18	—	718
32190	66.75–67.00	87	600	—	—	—	—	—	296	170	0.15	—	635
32195	68.00–68.25	110	720	—	—	—	—	—	399	220	0.15	—	645
32199	69.00–69.25	16	17	—	—	—	—	—	119	110	0.94	—	520
32203	70.00–70.25	6	8	—	—	—	—	—	159	130	0.75	—	550
32294	75.00–76.00	4	6	—	—	—	—	—	101	500	0.66	—	168
32299	80.00–81.00	5	7	—	—	—	—	—	77	510	0.71	—	131
32317	85.00–86.00	5	7	—	—	—	—	—	32	500	0.71	—	60
32322	90.00–91.00	<2	3	—	—	—	—	—	73	510	<0.66	—	125
32219	100.00–100.25	2	2	—	—	—	—	—	55	130	1.00	—	297
32363	120.00–121.00	4	6	—	—	—	—	—	44	1900	0.66	—	23
32383	140.00–141.00	5	4	—	—	—	—	—	55	1600	1.25	—	33
32403	160.00–161.00	2	1	—	—	—	—	—	42	640	2.00	—	62
32410	180.00–181.00	2	2	—	—	—	—	—	37	580	1.00	—	60
32430	200.00–201.00	6	4	—	—	—	—	—	31	760	1.50	—	39
32450	220.00–221.00	3	7	—	—	—	—	—	37	1100	0.43	—	33
32338	240.00–241.00	3	2	—	—	—	—	—	43	1400	1.50	—	30

Diamond-drillhole data (DDH MMD 1) kindly provided by Hunter Resources Ltd. Platinum and Pd determined by fire-assay–atomic-absorption spectrophotometry (FA-AAS); Cu and Ni by atomic-absorption spectrophotometry by SGS Australia Pty Ltd; Ir, Os, Ru, Rh, and Au by fire-assay–neutron activation (FA-NA) by Nuclear Activation Services Ltd, Ontario. — = not determined. Rock types drilled include gabbronorite (GZ), and porphyritic plagioclase websterite, olivine websterite, and serpentinised dunite (UZ).

— spinel-bearing orthopyroxenite blocks are depleted in Pt, Ir, and Au relative to the surrounding rocks, which supports the view that they are of accidental origin;
— chromitites contain low precious-metal contents relative to the enclosing porphyritic websterite layer, indicating that in a S-saturated magma, Pt, Pd, Ir, and Au will partition with S rather than Cr; and
— talc-carbonate-chlorite shears which traverse the mineralised websterite layer are enriched in Pt, Au, and, to a lesser degree Pd. Iridium shows no enrichment in the shear zone, which may indicate that under certain low-temperature conditions, Pt and Au are more mobile than Ir.

The ternary plots of Figures 55A–B highlight the dominance of Pt and Pd over Ir and Au in the ultramafic and gabbroic zone rocks and the Ir-poor nature of the latter rocks. Figure 55C shows that the gabbroic zone rocks have a higher S component than the ultramafic zone rocks, and the Pt and Pd contents of the unmineralised ultramafic rocks show a parallel relationship with S. This contrasts with the poor correlation of Ir with respect to S in Figure 55D. In the ternary plots of Figure 55, the mineralised porphyritic websterite has contrasting precious-metal and S contents relative to the other ultramafic zone rocks. This reflects the different behaviour of PGEs in S-undersaturated and S-saturated conditions. Similarly, the orthopyroxenites generally plot in separate fields, testifying to their accidental origin.

Copper, nickel, platinum, palladium, gold, iridium across the ultramafic/gabbroic zone contact. Platinum, Pd, Cu, and Ni trends in the vicinity of the zone contact are shown in the drillhole profiles of DDH MMD 1 and DDH MMD 5 (Fig. 56; note: 'up-hole' is also 'up-stratigraphy'). No surface samples were analysed for the PGEs over the stratigraphic interval 1723–1838 m due to poor exposure, and the increase in Pt and Pd above 1723 m is actually more abrupt than that shown in Figure 54A, as indicated by the drillhole data.

In DDH MMD 1 (Table 14; also Fig. 56A), Cu over the interval 240 to 76 m shows a weak increasing upward trend from 31 to 77 ppm, but above 76 m it rapidly increases and reaches a maximum of 4200 ppm at 64 m (7 m below the zone contact). Sulphur saturation, as indicated by the presence of cumulus sulphides and the rapid increase in Cu concentrations, occurs approximately above the 76 m level in DDH MMD 1 (equivalent to the ~ 1830 m stratigraphic level in the intrusion). Nickel on the other hand shows a more erratic trend upwards, and only above 65.75 m does it show any systematic increase in concentration upwards and sympathetic trends with Cu. Nickel and Cu attain their maximum concentrations of 1500 and 4200 ppm, respectively, at the 64 m level, indicating that both metals have similar sulphide/silicate partitioning coefficients (e.g. ~ 250–275: Naldrett, 1989). Across the ultramafic/gabbroic zone contact, Cu and Ni concentrations in gabbronorites decrease abruptly to < 420 ppm and < 280 ppm, respectively.

Platinum and Pd concentrations increase rapidly above the 70 m level in DDH MMD 1 (Table 14). Palladium is more chalcophile than Pt: it reaches its maximum concentration (2560 ppb) prior to Pt (2200 ppb) and the Pt/Pd ratio increases steadily upward from about 0.2 at the 67 m level to 1.0 at the 64 m level. The mineralised websterite is enriched in Pt and Pd by factors of approximately 10^3 relative to the unmineralised ultramafic zone rocks. For the most strongly mineralised 3 m-wide interval, 66.75–63.75 m, Pt and Pd average 1.11 and 1.82 ppm respectively. Both elements drop sharply to background concentrations immediately above the mineralised layer, whereas Cu and Ni continue to increase upwards. The dramatic increasing and decreasing trends of Pt and Pd during the initial stages of S build-up (as reflected by the trends of Cu and Cu/(Cu + Ni)) testify to the very high partitioning coefficients (10^4 to 10^5) of these elements from the silicate melt into sulphide liquid, as suggested by Campbell & Barnes (1984), Peach & others (1989), and Stone & others (1990). The slight displacement between Pt and Pd peaks, the decoupling of the precious metals from the base metals, and the increasing Pt/Pd ratio with increasing fractionation, are consistent with the trends observed in the PGE-rich horizons in the Wedza (Prendergast & Keays, 1989) and Darwendale (Wilson & Tredoux, 1990) subchambers of the Great Dyke of Zimbabwe, as well as the trends predicted in the S-saturated stages of a fractionation model proposed by Wilson & others (1989: see fig. 5).

Table 15. Pearson correlation coefficients for mineralised drill core from subzone I of the Munni Munni Complex

	Pt	*Pd*	*Cu*	*Ni*
Pt	—	0.79	0.13	0.21
Pd	—	—	−0.09	−0.07
Cu	—	—	—	0.96
Ni	—	—	—	—

The Pearson correlation coefficients for 20 drill core samples (Table 15) highlight the strong association of Cu with Ni and the decoupling of Pt and Pd from the base metals in the mineralised porphyritic websterite layer.

Relatively low concentrations of Au and Ir (maximum concentrations of 490 ppb and 37 ppb, and average concentrations of 148 ppb and 21 ppb, respectively, for the mineralised interval 66.25–64.00 m) are associated with the Pd and Pt mineralisation (Table 14). Gold has sympathetic trends with Cu and Ni, whereas Ir has antipathetic trends with the base metals. The most anomalous Au concentrations occur at the bottom and top of the high Pd-Pt interval, whereas the highest Ir concentrations are near the middle of the mineralised interval.

DDH MMD 5 (Fig. 56B), 1.5 km along strike from DDH MMD 1, shows similar geochemical trends to those in DDH MMD 1. Platinum and Pd contents increase rapidly during the early build-up of Cu and Ni and decrease abruptly to background concentrations before the base-metal concentrations peak. Additional drilling along a 7.5 km strike length of the porphyritic websterite layer has indicated considerable lateral uniformity for the PGE mineralisation. The main Pt- and Pd-enriched zone is restricted to within 20 m of the ultramafic/gabbroic zone contact, although some localised Pd-Cu-Ni enrichment (2 m @ 800 ppb Pd, 60 ppb Pt) may be present up to 45 m below the contact. This uniformity of mineralisation is also seen in a vertical sense as shown by the drillhole section of Figure 57. The spatial setting of the PGE mineralisation relative to the zone contact, the attitude of the mineralised zone, and the thickness of the porphyritic websterite layer are consistent to vertical depths of at least 550 m. There is an indication that the bulk PGE content (grade × thickness of intersection) increases at depth near the

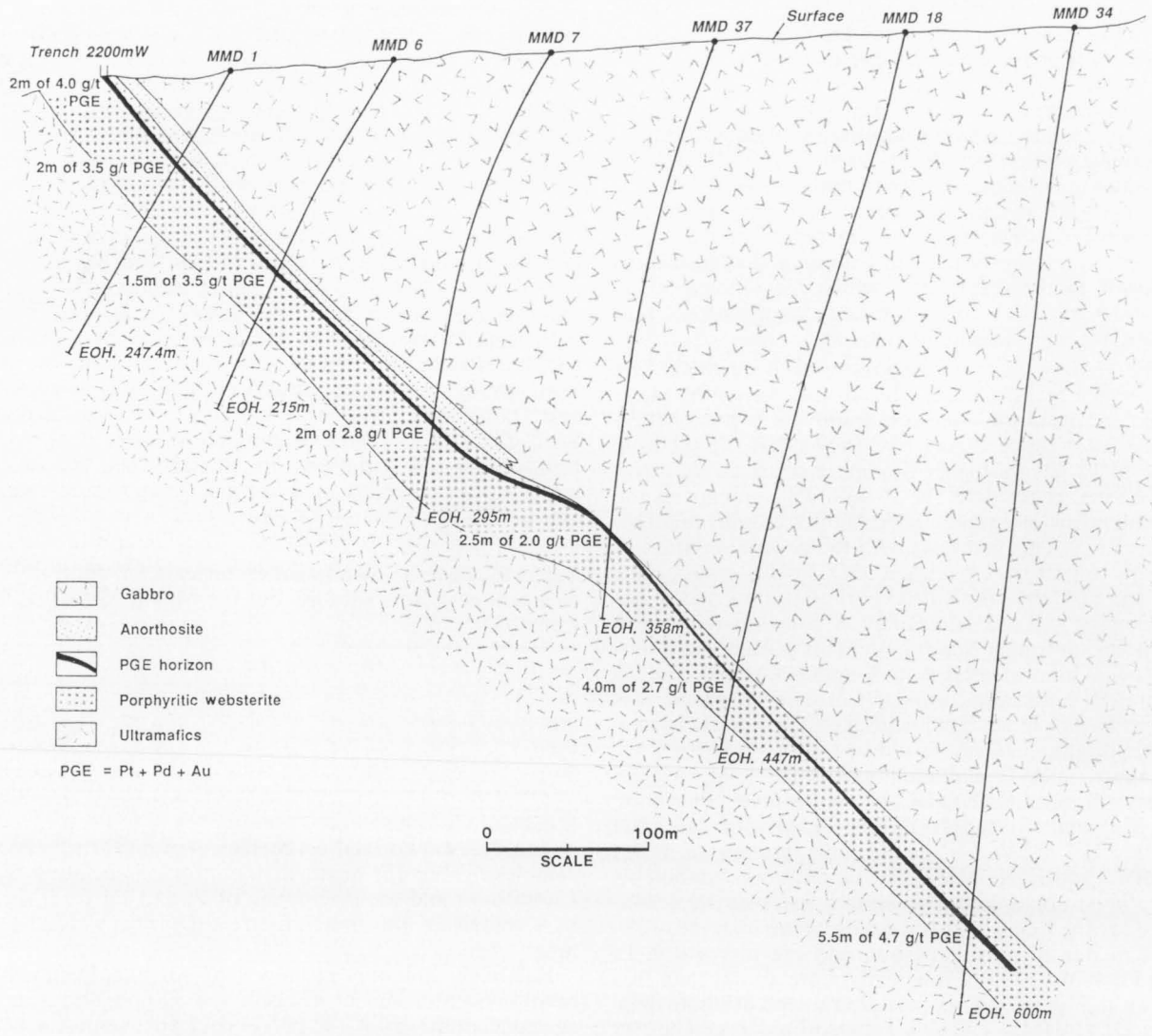

Fig. 57. Munni Munni Complex: diamond-drillhole profile of holes drilled to intersect the mineralised porphyritic websterite layer of subzone I, in the central part of the Munni Munni Complex. The profile highlights the persistent stratigraphic position of the Pt + Pd + Au mineralisation to vertical depths of at least 550 m. Drilling carried out by Hunter Resources Ltd. Figure modified from Williams & others (1990).

central axis of the intrusion, although further drilling would be required to substantiate this.

The vertical and lateral distribution of sulphides and PGEs in the porphyritic websterite layer is discussed in more detail by Barnes & others (1992).

Osmium, ruthenium, rhodium across the ultramafic/gabbroic zone contact. The mineralised porphyritic plagioclase websterite layer is less enriched in Os ($\leq$ 9 ppb), Ru ($\leq$ 130 ppb), and Rh ($\leq$ 180 ppb) relative to the other precious metals (Table 14). Osmium, Ru, and Rh have similar distribution trends to those of Ir and to a lesser degree Pd: their highest concentrations occur in the middle of the mineralised interval and decrease consistently above and below this interval. These elements were not analysed outside the main zone of Pd-Pt enrichment, so that their distribution trends in unmineralised rocks are not known.

The precious and base metals fall into four groups that show subtle differences in distribution trends in the mineralised websterite layer owing to their different partition coefficients between sulphide liquid and magma. These include: (1) Pd contents consistently decrease above, and below, the main mineralised interval; (2) Pt trends are similar to Pd, except they peak at a later stage; (3) Cu and Ni contents generally increase upwards and attain their maximum concentrations well above the highest Pd, Pt, and Au concentrations; and (4) Ir, Os, Ru, and Rh generally have highest concentrations in the middle of the mineralised interval. The sequence of selective removal of metals from the magma in the mineralised environment, and therefore the order of enrichment in sulphide, is believed to be: Ir $\sim$ Pd $\sim$ Rh $\sim$ Ru $>$ Pt $>$ Au $\gg$ Cu $\sim$ Ni. The position of Os in this sequence is uncertain because of its low concentrations, but it may be similar to the most chalcophile metals, Pd, Rh, and Ru. Palladium and Pt are known to have distribution coefficients of the order of 10^4 to 10^5 (Campbell & Barnes, 1984; Peach & others, 1989; Stone & others, 1990) and Cu has a much lower value, about 250 (Keays & Campbell, 1981; Naldrett 1989). Thus it is suggested that Au has a partition coefficient for S-bearing liquid somewhere between these two extremes. This is consistent with the recent results of Stone & others (1990), who determined partition

coefficients between a sulphide liquid and basaltic melt at 1200°C to be (9 ± 7) x 10^4 for Pd, (1 ± 0.7) x 10^5 for Ir, (9 ± 6) x 10^3 for Pt, and (1 ± 0.9) x 10^3 for Au.

Outside the S-rich environment, the partitioning coefficients of the precious and base metals are affected by the physical and chemical parameters of the magma. Rajamani & Naldrett (1978) have shown that the partitioning of Cu increases with decreasing temperature, and the partitioning of Ni increases with both decreasing temperature and decreasing MgO content of the magma. The effects of temperature and magma composition on the partition coefficients of the precious metals have not been determined experimentally; however, they are likely to vary under natural conditions, such as changes in the fO_2/fS_2 ratio of the magma (Prendergast & Keays, 1989).

In summary, the mineralised porphyritic websterite layer is strongly enriched in Pd, Pt, and Cu, and moderately enriched in Au, Rh, and Ni, and contains relatively low concentrations of Ru, Ir, and Os. Comparisons of the Munni Munni mineralised layer with PGE-enriched layers from other layered intrusions are shown in Figure 107 and discussed in the chapter on Petrogenesis (p. 165).

Incompatible trace elements selenium, cesium, rubidium, strontium, zirconium. Selenium, with its strong chalcophile properties, follows S in the magmatic cycle and is enriched in sulphides derived from a wide range of magma types (Loftus Hills & Solomon, 1967). Most igneous rocks have S/Se ratios of about 6000 (Stanton, 1972), but during weathering, S and Se are generally fractionated; S is removed as an oxidised species and Se remains behind as metallic Se adsorbed onto hydrous iron oxides (McGoldrick & Keays, 1981). The Eh-pH diagrams constructed by Yamamoto (1976) indicate that S is mobile under most low-temperature alteration processes involving a hydrous phase. As S is often depleted during weathering, Se was determined (by RNAA) to estimate the possible loss of S.

In the Munni Munni Complex, Se appears to parallel the trends of S for most of the ultramafic zone, although the relationship is unclear in the centre of the zone where Se is below the 5 ppb detection limit (Fig. 54B). Above the 1180 m stratigraphic level, Se progressively increases towards the zone contact and reaches a maximum of 1630 ppb in the mineralised websterite layer. In contrast to S, Se shows a weak decreasing trend in the lower 750 m of the gabbroic zone, whereas above 2377 m, Se and S once again show parallel increases through the middle and upper parts of the zone.

The gabbroic rocks along the basal contact of the Munni Munni ultramafic zone are S-rich (up to 12 420 ppm), but pyroxenite and peridotite in the central part of the ultramafic zone have low S contents (≤ 37 ppm). In contrast, the S contents of the gabbroic zone rocks are high, ranging from 280 to 836 ppm. Most Munni Munni rocks in the ultramafic and gabbroic zones have S/Se ratios between 2200 and 5900. These ratios indicate that there may have been some loss of S from those rocks with low S/Se ratios, while a more significant loss of up to 85% S is indicated for some serpentinised peridotites which have S/Se ratios as low as 800.

The variations of the incompatible elements Cs and Zr (Fig. 58) are similar to those of Pt, Pd, Au, Cu, S, and Se, in that all increase in concentration towards both the upper and lower contacts of the ultramafic zone. Strontium and Rb distributions in the ultramafic zone are also largely controlled by the amount of intercumulus liquid, i.e. by plagioclase and phlogopite-biotite, respectively, near the base and top of the ultramafic zone. In subzone A of the gabbroic zone, plagioclase is

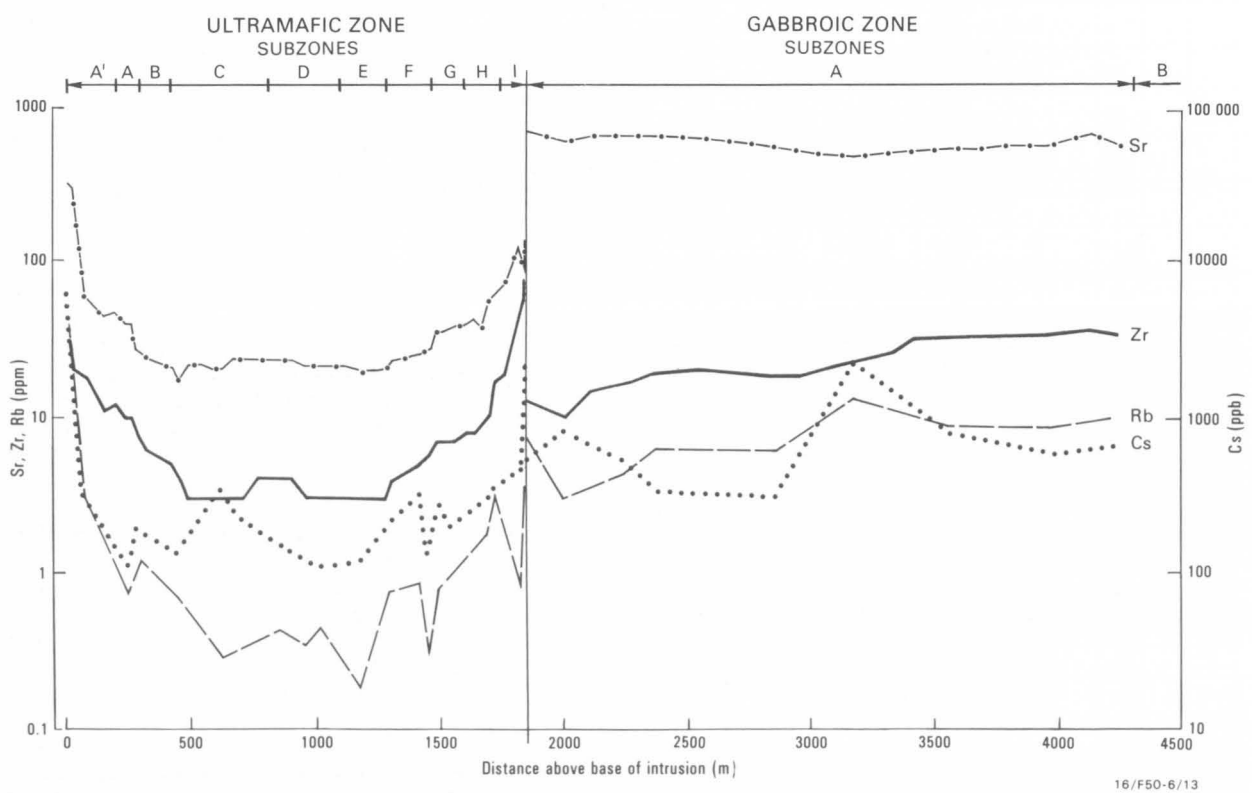

Fig. 58. Munni Munni Complex: profiles of Cs, Rb, Zr, and Sr through the ultramafic and gabbroic zones. A moving average of five sample points was used for the Zr and Sr data.

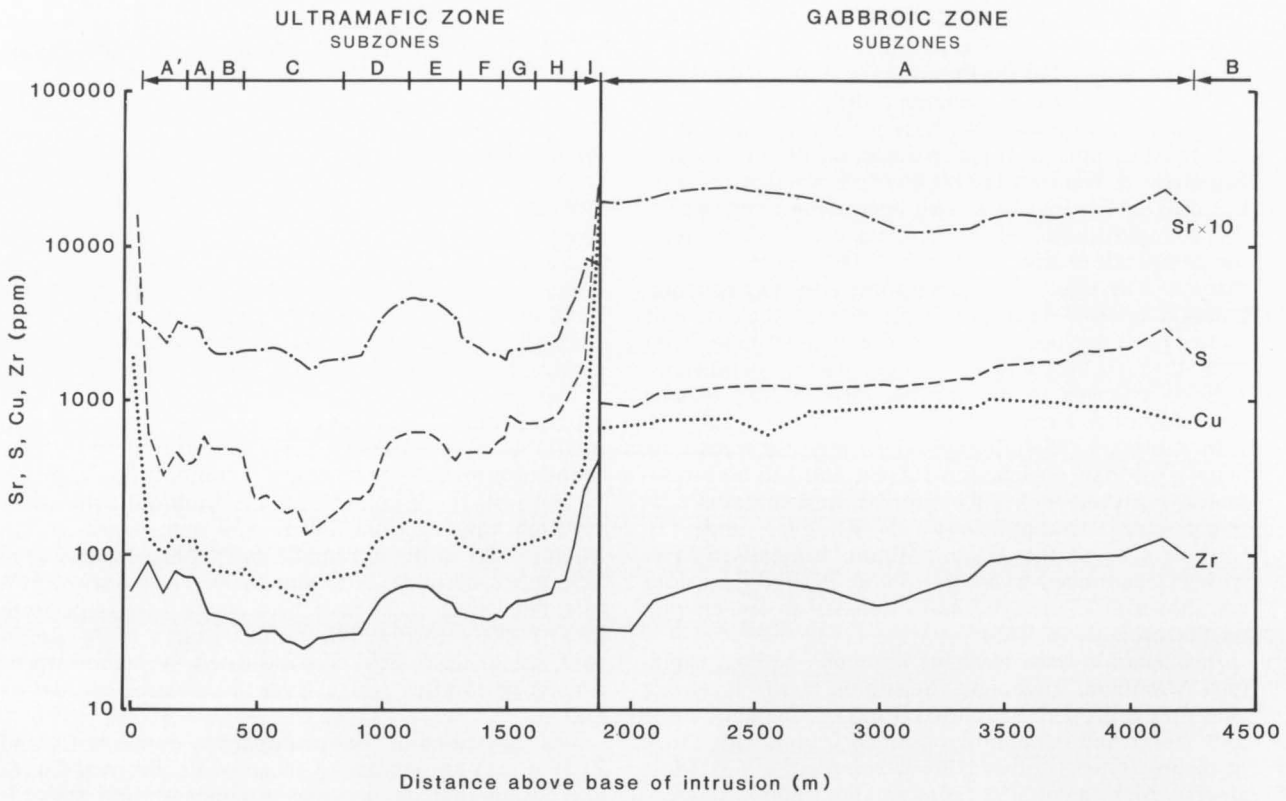

Fig. 59. Munni Munni Complex: profiles of the incompatible elements Sr, S, Cu, and Zr through the ultramafic and gabbroic zones. Element concentrations have been normalised to 100% melt based on the proportion of intercumulus minerals (from point counts) in the cumulate rocks. A moving average of five sample points was used to plot the data. Sulphur saturation occurs at the base of the ultramafic zone and from above the ~ 1830 m stratigraphic level.

of cumulus origin and biotite becomes a prominent intercumulus mineral at high stratigraphic levels. These mineral trends are reflected in the decreasing Sr and increasing Rb concentrations toward the top of the zone.

When assessing the incompatible element variations in Figure 58, it is important to ascertain whether the trends are due to changes in amounts of intercumulus melt in the rocks, or to magmatic processes such as crystal fractionation or magma mixing. One method of determining the relative importance of variable melt components versus magmatic processes is to normalise the trace element abundances to 100% melt based on estimates of the porosities of the cumulates. It should be pointed out that such a procedure has limitations for low-porosity cumulates, e.g. adcumulates, since it is unlikely that the intercumulus minerals preserve the trace element concentrations of the liquid, and certain assumptions about the amount of adcumulus growth in these cumulates have to be made. Despite these limitations the normalisation method is useful for evaluating gross geochemical features. For the Munni Munni Complex, the normalised trends (Fig. 59) are generally similar to the unnormalised trends of Figure 58, but with three differences:

(1) the decrease in Zr and Sr concentrations from the base of the ultramafic zone to the 500 m stratigraphic level is less pronounced than with the unnormalised trends. This indicates that the enrichment of Zr and Sr in the basal rocks (Fig. 58), is partly due to a higher proportion of intercumulus melt. However, Cu and S still show a well-defined decrease in concentration to the 700 m level. Thus, the increase in the concentration of the chalcophile elements along the basal contact is not related to differing amounts of intercumulus melt, but to some other process such as S-saturation induced by cooling or contamination;

(2) in the normalised trends for the stratigraphic interval 900–1300 m a 'hump' in the curves for all elements coincides with the clinopyroxenite adcumulates of subzone E, which have the lowest melt component (< 4%) of all cumulates in the complex. This feature implies that the subzone E clinopyroxenites were derived from a magma pulse enriched in incompatible elements, or, alternatively, it may reflect uncertainties in estimating such low porosities due to postcumulus growth of the clinopyroxene grains; and

(3) there is a sympathetic increase in the normalised incompatible-element concentrations above 700 m and more significantly above 1400 m, to the 1850 m level, which reflects the importance of crystal fractionation as a concentrating mechanism.

Ratios, correlation coefficients, and chondrite-normalised trends of the precious metals and trace elements

The flat trends of Cu/Zr and to a lesser degree (Pt + Pd)/Cs ratios in the ultramafic zone (Fig. 60) suggest similar incompatible behaviour of these elements. Moreover, there are sharp changes in these ratios at about the 1830 m level, coinciding with the introduction of cumulus sulphides. Cu/Zr increases and (Pt + Pd)/Cs declines, highlighting the different behaviour of these elements in S-undersaturated (ultramafic zone) and S-saturated (gabbroic zone) magmas. Ratios such as (Pt + Pd)/Ir and Cu/(Cu + Ni) are useful fraction-

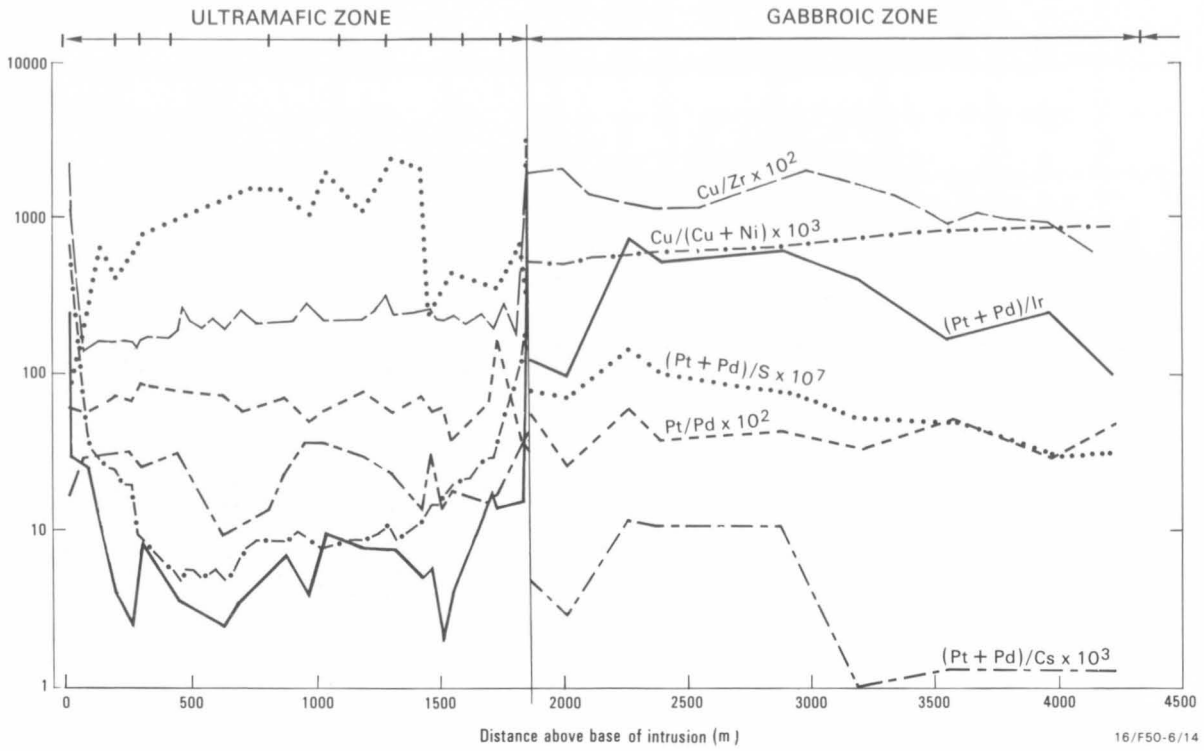

Fig. 60. Munni Munni Complex: profiles of Pt/Pd, (Pt + Pd)/Ir, (Pt + Pd)S, (Pt + Pd)/Cs, Cu/(Cu + Ni), and Cu/Zr through the ultramafic and gabbroic zones.

ation indices in the S-undersaturated ultramafic zone (Fig. 60). These ratios increase toward the main mineralised layer because Pt, Pd, and Cu are concentrated in the melt during fractionation, whereas Ir and Ni are removed with early crystallising olivine. The ratio (Pt + Pd)/Se (or (Pt + Pd)/S if there has been no loss of S during weathering or metamorphism) provides a good indication of the status of S-saturation of the magmas. For example, the ultramafic zone cumulates have much higher (Pt + Pd)/Se ratios (0.11–0.59) than the gabbroic zone cumulates (0.01–0.06). From an exploration point of view the Munni Munni Complex is a good example of how discontinuities in the (Pt + Pd)/Se, (Pt + Pd)/Cs, and Cu/Zr trends may indicate possible new magma pulses and stratigraphic levels of potential mineralisation.

Pearson correlation coefficients for element pairs in S-undersaturated ultramafic and S-saturated gabbroic rocks are listed in Table 16. Elements having the most significant positive correlations (coefficients > 0.44 and < -0.44, and > 0.66 and < -0.66 are statistically significant at the 95% confidence level for the 20 ultramafic and 9 gabbroic samples, respectively: Koch & Link, 1971) can be divided into six subgroups (Table 17) on the basis of their compatibility or incompatibility with cumulus silicate minerals in a S-undersaturated or S-saturated magma.

These correlations reflect the sympathetic enrichment of the incompatible elements (subgroups I, IV, and V) and those elements related to cumulus silicate minerals during fractionation (subgroups II, III, and VI). For the S-undersaturated ultramafic rocks, Ir shows a weak positive correlation with mg (0.32) followed by Ni (0.31) and an insignificant or negative correlation with all other elements. This indicates an affinity between Ir and those elements related to the crystallisation of olivine. In the S-saturated gabbroic zone, Ir displays a weak negative correlation with mg (-0.30) and Ni (-0.46), and a weak positive correlation with S (0.36). This is the reverse of the situation in the ultramafic zone. It is therefore suggested that in the absence of cumulus olivine, and in S-saturated conditions, Ir behaves in a chalcophile manner. A feature of both zones is the strong positive correlation of Pt and Au (0.75 and 0.98, respectively, for the ultramafic and gabbroic rocks). This seems to be unusual, since in the Jimberlana Dyke (Keays & Campbell, 1981), and in the Great Dyke (Prendergast & Keays, 1989) Au commonly follows Cu rather than Pt.

Figure 61 shows the chondrite-normalised whole rock Ir, Pt, Pd, and Au patterns for the various Munni Munni rock groups together with the mantle nodule field. The data have not been normalised to 100% sulphides since, as summarised by Barnes & others (1988), there are assumptions inherent in this procedure that may not be necessarily valid. Firstly, normalising to 100% sulphides assumes that during fractional crystallisation of the rocks all the precious metals entered a sulphide liquid containing 36–38% S. As has been been previously discussed, Ir and probably Os and Ru show a close association with olivine and chromite. Secondly, it assumes that the present S content of the rock represents the original igneous value. However, low S/Se ratios suggest that some Munni Munni peridotites have suffered a significant loss of S (up to 85%). In addition, the Munni Munni ultramafic cumulates generally have very low S contents (< 34 ppm); thus any normalisation manipulations to 36–38% S contents would greatly magnify analytical and sampling uncertainties.

The mantle nodules field (Fig. 61) has a characteristic flat pattern, with all PGEs and Au approximately 0.01 times chondrite abundances. In contrast, the Munni Munni rocks have more fractionated patterns, the rel-

Table 16. Pearson correlation coefficients for rock types from the ultramafic and gabbroic zones, Munni Munni Complex

	Pt	*Pd*	*Ir*	*Au*	*Se*	*S*	*Cs*	*Rb*	*Cu*	*Cr*	*Ni*	*Co*	*Zr*	*Sr*	*Ti*	*V*	*mg*
Sulphur-undersaturated ultramafic-zone rocks (n = 20)																	
Pt		0.37	−0.39	**0.75**	0.52	0.56	0.19	**0.81**	0.50	−0.23	−0.33	−0.26	0.64	**0.68**	0.55	0.18	−0.42
Pd	**0.91**		−0.44	−0.02	**0.80**	0.38	0.43	0.11	**0.93**	−0.41	−0.36	−0.05	0.52	0.30	0.64	0.51	−0.75
Ir	−0.26	−0.32		−0.15	−0.36	−0.26	−0.34	−0.33	−0.39	0.18	0.31	0.17	−0.31	−0.21	−0.33	−0.16	0.32
Au	**0.98**	**0.86**	−0.21		0.29	0.59	0.23	**0.69**	0.21	−0.04	−0.11	−0.21	0.31	0.40	0.16	−0.15	−0.03
Se	−0.41	−0.49	0.05	−0.36		**0.69**	0.38	0.30	**0.85**	−0.53	−0.11	0.14	**0.73**	0.59	**0.66**	0.31	−0.77
S	−0.26	−0.34	0.36	−0.25	**0.74**		0.26	0.58	0.54	−0.20	−0.11	−0.05	**0.72**	**0.67**	0.53	0	−0.41
Cs	−0.17	−0.02	0.13	−0.07	0.41	0.37		0.36	0.44	0.23	−0.45	−0.36	0.33	0.03	0.43	−0.05	0.01
Rb	−0.24	−0.24	0.02	−0.17	**0.69**	**0.80**	**0.67**		0.25	0.09	−0.41	−0.43	**0.74**	**0.75**	0.61	−0.03	−0.15
Cu	−0.26	−0.20	−0.07	−0.22	**0.89**	**0.67**	**0.66**	**0.78**		−0.40	−0.47	−0.19	**0.66**	0.49	**0.77**	0.57	−0.77
Cr	−0.07	−0.07	−0.10	−0.05	−0.51	−0.83	−0.30	−0.76	−0.57		−0.27	−0.55	−0.18	−0.21	−0.15	−0.54	**0.73**
Ni	0.20	0.27	−0.46	0.24	−0.59	−0.94	−0.13	−0.60	−0.50	**0.84**		**0.90**	−0.43	−0.28	−0.68	−0.54	0.20
Co	−0.39	−0.34	0.12	−0.42	**0.83**	**0.86**	0.38	**0.69**	**0.84**	−0.67	−0.80		−0.25	−0.19	−0.45	−0.23	−0.10
Zr	−0.10	−0.23	0.41	−0.13	**0.65**	**0.86**	0.02	0.53	0.53	−0.80	−0.94	**0.74**		**0.93**	**0.92**	0.35	−0.61
Sr	0.32	0.25	−0.27	0.32	−0.79	−0.72	−0.54	−0.51	−0.78	0.52	**0.65**	−0.85	−0.57		**0.79**	0.29	−0.57
Ti	−0.38	−0.40	0.30	−0.38	**0.85**	**0.96**	0.39	**0.75**	**0.80**	−0.75	−0.89	**0.96**	**0.85**	−0.83		0.57	−0.64
V	−0.19	−0.08	−0.09	−0.17	**0.78**	0.56	0.58	**0.66**	**0.96**	−0.49	−0.43	**0.80**	0.50	−0.69	**0.72**		−0.70
mg	0.28	0.32	−0.30	0.31	−0.77	−0.94	−0.26	−0.69	−0.73	**0.76**	**0.92**	−0.94	−0.90	**0.73**	−0.98	−0.70	
Sulphur-saturated gabbroic-zone rocks (n = 9)																	

Significant positive correlations are shown in bold. The correlation coefficients are from data shown in Table 12.

Table 17. Major geochemical subgroups with similar Pearson correlation coefficients, Munni Munni Complex

S-undersaturated ultramafic-zone rocks	*S-saturated gabbroic-zone rocks*
I— Cu-Pd-Se; Zr-Sr-Ti; Pt-Au-Rb-Sr	IV— Cu-Co-S-Se-Rb-Ti-V-Zr
II— mg-Cr	V— Pt-Pd-Au
III— Ni-Co	VI— Cr-Ni-mg

ative enrichment of the elements being Pd > Au > Pt ≫ Ir. The mineralised basal gabbronorite (trend B) of subzone A′ and porphyritic websterite (trend A) of subzone I are enriched in Pt, Pd, and Au, but depleted in Ir relative to the mantle nodules field. The overall pattern of the mineralised websterite displays characteristics similar to those of the Merensky and J-M reefs (discussed in the Petrogenesis chapter, p. 165). The unmineralised rocks generally have similar normalised patterns to the mineralised rocks, but are depleted in Pt, Pd, and Ir relative to mantle nodules.

The strong Ir depletion features of the olivine-free rocks (trends A, B, F, and H) and the highest Ir/Pt ratios in the lherzolites (trend G) suggest Ir behaved compatibly and was probably retained along with residual olivine in the mantle or removed with olivine during fractionation in the crustal magma chamber. In their study of Western Australian komatiites, Ross & Keays (1979) found Pd and Ir concentrations of 0.21 and 5.7 ppb, respectively, in olivine, and 10 and 1.4 ppb, respectively, in the parent liquid. This indicates that Ir partitions with olivine relative to a silicate melt, whereas the opposite is true for Pd. The Munni Munni data are generally consistent with this observation, although other phases such as Ir-Os alloys and chromite might also be important for the partitioning of Ir (Mitchell & Keays, 1981).

Gabbronorite (trend A) from the basal contact and mineralised websterite (trend B) near the top of the ultramafic zone have similar normalised patterns. Hence, despite the fractionation that occurred during the formation of the ultramafic zone cumulates, the Pt, Pd, Au to Ir ratios did not significantly change. This suggests the magma chamber was continually being topped up with new pulses of primitive magma and new supplies of Ir. An open system of magma replenishment operated for most of the ultramafic zone, but a dramatic drop in Ir contents from above the 1500 m level (Fig. 54A) coincides with the change from an open to a closed system, as defined by the chemical trends of cumulus minerals. The olivine-free rocks (trends A, B, F, and H), that are from different levels in the intrusion, have similar normalised PGE and Au patterns. This supports the view that the parent magmas that formed the ultramafic and gabbroic zones were probably genetically related.

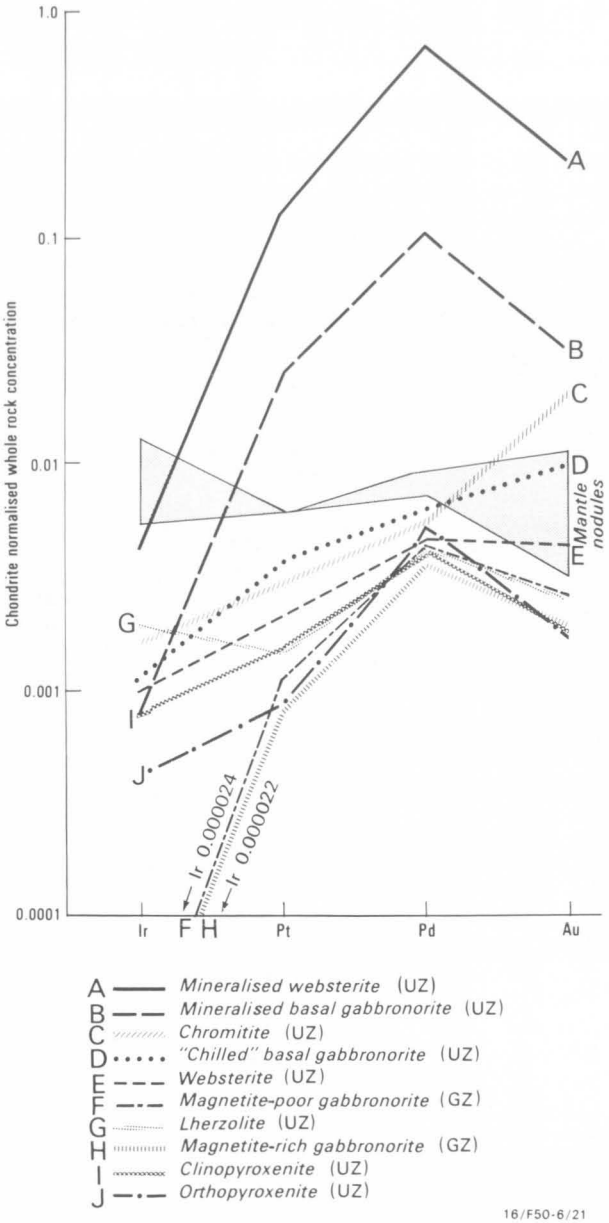

Fig. 61. Munni Munni Complex: chondrite-normalised Pt, Pd, Ir, and Au patterns for mineralised and unmineralised rock types from the ultramafic zone (UZ) and gabbroic zone (GZ). Total number of samples represented by the 10 profiles is 37. The C1 chondrite-normalised and mantle-nodule data are from a number of sources quoted by Naldrett & Duke (1980) and Barnes & others (1985).

FIELD RELATIONSHIPS, PETROGRAPHY, AND GEOCHEMISTRY OF THE MOUNT SHOLL COMPLEX *(DMH)*

Introduction

The Mount Sholl Complex is 22 km south of Karratha and 20 km north of the Munni Munni Complex, at latitude 20°56′S and longitude 116°54′E, on the Dampier 1 : 100 000 Topographic Sheet 2256 and Dampier & Barrow Island 1 : 250 000 Geological Sheet SF/50-2. Its broad geological setting is similar to the Munni Munni Complex, but it differs in having a smaller proportion of ultramafic rocks, in being more extensively tectonised, and in having Ni-Cu sulphide mineralisation near the basal contact.

Size and age

The Mount Sholl Complex has an irregular 'bow-tie'-shaped outcrop measuring 3 by 6 km (Fig. 62 & appended map sheet). Like most other west Pilbara layered intrusions, the Mount Sholl Complex has a northeasterly trend and contains dominantly metagabbroic rocks, with intensely serpentinised ultramafic rocks restricted to the northern half of the intrusion. Mafic rocks form low hills (up to 30% outcrop) in the northern part of the intrusion. Exposure at the southern end is restricted to the margins of the intrusion, and the central region is covered by gabbroic rubble and skeletal soils (Fig. 63A, B). The irregular 'bow-tie' shape of the outcrop of the intrusion is partly due to a complex interplay of strike-slip and dip-slip faulting, and also reflects the shallow dip of the intrusion. The relatively thin, sheet-like geometry of the intrusion is also indicated by the absence of any obvious gravity signature (Dampier 1 : 250 000 BMR Bouguer Anomalies Sheet F50/B2-2, 1972). Aeromagnetic data (Dampier 1 : 250 000 AGSO Total Magnetic Intensity Sheet 22-1/F50-2/1, in prep.) show that there are no significant subsurface extensions (in contrast to the Munni Munni Complex). The ultramafic rocks along the northwestern side of the intrusion have prominent aeromagnetic high anomalies attaining 800 nT, whereas the mafic rocks have anomalies of only 150 nT.

The tectonised complex intrudes Warrawoona Group country rocks that have been subdivided into intermediate and acid metavolcanics and associated pyroclastics tentatively assigned to the Duffer Formation, and mafic to intermediate metavolcanics tentatively assigned to the older Talga Talga Subgroup. Unlike the other west Pilbara intrusions studied, no granitic rocks occur in the vicinity of the Mount Sholl Complex. The Duffer Formation includes metarhyolite, metarhyodacite, meta-andesite, ash-fall tuffs, crystal tuffs, and minor agglomerates. The fine-grained pyroclastics locally have thin, size-graded ash layers that drape over crystal-rich blocks, and pumice-rich horizons, indicating an ash-fall origin. The Talga Talga Subgroup consists of aphanitic pillowed metabasalt, meta-andesite, and conformable microporphyritic metadolerite sills. The metabasalt pillows rarely exceed 30 cm, are strongly deformed, and have thin (< 3 mm) glassy selvedges (Fig. 63C). The pillows range from ovoid to crescent-shaped to flattened lenticular bodies.

The chronological framework for the Mount Sholl Complex is poorly constrained: no isotopic ages have been determined for the intrusion or surrounding rocks. The complex is younger than the Warrawoona Group, as shown by the chilling of marginal gabbroic rocks and gabbroic veins intruding hornfelsed volcanics. To the south, the Mount Roe Basalt, the basal formation of the Fortescue Group, unconformably overlies Duffer Formation metavolcanics of the Warrawoona Group. Unfortunately the Fortescue Group is not in contact with the Mount Sholl Complex. The intrusive relationship with the Warrawoona Group metavolcanics gives a maximum apparent age of 3300–3500 Ma for the Mount Sholl intrusion. However, if Horwitz (1988, 1990b) is correct and the metavolcanics of the Sholl Belt are part of the younger Whim Creek Group (~ 2900–3100 Ma) and not the Warrawoona Group, a maximum age of about 2900 Ma is indicated for the intrusion, i.e. similar to the Munni Munni Complex.

Distribution of rock types and stratigraphic relationships

Most of the intrusion is a monotonous poorly-layered gabbroic sequence. The mafic rocks have been subdivided into three subgroups: (1) a metagabbroic sequence that forms the main part of the intrusion; (2) a fine-grained, partly microporphyritic metagabbro; and (3) an aphanitic to fine-grained magnetite-rich ferrogabbro.

(1) Fine-to-medium-grained metagabbro, metagabbronorite, plagioclase metaclinopyroxenite, and minor anorthositic metagabbro are the dominant mafic rocks of the complex. These units are difficult to distinguish in the field, with no obvious compositional changes along, and across, the intrusion. The main rock type is a medium-grained, intergranular-textured metagabbro, commonly intensely tremolitised and sericitised. A 3–5 m-wide chill zone separates the medium-grained metagabbros from the metavolcanic country rocks and is particular prominent along parts of the southeastern and northwestern sides of the intrusion where metagabbro abuts intermediate and acidic metavolcanics. Acidic metavolcanic blocks up to 100 m long are locally incorporated in the marginal metagabbroic rocks. Thin (< 5 cm), irregular gabbroic veinlets, that thicken and thin markedly along strike, intrude the metavolcanics for up to 0.5 m (Fig. 63D). The hornfelsed metavolcanics are also locally fractured and brecciated near the contact.

The metagabbros have no significant cyclicity or macrorhythmic layering, although locally the plagioclase content increases upwards and the rock becomes an anorthositic metagabbro or meta-anorthosite. These more felsic rocks are of limited distribution, with strike lengths less than 10 m. Rare layering in the metagabbroic units takes the form of thin wispy segregations and thin modally-graded layers (Fig. 63E) of intercumulus plagioclase that have no lateral continuity or obvious relationships with major structural elements in the intrusion.

(2) Microporphyritic clinopyroxene (up to 2 mm) within a fine-grained matrix, and intense uralitisation and chloritisation alteration distinguish metagabbroic rocks of subgroup 2 from the subgroup 1 metagabbros. Subgroup 2 has a restricted distribution north of a dyke-like body of subgroup 1 metagabbro and serpentinised peridotite at the northeastern end of the intrusion. Quartz-filled shear zones containing chrysocolla, malachite, and ?cuprite occur at the western end of the gabbro outcrop. The relationships between the metagabbro subgroups are unknown because of poor outcrop.

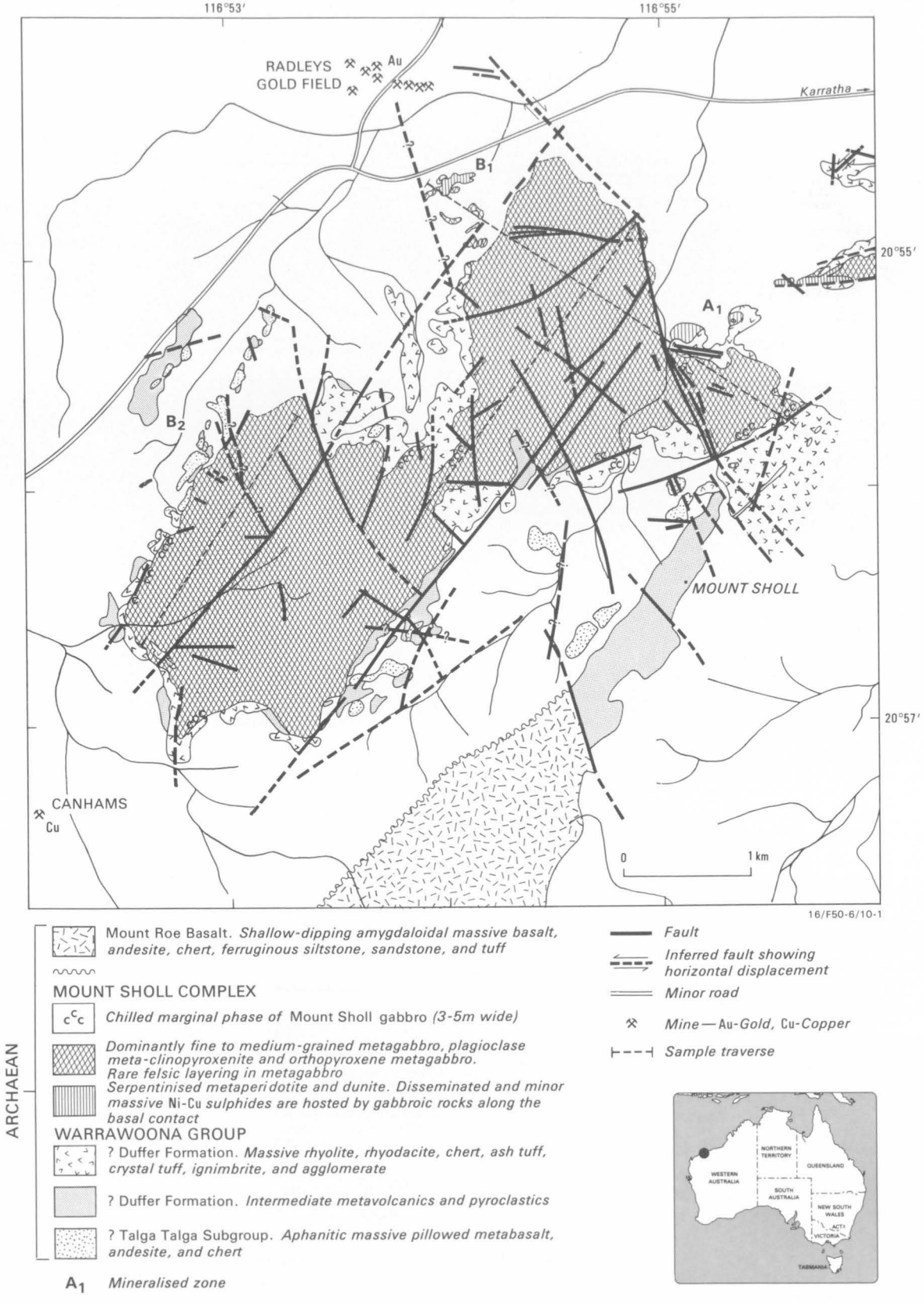

Fig. 62. Geology of the Mount Sholl Complex (simplified from appended map sheet).

(3) Aphanitic to fine-grained magnetite-rich ferrogabbros are spatially associated with faults in the eastern half of the intrusion. They are commonly related to long north- to northeast-trending faults that traverse metagabbros of subgroup 1 or metavolcanic country rocks adjacent to the intrusion. Along a major northeast-trending fault on the southeastern side of the intrusion, the ferrogabbros extend for over 4 km in metagabbro and intermediate metavolcanics (see appended map sheet). They characteristically form strongly

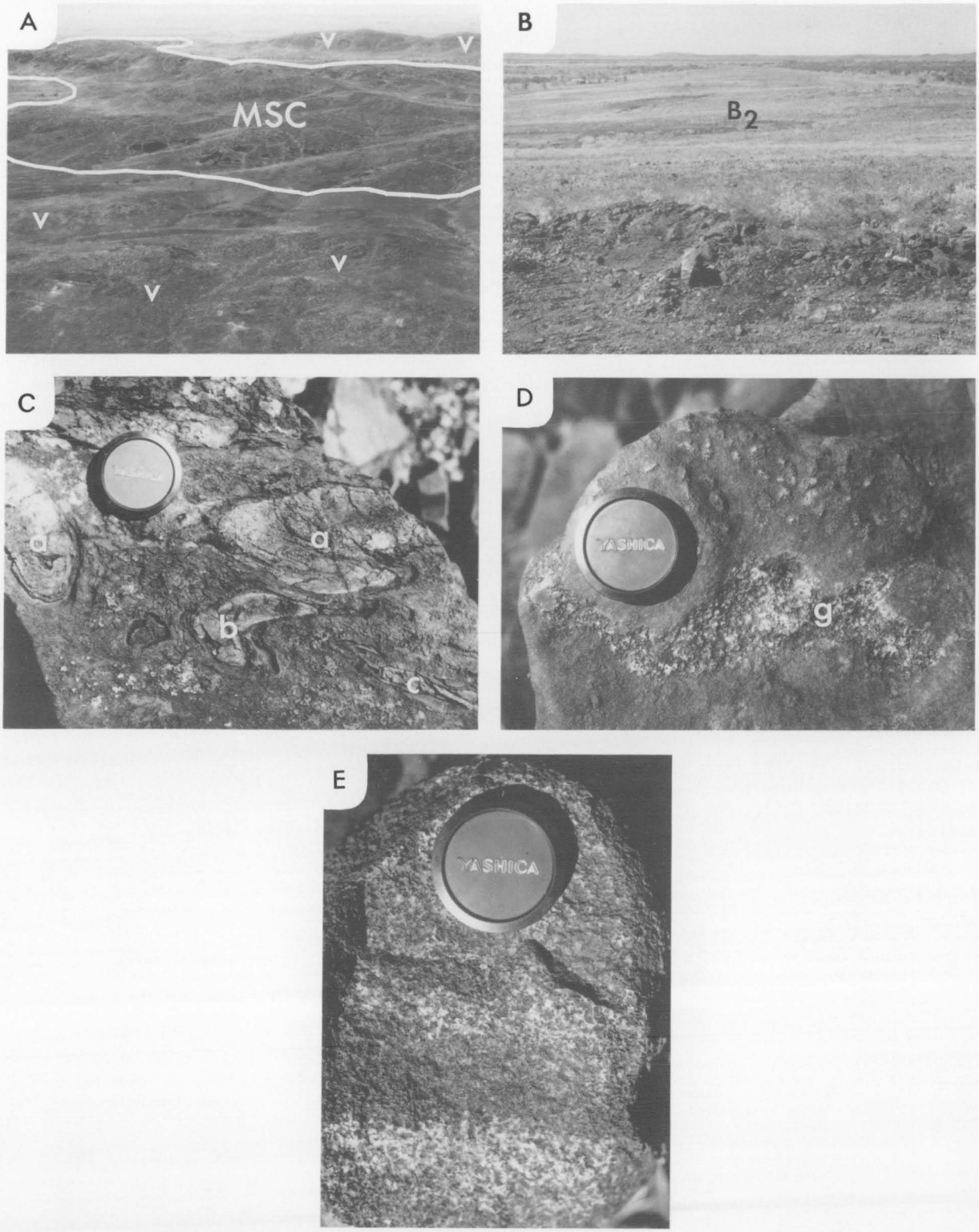

Fig. 63A–E. Mount Sholl Complex: aerial view and rock types. A—Aerial view looking east across the Mount Sholl Complex(MSC). Warrawoona Group intermediate to mafic metavolcanic units(v) are in the foreground and Mount Roe Basalt volcanics and intercalated sediments(v) define the ridge in the top right-hand corner. B—View along the northerly strike of the blind B_2 mineralised trend. The slight linear arch along the trend may be attributed to hornfelsing of the metavolcanic country rocks by the Mount Sholl Complex, which is located to the right of the photo. The longitudinal axis of the arch approximates to the contact between the intrusive complex and the metavolcanic units. It is not known if the absence of vegetation along the B_2 trend was caused by exploration activities or is a genuine geobotanical anomaly. C—Pillowed ?Talga Talga Subgroup metabasalt from the B_2 mineralised region. The small pillows have thin glassy selvedges and have been compressed and rotated during deformation. They range from ovoid(a), to crescent-shaped(b), to flattened lenticular bodies(c). D—Contorted gabbroic vein(g) intruding intermediate metavolcanic country rock; E—rare rhythmic layering in metagabbro unit defined by 10 cm thick modally-graded cyclic layers containing increasing amounts of intercumulus plagioclase up the cycle.

magnetic, rounded outcrops along the faults. Thin (< 2 m) chilled zones are locally present where they abut metagabbro. The strong structural association, their restriction to the intrusion, and the Fe-rich compositions indicate the ferrogabbros were possibly derived from highly-fractionated residual components of the magma that formed the subgroup 1 metagabbros.

Ultramafic rocks crop out locally on the northern (B_1 area) and northeastern (A_1 area) sides of the Mount Sholl Complex (Fig. 62 and appended map sheet). Ultramafic rocks are not exposed along the northwestern contact area (B_2 area), but drilling has defined a ~ 200 m-thick interlayered metaperidotite, metapyroxenite, and metagabbro sequence that contains the largest concentration of Ni-Cu sulphides in the complex (see p. 7). At the northern corner of the intrusion (B_1 area), metaperidotites are poorly exposed over a 150 by 300 m area and are about 100 m thick. They are intensely altered to serpentine and carbonate minerals and primary textures are largely destroyed. In contrast to the metagabbroic rocks, there appears to be a cyclic sequence of interlayered metaperidotite and metagabbro units up-section towards the southeast. The ultramafic component thins upwards relative to the metagabbro component, with the ultramafic rocks also thinning out along strike and possibly forming lenses. Trace Fe-Cu sulphide disseminations and secondary Cu carbonates on fractures and in veins at the surface indicate an association of ultramafic rocks and sulphide mineralisation at depth. The occurrence of sulphide mineralisation with mafic and ultramafic units near the basal contact is very similar to that in the nearby Radio Hill intrusion.

In contrast, ultramafic rocks on the northeastern side have pod-like and dyke-like forms (A_1 area of Fig. 62). They extend over a 1.5 km strike and are aligned along an east-northeast trend that is offset from the northeast-trending longitudinal axis of the intrusion. Two podiform outcrops of serpentinised peridotite partly enclosed by basement metavolcanics contain small gabbroic enclaves. Northeast of these podiform bodies, a fault-bounded dyke-like body of serpentinised peridotite wraps around a core of metagabbroic rocks that form a prominent ridge. At the western end of the ridge, the ultramafics are extensively sheared, with magnesite and chrysotile zones prominent. Shallow pits have been dug along the chrysotile zones and in sheared peridotite containing secondary Cu carbonates. A major southeast-trending dextral inferred fault separates the northeastern ultramafics from the complex; thus the northeastern ultramafics may be a displaced, rotated block of the northwestern ultramafics, although the different intrusive relationships of the ultramafics with the metagabbros in each area indicate this is unlikely. The northeastern ultramafics are interpreted as steeply-dipping podiform and dyke-like bodies which may be related to the Mount Sholl Complex as feeders, or late olivine-rich magmas that have been expelled during the emplacement of the larger volume of gabbroic magma.

Dykes and veins are common, but except for the ubiquitous ?Early Proterozoic metadolerites, strike lengths and thicknesses are generally less than 20 m and 1 m, respectively. Compositions range from quartz, aplite, quartz-feldspar-carbonate, and quartz-epidote, to quartz-bearing anorthosite, anorthosite, and anorthositic gabbro. The anorthositic dykes are restricted to the southern parts of the intrusion and are probably comagmatic with the subgroup 1 metagabbros. A distinctive northwest-trending, fragmental, quartz-bearing pyroxenite dyke traverses the Mount Roe Basalt, basement metavolcanics, the centre of the complex, and then back into metavolcanics. Across the complex, the trend of the dyke is deflected towards the north by faults and at the contact between the complex and the metavolcanics. The 2–5 m-wide central part of the microporphyritic ?orthopyroxene-bearing dyke contains abundant elongated and subangular fragments of quartz, aplite, and laminated chert, whereas the 0.2 m-wide chilled margins have only rare fragments. The partly resorbed fragments are poorly sorted with respect to their sizes, but strongly aligned parallel to the walls of the dyke, through flowage-differentiation.

Close-spaced drilling (Mathison & Marshall, 1981) has shown that the nature of the marginal contact of the intrusion varies along strike. The variations comprise wedge-shaped configurations of peridotite cores enclosed by thin gabbroic envelopes, to simple sheet-like arrangements of a lower gabbroic unit overlain by an ultramafic unit. A wedge-shaped configuration for the contact is indicated in the B_2 area where the average dip of the floor of the intrusion ('footwall') is about 25° towards the southeast and the 'hangingwall' dips moderately towards the northwest. The angle between the 'footwall' and 'hangingwall' varies from about 45° to 80° along strike, the angle generally increasing towards the north-northeast. At the northeastern end of the B_2 area there is a sharp break in this trend with both the floor and hangingwall contacts dipping outwards towards the northwest. Mathison & Marshall (1981) have interpreted the contact relationships at B_1 as a sheet-like extension of the contact at B_2, with an uplifted metavolcanic block separating the two areas.

Structure

Layering and structural features are everywhere poorly developed; thus, younging criteria for the intrusion are largely based on mineralogical and geochemical trends along sample traverses A and B (Fig. 62). These trends indicate the intrusion is a synform that plunges gently towards the northeast and is largely composed of a western limb which dips towards the southeast. The northeast-trending fold axis lies along the southeastern margin of the intrusion, and coincides with the large fault which has ferrogabbro along its length. The eastern limb of the synform is a faulted block at the northeastern corner of the intrusion (Fig. 62 & appended map sheet). Field relationships are also consistent with the interpretation that the complex is a southeasterly-dipping, gently folded sheet. These features include: the position of the ultramafics and associated sulphide mineralisation, along the northwestern margin, relative to the metagabbroic rocks; the shallow southeasterly-dipping footwall contact of the intrusion in the B_2 area; and minor granophyre east of the synformal fold axis (Mathison & Marshall, 1981).

Faulting has played an important role in determining the structure and shape of the complex. Three generations of faults are evident. The earliest phase is represented by two parallel northeast-trending faults that define in part the northwestern and southeastern margins. Movement along these regional steeply-dipping faults was dominantly dip-slip. They were probably active during, and after, emplacement, since they have partly controlled the regional extent of the complex and subgroup (3) ferrogabbros occur along parts of their length. A post-intrusive phase of faulting has a dominant northwest trend and involves both dip-slip and strike-slip movements. These faults have strike extents of less than 2 km and strike-slip displacements of up

to 600 m, and have caused numerous offsets of the contact between the complex and the metavolcanics. They are particularly prominent in the centre of the intrusion, where an intricate interplay of movements has made the outcrop of the complex narrow (150 m) and irregular. A block of basement metavolcanics separating the B_2 and B_1 mineralised zones has been uplifted via these second-generation faults. A third phase of faulting is represented by an extensive northwest-trending fault filled by the quartz-xenolith-bearing pyroxenite dyke discussed above. Movement has been largely dip-slip and postdates the deposition of the Mount Roe Basalt, i.e. younger than 2765 Ma, as can be seen where the fault traverses the Mount Roe Basalt ridge south of the Mount Sholl intrusion (see appended map sheet). Here the steeply-dipping fault separates a downthrown block of Mount Roe Basalt to the southwest from an upthrown block of intermediate metavolcanics to the northeast, from which the overlying Mount Roe Basalt has been eroded. None of the three generations of faulting at Mount Sholl appear to be related to the major east-west-trending Sholl Shear Zone, lying about 1 km to the north of the intrusion.

Mineralisation

There is a broad zonal distribution of precious- and base-metal mineralisation in the vicinity of the Mount Sholl Complex, namely: (1) auriferous quartz veins intrude basement metavoclanics furthest from the intrusion; (2) Cu ± Au ± Pb-bearing quartz veins in basement metavolcanics close to the intrusion; and (3) disseminated Fe-Cu-Ni sulphides in metagabbro and metaperidotite within the intrusion. The spatial association of subgroups 1 and 2 with the Mount Sholl Complex suggests the intrusion may have provided a heat source for the mobilisation of mineralising fluids into structurally favourable sites.

(1) Auriferous quartz veins occur within 600 m of the northern and northwestern contacts of the intrusion. All occurrences are defined by shallow pits along the strike extent of the veins. Most deposits are simple vein systems in metavolcanics, and in particular near shear zones that traverse intermediate and mafic metavolcanics. The largest mineralised vein system is at Radleys Gold Field, 600 m north of the complex, and midway between the complex and the Sholl Shear Zone (see appended map sheet). Mineralisation is discontinuous along a 0.5–1 m wide east-west-trending quartz vein system that intrudes amphibolitised schist for over 1100 m. The deepest workings are 20 m, with total recorded production about 317 g from 32 t of ore (Karratha 1 : 50 000 Urban Geology Series Map, GSWA 2256 11, 1979).

(2) Close to the complex are small quartz veins containing primary and secondary Cu mineralisation. The veins rarely exceed 25 m in strike extent and 1 m in width, and are largely restricted to the mafic metavolcanics. A little Cu has been produced from some of the occurrences. Some Cu-bearing veins further from the intrusion have associated Pb and Au (Karratha 1 : 50 000 Urban Geology Series Map, GSWA 2256 11, 1979), which highlights the more distal nature of Au mineralisation. One of the larger Cu occurrences is the Canhams deposit, situated near a major northeast-trending fault that traverses the intrusion (see appended map sheet). A small pod of quartz-goethite-malachite-chrysocolla mineralisation occurs along a northwest-striking contact between strongly recrystallised feldspathic metabasalt and porphyritic metarhyodacite. Pyrite is also associated with both rock types (Marston, 1979). The Cu in these deposits may have been leached from the surrounding mafic volcanics by hydrothermal SiO_2-rich fluids during regional metamorphism, or alternatively may have been remobilised from the metavolcanics during emplacement of the Mount Sholl Complex. Most of the deposits are characterised by secondary mineral assemblages formed by supergene enrichment.

(3) Three major areas of Fe-Cu-Ni sulphide mineralisation have been delineated by drilling in the Mount Sholl Complex. They are, in order of decreasing economic importance, the B_2, B_1, and A_1 areas (see appended map sheet). In all three areas, mineralisation occurs where gabbroic rocks are in close association with ultramafic rocks, and near basement metavolcanic sequences. The surface expression of the mineralisation is only slight. Malachite, azurite, chrysocolla, and ?cuprite stainings occur with limonite on fractures in sheared metagabbro and metaperidotite and in quartz veins at B_1 and A_1. The mineralisation at B_2 is blind and was found through various geophysical techniques (see p. 7). The northwestern contact of the complex in the B_2 area is indicated by a slight doming of the surface due to the hornfelsing effects of the metavolcanic country rocks.

Mineralisation at B_2 is masked at the surface by a north-northeast-striking sequence of intercalated massive and pillowed mafic metavolcanics, intermediate metavolcanics, and metadolerite sills (Warrawoona Group). Drilling has delineated mineralisation over a 2.5 km strike length at depths between 20 and 150 m. The depth to mineralisation steadily decreases towards the north-northeast. The northeasterly plunge of the intrusion indicates that the mineralisation may continue further to the south-southwest (i.e. sulphides concentrated at the lowest stratigraphic level), but it is terminated to the north-northeast by an upfaulted block of basement metavolcanics.

The distribution and nature of sulphide mineralisation at B_2 has been documented by Mathison & Marshall (1981). They noted that it is confined to a wedge-shaped closure consisting of a central zone of serpentinised peridotite and an outer envelope of metagabbroic rocks that has a thin chilled margin. Most sulphide mineralisation occurs immediately above the metavolcanic footwall contact in metagabbro and plagioclase-bearing pyroxenites for distances of up to 20 m. Disseminated and minor massive pyrrhotite-pentlandite-chalcopyrite persist irregularly to higher stratigraphic levels in the peridotite. Along strike the sulphides generally increase in concentration towards the north-northeast. Sulphides at B_1, by contrast, are largely hosted by peridotite in a thin sheet-like extension of the intrusion.

Petrography and mineralogy

The petrology and geochemistry of the Mount Sholl Complex have been documented in detail by Mathison & Marshall (1981) and summarised by Marston (1979, 1984). They will be discussed only briefly here. Two major problems were addressed in this study, namely (1) to define the orientation of the intrusion by mineralogical and geochemical trends, and (2) to investigate the PGE character of different settings of Ni-Cu sulphide mineralisation in the intrusion.

Metaperidotite (ol ± cpx)

Metaperidotites crop out locally on the northwestern and northeastern sides of the intrusion, but intense serpentinisation and carbonatisation has destroyed the primary mineralogy and textures. The following summary is, in part, from Mathison & Marshall's (1981) study of drill core from the northwestern contact of the intrusion (B_2 area). The metaperidotites are medium-grained (0.5–1 mm) mesocumulates and orthocumulates that contain cumulus olivine and clinopyroxene, and intercumulus plagioclase and orthopyroxene. The minerals in order of decreasing abundance are olivine, clinopyroxene, plagioclase, orthopyroxene, sulphide, biotite, magnetite, and ilmenite. The paragenetic sequence of olivine, clinopyroxene, orthopyroxene, plagioclase, sulphides, and biotite is similar to that of peridotites of the Munni Munni and Radio Hill complexes. Mineral compositions of selected Mount Sholl peridotites, e.g. olivine (mg_{76}; 0.33% Ni), clinopyroxene (mg_{83}; $Ca_{38}Mg_{51}Fe_{11}$), orthopyroxene (En_{75}), and plagioclase (An_{37-24}), are similar to those in the lower and upper parts of the Munni Munni ultramafic zone. Serpentine, magnetite, talc, actinolite-tremolite, hornblende, calcite, and chlorite are the major secondary minerals.

Sulphides occur as disseminations and local massive segregations in gabbroic rocks that form a thin basal veneer to the metaperidotite sequence. Pyrrhotite, pentlandite, and chalcopyrite typically fill intercumulus spaces, and their textures range from magmatic igneous to metamorphic, showing various stages of modification caused by the alteration of clinopyroxene to tremolite. Mathison & Marshall (1981) believe the modified textures reflect metamorphic readjustment rather than replacement. Similar features are seen in the sulphide-bearing gabbroic units of subzone A′ in the Munni Munni Complex (p. 38).

Massive and disseminated sulphides from the basal contact of the Mount Sholl Complex have $\partial^{34}S$ values of +2.3 to +3.7‰ (Table 34). These compositions are similar to those documented for other sulphide units in the west Pilbara intrusions. Sulphur isotopes are discussed on pp. 161–162.

Metagabbro (cpx + opx ± plag; cpx + plag + mt-ilm)

The poorly-layered mafic rocks in the intrusion have been subdivided into three subgroups, namely (1) a metagabbroic sequence which forms the bulk of the complex, (2) a fine-grained partly microporphyritic metagabbro, and (3) an aphanitic magnetite-rich ferrogabbro.

(1) Metagabbro, metagabbronorite, plagioclase metaclinopyroxenite, and minor anorthositic metagabbro are the dominant rocks of the mafic sequence. Clinopyroxene and plagioclase generally have similar abundances (45–65 vol. %) in the metagabbros, with minor orthopyroxene (< 5%), ilmenite-magnetite (< 1.0%), biotite (< 0.5%), and trace inverted pigeonite, alkali feldspar, quartz, sulphide, rutile, and apatite. Orthopyroxene locally attains 20 vol. % at the expense of clinopyroxene in metagabbronorite at high levels in the mafic sequence. Plagioclase contents also increase slightly for the more orthopyroxene-rich gabbroic rocks. Orthopyroxene and inverted pigeonite have restricted distributions in the gabbroic rocks. The Ca-poor pyroxene fractionation trend of bronzite, to hypersthene, to inverted pigeonite that is seen in the Munni Munni Complex is not as well developed in the Mount Sholl Complex.

Clinopyroxene and orthopyroxene are cumulus, whereas plagioclase, alkali feldspar, and Fe-Ti oxides are generally intercumulus. In some plagioclase-rich gabbros plagioclase may be of cumulus status. The late crystallisation of plagioclase is a major distinction from the Munni Munni gabbroic rocks. The average compositions of clinopyroxene (mg_{79}; $Ca_{38}Mg_{49}Fe_{13}$) and plagioclase (An_{32-12}) in the gabbroic rocks (Mathison & Marshall, 1981) indicate that the clinopyroxene is more primitive and the plagioclase more sodic than those in the Munni Munni gabbroic zone. Granular textures dominate the Mount Sholl gabbros: clinopyroxene forms subhedral to anhedral grains (1.0 x 2.0 mm) and orthopyroxene forms anhedra of similar size to the clinopyroxene. Apatite needles up to 1.2 mm long are commonly associated with plagioclase in the more fractionated gabbroic rocks. Fine-grained disseminations of chalcopyrite, pyrite, and pyrrhotite, and veinlets of chalcopyrite, characterise most gabbroic rocks, indicating a S-saturated parent magma. The pyroxenes are partly altered to clinoamphibole and chlorite, and plagioclase is invariably altered to sericite, chlorite, epidote, and carbonates.

Variations in modal abundances are more pronounced along sample traverse B than sample traverse A. These trends and plagioclase compositions suggest the intrusion is tilted toward the southeast. Decreasing clinopyroxene and inverted-pigeonite abundances, and increasing plagioclase, quartz, apatite, and ilmenite-magnetite, towards the southeast are consistent with the intrusion younging towards the southeast. Modal variation trends are not as clear at the southeastern end of traverse B (samples 84770174–178 on the appended map sheet), and, as discussed below on p. 98, this complication may be due to a structural repetition of the stratigraphy. Plagioclase compositions generally become more sodic, from An_{48} to An_{35}, towards the southeast, which is consistent with the modal trends.

(2) Metagabbros of subgroup 2 are distinguished from subgroup 1 metagabbros by their porphyritic character, more intense uralitisation, and lower quartz and apatite contents. Clinopyroxene is bimodal, comprising large subhedra (1.0 x 2.0 mm) set amongst more common smaller subhedra (0.3 x 0.5 mm). Clinopyroxene and intercumulus plagioclase are extensively altered to clinoamphibole, chlorite, and clinozoisite. Accessory minerals include biotite, quartz, apatite, and opaques.

(3) Magnetite-bearing ferrogabbros crop out along major faults in the eastern part of the intrusion. The ferrogabbros have intergranular textures and consist of cumulus clinopyroxene (40–50 vol. %), plagioclase (40%), magnetite-ilmenite (10%), and intercumulus orthopyroxene (2%). Accessory minerals include quartz, apatite, biotite, chalcopyrite, and pyrite. The disseminated magnetite-ilmenite subhedra range in size from 0.2 to 2.0 mm, have embayed margins, and are altered to maghemite. Their abundance, and the brown colour of clinopyroxene, attests to an evolved Fe-rich parent magma.

Geochemistry and orientation of the Mount Sholl Complex

Layering and structures are poorly developed in the Mount Sholl rocks. The relative position of the ultramafic sequence (B_2 area) in relation to the gabbroic rocks, and the occurrence of minor granophyre on the southeastern side of the intrusion, tentatively indicates that the complex youngs to the southeast. However, the

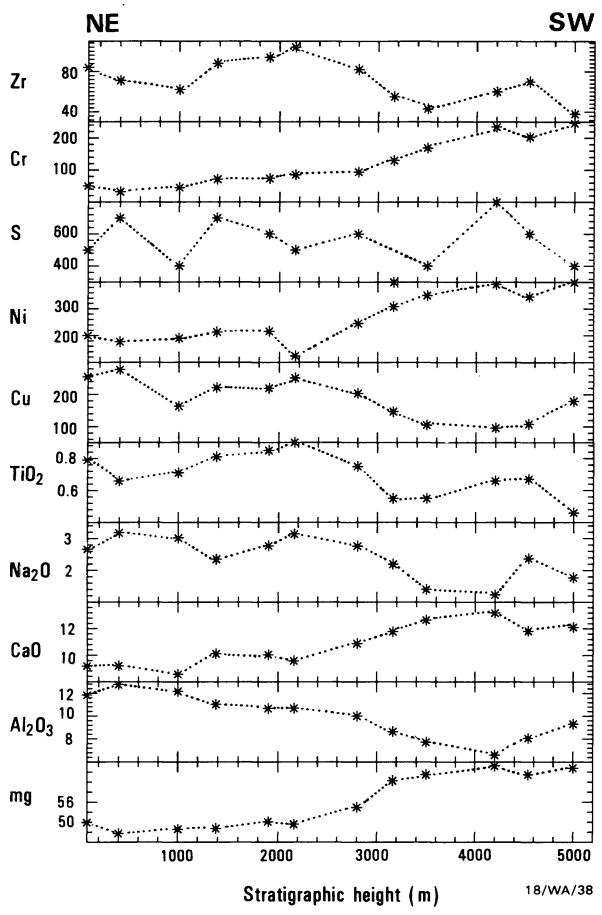

Fig. 64. Major- and trace-element whole-rock variations along traverse A (along strike) of the Mount Sholl Complex (location in Figure 62). Sample locations are indicated on the appended map sheet. 'Stratigraphic height' is apparent height.

detailed shape of the body cannot be determined from field evidence. Although it is recognised that major and trace element geochemistry has limited application in the interpretation of cumulate rocks, gross chemical variations along the sample traverses provide some insight into the orientation of the intrusion. Geochemical profiles of 21 samples (84770140–178) from traverses A and B are shown in Figures 64 & 65, and the data are given in Appendix 3. The stratigraphic height shown is apparent height.

Major and trace elements

Geochemical variations for traverse A show a consistent increase in mg, CaO, Ni, and Cr towards the southwest, whereas Al_2O_3, Na_2O, TiO_2, Cu, and Zr generally decrease. Sulphur has an erratic trend, which largely reflects secondary mobilisation. Traverse A trends highlight the more compatible behaviour of Cr and Ni relative to Ti, Cu, and Zr during fractionation, and indicate that the gabbros at the southwestern end of the intrusion are more primitive than those at the northeastern end. The association of these more primitive gabbros with the B_2 ultramafic sequence and the related basal segregations of sulphide suggest that the B_2 area and its south-southwestern extension (under cover) represent the lowest part of the Mount Sholl stratigraphy.

Geochemical trends for traverse B show a crude symmetrical pattern centred very broadly at about the 1700 m position. Correlations of the various elements with mg are the same as those seen in traverse A. The more marked variation in mg for traverse B (21 mg units) relative to traverse A (13 mg units) suggests that the strike direction of the gabbros is northeast, i.e. parallel to the length of the complex. There is no field evidence to indicate a new batch of magma above the ~ 1700 m position, although a major north-northwest-trending fault is present in this area (Fig. 62). The U-shaped trends of mg, CaO, Ni, and Cr are believed to reflect a synformal configuration of the complex.

Mineralogical and geochemical trends indicate that the Mount Sholl Complex is a synformal body that plunges gently towards the northeast and is largely composed of a western limb that dips towards the southeast. The northeast-trending fold axis is situated along the southeastern margin of the intrusion, and the eastern limb of the synform is defined by a small triangular block at the northeastern corner of the intrusion (Fig. 62 & appended map sheet).

Platinum, palladium, iridium, gold. The PGE concentrations of three settings of Fe-Ni-Cu sulphide mineralisation were investigated in the Mount Sholl Complex (Table 18). These comprise the western (B_2 mineralised zone), northern (B_1 mineralised zone), and northeastern margins (A_1 mineralised zone) of the intrusion. Sulphides in the B_2 area occur in a wedge-shaped closure, comprising a central zone of serpentinised metaperidotite and an outer envelope of metagabbroic rocks. At B_1, sulphides are largely hosted by metaperidotite in a thin sheet-like extension of the intrusion, and at A_1 they occur in steeply-dipping podiform and dyke-like metaperidotite bodies adjacent to the intrusion.

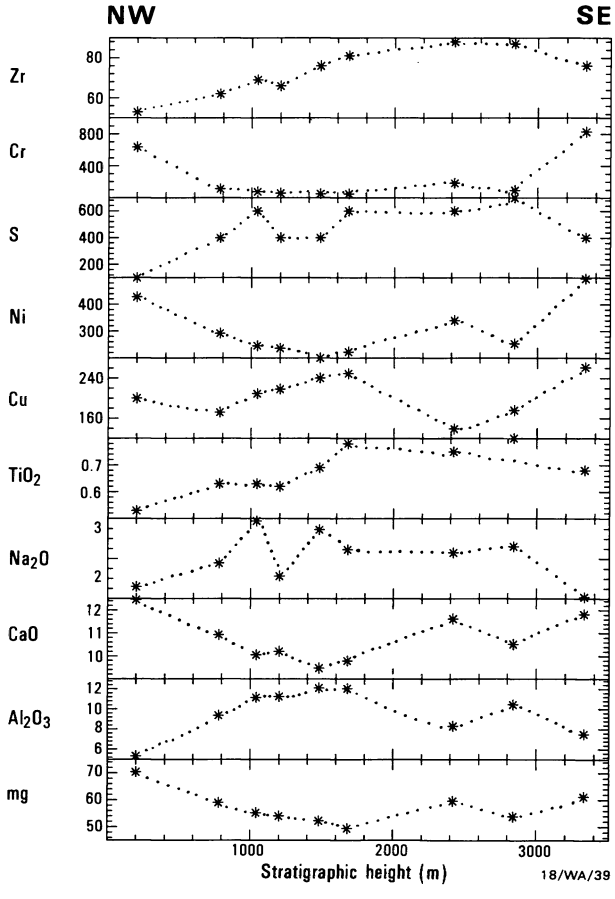

Fig. 65. Major- and trace-element whole-rock variations along traverse B (across strike) of the Mount Sholl Complex (location in Figure 62). Sample locations are indicated on the appended map sheet. 'Stratigraphic height' is apparent height.

Table 18. Precious-metal and trace-element geochemistry of the Mount Sholl Complex

Sample number	*Interval down hole (m)*	*Lithology*	*Style of mineralisation*	*Pt (ppb)*	*Pd (ppb)*	*Ir (ppb)*	*Au (ppb)*	*S (%)*	*Cu (ppm)*	*Ni (ppm)*	*Cr (ppm)*	*Zr (ppm)*	*Sr (ppm)*	$\frac{Pt}{Pd}$	$\frac{Pt+Pd}{S}\times 10^6$	$\frac{Pt+Pd}{Ir}$	$\frac{Cu}{Cu+Ni}\times 10^3$
B_2 mineralisation																	
DDH 72-5																	
84770200	37.80–40.80	Chilled gabbro	Trace disseminated s	—	—	—	—	1.10	314	801	342	80	166	—	—	—	282
84770201	87.00–88.50	Altered gabbro	Minor disseminated and vein s	91.6	325.0	6.59	13.37	2.00	4133	2983	411	34	83	0.28	20.82	63.2	581
84770202	88.50–90.00	Altered peridotite	Minor disseminated and vein s	123.3	165.7	1.62	10.92	2.22	2357	2798	342	39	60	0.74	13.02	178.40	457
84770203	90.00–91.50	Massive sulphide	Massive s	163.8	263.0	43.2	6.25	4.28	6751	36450	137	33	28	0.62	9.97	9.88	156
84770204	91.50–93.00	Altered peridotite	Trace disseminated s	62.8	243.0	5.46	9.61	3.16	2868	2704	411	39	44	0.26	9.68	56.03	515
84770205	93.00–94.50	Altered peridotite	Trace disseminated s	71.1	172.9	1.60	12.68	1.11	2515	2681	410	42	18	0.41	21.98	152.50	484
B_1 mineralisation																	
DDH 72-19																	
84770206	124.00–127.00	Altered peridotite	Minor disseminated s	—	—	—	—	1.07	2253	3008	411	37	26	—	—	—	428
84770207	130.00–133.00	Altered peridotite	Minor disseminated s	180.2	356.0	9.91	30.82	2.04	3297	4557	753	41	37	0.51	26.27	54.08	420
A_1 mineralisation																	
DDH 72-11																	
84770208	82.00–86.50	Chilled gabbro	Trace disseminated s	20.7	66.9	1.27	2.52	0.45	531	1714	479	45	26	0.31	19.47	69.00	237
84770209	86.50–89.50	Altered peridotite	Minor disseminated s	56.7	117.8	0.36	11.70	1.16	1540	2047	411	28	30	0.48	15.04	484.72	429
84770210	89.50–92.50	Altered peridotite	Minor disseminated s	48.3	99.8	0.62	10.89	0.68	1187	2432	410	29	30	0.48	21.78	238.87	328
84770211	92.50–95.50	Altered peridotite	Trace disseminated s	67.3	112.4	0.50	16.29	1.17	1354	2439	480	30	46	0.60	15.36	359.40	357
84770212	95.50–98.50	Altered peridotite	Trace disseminated s	50.8	104.9	0.44	11.25	0.67	1756	2635	341	28	22	0.48	23.24	353.86	400

s = sulphides (pyrrhotite, pentlandite, chalcopyrite). Platinum, Pd, Ir, Au determined by RNAA; Cr, Zr, Sr by XRFS; Cu, Ni by AAS; S by Leco titration. — = not determined.

Basal sulphide segregations in the Mount Sholl Complex are characterised by fairly low Pt (20–180 ppb), Pd (66–356 ppb), and Au (2.5–30 ppb) concentrations. In comparison to the Munni Munni Complex, they are slightly higher than the basal sulphides of subzone A′ (Table 12), but significantly lower than the PGE-enriched websterite layer of subzone I (Table 14). Only Ir (0.4–43 ppb) has similar concentrations in both intrusions. Platinum/Pd ratios at Mount Sholl display a restricted range (0.26–0.74) indicating that the three mineralised settings formed through similar magmatic processes related to the intrusion. The higher (Pt + Pd)/Ir ratios of the A_1 area (up to 485) compared to the B_1 and B_2 areas (10–178) may indicate that the sulphide melts associated with the A_1 dyke-like peridotite bodies were more fractionated than those of the B_1 and B_2 areas. This is consistent with the peridotite dykes being interpreted as late-crystallising features, compared to the B_1 and B_2 deposits that formed at earlier stages in the evolution of the intrusion.

The highest Pt, Pd, and Ir contents in the B_2 area occur in massive sulphides (3.6% Ni, 0.7% Cu, 4.3% S), whereas the highest Au contents characterise disseminated, rather than massive, sulphides (Table 18). Platinum, Pd, and Ir contents appear to be largely independent of the host rock: similar amounts occur in both gabbro and metaperidotite. The higher Cu/(Cu + Ni) ratios of the disseminated sulphides relative to the massive sulphides suggest that chalcopyrite is a more dominant component of the former.

Peridotites with disseminated sulphides in the B_1 area have the highest Pt, Pd, and Au contents. The similar Cu/(Cu + Ni) ratios to the other two mineralised areas suggest PGE enrichment was not simply due to fractionation processes. Mineralisation at A_1 is generally similar geochemically to that at B_1 and B_2, except for lower Ir and S.

In summary, there is no evidence of significant lateral variations in PGE contents of the basal Ni-Cu mineralisation in the Mount Sholl Complex. Minor differences, such as the high (Pt + Pd)/Ir ratios in the A_1 area, may be due to localised fractionation that occurred in a late-crystallising olivine-rich magma. This magma may have been expelled from the magma chamber during the emplacement of the gabbroic magma, to form dykes adjacent to the complex. The high S contents of chilled gabbroic rocks (0.45–1.10%), of the hangingwall peridotite units (0.67–3.16%), and of the gabbroic rocks (average of 600 ppm: Figs 64 & 65) from the upper parts of the intrusion indicate that the Mount Sholl Complex formed from a S-saturated parent magma. Mathison & Marshall (1981) have proposed that the parent magma was a basaltic komatiite, similar to those documented for other west Pilbara layered intrusions (Table 30). The S-saturated character of the Mount Sholl rocks indicates there is little likelihood of a PGE-enriched layer occurring in the higher stratigraphic levels of the gabbroic sequence. The processes of early S-saturation of the magmas and gravitational settling of immiscible sulphides, which operated in the nearby Radio Hill Complex, are believed to be generally applicable also to the Mount Sholl Complex (see p. 111–116).

FIELD RELATIONSHIPS, PETROGRAPHY, AND GEOCHEMISTRY OF THE RADIO HILL COMPLEX (*DMH*)

Introduction

The Radio Hill Complex is 28 km south of Karratha and 14 km north of the Munni Munni Complex, at latitude 20°59′30″S and longitude 116°52′30″E, on the Dampier 1 : 100 000 Topographic Sheet 2256 and Dampier & Barrow Island 1 : 250 000 Geological Sheet SF/50-2. The Radio Hill Complex is the smallest intrusion investigated in this study, but it contains the most economically significant Ni-Cu resource associated with a layered intrusion in the west Pilbara Block.

Size and age

The Radio Hill mafic-ultramafic complex (Figs 66 & 67A–B) consists of a 330 m-thick ultramafic zone and an overlying 870+ m-thick gabbroic zone (Table 19). The complex crops out over about 1.8 by 2 km and forms one of the most prominent hills (height ~ 180 m) in the west Pilbara. It intrudes intermediate and mafic metavolcanics along the northeastern and northwestern margins, whereas the southeastern margin is obscured by alluvium. Aeromagnetics and diamond-drilling indicate that the gabbroic rocks extend for at least another 700 m towards the southeast. The thickness ratio of the ultramafic and mafic components is similar (0.4) to the Munni Munni Complex (0.5), but much lower than the Andover Complex (1.6). The poorly-exposed ultramafic zone comprises an interlayered peridotite-pyroxenite sequence that is restricted to the northwestern side of the intrusion. The spatial arrangement of an ultramafic cumulate sequence on the northern side of a younger mafic sequence is also seen in the Munni Munni, Mount Sholl, and Andover complexes. This suggests that the intrusions had similar post-emplacement tectonic histories, with shallow tilting of the west Pilbara Block to the southwest and south-southeast prior to the deposition of the Fortescue Group platform cover.

No geochronological data exist for the Radio Hill Complex. It is chilled against intermediate and mafic metavolcanics that have been tentatively correlated with various formations belonging to the Warrawoona Group (3300–3500 Ma). However, if the metavolcanic sequences of the Sholl Belt belong to the younger Whim Creek Group and not the Warrawoona Group, as suggested by Horwitz (1988, 1990b), the maximum age of the Radio Hill intrusion is ~ 2900–3100 Ma. The Radio Hill Complex has very similar stratigraphy and mineralisation to the Mount Sholl Complex, and these intrusions are believed to be cogenetic with the nearby 2927 ± 13 Ma Munni Munni Complex.

The Radio Hill Complex is located at a regional triple junction between two different metavolcanic successions and granites (see appended map sheet). Along its northeastern margin, the complex intrudes an intercalated sequence of mainly rhyodacite, rhyolite, chert, and minor mafic metavolcanics (?Duffer Formation), whereas a more monotonous sequence of pillowed metabasalt and minor rhyolite (?Talga Talga Subgroup) occurs along the northwestern margin. Leucocratic granites crop out along the eastern margin of the alluvial plain to the southeast of the complex. This regional structural control for the Radio Hill Complex is also a feature of the other west Pilbara intrusions which were preferentially emplaced along unconformities and major lithological contacts of metavolcanic sequences, or between granitic and metavolcanic sequences.

Distribution of rock types and stratigraphic relationships

Ultramafic zone

The surface expression of the ultramafic zone is restricted to localised outcrops of intensely altered peridotite and minor pyroxenite in shallow gravel pits at the northern end of the intrusion. Ferruginous sand and shallow *in situ* skeletal soil mask most of the zone. The distribution and subdivision of the ultramafic zone is based largely on aeromagnetics and drilling carried out by Agip Australia Pty Ltd (de Angelis & others, 1987). The ultramafic zone is a north-northeast-trending lenticular body 800 m long by 200 m wide along the northwestern margin of the intrusion. It has been subdivided into seven subzones (A to G) on the basis of different relative proportions of olivine-rich and clinopyroxene-rich cumulates (Table 19).

The dominant rock types of the ultramafic zone include lherzolite, dunite, olivine websterite, plagioclase websterite, and websterite, with subordinate gabbroic lithologies in the basal parts and clinopyroxenite and plagioclase websterite in the upper parts of the zone. Lateral variations of rock types and structural complications due to faulting indicate that the ultramafic stratigraphy is more complex than that shown in Table 19. Subzone A contains the most fractionated and economically significant rock types in the zone. Plagioclase abundances in the gabbroic and pyroxenitic rocks of subzone A decrease steadily upward, and then decrease sharply across the contact with the overlying plagioclase-poor peridotites of subzone B. Rhythmically layered serpentinised lherzolite, wehrlite, and minor dunite dominate this most olivine-rich subzone of the ultramafic zone. Subzone C consists of a distinctive porphyritic plagioclase websterite unit, which texturally resembles the mineralised websterite layer of subzone I in the Munni Munni Complex. Subzones D to G comprise alternating peridotite and plagioclase-bearing pyroxenite cycles of varying thickness. Plagioclase and clinopyroxene abundances consistently increase upwards in subzones F and G at the expense of olivine. The occurrence of a stacked cyclic sequence of olivine- and clinopyroxene-rich cumulates underlain by a thin basal veneer of plagioclase-bearing rocks is similar to that seen in the Munni Munni and Mount Sholl ultramafic zones. The reappearance of olivine-rich cycles up the sequence is believed to reflect an open system that involved the emplacement of new pulses of primitive magma into an upward expanding magma chamber.

Gabbroic zone

The mafic rocks of the Radio Hill Complex have been subdivided into two subzones (Table 19) on the basis of mineralogy, layering, texture, and physiography. The contact between the ultramafic and gabbroic zones is covered by alluvium, but drill core shows that the basal gabbros have a marked increase in the intercumulus plagioclase content compared with the plagioclase-bearing pyroxenites in the upper parts of the ultramafic zone. The gabbroic rocks are locally chilled against intermediate metavolcanics along the north-

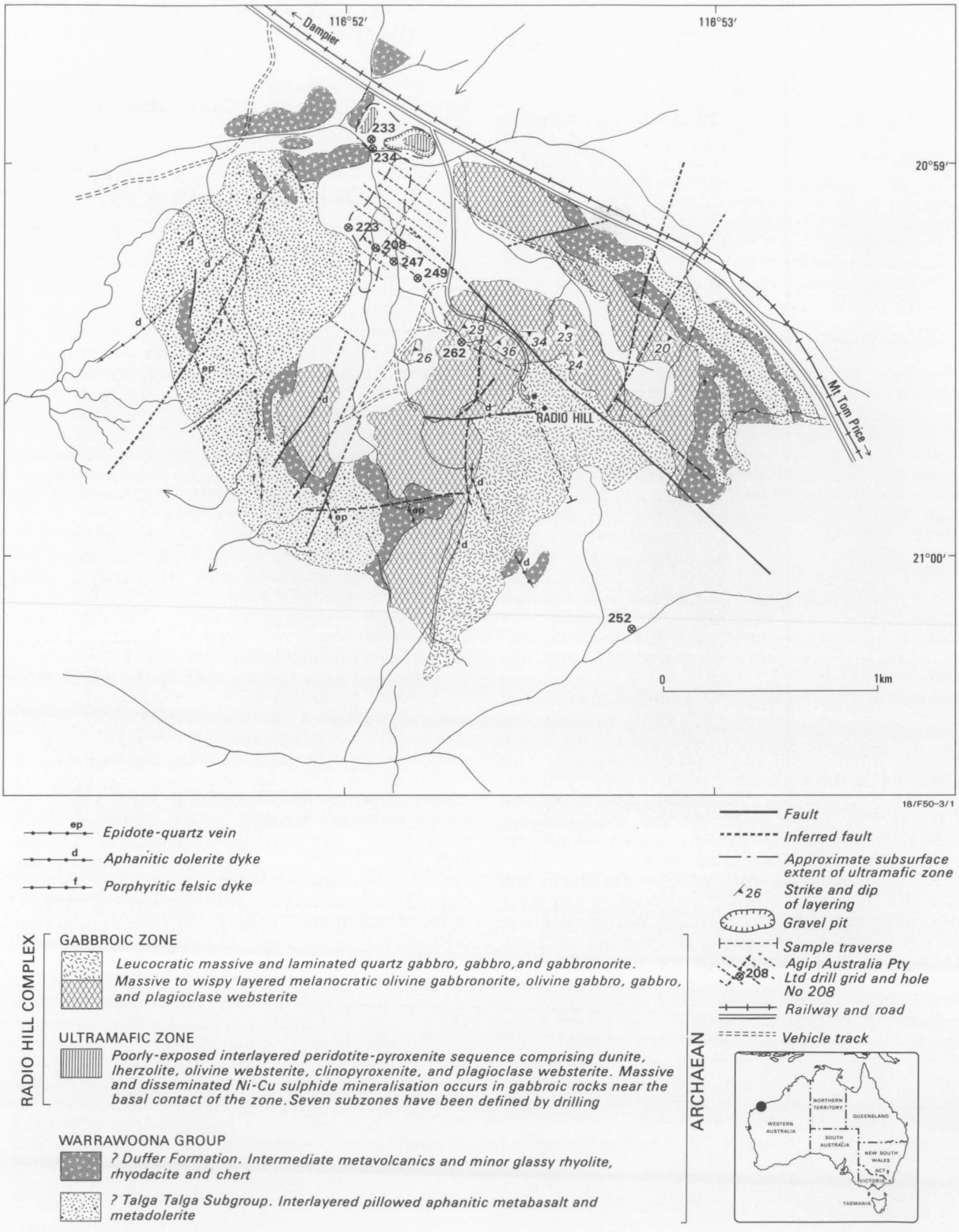

Fig. 66. Geology of the Radio Hill Complex (simplified from appended map sheet).

western margin of the intrusion. The basal parts of subzone A (total thickness 440 m) crop out on the lower slopes of Radio Hill as a monotonous sequence of massive melanocratic gabbro and gabbronorite. Wispy layering, defined by thin (5 cm) discontinuous plagioclase layers and rare thicker (0.5 m) anorthosite lenses, becomes more pronounced in olivine gabbro and olivine gabbronorite in the middle and upper parts of the subzone (Fig. 67C). The plagioclase segregations have strike extents of less than 2 m and are similar to those in the gabbroic rocks of the Mount Sholl Complex. Trace amounts of disseminated sulphide are found in

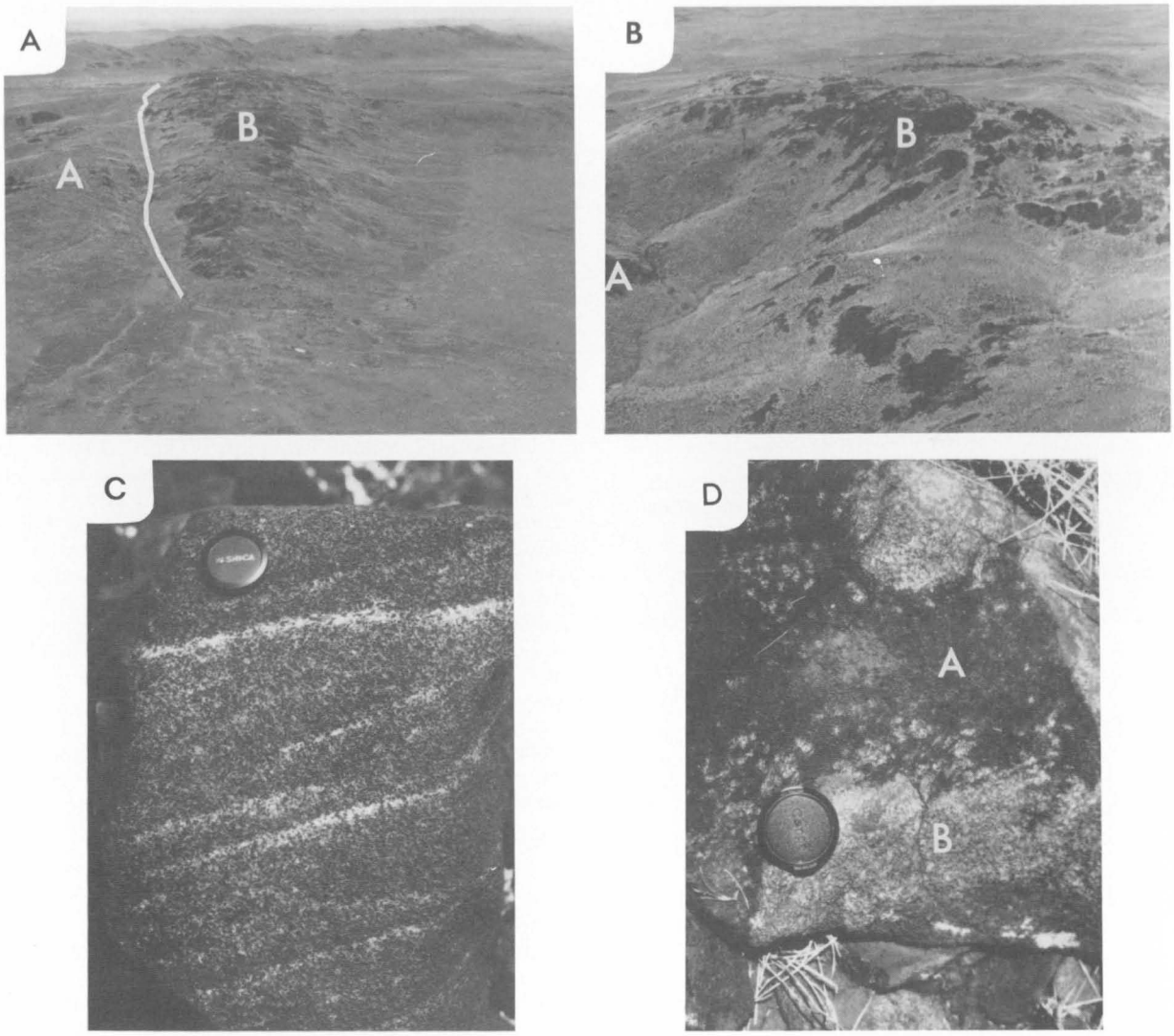

Fig. 67A–D. Radio Hill Complex: aerial views and rock types. A—Aerial view looking northeast along the strike of the subzone B gabbroic sequence of the complex. The approximate contact of this subzone with the underlying gabbroic sequence of subzone A is indicated by the full line. Subzone B extends beneath the alluvial plain to the right of the main ridge. B—Close-up aerial view of the subzone B gabbroic sequence, which defines the main ridge at Radio Hill. C—Wispy plagioclase layering in a melagabbro from the middle parts of the subzone A mafic sequence. D—Commingling of magmas that formed the glomeroporphyritic gabbroic unit(A) of subzone A and the overlying leucocratic quartz gabbro(B) of subzone B.

most gabbroic rocks of subzone A. A thin (~ 5 m) glomeroporphyritic gabbroic unit defined by ?plagioclase clusters up to 1 cm in diameter marks the upper contact of subzone A. This distinctive unit can be traced along the western side of Radio Hill and indicates localised mixing between the two gabbroic sequences (Fig. 67D).

Subzone B comprises a leucocratic mafic sequence (thickness 430+m) of quartz gabbro, gabbro, and gabbronorite. These rocks contrast with the subzone A gabbroic rocks in their more fractionated compositions, laminated textures, absence of compositional layering, and pronounced vertical jointing. They crop out along the main ridge of Radio Hill and are enclosed along the northwestern and northeastern margins by subzone A gabbros. Along the northwestern contact, the subzone B rocks have a sheared intrusive contact with the fractionated gabbros of subzone A. Locally there is evidence of mixing of magmas along the contact (Fig. 67D). Gabbroic rocks along the axis of the Radio Hill ridge are equigranular and strongly jointed, whereas those on the sides of the ridge just above the contact with the subzone A rocks are laminated. The spatial distribution of these textures suggests that flowage-differentiation and tectonics were important in the emplacement of the subzone B gabbroic rocks. The subzone B sequence was interpreted by de Angelis & others (1987) as a late, sub-vertical feeder dyke that has transected the layered sequences of the complex. They have shown (their Fig. 3) that the subzone A gabbroic sequence reappears southeast of their inferred dyke, but this study indicates that the subzone B rocks extend in outcrop as far as the alluvium on the southeastern side of the intrusion and are likely to be comagmatic with the subzone A gabbros. Aeromagnetics and the oxide-rich gabbroic sequence drilled in 86 RHPD 252 (Fig. 66) reveal that mafic intrusive units extend beneath the alluvium southeast of Radio Hill.

Table 19. Generalised stratigraphy of the Radio Hill Complex

Subzone (thickness)	*Dominant rock types*
Gabbroic zone	
B(430+ m)	Leucocratic mafic sequence of massive and laminated quartz gabbro, quartz gabbronorite, gabbronorite
A(440 m)	Melanocratic mafic sequence of massive to wispy layered olivine gabbronorite, olivine gabbro, gabbro, plagioclase websterite
Ultramafic zone	
G(120 m)	Websterite, plagioclase websterite, plagioclase clinopyroxenite
F(110 m)	Lherzolite, dunite, olivine websterite, plagioclase olivine websterite, olivine gabbronorite
E(25m)	Plagioclase websterite, websterite
D(10 m)	Olivine websterite, plagioclase olivine websterite
C(10 m)	Porphyritic plagioclase websterite, porphyritic plagioclase olivine websterite
B(25 m)	Lherzolite, dunite, wehrlite, olivine websterite, plagioclase websterite
A(30 m)	Chilled gabbro, gabbronorite, and plagioclase websterite containing massive, disseminated, veined, and brecciated pyrrhotite-pentlandite-chalcopyrite-magnetite mineralisation

The stratigraphy of the ultramafic zone was determined from DDH 84 RHPD 208, and that of the gabbroic zone from DDHs 86 RHPD 249, 87 RHPD 262, and outcrop (see appended map sheet for drillhole and sample locations).

Structure

The Radio Hill Complex is interpreted as a shallow-dipping basinal structure, consisting of a conformable lens-shaped ultramafic zone, transitional to an overlying thicker gabbroic sequence, which is in turn truncated by a steeply-dipping gabbroic body. The subzone A gabbros are largely conformable with the basement metavolcanics on the northeastern side of the intrusion, whereas low-angle crosscutting relationships characterise the northwestern side. Wispy layering in the upper parts of these gabbros on the western side of the main ridge dips between 26 and 36° towards the east and southeast (Fig. 66 & appended map sheet). The dip direction of the layering progressively swings towards the south and south-southwest around the northern and northeastern sides of the intrusion, but the dips remain between 18 and 34°.

The contact between the intrusion and the basement metavolcanics on the northeastern margin dips at 20–30° inwards towards the centre of the complex, whereas the contact on the northwestern side ranges from shallow-dipping to sub-vertical and in some places is overturned. Drilling indicates that this flexured contact flattens out to less than 30° towards the centre of the intrusion at depths of about 200 m. The general structural configuration, of a shallow-dipping sheet with steeper variable attitudes for the base of the intrusion, is very similar to that of the Mount Sholl Complex.

Three dominant fault trends are recognised in the Radio Hill region, namely (1) north-northeast to northeast, (2) northwest, and (3) east. Subgroup 1 faults cut the strike of the basement metavolcanics and subzone A gabbroic rocks at high angles. Some of these faults appear to predate the emplacement of the subzone B gabbros, since they terminate at the contact between the two gabbroic sequences. Their north-northeast to northeast strike direction is the dominant structural orientation in the Pilbara Block. Crustal weaknesses along this trend have acted as deep-seated conduits for the emplacement of various amounts of mafic magma, as evidenced by thin (< 1 m wide) dolerite dykes, larger gabbronorite dykes, such as the Pinderi Hills Dyke (100 m), and large differentiated intrusions, such as the Munni Munni Complex (9 km). Two major northwest-trending regional faults belong to subgroup 2. The most prominent of these, the Railway Fault (coincident with the Dampier railway line: see Fig. 2 of de Angelis & others, 1987) has a strike extent of over 15 km, and the second fault is near the northeastern contact of the subzone A and B gabbros. Smaller faults in this subgroup are infilled by porphyritic felsic and doleritic dykes and quartz-epidote veins. The Gaffs Well fault of subgroup 3 is a 100–200 m wide east-west-trending zone of fracturing and brecciation cutting the northern part of the Radio Hill Complex. This sinistral fault has truncated the northern part of the elongated ultramafic zone and associated sulphide mineralisation.

Mineralisation

The economic potential of the Radio Hill Complex became apparent in 1969 when Ni-Cu sulphide mineralisation was discovered by Whim Creek Consolidated NL in the nearby Mount Sholl Complex and Ruth Well Synclinorium. During the initial phases of exploration an aeromagnetic anomaly with coincident weak Ni-Cu soil anomalies was defined, but it was not until 1985 that the sulphide zones of economic significance were discovered by Agip Australia Pty Ltd. The mineralisation has no surface expression, and various ground geophysical techniques, such as magnetics, Sirotem, applied potential, and electromagnetics were successfully employed in locating and delineating the sulphide zones (Peters & de Angelis, 1987).

Detailed drilling (50 m spacing) has defined a resource with proved and probable reserves of 1.1 Mt @ 2.5% Ni and 1.8% Cu. Underground mining commenced in late 1991 at a proposed rate of 150 000 t/year over a seven-year period, but partly because of the depressed nickel price, the mine was subsequently placed on care-and-maintenance.

Massive, disseminated, vein, and brecciated pyrrhotite-pentlandite-chalcopyrite mineralisation is hosted by gabbro, gabbronorite, and plagioclase-bearing pyroxenite in the basal parts (subzone A) of the ultramafic sequence (Fig. 68). The mineralisation has a strike length of 600 m, a width of 25 m, has variable shallow-to-moderate dips to the southeast, and plunges 20° to the southwest from a vertical depth of 17 m in the northeast to 300 m in the southwest (de Angelis & others, 1987). In the mineralised zone, a composite sequence of thin massive-sulphide layers occurs within a few metres of, or next to, the basal contact of the intrusion. Disseminated sulphides are more typical of the peridotites and plagioclase-poor pyroxenites from

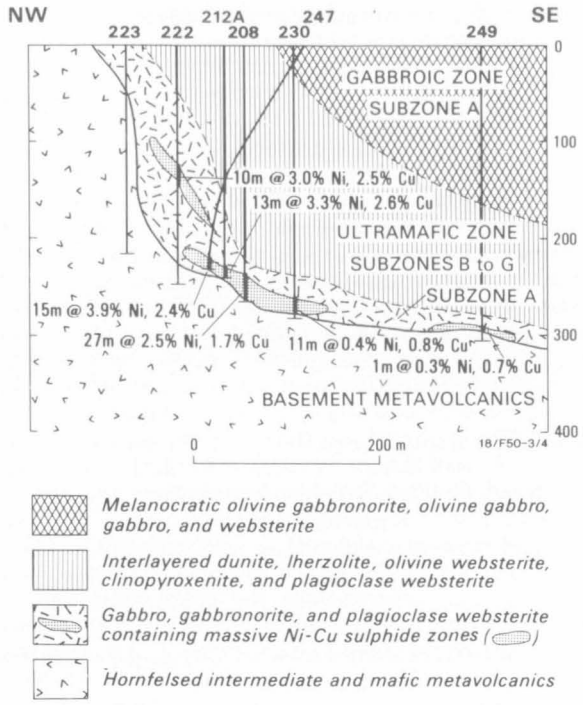

Fig. 68. Drillhole profile through the mineralised basal contact of the Radio Hill Complex. Drillhole data from de Angelis & others (1987; 1988).

higher stratigraphic levels. Carbonate-quartz-chlorite-epidote-chalcopyrite veins intrude the hornfelsed footwall metavolcanics for up to 0.5 m below the contact. Localised massive and disseminated chalcopyrite-dominant sulphides occur 200 m to the northwest of the northern end of the main Fe-rich sulphide zone (see holes 233 and 234 in Fig. 66). The Cu-rich mineralisation has a similar setting to the Fe-rich sulphide zone, but the spatial and genetic relationships of the two mineralised zones are not well understood.

Petrography and mineralogy

The mafic-ultramafic lithologies of the Radio Hill Complex have similar cumulus assemblages, mineralisation, and alteration to the nearby Mount Sholl Complex. Cumulus olivine, clinopyroxene, orthopyroxene, and intercumulus plagioclase characterise the ultramafic and gabbroic subzone A rocks, whereas olivine is absent and plagioclase is cumulus in the subzone B gabbroic sequence. Textural trends and mineral compositions are generally transitional upwards through the cyclic units of the ultramafic and lower gabbroic sequences, but there is a major transformation between gabbroic subzones A and B, indicating a significant change in the evolution of the Radio Hill intrusion.

Sulphide-bearing microgabbro, gabbronorite, plagioclase websterite (cpx ± opx)

Massive, disseminated, remobilised-vein and brecciated sulphides are hosted by microgabbro, gabbronorite, and plagioclase websterite along the basal contact of the ultramafic zone (subzone A). Four styles of primary and remobilised sulphide mineralisation have been recognised in these plagioclase-rich rocks:

(1) massive pyrrhotite-pentlandite and pyrrhotite-chalcopyrite-pentlandite-magnetite, associated with tremolite-actinolite-carbonate-biotite-?stilpnomelane alteration, close to, or abutting, the basement metavolcanics;
(2) massive chalcopyrite ± pentlandite ± pyrrhotite enriched in Pt, Pd, Au, and Ag close to, or abutting, the basement metavolcanics;
(3) disseminated and stringer pyrrhotite and pyrrhotite-chalcopyrite ± pentlandite ± magnetite ± pyrite in gabbroic (and peridotite) units above the massive sulphides; and
(4) remobilised chalcopyrite-pyrrhotite ± pentlandite veins associated with carbonate-quartz-chlorite-epidote at the basal contact of the massive sulphides and in basement metavolcanics.

Pyrrhotite in association 1 forms medium-to-coarse granular aggregates that enclose later-crystallising chains of anhedral pentlandite and chalcopyrite. Minor subhedral magnetite and trace pyrite are often associated with chalcopyrite. In contrast to the basal Fe-rich sulphides in the Munni Munni Complex, the pyrrhotite is massively textured and rarely contains exsolved spindle or flame-like lamellae of pentlandite. Thin layers of pentlandite often separate the pyrrhotite from abutting altered silicates and carbonates of the basement metavolcanics or gabbroic host. Prismatic tremolite-actinolite aggregates and radial sprays of brown ?stilpnomelane needles preferentially fringe the margins of chalcopyrite and pyrrhotite grains or are associated with late carbonate veins. Tellurides of Pd, Bi, and Pb were identified in pyrrhotite by de Angelis & others (1987), but no Pt-bearing minerals were located. Sulphide association 2 is characterised by massive chalcopyrite and minor (2–10 vol. %) associated Fe-rich sulphides. Very small (< 10 μm) highly reflective precious-metal and base-metal grains (e.g. PGMs and ?galena) occur in chalcopyrite and pyrrhotite and at the boundaries of sulphide and silicate grains. The gabbroic and peridotite units in the hangingwall contain fine- to medium-grained disseminated Fe-rich sulphides of association 3. These sulphides are interstitial to cumulus olivine and pyroxene grains, have experienced little remobilisation, and have well-preserved sulphide-silicate textures interpreted as magmatic. The basal parts of the Fe-rich massive sulphides are often brecciated and contain chalcopyrite-bearing carbonate-quartz veins and veinlets of association 4. Textural relationships indicate that the chalcopyrite was largely remobilised from the overlying massive sulphides, and the carbonate in the veins may have been derived from the contact metamorphism of the basement metavolcanics. The mafic host rocks to the sulphides are fine-grained orthocumulates that contain subhedral cumulus clinopyroxene (30–60 vol. %), intercumulus plagioclase (20–60%; An_{35-30}), and minor cumulus orthopyroxene, biotite, magnetite, and ilmenite. Microprobe analyses (by D. A. Wallace, AGSO) indicate salite to calcic augite compositions for clinopyroxene (mg_{66-63}; $Ca_{46}Mg_{35}Fe_{19}$). Chlorite, clinoamphibole, carbonate, and talc alteration of the ferromagnesian minerals is variable and plagioclase is altered to sericite, chlorite, and ?grossular garnet. Sulphide-silicate textures and alteration features are similar to the basal mineralised gabbroic rocks of the ultramafic zone of the Munni Munni Complex.

The mineralogy of the PGMs at the Radio Hill and Munni Munni complexes is currently the subject of a detailed collaborative study between AGSO and BRGM, France.

Dunite, lherzolite, wehrlite, olivine websterite, plagioclase olivine websterite (ol + cpx ± opx)

The peridotites (e.g. dunite, lherzolite, and wehrlite) and olivine-bearing websterites of the ultramafic zone consist of cumulus olivine (30–90 vol. %), clinopyroxene (10–50%), and orthopyroxene (0–20%), intercumulus plagioclase (2–20%), and minor phlogopite, sulphides, magnetite, and ilmenite. Peridotites are generally medium-grained adcumulates comprising olivine and orthopyroxene subhedra and smaller clinopyroxene subhedra, whereas the olivine-bearing websterites contain greater amounts of intercumulus plagioclase and are more mesocumulus in character. Orthopyroxene also locally forms large (2 x 5 mm) oikocrysts containing anhedral olivine and clinopyroxene inclusions. The intensity of serpentinisation is variable and generally proportional to the modal olivine content of the cumulate. Olivine (mg_{78-76}), clinopyroxene (mg_{84-80}; $Ca_{44-43}Mg_{46}Fe_{10-11}$), and orthopyroxene ($mg_{80-79}$; $Ca_2Mg_{78}Fe_{20}$) compositions for the two groups of olivine-bearing cumulates are identical, indicating that the two groups are comagmatic. Their restricted range of compositions suggests that fractionation in the ultramafic zone may have been inhibited by repeated influxes of primitive magma. Plagioclase changes to more calcic compositions (An_{52-40}) relative to the basal gabbros of subzone A, which is consistent with the trends at the base of the Munni Munni ultramafic zone. Disseminated pyrrhotite-chalcopyrite-pentlandite ± magnetite anhedra (sulphides up to 10%) are interstitial to olivine and pyroxene grains and range in size from 0.1 to 3 mm. Rare fine-scale modal layering defined by alternating olivine- and clinopyroxene-rich laminations is evident in some peridotites.

Plagioclase websterite, websterite, plagioclase clinopyroxenite, clinopyroxenite (cpx + opx ± ol)

Pyroxenites of the ultramafic zone contain cumulus clinopyroxene (25–95%), orthopyroxene (0–20%), and intercumulus plagioclase (1–30%; An_{49-36}), and minor cumulus olivine, biotite, quartz, sulphides, magnetite, and ilmenite. The high clinopyroxene/orthopyroxene ratio of these cumulates is consistent with the ultramafic sequences of the Munni Munni, Mount Sholl, and Maitland intrusions. Textures range from strongly porphyritic orthocumulates to equigranular adcumulates. Uralitisation and chloritisation alteration of the pyroxene-plagioclase assemblages is locally intense, but cumulus textures are generally well preserved. Disseminated pyrrhotite and chalcopyrite blebs indicate that the total ultramafic sequence crystallised from S-saturated magmas.

A distinctive porphyritic plagioclase websterite orthocumulate unit in the upper parts of subzone C has textures similar to the mineralised websterite layer of the Munni Munni Complex. It contains large (3 x 5 mm) orthopyroxene subhedra mantled by thin veneers of plagioclase (An_{46-42}), small granular clinopyroxene anhedra, and trace olivine, biotite, magnetite, and sulphides. Medium-to-coarse plagioclase clinopyroxenite and websterite adcumulates characterise the upper parts (subzone G) of the ultramafic zone. Their low residual porosities and coarse equigranular textures are attributed to extensive adcumulus growth during slow crystallisation in the upper parts of the cumulus pile.

Gabbro, gabbronorite, olivine gabbro, olivine gabbronorite (cpx ± ol ± opx)

The Radio Hill Complex is one of the few layered intrusions in the west Pilbara to contain a thick sequence of olivine-bearing mafic cumulates. The subzone A sequence of gabbro, gabbronorite, olivine gabbro, olivine gabbronorite, and minor plagioclase websterite comprises mineral assemblages transitional between the more primitive ultramafic zone cumulates and the quartz-bearing mafic cumulates of subzone B. They form medium-grained clinopyroxene-plagioclase-rich orthocumulates and mesocumulates consisting of cumulus clinopyroxene (65–85 vol. %), orthopyroxene (0–10%), and olivine (0–8%) grains enclosed by interlocking intercumulus plagioclase (10–35%). Inverted pigeonite is a minor phase (0–2%) above the 550 m stratigraphic level, and olivine attains maximum abundance in the upper parts of the subzone (above 640 m). Biotite, magnetite, ilmenite, quartz, chalcopyrite, and pyrrhotite are accessory minerals throughout the subzone. Clinopyroxene is extensively replaced by tremolite and hornblende, whereas olivine is often well preserved where enclosed by plagioclase.

The presence of olivine and paucity of Fe-Ti oxides, inverted pigeonite, and biotite reflects the more primitive character of these gabbroic orthocumulates compared to the gabbros along the basal contact of the ultramafic zone. This is also reflected in the range of compositions for clinopyroxene (mg_{71-66}; $Ca_{44-40}Mg_{38-43}Fe_{18-17}$), olivine ($mg_{59-53}$), and orthopyroxene ($mg_{64-60}$; $Ca_3Mg_{62-58}Fe_{35-39}$) throughout the zone. There is a consistent upward trend of sodic enrichment in plagioclase from An_{46} near the base of subzone A to An_{29} in the upper parts of the subzone.

Quartz gabbro, quartz gabbronorite (plag ± cpx ± opx)

The most fractionated cumulates in the complex are quartz gabbro, quartz gabbronorite, and gabbronorite belonging to subzone B of the gabbroic zone. Quartz gabbros commonly contain biotite and plagioclase more sodic than An_{50}; thus these rocks could also be classified as diorites (Streckeisen, 1973). However, since they are closely associated with olivine- and pyroxene-bearing cumulates in a layered intrusion they are treated here as gabbros.

The mafic cumulates of subzone B are markedly different in mineralogy and texture from the underlying gabbroic sequences. Olivine and inverted pigeonite are absent, quartz, Fe-Ti oxides, and apatite are important accessory minerals, plagioclase changes from intercumulus to cumulus, and coarse laminated textures replace the medium-grained intergranular textures more typical of the subzone A gabbroic cumulates. The subzone B gabbros consist of plagioclase (65–75 vol. %), clinopyroxene (25–35%), orthopyroxene (0–10%), quartz (0–1%), and trace magnetite, ilmenite, apatite, biotite, pyrrhotite, and chalcopyrite. Quartz forms 0.1 to 0.8 mm anhedra wedged between interlocking plagioclase laths and apatite euhedra become more prominent up the sequence. Disseminated titanomagnetite aggregates are of trace abundance for most of the subzone, but at the 1200 m level they reach 3% (88770135). The increasing abundance of apatite and Fe-Ti oxides up the sequence reflects the enrichment of P and Fe-Ti in the magma during crystal fractionation. The laminated textures are defined by the crystallographic orientation of long, slender (up to 2 x 7 mm) plagioclase laths and subhedral clinopyroxene prisms. In contrast to the subzone A gabbros, clinopyroxene in these rocks is more commonly altered to olive-green-brown hornblende rather than tremolite-actinolite.

Plagioclase compositions near the base of subzone B appear to be more calcic (An_{52}) compared to the upper

parts of subzone A (An_{29}); however, further microprobe analyses are needed to confirm this. In the middle to upper parts of the subzone, plagioclase (An_{46-30}) has similar andesine compositions to that documented in subzone A. Clinopyroxene (mg_{63-59}; $Ca_{40-43}Mg_{38-34}Fe_{22-23}$) has a consistent upward fractionation trend that appears to be a continuation of the trend established by clinopyroxene in the subzone A gabbroic rocks. In this respect the subzone B gabbros appear to be an advanced differentiate of the subzone A mafic sequence.

Geochemistry

Whole-rock major and trace-element analyses (see Appendix 3) were obtained for 74 drill core and 13 surface samples (88770051–137) along a 1800 m northwest-southeast traverse extending from the base of the ultramafic zone to the upper parts of subzone B of the gabbroic zone (traverse and sample locations are shown on the appended map sheet). Rock types analysed range in composition from lherzolite to plagioclase websterite in the ultramafic zone and from olivine gabbro to quartz gabbro in the gabbroic zone. Platinum-group-element (Pt, Pd, Ir, Ru) and Au determinations were carried out on basal massive and disseminated sulphides and at regular intervals through the overlying ultramafic and mafic cumulates.

Major elements

Despite the limitations of using whole-rock major-element compositions of cumulates as petrogenetic indicators (because they do not represent parent liquid compositions) they are useful for defining gross geochemical features of layered intrusions. The Radio Hill Complex has similar major-element variation trends

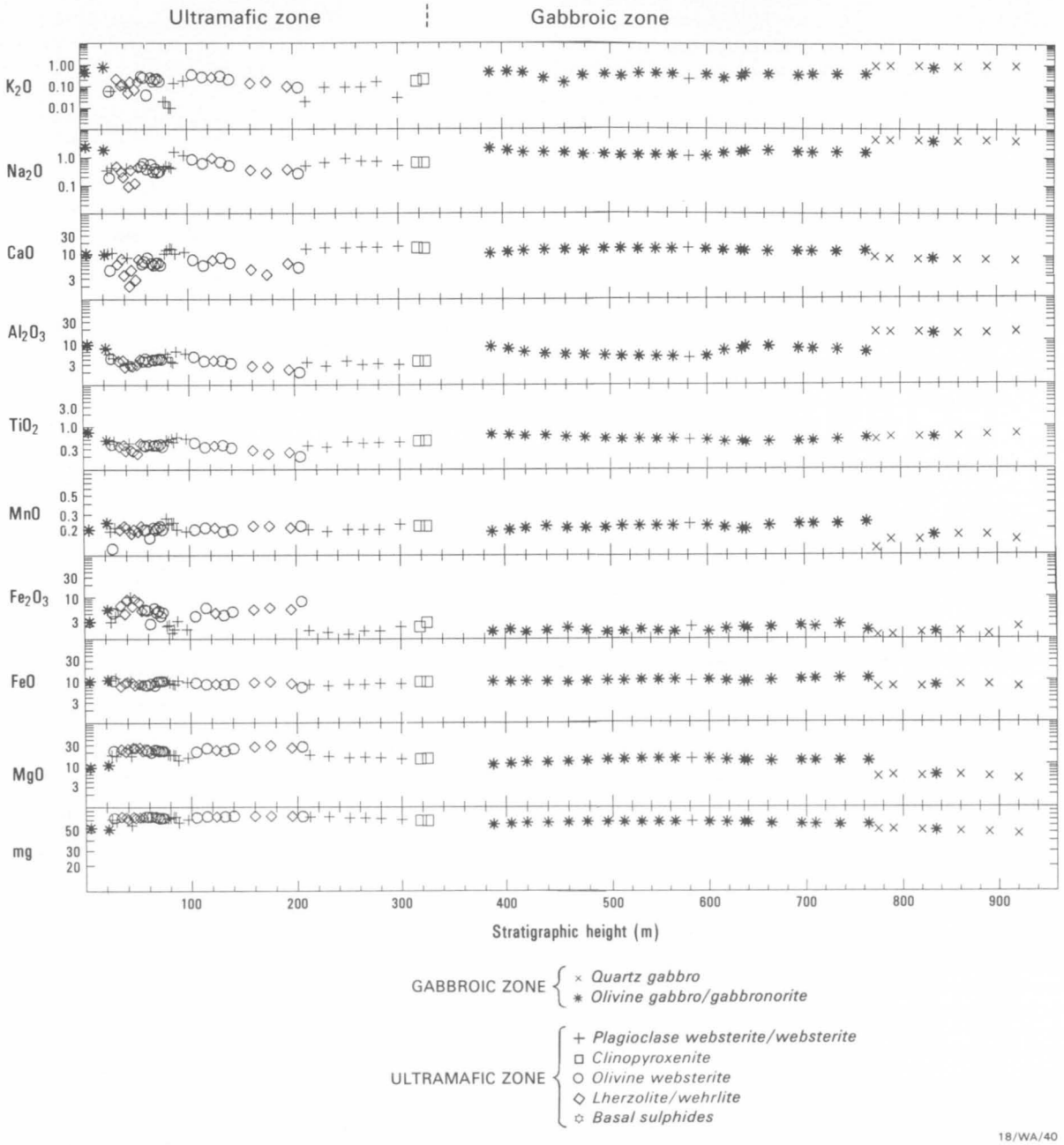

Fig. 69. Radio Hill Complex: variations in whole-rock major-element compositions (weight %) with stratigraphic height.

(Fig. 69) to the Munni Munni Complex, namely the occurrence of fractionated plagioclase-rich rocks along the basal contact, fairly flat fractionation trends for the cyclic peridotite and pyroxenite units in the ultramafic zone, and gently sloping fractionation trends for the overlying gabbros. There is a major disruption to the gross chemical trends at the contact of subzones A and B of the gabbroic zone, which reflects a significant change in the evolution of the intrusion.

Peridotites ($mg_{78.2-71.8}$), pyroxenites ($mg_{76.3-60.4}$), and subzone A gabbros ($mg_{67.5-62.0}$) of the gabbroic zone have consistent mg trends up the sequence, indicating that they are probably comagmatic and represent a continuous fractionation sequence. In contrast, two gabbro samples from near the base of the ultramafic zone have more fractionated compositions than the overlying ultramafic cumulates, as indicated by their lower mg (56.3–54.3), and higher FeO, MnO, TiO_2, Al_2O_3, Na_2O, and K_2O contents. These reverse fractionation trends are a common feature of the west Pilbara layered intrusions and are believed to be due to cooling and localised contamination, and greater amounts of melt components in the rocks, at the basal contact.

Peridotite and pyroxenite cumulates in the lower two-thirds of the ultramafic zone have generally flat mg trends, whereas from above the 212 m level the websterites and clinopyroxenites show weak decreasing mg trends as MnO and TiO_2 contents generally increase with height. This may reflect a change from steady-state magma replenishment in the lower levels to a more-closed system of restricted magma input in the upper levels of the ultramafic zone. The contrasting chemical trends would also be a function of variable cooling rates and amounts of trapped liquid, and fractionating minerals with different partition coefficients. The closed-system fractionation conditions appear to persist through to the lower parts of subzone A of the gabbroic zone, most elements showing consistent and gently sloping trends. However, there are some subtle irregularities in the Al_2O_3, Na_2O, MnO, and MgO trends above the 600 m level that may be due to changes in cumulate porosities or minor new pulses of fractionated magma. The TiO_2 contents of the subzone A gabbros display variable trends by initially decreasing to the 640 m level, and thereafter steadily increasing up the sequence.

With the exception of TiO_2, all major elements show a break in regional trends across the contact of the mafic subzones A and B (Fig. 69). The quartz gabbros from subzone B (above the 770 m level) differ from the more primitive subzone A gabbros in their lower mg (53.9–31.9), MgO, FeO, MnO, CaO, and higher Al_2O_3, Na_2O, and K_2O contents. These features reflect the absence of olivine and the marked increase in sodic plagioclase abundances in the upper mafic sequence. The increasing TiO_2 trend established in the upper part of subzone A continues up the subzone B sequence. The presence of the most magnetite-ilmenite-rich gabbro in the intrusion at the 1200 m level (88770135; not shown in Fig. 69) indicates that favourable conditions (e.g. magma composition and/or oxygen fugacity) prevailed in the upper levels of subzone B for the crystallisation of Fe-Ti oxides. The general transition to more closed-crystallisation conditions up the Radio Hill ultramafic-mafic sequence is a feature common to the west Pilbara layered intrusions.

The Radio Hill mafic and ultramafic cumulates show similar gross tholeiitic fractionation trends (Fig. 70), of increasing total FeO and Al_2O_3 and weak alkali enrichment, to the Munni Munni Complex (Fig. 49). However, in detail, the Radio Hill peridotites are more Fe-rich than their Munni Munni counterparts, and the subzone A gabbroic units are more primitive (shown by MgO versus total FeO contents) and less aluminous than the subzone A gabbronorites in the Munni Munni Complex. Interestingly, the fractionated subzone B quartz gabbros at Radio Hill fall in similar fields on the ternary plots (Fig. 70) to the subzone A gabbronorites of the Munni Munni Complex (Fig. 49).

Trace elements

The variations of Cu, Ni, Zn, S, Rb, Sr, Ba, Zr, Cr, Co, V, Ga, La, Nd, Ce, and Y abundances with stratigraphic height are summarised in Figures 71 & 72. The dominant control on the distributions of these trace

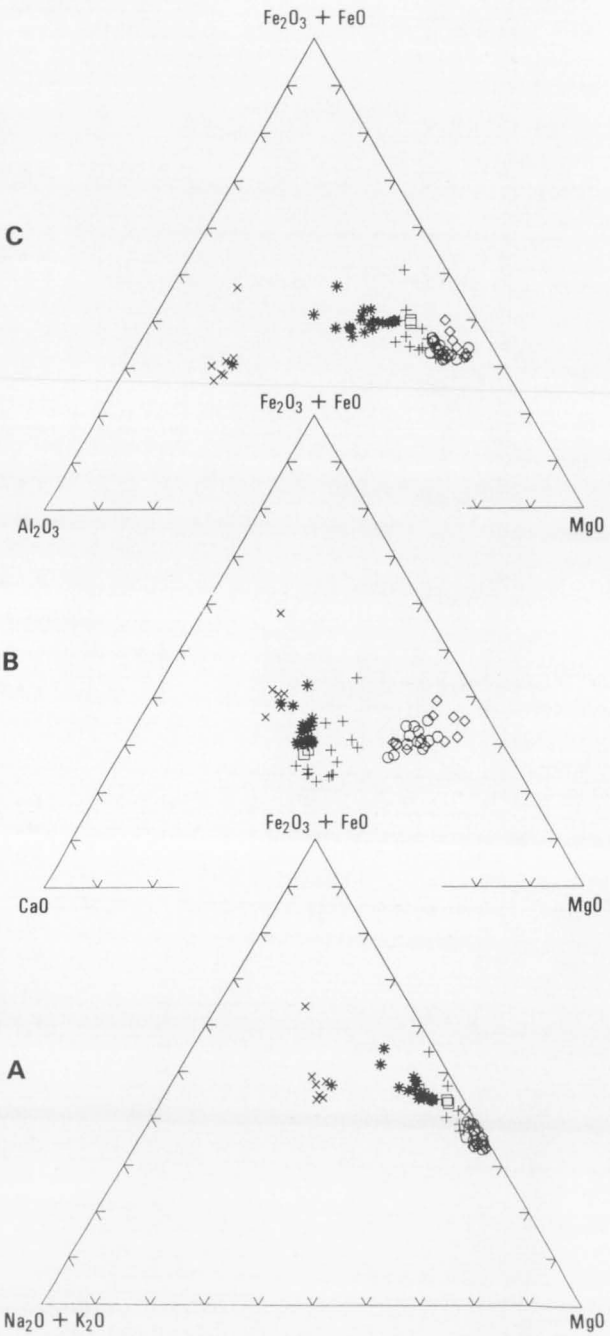

Fig. 70A–C. Radio Hill Complex: ternary plots showing variations in whole-rock major-element compositions (weight %). Symbols as in Figure 69.

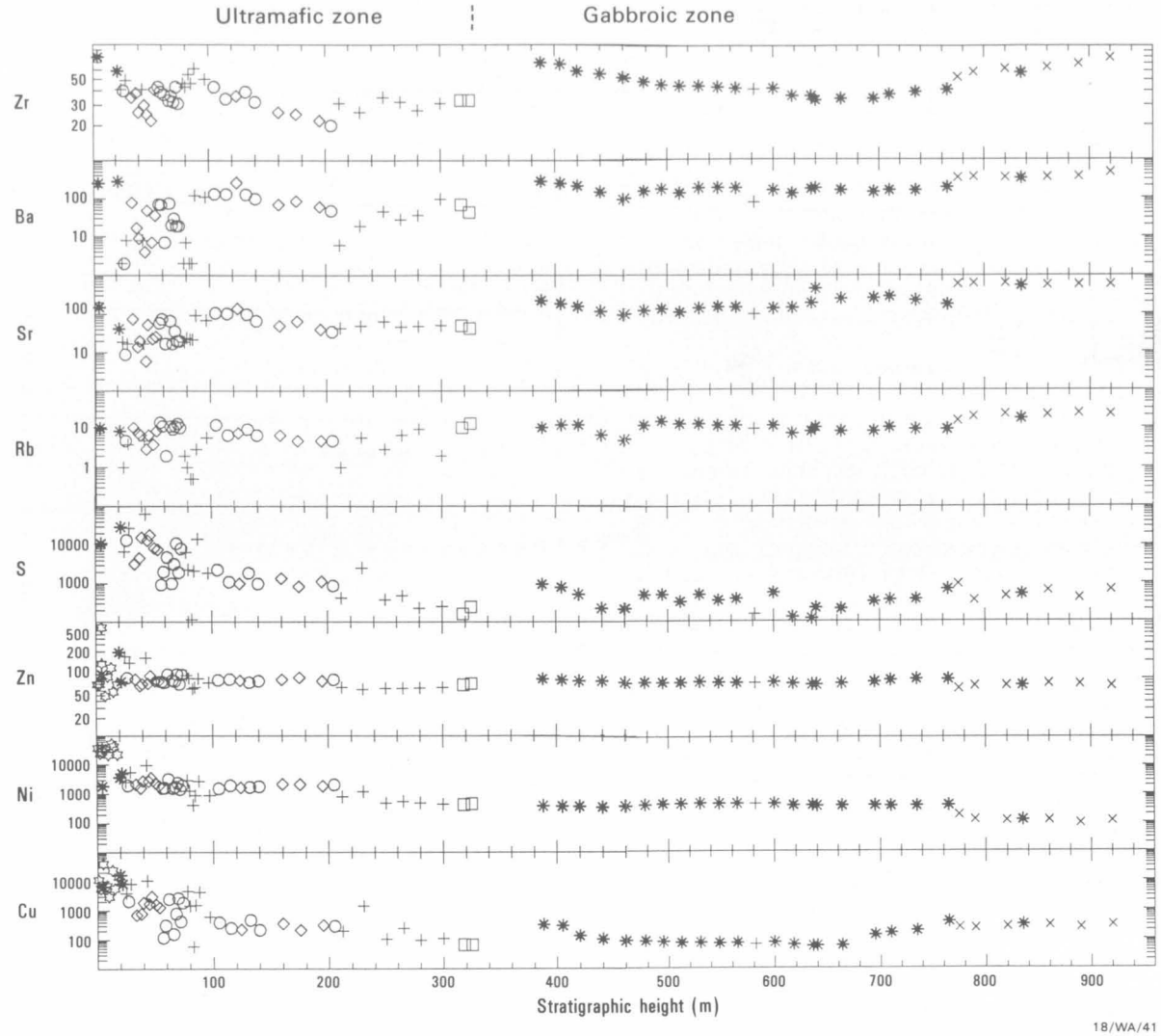

Fig. 71. Radio Hill Complex: variations in whole-rock trace-element compositions (ppm) with stratigraphic height. Symbols as in Figure 69.

elements is their degree of compatibility with cumulus sulphides, olivine, clinopyroxene, orthopyroxene, and plagioclase. Most 'unmineralised' ultramafic and mafic cumulates have S contents ranging from 400 to 2000 ppm and 200 to 1000 ppm, respectively, indicating that the total Radio Hill sequence formed from magmas that were S-saturated. Copper and Ni have sympathetic trends with S throughout the intrusion, the basal gabbroic rocks of the ultramafic zone being enriched in these elements, and thereafter Cu and Ni are depleted up the sequence. This contrasts with the Munni Munni Complex where Cu and Ni abundances are decoupled from each other in the ultramafic zone because of the preferential partitioning of Ni into olivine and Cu into the melt under S-undersaturated conditions. In the S-saturated Radio Hill sequence, both Ni and Cu partitioned into sulphides and the effect of olivine on the distribution of Ni is negligible. Cobalt shows similar chalcophile behaviour to Cu and Ni and its distribution appears to be largely controlled by pentlandite. Because the mafic and ultramafic cumulates formed from S-saturated magmas, there is no marked enrichment of the chalcophile elements due to crystal fractionation processes above the basal contact of the intrusion.

Discontinuities in the gross trends of the more incompatible elements Zr, Y, Nd, and Ce at the 212 m level support the suggestion from major-element data, that the pyroxenites in the upper part of the ultramafic zone (subzone G) formed from a large new pulse of magma. With the exception of Zr, Ba, and Sr, the trace elements generally have consistent trends across the ultramafic/gabbroic zone contact (330 m level), but show an abrupt break at the contact (770 m) of the subzone A and B mafic sequences. This discordance may be due to marked changes in porosity and/or mineralogy in a single magma type across the contact, or to the involvement of a new magma of different composition in the formation of the subzone B rocks. To explore these alternatives further, Figure 73 shows that for a given Zr value, the TiO_2, P_2O_5, Th, Nb, Y, La, Ce, and Nd contents of the subzone A cumulates are generally similar to the subzone B cumulates. These similar incompatible-element trends support a common origin for the subzone A and B mafic sequences, but detailed mineralogical and isotopic data are required to substantiate this.

Platinum, palladium, iridium, ruthenium, gold, silver. The precious-metal geochemistry of the mafic-ultramafic sequence is summarised in Table 20 and Figure

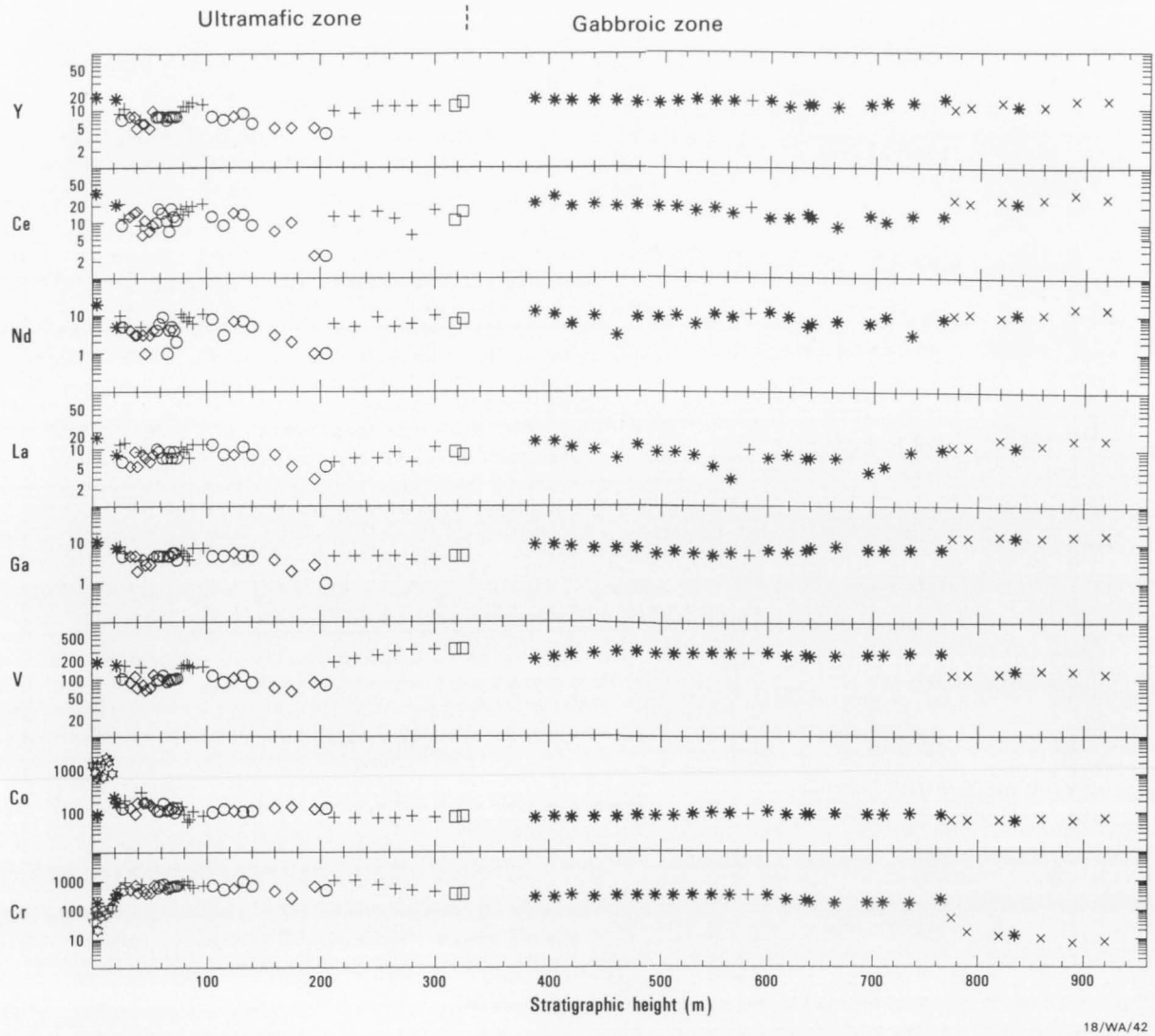

Fig. 72. Radio Hill Complex: variations in whole-rock trace-element compositions (ppm) with stratigraphic height. Symbols as in Figure 69.

74. Platinum, Pd, Ir, Ru, and Au generally show sympathetic distributions throughout the total sequence; this is consistent with their chalcophile behaviour during S-saturated magma conditions. The basal rocks are enriched in the precious metals (discussed in detail below) in the order Pd > Pt ≫ Ru > Ir > Au, and these metals progressively decrease in abundance with stratigraphic height. The depletion rate of precious-metal abundances to the 100 m level is rapid, and parallels the marked decline in S abundances. Palladium and Pt contents remain surprisingly high in the overlying S-saturated ultramafic (40.6–62.5 ppb Pd, 14.60–42.3 ppb Pd) and gabbroic (2.21–66.9 ppb Pd, 2.57–25.20 ppb Pt) cumulates. The high PGE contents of the latter cumulates contrast with the S-saturated gabbroic zone cumulates of the Munni Munni Complex, which have Pt + Pd contents of less than 3 ppb. Iridium and Ru contents are similarly high relative to the Munni Munni Complex. Gold is the only precious metal that shows upward enrichment trends over any significant part of the Radio Hill layered sequence (e.g. interval 640–765 m).

Most precious-metal abundances and ratios (Fig. 74) display fairly consistent trends across the ultramafic/gabbroic zone contact, which supports the suggestion that the subzone A mafic cumulates have differentiated from the ultramafic zone cumulates. There is a subtle increase in the Pt/Pd ratio from 0.15–0.51 for the ultramafic cumulates to 0.28–0.72 for the mafic cumulates, which may reflect the greater partitioning of Pd relative to that of Pt for S. The (Pd x 10^6)/S ratio should decrease for a fractionating S-saturated sequence in a closed magma chamber. However, there are some fluctuations in this ratio in the upper part of mafic subzone A and at the contact between mafic subzones A and B that suggest possible influxes of new magma. The decrease in this ratio at the interface of subzones A and B highlights the PGE-poor character of the S-saturated subzone A quartz gabbros compared to the underlying gabbros.

The steadily increasing Pt/Pd ratio with increasing fractionation, and the sympathetic chalcophile behaviour of the precious metals for all rock types in the Radio Hill Complex, is indicated by the positive trends in Figure 75. Palladium and Pt show the most sympathetic trends with S, followed by Au, Ru, and Ir. The subzone A gabbros, pyroxenites, peridotites, and basal units show a well-defined trend of increasing Cu with increasing Ni, but the subzone B gabbros have anomalously high Cu/Ni contents.

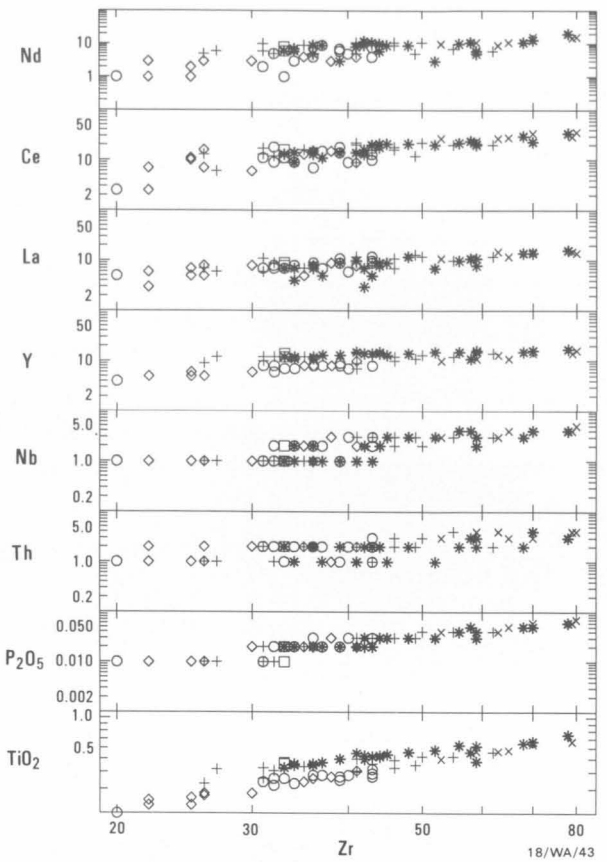

Fig. 73. Radio Hill Complex: variations in major and trace elements against Zr. Symbols as in Figure 69.

The Ni-Cu (Table 21; Fig. 76A) and Cu-Ni (Table 22; Fig. 76B) sulphide mineralisation at the base of the ultramafic zone is characterised by contrasting abundances and ratios of the precious and base metals. The Pt and Pd contents of the Ni-Cu-mineralised sequence (Fig. 76A) increase rapidly immediately above the basal contact of the intrusion and high abundances of about 0.32–1.90 ppm Pd and 0.29–0.84 ppm Pt are maintained for the overlying 15 m-thick mineralised interval. Platinum/Pd ratios (0.21–0.97) show no systematic trends, but the Cu/(Cu + Ni) ratio (0.28–0.57) steadily increases upwards in the top part of the mineralised interval. Copper has a crudely stepped distribution (two possible cycles) as it increases up the sequence, which may be due to influxes of new magma. Variable Ir (1.37–491 ppb) and Ru (30.5–459 ppb) and high Co (up to 2800 ppm) contents characterise the Ni-Cu mineralised zone. The low Ni/Cu ratios (0.8–2.6) are similar to other gabbroic-hosted Ni-Cu deposits in Western Australia (e.g. Mount Sholl, Carr Boyd Rocks, Sally Malay), which have Ni/Cu less than 7 (Marston, 1984).

The Cu-Ni mineralised sequence, which occurs at least 6 m above the basal contact (extrapolated 99.0 m level in Fig. 76B), has high Cu/(Cu + Ni) ratios (0.61–0.89) and is depleted in Pt and enriched in Au and Zn relative to the Ni-Cu mineralised sequence. Platinum/Pd ratios (0.04–0.33) are consistently lower, and Au contents (0.04–0.88 ppm) are an order of magnitude greater, than in the Ni-Cu mineralised zone. In addition, Pt and Pd show more marked depletion trends that closely parallel S up the sequence. Highest Ag contents (4–16 ppm) are generally associated with the Au-enriched intervals. A 1 m-thick massive chalcopyrite layer at 84.5 m is the most anomalous precious-metal intersection (6.58 ppm Pd, 1.80 ppm Pt, 23.80 ppm Au, 54 ppm Ag) reported at Radio Hill.

Discussion and origin of sulphide mineralisation

The Radio Hill Complex has similar stratigraphy and mineralisation to other Australian Precambrian mafic intrusions, including Mount Sholl (this study), Sally Malay (Thornett, 1981), and Carr Boyd Rocks (Purvis & others, 1972), and to the Early Proterozoic layered mafic intrusions of central and northern Finland (Papunen & others, 1979; Alapieti & Lahtinen, 1989). A common feature of these intrusions is the concentration of massive and disseminated PGE-bearing Ni-Cu sulphides near the basal contact. Various origins have been proposed for the formation of the sulphides, including such magmatic processes as gravitational accumulation of an immiscible sulphide liquid, upward expulsion of interstitial fluid (infiltration metasomatism of Irvine, 1980b), periodic magma replenishment, and fractional crystallisation (Ripley, 1986), as well as non-magmatic processes, such as the devolatilisation of underlying country rocks (Tyson & Chang, 1984), and infiltration of hydrothermal fluids (Mogessie & others, 1991).

The presence of massive sulphide layers, the uniformity of the base- and precious-metal depletion trends up the total layered sequence, the upward increasing Cu/(Cu + Ni) ratios, and primary magmatic sulphide-silicate textures collectively indicate that the massive

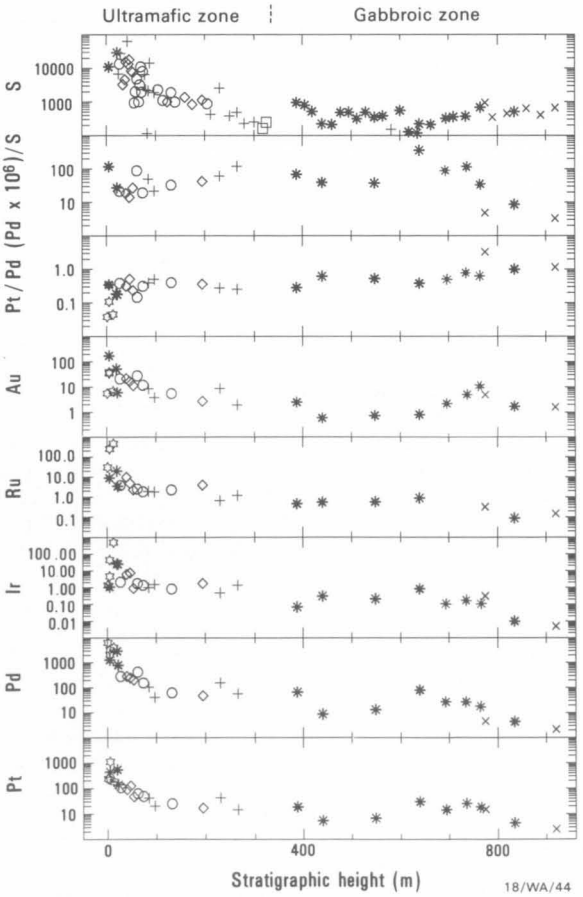

Fig. 74. Radio Hill Complex: variations in Pt, Pd, Ir, Ru, Au (ppb), Pt/Pd, Pd/S and S (ppm) with stratigraphic height. Symbols as in Figure 69.

Table 20. Precious-metal and trace-element geochemistry of the Radio Hill Complex

Sample number	*Stratigraphic level (m) and subzone*	*Lithology*	*Pt (ppb)*	*Pd (ppb)*	*Ir (ppb)*	*Ru (ppb)*	*Au (ppb)*	*Ag (ppm)*	*Cu (ppm)*	*Ni (ppm)*	*S (ppm)*	*Pt/Pd*	*(Pt + Pd) × 10^6/S*	*Cu × 10^3/(Cu + Ni)*
Ultramafic zone														
Basal Ni–Cu massive sulphides (see Table 21)														
0053	1, A	Massive sulphide	243	6312	1.37	30.5	5.60	9	11 190	36 750	—	0.04	—	233
0055	5, A	Massive sulphide	220	2025	44.6	254	34.7	13	6965	33 440	—	0.11	—	676
0058	13, A	Massive sulphide	184	4071	491	459	6.94	9	23 880	52 650	—	0.05	—	312
Basal Cu–Ni massive sulphides (see Table 22)														
0136	5, A	Massive sulphide	1127	3334	4.67	259	39.04	—	143 800	27 810	—	0.34	—	838
0137	5, A	Massive sulphide	453	1299	1.10	4.00	174	—	6539	1835	11 038	0.35	158.72	781
Hangingwall units with disseminated sulphides														
0061	20, A	Gabbronorite	550	2959	26.25	20.30	52.5	9	16 665	3642	—	0.19	—	821
0062	22, A	Gabbronorite	143	799	25.48	3.51	6.01	—	8273	5033	29 320	0.18	32.13	622
0064	27, A	Pyroxenite	110	287	2.13	3.88	21.16	—	2119	1957	13 452	0.38	29.51	520
0068	40, B	Lherzolite	91	288	6.15	9.91	21.60	—	1886	2705	15 568	0.32	24.34	411
0071	47, B	Lherzolite	127	250	7.53	4.95	16.94	—	3055	3493	17 968	0.51	20.98	466
0073	54, B	Lherzolite	47.6	205	0.91	2.30	11.54	—	1289	1891	7596	0.23	33.25	405
0076	62, C	Plag websterite	62.7	428	1.76	2.54	28.13	—	2496	3189	4852	0.15	101.13	439
0081	74, D	Ol websterite	48.7	156	1.38	1.88	11.80	—	1878	1945	8124	0.31	25.20	491
0085	85, E	Plag websterite	41.4	106	0.98	1.94	8.38	—	1536	891	2141	0.39	68.84	633
0087	97, E	Plag websterite	20.25	40.6	1.51	1.81	3.79	—	604	880	1885	0.50	32.28	407
0091	132, F	Ol websterite	25.09	62.5	0.83	2.31	5.53	—	479	1716	1905	0.40	45.98	218
0095	195, F	Lherzolite	17.25	47.8	1.78	3.96	2.69	—	321	1890	1136	0.36	57.26	145
0098	230, G	Websterite	42.3	155	0.48	0.66	8.56	—	1454	1209	2571	0.27	76.74	546
0100	265, G	Plag websterite	14.60	57.4	1.35	1.19	1.93	—	250	554	483	0.25	149.07	31
Gabbroic zone														
0107	388, A	Gabbro	18.89	66.9	0.07	0.46	2.52	—	332	391	965	0.28	88.90	459
0110	440, A	Gabbro	5.49	8.82	0.31	0.55	0.60	—	105	350	223	0.62	64.17	231
0116	548, A	Ol gabbronorite	6.96	13.25	0.21	0.58	0.74	—	74	460	351	0.53	57.57	139
0122	640, A	Ol gabbronorite	30.5	79.9	0.83	0.89	0.81	—	59	380	222	0.38	497.30	134
0124	695, A	Ol gabbronorite	17.70	33.5	0.07	—	5.17	—	139	394	325	0.53	235.08	261
0126	735, A	Ol gabbro	25.20	35.2	0.15	—	6.29	—	195	387	375	0.72	161.07	335
0127	765, A	Ol gabbronorite	18.20	29.00	0.08	—	6.67	—	395	403	694	0.63	68.01	495
0128	775, B	Gabbro	15.19	4.63	0.32	0.33	4.94	—	253	186	949	3.28	20.89	576
0131	835, B	Gabbronorite	4.46	4.42	0.01	0.09	1.72	—	312	124	511	1.01	17.38	716
0134	920, B	Quartz gabbro	2.57	2.21	0.01	0.15	1.61	—	312	116	667	1.16	7.17	729

Sample numbers are prefixed by AGSO reference numbers 8877. Ol = olivine, Plag = plagioclase. Analytical techniques for the precious metals (analyses by S. Reeves, School of Earth Sciences, University of Melbourne) involved a fire-assay nickel preconcentration (25 g charge) followed by instrumental neutron-activation analysis (Pt, Pd, Ir, Ru, Au). The other elements were determined at the AGSO by AAS (Ag, Cu, Ni) and XRFS (S). — = not determined.

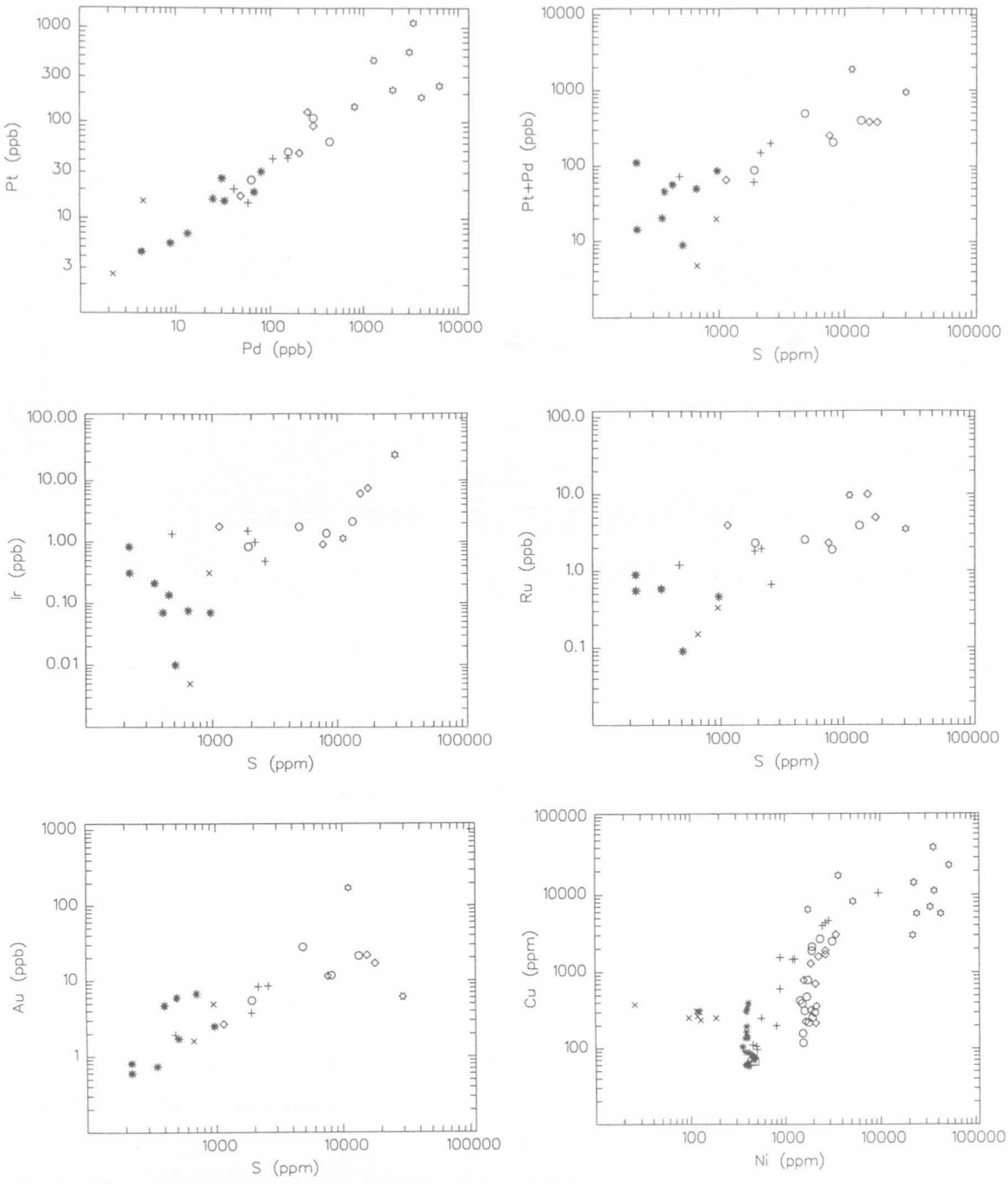

Fig. 75. Radio Hill Complex: variations in Pt against Pd, and precious metals and trace elements against S and Ni. Symbols as in Figure 69.

and disseminated sulphides in the Radio Hill Complex are largely of magmatic origin. Basal Ni-Cu sulphide zones of magmatic origin must invoke an efficient mineralising mechanism (e.g. gravitational settling or wide-scale magma mixing in the chamber) where large amounts of immiscible sulphides are derived from the silicate melt. De Angelis & others (1987) proposed that the stringer and massive sulphides along the basal contact were formed from the remobilisation and redeposition of primary sulphides by the intrusion of overlying gabbroic units. However, the concentration of the massive sulphide layers in the lowest and thickest parts of the elongated ultramafic zone, the widespread occurrence of primary disseminated sulphides, and the consistent metal ratios up the sequence indicate that large-scale primary processes, such as gravitational settling and structural controls (e.g. basinal depressions), were important for the accumulation of immiscible sulphides from magmas saturated in S. In addition, similar relationships between mineralisation and basinal structures are seen at the base of the Mount Sholl and Munni Munni ultramafic zones. Remobilisation of primary sulphides in the Radio Hill Complex is largely restricted to the immediate vicinity of the basal contact. Sulphide-bearing veins and brecciated massive sulphides along the basal contact are believed to reflect localised hydrothermal activity and movement during the emplacement of the overlying cyclic units, respectively. Brecciation along the basal contact may have been enhanced by the marked differences in competency between the indurated basement metavolcanics and the abutting massive sulphides.

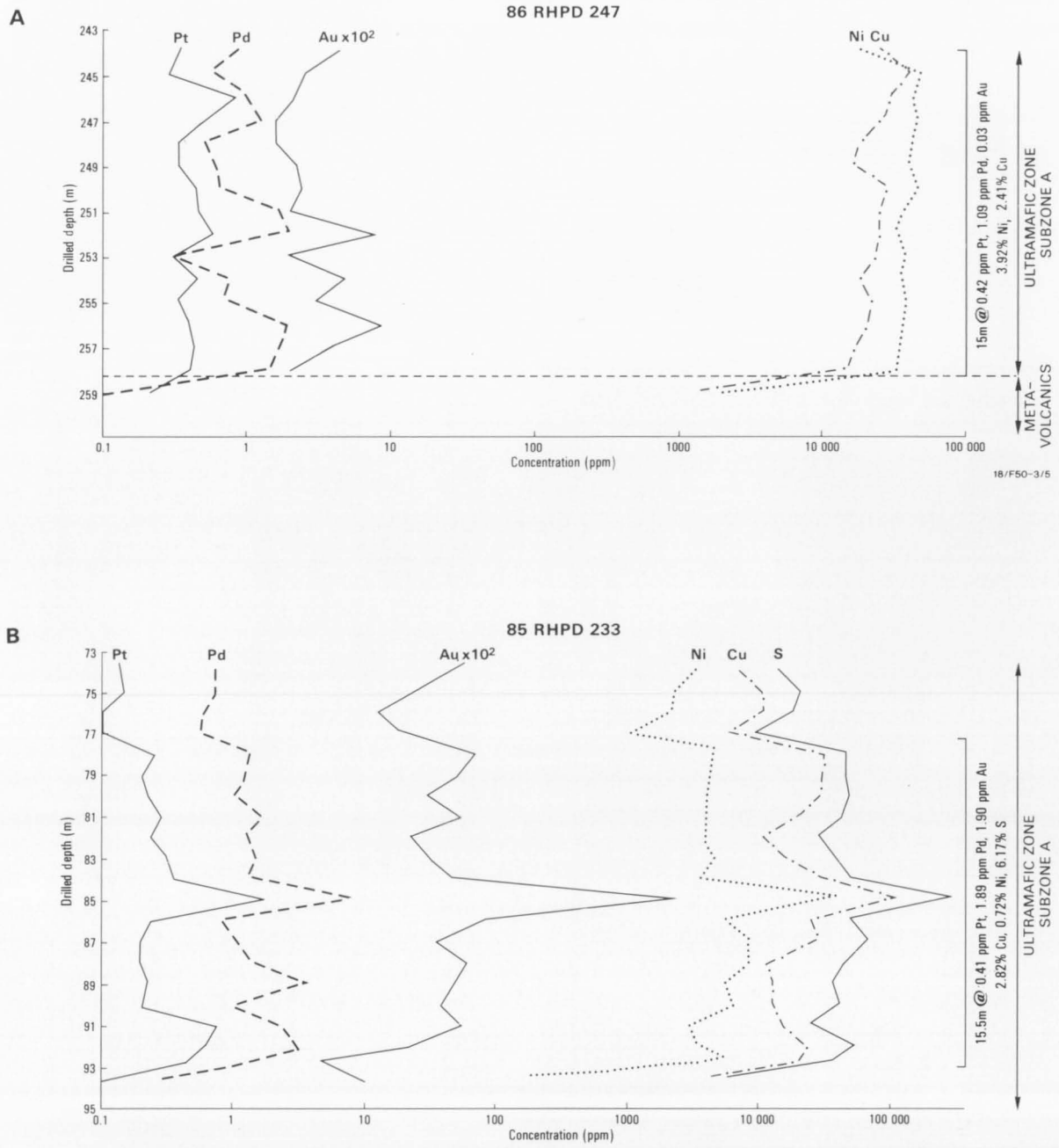

Fig. 76A–B. Precious-metal geochemistry of (A) Ni-Cu and (B) Cu-Ni sulphide mineralisation at the basal contact of the Radio Hill Complex. Drillhole data from Agip Australia Pty Ltd.

The primary mineralising processes at Radio Hill are believed to be similar in some broad respects to the magmatic accumulation models that were proposed for Archaean komatiitic volcanogenic Ni-Cu deposits (Ewers & Hudson, 1972; Green & Naldrett, 1981). These models involve the gravitational settling and accumulation of immiscible sulphides separating from an evolving komatiitic magma. This results in a typical stratigraphic sequence, similar to that seen at Radio Hill, of a basal layer of massive sulphides, overlain by a mixture of sulphides, olivine, and pyroxene, and an uppermost layer lacking olivine. In contrast to the volcanogenic environments, the paucity of associated minor rock types, and the absence of major lithological discontinuities in the mineralised sequences at Radio Hill, suggest that the sulphides formed from a continuum of magmatic processes and no major hiatuses were involved. Whole-rock and mineral compositional trends support the suggestion that the lower part of the magma chamber was quickly filled with repeated new pulses of primitive magma.

The more fractionated trends of clinopyroxene (i.e. more Fe-rich) and plagioclase (more sodic) compositions towards the basal contact, the absence of olivine in the basal rocks, and the increase of whole-rock SiO_2, Al_2O_3, Na_2O, K_2O with depth, are features seen in the other west Pilbara intrusions and are believed to reflect rapid cooling, different amounts of melt components in the marginal rocks, and minor localised contamination of the basaltic parent magmas along the basal contact. There is no field or chemical evidence to indicate that Cu, Fe, S, and other volatiles were derived through

large-scale partial melting and contamination involving the underlying basement metavolcanics, as has been proposed by Tyson & Chang (1984) for the Partridge River Troctolite of the Duluth Complex, Minnesota. Mass-balance relationships that incorporate a 1200 m thick mafic-ultramafic column averaging 500 ppm S show that it is not feasible to generate the large amounts of S and metals from the '*in situ* devolatilisation' of the basement metavolcanics, which are unlikely to have more than a few hundred ppm S.

Table 21. Precious-metal and trace-element geochemistry of the basal Ni-Cu sulphide mineralisation in the Radio Hill Complex

Depth down hole (m)	*Pt (ppm)*	*Pd (ppm)*	*Au (ppm)*	*Cu (%)*	*Ni (%)*	$\frac{Pt}{Pd}$	$\frac{Cu \times 10^3}{(Cu + Ni)}$
86 RHPD 247							
243.65–244.65	0.33	0.88	0.05	2.56	1.95	0.38	568
244.65–245.65	0.29	0.56	0.03	4.38	4.82	0.52	476
245.65–246.65	0.84	0.99	0.02	3.15	4.43	0.85	416
246.65–247.65	0.51	1.28	0.02	2.77	4.66	0.40	373
247.65–248.65	0.33	0.51	0.02	1.91	4.36	0.65	305
248.65–249.65	0.33	0.62	0.02	1.65	4.26	0.53	279
249.65–250.65	0.44	0.67	0.02	2.77	4.75	0.66	368
250.65–251.65	0.46	1.70	0.02	2.64	3.79	0.23	410
251.65–252.65	0.48	1.88	0.08	2.58	3.32	0.26	437
252.65–253.65	0.31	0.32	0.02	2.39	3.84	0.97	384
253.65–254.65	0.46	0.74	0.05	1.93	3.74	0.62	340
254.65–255.65	0.33	0.68	0.03	2.17	3.93	0.49	356
255.65–256.65	0.40	1.90	0.08	2.08	3.84	0.21	351
256.65–257.65	0.42	1.73	0.04	1.65	3.69	0.24	309
257.65–258.65	0.40	1.40	0.02	1.53	3.48	0.29	305
258.65–259.65	0.22	0.05	—	0.13	0.25	4.40	342

The diamond-drillhole data were kindly provided by Agip Australia Pty Ltd. The drilled sequence shown above is from the basal parts of subzone A of the ultramafic zone. Rock types include sulphide-bearing gabbro and gabbronorite. Basement metavolcanics occur at the 258.65 m drillhole level. Analytical techniques for the precious metals (by Resource Development Laboratories, Perth) involved a fire-assay lead preconcentration (50 g charge) followed by carbon-rod atomisation (Pt), atomic-absorption spectrophotometry (AAS—Pd), and fire-assay fusion—AAS (Au). The other elements were determined by AAS (Cu, Ni). — = not determined.

The contrasting precious-metal geochemistry and elevated level of the Cu-Ni sulphide mineralisation just above the basal contact at Radio Hill indicate a different origin to that proposed for the massive Ni-Cu sulphides that abut the footwall contact. Pasteris (1984) and Ripley (1986) have proposed mechanisms of Cu enrichment in the melt that involve upward migration of metals during fractional crystallisation. The mechanism includes enrichment of Cu in the residual melt, upward movement of the interstitial liquid during infiltration metasomatism (Irvine, 1980b), and periodic addition of new magma. Repetition of this sequence has the potential of producing a liquid strongly enriched in Cu that can ultimately form Cu-rich sulphide zones above Cu-depleted zones. It is unlikely there was a significant increase in the Cu contents of the residual melt by crystal fractionation at Radio Hill since the basal sequence contains copious amounts of sulphides (i.e. it is S saturated). However, the latter components of the model (infiltration metasomatism and periodic magma replenishment) may be relevant to the formation of the Cu-rich sulphide zone. The high Cu/(Cu + Ni) ratios and Au contents may be attributed to the decoupling of Cu and Au from Ni during metasomatism and/or to a highly-evolved magma pulse enriched in Cu and Au that was emplaced several metres above the basal contact of the intrusion.

Sulphur isotopes for the different styles of sulphide mineralisation in the Radio Hill Complex (Table 34) show a fairly restricted range (+1.1 to +4.8‰) that is typical of the west Pilbara layered intrusions. There appears to be a progressive increase in the $\partial^{34}S$ values from disseminated Fe-rich sulphides (+1.1 to +1.5‰), to massive chalcopyrite (+2.0 to +3.2), to massive pyrrhotite-pentlandite-chalcopyrite (+4.5 to +4.8). Remobilised chalcopyrite-rich veins along the basal con-

Table 22. Precious-metal and trace-element geochemistry of the basal Cu-Ni sulphide mineralisation in the Radio Hill Complex

Depth down hole (m)	*Pt (ppm)*	*Pd (ppm)*	*Au (ppm)*	*Ag (ppm)*	*Cu (%)*	*Ni (%)*	*S (%)*	*Pt/Pd*	$\frac{(Pt + Pd) \times 10^6}{S}$	$\frac{Cu \times 10^3}{(Cu + Ni)}$
85 RHPD 233										
73.5–74.5	0.14	0.74	0.47	5	0.79	0.34	1.55	0.19	56.77	699
74.5–75.5	0.15	0.73	0.27	8	1.34	0.24	2.08	0.21	42.31	848
75.5–76.5	0.10	0.61	0.14	7	1.37	0.22	1.81	0.16	39.23	862
76.5–77.5	0.10	0.57	0.19	4	0.65	0.11	0.98	0.18	68.37	855
77.5–78.5	0.26	1.41	0.71	16	3.25	0.42	4.95	0.18	33.74	886
78.5–79.5	0.21	1.27	0.57	15	3.21	0.41	4.78	0.17	30.96	887
79.5–80.5	0.23	1.08	0.30	14	2.96	0.41	5.00	0.21	26.20	878
80.5–81.5	0.29	1.60	0.53	9	2.00	0.92	4.47	0.18	42.28	685
81.5–82.5	0.24	1.21	0.22	6	1.07	0.37	2.81	0.20	51.60	743
82.5–83.5	0.32	1.39	0.31	8	1.59	0.44	3.65	0.23	46.85	783
83.5–84.5	0.36	1.30	0.47	14	2.94	0.37	4.65	0.28	35.70	888
84.5–85.5	1.80	6.58	23.80	54	12.40	3.67	32.9	0.27	25.47	772
85.5–86.5	0.24	0.84	0.88	13	2.75	0.57	4.83	0.29	22.36	828
86.5–87.5	0.20	1.01	0.34	14	3.02	0.86	6.56	0.20	18.45	778
87.5–88.5	0.20	1.37	0.60	7	1.27	0.81	4.51	0.15	34.81	611
88.5–89.5	0.22	3.24	0.48	7	1.28	0.55	3.74	0.04	92.51	699
89.5–90.5	0.20	0.96	0.38	8	1.31	0.65	4.13	0.21	28.09	668
90.5–91.5	0.72	2.40	0.58	8	1.57	0.29	2.54	0.30	12.28	855
91.5–92.5	0.60	3.24	0.23	10	2.41	0.35	5.41	0.19	70.98	873
92.5–93.0	0.44	1.33	0.04	8	2.02	0.42	3.76	0.33	47.07	828

The diamond-drillhole data were kindly provided by Agip Australia Pty Ltd. The drilled sequence shown above is from the basal parts of subzone A of the ultramafic zone. Rock types include sulphide-bearing gabbro and gabbronorite, with massive sulphides for the interval 84.5–85.5 m and basement metavolcanics at the 99.0 m drillhole level. Silver was analysed by XRFS and S was determined by iodometric Leco titration; the other elements were determined by the analytical techniques indicated in Table 21.

tact of the latter massive sulphides have a $\partial^{34}S$ value of +3.2‰. Unfortunately these data provide little insight into the origin of the S, since any sulphides that may be present in the Archaean basement metavolcanics will have magmatic S isotope signatures.

The Ni-Cu-(PGE) potential of the basal sulphides is well recognised in the Radio Hill Complex, but the PGE potential at higher stratigraphic levels has not been assessed. The trace-element profiles have highlighted the S-saturated character of the cumulates and the gross precious-metal depletion trends through the total stratigraphic succession. Because of these features (despite the coarse-sampling interval), it is believed the Radio Hill Complex is unlikely to host a laterally extensive PGE-enriched layer at high stratigraphic levels similar to that seen in the Munni Munni Complex. The widespread occurrence of early-crystallising clinopyroxene compared to that of orthopyroxene in the ultramafic and mafic units would have inhibited the formation of chromitite layers (see p. 55), thus downgrading the potential for a PGE-chromite deposit. However, the high background Pd + Pt concentrations throughout the stratigraphy would favour the formation of a structurally-controlled hydrothermally-remobilised PGE deposit. Shear zones that traverse serpentinised ultramafic cumulates and regions with widespread alteration features in the gabbroic zone should be a focus for such investigations.

FIELD RELATIONSHIPS, PETROGRAPHY, AND GEOCHEMISTRY OF THE MAITLAND COMPLEX *(DMH)*

Introduction

The Maitland Complex is 37 km south of Karratha and 8 km northeast of the Munni Munni Complex, at latitude 21°04′S and longitude 116°53′35″E, on the Pinderi Hills 1 : 100 000 Topographic Sheet 2255 and Yarraloola 1 : 250 000 Geological Sheet SF/50-6. This small, intensely-faulted mafic body is distinguished from the other west Pilbara intrusions by the high proportion of anorthosites and relative absence of ultramafic cumulates in the layered stratigraphy.

Size and age

The Maitland Complex (Fig. 77) is a small mafic intrusion exposed over an area of approximately 3.5 by 4 km. It has intruded the contact between metavolcanics of the ?Warrawoona Group (eastern margin of intrusion) and leucocratic biotite-muscovite granite and granodiorite (southern and western margins). The northern margin is masked by siliceous sands and gravels derived from granite, so there are unlikely to be significant subsurface extensions of the complex. The presence of uplifted fault blocks of basement granite in the mafic stratigraphy suggests the intrusion is a thin sheet. The thin vertical dimension is believed to be largely primary, although it is not known how much of the complex has been eroded. The total thickness of the mafic sequence is estimated at about 2 km.

No geochronological data exist for the Maitland Complex, and there are no chilled margins of the mafic rocks against the metavolcanics and granite. However, disseminated sulphides, quartz-feldspar intergrowths, and pegmatoidal segregations in a distinctive gabbroic unit along the eastern margin of the intrusion are believed to have been derived from the contamination of the mafic magma against an older felsic and intermediate metavolcanic sequence. The plagioclase-rich compositions, coexistence of disseminated sulphides and oxides, and alteration styles in these rocks are similar to those seen in the basal sulphide-bearing rocks of other west Pilbara intrusions. This supports the idea that the eastern margin of the complex is its basal contact. The occurrence of rare metavolcanic blocks hosted by gabbro, and the location of the intrusion along a regional lithological contact between the metavolcanics and granites, also testifies to the younger age of the intrusion relative to the surrounding rocks. The Maitland Complex is tentatively correlated with the nearby 2927 ± 13 Ma Munni Munni Complex.

Distribution of rock types and stratigraphic relationships

The Maitland Complex (Fig. 77) contains the highest ratio of mafic to ultramafic rocks of any of the layered intrusions investigated in this study. The mafic rocks form a bimodal cyclic sequence of gabbroic and anorthositic cyclic units, with the latter cumulates constituting about 25% of the stratigraphy. Ultramafic cumulates have a restricted distribution in the western half of the intrusion, where they form plugs and rarer conformable lenses.

The gabbroic units consist of an undivided monotonous sequence of gabbro, uralitised gabbro, gabbronorite, and minor norite. In the absence of interlayered anorthositic cyclic units, it is difficult to determine any systematic subdivision for the weakly layered gabbroic units. Layering is restricted to rare modal- and size-graded layers (Fig. 78A) in the more mafic gabbroic variants, and norites (samples 88770028–032) in the central part of the intrusion display a pervasive mineral lamination along an east-west strike trend for several hundreds of metres. The most sulphide-rich horizon documented in the intrusion is a distinctive sulphide-bearing quartz melagabbroic unit (88770021–023) that extends for 2.5 km along the eastern margin of the complex. The unit only occurs where the complex intrudes metavolcanics and it is absent from the other margins where the country rocks are leucocratic biotite-muscovite granites. The melagabbro (Fig. 78B) is characterised by irregular coarse-grained pegmatoidal patches of quartz-feldspar-amphibole intergrowths and disseminated trace Fe-rich sulphides (0.5 vol. %). The quartz and sulphide contents consistently decrease away from the contact towards the centre of the intrusion.

The anorthositic units consist largely of mottled anorthosite (Fig. 78C) with minor anorthositic gabbro and gabbro. They have sharp contacts with the gabbroic cycles and range in thickness from a few metres up to 200 m. Layering is poorly developed and the most distinctive feature is their mottled texture, defined by centimetre-sized clusters of intercumulus pyroxene in a matrix of sericitised cumulus plagioclase. The gabbroic and anorthositic cyclic sequences are best developed in the southeastern corner of the intrusion. Three anorthosite cycles of variable thickness show an arcuate strike trend sub-parallel to the eastern margin of the intrusion (see appended map sheet). Their distribution is partly controlled by two sets of steeply-dipping faults that trend northeast and east-southeast.

Ultramafic units that display both discordant and conformable relationships with the mafic sequences form a minor component of the Maitland Complex. Eleven plug-like ultramafic bodies (88770036, 037, 041) ranging from 5 to 600 m across form prominent conical hills in the western half of the intrusion. The smaller bodies have subcircular to elongated outcrop patterns, whereas the larger intrusions have more irregular patterns due to post-emplacement faulting. Uplifted fault-bounded blocks of basement aplitic microgranite locally abut the larger ultramafic bodies. Massive lherzolite, wehrlite, and harzburgite are the major rock types, and pyroxenite flanks the northeastern and southern margins of the largest body on the northern side of the intrusion (see appended map sheet). The serpentinised ultramafic cumulates contain trace (0.2 vol. %) disseminated chromite, but no chromitite layers were located. The ultramafic bodies appear to truncate the cyclic mafic units and their subrounded configurations suggest that they formed late in the evolution of the intrusion. The peridotite plugs are believed to have formed from new pulses of primitive magma that were forcibly injected upwards along the intersection of major sets of steeply-dipping faults.

Thin conformable clinopyroxenite lenses (88770014, 048) are locally associated with mafic cycles in the western half of the intrusion. They have strike lengths of up to 400 m and are probably comagmatic with the cyclic mafic sequences. A rare olivine gabbronorite (88770018) is associated with a ?clinopyroxenite lens on the northern margin of the intrusion. An unusual

Fig. 77. Geology of the Maitland Complex (simplified from appended map sheet).

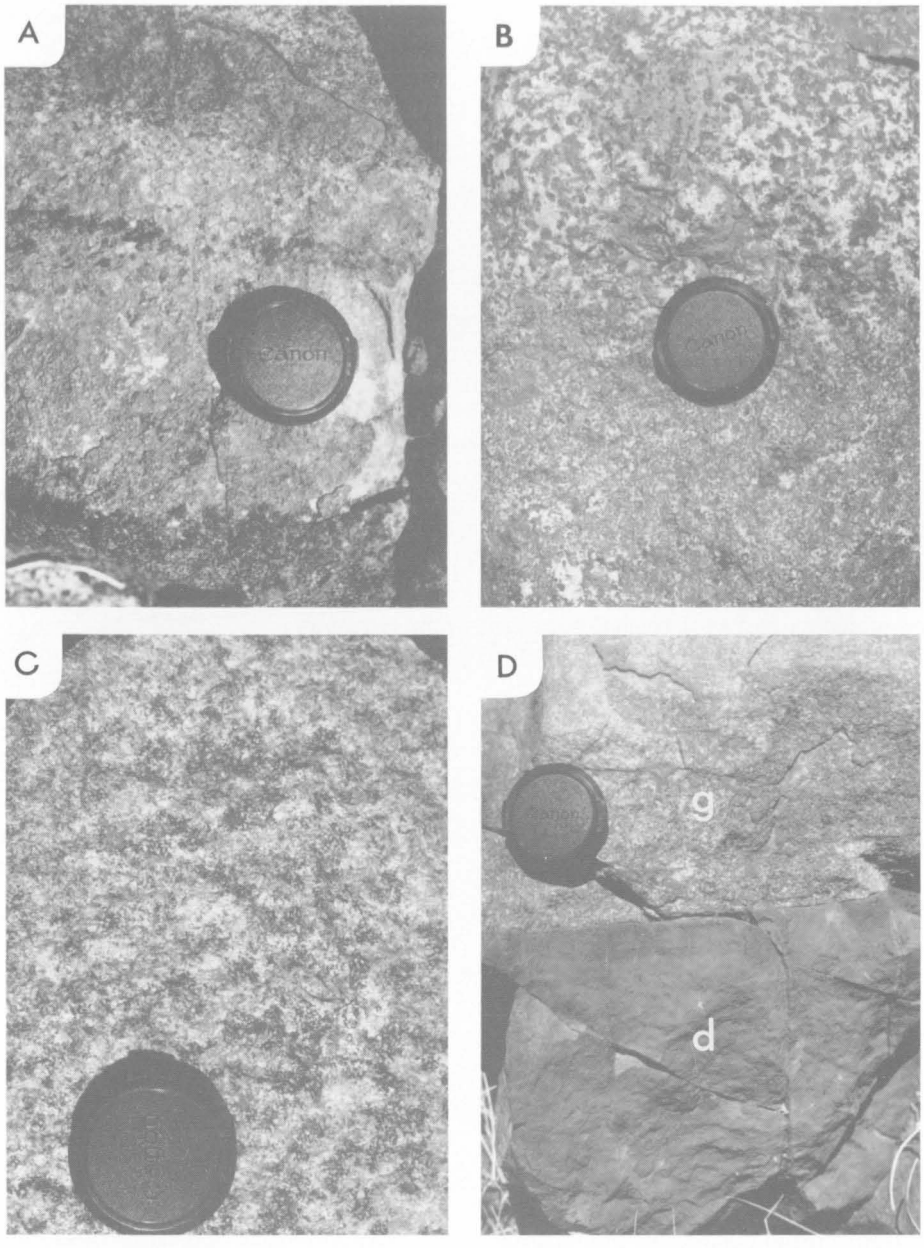

Fig. 78A–D. Maitland Complex: layering and rock types. A—Rare modal layering (clinopyroxene and plagioclase) in gabbro unit. B—Sulphide-bearing pegmatoidal phase of melagabbro unit along eastern contact of intrusion. C—Distinctive mottled texture (cumulus plagioclase and oikocrystic clinopyroxene) of anorthosite unit. D—Sharp contact between aphanitic ?Proterozoic dolerite dyke(d) and fine-grained gabbro(g).

cumulus mineral assemblage and reaction features in this orthocumulate indicate that it may be an accidental block of deep-crustal origin (see Discussion section, pp. 124–125).

Dykes of various ages and compositions intrude the Maitland Complex. The largest of these is an altered porphyritic gabbro that forms a 2.5 km ridge along the contact between a finger-like appendage of the complex and intermediate metavolcanics on the northeastern side of the complex (Fig. 77 & appended map sheet). Textures range from equigranular, to weakly porphyritic, to strongly porphyritic (euhedral plagioclase laths up to 3 x 5 mm). The dyke is probably a late intrusive phase related to the complex. Leucocratic microgranite, aplitic granite, aplite, and quartz blocks and dykes are common in the western half of the complex. The distribution of the felsic blocks and dykes coincides with the inferred subsurface distribution of granitic basement rocks beneath the intrusion. The granitic blocks are believed to be fault-bounded bodies that were uplifted into the overlying intrusive sequence along steeply-dipping faults; the dykes probably crystallised from partial melts formed by melting of the basement granites by the intrusion, which back-intruded the mafic units along fractures and faults. The felsic dykes have random orientations and short strike extents, which contrasts with the mafic dykes.

The various generations of mafic dykes are structurally controlled across the whole complex. Thin (< 1 m) postmagmatic aphanitic dolerite (Fig. 78D) and spotted metadolerite dykes generally have sharp, unchilled, contacts with the mafic cyclic units and strike trends parallel to the large northeast-trending Pinderi Hills Dyke on the northwestern side of the complex. Pyroxenitic and gabbroic dykes that are possibly comagmatic with the complex pinch and swell along their northeast

and east-southeast strike trends. The dykes are thickest, about 8 m, in the central part of the intrusion, and were interpreted by de Angelis & others (1987) as possible thermally metamorphosed feeders to the complex. Their thickness is exaggerated in Figure 77.

Structure

The poor develoment of layering, absence of distinctive laterally continuous stratigraphic units, and the intensity of faulting inhibits detailed structural interpretations. Younging criteria by geochemical trends are not definitive (see Geochemistry section, p. 122), so that it is very difficult to ascertain the geometry of the intrusion. The complex structure is highlighted in the southeastern quadrant of the intrusion where transposed anorthosite cycles are at a high angle to the main layering trend as a result of the combined effects of block faulting, uplift, and rotations by up to 90°. The crude concentric arrangement of cyclic units in this region suggests that the stratigraphy is not flat-lying and the overall equidimensional shape of the complex precludes a steeply-dipping attitude. The southeastern quadrant is interpreted as part of a basinal body that has shallow to moderate (20–50°) inward dips towards the centre of the intrusion. The basinal configuration on the southwestern quadrant is less pronounced owing to the disruption of the stratigraphy by faulting and the emplacement of the discordant ultramafic bodies. A major northeast-trending sinistral fault near the western side of the intrusion is believed to be the northern extension of the Munni Munni Fault (see appended map sheet). It has displaced a major east-trending pyroxenite dyke, the largest ultramafic plug, and an abutting thick anorthosite cycle about 350 m to the southwest. The inferred configuration of the anorthosite cycle prior to its sinistral displacement is a symmetrical U-shaped unit in the northern half of the intrusion. This feature and the basinal structure to the south may reflect an irregular magma-chamber floor that comprised contiguous sub-basins separated by a thin east-trending basement ridge. Alternatively, the different structural configurations may be due to interference patterns during folding.

The ?multichambered basinal body is believed to have behaved brittly after emplacement. This was facilitated by the thin sheet-like nature of the intrusion, which in turn assisted the upward movement of migrating felsic, mafic, and ultramafic magmas that formed the plugs and dykes. The dominant dip-slip displacements along the steeply-dipping faults and the upward emplacement of granite blocks and plugs indicate that vertical tectonic processes played an important role in the evolution of the Maitland Complex. This vertical movement was more pronouced than that seen in the other Pilbara intrusions investigated in this study.

Petrography

The cyclic mafic units of the Maitland Complex range in composition from melagabbro and gabbronorite, through leucogabbro and leucogabbronorite, to anorthositic gabbro and anorthosite. They are dominated by cumulus plagioclase and clinopyroxene assemblages, whereas orthopyroxene-rich gabbronorite and norite have a restricted distribution in the central part of the intrusion. The mafic units differ from the gabbroic zone cumulates of the Munni Munni Complex in their cyclic nature, absence of inverted pigeonite and apatite, lower titanomagnetite and biotite contents, and less pronounced exsolution in pyroxene and Fe-Ti oxides. Relative to the Munni Munni Complex, these features collectively reflect a more open system of steady-state magma replenishment for the upper parts of the chamber which inhibited protracted fractional crystallisation.

Melagabbro, melagabbronorite, leucogabbro, leucogabbronorite (plag ± cpx)

Intensely uralitised quartz-bearing gabbros and gabbronorites containing various amounts of cumulus plagioclase and clinopyroxene characterise the mafic rocks along the eastern margin of the intrusion. Clinopyroxene is altered to dark-green hornblende, pale-green actinolite, Mg-rich chlorite, and interstitial quartz, and plagioclase is totally sericitised and kaolinised. Cumulus textures are generally preserved, but in places foliated hornblende-quartz-plagioclase rocks are prominent owing to increased deformation and volatile activity along the contact. In these rocks, hornblende and quartz display deformational twins and undulose extinction, respectively. The intensity of alteration and the hornblende-quartz component of the alteration assemblage decreases away from the contact towards the centre of the intrusion.

The distinctive sulphide-bearing quartz melagabbroic unit along the eastern margin of the intrusion consists of hornblende (60 vol. %), plagioclase (15%), ?microcline (10%), quartz (10%), titanomagnetite (5%), and trace sulphides and biotite. The melagabbro varies markedly in grainsize (0.5--5 mm) and contains irregular swirling pegmatoidal patches of coarse-grained twinned hornblende plates that are commonly 'sieved' with small quartz inclusions, sericitised plagioclase and ?microcline subhedra, and strained-quartz anhedra. Pyrite and rarer chalcopyrite form small disseminated anhedra and remobilised veinlets in the silicates and oxides. Disseminated titanomagnetite aggregates (0.5 mm) containing subgrains and exsolved lamellae of ilmenite are fragmented and often spatially close to hornblende.

Gabbroic rocks distant to the margins of the intrusion form equigranular medium-grained (2–3 mm) cumulates. Cumulus plagioclase and clinopyroxene, which may be cumulus or intercumulus, are associated with minor orthopyroxene, quartz, biotite, alkali feldspar, magnetite, ilmenite, pyrite, and chalcopyrite. Uralitisation, chloritisation, and saussuritisation are widespread and pervasive, resulting in assemblages of actinolite-tremolite, hornblende, ?anthophyllite, Mg and Fe-rich chlorites, calcite, dolomite, epidote, rutile, and clinozoisite. Mesocumulates and adcumulates appear prominent, although the alteration products have largely masked the cumulus-intercumulus relationships of the minerals and it is difficult to estimate the volume of the residual melt components of the cumulates. Disseminated primary sulphide anhedra and remobilised sulphide veinlets occur in all cumulates, indicating that the rocks formed from S-saturated parent magmas.

Anorthosite, anorthositic gabbro (plag)

The most plagioclase-rich cumulates in the Maitland Complex are fine- to coarse-grained (0.5–4 mm) mottled anorthosites and anorthositic gabbros that consist of blocky cumulus plagioclase grains (70–95 vol. %) and large clinopyroxene oikocrysts (5–25%). Accessory minerals include late-crystallising strained quartz, chloritised biotite, titanomagnetite, rutile, pyrite, and chalcopyrite. The mottled textures are defined by clusters of uralitised clinopyroxene anhedra enclosing subhedral plagioclase, titanomagnetite, and rare quartz

inclusions. Clinopyroxene is altered to fine prismatic clinoamphibole, which was subsequently partly replaced by granular aggregates of Mg-bearing chlorite, clinozoisite, and epidote. Plagioclase has a range of calcic compositions from andesine (An_{45}) to labradorite (An_{62}).

Norite (plag + opx ± cpx)

Medium-grained (1–2 mm) orthopyroxene-rich cumulates are characterised by their well-developed laminated fabrics, low porosities, and paucity of alteration. Norite and orthopyroxene-rich gabbronorite adcumulates consist of cumulus plagioclase (60–70 vol. %) and orthopyroxene (10–40%), intercumulus clinopyroxene (0–30%), and trace magnetite, pyrite, and chalcopyrite. In the clinopyroxene-rich variants, clinopyroxene grains strongly modified by adcumulus growth may have originally been of cumulus status. This is supported by these grains having exsolved Fe-rich pyroxene material along {100} cleavages. The lamination is defined by the crystallographic alignment of euhedral plagioclase laths (An_{57-64}) and subhedral orthopyroxene grains which display fine exsolved Ca-rich clinopyroxene lamellae parallel to {100}. There is no evidence of deformation and it is believed the lamination may be due to flowage differentiation in the central part of the intrusion.

Olivine gabbronorite (opx + ol)

The olivine gabbronorite accidental block on the northern side of the complex is the only known occurrence of coexisting olivine and plagioclase in the complex. The weakly altered coarse (2–4 mm) orthocumulate consists of cumulus orthopyroxene (55 vol. %) and olivine (5%), and intercumulus plagioclase (30%) and clinopyroxene (10%). Olivine forms 1–2 mm subrounded grains rimmed by pyroxene-spinel reaction coronas where they abut plagioclase (An_{62}), but not pyroxene. Each corona consists of a partly resorbed olivine grain surrounded by a thin continuous halo of orthopyroxene that abruptly passes into an outer halo of pale-green diopside, which in turn merges into an outer radiating fringe of diopside and extremely fine-grained vermicular spinel. Similar concentric arrangements of reaction products have been widely documented in metagabbroic and similar rocks from New Zealand (Price & Wallace, 1976), Scotland (Mongkoltip & Ashworth, 1983), Norway (Griffin & others, 1985; Ashworth, 1986), and Australia (Ballhaus & Berry, 1991).

Peridotite (ol ± cpx ± opx ± chrom)

Peridotites comprising the discordant ultramafic pluglike intrusions range in composition from intensely serpentinised wehrlite, lherzolite, and orthopyroxene-rich lherzolite, to rare harzburgite. The coarse lherzolite and wehrlite cumulates consist of 2 to 4 mm equigranular cumulus olivine grains (50–90 vol. %), 2 to 3 mm cumulus or intercumulus clinopyroxene subhedra (5–30%), minor intercumulus orthopyroxene (0–2%), and trace disseminated cumulus chromite (0–0.2%). Orthopyroxene (0–20%) is a minor cumulus phase in the more orthopyroxene-rich lherzolites and harzburgites. Dark-brown to opaque chromite subhedra (0.1–0.2 mm) are rimmed by magnetite, and occur between, and within, olivine and clinopyroxene grains. One harzburgite sample (88770037) contained a rare sodic (~ An_{20}) plagioclase anhedron that may be a metasomatised xenocryst derived from the surrounding gabbroic units. If this is true, its presence suggests that the ultramafic intrusions postdate the cyclic mafic sequences.

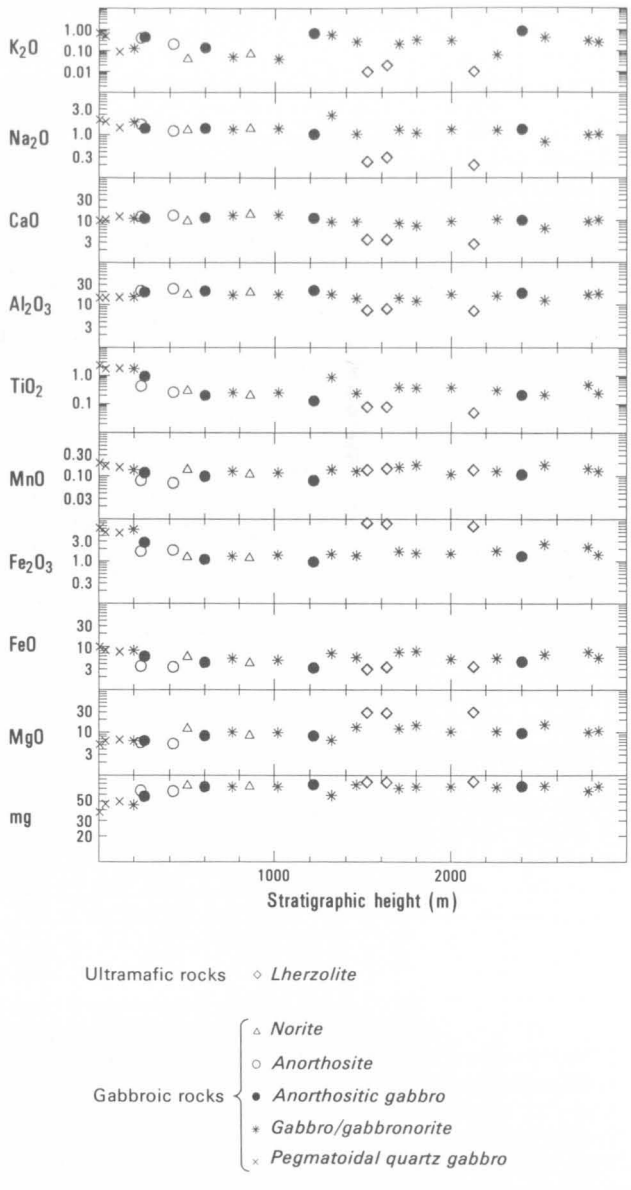

Fig. 79. Maitland Complex: variations in whole-rock major-element compositions (weight %) with stratigraphic height. 'Stratigraphic height' is apparent height.

Thick, curved trains of secondary magnetite traverse the totally serpentinised olivine grains, and clinopyroxene is replaced by colourless aggregates of tremolite, which contrasts with the more common secondary minerals of actinolite and hornblende in the mafic rocks. The absence of sulphides in the ultramafic cumulates (if originally present) is attributed to the intense and pervasive nature of serpentinisation and uralitisation.

Geochemistry

Whole-rock major and trace-element analyses (see Appendix 3) were carried out on 50 surface samples (88770001–050), of which 47 samples were obtained along two east-west traverses, A and B, that extend across the whole intrusion (traverses and sample locations are shown on the appended map sheet). It was hoped that the gross geochemical trends along the trav-

Table 23. Precious-metal and trace-element geochemistry of the Maitland Complex

Sample number	*Apparent height (m)*	*Lithology*	*Pt (ppb)*	*Pd (ppb)*	*Ir (ppb)*	*Ru (ppb)*	*Au (ppb)*	*Cu (ppm)*	*Ni (ppm)*	*S (ppm)*	*Pt/Pd*	$\frac{(Pt + Pd) \times 10^6}{S}$	$\frac{Cu \times 10^3}{(Cu + Ni)}$
0021	5	Quartz gabbro	4.25	2.63	0.06	0.06	3.47	129	8	3338	1.62	2.06	942
0023	120	Quartz gabbro	2.05	1.54	0.01	0.09	1.57	166	110	1665	1.33	2.16	601
0024	200	Gabbro	4.71	1.20	0.01	0.03	6.22	248	91	2400	3.93	2.46	732
0026	260	Anorth gabbro	3.36	5.93	0.05	0.52	0.51	23	77	791	0.57	11.74	230
0027	420	Anorthosite	2.47	1.89	0.06	0.53	0.43	28	167	432	1.31	10.09	144
0028	500	Norite	7.51	3.37	0.12	0.18	1.31	38	119	239	2.23	45.52	242
0030	760	Gabbronorite	3.66	2.04	0.01	0.17	1.10	216	152	1422	1.79	4.01	587
0032	1020	Gabbronorite	2.17	1.77	0.02	0.23	0.69	180	108	488	1.23	6.84	625
0034	1320	Gabbro	2.61	2.77	0.02	0.58	0.67	78	104	1029	0.94	5.23	428
0037*	1630	Lherzolite	9.01	14.59	0.34	1.05	0.61	2	1262	156	0.62	151.28	2
0038	1700	Gabbro	5.07	4.20	0.04	0.17	1.01	99	250	518	1.21	17.90	284
0040	2000	Gabbro	0.64	0.50	0.01	0.32	0.61	43	243	339	1.28	3.36	174
0042	2260	Gabbro	2.88	4.31	0.07	0.48	1.31	104	217	453	0.67	15.87	324
0043	2400	Anorth gabbro	6.07	7.72	0.01	0.16	1.43	93	255	144	0.79	95.76	273

Sample numbers are prefixed by AGSO reference numbers 8877. Anorth = anorthositic, * = intensely serpentinised sample. Analytical techniques for the precious metals (analyses by S. Reeves, School of Earth Sciences, University of Melbourne) involved a fire-assay nickel preconcentration (25 g charge) followed by instrumental neutron-activation analysis (Pt, Pd, Ir, Ru, Au). The other elements were determined at the AGSO by AAS (Cu, Ni) and XRFS (S).

erses would assist in the interpretation of the geometry of the intrusion, and provide an insight into its PGE potential. The geochemical-variation-versus-stratigraphic-height plots (Figs 79–82) for the Maitland Complex are from traverse B (samples 021–047) and they look toward the south. The 2840 m stratigraphic interval shown is an apparent height and not a true stratigraphic height. Rock types analysed from traverse B range in composition from quartz gabbro at the basal contact, to norite, gabbro, and anorthosite in the layered mafic sequence, to lherzolite in the discordant ultramafic intrusions. Platinum-group-element (Pt, Pd, Ir, Ru) and Au determinations were carried out at regular intervals through the layered mafic sequence (Table 23).

Major elements

The distribution of major elements (Fig. 79) in the mafic cumulates of the Maitland Complex is largely controlled by the dominant early-crystallising plagioclase and clinopyroxene, but it is evident that serpentinisation, uralitisation, and weathering have played important roles. Pegmatoidal quartz gabbros along the eastern basal contact are the most fractionated rocks in the intrusion, with $mg_{50.2-37.6}$ and TiO_2 contents up to 2.32%, whereas most gabbros, anorthosites, anorthositic gabbros, and norites, which form the bulk of the intrusion, have more primitive compositions, of $mg_{77.0-65.0}$ and TiO_2 contents less than 0.90%. The fractionated compositions persist up to the 200 m level, and indicate that contamination and hybridisation were extensive along the basal contact of the intrusion. The fairly flat major-element fractionation trends for the overlying mafic cumulates contrast with the gently sloping fractionation trends seen in the mafic sequences of the other west Pilbara layered intrusions. There is a suggestion that TiO_2, K_2O, and Na_2O may have weak cyclic distributions in the middle and upper parts of the intrusion, although the crude sawtooth patterns of the more mobile elements K_2O and Na_2O may reflect variable intensities of sericitisation and uralitisation alteration in mafic rocks containing different proportions of minerals. With the exception of lower Na_2O contents due to alteration, the major-element chemistry of the mafic cumulates is generally similar to that of the gabbroic units of the other west Pilbara intrusions.

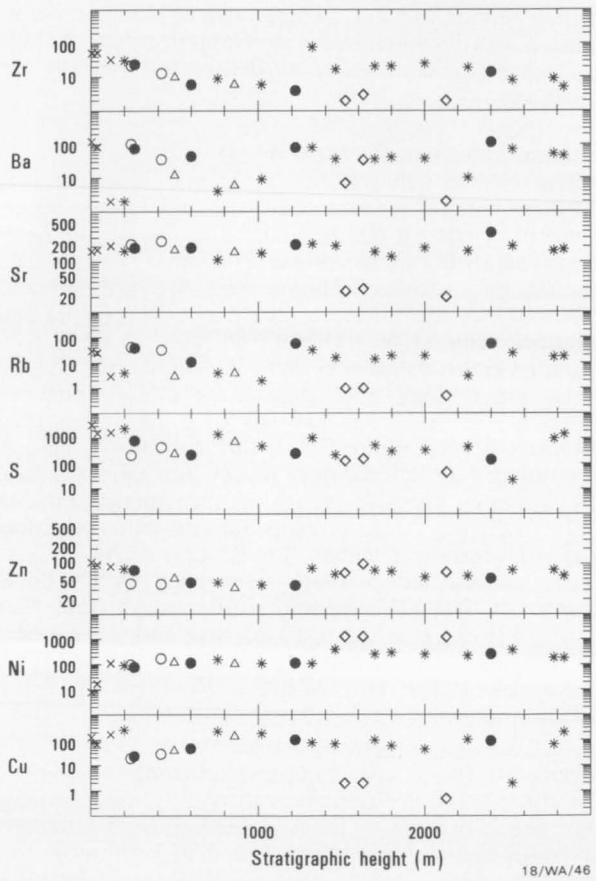

Fig. 80. Maitland Complex: variations in whole-rock trace-element compositions (ppm) with stratigraphic height. Symbols as in Figure 79. 'Stratigraphic height' is apparent height.

Lherzolite and harzburgite ($mg_{84.8-83.0}$) in the discordant plug-like intrusions are extensively oxidised (e.g. high $Fe^{3+}/(Fe^{3+} + Fe^{2+})$ ratios of ~ 0.70 and loss on ignition values of ~ 10%) relative to the mafic cumulates. The major-element chemistry of the peridotites reflects the dominance of secondary assemblages of serpentine, magnetite, chlorite, and clinoamphibole.

The absence of marked systematic variations in ma-

jor elements up the mafic stratigraphy of the Maitland Complex reflects the open system of periodic magma replenishment into the chamber, the fairly shallow-dipping attitude of the intrusion, and the intense alteration of the cumulates.

Trace elements

The variations in Cu, Ni, Zn, S, Rb, Sr, Ba, Zr, Cr, Co, V, Ga, La, Nd, Sc, and Y abundances with stratigraphic height are summarised in Figures 80 & 81. Many of the trace elements have erratic regional trends that indicate varying degrees of secondary mobility during alteration and weathering. Elements that show systematic abundance trends with height for the mafic units include Zr, Zn, La, Y, Ni, and Ga. The first four elements show sympathetic trends of steadily decreasing concentrations up the sequence, but at the 1320 m level there is an abrupt change to higher concentrations, which subsequently decrease again with increasing height. The 1320 m level represents a major geochemical (but not lithological) break in the evolution of the mafic sequences. Nickel displays flat fractionation trends with a minor increase in concentrations at the 1460 m level, and Ga consistently decreases up the sequence. The persistent high Sr and Sc concentrations testify to the plagioclase- and clinopyroxene-rich compositions of the mafic cumulates.

The basal gabbros have the highest S (up to 3340 ppm), Cu (248 ppm), and V (770 ppm) contents in the intrusion, which reflects the mutual association of sulphides and titanomagnetite in these rocks. The high, but variable (due to secondary mobilisation) S contents

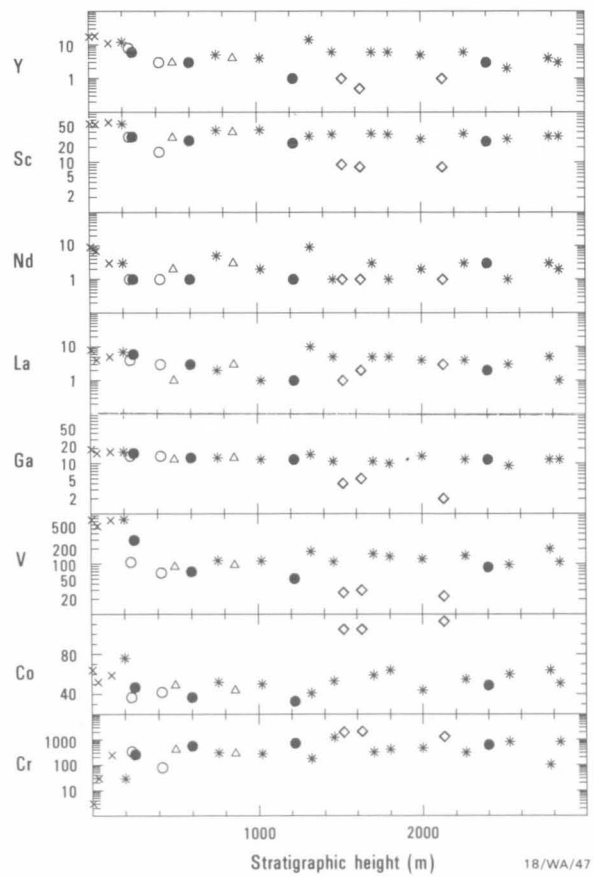

Fig. 81. Maitland Complex: variations in whole-rock trace-element compositions (ppm) with stratigraphic height. Symbols as in Figure 79. 'Stratigraphic height' is apparent height.

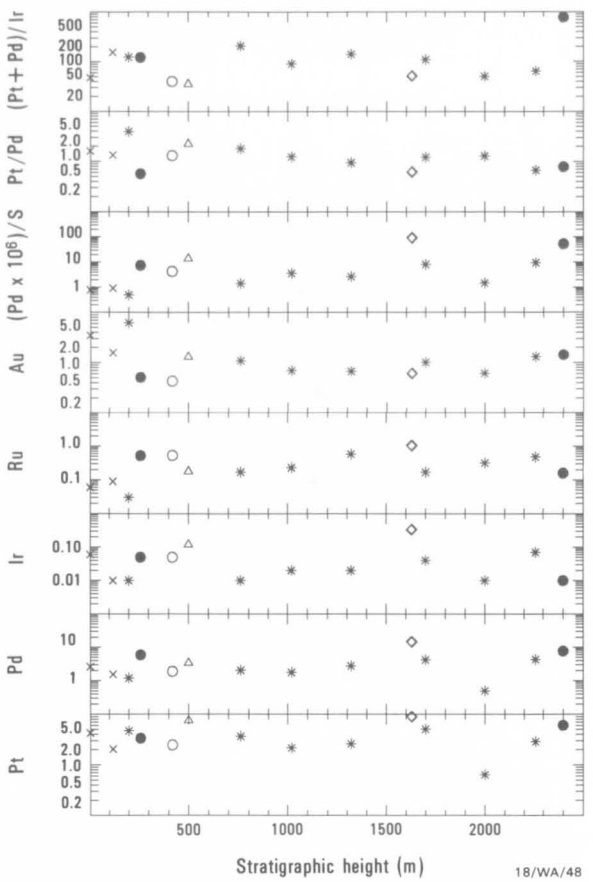

Fig. 82. Maitland Complex: variations in Pt, Pd, Ir, Ru, Au (ppb), Pd/S, Pt/Pd, (Pt + Pd)/Ir with stratigraphic height. Symbols as in Figure 79. 'Stratigraphic height' is apparent height.

(210–1490 ppm) of the overlying mafic cumulates indicate that S-saturated conditions prevailed throughout the intrusion. Consequently, Cu and Ni show no evidence of increasing concentrations up the sequence by crystal fractionation. As expected, the peridotites (Figs 80 & 81) are enriched in the compatible elements Cr (up to 2090 ppm), Co (105 ppm), and Ni (1265 ppm) and depleted in most other trace elements relative to the mafic cumulates.

Platinum, palladium, iridium, ruthenium, gold. Low precious-metal concentrations (Table 23; Fig. 82) characterise the mafic and ultramafic cumulates of the Maitland Complex. Gabbroic cumulates contain precious-metal concentrations (0.64–7.51 ppb Pt, 0.50–7.72 ppb Pd, 0.01–0.12 ppb Ir, 0.03–0.58 ppb Ru, 0.43–6.22 ppb Au) that are typical of the S-saturated mafic rocks of the west Pilbara layered intrusions. Maximum Pt (9.01 ppb), Pd (14.59 ppb), Ir (0.34 ppb), and Ru (1.05 ppb) concentrations occur in lherzolite, and the basal gabbros are weakly enriched in Au (up to 6.22 ppb) relative to the overlying cumulates. The precious metals are not enriched up the sequence and the variable Pt/Pd ratios (0.57–3.93) may reflect some decoupling of Pt and Pd during the different types of alteration in the mafic and ultramafic cumulates. The low (Pd x 10^6)/S ratios of less than 10 (Fig. 82) for most of the mafic cumulates indicate that S-saturation prevailed throughout the intrusion. The ternary diagrams of Figure 83 show the dominance of Pt and Pd relative to Ir, Ru, and Au.

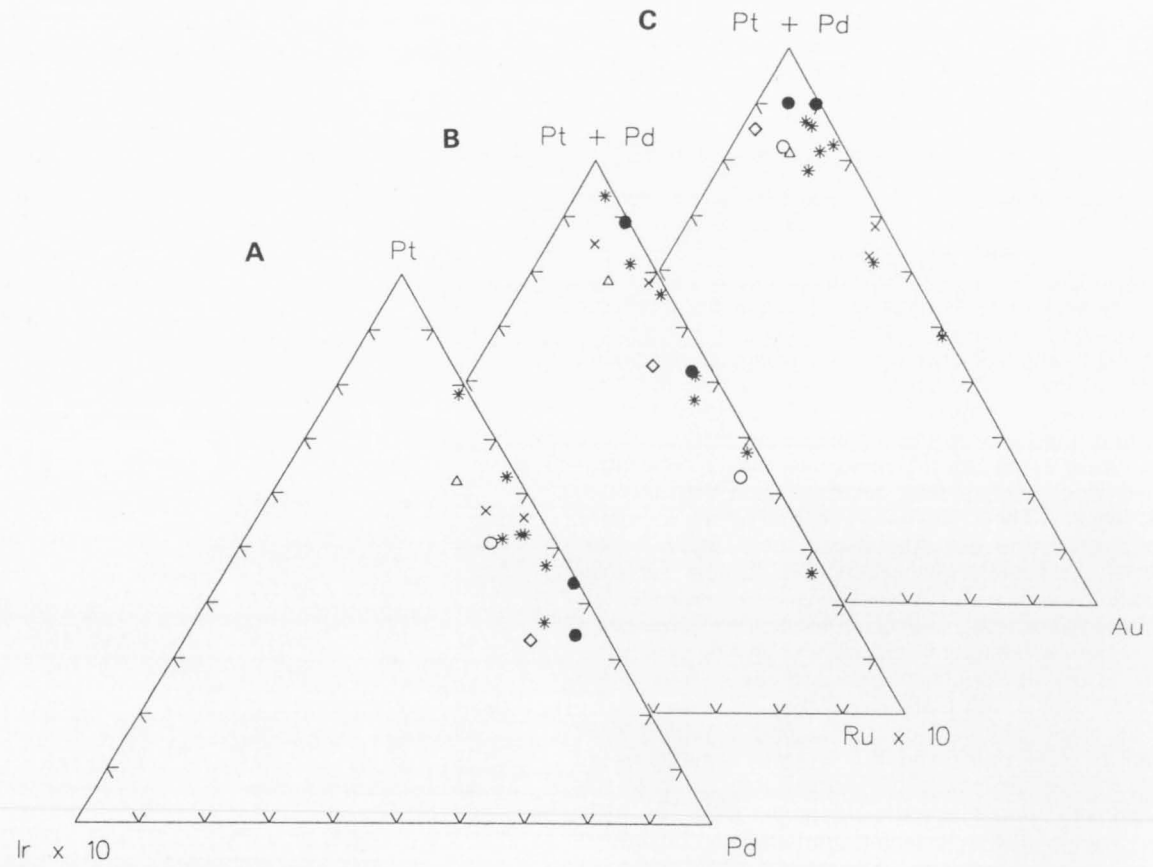

Fig. 83A–C. Maitland Complex: ternary plots showing variations in whole-rock precious-metal contents (ppb). Symbols as in Figure 79.

Discussion

The Maitland Complex contrasts with the other layered mafic-ultramafic intrusions of the west Pilbara Block in several ways. These include the high ratio of mafic to ultramafic cumulates, the widespread occurrence of anorthosite, the cyclic distribution and shallow-dipping attitude of the mafic cumulates, the presence of discordant plug-like ultramafic intrusions, and the apparent absence of significant precious- and base-metal mineralisation. However, the similar mineralogical and geochemical features indicate that the Maitland Complex is most likely related to the other west Pilbara layered intrusions. This is also supported by its regional setting near the other intrusions, and its preferential emplacement along a major lithological contact, a common feature of all the west Pilbara intrusions investigated.

It is postulated that the magmas that formed the Maitland Complex were emplaced into a small subchamber at a zone of discontinuity in the upper crust (probably at higher levels than the other west Pilbara intrusions). The mafic cumulates of the Maitland Complex have more primitive compositions ($mg_{77.0-65.0}$) than the gabbroic zone cumulates of the Munni Munni ($mg_{65.0-31.0}$) and Radio Hill ($mg_{67.5-31.9}$) complexes. They correlate more closely in composition with the S-saturated plagioclase-bearing pyroxenites ($mg_{76.9-63.5}$) near the top of the Munni Munni Complex ultramafic zone and the S-saturated cyclic anorthositic units ($mg_{78.8-72.9}$) in the ultramafic zone of the Andover Complex. It is believed the Maitland mafic magmas were either tapped directly from the Munni Munni Complex chamber, or from a deeper common magma chamber at a similar time when the more fractionated magmas were being emplaced into the upper levels of the Munni Munni Complex ultramafic zone. In contrast to the Munni Munni Complex, the magmas were S-saturated before they were emplaced into the sub-chamber. This early evolution of S-saturation resulted in a mafic sequence depleted in PGEs, and the cyclic emplacement of the magma pulses would have inhibited the possible formation of a PGE-enriched layer by crystal fractionation. The Maitland Complex is therefore believed to have limited potential for hosting a PGE-enriched layer similar to that seen in the nearby Munni Munni Complex. In addition, the absence of a thick olivine-rich cumulate sequence associated with the mafic cumulates (e.g. as seen at the Radio Hill and Mount Sholl intrusions) significantly decreases the likelihood of basal segregations of Ni-Cu sulphides.

The olivine gabbronorite accidental block on the northern side of the intrusion, which contains distinctive corona textures, is obviously of different origin to the enclosing layered mafic cumulates. Corona textures between two minerals are a common feature of high-grade metamorphic rocks, and form in response to changing pressure, temperature, and activities of volatile components. The orthopyroxene-clinopyroxene-spinel coronas in the olivine gabbronorite are believed to reflect the following subsolidus reaction between olivine and plagioclase at high-pressure and decreasing temperature:

$2Mg_2SiO_4$ (olivine) + $CaAl_2Si_2O_8$ (plagioclase) → $2MgSiO_3$ (enstatite) + $CaMgSi_2O_6$ (diopside) + $MgAl_2O_4$ (spinel)

The pressure-temperature conditions at which this reaction is initiated range from 11 kb at 1150°C for

olivine gabbros (Price & Wallace, 1976), to 10–11 kb at 900–950°C for anorthositic gabbros (Griffin & others, 1985), to 6.2 kb at 700–825°C for gabbros (Ballhaus & Berry, 1991). These pressures imply middle to lower crustal depths of 22 to 40 km, which are difficult to reconcile with the upper crustal (pressure of ~ 3.5 to 5 kb at 1100°C; see pp. 159–161) emplacement of the nearby and ?related Munni Munni Complex. The cumulus and replacement textures in the olivine gabbronorite orthocumulate suggest that it formed in a high-pressure magma chamber in the lower parts of the crust. It is postulated that the accidental block was uplifted to the upper crust (mechanism unknown) where it was detached some time later from the country rocks by the invading mafic magma that formed the Maitland Complex. The large size of the accidental block precludes the ascending mafic magma from directly transporting the block upwards for any significant distance from the lower crust. The accidental origin of the olivine gabbronorite is also supported by its orthopyroxene-rich character and it is the only known cumulate in the intrusion containing coexisting plagioclase and olivine. Corona textures between olivine and plagioclase are absent from the mafic cumulates of the nearby Radio Hill Complex, since these minerals experienced no significant changes in pressure and/or temperature during their '*in situ* crystallisation' in the upper crust.

FIELD RELATIONSHIPS, PETROGRAPHY, MINERALOGY, AND GEOCHEMISTRY OF THE ANDOVER COMPLEX *(DAW)*

Introduction

The Andover Complex (Figs 84, 85) is 3 km south of Roebourne, at latitude 20°50′S and longitude 117°10′E, on the Roebourne 1 : 100 000 Topographic Sheet 2356 and Roebourne 1 : 250 000 Geological Sheet SF/50-3. It has a similar geological setting to the Munni Munni Complex, but has some significant mineralogical differences.

The complex, with an outcrop extending over an area of 7 by 20 km, is one of the largest mafic-ultramafic intrusions in the west Pilbara Block (Fig. 4). It is broadly similar to the other Pilbara intrusions and major overseas stratiform complexes, such as the Bushveld Complex (South Africa) and Stillwater Complex (USA). Because of this, and particularly in light of the promising exploration results from the nearby Munni Munni Complex, exploration interest has recently focused on the Cu, Ni and precious metal potential of the complex.

The Roebourne district has a long history of mining, mainly for Cu and Au, dating from the 1870s. Numerous reports issued by the Western Australia Geological Survey cover this. Maitland (1909) presented the first reasonably accurate geological map of the Roebourne area, in which the Andover Complex is distinguished as a coherent mafic-ultramafic mass. He described the Andover Complex as consisting of serpentinite, gabbro, and dolerite, intruded by greenstone dykes.

The complex was first mapped systematically by Ryan & others in 1962–63, and is included in the Roebourne 1 : 250 000 Geological Series Sheet SF/50-3, published in 1965 by the Geological Survey of Western Australia (Ryan, 1966). The complex was subsequently remapped in 1976 by Archer as part of the Roebourne 1 : 50 000 Urban Geology Series Sheet 2356 III special map, issued by the Western Australia Geological Survey (Archer, 1979).

The 1960s mapping confirmed that the complex was a layered mafic-ultramafic intrusive of Archaean age. Hickman (1983) described the complex as consisting of sheets of dunite, peridotite, pyroxenite, gabbro, and minor anorthosite, with a total estimated thickness of 2 km. It was also believed that these units had a general rhythmic lithostratigraphy, which conformed to a typical layered-complex magmatic differentiation trend. Individual cycles were estimated as approximately 100 to 200 m thick.

Mining

The mineral potential of the Roebourne area was first recognised in 1872 when Cu and Pb were discovered, followed by rich Au-bearing quartz reefs in 1877 (Woodward, 1890, 1911). The apparent potential of the area, however, was not realised: no other significant mineral discoveries were subsequently made near Roebourne. Mining declined after the early 1900s, but there was a short-lived revival in the 1960s. Although the Carlow Castle Cu-Au mine is less than 2 km from the Andover Complex, and the Goodluck and Fortune Cu-Au mines are in gabbros at the northern margin of the complex, there appears to be no unequivocal genetic linkage between Cu-Au mineralisation and the complex (Marston, 1979). Further along the margin of the complex to the east (2 km south of Roebourne), scattered

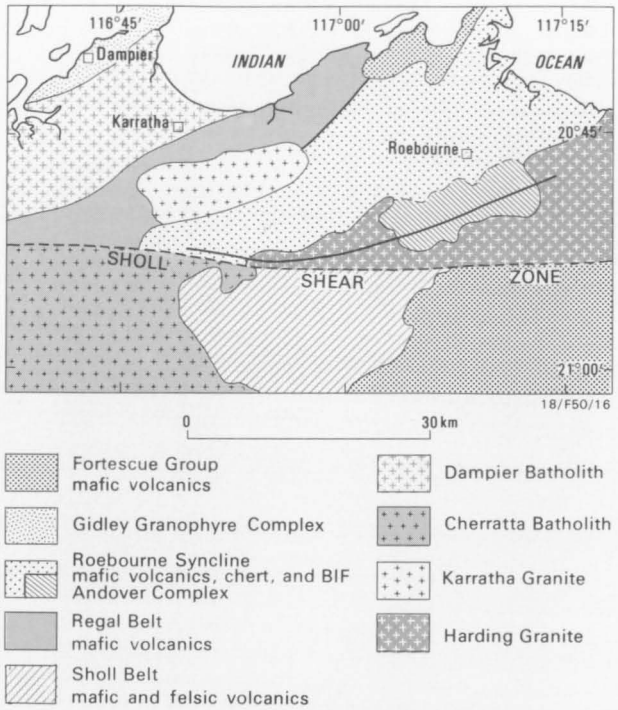

Fig. 84. Major structural units of the Roebourne–Karratha region. Structural units after Hickman (1983).

corundum rubble on the alluvial flat adjacent to serpentinite of the complex indicates that a corundum deposit underlies the alluvium. This was investigated by Greater Pacific Investments in 1986–87, but the deposit was found to be uneconomic.

Lead mining in the Roebourne area was confined to the Andover mine, in a small lode close to the southern margin of the Andover Complex, 4 km north of Woodbrook. The lode, which also yielded Zn and Ag, occurred as a galena-rich quartz pegmatite vein at an intrusive contact between granite and metavolcanics.

Within the Andover Complex, chrysotile asbestos and Cr-bearing beryl have been mined. Chrysotile occurs pervasively as veinlets, and more rarely, as seams up to 1 m thick throughout serpentinite in the eastern part of the complex. Some of these larger seams were mined on a small scale, producing less than 5 t of asbestos. A total of 106 t of beryl was mined during the 1960s from several localities in the northeastern part of the complex. The beryl occurred as both disseminations and massive crystals, intimately associated with albite and quartz, within some of the numerous pegmatite veins which intrude highly sheared serpentinite in the area. No gem-quality beryl was recorded. Small quantities of tantalite, tantalite-columbite, and cassiterite were also obtained from alluvium derived from these pegmatites, which also contain minor quantities of Li-rich minerals, notably zinnwaldite, spodumene, and lepidolite mica.

Massive, vanadiferous titanomagnetite deposits at the western end of the complex constitute an estimated resource of 3 Mt averaging 0.92% V_2O_5 (Connolly, 1959). Seventeen vanadium-bearing titaniferous magnetite lenses, up to 200 m long and 2 to 5 m thick, occur in a saussuritised metagabbro that contains both

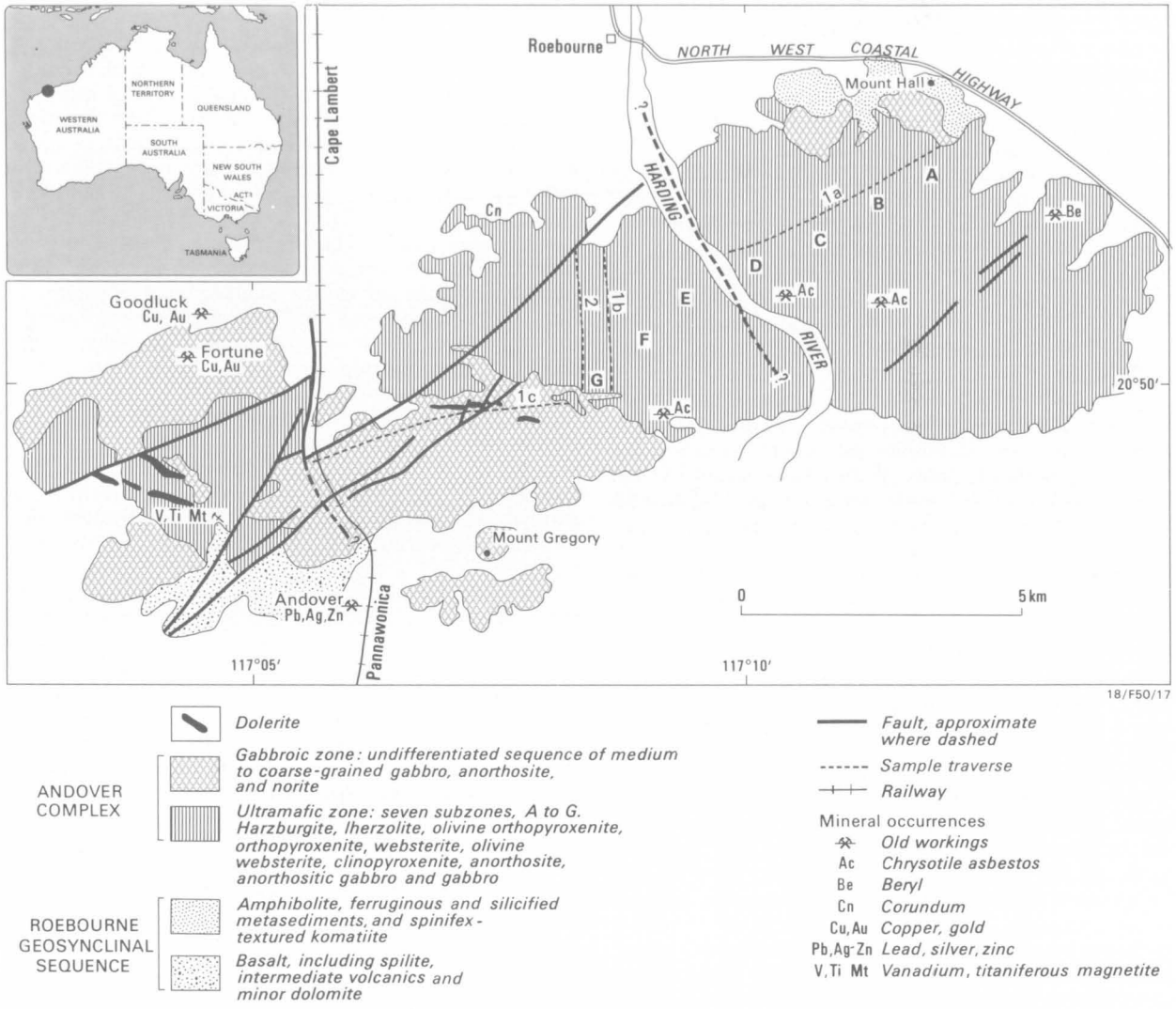

Fig. 85. Andover Complex: geology and mineral occurrences. Sample traverses are indicated by fine broken lines and approximate widths of subzones by the letters A to G.

cumulus and intercumulus magnetite, feldspar, ilmenite, sphene, and pyrite. The metagabbro is intruded by a younger gabbro containing no magnetite and the whole succession is intruded by aplite veins (Baxter, 1978). Iron, Ti, and V are potentially recoverable from the deposit, but the low tonnages and discontinuous nature of the magnetite make the deposit subeconomic.

Regional setting

The Andover Complex occupies part of the Roebourne Syncline (Fig. 84) which Hickman (1983) defined as a major structural unit in the west Pilbara, comprising a triangular geosynclinal block extending south from the coast to the Sholl Shear Zone. The Andover Complex is the only mafic-ultramafic intrusion investigated in this study which is north of the Sholl Shear Zone. The other intrusions are concentrated near the eastern margin of the Cherratta Batholith, south of the Sholl Shear Zone.

Ryan & Kriewaldt (1963) interpreted the structure of the area now identified as the Roebourne Syncline, as folded east-to-northeast-trending strata (which they called Roebourne Group), lying between, and partly incorporated into, two broad granitic domes. From the coast south to the Sholl Shear Zone the structure consists of tight synclines, and broad domes and ridges with granite cores. These synclines are segmented and displaced along a series of northwest-striking faults. The Roebourne Group units have since been included in the Pilbara Supergroup (Hickman, 1983), viz: (1) banded-iron formations are assigned to the Gorge Creek Group, and (2) amphibolite, ultramafic rocks, felsic volcanics, mafic volcanics, chert and clastic sediments to the Warrawoona Group (Table 3).

Ryan & Kriewaldt (1963) showed that the Andover Complex occupies a shallow, faulted, synform. On the Roebourne 1 : 250 000 Geological Sheet, a diagrammatic cross-section through the synform suggests, firstly, that the ultramafics were intruded along the axis of the synform, and secondly, that the Andover Complex was emplaced in two separate episodes, as shown by cross-cutting relationships with earlier intruded material. The floor of the synform consists of two lithological sequences: (a) amphibolite, and (b) a varied sequence of calc-metasediments, chert, schists, tuffs, and lavas (Towers Formation). These horizons overlie granitic basement. Further west, this synform coincides with the southernmost recognisable limit of the Ruth Well Syncline, which has been truncated by the east-trending

Sholl Shear Zone (Fig. 84). The synform and the Andover Complex were later intruded by post-tectonic granite, tonalite, gabbro, and aplite. Pre- and post-tectonic granite and tonalite crop out along the southern, eastern, and western margins of the complex. Aplite, gabbro, and dolerite extensively intrude the complex as dykes and sills, particularly in its eastern half.

According to Hickman (1983) the Ruth Well Syncline was formed during an early episode of deformation, which began about 3.5–3.45 Ga ago, during which the dominant structural elements of the region, the granitic domes and greenstone synclines, were formed. The Pb-Pb isochron age of 2960 ± 20 Ma reported by Korsch & Gulson (1986) from the 'Millindinna Complex' of the Roebourne area is consistent with the zircon age of 2925 ± 16 Ma (Arndt & others, 1991) and Sm/Nd mineral isochron age of 2927 ± 13 Ma (Sun & Hoatson, this Bulletin) for the Munni Munni Complex. Since the Andover Complex cumulates have similar initial εNd values to those of the Munni Munni Complex, and its 'chilled' rocks have similar major and trace-element characteristics (Sun & Hoatson, this Bulletin), it is most likely that the Andover Complex was emplaced into the crust at about the same time as the Munni Munni Complex. The estimated age of the Andover Complex also agrees closely with the 2.95 Ga metamorphic event recognised by Oversby (1976) as a major tectonic event within the D2 deformation episode.

The Sholl Shear Zone, a major crustal dislocation with a sinistral displacement of between 20 and 30 km in the Roebourne area, is a significant D2 fault. The Andover Complex has not been folded. The structural relationship between the Andover Complex and the folded synformal country rock metasediments, therefore, suggests either that the complex was intruded synchronously with the D2 deformation or after the deformation. In both cases a strong structural control on the intrusion is implied. The emplacement of the complex thus may be related to the precursory stress which was eventually relieved along the Sholl Shear Zone. Many examples of structurally controlled emplacement of ultramafic intrusions have been documented in the east Pilbara, e.g. peridotites in the Bamboo Creek–Pear Creek area, Mosquito Creek Synclinorium, Pilgangoora Syncline, Indee Syncline, Kangan Syncline, and Wodgina Belt (Hickman, 1983: p. 167, 168).

Structure

The Andover Complex (Fig. 85) is interpreted as a trough-shaped lopolith, with an east-northeasterly axis, roughly coinciding with the synclinal axis shown in Figure 84. The intrusion is tilted at an angle of about 10° to the southwest; locally steeper attitudes are attributed to faulting. The lowermost units crop out in the north and east of the complex and the uppermost units in the southwest. The complex has been subjected to a series of dislocations along faults of various generations. The principal fault directions are northerly and northeasterly. The north-trending faults extending to the Sholl Shear Zone have significantly displaced the geosynclinal succession and are the younger of the two sets of faults. Two of these faults intersect the complex. The larger and more westerly of these extends south from the coastline, intersecting the complex approximately along a fault coincident with the Cape Lambert–Pannawonica railway. To the east, another major north-trending fault cuts the complex along a plane coinciding with the Harding River.

Country rocks

The Roebourne Syncline sequence is exposed in the Mount Hall area on the northern margin of the Andover Complex and west of the Andover lead mine on the southern margin. In the Mount Hall area the complex cuts interbedded volcanic and sedimentary units and amphibolite. This sequence crops out over a distance of about 2.5 km between the complex and the North West Coastal Highway, as low-lying, undulating, east-trending ridges. The amphibolite abuts the complex as a narrow contact aureole, which, going away from the complex, gives way to a sequence of interbedded schist, ferruginous and silicified metasediments, thin chert, and spinifex-textured komatiitic lavas. Thin aplite stringers intrude these rocks near Mount Hall. The corundum deposit, at the margin of the complex further to the west, is also considered to be part of the contact aureole. The presence of sillimanite in the hornfels accompanying corundum suggests that the corundum was probably derived by thermal metamorphism of a silica-poor, alumina-rich argillite in the synclinal sequence during emplacement of the Andover Complex.

The komatiites are now tremolite-chlorite-antigorite rocks, in which spinifex textures are well preserved in places. The komatiites are depleted in Al (Al_2O_3/TiO_2 = 13), which is quite different from the Al-normal komatiites (Al_2O_3/TiO_2 = 27–30) of the 3.5 Ga Warrawoona volcanics. This depletion in Al, together with the spinifex textures and associated metasedimentary horizons, is characteristic of the Ruth Well sequence (Nisbet & Chinner, 1981; Sieber & others, 1990). On this basis the Mount Hall sequence is regarded as an easterly outlier of the Ruth Well geosynclinal sequence.

The Roebourne Syncline rocks north and west of the Andover mine form low-lying rubbly outcrops. These were only briefly examined but have been described by Archer (1979) as consisting mainly of altered basalts, some spilitic, together with intermediate volcanics and minor dolomitic horizons.

Tonalite crops out sparsely along the northern margin of the complex, west of Mount Hall. Tonalite, granodiorite, and leucocratic granite also crop out along the southern boundary of the complex and extend south to the Sholl Shear Zone. In places these granitoids are strongly contaminated by metasomatised xenoliths, described by Ryan (1966) as zones of hybridisation. The xenoliths are derived from a wide variety of country rocks, including the metasediments. However, incorporation of ultramafic xenoliths derived from the Andover Complex indicates that some of these granitoids post-date the complex.

Stratigraphy

The Andover Complex (Figs 85, 86A) comprises a lower ultramafic zone and an overlying gabbroic zone, and is made up of rocks typical of a differentiated ultramafic-mafic layered series (Table 24). The complex has an estimated minimum thickness of 2.1 km. The shallow dip of the layered sequence (about 10°), combined with its subdued topography, faulting and alteration, make it difficult to distinguish the various lithological units and to correlate them over appreciable distances. Thus the complex cannot be subdivided with the same degree of confidence and accuracy as has been done for the more steeply-dipping Munni Munni Complex (see appended map sheet).

Because of the gentle dip of the layering it is difficult

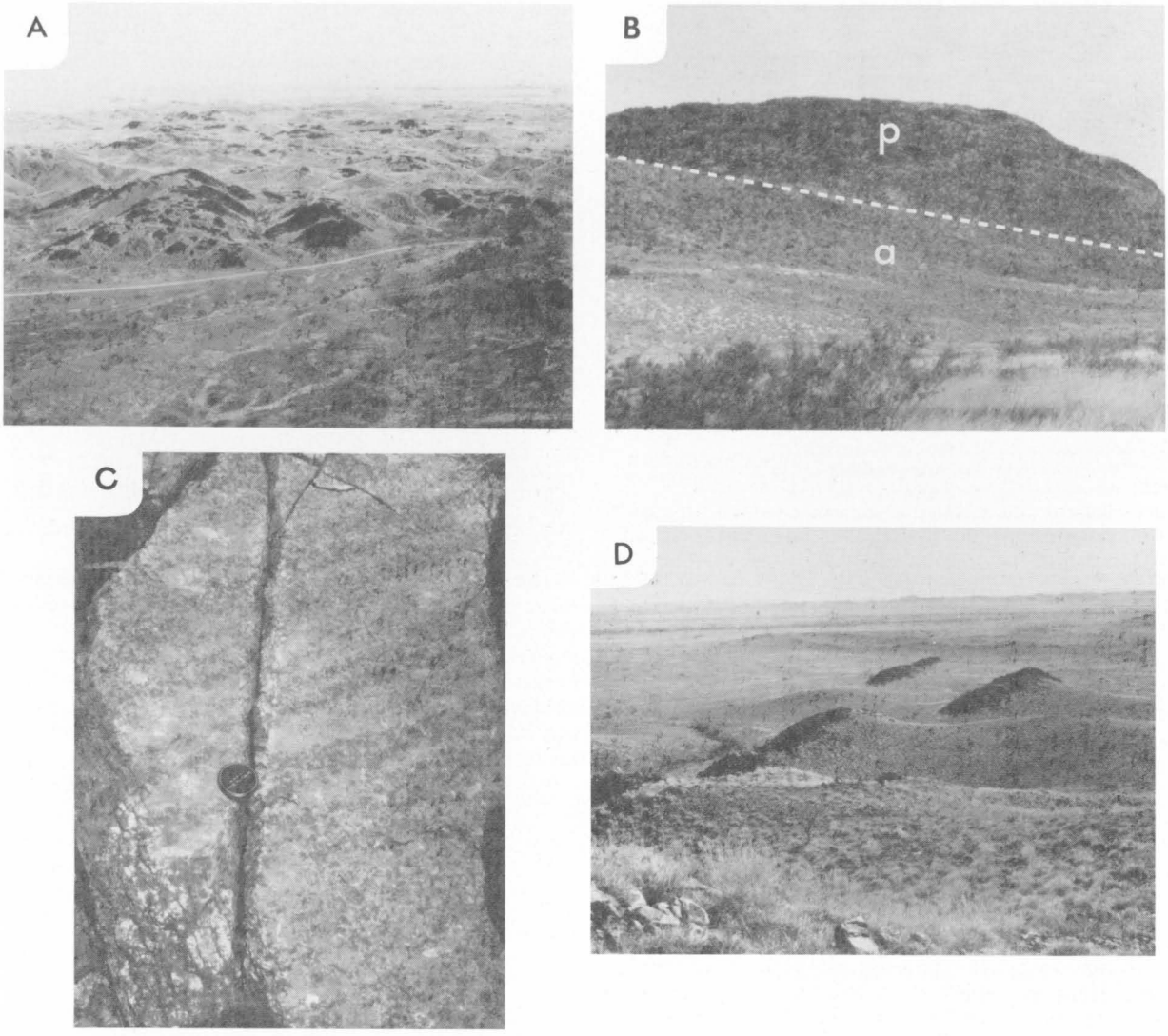

Fig. 86A–D. Andover Complex: aerial view, rock types and layering. A—Aerial view looking northwest across the gabbroic zone. Gabbroic units form low hills and granite underlies the alluvial plain in the foreground. Roebourne–Harding River Dam road runs through the centre of the Figure. B—Section from the eastern end of the ultramafic zone showing shallow-dipping basal peridotite(p) from subzone C overlying anorthosite(a) from the upper part of subzone B. C—Rare modal layering and size grading of pyroxene(dark) and feldspar(light) grains in a anorthositic gabbro from subzone C, east of the Harding River. D—?Proterozoic dolerite dykes intruding poorly-outcropping gabbroic units in the southwestern part of the complex.

to estimate how far the complex extends at depth. However, unpublished aeromagnetic data by Greater Pacific Investments Ltd showed that there are unlikely to be any major lateral sub-surface extensions.

Over 200 surface samples were collected from the complex along several semi-detailed traverses (Fig. 85). These traverses were aimed at establishing the broad lithostratigraphy (Table 24). Rock nomenclature follows the scheme for mafic-ultramafic intrusive rocks proposed by Streckeisen (1973, 1976), based on modal proportions of olivine, clinopyroxene, orthopyroxene and plagioclase.

The *ultramafic zone* consists of an estimated 1300 m-thick series of rhythmically layered horizons, consisting in whole or in part of peridotite, lherzolite, olivine websterite, clinopyroxenite, olivine orthopyroxenite, orthopyroxenite, clinopyroxenite, and websterite, together with interlayered anorthosite, anorthositic gabbro, and gabbro. On the basis of geochemical profiling of peridotites through the ultramafic zone, the ultramafic zone has been subdivided into seven subzones, A to G. In these subzones, cyclic units ranging from several centimetres to several metres in thickness can be recognised in places.

The subzones represent a series of cyclic sequences comprising harzburgite ± lherzolite, orthopyroxenite ± websterite ± clinopyroxenite, and anorthositic gabbro/anorthosite ± gabbro (Fig. 86B). Cumulus mineral trends follow a crystallisation order olivine + chromite, olivine + orthopyroxene + chromite, orthopyroxene ± chromite, orthopyroxene ± clinopyroxene, and plagioclase + clinopyroxene. Broadly, the cyclic pattern, crystallisation order, and mineralogy of the layered sequence are similar in some respects to those documented for other layered intrusions such as the Bushveld and Stillwater complexes. In contrast, the ultramafic zone of the Munni Munni Complex is characterised by cumulus-olivine-clinopyroxene-dominant mineral assemblages in the order: olivine, olivine + clinopyroxene, clinopyroxene + olivine, clinopyroxene, and clinopyroxene + orthopyroxene (Hoatson & Keays, 1989). Mafic units in the ultramafic zone display rare

Table 24. Stratigraphy of the Andover Complex

		Estimated thickness(m)
Gabbroic zone		
	Undifferentiated series of medium to coarse gabbro and anorthosite; norite at contact with ultramafic zone	800+
Ultramafic zone		
Subzone		
G	Series of peridotite horizons (Cr 0.13–0.25%) interlayered with orthopyroxenite, websterite, clinopyroxenite, olivine websterite and olivine orthopyroxenite horizons. Interfingering gabbro lenses are slivers of the gabbroic zone. Olivine orthopyroxenite and orthopyroxenite are the uppermost horizons in some places and websterite in others. Olivine orthopyroxenites contain up to 1% disseminated chromite. Orthopyroxenites also contain relatively high Cr (0.4–0.6%)	150
F	Series of interlayered peridotite horizons (Cr 0.12–0.27%), lherzolite, and olivine websterite	170
E	Series of peridotite horizons (Cr 0.21–0.32%), lherzolite, anorthosite, and massive anorthositic gabbro	200
D	Series of interlayered horizons of peridotite (Cr 0.26-0.36%), low-Cr (< 0.3% Cr), sulphide-bearing orthopyroxenite, lherzolite; overlain by minor olivine websterite, websterite	180
C	Series of peridotite horizons (Cr 0.25–0.41%), and minor lherzolite, orthopyroxenite, websterite layers, clinopyroxenite, gabbro, anorthosite, and anorthositic gabbro	200
B	Series of peridotite horizons (Cr 0.30–0.46%), minor gabbro, massive, laterally widespread anorthositic gabbro, and norite	230
A	Series of peridotite horizons (Cr 0.41–0.52%); up to 0.6% finely disseminated chromite in places; minor lenses of clinopyroxenite, websterite and gabbro; sulphide-bearing norite at base	170
	Total estimated thickness of ultramafic zone	1300

modal layering and size grading of pyroxene grains (Fig. 86C).

The *gabbroic zone*, with an estimated thickness of at least 800 m, is defined by the first appearance of cumulus plagioclase, and consists of a mixed series of massive, undifferentiated gabbro, anorthositic gabbro, and anorthosite. The gabbroic zone is exposed over an extensive area in the western sector of the complex, but was not examined in enough detail to enable it to be subdivided. The gabbroic zone was probably much thicker originally and has been eroded. However, because of the subhorizontal attitude of the intrusion this is difficult to assess.

The seven subzones of the ultramafic zone range from 150 m to over 300 m in thickness. Subzones A to D lie to the east of the Harding River, which coincides approximately with the boundary between subzones D and E. This boundary is also obscured by the major Harding River fault and alluvium. Subzones A to F are dominated by a series of peridotites (comprising over 50% of all rock types sampled on a systematic basis), accompanied by generally minor proportions of pyroxenite, gabbro, anorthositic gabbro, and anorthosite. Pyroxenites volumetrically form a much lower proportion of ultramafic rocks in subzones A to F than peridotites, except in subzone D, where orthopyroxenite, websterite, and olivine websterite are more common. In contrast, subzone G is characterised by a wider variety of interlayered pyroxenites, interspersed with a lesser proportion of peridotite. Subzone G is also characterised by olivine-bearing pyroxenites, including the first occurrence of olivine orthopyroxenite. Clinopyroxenite horizons were identified in subzones A, C, and G. The recurrence of peridotite at different levels indicates that subzone G could be further subdivided after more detailed work.

Anorthositic gabbro and anorthosite occur in all subzones, except possibly for subzones A, F, and G. Gabbros are minor in all subzones. Norites are present at the base of the intrusion, in subzone C, and at the contact between the ultramafic and gabbroic zones. The norites are remarkably fresh rocks which crop out with high relief over relatively small areas. The basal norite was recently quarried for road aggregate.

Aplite (microcline + mica + quartz) pervasively intrudes the southern part of the complex along a broad east-west 'corridor'. The aplites crop out over short distances east of the Harding River as massive tabular bodies up to several metres thick. West of the river the corridor narrows to several narrow dykes, extending almost up to the ultramafic zone/gabbroic zone contact. Contacts of the aplite with the ultramafic rocks are usually bounded by thin mica(lepidolite) schists, enriched in Rb and Li. Aplite outcrop also coincides with areas of pervasive asbestos serpentinisation. The aplite intrusions and the most intense serpentinisation coincide with the axial trace of the Roebourne Syncline. Dolerite and gabbroic dykes, which are common throughout the complex, locally form prominent ridges in the recessive mafic units (Fig. 86D).

Petrography

Peridotite (ol ± opx)

Peridotites are completely serpentinised cumulates, originally consisting of olivine and orthopyroxene. Textures are well preserved despite extensive hydration, and the major minerals are usually recognisable as pseudomorphs. Olivine is present as granular cumulus grains amounting to up to 70% of the rock. Orthopyroxene is predominantly intercumulus and is commonly poikilitic. Clinopyroxene, where present, occurs only in trace amounts. Modally and normatively these rocks are harzburgites. Finely disseminated chromite grains are present in most peridotites.

Lherzolites are also extensively hydrated, differing compositionally from the harzburgites by lesser modal olivine and the presence of 10 vol.% or more of clinopyroxene. Rare relict areas of unaltered clinopyroxene may be preserved in some lherzolites. Sample 092 contains finely disseminated chromite.

Pyroxenite (opx ± ol ± cpx; cpx)

With relatively few exceptions, pyroxenites are orthopyroxene-dominant cumulates, continuing the orthopyroxene-dominant character shown by earlier-crystallising harzburgites. Of six rocks classified as clinopyroxenites, three contain significant intercumulus orthopyroxene (up to 10 vol.%), including pleochroic hypersthene. Olivine-free pyroxenites, notably orthopyroxenites and websterites with high proportions of orthopyroxene, are generally the least-altered rock types. Of these, orthopyroxenites tend to be particularly well preserved, with some samples, e.g. 043, showing only minimal alteration along margins of cumulus orthopyroxene. Orthopyroxene tends to become altered to talc, and clinopyroxene is more commonly uralitised, with common retrogressive alteration of this amphibole to chlorite. Olivine-bearing pyroxenites (olivine orthopyroxenite, olivine websterite) on the other hand, are rarely unaltered, owing to the relatively greater susceptibility of olivine to hydration, resulting in greater penetration of the rock fabric.

Exsolution textures in clinopyroxene are either absent or poorly developed. In contrast, typical 'Bushveld' type exsolution in orthopyroxene, characterised by well-developed, thin, daughter lamellae of exsolved diopsidic augite in the {100} plane, is ubiquitous in most Andover ultramafic cumulates.

Plagioclase is present in all pyroxenites as a minor intercumulus phase, but only rarely is it unaltered; microprobe analyses of relict plagioclase show consistent bytownite compositions. Minor interstitial quartz and traces of biotite are present in some websterites, e.g. sample 204. Olivine orthopyroxenite and orthopyroxenite commonly contain finely disseminated chromite (up to 1% Cr in sample 018).

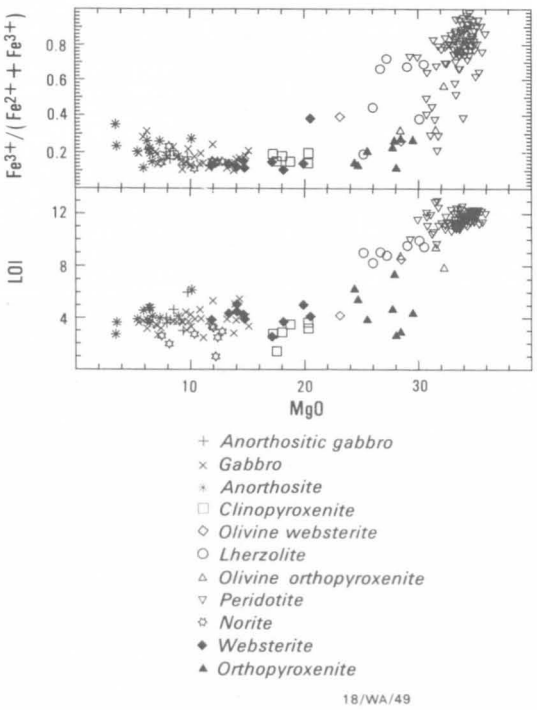

Fig. 87. Andover Complex: intensities of hydration (denoted by loss on ignition—LOI) and oxidation (denoted by $Fe^{3+}/(Fe^{2+} + Fe^{3+})$ for various mafic and ultramafic rocks. The olivine-bearing rocks are the most intensely altered.

Gabbro, anorthositic gabbro, anorthosite (plag ± opx ± cpx)

These rocks are invariably completely saussuritised. Ferromagnesian minerals are commonly uralitised and amphibole is commonly altered to chlorite. Traces of micrographically intergrown plagioclase and quartz are rarely visible, as are pseudomorphs after glomeroporphyritic pyroxene. In contrast norites are commonly relatively fresh, two-pyroxene (hypersthene and salite) rocks, in which feldspar (bytownite) is partly preserved.

Alteration

Rocks are mostly hydrated to some extent and many are also oxidised. Most rocks have undergone some form of alteration due to low-grade greenschist-facies metamorphism, characterised by chlorite, talc, sericite, epidote, and tremolite-actinolite products. Processes such as hydration, carbonation, silicification, and recrystallisation have selectively affected some rock types more than others.

Figure 87 shows that the rocks most affected by hydration (indicated by analysed loss on ignition), which are also the most oxidised (indicated by $Fe^{3+}/(Fe^{2+} + Fe^{3+})$ ratios), are the olivine-bearing peridotites (harzburgite and lherzolite), reflecting the relatively greater propensity of olivine to break down under such processes compared to pyroxene. Where modal proportions of olivine, indicated by MgO content in Figure 87, are lower, e.g. in olivine orthopyroxenite and olivine websterite, the degree of alteration by these processes becomes less significant. As a result of such alteration, peridotites are totally hydrated, but cumulus textures are generally preserved as serpentinised pseudomorphs after olivine, usually rimmed by Fe oxides.

Clinopyroxene is commonly uralitised. Orthopyroxene, occurring as cumulus and intercumulus phases in the peridotites, is invariably serpentinised, together with associated cumulus olivine grains. In pyroxenites, however, orthopyroxene is always partly or completely altered to talc instead of chlorite. However, some orthopyroxenites (e.g. 043) are remarkably fresh.

Figure 87 also shows that the more evolved pyroxenites and gabbroic rocks are, in general, markedly less hydrated and oxidised, having average loss-on-ignition values of about 4% and $Fe^{3+}/(Fe^{2+} + Fe^{3+})$ ratios of 0.2. The lowest analysed $Fe^{3+}/(Fe^{2+} + Fe^{3+})$ ratio, of 0.1, for a number of the more evolved rocks suggests that this figure may reflect the natural oxidation ratio for the intrusion. For the purpose of this investigation, however, the more commonly used $Fe^{3+}/(Fe^{2+} + Fe^{3+})$ ratio of 0.15, corresponding to the Irvine & Baragar (1971) estimate for non-oxidised basaltic lavas, has been used for geochemical calculations.

The differing levels of element mobility and redistribution behaviour in response to secondary processes makes interpretation of certain element dispersion patterns difficult. For example, it is well known that alkalis and alkaline-earths such as Na, K, Rb, Sr, and Ba are mobile during weathering and hydrothermal and metamorphic alteration, and are therefore unsuitable as petrogenetic indicators in altered rocks. However, Al and high-field-strength (HFS) cations such as Sc, Y, REE, Cr, V, Ti, Zr, and Nb, have been shown to be relatively immobile under most metamorphic conditions and can be used as petrogenetic indicators (e.g. Pearce & Cann, 1973; Beswick, 1982).

In order to assess the suitability of the samples for geochemical comparison it is necessary to determine, at least qualitatively, the extent to which elements have

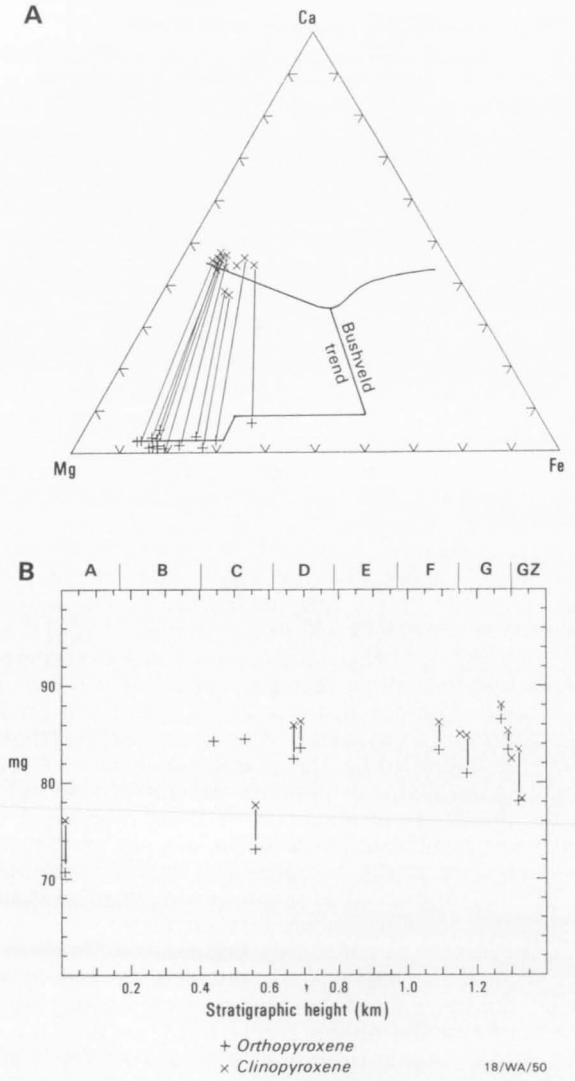

Fig. 88A–B. (A) Pyroxene ternary plot showing the fractionation trends of Ca-rich and Ca-poor pyroxenes from the Andover and Bushveld complexes, and (B) variations in mg of coexisting Ca-rich and Ca-poor pyroxenes plotted against stratigraphic height.

been redistributed. Several schemes to determine and evaluate the degree of rock alteration have been proposed for volcanic rocks, e.g. Floyd & Winchester (1978) and Beswick & Soucie (1978). These schemes are not, however, generally applicable to cumulate rocks. For these rocks more general qualitative criteria are employed, such as the preservation of primary mineralogy and textures.

For this study a combination of petrographic evaluation and evidence of geochemical consistency was used to assess the suitability of samples for geochemical comparison. It was found that even the most strongly altered rocks, such as the serpentinites, where the primary mineralogy has been totally altered, satisfy the criteria for geochemical consistency.

The role of alteration in the ultramafic-zone rocks (in particular the ubiquitous serpentinisation of peridotite sequences throughout the Andover Complex) in successfully discriminating ultramafic and gabbroic terranes by remote sensing, is discussed by Macias & Simpson later in this Bulletin.

Mineralogy

Systematic examination of mineral assemblages in the Andover Complex is inhibited by the widespread alteration of most rocks. Pyroxenes are generally the only major minerals well enough preserved in most rocks to allow comparative analysis throughout the ultramafic zone. Analysed pyroxenes are listed in Appendix 2.

Microprobe analyses of coexisting orthopyroxene and clinopyroxene from a variety of representative rocks from different stratigraphic levels (basal norite, subzones C, D, F, G, and gabbroic zone) show a range of compositions, which fall into well-constrained fields in the pyroxene quadrilateral (Fig. 88A). Figure 88A and Appendix 2 show that the pyroxenes in most of the ultramafic rocks consist of relatively primitive, equilibrated, bronzite-chromian diopside assemblages, with mg in the range 80–85. In more fractionated rocks, equilibrium pyroxene assemblages consist of either salite or augite, associated with more Fe-rich bronzite. The compositions and fractionation trends of Andover pyroxene assemblages are similar to the initial pyroxene fractionation trends of the Bushveld Complex.

In Figure 88B the most fractionated pyroxene assemblages are those of basal norite (119) (mg(cpx) = 76; mg(opx) = 71), clinopyroxenite (213) from subzone C (mg(cpx) = 78; mg(opx) = 73), norite (197) (mg(cpx) = 82; mg(opx) = 78), and gabbro (069) (mg(cpx) = 78), both from the base of the gabbroic zone. Pyroxenes having the most primitive compositions (mg(cpx) = 88; mg(opx) = 87) are those from orthopyroxenite sample 209, located in subzone G, in the centre of the complex.

Geochemistry

Major and trace element whole-rock analyses are listed in Appendix 3.

Geochemical trends along profiles through the layered complex (traverses 1a, 1b, 1c, and 2) show that the ultramafic zone can be subdivided into seven subzones. The subzones are particularly well highlighted by the systematic variation trends of Cr and Ni content, and mg (particularly peridotites) with stratigraphic height (Fig. 89).

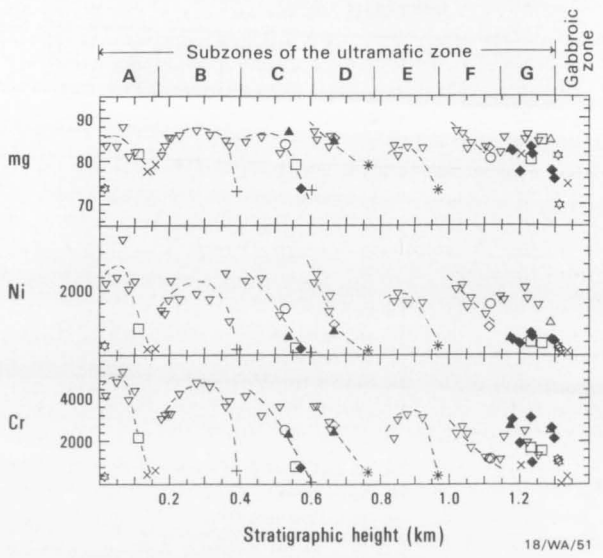

Fig. 89. Andover Complex: whole-rock variations in Cr, Ni (ppm), and mg plotted against stratigraphic height. The relatively more complex trends in subzone G indicate that this subzone could be further subdivided. Symbols as in Figure 87.

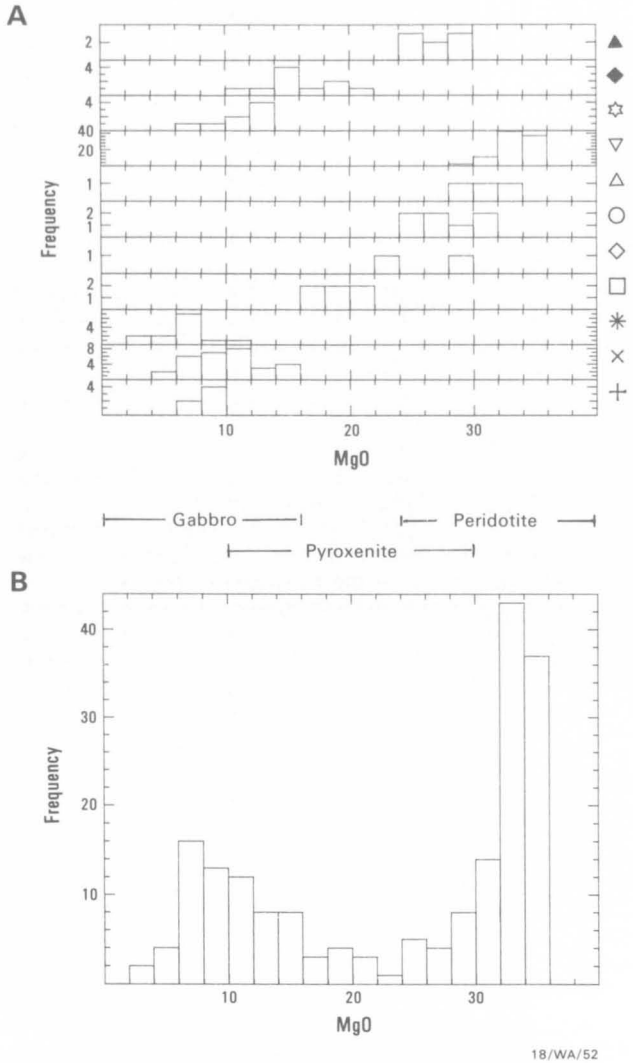

Fig. 90A–B. Andover Complex: histograms of MgO (weight %) contents for different rock types. Symbols as in Figure 87.

Figure 90 shows that peridotites account for over 50% of the rock types in the ultramafic zone. Harzburgites comprise by far the greatest proportion of these peridotites; lherzolites are subordinate. The relative proportions and compositions of the various rock groups making up the complex are also shown in Figure 91A, which also compares the compositions of the Andover Complex rocks with those of the Munni Munni Complex.

It is readily seen from Figure 91 that, with the exception of the Andover clinopyroxenites, the complete range of Andover rock compositions, from peridotite through pyroxenite to gabbro, are substantially richer in MgO (reflected by higher MgO/Al_2O_3 ratios) than the Munni Munni ultramafic-mafic suite. This striking difference between the two intrusions is expressed in the orthopyroxene-dominant mineralogy of the Andover Complex and the clinopyroxene-dominant mineralogy of the Munni Munni Complex. This fundamental difference is also illustrated by Figure 91B, where Munni Munni pyroxenites all reflect olivine-clinopyroxene control and Andover pyroxenites are more closely associated with the olivine-orthopyroxene control line. In the Munni Munni Complex, anorthosite forms a very minor component of the gabbroic zone. In the Andover Complex, by contrast, anorthosites and anorthositic gabbro horizons are ubiquitous within all subzones of the ultramafic zone, with the possible exception of subzone D, and are also substantially present in the gabbroic zone.

Despite these differences, Sun & others (1991) showed that the Munni Munni and Andover parental magmas are siliceous high-magnesian basalts (SHMB) of very similar composition, that are believed to be derived by contamination of komatiite by tonalitic Archaean crust.

The differences between the clinopyroxene-dominant Munni Munni rocks and the orthopyroxene-dominant Andover rocks can be explained if the Andover magmas had assimilated greater amounts of felsic crustal material, sufficient to change the crystallisation path

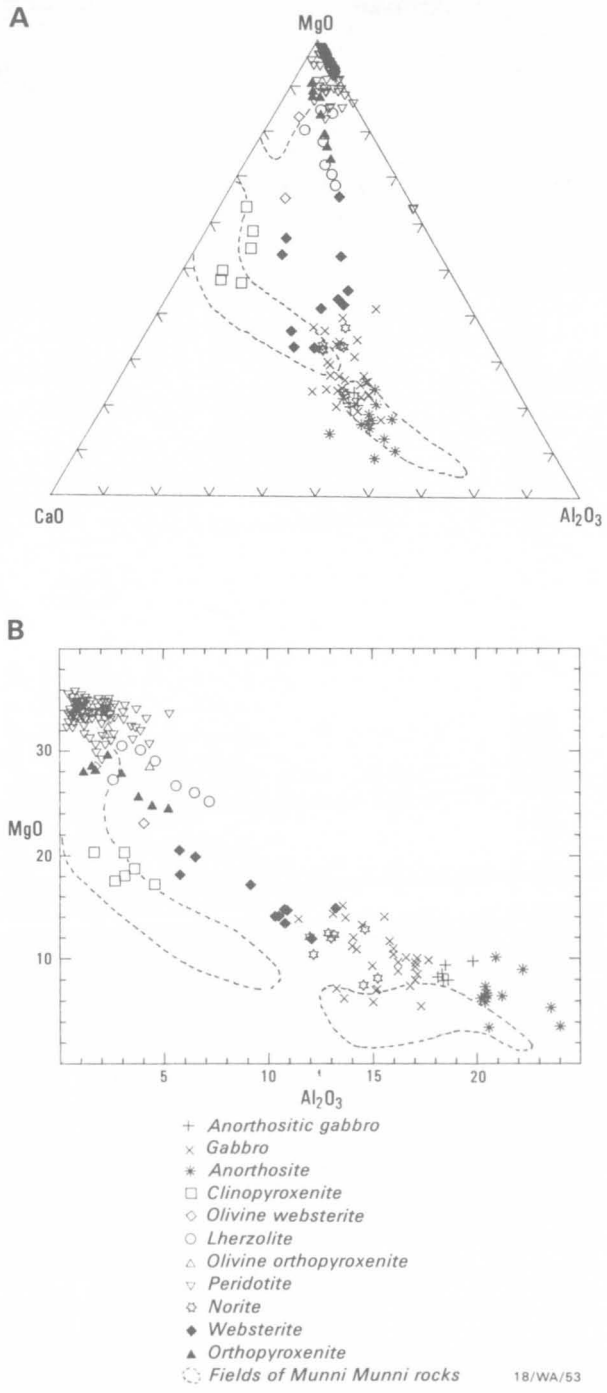

Fig. 91A–B. (A) Whole-rock variations in MgO, Al_2O_3, and CaO (weight %), and (B) MgO versus Al_2O_3 (weight %) from the Andover and Munni Munni complexes.

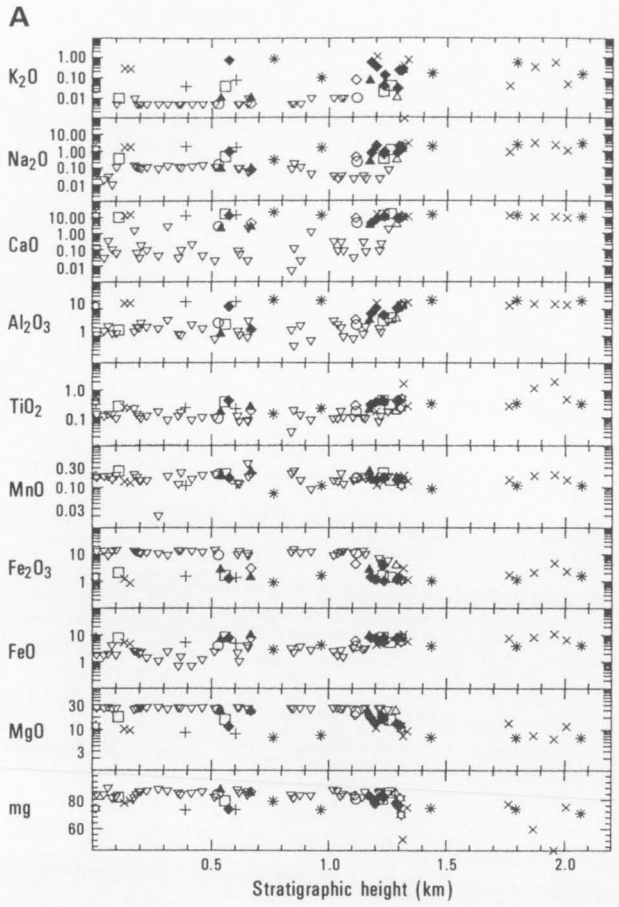

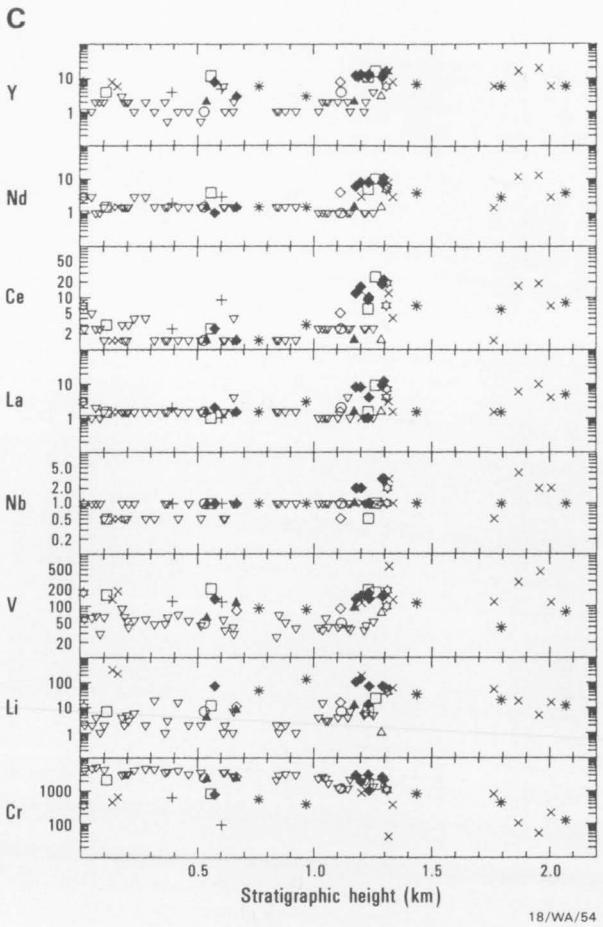

Fig. 92A–C. Andover Complex: whole-rock variations in major-element (weight %) and trace-element (ppm) compositions with stratigraphic height. Symbols as in Figure 87.

from Ca-rich pyroxene towards prior crystallisation of Ca-poor pyroxene (Longhi, 1981). The early appearance of Ca-poor pyroxene in the crystallisation sequence of the Andover intrusion may also suggest that such SiO_2 enrichment could have occurred at an early stage, before entry into the magma chamber (Campbell, 1985).

Major elements

The greatest variations in major-oxide concentrations largely reflect the gross mineralogical differences between the cumulates of the ultramafic and gabbroic zones (Fig. 92A).

Higher CaO, Na_2O, K_2O, and Al_2O_3, and lower MgO and mg, all distinguish the more plagioclase-rich, fractionated gabbroic rocks from the ultramafic rocks. Variations of Na_2O and K_2O in gabbros may, in part, reflect mobilisation of these elements by secondary alteration.

Higher TiO_2 contents in some fractionated gabbroic rocks reflect increased abundances of cumulus and intercumulus Fe-Ti oxides. In some gabbros at the south-western end of the complex, titanomagnetite layers are subeconomic with respect to their Ti, V, and Fe concentrations (Baxter, 1978).

The mg of the ultramafic-zone rocks ranges between 88 and 70, reflecting a relatively restricted geochemical range with time throughout the ultramafic sequence. Within this range, however, the olivine-rich character and more primitive composition of peridotites are shown by their relatively higher MgO concentrations (and mg), compared to pyroxenites and gabbroic rocks.

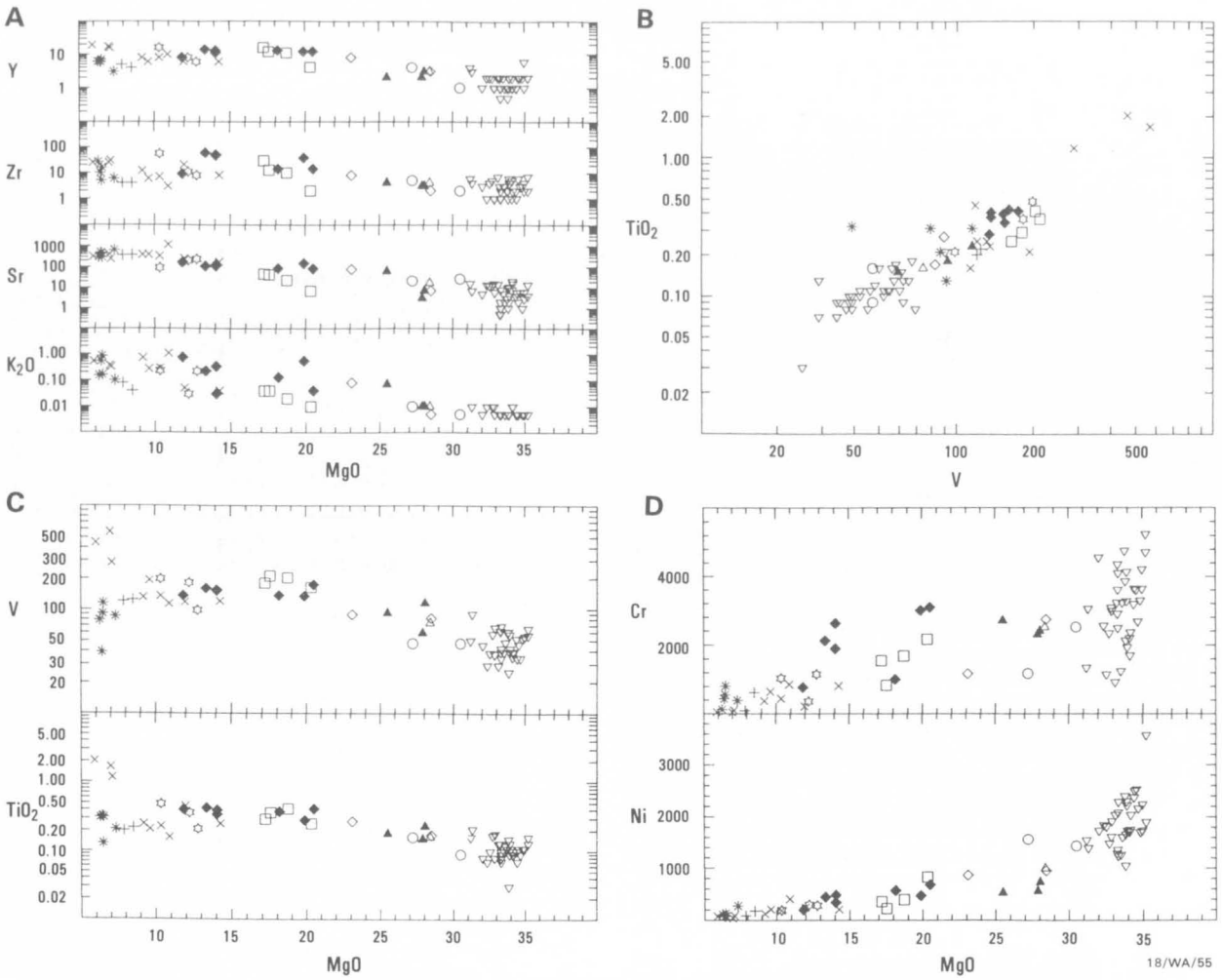

Fig. 93A–D. Andover Complex: whole-rock variations in (A) K_2O, Sr, Zr, and Y versus MgO; (B) TiO_2 versus V; (C) TiO_2 and V versus MgO; and (D) Ni and Cr versus MgO. Symbols as in Figure 87.

The highly oxidised nature of the peridotites, in comparison to other rocks, is shown by their high Fe_2O_3. The least oxidised peridotites occur in subzone G.

Pyroxenites in subzone G are the most alkaline, Mg-poor cumulates identified in the ultramafic zone. The ultramafic affinities of these pyroxenites are, however, shown geochemically by their relatively primitive mg, and petrographically by their intercumulus rather than cumulus feldspar. The location, and transitional nature of these more fractionated ultramafic rock types, defines a significant change in magma chemistry that culminates in the crystallisation of the mafic rocks.

Trace elements

Figure 92B–C shows that most trace-element abundances are different in the ultramafic and mafic rocks. As with the major oxides, the most marked and abrupt changes occur in subzone G, where abundances of some of the most incompatible elements, such as Ba and Rb, increase by more than 10 times in some evolved pyroxenites in subzone G and in the succeeding gabbroic zone. These variations in abundances largely reflect changes in the compatibility of these elements with evolving liquid compositions and associated cumulus mineral assemblages. For example, Figure 93A illustrates the varying extent of fractionation control on a range of trace elements, represented in order of incompatibility by K, Sr, Zr, and Y. Strontium and K are increasingly partitioned into plagioclase as rocks become more evolved. Yttrium and Zr, representing the least compatible elements, are, in contrast, partitioned preferably into clinopyroxene in mafic and ultramafic rocks. Although Zr has a similar partition coefficient for orthopyroxene and clinopyroxene, Y is highly incompatible with respect to orthopyroxene (Kd = 0.01) compared with clinopyroxene (Kd = 0.6) (Sheraton & Simons, 1988). Yttrium enrichment trends therefore reflect the rarity of clinopyroxene as an early crystallising phase in the ultramafic zone. Rare earths (La, Ce, and Nd), Rb, Sr, Ba, Li, Zr, Nb, Y, V, and Zn, are all relatively enriched to varying degrees in the mafic rocks.

Copper is more abundant in mafic rocks and pyroxenites than in peridotites. The Cu content of peridotites shows two markedly different distribution trends throughout the ultramafic zone, characterised by (a) a highly variable distribution, ranging from < 1 ppm to almost 600 ppm, within subzones A to D, and (b) a less variable trend of lower concentrations (3–53 ppm) within subzones E to G. Loss of Cu contained in sulphides, due to alteration, may account for low Cu values in some serpentinites.

A positive correlation between Ti and V reflects their closely related compatible behaviour with the crystallisation of titaniferous magnetite (Fig. 93B). Figure 93C shows that Ti and V behaved incompatibly in ultra-

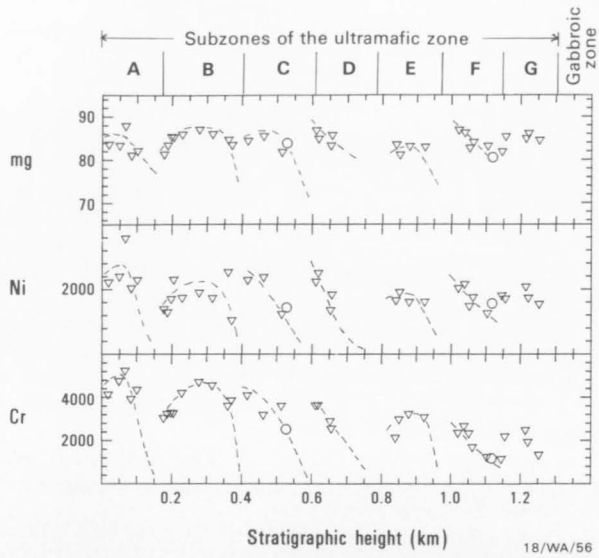

Fig. 94. Andover Complex: whole-rock variations in Cr, Ni (ppm), and mg with stratigraphic height for peridotites. Symbols as in Figure 87. Fractionation trends shown by dashed lines are from general rock trends in Figure 89.

mafic rocks (no crystallisation of Ti-magnetite) with MgO between 15% to 20%, and that Ti-magnetite was precipitated from the melt as rocks became more evolved, above subzone F. Anorthosites are the most Ti- and V-depleted rocks, whereas substantial Ti-magnetite accumulation is present in several gabbros.

Nickel and chrome show compatible-element behaviour during fractionation and are depleted in the mafic differentiates (Fig. 93D). Depletion of Ni with decreasing MgO is consistent with olivine fractionation. Nickel abundances decrease by a factor of about 3 in the ultramafic zone. Trends of Cr vs MgO, whilst having an overall depletion trend, consistent with fractionation and separation of chromite and/or chrome diopside, are less well defined.

Contrasting with the amount of Ni depletion, depletion of Cr, particularly within peridotites, amounts to a factor of about 5. Within this trend Cr, Ni, and the mg of the rocks vary cyclically, the seven identified cycles displaying sawtooth patterns in Cr, Ni, and mg, which are typical of fractionation trends brought about by influxes of fresh magma (Fig. 89). The lowest mg of the most fractionated end-members in the cycles of the ultramafic zone is over 70, suggesting that magmas were only moderately evolved. In peridotites, mg varies only within the relatively restricted range of 88–80 and, unlike Cr, Ni does not diminish significantly going upsequence (Fig. 94).

Discussion of results

Field observations, geochemical whole-rock data, and mineral-probe data support the conclusion that the ultramafic zone formed from a cyclic series of magmas that followed fractionation paths along the general crystallisation trend of peridotite → pyroxenite → anorthosite/gabbro. The repetition of these units, together with the presence of mg variation trends showing a resetting to more primitive compositions, implies that the cycles were formed in an open system, as a result of repeated injections of magma into an evolving magma chamber. Successive cyclic units were possibly formed either (a) wholly as a result of injection and fractionation of fresh magma batches, or (b) by mixing of batches of fresh magma with residues of earlier magma. The systematics of formation of the ultramafic zone are interpreted as similar to that described for the Class III layered sequence of the Muskox Intrusion (Irvine & Smith, 1967; Irvine, 1970).

The common occurrence of chromite in the ultramafic-zone cumulates may reflect the absence or scarcity of clinopyroxene as an early-crystallising phase in most rocks. Calculations from mineral-probe analyses (Appendix 2) suggest a clinopyroxene/orthopyroxene Kd factor for Cr of at least 9.

The sawtooth patterns of Cr, Ni, and mg (Fig. 94) show that Cr abundances are closely linked to fractionation, in particular to the fractional crystallisation of olivine, as reflected by Ni. These relationships are explicable in terms of the MgO-Cr_2O_3-SiO_2 phase-diagram model proposed by Irvine (1975; 1977) to explain the origin of chromite in stratiform intrusives. In this model the curvature of the olivine-chromite cotectic is such that, when the two minerals co-precipitate, the ratio of chromite to olivine gradually decreases with fractionation. The decreasing chromite/olivine ratios of successive cycles can also be achieved in this model by increasing the SiO_2 content of the magma, through salic contamination, and/or mixing with evolved liquids to create hybrid magmas. A plot (Fig. 95) of normative quartz against Cr of average peridotite compositions from each of the ultramafic subzones suggests that such progressive SiO_2 enrichment occurred during the development of the Andover cyclic sequence. Figure 95 suggests (a) that hybrid liquid E was dominated by an influx of relatively primitive magma, and (b) that the subzone G magma was more silicic than the earlier hybrid magmas of the layered sequence. The complexities of the possible processes involved in the evolution of the ultramafic-zone rocks are consistent with the periodically replenished, tapped, and fractionated (RTF) model of O'Hara (1977) and O'Hara & Mathews (1981). In this model, geochemical evolution is controlled by a cyclical sequence of magma replenishment, magma mixing, and fractional crystallisation. Although no stratiform chromite layers were found during

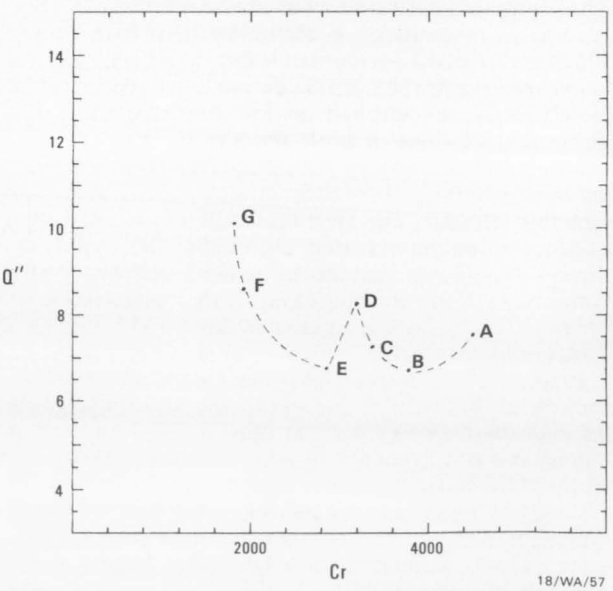

Fig. 95. Andover Complex: normative quartz (Q″) content of average peridotite compositions from subzones A to G, versus their average Cr content (ppm). Q″ is calculated normatively as Q + 0.3 x enstatite + 0.23 x ferrosilite (Sheraton & Simons, 1988).

this investigation, the geochemistry and mineralogy of the Andover Complex may be favourable for chromite under the circumstances of magmatic mixing suggested by Irvine's (1975; 1977) MgO-Cr_2O_3-SiO_2 mixing model.

Distribution of platinum, palladium, iridium, ruthenium, gold

Platinum, Pd, Ir, Ru, and Au data on 14 rocks from traverses 1a and 1b through the ultramafic zone are shown in Figure 96A,B and Table 25. Reflecting their relative proportions in the ultramafic zone, half of these rocks are peridotites and the rest are either pyroxenites or gabbroic rocks. Norites 197 and 199a, representing the earliest-crystallising stage of the gabbroic zone, were the only samples analysed from this zone.

Platinum, Pd, Ir, Ru, and Au have broadly similar trends through the ultramafic zone. Small increases in Pt, Pd, and Au abundances in peridotites, up to the 200 m stratigraphic level, are followed by an overall depletion trend in later peridotite horizons. Precious-metal abundances in peridotites up to the 600 m level exceed estimated values for fertile mantle (Sun & others, 1991), but abundances in peridotites above 600 m are lower. Precious-metal abundances in the more fractionated rocks are more variable. With the exception of clinopyroxenite 139 at the 100 m stratigraphic level, which has significantly lower precious-metal abundances, these rocks have similar or higher abundances of precious metals compared to peridotites from adjacent stratigraphic levels. Relative to the peridotite trend (dashed lines in Fig. 96), websterites 202 and 204 in subzone G, and norite 199a at the gabbroic zone contact, are enriched in Pt, Pd, and Ir.

Platinum, Pd, and Ru are lithophile elements in the absence of sulphides and chromite, and for this reason remain largely in the melt during crystallisation. As the analysed samples consist of a variety of adcumulates and mesocumulates, in which the proportion of intercumulus melt ranges up to 25%, a more realistic appraisal of precious-metal abundances can be obtained by relating the analysed whole-rock values to the proportion of intercumulus melt in the cumulates. Semi-quantitative estimates of these abundances can be derived by point-counting of intercumulus material in the cumulate (Hoatson & Keays, 1989), from which estimated porosity factors can be derived, e.g. where intercumulus material amounts to 5%, the porosity factor for the rock is 100/5 = 20, and the concentration of incompatible element (x) in the melt is 20 x. Porosity factors are listed in Table 25.

Zirconium also provides a reasonable measure of the amount of trapped melt in a cumulate because it is incompatible, and immobile under alteration and weathering (Hoatson & Keays, 1989). As shown in Figure 92B, Zr has a relatively flat variation trend through the ultramafic zone up to about the 1200 m stratigraphic level (subzone G), where its abundance is significantly higher in some mesocumulates. The flat Zr profile further substantiates the open-system of multiple magma influx and magma mixing characteristic of the Andover Complex.

When precious metals are normalised to Zr (Fig. 96B), most samples lie along a coherent trend for each element, indicating a direct relationship between element abundances and the volume of trapped melt. Figure 96B shows that, relative to values in the lowermost levels of the ultramafic zone, Pt, Pd, Ru, and Au in the upper peridotite horizons are depleted by up to 60 times, and Ir by about 150 times. The relatively higher depletion trend for Ir reflects its more compatible character compared to other PGEs, being largely fractionated with early-crystallising phases, notably olivine and chromite. Ruthenium behaves similarly to Ir, but has a proportionately lower fractionation factor. Exceptions are clinopyroxenite 139 and orthopyroxenite 043 from the 110 m and 670 m stratigraphic levels respectively. The clinopyroxenite is markedly deficient in all of the precious metals compared to abundances in peridotites around this stratigraphic level. Orthopyroxenite 043, in contrast, contains comparatively high Pt and Au, and has a similar Pd content. Lower Ir and Ru abundances reflect the absence of olivine in both of these pyroxenites, owing to their more evolved character. The gabbroic-zone norites have lower precious-metal abundances than the ultramafic zone cumulates.

The trend in precious-metal abundances through the ultramafic zone suggests that they became depleted as the ultramafic layered series evolved. The trend mirrors that shown in Figures 89 and 94 by Cr, suggesting that the depletion of the precious metals may also be controlled to some extent by RTF mixing and fractionation. Figure 96C, however, shows that the rate of precious-metal depletion is significantly greater than the rate of Cr depletion.

Role of sulphur

Sulphide saturation is the most obvious factor which could cause depletion in precious metals. Because of their very high partition coefficients, sulfides are very efficient scavengers of PGEs, and the importance of this mechanism as a determinant of PGE potential has been well documented for various layered intrusions (Campbell & others, 1983). When magmas are S-undersaturated, Pt, Pd, and Au behave incompatibly, resulting in their progressive *enrichment* towards the upper levels of fractionating sequences, as in the Munni Munni Complex (Hoatson & Keays, 1989). The Andover depletion trend, however, suggests a predominantly *compatible* behaviour of precious metals, consistent with continuous, systematic loss, due to extraction by sulphides, and, to a lesser degree, by chromite.

The S contents of the fourteen samples analysed for precious metals range from 40 to 1100 ppm (Table 25), which lies within the range of S determinations for the Andover Complex as a whole (Fig. 92B). Ultramafic rocks generally have the lowest S, and gabbros are generally more S-rich. Including most of the gabbroic-zone samples, many Andover rocks have greater than 1000 ppm S, estimated as the threshold for S-saturation in mafic magmas (Hoatson & Keays, 1989; Sun & others, 1991).

When porosity factors are taken into account, the S abundances in the cumulates are increased by factors of four to more than 10. This normalisation procedure provides a more realistic estimate of the S abundances in the primary melt. Except for some peridotites, these estimates range upwards from 600 ppm S. As most rocks are altered to some extent, particularly the serpentinised peridotites, these S abundances have to be considered as minimum values, as sulphides are highly mobile during such alteration. In the light of these normalised S abundances the ultramafic-zone rocks are believed to have been formed from magmas that were largely S-saturated.

Under the S-saturated conditions, precious metals behaved compatibly and were not progressively enriched in the melt. Instead, due to their strong affinities with sulphides and chromite, they were depleted during fractionation throughout the ultramafic zone. An ex-

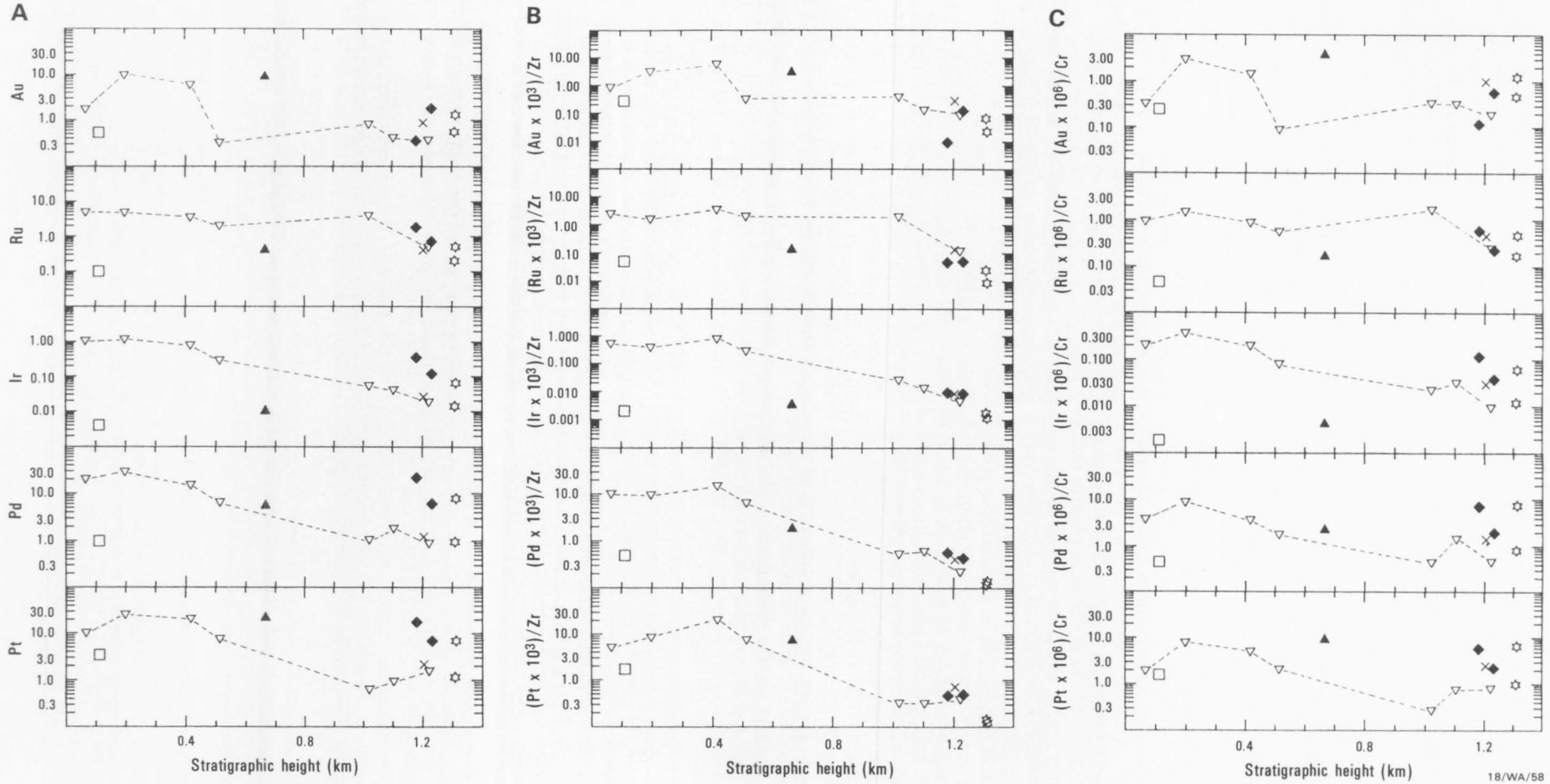

Fig. 96A–C. Andover Complex: whole-rock variations in precious-metal abundances (ppb) with stratigraphic height. A–Absolute abundances. B–Normalised against Zr (ppm). C–Normalised against Cr (ppm). Symbols as in Figure 87.

Table 25. Precious-metal and trace-element geochemistry of the Andover Complex

Sample number	*88330181*	*87330139*	*87330145*	*87330147*	*87330149*	*86330043*	*88330188*
Lithology	*peridotite*	*clinopyxte*	*peridotite*	*peridotite*	*peridotite*	*orthopyxte*	*peridotite*
Subzone	*A*	*A*	*B*	*C*	*C*	*D*	*F*
Strat. ht (km)	*0.07*	*0.11*	*0.20*	*0.42*	*0.51*	*0.67*	*1.02*
				Trace elements (ppb)			
Pt	10.50	3.42	26.40	21.30	7.75	21.80	0.66
Pd	20.70	0.98	29.70	15.40	6.65	5.44	1.09
Ir	1.10	n.d.	1.22	0.83	0.30	0.01	0.05
Ru	5.10	0.10	5.00	3.70	2.10	0.40	4.10
Au	1.77	0.53	10.10	6.11	0.33	8.94	0.84
Pt + Pd/Ir	28.36	1100.00	45.98	44.32	47.84	2724.00	31.82
(Pt + Pd) × 10^3/Zr	15.60	2.20	18.70	~36.70	~14.40	9.08	0.88
Porosity factor	10	altered	5	4	4	>10	4
				Trace elements (ppm)			
Zr	2	2	3	<2	<2	3	2
Cr	5243	2166	3295	4097	3611	2403	2362
Ni	3579	827	1707	2288	1236	730	2038
Cu	6	366	201	252	16	312	7
S	280	50	60	50	50	1100	160
mg	88	82	85	84	82	84	87
Sample number	*88330193*	*88330204*	*88330206*	*88330202*	*88330200*	*88330197*	*88330199a*
Lithology	*peridotite*	*websterite*	*gabbro*	*websterite*	*peridotite*	*norite*	*norite*
Subzone	*F*	*G*	*G*	*G*	*G*	*GZ*	*GZ*
Strat. ht (km)	*1.10*	*1.18*	*1.20*	*1.23*	*1.22*	*1.31*	*1.31*
				Trace elements (ppb)			
Pt	0.98	17.60	2.15	6.84	1.61	1.16	6.96
Pd	1.88	21.50	1.23	6.04	0.92	0.96	7.91
Ir	0.04	0.35	0.03	0.12	0.02	0.01	0.06
Ru	0.00	1.80	0.40	0.70	0.50	0.20	0.50
Au	0.42	0.35	0.87	1.79	0.38	0.56	1.30
Pt + Pd/Ir	68.10	111.08	130.00	108.24	133.16	151.43	228.77
(Pt + Pd) × 10^3/Zr	0.95	1.03	1.13	0.92	0.63	0.26	0.27
Porosity factor	10	5	5	5	10	3	3
				Trace elements (ppm)			
Zr	3	38	3	14	4	8	56
Cr	1244	3001	860	3091	1935	1156	1039
Ni	1261	470	406	678	1735	281	189
Cu	15	63	160	354	3	66	68
S	90	40	170	120	210	740	680
mg	83	82	81	83	86	81	70

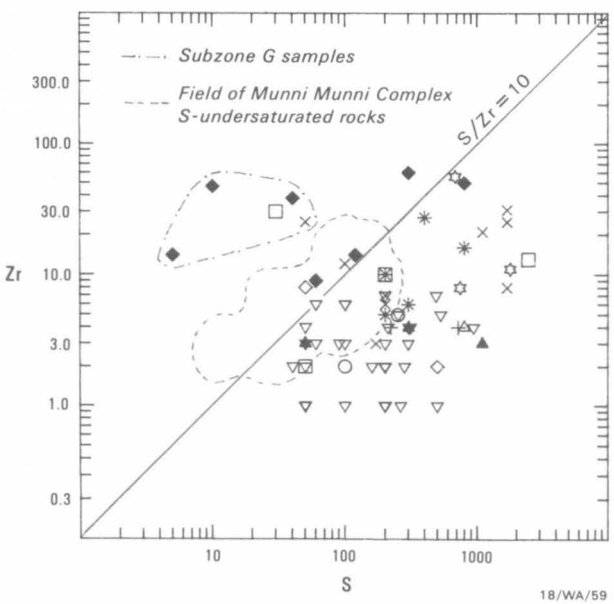

Fig. 97. Variations of Zr against S (ppm) for cumulates from the Andover and Munni Munni complexes. The plot shows that most Andover rocks fall in the field of S-saturation, as determined for various cumulates from the Munni Munni Complex (Hoatson & Keays, 1989: figure 12). Exceptions are rocks from subzone G, which may have crystallised from a late-stage S-undersaturated magma. Symbols as in Figure 87.

ample of such localised dissemination is the sulphide-bearing orthopyroxenite horizon in subzone D (S = 1100 ppm), containing anomalous Pt (21.8 ppb) and Au (8.94 ppb). Figure 96A implies that the most enriched precious-metal horizons may occur near the base of the ultramafic zone. Such a basal concentration of PGEs would be similar to those seen in the nearby S-saturated Radio Hill and Mount Sholl intrusions.

Platinum-group-element potential

Figure 97 shows that most of the Andover rocks fall on the S-rich side of the Munni Munni S-undersaturated trend. Several subzone G rocks, including websterite 204, fall in the S-poor field, suggesting that appropriate localised S-undersaturated conditions for accumulation of precious metals may have occurred in the final stages of the ultramafic zone. The scale of any

such accumulation, however, is likely to be small, given the unfavourable, pervasive, S-saturated character of precursory magma pulses, which would have resulted in the earlier extraction of precious metals from the system. Investigations by Greater Pacific Investments at the subzone G gabbroic zone contact during 1987–88 found no significant precious-metal anomalies.

Because of the PGE depletion trends, and the widespread faulting, the potential for a laterally continuous, stratabound, PGE-enriched horizon (e.g. Merensky Reef, J-M Reef) is greatly reduced. Potential, however, may exist for mineralisation resulting from secondary processes. Deposits associated with serpentinisation, such as those documented at Hitura, Finland (Hakli & others, 1976), the New Rambler mine, USA (McCallum & others, 1976) and the Hochgrössen Massif, Austria (Thalhammer & Stumpfl, 1988) demonstrate the effectiveness of serpentinisation as a concentrating process for PGEs. Rathbun Lake, Ontario (Rowell & Edgar, 1986) exemplifies a fault-controlled hydrothermal concentration system, which could also be relevant to the more sheared parts of the Andover Complex.

In the Andover Complex, serpentinisation, local and regional faulting, and intrusion by mafic rocks and aplites all provide conditions which could favour mobilisation, transport, and deposition of PGEs from hydrous solutions. Prospective areas for PGEs associated with serpentinisation could be those delineated by old asbestos workings, where serpentinisation was most intense (Fig. 85). Lithium- and Rb-enriched mica schists occurring at contacts between aplite and the ultramafic rocks, mainly east of the Harding River, may also be prospective areas for PGEs, together with fault zones, particularly in the western sector of the complex.

Acknowledgements

The helpful advice and time given by Dean Hoatson, Taro Macias, Colin Simpson, Shen-Su Sun, and John Sheraton, all of AGSO, is gratefully acknowledged. Petrographic data provided by Greater Pacific Investments and helpful discussions with John Ferguson and Dick England are also acknowledged.

CHEMICAL AND ISOTOPIC CHARACTERISTICS OF PARENT MAGMAS OF THE WEST PILBARA LAYERED INTRUSIONS: IMPLICATIONS FOR PETROGENESIS, MAGMA MIXING, AND PGE MINERALISATION IN LAYERED INTRUSIONS (*S-SS & DMH*)

Introduction

This chapter summarises some of the more important genetic issues relating to the ~ 2.9 Ga layered complexes in the west Pilbara Block. It will focus on the following questions, which are also relevant to the more general issues of PGE abundances in the mantle, and the mechanisms of PGE transport during magma generation and PGE concentration in the magma chamber:

— Were the siliceous high-magnesium basalt (SHMB) parent magmas proposed for these complexes (pp. 151-154) derived from komatiitic magma through crustal contamination, or are they of boninitic affinity and derived from melting of refractory lithospheric mantle?
— Were the parent magmas for the PGE-bearing Munni Munni Complex derived from a PGE-enriched mantle?
— Did PGE mineralisation in the Munni Munni Complex result from the mixing of two compositionally different types of magmas, as has been proposed for the Bushveld and Stillwater complexes?

Chemical and isotopic data presented in this chapter are integrated with field and petrological information described in previous chapters. Some of these issues have been addressed by Hoatson & Keays (1987, 1989) and Sun & others (1989, 1991).

Methods of approach

In this study, fine-grained 'chilled' marginal rocks of the complexes were used to define chemical and isotopic characteristics of the parent magmas, to formulate petrogenetic models, and to facilitate regional correlation. There are a number of possible shortcomings associated with a study of marginal samples. For example, these rocks often contain a cumulus component (e.g. high Al_2O_3, and positive Eu anomalies reflecting plagioclase accumulation and high Sc and Cr due to cumulus clinopyroxene) and thus are not necessarily representative of the primary magma. Furthermore, chilled marginal rocks are often contaminated by the country rocks during intrusion and post-intrusive metamorphism. Again, 'chilled' samples may represent magmas in various stages in the evolution of a magma chamber or even later dykes. To alleviate these problems, marginal rocks in direct contact with country rocks were avoided, in favour of marginal phases of magma intrusive into already solidified rock of the same kind; and petrographic and chemical criteria were used to avoid samples containing abundant cumulus grains. The results of this approach were integrated with a study of the chemistry of mesocumulates containing more than 7–25 vol. % trapped melt (which subsequently form intercumulus minerals), to maximise the amount of retrievable information.

Element ratios and isotope compositions of cumulates from different stratigraphic levels in the Munni Munni Complex are compared later in this chapter with data for 'chilled' samples and the Cadgerina Dyke, to test the models of multiple-magma-pulse injection and magma mixing at the top of the ultramafic zone (UZ) of the Munni Munni Complex. Chemical and Nd-isotope data for eight samples from various stratigraphic levels of the Andover Complex are used in comparison with more detailed data from the Munni Munni Complex to evaluate possible causes for their petrological differences which have been discussed by Wallace in this publication. They are also used to evaluate the magma mixing model. Finally, we apply knowledge obtained from this study to discuss the origin of different types of parent magmas observed in layered complexes in general.

Neodymium and Sr isotope analytical methods

Neodymium and Sr isotope compositions and Sm, Nd, Rb, and Sr concentrations were determined at the Research School of Earth Sciences, Australian National University, with a multi-collector Finnigan MAT 261 mass spectrometer operated in static multi-collector mode. Chemical separation procedures were similar to those described by McCulloch & Chappell (1982) and Maas & McCulloch (1991). Powdered samples (100–200 mg) were spiked with ^{147}Sm–^{150}Nd and ^{85}Rb–^{84}Sr tracers and then decomposed with an HF-HCl mixture in Teflon bombs. For mineral separates Savillex beakers with sealed caps were used for preliminary decomposition before Teflon bomb treatment. Separation of Sm and Nd was carried out using Kel-F/HDEHP coated ion-exchange columns. For mass fractionation correction the reported $^{143}Nd/^{144}Nd$ ratios have been normalised to $^{146}Nd/^{144}Nd = 0.7219$. Average $^{143}Nd/^{144}Nd$ values for La Jolla and BCR-1 standards are 0.511872 ± 2 and 0.512653 ± 5 (2σ), respectively. $^{87}Sr/^{86}Sr$ values were normalised to $^{88}Sr/^{86}Sr = 0.11940$ and the $^{87}Sr/^{86}Sr$ value for NBS 987 standard is 0.710219 ± 4 (2σ) during this study. Neodymium and Sr procedure blanks were less than 50 and 100 picograms, respectively. Reproducibility of routine measurements for the reported $^{143}Nd/^{144}Nd$ value is about 0.001% (i.e. 0.1 εNd unit). Reproducibility of the $^{147}Sm/^{144}Nd$ value for separate decompositions of the same sample is generally better than 0.2%. Thus, a realistic estimate for the reproducibility of initial $^{143}Nd/^{144}Nd$ at 2.9 Ga is 0.2 εNd unit. Since the total range of initial $^{143}Nd/^{144}Nd$ observed in the Munni Munni Complex at 2.9 Ga is small (0.7 εNd unit), duplicate analyses were carried out for several critical samples.

Sun & others (1991) have reported Nd isotope data for three samples from the Munni Munni Complex and one sample from the Dingo Complex using a different mass spectrometer (ANU-MSZ) and a different normalisation scheme with $^{146}Nd/^{142}Nd = 0.636151$. McCulloch has observed that there is a systematic difference in reported εNd values between this and the present approach. For comparison, about 0.6 εNd units has to be added to the data reported in Sun & others (1991). The three Munni Munni Complex samples have been reanalysed in this study.

Age of the Munni Munni Complex

Arndt & others (1991) have used the SHRIMP ion probe (ANU) to date zircons from a ferrogabbro pegmatite near the top of the ultramafic zone of the Munni

Table 26. Neodymium isotope compositions of minerals and whole-rock samples from the Munni Munni Complex

*Sample**	*Height (m)*	*Lithology**	$^{143}Nd/^{144}Nd$	$\pm 2\sigma_m$	*Sm (ppm)*	*Nd (ppm)*	$^{147}Sm/^{144}Nd$	*εNd*	*εNd @ 2.93 Ga*
84770052 wr	2377	GabN	0.511718	7	0.980	3.985	0.14862	−18.18	−0.04
clinopyroxene			0.512128	6	2.958	10.51	0.17014	−10.18	−0.16
plagioclase			0.510086	9	0.135	1.271	0.06436	−50.01	−0.07
84770061 wr	3553	GabN	0.511468	7	1.689	7.491	0.13630	−23.06	−0.26
clinopyroxene			0.511692	6	5.590	22.93	0.14739	−18.69	−0.08
plagioclase			0.510085	9	0.126	1.178	0.06465	−50.03	−0.20
84770094 wr	1846	Min. plag web	0.511490	6	3.329	14.66	0.13723	−22.63	−0.19
			0.511484	7	3.324	14.26	0.13735	−22.74	−0.35
clinopyroxene			0.511542	7	5.524	23.81	0.14021	−21.61	−0.30
			0.511551	5	5.591	24.15	0.13994	−21.44	−0.02
orthopyroxene			0.511822	8	0.895	3.512	0.15409	−16.15	−0.07
plagioclase			0.509781	7	0.096	1.199	0.04836	−55.96	+0.02

*wr = whole rock, GabN = gabbronorite,
Min. plag web = mineralised plagioclase websterite.

Munni Complex. They reported an age of 2925 ± 16 Ma.

Mineral separates of clinopyroxene, plagioclase, and orthopyroxene from three samples have been analysed for Sm/Nd mineral isochrons (Table 26). Sample 84770094 is a mineralised porphyritic websterite from the top of the UZ (subzone I) shown in Figure 98, and samples 84770052 and 84770061 are gabbronorites from the gabbroic zone (GZ; subzone A). As shown in Table 26, the total range of variation is 40 εNd units, plagioclase having the lowest values, whereas clinopyroxene, orthopyroxene, and whole rock have similar values. Analytical uncertainty of 0.2 εNd units corrresponds to about 15 Ma in age. Using a 'Yorkfit' regression program (Ludwig, 1990) with assigned errors for $^{147}Sm/^{144}Nd$ = 0.3% and $^{143}Nd/^{144}Nd$ = measured 2σ uncertainty, mineral isochron model-1 ages obtained for these three samples are quite consistent: 2915 ± 29 (2σ) Ma (with MSWD = 2.11 and initial εNd = −0.3) for sample 84770094, 2927 ± 19 Ma (with MSWD = 0.55 and initial εNd = −0.2) for sample 84770052, and 2935 ± 23 Ma (with MSWD = 1.52 and initial εNd = −0.2) for sample 84770061. Their weighted mean age is 2927 ± 13 Ma (2σ), which is within uncertainty of the zircon age (2925 ± 16 Ma) reported by Arndt & others (1991).

Chemical and isotopic characteristics of parent magmas

As discussed earlier, 'chilled' marginal samples and selected mesocumulates can be used to define the chemical and isotopic characteristics of parent magmas, to identify different magma types, to explore potential PGE fertility of the parent magmas, and to formulate petrogenetic models.

It is pointed out by Sun & others (1991: table 1) and in the next chapter of this Bulletin that parent magmas for the 2.9 Ga layered complexes of the west Pilbara Block are believed to be SHMB. 'Chilled' rocks of the Munni Munni, Andover, Mount Sholl, and Radio Hill complexes have consistently high silica (~ 53%), MgO (~ 10%), and total FeO (~ 11.5%), and are enriched in light-rare-earth elements (LREE with La ~ 17 ppm). They are depleted in Al_2O_3 (~ 9.5%), and heavy-rare-earth elements (HREE), Y (~ 15 ppm), Sc (~ 24 ppm), and have low Al_2O_3/TiO_2 (~ 11, which is about half of the chondrite value). On this basis the west Pilbara intrusions are believed to have been derived from SHMB parent magmas with similar compositions. However, in detail there are minor but significant chemical variations within and between complexes. As shown on the mantle-normalised trace-element spidergrams for Archaean SHMB (Fig. 99), sample 83330141 of the Munni Munni Complex has a very similar pattern to sample 83330172 from the Andover Complex, except that the latter sample has higher abundances of Nb (6 versus 4 ppm), and Zr (106 versus 65 ppm), and much higher Zr/Nd ratios (6.6 versus 3.6). Low Zr/Nd ratios (3.1–4.2) characterise 'chilled' rocks and mesocumulates associated with the Munni Munni UZ (Fig. 98). In contrast, Zr/Nd values for 'chilled' samples of the Cadgerina Dyke (5.4–5.9) on the northwestern side of the Munni Munni Complex, and gabbronorites (4.9–5.6) of the GZ, are closer to the Andover samples. 'Chilled' samples of the Cadgerina Dyke also have similar LREE (La = 18 ppm) and Zr (~ 94 versus 106 ppm) abundances, but different Nb (4 versus 6 ppm) abundances from the Andover 'chilled' samples.

Table 27 presents Sm-Nd concentrations and Nd isotope data for the Munni Munni and Andover complexes. Table 28 contains Rb-Sr concentrations and $^{87}Sr/^{86}Sr$ isotope data for mineral separates. Initial εNd values at 2.93 Ga range from 0.0 to −0.65 and +0.1 to −1.1 for the Munni Munni and Andover complexes, respectively. Two samples of granite intruded by the Munni Munni Complex have initial εNd values of 0.0 and −0.60, which are within the range of data for rocks of the complex. Estimated initial $^{87}Sr/^{86}Sr$ values at 2.93 Ga range from ~ 0.7015 to 0.7019 for plagioclase and clinopyroxene for the Munni Munni Complex. Clinopyroxene samples show open-system behaviour, as exemplified by two separate analyses of sample 84770094, which gave $^{87}Sr/^{86}Sr$ initial values of 0.6970 and 0.6996, much lower than the expected value of ~ 0.7006 (with εNd ~ +4) for the depleted mantle at 2.9 Ga. A value of 0.6970 is even lower than the initial value of 0.6989 for the earth at 4.56 Ga. Two separate clinopyroxene analyses for sample 84770021 gave $^{87}Sr/^{86}Sr$ values of 0.70174 and 0.70164, whereas calculated initial values are 0.70115 and 0.70092. It is proposed that the correct initial value for this sample should be between 0.7016 and 0.7012, and is most likely ~ 0.7015 (with initial εNd value of +0.1). If the generally observed negative correlation betweeen initial εNd and $^{87}Sr/^{86}Sr$ values is also applicable for the Munni Munni Complex, data in Table 28 would suggest that the calculated initial value of 0.7019 for sample 84770094 is slightly higher (~ 0.0002?) than expected. Thus, the best estimates of the initial

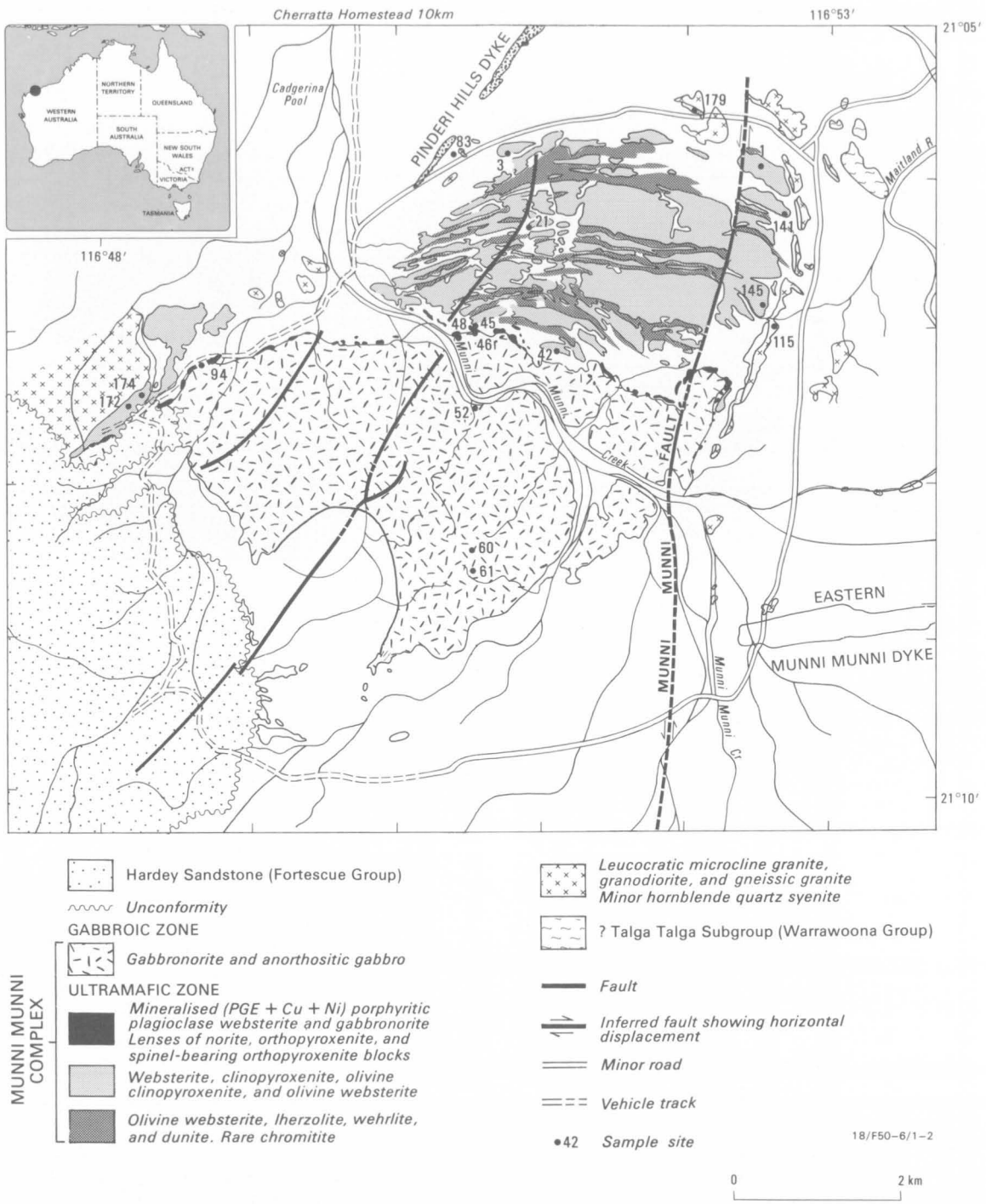

Fig. 98. Locations of samples used for isotope analysis from the Munni Munni Complex.

$^{87}Sr/^{86}Sr$ value for the Munni Munni Complex range from 0.7015 to 0.7017, corresponding to the observed initial εNd values of +0.1 to −0.2. These $^{87}Sr/^{86}Sr$ initial values are the lowest reported in the literature for Archaean layered complexes. Calculated initial $^{87}Sr/^{86}Sr$ values (0.69872 and 0.70103) at 2.93 Ga for two samples of the granite intruded by the Munni Munni Complex are also very low, suggesting that they have been disturbed since formation.

The initial εNd values reported for the Munni Munni Complex in Table 27 indicate the differences between $^{143}Nd/^{144}Nd$ values for the samples and average chondrite at 2.93 Ga ago. εNd is defined as $(((^{143}Nd/^{144}Nd)_{sample}/(^{143}Nd/^{144}Nd)_{chondrite} - 1) \times 10^4$. The geological significance of a positive initial εNd value for a basalt is that the time-integrated Sm/Nd ratio of the magma sources is higher than the chondrite value, suggesting a long-term LREE-depleted mantle source. A negative initial εNd suggests that either the magma source has a time-integrated LREE-enriched character or the parent magma has been contaminated by felsic crust with negative εNd during magma ascent and/or during emplacement. The significance of the negative initial eNd values needs to be interpreted in association with other petrological and geochemical data. On the basis of published data, initial εNd values for the de-

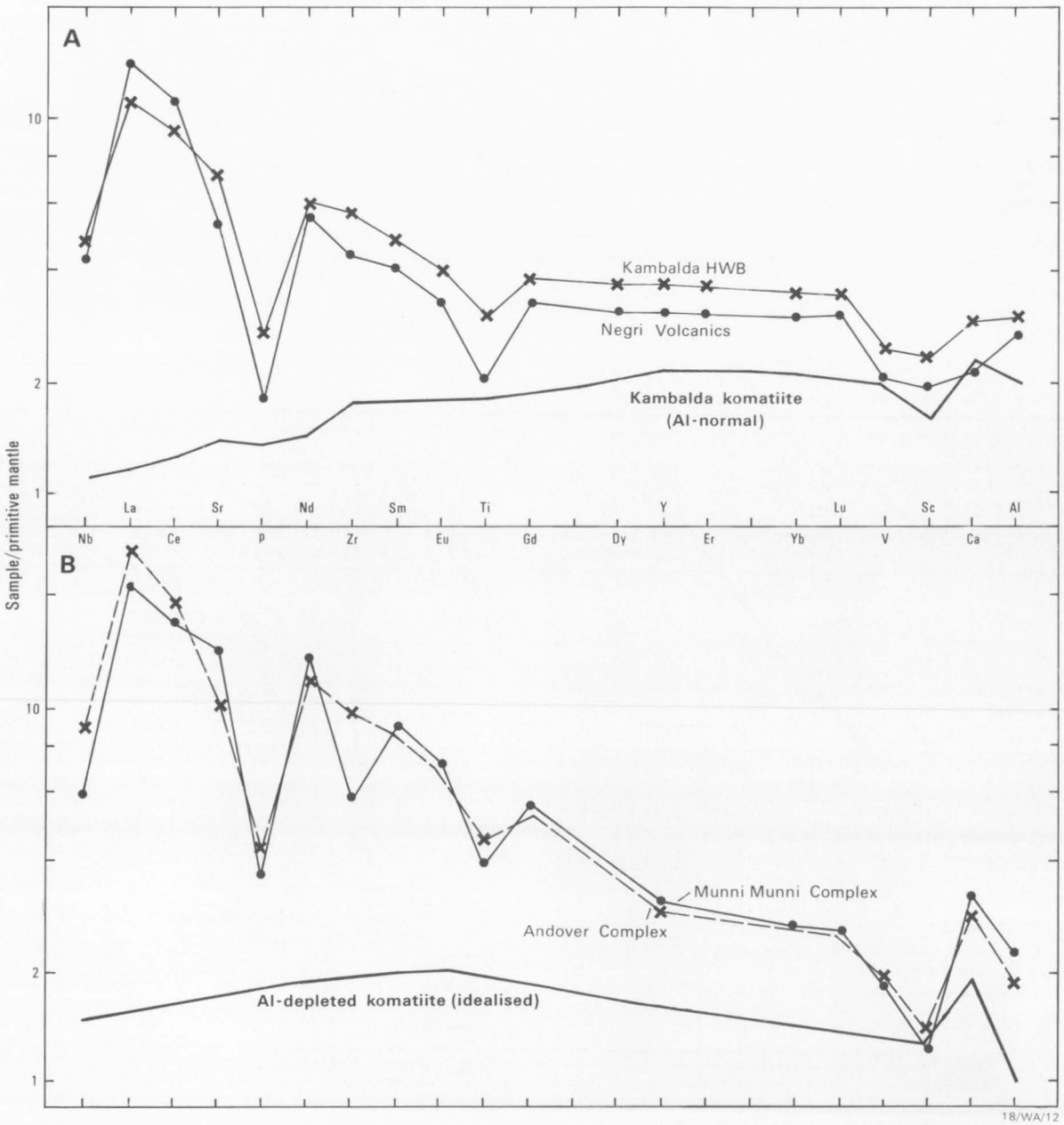

Fig. 99. Primitive-mantle-normalised trace-element diagrams for late-Archaean SHMB (e.g. Kambalda hangingwall basalt, Eastern Goldfields, and Negri Volcanics, west Pilbara, compared with idealised Kambalda komatiite with 24% MgO) and Munni Munni and Andover complexes, west Pilbara. Idealised pattern for Al-depleted-type komatiite is also shown. Abundance data for komatiites and the primitive mantle are from Arndt & Jenner (1986); Sun & McDonough (1989); and Sun & others (1989). The Munni Munni Complex chilled sample (83330141) shown in the figure is from the ultramafic zone. It has a lower Zr abundance (64 versus 95 ppm) and Zr/Nd ratio (3.6 versus 5.5) than chilled samples (85770172, 174) from the Cadgerina Dyke on the northwestern side of the complex. Relative abundances for the other trace elements shown in the figure are similar. The Andover Complex sample shown (83330172) has a higher Zr content (106 ppm) and Zr/Nd ratio (6.6) than the samples from the Munni Munni Complex.

pleted convective mantle at 2.9 Ga ago are likely to be $\sim +3$, whereas 3.5 Ga granodiorite and tonalite are likely to have values of -3 to -4. $^{87}Sr/^{86}Sr$ initial ratios for the depleted mantle at 2.9 Ga are likely to be close to 0.7006, whereas 3.5 Ga tonalite with low $^{87}Rb/^{86}Sr = 0.19$ (Rb = 35 ppm, Sr = 510 ppm) has initial $^{87}Sr/^{86}Sr \sim 0.7022$. Granodiorite and adamellite with higher Rb/Sr values are also expected to have higher initial $^{87}Sr/^{86}Sr$ values.

Proposed petrogenetic model for the SHMB parent magma

Chemical data (Fig. 99: see also next chapter) for SHMB of the Munni Munni and Andover complexes show 'crustal' characteristics. This could be a result of either crustal recycling through subduction or crustal contamination. Sun & others (1991) have shown that high FeO (11.5%) and low Al_2O_3/TiO_2 ($\sim$ 11) ratios for these SHMB rule out an origin by melting of a metasomatised refractory (poor in Fe and Ti) lithospheric mantle

Table 27. Samarium and Nd whole-rock data for samples from the Munni Munni and Andover complexes

*Sample**	*Height (m)*	*Lithology**	$^{143}Nd/^{144}Nd$	$\pm 2\sigma_m$	*Sm (ppm)*	*Nd (ppm)*	$^{147}Sm/^{144}Nd$	ε_{Nd}	ε_{Nd} @2.93 Ga
Munni Munni Complex									
84770003	174	Ol. web	0.511952	7	1.066	3.990	0.1615	−13.62	−0.33
84770021wr	910	Cpxenite	0.512598	6	0.539	1.677	0.1943	−1.01	−0.11
cpx			0.512606	7	0.542	1.688	0.1942	−0.86	+0.08
84770042wr	1723	Web	0.512145	6	0.985	3.466	0.1717	−9.85	−0.42
cpx			0.512128	8	1.136	4.028	0.1706	−10.18	−0.32
84770045	1811	Plag web	0.511596	7	2.245	9.427	0.1440	−20.56	−0.67
		"	0.511602	7	2.290	9.608	0.1441	−20.44	−0.58
84770094	1846	Min. plag web	0.511490	6	3.329	14.66	0.1372	−22.63	−0.19
		"	0.511484	7	3.240	14.26	0.1374	−22.74	−0.35
84770046	1840	Opx block	0.513931	10	0.117	0.270	0.2635	+24.99	−0.24
84770048	1851	GabN	0.511838	6	0.544	2.110	0.1558	−15.84	−0.39
		"	0.511850	7	0.568	2.205	0.1558	−15.61	−0.17
84770052	2377	GabN	0.511718	7	0.980	3.985	0.1486	−18.18	−0.04
84770060	3425	GabN	0.511496	6	1.666	7.299	0.1380	−22.51	−0.35
84770061	3553	GabN	0.511468	7	1.689	7.491	0.1363	−23.06	−0.26
83330136		GabN	0.511870	6	5.343	20.57	0.1571	−15.22	−0.26
85770179 chill	1	Ol. GabN	0.511225	7	3.746	18.36	0.1233	−27.80	−0.10
83330145		Ol. web	0.512107	7	1.209	4.305	0.1698	−10.59	−0.43
83330141 chill		Web	0.511304	7	3.902	18.48	0.1277	−26.26	−0.20
85770172 chill	1	GabN	0.511249	6	3.878	18.67	0.1255	−27.33	−0.48
85770174 chill	1	Plag web	0.511434	6	2.584	11.60	0.1347	−23.72	−0.31
84770083		Granite	0.510669	5	4.257	26.84	0.0959	−38.64	−0.60
84770115		Granite	0.510319	20	4.190	33.28	0.0762	−45.47	+0.02
Andover Complex									
88330213		Cpxenite	0.512636	6	1.858	5.712	0.1966	−0.27	−0.25
86330008		Web	0.511492	6	0.961	4.161	0.1397	−22.59	−1.07
87330127		GabN	0.511789	7	3.531	14.06	0.1518	−16.80	+0.15
87330205		Web	0.511383	6	1.607	7.26	0.1338	−24.71	−0.98
86330020		Later dyke	0.512195	6	5.001	20.18	0.1499	−8.88	+8.87
83330172 chill		GabN	0.511261	5	3.775	17.84	0.1279	−27.09	−1.14
88330196		Norite	0.511403	5	1.782	7.911	0.1362	−24.32	−1.49
86330069		GabN	0.512035	5	1.224	4.483	0.1651	−12.00	−0.06

*wr = whole rock, cpx = clinopyroxene, Ol. web = olivine websterite, Cpxenite = clinopyroxenite, Min. plag web = mineralised plagioclase websterite, GabN = gabbronorite, Web = websterite, Opx block = orthopyroxenite block.

Table 28. Rubidium, Sr, and Nd data for minerals from the Munni Munni Complex and granite country rock

Sample		*Rb (ppm)*	*Sr (ppm)*	$^{87}Rb/^{86}Sr$	$^{87}Sr/^{86}Sr$	$\pm 2\sigma_m$	$(^{87}Sr/^{86}Sr)_i$	ε_{Nd}*
84770021	clinopyroxene	0.129	26.90	0.01386	0.701736	12	0.70115	+0.1
	clinopyroxene	0.136	23.05	0.01695	0.701642	10	0.70092	
84770042	clinopyroxene	0.198	36.33	0.01579	0.702203	11	0.70153	−0.3
84770094	clinopyroxene	0.877	13.30	0.1902	0.705086	15	0.69701	−0.3
	clinopyroxene	1.187	12.63	0.2712	0.711154	14	0.69963	
	plagioclase	6.587	412.1	0.04609	0.703851	11	0.70189	−0.3
84770061	plagioclase	8.997	937.2	0.02775	0.702942	13	0.70176	
	plagioclase	8.034	719.9	0.03218	0.703058	13	0.70169	−0.2
84770052	plagioclase	3.913	977.7	0.01154	0.702087	10	0.70160	−0.2
84770083	granite	170.1	144.7	3.446	0.845121	14	0.69872	
84770115	granite	104	373	0.806	0.735260	40	0.70103	

ε_{Nd}* = initial ε_{Nd} values calculated at 2.93 Ga.

(i.e. the boninite model of Hamlyn & Keays, 1986). Sun & others (1991) suggested that the paradoxical combination in this magma type of high silica (reflecting low-pressure magma generation conditions) with depletion of some elements (Y, heavy REE, Al, and Sc), favoured by the crystallisation of garnet (reflecting high-pressure magma generation conditions), offers strong support for the crustal contamination model. This conclusion further supports the assimilation-fractional-crystallisation (AFC) model for Archaean SHMB in general (e.g. Arndt & Jenner, 1986; Sun & others, 1991). It has been shown that in terms of this model, 2.7 Ga SHMB from Kambalda with 10% MgO (Fig. 99) and initial εNd of −2 could be derived from komatiitic magmas with 24% MgO (with initial εNd of +4) by assimilation (~ 15%) of 3.5 Ga granodioritic crust (with initial εNd = −4.5). This could have occurred at depth, followed by ~ 35% crystal fractionation (Chauvel & others, 1985; Sun & others, 1991). Differences in compositions of komatiite, felsic crust, and extent of assimilation and crystal fractionation could explain variations observed in the SHMB.

The Al-depleted character of the 2.9 Ga SHMB magmas that fed the layered complexes of the west Pilbara requires that their komatiitic parent magmas must also have been depleted in Al. It is interesting to note that Al-depleted komatiites (~ 3.0 Ga?) with Al_2O_3/TiO_2 = 10 occur at Ruth Well (Nesbitt & others, 1979), west of the Andover Complex. In terms of the AFC model, consistent chemical and isotope characters observed in 'chilled' rocks and cumulates in these layered complexes would suggest that crustal assimilation mainly

took place at great depths (> 10–15 km?) before the magma was emplaced into the chambers. Two granite wallrock samples analysed have higher Zr/Nd values (5.3 versus 3.6), but considerably lower $^{147}Sm/^{144}Nd$ values (~ 0.09 versus 0.125) compared with the basal 'chilled' phases of the Munni Munni Complex. However, they have similar initial εNd values (Table 26). These basal 'chilled' phases have the same Zr/Nd ratios as mesocumulates of the UZ and very similar chemical compositions to other 'chilled' rocks of the Munni Munni Complex. Based on these observations it is suggested that the effects of wall-rock contamination on magma composition appear to have been minor. Consequently, differences in Zr/Nd ratios and slightly different Nd isotope compositions observed in 'chilled' rocks and mesocumulates discussed above could be mainly due to changes in the composition of the felsic crust contaminant at great depths, the effects of different extent of assimilation and crystal fractionation being only minor.

Compared with the 2.7 Ga Kambalda SHMB of the Yilgarn Block (Fig. 99), the Munni Munni and Andover samples have higher Ti, Sr, and LREE (a factor of two for Nd), and minor Eu anomalies, but similar initial εNd values, at 2.7 Ga (−2). These contrasting spidergram patterns could be due to differences in the chemical compositions of mantle-derived parent magmas, or to different crustal contaminants or amounts of crustal contaminants. In terms of the komatiite-crustal-contamination model, larger amounts of LREE and Sr from the contaminant are required for the Munni Munni Complex. However, this complex has low $^{87}Sr/^{86}Sr$ initial values (0.7015) and similar initial εNd (~−2) to the Kambalda SHMB at 2.7 Ga. These Sr and Nd isotope data would suggest that the crustal contaminant is most likely to be 3.3 Ga old or younger, and of tonalite-granodiorite composition, with initial εNd about −2 and $^{87}Sr/^{86}Sr \leq 0.7020$ (i.e. with low Rb/Sr ratios).

Platinum-group-element contents and Ti/Pd ratios estimated for the SHMB parent magma of the Munni Munni Complex (Pd = 15–20 ppb, Pt = 10–15 ppb, Au = 2–4 ppb and Ti/Pd = 2.2 x 10^5) by Hoatson & Keays (1987) and Sun & others (1991) also support the komatiite-crustal-contamination model. These PGE abundances and Ti/Pd ratio are similar to those seen in other Archaean SHMB, and are consistent with their derivation from a 'normal' mantle with Pd ~ 4 ppb, Pt ~ 6 ppb, and Au ~ 1 ppb. Sun & others (1991) have also summarised chemical data, including PGE contents of rocks from various geological settings, and concluded that the mafic-ultramafic magmas of layered intrusions are not derived from a PGE-enriched mantle.

An apparent exception to this komatiite-crustal-contamination model is the petrogenesis of the Stillwater Complex. Osmium isotope studies by Lambert & others (1989, 1991) showed that several chromitite layers within the ultramafic zone of the Stillwater Complex have initial $^{187}Os/^{186}Os$ ratios (0.87 ± 0.03) substantially lower than the chondritic ratio of 0.90, suggesting derivation of magma from a very refractory, early Archaean mantle with an Re/Os ratio much lower than chondrite. This observation supports the second-stage melting model of Hamlyn & Keays (1986), which may also explain the very high estimated Pt content (≥ 40 ppb) in the parent magma of the Stillwater Complex (P.R.Hamlyn, personal communication, 1990). The different parent magma compositions that have been proposed for the Stillwater Complex do not limit the application of the AFC model discussed above.

Variations in Nd and Sr isotope compositions and Zr/Nd ratios in the Munni Munni Complex: implications for magma-chamber processes

Hoatson (p. 63) has indicated that the ultramafic zone (UZ) of the Munni Munni Complex formed from repeated injections of S-undersaturated SHMB into an expanding magma chamber. Magma mixing through fountain injection was an important process and is believed to have led to the formation of the PGE-bearing porphyritic websterite layer (PWL). Different Zr/Nd ratios observed in 'chilled' rocks and websterite of the UZ (~ 3.5) and PWL, gabbroic zone (GZ), and Cadgerina Dyke (~ 5.5) suggest a change in magma composition during formation of the PWL, from SHMB with Zr/Nd ~ 3.5 to Zr/Nd ~ 5.5. However, one should be cautious when using the observed Zr/Nd values, since Zr and Nd abundances in the UZ are controlled by the amounts of clinopyroxene and trapped melt, and the effect of clinopyroxene on Zr and Nd has to be taken into consideration. Fujimaki & others (1984) reported that the Zr distribution coefficient (Kd) for clinopyroxene/melt in tholeiitic magmas is about half of that for Nd. This is consistent with the data for clinopyroxenite adcumulate from the Munni Munni Complex, namely low ~ 3 ppm Zr and ~ 1.5 ppm Nd (with mineral/melt Kd values of 0.05–0.10 and 0.10–0.20 for Zr and Nd, respectively). Accordingly, Zr/Nd ratios for websterite samples used in this study with > 12 ppm Zr should represent the Zr/Nd ratios of the trapped melt. In a steady-state magma chamber, crystal fractionation of clinopyroxene will increase the Zr/Nd ratio in the residual magma. It will also increase the abundance of incompatible elements (e.g. La, Ce, Nb) and some ratios (e.g. La/Nd, Nd/Y). However, such variations are not found between 'chilled' rocks associated with the UZ and Cadgerina Dyke close to the PWL. On the basis of the above it can be concluded that different Zr/Nd ratios observed in 'chilled' rocks represent the character of their parent SHMB magma.

Only small variations of initial εNd values (0.7 unit) have been observed in the Munni Munni Complex. There are no obvious systematic differences between 'chilled' marginal rocks and UZ and GZ cumulates. The enigmatic orthopyroxenite block sample (046) hosted by the PWL, has a very high εNd value of +24.99, but an initial εNd value of −0.24 at 2.93 Ga, similar to other samples from the complex. This Nd isotope composition may indicate a genetic connection of the orthopyroxenite to the Munni Munni Complex. Early crystallisation and accumulation of orthopyroxene could have been caused by interaction of the SHMB with roof and/or side-wall granite with similar Nd isotope composition.

Variations in initial εNd values observed in samples from different stratigraphic levels reflect the effect of multiple magma injections: −0.33 (174 m), 0.0 (910 m), −0.38 (1723 m), −0.65 (1811 m, base of the PWL), −0.27 (1846 m), and very limited variation, −0.2 ± 0.1, for gabbronorites (1851 to 3553 m). Such Nd isotopic variations are consistent with mineralogical and chemical trends observed in the Munni Munni Complex, as shown on p.51. There it was suggested that a near 'steady-state' condition of balanced fractionation and new magma influx was maintained in the lower part of the magma chamber, which resulted in restricted cumulus mineral compositions. In contrast,

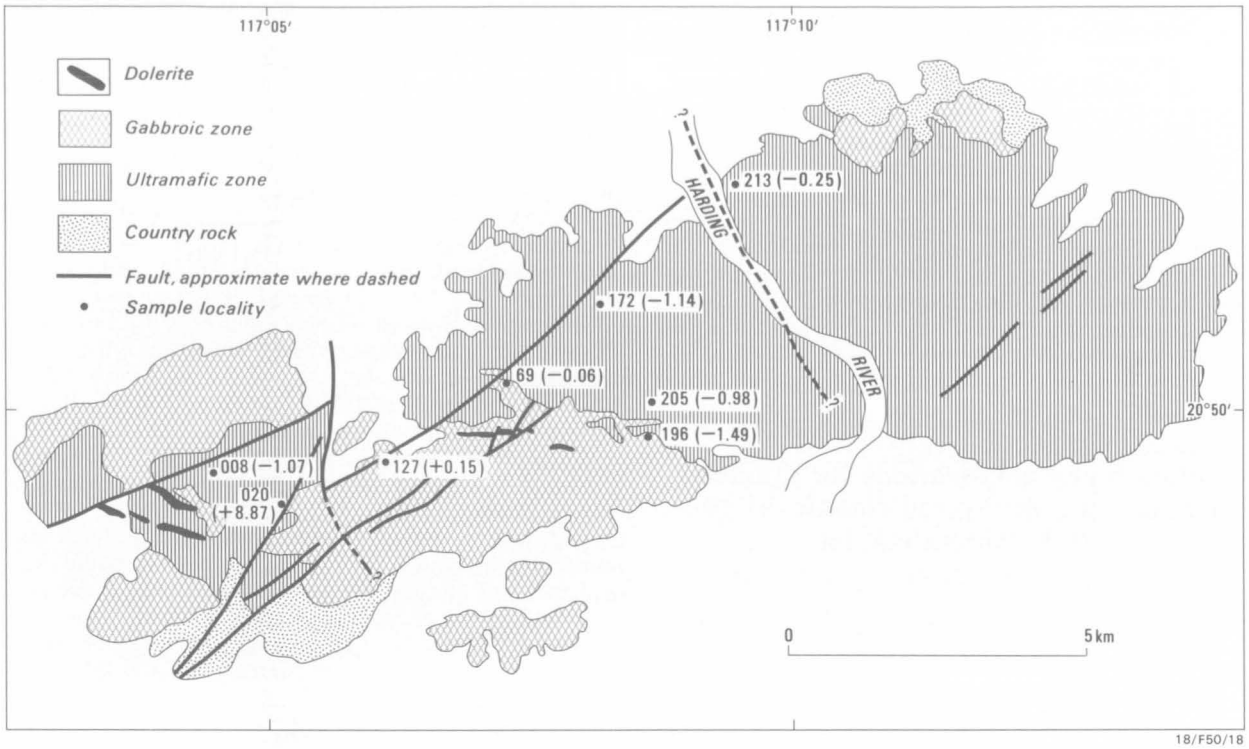

Fig. 100. Locations of samples used for isotope analysis from the Andover Complex (initial εNd values in brackets).

chemical and mineralogical trends observed in the GZ suggest a closed-system magma differentiation. To account for the magma-mixing effect, it is expected that εNd variations in the magma pulses were greater than the 0.7 unit observed. Sample 045 (1811 m), at the base of the PWL, with the lowest initial εNd (−0.65), probably represents a cumulate derived from a magma pulse starting at ~ 1745 m. Above this level, an iron-enrichment trend is maintained to the PWL. Sample 094 (1846 m) from the top of the PWL has the same initial εNd value as the GZ. These Nd isotope data seem to support the hypothesis that the bulk of the PWL is derived from a hybrid mixture between the resident magma which formed the UZ, and a new pulse of magma which generated the GZ.

To be consistent with the Zr/Nd criterion discussed above, Nd isotope data for the Munni Munni Complex could be interpreted in terms of the models proposed by Hoatson & Keays (1989; a modified version of Model 1 is shown in Fig. 104) and Barnes & others (1990; in press). A steady-state small magma chamber was maintained during formation of the UZ, by frequent injections of magnesium-rich (M type) SHMB, with Zr/Nd ~ 3.5 and tapping of the resident magma out of the chamber. A major influx of more fractionated gabbroic magma (G type), also genetically related to SHMB with Zr/Nd ~ 5.5, formed a fountain and inflated the small magma chamber and induced magma mixing, which resulted in the formation of the mineralised PWL. In terms of this model, PGE mineralisation in the PWL may either be derived from the residual, resident, PGE-fertile M magma or the new influx of G magma. On the basis of Zr/Nd ratios (~ 5.5) the Cadgerina Dyke is considered to be derived from the G magma. Chilled sample 172 of the Cadgerina Dyke is fertile in Pt, Pd, and Au (Hoatson & Keays, 1989), suggesting derivation from a S-undersaturated fertile magma. This and neighbouring chilled and cumulate samples, however, have higher MgO contents and mg numbers than would be expected for the G magma responsible for the GZ cumulates. Since the total GZ sequence is S-saturated, it seems likely that the resident residual M magma was the main source of the PGE mineralisation. However, if the earlier influx of G magma had a composition similar to the Cadgerina Dyke, then the G magma contribution to PGE mineralisation could have been more important.

Neodymium isotope data for the Andover Complex: a comparison with the Munni Munni Complex

With the exception of the Zr/Nd ratio, the Andover 'chilled' rocks have very similar major and trace-element spidergrams to 'chilled' rocks of the Munni Munni Complex (Fig. 99). A genetic connection can be suggested. In contrast to the Munni Munni Complex, crystallisation of orthopyroxene generally preceded clinopyroxene in cumulates from the UZ, which suggests that their SHMB parent magmas were more siliceous.

Except for a dolerite dyke (86330020), initial εNd values for eight samples from various parts of the Andover Complex (Fig. 100 & Table 27) range from +0.1 to −1.1. The dolerite dyke had a prohibitively high εNd at 2.93 Ga of +8.9, and is thus clearly younger (possibly ~ 2.0 Ga; with initial εNd +3.1) and not related to the Andover Complex. Initial εNd values of −0.99 and −1.06 for two websterite samples (87330205 and 86330008) are lower than for websterites (−0.2 to −0.7) from the Munni Munni Complex. This is consistent with the idea that their parent magmas may have assimilated more felsic crustal material. A norite sample (196) near the contact of the zones (Fig. 100) has an initial εNd value of −1.49, similar to the websterites, and chemical and mineralogical affini-

ties to the websterites (see p. 136). A clinopyroxenite sample (88330213) containing cumulus clinopyroxene and intercumulus orthopyroxene has an initial εNd value of −0.24, comparable with the Munni Munni Complex. Initial εNd values of +0.2 and −0.1 for two gabbronorites (87330127 and 86330069) are considerably higher than for the underlying websterite (−1), but similar to clinopyroxenite from the Andover Complex and gabbronorites from the Munni Munni Complex GZ. If these different values are not caused by the pervasive alteration in the Andover Complex, they would argue against a direct differentiation relationship between the GZ and UZ. The Andover Complex GZ may represent a separate influx of G-type magma similar to that proposed for the Munni Munni Complex.

Genetic connection between M and G magma types: implications for different magma types of layered complexes and PGE mineralisation

The concept of U (ultramafic) and A (anorthositic) magma types is well established for the Bushveld and Stillwater complexes (e.g. Barnes & Naldrett, 1986; Lambert & Simmons, 1987, 1988). The U-type magma is responsible for the lower ultramafic zones and its chemical composition is most likely to be magnesium-rich (i.e. M-type) tholeiite or picrite (Barnes & Naldrett, 1986). Thus, the main contrast between U-A and M-G magma-type associations is between A- and G-type magmas. In the present study a petrogenetic connection between M and G magma types for the Munni Munni Complex has been established. It is tempting to suggest that a genetic connection also exists between the U and A magma association observed in other layered complexes. Such a connection has in fact already been proposed by Barnes & Naldrett (1986). They suggested that in a deep-level magma chamber, under high pressures (> 6 kb), plagioclase crystallisation will be retarded in M-type magma and lead to plagioclase enrichment in the more evolved residual magma. This A-type magma is then available for later injection to a higher-level magma chamber. This suggestion was supported by a study of the ~ 1.2 Ga Giles intrusions of central Australia by Gray (1987) and a Pb isotope study of the Stillwater Complex (Wooden & others, 1991). Anorthositic layers become more abundant towards the top of the Giles intrusions (AGSO Project 211.14), which were emplaced into the continental crust at ~ 20 km depth (6–7 kb). The increase in anorthosite is accompanied by a decrease of $^{87}Sr/^{86}Sr$ initial ratios from 0.708 to 0.704 (Gray, 1987), and an increase of initial εNd values from −2 to +2 (Sun, unpublished data), as a result of progressive reduction of magma-wallrock interaction. In the Stillwater Complex, Wooden & others (1991) showed that samples from different stratigraphic levels have the same Pb isotope compositions, despite variations of initial Sr, Nd, and Os isotope compositions (e.g. Lambert & others, 1989; 1991). It is likely that the added crustal component, through subduction or crustal contamination, affected the isotopic compositions of different elements to varying extents (with Pb most affected), depending on the abundance of each element in the contaminant and in the evolving magma.

The difference between M-G and M-A type magma associations may be related to their Al-depleted (Munni Munni) versus Al-normal komatiitic parent magma derived from the mantle. Density differences between the A- and G-type magmas may result in contrasting fluid dynamics (plume versus fountain?) during their injection into the magma chamber.

A genetic connection between U-M and A-G magma types also has implications for PGE mineralisation in layered complexes. To generate Merensky Reef-style mineralisation, PGE-fertile, S-undersaturated magma, either resident or newly injected, is required. Since A- and G-type magmas are more fractionated than their associated U- and M-type magmas, they are more likely to be S-saturated, and contain less PGEs, and consequently are less likely to be the PGE source for the mineralisation. However, if new input of A or G magma is S-undersaturated and less fractionated than the resident magma, it may be a potential source of PGE mineralisation (e.g. Naldrett & von Gruenewaldt, 1989). Recently Os isotope studies of the Stillwater and Bushveld complexes by Lambert & others (1989, 1991) and McCandless & Ruiz (1991) suggest that A-type magmas may be the main PGE source for the J-M Reef, UG-1 chromitite and Merensky Reef mineralisation. Such an interpretation, however, is not unique: Os could be depleted and decoupled from Pt and Pd under S-undersaturated conditions through crystallisation of olivine and chromite. Thus, Os isotope compositions do not necessarily reflect the source of Pt and Pd.

Conclusions

When Nd isotope data are combined with geochemistry, mineralogy and field relationships, it is suggested that the west Pilbara intrusions belong to a cogenetic suite that was emplaced into the crust at about 2.93 Ga. Although this Nd isotope study has no direct application to PGE exploration, it constrains the genetic models of these intrusions and is an important tool for better understanding the regional distribution and processes involved in PGE mineralisation.

It has been demonstrated that SHMB parent magmas for the west Pilbara ~ 2.93 Ga layered complexes were most likely derived from Al-depleted komatiites with 'normal' mantle PGE abundances and Ti/Pd ~ 3×10^5. The komatiites are believed to have been contaminated by ~ 3.3 Ga early Archaean tonalitic to granodioritic crust before being emplaced into the high-level magma chambers. These resulting SHMB magmas were fertile in Pd (15–20 ppb), Pt (10–15 ppb), and Au (2–4 ppb), which behaved incompatibly during magma generation and crustal assimilation under S-undersaturated conditions. The age of the Munni Munni Complex (2927 ± 13 Ma) has been determined by an Sm/Nd isotope study of mineral separates of three samples and the results agree well with the U/Pb zircon age of 2925 ± 16 Ma reported by Arndt & others (1991). Samples from the UZ and GZ of the Andover Complex have consistently different initial εNd values (−1.0 versus 0.0, respectively), suggesting that they cannot be directly related by magmatic differentiation in the magma chamber. Two magma types, M (magnesium) for the UZ and G (gabbroic) for the GZ, are proposed. In the case of the Munni Munni Complex, despite the similarity in Nd isotope compositions, inferred parent magma compositions for the UZ and GZ have quite different Zr/Nd ratios (3.5 versus 5.5), suggesting a situation similar to the Andover Complex. Different magma pulses during generation of the lower 1850 m-thick UZ show minor, but experimentally reproducible, variations of initial εNd values. At the base of the 20–80 m thick PWL, a new magma pulse with a low initial εNd value (< −0.6) was introduced into the magma

chamber which contained a resident magma with a higher initial εNd value (> -0.3). This new magma pulse may have triggered instability in the chamber and resulted in magma mixing, leading in turn to S-saturation and PGE mineralisation near the top of the PWL. Nearly constant initial εNd values (-0.2) and Zr/Nd ($\sim$ 5.3) characterise the overlying GZ. These results support the conclusion reached on p. 54 that closed magma differentiation conditions largely prevailed above the PWL.

These chemical and Nd isotope data support a model in which a steady-state, small magma chamber was maintained during formation of the UZ under S-undersaturated conditions by frequent injections of SHMB with Zr/Nd $\sim$3.5, and tapping of the residual magma out of the chamber. A major influx of more fractionated, gabbroic magma related to the SHMB, with Zr/Nd $\sim$ 5.5, inflated the small-magma chamber and induced magma mixing, and formed the mineralised PWL and the GZ. In terms of this model, PGE mineralisation in the PWL may either have been derived from the residual, resident, PGE-fertile M-magma or the new influx of G-magma. On the basis of its Zr/Nd ratio, the Cadgerina Dyke is considered to be derived from the G-magma. Chilled samples of the Cadgerina Dyke are fertile in Pt, Pd, and Au, suggesting derivation from a S-undersaturated magma. Chilled and cumulate rocks of the dyke, however, have MgO contents and mg numbers for mafic minerals higher than would be expected for the G-magma responsible for the GZ cumulates. Since the total GZ sequence is S-saturated it seems likely that the resident, residual M-magma was the main PGE source for mineralisation. However, if an earlier influx of G-magma had a composition similar to the Cadgerina Dyke, G-magma contribution to PGE mineralisation could have been more important.

The association of M- and G-magma types for the Munni Munni and Andover complexes is analogous to the U (ultramafic) and A (anorthositic) magma association suggested for the Stillwater and Bushveld complexes. On the basis of isotope and petrological studies of the Giles intrusions, central Australia, and the Stillwater Complex it is suggested that the different magma types originated from a common parent magma, in each case through magmatic differentiation and assimilation that took place deep in the crust. A genetic connection between U-M and A-G magma types also has implications for PGE mineralisation in layered complexes. To generate Merensky Reef-style mineralisation, PGE-fertile, S-undersaturated magma, either resident or newly injected, is required. It has been shown that Archaean S-undersaturated SHMB generally have Pt and Pd $\sim$ 15 ppb and Ti/ Pd $\sim 3 \times 10^5$. Since A- and G-type magmas are more fractionated than their associated U and M types they are more likely to be S-saturated, contain less PGEs, and, consequently are less likely to be the main source for PGE mineralisation.

PETROGENESIS OF THE WEST PILBARA LAYERED MAFIC-ULTRAMAFIC INTRUSIONS *(DMH, S-SS, & RRK)*

Introduction

The major layered mafic-ultramafic intrusions of the west Pilbara Block are believed to be genetically related, and, together with a slightly younger easterly-trending suite of large mafic dykes (Eastern Munni Munni and Zebra Hill), record a period of extensive mafic magmatism during the evolution of the west Pilbara Block in the late Archaean. The age of the intrusions (~ 2925 Ma) implies prolonged stabilisation (about 160 Ma) of the western parts of the Pilbara craton before deposition of the basal ~ 2765 Ma Fortescue Group of the Hamersley Basin platform sequence. Fitton & others (1975) grouped many of these Pilbara intrusions into one major complex, the 'Millindinna Complex'; they believed that this extensive differentiated complex, covering 40 000 km^2, was emplaced along a regional unconformity between upper and lower Archaean cratonic successions. However, the results of the present study indicate that the magmas which formed the west Pilbara intrusions were emplaced along unconformities and major lithological contacts of metavolcanic sequences or between granitic and metavolcanic sequences (i.e. at different levels in the upper crust) and experienced different amounts of crustal contamination; thus the concept of a single intrusive sheet occupying one particular stratigraphic level should be rejected.

The different settings of sulphide mineralisation in the west Pilbara intrusions show that the timing and mechanism of the S-saturation event are critical in the development of PGE-enriched sulphide-bearing units in layered intrusions. Field relationships and geochemical trends indicate that PGE mineralisation in the Munni Munni Complex resulted from crystal fractionation and magma mixing in a chamber that involved both S-undersaturated and S-saturated magmas, whereas in the Radio Hill and Mount Sholl intrusions gravitational and structural controls were important for the concentration of Ni-Cu sulphides from magmas which had an early history of S-saturation.

The Munni Munni Complex is one of the best preserved Archaean layered mafic-ultramafic intrusions in Australia. Although it is broadly similar in geological setting to the major PGE-bearing layered intrusions overseas, such as the Bushveld and Stillwater complexes, the Munni Munni Complex has several contrasting features that are significant for the classification of mineralised layered intrusions as a whole. These include the geometry of the intrusion, the fractionated nature of the parent magma, the early crystallisation of clinopyroxene relative to orthopyroxene, the rarity of chromitite layers, and the stratigraphic level of PGE enrichment. With respect to the other west Pilbara layered intrusions, the Munni Munni Complex is atypical in its S-undersaturated ultramafic cumulate sequence and PGE mineralisation. The following section covers some of the more important genetic points that relate to this intrusion.

Munni Munni Complex

Evidence for magma mixing at the ultramafic/gabbroic zone contact

Rocks in subzone I are markedly different mineralogically and texturally from the underlying cumulates of the ultramafic zone. These differences include the appearance of cumulus orthopyroxene at the expense of cumulus olivine, introduction of spinel-rich cyclic units, increasing prominence of intercumulus plagioclase, biotite, and sulphides, and the transition from equigranular adcumulates and mesocumulates to porphyritic orthocumulates. Field and mineralogical evidence suggests that some of these features can be explained by the mixing of M (parent magma to ultramafic zone) and G (parent magma to gabbroic zone) magmas (see previous chapter) at the ultramafic/gabbroic zone contact. Some of the various features that suggest magma mixing are described below:

(1) The mineralised porphyritic plagioclase websterite layer is a poorly-layered horizon which closely parallels the zone contact, across the width and up the sides of the intrusion (see appended map sheet). This is consistent with the genesis of a hybrid, mixed zone at the interface between the ultramafic and gabbroic zones. Platinum-group elements are enriched in the upper levels of the porphyritic websterite layer and this enrichment shows no temporal or spatial relationship with cyclic units.

(2) The base of the porphyritic websterite layer is discordant with the regional arcuate layering trends in the ultramafic zone (Fig. 12), indicating magmatic erosion may have occurred in the upper parts of the ultramafic zone.

(3) Various mafic and ultramafic rock types form interfingering lenses and pods in the upper parts of the porphyritic websterite layer (Fig. 12) and thicken and thin markedly along strike. These laterally diverse and lensing rock types, which are also seen in the J-M Reef of the Stillwater Complex (Bow & others, 1982; Irvine & others, 1983), are interpreted to have formed from small components of M- and G-magmas that did not homogenise during the main mixing cycle.

(4) Rock relationships (Figs 13B–D) interpreted as reflecting magma mixing are confined to the upper part of the porphyritic websterite layer. These features, which are not seen at any other stratigraphic level in the intrusion, include narrow discontinuous websterite layers with cuspate lower surface and flat upper surface, detached and partly assimilated websterite blocks invaded by G-magma, and pods of mixed rock consisting of irregular discontinuous orthopyroxenite layers in norite.

(5) Laminated textures in the basal gabbronorites of the gabbroic zone may be related to the turbulent mixing of magmas that occurred directly below, or may be the result of movement along the contact soon after emplacement of the G-magma. The textures suggest that the deformation occurred when the G-magma was in a fluid or semi-fluid state.

(6) Thin, spinel-bearing orthopyroxenite lenses and elongated blocks are enclosed by the mineralised websterite layer of subzone I close to the ultramafic/gabbroic zone contact. The spinels have unusual aluminous and Cr-poor (~ 49% Al_2O_3 and ~ 14% Cr_2O_3) compositions. Irvine & Sharpe (1986a,b) have shown that the mixing of an A (anorthositic)-type magma with a U (ultramafic)-type magma can drive the hybrid magma into an aluminous spinel crystallisation field. However, the spinels are unlikely to have formed as a result of magma mixing since coexisting orthopyroxene compositions are inconsistent with their stratigraphic level in the ultramafic zone. The mg (87–85) of these orthopy-

roxenes represents the most primitive composition of any orthopyroxene in the intrusion, and is particularly anomalous when contrasted with orthopyroxene of mg_{75-64} in the enclosing porphyritic websterite layer. The strongly adcumulus character and layering fabrics of the orthopyroxenites suggest they are of cumulus origin, but they did not crystallise *in situ*. They are interpreted as accidental blocks that were incorporated into the mineralised websterite layer from higher levels in the chamber during magma mixing. Smaller recrystallised gabbroic xenoliths are also associated with the orthopyroxenite blocks and collectively form a slump-like deposit concentrated in the central part of the intrusion.

(7) Cumulus clinopyroxenes show marked changes in mg across the ultramafic/gabbroic contact. Over the stratigraphic interval 1810–1849 m there is a consistent decrease in mg from 84 to 58, but at the 1850 m level (base of gabbroic zone) the mg jumps abruptly to 75. This abrupt reversal is unlikely to reflect normal fractionation, but it may reflect the protracted crystallisation of clinopyroxene in localised pockets of magma that became trapped beneath the plagioclase-rich cumulates of the gabbroic zone. The trapped magma was possibly driven upwards by the filter pressing of the hybrid magma and continued to fractionate in stagnated conditions well after the crystallisation of the surrounding cumulates.

(8) The Pt/Pd ratio in the complex generally decreases with increasing stratigraphic height (Fig. 60). The most prominent reversals in Pt/Pd occur in the stratigraphic interval 1700 to 2250 m, i.e. centred around the mineralised websterite layer. These reversals may be caused by a new magma pulse and subsequent magma mixing or may reflect subtle differences in the behaviour of Pt and Pd under S-undersaturated and S-saturated conditions. Page & others (1972, 1976, 1980) noted increasing Pt/(Pt + Pd) ratios up the Stillwater and Fiskenaesset sequences, whereas Page & others (1982) noted a general decrease up the Bushveld sequence, as well as reversals at various mineralised units. They interpreted the reversals as indicating possible new batches of magma having different relative concentrations of Pt and Pd.

Composition of the parent magma for the ultramafic zone

The whole-rock compositions of chilled-margin samples, the high incompatible-element contents of cumulates throughout the ultramafic zone (Fig. 58), the most primitive olivine and clinopyroxene compositions in the intrusion, and the PGE ratios in the mineralised layer, all indicate that the parent magma to the ultramafic zone (M magma) was more mafic than ultramafic. Its mafic character is highlighted by the analyses of nine chilled olivine plagioclase websterite and gabbronorite samples from the northern (basal) contact of the ultramafic zone and northwestern contact of the Cadgerina Dyke feeder zone (Appendix 3). Samples 85770167, 170, 172, and 179 are believed to be the closest approximations to liquid magma compositions (some of the other chill samples have a minor cumulus clinopyroxene component, as shown by their high CaO/Al_2O_3 ratios and Cr and Sc contents). The mean average analysis of these four samples is given in Table 29.

Some of the data in Table 29 is similar to that of the boninite-type parental magma of the Bushveld Complex (B1 group of the marginal rocks of Hatton & Sharpe, 1989), e.g. high in SiO_2 (52–56%), MgO (10–16%), Cr (600–1500 ppm) and incompatible elements Rb (20–50 ppm) and Zr (60–110 ppm). However, boninites typically have lower Sr (150–200 ppm), TiO_2 (0.1–0.4%), Na_2O (1.50–1.75%), total FeO, and Ti/Zr than the Munni Munni marginal rocks. The compositions of the Munni Munni chill rocks show a greater similarity to an Al-poor, siliceous, high-magnesium basalt (SHMB) of komatiitic affinity. They show a striking resemblance in composition to the Barberton-type basaltic komatiites of South Africa, various Archaean quench-textured high-Mg basalts from the Pilbara Block (Nesbitt & others, 1979; Glikson & others, 1986), and chilled rocks from the Radio Hill and Mount Sholl intrusions (Table 30).

Sun & others (1991) have postulated that the late Archaean layered intrusions of the west Pilbara were derived from komatiite parent magmas by a combination of crustal contamination and fractional crystallisation. On the basis of Nd isotope data the contaminants are believed to have been felsic basement rocks, e.g.

Table 29. Estimated composition of the parent magma to the ultramafic zone of the Munni Munni Complex

	Mean (%)	*Range (%)*		*Mean (ppm)*	*Range (ppm)*
SiO_2	52.70	51.82–53.23	Ba	673	461–906
TiO_2	0.83	0.79–0.87	Rb	38	35–45
Al_2O_3	9.25	7.89–9.96	Sr	310	275–350
Fe_2O_3	1.94	1.22–3.46	Pb	7	6–8
FeO	9.91	8.61–10.47	Th	3	< 1–4
MnO	0.21	0.20–0.24	Zr	82	56–94
MgO	9.80	8.42–12.48	Nb	3	2–4
CaO	9.96	9.42–10.47	Y	17	14–19
Na_2O	2.63	2.34–2.99	La	17	14–18
K_2O	0.87	0.64–0.98	Ce	34	30–37
P_2O_5	0.07	0.05–0.08	Nd	16	15–17
LOI	1.63	1.51–1.79	Sc	24	21–26
100 × Mg/(Mg + Fe*)	59.6	56.5–65.5	V	169	154–181
			Cr	489	231–1153
			Co	63	62–67
			Ni	366	290–494
			Cu	149	143–159
			Zn	101	95–106
			Ga	13	11–14
			S	603	387–871
			Cs	10	6–14

* Total Fe. LOI = loss on ignition. Estimated composition is the mean average analysis of the four most representative chill samples (85770167, 170, 172, 179).

Table 30. Comparison of chilled rocks having siliceous high-magnesium komatiitic affinities

	Barberton-type basalts[1]	*Radio Hill chill*[2]	*Mount Sholl chill*[3]	*Munni Munni chill*[4]
SiO_2	52.73	53.4	53.4	52.70
TiO_2	0.85	0.8	0.9	0.83
Al_2O_3	9.83	9.1	10.1	9.25
Fe_2O_3	1.23	1.8	1.4	1.94
FeO	9.70	10.4	10.0	9.91
MnO	0.22	0.2	0.2	0.21
MgO	10.10	9.9	9.4	9.80
CaO	9.99	11.7	10.9	9.96
Na_2O	2.65	2.1	2.9	2.63
K_2O	0.46	0.5	0.5	0.87
P_2O_5	0.06	0.1	0.1	0.07
S	—	—	0.2	0.06
H_2O^+	1.87	2.1	1.9	1.69
100Mg/(Mg + Fe*)	62	60	60	60
CIPW norms				
Quartz	0.4	1.8	0.0	0.0
Orthoclase	2.8	2.9	3.0	5.2
Albite	22.9	17.8	24.6	22.7
Anorthite	13.9	13.9	13.1	11.1
Diopside	29.6	35.5	33.0	31.6
Hypersthene	25.9	23.4	20.3	23.3
Olivine	0.0	0.0	1.4	1.4
Magnetite	2.7	2.9	2.8	2.9
Ilmenite	1.6	1.5	1.7	1.6
Apatite	0.1	0.2	0.2	0.2

1—Viljoen & Viljoen (1971); 2—Richardson (1976); 3—Mathison & Marshall (1981); 4—average of four chill samples from this study; *—Total Fe; CIPW norms calculated by Hoatson. —= not determined.

possibly tonalites of early Archaean age. Sun & others (1991) believe the SHMB magmas that formed from these processes contained 9–15% MgO, Barberton-type low Al ($Al_2O_3/TiO_2 \sim 11$, i.e. about half chondrite concentrations), 14–24 ppm Sc, and 10–18 ppm Y, and were enriched in light-rare-earth elements (REE) relative to heavy REE (chondrite-normalised La/Sm ~ 2.7, La/Lu ~ 9).

The similar parent-magma compositions of the Munni Munni, Mount Sholl, and Radio Hill complexes strongly supports the suggestion that these intrusions are genetically related. However, the Andover Complex is characterised by the early crystallisation of orthopyroxene relative to clinopyroxene, the presence of chromite, and anorthosite in the upper parts of the cyclic units of the ultramafic zone. The orthopyroxene-chromite association suggests that the Andover parent magma was contaminated by felsic-crustal material and the anorthosites are believed to reflect more protracted crystal fractionation processes in the ultramafic zone compared to the other west Pilbara intrusions. Neodymium studies (p. 147) suggest that the parent magma of the Andover Complex was more crustally contaminated than the parent magma of the Munni Munni Complex.

Sun & others (1989) have noted that there are major chemical differences between Archaean SHMB and modern boninites. They concluded that the mantle sources of the former rocks are much less refractory than those of boninites. Siliceous high-magnesium basalts with 10–12% MgO have higher total FeO (10% versus 6%) and higher abundances of heavy REE and Y (15 ppm versus 8 ppm) than boninites. In addition, Al-normal and Al-depleted SHMB have Al_2O_3/TiO_2 of 20–30 and ~ 10, respectively, and Sc/Y of 2–3, whereas boninites have much higher ratios of 30–60 and 5–8 respectively, indicating a highly refractory source. Green (1975), Sun & Nesbitt (1978), and Arndt (1986) have suggested that during the generation of komatiitic magmas at high pressures, garnet (majorite) may separate from the magma. This would result in the depletion of Al, heavy REE, Y, and Sc in the residual magma and would account for the depletion in Al of the parent magmas that formed the ultramafic components of the west Pilbara layered intrusions (e.g. Al_2O_3/TiO_2 of 11 for Munni Munni). The paradoxical combination of high silica in the komatiitic magmas (reflecting low-pressure conditions) and depletion of elements favoured by garnet (reflecting high-pressure) suggests that the magmas were contaminated by crustal components (Sun & others, 1991).

Barnes (1989) has used whole-rock major- and incompatible-element plots of samples believed to represent liquid compositions to highlight different compositional features of Bushveld ultramafic-type parent magmas, boninites, and SHMB from around the world. Although there is some overlap in composition, the plots illustrate broad geochemical differences (Fig. 101). Most of the Munni Munni chill samples fall within the SHMB field, although some with slightly higher SiO_2 and lower TiO_2 relative to MgO fall in the ultramafic field. The variation diagrams also show that the Munni Munni chilled rocks have low Al_2O_3 relative to TiO_2 compared to other SHMB and have contrasting major- and trace-element geochemistry to that of boninites.

Experimental studies on both terrestrial basalt (Roeder & Emslie, 1970; Ford & others, 1983) and lunar basalt (Longhi & others, 1978) have shown that the Fe^{2+}/Mg partitioning between olivine and liquid $((Fe^{2+}/Mg)_{olivine} / (Fe^{2+}/Mg)_{liquid})$ is equal to 0.3 ± 0.03 and is largely independent of temperature and magma composition. This means that the most primitive olivine compositions in the Munni Munni ultramafic zone can be used to constrain the mg ratio of the zone's parent magma. Liquid in equilibrium with the most primitive olivine analysed in the complex (mg_{83}) would have a 100Mg/(Mg + Fe) ratio of 59, which is almost identical to the mg of the proposed parent magma detemined from the averaged composition of the chill rocks ($mg_{59.6}$ in Table 29). This shows that the proposed M-magma

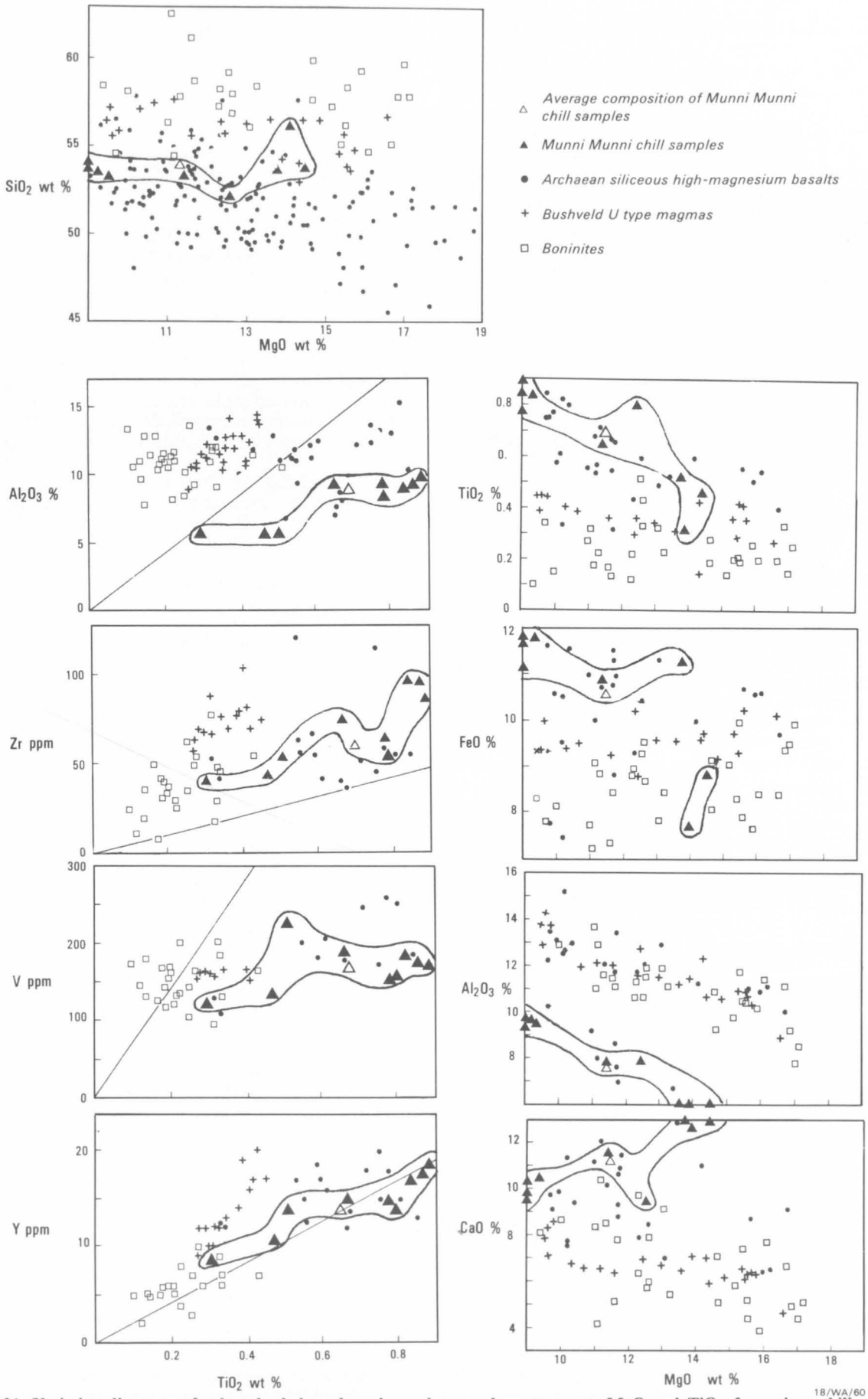

Fig. 101. Variation diagrams of selected whole-rock major and trace elements versus MgO and TiO_2 for various chill rocks believed to represent liquid compositions. Data for the boninites, siliceous high-magnesium basalts, and Bushveld U-type magmas are from Barnes (1989). Diagonal lines show chondritic ratios assumed to be representative of undepleted upper mantle. Modified from Barnes (1989).

was capable of crystallising such fractionated olivine. Olivine in the basal chill zone of the ultramafic zone (average mg_{73}) is predicted to have crystallised from a parent magma of mg_{45}. For lower K_d values of 0.27 that have been determined in glass-microphenocryst pairs in MORB-type rocks (Bryan & Moore, 1977; Rhodes & others, 1979), the mg of the parent magma that would have crystallised the most primitive olivine in the Munni Munni Complex would have been 57. The Munni Munni M magma with an mg of 59 ± 2 was considerably more fractionated than the magmas that formed other major layered intrusions (Table 36). This is also illustrated by the most primitive olivine compositions documented in these intrusions, namely: Fo_{90}—Bushveld (Cameron, 1980), Fo_{88}—Stillwater (Todd & others, 1982), Fo_{92}—Great Dyke (Wilson, 1982), Fo_{91}—Panton Sill (Hamlyn & Keays, 1979; Hamlyn, 1980), Fo_{89}—Wingellina Hills (Ballhaus & Glikson, 1989), and Fo_{84}—Lac des Iles (Sutcliffe & others, 1989).

The mg at which olivine is replaced by orthopyroxene provides a qualitative estimate of the degree of silica saturation and some indication of the chemical affinity of the parent magma. In their study of the Wingellina Hills intrusion, Giles Complex, central Australia, Ballhaus & Glikson (1989) noted that the compositions of the most evolved olivines, just before orthopyroxene becomes a liquidus phase at the expense of olivine, is Fo_{78-77}. This compares very closely to the Munni Munni Complex, where the mg of the most evolved olivine determined from the 1695 m stratigraphic level is 78. This is a maximum value since olivine is not replaced by cumulus orthopyroxene until about the 1800–1830 m level. In other mafic-ultramafic bodies, olivine in the Bushveld Complex and Great Dyke ceased to crystallise at an mg of around 85 (Cameron, 1982; Wilson, 1982), and in smaller, more alkaline, intrusions, such as Fongen-Hyllingen and Skaergaard, olivine persists to Fo_{71} and Fo_{54}, respectively (Wager & Brown, 1968; Wilson & others, 1981). This suggests that the silica activity of the Munni Munni M magma may have been similar to that at Wingellina Hills, but significantly lower than that in the Bushveld Complex and Great Dyke.

High (Pt + Pd)/(Ir + Os + Ru) ratios of 15 to > 135 (Table 14) in the PGE-rich zone of the mineralised websterite layer are consistent with Naldrett & Duke's (1980) suggestion that sulphides that have segregated from gabbroic or basaltic magmas have (Pt + Pd)/(Ir + Os + Ru) of > 13, while ultramafic komatiitic magmas with > 20% MgO have ratios of < 2. Naldrett & Duke (1980) propose that the (Pt + Pd)/(Ir + Os + Ru) ratio of the sulphide reflects the degree of partial melting involved in producing the parent magma, because, under S-undersaturated conditions, Pt and Pd are preferentially incorporated in early partial melts, whereas Ir, Os, and Ru are largely retained in residual olivine in the mantle.

The S-saturated gabbronorites along the base of the ultramafic zone contain elevated Pt (15.0–35.0 ppb), Pd (57.5 ppb), Au (4.79–5.06 ppb) and Cu (843–1575 ppm) contents, indicating that the M magma contained appreciable amounts of these elements. However, these marginal rocks do not necessarily give an accurate indication of the PGE content of the parent magma, since localised processes such as S-saturation along the contacts will significantly concentrate PGEs; moreover, they may not represent true melts since they commonly contain a significant cumulus component. More reliable estimates of the PGE content of the parent magma were determined by three independent normalising procedures using weakly fractionated, S-undersaturated mesocumulates in the 200–700 m stratigraphic interval of the ultramafic zone. The methods involved the following:

(1) Determining the porosities of the mesocumulates by point-counting the cumulus and melt components, and, by using these data, normalising the PGE concentrations of the cumulates to 100 vol.% melt. The unaltered mesocumulates used were not strongly modified by adcumulus growth, and estimates of the melt component are believed to be accurate to ± 5 vol.%.

(2) Comparing the concentration of an incompatible immobile element in the mesocumulates to its average concentration in the chill samples. Zirconium is ideal for this purpose since it has low partition coefficents of < 0.1 for olivine and pyroxene, is relatively stable during alteration, and is abundant in the chill samples (average concentration in nine chill samples is 62 ppm). The PGE concentrations of the mesocumulates were multiplied by the ratio 62/(Zr content of mesocumulate).

(3) Normalising the PGE concentrations of the mesocumulates by comparing the S contents of unaltered mesocumulates to the average S content of 530 ppm for the M magma, as determined by S/Se ratios (see pp. 155–156).

The precious-metal concentrations for the different methods are remarkably consistent, namely:

(1) 12.0 ppb Pt, 17.4 ppb Pd, and 2.5 ppb Au;
(2) 13.4 ppb Pt, 16.9 ppb Pd, and 2.4 ppb Au; and
(3) 13.7 ppb Pt, 17.5 ppb Pd, and 2.4 ppb Au.

Applying the same methods for Ir, a concentration of 5 to 10 ppb in the M-magma is indicated. However, this is about 10 times higher than the Ir contents of the fine-grained samples 85770167 and 179 (0.16 and 0.60 ppb, respectively), suggesting that Ir did not behave as an incompatible element during fractionation.

It is suggested that the parent magma of the ultramafic zone (M-magma) contained 10–15 ppb Pt, 15–20 ppb Pd, 2–3 ppb Au, 85–145 ppm Cu, 62 ppm Zr, and 530 ppm S. These values are similar to those reported by Davies & Tredoux (1985) for the magnesium-basalt parent magma (MgO ~ 12%) of the Bushveld Complex. The Zr content of the Munni Munni M-magma (average of nine chill samples is 62 ± 24 ppm) is comparable to the 40–80 ppm Zr that has been proposed for similar parent liquids in the Bushveld Complex (Sharpe, 1981) and the 50 ppm Zr for the Stillwater parent magma (Barnes & Naldrett, 1986).

Role of sulphur saturation during magma evolution

Sulphur solubility in a silicate melt increases with increasing temperature, FeO content, and fS_2, and with decreasing fO_2 and pressure (Haughton & others, 1974; Wendlandt, 1982). Haughton & others (1974) showed that the principal compositional control of S-solubility is the ferrous iron content of the magma. The maximum S-solubility for a basaltic melt at 1200°C was found to vary from 0.05–0.2% as the FeO content increased from 5–20%. These results were confirmed by a study of the S contents of submarine basalts by Czamanske & Moore (1977). They found the S contents of these basalts increased from 0.084 to 0.137% as their FeO increased from 8.0–12.6%. Buchanan & others (1983) found that at constant fO_2 and fS_2, the dissolved S content in a basaltic melt which contained 17% FeO increased by a factor of about 8.5 times per 100°C at

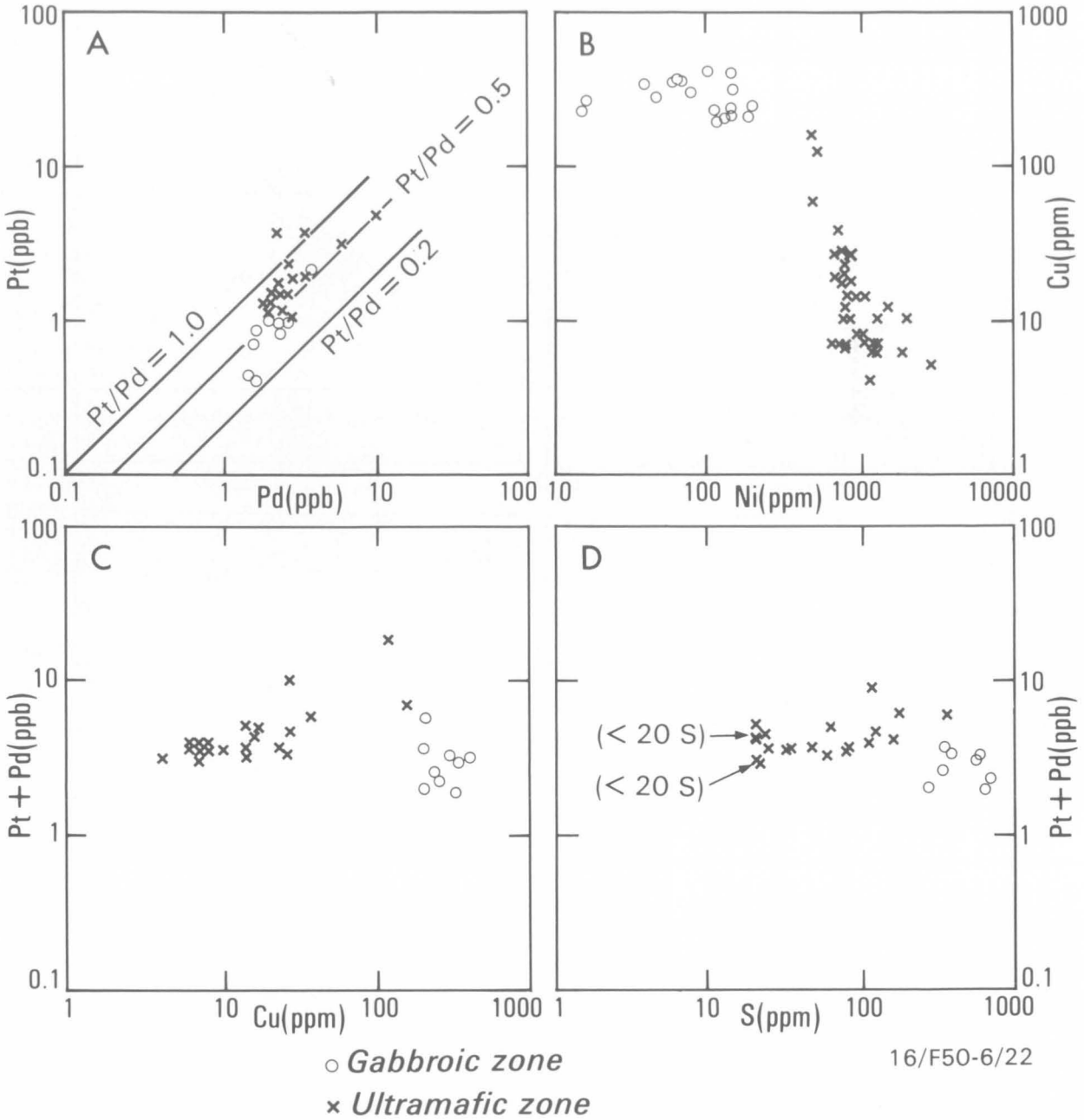

Fig. 102A–D. Munni Munni Complex: variations of Pt against Pd, Cu against Ni, Pt + Pd against Cu, and Pt + Pd against S for S-undersaturated ultramafic and S-saturated gabbroic rocks from the regional sample traverse.

1000°C, but by a factor of only 3 times per 100°C at 1400°C. These results are consistent with experiments by Haughton & others (1974) which showed that with each temperature rise of 100°C from 1000°C to 1400°C, the S-capacity of the magma increased by a factor of 5 to 7, assuming a constant ratio of fO_2 to fS_2. In their study of the system Fe-Si-S-O at 32 kb, Huang & Williams (1980) found that the miscibility gap between sulphide and silicate liquids expands with increasing pressure. This is supported by Wendlandt's (1982) experiments which indicate a negative relationship between S-solubility and pressure for melts of different FeO contents at a temperature of 1420°C.

To determine whether a cumulate rock has formed from a S-saturated magma requires a knowledge of both the amount of trapped intercumulus melt and the S content of the cumulate. For example, an adcumulate rock with 5 vol.% intercumulus material and 100 ppm S would have been formed from a tholeiitic magma at 1000°C with 100 ÷ 0.05 = 2000 ppm S, if all the S in the rock was contained in the intercumulus material. Hence, the magma would have been S-saturated. By contrast, a chilled magma having no cumulus component and 500 ppm S would probably have been S-undersaturated. In general, most mafic rocks containing > 1000 ppm S have formed from S-saturated magmas (Hoatson & Keays, 1989). It should be emphasised that this method provides a crude estimate of the original S content of the melt since S is very mobile during alteration and postcumulus processes.

A more reliable semi-quantitative estimate of the S content of the primary magma can be obtained by evaluating porosities in association with S/Se ratios of cumulates. The intercumulus component of unaltered ultramafic cumulates from subzones A to H of the Munni Munni Complex averages about 12 vol.% (from

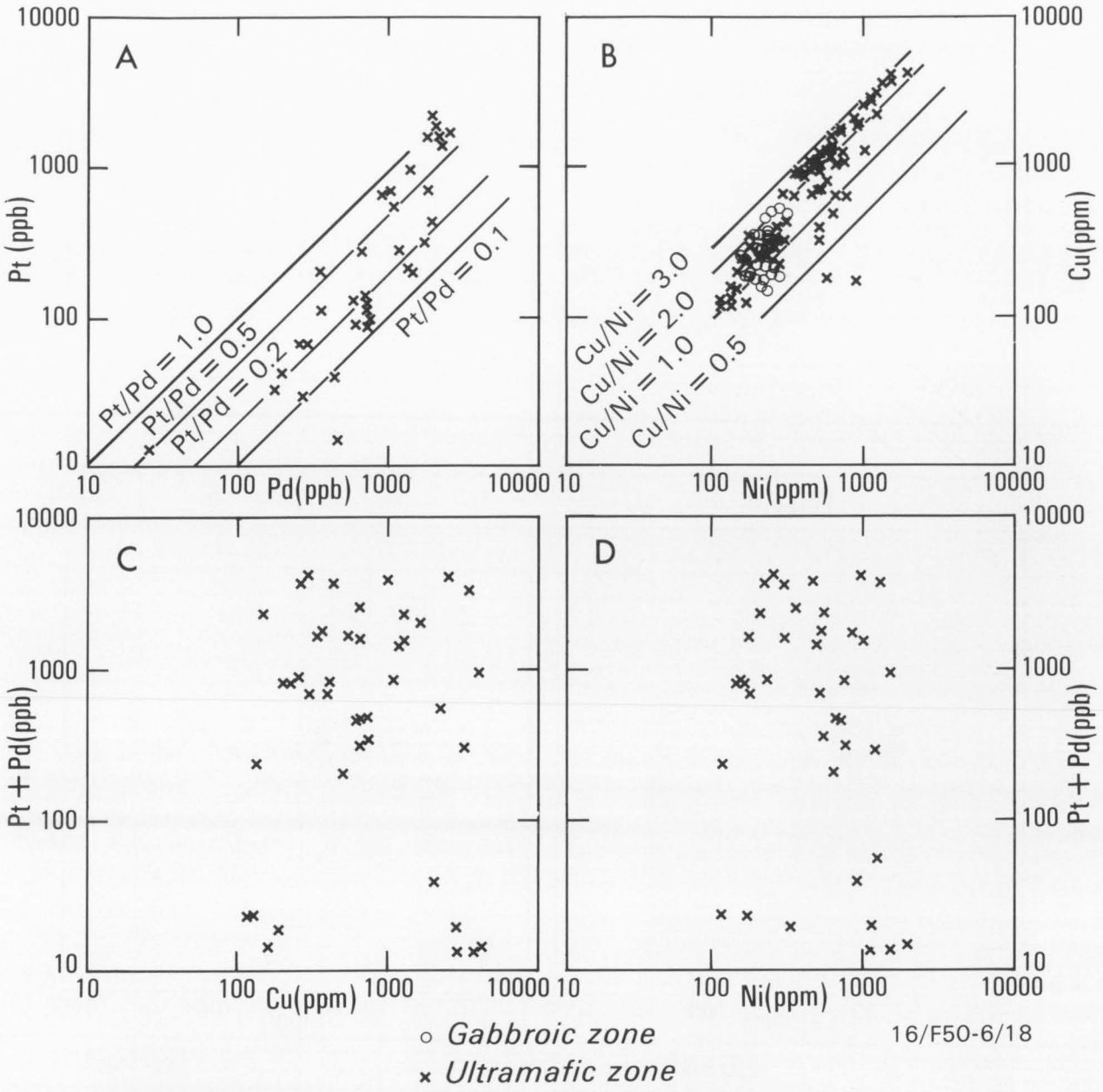

Fig. 103A–D. Munni Munni Complex: variations of Pt against Pd, Cu against Ni, Pt + Pd against Cu, and Pt + Pd against Ni for S-saturated ultramafic and gabbroic rocks in and near the mineralised zone (DDHs MMD 1 and MMD 5). Most gabbroic rocks have Pt + Pd contents ≤ 10 ppb and are not shown in A, C, and D.

modal point counts). The average S and Se contents of the mesocumulates is 62.6 ppm and 15.8 ppb, respectively. Assuming that the S/Se was initially 4000 (close to the average of most igneous rocks), then their original S content would have been about 63 ppm. Normalising to 100% melt, this is equivalent to about 530 ppm S for the M-magma. This is consistent with the averaged S content of the chill samples of the ultramafic zone (e.g. 600 ppm; see Table 29). In contrast, the gabbroic zone rocks have average S and Se values of 462 ppm and 127 ppb, an average S/Se ratio of 3610, and 20–30 vol.% intercumulus minerals. Assuming that the original S/Se ratio was also 4000, then the average S content would have been about 510 ppm. Normalising to 100% melt, this corresponds to approximately 1700–2600 ppm S. These S concentrations suggest that the G-magma was S-saturated, in contrast to the M-magma.

The different behaviour of Pt, Pd, Cu, and Ni in the S-undersaturated ultramafic rocks and the S-saturated ultramafic and gabbroic rocks is highlighted in Figures 102 & 103, respectively. Platinum/Pd ratios for S-undersaturated ultramafic cumulates (Fig. 102A) range from 0.4–1.7, whereas the S-saturated ultramafic (Fig. 103A) and gabbroic (Fig. 102A) cumulates range from 0.1–1.1 and 0.2–0.6, respectively. There is an increase in the Pt/Pd ratio with increasing Pd content for both groups of cumulates. For the S-undersaturated ultramafic cumulates, Cu shows a negative correlation with Ni (Fig. 102B), because Ni is partitioned into early-crystallising olivine, whereas Cu increases with S in the melt during fractionation. In the olivine-free, S-rich rocks (Fig. 103B), Cu and Ni show a positive correlation, since both elements partitioned into sulphide minerals. Under S-undersaturated conditions, precious metals in the ultramafic rocks display weak positive

correlations with Cu and S (Fig. 102C–D), since the concentrations of these incompatible elements increase during fractionation of the magma. In the S-saturated magmas, Pt + Pd is independent of Cu and Ni content (Fig. 103C–D), because once the magma is S-saturated, the PGEs are depleted more rapidly than the base metals.

Formation of the basal-contact sulphide zone

Sulphide-saturated chilled margins are common in many major layered intrusions, e.g. Bushveld, Sudbury, Stillwater, and Duluth. Sulphide precipitation and the role of contamination along the basal contact of the Bushveld Complex have been discussed by Liebenberg (1970), de Waal (1977), von Gruenewaldt (1979), Grunshaw (1983), Buchanan & Rouse (1984), and Cawthorn & others (1985a,b). Various mechanisms, such as the direct addition of S by assimilation of sulphides (sulphurisation) or H_2S- or SO_2-bearing material from the basement rocks, and an increase in fO_2 by addition of oxygen or water, have been proposed for driving mafic magmas towards S-saturation (Haughton & others, 1974).

Basal sulphide-rich layers in layered intrusions are often taken to indicate that the parent magma was S-saturated prior to emplacement. As the M-magma of the Munni Munni Complex was S-undersaturated, the precipitation of sulphides along the basal contact was due to a local process. Sulphide saturation was believed to have been induced by rapid chilling (similar to that documented in the Jimberlana Dyke, Keays & Campbell, 1981) and possibly minor contamination from the country rocks. As indicated by the estimated S content of the M-magma (530–600 ppm: see p. 156), the magma that fed the ultramafic zone was not significantly undersaturated in S. The moderately high S content of the parent magma assisted the S-saturation process along the basal contact. The sulphide content of the marginal ultramafic-zone rocks generally ranges from around 1.0 vol.% at the northern basal contact to < 0.2 vol.% at the southwest end of the northwestern contact. The sympathetic trends of decreasing S and modal quartz contents of the marginal rocks up the intrusion suggest that temperature and SiO_2 may have been important parameters for sulphide precipitation in the lower parts of the intrusion. Assimilation of granitic material along the northeastern and southeastern contacts of the intrusion is reflected by the net-vein textures, silicic-hydrous-alkali alteration, graphic intergrowth of quartz and feldspar, and the enhanced Rb and Cs contents of the marginal pyroxenites. The isotopic compositions and S/Se ratios of the basal sulphides are discussed on pp. 161–162.

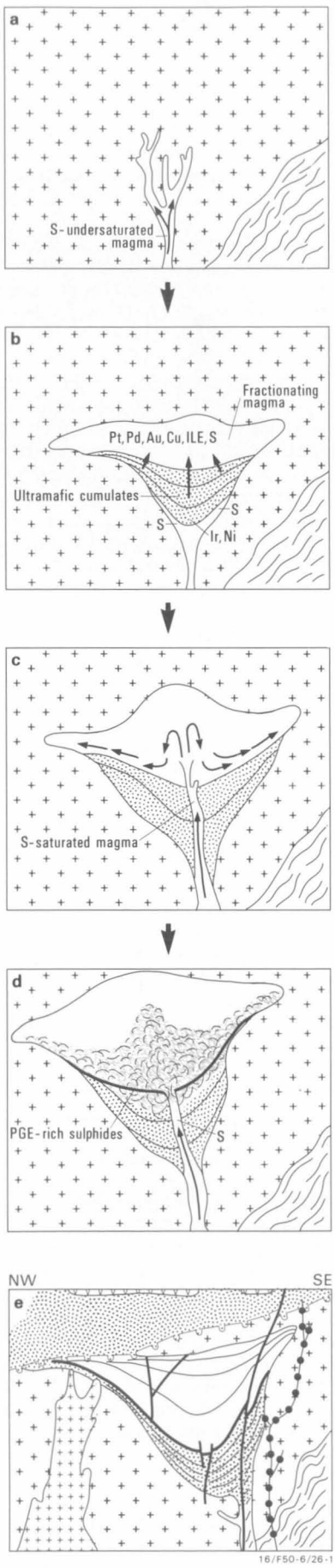

Fig. 104. Schematic diagram showing proposed sequence of events for the evolution of the Munni Munni Complex. The model involves the mixing by fountaining processes of the fractionated components of a S-undersaturated magma of basaltic-komatiitic composition enriched in Pt, Pd, Au, Cu, S, and the incompatible lithophile elements (ILE), with a new pulse of S-saturated gabbroic magma. Details of the various stages of the model are given in the text. For the final stage(E), the mineralised porphyritic websterite layer is represented by the full dark line at the contact of the ultramafic and gabbroic zones, ?Talga Talga metavolcanics by the wavy discontinuous lines, granite by the large '+' symbol, younger hornblende syenites by the small '+' symbol, dolerite dykes by the lines with large dots, and Fortescue Group sediments and volcanics by the fine stipples and 'v'.

Genesis of PGE mineralisation in the porphyritic websterite layer

The following model prescribes the enrichment of PGEs and incompatible trace elements in the porphyritic websterite layer by crystal fractionation processes and the mixing of two chemically distinct, but probably genetically related, magmas. Other similar models involving magma mixing have been described by Hoatson & Keays (1987, 1989) and Barnes & others (1990, 1992).

An incoming, S-undersaturated, M-magma pulse of SHMB composition (Fig. 104A) was emplaced into an evolving magma chamber in the upper crust (at pressures of 3.5— 5 kb; see p. 161). This pulse was chilled against the chamber walls and, together with localised contamination from the granitic country rocks, caused S-saturation and formation of high-Fe, low-PGE-bearing sulphides because of rapid precipitation (i.e. a low R factor—a small volume of silicate melt equilibrated with the immiscible sulphides: Campbell & Naldrett, 1979; Campbell & others, 1983). The host rocks for the Fe-rich sulphides are dominantly gabbroic and significantly more evolved ($mg_{76.4-55.6}$) than the overlying ultramafic cumulates ($mg_{84.9-78.0}$). The heterogeneity in sulphide content, hydrous-alkali alteration, and variable amounts of granitic melt components in the fractionated marginal gabbroic rocks all indicate that temperature gradients and contamination were not uniform in the contact rocks of the ultramafic zone.

Repeated S-undersaturated SHMB magma pulses containing ~ 530 ppm S were emplaced into the lower parts of the chamber. The primitive character of these pulses was preserved and buffered from the chilling and contamination that occurred along the contacts of the intrusion by the thin 'veneer' of hot, marginal, fractionated gabbroic rocks. At this stage in the evolution of the intrusion, the magma chamber was an open system and rapidly growing as a result of the addition of new pulses of primitive magma. Depending on their fluid-dynamic properties, the new injections of hot, primitive magma ponded out along the floor of the chamber and had limited interaction with the resident magma, or experienced small-scale mixing with the resident magma. It is believed that the initial growth of the chamber was largely vertical and was accommodated by the floating and raising of the roof rocks and/or by subsidence of the floor (isostatic readjustment). An ultramafic cumulate pile characterised by poorly-defined cyclic units comprising varying proportions of olivine and clinopyroxene cumulates formed along the floor of the chamber. The crystallisation path of the M-magma oscillated from within the olivine stability field to the cotectic between olivine and clinopyroxene (also for the peridotites of the Radio Hill and Mount Sholl complexes). The rarity of cumulus orthopyroxene in the ultramafic zone suggests that the liquid phase of the M-magma did not reach the olivine/orthopyroxene boundary on the liquidus. The irregular and 'beheaded' nature of the ultramafic-zone cyclic units and the unsystematic layering within the units indicate that the system was very dynamic and continually being modified by new influxes of primitive magma of similar composition and localised mixing. The cyclic units thickened along the central axis of the chamber as the cumulate pile sagged, but thinned upwards against the walls of the chamber.

In the S-undersaturated conditions of the ultramafic zone, Pt, Pd, Au, Cu, S, and Se all behaved incompatibly and increased in concentration during crystal fractionation, whereas Ir and Ni partitioned largely with early-crystallising olivine (Fig. 104B). The increase in concentration of the incompatible elements in the lower 1400 m of the zone was minimal since fractionation was continually being forestalled by the new pulses of primitive magma. Consequently there was no widescale enrichment at this stage.

The development of PGE mineralisation directly below the ultramafic/gabbroic zone contact was principally controlled by the timing of S-saturation. If the resident M-magma had been S-saturated prior to emplacement, there would have been no enrichment of the PGEs in the residual melt during differentiation, because of the extremely high sulphide-silicate partition coefficients of these elements, e.g. ~ 10^4 to 10^5 (Campbell & others, 1983; Campbell & Barnes, 1984; Peach & others, 1989; Stone & others, 1990). Incompatible-element trends (Fig. 59) and olivine and clinopyroxene compositional trends (Fig. 25) indicate that from above the ~ 1400 m stratigraphic level, the magma chamber evolved from an open system to a more closed system that had limited, irregular supplies of primitive magma. This change in rate of magma input into the chamber was important, since, in contrast to the lower part of the zone, it allowed the concentrations of S and other incompatible elements in the melt (Fig. 59) to significantly increase with crystal fractionation. Above the 1400 m level, magma input into the chamber was greatly reduced, essentially closed-system fractional crystallisation being interrupted by rare pulses of new magma. This resulted in the M-magma being on the verge of S-saturation just prior to the emplacement of the G-magma, which is an important requirement for the formation of stratiform PGE-enriched layers. The increase in whole-rock Zr, Cs, Rb, and Sr contents and Cu/(Cu + Ni) ratio upwards in the upper parts of the ultramafic zone is consistent with crystal fractionation being an important concentrating mechanism.

A large, major new pulse of dense, S-saturated (1700–2600 ppm S) G-magma, that was probably genetically related to the M-magma, reactivated the access conduit and was emplaced into the magma chamber as a fountain. The magma chamber increased rapidly in size both vertically and laterally. The new magma spread out for at least 12 km along the floor and up the sloping walls of the chamber (Fig. 104C) and mixed with the fractionated PGE-enriched, supernatant, resident magma to form the hybrid layer (Fig. 104D). The mixing eroded the upper stratigraphic levels of the ultramafic zone and caused S-saturation in the hybrid layer.

The main product of the mixing was the hybrid porphyritic websterite layer of subzone I (Fig. 104E), which hosts the PGE-enriched zone up to 20 m below the ultramafic/gabbroic zone contact. The mineralised layer is enriched in Pt and Pd by a factor of 1000 compared to the underlying cumulates (i.e. from background concentrations of about 3 ppb to 3 ppm) and contains sulphides dominated by chalcopyrite, with lesser amounts of pentlandite and pyrrhotite. Thin, weakly mineralised zones also occur 45 m below the contact, but the relatively PGE-poor character and the lateral discontinuity of these lower zones suggest a different mineralisation process, e.g. possibly reflecting low R conditions during mixing.

The porphyritic websterite layer contains lenses of norite, mixed norite-orthopyroxenite rock, and various hybrid rock types which are believed to have crystallised from partly mixed magma during the main mixing cycle. Accidental blocks of aluminous-spinel-bearing orthopyroxenite and smaller granoblastic mafic xenoliths of unknown origin from higher levels in the chamber

intermixed with the porphyritic websterite layer. The orthopyroxenite blocks have strongly developed igneous adcumulus textures (which include thin, cyclic spinel layers), no evidence of chemical modification by metamorphism or alteration, and a much finer grainsize (< 1 mm) than the other Munni Munni rocks. They may represent small pockets of primitive magma that migrated to the upper parts of the chamber, and the crystallisation of spinel may have been induced by siliceous contaminants derived by the partial melting of the roof rocks. However, it is difficult to explain the primitive compositions of the orthopyroxenes and high-alumina contents of the spinels, suggesting crystallisation at high pressures.

The subeconomic tenor of the mineralisation along the strike length of the porphyritic websterite layer may indicate that only a moderately-high R factor (but much lower than that believed to have occurred for the Merensky and J-M reefs) was achieved during magma mixing. Optimum conditions for a high R factor are when the density difference between the two magmas is small and the mixing is of turbulent plume-like character (Campbell & others, 1983). From an economic perspective, the real problem with the Munni Munni mineralisation is that it is spread over a substantial stratigraphic interval compared with, e.g., the Merensky Reef where the mineralised interval is around 0.8 m thick and has an average PGE grade of 8.1 ppm (Naldrett, 1989). At Munni Munni, Pt and Pd average 1.11 and 1.82 ppm, respectively over the 3 m-wide interval 63.75–66.75 m in DDH MMD 1. If the PGEs were compressed into a 0.8 m interval, they would average 4.16 ppm Pt and 6.84 ppm Pd, and would be an attractive target.

The lateral extent of the mineralisation (> 12 km), its general consistency of grade, stratigraphic position and lithological control, and the evolution of S, PGEs, and incompatible lithophile elements that can be explained by fractional crystallisation of silicate and sulphide phases, collectively suggest that the Munni Munni PGE mineralisation is largely of primary magmatic origin. The presence of PGE-bearing sulphide horizons below the main mineralised layer (e.g. in DDH MMD 1) is also inconsistent with hydrothermal models that involve PGE enhancement by postcumulus upward migration of fluids and volatiles (Ballhaus & Stumpfl, 1986; Boudreau, 1990a, b). Transgressive alteration and mineralisation zones, as observed in the Picket Pin deposit (Boudreau & McCallum, 1985, 1986), have not been observed at Munni Munni, and Cu/Ni and Pd/Pt ratios are lower than those documented in hydrothermal environments. In addition, the 'ascending-hydrothermal' models suggest that PGE grades should peak above the thickest parts of the cumulus pile, but at Munni Munni strongly anomalous PGE concentrations also occur in the porphyritic websterite along the margins of the intrusion (Barnes & others, 1992).

Volatiles that were possibly liberated from the crystallisation of the cumulus pile or were derived from high levels in the chamber, and which were responsible for the sulphide-silicate intergrowth textures, produced only a local low-temperature redistribution of the PGMs. This localised redistribution on a millimetre scale is reflected by the high percentage of PGMs that have a strong association with altered sulphide grains, and the development of low-temperature Bi, Cu, and Hg telluride assemblages. A later and more extensive remobilisation of PGMs is indicated by various Pt-arsenide minerals in talc-carbonate-chlorite shears traversing the mineralised websterite layer.

The association of PGMs and sulphides with hydrous silicates (as seen at Munni Munni) has been used as evidence supporting the role of widescale hydrothermal mineralising fluids in many overseas intrusions. Barnes & Campbell (1988) have noted that the intergrowth of amphibole and biotite with sulphides is a common postcumulus feature of sulphide-bearing gabbros, including all the Pilbara intrusions investigated in this study. The immiscible sulphide liquid solidifies at near-solidus temperatures in the pore space between early-crystallising silicate minerals, and is forced into areas occupied by late-crystallising Cl-bearing silicates. Prendergast (1990) also attributed identical postcumulus alteration textures in the Great Dyke to the *in situ* evolution of intercumulus silicate and sulphide liquids and volatile fluids and their continuous reaction with each other and with primary silicates.

Conditions of crystallisation

Temperature, oxygen fugacity, and P_{H_2O}. Estimated crystallisation temperatures have been determined for primary clinopyroxene-orthopyroxene pairs from the ultramafic and gabbroic zones using the semi-empirical geothermometer methods of Wood & Banno (1973) and Wells (1977), and the graphical method of Lindsley (1983). The three methods are reported to reproduce most of the experimental data for multicomponent systems to within ~ 50–70°C. Temperatures are shown in Table 31 for both cumulus-cumulus and cumulus-intercumulus pyroxene pairs, since, except in the basal part of the ultramafic zone, clinopyroxene and orthopyroxene crystallised in equilibrium throughout the intrusion (see Fig. 29). Estimates by the Wood & Banno (1973) method show the greatest consistency, with temperatures ranging from 1010 to 1100°C (average 1050 ± 32°C) for the cumulus pyroxene pairs, and from 990 to 1135°C (average 1080 ± 38°C) for the cumulus-intercumulus pyroxene pairs. The overlap in temperature

Table 31. Calculated equilibration temperatures for coexisting clinopyroxene and orthopyroxene pairs

Sample number	*Strat. height(m)*	*T°C(W&B)*	*T°C(W)*	*T°C(L)*
Cumulus clinopyroxene-cumulus orthopyroxene pairs (ultramafic and gabbroic zones)				
84770055*	2859	1102	1312	1050
84770053*	2551	1076	1246	1040
84770052*	2377	1090	1264	1040
84770094a	1846	1069	1200	930
84770094b	1846	1020	1119	800
84770047	1839	1009	1083	910
84770044	1838	1025	1071	870
84770045a	1811	1043	1038	920
84770045b	1811	1038	1068	920
84770102a	2	1012	1136	850
84770102b	2	1028	1162	700
Cumulus clinopyroxene-intercumulus orthopyroxene pairs (ultramafic zone)				
84770042	1723	1135	1152	1120
84770037	1538	1031	1000	930
84770032a	1417	1095	1076	1020
84770032b	1417	1097	1079	1020
84770020a	867	1071	1045	940
84770020b	867	1064	1035	1000
84770019	748	992	949	890
84770018a	690	1090	1070	980
84770018b	690	1091	1081	980
84770007	285	1049	1015	1000
84770002a	128	1111	1138	1060
84770002b	128	1096	1116	1020

W&B = Wood & Banno (1973); W = Wells (1977); L = Lindsley (1983); 'a' and 'b' are different orthopyroxene-clinopyroxene pairs in the same rock; * temperatures obtained from re-calculated bulk compositions of inverted pigeonite and coexisting clinopyroxene grains.

Table 32. Calculated equilibration temperatures and oxygen fugacities for coexisting magnetite and ilmenite pairs

Sample no.	*Strat. height (m)*	*T °C (S&L; S)*	*fO_2 (S&L; S)*	*T °C (A&L)*	*fO_2 (A&L)*
84770066	4222	702	−15.46	704	−16.01
84770062	3676	754	−14.62	754	−15.15
84770060a	3425	756	−15.42	763	−15.74
84770060b	3425	693	−15.59	691	−16.22
84770060c	3425	741	−14.98	744	−15.42
84770058a	3181	701	−17.32	699	−17.74
84770058b	3181	634	−19.93	624	−20.90
84770057	3052	523	−22.26	515	−23.35
84770055a	2859	630	−18.08	624	−19.07
84770055b	2859	701	−16.74	699	−17.36

S&L; S = combined method after Spencer & Lindsley (1981) and Stormer (1983); A & L = Andersen & Lindsley (1985). 'a', 'b', and 'c' are different magnetite-ilmenite pairs in the same rock.

supports the suggestion that intercumulus orthopyroxene crystallised in equilibrium with, and at a similar time to, cumulus clinopyroxene in the ultramafic zone. There are no apparent systematic trends in temperature with increasing stratigraphic height for the Wood & Banno (1983) results.

Estimates using Wells's (1977) calibration are generally within 30°C of the results from the Wood & Banno (1973) method for pyroxene pairs below the 1830 m level, but above this level they are considerably higher and increase up the succession. This unlikely upward trend suggests the Wells (1977) geothermometer may not be accurately calibrated for Fe-rich pyroxenes (e.g. $Fe^{2+}/(Fe^{2+}+Mg) > 0.20$), such as those found in the high levels of the Munni Munni Complex. The consistently lower temperatures from Lindsley's (1983) 5 kb geothermometer relative to the other two methods are believed to indicate the greater sensitivity of this graphical method to the determined Ca content of the pyroxene.

Temperatures of 1050–1100°C obtained from the Wood & Banno (1973) and Lindsley (1983) geothermometers for the three inverted-pigeonite and clinopyroxene pairs (re-calculated bulk grain compositions for samples 84770052, 053, 055) from the middle parts of the gabbroic zone, are believed to represent the closest approximations to magmatic temperatures. Estimated two-pyroxene equilibration temperatures below 1050°C largely reflect progressive cooling below magmatic temperatures. Liquidus temperatures for the M-magma (~ 9.80% MgO) are likely to be in the order of 1200–1250°C. Magmatic temperatures for the Munni Munni gabbroic zone are slightly lower than the liquidus temperatures of 1100–1300°C documented for other layered gabbroic intrusions (Williams, 1971; Biggar, 1974; McGuire & Coleman, 1986; Mathison & Hamlyn, 1987; Ballhaus & Glikson, 1989).

Podpora & Lindsley (1979) and Lindsley (1983) have shown experimentally that the minimum temperature of pigeonite stability is 825°C. It is independent of pressure, although the composition of pigeonite is pressure-dependent. The bulk composition of inverted pigeonite from the 2377 m level of the Munni Munni Complex corrected according to the scheme outlined in Lindsley (1983) is $Wo_{15}En_{50}Fe_{35}$. When plotted on the 5 kb pyroxene quadrilateral diagram of Lindsley (1983), this composition equates with the ~ 1080°C temperature isotherm for the inversion of orthopyroxene to inverted pigeonite. This temperature is consistent with the estimated magmatic temperatures obtained from the three geothermometric methods detailed above.

Temperatures and oxygen fugacities of coexisting magnetite-ilmenite pairs from the middle and upper parts of the gabbroic zone are shown in Table 32. These are based on a modified method from Spencer & Lindsley (1981) and Stormer (1983), and also Andersen & Lindsley (1985). Temperatures ranging from 515 to 765°C (average 680 ± 70°C) for the two methods are considerably lower than the two-pyroxene temperature estimates, which is believed to reflect subsolidus re-equilibration processes of the magnetite-ilmenite aggregates. Oxygen fugacities range from −14.62 to −23.35 (average −17.37 ± 2.52), which bracket the fayalite-magnetite-quartz (FMQ) buffer. These low fO_2 values are consistent with the late-crystallisation of Fe-Ti oxides in the gabbroic succession. $LogfO_2$ versus temperature relationships for magnetite-ilmenite pairs in the Munni Munni Complex are similar to those documented for other major layered intrusions (Fig. 105).

Other crystallisation parameters are not well defined, although the scarcity of primary hydrous minerals, the early crystallisation of intercumulus plagioclase in the basal parts of the ultramafic zone, and the late cumulus crystallisation of Fe-Ti oxides in the gabbroic zone, collectively suggest that low P_{H_2O} prevailed during the crystallisation of the mafic-ultramafic cumulate sequence. The pronounced Fe-enrichment trends of clinopyroxene from the Munni Munni gabbroic zone contrast with the more restricted fractionation trends documented for hydrous-gabbroic intrusions, such as the Dutchmans Creek Gabbro, South Carolina (McSween & Nystrom, 1979), Marangudzi ring complex, Zimbabwe (Hossain, 1977), and the Guadalupe Com-

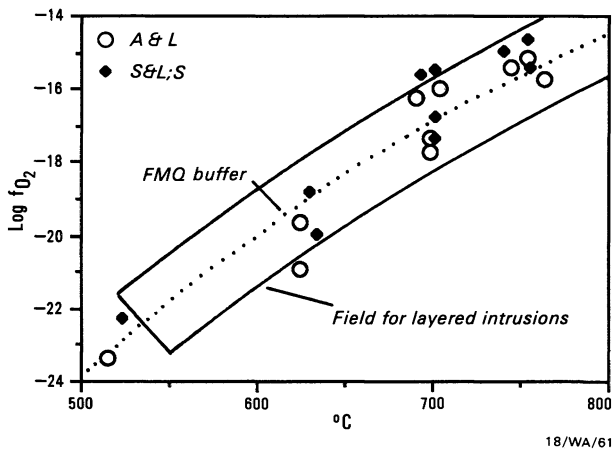

Fig. 105. Relationship of temperature versus $logfO_2$ for coexisting magnetite and ilmenite pairs from the Munni Munni gabbroic zone. The fayalite-magnetite-quartz (FMQ) buffer, which is corrected to 5 kb, and the field for layered intrusions are from Haggerty (1976). Temperatures and fugacities were determined using the methods of Andersen & Lindsley (1985) ('A&L'), and a modified method after Spencer & Lindsley (1981) and Stormer (1983) ('S&L; S').

plex, California (Best & Mercy, 1967). In these hydrous magmas, clinopyroxene was a stable liquidus phase for only a short crystallisation interval, after which hornblende and biotite became stable phases (Best & Mercy, 1967).

Pressure. The depth of emplacement of the Munni Munni Complex is difficult to establish because of the absence of suitable primary mineral assemblages for pressure determinations in both the contact granites and the mafic-ultramafic rocks of the complex. Various geobarometers (Ellis & Green, 1979; Harley, 1984) require coexisting assemblages of garnet, plagioclase, pyroxene, quartz, and/or primary amphibole. However, in the Munni Munni Complex, garnet is absent, quartz has a restricted distribution, and hornblende is invariably secondary.

Ellis (1980) has noted that for the assemblage plagioclase-clinopyroxene-quartz the reaction

$$\underset{CaAl_2Si_2O_8}{\text{Anorthite}} = \underset{CaAl_2SiO_6}{\text{Ca Tschermak's molecule}} + \underset{SiO_2}{\text{Quartz}}$$

provides a useful geobarometer. Quartz forms a minor interstitial phase (0.2--2 vol.%) with plagioclase and clinopyroxene in the middle and upper parts of the gabbroic zone. The clinopyroxenes contain between 1.23 and 1.69% Al_2O_3 (average 1.39 ± 0.19%), with an average Ca Tschermak's molecule content of ~ 2% (X_{CaTs} = 0.02, Table 33). At estimated magmatic temperatures of 1050°C (determined above), and in equilibrium with plagioclase compositions of An_{43} to An_{35} (Appendix 2), the Ellis (1980) geobarometer yields pressures of equilibration that range from 3.6 to 6.2 kb (average of 5.1 ± 0.79 kb). Some caution is required for the interpretation of the data in Table 33, because this geobarometer is extremely sensitive to variations in the Al_2O_3 content of clinopyroxene.

An upper limit to the pressure of emplacement is indicated by the coexistence of plagioclase and olivine in subzone A′ and in the lower parts of subzone I of the ultramafic zone. Green & Hibberson (1970) have experimentally shown that forsterite and anorthite are stable at less than 8.5 ± 0.5 kb at 1250°C, but forsterite-orthopyroxene-clinopyroxene-spinel is the stable assemblage at higher pressures. Olivine-spinel, orthopyroxene-clinopyroxene-spinel symplectite, and corona textures that reflect high-pressure crystallisation in the Giles Complex (Ballhaus & Berry, 1991), are absent in the Munni Munni Complex. In addition, Donaldson (1974) suggested that both the low Al_2O_3 content of pyroxene and the crystallisation sequence of the cumulus minerals indicate low-pressure crystallisation for the Munni Munni Complex. Cumulus clinopyroxene and orthopyroxene in the Munni Munni Complex have Al_2O_3 contents of < 2.20% and < 1.20%, respectively. Green (1964) attributed low Al_2O_3 contents of 2–3% in orthopyroxene from the Lizard Complex, Cornwall, to low-pressure crystallisation, although other factors, such as the activity of SiO_2 and temperature, are also important. Cawthorn & Davies (1983) have shown experimentally that the crystallisation sequence of olivine to clinopyroxene to orthopyroxene to plagioclase can be obtained by the crystallisation of a melt of similar composition (mg_{61} for sample 2, in table 1 of Cawthorn & Davies, 1983) to the Munni Munni M-magma at a pressure of 3 kb and temperatures of 1120 and 1150°C. Orthopyroxene crystallised before clinopyroxene in melts of various compositions at pressures of 3–10 kb and temperatures greater than 1150°C (see table 2 of Cawthorn & Davies, 1983).

Table 33. Pressure estimates based on the Ca Tschermak's molecule in clinopyroxene (after Ellis, 1980)

Sample number	*Strat. height (m)*	X_{CaTs}	*P (kb)*
84770064	3965	0.020	4.9
84770061a	3553	0.020	5.4
84770061b	3553	0.020	5.5
84770059a	3341	0.021	5.2
84770059b	3341	0.021	5.0
84770055	2859	0.024	3.6
84770053	2551	0.028	6.2

'a' and 'b' are different clinopyroxene-plagioclase pairs in the same rock.
X_{CaTs} determined from averaged bulk compositions of clinopyroxenes by raster analysis.
Pressures determined using 0.5 x Al rather than Al^{VI} in the equations of Ellis (1980); this gives a maximum estimate of pressure.

The fractionation trends and subsolidus textures of the pyroxene and Fe-Ti oxide minerals in the Munni Munni Complex are similar to those in the Bushveld and Stillwater complexes, which were emplaced into the upper crust at pressures of 4 to 5 kb (Nell, 1985) and 3 to 4 kb (Labotka, 1985), respectively. It is proposed that the Munni Munni Complex was emplaced into the upper crust at similar pressures (3.5--5 kb) to these major intrusions.

In summary, the Munni Munni Complex is believed to have crystallised at upper crustal pressures of 3.5--5 kb and temperatures of 1050 to 1100°C (for the gabbroic zone), and at oxygen fugacities equivalent to the fayalite-magnetite-quartz buffer, and under low P_{H_2O} conditions.

Sulphur isotope geochemistry of the west Pilbara layered intrusions

Isotopic compositions of S were determined for sulphide-rich units from various stratigraphic levels in the Munni Munni, Mount Sholl, and Radio Hill intrusions (Table 34). The isotopic compositions were determined by the procedures outlined in Appendix 1.4.

The most striking feature of the isotopic compositions is their uniformity. This applies both among the different intrusions and among the different mineralised zones within the intrusions. Sulphides in the west Pilbara intrusions have small positive $\partial^{34}S$ values that range from +1.1 to +4.8‰ (mean of +2.7‰, standard deviation of 1.0), with individual intrusions having $\partial^{34}S$ values between +2.1 and +2.5‰ (Munni Munni), +2.3 and +3.7‰ (Mount Sholl), and +1.1 and +4.8‰ (Radio Hill).

The $\partial^{34}S$ values appear to be largely independent of host rock (gabbro, websterite, or peridotite), and stratigraphic level (basal contact of the ultramafic zone, contact between the ultramafic and gabbroic zones, and in the gabbroic zone). However, there is a possible relationship with the style and composition of mineralisation; e.g. disseminated Fe-rich sulphides in the gabbroic zone of the Radio Hill Complex have lower $\partial^{34}S$ values (+1.1‰ and +1.5‰) than Cu-rich (+2.0‰ and +3.2‰) and Fe-rich (+4.5‰ and +4.8‰) massive sulphides hosted by gabbroic rocks at the base of the ultramafic zone, but further analyses are required to confirm this.

The uniformity of S-isotope compositions in the Munni Munni Complex contrasts with the Stillwater Complex, where Zientek & Ripley (1990) documented lower isotopic ratios (−0.2‰) in the basal sulphides

Table 34. Summary of sulphur-isotope compositions of west Pilbara layered intrusions

Intrusion	*Sample number*	*Subzone*	*Mineralisation**	*Host rock*	$\partial^{34}S$ (‰)
Munni Munni	84770100	A′	Diss Po-Pent-Cpy	Gabbronorite	+2.4
	84770102	A′	Diss Po-Pent-Cpy	Gabbronorite	+2.5
	84770094	I	Diss Cpy-Po-Pent	Plag websterite	+2.4
	84770094*	I	Diss Cpy-Po-Pent	Plag websterite	+2.1
Mount Sholl	84770203	UZ	Mass Po-Pent-Cpy	Peridotite	+3.7
	84770203*	UZ	Mass Po-Pent-Cpy	Peridotite	+2.3
	84770207	UZ	Diss Po-Pent-Cpy	Peridotite	+2.8
Radio Hill	88770052	A	Veined Cpy	Metavolcanic	+3.2
	88770055	A	Mass Po-Pent-Cpy	Gabbro	+4.8
	88770058	A	Mass Po-Pent-Cpy	Gabbro	+4.5
	88770061	A	Diss Po-Cpy-Pent	Gabbronorite	+1.1
	88770082	E	Diss Po-Cpy-Pent	Plag websterite	+1.5
	88770136	A	Mass Cpy	Gabbro	+3.2
	88770137	A	Mass Cpy	Gabbro	+2.0

* Repeat of different sulphide samples from the same rock; UZ = ultramafic zone; Diss = disseminated; Mass = massive; Plag = plagioclase; Po = pyrrhotite; Pent = pentlandite; Cpy = chalcopyrite.

than in the sulphides higher up in the intrusion, such as the J-M Reef (+1.0‰) and the Picket Pin deposit (+2.4‰). On the basis of the Fe, Cu, and Ni compositions of the basal sulphides, they proposed that the shift to more negative isotopic compositions for the basal sulphides was attributable to the assimilation of crustal S from the country rocks.

Naldrett (1981) and Ripley (1983) have documented possible S isotope fractionation features for different ores in the Sudbury (Ontario) and Deer Lake (Minnesota) complexes. This does not appear to be the case with the Munni Munni Complex. Basal pyrrhotite-rich sulphides at Munni Munni have the same $\partial^{34}S$ values (+2.4‰ and +2.5‰) as the chalcopyrite-rich sulphides in the porphyritic plagioclase websterite layer directly below the ultramafic/gabbroic zone contact (+2.4‰). The uniformity of isotopic compositions of the sulphides, which are separated by 1.85 km of ultramafic stratigraphy, indicates that the S was most likely derived from a common mantle source and the S isotopes have not been fractionated (e.g. enrichment of the heavier ^{34}S isotope relative to the lighter ^{32}S isotope) during the evolution of the intrusion.

An important question relates to the source of S in the west Pilbara layered intrusions. The major, alternative sources in ore deposits are either deep-seated (mantle or crust), or derived from local country rocks, or from sea water or marine evaporites (Rye & Ohmoto, 1974; Ohmoto, 1986). Lambert & Donnelly (1990) have shown that more than 80% of the Archaean (pre-2500 Ma) sedimentary and igneous rocks they have analysed have $\partial^{34}S$ values in the range of −4 to +4‰, whereas sulphides in Proterozoic sedimentary and exhalative rocks have a much wider spread, between −10 and +20‰. From about 2400 to 2000 Ma there was a transition to a largely oxidising hydrosphere, increasing oxygenation of the atmosphere, and proliferation of sulphate-reducing bacteria. Thus, in rocks younger than about 2400 Ma, the $\partial^{34}S$ values of sulphide minerals derived from bacteriogenic H_2S can provide a record of the presence of sulphate-reducing bacteria in sedimentary rocks, usually manifested by a spread of $\partial^{34}S$ values that show an increase in ^{32}S relative to mantle values (Zientek & Ripley, 1990). This allows greater scope for discriminating between magmatic and sedimentary sources of S in Proterozoic and younger rocks. The spread of $\partial^{34}S$ values is particularly well documented for mafic-ultramafic intrusions generally younger than ~ 2200 Ma, e.g. the Muskox Intrusion (0 to +17‰; see fig. 21 in Ohmoto, 1986), the Duluth Complex (0 to +15‰: Mainwaring & Naldrett, 1977; Ripley, 1981), the Noril'sk intrusions (+7 to +17‰: Godlevskii & Grinenko, 1963), and the Bushveld Complex (−9 to −6‰: Liebenberg, 1970, as quoted in Ohmoto, 1986). However, for Archaean layered intrusions, including the ~ 2925 Ma west Pilbara intrusions, the $\partial^{34}S$ values of the sulphides will have magmatic signatures irrespective of the nature of the source of the S. The range (+1.1 to +4.8‰) and low variance (mean of +2.7‰, standard deviation and variance of 1.0) of $\partial^{34}S$ values for the Pilbara intrusions are typical of Archaean sulphide deposits, such as Kambalda and Golden Grove, Yilgarn Block (Lambert & Donnelly, 1990). The source problem is also compounded by the abundance of Archaean igneous rocks (intrusive, volcanic, and pyroclastic) surrounding the Pilbara intrusions. Any sulphides that may have been assimilated from such country rocks will therefore have magmatic isotopic signatures.

Some insight into the possible source of the S can be gained from the S/Se ratios of the sulphide ores. Sulphur/Se ratios of 2000–10 000 are regarded as normal for uncontaminated magmatic sulphide ores, whereas ratios of > 20 000 are typical of sedimentary sulphides (Naldrett, 1981). The sulphide-rich rocks along the basal contact of the Munni Munni ultramafic zone have S/Se ratios ranging from 4500–5900, the mineralised porphyritic websterite a S/Se ratio of 2420, and the S-saturated gabbroic-zone rocks 2600–5600. These ratios are all consistent with a magmatic source for S in the Munni Munni Complex. In addition, most of the Munni Munni ultramafic zone is S-undersaturated, which suggests that no significant amounts of S were assimilated from the country rocks.

In summary, S isotopes and whole-rock S/Se ratios indicate that, for the west Pilbara layered intrusions,

- S appears to be largely magmatic and there was no significant external component of sedimentary S from the country rocks;
- various processes within the magma chamber, such as different cooling rates of the magma near the margins, crystal fractionation, magma mixing, gravitational settling, etc., are believed to have largely controlled the distribution of sulphides; and
- except possibly for the Radio Hill Complex, S-isotope compositions appear to be independent of host rock, style of mineralisation, relative proportions of sulphide minerals, and stratigraphic level, and there is no unequivocal evidence to support S-isotope fractionation.

Comparison with well-known PGE-bearing layered mafic-ultramafic intrusions outside Australia

The Munni Munni Complex is broadly similar to other major PGE-bearing layered intrusions, such as the Bushveld and Stillwater complexes and, in particular, the Great Dyke of Zimbabwe. These intrusions are commonly characterised by:

— lopolithic or dyke-like forms, and thick sequences (> 5 km) of mafic-ultramafic cumulates that encompass a wide variety of compositions from dunite to granophyre. Layering and cyclic units often have great lateral continuity;
— PGE mineralisation that may be associated with chromite and/or sulphides near the base of cyclic units or near the interface of the ultramafic and mafic parts of the stratigraphy;
— intrusive ages between 2.0 Ga and 3.0 Ga; and
— emplacement into tectonically stable Precambrian granite and/or greenstone terranes.

The intrusions range in shape from broad, shallow-dipping basins (e.g. Bushveld) and funnel-shaped lopoliths (e.g. Muskox), to steeply-dipping saucer-shaped bodies (e.g. Stillwater) and elongate dyke-like bodies (Great Dyke). With its elongate shape, and thinning and deflection upwards of cyclic units along the margins of the intrusion, the Munni Munni Complex is similar to the Great Dyke (Wilson, 1982; Wilson & others, 1989). However, the Great Dyke has a much greater length to width ratio of ~ 70, and has two major magma chambers and several subchambers. The Munni Munni Complex has a length to width ratio of only 2.8, is single-chambered (although other chambers may exist below the Fortescue platform cover), and has been tilted. Neither the Munni Munni Complex nor the Great Dyke are dykes in the true sense—the term merely indicates their shape in plan view. The Mount Sholl, Radio Hill, Maitland, and Andover intrusions are shallow-dipping (10–40°) sheets with smaller length to width ratios (in plan) than the Munni Munni Complex.

Except for the Andover Complex, the west Pilbara intrusions investigated have a greater thickness of mafic than ultramafic cumulates, i.e. similar to the Bushveld and Stillwater complexes (Fig. 106).

The crystallisation order of the cumulus minerals in the west Pilbara intrusions differs from that of the major PGE-bearing intrusions in which orthopyroxene generally precedes clinopyroxene (Table 35). The early crystallisation of clinopyroxene relative to orthopyroxene indicates that the primary magma was silica-undersaturated and there was no widespread silica contamination from the crust during emplacement. Campbell (1985) suggests that the abundance of orthopyroxene in most continental layered intrusions indicates that these intrusions crystallised from magmas that have assimilated continental crust. Campbell (1985) believes that, since orthopyroxene was an early-crystallising mineral in many layered intrusions, the assimilation may have been early, before the magma entered the chamber. This may be the case with the Andover Complex, where orthopyroxene appears to have crystallised before clinopyroxene. The early crystallisation of clinopyroxene that characterises the west Pilbara intrusions (except Andover) also accounts for the scarcity of cumulus chromite, since Cr is partitioned more strongly into clinopyroxene (up to 0.78% Cr_2O_3 at Munni Munni) than into orthopyroxene (up to 0.29% Cr_2O_3) during crystal fractionation. This depleted the melt in Cr and inhibited the formation of potential PGE-hosting chromitite layers.

Table 35. Sequences of cumulus minerals from various mafic-ultramafic geological settings (modified after Naldrett & Cabri, 1976)

Intrusion	*Cumulus assemblages*
Munni Munni	ol, ol+cpx, cpx+ol, cpx, cpx+opx, plag+opx+cpx, plag+cpx+opx+mt-ilm
Bushveld	opx+ol, opx+ol+chr, plag+opx+chr+cpx(+ol), plag+cpx(+opx), plag+cpx+mt, plag+cpx+mt+ol
Stillwater	ol, ol+opx, ol+opx+chr, plag+opx, plag+cpx+opx, plag+cpx+(opx+ol), plag+cpx+opx
Sudbury	plag+opx, plag+opx+cpx, plag+cpx, plag+cpx+mt
Duke Island	ol+chr, ol+cpx, cpx+mt, cpx+mt+plag
Pechenga	ol, cpx, cpx+mt, plag+cpx+mt
Dundonald sill	ol, cpx, plag+cpx+mt, plag+cpx(+hyp?)
Komatiites	ol, ol+cpx(opx), cpx+plag(+ol)

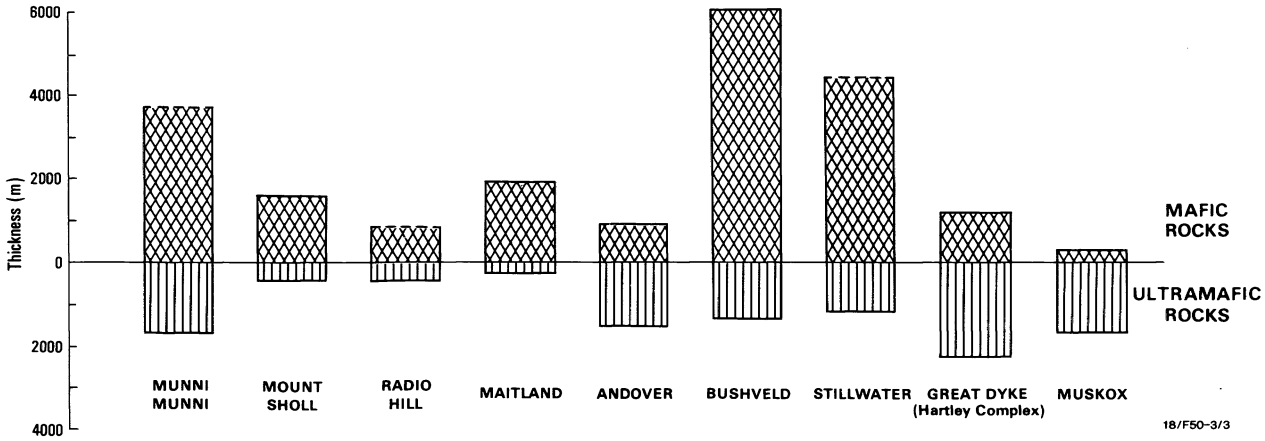

Fig. 106. Comparative thicknesses of mafic and ultramafic rocks in major layered mafic-ultramafic intrusions.

The parent magmas for the west Pilbara intrusions were compositionally very similar; they are believed to have been SHMB, of Al-depleted komatiitic affinity, derived through crustal contamination and fractional crystallisation. Although the parent magmas have some broad major-element features similar to the SHMB parent magmas proposed for other major layered intrusions (Table 36), there are some marked differences.

The major differences include: a more fractionated character (mg_{60}); lower Al_2O_3 contents; high normative diopside content relative to hypersthene; the sodic composition of normative plagioclase; and the low normative olivine content, which indicates the parent magmas were almost quartz-normative. The high normative diopside/orthopyroxene ratios are a distinctive feature of the west Pilbara intrusions (Table 30). The low Al_2O_3 contents may be due to the high-pressure crystallisation of garnet in komatiitic magmas, as discussed on p. 152.

According to Naldrett's (1981, 1989) classification scheme of mafic-ultramafic intrusions, the Munni Munni Complex falls into the category of large dyke-like layered intrusions of cratonic areas and the other west Pilbara complexes are sheet-like intrusions. The Munni Munni PGE mineralisation falls within the magma-mixing subclass of the orthomagmatic class in MacDonald's (1987) petrogenetic classification of PGE deposits. Such deposits are often of great economic importance and include the Merensky Reef of the Bushveld Complex, the J-M Reef of the Stillwater Complex, and various sulphide-bearing layers in the Great Dyke and the Lac des Iles Complex. These mineralised zones commonly define the first major development of sulphides in the layered sequences and crystal fractionation and magma mixing are generally believed to be some of the dominant mechanisms for PGE enrichment of the sulphides.

The stratigraphic level of PGE mineralisation in the Munni Munni Complex differs from that in the Merensky and J-M reefs, in that it coincides with the appearance of cumulus orthopyroxene in addition to cumulus clinopyroxene and just precedes the introduction of cumulus plagioclase. In the Bushveld and Stillwater complexes, the main PGE mineralisation occurs 400–500 m above the first appearance of cumulus plagioclase and in the vicinity of cumulus clinopyroxene joining cumulus orthopyroxene. Naldrett & others (1987) have also noted that mineralisation in the Penikat intrusion of Finland is underlain by up to 600 m of plagioclase cumulates.

The stratigraphic level of PGE mineralisation in the Munni Munni Complex is similar to the Great Dyke (Prendergast & Keays, 1987, 1989; Wilson & others, 1989; Wilson & Tredoux, 1990), where high PGE contents coincide with cumulus augite and cumulus bronzite-hypersthene directly below the appearance of cumulus plagioclase in the gabbros. The contrasting positions of PGE enrichment relative to the stratigraphic level of cumulus plagioclase crystallisation in these intrusions may have depended on the fluid dynamics (e.g. turbulent plume versus fountaining, versus quiet ponding on the chamber floor), compositional control (Al-depleted versus Al-normal character of parent magma may dictate when plagioclase becomes a cumulus phase), and/or thermal regime that obtained in the magma chamber. Prendergast & Keays (1989) proposed that the narrow width of the Great Dyke magma chamber may have induced faster cooling rates of the magma. This accelerated S-saturation, and set up steeper transverse gradients in temperature and composition between the margins and axes of the intrusion compared to the Bushveld and Stillwater complexes. The Munni Munni and Great Dyke intrusions are of similar dyke-like shape and have greater length to width ratios than the Bushveld Complex. This may indicate that thermal regimes as well as fluid dynamic processes may have played important roles in determining the stratigraphic level of S-saturation and PGE enrichment in the Munni Munni and Great Dyke intrusions.

Other features common to the Munni Munni and Great Dyke intrusions include: the occurrence of subsidiary PGE-bearing horizons below the main mineralised layer; the decoupling of the Pt and Pd peaks from those of Cu and Ni; the increase in Pt/Pd ratios up the PGE-enriched intervals; and the rapid decrease in mg of pyroxene upwards towards the ultramafic/gabbroic zone interface.

Table 36. Compositions (recalculated as anhydrous) of high-magnesium, high-silica parent magmas proposed for different layered intrusions (modified after Barnes, 1989)

	Bushveld[1]	*Great Dyke*[2]	*Stillwater*[3]	*Jimberlana*[4]	*Munni Munni*[5]
SiO_2	56.19	53.09	52.27	53.03	53.79
TiO_2	0.34	0.55	0.80	0.46	0.85
Al_2O_3	11.50	11.06	11.27	13.00	9.44
FeO*	9.55	9.49	10.40	9.46	11.90
MnO	0.18	0.14	0.21	0.17	0.21
MgO	12.99	15.51	13.08	11.98	10.00
CaO	6.69	7.68	9.33	9.25	10.17
Na_2O	1.68	1.79	1.96	2.10	2.68
K_2O	0.80	0.69	0.67	0.55	0.89
Mg/(Mg + Fe*)	0.71	0.74	0.69	0.69	0.60
CIPW norms					
Quartz	6.1	0.0	0.0	0.0	0.0
Orthoclase	4.7	4.1	3.9	3.2	5.2
Albite	14.2	15.1	16.6	17.7	22.6
Anorthite	21.5	20.0	19.9	24.4	11.1
Diopside	9.4	14.3	21.2	17.3	32.0
Hypersthene	41.1	39.4	29.7	33.5	22.8
Olivine	0.0	3.3	4.6	0.6	1.7
Magnetite	2.3	2.3	2.5	2.3	2.9
Ilmenite	0.6	1.5	1.5	0.9	1.6

1—Sharpe & Hulbert (1985); 2—Wilson (1982); 3—Longhi & others (1983); 4—Campbell (1977); 5—average of four chill samples from this study; *—total Fe; CIPW norms calculated by Hoatson.

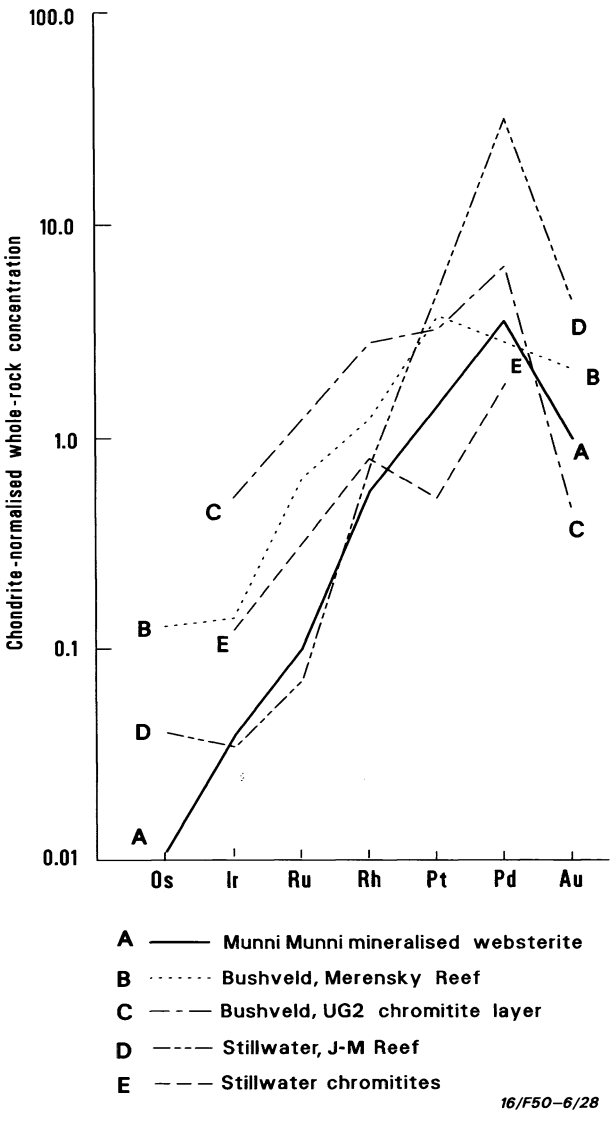

Fig. 107. Chondrite-normalised PGE and Au patterns for mineralised units, Munni Munni, Bushveld, and Stillwater complexes. The chondrite-normalising data are from a number of sources quoted by Naldrett & Duke (1980), and the Bushveld and Stillwater patterns are from Barnes & others (1985).

The similar PGE character of the Munni Munni mineralised porphyritic websterite layer (DDH MMD 1: 64.00–66.50 m) to major PGE-bearing units in other intrusions is illustrated by the chondrite-normalised trends in Figure 107. The PGE patterns for the sulphide-bearing horizons, such as the Munni Munni websterite, J-M Reef, and Merensky Reef, are characteristically steeper than those of chromite layers from the Bushveld and Stillwater complexes. Naldrett & Duke (1980) and Barnes & others (1985) concluded these patterns indicate that magmas from which these rocks crystallised were derived by low degrees of partial melting of upper-mantle peridotite, resulting in the enrichment of Pt and Pd relative to Ir, Ru, and Os. Alternatively, this could also reflect a more fractionated composition of the parent magma. The Munni Munni mineralised layer contains similar amounts of Ir, Ru, Rh, and Au contents to the J-M Reef, although the latter has anomalously high Pd compared to most layered intrusions.

Implications for exploring layered mafic-ultramafic intrusions

Much effort has been expended in searching for Merensky Reef-type mineralisation in layered mafic-ultramafic intrusions. Although these 'stratabound layers' often have great lateral persistence, they are difficult targets because they are thin (e.g. the Merensky Reef is an 0.8 m-thick layer in a 9000 m-thick mafic-ultramafic sequence), and do not have strong geochemical or geophysical signatures (the Merensky and J-M reefs generally have less than 2.0 vol.% disseminated sulphides). Also, there are no definitive geochemical or geophysical criteria to discriminate between barren and mineralised intrusions.

Historically, analyses of chilled contact rocks have been used to help determine the parental magmas and PGE potential of layered intrusions. However, as reflected by the many studies on the Bushveld Complex's marginal rocks and sills, there is disagreement about the composition of the parental magma(s) and the genetic implications of these magmas for PGE mineralisation. Various magma types (Willemse, 1969; Gijbels & others, 1974; Cameron, 1978; McCarthy & Cawthorn, 1980; Cawthorn & others, 1981; Sharpe & Irvine, 1983; Hamlyn & Keays, 1986; Irvine & others, 1983; Sharpe, 1981, 1985; Sharpe & Hulbert, 1985; Barnes, 1989; Hatton & Sharpe, 1989) have been proposed for the Bushveld, including ultramafic (MgO ~ 30%), high-magnesium basalt (MgO ~ 20%), magnesium basalt (MgO ~ 12%), olivine tholeiite, tholeiite, and high-alumina basalt (SiO_2 ~ 49–52%, MgO ~ 6–10%), contaminated komatiite, and combinations of magmas having boninitic (SiO_2 ~ 52–56%, MgO ~ 10–16%) and anorthositic affinities. In addition, chilled marginal rocks are commonly contaminated, have variable compositions at different stratigraphic levels in the magma chamber, and are not always representative of original melt compositions since they commonly have some cumulus character.

One of the most important criteria in evaluating the PGE potential of a layered intrusion is to establish whether the magma that formed the complex was ever S-saturated. This can be achieved by comparing the S contents of chilled rocks believed to represent the parent magma of the intrusion with the results of experimental studies on S solubility in fractionating magmas. However, as described above, chilled rocks are not always available or reliable. Alternatively, an estimate of the initial S content of the parent magma can be obtained by normalising average S contents of orthocumulates and mesocumulates to 100% melt and relating this to S/Se ratios to determine if there has been any loss of S during metamorphism or alteration. This method only provides a semi-quantitative estimate of the S content of the primary magma because such processes as subliquidus re-equilibration, infiltration metasomatism, and subsolidus re-equilibration may have a significant effect on trace element distributions in cumulate rocks. Determination of (Pt + Pd)/Se ratios (or (Pt + Pd)/S if there has been no loss of S) through a layered intrusion will indicate if, and where, S-saturation occurred, and thus represents a rapid technique in assessing the PGE potential of the intrusion. For example, the Munni Munni S-undersaturated ultramafic rocks have a (Pt + Pd)/Se range of 0.11–0.59, while the S-saturated gabbroic rocks have a range of 0.01–0.06. The break between these trends marks the stratigraphic level of S-saturation and PGE enrichment.

The Munni Munni data have shown that variations in the ratios of the precious metals and the trends of the incompatible lithophile and chalcophile elements are valuable in understanding the S evolution and PGE potential of the magmas. Marked discontinuities in stratigraphic profiles of Cs, Zr, Rb, Sr, S, Se, Cu, (Pt + Pd)/Se, (Pt + Pd)/S, (Pt + Pd)/Cs, (Pt + Pd)/Zr, (Pt + Pd)/Ir, and Cu/Zr may indicate new magma pulses and/or mineralised stratigraphic layers that resulted from magma mixing. When assessing the gross incompatible-element variations, it is important to ascertain whether the trends are due to changes in the amount of intercumulus melt in the cumulates or to processes such as crystal fractionation. The first factor can be partly corrected for by re-calculation of the element concentrations to 100% melt. Once again, some caution is required for the interpretation of these normalised results because of the influence of subliquidus and postcumulus crystallisation on the distribution of trace elements.

These chemical parameters should be used in association with field and mineralogical evidence that may indicate potential PGE-enrichment processes, such as crystal fractionation and/or magma mixing. This evidence may include

- rapid changes in composition of cumulus minerals, rock porosity (as shown by the intercumulus component and the incompatible-element trends), and contents of hydrous and sulphide minerals;
- transition from Fe-rich to Cu-rich sulphide assemblages with stratigraphic height;
- mineral compositional trends that may indicate changes from open- to more closed-fractionation systems;
- the close spatial association of hybrid rocks and accidental blocks in slump deposits;
- lateral variation of different rock types that show interfingering, thinning, or thickening;
- the development of porphyritic, pegmatoidal, and orthocumulus textures; and
- unconformities that may represent magmatic erosion.

The Munni Munni and Great Dyke complexes appear to represent a distinct class of mineralised layered intrusion. In contrast to the Bushveld, Stillwater, and Penikat intrusions, PGE enrichment occurred before cumulus plagioclase crystallised and has no spatial or genetic relationship with cyclic units. It is suggested that the magma-mixing class of MacDonald's (1987) petrogenetic classification of PGE deposits should be subdivided into two subclasses, to highlight the different stratigraphic level of PGE enrichment with respect to plagioclase crystallisation in large sheet-like and dyke-like intrusions. Various field, petrological, and geochemical criteria obtained from this study can be equally applied to evaluate the PGE potential of both proposed subclasses of layered intrusions.

This study has showed that PGE-sulphide mineralisation of potential economic significance

- is not restricted to layered intrusions of large areal extent;
- can occur in the upper parts of the ultramafic stratigraphy before the crystallisation of cumulus plagioclase, and is closely associated with a major compositional transformation in the intrusion, i.e. in the vicinity of the ultramafic/gabbroic zone contact;
- may persist across the total width of the intrusion from the margins to the centre of the body, and is not dependent on the thickness of the immediately underlying cumulate sequence;
- may occur in 'hybrid cross-cutting layers' rather than basal parts of cyclic units;
- is not dependent on the order of crystallisation of orthopyroxene with respect to clinopyroxene; and
- may be related to more fractionated parent magmas (e.g. Mg/(Mg + total Fe) ratio of 0.60) than those of the Bushveld, Stillwater, and Great Dyke intrusions.

In general, thick (> 3 km) layered mafic-ultramafic intrusions that have strong fractionation features and late S-saturation, will have higher potential for Merensky Reef-style mineralisation than smaller, homogeneous intrusions in which S was saturated early. It is likely that magmas which attained S-saturation prior to emplacement into the crust and had only limited equilibration of the silicate melt with large amounts of immiscible sulphides (i.e. a low R factor), will generate basal Ni-Cu mineralisation that has relatively low PGE contents, similar to the Mount Sholl and Radio Hill deposits to the north of the Munni Munni Complex.

GEOLOGICAL REMOTE SENSING OF THE MUNNI MUNNI AND ANDOVER COMPLEXES *(LFM & CJS)*

Introduction

To support AGSO mapping of Archaean layered mafic-ultramafic complexes in the west Pilbara, AGSO's Remote Sensing Group investigated the application of remote-sensing systems in discriminating the mafic and ultramafic rocks of the Munni Munni and Andover complexes. Raines & Wynn (1982) and Rothery (1984a,b) demonstrated that Landsat MSS (multispectral scanner sensing) data had considerable potential for ultramafic rock discrimination; however, these studies were of environments climatically quite different from northwestern Australia and no similar investigations had been undertaken in the Pilbara Block. Studies on multispectral scanner sensing in mafic-ultramafic terranes have been published by Abrams (1986), Sultan & others (1986), Macias & others (1987), Rothery (1987), Abrams & others (1988), Macias & Simpson (1990), and Pontual (1990).

Acquisition of scanner data over the Munni Munni Complex was carried out in October 1985, by the US National Aeronautics & Space Administration (NASA) advanced-remote-sensing research aircraft, brought to Australia by the United States–Australia Joint Scanner Project. At that time Landsat Thematic Mapper (TM) data were not available for Australia and the NASA scanners would allow the collection and assessment of data spectrally similar to TM data. Three advanced scanners were used (Huntington & Simpson, 1985; Simpson, 1986):

— Thematic Mapper Simulator NS001 (aircraft version of the Landsat TM scanner),
— Thermal Infrared Multispectral Scanner (TIMS), and
— Airborne Imaging Spectrometer (AIS).

Data were recorded at 54 target sites during the Project (Gabell & others, 1985), and archived at the Australian Centre for Remote Sensing (ACRES), Canberra.

All three instruments collected data over the Munni Munni Complex (test site 726), at the local time of 1045 am, on one flight-line which crossed the complex in a SSW direction, 4100 m above ground level. This resulted in the recording of simultaneous data strips approximately 25 km long and 6 km wide for the NS001 and TIMS, and 250 m wide for the AIS. Infrared aerial photography was acquired to assist flight-line location. NS001 and TIMS data were processed to discriminate and map mafic, ultramafic, granitic, and volcanic rocks. AIS data were not used because the data were found to have been corrupted during acquisition.

Based on this experience, studies were later conducted on Landsat TM data, which had by then become available, over the Munni Munni area, and over the Andover Complex.

The complexes are located in a semi-arid area and geological mapping of mafic and ultramafic rocks is particularly difficult because of the combined effects of weathering, soil, and extensive vegetation in the form of spinifex and black lichen. Weathering can produce a ferruginous crust up to 1 cm thick, such that mafic and ultramafic rocks often look the same, and outcrops must be broken to a fresh exposure.

Correlation between geology and vegetation is minimal. Vegetation types are similar at both Munni Munni and Andover. Large trees are normally restricted to stream courses; hills and scree slopes are up to 60–70% covered by low-growing spinifex species. At Munni Munni, black lichen completely covers most large outcrops. The lichen masks the spectral response of the rocks and inhibits their discrimination in scanner data. At Andover, the outcrops are generally not as massive as at Munni Munni, and both spinifex and lichen are comparably sparse. The relative lack of spinifex and lichen is attributed to more frequent burning of spinifex due to the proximity of Roebourne. Human access via numerous vehicle tracks, coupled with the relatively flat topography, would allow fire to reach almost all parts of the complex.

Preliminary processed imagery was used for field reconnaissance and spectral data collection. The spectral data were used to develop the image-processing methodology suitable for mafic and ultramafic rock discrimination. Analysis of spectral curves of ultramafic rock samples indicated the presence of serpentine, actinolite, carbonates, and clays (saponite); spectra of gabbro indicated the presence of epidote, chlorite, clays, and carbonates. Thus, the analysis suggested that there were sufficient mineralogical differences between the products resulting from primary alteration, between secondary weathering products, and between both these groups, to allow discrimination with the sensing bands available on the NS001 and TM.

Some of the results obtained here led to different concepts of local geological relationships that need further field checking.

Two wavelength units are used throughout this chapter: micrometres (μm) and nanometres (nm) (1 μm = 1000 nm).

General geology

Munni Munni Complex

The Munni Munni Complex was selected as a target for airborne remote-sensing studies because it contains a variety of lithologies, it is of relatively small size, and it had been mapped in detail (see appended map sheet). Also, it contains subeconomic PGEs in a fairly persistent layer of porphyritic plagioclase websterite, along the contact between the ultramafic and gabbroic zones (Hoatson & England, 1986).

The complex (Fig. 111, modified from Hoatson, this Bulletin) has an exposed area of 4 km by 9 km and consists of a basal ultramafic zone that contains rhythmically layered dunite, lherzolite, olivine websterite, clinopyroxenite, and websterite, and an overlying mafic zone consisting of gabbronorite and minor anorthositic gabbro. The more erosion-resistant rock types (e.g. pyroxenite) give rise to about 30–50% outcrop. Peridotitic rock types hardly crop out and are typified by recessive topographic areas covered by *in situ* soils. Where streams draining the ultramafic rocks meet the sandy plains on the western and northwestern sides of the ultramafic zone, extensive sandy-soil-hosted calcrete deposits have developed, typically as coalescing fans visible on aerial photographs and remotely-sensed imagery (Figs 113, 114, & 116). Incised drainage shows the calcrete to be at least 1.5 m thick; it appears to have formed by surface and groundwater leaching of calcium carbonate from ultramafic rocks (resulting from primary alteration of pyroxenes). No similar carbonate deposition is associated with drainage from the mafic rocks.

Andover Complex

The Andover Complex (Fig. 117, after Wallace, this Bulletin) covers an area of about 7 km by 20 km, and comprises a layered ultramafic zone about 1300 m thick, overlain by a mafic zone some 800 m thick. The ultramafic zone consists of peridotite, orthopyroxenite, clinopyroxenite, olivine websterite, olivine orthopyroxenite, and websterite, with interlayered anorthositic gabbro and anorthosite. The mafic zone consists of gabbro, anorthositic gabbro, and anorthosite. The complex is intruded by dolerite, granitic rocks, and pegmatites.

Comparison of the ultramafic rocks from Andover and Munni Munni shows them to have different dominant mineralogies. The Andover ultramafic sequence is olivine- and orthopyroxene-rich whereas the Munni Munni ultramafic sequence has a greater abundance of clinopyroxene-dominant rocks. Oxidation (Fig. 108A) and hydration analyses (Fig. 108B) indicate that, at Andover, primary alteration of olivine-rich rocks is more advanced than that of pyroxene-bearing rocks, and that, overall, primary alteration has been more extensive at Andover than at Munni Munni. The products of the primary mineral breakdown are as follows:

(1) olivine → serpentine + magnetite → talc, carbonates, clays (saponite)

(2) clinopyroxene → clinoamphibole, chlorite, epidote, carbonates, saponite

No significant calcrete development has been noted at Andover; this absence would be expected with an assemblage poor in clinopyroxene. Minor magnesium-calcium carbonate is present in soils, and spectral reflectance analysis shows that it has a composition between dolomite and magnesite, indicating it has been derived from the breakdown of peridotites.

Scanner data characteristics

The NS001 scanner had eight sensing bands, compared to seven on the Landsat-5 TM (Table 37); ground pixel size was 10 m x 10 m for NS001 (at the altitude flown) and 30 m x 30 m for TM. The TM data are rated as low-resolution, and the NS001 data as high-resolution.

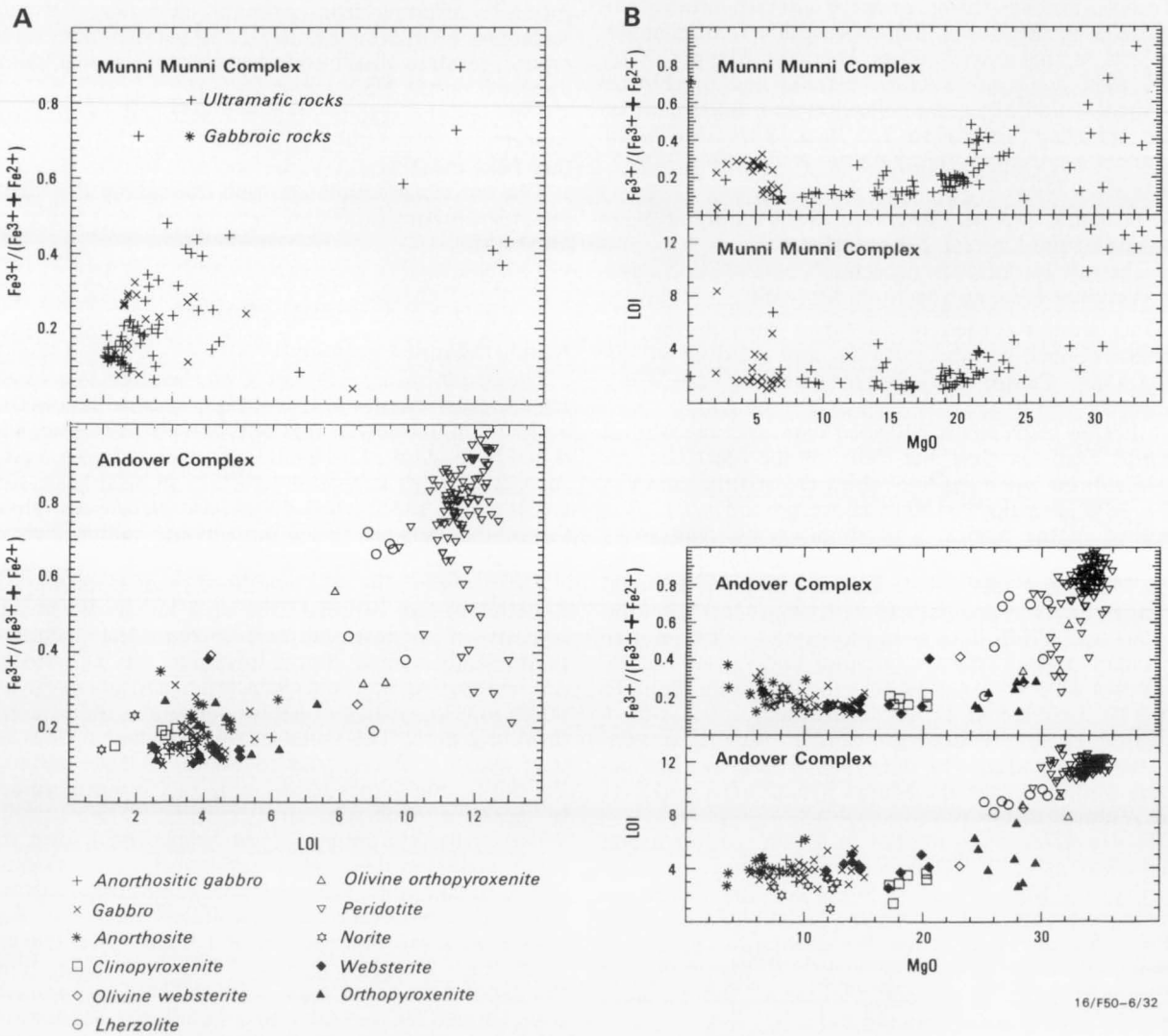

Fig. 108A, B. Alteration (oxidation and hydration) of ultramafic rocks, Munni Munni and Andover complexes. ('LOI' = loss on ignition.)

Three sets of Landsat-5 TM data were used for Munni Munni. The first was the radiometrically uncorrected Standard-Frame Scene, Path 113, Row 75 (AMIRA Signal Processing Experiment 84/P203). The second set, used for both Munni Munni and Andover, was the Non-Standard-Frame Scene, Path 113, Row 75; the second set included radiometric corrections (varying detector responses) applied by ACRES. The third set was the radiometrically uncorrected Standard-Frame Scene, Path 114, Row 75.

The TIMS scanner recorded six bands in the thermal-infrared wavelength region from 8.2 μm–12.2 μm (Table 38), with ground pixel size of 10 m x 10 m.

Table 37. Wavelengths recorded by Landsat-5 TM and NS001 scanners

Landsat-5 TM			*NS001*		
Band	*nm*	*CL*	*Band*	*nm*	*CL*
1	450–520	485	1	450–520	485
2	520–600	560	2	520–600	560
3	630–690	660	3	630–690	660
4	760–900	835	4	760–900	835
			5	1120–1370	1245
5	1550–1750	1650	6	1550–1750	1650
7	2080–2350	2215	7	2080–2350	2215
6	10 400–12 500	11 450	8	10 400–12 500	11 450

CL: centre line. Note: NS001 Band 5 has no equivalent on the Landsat-5 TM.

Table 38. Wavelengths recorded by TIMS scanner

Band	*Wavelength (μm)*
1	8.2–8.6
2	8.6–9.0
3	9.0–9.4
4	9.4–10.2
5	10.2–11.2

Spectral reflectance

Spectral-reflectance measurements of freshly-broken, weathered and lichen-covered rocks and soils from Munni Munni and Andover were carried out both in the field and in the laboratory using the InfraRed Intelligent Spectroradiometer (IRIS; manufactured by Geophysical Environmental Research, USA). Spectra are relative to a Halon standard.

Figure 109 shows spectral curves of representative mafic and ultramafic rocks. The spectral reflectance of fresh ultramafic rocks ranges from 8% to 14% in the 600–900 nm region, dropping to 6% in the 2200–2400 nm region. Some of the spectra show absorption features centred at 640–650 nm, 1020–1050 nm, and 2300 nm, indicating clinopyroxene; other spectra show broad absorption features centred at 630 nm and 1030–1050 nm, indicating olivine. These interpretations are supported by the mineral spectra of Adams (1975). Fresh mafic rocks have a higher reflectance than ultramafic rocks, with maxima ranging from 10% to 30% in the 1500–1800 nm region. Although reflectance drops towards the ultraviolet region (400 nm), it shows broad absorption features at 1030 nm, with slight increases in the 600 nm region. Reflectance falls sharply toward the far-infrared; absorption features at 2250 nm and 2332 nm indicate the presence of epidote. The spectral measurements differ markedly from those published in the benchmark work by Hunt & others (1974). Hunt & others' results, derived from laboratory measurements

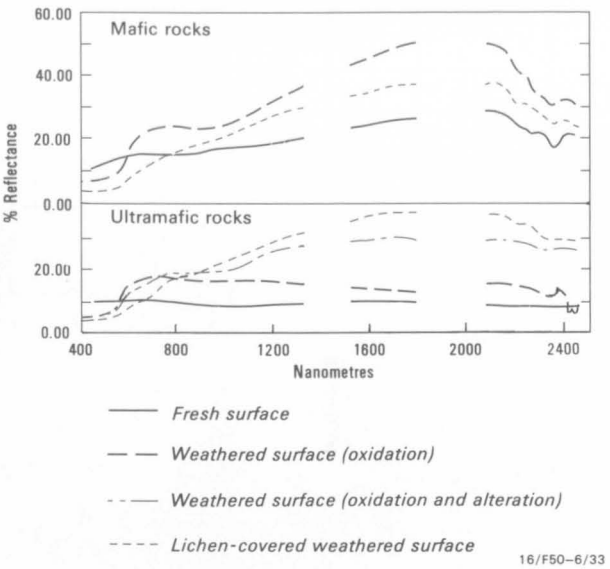

Fig. 109. Remote-sensing spectra of representative mafic and ultramafic rocks, Andover and Munni Munni complexes.

of powdered materials and reproduced in Figure 110, indicate that ultramafic rocks have a higher reflectance than mafic rocks, whereas our field and laboratory measurements on fresh and weathered surfaces show that mafic rocks have a higher reflectance than ultramafic rocks.

Spectra of both weathered mafic and ultramafic rocks (Fig. 109) are strongly influenced by the presence of iron in the 800–1000 nm region, which relates to the surface concentration of iron oxides from weathering. The analysis of all available reflectance curves of ultramafic rocks (not shown in Fig. 109) showed two discrete types: in the first case reflectance maxima range from 18% to 24% in the 900–1300 nm region, dropping to about 6% towards the ultraviolet, and to about 12% towards the 2300 nm region; in the second case, reflectance maxima range from 24% to 32% (exceptionally to 78%) in the 1200–1800 nm region, dropping to about 20% toward the 900–1100 nm region, where they display broad absorption features, and then to about 6% towards the ultraviolet. Reflectance drops evenly to a 25% average in the 2300 nm region.

In weathered gabbros, reflectance has an average maximum of 60% in the 2000–2100 nm region, dropping to about 30%–40% near 2500 nm, and to 5%–10% in the 400 nm region.

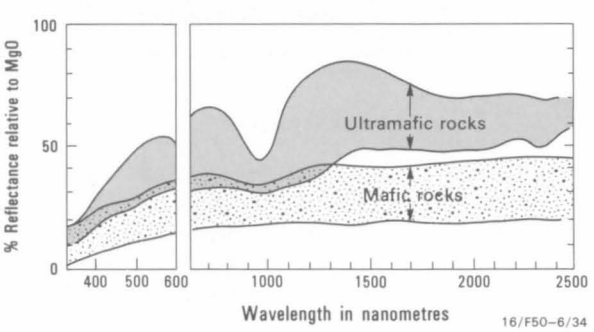

Fig. 110. Reflectance versus wavelength area diagram for 0–74 μm particle size range samples (modified after Hunt & others, 1974). The break in the Figure indicates a change in the horizontal scale.

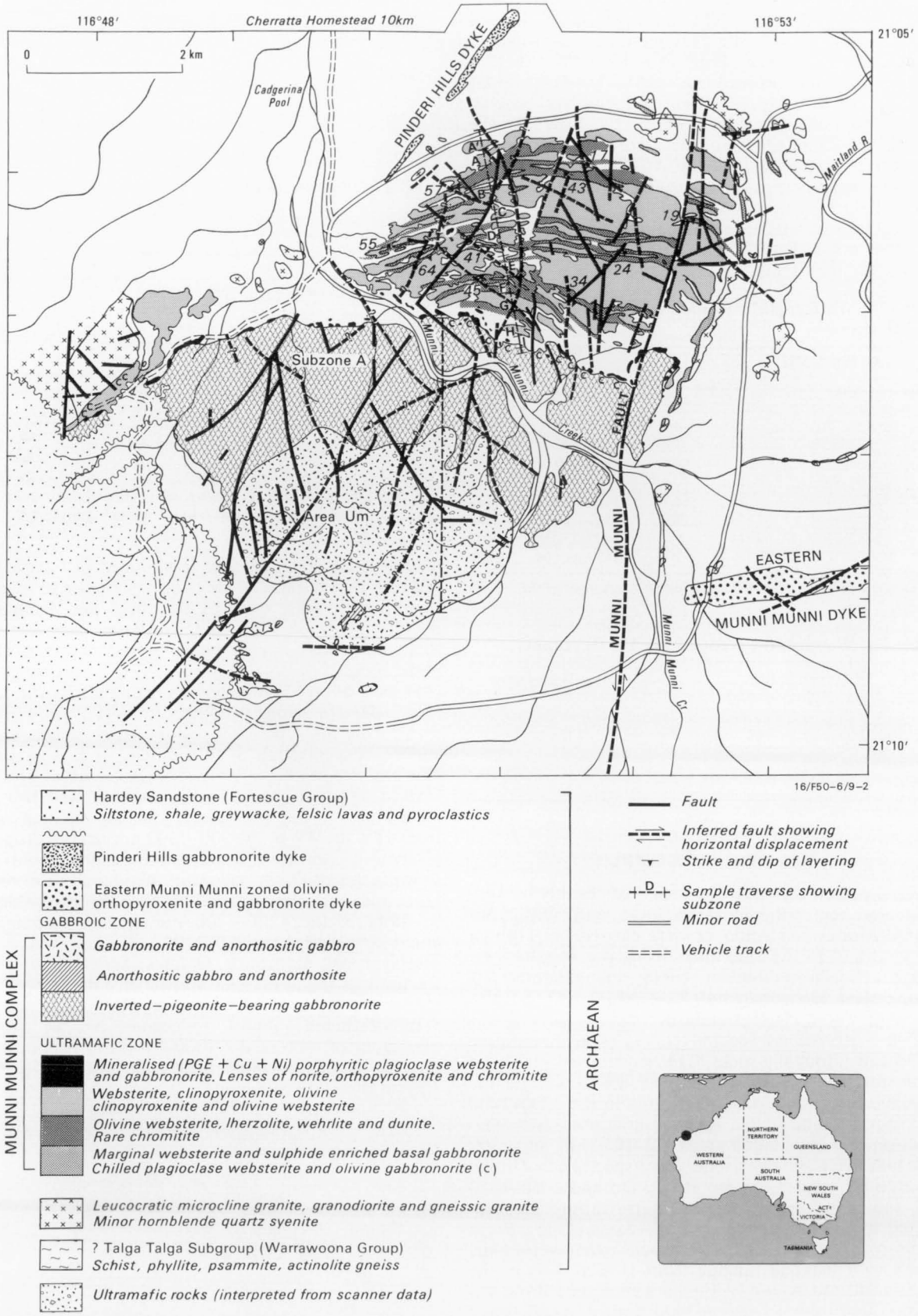

Fig. 111. Modified geological map of the Munni Munni Complex (after Hoatson, Fig. 7, this Bulletin).

The spectral curves of lichen-covered samples, of both mafic and ultramafic rocks, show lichen-masking effects on spectral features in the 400–2000 nm region; however, some absorption features deriving from the underlying mineralogy are discernible in the 2100–2400 nm region.

At Andover the spectral reflectance of volcanics, both freshly broken and weathered samples, is similar to

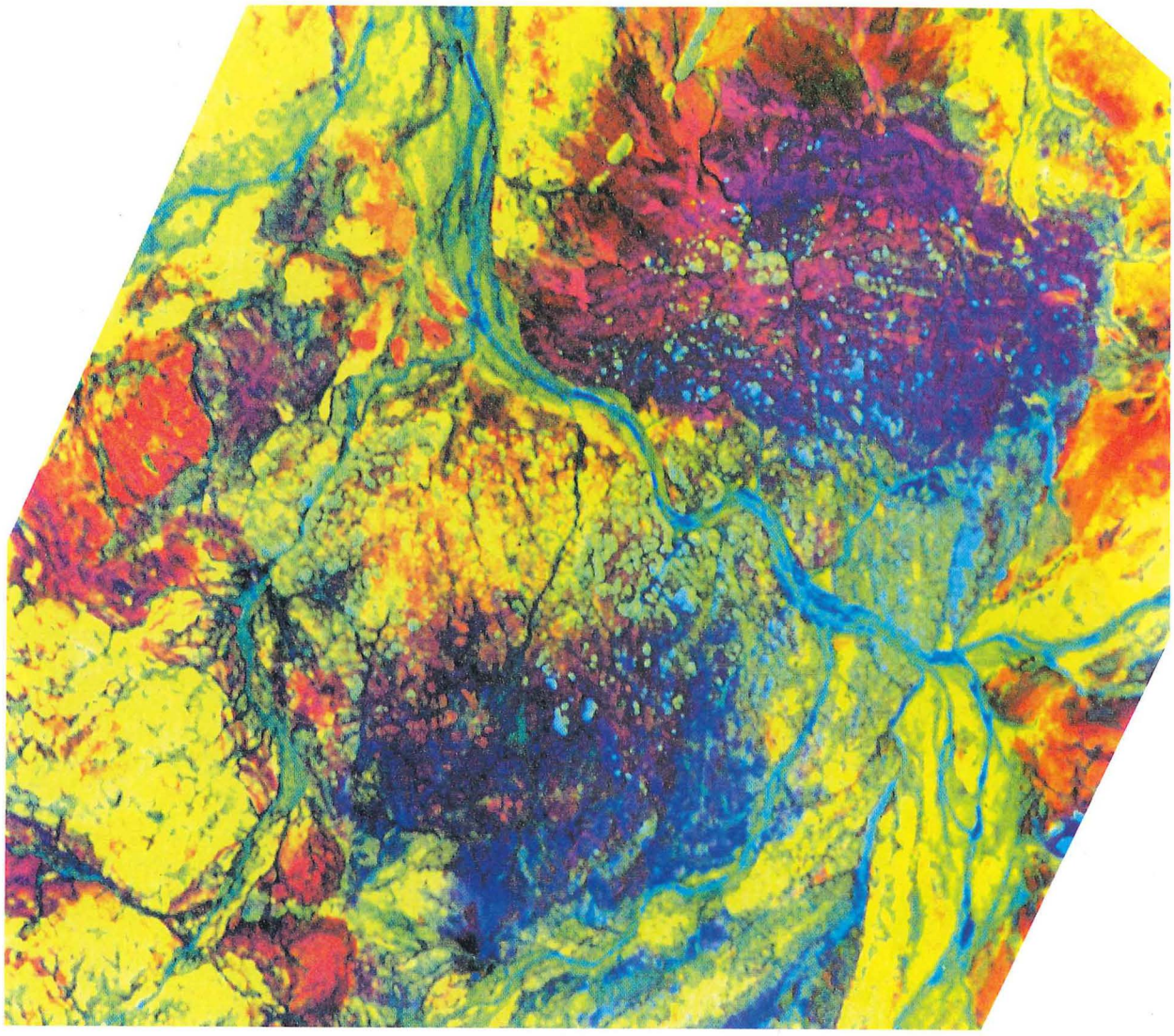

Fig. 112. NS001(NASA airborne Thematic Mapper Simulator) composite image using band ratios 3/2, 6/3, −5/6 shown as RGB (red, green, and blue), respectively, for the Munni Munni Complex.

that of gabbros, with an average maximum reflectance of about 50% in the 2000–2100 nm region.

Digital data processing

Initial processing of all data involved the subtraction of dark pixel values from every band, to correct for additive atmospheric scatter. The data were then calibrated by the radiance-to-reflectance conversion method of Honey & others (1974). Various image-processing techniques were assessed, including principal-component analysis; however, emphasis was placed on band ratioing to enhance spectral differences determined from field spectral reflectance information. Only those methods which proved of particular value are discussed here.

Munni Munni Complex

NS001 scanner data. Figure 112 is the NS001 composite ratio-image 660 μm/560 μm (3/2), 1650 μm/660 μm (6/3), −(1245) μm/660 μm (−5/6) displayed as red, green, and blue (RGB) respectively. Band −5, or negative 1245 nm, means the reversal of band 5 and equals 255 DN minus band 5 DN values. Selection of band ratios was based on spectral reflectance curves: ratio 3/2 was selected to show Fe, ratio 6/3 to discriminate gabbro, and ratio −5/6 to discriminate ultramafic rocks.

Although vegetation to some extent still masks the various spectral responses, the composite ratio-image proved to be particularly effective in discriminating the ultramafic rocks shown as magenta and blue, and the mafic rocks shown as yellow. It should be noted that, as other non-mafic materials, such as sand plains, are also displayed as yellow, the ratio-image cannot discriminate mafic material from sand plains (Macias & others, 1987).

The composite ratio-image has succeeded in discriminating the major ultramafic rock units (pyroxenites and peridotites) mapped in the field (see appended map sheet). The recessive areas, underlain by *in situ* soils, derived from peridotites are dominated by red and magenta, and the pyroxenite-rich areas by blue and green. The carbonate-rich soils north and west of the ultramafic zone are shown as deep-red to red-magenta. Discrimination within the ultramafic rocks is given by

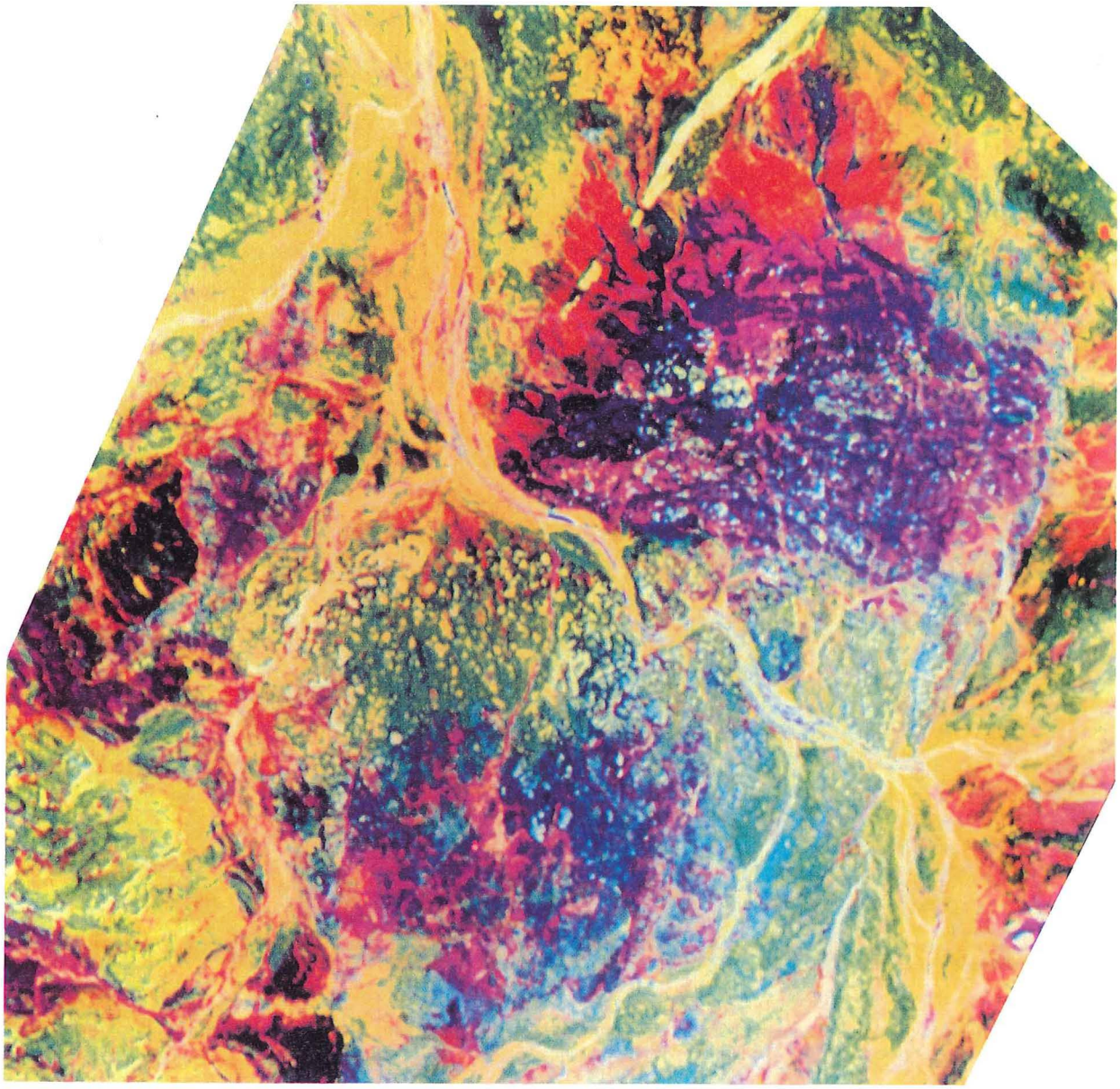

Fig. 113. NS001 composite image using principal component PC4, and band ratios 6/3 and −5/6, shown as RGB (red, green, and blue) respectively, for the Munni Munni Complex.

the blue component of ratio −5/6, which has no equivalent in TM data. No combination of NS001 image processing was found that could discriminate the PGE-bearing layer between the mafic and ultramafic rocks. Granitic rocks are shown as orange and yellow. Fire-burn areas, in which the spinifex cover has been reduced, are dark-green.

Integration of the field mapping results (Fig. 111), the NS001 composite ratio-image (Fig. 112), and large-scale conventional-colour aerial photography, reveals that the composite ratio-image displays large, individual outcrops of both mafic and ultramafic rocks as an almost identical green-blue. Thus NS001 ratio-imagery could not readily discriminate large, individual outcrops of mafic rocks from ultramafic rocks (Macias & others, 1987). In the early stages of image analysis we attributed this problem to the presence of a weathering crust giving a similar spectral response from both rock types. Later, field work, supported by spectral measurements, showed that dense, black lichen is masking the rock or mineral reflectance, and the green-blue display in the NS001 imagery represents lichen. This highlights a significant problem associated with image-processing procedures that attempt to derive spectral 'signatures' from remotely sensed data by the direct examination of digital values over major rock outcrops. Without a knowledge of local environmental characteristics, these procedures would lead to erroneous interpretation of results. Field observation established that lichen is absent from rock surfaces that are exposed to fire or substantial heat generated by periodic spinifex burning (Simpson, 1990). It is significant that the major lithological discriminations achieved with NS001 data were in areas of subcrop, rubble, and soil, i.e. where weathering has been at a maximum and where lichen could not become established because of periodic fire.

Additional implications from NS001 data interpretation. Over the gabbroic subzone A of the Munni Munni

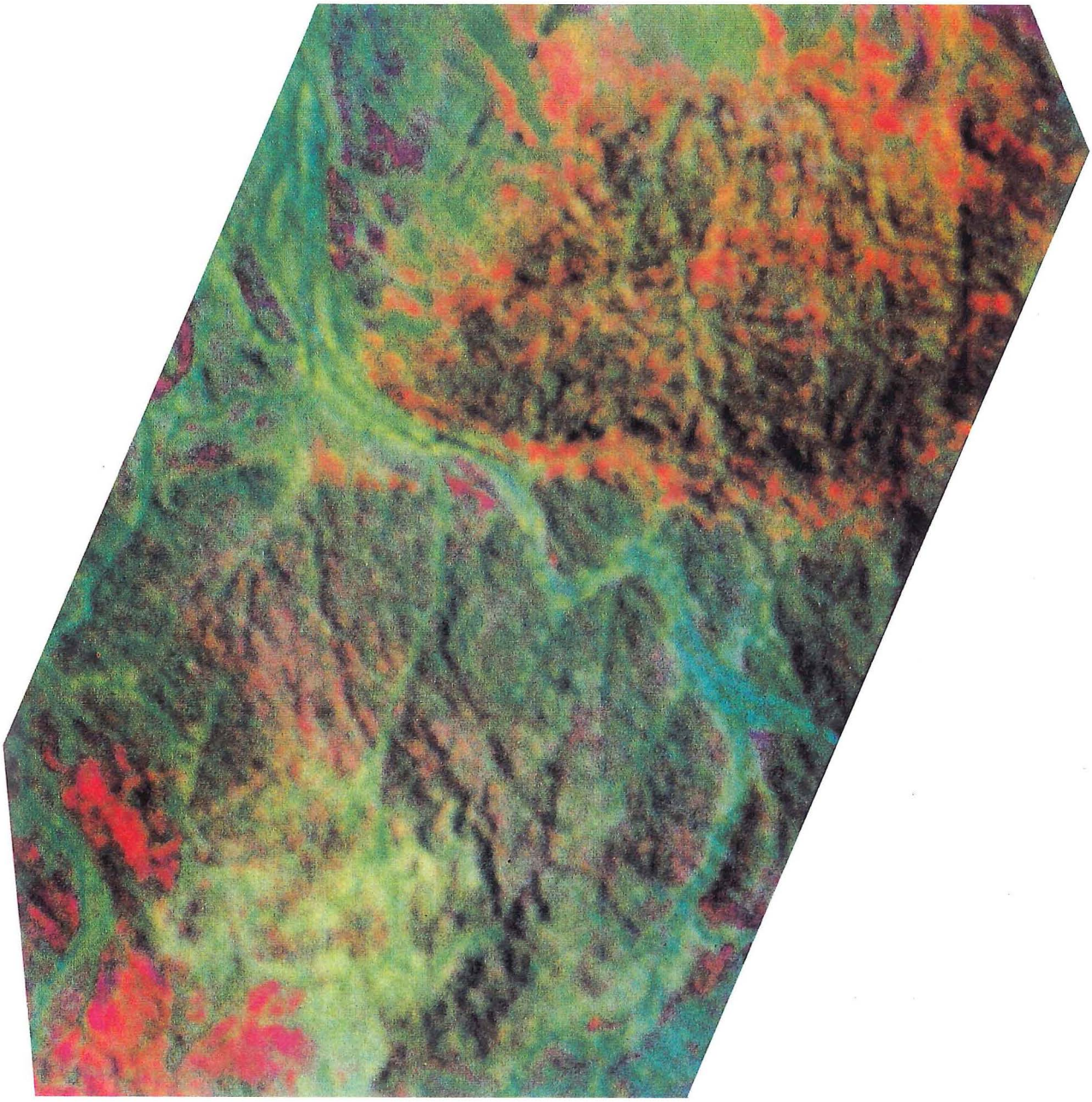

Fig. 114. TIMS(NASA airborne Thermal-Infrared Multispectral Scanner) composite image using bands 1, 4, and 6 shown as RGB (red, green, and blue) respectively, for the Munni Munni Complex.

Complex (Fig. 111), the NS001 ratio image shows, to the north, patches of brown-red that are identified as ultramafic rocks; in the southern part of subzone A, the image shows a distinctive area, named 'area Um', displayed in red, dark-blue and minor yellow and cyan, similar to colours typical of the ultramafic zone north of Munni Munni Creek. Field inspection showed that area Um is mostly covered by soil, almost devoid of outcrop, and in places densely covered by spinifex. Study of conventional-colour aerial photography showed that area Um coincides with a large circular region, topographically lower than the mafic hills to the north and west. However, area Um could not be distinguished lithologically within subzone A. Study of false-colour-infrared aerial photography shows discrete white areas of carbonate-rich soil associated with area Um. Spectral-reflectance analyses of soil samples from area Um indicate that some of the soils are abundant in calcium carbonate and similar to the calcretes west of the ultramafic zone. One rock sample collected in area Um has been identified spectrally as ultramafic.

Figure 113 is a composite image of principal component PC4, and band ratios 6/3 and −5/6, displayed as RGB. Here, PC4 replaces ratio 3/2 (the red band of Fig. 112), for on inspection it was found to enhance secondary carbonates. In Figure 114, carbonate-rich soils, shown as red to deep-red, are seen to be associated with all areas of ultramafic rocks, including the relatively narrow mafic-ultramafic contact zone south of Munni Munni Creek. Red areas, associated mainly with drainage, occur in area Um too, and indicate carbonate-rich material. Ultramafic rocks are shown as red-magenta and blue-magenta, and lichen-covered ultramafic outcrops are shown as cyan. Mafic rocks are light-green, and lichen-covered mafic outcrops are various yellows; some gabbros show up as cyan in the

eastern portion of the mafic zone, at the ultramafic contact. Granitic rocks are shown as green, to dark-green, to black; the upper part of the Fortescue Group preserved here is shown as yellow and green, while outcrops lower in the section are shown as red and magenta.

Airborne magnetics (Fig. 8) show a local magnetic high almost coinciding with the centre of area Um.

Observations on area Um thus include:

— remote-sensing images showing carbonate-rich soils characteristic of ultramafic rocks;
— its coincidence with a circular topographic low, i.e. erosionally recessive, suggestive of peridotite; and
— its coincidence with a local magnetic high.

From this we conclude that area Um may be underlain by ultramafic rocks, possibly a late-intrusive phase. Further field work is required to verify this.

TIMS data. No thermal emissivity data on Munni Munni were available at the time of processing. Emissivity curves published by Lyon & Patterson (1966) show that with decreasing silica content there is a systematic shift of emissivity minima towards the longer wavelengths. These curves also indicate that mafic rocks have emissivity minima between 9.0 and 10.0 μm, which corresponds with TIMS band 4 (Table 38), and peridotite/serpentine-rich rocks have minima between 10.0 and 10.5 μm., corresponding with TIMS band 5. Processing methods concentrated on attempting to discriminate the dominant rock types by using the expected emissivity differences between bands 4, 5, and the other bands. As TIMS bands are highly correlated, the decorrelation stretch technique (inverse principal component transformation: Kahle & others, 1980) was used.

The TIMS composite image in Figure 114 shows bands 1, 4, and 6 as red, green, and blue respectively. It discriminates ultramafic rocks as light- to dark-green, mafic rocks as pink-green and dark-green, and sandy soils as yellow to blue-green. The image maps the distribution of gabbroic rocks more precisely than the NS001 composite ratio-image (Fig. 112), in which gabbros and sandy soils are shown in yellow hues. Area Um is shown as light yellow-green, and its coinciding circular topographic low is quite distinct; however, there are no colour displays similar to those from ultramafic rocks or their weathering products.

Landsat TM data. A basic TM composite image, using bands 1, 4, and 7, and displayed as RGB (Fig. 115), was first produced to discriminate the major rock types. It discriminates to some extent between gabbro (magenta to dark-brown) and ultramafic rocks (light-brown). However, the discrimination is significantly hindered by the spectral response of vegetation, in particular by recent fireburns (areas of olive-green on the ultramafic rocks and blue on the gabbro). (A NS001 composite image 147 does not show the fireburns, indicating that the fires occurred after October 1985.) The colours are due to a mixed spectral response from rocks and from spinifex regrowth. The olive-green burn area on ultramafic rocks suggests the presence of healthy spinifex regrowth and may represent a somewhat older fireburn, whereas the blue area on gabbro suggests scattered, and/or less dense, recent regrowth.

Figure 116 is a TM composite ratio-image 1650 μm/2215 μm (5/7), 1650 μm/660 μm (5/3), 2215 μm/835 μm (7/4), displayed as RGB, selected to discriminate, and to enhance differences in, ultramafic rocks, and to differentiate gabbros and doleritic rocks. It discriminates adequately between ultramafic rocks (red-brown) and-mafic rocks (blue), with some discrimination of the layering in the ultramafic rocks. As with the NS001 data, the TM data did not discriminate between rocks over outcrops extensively covered by lichen.

Andover Complex

Landsat TM data. Figure 118 is a TM composite ratio-image 5/7, 5/3, 7/4 displayed as RGB. The image provided excellent discrimination of ultramafic rocks (deep-red-brown) and gabbros (green to yellow), adequate discrimination of doleritic dykes (pale-blue) and granite (greenish-blue), and poor discrimination of volcanics. Field checking confirmed that the discrimination of ultramafic rocks was accurate, and a new interpretation of the attitude of the body can now be proposed. Previously, the major ultramafic body was believed to dip to the northwest at 40–60° (Hickman, 1983). Examination of TM images, focusing on the distribution of ultramafic outcrops in the northeastern half of the complex, combined with patterns indicative of flat-lying lithological units, led to the interpretation that this part of the body is relatively thin and essentially flat-lying. This was corroborated by subsequent field work (Wallace, this Bulletin).

Discrimination of mafic and ultramafic rocks using the low-resolution TM data was most successful for the Andover Complex; it is significant that Andover has less spinifex and lichen cover than Munni Munni.

Discussion

We have successfully discriminated mafic and ultramafic rocks in the Munni Munni and Andover complexes by using Landsat-5 satellite TM and airborne scanner imagery. The scanner imagery can assist, substantially and cost-effectively, the mapping of layered mafic-ultramafic complexes in the west Pilbara Block. Landsat MSS data on the other hand have limited application in the discrimination of mafic-ultramafic rocks. Prior knowledge of the vegetation characteristics of the region is crucial for reliable interpretation and mapping from processed imagery.

Processing of raw, uncalibrated TM (e.g. band-ratio 5/3, 5/1, 4/7 as RGB) will allow some discrimination of ultramafic rocks (as blue). To achieve the maximum degree of discrimination among rock types, it is important to correct and calibrate the data before predictive ratioing. The usefulness of TM may be limited by its 30-m pixel size, as many peridotite and pyroxenite layers can be thinner than the 30-m resolution.

High-resolution aircraft scanner data are essential if reliable subdivision at larger scales is required. NS001 imagery discriminated the major ultramafic units, selected from field observations by Hoatson (see appended map sheet) as being suitable for geological mapping. Lithological discrimination was mainly via the different weathering products of the various ultramafic rock types. The degree and type of weathering affecting the Munni Munni Complex site was obviously critical in determining the success of the NS001 application, and this must be borne in mind when attempting to use the processing techniques described above for similar rock types in different environments.

The NS001 band-ratios, which provided excellent mafic-ultramafic discrimination, could not be reproduced in the TM data. This relates to both the better pixel resolution (10 m) and spectral resolution (additional band 5) of the NS001 scanner, and to the influence of different atmospheric conditions on data recorded on different dates at different aircraft or satellite altitudes. Given the uncertainties involved with

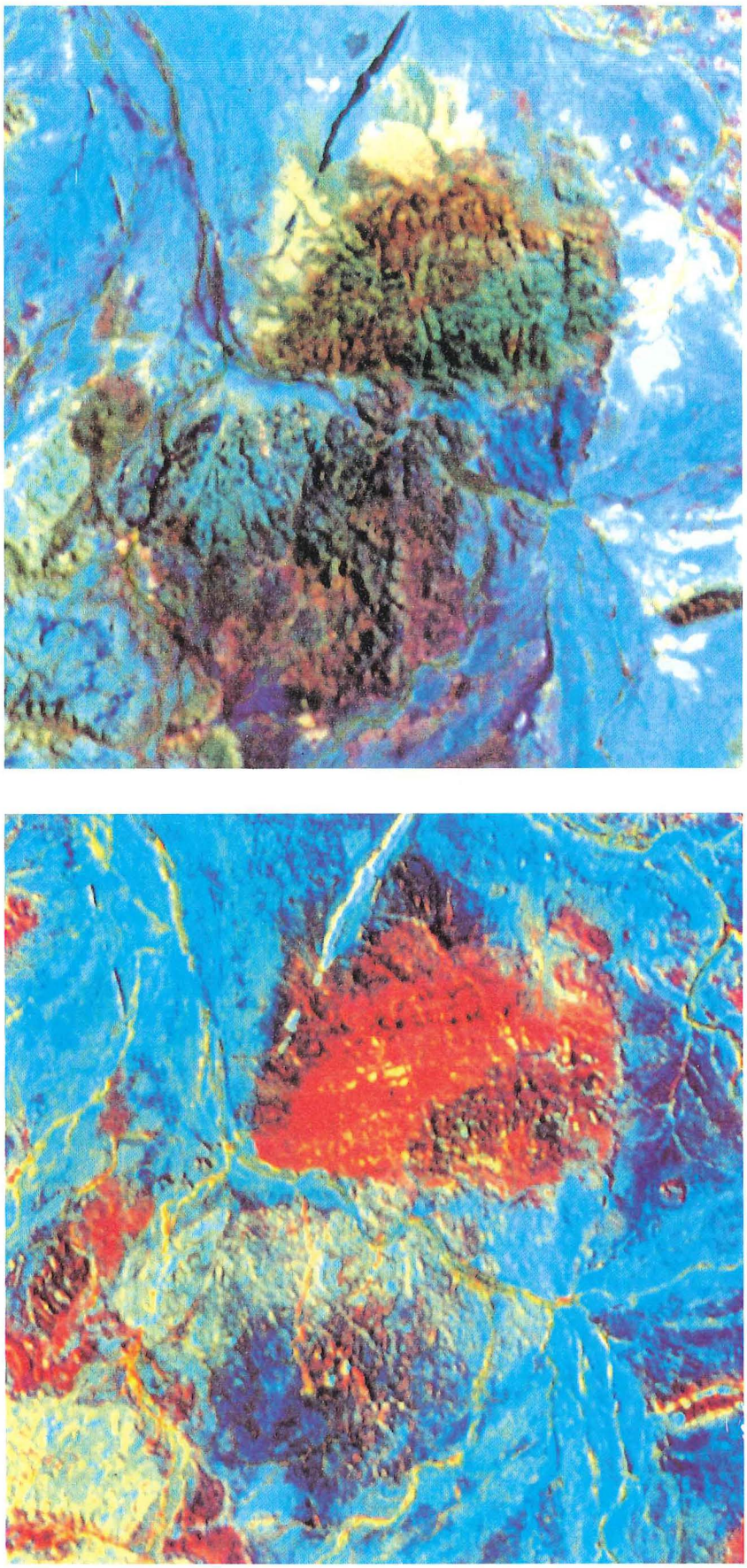

Fig. 115 (top). TM composite image using bands 1, 4, and 7 shown as RGB (red, green, and blue), respectively, for the Munni Munni Complex. Fig. 116 (lower). TM composite image using band ratios 5/7, 5/3, and 7/4 shown as RGB (red, green, and blue) respectively, for the Munni Munni Complex.

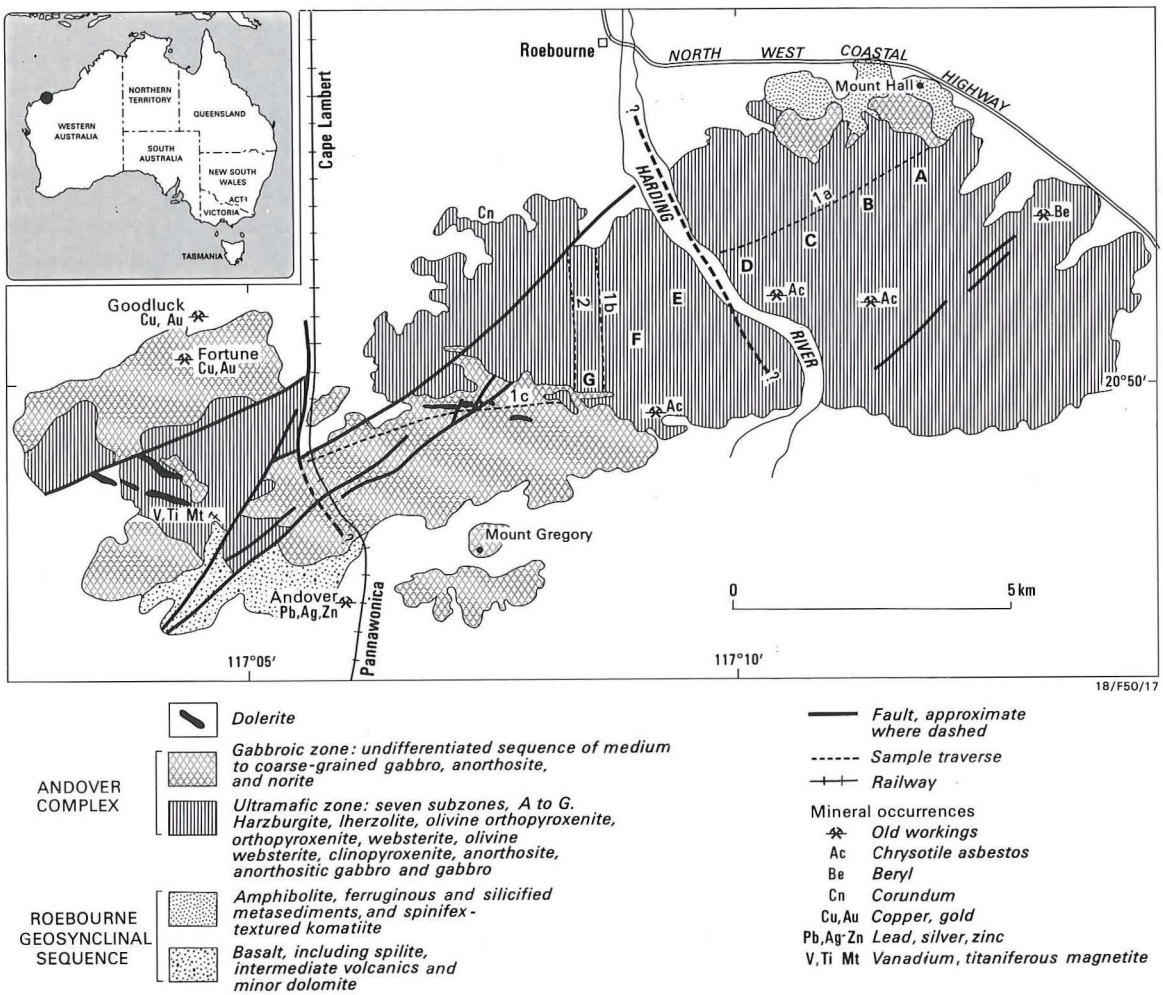

Fig. 117. Geological map of the Andover Complex (after Wallace, Fig. 85, this Bulletin).

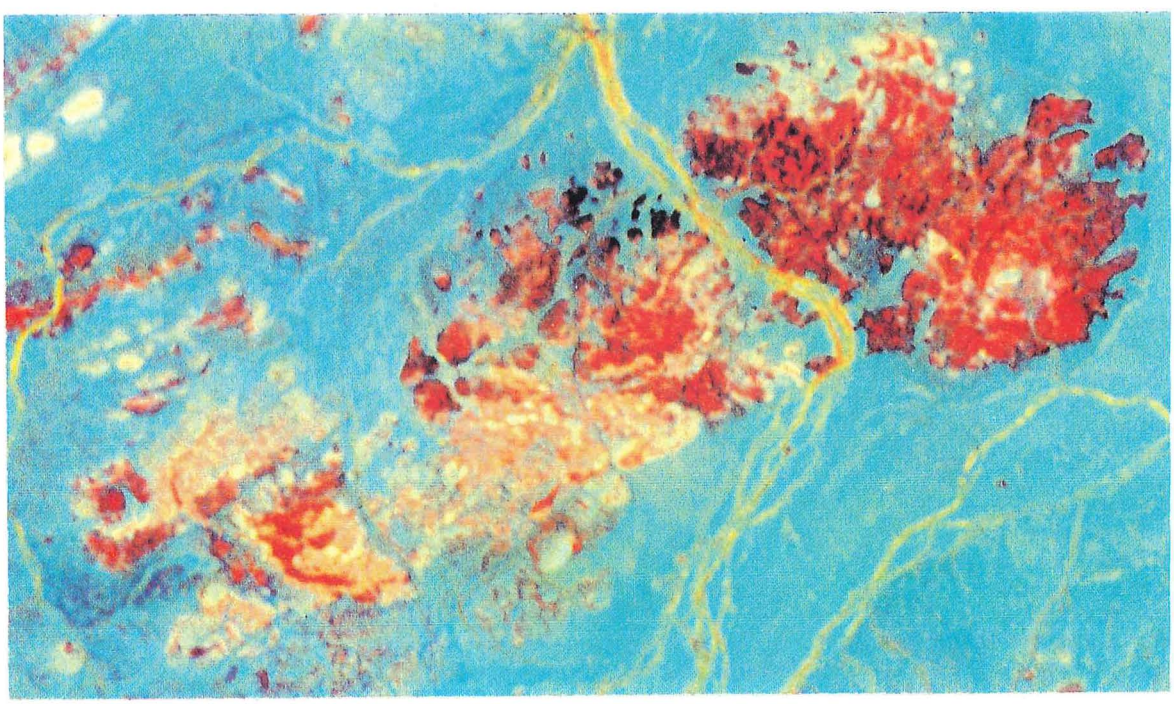

Fig. 118. TM composite image using band ratios 5/7, 5/3, and 7/4 shown as RGB (red, green, and blue) respectively, for the Andover Complex.

this type of data, acquired for the localities investigated, it is important that adequate corrections be carried out. However, currently, systematic correction routines are not readily applicable. The most suitable combinations of calibrated TM data selected for discrimination of mafic and ultramafic rocks at Andover did not involve any of the equivalent NS001 ratios used on Munni Munni.

Airborne thermal infrared (TIMS type) imagery would be useful in the initial stages of a survey to discriminate the major rock types. However, for further subdivision of rock types high-resolution aircraft scanner imagery (NS001-type) is more suitable.

The influence of the black-lichen and spinifex cover was unforeseen. Lichen covering even less than half of the rock surface can effectively mask most of the spectral response from the rock underneath. Similarly, spinifex density has a more significant influence on ground reflectance than was initially thought: field measurements, using IRIS, in the Munni Munni Complex show that spinifex density of between 30% and 40% can totally mask the reflectance from underlying soil and/or rock. This may be due to scattering from spinifex spines, combined with the fairly uniform separation between individual plants. Even in areas where burning has reduced the density of spinifex, interpretation is hampered by patterns of fireburns of different ages (Simpson, 1990). Both these factors influenced the effectiveness of remote sensing over the Munni Munni Complex, where ratioing processing, although it helped to discriminate between rock types, and reduced the effect of fireburns in spinifex on ultramafic rocks, was less successful than over the Andover Complex.

As rock discrimination is severely hampered by dense spinifex, one should be cautious when applying processing routines to areas with different vegetation characteristics. Application of the TM band combinations used successfully in the west Pilbara did not help in the discrimination of the densely-spinifex-covered mafic-ultramafic sequences of the Giles Complex in the Musgrave Block, central Australia (Macias & Simpson, 1990).

Availability of spectral instrumentation

Airborne multispectral scanners

Because NS001 and TIMS scanners are NASA scientific research instruments not routinely available in Australia, some comments on the availability of alternative scanners are given below.

Two airborne multispectral scanners are commercially available in Australia (1992). They are the Geoscan Mark 2 operated by Geoscan Pty Ltd, PO Box 1017, West Perth, WA, 6005, and the Daedalus 1268 Airborne Thematic Mapper operated by CSIRO's Office of Space Science & Applications (COSSA), GPO Box 3023, Canberra, ACT, 2600.

— **Geoscan Mark 2.** This scanner records up to 24 wavelength bands selected by the client from 46 detector channels. The 46 channels comprise 32 channels in the very-near infrared (VNIR : 490–1090 nm), 8 in the short-wave infrared (SWIR : 2020–2370 nm), and 6 in the thermal infrared (TIR : 8500–12 000 nm). The pixel size is variable from 2 m to 20 m (depending on flight altitude chosen). It is the only instrument currently available which has six bands in the thermal infrared region (from 8500–12 000 nm) and thus has the same capability as the NASA TIMS instrument discussed above.

— **Daedalus 1268 Airborne Thematic Mapper.** This scanner is capable of recording up to 11 separate bands, depending on the detector heads selected (Table 39). It records six bands in the VNIR and SWIR wavelengths, similar to those of Landsat TM, plus additional bands as shown in Table 39. From an altitude of 2000 m the pixel resolution is either 5 m or 2.5 m.

Table 39. Daedalus 1268 band combinations

Band	*Combination 1 (μm)*	*Combination 2 (μm)*
1	0.420–0.450	0.420–0.450
2	0.450–0.520	0.450–0.520
3	0.520–0.600	0.520–0.600
4	0.605–0.625	0.605–0.625
5	0.630–0.690	0.630–0.690
6	0.695–0.750	0.695–0.750
7	0.760–0.900	0.760–0.900
8	0.910–1.050	0.910–1.050
9	1.550–1.750	1.550–1.750
10	2.080–2.350	Not applicable
11	8.5–13.0	3.0–5.0
12	8.5–13.0 (*)	8.5–13.0

(*) Differential gain.

Airborne imaging spectrometers (AIS)

These are narrow-bandpass instruments which record a large number of bands (between 100 and 200) for each pixel. The data allow a spectral curve to be plotted for each pixel; thus they have the potential to positively identify the dominant material within the pixel area. The NASA AIS was operational during flights in the west Pilbara; however, the data were not used because of data-corruption problems. It is expected that airborne imaging spectrometers will become available for commercial and scientific use in Australia by 1994, and satellite-based systems will become available in the late 1990s.

Field spectrometers

The reflectance curves of mafic and ultramafic rocks are sufficiently distinct such that, if a portable field spectrometer were available, they could provide a rapid identification method for mineral mapping purposes.

The IRIS is not a readily available, truly portable field instrument for spectral measurements. However, two 'hand-held' field spectrometers are available:

— The Portable Infra-Red Mineral Analyser (PIMA) that operates in the 1300–2500 nm wavelength interval. PIMA is manufactured by Integrated Spectronics Pty Ltd, Sydney, NSW, Australia.

— The Personal Spectrometer II (PSII) that operates in the 350–1050 nm wavelength interval (Goetz & others, 1991). PSII is manufactured by Analytical Spectral Devices Inc., Boulder, Colorado USA.

Acknowledgements

We are indebted to Dean Hoatson and David Wallace for providing all necessary geological information on both complexes, and for helpful discussions. We acknowledge Hunter Resources Ltd for access to diamond-drill core. We thank John Creasey of AGSO's Image Processing Centre, whose comments improved the text.

REFERENCES

ABBEY, S., 1983—Studies in 'standard samples' of silicate rocks and minerals, 1969–1982. *Geological Survey of Canada, Paper* 83, 15.

ABRAMS, M. J., 1986—Mapping the Oman Ophiolite using TM data. Proceedings of the 5th Thematic Conference, *Remote Sensing for Exploration Geology*, 85–95.

ABRAMS, M. J., ROTHERY, D. A., & PONTUAL, A., 1988—Mapping in the Oman Ophiolite using enhanced TM images. *Tectonophysics*, 151, 387–401.

ADAMS, J. B., 1975—Interpretation of visible and near-infrared diffuse reflectance spectra of pyroxenes and other rock-forming minerals. *In* KARR, C. (Editor)—INFRARED AND RAMAN SPECTROSCOPY OF LUNAR AND TERRESTRIAL MINERALS. *Academic Press*, 91–115.

ALAPIETI, T. T., & LAHTINEN, J. J., 1989—Early Proterozoic layered intrusions in the northern part of the Fennoscandian Shield. *In* PAPUNEN, H. (Editor)—5th International Platinum Symposium, Abstracts. *Bulletin of the Geological Society of Finland*, 61, Part 1, 1989, 59.

ALAPIETI, T. T., & PIIRAINEN, T., 1984—Cu-Ni-PGE mineralization in the marginal series of the Early Proterozoic Koillismaa layered igneous complex, northeast Finland. *In* BUCHANAN, D. L., & JONES, M. J. (Editors)—SULFIDE DEPOSITS IN MAFIC AND ULTRAMAFIC ROCKS. Proceedings of IGCP Projects 161 & 91, Third Nickel Sulphide Field Conference, Perth, WA, 23–25 May 1982. *Institution of Mining & Metallurgy, London*, 123–131.

ANDERSEN, D. J., & LINDSLEY, D. H., 1985—New (and final!) models for the Ti-magnetite/ilmenite geothermometer and oxygen barometer. *EOS*, 66, 416.

ANHAEUSSER, C. R., 1983—Archaean layered ultramafic complexes in the Barberton Mountain Land, South Africa. Information Circular 161. University of the Witwatersrand, Johannesburg, South Africa, 1–30.

ARCHER, R. H., 1979—Roebourne Urban Geology 2356 III (map). *Western Australia Geological Survey, 1 : 50 000 Urban Geology Series Map.*

ARNDT, N. T., 1977—The partitioning of nickel between olivine and ultrabasic and basic komatiite liquids. *Carnegie Institution of Washington, Year Book, 1976*, 553–557.

ARNDT, N. T., 1986—Komatiites: a dirty window to the Archaean mantle. *Terra Cognita*, 6, 59–66.

ARNDT, N. T., & JENNER, G. A., 1986—Crustally contaminated komatiites and basalts from Kambalda, Western Australia. *Chemical Geology*, 56, 229–255.

ARNDT, N. T., NELSON, D. R., COMPSTON, W., TRENDALL, A. F., & THORNE, A. M., 1991—The age of the Fortescue Group, Hamersley Basin, Western Australia, from ion microprobe zircon U-Pb results. *Australian Journal of Earth Sciences*, 38, 261–281.

ASHWORTH, J. R., 1986—The role of magmatic reaction, diffusion and annealing in the evolution of coronitic microstructure in troctolitic gabbro from Risör, Norway: a discussion. *Mineralogical Magazine*, 50, 469–473.

ATKINS, F. B., 1969—Pyroxenes of the Bushveld Intrusion, South Africa. *Journal of Petrology*, 10, 222–249.

AURET, J. M., HARMER, R. E., EGLINGTON, B. M., & SHARPE, M. R., 1989—Pb isotope systematics in the Eastern Bushveld Complex. *In* ORIGIN OF MINERALIZATION IN SOUTHERN AFRICAN LAYERED COMPLEXES. *University of Witwatersrand, Johannesburg, South Africa, Abstracts*, 21–22.

BALLHAUS, C. G., & BERRY, R. F., 1991—Crystallization pressure and cooling history of the Giles layered igneous complex, central Australia. *Journal of Petrology*, 32, 1–28.

BALLHAUS, C. G., & GLIKSON, A. Y., 1989—Magma mixing and intraplutonic quenching in the Wingellina Hills intrusion, Giles Complex, central Australia. *Journal of Petrology*, 30, 1443–1469.

BALLHAUS, C. G., & STUMPFL, E. F., 1986—Sulfide and platinum mineralization in the Merensky Reef: evidence from hydrous silicates and fluid inclusions. *Contributions to Mineralogy & Petrology*, 94, 193–204.

BARLEY, M. E., 1984—Volcanism and hydrothermal alteration, Warrawoona Group, East Pilbara. *In* MUHLING, J. R., GROVES, D. I., & BLAKE, T. S. (Editors)—Archaean and Proterozoic basins of the Pilbara, Western Australia: evolution and mineralization potential. *The Geology Department and University Extension, University of Western Australia, Publication* 9, 23–36.

BARLEY, M. E., 1987—The Archaean Whim Creek Belt, an ensialic fault-bounded basin in the Pilbara Block, Australia. *Precambrian Research*, 37, 199–215.

BARLEY, M. E., & MCNAUGHTON, N. J., 1988—The tectonic evolution of greenstone belts and setting of Archaean gold mineralization in Western Australia: geochronological constraints on conceptual models. *In* HO, S. E., & GROVES, D. I. (Editors)—Advances in understanding Precambrian gold deposits, Vol. II. *The Geology Department and University Extension, University of Western Australia, Publication* 12, 23–40.

BARLEY, M. E., SYLVESTER, G. C., GROVES, D. I., BARLEY, G. D., & ROGERS, N., 1984—Archaean cal-alkaline volcanism in the Pilbara Block, Western Australia. *Precambrian Research*, 24, 285–320.

BARNES, SARAH-JANE, BOYD, R., KORNELIUSSEN, A., NILSSON, L. P., OFTEN, M., PEDERSEN, R. B., & ROBINS, B., 1988—The use of mantle normalization and metal ratios in discriminating between the effects of partial melting, crystal fractionation and sulphide segregation on platinum-group elements, gold, nickel and copper: examples from Norway. *In* PRICHARD, H. M., POTTS, P. J., BOWLES, J. F. W., & CRIBB, S. J. (Editors)—GEO-PLATINUM 87. 22–23 April 1987, Open University, Milton Keynes, United Kingdom. *Elsevier, England*, 113–143.

BARNES, SARAH-JANE, NALDRETT, A. J., & GORTON, M. P., 1985—The origin of the fractionation of platinum group elements in terrestrial magmas. *Chemical Geology*, 53, 303–323.

BARNES, STEPHEN J., 1989—Are Bushveld U-type parent magmas boninites or contaminated komatiites? *Contributions to Mineralogy & Petrology*, 101, 447–457.

BARNES, STEPHEN J., & CAMPBELL, I. H., 1988—Role of late magmatic fluids in Merensky-type platinum deposits: a discussion. *Geology*, 16, 488–491.

BARNES, STEPHEN J., HOATSON, D. M., & MCINTYRE, J. R., 1991—The Munni Munni Complex. *In* BARNES, STEPHEN J., & HILL, R. E. T. (Editors)—Mafic-ultramafic complexes of Western Australia. Excursion Guidebook No. 3. Sixth International Platinum Symposium, July 1991, Perth, WA. *IAGOD and the Geological Society of Australia*, 77–96.

BARNES, STEPHEN J., KEAYS, R. R., & HOATSON, D. M., 1992—Distribution of sulphides and PGE within the porphyritic websterite zone of the Munni Munni Complex, Western Australia. *Australian Journal of Earth Sciences*, 39, 289–302.

BARNES, STEPHEN J., MCINTYRE, J. R., NISBET, B. W., & WILLIAMS, C. R., 1990—Platinum group element mineralisation in the Munni Munni Complex, Western Australia. *Mineralogy & Petrology*, 42, 141–164.

BARNES, STEPHEN J., & NALDRETT, A. J., 1985—Geochemistry of the J-M (Howland) Reef of the Stillwater Complex, Minneapolis Adit Area. I. Sulfide chemistry and sulfide-olivine equilibrium. *Economic Geology*, 80, 627–645.

BARNES, STEPHEN J., & NALDRETT, A. J., 1986—Geochemistry of the J-M (Howland) Reef of the Stillwater Complex, Minneapolis Adit Area. II. Silicate mineral chemistry and petrogenesis. *Journal of Petrology*, 27, 791–825.

BARRIERE, M., 1976—Flowage differentiation: limitation of the 'Bagnold Effect' to narrow intrusions. *Contributions to Mineralogy & Petrology*, 55, 139–145.

BARTON, J. M., JR., CAWTHORN, R. G., & WHITE, J., 1986—The role of contamination in the evolution of the Platreef of the Bushveld Complex. *Economic Geology*, 81, 1096–1104.

BAXTER, J. L., 1978—Molybdenum, tungsten, vanadium and chromium in Western Australia. *Western Australia Geological Survey, Mineral Resources Bulletin* 11, 140 pp.

BEAUDOIN, G., LAURENT, R., & OHNENSTETTER, D., 1990—First report of platinum-group minerals at Blue Lake, Labrador Trough, Quebec. *Canadian Mineralogist*, 28, 409–418.

BEST, M. G., & MERCY, E. L. P., 1967—Composition and crystallization of mafic minerals in the Guadalupe igneous complex, California. *American Mineralogist*, 52, 436–474.

BESWICK, A. E., 1982—Some geochemical aspects of alteration and genetic relations in komatiitic suites. *In* ARNDT, N. T., & NESBIT, E. G. (Editors)—KOMATIITES. *Allen & Unwin, London.*

BESWICK, A. E., & SOUCIE, G., 1978—A correction procedure for metasomatism in an Archaean greenstone belt. *Precambrian Research*, 6, 235–248.

BETTENAY, L. F., BICKEL, M. J., BOULTER, C. A., GROVES, D. I., MORANT, P., BLAKE, T. S., & JAMES, B. A., 1981—Evolution of the Shaw Batholith—an Archaean granitoid-gneiss dome in the eastern Pilbara, Western Australia. *In* GLOVER, J. E., & GROVES, D. I. (Editors)—ARCHAEAN GEOLOGY. Second International Archaean Symposium, Perth, 1980. *Geological Society of Australia, Special Publication* 7, 361–372.

BHATTACHARJI, S., 1967—Mechanics of flow differentiation in ultramafic and mafic sills. *Journal of Geology*, 75, 101–112.

BHATTACHARJI, S., & SMITH, C. H., 1964—Flowage differentiation. *Science*, 145, 150–153.

BICKEL, M. J., BETTENAY, L. F., BOULTER, C. A., GROVES, D. I., & MORANT, P., 1980—Horizontal tectonic interaction of an Archaean gneiss belt and greenstones, Pilbara Block, Western Australia. *Geology*, 8, 525–529.

BICKEL, M. J., MORANT, P., BETTENAY, L. F., BOULTER, C. A., BLAKE, T. S., & GROVES, D. I., 1985—Archaean tectonics of the Shaw Batholith, Pilbara Block, Western Australia—structural and metamorphic tests of the Batholith concept. *In* AYRES, L. D., THUR-

STON, P. C., CARD, K. D., & WEBSTER, W. (Editors)—Evolution of Archaean supracrustal sequences. *Geological Association of Canada, Special Paper* 28, 325–341.

BIGGAR, G. M., 1974—Phase equilibrium studies of the chilled margins of some layered intrusions. *Contributions to Mineralogy & Petrology*, 46, 159–167.

BLAKE, D. H., 1981—Intrusive felsic-mafic net-veined complexes in north Queensland. *BMR Journal of Australian Geology & Geophysics*, 6, 95–99.

BLAKE, T. S., 1984—Evidence for the stabilization of the Pilbara Block, Australia. *Nature*, 307, 721–723.

BLAKE, T. S., 1990—Fortescue Group stratigraphy, palaeogeography and tectonics. *In* Recent advances in understanding the Archaean and Early Proterozoic geology of the Pilbara Craton, Abstracts. One-day seminar, 16 September 1990. *The Geology Department and University Extension, University of Western Australia*, 18–24.

BLAKE, T. S., & MCNAUGHTON, N. J., 1984—A geochronological framework for the Pilbara region. *In* MUHLING, J. R., GROVES, D. I., & BLAKE, T. S. (Editors)—Archaean and Proterozoic basins of the Pilbara, Western Australia: evolution and mineralization potential. *The Geology Department and University Extension, University of Western Australia, Publication* 9, 1–22.

BOUDREAU, A. E., 1990a—A review of the evidence for the high temperature hydrothermal concentration of the platinum-group elements in layered intrusions. *In* R. L. STANTON SYMPOSIUM: GONDWANA TERRANES AND RESOURCES. *Geological Society of Australia, Tenth Australian Geological Convention, Hobart, 1990, Abstracts 25*, 131–132.

BOUDREAU, A. E., 1990b—The chlorine connection and a hydromagmatic model for the concentration of the platinum-group elements in the Stillwater Complex, Montana. *In* R. L. STANTON SYMPOSIUM: GONDWANA TERRANES AND RESOURCES. *Geological Society of Australia, Tenth Australian Geological Convention, Hobart, 1990, Abstracts 25*, 141–142.

BOUDREAU, A. E., MATHEZ, E. A., & MCCALLUM, I. S., 1986—Halogen geochemistry of the Stillwater and Bushveld Complexes: evidence for transport of the platinum-group elements by Cl-rich fluids. *Journal of Petrology*, 27, 967–986.

BOUDREAU, A. E., & MCCALLUM, I. S., 1985—Features of the Picket Pin Pt-Pd deposit. *In* CZAMANSKE, G. K., & ZIENTEK, M. L. (Editors)—The Stillwater Complex, Montana: geology and guide. *Montana Bureau of Mines & Geology, Special Publication 92, IGCP Project 161*, 346–357.

BOUDREAU, A. E., & MCCALLUM, I. S., 1986—Investigations of the Stillwater Complex: III. The Picket Pin deposit. *Economic Geology*, 81, 1953–1975.

BOW, C., WOLFGRAM, D., TURNER, A., BARNES, STEPHEN J., EVANS, J., ZDEPSKI, M., & BOUDREAU, A., 1982—Investigations of the Howland reef of the Stillwater Complex, Minneapolis adit area: stratigraphy, structure, and mineralization. *Economic Geology*, 77, 1481–1492.

BRUGMANN, G. E., NALDRETT, A. J., & MACDONALD, A. J., 1989—Magma mixing and constitutional zone refining in the Lac des Iles Complex, Ontario: genesis of platinum-group element mineralization. *Economic Geology*, 84, 1557–1573.

BRYAN, W. B., & MOORE, J. G., 1977—Compositional variations of young basalts in the Mid-Atlantic Ridge rift valley near lat. 36°49'N. *Bulletin of the Geological Society of America*, 88, 556–570.

BUCHANAN, D. L., NOLAN, J., WILKINSON, N., & DE VILLIERS, J. R. R., 1983—An experimental investigation of sulfur solubility as a function of temperature in synthetic silicate melts. *Geological Society of South Africa, Special Publication* 7, 383–391.

BUCHANAN, D. L., & ROUSE, J. E., 1984—Role of contamination in the precipitation of sulfides in the Platreef of the Bushveld Complex. *In* BUCHANAN, D. L., & JONES, M. L. (Editors)—SULFIDE DEPOSITS IN MAFIC AND ULTRAMAFIC ROCKS. Proceedings of IGCP Projects 161 & 91, Third Nickel Sulphide Field Conference, Perth, WA, 23–25 May 1982. *Institution of Mining & Metallurgy, London*, 141–146.

BUDDINGTON, A. F., & LINDSLEY, D. H., 1964—Iron-titanium oxide minerals and synthetic equivalents. *Journal of Petrology*, 5, 310–357.

CABRI, L. J., & LAFLAMME, J. H. G., 1981—Analyses of minerals containing platinum-group elements. *In* CABRI, L. J. (Editor)—PLATINUM-GROUP ELEMENTS: MINERALOGY, GEOLOGY, RECOVERY. *Canadian Institute of Mining & Metallurgy, Special Volume 23*, 153–173.

CAMERON, E. N., 1978—The Lower Zone of the Eastern Bushveld Complex in the Olifants River trough. *Journal of Petrology*, 19, 437–462.

CAMERON, E. N., 1980—Evolution of the Lower Critical Zone, central sector, Eastern Bushveld Complex, and its chromite deposits. *Economic Geology*, 75, 845–871.

CAMERON, E. N., 1982—The upper critical zone of the eastern Bushveld Complex—precursor of the Merensky Reef. *Economic Geology*, 77, 1307–1327.

CAMPBELL, I. H., 1977—A study of macro-rhythmic layering and cumulate processes in the Jimberlana Intrusion, Western Australia. Part I: the upper layered series. *Journal of Petrology*, 18, 183–215.

CAMPBELL, I. H., 1978—Some problems with the cumulus theory. *Lithos*, 11, 311–323.

CAMPBELL, I. H., 1985—The difference between oceanic and continental tholeiites: a fluid dynamic explanation. *Contributions to Mineralogy & Petrology*, 91, 37–43.

CAMPBELL, I. H., 1986—A fluid dynamic model for the potholes of the Merensky Reef. *Economic Geology*, 81, 1118–1125.

CAMPBELL, I. H., & BARNES, STEPHEN J., 1984—A model for the geochemistry of the platinum group elements in magmatic sulfide deposits. *Canadian Mineralogist*, 22, 151–160.

CAMPBELL, I. H., & BORLEY, G. D., 1974—The geochemistry of pyroxenes from the Lower Layered Series of the Jimberlana Intrusion, Western Australia. *Contributions to Mineralogy & Petrology*, 47, 281–297.

CAMPBELL, I. H., & NALDRETT, A. J., 1979—The influence of silicate:sulfide ratios on the geochemistry of magmatic sulfides. *Economic Geology*, 74, 1503–1506.

CAMPBELL, I. H., NALDRETT, A. J., & BARNES, STEPHEN J., 1983—A model for the origin of the platinum-rich sulfide horizons in the Bushveld and Stillwater Complexes. *Journal of Petrology*, 24, 133–165.

CAMPBELL, I. H., & NOLAN, J., 1974—Factors effecting the stability field of Ca-poor pyroxene and the origin of the Ca-poor minimum in Ca-rich pyroxenes from tholeiitic intrusions. *Contributions to Mineralogy & Petrology*, 48, 205–219.

CAMPBELL, I. H., & TURNER, J. S., 1986a—The influence of viscosity on fountains in magma chambers. *Journal of Petrology*, 27, 1–30.

CAMPBELL, I. H., & TURNER, J. S., 1986b—The role of convection in the formation of platinum and chromitite deposits in layered intrusions. *In* SCARFE, C. M. (Editor)—Short course in silicate melts. Mineralogical Association of Canada, May 1986, Ottawa, Canada, 236–278.

CAWTHORN, R. G., BARTON, J. M., JR., & VILJOEN, M. J., 1985a—Interaction of floor rocks with the Platreef on Overysel, Potgietersrus, Northern Transvaal. *Economic Geology*, 80, 988–1006.

CAWTHORN, R. G., BARTON, J. R., JR., WHITE, J., & VILJOEN, M. J., 1985b—The role of contamination in the evolution of the Platreef of the Bushveld Complex. Fourth International Platinum Symposium, Abstracts, 14–31 July 1985, Toronto, Canada. *IGCP Project 161. Canadian Mineralogist*, 23, 298–299.

CAWTHORN, R. G., & DAVIES, G., 1983—Experimental data at 3 kbars pressure on parental magma to the Bushveld Complex. *Contributions to Mineralogy & Petrology*, 83, 128–135.

CAWTHORN, R. G., DAVIES, G., CLUBLEY-ARMSTRONG, A., & MCCARTHY, T. S., 1981—Sills associated with the Bushveld Complex, South Africa: an estimate of the parental magma composition. *Lithos*, 14, 1–15.

CAWTHORN, R. G., MYER, P. S., & KRUGER, F. J., 1991—Major addition of magma at the Pyroxenite Marker in the western Bushveld Complex, South Africa. *Journal of Petrology*, 32, 739–763.

CHALOKWU, C. I., & GRANT, N. K., 1987—Re-equilibration of olivine with trapped liquid in the Duluth complex, Minnesota. *Geology*, 15, 71–74.

CHAUVEL, C., DUPRE, B., & JENNER, G. A., 1985—The Sm-Nd age of Kambalda volcanics is 500 Ma too old! *Earth & Planetary Science Letters*, 74, 315–324.

CHEN, C. F., & TURNER, J. S., 1980—Crystallization in a double-diffusive system. *Journal of Geophysical Research*, 85, 2573–2593.

COLLERSON, K. D., & MCCULLOCH, M. T., 1983—Field and Sm-Nd isotopic constraints on Archaean crust and mantle evolution in the east Pilbara Block, Western Australia. *Geological Society of Australia, Abstracts* 9, 167–168.

COMPSTON, W., & ARRIENS, P. A., 1968—The Precambrian geochronology of Australia. *Canadian Journal of Earth Sciences*, 5, 561–583.

CONNOLLY, R. R., 1959—Iron ores in Western Australia. *Western Australia Geological Survey, Mineral Resources Bulletin* 7, 103 pp.

COOPER, J. A., JAMES, P. R., & RUTLAND, R. W. R., 1982—Isotopic dating and structural relationships of granitoids and greenstones in the east Pilbara, Western Australia. *Precambrian Research*, 18, 199–236.

COUSINS, C. A., 1973—Notes on the geochemistry of the platinum group elements. *Geological Society of South Africa, Transactions*, 76, 77–81.

COX, K. G., BELL, J. D., & PANKHURST, R. J., 1984—THE INTERPRETATION OF IGNEOUS ROCKS. *George Allen & Unwin, London*, 450 pp.

CZAMANSKE, G. K., & MOORE, J. G., 1977—Composition and phase chemistry of sulfide globules in basalt from the Mid-Atlantic Ridge rift valley near 37°N latitude. *Bulletin of the Geological Society of America*, 88, 587–599.

DANCHIN, R. V., & FERGUSON, J., 1970—The geochemistry of the Losberg Intrusion, Fochville, Transvaal. *In* VISSER, D. J. L., & VON GRUENEWALDT, G. (Editors)—SYMPOSIUM ON THE BUSHVELD IGNEOUS COMPLEX AND OTHER LAYERED INTRUSIONS. *Geological Society of South Africa, Special Publication* 1, 689–714.

DAVIES, G., & TREDOUX, M., 1985—The platinum-group element and gold contents of the marginal rocks and sills of the Bushveld Complex. *Economic Geology*, 80, 838–848.

DE ANGELIS, M., HOYLE, M. W. H., PETERS, W. S., & WIGHTMAN, D., 1987—The nickel-copper deposit at Radio Hill, Karratha, Western Australia. *Australasian Institute of Mining & Metallurgy, Bulletin & Proceedings*, 292, 61–74.

DE ANGELIS, M., HOYLE, M. W. H., & VOERMANS, F. M., 1988—The Radio Hill Ni-Cu deposit and the Mount Sholl–Munni Munni mafic-ultramafic metallogenic province: a case of integrated exploration technique. *In* Second International Conference on Prospecting in Arid Terrain, April 1988, Perth, Western Australia. *Australasian Institute of Mining & Metallurgy*, 51–58.

DEER, W. A., HOWIE, R. A., & ZUSSMAN, J., 1978—AN INTRODUCTION TO THE ROCK-FORMING MINERALS. *Longman, London*, 528 pp.

DE LAETER, J. R., & TRENDALL, A. F., 1971—The age of the Gidley Granophyre. *Western Australia Geological Survey, Annual Report*, 1970, 62–67.

DEPAOLO, D. J., 1985—Isotopic studies of processes in mafic magma chambers: I. The Kiglapait intrusion, Labrador. *Journal of Petrology*, 26, 925–951.

DE WAAL, S. A., 1977—Carbon dioxide and water from metamorphic reactions as agents for sulfide and spinel precipitation in mafic magmas. *Geological Society of South Africa, Transactions*, 80, 193–196.

DICKEY, J. S., JR., 1975—A hypothesis of origin for podiform chromite deposits. *Geochimica et Cosmochimica Acta*, 39, 1061–1074.

DONALDSON, M. J., 1974—Petrology of the Munni Munni Complex, Roebourne, Western Australia. *Journal of the Geological Society of Australia*, 21, 1–16.

DRUMMOND, B. J., 1981—Crustal structures of the Precambrian terrains of northwest Australia from seismic refraction data. *BMR Journal of Australian Geology & Geophysics*, 6, 123–135.

DRUMMOND, B. J., 1982—Seismic constraints on the chemical composition of the crust of the Pilbara craton, northwest Australia. *Revista Brasileira de Geociencias*, 12, 113–120.

DRUMMOND, B. J., 1988—A review of crust/upper mantle structure in the Precambrian areas of Australia and implications for Precambrian crustal evolution. *Precambrian Research*, 40/41, 101–116.

DUCHESNE, J. C., 1972a—Iron-titanium oxide minerals in the Bjerkrem-Sogndal Massif, south-western Norway. *Journal of Petrology*, 13, 57–81.

DUCHESNE, J. C., 1972b—Pyroxenes et olivines dans le massif de Bjerkrem-Sogndal (Norvège méridionale). Contribution à l'étude de la série anorthosite-mangérite. *Report, 24th International Geological Congress, 1972*, Section 2, 320–328.

DUKE, J. M., 1988—Magmatic segregation deposits of chromite. *In* ROBERTS, R. G., & SHEAHAN, P. A. (Editors)—ORE DEPOSIT MODELS. *Geoscience Canada, Reprint Series* 3, 133–143.

DUNNING, G. R., WATKINSON, D. H., & MAINWARING, P. R., 1981—Correlation of platinum-group elements, copper and nickel with lithology in the Lac des Iles Complex, Canada. *In* Proceedings of the International Symposium on Metallogeny of Mafic and Ultramafic Complexes: eastern Mediterranean, western Asia area, and its comparison with similar metallogenic environments in the world. *IGCP Project 169, Athens, Greece, October 9–11, 1980*, 83–102.

EALES, H. V., DE KLERK, W. J., BUTCHER, A. R., & KRUGER, F. J., 1990a—The cyclic unit beneath the UG1 chromitite (UG1FW unit) at RPM Union Section Platinum Mine—Rosetta Stone of the Bushveld Upper Critical Zone? *Mineralogical Magazine*, 54, 23–43.

EALES, H. V., DE KLERK, W. J., & TEIGLER, B., 1990b—Evidence for magma mixing processes within the Critical and Lower Zones of the northwestern Bushveld Complex, South Africa. *Chemical Geology*, 88, 261–278.

EALES, H. V., FIELD, M., DE KLERK, W. J., & SCOON, R. N., 1988—Regional trends of chemical variation and thermal erosion in the Upper Critical Zone, western Bushveld Complex. *Mineralogical Magazine*, 52, 63–79.

EALES, H. V., & MARSH, J. S., 1983—Al/Cr ratios of coexisting pyroxenes and spinellids in some ultramafic rocks. *Chemical Geology*, 38, 57–74.

ELLIOT, W. C., GRANDSTAFF, D. E., ULPMER, G. C., BUNTIN, T. J., & GOLD, D. P., 1982—An intrinsic oxygen fugacity study of the platinum-carbon associations in layered intrusions. *Economic Geology*, 77, 1493–1510.

ELLIS, D. J., 1980—Osumilite-sapphirine-quartz granulites from Enderby Land, Antarctica: P-T conditions of metamorphism, implications for garnet-corderite equilibria and the evolution of the deep crust. *Contributions to Mineralogy & Petrology*, 74, 201–210.

ELLIS, D. J., & GREEN, D. H., 1979—An experimental study of the effect of Ca upon garnet-clinopyroxene Fe-Mg exchange equilibria. *Contributions to Mineralogy & Petrology*, 71, 13–22.

EWERS, G. R., 1975—Volatile and precious metal zoning in the Broadlands Geothermal Field, New Zealand. Ph.D thesis, University of Melbourne (unpublished), 218 pp.

EWERS, W. E., & HUDSON, D. R., 1972—An interpretive study of a nickel-iron sulfide ore intersection, Lunnon shoot, Kambalda, Western Australia. *Economic Geology*, 67, 1075–1092.

FITTON, M. J., HORWITZ, R. C., & SYLVESTER, G., 1975—Stratigraphy of the early Precambrian in the west Pilbara, Western Australia. *Commonwealth Scientific & Industrial Research Organisation, Minerals Research Laboratories, Report* FP11.

FLOYD, P. A., & WINCHESTER, J. A., 1978—Identification and discrimination of altered and metamorphosed rocks using immobile elements. *Chemical Geology*, 21, 291–306.

FORD, C. E., RUSSELL, D. G., CRAVEN, J. A., & FISK, M. R., 1983—Olivine-liquid equilibria: temperature, pressure and composition dependence of the crystal/liquid cation partition coefficients for Mg, Fe^{2+}, Ca and Mn. *Journal of Petrology*, 24, 256–265.

FUJIMAKI, H., TATSUMOTO, M., & AOKI, K., 1984—Partition coefficients of Hf, Zr, and REE between phenocrysts and groundmasses. Proceedings of the 14th Lunar Planetary Science Conference. *Journal of Geophysical Research*, 89, Supplement, B662–B672.

GABELL, A. R., HUNTINGTON, J. F., & GREEN, A. A., 1985—The US/Australia Joint Scanner Project, Vol. II. Summary of data acquired. Commonwealth Scientific & Industrial Research Organisation, Australia.

GAIN, S. B., 1985—The geological setting of the platiniferous UG-2 chromitite layer on the farm Maandagshoek, Eastern Bushveld Complex. *Economic Geology*, 80, 925–943.

GIJBELS, R. H., MILLARD, H. T., JR., DESBOROUGH, G. A., & BARTEL. A. J., 1974—Osmium, ruthenium, iridium and uranium in silicates and chromite from the eastern Bushveld Complex, South Africa. *Geochimica et Cosmochimica Acta*, 38, 319–337.

GLIKSON, A. Y., 1986—The oldest age determined for Pilbara greenstones. *BMR Research Newsletter*, 4, 7.

GLIKSON, A. Y., & BALLHAUS, C., 1989—Significance of ultrabasic components of the Giles Complex, central Australia. *BMR Research Newsletter*, 10, 4–6.

GLIKSON, A. Y., DAVY, R., & HICKMAN, A. H., 1986—Geochemical data files of Archaean volcanic rocks, Pilbara Block, Western Australia. *Bureau of Mineral Resources, Australia, Record* 1986/14, 1–2.

GODLEVSKII, M. N., & GRINENKO, L. N., 1963—Some data on the isotopic composition of sulfur in the sulfides of the Noril'sk Deposit. *Geochemistry*, 1, 35–41.

GOETZ, A. F. H., HAUFF, P., & SHIPPERT, M., 1991—Rapid detection and identification of OH-bearing minerals in the 0.9–1.0 μm region using a new portable field spectrometer. Eighth Thematic Conference on Geologic Remote Sensing. *Environmental Research Institute of Michigan, Ann Arbor, Michigan*, 1–11.

GOODE, A. D. T., 1976—Small scale primary cumulus igneous layering in the Kalka layered intrusion, Giles Complex, central Australia. *Journal of Petrology*, 17, 379–397.

GOTTFRIED, D., FROELICH, A. J., RAIT, N., & ARUSCAVAGE, P. J., 1990—Fractionation of palladium and platinum in a Mesozoic diabase sheet, Gettysburg basin, Pennsylvania: implications for mineral exploration. *Journal of Geochemical Exploration*, 37, 75–89.

GRANT, N. K., & MOLLING, P. A., 1981—A strontium isotope and trace element profile through the Partridge River troctolite, Duluth complex, Minnesota. *Contributions to Mineralogy & Petrology*, 77, 296–305.

GRAY, C. M., 1987—Strontium isotopic constraints on the origin of Proterozoic anorthosites. *Precambrian Research*, 37, 173–189.

GREEN, A. H., & NALDRETT, A. J., 1981—The Langmuir volcanic peridotite-associated nickel deposits: Canadian equivalents of the Western Australian occurrences. *Economic Geology*, 76, 1503–1523.

GREEN, D. H., 1964—The petrogenesis of the high-temperature peridotite intrusion in the Lizard area, Cornwall. *Journal of Petrology*, 5, 134–188.

GREEN, D. H., 1975—Genesis of Archaean peridotite magmas and constraints on Archaean geothermal gradients and tectonics. *Geology*, 3, 15–18.

GREEN, D. H., & HIBBERSON, W. O., 1970—The instability of plagioclase at high pressure. *Lithos*, 3, 209–221.

GREENLAND, L. P., 1971—Variation of iridium in a differientated tholeiitic dolerite. *Geochimica et Cosmochimica Acta*, 35, 319–322.

GREGORY, F. T., 1861—On the geology of parts of Western Australia. *Quarterly Journal of the Geological Society of London*, 17, 475–483.

GRIFFIN, T. J., 1990—North Pilbara granite-greenstone terrane. *In* GEOLOGY AND MINERAL RESOURCES OF WESTERN AUSTRALIA. *Western Australia Geological Survey, Memoir* 3, 128–158.

GRIFFIN, W. L., MELLINI, M., OBERTI, R., & ROSSI, G., 1985—Evolution of coronas in Norwegian anorthosites: re-evaluation based on crystal-chemistry and microstructures. *Contributions to Mineralogy & Petrology*, 91, 330–339.

GRUAU, G., JAHN, B. M., GLIKSON, A. Y., DAVY, R., HICKMAN, A. H., & CHAUVEL, C., 1987—Age of the Archean Talga-Talga Subgroup, Pilbara Block, Western Australia, and early evolution of the mantle: new Sm-Nd isotopic evidence. *Earth & Planetary Science Letters*, 85, 105–116.

GRUNSHAW, D., 1983—Sulfide mineralization at the basal contacts of the Bushveld Complex, Marico District, Western Transvaal. *In* Symposium on the Bushveld Complex, Abstracts. Institute for Geological Research on the Bushveld Complex, University of Pretoria, 31 October–2 November, 1983, 29.

HAGGERTY, S. E., 1976—Opaque mineral oxides in terrestrial igneous rocks. *In* RUMBLE, D. (Editor)—REVIEWS IN MINERALOGY—OXIDE MINERALS. Volume 3. *Mineralogical Society of America*, Hg101–Hg300.

HAKLI, T. A., HANNINEN, E., VUORELAINEN, Y., & PAPUNEN, H., 1976—Platinum-group minerals in the Hitura nickel deposit, Finland. *Economic Geology*, 71, 1206–1213.

HAMILTON, P. J., EVENSEN, N. M., O'NIONS, R. K., GLIKSON, A. Y., & HICKMAN, A. H., 1981—Sm-Nd dating of the North Star Basalt, Warrawoona Group, Pilbara Block, Western Australia. *In* GLOVER, J. E., & GROVES, D. I. (Editors)—ARCHAEAN GEOLOGY. Second International Archaean Symposium, Perth, 1980. *Geological Society of Australia, Special Publication* 7, 187–192.

HAMLYN, P. R., 1980—Equilibration history and phase chemistry of the Panton Sill, Western Australia. *American Journal of Science*, 280, 631–668.

HAMLYN, P. R., & KEAYS, R. R., 1979—Origin of chromite compositional variation in the Panton Sill, Western Australia. *Contributions to Mineralogy & Petrology*, 69, 75–82.

HAMLYN, P. R., & KEAYS, R. R., 1986—Sulfur saturation and second-stage melts: application to the Bushveld platinum metal deposits. *Economic Geology*, 81, 1431–1445.

HAMLYN, P. R., KEAYS, R. R., CAMERON, W. E., CRAWFORD, A. J., & WALDRON, H. M., 1985—Precious metals in magnesian low-Ti lavas: implications for metallogenesis and sulfur saturation in primary magmas. *Geochimica et Cosmochimica Acta*, 49, 1797–1811.

HANSON, G. N., 1980—Rare earth elements in petrogenetic studies of igneous systems. *Annual Review of Earth & Planetary Sciences*, 8, 307–406.

HARLEY, S. L., 1984—Comparison of the garnet-orthopyroxene geobarometer with recent experimental studies, and applications to natural assemblages. *Journal of Petrology*, 25, 697–712.

HART, S. R., & KINLOCH, E. D., 1989—Osmium isotope systematics in Witwatersrand and Bushveld ore deposits. *Economic Geology*, 84, 1651–1655.

HASKIN, L. A., & KOROTEV, R. A., 1977—Test of a model for trace element partitioning during closed-system solidification of a silicate liquid. *Geochimica et Cosmochimica Acta*, 41, 921–939.

HATTON, C. J., & SHARPE, M. R., 1989—Significance and origin of boninite-like rocks associated with the Bushveld Complex. *In* CRAWFORD, A. J. (Editor)—BONINITE AND RELATED ROCKS. *Unwin Hyman, London*, 174–207.

HATTON, C. J., & VON GRUENEWALDT, G., 1987—The geological setting and petrogenesis of the Bushveld chromitite layers. *In* STOWE, C. W. (Editor)—EVOLUTION OF CHROMIUM ORE FIELDS. *Van Nostrand Reinhold, New York*, 109–143.

HATTORI, K., CABRI, L. J., & HART, S. R., 1991—Osmium isotope ratios of PGM grains associated with the Freetown layered complex, Sierra Leone, and their origin. *Contributions to Mineralogy & Petrology*, 109, 10–18.

HAUGHTON, D. R., ROEDER, P. L., & SKINNER, B. J., 1974—Solubility of sulfur in mafic magmas. *Economic Geology*, 69, 451–467.

HAWKES, D. D., 1967—Order of abundant crystal nucleation in a natural magma. *Geological Magazine*, 104, 473–486.

HENDERSON, P., 1975—Reaction trends shown by chrome-spinels of the Rhum layered intrusion. *Geochimica et Cosmochimica Acta*, 39, 1035–1044.

HENDERSON, P., & SUDDABY, P., 1971—The nature and origin of the chrome-spinel of the Rhum layered intrusion. *Contributions to Mineralogy & Petrology*, 33, 21–31.

HESS, H. H., 1960—Stillwater igneous complex, Montana: a quantitative mineralogical study. *Geological Society of America, Memoir* 80, 230 pp.

HICKMAN, A. H., 1981—Crustal evolution of the Pilbara Block. *In* GLOVER, J. E., & GROVES, D. I. (Editors)—ARCHAEAN GEOLOGY. *Geological Society of Australia, Special Publication* 7, 57–69.

HICKMAN, A. H., 1983—Geology of the Pilbara Block and its environs. *Western Australia Geological Survey, Bulletin* 127, 268 pp.

HICKMAN, A. H., & DE LAETER, J. R., 1977—The depositional environment and age of a shale within the Hardey Sandstone of the Fortescue Group. *Western Australia Geological Survey, Annual Report, 1976*, 62–68.

HIMMELBERG, G. R., & FORD, A. B., 1976—Pyroxenes of the Dufek intrusion, Antarctica. *Journal of Petrology*, 17, 219–243.

HOATSON, D. M., 1984—Potential for platinum group mineralisation in Australia: a review. *Bureau of Mineral Resources, Australia, Record* 1984/1, 84 pp.

HOATSON, D. M., 1990a—Platinum group element mineralisation and potential in Australia. *In* HUGHES, F. E. (Editor)—GEOLOGY OF THE MINERAL DEPOSITS OF AUSTRALIA AND PAPUA NEW GUINEA. Monograph 14, Volume 1. *Australasian Institute of Mining & Metallurgy, Melbourne*, 85–98.

HOATSON, D. M., 1990b—Potential for platinum-group element mineralisation. National Agricultural & Resources Outlook Conference 1990 (NAROC '90). Australian Bureau of Agricultural & Resource Economics, 30 January to 1 February 1990, Canberra, 1–10.

HOATSON, D. M., 1991—The petrology and platinum-group element geochemistry of the Munni Munni and Mount Sholl layered mafic-ultramafic intrusions of the west Pilbara Block, Western Australia. Ph.D thesis, University of Melbourne (unpublished), 510 pp.

HOATSON, D. M., & BARNES, Stephen J., 1991—Mafic-ultramafic intrusions of the west Pilbara Block. *In* BARNES, STEPHEN J., & HILL, R. E. T. (Editors)—Mafic-ultramafic complexes of Western Australia. Excursion Guidebook No. 3. Sixth International Platinum Symposium, July 1991, Perth, WA. *IAGOD and the Geological Society of Australia*, 7–10.

HOATSON, D. M., & ENGLAND, R. N., 1986—Platinum group minerals from a layer in the Munni Munni Complex of the Pilbara Block. *BMR Research Newsletter*, 5, 1–2.

HOATSON, D. M., & GLASER, L. M., 1989—Geology and economics of platinum-group metals in Australia. *Bureau of Mineral Resources, Australia, Resource Report* 5, 81 pp.

HOATSON, D. M., & KEAYS, R. R., 1987—Platinum group geochemistry of the Munni Munni layered intrusion, west Pilbara Block, Western Australia: an example of the formation of platiniferous horizons by crystal fractionation and magma mixing. *In* VON GRUENEWALDT, G., KEAYS, R. R., & HOATSON, D. M. (Compilers)—Platinum-group element deposits. Sydney 6–8 October 1987. *Workshop, Earth Resources Foundation, University of Sydney*, 1–50.

HOATSON, D. M., & KEAYS, R. R., 1989—Formation of platiniferous sulfide horizons by crystal fractionation and magma mixing in the Munni Munni layered intrusion, west Pilbara Block, Western Australia. *Economic Geology*, 84, 1775–1804.

HODGES, F. N., & PAPIKE, J. J., 1976—DSDP Site 334: magmatic cumulates from oceanic layer 3. *Journal of Geophysical Research*, 81, 4135–4151.

HONEY, F. R., PRELAT, A., & LYON, R. J. P., 1974—Stansort: Stanford Remote Sensing Laboratory pattern recognition and classification system. Proceedings of the 9th International Symposium on Remote Sensing of Environment, 2. *Environmental Research Institute of Michigan, Ann Arbor, Michigan*, 897–905.

HORWITZ, R. C., 1988—Contributed discussion to 'The nickel-copper deposit at Radio Hill, Karratha, Western Australia' by de Angelis, Hoyle, Peters & Wightman. *Australasian Institute of Mining & Metallurgy, Bulletin & Proceedings*, 293, 57–58.

HORWITZ, R. C., 1990a—Evolution of the Pilbara Craton. *In* GLOVER, J. E., & HO, S. E. (Compilers)—Third International Archaean Symposium, Extended Abstracts. *Geoconferences (WA) Incorporated, Perth*, 1990, 79.

HORWITZ, R. C., 1990b—Palaeogeography, tectonic evolution and stratigraphic status of the Gorge Creek and Whim Creek Groups. *In* Recent advances in understanding the Archaean and Early Proterozoic geology of the Pilbara Craton, Abstracts. One-day seminar, 16 September 1990. *The Geology Department and University Extension, University of Western Australia*, 10–11.

HOSSAIN, M. T., 1977—Pyroxenes from the gabbros of the Marangudzi ring complex, Rhodesia. *Mineralogical Magazine*, 41, 111–119.

HUANG, W. L., & WILLIAMS, R. J., 1980—Melting relations of portions of the system Fe-S-Si-O to 32 kb with implications for the nature of the mantle/core boundary. Abstract. *Lunar & Planet Sc. XI, Lunar & Planetary Institute, Houston*, 486–488.

HUDSON, D. R., & HORWITZ, R. C., 1985—Mineralogy and geological setting of a new occurrence of platinum group minerals, between Roebourne and Karratha, Western Australia. *Commonwealth Scientific & Industrial Research Organisation, Division of Mineralogy & Geochemistry, Research Review*, 1985, 79–80.

HUGHES, T. C., 1978—The geochemistry of sulphur, selenium, tellurium, mercury, thallium, and bismuth—their determination by thermal neutron activation analysis and their geochemical significance. Ph.D thesis, University of Melbourne, Australia (unpublished), 293 pp.

HUGHES, T. C., & HANNAKER, P., 1978—The determination of carbon and hydrogen in geological materials by thermal decomposition. *Chemical Geology*, 22, 331–339.

HUNT, G. R., SALISBURY, J. W., & LENHOFF, C. J., 1974—Visible and near-infrared spectra of minerals and rocks: IX. Basic and ultrabasic igneous rocks. *Modern Geology*, 5, 15–22.

HUNTINGTON, J. F., & SIMPSON, C. J., 1985—Major new Australian/US remote sensing initiative. *The Australian Geologist*, 57, 34–35.

HUPPERT, H. E., & SPARKS, R. S. J., 1980—The fluid dynamics of a basaltic magma chamber. *Contributions to Mineralogy & Petrology*, 75, 279–289.

HUPPERT, H. E., & SPARKS, R. S. J., 1984—Double diffusive convection due to crystallisation in magmas. *Annual Reviews, Earth & Planetary Science*, 12, 11–37.

HUPPERT, H. E., SPARKS, R. S. J., WILSON, J. R., HALLWORTH, M. A., & LEITCH, A. M., 1987—Laboratory experiments with aqueous solutions modelling magma chamber processes—II. Cooling and crystallisation along inclined planes. *In* PARSONS, I. (Editor)—ORIGINS

OF IGNEOUS LAYERING. NATO Advanced Science Series, 196. *D. Reidel Publishing Company, Dordrecht*, 539–568.

HUPPERT, H. E., & TURNER, J. S., 1981a—A laboratory model of a replenished magma chamber. *Earth & Planetary Science Letters*, 54, 144–152.

HUPPERT, H. E., & TURNER, J. S., 1981b—Double-diffusive convection. *Journal of Fluid Mechanics*, 106, 299–329.

IRVINE, T. N., 1965—Sedimentary structures in igneous intrusions with particular reference to the Duke Island ultramafic complex. *In* MIDDLETON, G. V. (Editor)—PRIMARY SEDIMENTARY STRUCTURES AND THEIR HYDRODYNAMIC INTERPRETATION. *Society of Economic Palaeontologists & Mineralogists*, Special Publication 12, 220–232.

IRVINE, T. N., 1970—Crystallization sequences in the Muskox intrusion and other layered intrusions—I. Olivine-pyroxene-plagioclase relations. *Geological Society of South Africa, Special Publication* 1, 441–476.

IRVINE, T. N., 1974a—Petrology of the Duke Island Ultramafic Complex, southeastern Alaska. *Geological Society of America, Memoir* 138, 240 pp.

IRVINE, T. N., 1974b—*Carnegie Institution of Washington, Year Book, 1973*, 300–316.

IRVINE, T. N., 1975—Crystallization sequences of the Muskox intrusion and other layered intrusions—II. Origin of chromitite layers and similar deposits of other magmatic ores. *Geochimica et Cosmochimica Acta*, 39, 991–1020.

IRVINE, T. N., 1977—Origin of chromitite layers in the Muskox intrusion and other stratiform intrusions: a new interpretation. *Geology*, 5, 273–277.

IRVINE, T. N., 1979—Rocks whose compositions are determined by crystal accumulation and sorting. *In* YODER, H. S., JR. (Editor)—EVOLUTION OF THE IGNEOUS ROCKS: FIFTIETH ANNIVERSARY PERSPECTIVES. *Princeton University Press*, Princeton, NJ, 245–306.

IRVINE, T. N., 1980a—Experimental modelling of convection in layered intrusions. *Carnegie Institution of Washington, Year Book, 1979*, 247–251.

IRVINE, T. N., 1980b—Magmatic infiltration metasomatism, double-diffusive fractional crystallization, and adcumulus growth in the Muskox intrusion and other layered intrusions. *In* HARGRAVES, R. B. (Editor)—PHYSICS OF MAGMATIC PROCESSES. *Princeton University Press, Princeton, NJ*, 325–383.

IRVINE, T. N., 1980c—Convection and mixing in layered liquids. *Carnegie Institution of Washington, Year Book, 1979*, 251–256.

IRVINE, T. N., 1980d—Observations on layering in the Skaergaard intrusion. *Carnegie Institution of Washington, Year Book, 1979*, 257–262.

IRVINE, T. N., 1980e—Magmatic density currents and cumulus processes. *American Journal of Science*, 280A, 1–58.

IRVINE, T. N., 1982—Terminology for layered intrusions. *Journal of Petrology*, 23, 127–162.

IRVINE, T. N., 1983—Observations on the origin of Skaergaard layering. *Carnegie Institution of Washington, Year Book, 1982*, 284–292.

IRVINE, T. N., 1987a—Layering and related structures in the Duke Island and Skaergaard intrusions: similarities, differences, and origins. *In* PARSONS, I. (Editor)—ORIGINS OF IGNEOUS LAYERING. NATO Advanced Science Series, 196. *D. Reidel Publishing Company, Dordrecht*, 185–245.

IRVINE, T. N., 1987b—Appendix 1. Glossary of terms for layered intrusions. *In* PARSONS, I. (Editor)—ORIGINS OF IGNEOUS LAYERING. NATO Advanced Science Series, 196. *D. Reidel Publishing Company, Dordrecht*, 641–647.

IRVINE, T. N., & BARAGAR, W. R. A., 1971—A guide to the chemical classification of the common volcanic rocks. *Canadian Journal of Earth Science*, 8, 523–548.

IRVINE, T. N., & SHARPE, M. R., 1986a—Magma mixing and the origin of stratiform oxide ore zones in the Bushveld and Stillwater complexes. *In* GALLAGHER, M. J., IXER, R. A., NEARY, C. R., & PRICHARD, H. M. (Editors)—METALLOGENY OF BASIC AND ULTRABASIC ROCKS. *Institution of Mining & Metallurgy, London*, 183–198.

IRVINE, T. N., & SHARPE, M. R., 1986b—Magma mixing and the origin of stratiform oxide ore zones in the Bushveld Complex. Geocongress '86, Extended Abstracts, 599-602.

IRVINE, T. N., & SMITH. C. H., 1967—III. The ultramafic rocks of the Muskox intrusion, Northwest Territories, Canada. *In* WYLLIE, P. J. (Editor)—ULTRAMAFIC AND RELATED ROCKS. *John Wiley & Sons, New York*, 38–49.

IRVINE, T. N., KEITH, D. W., & TODD, S. G., 1983—The J-M platinum-palladium reef of the Stillwater Complex, Montana—II. Origin by double-diffusive convective magma mixing and implications for the Bushveld Complex. *Economic Geology*, 78, 1287–1334.

JACKSON, E. D., 1961—Primary textures and mineral asociations in the Ultramafic Zone of the Stillwater Complex, Montana. *United States Geological Survey, Professional Paper* 358, 106 pp.

JACKSON, E. D., 1967—Ultramafic cumulates in the Stillwater, Great Dyke and Bushveld intrusions. *In* WYLLIE, P. J. (Editor)—ULTRAMAFIC AND RELATED ROCKS. *John Wiley & Sons, New York*, 20–38.

JACKSON, E. D., 1970—The cyclic units in layered intrusions—a comparison of repetitive stratigraphy in the ultramafic parts of the Stillwater, Muskox, Great Dyke, and Bushveld Complexes. *Geological Society of South Africa, Special Publication* 1, 391–424.

JAQUES, A. L., 1981—Petrology and petrogenesis of cumulate peridotites and gabbros from the Marum ophiolite complex, northern Papua New Guinea. *Journal of Petrology*, 22, 1–40.

JENKINS, R., & DE VRIES, J. L., 1967—PRACTICAL X-RAY SPECTROMETRY. *Philips, Eindhoven.*

JOHANNES, W., 1978—Melting of plagioclase in the system Ab-An-H_2O and Qz-Ab-An-H_2O at P_{H_2O} = 5 kbars, an equilibrium problem. *Contributions to Mineralogy & Petrology*, 66, 295–303.

KAHLE, A. B., MADURA, D. P., & SOHA, J. M., 1980—Middle infrared multispectral aircraft scanner data: analysis for geological applications. *Applied Optics*, 19 (14), 2279–2290.

KEAYS, R. R., & CAMPBELL, I. H., 1981—Precious metals in the Jimberlana Intrusion, Western Australia: implications for the genesis of platiniferous ores in layered intrusions. *Economic Geology*, 76, 1118–1141.

KEAYS, R. R., GANAPATHY, J. C., LAUL, J. C., KRAHENBUHL, U., & MORGAN, J. W., 1974—The simultaneous determination of 20 trace elements in terrestrial, lunar and meteoric material by radiochemical neutron activation analysis. *Analytica Chimica Acta*, 72, 1–29.

KEAYS, R. R., NICKEL, E. H., GROVES, D. I., & MCGOLDRICK, P. J., 1982—Iridium and palladium as discriminants of volcanic-exhalative, hydrothermal, and magmatic nickel sulfide mineralization. *Economic Geology*, 77, 1535–1547.

KINLOCH, E. D., 1982—Regional trends in the platinum-group mineralogy of the critical zone of the Bushveld Complex, South Africa. *Economic Geology*, 77, 1328–1347.

KOCH, G. S., & LINK, R. F., 1971—STATISTICAL ANALYSIS OF GEOLOGICAL DATA. *Wiley, New York*, 11, 438 pp.

KOMAR, P. D., 1972a—Mechanical interactions of phenocrysts and flow differentiation of igneous dikes and sills. *Bulletin of the Geological Society of America*, 83, 973–988.

KOMAR, P. D., 1972b—Flow differentiation of igneous dikes and sills: profiles of velocity and phenocryst concentration. *Bulletin of the Geological Society of America*, 83, 3443–3448.

KORSCH, M. J., & GULSON, B. L., 1986—Nd and Pb isotopic studies of an Archaean layered mafic–ultramafic complex, Western Australia, and implications for mantle heterogeneity. *Geochimica et Cosmochimica Acta*, 50, 1–10.

KRAPEZ, B., & BARLEY, M. E., 1987—Archaean strike-slip faulting and related ensialic basins: evidence from the Pilbara Block, Australia. *Geological Magazine*, 124, 555–567.

KRAPEZ, B., BLAKE, T. S., & BARLEY, M. E., 1990—Origin and reactivation of lineaments in the Pilbara Craton, Western Australia. *In* GLOVER, J. E., & HO, S. E. (Compilers)—Third International Archaean Symposium, Extended Abstracts. *Geoconferences (WA) Incorporated, Perth*, 1990, 23–24.

KRIEWALDT, M. J. B., 1964—Dampier and Barrow Island, Western Australia—1 : 250 000 Geological Series. *Western Australia Geological Survey, Explanatory Notes* SF/50-2, SF/50-1.

KRUGER, F. J., 1989—The Sr-isotopic stratigraphy of the Bushveld Complex: significance for models of PGE mineralization. *In* PAPUNEN, H. (Editor)—5th International Platinum Symposium, Abstracts. *Bulletin of the Geological Society of Finland*, 61, Part 1, 1989, 15–16.

KRUGER, F. J., & MARSH, J. S., 1982—Significance of $^{87}Sr/^{86}Sr$ ratios in the Merensky cyclic unit of the Bushveld Complex. *Nature*, 298, 53–55.

KRUGER, F. J., & MARSH, J. S., 1985—The mineralogy, petrology and origin of the Merensky cyclic unit in the western Bushveld Complex. *Economic Geology*, 80, 958–974.

LABOTKA, T. C., 1985—Petrogenesis of metamorphic rocks beneath the Stillwater Complex: assemblages and conditions of metamorphism. *In* CZAMANSKE, G. K. & ZIENTEK, M. L. (Editors)—THE STILLWATER COMPLEX, MONTANA: GEOLOGY AND GUIDE. *Montana Bureau of Mines & Geology, Special Publication 92, IGCP Project 161*, 70–76.

LAMBERT, D. D., MORGAN, J. W., WALKER, R. J., SHIREY, S. B., CARLSON, R. W., ZIENTEK, M. L., & KOSKI, M. S., 1989—Rhenium-osmium and samarium-neodymium isotopic systematics of the Stillwater Complex, Montana. *Science*, 244, 1169–1174.

LAMBERT, D. D., SHIREY, S. B., CARLSON, R. W., WALKER, R. J., & MORGAN, J. W., 1990—Re-Os and Sm-Nd isotope geochemistry of the Stillwater Complex, Montana: the role of crustal versus lithospheric mantle sources in layered intrusions. *In* GLOVER, J. E., & HO, S. E. (Compilers)—Third International Archaean Symposium, Extended Abstracts. *Geoconferences (WA) Incorporated, Perth*, 1990, 153–155.

LAMBERT, D. D., SHIREY, S. B., CARLSON, R. W., WALKER, R. J., MORGAN, J. W., & ZIENTEK, M. L., 1991—Applications of the Re-Os isotopic system to platinum-group element ore genesis in the Stillwater Complex, Montana (USA). *In* BARNES, Stephen J. (Editor)—Sixth International Platinum Symposium, Abstracts, July 1991, Perth, WA. *IAGOD and the Geological Society of Australia*, 30.

LAMBERT, D. D., & SIMMONS, E. C., 1980—Cumulate minerals as liquid analogues, a new approach to modelling trace elements in mafic layered intrusions: applications to the Stillwater Complex, Montana. *EOS*, 61, 410.

LAMBERT, D. D., & SIMMONS, E. C., 1987—Magma evolution in the Stillwater Complex, Montana—I. Rare-earth element evidence for the formation of the ultramafic series. *American Journal of Science*, 287, 1–32.

LAMBERT, D. D., & SIMMONS, E. C., 1988—Magma evolution in the Stillwater Complex—II. Rare-earth element evidence for the formation of the J-M Reef. *Economic Geology*, 83, 1109–1126.

LAMBERT, D. D., UNRUH, D. M., & GILBERT, M. C., 1988—Rb-Sr and Sm-Nd isotopic study of the Glen Mountains layered complex: initiation of rifting within the southern Oklahoma aulacogen. *Geology*, 16, 13–17.

LAMBERT, D. D., UNRUH, D. M., & SIMMONS, E. C., 1985—Isotopic investigations of the Stillwater complex: a review. *In* CZAMANSKE, G. K., & ZIENTEK, M. L. (Editors)—THE STILLWATER COMPLEX, MONTANA: GEOLOGY AND GUIDE. *Montana Bureau of Mines & Geology, Special Publication 92, IGCP Project 161*, 46–54.

LAMBERT, I. B., & DONNELLY, T. H., 1990—The paleoenvironmental significance of trends in sulfur isotope compositions in the Precambrian: a critical review. *In* HERBERT, H. K. & HO, S. E. (Editors)—STABLE ISOTOPES AND FLUID PROCESSES IN MINERALISATION. *Geology Department, University of Western Australia, Special Publication 23*, 260–268.

LEBLANC, M., 1987—Chromite in oceanic arc environments: New Caledonia. *In* STOWE, C. W. (Editor)—EVOLUTION OF CHROMIUM ORE FIELDS. *Van Nostrand Reinhold, New York*, 265–296.

LEE, C. A., 1983—Trace and platinum-group element geochemistry and the development of the Merensky Unit of the Western Bushveld Complex. *Mineralium Deposita*, 18, 173–190.

LEE, C. A., CAWTHORN, R. G., & BARTON, J. M., JR., 1989—Further Sr-isotope and trace element studies on the Platreef, Bushveld Complex. *In* PAPUNEN, H. (Editor)—5th International Platinum Symposium, Abstracts. *Bulletin of the Geological Society of Finland*, 61, Part 1, 1989, 21.

LEE, C. A., & TREDOUX, M., 1986—Platinum-group element abundances in the Lower and Lower Critical zones of the Eastern Bushveld Complex. *Economic Geology*, 81, 1087–1095.

LEGGO, P. J., COMPSTON, W., & TRENDALL, A. F., 1965—Radiometric ages of some Precambrian rocks from the northwest division of Western Australia. *Journal of the Geological Society of Australia*, 12, 53–65.

LEWIS, J. D., ROSMAN, K. J. R., & DE LAETER, J. R., 1975—The age and metamorphic effects of the Black Range dolerite dyke. *Western Australia Geological Survey, Annual Report*, 1974, 80–88.

LIEBENBERG, L., 1970—The sulfides in the layered sequence of the Bushveld Igneous Complex. *In* VISSER, D. J. L., & VON GRUENEWALDT, G. (Editors)—SYMPOSIUM ON THE BUSHVELD IGNEOUS COMPLEX AND OTHER LAYERED INTRUSIONS. *Geological Society of South Africa, Special Publication* 1, 108–207.

LIGHTFOOT, P. C., & NALDRETT, A. J., 1984—Chemical variation in the Insizwa Complex, Transkei, and the nature of the parent magma. *Canadian Mineralogist*, 22, 111–123.

LINDSLEY, D. H., 1983—Pyroxene thermometry. *American Mineralogist*, 68, 477–493.

LOFTUS-HILLS, G., & SOLOMON, M., 1967—Cobalt, nickel, and selenium in sulfides as indicators of ore genesis. *Mineralium Deposita*, 2, 228–242.

LONGHI, J., 1981—Multicomponent phase diagrams and the phase equilibria of basalts. *In* Workshop on magmatic processes of early planetary crusts. *Lunar & Planetary Institute, Technical Report* 82–01, 90–94.

LONGHI, J., WALKER, D., & HAYS, L. F., 1978—The distribution of Fe and Mg between olivine and lunar basaltic liquids. *Geochimica et Cosmochimica Acta*, 42, 1545–1558.

LONGHI, J., WOODEN, J. L., & COPPINGER, K. D., 1983—The petrology of high-Mg dikes from the Beartooth Mountains, Montana: a search for the parent magma of the Stillwater Complex. *Journal of Geophysical Research, Supplement*, 88, B53–B69.

LOUTHEAN, R., & SEIDEL, H., 1988—Platinum. *In* LOUTHEAN, R. (Editor)—REGISTER OF AUSTRALIAN MINING, 1988–1989. *Resource Information Unit Ltd, Perth*, 217–232.

LUDWIG, K. R., 1990—ISOPLOT—A plotting and regression program for radiogenic-isotope data for IBM-PC compatible computers, version 2.11. *United States Geological Survey, Open File Report* 88–557, Revision of August 7, 1990, 33 pp.

LYON, R. J. P., & PATTERSON, J. W., 1966—Infrared spectral signatures—a field geological tool. *Proceedings of the 4th International Symposium on Remote Sensing of the Environment*, 215–230.

MAALØE, S., 1978—The origin of rhythmic layering. *Mineralogical Magazine*, 42, 337–345.

MAALØE, S., 1987—Rhythmic layering of the Skaergaard intrusion. *In* PARSONS, I. (Editor)—ORIGINS OF IGNEOUS LAYERING. NATO Advanced Science Series, 196. *D. Reidel Publishing Company, Dordrecht*, 247–262.

MAAS, R., & MCCULLOCH, M. T., 1991—The provenance of Archean clastic metasediments in the Narryer Gneiss Complex, Western Australia: trace element geochemistry, Nd isotopes, and U-Pb ages for detrital zircons. *Geochimica et Cosmochimica Acta*, 55, 1915–1932.

MACDONALD, A. J., 1987—The platinum group element deposits: classification and genesis. *Geoscience Canada*, 14, 155–166.

MACIAS, L. F., & SIMPSON, C. J., 1990—Image processing of TM data over ultramafic complexes. Proceedings of the 5th Australasian Remote Sensing Conference, 1. *Committee of the 5th Australasian Remote Sensing Conference Incorporated 1990, Western Australia*, 616–627.

MACIAS, L. F., SIMPSON, C. J., & MOORE, R. F., 1987—Differentiation of mafic and ultramafic rock types using NS001 and TIMS data. *In* BRUCE, D. (Editor)—Proceedings of the 4th International Remote Sensing Conference, 1. *Committee of the 4th Australasian Remote Sensing Conference Incorporated 1987*, 364–370.

MAINWARING, P. R., & NALDRETT, A. J., 1977—Country-rock assimilation and the genesis of Cu-Ni sulfides in the Water Hen intrusion, Duluth Complex, Minnesota. *Economic Geology*, 72, 1269–1284.

MAITLAND, A. G., 1909—Geological investigations in the country lying between 21° 30′ and 25° 30′S latitude and 113° 30′ and 118° 30′ E longitude, embracing parts of the Gascoyne, Ashburton and West Pilbara Goldfields. *Western Australia Geological Survey, Bulletin* 33, 184 pp.

MARKGRAAFF, J., 1976—Pyroxenes of the Bushveld Complex, South Africa. *Transactions of the Geological Society of South Africa*, 79, 217–224.

MARSTON, R. J., 1979—Copper mineralization in Western Australia. *Western Australia Geological Survey, Mineral Resources Bulletin* 13, 208 pp.

MARSTON, R. J., 1984—Nickel mineralization in Western Australia. *Western Australia Geological Survey, Mineral Resources Bulletin* 14, 271 pp.

MARTIN, C. E., 1989—Re-Os isotopic investigation of the Stillwater Complex, Montana. *Earth & Planetary Science Letters*, 93, 336–344.

MATHISON, C. I., 1989—Petrological encoding of cumulates. *Transactions of the Institution of Mining & Metallurgy, London,* Section B, January–April, 98, B18–B23.

MATHISON, C. I., & BOOTH, R. A., 1990—Macrorhythmically layered gabbronorite in the Windimurra gabbroid complex, Western Australia. *Lithos*, 24, 171–180.

MATHISON, C. I., & HAMLYN, P. R., 1987—The McIntosh layered troctolite-olivine gabbro intrusion, east Kimberley, Western Australia. *Journal of Petrology*, 28, 211–234.

MATHISON, C. I., & MARSHALL, A. E., 1981—Ni-Cu sulfides and their host mafic-ultramafic rocks in the Mt. Sholl intrusion, Pilbara region, Western Australia. *Economic Geology*, 76, 1581–1596.

MATHISON, C. I., PERRING, R. J., VOGT, J. H., PARKS, J., HILL, R. E. T., & AHMAT, A. L., 1991—The Windimurra Complex. *In* BARNES, STEPHEN J., & HILL, R. E. T. (Editors)—Mafic-ultramafic complexes of Western Australia, Excursion Guidebook No. 3. Sixth International Platinum Symposium, July 1991, Perth, WA. *IAGOD and the Geological Society of Australia*, 45–76.

MATTEY, D. P., MARSH, N. G., & TARNEY, J., 1981—The geochemistry, mineralogy and petrology of basalts from the West Philippine and Parece Vela basins and from the Palau-Kyushu and west Mariana ridges. *Deep Sea Drilling Project, Leg 59, Initial Reports*, 59, 753–797.

MCBIRNEY, A. R., 1985—Further considerations of double-diffusive stratification and layering in the Skaergaard intrusion. *Journal of Petrology*, 26, 993–1001.

MCBIRNEY, A. R., 1987—Constitutional zone refining of layered intrusions. *In* PARSONS, I. (Editor)—ORIGINS OF IGNEOUS LAYERING. NATO Advanced Science Series, 196. *D. Reidel Publishing Company, Dordrecht*, 437–452.

MCBIRNEY, A. R., & NOYES, R. M., 1979—Crystallization and layering of the Skaergaard intrusion. *Journal of Petrology*, 20, 487–554.

MCCALLUM, M. E., LOUCKS, R. R., CARLSON, R. R., COOLEY, E. F., & DOERGE, T. A., 1976—Platinum metals associated with hydrothermal copper ores of the New Rambler Mine, Medicine Bow Mountains, Wyoming. *Economic Geology*, 71, 1429–1450.

MCCANDLESS, T. E., & RUIZ, J., 1991—Osmium isotopes and crustal sources for platinum-group mineralization in the Bushveld Complex, South Africa. *Geology*, 19, 1225–1228.

MCCARTHY, T. S., & CAWTHORN, R. G., 1980—changes in initial $^{87}Sr/^{86}Sr$ ratio during protracted fractionation in igneous complexes. *Journal of Petrology*, 21, 245–264.

MCCARTHY, T. S., LEE, C. A., FESQ, H. W., KABLE, E. J. D., & ERASMUS, C. S., 1984—Sulphur saturation in the lower and critical zones of the Eastern Bushveld Complex. *Geochimica et Cosmochimica Acta*, 48, 1005–1019.

MCCULLOCH, M. T., & CHAPPELL, B. W., 1982—Nd isotopic characteristics of S- and I-type granites. *Earth & Planetary Science Letters*, 58, 51–64.

MCDONALD, J. A., 1965—Liquid immiscibility as one factor in chromitite seam formation in the Bushveld Complex. *Economic Geology*, 60, 1674–1685.

McDONALD, J. A., 1967—Evolution of part of the lower Critical Zone, Farm Ruighoek, Western Bushveld. *Journal of Petrology*, 8, 165–209.

McGOLDRICK, P. J., 1986—Volatile and precious metal geochemistry of the Mount Isa ores and host rocks. Ph.D thesis, University of Melbourne (unpublished), 328 pp.

McGOLDRICK, P. J., & KEAYS, R. R., 1981—Precious and volatile metals in the Perseverance nickel deposit gossan: implications for exploration in weathered terrains. *Economic Geology*, 76, 1752–1763.

McGUIRE, A. V., & COLEMAN, R. G., 1986—The Jabal Tirf layered gabbro and associated rocks of the Tihama Asir Complex, SW Saudi Arabia. *Journal of Geology*, 94, 651–665.

McSWEEN, H. Y., JR., & NYSTROM, P. G., JR., 1979—Mineralogy and petrology of the Dutchmans Creek gabbroic intrusion, South Carolina. *American Mineralogist*, 64, 531–545.

MEDARIS, L. G., 1969—Partitioning of Fe^{++} and Mg^{++} between coexisting synthetic olivine and orthopyroxene. *American Journal of Science*, 267, 945–968.

MILLER, L. J., 1975—The Archaean eugeosyncline of the Pilbara. *In* KNIGHT, C. L. (Editor)—ECONOMIC GEOLOGY OF AUSTRALIA AND PAPUA NEW GUINEA. 1. Metals. *Australasian Institute of Mining & Metallurgy, Monograph* 5, 55–63.

MILLER, L. J., & SMITH, M. E., 1975—Sherlock Bay nickel-copper. *In* KNIGHT, C. L. (Editor)—ECONOMIC GEOLOGY OF AUSTRALIA AND PAPUA NEW GUINEA. 1. Metals. *Australasian Institute of Mining & Metallurgy, Monograph* 5, 168–174.

MITCHELL, R. H., & KEAYS, R. R., 1981—Abundance and distribution of gold, palladium and iridium in some spinel and garnet lherzolites: implications for the nature and origin of precious metal-rich intergranular components in the upper mantle. *Geochimica et Cosmochimica Acta*, 45, 2425–2442.

MOGESSIE, A., STUMPFL, E. F., & WEIBLEN, P. W., 1991—The role of fluids in the formation of platinum-group minerals, Duluth Complex, Minnesota: mineralogic, textural, and chemical evidence. *Economic Geology*, 86, 1506–1518.

MONGKOLTIP, P., & ASHWORTH, J. R., 1983—Quantitative estimation of an open-system symplectite-forming reaction: restricted diffusion of Al and Si in coronas around olivine. *Journal of Petrology*, 24, 635–661.

MORSE, S. A., 1979—Kiglapait geochemistry I: systematics, sampling, and density. *Journal of Petrology*, 20, 555–590.

NALDRETT, A. J., 1981—Nickel sulfide deposits: classification, composition, and genesis. *Economic Geology*, 75th Anniversary Volume, 628–685.

NALDRETT, A. J., 1989—MAGMATIC SULFIDE DEPOSITS. *Clarendon Press; Oxford University Press, New York*, 177 pp.

NALDRETT, A. J., BRAY, J. G., GASPARRINI, E. L., PODOLSKY, T., & RUCKLIDGE, J. C., 1970—Cryptic variation and the petrology of the Sudbury Nickel Irruptive. *Economic Geology*, 65, 122–155.

NALDRETT, A. J., BRUGMANN, G. E., & WILSON, A. H., 1990—Models for the concentration of PGE in layered intrusions. *Canadian Mineralogist*, 28, 389–408.

NALDRETT, A. J., & CABRI, L. J., 1976—Ultramafic and related rocks: their classification and genesis with special reference to the concentration of nickel sulfides and platinum-group elements. *Economic Geology*, 71, 1131–1158.

NALDRETT, A. J., CAMERON, G., VON GRUENEWALDT, G., & SHARPE, M. R., 1987—The formation of stratiform PGE deposits in layered intrusions. *In* PARSONS, I. (Editor)—ORIGINS OF IGNEOUS LAYERING. NATO Advanced Science Series, 196. *D. Reidel Publishing Company, Dordrecht*, 313–398.

NALDRETT, A. J., & DUKE, J. M., 1980—Platinum metals in magmatic sulfide ores. *Science*, 208, 1417–1424.

NALDRETT, A. J., GASPARRINI, E. C., BARNES, STEPHEN J., VON GRUENEWALDT, G., & SHARPE, M. R., 1986—The upper critical zone of the Bushveld Complex and the origin of Merensky-type ores. *Economic Geology*, 81, 1105–1117.

NALDRETT, A. J., & VON GRUENEWALDT, G., 1989—Association of platinum-group elements with chromitite in layered intrusions and ophiolite complexes. *Economic Geology*, 84, 180–187.

NELL, J., 1985—The Bushveld metamorphic aureole in the Potgietersrus area: evidence for a two-stage metamorphic event. *Economic Geology*, 80, 1129–1152.

NESBITT, R. W., GOODE, A. D. T., MOORE, A. C., & HOPWOOD, T. P., 1970—The Giles Complex, central Australia: a stratified sequence of mafic and ultramafic intrusions. *In* VISSER, D. J. L., & VON GRUENEWALDT, G. (Editors)—SYMPOSIUM ON THE BUSHVELD IGNEOUS COMPLEX AND OTHER LAYERED INTRUSIONS. *Geological Society of South Africa, Johannesburg. Special Publication 1*, 547–564.

NESBITT, R. W., SUN, S-S., & PURVIS, A. C., 1979—Komatiites: geochemistry and genesis. *Canadian Mineralogist*, 17, 165–186.

NIENABER-ROBERTS, C. J., 1986—A mineralogical and petrographic investigation of the Upper Zone of the Bushveld Complex, northwest of Potgietersrus. *Department of Mineral & Energy Affairs, Republic of South Africa, Bulletin* 80, 34 pp.

NISBET, E. G., & CHINNER, G. A., 1981—Controls on the eruption of mafic and ultramafic lavas, Ruth Well Ni-Cu prospect, West Pilbara. *Economic Geology*, 76, 1729–1735.

NORRISH, K., & CHAPPELL, B., 1977—X-ray fluorescence spectrography. *In* ZUSSMAN, J. (Editor)—PHYSICAL METHODS IN DETERMINATIVE MINERALOGY, 161–214, *Academic Press, London.*

NORRISH, K., & HUTTON, J. T., 1969—An accurate X-ray spectrographic method for the analysis of a wide range of geological samples. *Geochimica et Cosmochimica Acta*, 33, 431–453.

NWE, Y. Y., 1976—Electron-probe studies of the earlier pyroxenes and olivines from the Skaergaard Intrusion, East Greenland. *Contributions to Mineralogy & Petrology*, 55, 105–126.

O'HARA, M. J., 1977—Geochemical evolution during fractional crystallization of a periodically refilled magma chamber. *Nature*, 266, 506–507.

O'HARA, M. J., & MATHEWS, R. E., 1981—Geochemical evolution in an advancing, periodically replenished, periodically tapped, continuously fractionated magma chamber. *Journal of the Geological Society of London*, 138, 237–277.

OHMOTO, H., 1986—Stable isotope geochemistry of ore deposits. *In* VALLEY, J. W., TAYLOR, H. P., & O'NEIL, J. R. (Editors)—REVIEWS IN MINERALOGY—STABLE ISOTOPES. Volume 16. *Mineralogical Society of America*, 491–559.

OVERSBY, V. M., 1976—Isotopic ages and geochemistry of Archaean acid igneous rocks from the Pilbara, Western Australia. *Geochimica et Cosmochimica Acta*, 40, 817–829.

PAGE, N. J., MYERS, J. S., HAFFTY, J., SIMON, F. O., & ARUSCAVAGE, P. J., 1980—Platinum, palladium, and rhodium in the Fiskenaesset Complex, Southwestern Greenland. *Economic Geology*, 75, 907–915.

PAGE, N. J., RILEY, L. B., & HAFFTY, J., 1972—Vertical and lateral variation of platinum, palladium, and rhodium in the Stillwater Complex, Montana. *Economic Geology*, 67, 915–923.

PAGE, N. J., ROWE, J. J., & HAFFTY, J., 1976—Platinum metals in the Stillwater Complex, Montana. *Economic Geology*, 71, 1352–1363.

PAGE, N. J., VON GRUENEWALDT, G., HAFFTY, J., & ARUSCAVAGE, P. J., 1982—Comparison of platinum, palladium, and rhodium distributions in some layered intrusions with special reference to the late differentiates (Upper Zone) of the Bushveld Complex, South Africa. *Economic Geology*, 77, 1405–1418.

PALACZ, Z. A., & TAIT, S. R., 1985—Isotopic and geochemical investigation of unit 10 from the eastern layered series of the Rhum intrusion, Northwest Scotland. *Mineralogical Magazine*, 122, 485–490.

PAPUNEN, H., HAKLI, T. A., & IDMAN, H., 1979—Geological, geochemical and mineralogical features of sulfide-bearing ultramafic rocks in Finland. *Canadian Mineralogist*, 17, 217–232.

PARSONS, I., 1979—The Klokken gabbro-syenite complex, South Greenland: cryptic variation and origin of inversely graded layering. *Journal of Petrology*, 20, 653–694.

PASTERIS, J. D., 1984—Further interpretation of the Cu-Fe-Ni sulfide mineralization in the Duluth Complex, northeastern Minnesota. *Canadian Mineralogist*, 22, 39–53.

PEACH, C. L., MATHEZ, E. A., & KEAYS, R. R., 1989—Sulfide melt-silicate melt distribution coefficients for the noble metals as deduced from MORBs. *In* PAPUNEN, H. (Editor)—5th International Platinum Symposium, Abstracts. *Bulletin of the Geological Society of Finland*, 61, Part 1, 1989, 58.

PEARCE, J. A., & CANN, J. R., 1973—Tectonic setting of basic volcanic rocks using trace element analysis. *Earth & Planetary Science Letters*, 19, 290–300.

PECK, D. C., & KEAYS, R. R., 1990a—Geology, geochemistry, and origin of platinum-group element-chromitite occurrences in the Heazlewood River Complex, Tasmania. *Economic Geology*, 85, 765–793.

PECK, D. C., & KEAYS, R. R., 1990b—Insights into the behaviour of precious metals in primitive, S-undersaturated magmas: evidence from the Heazlewood River Complex, Tasmania. *Canadian Mineralogist*, 28, 553–577.

PETERS, W. S., & DE ANGELIS, M., 1987—The Radio Hill Ni-Cu massive sulphide deposit. A geophysical case history. *Exploration Geophysics*, 18, 160–166.

PETERSEN, J. S., 1987—Solidification contraction: another approach to cumulus processes and the origin of igneous layering. *In* PARSONS, I. (Editor)—ORIGINS OF IGNEOUS LAYERING. NATO Advanced Science Series, 196. *D. Reidel Publishing Company, Dordrecht*, 505–526.

PIDGEON, R. T., 1978—3450 M.y. old volcanics in the Archaean layered greenstone succession of the Pilbara Block, Western Australia. *Earth & Planetary Science Letters*, 37, 421–428.

PIDGEON, R. T., 1984—Geochronological constraints on early volcanic evolution of the Pilbara Block, Western Australia. *Australian Journal of Earth Sciences*, 31, 237–242.

POLDERVAART, A., & HESS, H. H., 1951—Pyroxenes in the crystallization of basaltic magma. *Journal of Geology*, 59, 472–489.

PODPORA, C., & LINDSLEY, D. H., 1979—Fe-rich pigeonites: minimum temperatures of stability in the Ca-Mg-Fe quadrilateral. *EOS*, 60, 420–421.

PONTUAL, A., 1990—Constraining the patterns of hydrothermal circulation cells in ophiolitic terrain by application of digitally enhanced Landsat Thematic Mapper data. Proceedings of the 5th Australasian Remote Sensing Conference, 1. *Committee of the 5th Australasian*

Remote Sensing Conference Incorporated 1990, Western Australia, 628–635.

PRENDERGAST, M. D., 1990—Platinum-group minerals and hydrosilicate 'alteration' in Wedza–Mimosa platinum deposit, Great Dyke, Zimbabwe—genetic and metallurgical implications. *Transactions of the Institution of Mining & Metallurgy, London*, Section B, May–August, 99, B91–B105.

PRENDERGAST, M. D., & KEAYS, R. R., 1987—Precious metals in the pyroxenite no. 1 layer in the Wedza Complex of the Great Dyke, Zimbabwe. Abstracts, Magmatic Sulphides Field Conference, 5th IGCP, Project 161. *Geological Society of Zimbabwe*, 11.

PRENDERGA/ST, M. D., & KEAYS, R. R., 1989—Controls of platinum-group element mineralisation and the origin of the PGE-rich main sulphide zone in the Wedza subchamber of the Great Dyke, Zimbabwe: implications for the genesis of, and exploration for, stratiform PGE mineralisation in layered intrusions. *In* PRENDERGAST, M. D., & JONES, M. J. (Editors)—MAGMATIC SULPHIDES—THE ZIMBABWE VOLUME. *Institution of Mining & Metallurgy, London*, 21–69.

PRICE, R. C., & WALLACE, R. C., 1976—The significance of corona textured inclusions from a high pressure fractionated alkalic lava: North Otago, New Zealand. *Lithos*, 9, 319–329.

PURVIS, A. C., NESBITT, R. W., & HALLBERG, J. A., 1972—The geology of part of the Carr Boyd Rocks complex and its associated nickel mineralization. *Economic Geology*, 67, 1093–1113.

RAEDEKE, L. D., & MCCALLUM, I. S., 1980—A comparison of fractionation trends in lunar crust and the Stillwater Complex. *In* PAPIKE, J. J., & MERRILL, R. B. (Editors)—CONFERENCE ON LUNAR HIGHLANDS CRUST, PROCEEDINGS, SUPPLEMENT 12. *Pergamon Press, New York*, 133–153.

RAINES, G. L., & WYNN, J. C., 1982—Mapping of the ultramafic rocks in a heavily vegetated terrain using Landsat data. *Economic Geology*, 77, 1755–1769.

RAJAMANI, V., & NALDRETT, A. J., 1978—Partitioning of Fe, Co, Ni, and Cu between sulfide liquid and basaltic melts and the composition of Ni-Cu sulfide deposits. *Economic Geology*, 73, 82–93.

RAO, B. V., & RIPLEY, E. M., 1983—Petrochemical studies of the Dunka Road Cu-Ni Deposit, Duluth Complex, Minnesota. *Economic Geology*, 78, 1222–1238.

RHODES, J. M., DUNGAN, M. A., BLANCHARD, D. P., & LONG, P. E., 1979—Magma mixing at mid-ocean ridges: evidence from basalts drilled near 22°N on the Mid-Atlantic Ridge. *Tectonophysics*, 55, 35–61.

RICHARDS, J. R., 1981—Precambrian galena ages. *Australian National University, Research School of Earth Sciences, Annual Report, 1981*, 186–187.

RICHARDS, J. R., & BLOCKLEY, J. G., 1984—The base of the Fortescue Group, Western Australia: further galena lead isotope evidence on its age. *Australian Journal of Earth Sciences*, 31, 257–268.

RICHARDS, J. R., FLETCHER, I. R., & BLOCKLEY, J. G., 1981—Pilbara galenas: precise isotopic assay of the oldest Australian leads: model ages and growth-curve implications. *Mineralium Deposita*, 16, 7–30.

RICHARDSON, B. D., 1976—The geology of the Radio Hill layered intrusion. B.Sc. Honours thesis, University of Western Australia, Australia (unpublished), 52 pp.

RICHARDSON, J. M., DICKIN, A. P., MCNUTT, R. H., BENETEAU, S. B., & CROCKET, J. H., 1989—Application of Re-Os isotopic analyses to PGE deposits. *In* PAPUNEN, H. (Editor)—5th International Platinum Symposium, Abstracts. *Bulletin of the Geological Society of Finland*, 61, Part 1, 1989, 56–57.

RIPLEY, E. M., 1979—Sulfide petrology of basal chilled margins in layered sills of the Archean Deer Lake Complex, Minnesota. *Contributions to Mineralogy & Petrology*, 69, 345–354.

RIPLEY, E. M., 1981—Sulfur isotopic studies of the Dunka Road Cu-Ni deposit, Duluth Complex, Minnesota. *Economic Geology*, 76, 610–620.

RIPLEY, E. M., 1983—Sulfide mineralogy and sulfur isotope geochemistry of layered sills in the Deer Lake Complex, Minnesota. *Mineralium Deposita*, 18, 3–15.

RIPLEY, E. M., 1986—Origin and concentration mechanisms of copper and nickel in Duluth Complex sulfide zones—a dilemma. *Economic Geology*, 81, 974–978.

ROBERT, R. V. D., & VAN WYK, E., 1975—The efficiency of various matrix elements on the efficiency of the fire-assay procedure using nickel sulphide as the collector. *Johannesburg National Institute for Metallurgy, Report* 1705, 1–7.

ROBERT, R. V. D., VAN WYK, E., PALMER, R., & STEELE, T. W., 1971—Concentration of the noble metals by a fire-assay technique using nickel sulphide as the collector. *Johannesburg National Institute for Metallurgy, Report* 1371.

ROEDER, P. L., & EMSLIE, R. F., 1970—Olivine-liquid equilibrium. *Contributions to Mineralogy & Petrology*, 29, 275–289.

ROSS, J. R., & KEAYS, R. R., 1979—Precious metals in volcanic-type nickel sulfide deposits in Western Australia, 1. Relationship with the composition of the ores and their host rocks. *Canadian Mineralogist*, 17, 417–435.

ROTHERY, D. A., 1984a—The role of Landsat Multispectral Scanner (MSS) imagery in mapping the Oman Ophiolite. *In* GASS, I. G., LIPPARD, S. J., & SHELTON, A. W. (Editors)—OPHIOLITES AND OCEANIC LITHOSPHERE. *Geological Society of London, Special Publication* 13, 405–413.

ROTHERY, D. A., 1984b—Reflectance of ophiolite rocks in the Landsat MSS bands: relevance to lithological mapping by remote sensing. *Journal of the Geological Society of London*, 141, 933–969.

ROTHERY, D. A., 1987—Improved discrimination of rock units using Landsat Thematic Mapper Imagery of the Oman Ophiolite. *Journal of the Geological Society of London*, 144, 587–597.

ROTHERY, D. A., ABRAMS, M. J., & PONTUAL, A., 1988—Subdivision of mapped units in the Oman Ophiolite using enhanced Landsat Thematic Mapper images. *Proceedings, Troodos 87, Ophiolites & Oceanic Lithosphere, Nicosia, Cyprus*, 4–10.

ROWELL, W. F., & EDGAR, A. D., 1986—Platinum-group element mineralization in a hydrothermal Cu-Ni sulfide occurrence, Rathbun Lake, northeastern Ontario. *Economic Geology*, 81, 1272–1277.

RUTHERFORD, M. J., & HERMES, O. D., 1984—Melatroctolite-anorthositic gabbro complex, Cumberland, Rhode Island: petrology, origin and regional setting. *Bulletin of the Geological Society of America*, 95, 844–854.

RYAN, G. R., 1965—The geology of the Pilbara Block, Western Australia. *Australasian Institute of Mining & Metallurgy, Proceedings*, 214, 61–94.

RYAN, G. R., 1966—Roebourne, Western Australia—1 : 250 000 Geological Series. *Western Australia Geological Survey, Explanatory Notes* SF/50-3.

RYAN, G. R., & KRIEWALDT, M. J. B., 1963—Archaean stratigraphy in the Roebourne area, West Pilbara Goldfield. *Western Australia Geological Survey, Annual Report*, 1962, 38.

RYE, R. O., & OHMOTO, H., 1974—Sulfur and carbon isotopes and ore genesis: a review. *Economic Geology*, 69, 826–842.

SCHIFFRIES, C. M., 1982—The petrogenesis of a platiniferous dunite pipe in the Bushveld Complex: infiltration metasomatism by a chloride solution. *Economic Geology*, 77, 1439–1453.

SCHIFFRIES, C. M., & RYE, D. M., 1989—Stable isotopic systematics of the Bushveld Complex: I. Constraints of magmatic processes in layered intrusions. *American Journal of Science*, 289, 841–873.

SCHIFFRIES, C. M., & RYE, D. M., 1990—Stable isotopic systematics of the Bushveld Complex: II. Constraints on hydrothermal processes in layered intrusions. *American Journal of Science*, 290, 209–245.

SCHIFFRIES, C. M., & SKINNER, B. J., 1987—The Bushveld hydrothermal system. Field and petrologic evidence. *American Journal of Science*, 287, 566–596.

SHARPE, M. R., 1981—The chronology of magma influxes to the eastern compartment of the Bushveld Complex as exemplified by its marginal border groups. *Journal of the Geological Society of London*, 138, 307–326.

SHARPE, M. R., 1985—Strontium isotope evidence for preserved density stratification in the main zone of the Bushveld Complex. *Nature*, 316, 119–126.

SHARPE, M. R., & HULBERT, L. J., 1985—Ultramafic sills beneath the Eastern Bushveld Complex: mobilized suspensions of early lower zone cumulates in a parental magma with boninitic affinities. *Economic Geology*, 80, 849–871.

SHARPE, M. R., & IRVINE, T. N., 1983—Melting relations of two Bushveld chilled margin rocks and implications for the origin of chromitites. *Carnegie Institution of Washington, Yearbook 1982*, 295–300.

SHERATON, J. W., & SIMONS, L., 1988— Geochemical data analysis system reference manual. *Bureau of Mineral Resources, Australia, Record* 1988/45, 183 pp.

SIEBER, G., REISCHMANN, T., & ARNDT, N. T., 1990—Petrological and geochemical comparison of Archaean and Proterozoic-style volcanics from the Pilbara region, Western Australia. *In* CRUSTAL DYNAMICS: PATHWAYS AND RECORDS. *Terra Abstracts*, 2, 25.

SIMKIN, T., & SMITH, J. V., 1970—Minor element distribution in olivine. *Journal of Geology*, 78, 304–325.

SIMPSON, C. J., 1986—US/Australia Joint Scanner Project. *BMR Research Newsletter*, 4, 14–15.

SIMPSON, C. J., 1990—Deep weathering, vegetation and fireburn. Significant obstacles to geoscience remote sensing in Australia. *International Journal of Remote Sensing*, 11 (11), 2019–2034.

SMITH, C. H., & KAPP, H. E., 1963—The Muskox intrusion, a recently discovered layered intrusion in the Coppermine River area, Northwest Territories, Canada. *Mineralogical Society of America, Special Paper* 1, 30–35.

SMITH, J. V., 1974—FELDSPAR MINERALS. *Springer Verlag*, 2, 690 pp.

SPARKS, R. S. J., & HUPPERT, H. E., 1987—Laboratory experiments with aqueous solutions modelling magma chamber processes. I. Discussion of their validity and geological application. *In* PARSONS, I. (Editor)—ORIGINS OF IGNEOUS LAYERING. NATO Advanced Science Series, 196. *D. Reidel Publishing Company, Dordrecht*, 527–538.

SPARKS, R. S. J., HUPPERT, H. E., & TURNER, J. S., 1984—The fluid dynamics of evolving magma chambers. *Philosophical Transactions, Royal Society of London*, A 310, 511–534.

SPARKS, R. S. J., SIGURDSSON, H., & WILSON, L., 1977—Magma mixing: for triggering acid explosive eruptions. *Nature*, 267, 315–318.

SPENCER, K. H., & LINDSLEY, D. H., 1981—A solution model for coexisting iron-titanium oxides. *American Mineralogist*, 66, 1189–1201.

SPERA, F. J., YUEN, D. A., CLARK, S., & HONG, H. J., 1986—Double-diffusive convection in magma chambers: single or multiple layers. *Geophysical Research Letters*, 13, 153–156.

STANTON, R. L., 1972—ORE PETROLOGY. *McGraw-Hill, New York*, 713 pp.

STEWART, B. W., & DEPAOLO, D. J., 1990—Isotopic studies of processes in mafic magma chambers—II: The Skaergaard intrusion, East Greenland. *Contributions to Mineralogy & Petrology*, 104, 125–141.

STONE, W. E., CROCKET, J. H., & FLEET, M. E., 1990—Partitioning of palladium, iridium, platinum, and gold between sulfide liquid and basalt melt at 1200°C. *Geochimica et Cosmochimica Acta*, 54, 2341–2344.

STORMER, J. C., JR., 1983—The effects of recalculation on estimates of temperature and oxygen fugacity from analyses of multicomponent iron-titanium oxides. *American Mineralogist*, 68, 586–594.

STRECKEISEN, A. L., 1973—Plutonic rocks: classification and nomenclature recommended by the IUGS Subcommission on the systematics of igneous rocks. *Geotimes*, October 1973, 26–30.

STRECKEISEN, A. L., 1976—To each plutonic rock its proper name. *Earth Science Reviews*, 12, 1–33.

STUMPFL, E. F., 1986—Distribution, transport and concentration of platinum group elements. *In* GALLAGHER, M. J., IXER, R. A., NEARY, C. R., & PRICHARD, H. M. (Editors)—METALLOGENY OF BASIC AND ULTRABASIC ROCKS. *Institution of Mining & Metallurgy, London*, 379–394.

STUMPFL, E. F., 1990—Platinum geology: new developments and future prospects. *In* R. L. STANTON SYMPOSIUM. GONDWANA: TERRANES AND RESOURCES. *Geological Society of Australia, Tenth Australian Geological Convention, Hobart, 1990, Abstracts 25*, 15–16.

STUMPFL, E. F., & BALLHAUS, C. G., 1986—Stratiform platinum deposits: new data and concepts. *Fortschritte der Mineralogie*, 64, 205–214.

SULTAN, M., ARVIDSON, R. E., & STURCHIO, N. C., 1986—Mapping of serpentinites in the Eastern Desert of Egypt by using Landsat thematic mapper data. *Geology*, 14, 995–999.

SUN, S-S., & MCDONOUGH, W. F., 1989—Chemical and isotopic systematics of oceanic basalts: implication for mantle composition and processes. *In* SAUNDERS, A. D., & NORRY, M. J. (Editors)—MAGMATISM IN THE OCEAN BASINS. Geological Society Special Publication 42. *Blackwell Scientific Publications, Oxford*, 313–345.

SUN, S-S., & NESBITT, R. W., 1978—Petrogenesis of Archaean ultrabasic and basic volcanics: evidence from rare elements. *Contributions to Mineralogy & Petrology*, 65, 301–325.

SUN, S-S., NESBITT, R. W., & MCCULLOCH, M. T., 1989—Geochemistry and petrogenesis of siliceous high magnesian basalts of the Archaean and early Proterozoic. *In* CRAWFORD, A. J. (Editor)—BONINITES AND RELATED ROCKS. *Unwin Hyman, London*, 148–173.

SUN, S-S., WALLACE, D. A., HOATSON, D. M., GLIKSON, A. Y., & KEAYS, R. R., 1991—Use of geochemistry as a guide to platinum group element potential of mafic-ultramafic rocks: examples from the west Pilbara and Halls Creek Mobile Zone, Western Australia. *Precambrian Research, 50, 1–35.*

SUTCLIFFE, R. H., SWEENY, J. M., & EDGAR, A. D., 1989—The Lac des Iles Complex, Ontario: petrology and platinum-group-elements mineralization in an Archean mafic intrusion. *Canadian Journal of Earth Sciences*, 26, 1408–1427.

SYLVESTER, G. C., & DE LAETER, J. R., 1987—Geochronology of the Mons Cupri Archaean volcanic centre, Pilbara Block, Western Australia. *Journal of the Royal Society of Western Australia*, 70, 29–34.

TAIT, S. R., 1985—Fluid dynamic and geochemical evolution of cyclic unit 10, Rhum, eastern layered series. *Geological Magazine*, 122, 469–484.

TAIT, S. R., & KERR, R. C., 1987—Experimental modelling of interstitial melt convection in cumulus piles. *In* PARSONS, I. (Editor)—ORIGINS OF IGNEOUS LAYERING. NATO Advanced Science Series, 196. *D. Reidel Publishing Company, Dordrecht*, 569–587.

TALKINGTON, R. W., & WATKINSON, D. W., 1984—Trends in the distribution of the precious metals in the Lac des Iles Complex, Northwestern Ontario. *Canadian Mineralogist*, 22, 125–136.

TAYLOR, R. B., 1956—The Duluth gabbro complex, Duluth, Minnesota. *Annual Meeting, GSA, Guidebook, Field Trip No. 1*, 42–66.

THALHAMMER, O. A. R., & STUMPFL, E. F., 1988—Platinum-group minerals from Hochgrössen ultramafic massif, Styria: first reported occurrence of PGM in Austria. *Transactions of the Institution of Mining & Metallurgy, London*, 97, B77–82.

THOMPSON, J. F. H., & NALDRETT, A. J., 1984—Sulphide-silicate reactions as a guide to Ni-Cu-Co mineralization in central Maine, U.S.A. *In* BUCHANAN, D. L., & JONES, M. J. (Editors)—SULPHIDE DEPOSITS IN MAFIC AND ULTRAMAFIC ROCKS. Proceedings of IGCP Projects 161 & 91, Third Nickel Sulphide Field Conference, Perth, WA, 23–25 May 1982. *Transactions of the Institution of Mining & Metallurgy, London*, 103–113.

THORNETT, J. R., 1981—The Sally Malay deposit: gabbroid-associated nickel-copper sulfide mineralization in the Halls Creek mobile belt, Western Australia. *Economic Geology*, 76, 1565–1580.

TODD, S. G., KEITH, D. W., LE ROY, L. W., SCHISSEL, D. J., MANN, E. L., & IRVINE, T. N., 1982—The J-M platinum-palladium reef of the Stillwater Complex, Montana: stratigraphy and petrology. *Economic Geology*, 77, 1454–1480.

TRENDALL, A. F., 1983—The Hamersley Basin. *In* TRENDALL, A. F., & MORRIS, R. C. (Editors)—IRON-FORMATION FACTS AND PROBLEMS. Developments in Precambrian geology, 6. *Elsevier, Amsterdam*, 69–129.

TURNER, J. S., & GUSTAFSON, L. B., 1978—The flow of hot saline solutions from vents in the sea floor: some implications for exhalative sulfide and other ore deposits. *Economic Geology*, 73, 1082–1100.

TYSON, R. M., & CHANG, L. L. Y., 1984—The petrology and sulfide mineralization of the Partridge River Troctolite, Duluth Complex, Minnesota. *Canadian Mineralogist*, 22, 23–38.

VERMAAK, C. F., 1976—The Merensky Reef—thoughts on its environment and genesis. *Economic Geology*, 71, 1270–1298.

VILJOEN, M. J., THERON, J., UNDERWOOD, B., WALTERS, B. M., WEAVER. J., & PEYERL, W., 1986—The Amandelbult section of the Rustenburg Platinum Mines Limited, with reference to the Merensky Reef. *In* ANAEUSSER, C. R., & MASKE, S. (Editors)—MINERAL DEPOSITS OF SOUTHERN AFRICA, Volume II. *Geological Society of South Africa, Johannesburg*, 1041–1060.

VILJOEN, R. P., & VILJOEN, M. J., 1971—The geological and geochemical evolution of the Onverwacht volcanic group of the Barberton Mountain Land, South Africa. *Geological Society of Australia, Special Publication*, 3, 133–149.

VOLBORTH, A., TARKIAN, M., STUMPFL, E. F., & HOUSLEY, R. M., 1986—A survey of the Pd-Pt mineralization along the 35-km strike of the J-M Reef, Stillwater Complex, Montana. *Canadian Mineralogist*, 24, 329–346.

VON GRUENEWALDT, G., 1970—On the phase change orthopyroxene-pigeonite and the resulting textures in the main and upper zones of the Bushveld Complex in the eastern Transvaal. *In* VISSER, D. J. L., & VON GRUENEWALDT, G. (Editors)—SYMPOSIUM ON THE BUSHVELD IGNEOUS COMPLEX AND OTHER LAYERED INTRUSIONS. *Geological Society of South Africa, Special Publication* 1, 67–73.

VON GRUENEWALDT, G., 1971—A petrographical and mineralogical investigation of the rocks of the Bushveld Complex in the Tauteshoogte–Roossenekal area of the eastern Transvaal. D.Sc. thesis, University of Pretoria, South Africa (unpublished), 228 pp.

VON GRUENEWALDT, G., 1979—A review of some recent concepts of the Bushveld Complex, with particular reference to sulfide mineralization. *Canadian Mineralogist*, 17, 233–256.

VON GRUENEWALDT, G., SHARPE, M. R., & HATTON, C. J., 1985—The Bushveld Complex: introduction and review. *Economic Geology*, 80, 803–812.

WAGER, L. R., 1961—A note on the origin of ophitic texture in the chilled olivine gabbro of the Skaergaard intrusion. *Geological Magazine*, 98, 353–366.

WAGER, L. R., & BROWN, G. M., 1968—LAYERED IGNEOUS ROCKS. *Oliver & Boyd, Edinburgh & London*, 588 pp.

WAGER, L. R., BROWN, G. M., & WADSWORTH, W. J. , 1960—Types of igneous cumulates. *Journal of Petrology*, 1, 73–85.

WAGER, L. R., & MITCHELL, R. L., 1951—The distribution of trace elements during strong fractionation of basic magma—a further study of the Skaergaard intrusion, East Greenland. *Geochimica et Cosmochimica Acta*, 1, 129–208.

WALKER, K. R., WARE, N. G., & LOVERING, J. R., 1973—Compositional variations in the pyroxenes of the differentiated Palisades Sill, New Jersey. *Bulletin of the Geological Society of America*, 84, 89–110.

WALLACE, D. A., & HOATSON, D. M., 1990—Petrology and whole-rock geochemistry of selected mafic and ultramafic suites from the Pilbara Block and Halls Creek Mobile Zone, Western Australia. *Bureau of Mineral Resources, Australia, Record* 1990/46, 69 pp.

WATKINSON, D. H., & DUNNING, G. R., 1979—Geology and platinum-group mineralization, Lac-des-Iles complex, Northwestern Ontario. *Canadian Mineralogist*, 17, 453–462.

WELLS, P. R. A., 1977—Pyroxene thermometry in simple and complex systems. *Contributions to Mineralogy & Petrology*, 62, 129–139.

WENDLANDT, R. F., 1982—Sulfide saturation of basalt and andesite melts at high pressures and temperatures. *American Mineralogist*, 67, 877–885.

WESTERN AUSTRALIA GEOLOGICAL SURVEY, 1990—Geology and mineral resources of Western Australia. *Western Australia Geological Survey, Memoir* 3, 827 pp.

WILLEMSE, J., 1969—The geology of the Bushveld Igneous Complex, the largest repository of magmatic ore deposits in the world. *Economic Geology, Monograph* 4, 1–22.

WILLIAMS, C. R., NISBET, B. W., & HOATSON, D. M., 1990—Munni Munni Complex, platinum group mineralisation. *In* HUGHES, F. E. (Editor)—GEOLOGY OF THE MINERAL DEPOSITS OF AUSTRALIA AND PAPUA NEW GUINEA. Monograph 14, Volume 1, *Australasian Institute of Mining & Metallurgy, Melbourne*, 145–150.

WILLIAMS, I. R., 1968—Yarraloola, Western Australia—1 : 250 000 Geological Series. *Western Australia Geological Survey, Explanatory Notes* SF/50-6.

WILLIAMS, R. J., 1971—Reaction constraints in the system Fe-MgO-SiO_2-O_2: intensive parameters in the Skaergaard intrusion, East Greenland. *American Journal of Science*, 271, 132–146.

WILSON, A. H., 1982—The geology of the Great 'Dyke', Zimbabwe: the ultramafic rocks. *Journal of Petrology*, 23, 240–292.

WILSON, A. H., NALDRETT, A. J., & TREDOUX, M., 1989—Distribution and controls of platinum group element and base metal mineralization in the Darwendale subchamber of the Great Dyke, Zimbabwe. *Geology*, 17, 649–652.

WILSON, A. H., & PRENDERGAST, M. D., 1989—The Great Dyke of Zimbabwe—I: tectonic setting, stratigraphy, petrology, structure, emplacement and crystallization. *In* PRENDERGAST, M. D., & JONES, M. J. (Editors)—MAGMATIC SULPHIDES—THE ZIMBABWE VOLUME. *Institution of Mining & Metallurgy, London*, 1–20.

WILSON, A. H., & TREDOUX, M., 1990—Lateral and vertical distribution of platinum-group elements and petrogenetic controls on the sulfide mineralization in the P1 pyroxenite layer of the Darwendale subchamber of the Great Dyke, Zimbabwe. *Economic Geology*, 85, 556–584.

WILSON, J. R., ESBENSEN, K. H., & THY, P., 1981—Igneous petrology of the synorogenic Fongen-Hyllingen layered basic complex, south-central Scandinavian Caledonides. *Journal of Petrology*, 22, 584–627.

WOOD, B. J., & BANNO, S., 1973—Garnet-orthopyroxene and orthopyroxene-clinopyroxene relationships in simple and complex systems. *Contributions to Mineralogy & Petrology*, 42, 109–124.

WOODEN, J. L., CZAMANSKE, G. K., & ZIENTEK, M. L., 1991– A lead isotopic study of the Stillwater Complex: constraints on crustal contamination and source regions. *Contributions to Mineralogy & Petrology*, 107, 80–93.

WOODWARD, H. P., 1890—Report on Cossack, Roebourne, Mallina, Peawah, Croydon, the Pyramid and Woodbrook. *Western Australia Geological Survey, Annual Report*, 1888.

WOODWARD, H. P., 1894—Geological sketch map of Western Australia. *George Philip & Son, London & Liverpool.*

WOODWARD, H. P., 1911—The geology and ore deposits of the West Pilbara Goldfield. *Western Australia Geological Survey, Bulletin* 41, 142 pp.

YAMAMOTO, M., 1976—Relationships between Se/S and sulfur isotope ratios of hydrothermal sulfide minerals. *Mineralium Deposita*, 11, 197–209.

ZIENTEK, M. L., & RIPLEY, E. M., 1990—Sulphur isotope studies of the Stillwater Complex and associated rocks, Montana. *Economic Geology*, 85, 376–391.

APPENDIX 1. ANALYTICAL PROCEDURES

1.1. Radiochemical neutron-activation analysis (RNAA)

Radiochemical neutron-activation analysis offers several advantages over more conventional analytical techniques. It is more sensitive to sub-ppb concentrations of precious metals (Pt, Pd, Ir, Au), it does not require quantitative recovery of the element concerned, and it is not subject to post-irradiation contamination by reagents. However, the method is dependent on access to a suitable nuclear reactor, and, in the laboratory, on the equilibration of an activated radionuclide and a carrier. And, being labour-intensive, the process is slow and expensive.

In radiochemical neutron-activation analysis the isotope of interest is extracted or isolated by an involved sequence of acid digestions, ion exchange, and precipitation methods. The procedures for this study, which were carried out in the School of Earth Sciences, University of Melbourne, involved two techniques, namely fire-assay preconcentration of Pt, Pd, Ir, and Au into a nickel-sulphide button, and whole-rock powder analysis for Se, Cs, Rb, and Th (Table 40). The fire-assay method using nickel sulphide as a collector for the precious metals was modified after the techniques initially developed by Robert & others (1971) and Robert & van Wyk (1975). The radiochemical procedures used in this study were modified from the techniques described by Keays & others (1974), Ewers (1975), Hughes (1978), and McGoldrick (1986). Flowchart summaries of the radiochemical procedures used in the nickel-sulphide button and whole-rock powder techniques are shown in Figures 119 & 120, respectively, and details of both techniques are presented by Hoatson (1991). The nuclear parameters of the isotopes used and detection limits are summarised in Table 40.

Precious-metal data (Table 14; Figs 56A–B) for the mineralised porphyritic websterite layer were kindly provided by Hunter Resources Ltd. Fire-assay neutron-activation analysis (by Nuclear Activation Services Ltd, Ontario) was used for the determination of Os (detection limit of 3 ppb), Ir (0.1 ppb), Ru (5 ppb), Rh (1 ppb), Au (1 ppb), and Re (5 ppb), and fire-assay atomic-absorption spectrophotometry (by SGS Australia Pty Ltd) was used for the determination of Pt (2 ppb) and Pd (1 ppb).

Samples were selected for RNAA on the basis of petrographic and trace-element geochemical criteria (e.g. immobile incompatible-element trends such as Zr, and S/Se and Cu/Ni ratios). A moving average of five samples was used to smooth the S, Cu, Ni, Zr, and Sr data in Figures 54A–B & 58 (except for the S-rich samples at the base of the ultramafic zone and at the contact of the ultramafic and gabbroic zones). This process was not applied to the more widely spaced RNAA data.

1.2. X-ray fluorescence spectrometry (XRFS) and atomic-absorption spectrophotometry (AAS) for major- and trace-element analysis

Major and trace elements were determined by X-ray fluorescence spectrometry (XRFS) and atomic-absorption spectrophotometry (AAS) at AGSO in Canberra. The XRFS analyses were carried out using a Philips PW1450 sequential spectrometer, and some of the trace elements were determined by using a Varian AA-975 spectrophotometer. Ferrous oxide was determined by a titrimetric method and gravimetric analysis was used to determine H_2O^+ and CO_2. A summary of the chemical techniques used and of the operating conditions of the XRFS-AAS facilities at AGSO is presented below (B. Cruikshank, personal communication, 1986).

Major-element oxides (SiO_2, TiO_2, Al_2O_3, Fe_2O_3 (total), MnO, MgO, CaO, K_2O, and P_2O_5) were determined on glass fusion discs using the method of Norrish & Hutton (1969). Finely ground rock powder (0.709 g) was mixed with the Norrish Formula flux (3.8 g of a mixture of lithium tetraborate, lithium carbonate and lanthanum oxide) and fused at 460°C for 15 minutes in an electric furnace to convert S^{2-} to SO_4^{2-}. The powder was fused into a homogeneous glass for a further 15 minutes at a furnace temperature of 1100°C. After cooling, the glass was melted over an O_2/LPG flame for five minutes at 1200°C, and pressed into a preheated (200°C) graphite platten, forming a glass disc measuring 2 by 40 mm. Matrix corrections, with alpha factors for the rhodium tube, were applied to all major oxides. Calibration of the major oxides was against USGS and BMR rock standards, using SiO_2 and CaO blanks. The USGS standards included: GSP-1(granodiorite), AGV-1(andesite), BCR-1(basalt), W-1(diabase), PCC-1(peridotite), and DTS-1(dunite).

Table 40. Parameters of isotopes and detection limits for RNAA data

	Pd	*Ir*	*Pt*	*Au*	*Se*	*Cs*	*Rb*	*Th*
Stable isotope	^{108}Pd	^{191}Ir	^{198}Pt	^{197}Au	^{74}Se	^{133}Cs	^{85}Rb	^{232}Th
Natural % abundance	26.7	37.3	7.2	100.0	0.9	100.0	72.1	100.0
Cross-section (Barn)	12	624	27	99	52	27	1	7
Daughter isotope	^{109}Pd	^{192}Ir	^{199}Au	^{198}Au	^{75}Se	^{134}Cs	^{86}Rb	^{233}Pa
Half life	13.47 h	74.02 d	3.15 d	2.69 d	120.40 d	2.06 y	18.66 d	27.40 d
Gamma-ray energy peaks measured (keV)	22.1 88.1	468.0	158.3	411.8	121.1 136.0 264.6 279.5	604.7 795.8	1076.6	311.8
Detection limits (ppb)								
Whole-rock powder (0.4 g)	10	0.02	20	0.01	10	5	200	2000
Ni-S button precon. (25 g)	0.2	0.005	0.2	0.01	—	—	—	—

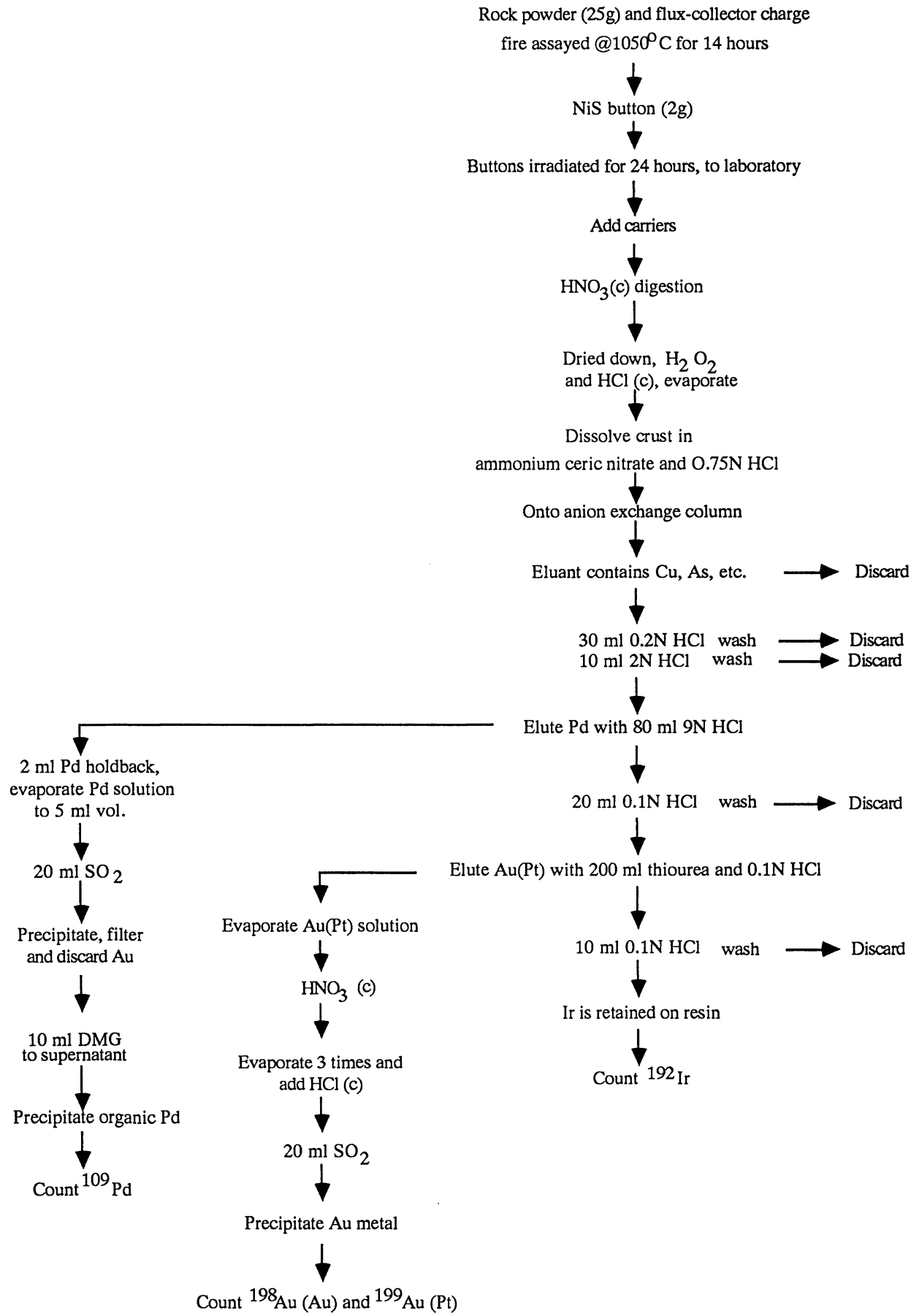

Fig. 119. RNAA (radiochemical neutron-activation analysis) flow chart for the nickel-sulphide-button technique.

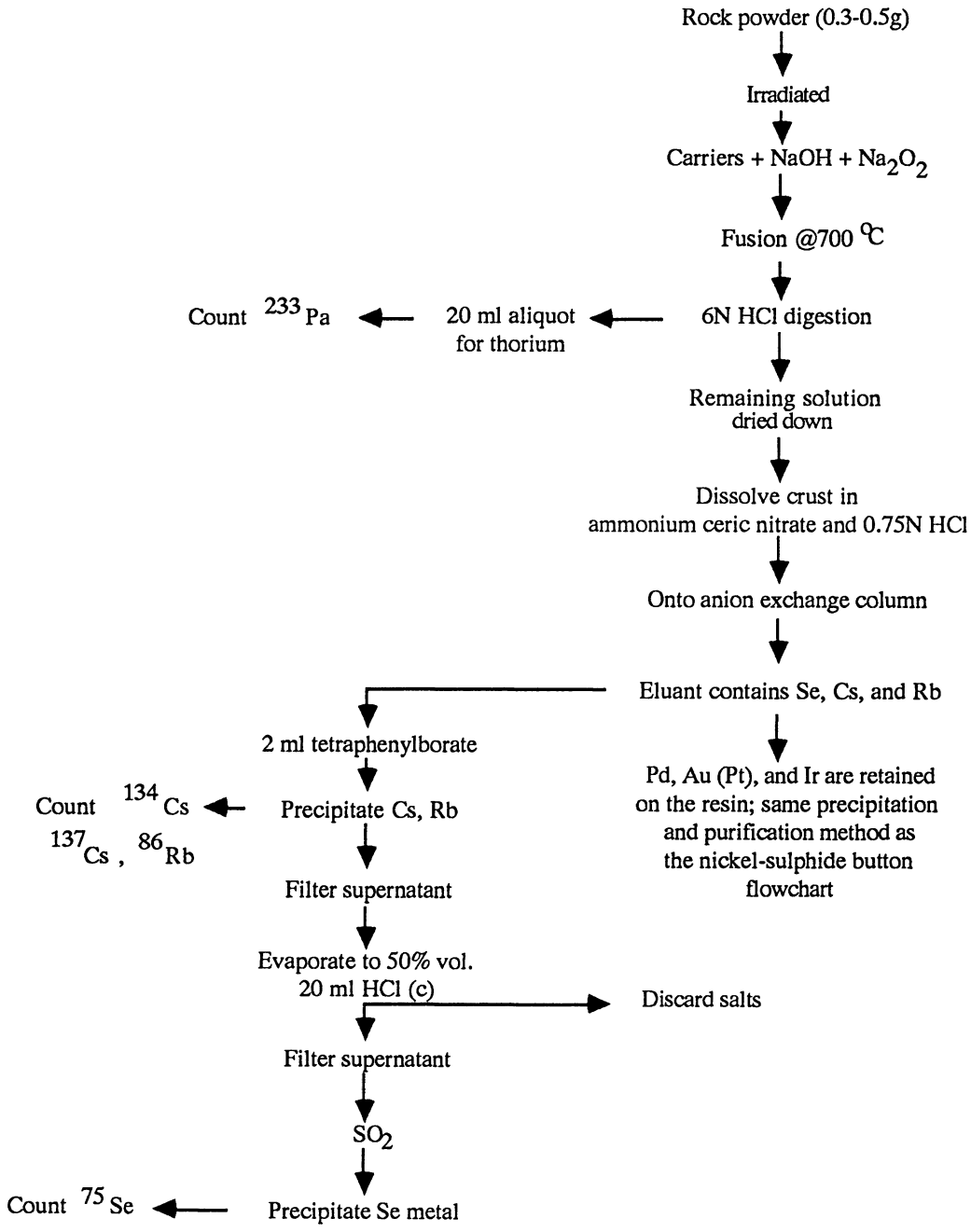

Fig. 120. RNAA (radiochemical neutron-activation analysis) flow chart for the whole-rock-powder technique.

A combined HF(10 mL, 40%)-$HClO_4$(5 mL, 1:1) acid digestion on 0.4 g of rock powder was used for the atomic-absorption analysis of Na_2O. The analyte solution contained controlled amounts of HCl acid and K^+, and calibration was against identical solutions prepared from AGSO rock standards. For the determination of FeO, a 0.5 g sample was digested in H_2SO_4 (10 mL, 1:3) and HF (5 mL, 40%) acid on a hotplate for 10 minutes. The digested solution was mixed with H_2O (300 mL), H_3BO_3 (15 g), and H_3PO_4 (10 mL, 1:1) before being titrated against standard $K_2Cr_2O_7$ solution (1 mL = 2.00 mg Fe^{2+}) using a Metrohm E536 potentiograph with a platinum reference electrode. Moisture water (H_2O^-) was measured by determining the loss in weight of a sample dried for two hours at 110°C. Lattice water (H_2O^+) and the CO_2 content were determined using the gravimetric method described by Hughes & Hannaker (1978). A 0.5 g powder sample was heated to 1100°C in a purified oxygen stream, with the evolved H_2O and CO_2 being trapped and weighed respectively on $MgClO_4.H_2O$ and soda-asbestos.

The trace elements (**As**, Ba, **Bi**, Ce, Cr, **Ga**, La, **Mo**, **Nb**, Nd, **Pb**, Pr, **Rb**, Sc, **Se**, **Sn**, **Sr**, **Th**, **U**, V, **Y** and **Zr**) were determined by XRFS using pressed-powder pellets as the sample medium. A mixture of 12 g of sample powder and approximately 30 drops of 7% aqueous alcohol PVA binding agent was pressed into a 40 x 6 mm pellet using a Specac hydraulic press to 2 ton pressure. Molybdenum, rhodium, and gold target X-ray tubes were used to give optimum excitation for different groups of elements. The elements indicated above in bold were determined using a mass-absorption

correction by the Compton Scatter method, whereas the determination of the other elements involved calculated mass-absorption coefficients. The XRFS counts were converted into element concentrations using a modification of the Norrish & Chappell (1977) method, and calibration was by synthetic standards and was verified against international and AGSO standards. The conversions were programmed through a Hewlett-Packard 86 computer. The trace elements Co, Cr, Cu, and Ni were determined by AAS after the acid digestion of a 1.0 g sample in HF(10 mL, 40%)-$HClO_4$(6 mL, 1:1) over a water bath. The solution was taken to dryness on a hotplate, taken up with HCl acid (10 mL, 1:1) and made up to 50 mL, before direct calibration against standard solutions on the AAS.

Table 41. Detection limits for major oxides (%) and trace elements (ppm) by XRFS and AAS

Element	*Detection limit*
SiO_2	0.006
TiO_2	0.008
Al_2O_3	0.007
Fe_2O_3	0.005
MnO	0.004
MgO	0.006
CaO	0.0014
Na_2O	0.02
K_2O	0.0004
P_2O_5	0.003
Ba	4
Li	1
Rb	1
Sr	2
Pb	1
Th	1
U	0.5
Zr	2
Nb	1
Y	2
La	2
Ce	2
Nd	2
Sc	3
V	2
Co	2
Cr	1
Ni	2
Cu	2
Zn	1
Mo	2
Ga	1
As	0.5
S	12
Cs	3

Estimated detection limits are given in Table 41. Those for elements determined by XRFS were calculated at the 95% confidence level for detection of peak-above-background, using the relation given by Jenkins & Vries (1967):

$$\text{detection limit} = \frac{3c}{(Rp-Rb)}\sqrt{\frac{Rb}{t}}$$

where, Rp = peak count rate (counts/sec)
Rb = background count rate (counts/sec)
t = backround counting time (secs)
c = element concentration

The detection limits given are twice these calculated theoretical values, and are considered to be more realistic. Detection limits for elements for which there are significant inter-element corrections (e.g. Ba, Ce, Sc, and Y) will probably be even higher.

The precision of the XRFS technique is generally good, as the effects of all but very short-term drift in machine conditions are practically eliminated by ratioing each measurement to a monitor standard. The precision (1 standard deviation level) for trace-element analyses is typically ±3% at the 30–100 ppm level. The corresponding precision for AAS analyses is between ±4% and ±6%.

Accuracy was assessed by analysing international rock standards. Comparisons of XRFS and AAS results for two standard rocks (GSP-1 and BCR-1) are given in Table 42.

Table 42. Accuracy of XRFS and AAS data: comparison of analyses of standard rocks with the recommended values of Abbey (1983)

	GSP-1 (see text)		*BCR-1 (see text)*	
	AGSO	*Recomm.*	*AGSO*	*Recomm.*
SiO_2	67.97 (0.29)*	67.32	54.42 (0.16)*	54.53
TiO_2	0.67 (0.004)*	0.66	2.26 (0.015)*	2.26
Al_2O_3	15.16 (0.08)*	15.28	13.51 (0.06)*	13.72
Fe_2O_3 (t)	4.26 (0.016)*	4.28	13.39 (0.03)*	13.44
FeO	2.25	2.32	8.89	8.96
MnO	0.04	0.04	0.17	0.18
MgO	0.99 (0.015)*	0.97	3.53 (0.012)*	3.48
CaO	1.97 (0.006)*	2.03	6.97 (0.06)*	6.97
Na_2O	2.74	2.81	3.27 (0.05)*	3.30
K_2O	5.56 (0.012)*	5.51	1.71 (0.010)*	1.70
P_2O_5	0.28	0.28	0.36	0.36
Ba	1300	1300	702	680
Li	25	30	11	14
Rb	253	250	46	47
Sr	237	240	329	330
Pb	54	54	14	14
Th	104	105	6	6
U	2.0	2.1	1.5	1.7
Zr	507	500	187	185
Nb	25	?23	13	?19
Y	28	29	37	40
La	165	195	29	27
Ce	391	360	55	53
Nd	187	?190	32	?26
Pr	46	?50	4	?7
Sc	8	7	31	33
V	49	54	416	420
Cr	11	12	6	15
Ni	7	9	7	10
Cu	30	33	17	16
Zn	91	105	117	125
Sn	8	?5	2	3
Ga	24	23	21	22
As	<0.5	<0.5	1.0	?0.8
S	400	?300	400	?400
F			500	500

* Standard deviation. See text, pp. 188 and 190–191, for elements analysed respectively by XRFS and AAS.

1.3. Leco titration for sulphur analysis

Sulphur determinations for the Munni Munni and Mount Sholl complexes were carried out by Leco induction furnace-titration analysis at the School of Earth Sciences, University of Melbourne. A detection limit of about 20 ppm was obtained.

A 1.0 to 1.1 g powder sample was dried for 4 hours at 105°C and placed in a 2 cm deep ceramic crucible with approximately 0.5 g of metallic tin and iron granules, which act as heat accelerators. Arrowroot starch (2 g) was dissolved in 50 mL of distilled water and then this was mixed with 150 mL of boiled distilled water and 6 g of KI. Dilute HCl acid was poured into a titration vessel. As shown by the following equation, free I_2 is released (starch solution turns blue) when a standard KIO_3 solution is added:

$$KIO_3 + 5KI + 6HCl = 6KCI + 3I_2$$

The sample in the crucible was combusted in a stream of oxygen to convert the rock sulphur to SO_2. The SO_2 from the ignited sample reacts with the free iodine to form the compound HI in the titration vessel, according to the reaction,

$$SO_2 + I_2 + 2H_2O = H_2SO_4 + 2HI$$

With the removal of I_2, the solution turned colourless. The blue colour of the starch was restored with the addition of further KIO_3 to form more free iodine. The amount of KIO_3 titrant used is therefore a function of the sulphur content of the sample. Calibration of the induction-titration procedure was determined through the regular combustion of iron rings with known sulphur contents.

1.4. Sulphur-isotope analysis

Sulphide samples from the Munni Munni, Mount Sholl, and Radio Hill layered intrusions, were submitted to the AGSO laboratories for sulphur-isotope determinations. Because of their small size (< 2 mm) and intergrowth textures, the pyrrhotite, pentlandite, and chalcopyrite grains were extracted as a composite sample using a diamond-tipped dental drill. 8.2 mg of sulphide sample and 50 mg of Cu_2O were weighed, mixed in a mortar and pestle, placed in vicor tubing (6 mm (I.D.) by 15 mm), and sealed under vacuum. These tubes were fired in a muffler furnace at 1020°C for one hour. The tubes were then placed in a break seal, and H_2O and CO_2 were cryogenically separated from the SO_2 on a vacuum line. The resultant SO_2 gas was measured against AGSO working sulphur standards, A and B, on a VG SIRA-12 mass spectrometer. The results are expressed in the usual delta notation relative to CDT (Canyon Diablo Troilite) in per mil:

$$\partial^{34}S = (R_{sample} - R_{std}) / R_{std} \times 1000$$

where R is the ratio of $^{34}S/^{32}S$. Reproducibility of results is < 0.1 per mil.

1.5. Electron-microprobe and scanning-electron-microscope analysis

Most of the cumulus and intercumulus mineral compositions from the Munni Munni Complex were determined at the Research School of Earth Sciences, Australian National University, by wavelength-dispersive microprobe analysis using a Camabex (Cameca) microbeam electron-probe microanalyser. A minor number of analyses were also carried out on a Cameca at the School of Earth Sciences, University of Melbourne. At the Research School, an accelerating voltage of 15 kV and a beam current of 40 nA (beam orientation and current determined on barium silicate) were used for all major-element programs. Counting time varied from two to three minutes for the major-element programs. Calibration and the monitoring of analytical quality was controlled through the use of natural standards such as olivine, wollastonite, augite, ilmenite, troilite, anorthite, and anorthoclase.

The bulk composition of the inverted-pigeonite grains was estimated by a process of integrated point-count analysis (see Appendix 2 for all point-count analyses and bulk-composition data). The inverted-pigeonite grains are commonly characterised by coarse (up to 0.2 mm) exsolution lamellae that often are unevenly distributed in the orthopyroxene host grain. This heterogeneity in grain composition indicated that a process involving multiple-focused-beam analysis of the host and lamellar components across the grain would provide a more representative estimation of the bulk composition than an analytical procedure involving defocusing the beam for a single analysis. Up to 61 point-analyses of the lamellar and host components were taken for each grain (e.g. sample 84770055). The analysed grain was photographed and enlarged, and an approximation of the relative volumes of the host and coarse lamellae were obtained by carefully cutting out and weighing the different parts of the grain. The bulk composition for each grain was determined by multiplying the averaged lamellar and host analyses by the relative volumes of the two components. Of course, this method provides only an approximation of the bulk composition since it assumes that the relative proportions of the two components as seen in two dimensions is the same as their actual volumetric proportions in three dimensions. Also, there is another generation of extremely small discontinuous lamellae trending at a high angle to the coarse lamellae, that cannot be taken into account when determining the relative volumes.

To determine the bulk composition of clinopyroxene grains in the gabbroic zone, which have narower lamellae (< 0.01 mm) than the inverted-pigeonite lamellae but wider than those in clinopyroxene in the ultramafic zone, energy-dispersive microprobe analysis incorporating a broad-beam raster scan was used. An accelerating voltage of 15 kV, a beam current of 40 nA, and a broad-beam scan covering an area of about 125 by 125 μm were employed during the 80-second counting times. The beam area was large enough to allow for the intergrated analysis of both the host and a representative number of exsolution lamellae. Multiple analyses within and between clinopyroxene grains for each rock were averaged and the results are presented in Appendix 2.

The platinum-group mineralogy was undertaken on a Jeol JSM 35 scanning-electron microscope (SEM) at the School of Earth Sciences, University of Melbourne, and at AGSO. Marked-up, polished thin-sections were particle-coated with carbon or gold prior to examination. Identification and semi-quantitative analysis of the platinum-group minerals were obtained using back-scatter electron images (Kevex energy-dispersive system) and a Robinson Detector facility.

APPENDIX 2. MINERAL CHEMISTRY OF THE MUNNI MUNNI AND ANDOVER INTRUSIONS

Minerals analysed from the Munni Munni Complex

Regional traverse (zone(s) shown in parenthesis):
- Olivine (UZ)
- Clinopyroxene (UZ and GZ)
  - Averaged bulk compositions (GZ)
- Orthopyroxene (UZ)
- Inverted pigeonite (GZ)
  - Averaged host and lamellae compositions
  - Averaged bulk compositions
- Plagioclase (UZ and GZ)
- Alkali feldspar (UZ)
- Biotite (UZ and GZ)
- Spinels (UZ and Eastern Munni Munni Dyke)
- Magnetite and ilmenite (GZ)
- Sulphides (UZ)

Detailed traverse across cycles 1–5 in subzones C and D (UZ):
- Olivine
- Clinopyroxene
- Orthopyroxene

Detailed traverse across ultramafic/gabbroic zone contact:
- Clinopyroxene (UZ and GZ)
- Clinopyroxene cores and rims (UZ and GZ)
- Plagioclase (UZ and GZ)

Minerals analysed from the Andover Complex

Regional traverse:
Clinopyroxene and orthopyroxene (UZ & GZ)

Explanation of attribute data and atomic ratios used in the mineral tables

Sample no: Eight-digits, comprising year of collection, AGSO project code, and four-digit sample number. Most samples are arranged in order of increasing stratigraphic height. Sample locations are indicated on the appended 1 : 20 000 geological maps for the Munni Munni, Mount Sholl, Maitland, and Radio Hill intrusions. Sample co-ordinates (AGM grid and longitude/latitude references) for the Andover Complex are given in Table 43, overleaf.

Analysis no: RSES (ANU) analyses have a five-digit number, and the Melbourne University analyses have three characters comprising a prefix (MU) and a number which indicates the grain analysed (e.g. MU2 = grain no. 2 analysed at Melbourne University). Most of the regional data was obtained at Melbourne University and all of the detailed traverse data was obtained from RSES.

Mineral: As indicated. The RSES analyses have a number after the mineral name, indicating the grain analysed (e.g. OLIVINE 2 = Olivine grain no. 2 analysed at RSES).

Description: Cumulus or intercumulus; core or rim; host or lamellae.

Lithology: As indicated.

Zone: Ultramafic or gabbroic, or as indicated if outside the complex.

Subzone: A′, A, B, C, D, E, F, G, H, I of the ultramafic zone and A, B of the gabbroic zone for the Munni Munni Complex, and C, D, F, G of the ultramafic zone for the Andover Complex.

Strat. ht (m): Estimated stratigraphic height in metres above the base of the intrusions.

Atomic ratios used:

Olivine
- mg number = mg = Mg/(Mg + Fe), where Fe = Total Fe

Pyroxene
- mg number = mg = Mg/(Mg + Fe), where Fe = Total Fe
- Mg′ = 100 x Mg/(Mg + Fe + Ca), where Fe = Total Fe
- Fe′ = 100 x Fe/(Mg + Fe + Ca), where Fe = Total Fe
- Ca′ = 100 x Ca/(Mg + Fe + Ca), where Fe = Total Fe

Plagioclase
- An = 100 x Ca/(Ca + Na + K)
- Ab = 100 x Na/(Ca + Na + K)
- Or = 100 x K/(Ca + Na + K)

Alkali feldspar
- Or = 100 x K/(Ca + Na + K + Ba)

Spinel
- mg number = mg = $Mg/(Mg + Fe^{2+})$
- Cr′ = $Cr/(Cr + Al + Fe^{3+})$
- Al′ = $Al/(Cr + Al + Fe^{3+})$
- $Fe^{3+\prime} = Fe^{3+}/(Cr + Al + Fe^{3+})$

Magnetite-ilmenite
- Ti′ = $Ti/(Ti + Fe^{2+} + Fe^{3+})$

Biotite
- mg number = mg = Mg/(Mg + Fe), where Fe = Total Fe
- Ti′ = Ti/(Ti + Fe), where Fe = Total Fe

Table 43. Locations of samples from the Andover Complex

Sample no.	*Gridref.*	*Lat.(°S)*	*Long.(°E)*	*Sample no.*	*Gridref.*	*Lat.(°S)*	*Long.(°E)*
86330033	175983	20.814716	117.168254	87330152	143958	20.837983	117.137648
86330042	174982	20.815783	117.166852	87330153	144957	20.838289	117.138648
86330043	174984	20.814410	117.167043	87330155	144960	20.836139	117.138867
86330044	174984	20.814220	117.166783	87330156	145961	20.835100	117.138952
86330049	167995	20.803989	117.160574	87330158	145964	20.831955	117.139555
86330053	166998	20.801486	117.159898	87330160	146968	20.829117	117.140542
86330061	149982	20.815569	117.143634	87330164	139954	20.840996	117.133181
86330100	151982	20.816300	117.144903	87330165	142958	20.837731	117.136744
86330102	150980	20.817900	117.143972	87330166	142957	20.838237	117.136341
86330106	150977	20.820882	117.143975	88330173	164997	20.802808	117.157219
86330107	150976	20.821081	117.144379	88330175	169001	20.799134	117.162807
86330109	160983	20.815425	117.153993	88330179	205003	20.797047	117.197330
86330119	209002	20.797938	117.200733	88330180	205002	20.797590	117.196860
87330125	102948	20.846422	117.098332	88330181	204002	20.798313	117.196217
87330126	105951	20.844144	117.101214	88330182	203001	20.798622	117.195228
87330127	108953	20.842480	117.103828	88330188	150971	20.826032	117.144460
87330128	113954	20.841745	117.108796	88330189	151970	20.826872	117.144778
87330130	119957	20.838931	117.114321	88330190	151969	20.827703	117.145298
87330131	117956	20.839546	117.112716	88330191	151969	20.828191	117.145385
87330133	191991	20.807968	117.183507	88330193	150966	20.830315	117.144436
87330134	193992	20.806755	117.185581	88330194	150965	20.831020	117.144379
87330135	195994	20.805443	117.187318	88330195	151964	20.832411	117.144678
87330137	196996	20.802876	117.188680	88330197	152956	20.839865	114.145742
87330138	197998	20.801394	117.188909	88330198	151957	20.838601	117.144751
87330139	202000	20.800005	117.194480	88330199a	152955	20.840461	117.146118
87330140	202001	20.799119	117.194441	88330199b	151958	20.838013	117.145395
87330141	201999	20.800576	117.193261	88330200	151958	20.837670	117.145202
87330142	200998	20.801182	117.191983	88330201	152959	20.837163	117.145999
87330143	198998	20.801066	117.190532	88330202	152959	20.836576	117.145980
87330144	197998	20.801095	117.189658	88330203	152960	20.835871	117.145902
87330145	197998	20.801095	117.189658	88330204	152961	20.835275	117.145757
87330146	189992	20.807076	117.181622	88330205	151962	20.834489	117.145122
87330147	187990	20.808533	117.179692	88330206	150962	20.833713	117.144429
87330148	185988	20.810143	117.177695	88330207	150963	20.833044	117.144419
87330149	183987	20.811835	117.175727	88330211	169992	20.807041	117.162460
87330150	179985	20.813275	117.171962	88330213	164995	20.803892	117.157143
87330151	176984	20.813856	117.169598				

Mineral analyses from the Munni Munni Complex

Regional traverse: olivine (UZ)

Sample no.	85770179	85770179	85770179	85770179	85770179	85770179	85770179	85770179	85770179	85770179	84770002	84770002
Analysis no.	MU1	57968	57967	57969	57970	57971	57972	57973	57974	MU2	MU4	MU3
Mineral	OLIVINE	OLIVINE 2	OLIVINE 1	OLIVINE 3	OLIVINE 4	OLIVINE 5	OLIVINE 6	OLIVINE 7	OLIVINE 8	OLIVINE	OLIVINE	OLIVINE
Description	CUMULUS, CORE	CUMULUS, CORE	CUMULUS, CORE	CUMULUS, CORE	CUMULUS, CORE	CUMULUS, CORE	CUMULUS, CORE	CUMULUS, CORE	CUMULUS, CORE	CUMULUS, CORE	CUMULUS, CORE	CUMULUS, CORE
Lithology	OLIVINE GABBRONOR. CHILL	OLIVINE GABBRONOR. CHILL	OLIVINE GABBRONOR. CHILL	OLIVINE GABBRONOR. CHILL	OLIVINE GABBRONOR. CHILL	OLIVINE GABBRONOR. CHILL	OLIVINE GABBRONOR. CHILL	OLIVINE GABBRONOR. CHILL	OLIVINE GABBRONOR. CHILL	OLIVINE GABBRONOR. CHILL	PLAGIOCLA. WEBSTERITE	PLAGIOCLA. WEBSTERITE
Zone	ULTRAMAFIC	ULTRAMAFIC	ULTRAMAFIC	ULTRAMAFIC	ULTRAMAFIC	ULTRAMAFIC	ULTRAMAFIC	ULTRAMAFIC	ULTRAMAFIC	ULTRAMAFIC	ULTRAMAFIC	ULTRAMAFIC
Subzone	A'	A'	A'	A'	A'	A'	A'	A'	A'	A'	A'	A'
Strat. ht (m)	1	1	1	1	1	1	1	1	1	1	128	128
SiO2	38.58	37.87	38.06	37.99	37.84	37.71	37.50	37.46	37.54	38.41	38.01	38.79
FeO	23.70	22.95	23.34	23.10	23.36	24.95	25.61	25.85	24.96	24.45	22.42	20.44
MnO	.37	.36	.39	.35	.37	.38	.40	.40	.39	.34	.18	.26
NiO	.37	.35	.37	.36	.31	.34	.30	.31	.34	.43	.41	.55
MgO	37.51	37.96	38.08	38.43	38.27	36.52	36.29	35.98	36.55	38.03	38.84	41.06
CaO	.03	<.02	<.02	<.02	<.02	<.02	<.02	<.02	<.02	<.02	.06	.06
Total	100.56	99.49	100.24	100.23	100.15	99.90	100.10	100.00	99.78	101.66	99.92	101.16
Atomic proportions												
Oxygens	4.0	4.0	4.0	4.0	4.0	4.0	4.0	4.0	4.0	4.0	4.0	4.0
Si	1.003	.996	.995	.992	.990	.997	.993	.994	.994	.993	.991	.991
Fe	.516	.505	.510	.505	.511	.552	.567	.574	.553	.529	.489	.437
Mn	.008	.008	.009	.008	.008	.009	.009	.009	.009	.007	.004	.006
Ni	.008	.007	.008	.008	.007	.007	.006	.007	.007	.009	.009	.011
Mg	1.454	1.488	1.484	1.496	1.493	1.439	1.432	1.423	1.443	1.465	1.509	1.563
Ca	.001	-	-	-	-	-	-	-	-	-	.002	.002
Total	2.990	3.004	3.005	3.008	3.010	3.003	3.007	3.006	3.006	3.003	3.004	3.009
mg number	74	75	74	75	74	72	72	71	72	73	76	78

Sample no.	84770002	84770002	84770003	84770003	84770003	84770003	84770004	84770005	84770006	84770006	84770007	84770010
Analysis no.	MU2	MU1	MU4	MU1	MU3	MU2	MU1	MU1	MU1	MU2	MU1	MU3
Mineral	OLIVINE	OLIVINE	OLIVINE	OLIVINE	OLIVINE	OLIVINE	OLIVINE	OLIVINE	OLIVINE	OLIVINE	OLIVINE	OLIVINE
Description	CUMULUS, CORE	CUMULUS, CORE	CUMULUS, RIM OF MU1	CUMULUS, CORE	CUMULUS, CORE	CUMULUS, RIM OF MU1	CUMULUS, CORE	CUMULUS, CORE	CUMULUS, CORE	CUMULUS, CORE	CUMULUS, CORE	CUMULUS, CORE
Lithology	PLAGIOCLA. WEBSTERITE	PLAGIOCLA. WEBSTERITE	OLIVINE WEBSTERITE	OLIVINE WEBSTERITE	OLIVINE WEBSTERITE	OLIVINE WEBSTERITE	OLIVINE WEBSTERITE	OLIVINE WEBSTERITE	OLIVINE WEBSTERITE	OLIVINE WEBSTERITE	WEBSTERITE	OLIVINE WEBSTERITE
Zone	ULTRAMAFIC	ULTRAMAFIC	ULTRAMAFIC	ULTRAMAFIC	ULTRAMAFIC	ULTRAMAFIC	ULTRAMAFIC	ULTRAMAFIC	ULTRAMAFIC	ULTRAMAFIC	ULTRAMAFIC	ULTRAMAFIC
Subzone	A'	A'	A'	A'	A'	A'	A	A	A	A	A	B
Strat. ht (m)	128	128	174	174	174	174	218	247	268	268	285	404
SiO2	38.07	38.60	38.26	38.16	38.56	38.56	37.96	37.99	39.21	38.80	38.87	38.72
FeO	22.23	21.92	21.11	21.74	20.87	21.03	20.48	20.08	18.88	19.37	18.43	17.77
MnO	.14	.31	.16	.22	.29	.26	.30	.32	.22	.34	.25	.25
NiO	.36	.38	.37	.45	.46	.45	.22	.21	.26	.11	.45	.55
MgO	37.79	39.65	40.04	39.79	40.26	39.64	40.45	40.44	42.27	42.02	43.20	43.35
CaO	.04	.06	.05	<.02	.05	.08	.05	.06	.08	.03	.04	.08
Total	98.63	100.92	99.99	100.36	100.49	100.02	99.46	99.10	100.92	100.67	101.24	100.72
Atomic proportions												
Oxygens	4.0	4.0	4.0	4.0	4.0	4.0	4.0	4.0	4.0	4.0	4.0	4.0
Si	1.003	.993	.989	.987	.991	.997	.985	.989	.992	.989	.982	.979
Fe	.490	.471	.456	.470	.448	.455	.445	.437	.400	.413	.389	.376
Mn	.003	.007	.004	.005	.006	.006	.007	.007	.005	.007	.005	.005
Ni	.008	.008	.008	.009	.010	.009	.005	.004	.005	.002	.009	.011
Mg	1.484	1.520	1.542	1.535	1.542	1.528	1.565	1.570	1.594	1.597	1.626	1.634
Ca	.001	.002	.001	-	.001	.002	.001	.002	.002	.001	.001	.002
Total	2.989	3.000	3.000	3.007	2.998	2.997	3.007	3.010	2.998	3.010	3.012	3.008
mg number	75	76	77	77	77	77	78	78	80	79	81	81

Sample no.	84770010	84770010	84770011	84770016	84770017	84770017	84770018	84770018	84770020	84770020	84770021	84770021
Analysis no.	MU2	MU1	MU1	MU1	MU2	MU1	MU2	MU1	MU1	MU2	MU1	MU3
Mineral	OLIVINE	OLIVINE	OLIVINE	OLIVINE	OLIVINE	OLIVINE	OLIVINE	OLIVINE	OLIVINE	OLIVINE	OLIVINE	OLIVINE
Description	CUMULUS, CORE	CUMULUS, CORE	CUMULUS, CORE	CUMULUS, CORE	CUMULUS, CORE	CUMULUS, CORE	CUMULUS, CORE	CUMULUS, CORE	CUMULUS, CORE	CUMULUS, CORE	CUMULUS, CORE	CUMULUS, CORE
Lithology	OLIVINE WEBSTERITE	OLIVINE WEBSTERITE	OLIVINE WEBSTERITE	OLIVINE WEBSTERITE	OLIVINE WEBSTERITE	OLIVINE WEBSTERITE	OLIVINE WEBSTERITE	OLIVINE WEBSTERITE	WEBSTERITE	WEBSTERITE	OLIVINE WEBSTERITE	OLIVINE WEBSTERITE
Zone	ULTRAMAFIC	ULTRAMAFIC	ULTRAMAFIC	ULTRAMAFIC	ULTRAMAFIC	ULTRAMAFIC	ULTRAMAFIC	ULTRAMAFIC	ULTRAMAFIC	ULTRAMAFIC	ULTRAMAFIC	ULTRAMAFIC
Subzone	B	B	C	C	C	C	C	C	D	D	D	D
Strat. ht (m)	404	404	440	620	655	655	690	690	867	867	910	910
SiO2	38.83	38.89	39.04	38.42	39.25	38.68	38.46	38.55	38.56	38.82	38.66	38.82
FeO	17.62	18.21	18.47	19.66	17.61	17.98	17.44	17.53	17.55	17.39	18.09	18.30
MnO	.30	.26	.29	.24	.22	.30	.25	.20	.24	.22	.28	.23
NiO	.46	.39	.42	.54	.41	.52	.62	.71	.51	.66	.51	.46
MgO	43.31	43.36	42.91	40.65	41.84	42.18	42.26	42.39	43.43	43.10	42.92	43.44
CaO	.04	.07	.04	.05	.10	.06	.04	.05	.04	.05	.04	.04
Total	100.56	101.18	101.17	99.56	99.43	99.72	99.07	99.43	100.33	100.24	100.50	101.29
Atomic proportions												
Oxygens	4.0	4.0	4.0	4.0	4.0	4.0	4.0	4.0	4.0	4.0	4.0	4.0
Si	.985	.982	.986	.994	1.001	.991	.990	.988	.979	.987	.982	.979
Fe	.374	.385	.390	.425	.376	.385	.376	.376	.373	.370	.384	.386
Mn	.006	.006	.006	.005	.005	.007	.005	.004	.005	.005	.006	.005
Ni	.009	.008	.009	.011	.008	.011	.013	.015	.010	.013	.010	.009
Mg	1.638	1.632	1.616	1.567	1.591	1.611	1.622	1.619	1.644	1.634	1.625	1.632
Ca	.001	.002	.001	.001	.003	.002	.001	.001	.001	.001	.001	.001
Total	3.014	3.014	3.008	3.004	2.983	3.007	3.008	3.002	3.012	3.010	3.008	3.012
mg number	81	81	81	79	81	81	81	81	82	82	81	81

Sample no.	84770021	84770022	84770022	84770024	84770024	84770028	84770029	84770030	84770031	84770032	84770032	84770032
Analysis no.	MU2	MU1	MU2	MU2	MU1	MU1	MU1	MU1	MU1	MU1	MU2	MU3
Mineral	OLIVINE	OLIVINE	OLIVINE	OLIVINE	OLIVINE	OLIVINE	OLIVINE	OLIVINE	OLIVINE	OLIVINE	OLIVINE	OLIVINE
Description	CUMULUS, CORE	CUMULUS, CORE	CUMULUS, CORE	CUMULUS, CORE	CUMULUS, CORE	CUMULUS, CORE	CUMULUS, CORE	CUMULUS, CORE	CUMULUS, CORE	CUMULUS, CORE	CUMULUS, CORE	CUMULUS, CORE
Lithology	OLIVINE WEBSTERITE	OLIVINE WEBSTERITE	OLIVINE WEBSTERITE	OLIVINE CLINOPYRO.	OLIVINE CLINOPYRO.	CLINOPYRO.	CLINOPYRO.	WEBSTERITE	OLIVINE WEBSTERITE	OLIVINE WEBSTERITE	OLIVINE WEBSTERITE	OLIVINE WEBSTERITE
Zone	ULTRAMAFIC	ULTRAMAFIC	ULTRAMAFIC	ULTRAMAFIC	ULTRAMAFIC	ULTRAMAFIC	ULTRAMAFIC	ULTRAMAFIC	ULTRAMAFIC	ULTRAMAFIC	ULTRAMAFIC	ULTRAMAFIC
Subzone	D	D	D	D	D	E	E	E	F	F	F	F
Strat. ht (m)	910	950	950	1020	1020	1180	1234	1278	1298	1417	1417	1417
SiO2	38.99	38.31	38.07	38.75	39.10	39.15	38.51	38.55	38.78	39.74	39.03	39.59
FeO	17.45	21.38	21.53	19.94	20.42	20.00	19.78	19.01	18.03	18.25	18.48	18.01
MnO	.31	.30	.29	.30	.25	.32	.21	.30	.11	.17	.28	.25
NiO	.47	.43	.54	.50	.41	.31	.42	.42	.27	.49	.31	.43
MgO	43.78	40.32	40.57	40.68	41.04	40.93	41.28	41.51	43.16	42.46	43.05	43.06
CaO	.06	.10	.07	.05	.04	.09	.03	.03	.05	<.02	<.02	.07
Total	101.06	100.84	101.07	100.22	101.26	100.80	100.23	99.82	100.40	101.11	101.15	101.41
Atomic proportions												
Oxygens	4.0	4.0	4.0	4.0	4.0	4.0	4.0	4.0	4.0	4.0	4.0	4.0
Si	.982	.984	.979	.996	.993	.998	.989	.990	.984	1.002	.986	.993
Fe	.368	.459	.463	.428	.434	.426	.425	.408	.383	.385	.390	.378
Mn	.007	.007	.006	.007	.005	.007	.005	.007	.002	.004	.006	.005
Ni	.010	.009	.011	.010	.008	.006	.009	.009	.006	.010	.006	.009
Mg	1.644	1.544	1.555	1.558	1.554	1.555	1.581	1.589	1.632	1.596	1.621	1.610
Ca	.002	.003	.002	.001	.001	.002	.001	.001	.001	-	-	.002
Total	3.012	3.005	3.016	3.000	2.996	2.995	3.009	3.003	3.008	2.997	3.009	2.998
mg number	82	77	77	78	78	78	79	80	81	81	81	81

Sample no.	84770035	84770035	84770036	84770037	84770040	84770041	84770041	84770041
Analysis no.	MU1	MU2	MU1	MU1	MU1	MU3	MU2	MU1
Mineral	OLIVINE	OLIVINE	OLIVINE	OLIVINE	OLIVINE	OLIVINE	OLIVINE	OLIVINE
Description	CUMULUS, CORE	CUMULUS, CORE	CUMULUS, CORE	CUMULUS, CORE	CUMULUS, CORE	CUMULUS, CORE	CUMULUS, CORE	CUMULUS, CORE
Lithology	OLIVINE WEBSTERITE	OLIVINE WEBSTERITE	OLIVINE WEBSTERITE	WEBSTERITE	WEBSTERITE	WEBSTERITE	WEBSTERITE	WEBSTERITE
Zone	ULTRAMAFIC	ULTRAMAFIC	ULTRAMAFIC	ULTRAMAFIC	ULTRAMAFIC	ULTRAMAFIC	ULTRAMAFIC	ULTRAMAFIC
Subzone	G	G	G	G	H	H	H	H
Strat. ht (m)	1474	1474	1500	1538	1666	1695	1695	1695
SiO2	38.66	38.78	38.08	38.66	39.29	39.08	38.49	38.40
FeO	18.61	18.20	17.71	19.15	19.45	20.22	20.03	20.44
MnO	.22	.24	.23	.28	.22	.21	.26	.31
NiO	.29	.42	.30	.46	.61	.36	.50	.38
MgO	42.22	41.95	41.93	41.43	40.69	41.21	40.81	41.04
CaO	.06	.06	.06	.04	.03	.04	.04	.05
Total	100.06	99.65	98.31	100.02	100.29	101.12	100.13	100.62
Atomic proportions								
Oxygens	4.0	4.0	4.0	4.0	4.0	4.0	4.0	4.0
Si	.988	.992	.988	.991	1.005	.996	.990	.985
Fe	.398	.389	.384	.411	.416	.431	.431	.438
Mn	.005	.005	.005	.006	.005	.005	.006	.007
Ni	.006	.009	.006	.009	.013	.007	.010	.008
Mg	1.609	1.599	1.621	1.583	1.551	1.565	1.564	1.569
Ca	.002	.002	.002	.001	.001	.001	.001	.001
Total	3.007	2.996	3.007	3.002	2.991	3.004	3.002	3.008
mg number	80	80	81	79	79	78	78	78

Regional traverse: clinopyroxene (UZ and GZ)

Sample no.	85770179	84770102	84770102	84770002	84770002	84770002	84770002	84770003	84770003	84770003	84770003	84770004
Analysis no.	MU1	MU2	MU1	MU1	MU2	MU4	MU3	MU4	MU3	MU2	MU1	MU2
Mineral	CLINOPYRO.	CLINOPYRO.	CLINOPYRO.	CLINOPYRO.	CLINOPYRO.	CLINOPYRO.	CLINOPYRO.	CLINOPYRO.	CLINOPYRO.	CLINOPYRO.	CLINOPYRO.	CLINOPYRO.
Description	CUMULUS, CORE	CUMULUS, CORE	CUMULUS, CORE	CUMULUS, CORE	CUMULUS, CORE	CUMULUS, RIM OF MU3	CUMULUS, CORE	CUMULUS, RIM OF MU3	CUMULUS, CORE	CUMULUS, RIM OF MU1	CUMULUS, CORE	CUMULUS, CORE
Lithology	OLIVINE GABBRONOR. CHILL	GABBRONOR.	GABBRONOR.	PLAGIOCLA. WEBSTERITE	PLAGIOCLA. WEBSTERITE	PLAGIOCLA. WEBSTERITE	PLAGIOCLA. WEBSTERITE	OLIVINE WEBSTERITE	OLIVINE WEBSTERITE	OLIVINE WEBSTERITE	OLIVINE WEBSTERITE	OLIVINE WEBSTERITE
Zone	ULTRAMAFIC	ULTRAMAFIC	ULTRAMAFIC	ULTRAMFIC	ULTRAMAFIC	ULTRAMAFIC	ULTRAMAFIC	ULTRAMAFIC	ULTRAMAFIC	ULTRAMAFIC	ULTRAMAFIC	ULTRAMAFIC
Subzone	A'	A'	A'	A'	A'	A'	A'	A'	A'	A'	A'	A
Strat. ht (m)	1	2	2	128	128	128	128	174	174	174	174	218
SiO2	52.43	51.64	52.62	53.74	53.48	53.53	53.09	52.81	53.19	52.83	52.95	53.09
TiO2	.77	.38	.43	.09	.39	.33	.23	.44	.34	.26	.19	.15
Al2O3	2.01	1.70	1.39	1.22	1.52	1.60	1.71	1.66	1.50	1.50	1.05	1.21
Cr2O3	.13	.11	.13	.30	.36	.40	.29	.47	.37	.43	.28	.17
FeO	10.29	10.34	9.80	6.59	6.81	6.12	6.10	6.72	5.97	5.51	5.04	6.80
MnO	.28	.22	.18	.15	.21	<.10	.11	.12	.13	.12	.12	.24
NiO	.03	.12	.09	.18	.05	.12	.12	.11	.21	.03	.16	.17
MgO	15.07	13.92	14.02	18.23	17.70	16.58	16.91	16.92	16.85	17.24	16.29	18.94
CaO	18.88	20.96	22.22	17.85	18.42	20.22	19.77	20.31	20.28	20.39	21.97	17.80
Na2O	.57	.50	.47	.32	.59	.55	.64	.50	.67	.67	.45	.53
Total	100.46	99.89	101.35	98.67	99.53	99.45	98.97	100.06	99.51	98.98	98.50	99.10
Atomic proportions												
Oxygens	6.0	6.0	6.0	6.0	6.0	6.0	6.0	6.0	6.0	6.0	6.0	6.0
Si	1.944	1.941	1.948	1.984	1.965	1.971	1.964	1.943	1.961	1.955	1.972	1.959
Ti	.021	.011	.012	.002	.011	.009	.006	.012	.009	.007	.005	.004
Al	.088	.075	.061	.053	.066	.069	.075	.072	.065	.065	.046	.053
Cr	.004	.003	.004	.009	.010	.012	.008	.014	.011	.013	.008	.005
Fe	.319	.325	.303	.203	.209	.188	.189	.207	.184	.171	.157	.210
Mn	.009	.007	.006	.005	.007	-	.003	.004	.004	.004	.004	.008
Ni	.001	.004	.003	.005	.001	.004	.004	.003	.006	.001	.005	.005
Mg	.833	.780	.774	1.003	.970	.910	.932	.928	.926	.951	.904	1.042
Ca	.750	.844	.881	.706	.725	.798	.784	.801	.801	.808	.877	.704
Na	.041	.036	.034	.023	.042	.039	.046	.036	.048	.048	.033	.038
Total	4.009	4.027	4.025	3.994	4.007	3.999	4.011	4.019	4.016	4.023	4.011	4.027
mg number	72	71	72	83	82	83	83	82	83	85	85	83
Mg'	44	40	40	52	51	48	49	48	48	49	47	53
Fe'	17	17	15	11	11	10	10	11	10	9	8	11
Ca'	39	43	45	37	38	42	41	41	42	42	45	36

Sample no.	84770004	84770005	84770005	84770006	84770007	84770010	84770010	84770010	84770013	84770013	84770016
Analysis no.	MU1	MU2	MU1	MU1	MU1	MU1	MU2	MU3	MU1	MU2	MU1
Mineral	CLINOPYRO.	CLINOPYRO.	CLINOPYRO.	CLINOPYRO.	CLINOPYRO.	CLINOPYRO.	CLINOPYRO.	CLINOPYRO.	CLINOPYRO.	CLINOPYRO.	CLINOPYRO.
Description	CUMULUS, CORE	CUMULUS, CORE	CUMULUS, CORE	CUMULUS, CORE	CUMULUS, CORE	CUMULUS, CORE	CUMULUS, RIM OF MU1	CUMULUS, CORE	CUMULUS, CORE	CUMULUS, CORE	CUMULUS, CORE
Lithology	OLIVINE WEBSTERITE	OLIVINE WEBSTERITE	OLIVINE WEBSTERITE	OLIVINE WEBSTERITE	WEBSTERITE	OLIVINE WEBSTERITE	OLIVINE WEBSTERITE	OLIVINE WEBSTERITE	OLIVINE WEBSTERITE	OLIVINE WEBSTERITE	OLIVINE WEBSTERITE
Zone	ULTRAMAFIC	ULTRAMAFIC	ULTRAMAFIC	ULTRAMAFIC	ULTRAMAFIC	ULTRAMAFIC	ULTRAMAFIC	ULTRAMAFIC	ULTRAMAFIC	ULTRAMAFIC	ULTRAMAFIC
Subzone	A	A	A	A	A	B	B	B	C	C	C
Strat. ht (m)	218	247	247	268	285	404	404	404	482	482	620
SiO2	53.20	53.15	53.52	53.97	51.82	53.40	54.45	53.84	53.00	53.14	53.10
TiO2	.33	.30	.20	.26	.28	.22	.16	.26	.30	.24	.23
Al2O3	1.24	1.77	1.33	1.11	1.63	1.04	1.18	1.10	1.25	.88	.79
Cr2O3	.44	<.10	.17	<.10	.49	.70	.78	.77	.13	.15	.34
FeO	7.09	5.76	6.73	6.56	4.89	5.59	4.89	5.08	5.86	5.98	6.47
MnO	.17	.18	.26	<.10	.21	.21	.19	.19	.19	.13	.19
NiO	.13	.22	.22	.09	.08	.06	.06	.09	.06	.05	.17
MgO	18.13	16.91	17.87	19.09	16.91	17.99	17.26	16.87	16.35	16.14	18.09
CaO	18.61	20.18	18.31	18.04	21.34	20.07	21.04	21.48	20.96	21.47	20.02
Na2O	.38	.44	.54	.22	.56	.35	.48	.44	.48	.53	.13
Total	99.72	98.91	99.15	99.34	98.21	99.63	100.49	100.12	98.58	98.71	99.53
Atomic proportions											
Oxygens	6.0	6.0	6.0	6.0	6.0	6.0	6.0	6.0	6.0	6.0	6.0
Si	1.957	1.965	1.974	1.976	1.938	1.961	1.978	1.970	1.972	1.979	1.959
Ti	.009	.008	.006	.007	.008	.006	.004	.007	.008	.007	.006
Al	.054	.077	.058	.048	.072	.045	.051	.047	.055	.039	.034
Cr	.013	-	.005	-	.014	.020	.022	.022	.004	.004	.010
Fe	.218	.178	.208	.201	.153	.172	.149	.155	.182	.186	.200
Mn	.005	.006	.008	-	.007	.007	.006	.006	.006	.004	.006
Ni	.004	.007	.007	.003	.002	.002	.002	.003	.002	.001	.005
Mg	.994	.932	.982	1.042	.942	.985	.934	.920	.907	.896	.995
Ca	.733	.799	.723	.708	.855	.790	.819	.842	.836	.857	.792
Na	.027	.032	.039	.016	.041	.025	.034	.031	.035	.038	.009
Total	4.014	4.004	4.009	4.000	4.032	4.012	3.998	4.004	4.007	4.012	4.017
mg number	82	84	83	84	86	85	86	86	83	83	83
Mg'	51	49	51	54	48	51	49	48	47	46	50
Fe'	11	9	11	10	8	9	8	8	9	10	10
Ca'	38	42	38	36	44	40	43	44	44	44	40

Sample no.	84770017	84770018	84770019	84770019	84770019	84770020	84770020	84770022	84770024	84770028
Analysis no.	MU1	MU1	MU1	MU2	MU3	MU1	MU2	MU2	MU1	MU1
Mineral	CLINOPYRO.	CLINOPYRO.	CLINOPYRO.	CLINOPYRO.	CLINOPYRO.	CLINOPYRO.	CLINOPYRO.	CLINOPYRO.	CLINOPYRO.	CLINOPYRO.
Description	CUMULUS, CORE	CUMULUS, CORE	CUMULUS, CORE	CUMULUS, CORE	CUMULUS, CORE	CUMULUS, CORE	CUMULUS, CORE	CUMULUS, CORE	CUMULUS, CORE	CUMULUS, CORE
Lithology	OLIVINE WEBSTERITE	OLIVINE WEBSTERITE	WEBSTERITE	WEBSTERITE	WEBSTERITE	WEBSTERITE	WEBSTERITE	OLIVINE WEBSTERITE	OLIVINE CLINOPYRO.	CLINOPYRO.
Zone	ULTRAMAFIC	ULTRAMAFIC	ULTRAMAFIC	ULTRAMAFIC	ULTRAMAFIC	ULTRAMAFIC	ULTRAMAFIC	ULTRAMAFIC	ULTRAMAFIC	ULTRAMAFIC
Subzone	C	C	C	C	C	D	D	D	D	E
Strat. ht (m)	655	690	748	748	748	867	867	950	1020	1180
SiO2	53.02	53.05	52.85	52.65	52.70	52.82	53.26	52.67	53.38	53.69
TiO2	.13	.20	.12	.20	.14	.25	.27	.24	.21	.06
Al2O3	.95	1.05	.94	.99	1.07	.97	1.00	.95	.82	1.06
Cr2O3	.42	.40	.55	.34	.46	.65	.63	.28	.21	.44
FeO	4.88	4.96	4.97	5.35	6.50	5.01	5.17	6.10	7.00	5.41
MnO	.21	.16	.15	.15	.12	.23	.10	.19	.17	.18
NiO	.10	.09	<.03	.03	.04	.07	.10	.21	.23	.19
MgO	16.69	16.84	16.48	16.92	18.20	16.98	16.85	16.98	18.52	16.69
CaO	22.29	20.98	22.54	21.45	18.72	21.63	21.10	21.47	18.87	21.47
Na2O	.67	.40	.38	.46	.25	.28	.53	.06	.34	.38
Total	99.36	98.13	98.98	98.54	98.20	98.89	99.01	99.15	99.75	99.57
Atomic proportions										
Oxygens	6.0	6.0	6.0	6.0	6.0	6.0	6.0	6.0	6.0	6.0
Si	1.962	1.976	1.963	1.962	1.963	1.960	1.971	1.957	1.964	1.977
Ti	.004	.006	.003	.006	.004	.007	.008	.007	.006	.002
Al	.041	.046	.041	.043	.047	.042	.044	.042	.036	.046
Cr	.012	.012	.016	.010	.014	.019	.018	.008	.006	.013
Fe	.151	.155	.154	.167	.203	.155	.160	.190	.215	.167
Mn	.007	.005	.005	.005	.004	.007	.003	.006	.005	.006
Ni	.003	.003	-	.001	.001	.002	.003	.006	.007	.006
Mg	.920	.935	.912	.940	1.011	.939	.929	.940	1.015	.916
Ca	.884	.837	.897	.856	.747	.860	.836	.855	.744	.847
Na	.048	.029	.027	.033	.018	.020	.038	.004	.024	.027
Total	4.032	4.004	4.019	4.022	4.011	4.012	4.010	4.014	4.022	4.006
mg number	86	86	86	85	83	86	85	83	83	85
Mg'	47	49	46	48	52	48	48	47	51	47
Fe'	8	8	8	8	10	8	8	10	11	9
Ca'	45	43	46	44	38	44	44	43	38	44

Sample no.	84770029	84770030	84770031	84770031	84770032	84770035	84770035	84770037	84770037	84770040	84770041	84770042
Analysis no.	MU1	MU1	MU2	MU1	MU1	MU2	MU1	MU1	MU2	MU1	MU1	MU1
Mineral	CLINOPYRO.	CLINOPYRO.	CLINOPYRO.	CLINOPYRO.	CLINOPYRO.	CLINOPYRO.	CLINOPYRO.	CLINOPYRO.	CLINOPYRO.	CLINOPYRO.	CLINOPYRO.	CLINOPYRO.
Description	CUMULUS, CORE	CUMULUS, CORE	CUMULUS, CORE	CUMULUS, CORE	CUMULUS, CORE	CUMULUS, CORE	CUMULUS, CORE	CUMULUS, CORE	CUMULUS, CORE	CUMULUS, CORE	CUMULUS, CORE	CUMULUS, CORE
Lithology	CLINOPYRO.	WEBSTERITE	OLIVINE WEBSTERITE	OLIVINE WEBSTERITE	OLIVINE WEBSTERITE	OLIVINE WEBSTERITE	OLIVINE WEBSTERITE	WEBSTERITE	WEBSTERITE	WEBSTERITE	WEBSTERITE	WEBSTERITE
Zone	ULTRAMAFIC	ULTRAMAFIC	ULTRAMAFIC	ULTRAMAFIC	ULTRAMAFIC	ULTRAMAFIC	ULTRAMAFIC	ULTRAMAFIC	ULTRAMAFIC	ULTRAMAFIC	ULTRAMAFIC	ULTRAMAFIC
Subzone	E	E	F	F	F	G	G	G	G	H	H	H
Strat. ht (m)	1234	1278	1298	1298	1417	1474	1474	1538	1538	1666	1695	1723
SiO2	52.80	53.54	54.23	52.92	53.34	52.17	52.71	53.54	54.54	52.98	53.76	53.19
TiO2	.20	.09	.33	.17	.24	.32	.18	.22	.15	.30	.17	.31
Al2O3	.75	.73	1.06	1.07	1.34	1.88	1.60	1.32	1.13	1.61	1.58	1.71
Cr2O3	.40	.31	.46	.39	.61	.72	.66	.46	.62	.40	.27	.25
FeO	7.39	6.82	5.33	5.79	5.45	4.93	5.30	5.98	4.88	6.33	6.06	6.71
MnO	.26	.22	.23	.18	.21	.19	.23	.15	.16	.20	.20	.22
NiO	.09	.08	<.03	.03	.08	.20	.07	.18	.03	<.03	.08	.08
MgO	18.90	19.21	17.94	17.62	17.31	16.59	17.18	17.87	16.88	17.99	18.01	17.42
CaO	18.57	17.99	21.41	20.63	20.92	21.22	20.01	19.80	21.92	18.79	19.21	19.19
Na2O	.29	.04	.49	.14	.51	.64	.60	.43	.74	.60	.66	.59
Total	99.65	99.03	101.48	98.94	100.01	98.86	98.54	99.95	101.05	99.20	100.00	99.67
Atomic proportions												
Oxygens	6.0	6.0	6.0	6.0	6.0	6.0	6.0	6.0	6.0	6.0	6.0	6.0
Si	1.949	1.974	1.958	1.960	1.956	1.938	1.957	1.961	1.976	1.954	1.964	1.956
Ti	.006	.002	.009	.005	.007	.009	.005	.006	.004	.008	.005	.009
Al	.033	.032	.045	.047	.058	.082	.070	.057	.048	.070	.068	.074
Cr	.012	.009	.013	.011	.018	.021	.019	.013	.018	.012	.008	.007
Fe	.228	.210	.161	.179	.167	.153	.165	.183	.148	.195	.185	.206
Mn	.008	.007	.007	.006	.007	.006	.007	.005	.005	.006	.006	.007
Ni	.003	.002	-	.001	.002	.006	.002	.005	.001	-	.002	.002
Mg	1.040	1.055	.965	.973	.946	.919	.951	.975	.911	.989	.981	.955
Ca	.735	.710	.828	.819	.822	.845	.796	.777	.851	.742	.752	.756
Na	.021	.003	.034	.010	.036	.046	.043	.031	.052	.043	.047	.042
Total	4.033	4.005	4.021	4.011	4.018	4.025	4.015	4.013	4.013	4.019	4.017	4.015
mg number	82	83	86	84	85	86	85	84	86	84	84	82
Mg'	52	53	49	49	49	48	50	50	48	51	51	50
Fe'	11	11	9	9	9	8	8	9	8	10	10	11
Ca'	37	36	42	42	42	44	42	41	44	39	39	39

Sample no.	84770045	84770044	84770047	84770094	84770094	84770048	84770048	84770049	84770050	84770051	84770052	84770052
Analysis no.	MU1	MU1	MU1	MU2	MU1	MU1	MU2	MU1	MU1	MU1	MU1	MU2
Mineral	CLINOPYRO.	CLINOPYRO.	CLINOPYRO.	CLINOPYRO.	CLINOPYRO.	CLINOPYRO.	CLINOPYRO.	CLINOPYRO.	CLINOPYRO.	CLINOPYRO.	CLINOPYRO.	CLINOPYRO.
Description	CUMULUS, CORE	CUMULUS, CORE	CUMULUS, CORE	CUMULUS, CORE	CUMULUS, CORE	CUMULUS, CORE	CUMULUS, CORE	CUMULUS, CORE	CUMULUS, CORE	CUMULUS, CORE	CUMULUS, CORE	CUMULUS, CORE
Lithology	PORPHYRIT. GABBRONOR.	PORPHYRIT. PLAG-WEBSTERITE	NORITE-ORTHOPYRO.	PORPHYRIT. PLAG-WEBSTERITE	PORPHYRIT. PLAG-WEBSTERITE	GABBRONOR.	GABBRONOR.	GABBRONOR.	GABBRONOR.	GABBRONOR.	GABBRONOR.	GABBRONOR.
Zone	ULTRAMAFIC	ULTRAMAFIC	ULTRAMAFIC	ULTRAMAFIC	ULTRAMAFIC	GABBROIC	GABBROIC	GABBROIC	GABBROIC	GABBROIC	GABBROIC	GABBROIC
Subzone	I	I	I	I	I	A	A	A	A	A	A	A
Strat. ht (m)	1811	1838	1839	1846	1846	1851	1851	1998	2094	2248	2377	2377
SiO2	52.02	52.68	51.41	50.85	51.90	50.85	50.73	50.65	50.99	51.30	50.41	50.12
TiO2	.41	.25	.64	.48	.65	.51	.42	.51	.35	.44	.54	.67
Al2O3	1.77	1.55	1.95	1.33	1.69	2.06	1.79	1.78	1.73	1.73	1.81	1.81
Cr2O3	.19	.10	.28	<.10	<.10	<.10	.14	<.10	.14	<.10	<.10	<.10
FeO	8.23	7.48	9.69	11.66	11.11	9.96	10.08	11.69	10.38	11.11	11.96	10.99
MnO	.19	.22	.17	.31	.26	.29	.35	.29	.28	.27	.29	.28
NiO	.12	.05	.06	.11	.07	.15	<.03	.18	.05	.10	<.03	.14
MgO	15.29	15.19	14.65	14.00	13.57	13.87	14.28	14.33	13.71	13.37	13.06	12.84
CaO	20.40	21.40	20.87	19.05	20.83	21.27	20.49	19.85	21.82	21.67	20.40	21.54
Na2O	.58	.39	.66	.68	.62	.37	.31	.38	.46	.39	.28	.43
Total	99.20	99.31	100.38	98.47	100.70	99.33	98.59	99.66	99.91	100.38	98.75	98.82
Atomic proportions												
Oxygens	6.0	6.0	6.0	6.0	6.0	6.0	6.0	6.0	6.0	6.0	6.0	6.0
Si	1.946	1.963	1.920	1.946	1.940	1.923	1.930	1.919	1.925	1.930	1.931	1.920
Ti	.012	.007	.018	.014	.018	.015	.012	.015	.010	.012	.016	.019
Al	.078	.068	.086	.060	.074	.092	.080	.079	.077	.077	.082	.082
Cr	.006	.003	.008	-	-	-	.004	-	.004	-	-	-
Fe	.258	.233	.303	.373	.347	.315	.321	.370	.328	.350	.383	.352
Mn	.006	.007	.005	.010	.008	.009	.011	.009	.009	.009	.009	.009
Ni	.004	.001	.002	.003	.002	.005	-	.005	.002	.003	-	.004
Mg	.853	.844	.815	.798	.756	.782	.810	.809	.771	.750	.745	.733
Ca	.818	.854	.835	.781	.834	.862	.835	.806	.882	.874	.837	.884
Na	.042	.028	.048	.050	.045	.027	.023	.028	.034	.028	.021	.032
Total	4.021	4.009	4.039	4.036	4.027	4.030	4.027	4.041	4.042	4.033	4.023	4.036
mg number	77	78	73	68	69	71	72	69	70	68	66	68
Mg'	44	44	42	41	39	40	41	41	39	38	38	37
Fe'	14	12	15	19	18	16	16	18	17	18	19	18
Ca'	42	44	43	40	43	44	43	41	44	44	43	45

Sample no.	84770053	84770054	84770055	84770057	84770059	84770060	84770061	84770062	84770063	84770064	84770065	84770066
Analysis no.	MU1	MU1	MU1	MU1	MU1	MU1	MU1	MU1	MU1	MU1	MU1	MU1
Mineral	CLINOPYRO.	CLINOPYRO.	CLINOPYRO.	CLINOPYRO.	CLINOPYRO.	CLINOPYRO.	CLINOPYRO.	CLINOPYRO.	CLINOPYRO.	CLINOPYRO.	CLINOPYRO.	CLINOPYRO.
Description	CUMULUS, CORE	CUMULUS, CORE	CUMULUS, CORE	CUMULUS, CORE	CUMULUS, CORE	CUMULUS, CORE	CUMULUS, CORE	CUMULUS, CORE	CUMULUS, CORE	CUMULUS, CORE	CUMULUS, CORE	CUMULUS, CORE
Lithology	GABBRONOR.	GABBRONOR.	GABBRONOR.	GABBRONOR.	GABBRONOR.	GABBRONOR.	GABBRONOR.	GABBRONOR.	GABBRONOR.	GABBRONOR.	GABBRONOR.	GABBRONOR.
Zone	GABBROIC	GABBROIC	GABBROIC	GABBROIC	GABBROIC	GABBROIC	GABBROIC	GABBROIC	GABBROIC	GABBROIC	GABBROIC	GABBROIC
Subzone	A	A	A	A	A	A	A	A	A	A	A	A
Strat. ht (m)	2551	2692	2859	3052	3341	3425	3553	3676	3798	3965	4125	4222
SiO2	50.86	50.51	50.87	50.11	49.79	51.11	51.48	50.00	50.66	49.45	49.75	49.12
TiO2	.72	.61	.36	.44	.44	.50	.22	.65	.36	.53	.43	.86
Al2O3	1.88	1.77	1.45	1.64	1.85	1.19	.81	1.75	1.36	.96	1.36	1.28
Cr2O3	<.10	<.10	.10	<.10	<.10	<.10	<.10	<.10	<.10	<.10	<.10	<.10
FeO	11.87	12.48	12.71	12.95	14.76	13.82	14.78	15.00	14.77	21.26	20.93	19.00
MnO	.35	.41	.24	.37	.35	.31	.35	.34	.28	.54	.48	.40
NiO	<.03	<.03	.03	.04	<.03	.04	.12	<.03	.07	<.03	<.03	<.03
MgO	12.16	12.20	12.16	12.60	11.69	11.66	11.21	11.13	11.15	11.47	10.65	10.56
CaO	21.66	21.12	21.13	20.71	19.49	21.18	20.34	20.35	20.25	15.39	15.10	17.37
Na2O	.35	.23	.26	.31	.55	.31	.41	.35	.25	.43	.31	.47
Total	99.85	99.33	99.31	99.17	98.92	100.12	99.72	99.57	99.15	100.03	99.01	99.06

Atomic proportions

Oxygens	6.0	6.0	6.0	6.0	6.0	6.0		6.0	6.0	6.0	6.0	6.0	6.0
Si	1.931	1.932	1.946	1.925	1.927	1.950	Si	1.975	1.928	1.955	1.931	1.953	1.928
Ti	.021	.018	.010	.013	.013	.014	Ti	.006	.019	.010	.016	.013	.025
Al	.084	.080	.065	.074	.084	.053	Al	.037	.080	.062	.044	.063	.059
Cr	-	-	.003	-	-	-	Fe	.474	.484	.477	.694	.687	.624
Fe	.377	.399	.407	.416	.478	.441	Mn	.011	.011	.009	.018	.016	.013
Mn	.011	.013	.008	.012	.011	.010	Ni	.004	-	.002	-	-	-
Ni	-	-	.001	.001	-	.001	Mg	.641	.640	.641	.668	.623	.618
Mg	.688	.695	.693	.721	.675	.663	Ca	.836	.841	.837	.644	.635	.731
Ca	.881	.865	.866	.852	.808	.866	Na	.031	.026	.019	.033	.024	.036
Na	.026	.017	.019	.023	.041	.023	Total	4.015	4.027	4.013	4.047	4.014	4.034
Total	4.019	4.019	4.019	4.037	4.038	4.021							
							mg number	57	57	57	49	48	50
mg number	65	64	63	63	59	60	Mg'	33	33	33	33	32	31
Mg'	36	35	35	36	34	34	Fe'	24	25	24	35	35	32
Fe'	19	20	21	21	24	22	Ca'	43	42	43	32	33	37
Ca'	45	45	44	43	42	44							

Regional traverse: average bulk compositions of clinopyroxene (GZ) by raster analysis

Sample no.	84770051	84770052	84770053	84770054	84770055	84770059	84770061	84770064	84770066
Mineral	CLINOPYRO.	CLINOPYRO.	CLINOPYRO.	CLINOPYRO.	CLINOPYRO.	CLINOPYRO.	CLINOPYRO.	CLINOPYRO.	CLINOPYRO.
Description	CUMULUS, CORE	CUMULUS, CORE	CUMULUS, CORE	CUMULUS CORE	CUMULUS, CORE	CUMULUS, CORE	CUMULUS, CORE	CUMULUS, CORE	CUMULUS, CORE
Lithology	GABBRONOR.	GABBRONOR.	GABBRONOR.	GABBRONOR.	GABBRONOR.	GABBRONOR.	GABBRONOR.	GABBRONOR.	GABBRONOR.
Zone	GABBROIC	GABBROIC	GABBROIC	GABBROIC	GABBROIC	GABBROIC	GABBROIC	GABBROIC	GABBROIC
Subzone	A	A	A	A	A	A	A	A	A
Strat. ht (m)	2248	2377	2551	2692	2859	3341	3553	3965	4222
SiO2	50.92	51.17	51.40	50.91	51.50	50.85	51.45	51.26	50.47
TiO2	.48	.42	.38	.38	.29	.36	.32	.38	.49
Al2O3	2.21	1.85	1.69	1.77	1.45	1.35	1.25	1.23	1.30
Cr2O3	<.11	<.11	<.11	<.11	.07	.05	.06	.05	.05
FeO	14.85	14.01	15.13	16.67	16.31	17.65	17.59	18.47	19.82
MnO	.19	.16	.18	.22	.18	.22	.15	.21	.26
MgO	13.92	13.59	13.32	13.25	12.96	12.26	11.55	11.46	10.93
CaO	17.11	18.58	18.41	16.57	18.03	16.84	18.06	17.41	16.74
Na2O	.23	.17	.22	.24	.19	.18	.08	.21	.25
K2O	<.06	<.05	<.06	<.05	<.06	<.06	<.06	<.06	<.06
Total	99.90	99.95	100.73	100.01	100.99	99.77	100.50	100.67	100.32
Atomic proportions									
Oxygens	6.0	6.0	6.0	6.0	6.0	6.0	6.0	6.0	6.0
Si	1.930	1.938	1.940	1.941	1.947	1.954	1.965	1.961	1.950
Ti	.014	.012	.011	.011	.008	.010	.009	.011	.014
Al	.099	.083	.075	.080	.065	.061	.056	.055	.059
Cr	-	-	-	-	.002	.002	.002	.002	.002
Fe	.471	.444	.478	.532	.516	.567	.562	.591	.640
Mn	.006	.005	.006	.007	.006	.007	.005	.007	.009
Mg	.786	.767	.750	.753	.730	.702	.657	.653	.629
Ca	.695	.754	.745	.677	.730	.693	.739	.714	.693
Na	.017	.012	.016	.018	.014	.014	.006	.015	.019
Total	4.016	4.015	4.019	4.017	4.018	4.011	4.000	4.008	4.015
mg number	63	63	61	59	59	55	54	53	50
Mg'	40	39	38	38	37	36	33	33	32
Fe'	24	23	24	27	26	29	29	30	33
Ca'	36	38	38	35	37	35	38	37	35
Number of analyses averaged	8	10	9	7	5	9	6	8	9

Regional traverse: orthopyroxene (UZ)

Sample no.	84770102	84770002	84770002	84770003	84770004	84770004	84770005	84770006	84770006	84770007	84770007
Analysis no.	MU1a	MU3a	MU1a	MU1a	MU1a	MU2a	MU1a	MU1a	MU2a	MU2a	MU1a
Mineral	ORTHOPYRO.	ORTHOPYRO.	ORTHOPYRO.	ORTHOPYRO.	ORTHOPYRO.	ORTHOPYRO.	ORTHOPYRO.	ORTHOPYRO.	ORTHOPYRO.	ORTHOPYRO.	ORTHOPYRO.
Description	INTERCUMU.	INTERCUMU.	INTERCUMU.	INTERCUMU.	INTERCUMU.	INTERCUMU.	INTERCUMU.	INTERCUMU.	INTERCUMU.	INTERCUMU.	INTERCUMU.
Lithology	GABBRONOR.	PLAGIOCLA. WEBSTERITE	PLAGIOCLA. WEBSTERITE	OLIVINE WEBSTERITE	OLIVINE WEBSTERITE	OLIVINE WEBSTERITE	OLIVINE WEBSTERITE	OLIVINE WEBSTERITE	OLIVINE WEBSTERITE	WEBSTERITE	WEBSTERITE
Zone	ULTRAMAFIC	ULTRAMAFIC	ULTRAMAFIC	ULTRAMAFIC	ULTRAMAFIC	ULTRAMAFIC	ULTRAMAFIC	ULTRAMAFIC	ULTRAMAFIC	ULTRAMAFIC	ULTRAMAFIC
Subzone	A'	A'	A'	A'	A	A	A	A	A	A	A
Strat. ht (m)	2	128	128	174	218	218	247	268	268	285	285
SiO2	51.66	55.08	54.76	54.66	54.26	55.45	54.71	54.60	56.03	55.24	54.86
TiO2	.23	.19	.12	.09	.14	.13	.25	.27	.18	.15	.10
Al2O3	.57	.92	1.01	.93	1.11	1.20	1.34	1.42	1.19	.96	1.05
Cr2O3	<.10	.14	.11	.14	.16	.12	<.10	<.10	<.10	.24	.22
FeO	25.09	13.54	13.15	12.63	12.37	13.31	12.47	11.40	12.04	11.82	11.19
MnO	.48	.19	.25	.14	.33	.13	.21	.32	.38	.31	.29
NiO	.13	.05	.21	.09	.05	<.03	.07	.06	.07	.17	.12
MgO	20.29	28.02	27.45	28.81	28.41	28.41	28.47	29.17	29.41	29.95	30.82
CaO	1.92	1.65	1.69	2.18	1.73	1.32	2.16	1.92	1.07	1.74	1.69
Na2O	.05	<.04	.17	<.04	.04	.13	.07	.12	.07	.04	.16
Total	100.42	99.78	98.92	99.67	98.60	100.20	99.75	99.28	100.44	100.62	100.50
Atomic proportions											
Oxygens	6.0	6.0	6.0	6.0	6.0	6.0	6.0	6.0	6.0	6.0	6.0
Si	1.955	1.975	1.981	1.960	1.964	1.975	1.958	1.954	1.978	1.955	1.941
Ti	.007	.005	.003	.002	.004	.003	.007	.007	.005	.004	.003
Al	.025	.039	.043	.039	.047	.050	.057	.060	.050	.040	.044
Cr	-	.004	.003	.004	.005	.003	-	-	-	.007	.006
Fe	.794	.406	.398	.379	.374	.396	.373	.341	.356	.350	.331
Mn	.015	.006	.008	.004	.010	.004	.006	.010	.011	.009	.009
Ni	.004	.001	.006	.003	.001	-	.002	.002	.002	.005	.003
Mg	1.145	1.498	1.480	1.540	1.533	1.508	1.519	1.556	1.548	1.580	1.625
Ca	.078	.063	.065	.084	.067	.050	.083	.074	.040	.066	.064
Na	.004	-	.012	-	.003	.009	.005	.008	.005	.003	.011
Total	4.027	3.998	3.999	4.016	4.008	3.999	4.009	4.013	3.995	4.019	4.037
mg number	59	79	79	80	80	79	80	82	81	82	83
Mg'	57	76	76	77	78	77	77	79	80	79	80
Fe'	39	21	20	19	19	20	19	17	18	18	17
Ca'	4	3	4	4	3	3	4	4	2	3	3

Sample no.	84770018	84770018	84770019	84770019	84770020	84770020	84770021	84770030	84770031	84770032	84770032	84770035
Analysis no.	MU1a	MU2a	MU2a	MU1a	MU1a	MU2a	MU1a	MU1a	MU1a	MU1a	MU2a	MU1a
Mineral	ORTHOPYRO.	ORTHOPYRO.	ORTHOPYRO.	ORTHOPYRO.	ORTHOPYRO.	ORTHOPYRO.	ORTHOPYRO.	ORTHOPYRO.	ORTHOPYRO.	ORTHOPYRO.	ORTHOPYRO.	ORTHOPYRO.
Description	INTERCUMU.	INTERCUMU.	INTERCUMU.	INTERCUMU.	INTERCUMU.	INTERCUMU.	INTERCUMU.	INTERCUMU.	INTERCUMU.	INTERCUMU.	INTERCUMU.	INTERCUMU.
Lithology	OLIVINE WEBSTERITE	OLIVINE WEBSTERITE	WEBSTERITE	WEBSTERITE	WEBSTERITE	WEBSTERITE	OLIVINE WEBSTERITE	WEBSTERITE	OLIVINE WEBSTERITE	OLIVINE WEBSTERITE	OLIVINE WEBSTERITE	OLIVINE WEBSTERITE
Zone	ULTRAMAFIC	ULTRAMAFIC	ULTRAMAFIC	ULTRAMAFIC	ULTRAMAFIC	ULTRAMAFIC	ULTRAMAFIC	ULTRAMAFIC	ULTRAMAFIC	ULTRAMAFIC	ULTRAMAFIC	ULTRAMAFIC
Subzone	C	C	C	C	D	D	D	E	F	F	F	G
Strat. ht (m)	690	690	748	748	867	867	910	1278	1298	1417	1417	1474
SiO2	55.24	55.33	54.72	54.85	55.87	55.49	54.97	55.29	56.32	55.63	55.94	54.67
TiO2	.12	.05	.20	.07	.12	.19	.19	.03	.27	.15	.05	.08
Al2O3	.63	.52	.67	.62	.75	.74	.69	.58	.84	.79	.80	1.01
Cr2O3	.27	.20	.10	.23	.21	.29	.26	.22	.26	.17	.28	.20
FeO	10.97	11.12	12.41	11.34	10.86	11.28	11.60	12.74	10.97	11.38	11.28	11.58
MnO	.28	.15	.22	.28	.22	.25	.28	.29	.24	.27	.20	.25
NiO	.11	.19	.11	.23	.10	.16	.10	.18	.19	.15	.07	.19
MgO	28.58	29.54	29.63	28.99	30.53	30.76	30.59	29.19	29.77	30.19	30.65	29.22
CaO	1.86	1.12	1.38	2.14	1.35	1.08	.96	1.73	2.01	1.81	1.65	1.84
Na2O	.19	.25	.13	<.04	.05	.19	.21	<.04	<.04	<.04	.05	.30
Total	98.25	98.47	99.57	98.75	100.06	100.43	99.85	100.25	100.87	100.54	100.97	99.34
Atomic proportions												
Oxygens	6.0	6.0	6.0	6.0	6.0	6.0	6.0	6.0	6.0	6.0	6.0	6.0
Si	1.992	1.989	1.961	1.976	1.974	1.960	1.956	1.971	1.977	1.965	1.964	1.960
Ti	.003	.001	.005	.002	.003	.005	.005	.001	.007	.004	.001	.002
Al	.027	.022	.028	.026	.031	.031	.029	.024	.035	.033	.033	.043
Cr	.008	.006	.003	.007	.006	.008	.007	.006	.007	.005	.008	.006
Fe	.331	.334	.372	.342	.321	.333	.345	.380	.322	.336	.331	.347
Mn	.009	.005	.007	.009	.007	.007	.008	.009	.007	.008	.006	.008
Ni	.003	.005	.003	.007	.003	.005	.003	.005	.005	.004	.002	.005
Mg	1.536	1.582	1.582	1.556	1.608	1.619	1.623	1.551	1.558	1.589	1.604	1.562
Ca	.072	.043	.053	.083	.051	.041	.037	.066	.076	.068	.062	.071
Na	.013	.017	.009	-	.003	.013	.014	-	-	-	.003	.021
Total	3.994	4.005	4.023	4.006	4.006	4.022	4.028	4.013	3.995	4.012	4.016	4.024
mg number	82	83	81	82	83	83	82	80	83	83	83	82
Mg'	79	81	79	79	81	81	81	78	80	80	80	79
Fe'	17	17	18	17	16	17	17	19	16	17	17	17
Ca'	4	2	3	4	3	2	2	3	4	3	3	4

Sample no.	84770036	84770037	84770040	84770041	84770042	84770045	84770045	85770159	85770159	85770159	84770044	84770047	84770094	84770046
Analysis no.	MU1a	MU1a	MU1a	MU1a	MU1a	MU2a	MU1a	MU2a	MU1a	MU3a	MU1a	MU1a	MU1a	MU1a
Mineral	ORTHOPYRO.	ORTHOPYRO.	ORTHOPYRO.	ORTHOPYRO.	ORTHOPYRO.	ORTHOPYRO.	ORTHOPYRO.	ORTHOPYRO.	ORTHOPYRO.	ORTHOPYRO.	ORTHOPYRO.	ORTHOPYRO.	ORTHOPYRO.	ORTHOPYRO.
Description	INTERCUMU.	INTERCUMU.	INTERCUMU.	INTERCUMU.	INTERCUMU.	CUMULUS	CUMULUS	CUMULUS	CUMULUS	CUMULUS	CUMULUS	CUMULUS	CUMULUS	CUMULUS
Lithology	OLIVINE WEBSTERITE	WEBSTERITE	WEBSTERITE	WEBSTERITE	WEBSTERITE	PORPHYRIT. GABBRONOR.	PORPHYRIT. GABBRONOR.	ORTHOPYRO.	ORTHOPYRO.	ORTHOPYRO.	PORPHYRIT. WEBSTERITE	NORITE-ORTHOPYRO.	PORPHYRIT. WEBSTERITE	ORTHOPYRO.
Zone	ULTRAMAFIC	ULTRAMAFIC	ULTRAMAFIC	ULTRAMAFIC	ULTRAMAFIC	ULTRAMAFIC	ULTRAMAFIC	ULTRAMAFIC	ULTRAMAFIC	ULTRAMAFIC	ULTRAMAFIC	ULTRAMAFIC	ULTRAMAFIC	ULTRAMAFIC
Subzone	G	G	H	H	H	I	I	I	I	I	I	I	I	I
Strat. ht (m)	1500	1538	1666	1695	1723	1811	1811	1836	1836	1836	1838	1839	1846	1848
SiO2	54.42	55.54	55.68	55.25	55.24	53.09	53.48	51.68	52.36	52.34	53.06	53.22	51.23	56.01
TiO2	.15	.19	.19	.10	.05	.28	.12	.11	.03	.15	.21	.14	.64	.20
Al2O3	1.00	1.11	.93	.96	.95	.91	1.21	5.49	5.34	5.10	1.08	1.20	.89	1.75
Cr2O3	.23	.29	.21	.22	<.10	<.10	.18	.35	.42	.60	<.10	.18	<.10	.56
FeO	11.34	11.80	11.93	11.89	12.33	16.35	15.25	9.57	9.48	10.00	17.14	20.33	21.66	8.26
MnO	.22	.31	.28	.21	.31	.38	.34	.27	.23	.18	.33	.41	.45	.20
NiO	.07	.12	.14	.16	.16	.12	.05	<.03	<.03	.11	<.03	<.03	.06	.17
MgO	30.13	29.93	29.18	28.74	28.84	25.73	25.68	30.41	30.81	30.90	24.37	22.88	21.75	32.00
CaO	1.50	.75	1.20	1.61	1.78	2.16	2.63	.33	.36	.26	2.90	1.22	2.99	1.41
Na2O	.21	.39	.09	<.04	.08	.33	.22	<.04	.11	<.04	.32	.30	.12	.04
Total	99.27	100.43	99.83	99.14	99.74	99.35	99.16	98.21	99.14	99.64	99.41	99.88	99.79	100.60
Atomic proportions														
Oxygens	6.0	6.0	6.0	6.0	6.0	6.0	6.0	6.0	6.0	6.0	6.0	6.0	6.0	6.0
Si	1.949	1.964	1.980	1.980	1.974	1.951	1.958	1.851	1.856	1.852	1.957	1.971	1.930	1.948
Ti	.004	.005	.005	.003	.001	.008	.003	.003	.001	.004	.006	.004	.018	.005
Al	.042	.046	.039	.041	.040	.039	.052	.232	.223	.213	.047	.052	.040	.072
Cr	.007	.008	.006	.006	-	-	.005	.010	.012	.017	-	.005	-	.015
Fe	.340	.349	.355	.356	.368	.502	.467	.287	.281	.296	.529	.630	.682	.240
Mn	.007	.009	.008	.006	.009	.012	.011	.008	.007	.005	.010	.013	.014	.006
Ni	.002	.003	.004	.005	.005	.004	.001	-	-	.003	-	-	.002	.005
Mg	1.608	1.577	1.547	1.535	1.536	1.409	1.401	1.623	1.628	1.630	1.340	1.263	1.221	1.659
Ca	.058	.028	.046	.062	.068	.085	.103	.013	.014	.010	.115	.048	.121	.053
Na	.015	.027	.006	-	.006	.024	.016	-	.008	-	.023	.022	.009	.003
Total	4.030	4.017	3.996	3.994	4.007	4.034	4.018	4.026	4.029	4.029	4.025	4.007	4.037	4.005
mg number	83	82	81	81	81	74	75	85	85	85	72	67	64	87
Mg'	80	81	79	79	78	71	71	84	84	84	67	65	60	85
Fe'	17	18	18	18	19	25	24	15	15	15	27	33	34	12
Ca'	3	1	3	3	3	4	5	1	1	1	6	2	6	3

Regional traverse: inverted pigeonite (GZ)

Sample no.	84770055	84770055	84770055	84770055	84770055	84770055	84770055	84770055	84770055	84770055	84770055	84770055
Analysis no.	59518	59519	59520	59521	59522	59523	59524	59525	59526	59527	59528	59529
Mineral	INVERTED PIGEONITE	INVERTED PIGEONITE	INVERTED PIGEONITE	INVERTED PIGEONITE	INVERTED PIGEONITE	INVERTED PIGEONITE	INVERTED PIGEONITE	INVERTED PIGEONITE	INVERTED PIGEONITE	INVERTED PIGEONITE	INVERTED PIGEONITE	INVERTED PIGEONITE
Description	CUMULUS, LAMELLAE	CUMULUS, LAMELLAE	CUMULUS, LAMELLAE	CUMULUS, LAMELLAE	CUMULUS, LAMELLAE	CUMULUS, LAMELLAE	CUMULUS, LAMELLAE	CUMULUS, LAMELLAE	CUMULUS, LAMELLAE	CUMULUS, LAMELLAE	CUMULUS, HOST	CUMULUS, HOST
Lithology	GABBRONOR.	GABBRONOR.	GABBRONOR.	GABBRONOR.	GABBRONOR.	GABBRONOR.	GABBRONOR.	GABBRONOR.	GABBRONOR.	GABBRONOR.	GABBRONOR.	GABBRONOR.
Zone	GABBROIC	GABBROIC	GABBROIC	GABBROIC	GABBROIC	GABBROIC	GABBROIC	GABBROIC	GABBROIC	GABBROIC	GABBROIC	GABBROIC
Subzone	A	A	A	A	A	A	A	A	A	A	A	A
Strat. ht (m)	2859	2859	2859	2859	2859	2859	2859	2859	2859	2859	2859	2859
SiO2	53.26	52.46	52.72	52.96	53.18	53.29	53.11	52.96	53.17	53.15	52.30	52.57
TiO2	.24	.29	.32	.34	.32	.32	.30	.33	.30	.31	.18	.19
Al2O3	1.45	1.35	1.33	1.30	1.27	1.24	1.28	1.30	1.31	1.36	.70	.62
Cr2O3	<.03	<.03	<.03	<.03	<.03	<.03	<.03	<.03	<.03	<.03	.03	.03
FeO	12.40	12.22	12.01	11.85	12.34	11.09	12.18	11.77	11.82	11.85	28.49	27.10
MnO	.23	.28	.30	.26	.23	.24	.29	.24	.23	.33	.60	.58
NiO	<.03	.07	.05	<.03	<.03	.03	.05	.05	.03	<.03	<.03	<.03
MgO	13.91	12.64	12.72	12.67	12.83	12.59	12.79	12.62	12.78	12.76	18.47	18.44
CaO	19.71	20.81	21.02	20.82	21.15	21.13	21.04	20.95	21.33	20.80	.91	.87
Na2O	.26	.36	.35	.36	.35	.33	.30	.35	.32	.34	.03	.02
Total	101.46	100.48	100.83	100.57	101.67	100.26	101.34	100.57	101.29	100.90	101.71	100.42
Atomic proportions												
Oxygens	6.0	6.0	6.0	6.0	6.0	6.0	6.0	6.0	6.0	6.0	6.0	6.0
Si	1.971	1.970	1.972	1.981	1.973	1.992	1.976	1.981	1.976	1.981	1.973	1.995
Ti	.007	.008	.009	.010	.009	.009	.008	.009	.008	.009	.005	.005
Al	.063	.060	.059	.057	.056	.055	.056	.057	.057	.060	.031	.028
Fe	.384	.384	.376	.371	.383	.347	-	-	-	-	.001	.001
Mn	.007	.009	.009	.008	.007	.008	.379	.368	.367	.369	.899	.860
Ni	-	.002	.002	-	-	.001	.009	.008	.007	.011	.019	.019
Mg	.768	.707	.709	.706	.709	.702	.001	.002	.001	-	-	-
Ca	.781	.837	.842	.835	.841	.846	.709	.704	.708	.709	1.039	1.043
Na	.018	.026	.025	.026	.025	.024	.838	.840	.850	.831	.037	.035
Total	4.000	4.005	4.003	3.994	4.003	3.983	.021	.026	.023	.024	.002	.001
							3.999	3.994	3.998	3.993	4.006	3.987
mg number	67	65	65	66	65	67						
Mg'	40	37	37	37	37	37	65	66	66	66	54	55
Fe'	20	20	19	19	20	18	36	37	37	37	53	54
Ca'	40	43	44	44	43	45	20	19	19	19	45	44
							44	44	44	44	2	2

Sample no.	84770055	84770055	84770055	84770055	84770055	84770055	84770055	84770055	84770055	84770055	84770055	84770055
Analysis no.	59530	59531	59532	59533	59534	59535	59536	59537	59538	59539	59540	59541
Mineral	INVERTED PIGEONITE	INVERTED PIGEONITE	INVERTED PIGEONITE	INVERTED PIGEONITE	INVERTED PIGEONITE	INVERTED PIGEONITE	INVERTED PIGEONITE	INVERTED PIGEONITE	INVERTED PIGEONITE	INVERTED PIGEONITE	INVERTED PIGEONITE	INVERTED PIGEONITE
Description	CUMULUS, HOST	CUMULUS, HOST	CUMULUS, HOST	CUMULUS, HOST	CUMULUS, HOST	CUMULUS, HOST	CUMULUS, HOST	CUMULUS, HOST	CUMULUS, HOST	CUMULUS, LAMELLAE	CUMULUS, LAMELLAE	CUMULUS, LAMELLAE
Lithology	GABBRONOR.	GABBRONOR.	GABBRONOR.	GABBRONOR.	GABBRONOR.	GABBRONOR.	GABBRONOR.	GABBRONOR.	GABBRONOR.	GABBRONOR.	GABBRONOR.	GABBRONOR.
Zone	GABBROIC	GABBROIC	GABBROIC	GABBROIC	GABBROIC	GABBROIC	GABBROIC	GABBROIC	GABBROIC	GABBROIC	GABBROIC	GABBROIC
Subzone	A	A	A	A	A	A	A	A	A	A	A	A
Strat. ht (m)	2859	2859	2859	2859	2859	2859	2859	2859	2859	2859	2859	2859
SiO2	52.21	52.72	51.99	51.57	51.64	51.60	51.95	51.39	52.06	52.56	52.75	52.79
TiO2	.17	.20	.21	.21	.21	.20	.22	.20	.16	.29	.29	.31
Al2O3	.68	.69	.70	.69	.70	.64	.68	.64	.55	1.17	1.26	1.26
Cr2O3	<.03	<.03	<.03	<.03	<.03	<.03	<.03	<.03	<.03	.04	<.03	<.03
FeO	28.50	27.83	27.84	28.23	28.44	27.22	28.55	26.56	27.91	11.50	11.87	11.58
MnO	.61	.63	.62	.60	.62	.57	.58	.59	.62	.29	.27	.28
NiO	<.03	<.03	.04	.03	<.03	.04	.04	<.03	.05	.05	.05	<.03
MgO	18.24	18.25	17.92	17.93	18.05	17.73	18.01	17.60	18.17	12.76	12.81	12.71
CaO	1.10	1.16	1.06	.98	.99	1.09	.99	1.22	1.20	20.11	20.31	20.33
Na2O	<.02	.02	<.02	<.02	<.02	.02	<.02	.02	<.02	.33	.32	.33
Total	101.50	101.51	100.38	100.24	100.63	99.10	101.02	98.22	100.71	99.11	99.93	99.59

Atomic proportions

Oxygens	6.0	6.0	6.0	6.0	6.0	6.0		6.0	6.0	6.0	6.0	6.0	6.0
Si	1.975	1.987	1.984	1.976	1.972	1.991	Si	1.976	1.996	1.982	1.990	1.984	1.989
Ti	.005	.006	.006	.006	.006	.006	Ti	.006	.006	.004	.008	.008	.009
Al	.030	.031	.032	.031	.031	.029	Al	.031	.029	.025	.052	.056	.056
Fe	.902	.877	.889	.905	.908	.878	Cr	-	-	-	.001	-	-
Mn	.020	.020	.020	.019	.020	.019	Fe	.908	.863	.889	.364	.373	.365
Ni	-	-	.001	.001	-	.001	Mn	.019	.020	.020	.009	.009	.009
Mg	1.029	1.025	1.019	1.024	1.028	1.020	Ni	.001	-	.001	.002	.001	-
Ca	.044	.047	.043	.040	.040	.045	Mg	1.021	1.019	1.031	.720	.718	.714
Na	-	.002	-	-	-	.002	Ca	.041	.051	.049	.816	.818	.821
Total	4.005	3.993	3.994	4.003	4.006	3.990	Na	-	.001	-	.025	.023	.024
							Total	4.002	3.984	4.001	3.987	3.991	3.986
mg number	53	54	53	53	53	54							
Mg'	52	53	52	52	52	52	mg number	53	54	54	66	66	66
Fe'	46	45	46	46	46	46	Mg'	52	53	53	38	38	38
Ca'	2	2	2	2	2	2	Fe'	46	45	45	19	20	19
							Ca'	2	2	2	43	42	43

Sample no.	84770055	84770055	84770055	84770055	84770055	84770055	84770055	84770055	84770055	84770055	84770055	84770055
Analysis no.	59542	59543	59544	59545	59546	59547	59548	59549	59550	59551	59552	59553
Mineral	INVERTED PIGEONITE	INVERTED PIGEONITE	INVERTED PIGEONITE	INVERTED PIGEONITE	INVERTED PIGEONITE	INVERTED PIGEONITE	INVERTED PIGEONITE	INVERTED PIGEONITE	INVERTED PIGEONITE	INVERTED PIGEONITE	INVERTED PIGEONITE	INVERTED PIGEONITE
Description	CUMULUS, LAMELLAE	CUMULUS, LAMELLAE	CUMULUS, LAMELLAE	CUMULUS, LAMELLAE	CUMULUS, LAMELLAE	CUMULUS, LAMELLAE	CUMULUS, LAMELLAE	CUMULUS, HOST	CUMULUS, HOST	CUMULUS, HOST	CUMULUS, HOST	CUMULUS, HOST
Lithology	GABBRONOR.	GABBRONOR.	GABBRONOR.	GABBRONOR.	GABBRONOR.	GABBRONOR.	GABBRONOR.	GABBRONOR.	GABBRONOR.	GABBRONOR.	GABBRONOR.	GABBRONOR.
Zone	GABBROIC	GABBROIC	GABBROIC	GABBROIC	GABBROIC	GABBROIC	GABBROIC	GABBROIC	GABBROIC	GABBROIC	GABBROIC	GABBROIC
Subzone	A	A	A	A	A	A	A	A	A	A	A	A
Strat. ht (m)	2859	2859	2859	2859	2859	2859	2859	2859	2859	2859	2859	2859
SiO2	52.08	52.51	52.09	52.44	52.50	52.44	52.29	51.58	52.23	51.95	51.42	51.40
TiO2	.33	.32	.34	.36	.30	.32	.32	.23	.17	.21	.19	.18
Al2O3	1.52	1.31	1.27	1.27	1.25	1.24	1.27	.69	.61	.65	.66	.66
Cr2O3	<.03	<.03	<.03	<.03	<.03	<.03	<.03	<.03	<.03	<.03	<.03	<.03
FeO	12.85	11.80	11.95	11.97	11.03	11.87	11.72	27.80	27.82	28.17	27.74	27.69
MnO	.36	.30	.31	.29	.26	.27	.26	.63	.61	.60	.58	.66
NiO	.05	.04	.05	<.03	.04	<.03	.04	.05	.04	<.03	.04	<.03
MgO	12.86	12.60	12.83	12.90	12.86	12.91	12.45	18.01	18.29	18.26	18.05	18.09
CaO	19.05	20.14	20.91	21.07	21.17	21.05	21.01	1.02	.72	.96	.91	.96
Na2O	.30	.32	.31	.33	.32	.32	.34	<.02	<.02	<.02	.02	<.02
Total	99.39	99.33	100.06	100.61	99.74	100.44	99.71	100.01	100.49	100.79	99.61	99.65
Atomic proportions												
Oxygens	6.0	6.0	6.0	6.0	6.0	6.0	6.0	6.0	6.0	6.0	6.0	6.0
Si	1.974	1.986	1.965	1.966	1.977	1.969	1.976	1.978	1.988	1.977	1.979	1.977
Ti	.009	.009	.010	.010	.009	.009	.009	.007	.005	.006	.005	.005
Al	.068	.058	.056	.056	.055	.055	.057	.031	.028	.029	.030	.030
Fe	.407	.373	.377	.375	.347	.373	.370	.892	.886	.896	.893	.891
Mn	.011	.010	.010	.009	.008	.009	.008	.020	.020	.019	.019	.022
Ni	.002	.001	.002	-	.001	-	.001	.001	.001	-	.001	-
Mg	.726	.710	.722	.721	.722	.723	.701	1.030	1.037	1.036	1.035	1.038
Ca	.774	.816	.845	.846	.854	.847	.851	.042	.029	.039	.038	.040
Na	.022	.023	.023	.024	.023	.024	.025	-	-	-	.002	-
Total	3.993	3.987	4.008	4.008	3.998	4.007	3.999	4.000	3.994	4.003	4.002	4.002
mg number	64	66	66	66	68	66	65	54	54	54	54	54
Mg'	38	37	37	37	38	37	37	53	53	53	53	53
Fe'	21	20	19	19	18	19	19	45	45	45	45	45
Ca'	41	43	44	44	44	44	44	2	2	2	2	2

Sample no.	84770055	84770055	84770055	84770055	84770055	84770055	84770055	84770055	84770055	84770055	84770055	84770055
Analysis no.	59554	59555	59556	59557	59558	59559	59560	59561	59562	59563	59564	59565
Mineral	INVERTED PIGEONITE	INVERTED PIGEONITE	INVERTED PIGEONITE	INVERTED PIGEONITE	INVERTED PIGEONITE	INVERTED PIGEONITE	INVERTED PIGEONITE	INVERTED PIGEONITE	INVERTED PIGEONITE	INVERTED PIGEONITE	INVERTED PIGEONITE	INVERTED PIGEONITE
Description	CUMULUS, HOST	CUMULUS, HOST	CUMULUS, HOST	CUMULUS, HOST	CUMULUS, HOST	CUMULUS, LAMELLAE	CUMULUS, LAMELLAE	CUMULUS, LAMELLAE	CUMULUS, LAMELLAE	CUMULUS, LAMELLAE	CUMULUS, LAMELLAE	CUMULUS, LAMELLAE
Lithology	GABBRONOR.	GABBRONOR.	GABBRONOR.	GABBRONOR.	GABBRONOR.	GABBRONOR.	GABBRONOR.	GABBRONOR.	GABBRONOR.	GABBRONOR.	GABBRONOR.	GABBRONOR.
Zone	GABBROIC	GABBROIC	GABBROIC	GABBROIC	GABBROIC	GABBROIC	GABBROIC	GABBROIC	GABBROIC	GABBROIC	GABBROIC	GABBROIC
Subzone	A	A	A	A	A	A	A	A	A	A	A	A
Strat. ht (m)	2859	2859	2859	2859	2859	2859	2859	2859	2859	2859	2859	2859
SiO2	51.57	51.84	51.61	51.77	51.31	52.21	52.37	51.66	52.12	52.40	52.22	52.21
TiO2	.24	.19	.21	.20	.20	.34	.34	.37	.31	.32	.30	.31
Al203	.77	.70	.61	.67	.66	1.28	1.24	1.52	1.30	1.18	1.23	1.29
Cr203	<.03	<.03	<.03	<.03	<.03	<.03	<.03	<.03	<.03	<.03	<.03	<.03
FeO	27.59	27.70	27.47	27.84	27.50	11.64	11.58	12.32	11.65	11.77	11.23	11.88
MnO	.60	.58	.62	.60	.65	.33	.31	.25	.28	.28	.28	.26
NiO	.05	.03	.04	<.03	<.03	<.03	<.03	.03	<.03	<.03	<.03	.03
MgO	17.83	18.04	18.16	18.16	18.07	12.66	12.66	12.76	12.71	12.66	12.66	12.63
CaO	1.10	1.00	.95	.98	.97	21.01	20.94	20.29	20.73	20.82	20.94	20.79
Na2O	<.02	.03	<.02	.02	<.02	.31	.33	.35	.33	.33	.34	.36
Total	99.74	100.10	99.68	100.25	99.35	99.78	99.77	99.56	99.43	99.76	99.20	99.76
Atomic proportions												
Oxygens	6.0	6.0	6.0	6.0	6.0	6.0	6.0	6.0	6.0	6.0	6.0	6.0
Si	1.980	1.983	1.982	1.979	1.978	1.972	1.976	1.959	1.974	1.978	1.979	1.973
Ti	.007	.006	.006	.006	.006	.010	.010	.010	.009	.009	.009	.009
Al	.035	.032	.027	.030	.030	.057	.055	.068	.058	.052	.055	.057
Fe	.886	.886	.882	.890	.887	.368	.365	.391	.369	.372	.356	.376
Mn	.019	.019	.020	.019	.021	.010	.010	.008	.009	.009	.009	.008
Ni	.002	.001	.001	-	-	-	-	.001	-	-	-	.001
Mg	1.021	1.028	1.040	1.035	1.038	.713	.712	.722	.717	.712	.715	.711
Ca	.045	.041	.039	.040	.040	.850	.847	.825	.841	.842	.850	.842
Na	-	.002	-	.001	-	.023	.024	.026	.024	.024	.025	.026
Total	3.995	3.997	3.998	4.001	4.001	4.002	3.999	4.009	4.001	3.999	3.997	4.003
mg number	54	54	54	54	54	66	66	65	66	66	67	65
Mg'	53	53	53	53	53	37	37	37	37	37	37	37
Fe'	45	45	45	45	45	19	19	20	19	19	19	19
Ca'	2	2	2	2	2	44	44	43	44	44	44	44

Sample no.	84770055	84770055	84770055	84770055	84770055	84770055	84770055	84770055	84770055	84770055	84770055	84770055
Analysis no.	59566	59567	59568	59569	59570	59571	59572	59573	59574	59575	59576	59577
Mineral	INVERTED PIGEONITE	INVERTED PIGEONITE	INVERTED PIGEONITE	INVERTED PIGEONITE	INVERTED PIGEONITE	INVERTED PIGEONITE	INVERTED PIGEONITE	INVERTED PIGEONITE	INVERTED PIGEONITE	INVERTED PIGEONITE	INVERTED PIGEONITE	INVERTED PIGEONITE
Description	CUMULUS, LAMELLAE	CUMULUS, LAMELLAE	CUMULUS, LAMELLAE	CUMULUS, HOST	CUMULUS, HOST	CUMULUS, HOST	CUMULUS, HOST	CUMULUS, HOST	CUMULUS, HOST	CUMULUS, HOST	CUMULUS, HOST	CUMULUS, HOST
Lithology	GABBRONOR.	GABBRONOR.	GABBRONOR.	GABBRONOR.	GABBRONOR.	GABBRONOR.	GABBRONOR.	GABBRONOR.	GABBRONOR.	GABBRONOR.	GABBRONOR.	GABBRONOR.
Zone	GABBROIC	GABBROIC	GABBROIC	GABBROIC	GABBROIC	GABBROIC	GABBROIC	GABBROIC	GABBROIC	GABBROIC	GABBROIC	GABBROIC
Subzone	A	A	A	A	A	A	A	A	A	A	A	A
Strat. ht (m)	2859	2859	2859	2859	2859	2859	2859	2859	2859	2859	2859	2859
SiO2	52.04	52.34	51.76	51.69	52.02	51.75	51.82	51.48	51.68	51.89	51.99	51.43
TiO2	.29	.28	.29	.20	.21	.19	.19	.20	.14	.20	.19	.22
Al2O3	1.25	1.31	1.22	.61	.64	.61	.61	.68	.55	.68	.54	.68
Cr2O3	<.03	<.03	<.03	<.03	<.03	<.03	<.03	<.03	.03	<.03	<.03	<.03
FeO	10.71	11.83	11.72	27.39	27.18	26.75	27.74	26.91	27.59	27.95	27.38	26.77
MnO	.27	.34	.30	.56	.60	.61	.57	.65	.63	.62	.58	.59
NiO	<.03	<.03	<.03	<.03	<.03	<.03	.04	.05	.03	<.03	.05	<.03
MgO	12.71	12.85	12.61	18.26	18.14	18.16	18.51	18.13	18.30	18.03	18.16	17.94
CaO	21.03	20.12	20.59	.88	.98	1.29	.99	.95	.85	1.07	.83	1.20
Na2O	.33	.32	.36	<.02	.03	<.02	<.02	<.02	<.02	<.02	<.02	<.02
Total	98.63	99.40	98.85	99.58	99.80	99.37	100.49	99.05	99.80	100.43	99.71	98.83

Atomic proportions

Oxygens	6.0	6.0	6.0	6.0	6.0	6.0		6.0	6.0	6.0	6.0	6.0	6.0
Si	1.980	1.980	1.973	1.984	1.990	1.988	Si	1.976	1.985	1.983	1.981	1.992	1.987
Ti	.008	.008	.008	.006	.006	.006	Ti	.006	.006	.004	.006	.005	.006
Al	.056	.059	.055	.028	.029	.027	Al	.027	.031	.025	.031	.024	.031
Fe	.341	.374	.374	.879	.870	.859	Cr	-	-	.001	-	-	-
Mn	.009	.011	.010	.018	.019	.020	Fe	.884	.868	.885	.892	.877	.865
Mg	.721	.725	.716	1.045	1.034	1.040	Mn	.018	.021	.020	.020	.019	.019
Ca	.857	.815	.841	.036	.040	.053	Ni	.001	.001	.001	-	.001	-
Na	.024	.023	.027	-	.002	-	Mg	1.052	1.042	1.047	1.026	1.037	1.033
Total	3.996	3.995	4.004	3.996	3.990	3.993	Ca	.041	.039	.035	.044	.034	.050
							Total	4.005	3.994	4.000	3.998	3.990	3.991
mg number	68	66	66	54	54	55							
Mg'	38	37	37	53	53	53	mg number	54	55	54	53	54	54
Fe'	18	20	19	45	45	44	Mg'	53	53	53	53	53	53
Ca'	44	43	44	2	2	3	Fe'	45	45	45	45	45	44
							Ca'	2	2	2	2	2	3

Sample no.	84770055	84770049	84770049	84770049	84770049	84770049	84770049	84770049	84770049	84770049	84770049	84770049
Analysis no.	59578	59579	59580	59581	59582	59583	59584	59585	59586	59587	59588	59589
Mineral	INVERTED PIGEONITE	INVERTED PIGEONITE	INVERTED PIGEONITE	INVERTED PIGEONITE	INVERTED PIGEONITE	INVERTED PIGEONITE	INVERTED PIGEONITE	INVERTED PIGEONITE	INVERTED PIGEONITE	INVERTED PIGEONITE	INVERTED PIGEONITE	INVERTED PIGEONITE
Description	CUMULUS, HOST	CUMULUS, LAMELLAE	CUMULUS, LAMELLAE	CUMULUS, LAMELLAE	CUMULUS, HOST	CUMULUS, HOST	CUMULUS, HOST	CUMULUS, LAMELLAE	CUMULUS, LAMELLAE	CUMULUS, LAMELLAE	CUMULUS, LAMELLAE	CUMULUS, HOST
Lithology	GABBRONOR.	GABBRONOR.	GABBRONOR.	GABBRONOR.	GABBRONOR.	GABBRONOR.	GABBRONOR.	GABBRONOR.	GABBRONOR.	GABBRONOR.	GABBRONOR.	GABBRONOR.
Zone	GABBROIC	GABBROIC	GABBROIC	GABBROIC	GABBROIC	GABBROIC	GABBROIC	GABBROIC	GABBROIC	GABBROIC	GABBROIC	GABBROIC
Subzone	A	A	A	A	A	A	A	A	A	A	A	A
Strat. ht (m)	2859	1998	1998	1998	1998	1998	1998	1998	1998	1998	1998	1998
SiO2	51.54	52.16	52.17	52.03	52.68	52.60	52.48	51.82	52.15	52.23	52.22	52.42
TiO2	.21	.40	.41	.43	.24	.22	.22	.35	.38	.39	.35	.21
Al2O3	.69	1.81	1.80	1.80	1.07	1.02	1.03	1.73	1.80	1.74	1.72	.94
Cr2O3	.03	<.03	<.03	<.03	<.02	<.03	<.03	<.03	<.03	<.03	<.03	<.03
FeO	27.37	9.58	9.32	9.07	22.15	22.12	22.31	9.07	9.41	8.88	9.37	21.79
MnO	.61	.28	.26	.26	.46	.48	.48	.29	.24	.25	.26	.48
NiO	<.03	<.03	.05	<.03	.04	.06	.06	.05	<.03	.05	.04	.08
MgO	18.37	14.07	13.85	14.09	22.07	21.91	22.08	14.10	14.07	14.44	14.26	21.89
CaO	1.06	20.76	20.95	21.00	1.11	.90	.93	20.96	21.01	21.00	20.90	1.04
Na2O	<.02	.28	.28	.26	<.02	.02	.02	.28	.27	.23	.25	<.01
Total	99.88	99.34	99.10	98.94	99.81	99.32	99.60	98.64	99.34	99.21	99.36	98.85

Atomic proportions

Oxygens	6.0	6.0	6.0	6.0	6.0	6.0		6.0	6.0	6.0	6.0	6.0	6.0
Si	1.975	1.958	1.962	1.958	1.968	1.974	Si	1.966	1.958	1.957	1.958	1.959	1.975
Ti	.006	.011	.012	.012	.007	.006	Ti	.006	.010	.011	.011	.010	.006
Al	.031	.080	.080	.080	.047	.045	Al	.045	.077	.080	.077	.076	.042
Cr	.001	-	-	-	-	-	Fe	.699	.286	.295	.279	.294	.686
Fe	.877	.301	.293	.285	.692	.694	Mn	.015	.009	.008	.008	.008	.015
Mn	.020	.009	.008	.008	.015	.015	Ni	.002	.001	-	.001	.001	.003
Ni	-	-	.002	-	.001	.002	Mg	1.233	.794	.787	.807	.797	1.229
Mg	1.049	.787	.776	.790	1.229	1.225	Ca	.037	.848	.845	.844	.840	.042
Ca	.044	.835	.844	.847	.044	.036	Na	.001	.020	.019	.017	.018	-
Na	-	.020	.021	.019	-	.001	Total	4.005	4.004	4.002	4.001	4.003	3.998
Total	4.003	4.001	3.997	4.000	4.002	3.998							
							mg number	64	73	73	74	73	64
mg number	54	72	73	73	64	64	Mg'	63	41	41	42	41	63
Mg'	53	41	41	41	63	63	Fe'	35	15	15	14	15	35
Fe'	45	16	15	15	35	35	Ca'	2	44	44	44	44	2
Ca'	2	43	44	44	2	2							

Sample no.	84770049	84770049	84770052	84770052	84770052	84770052	84770052	84770053	84770053	84770053	84770053	84770053
Analysis no.	59590	59592	59593	59594	59595	59598	59599	59601	59602	59603	59604	59605
Mineral	INVERTED PIGEONITE	INVERTED PIGEONITE	INVERTED PIGEONITE	INVERTED PIGEONITE	INVERTED PIGEONITE	INVERTED PIGEONITE	INVERTED PIGEONITE	INVERTED PIGEONITE	INVERTED PIGEONITE	INVERTED PIGEONITE	INVERTED PIGEONITE	INVERTED PIGEONITE
Description	CUMULUS, HOST	CUMULUS, HOST	CUMULUS, LAMELLAE	CUMULUS, LAMELLAE	CUMULUS, LAMELLAE	CUMULUS, HOST	CUMULUS, HOST	CUMULUS, HOST	CUMULUS, LAMELLAE	CUMULUS, LAMELLAE	CUMULUS, LAMELLAE	CUMULUS, HOST
Lithology	GABBRONOR.	GABBRONOR.	GABBRONOR.	GABBRONOR.	GABBRONOR.	GABBRONOR.	GABBRONOR.	GABBRONOR.	GABBRONOR.	GABBRONOR.	GABBRONOR.	GABBRONOR.
Zone	GABBROIC	GABBROIC	GABBROIC	GABBROIC	GABBROIC	GABBROIC	GABBROIC	GABBROIC	GABBROIC	GABBROIC	GABBROIC	GABBROIC
Subzone	A	A	A	A	A	A	A	A	A	A	A	A
Strat. ht (m)	1998	1998	2377	2377	2377	2377	2377	2551	2551	2551	2551	2551
SiO2	52.34	52.37	52.11	52.13	51.97	52.19	52.19	52.32	52.48	52.45	52.63	52.07
TiO2	.21	.23	.43	.43	.42	.24	.27	.25	.39	.40	.40	.27
Al2O3	.94	.98	1.50	1.42	1.50	.80	.75	.84	1.41	1.39	1.35	.72
Cr2O3	<.03	<.03	.02	<.03	<.03	<.03	<.03	<.03	<.03	.03	<.03	<.03
FeO	22.04	22.36	10.05	10.43	10.04	24.63	25.77	25.22	11.04	11.03	10.99	26.31
MnO	.42	.51	.27	.24	.23	.55	.55	.55	.26	.25	.27	.59
NiO	.06	.03	<.03	<.03	.04	.06	.04	.03	<.03	<.03	<.03	.04
MgO	21.91	21.95	13.08	13.33	13.11	19.95	20.03	20.12	13.25	13.07	13.19	19.20
CaO	1.21	1.10	21.29	21.40	21.05	.67	1.00	.96	21.41	21.30	21.40	1.10
Na2O	<.02	.02	.36	.36	.36	<.02	<.02	.02	.36	.38	.38	<.02
Total	99.14	99.54	99.11	99.73	98.74	99.10	100.60	100.29	100.61	100.30	100.62	100.31
Atomic proportions												
Oxygens	6.0	6.0	6.0	6.0	6.0	6.0	6.0	6.0	6.0	6.0	6.0	6.0
Si	1.969	1.965	1.968	1.961	1.970	1.985	1.968	1.973	1.961	1.966	1.966	1.976
Ti	.006	.007	.012	.012	.012	.007	.008	.007	.011	.011	.011	.008
Al	.042	.043	.067	.063	.067	.036	.033	.037	.062	.061	.059	.032
Cr	-	-	.001	-	-	-	-	-	-	.001	-	-
Fe	.694	.702	.318	.328	.318	.783	.813	.795	.345	.346	.343	.835
Mn	.013	.016	.009	.008	.007	.018	.018	.018	.008	.008	.009	.019
Ni	.002	.001	-	-	.001	.002	.001	.001	-	-	-	.001
Mg	1.229	1.228	.736	.748	.741	1.131	1.126	1.131	.738	.730	.734	1.086
Ca	.049	.044	.862	.863	.855	.027	.040	.039	.858	.855	.856	.045
Na	-	.001	.026	.026	.026	-	-	.001	.026	.027	.027	-
Total	4.004	4.007	3.999	4.008	3.998	3.990	4.007	4.002	4.010	4.006	4.007	4.001
mg number	64	64	70	69	70	59	58	59	68	68	68	57
Mg'	62	62	38	39	39	58	57	58	38	38	38	55
Fe'	36	36	17	17	17	40	41	40	18	18	18	42
Ca'	2	2	45	44	44	2	2	2	44	44	44	3

Sample no.	84770053	84770053	84770053	84770053	84770053	84770053	84770053	84770053
Analysis no.	59606	59607	59608	59609	59610	59612	59613	59614
Mineral	INVERTED PIGEONITE	INVERTED PIGEONITE	INVERTED PIGEONITE	INVERTED PIGEONITE	INVERTED PIGEONITE	INVERTED PIGEONITE	INVERTED PIGEONITE	INVERTED PIGEONITE
Description	CUMULUS, HOST	CUMULUS, HOST	CUMULUS, LAMELLAE	CUMULUS, LAMELLAE	CUMULUS, LAMELLAE	CUMULUS, HOST	CUMULUS, HOST	CUMULUS, HOST
Lithology	GABBRONOR.	GABBRONOR.	GABBRONOR.	GABBRONOR.	GABBRONOR.	GABBRONOR.	GABBRONOR.	GABBRONOR.
Zone	GABBROIC	GABBROIC	GABBROIC	GABBROIC	GABBROIC	GABBROIC	GABBROIC	GABBROIC
Subzone	A	A	A	A	A	A	A	A
Strat. ht (m)	2551	2551	2551	2551	2551	2551	2551	2551
SiO2	52.44	52.17	52.65	52.47	52.65	51.94	51.86	51.95
TiO2	.23	.22	.40	.39	.38	.22	.22	.15
Al2O3	.71	.67	1.39	1.41	1.33	.71	.70	.67
Cr2O3	<.03	<.03	<.03	<.03	<.03	<.03	<.03	<.03
FeO	26.75	26.68	12.05	11.22	11.09	26.21	26.52	26.30
MnO	.55	.60	.31	.32	.26	.56	.60	.54
NiO	.06	<.03	<.03	.05	<.03	<.03	<.03	<.03
MgO	19.66	19.43	13.25	12.90	13.05	19.28	19.23	19.27
CaO	.69	.87	20.91	21.43	21.25	.99	.96	.77
Na2O	<.02	<.02	.40	.37	.35	.02	.02	.02
Total	101.09	100.65	101.37	100.55	100.35	99.92	100.11	99.66

Atomic proportions

Oxygens	6.0	6.0	6.0	6.0	6.0	6.0		6.0	6.0
Si	1.974	1.974	1.959	1.965	1.971	1.976	Si	1.973	1.981
Ti	.007	.006	.011	.011	.011	.006	Ti	.006	.004
Al	.032	.030	.061	.062	.059	.032	Al	.032	.030
Fe	.842	.844	.375	.351	.347	.834	Fe	.844	.839
Mn	.017	.019	.010	.010	.008	.018	Mn	.019	.017
Ni	.002	-	-	.001	-	-	Mg	1.090	1.096
Mg	1.103	1.096	.735	.720	.728	1.093	Ca	.039	.031
Ca	.028	.035	.834	.860	.852	.040	Na	.002	.001
Na	-	-	.029	.027	.025	.001	Total	4.006	4.000
Total	4.004	4.005	4.014	4.007	4.002	4.002			
							mg number	56	57
mg number	57	56	66	67	68	57	Mg '	55	56
Mg '	56	55	38	37	38	56	Fe '	43	42
Fe '	43	43	19	18	18	42	Ca '	2	2
Ca '	1	2	43	45	44	2			

Regional traverse: average host and lamellae analyses of inverted pigeonite (GZ)

Sample no.	84770049	84770049	84770052	84770052	84770053	84770053	84770055	84770055
Analysis no.	59582	59581	59598	59595	59601	59602	59529	59526
Mineral	INVERTED PIGEONITE	INVERTED PIGEONITE	INVERTED PIGEONITE	INVERTED PIGEONITE	INVERTED PIGEONITE	INVERTED PIGEONITE	INVERTED PIGEONITE	INVERTED PIGEONITE
Description	CUMULUS, HOST	CUMULUS, LAMELLAE	CUMULUS, HOST	CUMULUS, LAMELLAE	CUMULUS, HOST	CUMULUS, LAMELLAE	CUMULUS, HOST	CUMULUS, LAMELLAE
Lithology	GABBRONOR.	GABBRONOR	GABBRONOR.	GABBRONOR.	GABBRONOR.	GABBRONOR.	GABBRONOR.	GABBRONOR.
Zone	GABBROIC	GABBROIC	GABBROIC	GABBROIC	GABBROIC	GABBROIC	GABBROIC	GABBROIC
Subzone	A	A	A	A	A	A	A	A
Strat. ht (m)	1998	1998	2377	2377	2551	2551	2859	2859
SiO2	52.48	52.11	52.19	52.07	52.11	52.56	51.80	52.53
TiO2	.22	.39	.25	.43	.22	.39	.20	.31
Al2O3	1.00	1.77	.77	1.47	.72	1.38	.65	1.29
Cr2O3	.01	.01	.01	.02	.01	.02	.02	.01
FeO	22.13	9.24	25.20	10.18	26.28	11.24	27.65	11.80
MnO	.47	.26	.55	.25	.57	.28	.61	.28
NiO	.06	.03	.05	.02	.03	.02	.03	.03
MgO	21.97	14.13	19.99	13.17	19.45	13.12	18.12	12.76
CaO	1.05	20.94	.84	21.25	.90	21.28	1.01	20.71
Na2O	.01	.26	.01	.36	.01	.37	.01	.33
Total	99.39	99.15	99.87	99.21	100.31	100.66	100.09	100.07
Atomic proportions								
Oxygens	6.0	6.0	6.0	6.0	6.0	6.0	6.0	6.0
Si	1.969	1.958	1.977	1.966	1.975	1.964	1.982	1.976
Ti	.006	.011	.007	.012	.006	.011	.006	.009
Al	.044	.078	.035	.066	.032	.061	.029	.057
Cr	-	-	-	.001	-	-	-	-
Fe	.694	.290	.798	.321	.833	.351	.884	.371
Mn	.015	.008	.018	.008	.018	.009	.020	.009
Ni	.002	.001	.002	.001	.001	.001	.001	.001
Mg	1.229	.791	1.128	.741	1.099	.731	1.033	.716
Ca	.042	.843	.034	.860	.037	.852	.041	.835
Na	.001	.019	.001	.026	.001	.027	.001	.024
Total	4.003	4.001	3.999	4.002	4.003	4.008	3.998	3.998
mg number	64	73	59	70	57	68	54	66
Mg'	63	41	57	39	56	38	53	37
Fe'	35	15	41	17	42	18	45	19
Ca'	2	44	2	44	2	44	2	44
Number of analyses averaged	6	7	2	3	7	6	31	30

Regional traverse: average bulk compositions of inverted pigeonite (GZ) by multiple point analyses

Sample no.	84770052	84770053	84770055
Mineral	INVERTED PIGEONITE	INVERTED PIGEONITE	INVERTED PIGEONITE
Description	CUMULUS, CORE	CUMULUS, CORE	CUMULUS, CORE
Lithology	Gabbronor.	Gabbronor.	Gabbronor.
Zone	Gabbroic	Gabbroic	Gabbroic
Subzone	A	A	A
Strat. ht (m)	2377	2551	2859
SiO2	52.16	52.23	51.96
TiO2	.29	.27	.22
Al2O3	.94	.90	.79
Cr2O3	.01	.01	.02
FeO	21.44	22.22	24.16
MnO	.47	.49	.54
NiO	.04	.03	.03
MgO	18.28	17.74	16.94
CaO	5.94	6.40	5.34
Na2O	.10	.11	.08
Total	99.67	100.40	100.08
Atomic proportions			
Oxygens	6.0	6.0	6.0
Si	1.975	1.972	1.981
Ti	.008	.008	.006
Al	.042	.040	.035
Cr	-	-	.001
Fe	.679	.702	.770
Mn	.015	.016	.017
Ni	.001	.001	.001
Mg	1.031	.998	.962
Ca	.241	.259	.218
Na	.007	.008	.006
Total	4.000	4.004	3.998
mg number	60	59	56
Mg'	53	51	49
Fe'	35	36	40
Ca'	12	13	11
Number of analyses averaged	5	13	61

Regional traverse: plagioclase (UZ and GZ)

Sample no.	85770179	85770179	84770102	84770102	84770102	84770102	84770003	84770003	84770045	84770045	84770044	84770047
Analysis no.	MU1	MU2	MU2	MU3	MU4	MU1	MU2	MU1	MU1	MU2	MU1	MU3
Mineral	PLAGIOCLA.	PLAGIOCLA.	PLAGIOCLA.	PLAGIOCLA.	PLAGIOCLA.	PLAGIOCLA.	PLAGIOCLA.	PLAGIOCLA.	PLAGIOCLA.	PLAGIOCLA.	PLAGIOCLA.	PLAGIOCLA.
Description	INTERCUMU.	INTERCUMU.	INTERCUMU.	INTERCUMU.	INTERCUMU.	INTERCUMU.	INTERCUMU.	INTERCUMU.	INTERCUMU.	INTERCUMU.	INTERCUMU.	INTERCUMU.
Lithology	OLIVINE GABBRONOR. CHILL	OLIVINE GABBRONOR. CHILL	GABBRONOR.	GABBRONOR.	GABBRONOR.	GABBRONOR.	OLIVINE WEBSTERITE	OLIVINE WEBSTERITE	PORPHYRIT. GABBRONOR.	PORPHYRIT. GABBRONOR.	PORPHYRIT. PLAG-WEBSTERITE	NORITE-ORTHOPYRO. IN OPX LAYER
Zone	ULTRAMAFIC	ULTRAMAFIC	ULTRAMAFIC	ULTRAMAFIC	ULTRAMAFIC	ULTRAMAFIC	ULTRAMAFIC	ULTRAMAFIC	ULTRAMAFIC	ULTRAMAFIC	ULTRAMAFIC	ULTRAMAFIC
Subzone	A'	A'	A'	A'	A'	A'	A'	A'	I	I	I	I
Strat. ht (m)	1	1	2	2	2	2	174	174	1811	1811	1838	1839
SiO2	60.35	62.06	58.40	57.22	57.60	57.22	60.37	60.92	58.25	59.15	57.12	56.00
TiO2	.10	.03	-	-	-	.05	.09	.12	<.03	.09	.08	<.03
Al2O3	24.19	24.04	26.60	27.17	26.55	26.15	23.31	24.17	24.98	24.19	25.87	26.67
FeO	.28	.25	.23	.19	.20	.27	1.22	.15	.14	.13	.37	.15
MgO	<.02	<.02	-	-	-	.03	.40	<.02	.05	.06	.03	.11
CaO	6.50	6.05	7.48	8.34	7.65	8.80	5.14	5.55	7.81	6.57	8.71	9.94
BaO	.23	.17	.04	.03	.05	.16	.28	.09	.15	.10	<.04	<.04
Na2O	7.91	8.30	6.71	6.29	6.40	6.54	7.60	8.27	6.91	7.31	6.35	5.62
K2O	.41	.46	.57	.59	.71	.67	1.43	.83	.78	.59	.83	.40
Total	99.97	101.36	100.03	99.83	99.16	99.89	99.84	100.10	99.07	98.19	99.36	98.89
Atomic proportions												
Oxygens	8.0	8.0	8.0	8.0	8.0	8.0	8.0	8.0	8.0	8.0	8.0	8.0
Si	2.700	2.731	2.611	2.571	2.601	2.582	2.719	2.717	2.641	2.690	2.589	2.548
Ti	.003	.001	-	-	-	.002	.003	.004	-	.003	.003	-
Al	1.275	1.247	1.402	1.439	1.413	1.391	1.238	1.270	1.335	1.296	1.382	1.430
Fe	.010	.009	.009	.007	.008	.010	.046	.006	.005	.005	.014	.006
Mg	-	-	-	-	-	.002	.027	-	.003	.004	.002	.007
Ca	.312	.285	.358	.401	.370	.425	.248	.265	.379	.320	.423	.485
Ba	.004	.003	.001	.001	.001	.003	.005	.002	.003	.002	-	-
Na	.686	.708	.582	.548	.560	.572	.664	.715	.607	.644	.558	.496
K	.023	.026	.033	.034	.041	.039	.082	.047	.045	.034	.048	.023
Total	5.014	5.011	4.995	5.001	4.993	5.026	5.032	5.025	5.018	4.999	5.020	4.996
An	31	28	37	41	38	41	25	26	37	32	41	48
Ab	67	69	60	56	58	55	67	70	59	65	54	49
Or	2	3	3	3	4	4	8	4	4	3	5	3

Sample no.	84770047	84770047	84770048	84770048	84770048	84770049	84770049	84770050	84770051	84770052	84770053
Analysis no.	MU2	MU1	MU3	MU2	MU1	MU1	MU2	MU1	MU1	MU1	MU1
Mineral	PLAGIOCLA. IN OPX LAYER	PLAGIOCLA. IN NORITE	PLAGIOCLA.	PLAGIOCLA	PLAGIOCLA.	PLAGIOCLA.	PLAGIOCLA.	PLAGIOCLA.	PLAGIOCLA.	PLAGIOCLA.	PLAGIOCLA.
Description	INTERCUMU.	CUMULUS	CUMULUS	CUMULUS	CUMULUS	CUMULUS	CUMULUS	CUMULUS	CUMULUS	CUMULUS	CUMULUS
Lithology	NORITE-ORTHOPYRO.	NORITE-ORTHOPYRO.	GABBRONOR.	GABBRONOR.	GABBRONOR.	GABBRONOR.	GABBRONOR.	GABBRONOR.	GABBRONOR.	GABBRONOR.	GABBRONOR.
Zone	ULTRAMAFIC	ULTRAMAFIC	GABBROIC	GABBROIC	GABBROIC	GABBROIC	GABBROIC	GABBROIC	GABBROIC	GABBROIC	GABBROIC
Subzone	I	I	A	A	A	A	A	A	A	A	A
Strat. ht (m)	1839	1839	1851	1851	1851	1998	1998	2094	2248	2377	2551
SiO2	54.89	53.84	54.94	55.25	55.25	55.46	55.62	56.43	56.29	56.96	57.34
TiO2	.09	.11	.09	.04	<.03	<.03	.03	<.03	.10	.07	.11
Al2O3	27.32	27.92	26.56	26.88	26.89	27.06	26.79	26.64	26.42	26.13	26.28
FeO	.33	.40	.35	.47	.35	.48	.38	.38	.37	.33	.22
MgO	.08	<.02	.10	.23	<.02	.02	.09	.06	.13	<.02	<.02
CaO	10.53	11.60	9.94	10.05	10.15	10.20	9.61	9.44	9.25	9.09	8.73
BaO	.26	<.04	.07	.12	<.04	<.04	.08	.22	.19	<.04	<.04
Na2O	5.83	4.86	5.93	5.45	5.52	5.81	6.00	6.11	6.07	6.16	6.11
K2O	.40	.19	.43	.39	.44	.41	.36	.49	.44	.52	.54
Total	99.73	98.92	98.41	98.88	98.60	99.44	98.96	99.77	99.26	99.26	99.33
Atomic proportions											
Oxygens	8.0	8.0	8.0	8.0	8.0	8.0	8.0	8.0	8.0	8.0	8.0
Si	2.496	2.464	2.524	2.523	2.528	2.521	2.536	2.553	2.557	2.581	2.590
Ti	.003	.004	.003	.001	-	-	.001	-	.003	.002	.004
Al	1.464	1.506	1.438	1.447	1.450	1.450	1.440	1.421	1.415	1.396	1.399
Fe	.013	.015	.013	.018	.013	.018	.014	.014	.014	.013	.008
Mg	.005	-	.007	.016	-	.001	.006	.004	.009	-	-
Ca	.513	.569	.489	.492	.498	.497	.469	.458	.450	.441	.422
Ba	.005	-	.001	.002	-	-	.001	.004	.003	-	-
Na	.514	.431	.528	.483	.490	.512	.530	.536	.535	.541	.535
K	.023	.011	.025	.023	.026	.024	.021	.028	.025	.030	.031
Total	5.037	5.000	5.030	5.004	5.005	5.022	5.019	5.018	5.012	5.004	4.990
An	49	56	47	49	49	48	46	45	45	44	43
Ab	49	43	51	48	48	50	52	52	52	53	54
Or	2	1	2	3	3	2	2	3	3	3	3

Sample no.	84770054	84770055	84770057	84770059	84770059	84770060	84770061	84770061	84770062	84770062	84770062
Analysis no.	MU1	MU1	MU1	MU1	MU2	MU1	MU2	MU1	MU3	MU2	MU1
Mineral	PLAGIOCLA.	PLAGIOCLA.	PLAGIOCLA.	PLAGIOCLA.	PLAGIOCLA.	PLAGIOCLA.	PLAGIOCLA.	PLAGIOCLA.	PLAGIOCLA.	PLAGIOCLA.	PLAGIOCLA.
Description	CUMULUS	CUMULUS	CUMULUS	CUMULUS	CUMULUS	CUMULUS	CUMULUS	CUMULUS	CUMULUS	CUMULUS	CUMULUS
Lithology	GABBRONOR.	GABBRONOR.	GABBRONOR.	GABBRONOR.	GABBRONOR.	GABBRONOR.	GABBRONOR.	GABBRONOR.	GABBRONOR.	GABBRONOR.	GABBRONOR.
Zone	GABBROIC	GABBROIC	GABBROIC	GABBROIC	GABBROIC	GABBROIC	GABBROIC	GABBROIC	GABBROIC	GABBROIC	GABBROIC
Subzone	A	A	A	A	A	A	A	A	A	A	A
Strat. ht (m)	2692	2859	3052	3341	3341	3425	3553	3553	3676	3676	3676
SiO2	57.85	57.99	57.97	58.33	57.77	58.00	59.99	59.23	59.03	59.41	59.96
TiO2	.03	.10	<.03	.07	.12	.09	.08	<.03	.07	.07	.10
Al2O3	25.65	25.23	25.16	25.15	24.88	25.30	25.40	25.33	24.68	25.21	25.26
FeO	.32	.39	.34	.26	.31	.19	.25	.27	.19	.16	.29
MgO	<.02	.15	.03	<.02	<.02	<.02	.09	<.02	.07	<.02	.03
CaO	8.20	8.25	8.01	7.67	7.66	7.75	7.30	7.65	6.84	7.17	7.24
BaO	.10	.15	.10	.10	<.04	.13	.25	<.04	<.04	.08	.06
Na2O	6.30	6.46	6.65	7.02	6.84	7.13	7.09	6.72	7.42	7.29	7.26
K2O	.66	.54	.61	.60	.72	.75	.84	.65	.75	.72	.73
Total	99.11	99.26	98.87	99.20	98.30	99.34	101.29	99.85	99.05	100.11	100.93
Atomic proportions											
Oxygens	8.0	8.0	8.0	8.0	8.0	8.0	8.0	8.0	8.0	8.0	8.0
Si	2.619	2.624	2.632	2.638	2.637	2.625	2.656	2.653	2.667	2.657	2.660
Ti	.001	.003	-	.002	.004	.003	.003	-	.002	.002	.003
Al	1.369	1.346	1.346	1.341	1.338	1.349	1.326	1.337	1.314	1.329	1.321
Fe	.012	.015	.013	.010	.012	.007	.009	.010	.007	.006	.011
Mg	-	.010	.002	-	-	-	.006	-	.005	-	.002
Ca	.398	.400	.390	.372	.375	.376	.346	.367	.331	.344	.344
Ba	.002	.003	.002	.002	-	.002	.004	-	-	.001	.001
Na	.553	.567	.585	.616	.605	.626	.609	.584	.650	.632	.625
K	.038	.031	.035	.035	.042	.043	.047	.037	.043	.041	.041
Total	4.991	4.999	5.005	5.014	5.013	5.032	5.006	4.989	5.020	5.013	5.009
An	40	40	39	36	37	36	35	37	33	34	34
Ab	56	57	58	60	59	60	61	59	63	62	62
Or	4	3	3	4	4	4	4	4	4	4	4

Sample no.	84770063	84770064	84770065	84770066
Analysis no.	MU1	MU1	MU1	MU1
Mineral	PLAGIOCLA.	PLAGIOCLA.	PLAGIOCLA.	PLAGIOCLA.
Description	CUMULUS	CUMULUS	CUMULUS	CUMULUS
Lithology	GABBRONOR.	GABBRONOR.	GABBRONOR.	GABBRONOR.
Zone	GABBROIC	GABBROIC	GABBROIC	GABBROIC
Subzone	A	A	A	A
Strat. ht (m)	3798	3965	4125	4222
SiO2	58.44	58.46	59.15	60.13
TiO2	.06	<.03	.06	.04
Al2O3	25.26	24.87	24.36	23.97
FeO	.33	.25	.59	.18
MgO	.03	.11	.06	.19
CaO	7.64	7.54	6.28	6.21
BaO	.08	.05	.07	<.04
Na2O	6.73	7.03	7.56	7.58
K2O	.80	.75	.84	.76
Total	99.37	99.06	98.97	99.06
Atomic proportions				
Oxygens	8.0	8.0	8.0	8.0
Si	2.638	2.647	2.679	2.708
Ti	.002	-	.002	.001
Al	1.344	1.327	1.300	1.272
Fe	.012	.009	.022	.007
Mg	.002	.007	.004	.013
Ca	.370	.366	.305	.300
Ba	.001	.001	.001	-
Na	.589	.617	.664	.662
K	.046	.043	.049	.044
Total	5.005	5.019	5.025	5.007
An	37	36	30	30
Ab	59	60	65	66
Or	4	4	5	4

Regional traverse: alkali feldspar (UZ)

Sample no.	84770006	84770006	84770007	84770035	84770035	84770041	84770042
Analysis no.	MU1	MU2	MU1	MU1	MU2	MU1	MU1
Mineral	ALKALI FELDSPAR	ALKALI FELDSPAR	ALKALI FELDSPAR	ALKALI FELDSPAR	ALKALI FELDSPAR	ALKALI FELDSPAR	ALKALI FELDSPAR
Description	INTERCUMU.	INTERCUMU.	INTERCUMU.	INTERCUMU.	INTERCUMU.	INTERCUMU.	INTERCUMU.
Lithology	OLIVINE WEBSTERITE	OLIVINE WEBSTERITE	WEBSTERITE	OLIVINE WEBSTERITE	OLIVINE WEBSTERITE	WEBSTERITE	WEBSTERITE
Zone	ULTRAMAFIC	ULTRAMAFIC	ULTRAMAFIC	ULTRAMAFIC	ULTRAMAFIC	ULTRAMAFIC	ULTRAMAFIC
Subzone	A	A	A	G	G	H	H
Strat. ht (m)	268	268	285	1474	1474	1695	1723
SiO2	64.03	64.84	65.00	61.09	62.94	62.85	62.73
TiO2	.03	.11	.08	.10	.10	.11	.06
Al2O3	19.64	19.63	20.17	19.65	19.71	19.78	19.99
FeO	.14	.12	.18	.16	.07	<.09	.70
MgO	.03	.04	<.02	<.02	.03	.05	.19
CaO	.66	.79	1.47	.92	.94	1.61	2.07
BaO	.89	.87	.11	2.27	.96	.65	.50
Na2O	3.45	3.23	4.58	2.01	4.11	3.98	5.26
K2O	11.25	11.25	9.76	12.74	9.92	10.14	8.16
Total	100.12	100.88	101.35	98.94	98.78	99.17	99.66
Atomic proportions							
Oxygens	8.0	8.0	8.0	8.0	8.0	8.0	8.0
Si	2.934	2.944	2.918	2.889	2.916	2.903	2.876
Ti	.001	.004	.003	.004	.003	.004	.002
Al	1.061	1.050	1.067	1.095	1.076	1.077	1.080
Fe	.005	.005	.007	.006	.003	-	.027
Mg	.002	.003	-	-	.002	.003	.013
Ca	.032	.038	.071	.047	.047	.080	.102
Ba	.016	.015	.002	.042	.017	.012	.009
Na	.307	.284	.399	.184	.369	.356	.468
K	.658	.652	.559	.769	.586	.597	.477
Total	5.016	4.995	5.025	5.036	5.020	5.032	5.054
Or	65	66	54	74	58	57	45

Regional traverse: biotite (UZ and GZ)

Sample no.	84770045	84770045	84770094	84770094	84770053	84770055		84770055	84770059	84770059	84770060	84770060	84770061
Analysis no.	MU1	MU2	MU1	MU2	MU1	MU1		MU2	MU1	MU2	MU1	MU2	MU1
Mineral	BIOTITE	BIOTITE	BIOTITE	BIOTITE	BIOTITE	BIOTITE		BIOTITE	BIOTITE	BIOTITE	BIOTITE	BIOTITE	BIOTITE
Lithology	PORPHYRIT. GABBRONOR.	PORPHYRIT. GABBRONOR.	PORPHYRIT. PLAG-WEBSTERITE	PORPHYRIT. PLAG-WEBSTERITE	GABBRONOR.	GABBRONOR.		GABBRONOR.	GABBRONOR.	GABBRONOR.	GABBRONOR.	GABBRONOR.	GABBRONOR.
Zone	ULTRAMAFIC	ULTRAMAFIC	ULTRAMAFIC	ULTRAMAFIC	GABBROIC	GABBROIC		GABBROIC	GABBROIC	GABBROIC	GABBROIC	GABBROIC	GABBROIC
Subzone	I	I	I	I	A	A		A	A	A	A	A	A
Strat. ht (m)	1811	1811	1846	1846	2551	2859		2859	3341	3341	3425	3425	3553
SiO2	37.35	36.25	35.81	35.15	35.20	36.85		37.17	34.83	34.42	34.55	33.64	35.30
TiO2	5.11	5.10	4.58	5.53	4.31	3.03		3.23	3.22	3.77	3.46	3.36	4.79
Al2O3	12.72	12.66	12.92	12.64	12.97	13.82		14.24	13.87	13.52	13.11	12.75	13.05
Cr2O3	.37	.18	<.10	<.10	.10	<.10		<.10	<.10	<.10	<.10	<.10	<.10
FeO	15.12	13.62	17.87	17.15	24.80	18.28		14.43	22.61	25.02	24.95	27.74	25.46
MnO	<.10	.10	<.10	<.10	.33	<.10		<.10	.12	.15	.11	.12	<.10
NiO	.23	.20	.32	.26	.24	.22		.14	.12	.11	.10	<.03	.03
MgO	13.87	14.80	12.93	13.49	8.85	12.90		15.67	9.26	7.78	9.04	7.70	7.48
CaO	<.02	<.02	<.02	<.02	<.02	<.02		<.02	<.02	<.02	<.02	<.02	<.02
Na2O	.11	.05	.27	.10	.16	<.04		.05	.04	.25	<.04	<.04	.21
K2O	9.95	9.81	9.60	9.44	9.39	9.55		10.14	9.40	9.17	8.52	8.24	9.12
Total	94.83	92.77	94.30	93.76	96.35	94.65		95.07	93.47	94.19	93.84	93.55	95.44

Atomic proportions

Oxygens	22.0	22.0	22.0	22.0	22.0	22.0		22.0	22.0	22.0	22.0	22.0	22.0
Si	5.656	5.586	5.538	5.456	5.513	5.651	Si	5.585	5.554	5.518	5.531	5.486	5.573
Ti	.582	.591	.533	.645	.508	.349	Ti	.365	.386	.454	.417	.412	.569
Al	2.270	2.299	2.355	2.312	2.394	2.498	Al	2.522	2.607	2.554	2.473	2.451	2.428
Cr	.044	.022	-	-	.012	-	Fe	1.813	3.015	3.354	3.340	3.783	3.361
Fe	1.915	1.755	2.311	2.226	3.248	2.344	Mn	-	.016	.020	.015	.017	-
Mn	-	.013	-	-	.044	-	Ni	.017	.015	.014	.013	-	.004
Ni	.028	.025	.040	.032	.030	.027	Mg	3.509	2.201	1.859	2.157	1.872	1.760
Mg	3.131	3.399	2.980	3.121	2.066	2.948	Na	.015	.012	.078	-	-	.064
Na	.032	.015	.081	.030	.049	-	K	1.943	1.912	1.875	1.740	1.714	1.837
K	1.922	1.928	1.894	1.869	1.876	1.868	Total	15.769	15.719	15.727	15.686	15.734	15.595
Total	15.582	15.634	15.732	15.692	15.739	15.685							
							mg number	66	42	36	39	33	34
mg number	62	66	56	58	39	56	Ti'	17	11	12	11	10	14
Ti'	23	25	19	22	14	13							

Sample no.	84770062	84770062	84770063	84770063	84770064	84770065	84770065	84770066
Analysis no.	MU1	MU2	MU1	MU2	MU1	MU1	MU2	MU1
Mineral	BIOTITE	BIOTITE	BIOTITE	BIOTITE	BIOTITE	BIOTITE	BIOTITE	BIOTITE
Lithology	GABBRONOR.	GABBRONOR.	GABBRONOR.	GABBRONOR.	GABBRONOR.	GABBRONOR.	GABBRONOR.	GABBRONOR.
Zone	GABBROIC	GABBROIC	GABBROIC	GABBROIC	GABBROIC	GABBROIC	GABBROIC	GABBROIC
Subzone	A	A	A	A	A	A	A	A
Strat. ht (m)	3676	3676	3798	3798	3965	4125	4125	4222
SiO2	35.15	33.43	34.23	33.67	34.18	33.72	35.45	35.45
TiO2	4.15	4.15	3.50	3.92	5.76	4.10	3.98	4.12
Al2O3	13.18	13.13	13.50	13.75	13.37	13.85	14.35	14.18
Cr2O3	<.10	<.10	<.10	<.10	<.10	<.10	<.10	<.10
FeO	22.79	27.11	26.30	26.73	26.04	24.21	21.18	20.53
MnO	.11	.12	.18	.14	.17	.11	<.10	.10
NiO	.08	.11	<.03	.11	<.03	<.03	<.03	.04
MgO	9.14	7.73	7.79	7.72	6.90	8.99	10.11	11.26
CaO	<.02	.16	.47	.45	.05	.24	<.02	<.02
Na2O	<.04	.24	.06	.26	.21	.34	.49	<.04
K2O	9.39	8.01	8.20	7.95	9.78	8.63	9.85	10.06
Total	93.99	94.19	94.23	94.70	96.46	94.19	95.41	95.74

Atomic proportions

Oxygens	22.0	22.0	22.0	22.0	22.0	22.0		22.0	22.0
Si	5.576	5.399	5.491	5.390	5.396	5.379	Si	5.500	5.467
Ti	.495	.504	.422	.472	.684	.492	Ti	.464	.478
Al	2.464	2.499	2.552	2.594	2.488	2.604	Al	2.624	2.577
Fe	3.024	3.662	3.528	3.579	3.438	3.230	Fe	2.748	2.648
Mn	.015	.016	.024	.019	.023	.015	Mn	-	.013
Ni	.010	.014	-	.014	-	-	Ni	-	.005
Mg	2.161	1.861	1.863	1.842	1.624	2.137	Mg	2.338	2.588
Ca	-	.028	.081	.077	.008	.041	Na	.147	-
Na	-	.075	.019	.081	.064	.105	K	1.950	1.979
K	1.900	1.650	1.678	1.624	1.969	1.756	Total	15.772	15.756
Total	15.646	15.710	15.659	15.693	15.693	15.758			
							mg number	46	49
mg number	42	34	35	34	32	40	Ti'	14	15
Ti'	14	12	11	12	17	13			

Regional traverse: spinels (UZ and Eastern Munni Munni Dyke)

Sample no.	85770156	85770156	85770156	85770156	85770156	85770156	85770156	85770156	85770159	85770159	85770159	85770159	85770159	85770159
Analysis no.	MU1	MU2	MU3	MU4	MU5	MU6	MU7	MU8	MU1	MU2	MU3	MU4	MU5	MU6
Mineral	CHROMITE	CHROMITE	CHROMITE	CHROMITE	CHROMITE	CHROMITE	CHROMITE	CHROMITE	CHROMITE	CHROMITE	CHROMITE	CHROMITE	CHROMITE	CHROMITE
Description	CUMULUS, CORE	CUMULUS, CORE	CUMULUS, CORE	CUMULUS, CORE	CUMULUS, CORE	CUMULUS, CORE	CUMULUS, CORE	CUMULUS, CORE	CUMULUS, CORE	CUMULUS, CORE	CUMULUS, CORE	CUMULUS, CORE	CUMULUS, CORE	CUMULUS, CORE
Lithology	DUNITE-CHROMITITE	DUNITE-CHROMITITE	DUNITE-CHROMITITE	DUNITE-CHROMITITE	DUNITE-CHROMITITE	DUNITE-CHROMITITE	DUNITE-CHROMITITE	DUNITE-CHROMITITE	ORTHOPYRO.	ORTHOPYRO.	ORTHOPYRO.	ORTHOPYRO.	ORTHOPYRO.	ORTHOPYRO.
Zone	ULTRAMAFIC	ULTRAMAFIC	ULTRAMAFIC	ULTRAMAFIC	ULTRAMAFIC	ULTRAMAFIC	ULTRAMAFIC	ULTRAMAFIC	ULTRAMAFIC	ULTRAMAFIC	ULTRAMAFIC	ULTRAMAFIC	ULTRAMAFIC	ULTRAMAFIC
Subzone	F	F	F	F	F	F	F	F	I	I	I	I	I	I
Strat. ht (m)	1460	1460	1460	1460	1460	1460	1460	1460	1836	1836	1836	1836	1836	1836
SiO2	.52	.06	.28	<.04	.41	.11	.32	.27	.21	.17	.37	.18	.10	.06
TiO2	1.18	.95	1.18	.81	1.23	1.02	1.17	1.14	.15	.15	.14	.06	.13	.16
Al2O3	14.07	14.49	15.01	15.56	14.89	14.88	15.17	14.77	47.90	47.01	48.48	48.86	50.19	49.95
Cr2O3	47.21	48.22	48.85	47.34	48.02	47.99	48.06	47.51	15.09	14.48	13.69	13.59	12.65	12.14
Fe2O3	4.76	5.09	4.45	5.02	4.16	4.16	4.53	4.74	5.91	5.69	5.40	5.71	4.94	5.09
FeO	21.84	20.91	21.81	20.69	21.64	20.92	22.24	22.01	15.30	15.16	15.20	14.46	14.37	14.57
MnO	.16	.15	.13	<.10	.11	.11	.12	<.10	.10	.15	.11	.14	.10	<.10
MgO	8.66	8.87	9.27	9.16	9.16	8.84	8.95	8.80	16.15	15.53	16.04	16.36	16.48	16.32
ZnO	.34	.28	<.10	<.10	.17	.36	<.10	<.10	.12	.18	.30	.20	.19	<.10
CaO	<.02	.02	<.02	.03	.02	.03	<.02	<.02	.02	.04	.03	.02	.02	<.02
Total	98.75	99.04	100.98	98.61	99.82	98.42	100.56	99.25	100.95	98.56	99.76	99.57	99.17	98.29
Atomic proportions														
Oxygens	4.0	4.0	4.0	4.0	4.0	4.0	4.0	4.0	4.0	4.0	4.0	4.0	4.0	4.0
Cations	3.0	3.0	3.0	3.0	3.0	3.0	3.0	3.0	3.0	3.0	3.0	3.0	3.0	3.0
Si	.017	.002	.009	-	.013	.004	.010	.009	.006	.005	.010	.005	.003	.002
Ti	.029	.024	.029	.020	.030	.025	.029	.028	.003	.003	.003	.001	.003	.003
Al	.550	.564	.571	.604	.572	.581	.580	.573	1.537	1.546	1.566	1.576	1.615	1.620
Cr	1.238	1.259	1.246	1.232	1.238	1.257	1.232	1.236	.325	.319	.297	.294	.273	.264
Fe3+	.119	.126	.108	.124	.102	.104	.111	.117	.121	.119	.111	.118	.101	.105
Fe2+	.606	.577	.588	.570	.590	.580	.603	.606	.348	.354	.348	.331	.328	.335
Mn	.004	.004	.004	-	.003	.003	.003	-	.002	.004	.003	.003	.002	-
Mg	.428	.436	.446	.449	.445	.437	.433	.432	.655	.646	.655	.667	.671	.670
Zn	.008	.007	-	-	.004	.009	-	-	.002	.004	.006	.004	.004	-
Ca	-	.001	-	.001	.001	.001	-	-	.001	.001	.001	.001	.001	-
Total	3.000	3.000	3.000	3.000	3.000	3.000	3.000	3.000	3.000	3.000	3.000	3.000	3.000	3.000
mg number	41	43	43	44	43	43	42	42	65	65	65	67	67	67
Cr'	65	65	65	63	65	65	64	64	16	16	15	15	14	13
Al'	29	29	30	31	30	30	30	30	78	78	79	79	81	82
Fe3+'	6	6	5	6	5	5	6	6	6	6	6	6	5	5

Sample no.	84770132	84770132	84770132	84770132	84770132	84770132	84770074	84770074	84770074	84770074	84770074	84770074
Analysis no.	MU1	MU2	MU3	MU4	MU5	MU6	MU1	MU2	MU3	MU4	MU5	MU6
Mineral	CHROMITE	CHROMITE	CHROMITE	CHROMITE	CHROMITE	CHROMITE	CHROMITE	CHROMITE	CHROMITE	CHROMITE	CHROMITE	CHROMITE
Description	CUMULUS, CORE	CUMULUS, CORE	CUMULUS, CORE	CUMULUS, CORE	CUMULUS, CORE	CUMULUS, CORE	CUMULUS, CORE	CUMULUS, CORE	CUMULUS, CORE	CUMULUS, CORE	CUMULUS, CORE	CUMULUS, CORE
Lithology	GABBRONOR.	GABBRONOR.	GABBRONOR.	GABBRONOR.	GABBRONOR.	GABBRONOR.	PLAG-OL-ORTHOPYRO.	PLAG-OL-ORTHOPYRO.	PLAG-OL-ORTHOPYRO.	PLAG-OL-ORTHOPYRO.	PLAG-OL-ORTHOPYRO.	PLAG-OL-ORTHOPYRO.
Zone	EASTERN MUNNI	EASTERN MUNNI	EASTERN MUNNI	EASTERN MUNNI	EASTERN MUNNI	EASTERN MUNNI	EASTERN MUNNI	EASTERN MUNNI	EASTERN MUNNI	EASTERN MUNNI	EASTERN MUNNI	EASTERN MUNNI
	MUNNI DYKE	MUNNI DYKE	MUNNI DYKE	MUNNI DYKE	MUNNI DYKE	MUNNI DYKE	MUNNI DYKE	MUNNI DYKE	MUNNI DYKE	MUNNI DYKE	MUNNI DYKE	MUNNI DYKE
SiO2	.29	.42	<.04	.12	<.04	.23	.10	.26	.35	<.04	.21	.43
TiO2	.51	.95	.42	.54	.44	1.74	2.98	2.78	3.56	2.36	1.39	2.91
Al2O3	12.66	15.80	11.06	17.07	10.79	13.31	8.16	13.91	8.28	12.41	17.30	14.50
Cr2O3	48.62	43.76	53.15	40.50	51.19	39.92	42.39	42.22	39.15	41.47	43.64	42.73
Fe2O3	9.31	8.98	6.01	10.63	7.46	13.01	13.63	8.86	15.70	12.03	7.76	7.41
FeO	21.12	22.93	20.15	22.26	22.57	24.26	26.80	23.74	28.47	25.40	20.41	23.15
MnO	.31	<.10	<.10	.11	.10	.12	<.10	<.10	.16	.26	<.10	.19
MgO	7.73	8.69	9.05	8.21	7.33	7.47	6.00	8.67	5.53	6.87	10.52	9.35
ZnO	<.10	.15	.11	.21	.24	.10	<.10	.17	.17	.11	.17	<.10
CaO	<.02	.02	<.02	.02	<.02	<.02	.02	.02	<.02	<.02	<.02	<.02
Total	100.55	101.70	99.95	99.68	100.13	100.15	100.07	100.63	101.37	100.90	101.40	100.67
Atomic proportions												
Oxygens	4.0	4.0	4.0	4.0	4.0	4.0	4.0	4.0	4.0	4.0	4.0	4.0
Cations	3.0	3.0	3.0	3.0	3.0	3.0	3.0	3.0	3.0	3.0	3.0	3.0
Si	.010	.013	-	.004	-	.008	.003	.009	.012	-	.007	.014
Ti	.013	.023	.010	.013	.011	.044	.077	.068	.091	.059	.033	.071
Al	.490	.598	.433	.658	.428	.522	.331	.536	.333	.487	.645	.554
Cr	1.263	1.112	1.396	1.047	1.361	1.050	1.154	1.092	1.057	1.093	1.091	1.095
Fe3+	.230	.217	.150	.262	.189	.326	.353	.218	.403	.302	.185	.181
Fe2+	.580	.616	.560	.608	.635	.675	.772	.649	.813	.708	.540	.628
Mn	.009	-	-	.003	.003	.003	-	-	.005	.007	-	.005
Mg	.378	.416	.448	.400	.367	.370	.308	.423	.281	.341	.496	.452
Zn	-	.004	.003	.005	.006	.002	-	.004	.004	.003	.004	-
Ca	-	.001	-	.001	-	-	.001	.001	-	-	-	-
Total	3.000	3.000	3.000	3.000	3.000	3.000	3.000	3.000	3.000	3.000	3.000	3.000
mg number	39	40	44	40	37	35	29	39	26	33	48	42
Cr'	64	58	71	53	69	55	63	59	59	58	57	60
Al'	25	31	22	34	22	28	18	29	19	26	34	30
Fe3+'	11	11	7	13	9	17	19	12	22	16	9	10

Regional traverse: magnetite and ilmenite (GZ)

Sample no.	84770052	84770052	84770054	84770054	84770054	84770055	84770055	84770055	84770055	84770055	84770057	84770057
Analysis no.	58786	58791	59199	59201	59203	59205	59206	59207	59208	59209	59210	59212
Mineral	ILMENITE 1	ILMENITE 2	ILMENITE 1	MAGNETITE 1	ILMENITE 3	MAGNETITE 1	ILMENITE 1	ILMENITE 2	MAGNETITE 2	ILMENITE 3	ILMENITE 1	ILMENITE 2
Description	CUMULUS	CUMULUS	CUMULUS	CUMULUS	CUMULUS	CUMULUS	CUMULUS	CUMULUS	CUMULUS	CUMULUS	CUMULUS	CUMULUS
Lithology	GABBRONOR.	GABBRONOR.	GABBRONOR.	GABBRONOR.	GABBRONOR.	GABBRONOR.	GABBRONOR.	GABBRONOR.	GABBRONOR.	GABBRONOR.	GABBRONOR.	GABBRONOR.
Zone	GABBROIC	GABBROIC	GABBROIC	GABBROIC	GABBROIC	GABBROIC	GABBROIC	GABBROIC	GABBROIC	GABBROIC	GABBROIC	GABBROIC
Subzone	A	A	A	A	A	A	A	A	A	A	A	A
Strat. ht (m)	2377	2377	2692	2692	2692	2859	2859	2859	2859	2859	3052	3052
SiO2	.04	<.02	<.02	.04	<.02	.06	.02	<.02	.06	<.02	<.02	<.02
TiO2	50.31	48.93	48.87	.14	46.86	3.84	50.73	50.23	8.86	50.15	51.59	51.55
Al2O3	.06	<.02	<.02	.12	<.02	.96	<.02	<.02	1.71	<.02	<.02	<.02
V2O3	<.06	<.06	<.06	1.42	<.06	1.82	<.06	<.06	1.61	<.06	<.06	<.06
Cr2O3	<.03	<.03	<.03	.08	.04	.14	<.03	<.03	.20	<.03	<.03	<.03
Fe2O3	5.40	7.17	7.64	67.89	12.02	59.10	4.50	5.69	49.27	5.58	2.79	2.25
FeO	39.33	37.73	39.31	31.54	38.01	34.97	43.71	43.02	39.76	42.94	43.73	43.67
MnO	5.62	6.14	4.58	<.03	4.03	.21	1.83	2.01	.43	2.13	2.55	2.55
NiO	<.04	<.04	<.04	.10	<.04	.07	.04	.06	.12	<.04	<.04	<.04
MgO	.04	<.02	<.02	<.02	.03	<.02	.03	.03	<.02	<.02	.04	.02
ZnO	.07	<.06	<.06	<.07	<.06	<.06	<.06	<.06	<.06	<.06	<.06	.07
CaO	.09	.04	<.01	.05	<.01	<.01	<.01	<.01	<.01	<.01	<.01	<.01
Total	100.96	100.02	100.39	101.38	100.99	101.17	100.85	101.05	102.00	100.80	100.71	100.12

Atomic proportions

Oxygens	6.0	6.0	6.0	4.0	6.0	4.0	6.0	6.0	4.0	6.0	6.0	6.0
Cations	4.0	4.0	4.0	3.0	4.0	3.0	4.0	4.0	3.0	4.0	4.0	4.0
Si	.002	-	-	.001	-	.002	.001	-	.002	-	-	-
Ti	1.895	1.863	1.855	.004	1.772	.109	1.914	1.893	.247	1.894	1.947	1.957
Al	.004	-	-	.006	-	.043	-	-	.075	-	-	-
V	-	-	-	.043	-	.055	-	-	.048	-	-	-
Cr	-	-	-	.002	.002	.004	-	-	.006	-	-	-
Fe3+	.204	.273	.290	1.938	.455	1.676	.170	.215	1.374	.211	.105	.086
Fe2+	1.647	1.598	1.659	1.001	1.598	1.102	1.834	1.803	1.232	1.804	1.836	1.844
Mn	.238	.263	.196	-	.171	.007	.078	.085	.014	.091	.108	.109
Ni	-	-	-	.003	-	.002	.001	.002	.003	-	-	-
Mg	.003	-	-	-	.002	-	.002	.002	-	-	.003	.001
Zn	.003	-	-	-	-	-	-	-	-	-	-	.003
Ca	.005	.002	-	.002	-	-	Total 4.000	4.000	3.000	4.000	4.000	4.000
Total	4.000	4.000	4.000	3.000	4.000	3.000						
							Ti' 49	48	9	48	50	50
Ti'	51	50	49	0	46	4						

Sample no.	84770057	84770057	84770057	84770057	84770058	84770058	84770058	84770058	84770058	84770060	84770060	84770060
Analysis no.	59214	59215	59216	59217	59218	59220	59222	59223	59224	59225	59226	59227
Mineral	ILMENITE 3	MAGNETITE 3	MAGNETITE 4	ILMENITE 4	MAGNETITE 1	ILMENITE 2	ILMENITE 3	MAGNETITE 4	ILMENITE 4	MAGNETITE 1	ILMENITE 1	MAGNETITE 2
Description	CUMULUS	CUMULUS	CUMULUS	CUMULUS	CUMULUS	CUMULUS	CUMULUS	CUMULUS	CUMULUS	CUMULUS	CUMULUS	CUMULUS
Lithology	GABBRONOR.	GABBRONOR.	GABBRONOR.	GABBRONOR.	GABBRONOR.	GABBRONOR.	GABBRONOR.	GABBRONOR.	GABBRONOR.	GABBRONOR.	GABBRONOR.	GABBRONOR.
Zone	GABBROIC	GABBROIC	GABBROIC	GABBROIC	GABBROIC	GABBROIC	GABBROIC	GABBROIC	GABBROIC	GABBROIC	GABBROIC	GABBROIC
Subzone	A	A	A	A	A	A	A	A	A	A	A	A
Strat. ht (m)	3052	3052	3052	3052	3181	3181	3181	3181	3181	3425	3425	3425
SiO2	<.02	.03	.07	<.02	.09	.04	.05	.08	<.02	.06	<.02	.09
TiO2	51.63	5.34	.63	51.65	11.28	50.37	49.74	10.65	50.68	12.75	48.95	3.53
Al2O3	<.02	1.99	.19	<.02	1.95	<.02	<.02	2.16	<.02	2.30	<.02	.83
V2O3	<.06	1.43	2.47	<.06	1.28	<.06	<.06	1.31	<.06	1.13	<.06	1.54
Cr2O3	<.03	<.03	<.03	<.03	<.03	<.03	<.03	<.03	<.03	.11	<.03	.09
Fe2O3	2.33	56.41	65.45	3.20	44.79	5.03	4.74	44.80	3.23	39.14	6.30	58.78
FeO	43.71	36.83	31.96	43.28	41.90	42.43	42.01	40.83	42.93	42.02	40.96	33.99
MnO	2.63	.26	<.03	3.03	.69	2.70	2.69	.66	2.50	.84	2.90	.22
NiO	<.04	.06	.08	<.04	<.04	<.04	<.03	.04	<.04	<.04	<.04	.05
MgO	.03	<.02	<.02	.04	<.02	.05	.02	.03	.05	<.02	.03	.02
ZnO	<.06	<.06	<.06	<.05	<.06	.09	<.06	<.06	<.06	<.06	.06	<.07
CaO	<.01	<.01	.02	.02	.02	.01	.02	.03	.02	.02	.02	.03
Total	100.33	102.35	100.87	101.23	102.01	100.72	99.26	100.60	99.40	98.37	99.22	99.17

Atomic proportions

Oxygens	6.0	4.0	4.0	6.0	4.0	6.0		6.0	4.0	6.0	4.0	6.0	4.0
Cations	4.0	3.0	3.0	4.0	3.0	4.0		4.0	3.0	4.0	3.0	4.0	3.0
Si	-	.001	.003	-	.003	.002	Si	.002	.003	-	.002	-	.003
Ti	1.956	.149	.018	1.940	.313	1.903	Ti	1.907	.300	1.938	.366	1.879	.102
Al	-	.087	.009	-	.085	-	Al	-	.095	-	.103	-	.038
V	-	.042	.075	-	.038	-	V	-	.039	-	.035	-	.047
Fe3+	.089	1.571	1.875	.120	1.244	.190	Cr	-	-	-	.003	-	.003
Fe2+	1.841	1.140	1.018	1.807	1.294	1.783	Fe3+	.182	1.261	.123	1.123	.242	1.702
Mn	.112	.008	-	.128	.022	.115	Fe2+	1.791	1.277	1.826	1.340	1.748	1.094
Ni	-	.002	.002	-	-	-	Mn	.116	.021	.108	.027	.125	.007
Mg	.002	-	-	.003	-	.003	Ni	-	.001	-	-	-	.002
Zn	-	-	-	-	-	.003	Mg	.001	.002	.004	-	.002	.001
Ca	-	-	.001	.001	.001	.001	Zn	-	-	-	-	.002	-
Total	4.000	3.000	3.000	4.000	3.000	4.000	Ca	.001	.001	.001	.001	.001	.001
							Total	4.000	3.000	4.000	3.000	4.000	3.000
Ti'	50	5	1	50	11	49							
							Ti'	49	11	50	13	49	4

Sample no.	84770060	84770060	84770060	84770062	84770062	84770062	84770062	84770064	84770064	84770064	84770066	84770066
Analysis no.	59228	59229	59230	59231	59232	59233	59236	59238	59240	59242	59243	59244
Mineral	ILMENITE 2	ILMENITE 3	MAGNETITE 3	MAGNETITE 1	ILMENITE 1	ILMENITE 2	ILMENITE 3	ILMENITE 1	ILMENITE 2	ILMENITE 3	MAGNETITE 1	ILMENITE 1
Description	CUMULUS	CUMULUS	CUMULUS	CUMULUS	CUMULUS	CUMULUS	CUMULUS	CUMULUS	CUMULUS	CUMULUS	CUMULUS	CUMULUS
Lithology	GABBRONOR.	GABBRONOR.	GABBRONOR.	GABBRONOR.	GABBRONOR.	GABBRONOR.	GABBRONOR.	GABBRONOR.	GABBRONOR.	GABBRONOR.	GABBRONOR.	GABBRONOR.
Zone	GABBROIC	GABBROIC	GABBROIC	GABBROIC	GABBROIC	GABBROIC	GABBROIC	GABBROIC	GABBROIC	GABBROIC	GABBROIC	GABBROIC
Subzone	A	A	A	A	A	A	A	A	A	A	A	A
Strat. ht (m)	3425	3425	3425	3676	3676	3676	3676	3965	3965	3965	4222	4222
SiO2	.03	<.02	.08	.09	<.02	.03	<.02	<.02	<.02	<.02	.10	<.02
TiO2	47.71	48.05	7.89	8.52	47.96	49.58	48.21	48.60	47.86	47.92	4.10	47.32
Al2O3	<.02	<.02	2.26	1.62	<.02	.03	<.02	<.02	<.02	<.02	4.00	.06
V2O3	<.06	<.06	1.32	1.22	<.06	<.06	<.06	<.06	<.06	<.06	.70	<.06
Cr2O3	<.03	<.03	.09	<.03	<.03	.05	<.03	<.03	<.03	<.03	<.03	<.03
Fe2O3	8.04	7.95	50.56	50.76	8.42	6.57	9.09	8.33	8.45	7.90	56.61	8.04
FeO	40.21	40.13	38.57	39.71	41.35	42.78	41.34	41.23	40.55	40.76	35.99	40.27
MnO	2.49	2.93	.42	.33	1.68	1.75	1.89	2.30	2.34	2.20	.21	2.21
NiO	<.04	<.04	.05	.07	<.04	<.04	<.04	<.03	.04	<.04	<.04	<.04
MgO	.03	<.02	.04	<.02	.03	<.02	.05	.04	.04	.04	.02	.03
ZnO	<.06	.10	.32	<.06	<.06	.08	<.06	.07	<.06	<.06	<.06	<.06
CaO	.12	.01	<.01	<.01	.02	<.01	<.01	<.01	<.01	.03	<.01	<.01
Total	98.63	99.17	101.59	102.34	99.46	100.86	100.57	100.57	99.29	98.85	101.73	97.93

Atomic proportions

Oxygens	6.0	6.0	4.0	4.0	6.0	6.0		6.0	6.0	6.0	6.0	4.0	6.0
Cations	4.0	4.0	3.0	3.0	4.0	4.0		4.0	4.0	4.0	4.0	3.0	4.0
Si	.001	-	.003	.003	-	.001	Si	-	-	-	-	.004	-
Ti	1.843	1.847	.220	.237	1.838	1.873	Ti	1.828	1.842	1.838	1.848	.114	1.842
Al	-	-	.099	.071	-	.002	Al	-	-	-	-	.174	.004
V	-	-	.039	.036	-	-	V	-	-	-	-	.021	-
Cr	-	-	.003	-	-	.002	Fe3+	.345	.316	.325	.305	1.571	.313
Fe3+	.311	.306	1.413	1.412	.323	.248	Fe2+	1.743	1.738	1.732	1.748	1.110	1.743
Fe2+	1.727	1.716	1.198	1.228	1.763	1.797	Mn	.081	.098	.101	.096	.007	.097
Mn	.109	.127	.013	.010	.073	.074	Ni	-	-	.002	-	-	-
Ni	-	-	.001	.002	-	-	Mg	.004	.003	.003	.003	.001	.002
Mg	.002	-	.002	-	.002	-	Zn	-	.003	-	-	-	-
Zn	-	.004	.009	-	-	.003	Ca	-	-	-	.002	-	-
Ca	.007	.001	-	-	.001	-	Total	4.000	4.000	4.000	4.000	3.000	4.000
Total	4.000	4.000	3.000	3.000	4.000	4.000							
							Ti	47	47	47	47	4	47
Ti'	47	48	8	8	47	48							

Regional traverse: sulphides (UZ)

Sample no.	84770102	84770102	84770102	84770102	84770102	84770102	84770102	84770102	84770102	84770100	84770100	84770102
Analysis no.	59793	59794	59795	59796	59797	59798	59808	59809	59810	59812	59813	59814
Mineral	PYRRHOTITE	PYRRHOTITE	PENTLANDI.	CHALCOPYR.	PENTLANDI.	CHALCOPYR.	PYRRHOTITE	CHALCOPYR.	PENTLANDI.	CHALCOPYR.	PYRRHOTITE	PYRRHOTITE
Description	CORE	CORE	CORE	CORE	CORE	CORE	CORE	CORE	CORE	CORE	CORE	CORE
Lithology	GABBRONOR.	GABBRONOR.	GABBRONOR.	GABBRONOR.	GABBRONOR.	GABBRONOR.	GABBRONOR.	GABBRONOR.	GABBRONOR.	GABBRONOR.	GABBRONOR.	GABBRONOR.
Zone	ULTRAMAFIC	ULTRAMAFIC	ULTRAMAFIC	ULTRAMAFIC	ULTRAMAFIC	ULTRAMAFIC	ULTRAMAFIC	ULTRAMAFIC	ULTRAMAFIC	ULTRAMAFIC	ULTRAMAFIC	ULTRAMAFIC
Subzone	A'	A'	A'	A'	A'	A'	A'	A'	A'	A'	A'	A'
Strat. ht (m)	2	2	2	2	2	2	2	2	2	2	2	2
Cu	.04	.02	.12	33.92	.01	34.38	.01	31.44	<.01	34.30	.01	<.01
Ni	.40	.45	33.95	.18	33.68	<.01	.49	.02	34.18	<.01	.60	.63
Fe	60.32	60.01	30.72	31.85	29.99	31.71	60.98	32.09	31.13	32.60	61.88	60.89
Co	<.01	<.01	4.43	.04	5.19	<.01	<.01	<.01	4.88	<.01	.04	.04
Zn	<.01	<.01	.01	<.01	<.01	<.01	<.01	.02	<.01	<.01	<.01	<.01
As	<.03	<.03	<.03	<.03	<.03	<.03	<.03	.03	<.03	<.03	<.03	<.03
S	37.61	37.45	31.00	32.81	30.57	32.64	38.70	33.66	32.50	34.03	38.94	38.92
Total	98.37	97.93	100.23	98.80	99.44	98.73	100.19	97.25	102.68	100.92	101.46	100.48

Atomic proportions

Oxygens	.0	.0	.0	.0	.0	.0		.0	.0	.0	.0	.0	.0
Cu	-	-	.001	.250	-	.254	Cu	-	.233	-	.247	-	-
Ni	.003	.003	.266	.001	.267	-	Ni	.004	-	.260	-	.004	.005
Fe	.478	.477	.253	.268	.250	.267	Fe	.473	.271	.249	.267	.475	.471
Co	-	-	.035	-	.041	-	Co	-	-	.037	-	-	-
Zn	-	-	-	-	-	-	Zn	-	-	-	-	-	-
S	.519	.519	.445	.480	.443	.479	As	-	-	-	-	-	-
Total	1.000	1.000	1.000	1.000	1.000	1.000	S	.523	.495	.453	.486	.520	.524
							Total	1.000	1.000	1.000	1.000	1.000	1.000
Cu/(Cu+Ni)	.09	.06	.00	.99	.00	1.00							
(Fe+Ni+Cu)/S	.93	.93	1.17	1.08	1.17	1.09	Cu/(Cu+Ni)	.03	1.00	.00	1.00	.02	.00
							(Fe+Ni+Cu)/S	.91	1.02	1.12	1.06	.92	.91

Sample no.	84770100	84770100	84770094	84770094	84770094	84770094	84770094	85770238	85770238	85770238	85770238	85770238	85770238
Analysis no.	59815	59817	59819	59820	59823	59825	59827	59832	59833	59834	59835	59836	59837
Mineral	PENTLANDI.	CHALCOPYR.	PYRRHOTITE	PYRRHOTITE	CHALCOPYR.	CHALCOPYR.	PYRRHOTITE	PYRRHOTITE	PYRRHOTITE	PYRRHOTITE	CHALCOPYR.	CHALCOPYR.	CHALCOPYR.
Description	CORE	CORE	CORE	CORE	CORE	CORE	CORE	CORE	CORE	CORE	CORE	CORE	CORE
Lithology	GABBRONOR.	GABBRONOR.	PLAGIOCLA. WEBSTERITE	PLAGIOCLA. WEBSTERITE	PLAGIOCLA. WEBSTERITE	PLAGIOCLA. WEBSTERITE	PLAGIOCLA. WEBSTERITE	PLAGIOCLA. WEBSTERITE	PLAGIOCLA. WEBSTERITE	PLAGIOCLA. WEBSTERITE	PLAGIOCLA. WEBSTERITE	PLAGIOCLA. WEBSTERITE	PLAGIOCLA. WEBSTERITE
Zone	ULTRAMAFIC	ULTRAMAFIC	ULTRAMAFIC	ULTRAMAFIC	ULTRAMAFIC	ULTRAMAFIC	ULTRAMAFIC	ULTRAMAFIC	ULTRAMAFIC	ULTRAMAFIC	ULTRAMAFIC	ULTRAMAFIC	ULTRAMAFIC
Subzone	A'	A'	I	I	I	I	I	I	I	I	I	I	I
Strat. ht (m)	2	2	1846	1846	1846	1846	1846	1845.40	1845.40	1845.40	1845.40	1845.40	1845.40
Cu	<.01	32.10	.15	.18	32.26	32.91	.18	<.01	<.01	.02	34.33	34.08	34.65
Ni	32.33	<.01	.15	.24	<.02	<.02	.22	.50	.33	.43	<.01	<.01	.03
Fe	29.60	31.68	60.59	59.30	32.85	32.23	60.43	60.55	60.90	60.63	32.48	32.25	32.13
Co	6.42	<.01	<.01	<.01	<.02	<.01	<.02	<.01	<.01	<.01	<.01	<.01	<.01
Zn	<.01	.02	<.01	<.01	.04	.04	<.01	<.01	<.01	<.01	<.01	.03	.03
As	<.03	<.03	<.03	<.03	<.03	<.03	<.03	<.03	<.03	<.03	<.03	<.03	<.03
S	32.55	33.82	39.11	38.80	34.94	34.28	39.05	39.34	38.90	38.77	34.27	34.16	33.96
Total	100.90	97.62	99.99	98.52	100.08	99.46	99.87	100.39	100.13	99.85	101.08	100.51	100.80

Atomic proportions

Oxygens	.0	.0	.0	.0	.0	.0		.0	.0	.0	.0	.0	.0	.0
Cu	-	.237	.001	.001	.232	.239	Cu	.001	-	-	-	.247	.246	.250
Ni	.250	-	.001	.002	-	-	Ni	.002	.004	.002	.003	-	-	-
Fe	.240	.267	.470	.466	.269	.267	Fe	.469	.467	.472	.472	.265	.265	.264
Co	.049	-	-	-	-	-	Zn	-	-	-	-	-	-	-
Zn	-	-	-	-	-	-	S	.528	.529	.525	.525	.488	.489	.486
S	.460	.496	.528	.531	.498	.494	Total	1.000	1.000	1.000	1.000	1.000	1.000	1.000
Total	1.000	1.000	1.000	1.000	1.000	1.000								
							Cu/(Cu+Ni)	.43	.00	.00	.03	1.00	1.00	1.00
Cu/(Cu+Ni)	.00	1.00	.48	.42	1.00	1.00	(Fe+Ni+Cu)/S	.89	.89	.90	.90	1.05	1.05	1.06
(Fe+Ni+Cu)/S	1.06	1.02	.89	.88	1.01	1.02								

Detailed traverse across cycles 1–5 in subzones C and D (UZ): olivine

Sample no.	85770189	85770189	85770189	85770190	85770190	85770190	85770191	85770191	85770191	85770192	85770192	85770192
Analysis no.	57653	57654	57655	57658	57659	57660	57661	57662	57663	57664	57665	57666
Mineral	OLIVINE 3	OLIVINE 1	OLIVINE 4	OLIVINE 4	OLIVINE 5	OLIVINE 3	OLIVINE 2	OLIVINE 4	OLIVINE 5	OLIVINE 1	OLIVINE 3	OLIVINE 4
Description	CUMULUS, CORE	CUMULUS, CORE	CUMULUS, CORE	CUMULUS, CORE	CUMULUS, CORE	CUMULUS, CORE	CUMULUS, CORE	CUMULUS, CORE	CUMULUS, CORE	CUMULUS, CORE	CUMULUS, CORE	CUMULUS, CORE
Lithology	OLIVINE WEBSTERITE	OLIVINE WEBSTERITE	OLIVINE WEBSTERITE	OLIVINE WEBSTERITE	OLIVINE WEBSTERITE	OLIVINE WEBSTERITE	LHERZOLITE	LHERZOLITE	LHERZOLITE	LHERZOLITE	LHERZOLITE	LHERZOLITE
Zone	ULTRAMAFIC	ULTRAMAFIC	ULTRAMAFIC	ULTRAMAFIC	ULTRAMAFIC	ULTRAMAFIC	ULTRAMAFIC	ULTRAMAFIC	ULTRAMAFIC	ULTRAMAFIC	ULTRAMAFIC	ULTRAMAFIC
Subzone	C	C	C	C	C	C	C	C	C	C	C	C
Cycle no.	1	1	1	1	1	1	2	2	2	2	2	2
Strat. ht (m)	664	664	664	671	671	671	685	685	685	692	692	692
SiO2	38.42	38.23	38.38	38.78	38.71	38.77	38.51	38.71	38.50	38.91	38.82	38.93
FeO	19.75	19.69	20.13	19.67	19.83	20.08	18.79	18.38	18.26	18.78	18.28	18.21
MnO	.28	.27	.29	.29	.27	.28	.29	.28	.28	.28	.29	.30
NiO	.42	.46	.45	.48	.49	.47	.46	.44	.46	.46	.46	.45
MgO	41.16	40.78	40.94	41.26	41.39	41.23	41.78	41.53	41.63	41.84	41.83	41.88
CaO	.04	.04	.05	.03	.02	.03	.06	.05	.06	.04	.05	.05
Total	100.07	99.46	100.23	100.50	100.72	100.86	99.89	99.39	99.19	100.32	99.73	99.82
Trace elements in parts per million												
Ni	3268	3617	3543	3754	3857	3704	3617	3479	3605	3589	3594	3547
Atomic proportions												
Oxygens	4.0	4.0	4.0	4.0	4.0	4.0	4.0	4.0	4.0	4.0	4.0	4.0
Si	.989	.991	.989	.993	.990	.991	.989	.996	.994	.994	.996	.997
Fe	.425	.427	.434	.421	.424	.429	.404	.396	.394	.401	.392	.390
Mn	.006	.006	.006	.006	.006	.006	.006	.006	.006	.006	.006	.006
Ni	.009	.010	.009	.010	.010	.010	.010	.009	.010	.009	.009	.009
Mg	1.580	1.575	1.572	1.575	1.578	1.571	1.600	1.593	1.601	1.594	1.599	1.599
Ca	.001	.001	.001	.001	.001	.001	.002	.001	.002	.001	.001	.001
Total	3.010	3.009	3.011	3.007	3.010	3.008	3.010	3.002	3.006	3.006	3.004	3.003
mg number	79	79	78	79	79	79	80	80	80	80	80	80

Cu contents for all olivine grains are < 45 ppm

Sample no.	85770193	85770193	85770193	85770194	85770194	85770195	85770195	85770195	85770195	85770196	85770196	85770196
Analysis no.	57667	57668	57669	57670	57671	57675	57676	57678	57679	57680	57681	57682
Mineral	OLIVINE 1	OLIVINE 2	OLIVINE 3	OLIVINE 3	OLIVINE 2	OLIVINE 1	OLIVINE 2	OLIVINE 4	OLIVINE 5	OLIVINE 3	OLIVINE 2	OLIVINE 1
Description	CUMULUS, CORE	CUMULUS, CORE	CUMULUS, CORE	CUMULUS, CORE	CUMULUS, CORE	CUMULUS, CORE	CUMULUS, CORE	CUMULUS, CORE	CUMULUS, CORE	CUMULUS, CORE	CUMULUS, CORE	CUMULUS, CORE
Lithology	LHERZOLITE	LHERZOLITE	LHERZOLITE	LHERZOLITE	LHERZOLITE	OLIVINE WEBSTERITE	OLIVINE WEBSTERITE	OLIVINE WEBSTERITE	OLIVINE WEBSTERITE	OLIVINE WEBSTERITE	OLIVINE WEBSTERITE	OLIVINE WEBSTERITE
Zone	ULTRAMAFIC	ULTRAMAFIC	ULTRAMAFIC	ULTRAMAFIC	ULTRAMAFIC	ULTRAMAFIC	ULTRAMAFIC	ULTRAMAFIC	ULTRAMAFIC	ULTRAMAFIC	ULTRAMAFIC	ULTRAMAFIC
Subzone	C	C	C	C	C	C	C	C	C	C	C	C
Cycle no.	2	2	2	2	2	2	2	2	2	2	2	2
Strat. ht (m)	700	700	700	703	703	707	707	707	707	714	714	714
SiO2	38.62	38.67	38.63	38.60	38.49	38.30	38.16	38.36	38.28	38.90	38.84	38.99
FeO	18.70	18.69	18.48	18.43	18.29	20.36	20.06	20.70	20.74	18.85	18.79	18.86
MnO	.27	.28	.29	.30	.28	.30	.29	.30	.28	.30	.29	.28
NiO	.46	.46	.45	.42	.45	.44	.46	.43	.44	.45	.45	.50
MgO	41.75	41.64	41.75	41.57	41.25	40.13	39.97	39.97	39.98	41.92	41.63	42.19
CaO	.05	.05	.06	.05	.04	.05	.03	.04	.05	.02	.03	.03
Total	99.85	99.79	99.65	99.37	98.81	99.58	98.97	99.80	99.78	100.44	100.03	100.86
Trace elements in parts per million												
Ni	3585	3620	3511	3324	3567	3473	3598	3378	3481	3539	3555	3940
Atomic proportions												
Oxygens	4.0	4.0	4.0	4.0	4.0	4.0	4.0	4.0	4.0	4.0	4.0	4.0
Si	.992	.993	.993	.995	.997	.994	.996	.995	.993	.993	.995	.991
Fe	.402	.402	.397	.397	.396	.442	.438	.449	.450	.402	.403	.401
Mn	.006	.006	.006	.006	.006	.007	.007	.007	.006	.006	.006	.006
Ni	.009	.010	.009	.009	.009	.009	.010	.009	.009	.009	.009	.010
Mg	1.598	1.594	1.600	1.597	1.593	1.552	1.554	1.545	1.546	1.595	1.590	1.599
Ca	.001	.001	.002	.001	.001	.001	.001	.001	.001	-	.001	.001
Total	3.008	3.006	3.007	3.005	3.003	3.006	3.004	3.005	3.006	3.007	3.005	3.008
mg number	80	80	80	80	80	78	78	77	77	80	80	80

Sample no.	85770196	85770197	85770197	85770197	85770197	85770198	85770198	85770198	85770198	85770201	85770201	85770201
Analysis no.	57683	57685	57686	57687	57688	57690	57691	57692	57693	57695	57696	57697
Mineral	OLIVINE 4	OLIVINE 1	OLIVINE 2	OLIVINE 3	OLIVINE 4	OLIVINE 1	OLIVINE 2	OLIVINE 3	OLIVINE 4	OLIVINE 3	OLIVINE 5	OLIVINE 4
Description	CUMULUS, CORE	CUMULUS, CORE	CUMULUS, CORE	CUMULUS, CORE	CUMULUS, CORE	CUMULUS, CORE	CUMULUS, CORE	CUMULUS, CORE	CUMULUS, CORE	CUMULUS, CORE	CUMULUS, CORE	CUMULUS, CORE
Lithology	OLIVINE WEBSTERITE	OLIVINE WEBSTERITE	OLIVINE WEBSTERITE	OLIVINE WEBSTERITE	OLIVINE WEBSTERITE	OLIVINE WEBSTERITE	OLIVINE WEBSTERITE	OLIVINE WEBSTERITE	OLIVINE WEBSTERITE	LHERZOLITE	LHERZOLITE	LHERZOLITE
Zone	ULTRAMAFIC	ULTRAMAFIC	ULTRAMAFIC	ULTRAMAFIC	ULTRAMAFIC	ULTRAMAFIC	ULTRAMAFIC	ULTRAMAFIC	ULTRAMAFIC	ULTRAMAFIC	ULTRAMAFIC	ULTRAMAFIC
Subzone	C	C	C	C	C	C	C	C	C	C	C	C
Cycle no.	2	2	2	2	2	2	2	2	2	3	3	3
Strat. ht (m)	714	728	728	728	728	749	749	749	749	784	784	784
SiO2	39.07	38.29	38.68	39.00	39.14	38.95	38.94	39.10	38.84	38.82	39.36	39.15
FeO	18.83	18.04	17.44	18.67	18.39	17.90	18.29	17.79	17.75	16.38	16.50	16.67
MnO	.28	.25	.24	.25	.25	.28	.26	.26	.25	.25	.25	.24
NiO	.47	.46	.49	.46	.53	.52	.49	.50	.47	.46	.45	.46
MgO	42.19	41.80	41.64	42.32	42.61	42.18	42.33	42.66	42.38	43.09	43.61	43.58
CaO	.04	.03	.02	.03	.03	.03	.04	.04	.03	.04	.05	.04
Total	100.88	98.88	98.53	100.73	100.94	99.87	100.35	100.35	99.73	99.04	100.23	100.15
Trace elements in parts per million												
Ni	3706	3625	3849	3651	4181	4112	3849	3900	3724	3627	3565	3611
Atomic proportions												
Oxygens	4.0	4.0	4.0	4.0	4.0	4.0	4.0	4.0	4.0	4.0	4.0	4.0
Si	.993	.991	1.000	.992	.992	.996	.992	.994	.994	.994	.995	.992
Fe	.400	.390	.377	.397	.390	.383	.390	.378	.380	.351	.349	.353
Mn	.006	.006	.005	.005	.005	.006	.006	.006	.005	.005	.005	.005
Ni	.010	.010	.010	.010	.011	.011	.010	.010	.010	.010	.009	.009
Mg	1.598	1.612	1.605	1.604	1.610	1.607	1.608	1.617	1.616	1.645	1.644	1.646
Ca	.001	.001	.001	.001	.001	.001	.001	.001	.001	.001	.001	.001
Total	3.007	3.009	3.000	3.008	3.008	3.004	3.007	3.006	3.006	3.006	3.004	3.008
mg number	80	81	81	80	81	81	80	81	81	82	82	82

Sample no.	85770201	85770202	85770202	85770202	85770202	85770203	85770203	85770203	85770203	85770204	85770204	85770204
Analysis no.	57698	57699	57700	57701	57702	57703	57704	57705	57706	57707	57708	57709
Mineral	OLIVINE 6	OLIVINE 3	OLIVINE 2	OLIVINE 1	OLIVINE 4	OLIVINE 4	OLIVINE 5	OLIVINE 1	OLIVINE 2	OLIVINE 2	OLIVINE 1	OLIVINE 3
Description	CUMULUS, CORE	CUMULUS, CORE	CUMULUS, CORE	CUMULUS, CORE	CUMULUS, CORE	CUMULUS, CORE	CUMULUS, CORE	CUMULUS, CORE	CUMULUS, CORE	CUMULUS, CORE	CUMULUS, CORE	CUMULUS, CORE
Lithology	LHERZOLITE	OLIVINE WEBSTERITE	OLIVINE WEBSTERITE	OLIVINE WEBSTERITE	OLIVINE WEBSTERITE	OLIVINE WEBSTERITE	OLIVINE WEBSTERITE	OLIVINE WEBSTERITE	OLIVINE WEBSTERITE	OLIVINE WEBSTERITE	OLIVINE WEBSTERITE	OLIVINE WEBSTERITE
Zone	ULTRAMAFIC	ULTRAMAFIC	ULTRAMAFIC	ULTRAMAFIC	ULTRAMAFIC	ULTRAMAFIC	ULTRAMAFIC	ULTRAMAFIC	ULTRAMAFIC	ULTRAMAFIC	ULTRAMAFIC	ULTRAMAFIC
Subzone	C	C	C	C	C	C	C	C	C	C	C	C
Cycle no.	3	3	3	3	3	3	3	3	3	3	3	3
Strat. ht (m)	784	791	791	791	791	798	798	798	798	827	827	827
SiO2	38.95	39.54	39.42	39.05	39.03	38.31	38.34	38.63	38.64	39.14	38.69	38.50
FeO	16.49	17.94	17.93	17.57	17.74	19.61	19.11	20.01	19.72	19.49	19.76	19.44
MnO	.24	.27	.25	.25	.26	.29	.27	.27	.28	.28	.28	.28
NiO	.49	.52	.51	.51	.48	.51	.51	.48	.51	.49	.45	.48
MgO	43.51	43.16	43.19	42.51	42.65	40.80	40.59	41.29	41.36	41.65	41.61	41.08
CaO	.04	.04	.05	.04	.04	.04	.03	.04	.04	.04	.03	.03
Total	99.72	101.47	101.35	99.93	100.20	99.56	98.85	100.71	100.55	101.10	100.82	99.81
Trace elements in parts per million												
Ni	3840	4099	4002	4016	3738	4009	4002	3745	4046	3885	3539	3792
Atomic proportions												
Oxygens	4.0	4.0	4.0	4.0	4.0	4.0	4.0	4.0	4.0	4.0	4.0	4.0
Si	.991	.994	.992	.996	.994	.992	.997	.989	.990	.995	.988	.992
Fe	.351	.377	.377	.375	.378	.424	.416	.429	.422	.414	.422	.419
Mn	.005	.006	.005	.005	.006	.006	.006	.006	.006	.006	.006	.006
Ni	.010	.011	.010	.010	.010	.011	.011	.010	.011	.010	.009	.010
Mg	1.650	1.617	1.621	1.616	1.618	1.574	1.573	1.576	1.579	1.578	1.585	1.579
Ca	.001	.001	.001	.001	.001	.001	.001	.001	.001	.001	.001	.001
Total	3.008	3.006	3.007	3.004	3.006	3.008	3.003	3.011	3.010	3.005	3.012	3.007
mg number	82	81	81	81	81	79	79	79	79	79	79	79

Sample no.	85770204	85770206	85770206	85770206	85770207	85770207	85770207	85770207	85770209	85770209	85770209	85770210
Analysis no.	57710	57711	57715	57717	57944	57945	57946	57947	57948	57949	57950	57951
Mineral	OLIVINE 4	OLIVINE 1	OLIVINE 4	OLIVINE 3	OLIVINE 1	OLIVINE 2	OLIVINE 3	OLIVINE 4	OLIVINE 1	OLIVINE 2	OLIVINE 3	OLIVINE 1
Description	CUMULUS, CORE	CUMULUS, CORE	CUMULUS, CORE	CUMULUS, CORE	CUMULUS, CORE	CUMULUS, CORE	CUMULUS, CORE	CUMULUS, CORE	CUMULUS, CORE	CUMULUS, CORE	CUMULUS, CORE	CUMULUS, CORE
Lithology	OLIVINE WEBSTERITE	LHERZOLITE	LHERZOLITE	LHERZOLITE	OLIVINE WEBSTERITE	OLIVINE WEBSTERITE	OLIVINE WEBSTERITE	OLIVINE WEBSTERITE	OLIVINE WEBSTERITE	OLIVINE WEBSTERITE	OLIVINE WEBSTERITE	LHERZOLITE
Zone	ULTRAMAFIC	ULTRAMAFIC	ULTRAMAFIC	ULTRAMAFIC	ULTRAMAFIC	ULTRAMAFIC	ULTRAMAFIC	ULTRAMAFIC	ULTRAMAFIC	ULTRAMAFIC	ULTRAMAFIC	ULTRAMAFIC
Subzone	C	D	D	D	D	D	D	D	D	D	D	D
Cycle no.	3	4	4	4	4	4	4	4	4	4	4	5
Strat. ht (m)	827	883	883	883	898	898	898	898	919	919	919	933
SiO2	38.53	38.82	38.84	38.90	39.08	38.83	38.20	38.74	38.95	38.79	38.75	39.01
FeO	19.15	17.66	17.98	17.89	18.38	18.06	17.92	18.06	18.60	18.53	18.48	17.35
MnO	.28	.27	.27	.29	.27	.27	.26	.28	.27	.26	.27	.26
NiO	.46	.47	.47	.46	.48	.47	.47	.47	.46	.47	.47	.47
MgO	41.36	42.45	42.47	42.80	42.64	42.35	41.63	42.56	41.87	42.16	42.38	42.91
CaO	.04	.05	.04	.03	.02	.04	.05	.05	.04	.05	.04	.05
Total	99.82	99.73	100.07	100.36	100.88	100.02	98.53	100.17	100.19	100.27	100.39	100.05
Trace elements in parts per million												
Ni	3618	3704	3660	3598	3745	3690	3658	3710	3609	3719	3671	3698
Atomic proportions												
Oxygens	4.0	4.0	4.0	4.0	4.0	4.0	4.0	4.0	4.0	4.0	4.0	4.0
Si	.992	.993	.991	.990	.991	.992	.991	.989	.995	.991	.989	.993
Fe	.412	.378	.384	.381	.390	.386	.389	.386	.398	.396	.394	.369
Mn	.006	.006	.006	.006	.006	.006	.006	.006	.006	.006	.006	.006
Ni	.010	.010	.010	.009	.010	.010	.010	.010	.009	.010	.010	.010
Mg	1.587	1.619	1.616	1.623	1.612	1.613	1.610	1.619	1.595	1.605	1.611	1.628
Ca	.001	.001	.001	.001	.001	.001	.001	.001	.001	.001	.001	.001
Total	3.008	3.006	3.008	3.010	3.009	3.007	3.006	3.011	3.004	3.008	3.011	3.007
mg number	79	81	81	81	81	81	81	81	80	80	80	82

Sample no.	85770210	85770210	85770211	85770211	85770211	85770211	85770212	85770212	85770212	85770212	85770212	85770213	85770213	85770213	85770213
Analysis no.	57952	57953	57954	57955	57956	57957	57958	57959	57960	57961	57962	57963	57964	57965	57966
Mineral	OLIVINE 2	OLIVINE 3	OLIVINE 1	OLIVINE 2	OLIVINE 3	OLIVINE 4	OLIVINE 1	OLIVINE 2	OLIVINE 5	OLIVINE 3	OLIVINE 4	OLIVINE 4	OLIVINE 5	OLIVINE 3	OLIVINE 1
Description	CUMULUS, CORE	CUMULUS, CORE	CUMULUS, CORE	CUMULUS, CORE	CUMULUS, CORE	CUMULUS, CORE	CUMULUS, CORE	CUMULUS, CORE	CUMULUS, CORE	CUMULUS, CORE	CUMULUS, CORE	CUMULUS, CORE	CUMULUS, CORE	CUMULUS, CORE	CUMULUS, CORE
Lithology	LHERZOLITE	LHERZOLITE	OLIVINE WEBSTERITE	OLIVINE WEBSTERITE	OLIVINE WEBSTERITE	OLIVINE WEBSTERITE	OLIVINE WEBSTERITE	OLIVINE WEBSTERITE	OLIVINE WEBSTERITE	OLIVINE WEBSTERITE	OLIVINE WEBSTERITE	OLIVINE WEBSTERITE	OLIVINE WEBSTERITE	OLIVINE WEBSTERITE	OLIVINE WEBSTERITE
Zone	ULTRAMAFIC	ULTRAMAFIC	ULTRAMAFIC	ULTRAMAFIC	ULTRAMAFIC	ULTRAMAFIC	ULTRAMAFIC	ULTRAMAFIC	ULTRAMAFIC	ULTRAMAFIC	ULTRAMAFIC	ULTRAMAFIC	ULTRAMAFIC	ULTRAMAFIC	ULTRAMAFIC
Subzone	D	D	D	D	D	D	D	D	D	D	D	D	D	D	D
Cycle no.	5	5	5	5	5	5	5	5	5	5	5	5	5	5	5
Strat. ht (m)	933	933	947	947	947	947	969	969	969	969	969	982	982	982	982
SiO2	38.99	38.96	39.42	39.30	39.00	39.08	38.72	38.88	38.73	38.79	38.34	37.81	37.84	38.07	38.06
FeO	17.35	17.36	17.07	16.95	16.34	16.90	21.47	20.92	21.58	21.55	21.31	21.10	21.06	21.17	21.28
MnO	.26	.27	.27	.26	.26	.25	.29	.31	.30	.31	.29	.30	.29	.30	.28
NiO	.47	.49	.52	.52	.53	.49	.42	.43	.41	.41	.43	.40	.41	.42	.43
MgO	42.88	42.87	43.36	43.63	43.16	43.09	39.91	40.11	40.21	40.22	39.77	39.41	39.29	39.70	39.68
CaO	.04	.06	.03	.04	.04	.03	.05	.04	.05	.05	.05	.05	.05	.05	.04
Total	100.00	100.01	100.68	100.69	99.34	99.83	100.86	100.68	101.28	101.35	100.18	99.06	98.94	99.71	99.77
Trace elements in parts per million															
Ni	3688	3819	4083	4079	4198	3823	3295	3349	3203	3260	3363	3143	3207	3264	3380
Atomic proportions															
Oxygens	4.0	4.0	4.0	4.0	4.0	4.0	4.0	4.0	4.0	4.0	4.0	4.0	4.0	4.0	4.0
Si	.993	.992	.995	.992	.995	.995	.996	.999	.992	.993	.993	.991	.993	.991	.990
Fe	.370	.370	.360	.358	.349	.360	.462	.449	.463	.461	.461	.463	.462	.461	.463
Mn	.006	.006	.006	.006	.006	.005	.006	.007	.007	.007	.006	.007	.006	.007	.006
Ni	.010	.010	.011	.011	.011	.010	.009	.009	.008	.009	.009	.008	.009	.009	.009
Mg	1.628	1.628	1.632	1.641	1.642	1.634	1.530	1.536	1.536	1.535	1.535	1.539	1.536	1.540	1.539
Ca	.001	.002	.001	.001	.001	.001	.001	.001	.001	.001	.001	.001	.001	.001	.001
Total	3.007	3.007	3.005	3.008	3.004	3.005	3.004	3.001	3.007	3.006	3.006	3.009	3.007	3.009	3.009
mg number	81	81	82	82	82	82	77	77	77	77	77	77	77	77	77

Detailed traverse across cycles 1–5 in subzones C and D (UZ): clinopyroxene

Sample no.	85770188	85770188	85770188	85770188	85770189	85770190	85770190	85770190	85770191	85770191	85770191	85770191
Analysis no.	56480	56481	56483	56484	56495	56505	56507	56508	56509	56510	56518	56519
Mineral	CLINOPYRO.	CLINOPYRO.	CLINOPYRO.	CLINOPYRO.	CLINOPYRO.	CLINOPYRO.	CLINOPYRO.	CLINOPYRO.	CLINOPYRO.	CLINOPYRO.	CLINOPYRO.	CLINOPYRO.
	1	2	3	4	2	1	2	3	1	2	3	5
Description	CUMULUS, CORE	CUMULUS, CORE	CUMULUS, CORE	CUMULUS, CORE	CUMULUS, CORE	CUMULUS, CORE	CUMULUS, CORE	CUMULUS, CORE	CUMULUS, CORE	CUMULUS, CORE	CUMULUS, CORE	CUMULUS, CORE
Lithology	WEBSTERITE	WEBSTERITE	WEBSTERITE	WEBSTERITE	OLIVINE WEBSTERITE	OLIVINE WEBSTERITE	OLIVINE WEBSTERITE	OLIVINE WEBSTERITE	LHERZOLITE	LHERZOLITE	LHERZOLITE	LHERZOLITE
Zone	ULTRAMAFIC	ULTRAMAFIC	ULTRAMAFIC	ULTRAMAFIC	ULTRAMAFIC	ULTRAMAFIC	ULTRAMAFIC	ULTRAMAFIC	ULTRAMAFIC	ULTRAMAFIC	ULTRAMAFIC	ULTRAMAFIC
Subzone	C	C	C	C	C	C	C	C	C	C	C	C
Cycle no.	1	1	1	1	1	1	1	1	2	2	2	2
Strat. ht (m)	650	650	650	650	664	671	671	671	685	685	685	685
SiO2	53.55	52.83	53.00	53.85	53.23	53.20	53.29	52.69	52.94	52.88	53.63	53.41
TiO2	.27	.25	.27	.26	.14	.19	.16	.17	.20	.19	.18	.17
Al2O3	1.61	1.55	1.56	1.52	.87	.88	.82	1.18	1.11	.90	.96	1.14
Cr2O3	.06	.04	.06	.07	.21	.26	.27	.25	.21	.20	.16	.19
FeO	6.50	6.35	6.13	6.71	5.42	5.33	5.17	5.12	5.08	4.90	5.10	5.21
MnO	.21	.19	.21	.20	.19	.21	.17	.15	.23	.17	.17	.14
NiO	.08	<.03	.08	.09	.05	.12	.09	.05	.07	.08	.07	.08
MgO	16.79	16.72	16.25	16.97	16.90	16.89	16.56	16.40	16.76	16.43	16.99	17.08
CaO	21.22	21.45	21.43	20.26	22.13	22.10	22.32	22.77	21.94	22.71	22.05	22.47
Na2O	.40	.46	.41	.39	.38	.38	.35	.40	.41	.40	.39	.43
Total	100.70	99.86	99.39	100.32	99.51	99.57	99.20	99.18	98.94	98.87	99.70	100.33
Atomic proportions												
Oxygens	6.0	6.0	6.0	6.0	6.0	6.0	6.0	6.0	6.0	6.0	6.0	6.0
Si	1.956	1.949	1.961	1.969	1.966	1.964	1.973	1.955	1.963	1.966	1.971	1.956
Ti	.007	.007	.007	.007	.004	.005	.005	.005	.006	.005	.005	.005
Al	.069	.067	.068	.065	.038	.038	.036	.052	.048	.040	.042	.049
Cr	.002	.001	.002	.002	.006	.008	.008	.007	.006	.006	.005	.006
Fe	.199	.196	.190	.205	.167	.165	.160	.159	.157	.152	.157	.160
Mn	.006	.006	.007	.006	.006	.007	.005	.005	.007	.005	.005	.004
Ni	.002	-	.002	.003	.001	.004	.003	.002	.002	.002	.002	.002
Mg	.914	.919	.896	.925	.930	.930	.914	.907	.926	.911	.931	.932
Ca	.831	.848	.849	.794	.876	.874	.885	.905	.872	.904	.868	.882
Na	.029	.033	.029	.028	.027	.027	.025	.029	.030	.029	.028	.030
Total	4.015	4.026	4.012	4.004	4.022	4.021	4.013	4.025	4.019	4.021	4.014	4.027
mg number	82	82	83	82	85	85	85	85	85	86	86	85
Mg'	47	47	46	48	47	47	47	46	47	46	48	47
Fe'	10	10	10	11	9	9	8	8	8	8	8	8
Ca'	43	43	44	41	44	44	45	46	45	46	44	45

Sample no.	85770191	85770192	85770192	85770193	85770193	85770193	85770194	85770194	85770194	85770195	85770196	85770196
Analysis no.	56521	56527	56533	56537	56538	56541	56548	56549	56550	56573	56582	56583
Mineral	CLINOPYRO. 4	CLINOPYRO. 1	CLINOPYRO. 3	CLINOPYRO. 1	CLINOPYRO. 2	CLINOPYRO. 3	CLINOPYRO. 2	CLINOPYRO. 3	CLINOPYRO. 4	CLINOPYRO. 1	CLINOPYRO. 1	CLINOPYRO. 2
Description	CUMULUS, CORE	CUMULUS, CORE	CUMULUS, CORE	CUMULUS, CORE	CUMULUS, CORE	CUMULUS, CORE	CUMULUS, CORE	CUMULUS, CORE	CUMULUS, CORE	CUMULUS, CORE	CUMULUS, CORE	CUMULUS, CORE
Lithology	LHERZOLITE	LHERZOLITE	LHERZOLITE	LHERZOLITE	LHERZOLITE	LHERZOLITE	LHERZOLITE	LHERZOLITE	LHERZOLITE	OLIVINE WEBSTERITE	OLIVINE WEBSTERITE	OLIVINE WEBSTERITE
Zone	ULTRAMAFIC	ULTRAMAFIC	ULTRAMAFIC	ULTRAMAFIC	ULTRAMAFIC	ULTRAMAFIC	ULTRAMAFIC	ULTRAMAFIC	ULTRAMAFIC	ULTRAMAFIC	ULTRAMAFIC	ULTRAMAFIC
Subzone	C	C	C	C	C	C	C	C	C	C	C	C
Cycle no.	2	2	2	2	2	2	2	2	2	2	2	2
Strat. ht (m)	685	692	692	700	700	700	703	703	703	707	714	714
SiO2	53.82	53.63	53.51	52.77	53.10	53.16	53.77	53.69	53.78	52.68	53.28	53.22
TiO2	.18	.16	.19	.17	.12	.19	.14	.15	.15	.23	.23	.20
Al2O3	1.22	.81	1.04	.97	.91	1.10	.81	.89	.80	1.32	1.54	1.52
Cr2O3	.18	.20	.23	.18	.13	.16	.33	.18	.24	.29	.44	.45
FeO	5.46	5.28	5.27	5.17	5.08	5.20	5.29	4.62	4.89	5.11	6.38	6.26
MnO	.15	.18	.19	.19	.21	.17	.20	.20	.18	.20	.19	.20
NiO	.06	.06	.07	.05	.05	.07	.08	.08	.07	.07	.08	.06
MgO	17.85	17.00	16.79	16.79	16.82	17.31	17.04	16.87	17.15	16.24	18.63	17.94
CaO	19.97	22.08	21.88	21.75	22.28	21.96	22.24	23.37	22.70	22.01	18.12	19.02
Na2O	.42	.36	.39	.37	.37	.35	.36	.36	.34	.48	.45	.46
Total	99.31	99.76	99.55	98.42	99.08	99.69	100.26	100.41	100.29	98.61	99.35	99.34

Atomic proportions

Oxygens	6.0	6.0	6.0	6.0	6.0	6.0	6.0	6.0	6.0	6.0	6.0	6.0
Si	1.976	1.972	1.971	1.967	1.967	1.957	1.970	1.964	1.968	1.962	1.957	1.959
Ti	.005	.004	.005	.005	.003	.005	.004	.004	.004	.006	.006	.006
Al	.053	.035	.045	.043	.040	.048	.035	.038	.034	.058	.067	.066
Cr	.005	.006	.007	.005	.004	.005	.010	.005	.007	.008	.013	.013
Fe	.168	.162	.162	.161	.158	.160	.162	.141	.150	.159	.196	.193
Mn	.005	.006	.006	.006	.007	.005	.006	.006	.006	.006	.006	.006
Ni	.002	.002	.002	.002	.002	.002	.002	.002	.002	.002	.002	.002
Mg	.977	.932	.922	.933	.929	.950	.931	.920	.935	.901	1.020	.984
Ca	.785	.870	.863	.869	.885	.866	.873	.916	.890	.878	.713	.750
Na	.030	.026	.028	.027	.027	.025	.026	.026	.024	.035	.032	.033
Total	4.005	4.016	4.012	4.017	4.021	4.024	4.017	4.023	4.020	4.016	4.013	4.012
mg number	85	85	85	85	85	86	85	87	86	85	84	84
Mg'	51	48	47	48	47	48	48	47	47	46	53	51
Fe'	8	8	9	8	8	8	8	7	8	8	10	10
Ca'	41	44	44	44	45	44	44	46	45	45	37	39

Sample no.	85770197	85770197	85770197	85770198	85770198	85770198	85770198	85770199	85770199	85770199	85770199	85770200
Analysis no.	56594	56596	56597	56603	56604	56605	56606	56608	56609	56610	56611	56612
Mineral	CLINOPYRO. 1	CLINOPYRO. 2	CLINOPYRO. 3	CLINOPYRO. 1	CLINOPYRO. 4	CLINOPYRO. 2	CLINOPYRO. 3	CLINOPYRO. 1	CLINOPYRO. 2	CLINOPYRO. 3	CLINOPYRO. 4	CLINOPYRO. 1
Description	CUMULUS, CORE	CUMULUS, CORE	CUMULUS, CORE	CUMULUS, CORE	CUMULUS, CORE	CUMULUS, CORE	CUMULUS, CORE	CUMULUS, CORE	CUMULUS, CORE	CUMULUS, CORE	CUMULUS, CORE	CUMULUS, CORE
Lithology	OLIVINE WEBSTERITE	OLIVINE WEBSTERITE	OLIVINE WEBSTERITE	OLIVINE WEBSTERITE	OLIVINE WEBSTERITE	OLIVINE WEBSTERITE	OLIVINE WEBSTERITE	LHERZOLITE	LHERZOLITE	LHERZOLITE	LHERZOLITE	LHERZOLITE
Zone	ULTRAMAFIC	ULTRAMAFIC	ULTRAMAFIC	ULTRAMAFIC	ULTRAMAFIC	ULTRAMAFIC	ULTRAMAFIC	ULTRAMAFIC	ULTRAMAFIC	ULTRAMAFIC	ULTRAMAFIC	ULTRAMAFIC
Subzone	C	C	C	C	C	C	C	C	C	C	C	C
Cycle no.	2	2	2	2	2	2	2	3	3	3	3	3
Strat. ht (m)	728	728	728	749	749	749	749	770	770	770	770	777
SiO2	53.14	52.84	52.70	53.21	53.69	53.36	53.10	52.68	53.09	53.79	53.26	53.68
TiO2	.20	.21	.20	.18	.17	.21	.24	.27	.33	.29	.35	.15
Al2O3	1.43	1.51	1.61	1.12	1.12	1.54	1.72	1.79	1.96	1.86	1.92	.90
Cr2O3	.53	.55	.58	.60	.55	.55	.55	.41	.45	.40	.39	.29
FeO	5.95	4.69	4.82	4.60	4.57	4.81	4.76	5.17	4.39	4.28	4.31	4.14
MnO	.16	.15	.17	.15	.17	.18	.14	.18	.12	.13	.18	.17
NiO	.07	.08	.07	.07	.06	.09	.06	.50	.08	.27	.08	.08
MgO	18.33	16.54	17.02	16.43	16.72	16.73	16.41	17.44	16.77	16.63	17.03	16.94
CaO	18.91	22.10	21.01	22.10	22.49	21.82	22.00	20.30	22.10	21.35	22.15	23.36
Na2O	.46	.53	.54	.53	.57	.56	.57	.56	.56	.55	.56	.36
Total	99.20	99.21	98.74	98.98	100.11	99.86	99.56	99.30	99.86	99.56	100.24	100.07
Atomic proportions												
Oxygens	6.0	6.0	6.0	6.0	6.0	6.0	6.0	6.0	6.0	6.0	6.0	6.0
Si	1.957	1.954	1.953	1.970	1.966	1.958	1.955	1.944	1.945	1.969	1.944	1.966
Ti	.006	.006	.006	.005	.005	.006	.007	.007	.009	.008	.009	.004
Al	.062	.066	.070	.049	.048	.066	.075	.078	.085	.080	.083	.039
Cr	.015	.016	.017	.017	.016	.016	.016	.012	.013	.012	.011	.008
Fe	.183	.145	.150	.142	.140	.148	.147	.160	.134	.131	.131	.127
Mn	.005	.005	.005	.005	.005	.006	.004	.005	.004	.004	.006	.005
Ni	.002	.002	.002	.002	.002	.003	.002	.015	.002	.008	.002	.002
Mg	1.006	.911	.940	.907	.912	.915	.901	.959	.916	.908	.927	.925
Ca	.746	.876	.834	.876	.882	.858	.868	.803	.868	.837	.866	.917
Na	.032	.038	.039	.038	.040	.040	.041	.040	.040	.039	.040	.026
Total	4.015	4.019	4.017	4.011	4.017	4.015	4.014	4.024	4.016	3.996	4.020	4.019
mg number	85	86	86	86	87	86	86	86	87	87	88	88
Mg'	52	47	49	47	47	47	47	50	48	48	48	47
Fe'	9	8	8	7	7	8	8	8	7	7	7	6
Ca'	39	45	43	46	46	45	45	42	45	45	45	47

Sample no.	85770200	85770200	85770200	85770201	85770201	85770201	85770202	85770202	85770202	85770203	85770203	85770203
Analysis no.	56613	56614	56616	56621	56625	56626	56737	56740	56741	56748	56749	56750
Mineral	CLINOPYRO. 2	CLINOPYRO. 3	CLINOPYRO. 5	CLINOPYRO. 1	CLINOPYRO. 2	CLINOPYRO. 3	CLINOPYRO. 1	CLINOPYRO. 2	CLINOPYRO. 3	CLINOPYRO. 1	CLINOPYRO. 2	CLINOPYRO. 3
Description	CUMULUS, CORE	CUMULUS, CORE	CUMULUS, CORE	CUMULUS, CORE	CUMULUS, CORE	CUMULUS, CORE	CUMULUS, CORE	CUMULUS, CORE	CUMULUS, CORE	CUMULUS, CORE	CUMULUS, CORE	CUMULUS, CORE
Lithology	LHERZOLITE	LHERZOLITE	LHERZOLITE	LHERZOLITE	LHERZOLITE	LHERZOLITE	OLIVINE WEBSTERITE	OLIVINE WEBSTERITE	OLIVINE WEBSTERITE	OLIVINE WEBSTERITE	OLIVINE WEBSTERITE	OLIVINE WEBSTERITE
Zone	ULTRAMAFIC	ULTRAMAFIC	ULTRAMAFIC	ULTRAMAFIC	ULTRAMAFIC	ULTRAMAFIC	ULTRAMAFIC	ULTRAMAFIC	ULTRAMAFIC	ULTRAMAFIC	ULTRAMAFIC	ULTRAMAFIC
Subzone	C	C	C	C	C	C	C	C	C	C	C	C
Cycle no.	3	3	3	3	3	3	3	3	3	3	3	3
Strat. ht (m)	777	777	777	784	784	784	791	791	791	798	798	798
SiO2	53.46	53.40	53.47	53.20	53.21	53.05	53.21	52.97	53.18	53.11	52.89	53.09
TiO2	.13	.11	.17	.21	.20	.24	.22	.23	.18	.18	.18	.17
Al2O3	.94	.80	1.01	1.29	1.35	1.81	1.40	1.58	1.11	.88	.92	.89
Cr2O3	.30	.28	.32	.58	.63	.61	.56	.54	.59	.19	.21	.23
FeO	4.92	3.70	4.51	4.68	4.47	4.62	5.28	5.58	4.55	5.66	5.60	5.78
MnO	.16	.23	.18	.16	.13	.18	.14	.19	.17	.17	.18	.23
NiO	.05	.03	.07	.08	.07	.08	.09	.13	.06	.08	.06	.07
MgO	17.67	17.04	17.27	16.95	17.43	16.87	17.29	17.66	16.83	16.84	16.64	16.85
CaO	21.44	23.47	22.43	22.18	21.46	21.92	20.64	20.12	22.12	22.26	21.90	21.90
Na2O	.34	.29	.37	.53	.54	.58	.50	.51	.47	.28	.31	.25
Total	99.41	99.34	99.80	99.86	99.49	99.96	99.34	99.51	99.27	99.66	98.89	99.47
Atomic proportions												
Oxygens	6.0	6.0	6.0	6.0	6.0	6.0	6.0	6.0	6.0	6.0	6.0	6.0
Si	1.967	1.967	1.963	1.954	1.955	1.945	1.960	1.950	1.963	1.962	1.967	1.964
Ti	.004	.003	.005	.006	.006	.007	.006	.006	.005	.005	.005	.005
Al	.041	.035	.044	.056	.059	.078	.061	.069	.048	.038	.040	.039
Cr	.009	.008	.009	.017	.018	.018	.016	.016	.017	.006	.006	.007
Fe	.151	.114	.138	.144	.137	.142	.163	.172	.140	.175	.174	.179
Mn	.005	.007	.006	.005	.004	.006	.004	.006	.005	.005	.006	.007
Ni	.002	.001	.002	.002	.002	.002	.003	.004	.002	.002	.002	.002
Mg	.969	.936	.945	.928	.955	.922	.949	.969	.926	.927	.922	.929
Ca	.845	.926	.882	.873	.845	.861	.815	.793	.875	.881	.873	.868
Na	.024	.021	.026	.038	.038	.041	.036	.036	.034	.020	.022	.018
Total	4.017	4.018	4.019	4.023	4.020	4.021	4.013	4.020	4.016	4.022	4.016	4.017
mg number	86	89	87	87	87	87	85	85	87	84	84	84
Mg'	49	47	48	48	49	48	49	50	48	47	47	47
Fe'	8	6	7	7	7	7	8	9	7	9	9	9
Ca'	43	47	45	45	44	45	43	41	45	44	44	44

Sample no.	85770204	85770204	85770204	85770205	85770205	85770205	85770205	85770205	85770206	85770206	85770206	85770207
Analysis no.	56757	56758	56759	56762	56763	56764	56765	56766	56772	56773	56774	56779
Mineral	CLINOPYRO. 1	CLINOPYRO. 2	CLINOPYRO. 3	CLINOPYRO. 1	CLINOPYRO. 2	CLINOPYRO. 3	CLINOPYRO. 4	CLINOPYRO. 5	CLINOPYRO. 1	CLINOPYRO. 2	CLINOPYRO. 3	CLINOPYRO. 1
Description	CUMULUS, CORE	CUMULUS, CORE	CUMULUS, CORE	CUMULUS, CORE	CUMULUS, CORE	CUMULUS, CORE	CUMULUS, CORE	CUMULUS, CORE	CUMULUS, CORE	CUMULUS, CORE	CUMULUS, CORE	CUMULUS, CORE
Lithology	OLIVINE WEBSTERITE	OLIVINE WEBSTERITE	OLIVINE WEBSTERITE	LHERZOLITE	LHERZOLITE	LHERZOLITE	LHERZOLITE	LHERZOLITE	LHERZOLITE	LHERZOLITE	LHERZOLITE	OLIVINE WEBSTERITE
Zone	ULTRAMAFIC	ULTRAMAFIC	ULTRAMAFIC	ULTRAMAFIC	ULTRAMAFIC	ULTRAMAFIC	ULTRAMAFIC	ULTRAMAFIC	ULTRAMAFIC	ULTRAMAFIC	ULTRAMAFIC	ULTRAMAFIC
Subzone	C	C	C	D	D	D	D	D	D	D	D	D
Cycle no.	3	3	3	4	4	4	4	4	4	4	4	4
Strat. ht (m)	827	827	827	869	869	869	869	869	883	883	883	898
SiO2	53.55	53.05	53.27	53.60	53.20	53.24	52.82	53.19	53.14	53.25	53.26	53.46
TiO2	.25	.23	.26	.15	.23	.24	.30	.20	.20	.26	.22	.16
Al2O3	1.75	1.78	1.58	.96	1.49	1.39	2.07	1.28	1.58	1.57	1.32	.96
Cr2O3	.31	.39	.35	.31	.25	.23	.31	.27	.50	.50	.56	.55
FeO	6.40	6.36	5.73	4.13	4.81	4.83	4.64	3.90	5.10	5.65	5.18	4.94
MnO	.18	.16	.18	.16	.19	.18	.17	.20	.16	.19	.20	.18
NiO	.06	.09	.06	.07	.04	.06	.07	.05	.07	.07	.09	.06
MgO	17.57	17.55	16.49	17.18	17.25	17.71	17.02	16.94	17.07	18.19	17.01	16.60
CaO	20.06	19.80	21.52	22.95	21.91	21.21	21.84	23.46	21.89	20.17	22.20	22.93
Na2O	.45	.46	.53	.44	.51	.47	.56	.45	.53	.50	.54	.48
Total	100.56	99.87	99.96	99.94	99.88	99.56	99.80	99.93	100.24	100.34	100.57	100.30
Atomic proportions												
Oxygens	6.0	6.0	6.0	6.0	6.0	6.0	6.0	6.0	6.0	6.0	6.0	6.0
Si	1.952	1.948	1.958	1.964	1.951	1.955	1.938	1.951	1.946	1.943	1.948	1.961
Ti	.007	.006	.007	.004	.006	.007	.008	.006	.006	.007	.006	.004
Al	.075	.077	.069	.041	.064	.060	.089	.055	.068	.068	.057	.041
Cr	.009	.011	.010	.009	.007	.007	.009	.008	.014	.014	.016	.016
Fe	.195	.195	.176	.126	.147	.148	.142	.120	.156	.172	.158	.152
Mn	.006	.005	.006	.005	.006	.006	.005	.006	.005	.006	.006	.006
Ni	.002	.003	.002	.002	.001	.002	.002	.002	.002	.002	.003	.002
Mg	.955	.961	.903	.938	.943	.969	.931	.926	.932	.989	.927	.907
Ca	.783	.779	.847	.901	.861	.834	.859	.922	.859	.789	.870	.901
Na	.032	.033	.038	.031	.037	.034	.040	.032	.038	.035	.038	.034
Total	4.015	4.018	4.015	4.022	4.025	4.022	4.024	4.028	4.026	4.026	4.029	4.024
mg number	83	83	84	88	86	87	87	89	86	85	85	86
Mg'	49	50	47	48	48	50	48	47	48	51	47	46
Fe'	10	10	9	6	8	7	8	6	8	9	9	8
Ca'	41	40	44	46	44	43	44	47	44	40	44	46

Sample no.	85770207	85770207	85770207	85770209	85770209	85770209	85770210	85770210	85770210	85770210	85770211	85770211
Analysis no.	56780	56781	56782	56874	56875	56876	56883	56884	56885	56886	56894	56895
Mineral	CLINOPYRO. 2	CLINOPYRO. 3	CLINOPYRO. 4	CLINOPYRO. 2	CLINOPYRO. 3	CLINOPYRO. 4	CLINOPYRO. 1	CLINOPYRO. 2	CLINOPYRO. 3	CLINOPYRO. 4	CLINOPYRO. 1	CLINOPYRO. 2
Description	CUMULUS, CORE	CUMULUS, CORE	CUMULUS, CORE	CUMULUS, CORE	CUMULUS, CORE	CUMULUS, CORE	CUMULUS, CORE	CUMULUS, CORE	CUMULUS, CORE	CUMULUS, CORE	CUMULUS, CORE	CUMULUS, CORE
Lithology	OLIVINE WEBSTERITE	OLIVINE WEBSTERITE	OLIVINE WEBSTERITE	OLIVINE WEBSTERITE	OLIVINE WEBSTERITE	OLIVINE WEBSTERITE	LHERZOLITE	LHERZOLITE	LHERZOLITE	LHERZOLITE	OLIVINE WEBSTERITE	OLIVINE WEBSTERITE
Zone	ULTRAMAFIC	ULTRAMAFIC	ULTRAMAFIC	ULTRAMAFIC	ULTRAMAFIC	ULTRAMAFIC	ULTRAMAFIC	ULTRAMAFIC	ULTRAMAFIC	ULTRAMAFIC	ULTRAMAFIC	ULTRAMAFIC
Subzone	D	D	D	D	D	D	D	D	D	D	D	D
Cycle no.	4	4	4	4	4	4	5	5	5	5	5	5
Strat. ht (m)	898	898	898	919	919	919	933	933	933	933	947	947
SiO2	52.96	53.20	53.08	53.33	52.98	52.94	52.36	52.39	52.80	53.03	53.62	53.35
TiO2	.25	.22	.21	.29	.27	.26	.27	.27	.27	.26	.18	.18
Al2O3	1.77	1.51	1.81	1.62	1.51	1.55	1.73	1.62	1.67	1.54	1.05	1.04
Cr2O3	.54	.51	.52	.48	.44	.50	.48	.44	.49	.49	.39	.44
FeO	5.42	4.99	5.34	4.97	5.35	5.20	4.87	4.64	5.43	4.89	4.86	5.61
MnO	.16	.17	.16	.20	.17	.16	.21	.20	.19	.17	.18	.18
NiO	.08	.10	.06	.07	.08	.09	.08	.07	.08	.09	.10	.09
MgO	16.95	16.86	16.79	16.69	17.04	16.79	17.12	17.37	18.33	17.11	17.45	18.34
CaO	21.38	22.06	21.49	22.15	21.17	21.60	21.33	21.57	20.28	22.36	22.26	20.67
Na2O	.52	.52	.52	.52	.57	.50	.56	.50	.52	.60	.39	.34
Total	100.04	100.14	100.00	100.32	99.60	99.60	99.00	99.06	100.06	100.52	100.46	100.24

Atomic proportions

Oxygens	6.0	6.0	6.0	6.0	6.0	6.0	6.0	6.0	6.0	6.0	6.0	6.0
Si	1.944	1.950	1.948	1.951	1.951	1.951	1.939	1.939	1.933	1.939	1.958	1.951
Ti	.007	.006	.006	.008	.008	.007	.008	.008	.007	.007	.005	.005
Al	.077	.065	.078	.070	.066	.067	.076	.070	.072	.066	.045	.045
Cr	.016	.015	.015	.014	.013	.015	.014	.013	.014	.014	.011	.013
Fe	.166	.153	.164	.152	.165	.160	.151	.144	.166	.149	.148	.172
Mn	.005	.005	.005	.006	.005	.005	.007	.006	.006	.005	.006	.006
Ni	.002	.003	.002	.002	.002	.003	.002	.002	.002	.003	.003	.003
Mg	.927	.921	.918	.910	.936	.922	.945	.958	1.000	.932	.949	1.000
Ca	.841	.867	.845	.868	.836	.853	.847	.855	.796	.876	.871	.810
Na	.037	.037	.037	.037	.040	.036	.040	.036	.037	.042	.027	.024
Total	4.022	4.022	4.018	4.018	4.022	4.019	4.028	4.030	4.034	4.035	4.023	4.027
mg number	85	86	85	86	85	85	86	87	86	86	86	85
Mg'	48	47	48	47	48	48	49	49	51	48	48	50
Fe'	9	8	8	8	9	8	7	7	8	7	8	9
Ca'	43	45	44	45	43	44	44	44	41	45	44	41

Sample no.	85770211	85770211	85770212	85770212	85770212	85770212	85770212	85770212	85770213	85770213	85770213	85770213
Analysis no.	56896	56898	56906	56907	56909	56910	56911	56912	56923	56925	56927	56928
Mineral	CLINOPYRO. 3	CLINOPYRO. 5	CLINOPYRO. 1	CLINOPYRO. 2	CLINOPYRO. 4	CLINOPYRO. 5	CLINOPYRO. 6	CLINOPYRO. 7	CLINOPYRO. 1	CLINOPYRO. 3	CLINOPYRO. 5	CLINOPYRO. 6
Description	CUMULUS, CORE	CUMULUS, CORE	CUMULUS, CORE	CUMULUS, CORE	CUMULUS, CORE	CUMULUS, CORE	CUMULUS, CORE	CUMULUS, CORE	CUMULUS, CORE	CUMULUS, CORE	CUMULUS, CORE	CUMULUS, CORE
Lithology	OLIVINE WEBSTERITE	OLIVINE WEBSTERITE	OLIVINE WEBSTERITE	OLIVINE WEBSTERITE	OLIVINE WEBSTERITE	OLIVINE WEBSTERITE	OLIVINE WEBSTERITE	OLIVINE WEBSTERITE	OLIVINE WEBSTERITE	OLIVINE WEBSTERITE	OLIVINE WEBSTERITE	OLIVINE WEBSTERITE
Zone	ULTRAMAFIC	ULTRAMAFIC	ULTRAMAFIC	ULTRAMAFIC	ULTRAMAFIC	ULTRAMAFIC	ULTRAMAFIC	ULTRAMAFIC	ULTRAMAFIC	ULTRAMAFIC	ULTRAMAFIC	ULTRAMAFIC
Subzone	D	D	D	D	D	D	D	D	D	D	D	D
Cycle no.	5	5	5	5	5	5	5	5	5	5	5	5
Strat. ht (m)	947	947	969	969	969	969	969	969	982	982	982	982
SiO2	53.19	53.10	53.02	53.01	52.86	52.69	53.02	52.52	53.02	53.04	53.33	53.19
TiO2	.18	.19	.20	.16	.15	.18	.21	.20	.21	.19	.17	.19
Al2O3	1.06	1.04	.88	.89	.85	.93	.87	.93	.92	.94	.92	.96
Cr2O3	.40	.40	.18	.18	.16	.19	.17	.17	.21	.20	.15	.13
FeO	5.08	5.04	5.75	6.11	6.28	6.18	7.26	6.25	5.60	5.68	5.97	5.75
MnO	.17	.21	.23	.22	.23	.20	.20	.20	.24	.19	.20	.17
NiO	.09	.07	.09	.07	.08	.06	.10	.05	.07	.09	.07	.06
MgO	17.76	17.53	17.48	17.25	17.84	17.16	18.59	17.76	16.72	16.88	17.19	17.13
CaO	21.87	22.18	21.83	21.98	21.36	21.93	19.23	21.01	23.34	22.99	22.41	22.71
Na2O	.37	.36	.28	.25	.24	.29	.26	.28	.28	.26	.29	.27
Total	100.18	100.11	99.94	100.12	100.03	99.80	99.92	99.36	100.61	100.46	100.69	100.58
Atomic proportions												
Oxygens	6.0	6.0	6.0	6.0	6.0	6.0	6.0	6.0	6.0	6.0	6.0	6.0
Si	1.949	1.949	1.953	1.952	1.948	1.948	1.952	1.947	1.947	1.949	1.953	1.950
Ti	.005	.005	.005	.004	.004	.005	.006	.006	.006	.005	.005	.005
Al	.046	.045	.038	.039	.037	.041	.038	.040	.040	.041	.040	.041
Cr	.012	.012	.005	.005	.005	.006	.005	.005	.006	.006	.004	.004
Fe	.156	.155	.177	.188	.193	.191	.223	.194	.172	.175	.183	.176
Mn	.005	.007	.007	.007	.007	.006	.006	.006	.007	.006	.006	.005
Ni	.003	.002	.003	.002	.002	.002	.003	.001	.002	.003	.002	.002
Mg	.970	.959	.960	.947	.980	.946	1.020	.981	.915	.924	.938	.936
Ca	.859	.872	.861	.867	.843	.869	.758	.835	.918	.905	.879	.892
Na	.026	.025	.020	.018	.017	.021	.019	.020	.020	.019	.020	.019
Total	4.030	4.031	4.030	4.030	4.036	4.034	4.031	4.035	4.034	4.032	4.030	4.032
mg number	86	86	84	83	84	83	82	84	84	84	84	84
Mg'	49	48	48	48	48	47	51	48	46	46	47	47
Fe'	8	8	9	9	10	10	11	10	9	9	9	9
Ca'	43	44	43	43	42	43	38	42	45	45	44	44

Detailed traverse across cycles 1–5 in subzones C and D (UZ): orthopyroxene

Sample no.	85770188	85770188	85770188	85770188	85770190	85770192	85770192	85770194	85770194	85770195	85770195	85770195
Analysis no.	56485	56487	56488	56489	56506	56528	56530	56551	56552	56574	56575	56576
Mineral	ORTHOPYRO.	ORTHOPYRO.	ORTHOPYRO.	ORTHOPYRO.	ORTHOPYRO.	ORTHOPYRO.	ORTHOPYRO.	ORTHOPYRO.	ORTHOPYRO.	ORTHOPYRO.	ORTHOPYRO.	ORTHOPYRO.
	1	2	3	4	1	1	2	1	2	1	2	4
Description	INTERCUMU.	INTERCUMU.	INTERCUMU.	INTERCUMU.	INTERCUMU.	INTERCUMU.	INTERCUMU.	INTERCUMU.	INTERCUMU.	INTERCUMU.	INTERCUMU.	INTERCUMU.
Lithology	WEBSTERITE	WEBSTERITE	WEBSTERITE	WEBSTERITE	OLIVINE WEBSTERITE	LHERZOLITE	LHERZOLITE	LHERZOLITE	LHERZOLITE	OLIVINE WEBSTERITE	OLIVINE WEBSTERITE	OLIVINE WEBSTERITE
Zone	ULTRAMAFIC	ULTRAMAFIC	ULTRAMAFIC	ULTRAMAFIC	ULTRAMAFIC	ULTRAMAFIC	ULTRAMAFIC	ULTRAMAFIC	ULTRAMAFIC	ULTRAMAFIC	ULTRAMAFIC	ULTRAMAFIC
Subzone	C	C	C	C	C	C	C	C	C	C	C	C
Cycle no.	1	1	1	1	1	2	2	2	2	2	2	2
Strat. ht (m)	650	650	650	650	671	692	692	703	703	707	707	707
SiO2	54.97	54.72	54.61	54.61	54.57	55.33	55.32	55.53	55.00	54.47	54.31	54.92
TiO2	.18	.14	.15	.17	.11	.14	.10	.09	.10	.10	.18	.14
Al2O3	.53	.67	.60	.61	.61	.71	.68	.66	.73	.83	.92	.92
Cr2O3	.04	<.02	.04	<.02	.12	.07	.06	.09	.12	.12	.13	.14
FeO	15.04	14.89	13.63	14.34	12.80	11.82	12.33	12.53	11.13	12.76	11.83	12.97
MnO	.30	.35	.32	.34	.27	.27	.31	.29	.31	.28	.33	.30
NiO	.12	.13	.14	.09	.14	.11	.12	.11	.11	.11	.12	.14
MgO	28.17	27.27	26.85	27.32	28.63	30.05	29.33	30.08	29.18	28.24	28.20	28.61
CaO	1.45	1.54	2.44	1.72	2.31	1.28	2.23	.81	1.59	2.11	2.25	2.20
Na2O	.02	.02	.03	.05	.07	<.01	.04	.02	.02	.03	.06	.04
Total	100.82	99.74	98.83	99.24	99.63	99.79	100.51	100.21	98.29	99.04	98.33	100.38
Atomic proportions												
Oxygens	6.0	6.0	6.0	6.0	6.0	6.0	6.0	6.0	6.0	6.0	6.0	6.0
Si	1.967	1.978	1.986	1.980	1.963	1.969	1.966	1.971	1.982	1.968	1.970	1.960
Ti	.005	.004	.004	.005	.003	.004	.003	.002	.003	.003	.005	.004
Al	.022	.029	.026	.026	.026	.030	.028	.028	.031	.035	.040	.039
Cr	.001	-	.001	-	.003	.002	.002	.003	.003	.003	.004	.004
Fe	.450	.450	.415	.435	.385	.352	.366	.372	.336	.385	.359	.387
Mn	.009	.011	.010	.010	.008	.008	.009	.009	.010	.009	.010	.009
Ni	.004	.004	.004	.003	.004	.003	.003	.003	.003	.003	.004	.004
Mg	1.502	1.469	1.455	1.476	1.535	1.594	1.553	1.592	1.568	1.521	1.524	1.522
Ca	.056	.060	.095	.067	.089	.049	.085	.031	.061	.082	.088	.084
Na	.001	.002	.002	.004	.005	-	.003	.002	.002	.002	.004	.003
Total	4.017	4.005	3.998	4.005	4.022	4.011	4.018	4.012	3.999	4.011	4.006	4.016
mg number	77	77	78	77	80	82	81	81	82	80	81	80
Mg'	75	74	74	75	77	80	78	80	80	77	78	77
Fe'	22	23	21	22	19	18	18	18	17	19	18	19
Ca'	3	3	5	3	4	2	4	2	3	4	4	4

Sample no.	85770195	85770196	85770196	85770197	85770197	85770198	85770198	85770198	85770201	85770201	85770201	85770202
Analysis no.	56579	56584	56585	56593	56595	56601	56602	56607	56622	56623	56624	56738
Mineral	ORTHOPYRO. 3	ORTHOPYRO. 1	ORTHOPYRO. 2	ORTHOPYRO. 1	ORTHOPYRO. 2	ORTHOPYRO. 1	ORTHOPYRO. 2	ORTHOPYRO. 3	ORTHOPYRO. 1	ORTHOPYRO. 2	ORTHOPYRO. 3	ORTHOPYRO. 1
Description	INTERCUMU.	INTERCUMU.	INTERCUMU.	INTERCUMU.	INTERCUMU.	INTERCUMU.	INTERCUMU.	INTERCUMU.	INTERCUMU.	INTERCUMU.	INTERCUMU.	INTERCUMU.
Lithology	OLIVINE WEBSTERITE	OLIVINE WEBSTERITE	OLIVINE WEBSTERITE	OLIVINE WEBSTERITE	OLIVINE WEBSTERITE	OLIVINE WEBSTERITE	OLIVINE WEBSTERITE	OLIVINE WEBSTERITE	LHERZOLITE	LHERZOLITE	LHERZOLITE	OLIVINE WEBSTERITE
Zone	ULTRAMAFIC	ULTRAMAFIC	ULTRAMAFIC	ULTRAMAFIC	ULTRAMAFIC	ULTRAMAFIC	ULTRAMAFIC	ULTRAMAFIC	ULTRAMAFIC	ULTRAMAFIC	ULTRAMAFIC	ULTRAMAFIC
Subzone	C	C	C	C	C	C	C	C	C	C	C	C
Cycle no.	2	2	2	2	2	2	2	2	3	3	3	3
Strat. ht (m)	707	714	714	728	728	749	749	749	784	784	784	791
SiO2	54.21	55.02	54.97	55.22	55.10	55.07	54.91	55.37	55.40	55.56	55.43	55.24
TiO2	.12	.14	.12	.14	.09	.15	.15	.13	.11	.12	.12	.14
Al2O3	.91	.83	.91	1.04	.81	.92	.82	.93	.99	.92	.91	.92
Cr2O3	.15	.18	.19	.19	.24	.25	.20	.20	.22	.22	.23	.22
FeO	12.84	12.10	12.03	11.51	11.43	10.74	11.14	11.36	11.02	10.86	11.02	11.31
MnO	.32	.28	.28	.25	.31	.28	.26	.26	.29	.27	.29	.22
NiO	.10	.13	.11	.09	.12	.12	.13	.11	.12	.15	.09	.11
MgO	28.81	29.33	28.58	29.94	29.20	29.16	29.25	29.89	30.62	30.26	30.22	29.83
CaO	1.85	1.36	2.60	1.44	1.90	2.43	1.99	1.64	1.17	1.68	1.80	1.57
Na2O	.03	.03	.08	.03	.03	.05	.04	.02	.04	.04	.04	.02
Total	99.34	99.39	99.87	99.85	99.21	99.17	98.90	99.91	99.98	100.09	100.15	99.58
Atomic proportions												
Oxygens	6.0	6.0	6.0	6.0	6.0	6.0	6.0	6.0	6.0	6.0	6.0	6.0
Si	1.954	1.970	1.965	1.963	1.973	1.970	1.971	1.966	1.961	1.966	1.962	1.967
Ti	.003	.004	.003	.004	.002	.004	.004	.003	.003	.003	.003	.004
Al	.038	.035	.038	.044	.034	.039	.035	.039	.041	.038	.038	.039
Cr	.004	.005	.005	.005	.007	.007	.006	.006	.006	.006	.007	.006
Fe	.387	.362	.360	.342	.342	.321	.335	.337	.326	.321	.326	.337
Mn	.010	.008	.009	.008	.009	.008	.008	.008	.009	.008	.009	.007
Ni	.003	.004	.003	.003	.003	.004	.004	.003	.003	.004	.003	.003
Mg	1.548	1.565	1.523	1.586	1.559	1.555	1.565	1.582	1.616	1.596	1.595	1.584
Ca	.072	.052	.100	.055	.073	.093	.077	.062	.044	.064	.068	.060
Na	.002	.002	.006	.002	.002	.003	.003	.002	.003	.003	.003	.001
Total	4.022	4.008	4.012	4.010	4.005	4.004	4.006	4.009	4.013	4.010	4.014	4.007
mg number	80	81	81	82	82	83	82	82	83	83	83	82
Mg'	77	79	77	80	79	79	79	80	81	81	80	80
Fe'	19	18	18	17	17	16	17	17	16	16	17	17
Ca'	4	3	5	3	4	5	4	3	3	3	3	3

Sample no.	85770202	85770202	85770204	85770204	85770206	85770206	85770206	85770207	85770207	85770209	85770209	85770209
Analysis no.	56739	56742	56760	56761	56770	56771	56775	56783	56784	56877	56878	56879
Mineral	ORTHOPYRO. 2	ORTHOPYRO. 3	ORTHOPYRO. 1	ORTHOPYRO. 2	ORTHOPYRO. 1	ORTHOPYRO. 2	ORTHOPYRO. 3	ORTHOPYRO. 1	ORTHOPYRO. 2	ORTHOPYRO. 1	ORTHOPYRO. 2	ORTHOPYRO. 3
Description	INTERCUMU.	INTERCUMU.	INTERCUMU.	INTERCUMU.	INTERCUMU.	INTERCUMU.	INTERCUMU.	INTERCUMU.	INTERCUMU.	INTERCUMU.	INTERCUMU.	INTERCUMU.
Lithology	OLIVINE WEBSTERITE	OLIVINE WEBSTERITE	OLIVINE WEBSTERITE	OLIVINE WEBSTERITE	LHERZOLITE	LHERZOLITE	LHERZOLITE	OLIVINE WEBSTERITE	OLIVINE WEBSTERITE	OLIVINE WEBSTERITE	OLIVINE WEBSTERITE	OLIVINE WEBSTERITE
Zone	ULTRAMAFIC	ULTRAMAFIC	ULTRAMAFIC	ULTRAMAFIC	ULTRAMAFIC	ULTRAMAFIC	ULTRAMAFIC	ULTRAMAFIC	ULTRAMAFIC	ULTRAMAFIC	ULTRAMAFIC	ULTRAMAFIC
Subzone	C	C	C	C	D	D	D	D	D	D	D	D
Cycle no.	3	3	3	3	4	4	4	4	4	4	4	4
Strat. ht (m)	791	791	827	827	883	883	883	898	898	919	919	919
SiO2	55.02	55.21	54.80	55.16	54.75	55.39	55.40	55.36	55.36	55.05	54.85	54.97
TiO2	.12	.13	.13	.14	.10	.15	.14	.12	.13	.14	.17	.17
Al2O3	.87	1.01	1.00	.97	1.00	.87	.92	.89	.96	.87	.87	.88
Cr2O3	.23	.27	.16	.18	.20	.22	.20	.19	.24	.21	.22	.20
FeO	10.69	11.26	12.65	12.24	11.64	10.97	11.16	10.99	11.26	11.41	11.47	11.06
MnO	.28	.25	.27	.24	.28	.30	.28	.31	.32	.27	.28	.30
NiO	.15	.12	.12	.08	.10	.10	.10	.13	.13	.14	.13	.15
MgO	29.25	29.65	28.91	28.92	30.08	29.90	29.89	28.58	29.33	29.26	29.50	29.03
CaO	2.59	2.38	1.82	2.05	.65	2.01	2.10	2.82	1.98	2.30	2.03	2.52
Na2O	.06	.04	.04	.03	.03	.06	.04	.08	.04	.05	.05	.06
Total	99.25	100.32	99.90	100.03	98.83	99.96	100.24	99.46	99.74	99.70	99.57	99.35
Atomic proportions												
Oxygens	6.0	6.0	6.0	6.0	6.0	6.0	6.0	6.0	6.0	6.0	6.0	6.0
Si	1.968	1.958	1.960	1.966	1.964	1.965	1.963	1.978	1.971	1.965	1.960	1.967
Ti	.003	.004	.003	.004	.003	.004	.004	.003	.003	.004	.005	.004
Al	.037	.042	.042	.041	.042	.036	.039	.038	.040	.037	.036	.037
Cr	.007	.008	.004	.005	.006	.006	.005	.005	.007	.006	.006	.006
Fe	.320	.334	.378	.365	.349	.326	.331	.328	.335	.341	.343	.331
Mn	.008	.007	.008	.007	.009	.009	.009	.009	.010	.008	.008	.009
Ni	.004	.003	.004	.002	.003	.003	.003	.004	.004	.004	.004	.004
Mg	1.560	1.567	1.541	1.537	1.608	1.582	1.578	1.522	1.556	1.557	1.572	1.549
Ca	.099	.090	.070	.078	.025	.076	.080	.108	.075	.088	.078	.096
Na	.004	.003	.003	.002	.002	.004	.003	.005	.003	.003	.003	.004
Total	4.009	4.015	4.015	4.008	4.010	4.012	4.013	4.000	4.004	4.012	4.016	4.009
mg number	83	82	80	81	82	83	83	82	82	82	82	82
Mg'	79	79	77	78	81	80	79	78	79	78	79	78
Fe'	16	17	19	18	18	16	17	17	17	17	17	17
Ca'	5	4	4	4	1	4	4	5	4	5	4	5

Sample no.	85770210	85770210	85770210	85770210	85770211	85770211	85770211
Analysis no.	56887	56888	56889	56890	56899	56900	56901
Mineral	ORTHOPYRO. 1	ORTHOPYRO. 2	ORTHOPYRO. 3	ORTHOPYRO. 4	ORTHOPYRO. 1	ORTHOPYRO. 2	ORTHOPYRO. 3
Description	INTERCUMU.	INTERCUMU.	INTERCUMU.	INTERCUMU.	INTERCUMU.	INTERCUMU.	INTERCUMU.
Lithology	LHERZOLITE	LHERZOLITE	LHERZOLITE	LHERZOLITE	OLIVINE WEBSTERITE	OLIVINE WEBSTERITE	OLIVINE WEBSTERITE
Zone	ULTRAMAFIC	ULTRAMAFIC	ULTRAMAFIC	ULTRAMAFIC	ULTRAMAFIC	ULTRAMAFIC	ULTRAMAFIC
Subzone	D	D	D	D	D	D	D
Cycle no.	5	5	5	5	5	5	5
Strat. ht (m)	933	933	933	933	947	947	947
SiO2	54.66	55.18	55.19	54.94	55.01	55.62	55.09
TiO2	.15	.15	.16	.16	.12	.11	.11
Al2O3	1.03	.95	.89	.95	.68	.72	.66
Cr2O3	.20	.20	.20	.19	.19	.20	.23
FeO	10.91	10.92	10.22	10.56	11.76	11.11	11.47
MnO	.26	.27	.28	.30	.30	.29	.31
NiO	.12	.12	.11	.14	.11	.14	.16
MgO	30.62	30.55	30.15	30.16	30.45	30.64	30.48
CaO	1.48	1.95	2.35	2.32	1.26	1.60	1.60
Na2O	.04	.04	.08	.06	<.01	.02	.03
Total	99.48	100.34	99.63	99.78	99.88	100.46	100.13
Atomic proportions							
Oxygens	6.0	6.0	6.0	6.0	6.0	6.0	6.0
Si	1.949	1.952	1.961	1.954	1.958	1.963	1.957
Ti	.004	.004	.004	.004	.003	.003	.003
Al	.043	.040	.037	.040	.028	.030	.028
Cr	.006	.005	.006	.005	.005	.006	.006
Fe	.325	.323	.304	.314	.350	.328	.341
Mn	.008	.008	.008	.009	.009	.009	.009
Ni	.004	.003	.003	.004	.003	.004	.004
Mg	1.627	1.611	1.597	1.599	1.616	1.612	1.613
Ca	.057	.074	.090	.088	.048	.060	.061
Na	.003	.003	.006	.004	-	.001	.002
Total	4.024	4.023	4.016	4.021	4.021	4.016	4.024
mg number	83	83	84	84	82	83	83
Mg'	81	80	80	80	80	81	80
Fe'	16	16	15	16	17	16	17
Ca'	3	4	5	4	3	3	3

Detailed traverse across ultramafic/gabbroic zone contact (UZ, GZ): clinopyroxene

Sample no.	85770214	85770214	85770214	85770214	85770215	85770215	85770215	85770215	85770216	85770216	85770216	85770216
Analysis no.	58330	58328	58327	58331	58323	58326	58325	58324	58333	58334	58335	58336
Mineral	CLINOPYRO. 4	CLINOPYRO. 2	CLINOPYRO. 1	CLINOPYRO. 5	CLINOPYRO. 1	CLINOPYRO. 4	CLINOPYRO. 3	CLINOPYRO. 2	CLINOPYRO. 1	CLINOPYRO. 2	CLINOPYRO. 3	CLINOPYRO. 4
Description	CUMULUS, CORE	CUMULUS, CORE	CUMULUS, CORE	CUMULUS, CORE	CLINOPYRO. CORE	CUMULUS, CORE	CUMULUS, CORE	CUMULUS, CORE	CUMULUS, CORE	CUMULUS, CORE	CUMULUS, CORE	CUMULUS, CORE
Lithology	DUNITE	DUNITE	DUNITE	DUNITE	OLIVINE-PLAGIOCLA. WEBSTERITE	PLAGIOCLA. WEBSTERITE	OLIVINE-PLAGIOCLA. WEBSTERITE	OLIVINE-PLAGIOCLA. WEBSTERITE	PLAGIOCLA. WEBSTERITE	PLAGIOCLA. WEBSTERITE	PLAGIOCLA. WEBSTERITE	PLAGIOCLA. WEBSTERITE
Zone	ULTRAMAFIC	ULTRAMAFIC	ULTRAMAFIC	ULTRAMAFIC	ULTRAMAFIC	ULTRAMAFIC	ULTRAMAFIC	ULTRAMAFIC	ULTRAMAFIC	ULTRAMAFIC	ULTRAMAFIC	ULTRAMAFIC
Subzone	I	I	I	I	I	I	I	I	I	I	I	I
Strat. ht (m)	1745	1745	1745	1745	1757	1757	1757	1757	1777	1777	1777	1777
SiO2	53.11	53.80	54.07	54.50	53.59	53.82	53.88	53.59	54.34	53.41	53.67	53.71
TiO2	.22	.15	.23	.27	.33	.25	.34	.36	.33	.33	.34	.30
Al2O3	1.34	1.02	1.31	1.50	1.93	1.85	1.70	1.77	1.94	1.56	1.64	1.55
Cr2O3	.44	.60	.47	.43	.39	.38	.41	.38	.31	.26	.29	.28
FeO	5.25	5.01	4.67	5.03	5.57	5.20	5.66	5.54	5.44	5.81	5.63	5.88
MnO	.19	.19	.17	.17	.17	.22	.21	.20	.19	.18	.19	.21
NiO	.06	.09	.06	.04	.08	<.03	.07	.08	.05	.09	.05	.04
MgO	17.03	17.55	16.39	16.64	16.54	16.10	16.43	16.52	16.47	16.54	16.24	16.62
CaO	20.75	20.60	21.37	21.78	21.03	21.64	21.50	21.00	21.28	20.41	21.33	20.41
Na2O	.61	.56	.64	.64	.54	.59	.55	.56	.52	.43	.52	.48
Total	98.99	99.57	99.39	101.00	100.16	100.04	100.76	100.01	100.85	99.02	99.90	99.47
Atomic proportions												
Oxygens	6.0	6.0	6.0	6.0	6.0	6.0	6.0	6.0	6.0	6.0	6.0	6.0
Si	1.964	1.974	1.985	1.973	1.959	1.969	1.962	1.962	1.969	1.973	1.969	1.975
Ti	.006	.004	.006	.007	.009	.007	.009	.010	.009	.009	.010	.008
Al	.058	.044	.057	.064	.083	.080	.073	.077	.083	.068	.071	.067
Cr	.013	.017	.014	.012	.011	.011	.012	.011	.009	.007	.008	.008
Fe	.162	.154	.144	.152	.170	.159	.172	.170	.165	.179	.173	.181
Mn	.006	.006	.005	.005	.005	.007	.006	.006	.006	.006	.006	.007
Ni	.002	.003	.002	.001	.002	-	.002	.002	.001	.003	.001	.001
Mg	.939	.960	.897	.898	.901	.878	.892	.902	.890	.911	.888	.911
Ca	.822	.810	.841	.845	.824	.848	.839	.824	.826	.808	.838	.804
Na	.044	.040	.045	.045	.038	.042	.039	.040	.037	.031	.037	.034
Total	4.016	4.011	3.996	4.004	4.004	4.000	4.006	4.004	3.994	3.995	4.000	3.996
mg number	85	86	86	86	84	85	84	84	84	84	84	83
Mg'	49	50	47	47	48	47	47	48	47	48	47	48
Fe'	8	8	8	8	9	8	9	9	9	9	9	10
Ca'	43	42	45	45	43	45	44	43	44	43	44	42

Sample no.	85770217	85770217	85770217	85770217	85770217	85770218	85770218	85770218	85770218	85770219	85770219	85770219
Analysis no.	58341	58340	58339	58338	58337	58345	58344	58343	58342	58346	58347	58348
Mineral	CLINOPYRO. 5	CLINOPYRO. 4	CLINOPYRO. 3	CLINOPYRO. 2	CLINOPYRO. 1	CLINOPYRO. 4	CLINOPYRO. 3	CLINOPYRO. 2	CLINOPYRO. 1	CLINOPYRO. 1	CLINOPYRO. 2	CLINOPYRO. 3
Description	CUMULUS, CORE	CUMULUS, CORE	CUMULUS, CORE	CUMULUS, CORE	CUMULUS, CORE	CUMULUS, CORE	CUMULUS, CORE	CUMULUS, CORE	CUMULUS, CORE	CUMULUS, CORE	CUMULUS, CORE	CUMULUS, CORE
Lithology	PLAGIOCLA. WEBSTERITE	PLAGIOCLA. WEBSTERITE	PLAGIOCLA. WEBSTERITE	PLAGIOCLA. WEBSTERITE	PLAGIOCLA. WEBSTERITE	OLIVINE-PLAGIOCLA. WEBSTERITE	OLIVINE-PLAGIOCLA. WEBSTERITE	OLIVINE-PLAGIOCLA. WEBSTERITE	OLIVINE-PLAGIOCLA. WEBSTERITE	WEBSTERITE	WEBSTERITE	WEBSTERITE
Zone	ULTRAMAFIC	ULTRAMAFIC	ULTRAMAFIC	ULTRAMAFIC	ULTRAMAFIC	ULTRAMAFIC	ULTRAMAFIC	ULTRAMAFIC	ULTRAMAFIC	ULTRAMAFIC	ULTRAMAFIC	ULTRAMAFIC
Subzone	I	I	I	I	I	I	I	I	I	I	I	I
Strat. ht (m)	1790	1790	1790	1790	1790	1798	1798	1798	1798	1808	1808	1808
SiO2	53.38	53.87	52.85	53.30	53.54	53.47	53.68	53.56	53.08	53.57	53.61	53.43
TiO2	.46	.23	.38	.39	.48	.30	.42	.45	.40	.49	.31	.46
Al2O3	1.80	1.47	1.85	1.71	1.66	1.65	1.87	1.92	1.98	1.57	1.87	1.52
Cr2O3	.34	.38	.37	.33	.31	.29	.29	.26	.25	.21	.19	.24
FeO	5.64	6.30	5.24	5.41	5.57	5.17	5.42	5.39	5.52	6.72	5.70	6.28
MnO	.17	.18	.18	.17	.16	.17	.18	.19	.21	.20	.24	.25
NiO	.07	.06	.06	.08	.07	.08	<.03	.09	.11	.06	.05	.04
MgO	16.47	17.13	15.93	16.02	16.59	16.33	16.27	16.58	16.87	16.70	15.52	15.96
CaO	20.24	19.76	20.97	21.47	20.42	21.76	21.37	20.97	20.97	20.27	21.88	20.95
Na2O	.56	.44	.53	.54	.52	.53	.57	.57	.56	.46	.56	.53
Total	99.13	99.82	98.36	99.41	99.31	99.74	100.06	99.99	99.95	100.25	99.94	99.66
Atomic proportions												
Oxygens	6.0	6.0	6.0	6.0	6.0	6.0	6.0	6.0	6.0	6.0	6.0	6.0
Si	1.968	1.974	1.966	1.965	1.970	1.964	1.964	1.960	1.947	1.962	1.969	1.970
Ti	.013	.006	.011	.011	.013	.008	.012	.012	.011	.013	.008	.013
Al	.078	.063	.081	.074	.072	.071	.080	.083	.086	.068	.081	.066
Cr	.010	.011	.011	.010	.009	.009	.008	.008	.007	.006	.006	.007
Fe	.174	.193	.163	.167	.172	.159	.166	.165	.169	.206	.175	.194
Mn	.005	.006	.006	.005	.005	.005	.006	.006	.007	.006	.008	.008
Ni	.002	.002	.002	.002	.002	.002	-	.003	.003	.002	.001	.001
Mg	.905	.935	.883	.881	.910	.894	.887	.904	.922	.912	.850	.877
Ca	.799	.776	.836	.848	.805	.856	.837	.822	.824	.795	.861	.828
Na	.040	.031	.038	.039	.037	.038	.040	.040	.039	.033	.040	.038
Total	3.995	3.998	3.996	4.002	3.995	4.007	4.001	4.003	4.016	4.004	3.999	4.000
mg number	84	83	84	84	84	85	84	85	84	82	83	82
Mg'	48	49	47	46	48	47	47	48	48	48	45	46
Fe'	9	10	9	9	9	8	9	9	9	10	9	10
Ca'	43	41	44	45	43	45	44	43	43	42	46	44

Sample no.	85770219	85770220	85770220	85770220	85770220	85770220	85770221	85770221	85770221	85770221	85770222	85770222
Analysis no.	58349	58355	58354	58353	58351	58350	58360	58359	58358	58357	58363	58364
Mineral	CLINOPYRO. 4	CLINOPYRO. 6	CLINOPYRO. 5	CLINOPYRO. 4	CLINOPYRO. 2	CLINOPYRO. 1	CLINOPYRO. 4	CLINOPYRO. 3	CLINOPYRO. 2	CLINOPYRO. 1	CLINOPYRO. 1	CLINOPYRO. 2
Description	CUMULUS, CORE	CUMULUS, CORE	CUMULUS, CORE	CUMULUS, CORE	CUMULUS, CORE	CUMULUS, CORE	CUMULUS, CORE	CUMULUS, CORE	CUMULUS, CORE	CUMULUS, CORE	CUMULUS, CORE	CUMULUS, CORE
Lithology	WEBSTERITE	WEBSTERITE	WEBSTERITE	WEBSTERITE	WEBSTERITE	WEBSTERITE	WEBSTERITE	WEBSTERITE	WEBSTERITE	WEBSTERITE	PLAGIOCLA. WEBSTERITE	PLAGIOCLA. WEBSTERITE
Zone	ULTRAMAFIC	ULTRAMAFIC	ULTRAMAFIC	ULTRAMAFIC	ULTRAMAFIC	ULTRAMAFIC	ULTRAMAFIC	ULTRAMAFIC	ULTRAMAFIC	ULTRAMAFIC	ULTRAMAFIC	ULTRAMAFIC
Subzone	I	I	I	I	I	I	I	I	I	I	I	I
Strat. ht (m)	1808	1814	1814	1814	1814	1814	1834	1834	1834	1834	1841	1841
SiO2	53.48	53.56	53.32	53.30	52.96	53.16	53.02	52.93	52.98	53.17	52.92	52.78
TiO2	.50	.36	.41	.42	.43	.33	.34	.34	.46	.39	.34	.37
Al2O3	1.52	1.83	1.73	1.57	1.59	1.67	1.08	.99	1.28	1.17	1.87	1.72
Cr2O3	.21	.21	.20	.17	.16	.20	.16	.15	.16	.17	.03	.03
FeO	6.73	6.25	6.12	6.55	7.12	6.29	7.63	8.68	7.45	7.42	7.19	7.88
MnO	.20	.20	.16	.23	.22	.21	.21	.24	.21	.21	.22	.22
NiO	.05	.10	<.03	.06	.08	.06	.11	.07	<.03	.04	.06	.05
MgO	16.37	15.74	15.91	15.92	16.53	15.93	15.36	15.83	15.41	15.36	15.03	15.16
CaO	20.68	21.59	21.13	20.97	20.05	21.27	21.34	20.17	20.95	21.50	21.58	21.32
Na2O	.47	.48	.46	.50	.44	.48	.38	.34	.40	.42	.40	.44
Total	100.21	100.31	99.44	99.70	99.57	99.62	99.64	99.74	99.29	99.86	99.63	99.97
Atomic proportions												
Oxygens	6.0	6.0	6.0	6.0	6.0	6.0	6.0	6.0	6.0	6.0	6.0	6.0
Si	1.963	1.963	1.967	1.967	1.958	1.963	1.971	1.968	1.971	1.970	1.962	1.956
Ti	.014	.010	.012	.012	.012	.009	.010	.010	.013	.011	.009	.010
Al	.066	.079	.075	.068	.069	.073	.047	.043	.056	.051	.082	.075
Cr	.006	.006	.006	.005	.005	.006	.005	.004	.005	.005	.001	.001
Fe	.207	.192	.189	.202	.220	.194	.237	.270	.232	.230	.223	.244
Mn	.006	.006	.005	.007	.007	.007	.007	.007	.007	.007	.007	.007
Ni	.001	.003	-	.002	.002	.002	.003	.002	-	.001	.002	.002
Mg	.896	.860	.875	.875	.911	.877	.851	.877	.854	.848	.830	.837
Ca	.813	.848	.835	.829	.794	.841	.850	.804	.835	.853	.857	.847
Na	.034	.034	.033	.036	.031	.035	.028	.025	.029	.030	.029	.031
Total	4.004	4.001	3.997	4.003	4.009	4.006	4.007	4.011	4.001	4.006	4.002	4.011
mg number	81	82	82	81	81	82	78	76	79	79	79	77
Mg'	47	45	46	46	47	46	44	45	44	44	43	43
Fe'	11	10	10	11	11	10	12	14	12	12	12	13
Ca'	42	45	44	43	42	44	44	41	44	44	45	44

Sample no.	85770222	85770222	85770223	85770223	85770223	85770223	85770224	85770224	85770224	85770224	85770236	85770236
Analysis no.	58365	58366	58370	58369	58368	58367	58371	58372	58373	58374	59186	59187
Mineral	CLINOPYRO. 3	CLINOPYRO. 4	CLINOPYRO. 4	CLINOPYRO. 3	CLINOPYRO. 2	CLINOPYRO. 1	CLINOPYRO. 1	CLINOPYRO. 2	CLINOPYRO. 3	CLINOPYRO. 4	CLINOPYRO. 1	CLINOPYRO. 2
Description	CUMULUS, CORE	CUMULUS, CORE	CUMULUS, CORE	CUMULUS, CORE	CUMULUS, CORE	CUMULUS, CORE	CUMULUS, CORE	CUMULUS, CORE	CUMULUS, CORE	CUMULUS, CORE	CUMULUS, CORE	CUMULUS, CORE
Lithology	PLAGIOCLA. WEBSTERITE	PLAGIOCLA. WEBSTERITE	WEBSTERITE	WEBSTERITE	WEBSTERITE	WEBSTERITE	WEBSTERITE	WEBSTERITE	WEBSTERITE	WEBSTERITE	PLAGIOCLA. WEBSTERITE	PLAGIOCLA. WEBSTERITE
Zone	ULTRAMAFIC	ULTRAMAFIC	ULTRAMAFIC	ULTRAMAFIC	ULTRAMAFIC	ULTRAMAFIC	ULTRAMAFIC	ULTRAMAFIC	ULTRAMAFIC	ULTRAMAFIC	ULTRAMAFIC	ULTRAMAFIC
Subzone	I	I	I	I	I	I	I	I	I	I	I	I
Strat. ht (m)	1841	1841	1842	1842	1842	1842	1843	1843	1843	1843	1843.30	1843.30
SiO2	52.84	52.77	53.37	53.08	52.01	52.24	52.40	53.00	52.94	52.72	52.77	53.15
TiO2	.46	.42	.21	.34	.46	.50	.31	.30	.32	.37	.33	.27
Al2O3	1.40	1.50	.75	1.24	1.73	2.16	2.22	1.87	1.81	1.90	2.03	2.24
Cr2O3	<.03	.04	.03	.05	.03	<.03	<.03	<.03	<.03	.04	.05	.06
FeO	7.24	7.57	7.60	8.10	7.58	7.68	7.67	7.75	7.21	7.74	7.78	8.07
MnO	.23	.19	.22	.22	.27	.25	.21	.23	.22	.21	.22	.24
NiO	.07	.08	.07	.09	.03	.06	.07	.07	.03	.07	.03	<.03
MgO	14.84	14.62	15.02	15.03	14.47	14.38	14.91	15.14	14.94	14.75	15.11	15.07
CaO	21.65	21.94	22.10	21.36	21.72	21.68	21.36	21.60	21.95	21.95	20.97	21.29
Na2O	.43	.46	.35	.42	.48	.48	.43	.41	.38	.41	.41	.45
Total	99.16	99.59	99.72	99.94	98.78	99.43	99.58	100.35	99.81	100.17	99.69	100.84
Atomic proportions												
Oxygens	6.0	6.0	6.0	6.0	6.0	6.0	6.0	6.0	6.0	6.0	6.0	6.0
Si	1.971	1.964	1.984	1.970	1.954	1.948	1.948	1.956	1.961	1.952	1.957	1.952
Ti	.013	.012	.006	.010	.013	.014	.009	.008	.009	.010	.009	.007
Al	.061	.066	.033	.054	.076	.095	.097	.081	.079	.083	.089	.097
Cr	-	.001	.001	.001	.001	-	-	-	-	.001	.001	.002
Fe	.226	.236	.236	.252	.238	.239	.238	.239	.223	.240	.241	.248
Mn	.007	.006	.007	.007	.009	.008	.007	.007	.007	.007	.007	.007
Ni	.002	.003	.002	.003	.001	.002	.002	.002	.001	.002	.001	-
Mg	.825	.811	.832	.832	.811	.800	.826	.833	.825	.814	.835	.825
Ca	.865	.875	.880	.850	.874	.866	.851	.854	.871	.871	.833	.838
Na	.031	.033	.025	.030	.035	.035	.031	.029	.028	.030	.029	.032
Total	4.001	4.007	4.006	4.008	4.012	4.007	4.010	4.010	4.004	4.010	4.003	4.008
mg number	79	77	78	77	77	77	78	78	79	77	78	77
Mg'	43	42	43	43	42	42	44	43	43	43	44	43
Fe'	12	12	12	13	13	13	12	12	12	12	12	13
Ca'	45	46	45	44	45	45	44	45	45	45	44	44

Sample no.	85770236	85770236	85770238	85770238	85770238	85770238	85770235	85770235	85770235	85770235	85770235	85770225
Analysis no.	59188	59189	59190	59191	59193	59194	59180	59181	59182	59184	59185	58766
Mineral	CLINOPYRO. 3	CLINOPYRO. 4	CLINOPYRO. 1	CLINOPYRO. 2	CLINOPYRO. 4	CLINOPYRO. 5	CLINOPYRO. 1	CLINOPYRO. 2	CLINOPYRO. 3	CLINOPYRO. 5	CLINOPYRO. 6	CLINOPYRO. 6
Description	CUMULUS, CORE	CUMULUS, CORE	CUMULUS, CORE	CUMULUS, CORE	CUMULUS, CORE	CUMULUS, CORE	CUMULUS, CORE	CUMULUS, CORE	CUMULUS, CORE	CUMULUS, CORE	CUMULUS, CORE	CUMULUS, CORE
Lithology	PLAGIOCLA. WEBSTERITE	PLAGIOCLA. WEBSTERITE	GABBRONOR.	GABBRONOR.	GABBRONOR.	GABBRONOR.	GABBRONOR.	GABBRONOR.	GABBRONOR.	GABBRONOR.	GABBRONOR.	PLAGIOCLA. WEBSTERITE
Zone	ULTRAMAFIC	ULTRAMAFIC	ULTRAMAFIC	ULTRAMAFIC	ULTRAMAFIC	ULTRAMAFIC	ULTRAMAFIC	ULTRAMAFIC	ULTRAMAFIC	ULTRAMAFIC	ULTRAMAFIC	ULTRAMAFIC
Subzone	I	I	I	I	I	I	I	I	I	I	I	I
Strat. ht (m)	1843.30	1843.30	1845.40	1845.40	1845.40	1845.40	1845.75	1845.75	1845.75	1845.75	1845.75	1846
SiO2	52.94	52.90	52.84	52.59	52.19	52.17	52.27	52.37	52.40	52.70	52.31	52.48
TiO2	.31	.41	.17	.18	.35	.23	.28	.35	.34	.24	.21	.42
Al2O3	2.03	1.92	.79	.86	1.29	1.03	1.26	1.24	1.21	1.10	.92	1.28
Cr2O3	.08	.05	.03	<.03	.03	<.03	<.03	<.03	<.03	<.03	<.03	<.03
FeO	7.87	8.13	10.46	10.66	10.90	10.46	10.55	11.00	10.95	10.66	11.71	10.40
MnO	.17	.27	.19	.24	.25	.23	.23	.25	.27	.24	.21	.26
NiO	.06	.03	.11	.11	.09	.09	.09	.10	.07	.06	.09	.08
MgO	15.44	15.19	13.39	13.17	13.20	13.22	13.08	12.94	13.00	13.05	13.13	13.54
CaO	21.09	20.93	21.33	21.06	20.78	20.77	21.55	21.25	21.12	21.52	20.71	21.45
Na2O	.40	.39	.46	.46	.57	.52	.45	.52	.53	.50	.47	.56
Total	100.39	100.22	99.76	99.35	99.64	98.73	99.76	100.01	99.89	100.07	99.75	100.48

Atomic proportions

Oxygens	6.0	6.0	6.0	6.0	6.0	6.0		6.0	6.0	6.0	6.0	6.0	6.0
Si	1.951	1.955	1.986	1.987	1.968	1.981	Si	1.969	1.970	1.972	1.978	1.976	1.961
Ti	.009	.011	.005	.005	.010	.007	Ti	.008	.010	.010	.007	.006	.012
Al	.088	.083	.035	.039	.057	.046	Al	.056	.055	.054	.049	.041	.056
Cr	.002	.001	.001	-	.001	-	Fe	.332	.346	.345	.335	.370	.325
Fe	.243	.251	.329	.337	.344	.332	Mn	.007	.008	.008	.008	.007	.008
Mn	.005	.008	.006	.008	.008	.008	Ni	.003	.003	.002	.002	.003	.002
Ni	.002	.001	.003	.003	.003	.003	Mg	.734	.725	.729	.730	.739	.754
Mg	.848	.837	.750	.741	.742	.748	Ca	.870	.856	.852	.865	.838	.859
Ca	.833	.829	.859	.852	.839	.845	Na	.033	.038	.038	.036	.034	.041
Na	.029	.028	.034	.034	.041	.039	Total	4.012	4.012	4.010	4.009	4.014	4.019
Total	4.010	4.005	4.008	4.006	4.013	4.008							
							mg number	69	68	68	69	67	70
mg number	78	77	70	69	68	69	Mg'	38	38	38	38	38	39
Mg'	44	44	39	39	39	39	Fe'	17	18	18	17	19	17
Fe'	13	13	17	17	17	17	Ca'	45	44	44	45	43	44
Ca'	43	43	44	44	44	44							

Sample no.	85770225	85770225	85770225	85770225	85770225	85770225	85770234	85770234	85770234	85770234	85770234	85770234
Analysis no.	58767	58768	58379	58378	58377	58375	59174	59175	59176	59177	59178	59179
Mineral	CLINOPYRO.	CLINOPYRO.	CLINOPYRO.	CLINOPYRO.	CLINOPYRO.	CLINOPYRO.	CLINOPYRO.	CLINOPYRO.	CLINOPYRO.	CLINOPYRO.	CLINOPYRO.	CLINOPYRO.
	7	8	5	4	3	1	3	4	5	6	7	8
Description	CUMULUS,	CUMULUS,	CUMULUS,	CUMULUS,	CUMULUS,	CUMULUS,	CUMULUS,	CUMULUS,	CUMULUS,	CUMULUS,	CUMULUS,	CUMULUS,
	CORE	CORE	CORE	CORE	CORE	CORE	CORE	CORE	CORE	CORE	CORE	CORE
Lithology	PLAGIOCLA.	PLAGIOCLA.	PLAGIOCLA.	PLAGIOCLA.	PLAGIOCLA.	PLAGIOCLA.	PLAGIOCLA.	PLAGIOCLA.	PLAGIOCLA.	PLAGIOCLA.	PLAGIOCLA.	PLAGIOCLA.
	WEBSTERITE	WEBSTERITE	WEBSTERITE	WEBSTERITE	WEBSTERITE	WEBSTERITE	WEBSTERITE	WEBSTERITE	WEBSTERITE	WEBSTERITE	WEBSTERITE	WEBSTERITE
Zone	ULTRAMAFIC	ULTRAMAFIC	ULTRAMAFIC	ULTRAMAFIC	ULTRAMAFIC	ULTRAMAFIC	ULTRAMAFIC	ULTRAMAFIC	ULTRAMAFIC	ULTRAMAFIC	ULTRAMAFIC	ULTRAMAFIC
Subzone	I	I	I	I	I	I	I	I	I	I	I	I
Strat. ht (m)	1846	1846	1846	1846	1846	1846	1849.75	1849.75	1849.75	1849.75	1849.75	1849.75
SiO2	52.81	52.25	52.35	52.47	51.66	51.89	52.13	51.50	52.11	50.94	51.70	51.24
TiO2	.16	.40	.44	.38	.62	.38	.09	.21	.31	.42	.14	.44
Al2O3	.95	1.23	1.31	1.38	2.02	1.25	.51	.81	.94	1.98	.58	2.02
Cr2O3	<.03	.03	<.03	<.03	<.03	<.03	.05	.06	.03	.08	.03	.03
FeO	10.31	10.38	9.66	10.02	9.90	10.00	14.20	13.90	14.20	14.04	14.06	13.00
MnO	.25	.25	.22	.25	.22	.22	.32	.32	.29	.32	.32	.31
NiO	.04	.07	.08	.10	.07	.07	<.03	<.03	.05	.05	.07	<.03
MgO	13.55	13.64	13.49	13.47	13.30	13.22	11.40	11.50	11.29	11.17	11.27	11.65
CaO	21.59	20.83	21.78	21.65	20.96	21.69	20.43	20.52	21.15	19.95	20.57	20.68
Na2O	.47	.51	.52	.53	.57	.52	.36	.45	.48	.49	.38	.44
Total	100.14	99.61	99.86	100.25	99.31	99.24	99.49	99.26	100.86	99.44	99.12	99.82
Atomic proportions												
Oxygens	6.0	6.0	6.0	6.0	6.0	6.0	6.0	6.0	6.0	6.0	6.0	6.0
Si	1.978	1.966	1.964	1.963	1.947	1.963	1.996	1.977	1.973	1.951	1.989	1.948
Ti	.005	.011	.013	.011	.018	.011	.003	.006	.009	.012	.004	.013
Al	.042	.055	.058	.061	.090	.056	.023	.037	.042	.089	.026	.091
Cr	-	.001	-	-	-	-	.001	.002	.001	.002	.001	.001
Fe	.323	.327	.303	.314	.312	.316	.455	.446	.450	.450	.452	.413
Mn	.008	.008	.007	.008	.007	.007	.010	.010	.009	.010	.010	.010
Ni	.001	.002	.002	.003	.002	.002	-	-	.002	.001	.002	-
Mg	.757	.765	.754	.751	.747	.746	.650	.658	.637	.638	.646	.660
Ca	.866	.840	.875	.868	.847	.879	.838	.844	.858	.819	.848	.842
Na	.034	.037	.038	.039	.042	.038	.027	.033	.035	.036	.029	.032
Total	4.014	4.013	4.014	4.016	4.011	4.017	4.003	4.014	4.015	4.009	4.008	4.010
mg number	70	70	71	71	71	70	59	60	59	59	59	61
Mg'	39	40	39	39	39	39	33	34	33	33	33	34
Fe'	17	17	16	16	16	16	23	23	23	24	23	22
Ca'	44	43	45	45	45	45	44	43	44	43	44	44

Sample no.	85770234	85770234	85770226	85770226	85770226	85770226	85770226	85770226	85770226	85770226	85770229	85770229
Analysis no.	59171	59173	58719	58717	58716	58715	58722	58718	58720	58721	58734	58735
Mineral	CLINOPYRO. 1	CLINOPYRO. 2	CLINOPYRO. 5	CLINOPYRO. 3	CLINOPYRO. 2	CLINOPYRO. 1	CLINOPYRO. 8	CLINOPYRO. 4	CLINOPYRO. 6	CLINOPYRO. 7	CLINOPYRO. 1	CLINOPYRO. 2
Description	CUMULUS, CORE	CUMULUS, CORE	CUMULUS, CORE	CUMULUS, CORE	CUMULUS, CORE	CUMULUS, CORE	CUMULUS, CORE	CUMULUS, CORE	CUMULUS, CORE	CUMULUS, CORE	CUMULUS, CORE	CUMULUS, CORE
Lithology	PLAGIOCLA. WEBSTERITE	PLAGIOCLA. WEBSTERITE	GABBRONOR.	GABBRONOR.	GABBRONOR.	GABBRONOR.	GABBRONOR.	GABBRONOR.	GABBRONOR.	GABBRONOR.	GABBRONOR.	GABBRONOR.
Zone	ULTRAMAFIC	ULTRAMAFIC	GABBROIC	GABBROIC	GABBROIC	GABBROIC	GABBROIC	GABBROIC	GABBROIC	GABBROIC	GABBROIC	GABBROIC
Subzone	I	I	A	A	A	A	A	A	A	A	A	A
Strat. ht (m)	1849.75	1849.75	1851	1851	1851	1851	1851	1851	1851	1851	1854.50	1854.50
SiO2	52.76	52.00	52.16	52.39	52.56	53.13	52.57	51.94	52.33	52.36	52.11	51.63
TiO2	.14	.11	.32	.42	.40	.05	.45	.42	.39	.43	.70	.70
Al2O3	.62	.54	2.05	2.15	2.11	1.77	1.99	2.90	2.10	2.02	1.74	2.07
Cr2O3	.03	<.03	<.03	.04	<.03	<.02	<.03	<.03	.04	<.03	.06	.07
FeO	14.71	15.26	9.31	9.81	9.34	7.72	9.36	8.74	8.76	8.66	8.37	8.52
MnO	.36	.33	.25	.27	.26	.20	.26	.23	.25	.24	.22	.23
NiO	.05	.04	.06	.06	<.03	.05	.04	.04	.05	.06	.04	<.03
MgO	11.48	11.70	15.14	15.13	14.95	14.66	14.95	14.87	14.66	14.86	14.09	14.55
CaO	20.89	19.44	19.62	19.40	20.07	21.75	19.85	20.09	21.19	20.25	22.01	21.46
Na2O	.37	.33	.31	.32	.37	.42	.36	.37	.33	.34	.38	.49
Total	101.41	99.75	99.21	99.98	100.05	99.75	99.82	99.59	100.10	99.22	99.70	99.71
Atomic proportions												
Oxygens	6.0	6.0	6.0	6.0	6.0	6.0	6.0	6.0	6.0	6.0	6.0	6.0
Si	1.987	1.990	1.952	1.948	1.951	1.972	1.955	1.933	1.945	1.956	1.947	1.930
Ti	.004	.003	.009	.012	.011	.001	.013	.012	.011	.012	.020	.020
Al	.028	.024	.091	.094	.093	.077	.087	.127	.092	.089	.076	.091
Cr	.001	-	-	.001	-	-	-	-	.001	-	.002	.002
Fe	.463	.489	.291	.305	.290	.239	.291	.272	.272	.271	.262	.266
Mn	.011	.011	.008	.009	.008	.006	.008	.007	.008	.008	.007	.007
Ni	.001	.001	.002	.002	-	.001	.001	.001	.002	.002	.001	-
Mg	.644	.667	.844	.838	.827	.811	.829	.825	.812	.827	.785	.811
Ca	.843	.797	.786	.773	.798	.865	.791	.801	.844	.810	.881	.859
Na	.027	.025	.022	.023	.026	.030	.026	.027	.024	.024	.028	.035
Total	4.008	4.007	4.005	4.004	4.005	4.003	4.001	4.005	4.010	4.000	4.008	4.022
mg number	58	58	74	73	74	77	74	75	75	75	75	75
Mg'	33	34	44	44	43	42	43	43	42	43	41	42
Fe'	24	25	15	16	15	13	15	14	14	14	14	14
Ca'	43	41	41	40	42	45	42	43	44	43	45	44

Sample no.	85770229	85770229	85770227	85770227	85770227	85770227	85770231	85770231	85770231	85770231	85770231	85770231
Analysis no.	58736	58737	58723	58726	58727	58725	58746	58747	58749	58748	58751	58750
Mineral	CLINOPYRO. 3	CLINOPYRO. 4	CLINOPYRO. 1	CLINOPYRO. 4	CLINOPYRO. 5	CLINOPYRO. 3	CLINOPYRO. 1	CLINOPYRO. 2	CLINOPYRO. 4	CLINOPYRO. 3	CLINOPYRO. 6	CLINOPYRO. 5
Description	CUMULUS, CORE	CUMULUS, CORE	CUMULUS, CORE	CUMULUS, CORE	CUMULUS, CORE	CUMULUS, CORE	CUMULUS, CORE	CUMULUS, CORE	CUMULUS, CORE	CUMULUS, CORE	CUMULUS, CORE	CUMULUS, CORE
Lithology	GABBRONOR.	GABBRONOR.	GABBRONOR.	GABBRONOR.	GABBRONOR.	GABBRONOR.	GABBRONOR.	GABBRONOR.	GABBRONOR.	GABBRONOR.	GABBRONOR.	GABBRONOR.
Zone	GABBROIC	GABBROIC	GABBROIC	GABBROIC	GABBROIC	GABBROIC	GABBROIC	GABBROIC	GABBROIC	GABBROIC	GABBROIC	GABBROIC
Subzone	A	A	A	A	A	A	A	A	A	A	A	A
Strat. ht (m)	1854.50	1854.50	1870	1870	1870	1870	1884	1884	1884	1884	1884	1884
SiO2	51.98	51.84	52.52	52.06	52.37	52.48	51.93	51.59	52.25	51.49	52.09	52.49
TiO2	.60	.41	.39	.40	.40	.46	.39	.36	.42	.43	.42	.44
Al2O3	1.57	2.10	1.97	1.80	1.80	1.91	1.63	1.76	2.04	1.70	1.89	1.90
Cr2O3	.07	.04	<.03	<.03	<.03	<.03	<.03	<.03	<.03	.03	<.03	<.03
FeO	8.53	8.51	8.45	8.46	8.63	7.91	8.20	8.76	8.55	8.62	8.61	9.36
MnO	.26	.21	.26	.29	.28	.25	.23	.28	.22	.25	.28	.25
NiO	<.03	.05	.05	.03	.08	.04	.05	.06	.06	.04	.08	.08
MgO	14.25	14.40	14.20	14.39	14.77	14.47	14.51	14.21	14.39	14.15	14.68	14.65
CaO	21.74	21.24	21.70	21.68	20.70	21.87	22.28	21.83	22.24	21.74	21.65	21.12
Na2O	.43	.48	.37	.32	.34	.33	.29	.36	.39	.34	.33	.36
Total	99.44	99.28	99.91	99.44	99.36	99.71	99.51	99.22	100.56	98.79	100.02	100.64
Atomic proportions												
Oxygens	6.0	6.0	6.0	6.0	6.0	6.0	6.0	6.0	6.0	6.0	6.0	6.0
Si	1.949	1.943	1.955	1.949	1.957	1.953	1.945	1.942	1.938	1.945	1.941	1.945
Ti	.017	.011	.011	.011	.011	.013	.011	.010	.012	.012	.012	.012
Al	.070	.093	.086	.079	.079	.084	.072	.078	.089	.076	.083	.083
Cr	.002	.001	-	-	-	-	-	-	-	.001	-	-
Fe	.268	.267	.263	.265	.270	.246	.257	.276	.265	.272	.268	.290
Mn	.008	.007	.008	.009	.009	.008	.007	.009	.007	.008	.009	.008
Ni	-	.001	.002	.001	.002	.001	.001	.002	.002	.001	.002	.002
Mg	.796	.804	.788	.803	.823	.803	.810	.797	.796	.797	.815	.809
Ca	.873	.853	.865	.870	.829	.872	.894	.881	.884	.880	.864	.838
Na	.031	.035	.027	.023	.024	.024	.021	.026	.028	.025	.024	.026
Total	4.014	4.016	4.005	4.011	4.004	4.004	4.019	4.021	4.020	4.017	4.018	4.014
mg number	75	75	75	75	75	77	76	74	75	75	75	74
Mg'	41	42	41	41	43	42	41	41	41	41	42	42
Fe'	14	14	14	14	14	13	13	14	14	14	14	15
Ca'	45	44	45	45	43	45	46	45	45	45	44	43

Sample no.	85770232	85770232	85770232	85770232	85770232	85770232		85770228	85770228	85770228	85770228	85770228	85770230
Analysis no.	58754	58752	58753	58755	58756	58758		58730	58733	58732	58731	58729	58742
Mineral	CLINOPYRO.	CLINOPYRO.	CLINOPYRO.	CLINOPYRO.	CLINOPYRO.	CLINOPYRO.		CLINOPYRO.	CLINOPYRO.	CLINOPYRO.	CLINOPYRO.	CLINOPYRO.	CLINOPYRO.
	3	1	2	4	5	7		2	5	4	3	1	4
Description	CUMULUS,	CUMULUS,	CUMULUS,	CUMULUS,	CUMULUS,	CUMULUS,		CUMULUS,	CUMULUS,	CUMULUS,	CUMULUS,	CUMULUS,	CUMULUS,
	CORE	CORE	CORE	CORE	CORE	CORE		CORE	CORE	CORE	CORE	CORE	CORE
Lithology	GABBRONOR.	GABBRONOR.	GABBRONOR.	GABBRONOR.	GABBRONOR.	GABBRONOR.		GABBRONOR.	GABBRONOR.	GABBRONOR.	GABBRONOR.	GABBRONOR.	GABBRONOR.
Zone	GABBROIC	GABBROIC	GABBROIC	GABBROIC	GABBROIC	GABBROIC		GABBROIC	GABBROIC	GABBROIC	GABBROIC	GABBROIC	GABBROIC
Subzone	A	A	A	A	A	A		A	A	A	A	A	A
Strat. ht (m)	1890	1890	1890	1890	1890	1890		1900	1900	1900	1900	1900	1950
SiO2	51.86	51.49	52.09	52.01	51.93	51.62		52.07	52.14	51.59	51.80	51.96	51.97
TiO2	.53	.47	.53	.54	.47	.48		.48	.47	.46	.43	.51	.45
Al2O3	1.97	2.08	1.96	2.16	1.96	2.06		1.83	2.05	1.86	1.77	1.91	1.83
Cr2O3	<.03	.04	<.03	.03	<.03	.03		<.03	<.03	<.03	<.03	<.03	<.03
FeO	9.52	8.82	10.04	9.73	9.26	8.94		9.11	8.86	9.20	9.05	8.87	9.92
MnO	.26	.29	.28	.28	.29	.29		.29	.27	.27	.28	.27	.29
NiO	.06	<.03	<.03	.04	.09	.03		<.03	.04	<.03	.05	<.03	.06
MgO	14.09	13.79	13.93	13.92	14.35	13.94		14.11	13.84	13.71	14.15	13.94	14.22
CaO	21.36	21.78	21.33	21.89	20.72	21.72		21.63	21.90	22.09	21.18	21.44	21.24
Na2O	.33	.39	.38	.43	.38	.40		.35	.41	.36	.36	.37	.36
Total	99.98	99.15	100.53	101.05	99.46	99.51		99.87	99.99	99.53	99.08	99.27	100.34

Atomic proportions

Oxygens	6.0	6.0	6.0	6.0	6.0	6.0		6.0	6.0	6.0	6.0	6.0	6.0
Si	1.939	1.939	1.941	1.929	1.947	1.938	Si	1.946	1.946	1.940	1.950	1.951	1.940
Ti	.015	.013	.015	.015	.013	.013	Ti	.013	.013	.013	.012	.014	.013
Al	.087	.092	.086	.095	.087	.091	Al	.081	.090	.082	.079	.084	.081
Cr	-	.001	-	.001	-	.001	Fe	.285	.277	.289	.285	.279	.310
Fe	.298	.278	.313	.302	.290	.281	Mn	.009	.008	.008	.009	.009	.009
Mn	.008	.009	.009	.009	.009	.009	Ni	-	.001	-	.001	-	.002
Ni	.002	-	-	.001	.003	.001	Mg	.786	.770	.769	.794	.780	.791
Mg	.786	.774	.774	.770	.802	.780	Ca	.866	.876	.890	.855	.862	.849
Ca	.856	.879	.852	.870	.832	.874	Na	.025	.030	.026	.027	.027	.026
Na	.024	.029	.028	.031	.027	.029	Total	4.013	4.011	4.019	4.012	4.006	4.020
Total	4.014	4.015	4.016	4.023	4.010	4.017							
							mg number	73	74	73	74	74	72
mg number	73	74	71	72	73	74	Mg'	40	40	39	41	40	40
Mg'	41	40	40	40	42	40	Fe'	15	14	15	15	15	16
Fe'	15	14	16	16	15	15	Ca'	45	46	46	44	45	44
Ca'	44	46	44	44	43	45							

Sample no.	85770230	85770230	85770230	85770230	85770233	85770233	85770233	85770233
Analysis no.	58745	58743	58739	58741	58763	58760	58764	58765
Mineral	CLINOPYRO.	CLINOPYRO.	CLINOPYRO.	CLINOPYRO.	CLINOPYRO.	CLINOPYRO.	CLINOPYRO.	CLINOPYRO.
	7	5	1	3	5	2	6	7
Description	CUMULUS,	CUMULUS,	CUMULUS,	CUMULUS,	CUMULUS,	CUMULUS,	CUMULUS,	CUMULUS,
	CORE	CORE	CORE	CORE	CORE	CORE	CORE	CORE
Lithology	GABBRONOR.	GABBRONOR.	GABBRONOR.	GABBRONOR.	GABBRONOR.	GABBRONOR.	GABBRONOR.	GABBRONOR.
Zone	GABBROIC	GABBROIC	GABBROIC	GABBROIC	GABBROIC	GABBROIC	GABBROIC	GABBROIC
Subzone	A	A	A	A	A	A	A	A
Strat. ht (m)	1950	1950	1950	1950	2000	2000	2000	2000
SiO2	51.85	51.46	51.79	51.61	51.89	51.92	51.91	51.67
TiO2	.47	.47	.45	.48	.47	.36	.43	.48
Al2O3	1.77	2.00	1.80	1.93	1.95	2.15	1.86	1.86
Cr2O3	<.03	.05	.03	.04	<.03	<.03	<.03	<.03
FeO	9.63	9.10	9.25	10.06	10.10	10.25	9.92	10.29
MnO	.26	.30	.22	.27	.22	.23	.31	.28
NiO	.04	.06	<.03	.03	.04	.03	.06	.04
MgO	14.03	13.92	13.85	14.06	13.98	14.05	14.25	14.17
CaO	21.52	21.93	22.08	21.05	21.48	21.00	21.05	20.53
Na2O	.36	.34	.36	.38	.33	.36	.26	.22
Total	99.94	99.64	99.82	99.90	100.45	100.37	100.05	99.54

Atomic proportions

Oxygens	6.0	6.0	6.0	6.0	6.0	6.0		6.0	6.0
Si	1.942	1.933	1.942	1.936	1.937	1.938	Si	1.942	1.943
Ti	.013	.013	.013	.013	.013	.010	Ti	.012	.013
Al	.078	.089	.079	.085	.086	.094	Al	.082	.083
Cr	-	.001	.001	.001	-	-	Fe	.310	.324
Fe	.302	.286	.290	.315	.315	.320	Mn	.010	.009
Mn	.008	.009	.007	.009	.007	.007	Ni	.002	.001
Ni	.001	.002	-	.001	.001	.001	Mg	.794	.794
Mg	.783	.779	.774	.786	.778	.782	Ca	.844	.827
Ca	.864	.883	.887	.846	.859	.840	Na	.019	.016
Na	.026	.025	.026	.027	.024	.026	Total	4.015	4.010
Total	4.019	4.021	4.019	4.021	4.020	4.018			
							mg number	72	71
mg number	72	73	73	71	71	71	Mg'	41	40
Mg'	40	40	40	40	40	40	Fe'	16	17
Fe'	15	15	15	16	16	16	Ca'	43	43
Ca'	45	45	45	44	44	44			

Detailed traverse across ultramafic/gabbroic zone contact (UZ, GZ): clinopyroxene cores and rims

Sample no.	85770215	85770215	85770215	85770215	85770222	85770222	85770222	85770222	85770238	85770238	85770238	85770238
Analysis no.	72002	72004	72005	72006	72007	72008	72011	72012	72029	72030	72031	72032
Mineral	CLINOPYRO. 1	CLINOPYRO. 1	CLINOPYRO. 2	CLINOPYRO. 2	CLINOPYRO. 1	CLINOPYRO. 1	CLINOPYRO. 2	CLINOPYRO. 2	CLINOPYRO. 1	CLINOPYRO. 1	CLINOPYRO. 2	CLINOPYRO. 2
Description	CUMULUS, CORE	CUMULUS, RIM	CUMULUS, CORE	CUMULUS, RIM	CUMULUS, CORE	CUMULUS, RIM	CUMULUS, CORE	CUMULUS, RIM	CUMULUS, CORE	CUMULUS, RIM	CUMULUS, CORE	CUMULUS, RIM
Lithology	OLIVINE-PLAGIOCLA. WEBSTERITE	OLIVINE-PLAGIOCLA. WEBSTERITE	OLIVINE-PLAGIOCLA. WEBSTERITE	OLIVINE-PLAGIOCLA. WEBSTERITE	PLAGIOCLA. WEBSTERITE	PLAGIOCLA. WEBSTERITE	PLAGIOCLA. WEBSTERITE	PLAGIOCLA. WEBSTERITE	GABBRONOR.	GABBRONOR.	GABBRONOR.	GABBRONOR.
Zone	ULTRAMAFIC	ULTRAMAFIC	ULTRAMAFIC	ULTRAMAFIC	ULTRAMAFIC	ULTRAMAFIC	ULTRAMAFIC	ULTRAMAFIC	ULTRAMAFIC	ULTRAMAFIC	ULTRAMAFIC	ULTRAMAFIC
Subzone	I	I	I	I	I	I	I	I	I	I	I	I
Strat. ht (m)	1757	1757	1757	1757	1841	1841	1841	1841	1845.5	1845.5	1845.5	1845.5
SiO2	53.24	53.13	52.92	52.76	51.49	51.49	52.17	51.98	51.84	52.60	52.13	51.88
TiO2	.34	.30	.37	.37	.50	.32	.39	.38	.16	.40	.40	.40
Al2O3	1.70	1.78	1.50	1.58	1.95	1.89	1.45	1.47	1.31	1.14	1.26	1.28
Cr2O3	.35	.36	.39	.39	.03	.06	<.03	<.03	<.03	<.03	.15	<.03
FeO	5.35	5.70	5.67	5.48	7.09	7.34	8.46	8.39	10.86	10.96	11.94	11.44
MnO	.17	.18	.18	.16	.19	.19	.19	.27	.26	.24	.29	.27
NiO	.07	.06	.05	.09	.03	.06	.09	.04	.05	.07	.08	.09
MgO	15.97	16.26	16.43	16.17	14.52	14.50	14.96	15.02	12.56	12.55	12.55	12.32
CaO	22.50	22.18	21.60	22.20	22.91	22.83	21.27	21.63	22.71	22.31	21.63	22.34
Na2O	.57	.52	.49	.50	.37	.40	.46	.41	.53	.53	.48	.48
Total	100.25	100.48	99.59	99.69	99.09	99.08	99.46	99.59	100.28	100.80	100.90	100.49
Atomic proportions												
Oxygens	6.0	6.0	6.0	6.0	6.0	6.0	6.0	6.0	6.0	6.0	6.0	6.0
Si	1.953	1.946	1.953	1.948	1.932	1.935	1.952	1.945	1.954	1.968	1.956	1.955
Ti	.009	.008	.010	.010	.014	.009	.011	.011	.004	.011	.011	.011
Al	.074	.077	.065	.069	.086	.083	.064	.065	.058	.050	.056	.057
Cr	.010	.010	.011	.011	.001	.002	-	-	-	-	.005	-
Fe	.164	.175	.175	.169	.222	.231	.265	.263	.342	.343	.375	.360
Mn	.005	.006	.006	.005	.006	.006	.006	.009	.008	.008	.009	.009
Ni	.002	.002	.001	.003	.001	.002	.003	.001	.001	.002	.002	.003
Mg	.873	.888	.904	.890	.812	.812	.834	.838	.706	.700	.702	.692
Ca	.884	.871	.854	.878	.921	.919	.853	.867	.917	.894	.870	.902
Na	.041	.037	.035	.036	.027	.029	.034	.030	.039	.038	.035	.035
Total	4.016	4.020	4.015	4.019	4.023	4.028	4.022	4.027	4.031	4.015	4.020	4.023
mg number	84	84	84	84	78	78	76	76	67	67	65	66
Mg'	45	46	47	46	42	41	43	43	36	36	36	36
Fe'	9	9	9	9	11	12	13	13	17	18	19	18
Ca'	46	45	44	45	47	47	44	44	47	46	45	46

Sample no.	85770238	85770238	85770235	85770235	85770235	85770225	85770225	85770225	85770225	85770225	85770225
Analysis no.	72033	72034	72035	72036	72038	72013	72014	72015	72016	72017	72018
Mineral	CLINOPYRO. 3	CLINOPYRO. 3	CLINOPYRO. 1	CLINOPYRO. 1	CLINOPYRO. 2	CLINOPYRO. 1	CLINOPYRO. 1	CLINOPYRO. 2	CLINOPYRO. 2	CLINOPYRO. 3	CLINOPYRO. 3
Description	CUMULUS, CORE	CUMULUS, RIM	CUMULUS, CORE	CUMULUS, RIM	CUMULUS, RIM	CUMULUS, CORE	CUMULUS, RIM	CUMULUS, CORE	CUMULUS, RIM	CUMULUS, CORE	CUMULUS, RIM
Lithology	GABBRONOR.	GABBRONOR.	GABBRONOR.	GABBRONOR.	GABBRONOR.	PLAGIOCLA. WEBSTERITE	PLAGIOCLA. WEBSTERITE	PLAGIOCLA. WEBSTERITE	PLAGIOCLA. WEBSTERITE	PLAGIOCLA. WEBSTERITE	PLAGIOCLA. WEBSTERITE
Zone	ULTRAMAFIC	ULTRAMAFIC	ULTRAMAFIC	ULTRAMAFIC	ULTRAMAFIC	ULTRAMAFIC	ULTRAMAFIC	ULTRAMAFIC	ULTRAMAFIC	ULTRAMAFIC	ULTRAMAFIC
Subzone	I	I	I	I	I	I	I	I	I	I	I
Strat. ht (m)	1845.5	1845.5	1845.75	1845.75	1845.75	1846	1846	1846	1846	1846	1846
SiO2	52.29	52.70	51.37	52.56	51.53	51.15	51.15	50.99	50.56	50.60	50.87
TiO2	.33	.32	.42	.20	.32	.50	.50	.51	.55	.48	.45
Al2O3	1.49	1.12	1.56	.70	1.10	1.60	1.46	1.98	1.85	1.92	1.62
Cr2O3	.04	.03	<.03	<.03	<.03	<.03	<.03	<.03	.03	<.03	<.03
FeO	10.50	11.33	11.61	11.64	11.36	10.03	9.49	9.46	10.04	11.43	10.54
MnO	.22	.26	.25	.25	.24	.20	.27	.23	.25	.28	.28
NiO	.05	.10	.06	.07	.05	.04	.05	.04	.06	.05	.06
MgO	12.74	12.67	12.66	12.69	12.26	13.04	13.07	13.36	12.97	13.60	13.28
CaO	22.39	22.32	21.91	22.14	22.10	22.80	22.81	22.42	22.35	20.66	21.83
Na2O	.58	.47	.60	.38	.47	.60	.54	.63	.58	.52	.52
Total	100.64	101.33	100.44	100.64	99.42	99.96	99.34	99.62	99.23	99.55	99.44

Atomic proportions

Oxygens	6.0	6.0	6.0	6.0	6.0	6.0	6.0	6.0	6.0	6.0	6.0
Si	1.957	1.965	1.938	1.975	1.961	1.931	1.939	1.925	1.923	1.921	1.931
Ti	.009	.009	.012	.006	.009	.014	.014	.015	.016	.014	.013
Al	.066	.049	.069	.031	.049	.071	.065	.088	.083	.086	.072
Cr	.001	.001	-	-	-	-	-	-	.001	-	-
Fe	.329	.353	.366	.366	.362	.317	.301	.299	.319	.363	.334
Mn	.007	.008	.008	.008	.008	.006	.009	.007	.008	.009	.009
Ni	.002	.003	.002	.002	.002	.001	.001	.001	.002	.002	.002
Mg	.711	.704	.712	.711	.695	.734	.739	.752	.735	.770	.752
Ca	.898	.891	.886	.892	.901	.922	.926	.907	.911	.840	.888
Na	.042	.034	.044	.028	.035	.044	.040	.046	.043	.038	.038
Total	4.021	4.018	4.037	4.018	4.022	4.041	4.034	4.039	4.041	4.042	4.039
mg number	68	67	66	66	66	70	71	72	70	68	69
Mg'	37	36	36	36	36	37	38	38	38	39	38
Fe'	17	18	19	19	18	16	15	16	16	18	17
Ca'	46	46	45	45	46	47	47	46	46	43	45

Sample no.	85770234	85770234	85770234	85770234	85770234	85770234	85770234	85770234	85770226	85770226	85770226	85770226
Analysis no.	72022	72042	72044	72045	72046	72047	72049	72050	72053	72054	72055	72056
Mineral	CLINOPYRO.	CLINOPYRO.	CLINOPYRO.	CLINOPYRO.	CLINOPYRO.	CLINOPYRO.	CLINOPYRO.	CLINOPYRO.	CLINOPYRO.	CLINOPYRO.	CLINOPYRO.	CLINOPYRO.
	1	1	2	2	3	3	4	4	1	1	2	2
Description	CUMULUS, CORE	CUMULUS, RIM	CUMULUS, CORE	CUMULUS, RIM	CUMULUS, CORE	CUMULUS, RIM	CUMULUS, CORE	CUMULUS, RIM	CUMULUS, CORE	CUMULUS, RIM	CUMULUS, CORE	CUMULUS, RIM
Lithology	PLAGIOCLA. WEBSTERITE	PLAGIOCLA. WEBSTERITE	PLAGIOCLA. WEBSTERITE	PLAGIOCLA. WEBSTERITE	PLAGIOCLA. WEBSTERITE	PLAGIOCLA. WEBSTERITE	PLAGIOCLA. WEBSTERITE	PLAGIOCLA. WEBSTERITE	GABBRONOR.	GABBRONOR.	GABBRONOR.	GABBRONOR.
Zone	ULTRAMAFIC	ULTRAMAFIC	ULTRAMAFIC	ULTRAMAFIC	ULTRAMAFIC	ULTRAMAFIC	ULTRAMAFIC	ULTRAMAFIC	GABBROIC	GABBROIC	GABBROIC	GABBROIC
Subzone	I	I	I	I	I	I	I	I	A	A	A	A
Strat. ht (m)	1849.75	1849.75	1849.75	1849.75	1849.75	1849.75	1849.75	1849.75	1851	1851	1851	1851
SiO2	49.48	52.24	52.10	51.91	51.75	51.29	51.68	52.00	52.43	52.75	51.71	52.84
TiO2	.49	.10	.33	.44	.35	.32	.42	.35	.38	.39	.28	.31
Al2O3	1.78	.49	1.06	1.08	.88	.85	1.50	.98	2.11	1.97	1.94	1.88
Cr2O3	.07	.05	<.03	.04	.03	.04	.04	.05	.03	<.03	.04	<.03
FeO	12.57	14.46	12.84	13.90	12.99	14.03	13.84	13.89	8.47	8.43	9.15	8.19
MnO	.28	.30	.25	.34	.24	.32	.33	.30	.25	.24	.22	.25
NiO	.04	<.03	<.03	.04	<.03	.06	<.03	.05	.06	.05	.07	.07
MgO	11.49	11.07	11.26	10.76	10.91	10.60	11.02	10.95	14.14	14.23	14.15	14.59
CaO	22.03	21.96	22.30	21.74	21.99	21.52	21.71	22.21	23.12	22.70	20.98	22.20
Na2O	.48	.36	.44	.45	.43	.43	.56	.45	.43	.32	.34	.34
Total	98.70	101.02	100.58	100.71	99.57	99.45	101.10	101.23	101.41	101.08	98.87	100.66
Atomic proportions												
Oxygens	6.0	6.0	6.0	6.0	6.0	6.0	6.0	6.0	6.0	6.0	6.0	6.0
Si	1.917	1.980	1.971	1.969	1.979	1.974	1.953	1.965	1.932	1.945	1.950	1.952
Ti	.014	.003	.009	.013	.010	.009	.012	.010	.011	.011	.008	.009
Al	.081	.022	.047	.048	.040	.038	.067	.044	.092	.086	.086	.082
Cr	.002	.002	-	.001	.001	.001	.001	.002	.001	-	.001	-
Fe	.407	.458	.406	.441	.415	.451	.437	.439	.261	.260	.289	.253
Mn	.009	.010	.008	.011	.008	.010	.011	.009	.008	.008	.007	.008
Ni	.001	-	-	.001	-	.002	-	.002	.002	.002	.002	.002
Mg	.664	.625	.635	.608	.622	.608	.621	.617	.777	.782	.795	.803
Ca	.915	.892	.904	.884	.901	.887	.879	.899	.913	.897	.848	.878
Na	.036	.026	.032	.033	.032	.032	.041	.033	.030	.023	.025	.024
Total	4.046	4.018	4.012	4.010	4.007	4.013	4.022	4.019	4.026	4.013	4.011	4.011
mg number	62	58	61	58	60	57	59	58	75	75	73	76
Mg'	33	32	33	31	32	31	32	32	40	40	41	42
Fe'	21	23	21	23	22	23	23	22	13	14	15	13
Ca'	46	45	46	46	46	46	45	46	47	46	44	45

Sample no.	85770227	85770227	85770227	85770227
Analysis no.	72057	72058	72061	72062
Mineral	CLINOPYRO. 1	CLINOPYRO. 1	CLINOPYRO. 2	CLINOPYRO. 2
Description	CUMULUS, CORE	CUMULUS, RIM	CUMULUS, CORE	CUMULUS, RIM
Lithology	GABBRONOR.	GABBRONOR.	GABBRONOR.	GABBRONOR.
Zone	GABBROIC	GABBROIC	GABBROIC	GABBROIC
Subzone	A	A	A	A
Strat. ht (m)	1870	1870	1870	1870
SiO2	52.51	52.48	52.37	52.44
TiO2	.40	.40	.43	.41
Al2O3	1.87	1.69	1.73	1.76
Cr2O3	<.03	<.03	.04	<.04
FeO	9.39	9.96	8.88	8.30
MnO	.24	.31	.24	.18
NiO	.05	.05	<.04	.07
MgO	14.25	14.02	14.34	13.87
CaO	20.86	19.61	21.60	22.92
Na2O	.32	.33	.34	.35
Total	99.89	98.84	99.97	100.30
Atomic proportions				
Oxygens	6.0	6.0	6.0	6.0
Si	1.958	1.975	1.952	1.950
Ti	.011	.011	.012	.012
Al	.082	.075	.076	.077
Cr	-	-	.001	-
Fe	.293	.314	.277	.258
Mn	.008	.010	.008	.006
Ni	.001	.001	-	.002
Mg	.792	.786	.797	.769
Ca	.833	.791	.863	.913
Na	.023	.024	.024	.025
Total	4.001	3.988	4.010	4.012
mg number	73	71	74	75
Mg'	41	42	41	40
Fe'	15	17	14	13
Ca'	44	41	45	47

Detailed traverse across ultramafic/gabbroic zone contact (UZ, GZ): plagioclase

Sample no.	85770215	85770215	85770215	85770215	85770216	85770216	85770216	85770216	85770218	85770218	85770218	85770218
Analysis no.	71918	71921	71920	71919	71925	71924	71923	71922	71927	71928	71929	71930
Mineral	PLAGIOCLA. 1	PLAGIOCLA. 4	PLAGIOCLA. 3	PLAGIOCLA. 2	PLAGIOCLA. 4	PLAGIOCLA. 3	PLAGIOCLA. 2	PLAGIOCLA. 1	PLAGIOCLA. 1	PLAGIOCLA. 2	PLAGIOCLA. 3	PLAGIOCLA. 4
Description	INTERCUMU.	INTERCUMU.	INTERCUMU.	INTERCUMU.	INTERCUMU.	INTERCUMU.	INTERCUMU.	INTERCUMU.	INTERCUMU.	INTERCUMU.	INTERCUMU.	INTERCUMU.
Lithology	OLIVINE-PLAGIOCLA. WEBSTERITE	OLIVINE-PLAGIOCLA. WEBSTERITE	OLIVINE-PLAGIOCLA. WEBSTERITE	OLIVINE-PLAGIOCLA. WEBSTERITE	PLAGIOCLA. WEBSTERITE	PLAGIOCLA. WEBSTERITE	PLAGIOCLA. WEBSTERITE	PLAGIOCLA. WEBSTERITE	OLIVINE-PLAGIOCLA. WEBSTERITE	OLIVINE-PLAGIOCLA. WEBSTERITE	OLIVINE-PLAGIOCLA. WEBSTERITE	OLIVINE-PLAGIOCLA. WEBSTERITE
Zone	ULTRAMAFIC	ULTRAMAFIC	ULTRAMAFIC	ULTRAMAFIC	ULTRAMAFIC	ULTRAMAFIC	ULTRAMAFIC	ULTRAMAFIC	ULTRAMAFIC	ULTRAMAFIC	ULTRAMAFIC	ULTRAMAFIC
Subzone	I	I	I	I	I	I	I	I	I	I	I	I
Strat. ht (m)	1757	1757	1757	1757	1777	1777	1777	1777	1798	1798	1798	1798
SiO2	59.44	60.13	60.57	60.21	60.93	60.52	60.03	60.37	58.03	58.65	58.78	58.92
Al2O3	25.43	25.13	25.35	25.48	25.56	25.44	25.85	25.69	26.76	26.22	26.46	26.24
FeO	.18	.12	.14	.07	.18	.11	.19	.14	.14	.22	.19	.11
CaO	6.09	5.82	5.68	5.85	5.92	5.92	6.37	6.28	7.59	6.79	7.07	6.71
SrO	.06	.06	.08	.05	.10	.09	.10	.08	.08	.10	.10	.11
BaO	.05	.06	.09	.05	.07	.12	.08	.06	.09	.08	.08	.08
Na2O	7.56	7.39	7.58	7.51	7.64	7.33	7.27	7.42	6.69	7.01	6.90	7.08
K2O	.66	.98	1.05	.90	.75	1.04	.88	.73	.56	.80	.73	.76
Total	99.46	99.70	100.54	100.12	101.14	100.57	100.77	100.77	99.93	99.86	100.32	100.02
Atomic proportions												
Oxygens	8.0	8.0	8.0	8.0	8.0	8.0	8.0	8.0	8.0	8.0	8.0	8.0
Si	2.666	2.689	2.688	2.680	2.686	2.685	2.662	2.672	2.600	2.629	2.622	2.634
Al	1.344	1.325	1.326	1.337	1.328	1.330	1.351	1.340	1.413	1.385	1.391	1.383
Fe	.007	.005	.005	.003	.006	.004	.007	.005	.005	.008	.007	.004
Ca	.293	.279	.270	.279	.280	.281	.303	.298	.364	.326	.338	.321
Sr	.002	.001	.002	.001	.002	.002	.003	.002	.002	.003	.003	.003
Ba	.001	.001	.002	.001	.001	.002	.001	.001	.002	.001	.001	.001
Na	.657	.641	.653	.649	.653	.631	.625	.637	.581	.609	.597	.614
K	.038	.056	.060	.051	.042	.059	.050	.041	.032	.046	.042	.043
Total	5.008	4.997	5.005	5.001	4.998	4.995	5.001	4.997	5.000	5.006	5.001	5.004
An	30	29	28	29	29	29	31	30	37	33	35	33
Ab	66	66	66	66	67	65	64	65	59	62	61	63
Or	4	5	6	5	4	6	5	5	4	5	4	4

Sample no.	85770222	85770222	85770222	85770238	85770238	85770238	85770238	85770238	85770235	85770235	85770235	85770239
Analysis no.	71933	71932	71931	71945	71944	71943	71942	71941	71946	71947	71949	71951
Mineral	PLAGIOCLA. 3	PLAGIOCLA. 2	PLAGIOCLA. 1	PLAGIOCLA. 5	PLAGIOCLA. 4	PLAGIOCLA. 3	PLAGIOCLA. 2	PLAGIOCLA. 1	PLAGIOCLA. 1	PLAGIOCLA. 2	PLAGIOCLA. 4	PLAGIOCLA. 1
Description	INTERCUMU.	INTERCUMU.	INTERCUMU.	INTERCUMU.	INTERCUMU.	INTERCUMU.	INTERCUMU.	INTERCUMU.	INTERCUMU.	INTERCUMU.	INTERCUMU.	INTERCUMU.
Lithology	PLAGIOCLA. WEBSTERITE	PLAGIOCLA. WEBSTERITE	PLAGIOCLA. WEBSTERITE	GABBRONOR.	GABBRONOR.	GABBRONOR.	GABBRONOR.	GABBRONOR.	GABBRONOR.	GABBRONOR.	GABBRONOR.	PLAGIOCLA. WEBSTERITE
Zone	ULTRAMAFIC	ULTRAMAFIC	ULTRAMAFIC	ULTRAMAFIC	ULTRAMAFIC	ULTRAMAFIC	ULTRAMAFIC	ULTRAMAFIC	ULTRAMAFIC	ULTRAMAFIC	ULTRAMAFIC	ULTRAMAFIC
Subzone	I	I	I	I	I	I	I	I	I	I	I	I
Strat. ht (m)	1841	1841	1841	1845.5	1845.5	1845.5	1845.5	1845.5	1845.75	1845.75	1845.75	1846
SiO2	56.57	56.09	56.46	62.44	62.51	62.95	62.56	60.27	60.33	60.66	60.53	62.80
Al2O3	27.29	27.66	27.82	23.61	23.33	23.15	23.48	25.35	24.73	24.58	24.73	23.71
FeO	.14	.17	.10	.23	.16	.14	.11	.16	.17	.16	.19	.19
CaO	8.23	8.76	8.83	4.02	4.02	3.73	3.97	5.74	5.59	5.32	5.49	4.22
SrO	.07	.05	.10	<.03	<.03	<.03	<.03	<.03	<.03	<.03	.07	<.03
BaO	.07	.07	.04	<.02	<.02	.04	.08	<.02	.08	.04	.13	.02
Na2O	6.08	5.95	5.89	8.83	8.80	8.67	8.86	7.84	7.64	7.77	7.74	8.86
K2O	.66	.65	.64	.26	.28	.74	.62	.49	.70	.72	.75	.34
Total	99.11	99.40	99.90	99.39	99.10	99.42	99.69	99.85	99.23	99.25	99.62	100.13
Atomic proportions												
Oxygens	8.0	8.0	8.0	8.0	8.0	8.0	8.0	8.0	8.0	8.0	8.0	8.0
Si	2.561	2.537	2.540	2.778	2.787	2.800	2.780	2.685	2.706	2.717	2.707	2.776
Al	1.456	1.475	1.475	1.238	1.226	1.214	1.230	1.331	1.307	1.298	1.303	1.235
Fe	.005	.006	.004	.009	.006	.005	.004	.006	.006	.006	.007	.007
Ca	.399	.425	.426	.191	.192	.178	.189	.274	.268	.255	.263	.200
Sr	.002	.001	.003	-	-	-	-	-	-	-	.002	-
Ba	.001	.001	.001	-	-	.001	.001	-	.001	.001	.002	-
Na	.534	.522	.514	.761	.761	.747	.764	.677	.665	.675	.671	.759
K	.038	.038	.037	.015	.016	.042	.035	.028	.040	.041	.043	.019
Total	4.997	5.004	4.998	4.992	4.988	4.987	5.004	5.002	4.993	4.992	4.998	4.996
An	41	43	44	20	20	18	19	28	28	27	27	20
Ab	55	53	53	78	78	78	77	69	68	69	69	78
Or	4	4	3	2	2	4	4	3	4	4	4	2

Sample no.	85770239	85770239	85770239	85770239	85770225	85770225	85770225	85770225	85770225	85770234	85770234	85770234
Analysis no.	71953	71955	71956	71957	71940	71939	71938	71937	71936	71961	71960	71959
Mineral	PLAGIOCLA. 3	PLAGIOCLA. 5	PLAGIOCLA. 6	PLAGIOCLA. 7	PLAGIOCLA. 5	PLAGIOCLA. 4	PLAGIOCLA. 3	PLAGIOCLA. 2	PLAGIOCLA. 1	PLAGIOCLA. 4	PLAGIOCLA. 3	PLAGIOCLA. 2
Description	INTERCUMU.	INTERCUMU.	INTERCUMU.	INTERCUMU.	INTERCUMU.	INTERCUMU.	INTERCUMU.	INTERCUMU.	INTERCUMU.	INTERCUMU.	INTERCUMU.	INTERCUMU.
Lithology	PLAGIOCLA. WEBSTERITE	PLAGIOCLA. WEBSTERITE	PLAGIOCLA. WEBSTERITE	PLAGIOCLA. WEBSTERITE	PLAGIOCLA. WEBSTERITE	PLAGIOCLA. WEBSTERITE	PLAGIOCLA. WEBSTERITE	PLAGIOCLA. WEBSTERITE	PLAGIOCLA. WEBSTERITE	PLAGIOCLA. WEBSTERITE	PLAGIOCLA. WEBSTERITE	PLAGIOCLA. WEBSTERITE
Zone	ULTRAMAFIC	ULTRAMAFIC	ULTRAMAFIC	ULTRAMAFIC	ULTRAMAFIC	ULTRAMAFIC	ULTRAMAFIC	ULTRAMAFIC	ULTRAMAFIC	ULTRAMAFIC	ULTRAMAFIC	ULTRAMAFIC
Subzone	I	I	I	I	I	I	I	I	I	I	I	I
Strat. ht (m)	1846	1846	1846	1846	1846	1846	1846	1846	1846	1849.75	1849.75	1849.75
SiO2	58.93	59.53	58.55	62.48	58.73	59.04	60.87	60.01	59.54	59.53	59.40	59.47
Al2O3	25.66	25.99	26.18	23.63	25.69	25.75	24.67	25.22	25.81	25.47	25.49	25.51
FeO	.22	.18	.16	.19	.14	.19	.17	.18	.20	.14	.21	.16
CaO	6.70	6.73	7.19	4.37	6.78	6.61	5.56	6.12	6.63	6.26	6.40	6.33
SrO	.04	<.03	.05	<.03	.06	.07	.03	.07	.06	.08	.08	.08
BaO	.06	.06	.04	.05	.09	.09	.12	.10	.08	.08	.08	.12
Na2O	7.12	7.21	6.98	8.64	7.09	7.16	7.73	7.55	7.31	7.39	7.44	7.51
K2O	.59	.56	.52	.42	.62	.58	.72	.69	.63	.54	.53	.48
Total	99.31	100.25	99.68	99.79	99.19	99.49	99.87	99.94	100.25	99.48	99.65	99.66
Atomic proportions												
Oxygens	8.0	8.0	8.0	8.0	8.0	8.0	8.0	8.0	8.0	8.0	8.0	8.0
Si	2.650	2.650	2.626	2.773	2.646	2.650	2.713	2.680	2.653	2.668	2.662	2.663
Al	1.360	1.364	1.384	1.236	1.364	1.362	1.296	1.327	1.355	1.345	1.346	1.347
Fe	.008	.007	.006	.007	.005	.007	.006	.007	.008	.005	.008	.006
Ca	.323	.321	.346	.208	.327	.318	.266	.293	.317	.301	.307	.304
Sr	.001	-	.001	-	.002	.002	.001	.002	.001	.002	.002	.002
Ba	.001	.001	.001	.001	.002	.002	.002	.002	.001	.001	.001	.002
Na	.621	.622	.607	.743	.619	.623	.668	.654	.631	.642	.647	.653
K	.034	.032	.030	.024	.036	.033	.041	.040	.036	.031	.031	.027
Total	4.997	4.995	5.000	4.992	5.000	4.997	4.993	5.003	5.003	4.995	5.004	5.003
An	33	33	35	21	33	33	27	30	32	31	31	31
Ab	64	64	62	76	63	64	69	66	64	66	66	66
Or	3	3	3	3	4	3	4	4	4	3	3	3

Sample no.	85770234	85770226	85770226	85770226	85770226	85770229	85770229	85770229	85770227	85770227	85770227	85770227
Analysis no.	71958	71962	71963	71964	71965	71976	71975	71974	71969	71968	71967	71966
Mineral	PLAGIOCLA. 1	PLAGIOCLA. 1	PLAGIOCLA. 2	PLAGIOCLA. 3	PLAGIOCLA. 4	PLAGIOCLA. 4	PLAGIOCLA. 3	PLAGIOCLA. 2	PLAGIOCLA. 4	PLAGIOCLA. 3	PLAGIOCLA. 2	PLAGIOCLA. 1
Description	INTERCUMU.	CUMULUS, CORE	CUMULUS, CORE	CUMULUS, CORE	CUMULUS, CORE	CUMULUS, CORE	CUMULUS, CORE	CUMULUS, CORE	CUMULUS, CORE	CUMULUS, CORE	CUMULUS, CORE	CUMULUS, CORE
Lithology	PLAGIOCLA. WEBSTERITE	GABBRONOR.	GABBRONOR.	GABBRONOR.	GABBRONOR.	GABBRONOR.	GABBRONOR.	GABBRONOR.	GABBRONOR.	GABBRONOR.	GABBRONOR.	GABBRONOR.
Zone	ULTRAMAFIC	GABBROIC	GABBROIC	GABBROIC	GABBROIC	GABBROIC	GABBROIC	GABBROIC	GABBROIC	GABBROIC	GABBROIC	GABBROIC
Subzone	I	A	A	A	A	A	A	A	A	A	A	A
Strat. ht (m)	1849.75	1851	1851	1851	1851	1854.5	1854.5	1854.5	1870	1870	1870	1870
SiO2	60.58	54.57	55.65	54.97	55.27	55.05	57.54	56.19	55.74	55.53	54.65	55.46
Al2O3	25.27	29.42	28.57	28.88	28.79	28.85	27.05	27.49	28.16	28.48	28.79	28.44
FeO	.15	.24	.27	.23	.24	.27	.16	.20	.31	.32	.35	.50
CaO	5.76	11.01	10.03	10.27	10.15	10.22	8.12	9.03	9.80	10.11	10.63	9.90
SrO	<.03	.08	.09	.08	.06	.07	.04	.07	.06	.07	.06	.06
BaO	.09	<.02	<.02	<.02	<.02	.03	<.02	.03	<.02	.03	<.02	<.02
Na2O	7.96	4.96	5.44	5.41	5.41	5.27	6.14	5.76	5.53	5.43	5.12	5.45
K2O	.49	.32	.39	.38	.37	.57	.79	.73	.42	.34	.35	.37
Total	100.29	100.61	100.44	100.22	100.29	100.33	99.83	99.50	100.02	100.31	99.95	100.18
Atomic proportions												
Oxygens	8.0	8.0	8.0	8.0	8.0	8.0	8.0	8.0	8.0	8.0	8.0	8.0
Si	2.690	2.450	2.496	2.474	2.484	2.477	2.583	2.541	2.509	2.495	2.469	2.496
Al	1.322	1.557	1.511	1.532	1.525	1.530	1.431	1.465	1.494	1.508	1.533	1.508
Fe	.005	.009	.010	.009	.009	.010	.006	.007	.012	.012	.013	.019
Ca	.274	.529	.482	.496	.489	.493	.390	.437	.473	.487	.514	.477
Sr	-	.002	.002	.002	.001	.002	.001	.002	.002	.002	.002	.002
Ba	.002	-	-	-	-	.001	-	.001	-	.001	-	-
Na	.685	.432	.473	.472	.472	.460	.535	.505	.483	.473	.449	.476
K	.028	.019	.022	.022	.021	.033	.045	.042	.024	.020	.020	.021
Total	5.005	4.997	4.996	5.007	5.000	5.004	4.991	5.001	4.997	4.995	4.999	4.998
An	28	54	49	50	50	50	40	45	48	50	52	49
Ab	69	44	48	48	48	47	55	51	49	48	46	49
Or	3	2	3	2	2	3	5	4	3	2	2	2

Sample no.	85770231	85770231	85770231	85770232	85770232	85770232	85770232	85770228	85770228	85770228	85770230	85770230
Analysis no.	71984	71983	71982	71988	71987	71986	71985	71972	71971	71970	71981	71980
Mineral	PLAGIOCLA.	PLAGIOCLA.	PLAGIOCLA.	PLAGIOCLA.	PLAGIOCLA.	PLAGIOCLA.	PLAGIOCLA.	PLAGIOCLA.	PLAGIOCLA.	PLAGIOCLA.	PLAGIOCLA.	PLAGIOCLA.
	3	2	1	4	3	2	1	3	2	1	4	3
Description	CUMULUS,	CUMULUS,	CUMULUS,	CUMULUS,	CUMULUS,	CUMULUS,	CUMULUS,	CUMULUS,	CUMULUS,	CUMULUS,	CUMULUS,	CUMULUS,
	CORE	CORE	CORE	CORE	CORE	CORE	CORE	CORE	CORE	CORE	CORE	CORE
Lithology	GABBRONOR.	GABBRONOR.	GABBRONOR.	GABBRONOR.	GABBRONOR.	GABBRONOR.	GABBRONOR.	GABBRONOR.	GABBRONOR.	GABBRONOR.	GABBRONOR.	GABBRONOR.
Zone	GABBROIC	GABBROIC	GABBROIC	GABBROIC	GABBROIC	GABBROIC	GABBROIC	GABBROIC	GABBROIC	GABBROIC	GABBROIC	GABBROIC
Subzone	A	A	A	A	A	A	A	A	A	A	A	A
Strat. ht (m)	1884	1884	1884	1890	1890	1890	1890	1900	1900	1900	1950	1950
SiO2	55.60	55.68	55.39	55.40	56.17	56.60	56.19	55.60	55.45	56.18	55.76	56.11
Al2O3	28.21	28.35	28.45	28.16	27.90	27.22	28.25	28.21	28.59	28.44	28.02	27.97
FeO	.35	.36	.35	.35	.34	.68	.42	.36	.39	.36	.42	.40
CaO	9.92	9.97	10.21	9.74	9.27	8.53	9.64	9.69	10.08	9.84	9.38	9.38
SrO	.07	.08	.06	.06	.07	.07	.09	.07	.09	.07	.06	.08
BaO	<.02	<.02	.03	.03	<.02	<.02	<.02	<.02	<.02	<.02	<.02	.03
Na2O	5.50	5.40	5.35	5.46	5.88	6.33	5.73	5.60	5.42	5.60	5.55	5.71
K2O	.37	.38	.35	.41	.41	.32	.43	.40	.37	.39	.41	.42
Total	100.02	100.23	100.19	99.63	100.05	99.74	100.75	99.94	100.38	100.87	99.58	100.10
Atomic proportions												
Oxygens	8.0	8.0	8.0	8.0	8.0	8.0	8.0	8.0	8.0	8.0	8.0	8.0
Si	2.504	2.503	2.493	2.504	2.526	2.552	2.513	2.506	2.491	2.508	2.519	2.523
Al	1.498	1.502	1.509	1.501	1.479	1.446	1.489	1.499	1.513	1.496	1.492	1.482
Fe	.013	.014	.013	.013	.013	.025	.016	.014	.015	.013	.016	.015
Ca	.479	.480	.492	.472	.447	.412	.462	.468	.485	.471	.454	.452
Sr	.002	.002	.002	.002	.002	.002	.002	.002	.002	.002	.001	.002
Ba	-	-	.001	.001	-	-	-	-	-	-	-	.001
Na	.480	.471	.467	.479	.513	.554	.497	.489	.472	.484	.486	.498
K	.021	.022	.020	.024	.024	.018	.025	.023	.021	.022	.024	.024
Total	4.997	4.993	4.996	4.995	5.003	5.009	5.003	5.000	4.999	4.997	4.990	4.997
An	49	49	50	49	45	42	47	48	50	48	47	46
Ab	49	49	48	49	52	56	51	50	48	50	50	51
Or	2	2	2	2	3	2	2	2	2	2	3	3

Sample no.	85770230	85770230	85770233	85770233	85770233	85770233
Analysis no.	71979	71978	71989	71990	71991	71992
Mineral	PLAGIOCLA. 2	PLAGIOCLA. 1	PLAGIOCLA. 1	PLAGIOCLA. 2	PLAGIOCLA. 3	PLAGIOCLA. 4
Description	CUMULUS, CORE	CUMULUS, CORE	CUMULUS, CORE	CUMULUS, CORE	CUMULUS, CORE	CUMULUS, CORE
Lithology	GABBRONOR.	GABBRONOR.	GABBRONOR.	GABBRONOR.	GABBRONOR.	GABBRONOR.
Zone	GABBROIC	GABBROIC	GABBROIC	GABBROIC	GABBROIC	GABBROIC
Subzone	A	A	A	A	A	A
Strat. ht (m)	1950	1950	2000	2000	2000	2000
SiO2	56.16	56.41	55.99	55.83	55.53	55.98
Al2O3	28.22	28.20	28.05	28.08	28.15	27.91
FeO	.32	.31	.25	.32	.28	.24
CaO	9.45	9.49	9.53	9.37	9.55	9.30
SrO	.06	.07	.05	.09	.05	.06
BaO	<.02	.03	.05	<.02	<.02	.04
Na2O	5.63	5.80	5.69	5.60	5.59	5.79
K2O	.41	.44	.38	.43	.35	.35
Total	100.26	100.74	99.98	99.71	99.50	99.67
Atomic proportions						
Oxygens	8.0	8.0	8.0	8.0	8.0	8.0
Si	2.519	2.520	2.519	2.518	2.510	2.525
Al	1.492	1.485	1.488	1.493	1.500	1.484
Fe	.012	.011	.009	.012	.011	.009
Ca	.454	.454	.459	.453	.463	.450
Sr	.002	.002	.001	.002	.001	.002
Ba	-	.001	.001	-	-	.001
Na	.490	.503	.496	.490	.490	.507
K	.024	.025	.022	.025	.020	.020
Total	4.992	5.001	4.996	4.993	4.995	4.997
An	47	46	47	47	48	46
Ab	51	51	51	51	50	52
Or	2	3	2	2	2	2

Pyroxene analyses from the Andover Complex

Sample number	119	119	057	053	213	213	043	043	038	038	162	162
Analysis number	10889	10891	10917	10850	9744	9739	10509	10506	10557	10546	10913	10911
Mineral name	CLINOPYRO.	ORTHOPYRO.	ORTHOPYRO.	ORTHOPYRO.	CLINOPYRO.	ORTHOPYRO.	CLINOPYRO.	ORTHOPYRO.	CLINOPYRO.	ORTHOPYRO.	CLINOPYRO.	ORTHOPYRO.
Description	INTERCUM.	CUMULUS	CUMULUS	CUMULUS	CUMULUS	CUMULUS	INTERCUM.	CUMULUS	CUMULUS	CUMULUS	CUMULUS	CUMULUS
Lithology	NORITE	NORITE	PERIDOTITE	LHERZOLITE	CLINO-PYROXENITE	CLINO-PYROXENITE	ORTHO-PYROXENITE	ORTHO-PYROXENITE	ORTHO-PYROXENITE	ORTHO-PYROXENITE	LHERZOLITE	LHERZOLITE
Zone	ULTRAMAFIC	ULTRAMAFIC	ULTRAMAFIC	ULTRAMAFIC	ULTRAMAFIC	ULTRAMAFIC	ULTRAMAFIC	ULTRAMAFIC	ULTRAMAFIC	ULTRAMAFIC	ULTRAMAFIC	ULTRAMAFIC
Subzone	BASE	BASE	C	C	C	C	D	D	D	D	F	F
Strat. ht (km)	0.01	0.01	.44	0.53	0.56	0.56	0.67	0.67	0.68	0.68	1.09	1.09
SiO2	50.58	53.10	55.61	54.11	53.04	54.73	51.79	55.27	51.55	55.96	51.34	55.10
TiO2	.68	.12	<.09	<.09	.31	<.09	.42	<.09	.29	<.09	.56	.20
Al2O3	2.31	.99	.63	2.02	1.54	.23	2.44	.91	2.32	.95	2.51	1.28
Cr2O3	.15	<.11	<.10	.10	.14	<.11	.68	<.10	1.07	<.11	.87	.26
FeO	8.13	18.65	10.57	10.10	8.90	17.61	4.87	11.75	4.61	11.00	4.52	10.59
MnO	<.11	.19	<.10	.12	.12	.19	<.11	<.10	<.11	<.11	<.11	<.10
MgO	14.54	25.28	31.87	30.91	17.38	26.82	16.70	31.02	16.33	31.47	15.90	29.76
CaO	22.99	1.49	.64	1.87	18.73	.59	22.31	.53	22.84	.78	23.40	2.84
Na2O	.26	<.17	<.16	<.16	<.15	<.16	.19	<.16	.26	<.17	.21	<.16
K2O	<.05	<.05	<.05	<.05	<.06	<.06	<.05	<.05	<.06	<.06	<.05	<.05
Total	99.64	99.82	99.32	99.24	100.16	100.17	99.41	99.48	99.28	100.16	99.33	100.03
Atomic proportions												
Oxygens	6.0	6.0	6.0	6.0	6.0	6.0	6.0	6.0	6.0	6.0	6.0	6.0
Si	1.899	1.953	1.970	1.926	1.953	1.986	1.913	1.965	1.911	1.969	1.904	1.952
Ti	.019	.003	-	-	.009	-	.012	-	.008	-	.016	.005
Al	.102	.043	.026	.085	.067	.010	.106	.038	.102	.039	.110	.054
Cr	.004	-	-	.003	.004	-	.020	-	.031	-	.026	.007
Fe	.255	.574	.313	.301	.274	.534	.150	.349	.143	.324	.140	.314
Mn	-	.006	-	.004	.004	.006	-	-	-	-	-	-
Mg	.814	1.386	1.683	1.640	.954	1.450	.920	1.644	.902	1.650	.879	1.572
Ca	.925	.059	.024	.071	.739	.023	.883	.020	.907	.029	.930	.108
Na	.019	-	-	-	-	-	.014	-	.019	-	.015	-
Total	4.038	4.023	4.017	4.030	4.003	4.009	4.019	4.016	4.024	4.011	4.020	4.012
mg number	76	71	84	84	78	73	86	82	86	84	86	83
Mg'	41	69	83	81	48	72	47	82	46	82	45	79
Fe'	13	28	16	15	14	27	8	17	7	16	7	16
Ca'	46	3	1	4	38	1	45	1	47	2	48	5

Sample number	074	158	158	209	209	068	068	153	197	197	069
Analysis number	10527	10536	10535	9595	9596	10517	10512	10542	9607	9601	10906
Mineral name	CLINOPYRO.	CLINOPYRO.	ORTHOPYRO.	ORTHOPYRO.	CLINOPYRO.	CLINOPYRO.	ORTHOPYRO.	ORTHOPYRO.	CLINOPYRO.	ORTHOPYRO.	CLINOPYRO.
Description	CUMULUS	CUMULUS	CUMULUS	CUMULUS	CUMULUS	CUMULUS	CUMULUS	CUMULUS	INTERCUM.	CUMULUS	CUMULUS
Lithology	CLINO-PYROXENITE	ORTHO-PYROXENITE	ORTHO-PYROXENITE	ORTHO-PYROXENITE	ORTHO-PYROXENITE	ORTHO-PYROXENITE	ORTHO-PYROXENITE	WEBSTERITE	NORITE	NORITE	GABBRO
Zone	ULTRAMAFIC	ULTRAMAFIC	ULTRAMAFIC	ULTRAMAFIC	ULTRAMAFIC	ULTRAMAFIC	ULTRAMAFIC	ULTRAMAFIC	GABBRO	GABBRO	GABBRO
Subzone	G	G	G	G	G	G	G	G	-	-	-
Strat. ht (km)	1.15	1.17	1.17	1.28	1.28	1.29	1.29	1.30	1.31	1.31	1.32
SiO2	51.62	52.21	55.06	56.23	52.84	51.40	55.68	51.90	52.28	55.81	51.09
TiO2	.19	.25	<.09	<.09	<.09	<.09	<.09	.10	.56	.11	.65
Al2O3	2.32	2.07	.94	.99	2.34	2.53	.60	2.80	1.79	.56	2.37
Cr2O3	.42	.73	<.10	.41	1.25	1.25	.15	.98	.48	<.11	.22
FeO	5.45	5.13	12.74	8.84	4.18	5.01	10.87	6.10	5.60	14.51	7.61
MnO	<.10	<.11	.12	<.11	<.11	<.11	<.11	<.11	<.11	<.11	<.11
MgO	17.37	16.13	30.36	31.93	17.23	16.37	30.61	16.11	15.81	28.97	15.40
CaO	21.91	23.17	.51	1.51	23.08	22.69	1.76	21.56	23.43	.90	22.04
Na2O	<.15	<.16	<.17	<.15	<.15	<.15	<.17	<.16	.19	<.16	<.16
K2O	<.05	<.06	<.06	<.05	<.06	<.05	<.06	<.06	<.05	<.06	<.05
Total	99.27	99.69	99.73	99.91	100.92	99.24	99.68	99.55	100.14	100.86	99.38
Atomic proportions											
Oxygens	6.0	6.0	6.0	6.0	6.0	6.0	6.0	6.0	6.0	6.0	6.0
Si	1.911	1.928	1.962	1.970	1.919	1.908	1.974	1.919	1.928	1.981	1.909
Ti	.005	.007	-	-	-	-	-	.003	.016	.003	.018
Al	.101	.090	.039	.041	.100	.111	.025	.122	.078	.023	.104
Cr	.012	.021	-	.011	.036	.037	.004	.029	.014	-	.007
Fe	.169	.158	.380	.259	.127	.156	.322	.189	.173	.431	.238
Mn	-	-	.004	-	-	-	-	-	-	-	-
Mg	.959	.888	1.613	1.667	.933	.906	1.618	.888	.869	1.533	.858
Ca	.869	.917	.019	.057	.898	.902	.067	.854	.926	.034	.883
Na	-	-	-	-	-	-	-	-	.014	-	-
Total	4.027	4.009	4.018	4.004	4.013	4.018	4.011	4.003	4.017	4.005	4.017
mg number	85	85	81	86	88	85	83	82	83	78	78
Mg'	48	45	80	84	48	46	81	46	44	77	43
Fe'	8	8	19	13	6	8	16	10	9	21	12
Ca'	44	47	1	3	46	46	3	44	47	2	45

APPENDIX 3. WHOLE-ROCK (MAJOR, TRACE, PGEs) GEOCHEMISTRY OF THE MUNNI MUNNI, MOUNT SHOLL, MAITLAND, RADIO HILL, AND ANDOVER INTRUSIONS

Explanation of attribute data and ratios used in the whole-rock tables

Sample no: Eight digits, comprising year of collection, AGSO project code, and four-digit sample number. Most samples are arranged in order of increasing stratigraphic height.

Intrusion: As indicated.

Locality: As indicated, and on the appended 1 : 20 000 geological maps for the Munni Munni, Mount Sholl, Maitland, and Radio Hill intrusions. Sample co-ordinates (AGM grid and longitude/latitude references) for the Andover Complex are given in Table 43.

Lithology: As indicated.

Zone: Ultramafic or gabbroic, or as indicated if outside the complex.

Subzone: As indicated.

Strat. ht (m): Estimated stratigraphic height in metres above the base of the Munni Munni, Radio Hill, and Andover complexes. The stratigraphic height indicated along sample traverses A and B for the Mount Sholl and Maitland complexes is an apparent height.

Ratio used: mg = mg number = (100 x MgO/40.32)/(FeO/71.85 + Fe_2O_3/79.85 + MgO/40.32).

Sample no.	84770001	84770002	84770003	84770004	84770005	84770006	84770007	84770008
Intrusion	Munni Munni Complex	Munni Munni Complex	Munni Munni Complex	Munni Munni Complex	Munni Munni Complex	Munni Munni Complex	Munni Munni Complex	Munni Munni Complex
Locality	Sample traverse	Sample traverse	Sample traverse	Sample traverse	Sample traverse	Sample traverse	Sample traverse	Sample traverse
Lithology	Plagiocla. olivine websterite	Plagiocla. websterite	Olivine websterite	Olivine websterite	Olivine websterite	Olivine websterite	Websterite	Lherzolite
Zone	Ultramafic	Ultramafic	Ultramafic	Ultramafic	Ultramafic	Ultramafic	Ultramafic	Ultramafic
Subzone	A'	A'	A'	A	A	A	A	B
Strat. ht (m)	64	128	174	218	247	268	285	313
SiO2	52.38	52.65	51.04	52.05	49.66	51.51	52.48	36.92
TiO2	.28	.24	.27	.21	.20	.23	.21	.05
Al2O3	2.16	1.56	1.93	1.31	1.34	1.46	1.43	.47
Fe2O3	1.06	1.09	1.62	1.05	3.40	1.68	1.16	14.65
FeO	6.97	6.66	7.21	6.97	5.85	6.13	5.81	1.55
MnO	.20	.19	.19	.20	.20	.20	.19	.15
MgO	18.10	18.87	20.66	19.53	21.33	20.10	19.73	33.14
CaO	16.14	16.77	14.97	16.86	14.72	16.49	16.61	.03
Na2O	.79	.55	.23	.40	.43	.37	.46	.18
K2O	.13	.05	.11	.01	.01	.02	.02	.04
P2O5	<.01	<.01	<.01	<.01	<.01	<.01	<.01	<.01
H2O+	.90	-	-	-	-	.97	-	-
H2O-	<.05	-	-	-	-	<.05	-	-
CO2	.36	-	-	-	-	.21	-	-
LOI	-	1.03	1.49	1.16	2.28	-	1.34	11.50
Rest	.57	.48	.49	.50	.46	.44	.56	.49
Total	100.04	100.14	100.21	100.25	99.88	99.81	100.00	99.17
O=F,S,Cl	.01	.00	.00	.00	.00	.00	.00	.00
Total	100.04	100.13	100.21	100.25	99.88	99.81	100.00	99.17
Trace elements in parts per million								
Ba	70	35	63	15	26	17	31	13
Rb	4	2	3	1	<1	1	1	<1
Sr	62	45	60	31	31	37	39	2
Pb	1	2	<1	1	<1	<1	2	1
Th	1	1	1	1	1	<1	1	<1
Zr	18	11	16	7	8	9	9	5
Nb	1	1	1	<1	1	<1	<1	<1
Y	7	6	6	6	7	6	5	1
La	4	2	2	<2	4	2	<2	2
Ce	5	4	2	2	3	6	2	3
Nd	4	3	3	2	4	4	3	<2
Sc	36	41	36	42	36	41	38	5
V	129	194	168	187	166	192	135	23
Cr	2777	2123	2058	2286	1833	1810	2745	486
Co	68	69	79	75	85	77	63	160
Ni	683	683	856	784	947	824	759	2916
Cu	27	19	26	12	14	14	17	5
Zn	55	50	58	51	61	48	47	83
Mo	4	4	3	4	4	4	4	2
Ga	3	3	3	2	2	3	2	1
As	<.5	<.5	1.0	.5	.5	.5	<.5	.5
S	118	62	82	30	60	41	64	63
Cs	<3	<3	<3	<3	<3	<3	<3	<3
Trace elements in parts per billion								
Pt	3.27	-	1.46	-	1.34	-	2.40	-
Pd	5.81	-	1.97	-	1.99	-	2.67	-
Ir	.31	-	.81	-	1.37	-	.63	-
Au	.50	-	.25	-	.20	-	.48	-
Se	29.0	-	-	-	26.0	-	12.0	-
Cs	298	-	-	-	104	-	188	-
Rb	3218	-	-	-	703	-	1202	-
mg	80.3	81.5	80.9	81.5	81.0	82.4	83.7	80.0

Sample no.	84770010	84770011	84770012	84770013	84770014	84770015	84770016	84770017
Intrusion	Munni Munni Complex	Munni Munni Complex	Munni Munni Complex	Munni Munni Complex	Munni Munni Complex	Munni Munni Complex	Munni Munni Complex	Munni Munni Complex
Locality	Sample traverse	Sample traverse	Sample traverse	Sample traverse	Sample traverse	Sample traverse	Sample traverse	Sample traverse
Lithology	Olivine websterite	Olivine websterite	Olivine websterite	Olivine websterite	Olivine websterite	Olivine websterite	Olivine websterite	Olivine websterite
Zone	Ultramafic	Ultramafic	Ultramafic	Ultramafic	Ultramafic	Ultramafic	Ultramafic	Ultramafic
Subzone	B	C	C	C	C	C	C	C
Strat. ht (m)	404	440	459	482	533	578	620	655
SiO2	47.44	49.44	49.32	48.93	50.27	49.26	50.65	50.05
TiO2	.12	.14	.15	.15	.14	.15	.15	.13
Al2O3	.77	.77	.77	.78	.73	.78	.73	.71
Fe2O3	4.39	3.73	3.65	4.35	3.47	3.81	4.31	3.59
FeO	4.87	4.80	5.28	5.04	4.68	5.30	4.19	4.64
MnO	.19	.19	.18	.20	.20	.20	.19	.19
MgO	24.09	22.19	20.72	21.55	21.30	21.45	20.89	22.17
CaO	12.11	14.53	14.87	14.33	15.25	14.73	15.51	14.82
Na2O	.36	.30	.26	.32	.38	.31	.26	.33
K2O	.01	.01	<.01	<.01	<.01	<.01	<.01	<.01
P2O5	<.01	<.01	<.01	<.01	<.01	<.01	<.01	<.01
H2O+	-	-	3.43	-	-	-	-	2.60
H2O-	-	-	.06	-	-	-	-	.05
CO2	-	-	.15	-	-	-	-	.08
LOI	4.68	3.39	-	3.73	3.56	3.89	2.84	-
Rest	.73	.42	.34	.35	.57	.35	.47	.54
Total	99.76	99.91	99.18	99.73	100.55	100.23	100.19	99.90
O=F,S,Cl	.01	.00	.00	.00	.00	.00	.00	.00
Total	99.75	99.91	99.18	99.73	100.55	100.23	100.19	99.90
Trace elements in parts per million								
Ba	21	9	11	7	11	18	14	8
Rb	1	1	<1	1	<1	1	<1	<1
Sr	19	22	22	22	22	22	21	20
Pb	1	<1	1	1	<1	<1	<1	1
Th	1	<1	<1	1	<1	1	<1	<1
Zr	3	2	4	4	3	3	3	3
Nb	1	<1	<1	<1	<1	<1	<1	<1
Y	3	5	5	4	4	4	4	5
La	<2	<2	3	<2	<2	3	<2	<2
Ce	<2	<2	<2	3	<2	<2	<2	<2
Nd	<2	<2	<2	<2	<2	2	<2	<2
Sc	27	35	35	37	34	36	36	33
V	81	123	153	152	119	153	138	113
Cr	3266	1408	899	893	2544	884	1840	2279
Co	98	89	92	103	87	97	85	87
Ni	1527	1250	1195	1218	1199	1210	1130	1199
Cu	12	7	6	9	6	7	4	7
Zn	57	52	48	56	54	55	51	56
Mo	3	4	3	3	4	4	4	4
Ga	1	1	2	1	1	1	2	1
As	.5	.5	<.5	.5	.5	.5	1.0	1.0
S	104	<20	27	23	<20	49	<20	<20
Cs	<3	<3	<3	<3	<3	<3	<3	<3
Trace elements in parts per billion								
Pt	-	1.77	-	-	-	-	1.38	-
Pd	-	2.27	-	-	-	-	1.84	-
Ir	-	1.14	-	-	-	-	1.30	-
Au	-	.35	-	-	-	-	.30	-
Se	-	7.0	-	-	-	-	16.0	-
Cs	-	128	-	-	-	-	336	-
Rb	-	696	-	-	-	-	289	-
mg	83.0	82.9	81.2	81.1	83.0	81.4	82.2	83.4

Sample no.	84770018	84770019	84770020	84770021	84770022	84770023	84770024	84770027
Intrusion	Munni Munni Complex	Munni Munni Complex	Munni Munni Complex	Munni Munni Complex	Munni Munni Complex	Munni Munni Complex	Munni Munni Complex	Munni Munni Complex
Locality	Sample traverse	Sample traverse	Sample traverse	Sample traverse	Sample traverse	Sample traverse	Sample traverse	Sample traverse
Lithology	Olivine websterite	Websterite	Websterite	Olivine websterite	Olivine websterite	Websterite	Olivine clinopyro.	Clinopyro.
Zone	Ultramafic	Ultramafic	Ultramafic	Ultramafic	Ultramafic	Ultramafic	Ultramafic	Ultramafic
Subzone	C	C	D	D	D	D	D	E
Strat. ht (m)	690	748	867	910	950	990	1020	1103
SiO2	51.82	53.54	52.98	49.59	50.95	52.65	50.69	52.25
TiO2	.15	.16	.15	.13	.14	.17	.14	.16
Al2O3	.79	.97	.87	.76	.72	.84	.71	.79
Fe2O3	1.70	1.56	1.29	2.81	2.69	1.73	2.63	1.57
FeO	5.32	5.36	5.33	5.53	6.09	5.58	6.29	5.69
MnO	.18	.19	.19	.20	.21	.20	.21	.20
MgO	21.09	19.88	20.41	23.31	20.85	18.65	21.83	19.30
CaO	16.10	16.31	16.45	13.49	15.51	17.42	14.88	17.05
Na2O	.31	.46	.41	.30	.33	.33	.28	.40
K2O	<.01	.01	<.01	<.01	<.01	.10	.01	<.01
P2O5	<.01	<.01	<.01	<.01	<.01	<.01	<.01	<.01
H2O+	-	-	-	-	1.86	-	-	-
H2O-	-	-	-	-	<.05	-	-	-
CO2	-	-	-	-	.07	-	-	-
LOI	1.77	1.59	1.52	3.18	-	1.75	2.21	2.40
Rest	.62	.54	.69	.55	.38	.34	.36	.33
Total	99.85	100.57	100.29	99.85	99.80	99.76	100.24	100.14
O=F,S,Cl	.00	.00	.00	.00	.00	.00	.00	.00
Total	99.85	100.57	100.28	99.85	99.80	99.76	100.24	100.14
Trace elements in parts per million								
Ba	6	15	15	4	9	5	11	4
Rb	1	1	<1	1	<1	<1	1	<1
Sr	22	28	24	20	20	22	20	21
Pb	<1	1	<1	1	<1	1	1	<1
Th	1	2	<1	<1	<1	<1	<1	<1
Zr	3	5	3	4	3	3	3	3
Nb	<1	<1	<1	<1	<1	1	1	<1
Y	5	4	4	4	5	6	4	5
La	2	2	<2	3	2	<2	2	<2
Ce	<2	<2	<2	5	2	3	<2	<2
Nd	<2	<2	<2	3	2	2	<2	<2
Sc	35	37	34	28	38	46	36	43
V	111	125	106	87	182	207	159	192
Cr	2970	2674	3628	2381	1242	1289	1120	1110
Co	76	65	66	83	85	66	88	70
Ni	1060	777	846	1272	1045	702	1040	791
Cu	7	10	10	10	8	7	8	7
Zn	46	44	42	56	53	42	55	40
Mo	4	4	4	4	4	3	3	4
Ga	1	2	2	2	1	2	2	1
As	.5	<.5	.5	.5	.5	.5	.5	<.5
S	20	37	24	<20	34	<20	20	37
Cs	<3	<3	<3	<3	<3	<3	<3	<3
Trace elements in parts per billion								
Pt	1.18	-	1.55	-	1.20	-	1.56	-
Pd	1.96	-	2.09	-	2.40	-	2.60	-
Ir	.85	-	.51	-	.92	-	.42	-
Au	.23	-	.27	-	.24	-	.26	-
Se	<5.0	-	<5.0	-	<5.0	-	<5.0	-
Cs	223	-	148	-	94	-	109	-
Rb	313	-	413	-	339	-	443	-
mg	84.6	84.0	84.9	83.8	81.4	82.3	81.8	82.8

Sample no.	84770028	84770029	84770030	84770031	84770032	84770034	84770035	84770036
Intrusion	Munni Munni Complex	Munni Munni Complex	Munni Munni Complex	Munni Munni Complex	Munni Munni Complex	Munni Munni Complex	Munni Munni Complex	Munni Munni Complex
Locality	Sample traverse	Sample traverse	Sample traverse	Sample traverse	Sample traverse	Sample traverse	Sample traverse	Sample traverse
Lithology	Clinopyro.	Clinopyro.	Websterite	Olivine websterite	Olivine websterite	Lherzolite	Olivine websterite	Olivine websterite
Zone	Ultramafic	Ultramafic	Ultramafic	Ultramafic	Ultramafic	Ultramafic	Ultramafic	Ultramafic
Subzone	E	E	E	F	F	F	G	G
Strat. ht (m)	1180	1234	1278	1298	1417	1453	1474	1500
SiO2	53.08	52.17	52.56	49.51	49.79	38.17	51.45	51.58
TiO2	.16	.15	.15	.14	.15	.10	.19	.18
Al2O3	.81	.74	.74	.81	1.01	.72	1.45	1.23
Fe2O3	1.20	1.39	1.57	3.04	2.02	5.25	1.42	1.33
FeO	6.01	6.40	5.56	5.58	5.52	6.22	5.28	5.47
MnO	.20	.21	.20	.20	.19	.21	.18	.18
MgO	19.05	20.32	20.27	23.72	21.49	29.75	19.85	20.10
CaO	17.39	16.24	16.68	13.47	14.52	5.65	16.08	16.08
Na2O	.24	.27	.32	.34	.45	.13	.37	.46
K2O	.03	<.01	<.01	<.01	.02	<.01	.04	.01
P2O5	<.01	<.01	<.01	<.01	<.01	<.01	<.01	<.01
H2O+	-	1.36	-	-	-	-	1.88	-
H2O-	-	<.05	-	-	-	-	.08	-
CO2	-	.07	-	-	-	-	.36	-
LOI	1.56	-	1.85	2.59	3.79	12.92	-	2.15
Rest	.48	.49	.50	.50	.69	.50	.76	.68
Total	100.21	99.81	100.40	99.90	99.64	99.62	99.39	99.45
O=F,S,Cl	.00	.00	.00	.00	.00	.01	.01	.01
Total	100.21	99.81	100.40	99.90	99.64	99.61	99.39	99.44
	Trace elements in parts per million							
Ba	7	8	7	15	18	10	26	14
Rb	<1	<1	<1	<1	1	<1	1	1
Sr	22	18	19	20	26	32	34	28
Pb	<1	<1	<1	2	1	1	1	1
Th	1	<1	<1	<1	<1	<1	1	<1
Zr	3	2	3	4	5	6	8	7
Nb	<1	1	<1	<1	<1	<1	<1	<1
Y	5	4	5	5	5	2	4	4
La	<2	2	<2	<2	<2	<2	2	3
Ce	<2	<2	<2	<2	2	<2	<2	3
Nd	<2	<2	<2	<2	<2	<2	<2	<2
Sc	42	39	39	29	30	14	36	34
V	183	166	158	110	105	50	115	115
Cr	2300	2238	2382	2118	3574	1354	4121	3549
Co	64	75	62	85	72	121	58	63
Ni	660	794	755	1110	910	1890	778	786
Cu	7	7	7	14	16	6	20	23
Zn	42	46	41	54	45	74	38	41
Mo	4	4	4	4	3	3	4	4
Ga	2	1	1	1	2	1	2	2
As	1.0	1.0	.5	<.5	.5	<.5	1.0	.5
S	32	23	<20	<20	23	164	116	113
Cs	<3	<3	<3	<3	<3	<3	<3	<3
	Trace elements in parts per billion							
Pt	1.58	-	-	1.99	1.89	1.53	-	1.52
Pd	2.01	-	-	3.30	2.59	2.59	-	2.40
Ir	.45	-	-	.67	.88	.69	-	1.90
Au	.29	-	-	.42	.74	.57	-	.55
Se	<5.0	-	-	22.0	10.0	42.0	-	12.0
Cs	117	-	-	207	311	124	-	269
Rb	176	-	-	741	876	310	-	793
mg	82.7	82.6	83.8	83.6	83.9	82.9	84.4	84.3

Sample no.	84770037	84770038	84770039	84770040	84770041	84770042	84770043	84770044
Intrusion	Munni Munni Complex	Munni Munni Complex	Munni Munni Complex	Munni Munni Complex	Munni Munni Complex	Munni Munni Complex	Munni Munni Complex	Munni Munni Complex
Locality	Sample traverse	Sample traverse	Sample traverse	Sample traverse	Sample traverse	Sample traverse	Sample traverse	Sample traverse
Lithology	Websterite	Websterite	Lherzolite	Websterite	Websterite	Websterite	Lherzolite	Porphyrit. websterite
Zone	Ultramafic	Ultramafic	Ultramafic	Ultramafic	Ultramafic	Ultramafic	Ultramafic	Ultramafic
Subzone	G	H	H	H	H	H	H	I
Strat. ht (m)	1538	1603	1622	1666	1695	1723	1760	1838
SiO2	51.75	52.36	38.78	52.14	52.28	52.05	40.01	52.40
TiO2	.19	.18	.08	.20	.22	.22	.15	.32
Al2O3	1.23	1.37	.65	1.55	1.65	1.66	.81	2.78
Fe2O3	1.55	1.37	5.22	1.63	1.49	1.51	9.66	1.22
FeO	5.80	5.45	6.84	5.44	5.77	5.88	6.18	9.09
MnO	.19	.19	.23	.19	.19	.20	.25	.25
MgO	20.36	19.38	32.29	19.69	18.96	18.77	29.53	16.40
CaO	15.97	16.49	2.56	16.14	16.39	16.32	2.57	15.64
Na2O	.42	.51	.14	.67	.44	.55	.20	.51
K2O	.02	.03	<.01	.05	.05	.07	<.01	.02
P2O5	<.01	<.01	<.01	<.01	<.01	<.01	<.01	<.01
H2O+	-	-	-	1.45	-	-	-	-
H2O-	-	-	-	.11	-	-	-	-
CO2	-	-	-	.25	-	-	-	-
LOI	1.84	2.19	12.48	-	2.04	2.58	9.82	1.57
Rest	.65	.60	.43	.58	.48	.43	.36	.24
Total	99.97	100.12	99.70	100.09	99.96	100.24	99.54	100.44
O=F,S,Cl	.00	.01	.00	.01	.01	.01	.00	.01
Total	99.96	100.12	99.69	100.09	99.95	100.23	99.54	100.43
Trace elements in parts per million								
Ba	18	23	7	35	35	37	8	16
Rb	1	1	<1	1	1	2	<1	1
Sr	31	36	20	39	45	51	5	45
Pb	1	1	<1	<1	<1	1	<1	1
Th	1	<1	1	<1	<1	1	1	1
Zr	7	8	6	10	11	12	9	16
Nb	<1	<1	<1	<1	1	1	<1	<1
Y	5	4	2	5	6	6	3	10
La	<2	<2	3	3	3	4	4	<2
Ce	2	2	3	<2	2	2	4	11
Nd	2	<2	2	<2	2	2	2	6
Sc	35	36	11	36	39	38	13	45
V	118	120	43	126	133	138	68	229
Cr	3288	3063	771	2841	2146	1715	359	439
Co	64	60	148	61	61	63	160	75
Ni	829	714	2062	798	735	727	1995	527
Cu	14	18	10	20	28	38	15	122
Zn	47	40	93	46	47	48	113	71
Mo	4	3	2	5	3	4	2	4
Ga	2	2	1	2	3	3	2	5
As	.5	.5	<.5	1.0	.5	.5	.5	1.0
S	83	134	39	119	125	180	26	144
Cs	<3	<3	<3	<3	<3	<3	<3	<3
Trace elements in parts per billion								
Pt	1.05	-	-	-	1.97	3.81	-	2.60
Pd	2.69	-	-	-	2.82	2.23	-	17.00
Ir	.86	-	-	-	.28	.42	-	.04
Au	.31	-	-	-	.57	1.72	-	.39
Se	<5.0	-	-	-	42.0	34.0	-	90
Cs	193	-	-	-	293	341	-	460
Rb	878	-	-	-	1745	3145	-	765
mg	83.5	83.8	83.3	83.6	82.6	82.2	78.0	74.2

Sample no.	84770045	84770046	84770047	84770048	84770049	84770050	84770051	84770052
Intrusion	Munni Munni Complex	Munni Munni Complex	Munni Munni Complex	Munni Munni Complex	Munni Munni Complex	Munni Munni Complex	Munni Munni Complex	Munni Munni Complex
Locality	Off sample traverse	Off sample traverse	Off sample traverse	Sample traverse	Sample traverse	Sample traverse	Sample traverse	Sample traverse
Lithology	Porphyrit. gabbronor.	Orthopyro.	Norite	Gabbronor.	Gabbronor.	Gabbronor.	Gabbronor.	Gabbronor.
Zone	Ultramafic	Ultramafic	Ultramafic	Gabbroic	Gabbroic	Gabbroic	Gabbroic	Gabbroic
Subzone	I	I	I	A	A	A	A	A
Strat. ht (m)	1811	1840	1837	1851	1998	2094	2248	2377
SiO2	52.13	53.35	51.61	53.12	54.04	53.20	53.64	54.24
TiO2	.44	.16	.15	.16	.17	.19	.22	.24
Al2O3	3.94	1.95	17.40	17.22	16.70	18.57	16.17	16.26
Fe2O3	.82	1.22	.60	.56	.58	.74	1.02	1.04
FeO	8.05	6.48	7.80	5.98	6.28	5.40	6.70	6.91
MnO	.21	.15	.16	.14	.14	.13	.15	.16
MgO	15.50	30.64	9.10	6.74	6.90	5.53	6.23	6.21
CaO	14.65	1.41	7.54	9.65	10.19	8.95	9.82	9.42
Na2O	1.02	.10	2.59	3.56	3.38	4.20	3.48	3.87
K2O	.28	.03	.42	.40	.23	.57	.30	.39
P2O5	.01	<.01	<.01	<.01	<.01	<.01	<.01	<.01
H2O+	1.38	-	-	-	-	2.18	-	-
H2O-	.11	-	-	-	-	.08	-	-
CO2	1.04	-	-	-	-	.26	-	-
LOI	-	4.19	2.47	2.03	1.44	-	1.51	1.10
Rest	.30	.68	.23	.23	.21	.23	.22	.23
Total	99.88	100.36	100.07	99.79	100.26	100.23	99.46	100.07
O=F,S,Cl	.01	.00	.01	.02	.01	.01	.02	.02
Total	99.87	100.36	100.06	99.77	100.25	100.22	99.44	100.05
Trace elements in parts per million								
Ba	114	4	132	173	149	286	184	231
Rb	9	1	8	7	2	7	3	5
Sr	128	2	491	669	587	700	604	662
Pb	2	<1	2	1	1	2	2	2
Th	1	1	1	<1	<1	1	1	1
Zr	41	3	9	12	10	16	18	19
Nb	1	<1	<1	<1	<1	<1	1	1
Y	12	2	2	4	4	4	5	5
La	9	<2	<2	3	2	2	3	2
Ce	16	<2	4	4	7	7	5	3
Nd	9	<2	<2	2	2	3	<2	<2
Sc	40	23	19	23	19	21	26	23
V	195	87	69	80	89	98	97	105
Cr	730	3728	321	47	77	17	27	14
Co	62	68	55	46	49	44	49	51
Ni	488	729	186	195	188	142	146	129
Cu	59	6	223	240	210	237	215	204
Zn	66	62	64	47	45	47	53	52
Mo	4	2	3	2	3	2	3	3
Ga	6	2	13	13	13	15	15	16
As	1.0	.5	.5	.5	.5	<.5	<.5	<.5
S	279	47	241	349	280	287	374	357
Cs	<3	<3	<3	<3	<3	<3	4	<3
Trace elements in parts per billion								
Pt	-	.88	-	.91	.42	-	2.22	1.03
Pd	-	2.88	-	1.66	1.59	-	3.71	2.62
Ir	-	.23	-	<.02	.02	-	.01	.01
Au	-	.26	-	.36	.20	-	.67	.32
Se	-	6.0	-	125	106	-	99	90
Cs	-	625	-	533	795	-	511	324
Rb	-	1085	-	7535	2955	-	4435	6010
mg	75.9	87.8	66.0	64.9	64.4	61.9	59.3	58.5

Sample no.	84770053	84770054	84770055	84770056	84770057	84770058	84770059	84770060
Intrusion	Munni Munni Complex	Munni Munni Complex	Munni Munni Complex	Munni Munni Complex	Munni Munni Complex	Munni Munni Complex	Munni Munni Complex	Munni Munni Complex
Locality	Sample traverse	Sample traverse	Sample traverse	Sample traverse	Sample traverse	Sample traverse	Sample traverse	Sample traverse
Lithology	Gabbronor.	Gabbronor.	Gabbronor.	Gabbronor.	Gabbronor.	Gabbronor.	Gabbronor.	Gabbronor.
Zone	Gabbroic	Gabbroic	Gabbroic	Gabbroic	Gabbroic	Gabbroic	Gabbroic	Gabbroic
Subzone	A	A	A	A	A	A	A	A
Strat. ht (m)	2551	2692	2859	2975	3052	3181	3341	3425
SiO2	54.60	54.47	51.84	49.35	48.02	49.63	50.81	51.12
TiO2	.25	.27	.94	1.48	1.54	1.62	1.37	1.36
Al2O3	16.67	15.80	15.32	13.79	13.58	13.62	14.12	13.90
Fe2O3	1.17	1.20	3.39	4.41	4.33	5.23	4.03	3.74
FeO	6.72	7.30	9.18	9.97	10.52	9.85	9.92	9.88
MnO	.15	.16	.18	.18	.18	.19	.19	.19
MgO	5.47	5.81	5.42	4.92	5.56	5.46	5.13	5.13
CaO	9.35	9.56	8.34	8.02	8.47	8.98	8.25	8.74
Na2O	3.94	3.88	3.85	3.54	3.11	3.42	3.65	3.69
K2O	.44	.40	.41	.38	.24	.36	.48	.51
P2O5	<.01	<.01	.01	<.01	.01	.01	.01	.02
H2O+	-	-	.67	-	-	-	-	1.17
H2O-	-	-	.09	-	-	-	-	.11
CO2	-	-	.24	-	-	-	-	.29
LOI	1.35	1.06	-	3.64	3.45	1.90	1.60	-
Rest	.22	.23	.31	.38	.35	.35	.30	.32
Total	100.33	100.14	100.19	100.06	99.36	100.62	99.86	100.17
O=F,S,Cl	.01	.02	.02	.03	.02	.03	.02	.03
Total	100.31	100.12	100.17	100.03	99.34	100.59	99.84	100.14
	Trace elements in parts per million							
Ba	238	255	235	175	132	192	252	280
Rb	5	5	4	5	2	8	11	10
Sr	668	624	597	447	414	499	526	510
Pb	3	2	3	2	2	3	4	6
Th	1	1	1	<1	<1	1	1	<1
Zr	21	21	21	14	11	21	31	36
Nb	<1	<1	1	<1	<1	1	1	1
Y	5	6	5	5	5	6	7	9
La	3	5	4	<2	3	4	4	5
Ce	10	8	6	6	7	6	14	13
Nd	5	5	3	2	4	2	6	7
Sc	19	22	20	24	24	25	24	25
V	104	117	454	835	791	587	467	443
Cr	11	16	43	6	<2	<2	<2	10
Co	48	51	71	81	82	78	74	72
Ni	114	111	144	148	142	102	78	68
Cu	193	229	311	405	399	410	297	357
Zn	51	51	59	87	87	93	80	80
Mo	3	3	3	4	3	4	3	3
Ga	17	16	18	17	18	19	18	17
As	<.5	.5	<.5	.5	<.5	<.5	<.5	<.5
S	273	398	405	530	499	614	456	581
Cs	<3	<3	<3	<3	<3	<3	<3	<3
	Trace elements in parts per billion							
Pt	-	-	.98	-	-	.84	-	-
Pd	-	-	2.28	-	-	2.37	-	-
Ir	-	-	<.01	-	-	.01	-	-
Au	-	-	.31	-	-	.33	-	-
Se	-	-	132	-	-	150	-	-
Cs	-	-	304	-	-	2200	-	-
Rb	-	-	5875	-	-	12520	-	-
mg	55.6	55.3	44.1	38.6	40.7	40.1	40.3	40.8

Sample no.	84770061	84770062	84770063	84770064	84770065	84770066	84770067	84770070
Intrusion	Munni Munni Complex	Munni Munni Complex	Munni Munni Complex	Munni Munni Complex	Munni Munni Complex	Munni Munni Complex	Southern Munni Munni Dyke	Zebra Hill Dyke
Locality	Sample traverse	Sample traverse	Sample traverse	Sample traverse	Sample traverse	Sample traverse	Off sample traverse	Off sample traverse
Lithology	Gabbronor.	Gabbronor.	Gabbronor.	Gabbronor.	Gabbronor.	Gabbronor.	Gabbronor.	Gabbronor.
Zone	Gabbroic	Gabbroic	Gabbroic	Gabbroic	Gabbroic	Gabbroic		
Subzone	A	A	A	A	A	A		
Strat. ht (m)	3553	3676	3798	3965	4125	4222		
SiO2	50.95	49.82	51.06	49.05	52.55	50.56	52.79	53.50
TiO2	1.54	1.91	1.65	1.93	1.42	1.76	.49	.39
Al2O3	14.31	13.87	15.71	13.41	17.28	15.56	4.60	13.14
Fe2O3	3.89	4.24	4.35	5.09	3.36	4.40	1.37	1.15
FeO	9.83	10.78	9.46	11.24	8.11	9.94	8.57	7.57
MnO	.18	.19	.17	.20	.13	.17	.22	.16
MgO	4.57	4.57	4.03	4.76	2.79	3.55	14.00	8.94
CaO	8.62	8.43	7.18	8.33	7.25	7.47	14.33	8.33
Na2O	3.89	3.79	4.41	3.73	4.99	4.20	1.32	1.46
K2O	.54	.53	.53	.47	.66	.58	.45	.85
P2O5	.02	.02	.02	.02	.03	.01	.02	.03
H2O+	-	-	-	-	1.24	-	-	-
H2O-	-	-	-	-	.09	-	-	-
CO2	-	-	-	-	.25	-	-	-
LOI	1.57	1.60	1.71	1.95	-	1.69	1.89	3.69
Rest	.32	.34	.30	.30	.29	.28	.20	.26
Total	100.23	100.09	100.58	100.48	100.44	100.17	100.25	99.47
O=F,S,Cl	.03	.03	.03	.03	.04	.04	.00	.00
Total	100.20	100.06	100.55	100.45	100.40	100.14	100.25	99.47
Trace elements in parts per million								
Ba	286	285	311	271	387	330	169	310
Rb	9	10	9	7	11	10	38	42
Sr	541	538	557	468	660	576	122	390
Pb	4	4	4	5	3	4	3	5
Th	1	1	1	<1	1	<1	<1	3
Zr	37	35	28	31	36	34	46	67
Nb	2	2	1	1	1	1	2	2
Y	8	8	6	8	6	7	12	15
La	9	5	7	7	7	6	8	9
Ce	14	13	12	12	14	12	19	19
Nd	8	5	4	6	6	4	9	8
Sc	23	23	17	23	14	19	38	26
V	412	490	362	337	157	193	176	146
Cr	3	<2	<2	<2	<2	2	205	590
Co	70	75	75	84	58	73	63	49
Ni	59	64	46	38	15	16	447	151
Cu	354	367	282	337	217	262	77	58
Zn	76	85	94	99	64	78	78	75
Mo	4	3	4	4	3	3	4	3
Ga	19	19	20	19	22	20	7	13
As	1.0	.5	<.5	.5	.5	<.5	.5	1.5
S	581	675	614	657	836	721	100	600
Cs	<3	<3	<3	<3	<3	<3	8	<3
Trace elements in parts per billion								
Pt	1.04	-	-	.46	-	.74	-	-
Pd	1.97	-	-	1.48	-	1.53	-	-
Ir	.02	-	-	.01	-	.02	-	-
Au	.38	-	-	.17	-	.28	-	-
Se	158	-	-	161	-	129	-	-
Cs	795	-	-	572	-	655	-	-
Rb	8595	-	-	8150	-	9615	-	-
mg	37.9	35.8	34.9	34.9	30.9	31.3	71.8	64.9

Sample no.	84770073	84770074	84770081	84770086	84770087	84770088	84770089	84770094
Intrusion	Eastern Munni Munni Dyke	Eastern Munni Munni Dyke	Pinderi Hills Dyke	Munni Munni Complex	Munni Munni Complex	Munni Munni Complex	Munni Munni Complex	Munni Munni Complex
Locality	Off sample traverse	Off sample traverse	Off sample traverse	Off sample traverse	Off sample traverse	Off sample traverse	Off sample traverse	Off sample traverse
Lithology	Gabbronor.	Plagiocla. olivine orthopyro.	Gabbronor.	Metagabbro xenolith	Olivine orthopyro.	Carbonate - quartz shear fill	Porphyrit. plagiocla. websterite	Mineralis. gabbronor.
Zone	Marginal	Core		Gabbroic	Ultramafic	Ultramafic	Ultramafic	Ultramafic
Subzone				A	I	I	I	I
Strat. ht (m)				1855	1837	1837	1812	1846
SiO2	53.66	47.46	53.61	47.91	52.78	38.35	51.74	51.91
TiO2	.37	.13	.44	.21	.21	.45	.37	.73
Al2O3	6.26	3.26	10.24	15.09	2.87	3.22	3.31	5.33
Fe2O3	1.11	1.34	1.03	.77	1.32	1.06	1.52	1.60
FeO	8.33	7.44	8.84	5.53	8.07	4.13	9.76	10.80
MnO	.19	.16	.18	.13	.18	.26	.24	.24
MgO	18.73	31.13	12.67	11.91	28.97	2.76	15.36	11.96
CaO	5.17	2.43	8.56	13.51	1.94	26.91	16.08	12.85
Na2O	1.10	.45	1.66	1.48	.30	<.01	.39	1.79
K2O	.59	.22	.70	.21	.03	.02	.08	.53
P2O5	.03	<.01	.05	<.01	<.01	<.01	<.01	.06
H2O+	-	-	-	-	-	-	-	1.10
H2O-	-	-	-	-	-	-	-	.08
CO2	-	-	-	-	-	-	-	.20
LOI	4.32	4.63	1.93	3.48	2.44	20.90	1.32	-
Rest	.58	1.06	.38	.23	.72	1.35	.33	1.01
Total	100.44	99.71	100.29	100.46	99.83	99.41	100.50	100.19
O=F,S,Cl	.00	.00	.00	.00	.00	.29	.00	.20
Total	100.44	99.71	100.29	100.46	99.83	99.12	100.50	100.00
Trace elements in parts per million								
Ba	141	65	230	30	29	5	42	251
Rb	31	7	30	5	1	<1	2	16
Sr	85	32	116	131	48	131	68	135
Pb	5	2	6	1	1	8	3	8
Th	3	1	2	<1	<1	1	<1	2
Zr	49	14	60	8	7	47	20	70
Nb	1	<1	2	<1	<1	2	<1	3
Y	10	4	15	5	4	13	11	17
La	8	3	10	2	<2	8	3	11
Ce	14	<2	15	<2	<2	9	6	21
Nd	7	<2	7	<2	<2	9	5	14
Sc	22	10	28	35	22	53	49	38
V	130	62	185	115	97	264	252	242
Cr	2944	6064	1460	890	3940	203	76	51
Co	65	91	59	45	72	114	80	82
Ni	457	973	333	282	707	1399	719	955
Cu	46	21	42	8	25	3685	1049	2808
Zn	76	59	79	29	79	36	74	97
Mo	3	2	3	3	2	5	4	5
Ga	8	4	13	11	5	5	5	10
As	.5	<.5	1.5	<.5	<.5	.5	.5	<.5
S	400	100	100	500	200	5750	1500	3940
Cs	9	<3	<3	<3	<3	3	<3	<3
Trace elements in parts per billion								
Pt	-	-	-	-	-	50.0	-	88.0
Pd	-	-	-	-	-	11.92	-	6.28
Ir	-	-	-	-	-	.16	-	.06
Au	-	-	-	-	-	20.33	-	44.7
Se	-	-	-	-	-	1655	-	1630
Cs	-	-	-	-	-	-	-	2060
Rb	-	-	-	-	-	-	-	15225
mg	78.2	86.5	69.8	77.3	84.8	49.2	71.1	63.5

Sample no.	84770100	84770102	84770106	84770121	84770125	84770127	84770129	84770131
Intrusion	Munni Munni Complex	Munni Munni Complex	Munni Munni Complex	Munni Munni Complex	Munni Munni Complex	Munni Munni Complex	Munni Munni Complex	Eastern Munni Munni Dyke
Locality	Sample traverse	Sample traverse	Off sample traverse	Off sample traverse	Off sample traverse	Off sample traverse	Sample traverse	Off sample traverse
Lithology	Gabbronor.	Gabbronor.	Metadoler. dyke	Plagiocla. websterite	Orthopyro.	Quartz-Pb-Cu vein	Anorthosi. gabbro	Gabbronor.
Zone	Ultramafic	Ultramafic	Ultramafic	Ultramafic	Ultramafic	Ultramafic	Gabbroic	Marginal
Subzone	A'	A'		I	C	A'	B	
Strat. ht (m)	2	2		1826	430		5220	
SiO2	50.28	50.04	50.68	52.68	53.96	91.81	45.61	53.02
TiO2	.40	.43	1.77	.36	.18	.01	2.50	.37
Al2O3	8.44	7.57	13.17	2.85	1.52	.15	14.70	11.65
Fe2O3	1.68	2.32	1.29	1.19	1.03	1.70	.72	.82
FeO	11.86	13.30	10.52	8.24	9.79	.62	15.60	7.32
MnO	.23	.24	.20	.22	.27	.02	.22	.15
MgO	10.59	10.79	6.86	16.71	24.85	.17	2.13	13.37
CaO	11.72	10.48	8.60	15.85	5.98	2.13	6.40	7.48
Na2O	1.84	2.01	3.60	.41	.40	<.01	3.94	1.92
K2O	.64	.42	.58	.06	.04	.02	.16	.98
P2O5	<.01	.01	.19	<.01	<.01	<.01	.03	.03
H2O+	1.22	1.04	-	-	-	-	-	-
H2O-	.07	.10	-	-	-	-	-	-
CO2	.24	.10	-	-	-	-	-	-
LOI	-	-	2.52	1.22	1.74	2.00	8.33	2.96
Rest	1.23	1.71	.31	.27	.46	1.30	.13	.49
Total	100.44	100.56	100.29	100.06	100.22	99.93	100.47	100.56
O=F,S,Cl	.41	.62	.00	.00	.00	.04	.01	.01
Total	100.02	99.94	100.29	100.06	100.22	99.89	100.45	100.54
	Trace elements in parts per million							
Ba	744	394	757	50	21	<20	37	240
Rb	36	20	36	2	1	<1	3	29
Sr	323	319	448	67	17	40	290	285
Pb	5	10	11	1	2	6545	6	7
Th	<1	1	<1	<1	1	<1	<1	3
Zr	21	31	143	21	11	18	39	51
Nb	<1	1	12	1	1	<1	2	2
Y	10	12	26	9	3	21	7	11
La	2	8	11	3	2	2	5	11
Ce	10	14	31	10	5	20	13	16
Nd	5	6	18	7	2	<2	5	6
Sc	35	31	29	43	20	3	23	24
V	214	187	276	198	86	10	99	133
Cr	266	212	222	794	2126	12	<2	1887
Co	98	110	47	71	94	7	69	56
Ni	362	609	95	509	794	25	5	389
Cu	843	1575	83	68	23	2389	51	58
Zn	83	123	110	63	83	1566	99	66
Mo	5	5	4	4	2	<2	4	2
Ga	9	10	19	5	3	<1	17	12
As	.5	1.0	<.5	1.0	.5	<.5	.5	.5
S	8310	12420	200	100	<100	827	265	281
Cs	6	6	13	<3	<3	<3	<3	<3
	Trace elements in parts per billion							
Pt	35.0	15.0	-	-	-	<10.00	-	5.78
Pd	57.5	-	-	-	-	2.61	-	4.01
Ir	.38	.51	-	-	-	<.02	-	.14
Au	4.79	5.06	-	-	-	1.06	-	.67
Se	1825	2460	-	-	-	2210	-	116
Cs	5555	-	-	-	-	-	-	1050
Rb	39530	-	-	-	-	-	-	28322
mg	58.5	55.6	51.1	76.2	80.5	12.4	18.9	74.7

Sample no.	85770139	85770140	85770141	85770142	85770143	85770148	85770149	85770151
Intrusion	Munni Munni Complex	Munni Munni Complex	Munni Munni Complex	Munni Munni Complex	Munni Munni Complex	Munni Munni Complex	Munni Munni Complex	Munni Munni Complex
Locality	Trench traverse	Trench traverse	Trench traverse	Trench traverse	Trench traverse	Trench traverse	Trench traverse	Trench traverse
Lithology	Porphyrit. websterite	Porphyrit. websterite	Porphyrit. websterite	Porphyrit. websterite	Porphyrit. websterite	Porphyrit. websterite	Porphyrit. websterite	Gabbronor.
Zone	Ultramafic	Ultramafic	Ultramafic	Ultramafic	Ultramafic	Ultramafic	Ultramafic	Gabbroic
Subzone	I	I	I	I	I	I	I	A
Strat. ht (m)	1830	1835	1838	1840	1842	1847	1848	1852
SiO2	49.88	51.95	52.77	52.63	50.63	50.81	48.76	49.42
TiO2	.28	.29	.35	.35	.34	.36	.36	.19
Al2O3	2.20	2.28	2.66	2.97	3.82	3.87	3.44	16.59
Fe2O3	1.49	1.76	1.79	1.60	2.56	2.41	1.81	1.27
FeO	7.02	6.04	7.24	8.13	7.52	8.16	8.24	3.63
MnO	.20	.19	.22	.23	.21	.23	.21	.10
MgO	21.54	18.70	16.57	16.67	14.65	14.41	14.06	6.24
CaO	13.72	15.46	16.14	15.85	17.10	16.41	18.23	13.81
Na2O	.80	.89	.62	.48	.40	.89	.70	2.67
K2O	.07	.14	.09	.05	.04	.04	.04	.81
P2O5	<.01	<.01	<.01	<.01	<.01	.01	<.01	<.01
H2O+	-	-	-	-	-	-	-	-
H2O-	-	-	-	-	-	-	-	-
CO2	-	-	-	-	-	-	-	-
LOI	2.07	1.99	1.08	1.13	3.03	2.61	4.40	5.17
Rest	.53	.46	.30	.30	.39	.42	.32	.26
Total	99.80	100.15	99.83	100.39	100.69	100.63	100.57	100.16
O=F,S,Cl	.01	.01	.01	.01	.01	.00	.01	.00
Total	99.80	100.13	99.83	100.38	100.69	100.63	100.57	100.15
	Trace elements in parts per million							
Ba	42	62	50	48	56	42	53	329
Rb	2	5	2	1	1	1	1	17
Sr	67	65	58	75	78	68	55	697
Pb	2	2	2	3	3	3	2	3
Th	<1	<1	1	1	<1	<1	<1	<1
Zr	20	20	23	21	20	20	25	17
Nb	<1	1	1	1	<1	1	1	<1
Y	7	7	10	9	10	10	12	5
La	2	4	4	<2	3	2	3	3
Ce	9	9	7	8	9	15	7	3
Nd	4	5	5	6	6	8	5	4
Sc	32	36	44	43	49	50	52	33
V	119	133	198	205	240	274	261	135
Cr	2128	1796	920	794	155	76	70	34
Co	82	65	68	72	80	79	82	36
Ni	1103	740	526	530	898	850	740	290
Cu	38	34	51	102	1232	1578	885	343
Zn	57	53	58	65	65	68	66	33
Mo	4	3	4	4	5	5	5	3
Ga	4	4	5	5	6	6	6	12
As	.5	<.5	<.5	<.5	.5	.5	<.5	<.5
S	149	295	176	241	105	92	106	83
Cs	<3	<3	<3	<3	<3	<3	3	<3
	Trace elements in parts per billion							
Pt	-	-	-	-	525	20.00	<20.00	-
Pd	-	-	-	-	1854	32.59	16.69	-
Ir	-	-	-	-	12.09	.07	<.02	-
Au	-	-	-	-	108	8.23	5.91	-
Se	-	-	-	-	237	146	258	-
Cs	-	-	-	-	-	-	-	-
Rb	-	-	-	-	-	-	-	-
mg	82.1	81.4	76.9	75.6	72.7	71.3	71.7	70.0

Sample no.	85770152	85770153	85770154	85770156	85770159	85770163	85770164	85770165
Intrusion	Munni Munni Complex	Munni Munni Complex	Munni Munni Complex	Munni Munni Complex	Munni Munni Complex	Munni Munni Complex	Munni Munni Complex	Munni Munni Complex
Locality	Trench traverse	Sample traverse	Sample traverse	Off sample traverse	Off sample traverse	Off sample traverse	Off sample traverse	Off sample traverse
Lithology	Gabbronor.	Gabbronor.	Gabbronor.	Dunite - chromitite	Orthopyr.- chromitite	Carbonat.- talc shear fill	Coarse - grained leucogabb.	Olivine - orthopyro. ?pipe
Zone	Gabbroic	Gabbroic	Gabbroic	Ultramafic	Ultramafic	Ultramafic	Gabbroic	Ultramafic
Subzone	A	A	A	F	I	I	A	I
Strat. ht (m)	1853	1870	1900	1460	1836		1855	1845
SiO2	52.73	53.33	53.47	35.32	44.65	66.97	56.02	38.77
TiO2	.15	.16	.16	.11	.09	.45	.30	.08
Al2O3	20.16	17.73	18.20	1.28	9.93	3.98	21.83	.65
Fe2O3	.99	.90	1.04	11.24	2.86	.66	.84	3.87
FeO	2.97	4.80	4.82	3.80	7.73	6.50	2.60	5.98
MnO	.09	.11	.12	.20	.24	.17	.08	.09
MgO	4.77	6.68	6.13	31.01	28.20	6.28	2.06	33.56
CaO	10.34	11.04	10.20	1.97	.24	7.39	5.99	2.57
Na2O	4.19	3.71	3.48	.29	.22	.26	5.93	.11
K2O	1.36	.23	.24	<.01	.03	.01	2.08	.01
P2O5	<.01	<.01	<.01	<.01	<.01	.02	.05	<.01
H2O+	-	-	-	-	-	-	-	-
H2O-	-	-	-	-	-	-	-	-
CO2	-	-	-	-	-	-	-	-
LOI	2.61	1.71	1.71	11.38	4.21	6.77	2.22	12.76
Rest	.25	.23	.23	2.94	1.59	.53	.41	.51
Total	100.61	100.63	99.80	99.54	99.99	99.99	100.41	98.96
O=F,S,Cl	.00	.02	.02	.00	.00	.06	.00	.00
Total	100.61	100.60	99.78	99.54	99.99	99.93	100.41	98.96
	Trace elements in parts per million							
Ba	519	118	134	28	10	7	1947	4
Rb	30	2	2	<1	2	<1	44	<1
Sr	829	651	701	9	4	21	1222	26
Pb	2	2	2	2	2	2	4	2
Th	<1	<1	<1	<1	<1	<1	2	<1
Zr	17	14	15	2	7	23	48	4
Nb	<1	<1	<1	<1	<1	<1	2	<1
Y	4	4	4	1	1	8	6	1
La	<2	<2	4	<2	<2	4	11	<2
Ce	5	3	6	<2	<2	10	17	2
Nd	2	<2	2	<2	<2	5	7	<2
Sc	23	22	19	6	19	56	9	6
V	105	83	74	68	103	363	27	11
Cr	23	16	14	17997	9913	97	17	1117
Co	29	43	42	116	55	84	18	125
Ni	215	250	225	2040	655	766	44	2466
Cu	186	197	245	5	22	1590	68	29
Zn	28	40	40	98	141	56	34	44
Mo	2	3	3	2	2	2	2	<2
Ga	13	13	14	3	6	6	21	2
As	<.5	<.5	<.5	<.5	<.5	<.5	<.5	<.5
S	32	440	424	33	46	1158	100	2200
Cs	<3	<3	<3	<3	<3	<3	<3	<3
	Trace elements in parts per billion							
Pt	-	-	-	<10.00	<20.00	<20.00	-	-
Pd	-	-	-	3.19	2.81	3.47	-	-
Ir	-	-	-	1.47	.32	<.02	-	-
Au	-	-	-	.32	5.88	7.61	-	-
Se	-	-	-	122	12.74	725	-	-
Cs	-	-	-	-	-	-	-	-
Rb	-	-	-	-	-	-	-	-
mg	68.8	68.0	65.5	79.9	83.0	61.2	52.2	86.3

Sample no.	85770166	85770167	85770168	85770169	85770170	85770171	85770172	85770173
Intrusion	Munni Munni Complex	Munni Munni Complex	Munni Munni Complex	Munni Munni Complex	Munni Munni Complex	Munni Munni Complex	Munni Munni Complex	Munni Munni Complex
Locality	Off sample traverse	Off sample traverse	Off sample traverse	Off sample traverse	Off sample traverse	Off sample traverse	Off sample traverse	Off sample traverse
Lithology	Orthopyro.	Chilled marginal pyroxenite	Chilled gabbronor.	Chilled gabbronor.	Chilled gabbronor.	Chilled gabbronor.	Chilled gabbronor.	Chilled plagiocla. websterite
Zone	Ultramafic	Ultramafic	Ultramafic	Ultramafic	Ultramafic	Ultramafic	Ultramafic	Ultramafic
Subzone	I							
Strat. ht (m)	1845							
SiO2	50.96	53.23	55.43	52.79	52.84	52.82	52.91	52.50
TiO2	.18	.87	.31	.65	.83	.45	.85	.36
Al2O3	8.24	9.96	5.30	7.83	9.32	5.18	9.82	2.54
Fe2O3	3.63	1.22	.88	1.25	1.60	1.09	1.47	1.54
FeO	7.23	10.47	6.88	9.72	10.25	7.82	10.33	9.55
MnO	.21	.20	.17	.20	.20	.20	.21	.25
MgO	23.00	8.42	13.97	11.31	9.41	14.35	8.90	16.19
CaO	2.95	9.90	12.71	11.64	10.47	14.19	10.04	15.00
Na2O	.38	2.99	2.19	2.22	2.43	1.68	2.78	.88
K2O	.60	.98	.46	.67	.88	.38	.97	.15
P2O5	<.01	.08	.03	.05	.07	.01	.07	<.01
H2O+	-	-	-	-	-	-	-	-
H2O-	-	-	-	-	-	-	-	-
CO2	-	-	-	-	-	-	-	-
LOI	2.31	1.79	1.63	1.50	1.53	1.11	1.51	1.28
Rest	.93	.31	.34	.28	.34	.50	.30	.28
Total	100.62	100.42	100.30	100.11	100.17	99.78	100.16	100.52
O=F,S,Cl	.00	.02	.00	.00	.03	.00	.00	.00
Total	100.62	100.40	100.30	100.11	100.14	99.78	100.16	100.52
	Trace elements in parts per million							
Ba	171	569	213	338	461	300	755	100
Rb	21	45	19	28	35	17	38	6
Sr	285	303	144	235	275	177	314	60
Pb	1	8	5	5	6	3	8	2
Th	<1	3	1	2	3	<1	4	<1
Zr	9	83	37	72	94	43	94	21
Nb	<1	4	1	3	4	2	4	<1
Y	2	19	9	14	17	10	18	10
La	2	18	10	11	17	7	18	3
Ce	<2	33	22	23	37	13	36	10
Nd	<2	15	10	13	16	7	17	6
Sc	32	24	31	31	26	33	25	45
V	108	169	121	181	181	143	171	224
Cr	5320	231	1112	457	324	2181	248	547
Co	50	62	57	67	62	59	62	83
Ni	445	290	570	430	365	480	315	629
Cu	4	143	78	108	145	76	148	180
Zn	75	106	66	93	102	68	102	76
Mo	3	4	3	4	3	4	4	4
Ga	7	14	9	11	13	8	14	5
As	<.5	.5	<.5	.5	.5	1.0	<.5	1.0
S	<100	387	200	600	555	500	600	300
Cs	3	14	8	10	8	<3	11	3
	Trace elements in parts per billion							
Pt	-	4.96	-	-	-	-	-	-
Pd	-	6.39	-	-	-	-	-	-
Ir	-	.16	-	-	-	-	-	-
Au	-	1.48	-	-	-	-	-	-
Se	-	-	-	-	-	-	-	-
Cs	-	-	-	-	-	-	-	-
Rb	-	-	-	-	-	-	-	-
mg	79.6	56.5	76.4	65.0	58.9	74.4	57.7	72.5

Sample no.	85770174	85770175	85770176	85770177	85770178	85770179
Intrusion	Munni Munni Complex	Western granite	Munni Munni Complex	Munni Munni Complex	Munni Munni Complex	Munni Munni Complex
Locality	Off sample traverse	Off sample traverse	Off sample traverse	Off sample traverse	Off sample traverse	Off sample traverse
Lithology	Chilled - ol - plag websterite	Microcline granite	Chilled gabbronor.	Gabbronor.	Plagiocla. olivine websterite	Chilled olivine gabbronor.
Zone	Ultramafic		Ultramafic	Ultramafic	Ultramafic	Ultramafic
Subzone			A'	A'	A'	A'
Strat. ht (m)						1
SiO2	52.92	73.50	61.34	56.94	52.34	51.82
TiO2	.52	.13	.20	.17	.29	.79
Al2O3	5.14	14.13	6.57	3.49	2.08	7.89
Fe2O3	1.54	.57	.93	.79	1.38	3.46
FeO	9.82	.71	6.52	5.04	7.26	8.61
MnO	.22	.01	.16	.15	.20	.24
MgO	13.80	.29	9.66	15.81	19.31	12.48
CaO	13.17	1.18	9.63	14.16	15.24	9.42
Na2O	1.15	4.40	2.36	1.27	.74	2.34
K2O	.55	4.24	1.35	.73	.11	.64
P2O5	.02	.01	<.01	<.01	<.01	.05
H2O+	-	-	-	-	-	1.69
H2O-	-	-	-	-	-	<.05
CO2	-	-	-	-	-	.09
LOI	1.25	.65	1.41	1.04	1.12	-
Rest	.29	.19	.27	.39	.36	.56
Total	100.39	100.01	100.40	99.98	100.43	100.08
O=F,S,Cl	.02	.00	.02	.00	.01	.04
Total	100.37	100.00	100.37	99.97	100.43	100.04
Trace elements in parts per million						
Ba	291	748	300	217	64	906
Rb	20	152	42	23	2	35
Sr	155	196	87	69	64	350
Pb	4	48	22	7	1	6
Th	3	47	5	3	<1	<1
Zr	54	119	30	21	19	56
Nb	2	4	<1	1	1	2
Y	13	8	7	4	7	14
La	8	51	7	6	<2	14
Ce	17	78	12	11	7	30
Nd	10	27	6	4	3	15
Sc	35	3	27	32	39	21
V	225	5	119	100	185	154
Cr	334	2	363	2060	1191	1153
Co	79	3	53	51	74	67
Ni	495	8	363	-	764	494
Cu	59	3	133	7	30	159
Zn	84	32	55	39	58	95
Mo	4	<2	<2	3	4	4
Ga	8	18	10	5	3	11
As	.5	<.5	.5	.5	<.5	.5
S	354	58	501	77	123	871
Cs	5	<3	3	<3	<3	6
Trace elements in parts per billion						
Pt	-	-	-	-	-	3.76
Pd	-	-	-	-	-	3.40
Ir	-	-	-	-	-	.60
Au	-	-	-	-	-	1.57
Se	-	-	-	-	-	148
Cs	-	-	-	-	-	5565
Rb	-	-	-	-	-	36360
mg	68.7	29.7	70.1	83.1	80.2	65.5

Sample no.	84770140	84770141	84770143	84770145	84770147	84770148	84770150	84770152
Intrusion	Mount Sholl Com.	Mount Sholl Com.	Mount Sholl Com.	Mount Sholl Com.	Mount Sholl Com.	Mount Sholl Com.	Mount Sholl Com.	Mount Sholl Com.
Locality	Sample traverse A	Sample traverse A	Sample traverse A	Sample traverse A	Sample traverse A	Sample traverse A	Sample traverse A	Sample traverse A
Lithology	Gabbro	Gabbro	Gabbro	Gabbro	Gabbro	Gabbro	Gabbro	Gabbro
Strat. ht (m)	80	400	1000	1380	1900	2160	2800	3160
SiO2	50.42	51.56	50.92	50.63	50.88	53.22	50.04	50.74
TiO2	.79	.66	.71	.81	.85	.90	.75	.55
Al2O3	11.83	12.75	12.17	11.03	10.67	10.69	10.00	8.64
Fe2O3	1.68	1.39	1.91	2.32	1.74	2.46	1.61	1.24
FeO	11.47	10.86	11.03	11.14	11.26	10.09	11.28	11.06
MnO	.20	.19	.21	.20	.21	.20	.21	.22
MgO	7.87	6.73	7.32	7.65	7.82	7.36	8.71	10.36
CaO	9.18	9.19	8.57	10.12	10.04	9.58	10.88	11.77
Na2O	2.66	3.18	3.02	2.35	2.77	3.14	2.76	2.19
K2O	.80	1.16	.70	.95	.87	1.17	.81	.69
P2O5	.05	.05	.02	.06	.06	.09	.06	.03
LOI	3.33	2.44	3.25	2.89	2.83	1.48	3.21	2.67
Rest	.28	.32	.25	.31	.29	.29	.31	.28
Total	100.56	100.48	100.08	100.46	100.29	100.67	100.63	100.44
O=F,S,Cl	.02	.03	.02	.03	.03	.02	.03	.01
Total	100.53	100.44	100.06	100.43	100.26	100.64	100.60	100.42
Trace elements in parts per million								
Ba	425	502	402	548	401	436	519	357
Rb	19	36	16	23	21	34	18	17
Sr	258	471	280	235	259	322	267	395
Pb	7	4	5	6	8	7	7	4
Th	3	3	2	4	4	4	2	1
Zr	84	71	62	88	94	104	82	55
Nb	3	3	2	4	4	5	3	2
Y	15	13	14	16	18	18	16	13
La	16	11	11	14	14	23	13	9
Ce	26	24	20	32	34	42	25	18
Nd	14	11	12	14	16	19	12	11
Sc	23	22	22	25	24	23	28	32
V	175	146	164	187	185	161	203	208
Cr	50	32	45	71	74	85	94	130
Co	77	69	60	71	71	71	76	77
Ni	200	177	190	213	216	124	245	308
Cu	255	277	163	221	219	251	203	147
Zn	114	96	114	110	110	104	114	99
Mo	4	4	4	5	4	4	5	4
Ga	14	15	15	15	15	15	13	11
As	3.5	2.5	21.0	12.0	1.5	.5	2.5	.5
S	500	700	400	700	600	500	600	300
Cs	<3	8	<3	<3	<3	5	<3	<3
Trace elements in parts per billion								
Pt	-	-	-	-	-	-	-	-
Pd	-	-	-	-	-	-	-	-
Ir	-	-	-	-	-	-	-	-
Au	-	-	-	-	-	-	-	-
mg	51.9	49.8	50.6	50.8	52.1	51.6	54.9	60.3

Sample no.	84770154	84770156	84770157	84770159	84770161	84770164	84770166	84770167
Intrusion	Mount Sholl Com.	Mount Sholl Com.	Mount Sholl Com.	Mount Sholl Com.	Mount Sholl Com.	Mount Sholl Com.	Mount Sholl Com.	Mount Sholl Com.
Locality	Sample traverse A	Sample traverse A	Sample traverse A	Sample traverse A	Sample traverse B	Sample traverse B	Sample traverse B	Sample traverse B
Lithology	Gabbro	Gabbro	Gabbro	Gabbro	Gabbro	Gabbro	Gabbro	Gabbro
Strat. ht (m)	3500	4200	4540	5000	200	780	1040	1200
SiO2	50.77	51.35	51.17	51.26	55.29	50.95	50.45	51.50
TiO2	.55	.66	.67	.46	.53	.63	.63	.62
Al2O3	7.72	6.60	8.07	9.30	5.33	9.38	11.14	11.25
Fe2O3	1.53	1.67	1.27	1.44	1.02	1.65	1.43	1.72
FeO	10.97	10.64	10.67	10.03	8.63	10.72	10.84	11.03
MnO	.21	.22	.21	.19	.23	.21	.20	.21
MgO	11.06	11.70	10.57	10.72	12.72	9.86	8.40	8.29
CaO	12.65	13.19	11.82	12.11	12.46	10.93	10.05	10.20
Na2O	1.40	1.23	2.37	1.77	1.84	2.31	3.15	2.05
K2O	.62	.48	.58	.44	.34	.48	.69	1.14
P2O5	<.01	.03	.04	<.01	.02	.04	.05	.04
LOI	2.58	2.23	2.72	2.71	1.90	2.94	2.96	2.33
Rest	.27	.32	.30	.26	.35	.27	.29	.26
Total	100.33	100.32	100.46	100.69	100.66	100.37	100.28	100.64
O=F,S,Cl	.02	.04	.03	.02	.00	.02	.03	.02
Total	100.31	100.28	100.43	100.67	100.65	100.35	100.25	100.62
	Trace elements in parts per million							
Ba	364	326	369	154	693	285	415	298
Rb	14	10	9	12	9	14	19	36
Sr	211	166	187	212	183	290	299	330
Pb	7	4	8	3	6	5	9	5
Th	1	2	2	1	1	2	2	3
Zr	43	60	70	38	53	62	69	66
Nb	1	2	2	1	3	3	3	2
Y	13	14	15	11	11	13	14	13
La	8	9	11	7	8	10	10	11
Ce	12	25	24	14	16	25	23	22
Nd	9	10	13	8	7	12	12	11
Sc	35	37	31	31	32	28	25	25
V	231	240	225	180	154	201	184	169
Cr	169	235	203	246	637	110	76	58
Co	79	80	76	75	61	81	74	71
Ni	350	392	345	399	428	292	245	236
Cu	105	96	108	179	200	172	209	218
Zn	93	93	101	90	77	103	101	99
Mo	4	5	4	4	4	4	3	3
Ga	10	9	11	11	7	12	14	13
As	1.5	1.5	3.5	2.5	1.5	14.0	3.5	1.0
S	400	800	600	400	100	400	600	400
Cs	<3	<3	<3	<3	<3	<3	<3	4
	Trace elements in parts per billion							
Pt	-	-	-	-	-	-	-	-
Pd	-	-	-	-	-	-	-	-
Ir	-	-	-	-	-	-	-	-
Au	-	-	-	-	-	-	-	-
mg	61.5	63.2	61.4	62.8	70.4	59.0	55.2	54.0

Sample no.	84770169	84770171	84770174	84770176	84770178	84770180	84770200	84770201
Intrusion	Mount Sholl Com.	Mount Sholl Com.	Mount Sholl Com.	Mount Sholl Com.	Mount Sholl Com.	Mount Sholl Com.	Mount Sholl Com.	Mount Sholl Com.
Locality	Sample traverse B	Sample traverse B	Sample traverse B	Sample traverse B	Sample traverse B	Off sample traverse	B2	B2
Lithology	Leucogabb.	Leucogabb.	Gabbro	Gabbro	Gabbro chill	Fine - grained gabbro	Gabbro chill trace sul.	Gabbro minor sulphides
Strat. ht (m)	1480	1680	2420	2840	3330			
Drill hole							DDH 72-5	DDH 72-5
Depth (m)							37.8-40.8	87.0-88.5
SiO2	51.39	50.22	51.60	51.02	50.59	48.14	48.73	42.63
TiO2	.69	.78	.75	.80	.68	1.26	.74	.32
Al2O3	12.11	12.03	8.30	10.43	7.51	14.54	8.54	3.62
Fe2O3	1.61	2.21	1.43	1.61	1.47	2.79	1.13	4.73
FeO	10.41	11.09	10.68	10.88	11.16	10.10	11.11	10.40
MnO	.19	.20	.21	.20	.22	.18	.21	.16
MgO	7.27	7.17	9.90	8.07	11.05	7.12	12.86	20.39
CaO	9.47	9.79	11.62	10.51	11.82	9.71	10.35	6.88
Na2O	2.98	2.58	2.52	2.64	1.63	2.51	2.04	.16
K2O	1.04	.84	.22	.92	.24	.18	.22	.08
P2O5	.05	.05	.06	.07	.05	.11	.07	.03
LOI	2.67	3.16	2.58	2.66	3.35	3.60	2.77	6.03
Rest	.31	.30	.30	.31	.37	.28	1.41	3.04
Total	100.19	100.42	100.17	100.12	100.14	100.52	100.18	98.47
O=F,S,Cl	.02	.03	.03	.03	.02	.03	.55	1.00
Total	100.17	100.39	100.14	100.08	100.12	100.49	99.63	97.47
	Trace elements in parts per million							
Ba	702	439	279	389	175	84	208	5
Rb	28	20	6	22	6	3	7	4
Sr	412	335	219	307	99	94	166	83
Pb	5	6	6	7	3	3	9	4
Th	2	3	2	3	3	<1	3	1
Zr	76	81	88	87	76	84	80	34
Nb	3	4	4	3	4	3	3	2
Y	13	16	17	17	16	30	14	6
La	11	16	13	15	14	6	20	7
Ce	25	30	31	29	24	15	26	13
Nd	12	14	15	15	10	10	14	6
Sc	22	22	30	26	30	36	24	16
V	163	174	213	193	178	290	165	81
Cr	49	48	185	93	827	309	288	475
Co	70	71	71	67	82	55	77	177
Ni	200	222	340	253	496	122	801	2983
Cu	240	249	139	176	261	269	314	4133
Zn	100	110	106	106	110	96	103	108
Mo	4	4	4	4	5	4	4	4
Ga	14	15	12	14	11	17	12	5
As	19.0	2.0	3.0	2.5	1.5	2.0	1.0	<.5
S	400	600	600	700	400	700	11000	20000
Cs	<3	<3	<3	<3	<3	<3	6	<3
	Trace elements in parts per billion							
Pt	-	-	-	-	-	-	-	91
Pd	-	-	-	-	-	-	-	324
Ir	-	-	-	-	-	-	-	6.59
Au	-	-	-	-	-	-	-	13.37
mg	52.2	49.4	59.6	53.8	61.2	50.2	65.4	71.3

Sample no.	84770202	84770203	84770204	84770205	84770206	84770207	84770208	84770209
Intrusion	Mount Sholl Com.	Mount Sholl Com.	Mount Sholl Com.	Mount Sholl Com.	Mount Sholl Com.	Mount Sholl Com.	Mount Sholl Com.	Mount Sholl Com.
Locality	B2	B2	B2	B2	B1	B1	A1	A1
Lithology	Peridotite minor sulphides	Massive po - pent - cpy	Peridotite trace sulphides	Peridotite trace sulphides	Peridotite minor sulphides	Peridotite minor sulphides	Gabbro - peridotite chill	Peridotite minor sulphides
Drill hole	DDH 72-5	DDH 72-5	DDH 72-5	DDH 72-5	DDH 72-19	DDH 72-19	DDH 72-19	DDH 72-19
Depth (m)	88.5-90.0	90.0-91.5	91.5-93.0	93.0-94.5	124-127	130-133	82.0-86.5	86.5-89.5
SiO2	43.67	6.46	41.97	44.10	42.50	41.97	45.60	42.70
TiO2	.35	.06	.37	.41	.32	.41	.41	.26
Al2O3	3.74	.98	4.56	4.54	3.90	4.36	4.69	3.22
Fe2O3	5.31	11.78	4.45	4.37	4.85	6.03	2.74	5.68
FeO	10.28	47.18	11.84	11.31	10.30	11.22	10.84	8.86
MnO	.14	.06	.15	.15	.21	.23	.21	.18
MgO	21.43	3.16	21.13	22.72	23.47	18.63	21.28	24.01
CaO	5.16	2.28	4.59	3.53	5.33	7.27	7.00	5.57
Na2O	.13	<.01	<.01	<.01	<.01	<.01	<.01	<.01
K2O	.09	.04	.13	.23	.03	.04	.02	.03
P2O5	.03	<.01	<.01	<.01	<.01	<.01	<.01	<.01
LOI	5.61	14.14	5.06	6.82	7.01	4.95	5.99	7.09
Rest	3.01	10.02	4.02	1.88	1.86	3.24	.87	1.75
Total	98.95	96.16	98.27	100.06	99.78	98.35	99.65	99.35
O=F,S,Cl	1.11	2.14	1.58	.55	.53	1.02	.22	.58
Total	97.84	94.03	96.69	99.52	99.25	97.33	99.43	98.77
	Trace elements in parts per million							
Ba	14	15	12	13	6	<3	<3	3
Rb	4	<1	6	12	3	2	1	3
Sr	60	28	44	18	26	37	26	30
Pb	4	16	3	3	3	6	3	4
Th	1	<1	<1	1	1	1	<1	<1
Zr	39	33	39	42	37	41	45	28
Nb	2	<1	2	3	2	2	2	1
Y	6	2	9	7	6	8	8	6
La	5	4	7	7	6	12	10	3
Ce	14	3	14	14	8	18	16	11
Nd	5	2	7	6	6	10	8	4
Sc	15	<2	16	14	14	22	21	16
V	88	29	100	94	88	134	110	75
Cr	488	86	558	418	456	847	488	538
Co	149	1691	170	154	144	215	111	121
Ni	2798	36450	2704	2681	3008	4557	1714	2047
Cu	2357	6751	2868	2515	2253	3297	531	1540
Zn	86	63	98	89	79	99	91	82
Mo	4	18	3	4	4	5	3	3
Ga	5	2	6	6	5	6	6	4
As	.5	34.0	.5	<.5	<.5	<.5	8.0	.5
S	22200	42800	31600	11000	10700	20400	4500	11600
Cs	<3	6	5	8	3	3	<3	<3
	Trace elements in parts per billion							
Pt	123	163	62.7	71.1	-	180	20.73	56.6
Pd	165	262	243	173	-	355	66.8	117
Ir	1.62	43.25	5.46	1.60	-	9.91	1.27	.36
Au	10.92	6.25	9.61	12.68	-	30.82	2.52	11.70
mg	71.7	8.9	70.4	72.6	74.0	66.6	74.0	75.4

Sample no.	84770210	84770211	84770212
Intrusion	Mount Sholl Com.	Mount Sholl Com.	Mount Sholl Com.
Locality	A1	A1	A1
Lithology	Peridotite minor sulphides	Peridotite minor sulphides	Peridotite minor sulphides
Drill hole	DDH 72-11	DDH 72-11	DDH 72-11
Depth (m)	89.5-92.5	92.5-95.5	95.5-98.5
SiO2	41.30	41.16	41.16
TiO2	.27	.29	.27
Al2O3	3.10	3.26	3.09
Fe2O3	7.11	7.19	6.95
FeO	8.26	7.97	8.57
MnO	.20	.19	.18
MgO	27.10	25.06	25.83
CaO	2.88	4.71	3.69
Na2O	<.01	<.01	<.01
K2O	.06	.03	.02
P2O5	<.01	<.01	<.01
LOI	8.36	7.68	8.32
Rest	1.27	1.79	1.36
Total	99.91	99.33	99.44
O=F,S,Cl	.34	.58	.33
Total	99.57	98.74	99.10
Trace elements in parts per million			
Ba	14	9	8
Rb	6	3	3
Sr	30	46	22
Pb	3	3	2
Th	<1	1	<1
Zr	29	30	28
Nb	2	1	1
Y	5	5	5
La	3	6	5
Ce	7	12	10
Nd	3	5	3
Sc	12	16	14
V	73	83	77
Cr	507	523	498
Co	147	145	168
Ni	2432	2439	2635
Cu	1187	1354	1756
Zn	88	82	73
Mo	3	2	3
Ga	4	5	5
As	<.5	<.5	<.5
S	6800	11700	6700
Cs	<3	3	<3
Trace elements in parts per billion			
Pt	48.3	67.3	50.8
Pd	99	112	104
Ir	.62	.50	.44
Au	10.89	16.29	11.25
mg	76.7	75.6	75.6

Sample no.	88770001	88770002	88770003	88770004	88770005	88770006	88770007	88770008
Intrusion	Maitland Complex	Maitland Complex	Maitland Complex	Maitland Complex	Maitland Complex	Maitland Complex	Maitland Complex	Maitland Complex
Locality	Sample traverse A	Sample traverse A	Sample traverse A	Sample traverse A	Sample traverse A	Sample traverse A	Sample traverse A	Sample traverse A
Lithology	Uralitised quartz gabbro	Uralitised quartz gabbro	Uralitised quartz gabbro	Uralitised gabbro	Uralitised gabbro	Uralitised anorthosi. gabbro	Uralitised anorthosi. gabbro	Uralitised gabbro
Zone	Gabbroic	Gabbroic	Gabbroic	Gabbroic	Gabbroic	Gabbroic	Gabbroic	Gabbroic
SiO2	56.21	54.16	50.26	47.09	51.36	47.97	48.22	47.38
TiO2	.88	.64	.37	.34	.43	.43	.44	.37
Al2O3	14.74	16.31	16.97	16.56	16.86	17.73	17.69	16.80
Fe2O3	2.86	2.20	1.82	1.57	1.33	1.63	1.27	1.62
FeO	5.93	5.34	5.73	5.95	5.56	6.08	6.13	6.70
MnO	.14	.12	.14	.12	.12	.14	.13	.13
MgO	5.03	6.64	9.51	12.86	9.18	9.96	10.03	10.94
CaO	8.50	8.88	9.30	8.80	9.54	10.13	8.90	9.51
Na2O	3.06	3.12	1.43	1.20	1.64	1.60	1.21	1.07
K2O	.37	.37	.53	.49	.56	.75	2.24	1.24
P2O5	.11	.07	.03	.03	.03	.04	.03	.03
LOI	1.85	1.98	3.72	4.81	3.24	3.32	3.53	3.96
Rest	.14	.14	.18	.21	.20	.18	.23	.20
Total	99.82	99.97	99.99	100.03	100.05	99.96	100.05	99.95
O=F,S,Cl	.01	.00	.00	.00	.00	.00	.00	.00
Total	99.82	99.96	99.98	100.03	100.05	99.95	100.05	99.95
	Trace elements in parts per million							
Ba	96	70	79	85	85	150	446	334
Rb	7	11	19	26	27	34	115	61
Sr	170	184	113	139	143	153	61	105
Pb	<1	2	<1	<1	<1	2	<1	2
Th	2	2	<1	2	<1	<1	<1	<1
Zr	124	81	38	37	48	36	45	32
Nb	6	4	2	2	2	2	2	2
Y	35	23	13	14	17	12	12	11
La	16	12	6	6	6	6	5	5
Ce	27	15	10	14	13	9	10	6
Nd	16	9	8	6	5	3	4	5
Sc	44	37	34	23	35	32	29	32
V	241	197	134	99	144	138	133	128
Cr	53	149	573	579	672	388	491	399
Co	62	62	42	57	47	52	51	55
Ni	29	48	96	371	109	208	254	249
Cu	2	<2	8	<2	5	<2	2	23
Zn	54	60	54	66	59	55	46	61
Ga	15	14	12	10	12	11	11	11
As	<.5	<.5	.5	1.0	1.0	<.5	.5	<.5
S	38	35	24	16	14	16	15	36
Cs	<3	<3	<3	<3	<3	<3	<3	<3
	Trace elements in parts per billion							
Pt	-	-	-	-	-	-	-	-
Pd	-	-	-	-	-	-	-	-
Ir	-	-	-	-	-	-	-	-
Ru	-	-	-	-	-	-	-	-
Au	-	-	-	-	-	-	-	-
mg	51.3	61.8	69.7	75.7	70.8	70.2	71.1	70.5

Sample no.	88770009	88770010	88770011	88770012	88770013	88770014	88770015	88770016
Intrusion	Maitland Complex	Maitland Complex	Maitland Complex	Maitland Complex	Maitland Complex	Maitland Complex	Maitland Complex	Maitland Complex
Locality	Sample traverse A	Sample traverse A	Sample traverse A	Sample traverse A	Sample traverse A	Sample traverse A	Sample traverse A	Sample traverse A
Lithology	Anorthosi.	Anorthosi.	Uralitised quartz gabbro	Uralitised quartz gabbro	Uralitised anorthosi. gabbro	Uralitised clinopyro.	Uralitised anorthosi. gabbro	Uralitised anorthosi. gabbro
Zone	Gabbroic	Gabbroic	Gabbroic	Gabbroic	Gabbroic	Ultramafic	Gabbroic	Gabbroic
SiO2	48.78	48.30	53.53	61.92	47.15	46.02	49.96	49.46
TiO2	.42	.36	.72	1.13	.57	.56	.21	.28
Al2O3	20.24	22.89	15.14	13.54	16.87	12.26	15.53	15.66
Fe2O3	1.54	1.07	2.67	4.54	1.62	1.88	.99	.73
FeO	4.78	3.37	6.02	4.35	5.99	8.48	5.49	5.38
MnO	.10	.07	.13	.12	.14	.16	.13	.12
MgO	7.31	6.09	6.17	2.47	7.76	14.27	12.95	13.53
CaO	11.12	11.81	9.06	6.00	13.81	11.49	8.03	8.43
Na2O	2.07	2.20	3.46	3.65	1.38	1.28	1.08	1.06
K2O	.38	.34	.73	.67	.53	.20	.71	.59
P2O5	.03	.04	.10	.16	.05	.05	.03	.02
LOI	3.08	3.53	2.15	1.32	4.01	2.93	4.42	4.46
Rest	.16	.16	.15	.16	.22	.33	.23	.25
Total	100.01	100.23	100.03	100.03	100.10	99.91	99.76	99.97
O=F,S,Cl	.00	.00	.01	.01	.03	.02	.00	.00
Total	100.01	100.22	100.02	100.02	100.07	99.89	99.76	99.97
Trace elements in parts per million								
Ba	63	58	151	218	102	78	114	100
Rb	25	18	31	22	35	11	46	25
Sr	184	199	176	144	109	57	206	187
Pb	<1	2	2	2	<1	<1	<1	2
Th	<1	<1	<1	5	<1	<1	<1	<1
Zr	31	33	68	220	43	45	15	13
Nb	<1	<1	4	12	<1	<1	<1	<1
Y	10	8	21	72	10	11	3	5
La	4	5	7	25	<2	<2	6	3
Ce	8	9	21	56	6	<5	6	7
Nd	7	4	8	30	3	4	2	<2
Sc	33	25	51	32	45	40	25	24
V	136	101	226	214	189	173	81	95
Cr	449	457	83	10	476	1339	730	877
Co	44	34	45	43	45	66	53	49
Ni	113	131	44	5	120	350	311	344
Cu	<2	<2	20	2	41	25	<2	<1
Zn	36	27	51	38	53	84	63	58
Ga	13	13	14	17	15	11	12	12
As	1.0	<.5	.5	.5	.5	.5	.5	1.0
S	12	11	50	26	423	70	36	24
Cs	<3	<3	<3	<3	<3	<3	<3	<3
Trace elements in parts per billion								
Pt	-	-	-	-	-	-	-	-
Pd	-	-	-	-	-	-	-	-
Ir	-	-	-	-	-	-	-	-
Ru	-	-	-	-	-	-	-	-
Au	-	-	-	-	-	-	-	-
mg	67.9	71.5	56.6	34.3	65.0	71.4	78.3	80.0

Sample no.	88770017	88770018	88770019	88770020	88770021	88770022	88770023	88770024
Intrusion	Maitland Complex	Maitland Complex	Maitland Complex	Maitland Complex	Maitland Complex	Maitland Complex	Maitland Complex	Maitland Complex
Locality	Sample traverse A	Sample traverse A	Sample traverse A	Sample traverse A	Sample traverse B	Sample traverse B	Sample traverse B	Sample traverse B
Lithology	Uralitised anorthosi. gabbro	Olivine gabbronor.	Uralitised anorthosi. gabbro	Uralitised gabbro	Pegmatoid. quartz gabbro	Pegmatoid. quartz gabbro	Pegmatoid. quartz gabbro	Uralitised gabbro
Zone	Gabbroic	Gabbroic	Gabbroic	Gabbroic	Gabbroic	Gabbroic	Gabbroic	Gabbroic
Strat. ht (m)					5	40	120	200
SiO2	49.07	50.18	45.94	46.14	45.63	47.52	45.74	45.10
TiO2	.19	.23	.30	.42	2.32	1.75	1.81	1.77
Al2O3	16.82	8.89	21.28	18.95	14.40	14.69	15.19	15.54
Fe2O3	1.04	1.98	1.61	2.08	6.20	4.93	4.79	5.82
FeO	5.43	8.23	3.73	6.10	9.85	8.25	7.65	8.19
MnO	.12	.19	.09	.13	.20	.17	.16	.14
MgO	12.06	19.76	7.01	8.63	5.21	6.30	6.76	6.33
CaO	10.08	7.37	13.66	10.61	9.87	10.45	12.60	11.29
Na2O	1.17	.59	1.63	1.74	2.24	2.02	1.47	1.97
K2O	.42	.04	.26	1.25	.67	.50	.09	.13
P2O5	-	-	.01	.02	.05	.11	.03	.02
LOI	3.44	2.12	4.34	3.91	2.71	2.76	3.35	3.20
Rest	.21	.33	.25	.14	.57	.35	.43	.48
Total	100.05	99.91	100.11	100.12	99.92	99.80	100.07	99.98
O=F,S,Cl	.01	.04	.04	.02	.19	.08	.09	.13
Total	100.04	99.87	100.07	100.10	99.73	99.71	99.98	99.85
	Trace elements in parts per million							
Ba	34	6	52	142	122	85	<4	<4
Rb	26	3	15	72	30	25	3	4
Sr	161	84	249	257	161	173	208	163
Pb	<1	<1	3	2	2	<1	<1	2
Th	<1	<1	<1	<1	<1	<1	<1	<1
Zr	7	6	8	9	52	53	33	31
Nb	<1	<1	<1	<1	3	3	<1	<1
Y	3	3	4	3	17	18	11	12
La	2	2	<2	3	8	4	5	7
Ce	<5	<5	6	<5	13	14	<5	6
Nd	2	<2	<2	2	9	7	3	3
Sc	30	38	33	28	58	57	62	58
V	79	109	99	87	748	560	734	769
Cr	682	957	480	44	3	30	247	29
Co	42	69	44	53	64	52	59	76
Ni	244	426	122	63	8	17	110	91
Cu	69	69	135	19	129	67	166	248
Zn	50	76	56	58	107	97	88	79
Ga	12	7	13	13	19	16	17	17
As	.5	.5	.5	.5	1.5	1.0	1.0	<.5
S	126	675	669	342	3338	1563	1665	2400
Cs	<3	<3	<3	<3	<3	<3	<3	<3
	Trace elements in parts per billion							
Pt	-	-	-	-	4.25	-	2.05	4.71
Pd	-	-	-	-	2.63	-	1.54	1.20
Ir	-	-	-	-	.06	-	.01	.01
Ru	-	-	-	-	.06	-	.09	.03
Au	-	-	-	-	3.47	-	1.57	6.22
mg	77.2	77.9	70.7	65.9	37.6	47.0	50.2	45.7

Sample no.	88770025	88770026	88770027	88770028	88770029	88770030	88770031	88770032
Intrusion	Maitland Complex	Maitland Complex	Maitland Complex	Maitland Complex	Maitland Complex	Maitland Complex	Maitland Complex	Maitland Complex
Locality	Sample traverse B	Sample traverse B	Sample traverse B	Sample traverse B	Sample traverse B	Sample traverse B	Sample traverse B	Sample traverse B
Lithology	Anorthosi.	Uralitised anorthosi. gabbro	Anorthosi.	Norite	Uralitised anorthosi. gabbro	Gabbronor.	Norite	Gabbronor.
Zone	Gabbroic	Gabbroic	Gabbroic	Gabbroic	Gabbroic	Gabbroic	Gabbroic	Gabbroic
Strat. ht (m)	240	260	420	500	600	760	860	1020
SiO2	47.46	46.22	44.93	50.00	47.99	49.76	48.98	49.63
TiO2	.43	.95	.26	.29	.20	.25	.20	.25
Al2O3	21.88	20.15	24.40	17.51	21.41	17.13	19.63	17.52
Fe2O3	1.75	2.85	1.87	1.26	1.12	1.33	1.21	1.42
FeO	3.54	5.94	3.37	5.79	4.32	5.34	4.17	4.86
MnO	.08	.12	.07	.14	.10	.13	.11	.12
MgO	5.78	6.41	5.41	12.09	8.36	10.17	8.45	9.83
CaO	12.62	11.32	13.45	9.68	11.72	13.12	13.98	13.47
Na2O	1.77	1.42	1.24	1.29	1.42	1.33	1.38	1.39
K2O	.41	.45	.21	.04	.14	.05	.07	.04
P2O5	.02	.02	.02	.01	-	-	-	-
LOI	4.05	3.98	4.88	1.57	2.84	.96	1.41	1.16
Rest	.17	.25	.15	.16	.18	.29	.20	.19
Total	99.96	100.08	100.26	99.83	99.80	99.86	99.79	99.88
O=F,S,Cl	.01	.05	.02	.01	.01	.07	.04	.03
Total	99.95	100.03	100.23	99.82	99.79	99.79	99.75	99.85
	Trace elements in parts per million							
Ba	103	75	36	12	44	4	6	9
Rb	43	39	33	3	11	4	4	2
Sr	223	189	258	171	190	110	156	148
Pb	<1	<1	<1	<1	<1	<1	<1	<1
Th	<1	<1	<1	<1	<1	<1	<1	<1
Zr	22	24	13	10	6	9	6	6
Nb	<1	<1	<1	<1	<1	<1	<1	<1
Y	8	6	3	3	3	5	4	4
La	4	6	3	<2	3	2	3	<2
Ce	7	6	<5	<5	<5	5	<5	<5
Nd	<2	<2	<2	2	<2	5	3	2
Sc	32	32	16	31	27	43	40	44
V	108	297	66	87	70	116	95	114
Cr	340	259	80	406	564	300	286	274
Co	37	47	42	49	37	52	44	50
Ni	96	77	167	119	113	152	105	108
Cu	19	23	28	38	46	216	140	180
Zn	40	74	39	51	42	42	33	38
Ga	14	16	14	12	13	13	13	12
As	<.5	.5	.5	1.0	1.0	1.0	.5	<.5
S	210	791	432	239	218	1422	722	488
Cs	<3	<3	<3	<3	<3	<3	<3	<3
	Trace elements in parts per billion							
Pt	-	3.36	2.47	7.51	-	3.66	-	2.17
Pd	-	5.93	1.89	3.37	-	2.04	-	1.77
Ir	-	.05	.05	.12	-	.01	-	.02
Ru	-	.52	.53	.18	-	.17	-	.23
Au	-	.51	.43	1.31	-	1.09	-	.69
mg	66.8	57.3	65.6	75.7	73.7	73.5	74.1	74.1

Sample no.	88770033	88770034	88770035	88770036	88770037	88770038	88770039	88770040
Intrusion	Maitland Complex	Maitland Complex	Maitland Complex	Maitland Complex	Maitland Complex	Maitland Complex	Maitland Complex	Maitland Complex
Locality	Sample traverse B	Sample traverse B	Sample traverse B	Sample traverse B	Sample traverse B	Sample traverse B	Sample traverse B	Sample traverse B
Lithology	Anorthosi. gabbro	Uralitised gabbro	Uralitised gabbro	Lherzolite	Harzburgi.	Gabbro	Gabbro	Gabbro
Zone	Gabbroic	Gabbroic	Gabbroic	Ultramafic	Ultramafic	Gabbroic	Gabbroic	Gabbroic
Strat. ht (m)	1220	1320	1460	1520	1630	1700	1800	2000
SiO2	46.70	50.43	49.84	37.12	37.15	49.96	50.61	49.16
TiO2	.13	.88	.24	.08	.08	.39	.37	.38
Al2O3	22.07	17.59	14.12	7.53	8.10	14.23	12.24	17.44
Fe2O3	.98	1.49	1.38	8.21	7.89	1.73	1.56	1.51
FeO	3.23	6.95	5.61	3.00	3.37	7.45	7.77	5.13
MnO	.08	.14	.13	.14	.15	.16	.18	.11
MgO	8.32	6.59	13.23	29.28	28.77	12.21	14.65	10.39
CaO	11.52	9.30	9.33	3.55	3.51	8.55	7.47	9.32
Na2O	1.03	2.85	1.03	.24	.30	1.30	1.09	1.31
K2O	.68	.57	.27	.01	.02	.21	.32	.29
P2O5	-	.14	.01	-	-	.03	.02	.03
LOI	5.00	2.85	4.51	10.15	10.09	3.41	3.30	4.65
Rest	.22	.26	.34	.50	.52	.22	.21	.21
Total	99.96	100.04	100.04	99.81	99.95	99.85	99.79	99.93
O=F,S,Cl	.01	.06	.01	.02	.02	.03	.02	.02
Total	99.95	99.98	100.02	99.79	99.93	99.83	99.77	99.91
Trace elements in parts per million								
Ba	80	80	36	7	34	36	41	37
Rb	59	32	16	1	1	14	19	19
Sr	219	224	206	26	29	157	126	186
Pb	<1	<1	<1	<1	<1	<1	<1	<1
Th	<1	<1	2	<1	<1	<1	<1	<1
Zr	4	78	17	2	3	21	21	25
Nb	<1	5	<1	<1	<1	<1	<1	<1
Y	1	14	6	1	<1	6	6	5
La	<2	10	5	<2	2	5	5	4
Ce	6	24	9	<5	<5	9	<5	5
Nd	<2	9	<2	<2	<2	3	<2	2
Sc	24	33	36	9	8	37	36	29
V	51	176	111	27	30	158	140	125
Cr	723	176	1227	1988	2089	317	404	467
Co	33	41	53	105	105	59	64	44
Ni	113	104	386	1265	1262	250	287	243
Cu	103	78	70	2	2	99	59	43
Zn	37	81	62	66	99	74	70	54
Ga	12	15	11	4	5	11	10	14
As	.5	1.5	1.5	.5	1.5	.5	.5	<.5
S	253	1029	215	129	156	518	305	339
Cs	<3	<3	<3	<3	<3	<3	<3	<3
Trace elements in parts per billion								
Pt	-	2.61	-	-	9.01	5.07	-	.64
Pd	-	2.77	-	-	14.59	4.20	-	.50
Ir	-	.02	-	-	.34	.04	-	.01
Ru	-	.58	-	-	1.05	.17	-	.32
Au	-	.67	-	-	.61	1.01	-	.61
mg	78.3	58.6	77.5	83.4	83.0	70.7	74.0	74.1

Sample no.	88770041	88770042	88770043	88770044	88770045	88770046	88770047	88770048
Intrusion	Maitland Complex	Maitland Complex	Maitland Complex	Maitland Complex	Maitland Complex	Maitland Complex	Maitland Complex	Maitland Complex
Locality	Sample traverse B	Sample traverse B	Sample traverse B	Sample traverse B	Sample traverse B	Sample traverse B	Sample traverse B	Off sample traverse
Lithology	Lherzolite	Gabbro	Anorthosi. gabbro	Gabbronor.	Quartz - mica - ?xenolith	Gabbronor.	Gabbro	Clinopyro.
Zone	Ultramafic	Gabbroic	Gabbroic	Gabbroic		Gabbroic	Gabbroic	Ultramafic
Strat. ht (m)	2130	2260	2400	2530		2780	2840	
SiO2	37.75	49.35	47.91	50.37	64.48	47.18	47.86	46.18
TiO2	.05	.30	.21	.21	.63	.47	.24	.34
Al2O3	7.18	16.14	18.83	12.60	15.91	17.10	17.97	11.61
Fe2O3	6.85	1.77	1.34	2.59	2.40	2.18	1.43	3.09
FeO	3.46	5.42	4.55	6.61	2.88	7.49	5.55	6.92
MnO	.14	.13	.11	.18	.04	.15	.13	.16
MgO	30.22	10.62	9.72	15.41	1.43	10.10	10.90	15.46
CaO	2.75	10.52	10.14	6.45	4.89	9.31	10.14	11.29
Na2O	.20	1.26	1.33	.68	3.81	.99	1.03	.95
K2O	.01	.06	.82	.40	.62	.29	.25	.10
P2O5	-	.02	.02	-	.18	.01	-	.01
LOI	10.76	4.06	4.71	4.26	2.44	4.29	3.90	3.38
Rest	.38	.20	.25	.25	.13	.24	.39	.36
Total	99.75	99.85	99.94	100.01	99.84	99.80	99.79	99.85
O=F,S,Cl	.01	.03	.01	.00	.00	.05	.08	.02
Total	99.74	99.83	99.93	100.00	99.83	99.74	99.71	99.84
	Trace elements in parts per million							
Ba	<4	10	114	71	189	52	46	142
Rb	<1	3	56	24	31	17	18	2
Sr	20	162	376	203	235	164	176	31
Pb	<1	<1	<1	2	7	<1	<1	<1
Th	<1	<1	<1	<1	6	<1	<1	<1
Zr	2	19	14	8	212	9	5	13
Nb	<1	<1	<1	<1	7	<1	<1	<1
Y	1	6	3	2	21	4	3	6
La	3	4	2	3	12	5	<2	2
Ce	<5	<5	<5	<5	35	5	<5	<5
Nd	<2	3	3	<2	17	3	2	<2
Sc	8	37	26	29	14	33	33	46
V	23	146	86	96	55	199	109	145
Cr	1325	309	625	818	7	103	823	1438
Co	113	55	49	60	65	64	51	78
Ni	1205	217	255	370	5	185	181	354
Cu	<2	104	93	2	<2	67	205	76
Zn	68	57	51	75	47	76	58	81
Ga	2	12	12	9	18	12	12	10
As	1.5	.5	.5	<.5	<.5	1.0	.5	.50
S	45	453	144	22	14	985	1492	219
Cs	<3	<3	3	<3	3	<3	<3	<3
	Trace elements in parts per billion							
Pt	-	2.88	6.07	-	-	-	-	-
Pd	-	4.31	7.72	-	-	-	-	-
Ir	-	.07	.01	-	-	-	-	-
Ru	-	.48	.16	-	-	-	-	-
Au	-	1.31	1.43	-	-	-	-	-
mg	84.8	73.0	75.1	75.4	33.6	65.6	74.0	74.0

Sample no.	88770049	88770050	88770051	88770052	88770053	88770054	88770055	88770056
Intrusion	Maitland Complex	Granite	Radio Hill Complex	Radio Hill Complex	Radio Hill Complex	Radio Hill Complex	Radio Hill Complex	Radio Hill Complex
Locality	Off sample traverse	Off sample traverse	Sample traverse	Sample traverse	Sample traverse	Sample traverse	Sample traverse	Sample traverse
Lithology	Gabbro	Biotite granite	Felsic metavolca.	Felsic metavolca.	Massive po - pent - cpy	Veined cpy - po - pent	Massive po - pent - cpy	Massive po - pent - cpy
Zone	Gabbroic				Ultramafic	Ultramafic	Ultramafic	Ultramafic
Subzone					A	A	A	A
Strat. ht (m)					1	3	5	8
Drill hole			84RHPD208	84RHPD208	84RHPD208	84RHPD208	84RHPD208	84RHPD208
Depth (m)			269.3	265.6	263.5	260.7	258.1	254.8
SiO2	49.71	74.09	71.95	21.06	-	-	-	-
TiO2	.48	.17	.48	.05	-	-	-	-
Al2O3	17.20	13.73	10.44	2.69	-	-	-	-
Fe2O3	1.40	.94	1.11	16.36	-	-	-	-
FeO	5.12	.33	3.77	4.14	-	-	-	-
MnO	.12	.03	.08	.09	-	-	-	-
MgO	9.42	.26	1.05	.75	-	-	-	-
CaO	10.05	.82	3.26	23.93	-	-	-	-
Na2O	2.00	3.85	4.10	.57	-	-	-	-
K2O	.99	4.81	.59	.13	-	-	-	-
P2O5	.03	.03	.09	.01	-	-	-	-
LOI	3.29	.63	2.45	-	-	-	-	-
Rest	.19	.26	.16	26.29	-	-	-	-
Total	100.00	99.95	99.53	96.07	-	-	-	-
O=F,S,Cl	.00	.00	.03	4.99	-	-	-	-
Total	100.00	99.95	99.50	91.08	-	-	-	-
Trace elements in parts per million								
Ba	150	1304	95	185	-	-	-	-
Rb	52	222	9	7	-	-	-	-
Sr	102	157	70	179	-	-	-	-
Pb	<1	39	<1	436	-	-	-	-
Th	<1	32	6	<1	-	-	-	-
Zr	52	169	343	50	-	-	-	-
Nb	3	8	15	3	-	-	-	-
Y	19	9	73	13	-	-	-	-
La	9	59	31	3	-	-	-	-
Ce	8	110	72	15	-	-	-	-
Nd	11	33	38	9	-	-	-	-
Sc	31	3	18	20	-	-	-	-
V	130	7	2	6	-	-	-	-
Cr	519	1	2	2	42	104	83	63
Co	46	53	49	494	1837	1187	1909	1622
Ni	200	<2	<2	24105	36750	24170	36090	33440
Cu	<2	4	27	97450	11190	5720	40295	6965
Zn	57	37	27	3569	78	78	184	49
Ga	11	21	11	3	-	-	-	-
As	1.0	<.5	.5	743	-	-	-	-
S	29	6	490	99990	-	-	-	-
Cs	<3	3	<3	<3	-	-	-	-
Trace elements in parts per billion								
Pt	-	-	-	-	243	-	220	-
Pd	-	-	-	-	6312	-	2025	-
Ir	-	-	-	-	1.37	-	44.6	-
Ru	-	-	-	-	30.48	-	254	-
Au	-	-	-	-	5.60	-	34.70	-
mg	72.5	28.3	28.2	6.6	-	-	-	-

Sample no.	88770057	88770058	88770059	88770060	88770061	88770062	88770063	88770064
Intrusion	Radio Hill Complex	Radio Hill Complex	Radio Hill Complex	Radio Hill Complex	Radio Hill Complex	Radio Hill Complex	Radio Hill Complex	Radio Hill Complex
Locality	Sample traverse	Sample traverse	Sample traverse	Sample traverse	Sample traverse	Sample traverse	Sample traverse	Sample traverse
Lithology	Massive po - pent - cpy	Massive po - pent - cpy	Massive po - pent - cpy	Massive po - pent - cpy	Gabbro	Gabbro	Plagiocla. pyroxenite	Pyroxenite
Zone	Ultramafic	Ultramafic	Ultramafic	Ultramafic	Ultramafic	Ultramafic	Ultramafic	Ultramafic
Subzone	A	A	A	A	A	A	A	A
Strat. ht (m)	10	13	15	18	20	22	25	27
Drill hole	84RHPD208	84RHPD208	84RHPD208	84RHPD208	84RHPD208	84RHPD208	84RHPD208	84RHPD208
Depth (m)	251.8	248.5	246.0	243.7	241.5	238.5	235.5	232.0
SiO2	-	-	-	-	-	46.47	45.52	45.94
TiO2	-	-	-	-	-	.48	.40	.38
Al2O3	-	-	-	-	-	7.25	5.26	4.20
Fe2O3	-	-	-	-	-	5.00	2.52	4.17
FeO	-	-	-	-	-	10.44	10.31	10.00
MnO	-	-	-	-	-	.24	.19	.12
MgO	-	-	-	-	-	9.96	17.21	21.74
CaO	-	-	-	-	-	10.89	11.49	4.68
Na2O	-	-	-	-	-	1.86	.34	.19
K2O	-	-	-	-	-	.78	-	.06
P2O5	-	-	-	-	-	.03	.02	.03
LOI	-	-	-	-	-	1.70	4.68	5.27
Rest	-	-	-	-	-	4.79	1.67	2.00
Total	-	-	-	-	-	99.89	99.61	98.78
O=F,S,Cl	-	-	-	-	-	1.47	.34	.67
Total	-	-	-	-	-	98.43	99.27	98.11
Trace elements in parts per million								
Ba	-	-	-	-	-	283	<4	<4
Rb	-	-	-	-	-	9	1	5
Sr	-	-	-	-	-	42	19	9
Pb	-	-	-	-	-	12	4	<1
Th	-	-	-	-	-	2	2	2
Zr	-	-	-	-	-	59	41	40
Nb	-	-	-	-	-	2	3	3
Y	-	-	-	-	-	16	9	7
La	-	-	-	-	-	8	12	6
Ce	-	-	-	-	-	21	22	9
Nd	-	-	-	-	-	5	10	5
Sc	-	-	-	-	-	26	23	18
V	-	-	-	-	-	180	114	103
Cr	104	83	125	125	271	399	595	528
Co	902	2805	2248	1101	260	185	144	137
Ni	21850	52650	43045	22515	3642	5035	2526	1957
Cu	2985	23880	5720	14185	16665	8275	3955	2119
Zn	107	155	58	78	291	88	243	102
Ga	-	-	-	-	-	8	9	5
As	-	-	-	-	-	1.0	1.5	.5
S	-	-	-	-	-	29320	6820	13450
Cs	-	-	-	-	-	<3	<3	<3
Trace elements in parts per billion								
Pt	-	184	-	-	550	143	-	110
Pd	-	4070	-	-	2960	799	-	287
Ir	-	491	-	-	26.25	25.48	-	2.13
Ru	-	459	-	-	20.30	3.51	-	3.88
Au	-	6.94	-	-	52.5	6.01	-	21.20
mg	-	-	-	-	-	54.3	70.9	73.8

Sample no.	88770065	88770066	88770067	88770068	88770069	88770070	88770071	88770072
Intrusion	Radio Hill Complex	Radio Hill Complex	Radio Hill Complex	Radio Hill Complex	Radio Hill Complex	Radio Hill Complex	Radio Hill Complex	Radio Hill Complex
Locality	Sample traverse	Sample traverse	Sample traverse	Sample traverse	Sample traverse	Sample traverse	Sample traverse	Sample traverse
Lithology	Plagiocla. pyroxenite	Lherzolite	Lherzolite	Lherzolite	Websterite	Lherzolite	Wehrlite	Lherzolite
Zone	Ultramafic	Ultramafic	Ultramafic	Ultramafic	Ultramafic	Ultramafic	Ultramafic	Ultramafic
Subzone	A	B	B	B	B	B	B	B
Strat. ht (m)	29	34	38	40	43	45	47	51
Drill hole	84RHPD208	84RHPD208	84RHPD208	84RHPD208	84RHPD208	84RHPD208	84RHPD208	84RHPD208
Depth (m)	228.3	225.3	221.0	217.5	215.0	212.8	209.8	205.2
SiO2	43.52	43.52	46.08	39.09	38.83	43.55	39.36	40.68
TiO2	.45	.34	.37	.27	.41	.28	.26	.23
Al2O3	4.27	3.64	3.75	2.62	3.12	2.85	2.76	2.98
Fe2O3	3.53	6.29	3.98	8.84	10.17	5.95	9.00	7.67
FeO	11.51	7.33	8.90	9.31	9.84	8.88	7.83	8.32
MnO	.21	.20	.22	.21	.20	.18	.20	.19
MgO	16.40	23.73	20.98	24.61	16.27	25.80	25.31	26.03
CaO	11.84	6.42	8.61	3.56	9.16	2.01	4.70	2.84
Na2O	.42	.47	.31	.20	.41	.09	.35	.12
K2O	.06	.22	.11	.12	.10	.05	.16	.07
P2O5	.03	.02	.03	.01	.03	.02	.01	.01
LOI	3.13	6.82	5.61	8.20	1.54	7.17	7.03	8.46
Rest	4.70	.84	.93	2.26	9.03	2.01	2.75	1.44
Total	100.07	99.84	99.88	99.30	99.11	98.84	99.72	99.04
O=F,S,Cl	1.37	.17	.23	.78	3.13	.66	.90	.42
Total	98.70	99.67	99.65	98.52	95.98	98.18	98.82	98.62
	Trace elements in parts per million							
Ba	8	79	17	9	8	4	49	7
Rb	4	11	8	7	5	3	7	4
Sr	17	75	14	20	17	6	53	23
Pb	5	2	<1	7	17	4	5	4
Th	2	2	<1	<1	2	2	<1	2
Zr	49	35	38	26	41	30	25	22
Nb	3	2	3	<1	3	<1	<1	<1
Y	11	8	8	5	7	6	6	5
La	13	5	9	5	9	8	7	6
Ce	12	13	15	16	9	6	11	7
Nd	5	4	3	3	5	3	<2	3
Sc	33	18	23	13	30	13	11	13
V	174	90	113	71	163	80	66	71
Cr	950	527	740	421	834	483	396	413
Co	219	137	98	187	353	191	194	170
Ni	5500	2119	1592	2705	9535	2713	3493	2294
Cu	8080	704	784	1886	10465	1697	3055	1582
Zn	186	96	74	79	232	81	111	89
Ga	6	5	5	2	4	4	3	3
As	.5	1.0	.5	1.0	.5	<.5	1.5	.5
S	27460	3285	4615	15570	62630	13195	17970	8315
Cs	<3	6	<3	<3	<3	<3	5	<3
	Trace elements in parts per billion							
Pt	-	-	-	91.3	-	-	127	-
Pd	-	-	-	288	-	-	250	-
Ir	-	-	-	6.14	-	-	7.53	-
Ru	-	-	-	9.91	-	-	4.95	-
Au	-	-	-	21.60	-	-	16.90	-
mg	66.6	76.5	75.0	71.8	60.4	76.4	73.9	75.3

Sample no.	88770073	88770074	88770075	88770076	88770077	88770078	88770079	88770080
Intrusion	Radio Hill Complex	Radio Hill Complex	Radio Hill Complex	Radio Hill Complex	Radio Hill Complex	Radio Hill Complex	Radio Hill Complex	Radio Hill Complex
Locality	Sample traverse	Sample traverse	Sample traverse	Sample traverse	Sample traverse	Sample traverse	Sample traverse	Sample traverse
Lithology	Wehrlite	Porphyrit. olivine websterite	Porphyrit. plagiocla. websterite	Porphyrit. plagiocla. websterite	Olivine websterite	Olivine websterite	Plagiocla. olivine websterite	Olivine websterite
Zone	Ultramafic	Ultramafic	Ultramafic	Ultramafic	Ultramafic	Ultramafic	Ultramafic	Ultramafic
Subzone	B	C	C	C	D	D	D	D
Strat. ht (m)	54	57	59	62	66	68	70	72
Drill hole	84RHPD208	84RHPD208	84RHPD208	84RHPD208	84RHPD208	84RHPD208	84RHPD208	84RHPD208
Depth (m)	203.0	199.2	196.5	193.5	190.0	188.1	185.0	182.7
SiO2	44.66	44.69	45.83	48.83	44.29	44.76	44.13	44.95
TiO2	.41	.37	.35	.38	.36	.38	.36	.39
Al2O3	3.96	3.61	4.12	3.61	3.94	3.85	4.04	4.16
Fe2O3	4.73	5.07	4.82	2.31	5.47	4.30	4.73	3.54
FeO	8.05	7.98	7.80	8.55	7.69	9.61	9.71	9.85
MnO	.22	.20	.20	.16	.21	.20	.21	.22
MgO	21.46	23.53	21.96	19.99	23.24	22.54	21.46	21.82
CaO	8.43	6.56	7.49	9.11	6.73	6.12	6.92	6.98
Na2O	.44	.48	.62	.38	.57	.31	.40	.29
K2O	.16	.29	.25	.04	.25	.17	.22	.23
P2O5	.02	.03	.02	.02	.02	.03	.02	.03
LOI	5.69	6.56	5.72	4.66	6.70	6.80	5.89	6.61
Rest	1.34	.47	.63	1.40	.48	.81	1.92	.60
Total	99.57	99.84	99.81	99.44	99.95	99.88	100.01	99.67
O=F,S,Cl	.38	.05	.10	.24	.05	.16	.55	.10
Total	99.19	99.80	99.71	99.20	99.89	99.71	99.46	99.57
	Trace elements in parts per million							
Ba	36	71	69	7	75	20	30	19
Rb	9	15	12	2	12	10	12	14
Sr	26	59	74	17	67	17	36	20
Pb	4	3	4	<1	<1	5	7	4
Th	2	2	<1	2	<1	2	2	3
Zr	41	43	39	37	33	36	32	43
Nb	2	2	<1	2	<1	2	2	3
Y	10	8	8	8	7	8	8	8
La	8	10	9	7	7	9	7	9
Ce	9	10	18	15	11	7	18	13
Nd	4	4	6	9	<2	4	5	4
Sc	25	18	22	23	18	20	21	21
V	121	98	100	117	92	100	100	102
Cr	748	624	758	827	593	662	693	711
Co	134	120	117	181	121	129	144	108
Ni	1891	1567	1625	3189	1554	1761	2386	1451
Cu	1289	119	314	2496	159	789	2676	429
Zn	88	88	84	117	92	89	118	79
Ga	5	5	5	5	5	5	6	6
As	<.5	<.5	.5	2.0	1.0	.5	.5	.5
S	7596	939	2019	4852	1006	3231	11039	1967
Cs	<3	7	<3	<3	3	3	<3	<3
	Trace elements in parts per billion							
Pt	47.60	-	-	62.7	-	-	-	-
Pd	205	-	-	428	-	-	-	-
Ir	.91	-	-	1.76	-	-	-	-
Ru	2.30	-	-	2.54	-	-	-	-
Au	11.54	-	-	28.10	-	-	-	-
mg	75.7	77.0	76.3	77.0	76.7	74.9	73.3	74.9

Sample no.	88770081	88770082	88770083	88770084	88770085	88770086	88770087	88770088
Intrusion	Radio Hill Complex	Radio Hill Complex	Radio Hill Complex	Radio Hill Complex	Radio Hill Complex	Radio Hill Complex	Radio Hill Complex	Radio Hill Complex
Locality	Sample traverse	Sample traverse	Sample traverse	Sample traverse	Sample traverse	Sample traverse	Sample traverse	Sample traverse
Lithology	Plagiocla. olivine websterite	Plagiocla. websterite	Websterite	Plagiocla. websterite	Plagiocla. websterite	Plagiocla. websterite	Plagiocla. websterite	Olivine websterite
Zone	Ultramafic	Ultramafic	Ultramafic	Ultramafic	Ultramafic	Ultramafic	Ultramafic	Ultramafic
Subzone	D	E	E	E	E	E	E	F
Strat. ht (m)	74	78	80	83	85	88	97	105
Drill hole	84RHPD208	84RHPD208	84RHPD208	84RHPD208	84RHPD208	86RHPD249	86RHPD249	86RHPD249
Depth (m)	178.8	175.3	172.0	169.2	167.9	300.0	290.0	280.0
SiO2	44.95	45.80	47.21	49.31	49.80	48.82	50.42	46.86
TiO2	.34	.49	.46	.52	.43	.56	.52	.42
Al2O3	3.98	5.38	4.55	3.57	3.32	6.09	5.41	4.58
Fe2O3	4.32	2.04	2.14	1.39	1.70	2.68	1.70	3.52
FeO	9.77	10.04	8.84	8.28	8.05	10.03	9.25	8.91
MnO	.20	.27	.23	.24	.24	.20	.19	.20
MgO	21.59	17.84	17.21	17.18	17.27	12.89	14.73	20.71
CaO	6.13	11.30	13.71	15.00	14.44	11.36	12.40	8.20
Na2O	.32	.39	.50	.46	.41	1.56	1.19	.85
K2O	.17	.02	.02	.01	.01	.14	.18	.35
P2O5	.01	.03	.03	.04	.03	.04	.04	.03
LOI	6.17	4.61	4.16	3.63	3.60	2.78	3.30	4.35
Rest	1.47	1.80	.78	.30	.70	2.50	.57	.67
Total	99.42	100.01	99.84	99.93	100.00	99.65	99.90	99.65
O=F,S,Cl	.41	.33	.12	.01	.11	.71	.10	.12
Total	99.01	99.68	99.71	99.92	99.89	98.94	99.81	99.53
Trace elements in parts per million								
Ba	19	<4	7	<4	<4	122	110	133
Rb	11	2	1	<1	<1	3	6	13
Sr	20	19	24	22	22	93	69	107
Pb	3	8	24	2	2	4	3	3
Th	2	3	<1	4	2	2	3	<1
Zr	31	46	43	55	46	62	50	43
Nb	<1	2	3	3	3	3	2	2
Y	8	10	12	12	12	14	13	8
La	7	11	9	10	7	12	12	12
Ce	11	18	14	20	16	20	22	13
Nd	2	11	9	7	9	6	11	8
Sc	21	32	39	40	41	31	35	24
V	105	158	175	182	172	160	166	117
Cr	726	825	819	1054	754	610	713	732
Co	140	150	96	61	71	113	87	108
Ni	1945	2917	1277	424	891	2704	880	1532
Cu	1878	4597	1469	59	1536	4323	604	393
Zn	116	113	100	65	69	99	84	93
Ga	4	7	6	5	4	8	8	5
As	<.5	2.0	2.0	.5	1.0	2.0	<.5	.5
S	8124	6476	2311	115	2141	14279	1885	2290
Cs	<3	<3	<3	<3	<3	<3	<3	<3
Trace elements in parts per billion								
Pt	48.70	-	-	-	41.40	-	20.25	-
Pd	156	-	-	-	106	-	40.60	-
Ir	1.38	-	-	-	.98	-	1.51	-
Ru	1.88	-	-	-	1.94	-	1.81	-
Au	11.79	-	-	-	8.38	-	3.78	-
mg	73.8	72.8	74.0	76.3	76.3	64.9	70.9	75.3

Sample no.	88770089	88770090	88770091	88770092	88770093	88770094	88770095	88770096
Intrusion	Radio Hill Complex	Radio Hill Complex	Radio Hill Complex	Radio Hill Complex	Radio Hill Complex	Radio Hill Complex	Radio Hill Complex	Radio Hill Complex
Locality	Sample traverse	Sample traverse	Sample traverse	Sample traverse	Sample traverse	Sample traverse	Sample traverse	Sample traverse
Lithology	Plagiocla. olivine websterite	Lherzolite	Plagiocla. olivine websterite	Plagiocla. olivine websterite	Lherzolite	Lherzolite	Lherzolite	Olivine websterite
Zone	Ultramafic	Ultramafic	Ultramafic	Ultramafic	Ultramafic	Ultramafic	Ultramafic	Ultramafic
Subzone	F	F	F	F	F	F	F	F
Strat. ht (m)	115	124	132	140	160	175	195	205
Drill hole	86RHPD249	86RHPD249	86RHPD249	86RHPD249	86RHPD249	86RHPD249	86RHPD249	86RHPD249
Depth (m)	270.0	260.0	250.0	240.0	220.0	200.0	180.0	170.0
SiO2	43.88	45.71	46.71	44.24	41.99	40.80	43.29	41.45
TiO2	.33	.36	.37	.32	.28	.23	.25	.20
Al2O3	3.65	3.73	3.70	3.23	2.76	2.66	2.29	1.99
Fe2O3	5.57	4.17	3.72	4.48	5.02	5.54	5.06	8.03
FeO	8.22	8.38	8.13	8.41	9.04	9.47	8.54	6.97
MnO	.21	.21	.19	.20	.22	.22	.21	.22
MgO	25.12	22.90	21.78	24.75	27.11	29.05	25.63	27.21
CaO	6.05	8.00	9.19	6.87	4.85	3.69	6.69	5.44
Na2O	.61	.94	.68	.51	.35	.28	.37	.27
K2O	.27	.26	.30	.21	.14	.16	.10	.09
P2O5	.02	.02	.02	.02	.01	.01	.01	.01
LOI	5.39	5.03	4.31	6.17	7.90	7.72	6.82	7.65
Rest	.56	.53	.70	.53	.59	.49	.55	.52
Total	99.88	100.24	99.80	99.94	100.26	100.32	99.81	100.05
O=F,S,Cl	.06	.05	.10	.05	.07	.05	.06	.05
Total	99.82	100.19	99.71	99.89	100.19	100.27	99.76	100.01
Trace elements in parts per million								
Ba	132	264	129	99	70	86	61	48
Rb	7	8	10	7	7	5	5	5
Sr	103	138	99	67	50	65	40	35
Pb	<1	3	3	3	5	2	<1	3
Th	2	2	<1	2	2	<1	<1	<1
Zr	34	36	39	32	26	25	22	20
Nb	2	<1	<1	<1	<1	<1	<1	<1
Y	7	8	9	6	5	5	5	4
La	8	8	11	8	8	5	3	5
Ce	9	15	14	9	7	10	<5	<5
Nd	3	7	7	5	3	2	<2	<2
Sc	17	23	25	19	14	11	20	15
V	90	106	116	89	71	62	89	80
Cr	535	589	996	711	466	261	665	500
Co	130	117	110	116	138	146	129	134
Ni	1960	1666	1716	1802	2167	2134	1890	2079
Cu	256	228	479	221	362	218	321	299
Zn	96	91	85	90	95	103	90	95
Ga	5	6	5	5	4	2	3	1
As	1.0	.5	.5	.5	1.0	<.5	1.5	.5
S	1116	1002	1905	995	1366	840	1136	882
Cs	<3	<3	<3	3	<3	<3	<3	<3
Trace elements in parts per billion								
Pt	-	-	25.09	-	-	-	17.25	-
Pd	-	-	62.4	-	-	-	47.80	-
Ir	-	-	.83	-	-	-	1.78	-
Ru	-	-	2.31	-	-	-	3.96	-
Au	-	-	5.53	-	-	-	2.70	-
mg	77.2	77.1	77.2	78.0	78.	78.2	77.7	77.4

Sample no.	88770097	88770098	88770099	88770100	88770101	88770102	88770103	88770104
Intrusion	Radio Hill Complex	Radio Hill Complex	Radio Hill Complex	Radio Hill Complex	Radio Hill Complex	Radio Hill Complex	Radio Hill Complex	Radio Hill Complex
Locality	Sample traverse	Sample traverse	Sample traverse	Sample traverse	Sample traverse	Sample traverse	Sample traverse	Sample traverse
Lithology	Websterite	Websterite	Plagiocla. websterite	Plagiocla. websterite	Websterite	Websterite	Clinopyro.	Clinopyro.
Zone	Ultramafic	Ultramafic	Ultramafic	Ultramafic	Ultramafic	Ultramafic	Ultramafic	Ultramafic
Subzone	G	G	G	G	G	G	G	G
Strat. ht (m)	212	230	250	265	280	300	318	325
Drill hole	86RHPD249	86RHPD249	86RHPD249	86RHPD249	86RHPD249	86RHPD249	86RHPD249	86RHPD249
Depth (m)	160.0	140.0	120.0	100.0	80.0	60.0	40.0	20.0
SiO2	49.80	51.87	52.18	51.82	51.68	51.78	50.57	49.96
TiO2	.36	.33	.44	.41	.42	.43	.46	.47
Al2O3	3.38	2.78	3.63	3.00	3.12	3.01	3.62	3.60
Fe2O3	1.61	1.44	1.30	1.56	1.55	1.98	1.95	2.48
FeO	8.14	7.56	8.12	8.12	8.51	8.42	9.39	9.37
MnO	.20	.19	.20	.20	.20	.23	.22	.22
MgO	17.20	16.00	14.67	15.15	14.84	13.88	13.90	14.15
CaO	14.61	15.74	15.51	16.28	15.89	16.69	15.49	15.11
Na2O	.50	.65	.90	.73	.71	.50	.65	.64
K2O	.02	.09	.09	.09	.16	.03	.17	.21
P2O5	.02	.01	.02	.01	.01	.01	.01	.02
LOI	3.72	2.47	2.66	2.37	2.55	2.80	3.05	3.30
Rest	.40	.84	.32	.33	.28	.28	.25	.26
Total	99.96	99.97	100.04	100.07	99.92	100.04	99.73	99.79
O=F,S,Cl	.02	.13	.02	.02	.01	.01	.01	.01
Total	99.94	99.84	100.02	100.05	99.90	100.02	99.72	99.78
Trace elements in parts per million								
Ba	6	19	46	28	36	98	70	44
Rb	1	6	3	7	10	2	11	14
Sr	43	49	64	47	48	51	51	43
Pb	<1	6	3	2	<1	<1	2	<1
Th	2	<1	2	<1	<1	2	2	2
Zr	31	26	35	32	27	31	33	33
Nb	<1	<1	<1	<1	<1	<1	<1	2
Y	10	9	12	12	12	12	12	14
La	6	7	7	9	6	11	9	8
Ce	13	13	16	12	6	17	11	16
Nd	6	5	9	5	6	10	6	8
Sc	40	50	51	58	57	58	54	55
V	201	231	263	311	328	332	335	337
Cr	1090	1096	749	541	491	443	362	367
Co	78	77	75	76	84	79	81	83
Ni	805	1209	490	554	500	449	434	469
Cu	200	1454	107	250	97	111	68	67
Zn	69	64	67	67	68	69	77	81
Ga	5	5	5	5	4	4	5	5
As	.5	.5	<.5	.5	1.0	.5	<.5	1.0
S	421	2571	381	483	229	251	161	246
Cs	<3	<3	<3	<3	<3	<3	<3	6
Trace elements in parts per billion								
Pt	-	42.30	-	14.60	-	-	-	-
Pd	-	155	-	57.4	-	-	-	-
Ir	-	.48	-	1.35	-	-	-	-
Ru	-	.66	-	1.19	-	-	-	-
Au	-	8.56	-	1.93	-	-	-	-
mg	76.2	76.3	73.8	73.9	72.8	70.8	69.0	68.5

Sample no.	88770105	88770106	88770107	88770108	88770109	88770110	88770111	88770112
Intrusion	Radio Hill Complex	Radio Hill Complex	Radio Hill Complex	Radio Hill Complex	Radio Hill Complex	Radio Hill Complex	Radio Hill Complex	Radio Hill Complex
Locality	Sample traverse	Sample traverse	Sample traverse	Sample traverse	Sample traverse	Sample traverse	Sample traverse	Sample traverse
Lithology	?Microgab.	?Microgab.	Gabbro	Gabbro	Gabbro	Gabbro	Gabbro	Gabbronor.
Zone	Gabbroic	Gabbroic	Gabbroic	Gabbroic	Gabbroic	Gabbroic	Gabbroic	Gabbroic
Subzone	A	A	A	A	A	A	A	A
Strat. ht (m)	350	370	388	405	420	440	460	478
Drill hole	87RHPD262	87RHPD262	87RHPD262	87RHPD262	87RHPD262	87RHPD262	87RHPD262	87RHPD262
Depth (m)	340.0	320.0	300.0	280.0	260.0	240.0	220.0	200.0
SiO2	48.06	47.25	51.78	51.77	51.86	51.53	51.16	50.82
TiO2	.93	1.06	.67	.65	.62	.63	.58	.56
Al2O3	16.39	15.76	7.97	7.10	6.00	5.44	5.23	5.15
Fe2O3	2.40	2.13	1.54	1.71	1.47	1.61	1.86	1.63
FeO	10.05	11.06	9.80	9.60	9.95	9.74	9.42	9.94
MnO	.24	.22	.19	.20	.21	.22	.21	.21
MgO	7.47	7.20	10.29	10.89	11.82	11.72	12.03	12.57
CaO	8.43	7.80	11.72	12.56	13.52	14.12	14.33	13.73
Na2O	1.87	2.71	2.13	1.81	1.54	1.54	1.49	1.26
K2O	.38	.37	.46	.49	.44	.24	.15	.32
P2O5	.13	.10	.05	.05	.04	.04	.03	.03
LOI	3.65	4.01	3.05	2.85	2.24	2.67	3.23	3.58
Rest	.17	2.25	.38	.35	.31	.25	.25	.29
Total	100.17	101.92	100.03	100.03	100.02	99.75	99.97	100.09
O=F,S,Cl	.01	1.04	.05	.04	.03	.01	.01	.03
Total	100.16	100.88	99.98	99.99	99.99	99.74	99.95	100.06
Trace elements in parts per million								
Ba	78	67	290	255	218	151	96	146
Rb	12	9	11	13	13	7	5	11
Sr	156	235	223	186	157	117	95	117
Pb	<1	<1	4	4	4	5	3	3
Th	<1	<1	4	2	3	2	<1	2
Zr	54	26	70	68	59	56	52	48
Nb	3	2	4	3	3	4	3	3
Y	17	11	16	15	15	15	15	14
La	8	<2	14	14	11	10	7	12
Ce	7	<5	23	30	20	22	20	21
Nd	7	2	13	11	6	10	3	9
Sc	58	61	37	41	46	45	49	50
V	282	377	225	247	274	285	302	297
Cr	80	23	293	289	348	293	320	323
Co	63	63	78	83	79	81	81	88
Ni	80	63	391	382	375	350	374	412
Cu	38	152	332	308	137	105	90	87
Zn	105	99	98	94	90	89	84	87
Ga	14	17	10	10	9	8	8	8
As	<.5	2.0	1.0	1.0	<.5	<.5	.5	.5
S	196	20757	965	800	522	223	213	489
Cs	<3	<3	<3	<3	<3	<3	<3	3
Trace elements in parts per billion								
Pt	-	-	18.89	-	-	5.49	-	-
Pd	-	-	66.9	-	-	8.82	-	-
Ir	-	-	.07	-	-	.31	-	-
Ru	-	-	.46	-	-	.55	-	-
Au	-	-	2.52	-	-	.60	-	-
mg	52.2	49.7	62.1	63.5	65.1	65.1	65.9	66.3

Sample no.	88770113	88770114	88770115	88770116	88770117	88770118	88770119	88770120
Intrusion	Radio Hill Complex	Radio Hill Complex	Radio Hill Complex	Radio Hill Complex	Radio Hill Complex	Radio Hill Complex	Radio Hill Complex	Radio Hill Complex
Locality	Sample traverse	Sample traverse	Sample traverse	Sample traverse	Sample traverse	Sample traverse	Sample traverse	Sample traverse
Lithology	Olivine gabbronor.	Gabbronor.	Olivine gabbronor.	Olivine gabbronor.	Olivine gabbronor.	Plagiocla. websterite	Olivine gabbronor.	Gabbronor.
Zone	Gabbroic	Gabbroic	Gabbroic	Gabbroic	Gabbroic	Gabbroic	Gabbroic	Gabbroic
Subzone	A	A	A	A	A	A	A	A
Strat. ht (m)	495	512	530	548	565	582	600	618
Drill hole	87RHPD262	87RHPD262	87RHPD262	87RHPD262	87RHPD262	87RHPD262	87RHPD262	87RHPD262
Depth (m)	180.0	160.0	140.0	120.0	100.0	80.0	60.0	40.0
SiO2	51.20	50.91	51.31	51.30	51.25	50.39	50.81	50.18
TiO2	.54	.52	.53	.52	.53	.50	.50	.45
Al2O3	4.89	4.66	4.62	4.55	4.55	4.22	4.64	6.18
Fe2O3	1.45	1.53	1.68	1.56	1.50	1.96	1.51	1.75
FeO	10.12	10.13	10.42	10.42	10.53	9.83	10.46	9.90
MnO	.21	.22	.22	.22	.22	.23	.22	.21
MgO	12.98	13.16	13.57	13.59	13.65	13.52	13.44	12.76
CaO	13.90	14.05	13.83	13.96	13.99	14.55	13.82	13.24
Na2O	1.28	1.16	1.20	1.22	1.22	1.09	1.15	1.43
K2O	.36	.29	.40	.39	.37	.21	.35	.24
P2O5	.03	.03	.03	.02	.03	.02	.02	.02
LOI	2.79	3.01	1.70	1.64	1.90	3.07	2.68	3.28
Rest	.29	.27	.30	.29	.29	.24	.31	.23
Total	100.04	99.94	99.81	99.68	100.03	99.83	99.91	99.87
O=F,S,Cl	.03	.02	.03	.02	.02	.01	.03	.01
Total	100.02	99.92	99.79	99.66	100.01	99.83	99.88	99.86
Trace elements in parts per million								
Ba	166	131	179	181	178	75	158	129
Rb	14	12	12	11	11	9	11	7
Sr	129	107	137	148	145	94	137	142
Pb	2	2	2	3	3	4	3	3
Th	<1	2	2	2	2	2	2	2
Zr	45	44	44	43	42	41	42	36
Nb	3	2	2	<1	2	<1	2	2
Y	13	14	15	14	14	14	14	11
La	9	9	8	5	3	10	7	8
Ce	21	21	18	20	16	20	13	13
Nd	9	10	6	11	9	11	12	9
Sc	47	48	50	51	49	49	51	43
V	299	294	299	303	299	297	303	270
Cr	321	322	336	331	323	323	320	231
Co	86	86	96	104	98	94	110	91
Ni	442	447	470	460	463	449	461	402
Cu	82	76	77	74	75	66	78	65
Zn	86	86	89	87	86	85	89	84
Ga	7	8	7	6	7	6	8	7
As	1.0	<.5	.5	<.5	.5	.5	1.0	.5
S	496	321	496	351	386	151	555	129
Cs	<3	<3	<3	<3	<3	<3	<3	<3
Trace elements in parts per billion								
Pt	-	-	-	6.96	-	-	-	-
Pd	-	-	-	13.25	-	-	-	-
Ir	-	-	-	.21	-	-	-	-
Ru	-	-	-	.58	-	-	-	-
Au	-	-	-	.74	-	-	-	-
mg	67.0	67.1	67.0	67.2	67.2	67.5	67.0	66.5

Sample no.	88770121	88770122	88770123	88770124	88770125	88770126	88770127	88770128
Intrusion	Radio Hill Complex	Radio Hill Complex	Radio Hill Complex	Radio Hill Complex	Radio Hill Complex	Radio Hill Complex	Radio Hill Complex	Radio Hill Complex
Locality	Sample traverse	Sample traverse	Sample traverse	Sample traverse	Sample traverse	Sample traverse	Sample traverse	Sample traverse
Lithology	Gabbronor.	Olivine gabbronor.	Olivine gabbronor.	Olivine gabbronor.	Olivine gabbronor.	Olivine gabbro	Olivine gabbronor.	Quartz gabbro
Zone	Gabbroic	Gabbroic	Gabbroic	Gabbroic	Gabbroic	Gabbroic	Gabbroic	Gabbroic
Subzone	A	A	A	A	A	A	A	B
Strat. ht (m)	636	640	664	695	710	735	765	775
Drill hole	87RHPD262							
Depth (m)	20.0							
SiO2	50.67	51.28	50.85	50.75	50.80	50.64	51.55	53.07
TiO2	.46	.43	.45	.46	.47	.50	.55	.50
Al2O3	6.64	7.66	7.63	6.82	6.58	6.35	5.64	16.28
Fe2O3	1.88	1.76	1.90	2.08	2.00	2.24	1.63	1.22
FeO	9.37	9.53	10.13	10.73	11.06	11.35	11.35	6.82
MnO	.20	.20	.22	.23	.23	.23	.24	.12
MgO	12.22	11.99	11.83	12.27	12.20	12.23	12.03	5.19
CaO	13.32	12.91	12.59	12.67	12.62	12.51	13.35	9.29
Na2O	1.55	1.69	1.76	1.56	1.50	1.54	1.48	4.09
K2O	.29	.41	.37	.33	.37	.37	.37	.90
P2O5	.02	.02	.02	.02	.02	.02	.02	.04
LOI	3.09	1.76	1.77	1.67	1.83	1.55	1.28	1.99
Rest	.23	.27	.24	.26	.27	.28	.34	.33
Total	99.94	99.91	99.76	99.85	99.95	99.81	99.83	99.84
O=F,S,Cl	.01	.01	.01	.02	.02	.02	.04	.05
Total	99.94	99.89	99.75	99.83	99.93	99.79	99.80	99.79
Trace elements in parts per million								
Ba	171	178	159	142	157	157	187	336
Rb	8	10	8	8	10	9	9	15
Sr	189	455	247	255	281	225	175	607
Pb	<1	<1	3	2	2	3	2	4
Th	2	2	<1	<1	<1	2	<1	3
Zr	36	33	34	34	37	39	41	53
Nb	<1	<1	<1	2	<1	<1	<1	3
Y	12	12	11	12	13	13	15	10
La	7	7	7	4	5	9	10	11
Ce	15	13	9	14	11	14	14	27
Nd	5	6	7	6	9	3	8	10
Sc	45	43	43	44	43	46	47	20
V	275	259	266	272	275	291	286	117
Cr	212	195	174	179	179	174	233	52
Co	92	91	96	90	90	95	88	64
Ni	404	380	386	394	385	387	403	186
Cu	58	59	61	139	164	195	395	253
Zn	80	80	84	89	95	99	98	68
Ga	8	9	10	8	8	8	8	16
As	2.0	.5	<.5	1.0	.5	.5	.5	.5
S	118	222	211	325	361	375	694	949
Cs	<3	<3	<3	<3	<3	<3	<3	<3
Trace elements in parts per billion								
Pt	-	30.50	-	17.70	-	25.20	18.20	15.19
Pd	-	79.9	-	33.5	-	35.2	29.00	4.63
Ir	-	.83	-	.07	-	.15	.08	.31
Ru	-	.89	-	-	-	-	-	.33
Au	-	.81	-	5.17	-	6.29	6.67	4.94
mg	66.3	65.8	64.0	63.4	62.8	62.0	62.6	53.9

Sample no.	88770129	88770130	88770131	88770132	88770133	88770134	88770135	88770136	88770137
Intrusion	Radio Hill Complex	Radio Hill Complex	Radio Hill Complex	Radio Hill Complex	Radio Hill Complex	Radio Hill Complex	Radio Hill Complex	Radio Hill Complex	Radio Hill Complex
Locality	Sample traverse	Sample traverse	Sample traverse	Sample traverse	Sample traverse	Sample traverse	Sample traverse	Off sample traverse	Off sample traverse
Lithology	Quartz gabbro	Quartz gabbro	Gabbronor.	Quartz gabbro	Quartz gabbro	Quartz gabbro	Quartz gabbro	Massive cpy - po - pent	Gabbro chill
Zone	Gabbroic	Gabbroic	Gabbroic	Gabbroic	Gabbroic	Gabbroic	Gabbroic	Ultramafic	Ultramafic
Subzone	B	B	B	B	B	B	B	A	A
Strat. ht (m)	790	820	835	860	890	920	~1200	5	5
Drill hole							86RHPD252	85RHPD233	85RHPD234
Depth (m)							200.0	85.3	92-99
SiO2	54.14	54.25	53.98	54.14	54.48	53.76	50.42	-	50.76
TiO2	.57	.57	.56	.58	.64	.67	1.87	-	.75
Al2O3	15.68	15.68	14.94	14.70	14.98	16.05	13.42	-	8.80
Fe2O3	1.26	1.42	1.48	1.53	1.31	1.95	4.43	-	2.57
FeO	7.20	7.08	7.70	8.05	7.95	7.11	11.05	-	9.73
MnO	.15	.15	.17	.17	.17	.15	.19	-	.20
MgO	5.60	5.38	5.77	5.64	5.23	4.65	3.95	-	8.71
CaO	8.34	8.24	8.69	8.25	8.26	8.04	7.27	-	11.25
Na2O	4.00	4.05	3.74	3.85	4.10	3.83	3.80	-	2.35
K2O	.92	.92	.74	.87	.96	.93	.92	-	.44
P2O5	.04	.04	.05	.05	.06	.06	.07	-	.06
LOI	1.82	1.93	1.80	1.71	1.83	2.35	2.15	-	2.07
Rest	.26	.27	.27	.29	.27	.31	.37	-	2.34
Total	99.98	99.98	99.89	99.83	100.24	99.86	99.91	-	100.03
O=F,S,Cl	.02	.02	.03	.03	.02	.03	.06	-	.55
Total	99.96	99.96	99.87	99.80	100.21	99.83	99.85	-	99.47
	Trace elements in parts per million								
Ba	354	340	325	349	364	467	433	-	253
Rb	19	22	17	21	23	22	24	-	11
Sr	632	636	544	570	586	589	422	-	151
Pb	5	5	4	5	6	5	8	-	119
Th	4	4	3	3	3	4	4	-	3
Zr	59	63	58	65	70	79	80	-	78
Nb	3	3	4	4	4	4	5	-	4
Y	11	13	11	11	14	14	16	-	17
La	11	15	11	12	15	15	14	-	16
Ce	24	27	24	28	34	29	36	-	34
Nd	11	9	11	11	16	15	16	-	20
Sc	21	19	21	23	22	19	23	-	32
V	119	122	138	141	137	121	284	-	200
Cr	17	12	13	10	7	8	14	21	193
Co	62	63	62	69	61	71	78	837	95
Ni	128	119	124	123	96	116	26	27810	1835
Cu	237	267	312	301	255	312	380	143800	6539
Zn	76	77	78	84	82	76	120	796	118
Ga	16	17	16	16	17	18	19	-	12
As	.5	<.5	<.5	<.5	<.5	1.5	.5	-	4.0
S	349	453	511	636	408	667	1167	-	11040
Cs	<3	<3	<3	<3	<3	<3	<3	-	<3
	Trace elements in parts per billion								
Pt	-	-	4.46	-	-	2.57	-	1127	453
Pd	-	-	4.42	-	-	2.21	-	3334	1299
Ir	-	-	.01	-	-	<.01	-	4.67	1.10
Ru	-	-	.09	-	-	.15	-	259	9.00
Au	-	-	1.72	-	-	1.61	-	39.04	174
mg	54.5	53.4	53.2	51.6	50.5	48.3	31.9	-	56.3

Sample number	86330119	88330179	88330180	88330181	88330182	87330140	87330139	87330141
Intrusion	Andover Complex	Andover Complex	Andover Complex	Andover Complex	Andover Complex	Andover Complex	Andover Complex	Andover Complex
Traverse	1a	1a	1a	1a	1a	1a	1a	1a
Lithology	Norite	Peridotite	Peridotite	Peridotite	Peridotite	Peridotite	Clino-pyroxenite	Gabbro
Zone	Ultramafic	Ultramafic	Ultramafic	Ultramafic	Ultramafic	Ultramafic	Ultramafic	Ultramafic
Subzone	Base	A	A	A	A	A	A	A
Strat. ht (km)	0.01	0.02	0.05	0.07	0.08	0.1	0.11	0.14
SiO2	50.41	37.38	36.82	37.44	36.22	36.37	54.24	48.55
TiO2	.36	.13	.11	.13	.13	.09	.25	.23
Al2O3	13.16	1.11	1.56	2.36	1.26	1.26	1.65	16.00
Fe2O3	1.42	13.43	13.74	9.06	13.46	14.85	2.10	1.23
FeO	7.87	1.81	1.72	1.95	4.08	1.79	7.71	5.18
MnO	.19	.18	.19	.19	.16	.20	.25	.14
MgO	12.24	33.93	33.79	35.22	33.14	33.31	20.36	10.37
CaO	12.29	.11	.03	.35	.10	.06	10.12	12.63
Na2O	1.18	.05	.02	.03	.01	.11	.37	1.67
K2O	.03	-	-	-	-	<.01	.01	.29
P2O5	<.01	.01	.01	.01	-	.01	.02	.02
LOI	.98	11.21	11.15	12.06	10.96	11.02	3.18	3.89
Rest	.37	.95	1.04	1.29	.90	.98	.53	.34
Total	100.50	100.30	100.18	100.09	100.42	100.05	100.79	100.54
O=F,S,Cl	.09	.02	.00	.01	.02	.01	.00	.01
Total	100.41	100.29	100.17	100.07	100.40	100.04	100.78	100.53
	Trace elements in parts per million							
Ba	30	44	12	36	19	13	22	389
Li	11	2	2	4	1	2	7	320
Rb	8	1	1	1	1	1	<1	130
Sr	207	11	3	14	15	1	7	334
Pb	1	<2	<2	<2	3	3	2	-
Th	<1	<2	<2	<2	<2	1	<1	1
U	<0.5	<0.5	1	<0.5	<0.5	0.5	0.5	0.5
Zr	11	4	2	2	7	<2	2	7
Nb	<2	<2	<2	<2	<2	<1	<1	<1
Y	8	1	1	2	2	2	4	8
La	3	<2	<2	2	<2	<3	<3	<3
Ce	7	<5	5	<5	<5	<3	3	<3
Nd	3	<2	3	<2	<2	<3	<3	<3
Sc	46	6	8	5	5	10	43	41
V	182	57	60	65	29	62	164	135
Cr	361	4137	4763	5243	3925	4358	2166	446
Ni	294	2223	2400	3579	2037	2292	827	184
Cu	82	16	13	6	8	<1	366	192
Zn	69	107	96	112	59	109	87	46
Ga	13	6	2	5	3	2	4	12
As	1	1.5	1.5	2	1	2.5	2	1
S	1800	310	40	280	490	200	50	200
mg	73.7	83.6	83.4	87.9	81.1	82.1	81.6	77.5

Sample number	87330142	87330143	87330144	87330145	87330137	87330138	87330135	87330134
Intrusion	Andover Complex	Andover Complex	Andover Complex	Andover Complex	Andover Complex	Andover Complex	Andover Complex	Andover Complex
Traverse	1a	1a	1a	1a	1a	1a	1a	1a
Lithology	Gabbro	Peridotite	Peridotite	Peridotite	Peridotite	Peridotite	Peridotite	Peridotite
Zone	Ultramafic	Ultramafic	Ultramafic	Ultramafic	Ultramafic	Ultramafic	Ultramafic	Ultramafic
Subzone	A	B	B	B	B	B	B	B
Strat. ht (km)	0.16	0.18	0.19	0.20	0.20	0.23	0.28	315
SiO2	48.67	37.95	37.11	36.30	36.13	36.23	36.60	37.20
TiO2	.21	.21	.13	.11	.09	.11	.16	.08
Al2O3	16.22	1.45	2.18	2.00	3.05	2.16	1.87	3.89
Fe2O3	.85	13.89	12.64	11.62	10.99	11.70	10.94	9.41
FeO	4.55	2.54	2.44	1.97	2.30	1.40	1.07	2.42
MnO	.13	.21	.18	.15	.15	.15	.02	.19
MgO	9.63	31.32	33.27	34.84	33.91	34.97	35.22	32.04
CaO	14.64	1.53	.06	.03	.18	.09	.04	2.71
Na2O	1.77	.14	.11	.11	.09	.11	.09	.13
K2O	.27	.01	<.01	<.01	<.01	<.01	<.01	<.01
P2O5	.02	.01	<.01	<.01	<.01	<.01	.01	<.01
LOI	3.03	10.63	11.38	12.26	11.85	12.22	12.36	11.33
Rest	.32	.69	.69	.75	.80	.86	.98	.95
Total	100.31	100.58	100.19	100.14	99.54	100.00	99.36	100.35
O=F,S,Cl	.01	.01	.01	.00	.00	.00	.01	.01
Total	100.30	100.57	100.18	100.14	99.54	100.00	99.35	100.33
	Trace elements in parts per million							
Ba	96	18	3	10	13	8	11	38
Li	223	4	2	5	3	6	2	19
Rb	79	2	2	<1	3	<1	3	1
Sr	395	7	<1	1	2	3	4	5
Pb	2	2	1	1	<1	1	1	1
Th	<1	<1	<1	<1	<1	1	<1	<1
U	<0.5	<0.5	<0.5	<0.5	<0.5	<0.5	<0.5	<0.5
Zr	6	4	3	3	6	4	7	3
Nb	<1	1	<1	<1	1	1	<1	<1
Y	6	3	2	2	2	1	2	1
La	<3	<3	<3	<3	<3	<3	<3	<3
Ce	<3	3	<3	<3	3	4	4	<3
Nd	<3	<3	<3	<3	<3	3	3	<3
Sc	47	16	9	9	7	9	9	11
V	193	90	62	52	39	54	56	45
Cr	650	3048	3234	3295	3278	4212	4718	4557
Ni	209	1391	1293	1707	2300	1737	1899	1733
Cu	114	15	67	201	<1	10	3	3
Zn	41	102	67	65	49	60	75	85
Ga	13	3	3	3	3	3	4	5
As	0.5	1.5	2	0.5	1.5	0.5	1	0.5
S	200	300	200	60	100	<100	200	300
mg	79.1	81.3	83.4	85.4	85.3	86.0	87.1	86.0

Sample number	87330133	87330146	88330175	87330147	87330148	87330149	86330053	86330049
Intrusion	Andover Complex	Andover Complex	Andover Complex	Andover Complex	Andover Complex	Andover Complex	Andover Complex	Andover Complex
Traverse	1a	1a	off trav.	1a	1a	1a	off trav.	off trav.
Lithology	Peridotite	Peridotite	Anorth. gabbro	Peridotite	Peridotite	Peridotite	Lherzolite	Ortho-pyroxenite
Zone	Ultramafic	Ultramafic	Ultramafic	Ultramafic	Ultramafic	Ultramafic	Ultramafic	Ultramafic
Subzone	B	B	B	C	C	C	C	C
Strat. ht (km)	0.36	0.37	0.39	0.42	0.46	0.51	0.53	0.54
SiO2	36.10	37.34	47.21	35.72	36.31	37.09	40.07	51.59
TiO2	.11	.15	.22	.08	.10	.10	.09	.15
Al2O3	1.18	1.06	18.33	2.62	1.85	.77	2.98	1.15
Fe2O3	13.79	13.90	1.52	13.53	12.22	14.64	9.48	2.62
FeO	.69	1.55	5.27	.69	1.22	2.41	3.83	6.71
MnO	.12	.23	.11	.16	.20	.21	.21	.20
MgO	34.56	33.84	8.53	33.35	34.40	33.33	30.51	27.90
CaO	.03	.09	12.18	.20	.04	.02	2.48	1.79
Na2O	.12	.10	1.86	.12	.14	.11	.15	.08
K2O	<.01	<.01	.04	<.01	<.01	<.01	<.01	.01
P2O5	.01	<.01	-	.01	.01	<.01	<.01	<.01
LOI	12.26	11.10	4.66	12.52	12.34	10.88	9.46	7.33
Rest	.88	.76	.24	.96	.83	.72	.62	.48
Total	99.85	100.12	100.17	99.96	99.66	100.28	99.88	100.01
O=F,S,Cl	.00	.01	.01	.00	.01	.00	.00	.00
Total	99.84	100.11	100.16	99.95	99.65	100.27	99.87	100.01
Trace elements in parts per million								
Ba	8	76	94	12	20	11	38	14
Li	1	3	-	16	2	2	7	4
Rb	3	1	1	1	<1	1	1	<1
Sr	2	10	374	1	4	<1	27	3
Pb	2	2	3	2	2	2	3	1
Th	<1	<1	<2	<1	1	<1	1	<1
U	<0.5	<0.5	1	<0.5	<0.5	0.5	<0.5	<0.5
Zr	6	2	4	<2	2	<2	2	3
Nb	1	1	<2	<1	1	<1	<2	<2
Y	2	<1	4	1	1	<1	1	2
La	<3	<3	2	<3	<3	<3	<3	<3
Ce	<3	<3	<5	<3	<3	<3	<3	<3
Nd	<3	<3	2	<3	<3	<3	<3	<3
Sc	6	6	35	9	8	4	11	18
V	46	61	124	69	52	42	47	59
Cr	3605	3863	625	4097	3186	3611	2520	2304
Ni	2530	1049	180	2288	2373	1236	1434	558
Cu	<1	27	70	252	96	16	204	401
Zn	57	124	54	77	99	105	82	76
Ga	2	3	15	3	2	2	3	3
As	<0.5	1	<0.5	0.5	1.5	2.5	<0.5	0.5
S	100	200	220	50	200	50	100	<100
mg	84.6	83.4	72.9	84.4	85.5	81.7	83.8	86.5

Sample number	88330213	88330211	88330173	87330150	87330151	86330042	86330044	86330043
Intrusion	Andover Complex	Andover Complex	Andover Complex	Andover Complex	Andover Complex	Andover Complex	Andover Complex	Andover Complex
Traverse	off trav.	off trav.	off trav.	1a	1a	1a	1a	1a
Lithology	Clino-pyroxenite	Websterite	Anorth. gabbro	Peridotite	Peridotite	Peridotite	Peridotite	Ortho-pyroxenite
Zone	Ultramafic	Ultramafic	Ultramafic	Ultramafic	Ultramafic	Ultramafic	Ultramafic	Ultramafic
Subzone	C	C	C	D	D	D	D	D
Strat. ht (km)	0.56	0.57	0.60	0.61	0.62	0.65	0.66	0.67
SiO2	51.68	48.31	48.23	38.98	36.80	38.04	37.95	53.09
TiO2	.36	.40	.20	.11	.07	.08	.07	.23
Al2O3	2.65	12.08	18.39	1.51	1.08	.89	3.66	1.72
Fe2O3	1.63	1.27	1.35	9.93	13.17	11.02	8.78	1.36
FeO	8.27	7.81	4.85	2.18	1.03	4.13	3.39	9.68
MnO	.21	.17	.12	.13	.12	.38	.18	.24
MgO	17.56	11.86	7.89	34.97	34.44	33.30	32.36	28.06
CaO	15.20	12.31	13.26	.08	.05	.02	1.93	2.27
Na2O	.45	.90	1.59	.09	.09	.06	.05	.08
K2O	.04	.74	.08	<.01	<.01	<.01	.01	.01
P2O5	.01	-	-	.03	.01	<.01	<.01	<.01
LOI	1.38	3.84	4.01	11.48	11.95	11.16	10.85	2.58
Rest	.49	.32	.19	.86	.89	.70	.66	.63
Total	99.93	100.01	100.16	100.35	99.70	99.78	99.89	99.95
O=F,S,Cl	.12	.00	.04	.01	.01	.00	.01	.05
Total	99.81	100.00	100.12	100.34	99.69	99.78	99.88	99.90
	Trace elements in parts per million							
Ba	<4	591	17	32	24	13	21	15
Li	12	72	-	1	2	<2	7	8
Rb	1	48	5	<1	1	<1	5	5
Sr	43	164	372	6	6	2	14	7
Pb	<2	7	<2	2	3	2	1	2
Th	<2	<2	<2	1	1	1	<1	<1
U	<0.5	0.5	<0.5	<0.5	<0.5	<0.5	0.5	<0.5
Zr	13	9	4	2	<2	<2	<2	3
Nb	<2	<2	<2	<1	<1	<2	<2	<2
Y	12	8	5	6	1	1	2	3
La	<2	2	<2	<3	<3	<3	4	<3
Ce	<5	<5	9	<3	<3	<3	4	<3
Nd	4	<2	3	<3	<3	<3	<3	<3
Sc	68	43	36	5	5	9	7	29
V	212	136	120	55	34	39	29	115
Cr	833	769	91	3637	3647	2903	2555	2403
Ni	223	199	85	2238	2503	1360	1842	730
Cu	211	174	44	<1	9	591	53	312
Zn	76	69	53	74	82	110	74	81
Ga	2	12	18	3	3	1	3	4
As	0.5	<0.5	<0.5	5	1	1	0.5	0.5
S	2470	60	720	200	200	<100	200	1100
mg	79.0	73.5	73.1	86.8	84.8	83.2	85.7	84.3

Sample number	86330033	86330109	86330061	86330100	86330102	86330106	86330107	88330188
Intrusion	Andover Complex	Andover Complex	Andover Complex	Andover Complex	Andover Complex	Andover Complex	Andover Complex	Andover Complex
Traverse	1a	off trav.	1b	1b	1b	1b	1b	1b
Lithology	Olivine websterite	Anortho-site	Peridotite	Peridotite	Peridotite	Peridotite	Anortho-site	Peridotite
Zone	Ultramafic	Ultramafic	Ultramafic	Ultramafic	Ultramafic	Ultramafic	Ultramafic	Ultramafic
Subzone	D	D	E	E	E	E	E	F
Strat. ht (km)	0.67	0.76	0.84	0.85	0.88	0.92	0.97	1.02
SiO2	45.65	45.29	36.61	36.99	36.52	36.33	48.21	37.27
TiO2	.17	.13	.03	.18	.12	.08	.21	.09
Al2O3	1.72	21.21	1.66	.43	2.43	.68	20.40	3.70
Fe2O3	3.01	.90	12.06	15.37	11.80	12.61	1.63	9.19
FeO	7.65	2.82	3.19	2.24	3.71	2.78	4.18	2.52
MnO	.22	.07	.22	.25	.15	.09	.11	.15
MgO	28.49	6.47	33.86	32.91	33.63	32.87	7.34	34.18
CaO	4.01	18.79	<.01	.11	.02	1.15	12.38	.29
Na2O	.07	.28	.08	.17	.10	.04	1.56	.03
K2O	<.01	.84	<.01	<.01	<.01	.01	.10	.01
P2O5	<.01	<.01	<.01	.01	.01	<.01	<.01	-
LOI	8.51	3.61	11.36	10.70	10.83	12.39	3.98	11.79
Rest	.62	.25	.55	.77	.70	.69	.28	.65
Total	100.12	100.66	99.62	100.13	100.02	99.72	100.38	99.87
O=F,S,Cl	.02	.01	.00	.02	.00	.00	.01	.01
Total	100.09	100.65	99.62	100.10	100.02	99.72	100.36	99.86
Trace elements in parts per million								
Ba	4	219	11	22	11	23	26	48
Li	11	48	2	<2	2	<2	135	4
Rb	20	73	<1	<1	<1	<1	11	1
Sr	7	441	1	6	2	16	640	16
Pb	3	1	2	2	1	2	13	<2
Th	1	<1	<1	31	1	<1	1	<2
U	<0.5	0.5	0.5	0.5	0.5	<0.5	<0.5	0.5
Zr	2	5	<2	<2	3	<2	6	2
Nb	<2	<2	<2	<2	<2	<2	<2	<2
Y	3	6	1	1	1	1	3	1
La	<3	<3	<3	<3	<3	<3	3	<2
Ce	<3	<3	<3	<3	<3	<3	3	<5
Nd	<3	<3	<3	<3	<3	<3	<3	<2
Sc	25	45	4	9	8	6	29	6
V	82	91	25	67	48	37	86	38
Cr	2743	559	2131	2993	3234	3084	392	2362
Ni	948	139	1659	1917	1609	1614	276	2038
Cu	65	76	9	14	17	18	138	7
Zn	80	20	109	107	76	72	44	67
Ga	3	14	3	3	3	1	17	4
As	<0.5	1	1	1.5	0.5	2.5	0.5	9
S	500	200	<100	500	<100	100	300	160
mg	85.2	78.8	83.4	81.1	83.1	82.9	73.1	86.9

Sample number	88330189	88330190	88330191	88330193	87330160	88330194	88330195	88330207
Intrusion	Andover Complex	Andover Complex	Andover Complex	Andover Complex	Andover Complex	Andover Complex	Andover Complex	Andover Complex
Traverse	1b	1b	1b	1b	2	1b	1b	1b
Lithology	Peridotite	Peridotite	Peridotite	Peridotite	Olivine websterite	Lherzolite	Peridotite	Peridotite
Zone	Ultramafic	Ultramafic	Ultramafic	Ultramafic	Ultramafic	Ultramafic	Ultramafic	Ultramafic
Subzone	F	F	F	F	F	F	G	G
Strat. ht (km)	1.04	1.05	1.06	1.10	1.11	1.12	1.15	1.16
SiO2	36.31	37.03	37.61	38.34	48.82	41.43	37.38	37.84
TiO2	.09	.17	.10	.10	.27	.16	.10	.09
Al2O3	2.65	2.02	.95	.80	4.04	2.55	1.18	2.19
Fe2O3	10.98	12.89	13.37	12.07	4.34	11.07	13.49	10.07
FeO	1.71	2.74	1.51	3.33	6.05	3.85	2.96	3.16
MnO	.14	.22	.12	.15	.17	.17	.19	.17
MgO	34.68	32.74	34.14	33.53	23.10	27.21	32.55	34.12
CaO	.08	.27	.08	.03	8.24	4.11	.27	.07
Na2O	.02	.03	-	.02	.43	.21	.03	.02
K2O	-	.01	.01	-	.08	.01	-	-
P2O5	-	.01	.01	-	.02	-	.02	-
LOI	12.31	11.32	11.56	11.35	4.19	8.80	11.43	11.60
Rest	.70	.62	.53	.38	.34	.43	.53	.59
Total	99.67	100.07	99.99	100.10	100.09	100.00	100.13	99.92
O=F,S,Cl	.00	.03	.01	.00	.00	.01	.05	.01
Total	99.67	100.04	99.98	100.09	100.09	99.99	100.08	99.91
	Trace elements in parts per million							
Ba	9	26	110	<4	69	11	24	13
Li	15	3	3	4	16	7	4	7
Rb	1	1	1	1	10	1	1	1
Sr	6	14	21	5	77	21	13	8
Pb	2	<2	<2	2	2	<2	<2	<2
Th	<2	<2	<2	<2	<1	<2	<2	<2
U	<0.5	0.5	0.5	1	<0.5	0.5	0.5	<0.5
Zr	3	5	5	3	8	5	4	1
Nb	<2	<2	<2	<2	<1	<2	<2	<2
Y	2	2	2	2	8	4	2	1
La	<2	<2	<2	<2	<3	2	4	<2
Ce	<5	<5	<5	<5	5	<5	<5	<5
Nd	<2	<2	<2	<2	4	<2	<2	<2
Sc	3	10	7	9	32	17	7	7
V	34	58	39	39	89	47	38	35
Cr	2680	2339	1700	1244	1170	1179	1153	2200
Ni	2161	1483	1758	1261	862	1563	1814	1712
Cu	12	10	7	15	<1	5	10	5
Zn	86	100	61	97	92	119	121	120
Ga	3	1	3	<1	6	<1	7	2
As	<0.5	1.5	3	4	1	4.5	4	1.5
S	100	530	250	90	<100	250	940	260
mg	86.2	82.7	84.1	83.2	82.9	80.5	81.8	85.4

Sample number	87330158	88330204	88330205	88330206	88330203	88330200	87330156	88330202
Intrusion	Andover Complex	Andover Complex	Andover Complex	Andover Complex	Andover Complex	Andover Complex	Andover Complex	Andover Complex
Traverse	2	1b	1b	1b	1b	1b	2	1b
Lithology	Ortho-pyroxenite	Websterite	Websterite	Gabbro	Peridotite	Peridotite	Clino-pyroxenite	Websterite
Zone	Ultramafic	Ultramafic	Ultramafic	Ultramafic	Ultramafic	Ultramafic	Ultramafic	Ultramafic
Subzone	G	G	G	G	G	G	G	G
Strat. ht (km)	1.17	1.18	1.20	1.21	1.22	1.22	1.23	1.23
SiO2	51.03	52.96	52.23	46.98	38.96	40.04	50.66	48.44
TiO2	.18	.28	.34	.16	.07	.11	.41	.41
Al2O3	3.79	6.51	10.35	15.99	1.88	1.38	3.59	5.74
Fe2O3	2.58	1.39	1.15	1.13	7.12	4.96	1.61	3.71
FeO	9.10	7.78	7.60	4.23	5.95	7.01	8.24	5.40
MnO	.24	.16	.15	.11	.13	.19	.22	.17
MgO	25.51	19.90	14.05	10.93	33.33	33.96	18.76	20.53
CaO	2.87	3.92	6.64	13.82	.08	.21	12.07	9.91
Na2O	.21	.71	1.96	1.07	.02	-	.33	.59
K2O	.07	.54	.33	1.07	-	-	.02	.04
P2O5	<.01	.02	.03	-	-	-	.02	-
LOI	3.82	5.04	4.49	3.94	11.83	11.60	3.49	4.12
Rest	.57	.64	.45	.50	.67	.55	.39	.67
Total	99.97	99.85	99.77	99.93	100.04	100.01	99.81	99.73
O=F,S,Cl	.01	.00	.00	.01	.00	.01	.01	.01
Total	99.95	99.85	99.77	99.93	100.04	100.00	99.80	99.72
	Trace elements in parts per million							
Ba	12	192	160	407	113	<4	12	48
Li	12	105	139	185	5	6	7	13
Rb	15	197	76	260	1	1	<1	3
Sr	61	148	110	1177	8	4	23	82
Pb	3	2	4	2	<2	<2	1	2
Th	<1	2	2	<2	<2	<2	<1	<2
U	<0.5	0.5	1	<0.5	<0.5	<0.5	<0.5	<0.5
Zr	4	38	47	3	2	4	10	14
Nb	1	2	2	<2	<2	<2	<1	<2
Y	2	12	13	10	1	2	11	12
La	<3	8	8	<2	<2	<2	<3	<2
Ce	<3	12	16	13	<5	<5	6	9
Nd	<3	6	8	3	<2	<2	5	8
Sc	25	24	28	37	3	9	57	45
V	92	134	154	113	34	42	203	174
Cr	2701	3001	1893	860	2490	1935	1687	3091
Ni	520	470	340	406	2082	1735	393	678
Cu	229	63	53	160	53	3	63	354
Zn	88	76	74	41	82	138	86	76
Ga	4	12	16	13	5	2	6	7
As	1	1	0.5	<0.5	1.5	0.5	0.5	1
S	300	40	10	170	50	210	200	120
mg	82.4	82.2	77.3	81.3	84.9	86.1	80.2	83.1

Sample number	88330201	88330198	88330199b	87330165	87330166	87330153	88330197	88330199a
Intrusion	Andover Complex	Andover Complex	Andover Complex	Andover Complex	Andover Complex	Andover Complex	Andover Complex	Andover Complex
Traverse	1b	1b	1b	2	2	2	1b	1b
Lithology	Websterite	Peridotite	Clino-pyroxenite	Olivine orthopyxte	Websterite	Websterite	Gabbro norite	Norite
Zone	Ultramafic	Ultramafic	Ultramafic	Ultramafic	Ultramafic	Ultramafic	Gabbro	Gabbro
Subzone	G	G	G	G	G	G		
Strat. ht (km)	1.24	1.25	1.26	1.29	1.29	1.30	1.31	1.31
SiO2	51.34	39.60	51.92	43.07	52.01	51.59	49.87	53.17
TiO2	.37	.16	.29	.16	.39	.42	.21	.48
Al2O3	5.77	3.52	4.57	4.34	10.52	10.82	14.64	12.16
Fe2O3	1.00	5.98	1.38	3.76	1.13	1.36	1.04	1.15
FeO	7.77	6.59	5.23	7.37	7.47	7.74	5.30	8.41
MnO	.17	.19	.15	.17	.15	.16	.11	.16
MgO	18.16	31.20	17.22	28.41	14.06	13.36	12.80	10.35
CaO	10.24	1.71	14.96	3.27	7.85	7.56	11.08	8.92
Na2O	.84	.07	1.10	.28	.76	1.78	1.21	1.77
K2O	.13	-	.04	.01	.03	.22	.22	.23
P2O5	.01	-	.03	.01	.04	.05	.01	.04
LOI	3.69	10.47	2.75	8.70	5.08	4.35	2.93	2.71
Rest	.31	.43	.36	.62	.62	.49	.38	.36
Total	99.80	99.92	100.00	100.17	100.11	99.90	99.80	99.91
O=F,S,Cl	.00	.00	.00	.04	.04	.01	.04	.03
Total	99.80	99.92	100.00	100.13	100.07	99.89	99.76	99.88
	Trace elements in parts per million							
Ba	61	<4	36	36	23	-	60	155
Li	70	5	23	1	70	67	58	41
Rb	26	1	<1	1	2	21	40	39
Sr	86	16	47	17	132	109	243	91
Pb	3	<2	2	1	10	14	2	7
Th	<2	<2	<2	<1	6	4	<2	2
U	<0.5	0.5	0.5	0.5	1	1.5	0.5	<0.5
Zr	14	6	30	4	50	60	8	56
Nb	<2	<2	<2	1	3	3	<2	2
Y	13	4	16	3	11	14	6	16
La	4	<2	9	<3	9	12	4	7
Ce	10	<5	25	<3	18	22	7	19
Nd	8	<2	10	<3	8	11	5	6
Sc	42	9	57	16	27	27	28	35
V	136	50	180	74	152	160	98	198
Cr	1005	1343	1552	2512	2621	2121	1156	1039
Ni	566	1544	356	993	479	442	281	189
Cu	7	4	40	129	56	59	66	68
Zn	106	119	69	86	68	71	58	83
Ga	7	4	7	6	12	13	20	14
As	<0.5	0.5	1	1.5	1.5	1.5	2	2
S	<10	60	30	800	800	300	740	680
mg	81.4	84.5	84.8	84.7	77.6	75.7	81.1	69.6

Sample number	87330155	87330152	87330164	87330130	87330131	87330128	87330127	87330126
Intrusion	Andover Complex	Andover Complex	Andover Complex	Andover Complex	Andover Complex	Andover Complex	Andover Complex	Andover Complex
Traverse	2	2	2	1c	1c	1c	1c	1c
Lithology	Gabbro	Gabbro	Anortho-site	Gabbro	Anortho-site	Gabbro	Gabbro	Gabbro
Zone	Gabbro	Gabbro	Gabbro	Gabbro	Gabbro	Gabbro	Gabbro	Gabbro
Subzone								
Strat. ht (km)	1.32	1.34	1.44	1.76	1.80	1.87	1.95	2.01
SiO2	46.00	49.59	47.21	44.78	46.03	49.33	44.63	49.39
TiO2	1.66	.25	.31	.25	.32	1.16	2.02	.45
Al2O3	15.14	17.04	20.51	13.09	20.38	15.22	15.02	14.08
Fe2O3	2.96	1.09	1.02	1.68	1.14	2.07	4.62	2.26
FeO	10.42	5.59	3.82	7.47	3.76	8.08	10.56	6.35
MnO	.19	.14	.09	.15	.11	.19	.20	.15
MgO	6.98	9.22	6.50	14.30	6.40	7.09	5.88	11.99
CaO	9.00	9.95	13.54	11.83	12.63	9.78	10.12	8.70
Na2O	83.00	2.57	1.90	.82	2.32	2.97	2.20	1.03
K2O	.36	.72	.16	.04	.54	.33	.53	.05
P2O5	.08	.02	.04	.02	.03	.12	.35	.05
LOI	3.47	3.75	4.81	5.49	4.79	3.37	3.75	5.35
Rest	.22	.22	.30	.40	.32	.33	.39	.28
Total	179.48	100.15	100.21	100.32	98.77	100.04	100.27	100.13
O=F,S,Cl	.00	.00	.04	.08	.01	.08	.08	.05
Total	179.48	100.15	100.17	100.24	98.76	99.96	100.18	100.07
	Trace elements in parts per million							
Ba	99	263	36	12	1139	166	353	21
Li	46	60	33	53	20	18	5	16
Rb	28	89	8	1	137	8	13	2
Sr	404	386	289	176	478	246	313	264
Pb	4	2	2	7	3	4	5	4
Th	<1	<1	1	<1	<1	1	<1	1
U	<0.5	<0.5	0.5	<0.5	<0.5	0.5	<0.5	0.5
Zr	25	12	16	8	10	31	25	21
Nb	3	1	1	<1	1	4	2	2
Y	17	8	7	6	6	16	19	6
La	3	<3	<3	<3	<3	6	10	4
Ce	12	4	7	<3	6	17	19	7
Nd	8	3	4	<3	3	12	13	3
Sc	43	38	31	37	15	39	35	28
V	565	131	115	120	39	287	445	118
Cr	41	375	817	814	439	103	51	215
Ni	36	122	82	209	72	85	72	238
Cu	<1	32	84	108	89	30	42	197
Zn	102	57	33	57	14	87	129	68
Ga	22	15	15	12	17	17	22	13
As	4.5	0.5	1	1	1.5	1	1	3.5
S	<100	100	800	1700	200	1700	1700	1100
mg	52.8	74.6	74.2	77.0	73.7	59.9	45.6	75.0

Sample number	87330125
Intrusion	Andover Complex
Traverse	1c
Lithology	Anortho-site
Zone	Gabbro
Subzone	
Strat. ht (km)	2.07
SiO2	51.07
TiO2	.31
Al2O3	20.19
Fe2O3	1.58
FeO	4.00
MnO	.11
MgO	6.25
CaO	9.77
Na2O	2.82
K2O	.15
P2O5	.05
LOI	3.83
Rest	.17
Total	100.30
O=F,S,Cl	.02
Total	100.28

Trace elements in parts per million

Ba	90
Li	12
Rb	3
Sr	293
Pb	3
Th	<1
U	0.5
Zr	27
Nb	1
Y	6
La	5
Ce	8
Nd	4
Sc	21
V	79
Cr	126
Ni	110
Cu	126
Zn	52
Ga	17
As	1.5
S	400
mg	70.7

LAYERED ARCHAEAN MAFIC–ULTRAMAFIC INTRUSIONS OF THE WEST PILBARA BLOCK, WESTERN AUSTRALIA

BMR GEOLOGY & GEOPHYSICS AUSTRALIA

by D. M. Hoatson
BMR 1991

Scale 1:20 000

1 0 1 Kilometre

TRANSVERSE MERCATOR PROJECTION
Brown numbered lines are 1000 metre intervals of the Australian Map Grid, Zone 50

Geology 1984–85, 88 by D. M. Hoatson, BMR
Compiled 1989–91 by D. M. Hoatson, T. W. Brown, BMR
Digital cartography by D. M. Hoatson, T. W. Brown, G. Butterworth, BMR)
(MT SHOLL, 1990–91 by D. M. Hoatson, T. W. Brown)
(MUNNI MUNNI block diagram by J. M. Mifsud, BMR)
Geophysical data compiled by R. Wellman, BMR.
Gravity overlays by J. Williams, BMR
Edited by J. W. Sheraton, A. J. Stewart, D.M. Pillinger, BMR
Cartography by T. W. Brown

Acknowledgments
Thanks for discussions on the geology of the west Pilbara and access to intrusions and diamond drill core material to:
A. Y. Gibson, A. L. Jaques, J. W. Sheraton, G–S. Sun, D. A. Wallace, BMR
R. Hallberg, Dr. R. Hill, Dr. A. H. Wilson, CSIRO
P. Monaghan, Mitsui Creek Consolidated NL
C. R. Williams, Hunter Resources Ltd (I. L. Andrews, CRA Exploration Pty Ltd)
R. R. Keays, University of Melbourne; C. I. Mathison, University of Western Australia
For remote sensing data: I. F. Mackie, C. J. Simpson, BMR
Core photography by the Geological Survey of Western Australia Department of Primary Industries and Energy, based under the authority of the Minister for Primary Industries and Energy
Base maps compiled by the BMR from 1:50 000 mining tenement maps supplied by the Australian Survey and Land Information Group and 1:100 000 topographic maps supplied by the Australian Land Information Group, Department of Administrative Services

© Commonwealth of Australia 1991

This map is accompanied by a text publication:
Hoatson, D. M., 1991
Petrology and platinum-group element geochemistry of layered Archaean mafic–ultramafic intrusions, west Pilbara Block, Western Australia
Bureau of Mineral Resources, Australia, Bulletin 242

It is recommended that this map be referred to as:
Hoatson, D. M., 1991–Layered Archaean mafic–ultramafic intrusions of the west Pilbara Block, Western Australia (1:20 000 scale map). *Bureau of Mineral Resources, Canberra*

Summary of Archaean layered mafic–ultramafic intrusions of the west Pilbara Block, Western Australia

Intrusion	Approx area (km²)	Approx thickness (km)	Form / orientation	Major rock types	Mineralisation	Comments	References
ANDOVER (35 km east–southeast of Karratha)	7×20	2×3	Sill-like body dipping 45°–60° NW	Harzburgite, lherzolite, websterite, olivine websterite, clinopyroxenite, orthopyroxenite, gabbro, anorthosite	Ni, Cu 3 Mt @ 0.92% Ni, 0.3% Cu	Possibly a large mafic–ultramafic intrusion that is extensively faulted and intruded by dolerite, granite, pegmatite, and aplite. Sometimes confused with the Munni Munni Complex, but the Andover body is lying on the west flank of the Hook Creek anticline and is separated from the eastern outcrops of the complex	Blockarama (1:250 000 map) Urban Geological Survey Hickman, A. H., 1983 Hoatson, D.M., & others (Bull 242)
BALLA BALLA (95 km east of Karratha)	1×6	1×3	Lower intrusion dipping 060°–080° dipping 30°N	Pyroxenite, gabbro, anorthositic gabbro, leucogabbro, olivine gabbro, diorite/granite	V, Ti 3 Mt @ 0.95% V_2O_5	Poorly exposed multi-intrusion body(?) between the Carlow Hill/Balla Balla and Nerring Bore–Andover mafic–ultramafic units. Trends NW/SE over a strike length of 6 km. Mafic rocks are faulted against granite and basalt of the Fortescue Group	Hamilton, P.J., 1978 Hoatson, D.M., & Keele, R.A., 1988 (Southern, P.J. & Keele) ms., 1988
DINGO	1.5×2	<0.5	Steeply dipping pipe-like body(?)	Harzburgite, orthopyroxenite, gabbro, gabbronorite	N_i, Cu, PGE	Group of small isolated ultramafic–mafic intrusions interlayered with acid and mafic metavolcanics. May represent plugs related to the komatiitic volcanics in the Mount Welcome area	Hamilton, P.J. & Macdonald, A.J., 1981 Hoatson, D.M., & others (Bull 242)
GIDLEY GRANOPHYRE (Dampier)	9×30	3	Large lower intrusion dipping 45°–60° W	Gabbro, diorite, quartz diorite, granophyre	—	Mostly the largest intrusion in the west Pilbara. Three principal phases: (1) gabbro–diorite, (2) granophyre, (3) granophyre with minor fine grained felsic porphyry. Intrusive into Karratha Volcanics and Archaean granitoids	Hickman, A. H., 1983 Nicholas, D.A. & Hoatson, D.M., 1990
MAITLAND	5×14	1?	Mainly sill-like intrusion comprising several differentiated units with variable dips	Harzburgite, olivine websterite, clinopyroxenite, norite, gabbro, anorthosite, gabbronorite	Cu, Ni_2	Internally deformed and faulted mafic–ultramafic which contains an unusually high proportion of pyroxenitic rocks. Younger plug-like intrusion called Maitland Gabbronorite. Anorthositic rocks cycle multi-units. Sulphide mineralisation occurs in a metamorphosed gossan which is exposed over a strike length of 3 km	Hoatson, D.M., & others (Bull 242)
MOUNT SHOLL	3×6	1×≥2	Westerly-dipping sill-like body with cyclic layering 30°to 80°, E,SE	Dunite, clinopyroxene harzburgite, lherzolite, olivine websterite, orthopyroxenite, gabbro, anorthositic gabbro	Cu, Ni, PGE 4 000 t Ni, 4 000 t Cu, 0.5 g/t Au	Poorly layered multi-ultramafic intrusion that has been extensively faulted and intruded by dolerite, granite, pegmatite, and aplite. Ni–Cu mineralisation is generally less than 0.5% Cu. Some of the sulphide mineralisation which is hosted by gabbroic rocks directly below an ultramafic–gabbro sequence	Markham, C.J. & Marshall, A.F., 1981 Hoatson, D.M., & others (Bull 242)
MUNNI MUNNI	9×25	≥0.5	Large layered intrusion dipping 30°to 80°, E,SE	Dunite, clinopyroxenite, lherzolite, olivine websterite, clinopyroxenite, orthopyroxenite, norite, gabbro, anorthositic gabbro, anorthosite	PGE, Cu, Ni_2, As 1 000 t Ni, 1 000 t Cu, 0.3 g/t Au, 0.2% As	Layered mafic–ultramafic intrusion consisting of a lower, ultramafic zone overlain by thicker, more gabbroic zone. Disseminated copper–nickel sulphide mineralisation directly below the ultramafic–gabbro contact. Also contains a stratiform platinum–palladium reef of PGE(+Au) mineralisation several m in a peridotitic–gabbroic sequence which has a strike extent of 12 km. Minor chromitite layers in orthopyroxenite and norite. Serpentinised	Davidson, M.J., 1978 Hoatson, D.M., & Keays, R.R., 1989 Hoatson, D.M., & Keays, R.R., 1987, 1989 Hoatson, D.M., & others (Bull 242) Hoatson, D.M., 1990 Williams, C.R., & others 1990 Harris, P.G., & others (Bull 242)
RADIO HILL	2×2	1×2	Near-circular pipe dipping 50°–70° E,SE	Lherzolite, olivine websterite, clinopyroxenite, harzburgite, olivine gabbro, gabbro	Ni, Cu, PGE 0.3% Ni, 0.15% Cu, 1 g/t $(Pt+Pd)$	Very similar geological setting to the nearby Mount Sholl intrusion. Ni–Cu sulphide mineralisation occurs in a metamorphosed gossan near the basal contact of the intrusion. These rocks are overlain by an interlayered peridotite and pyroxenite sequence, a very coarse-grained pegmatoidal pyroxenite sequence, and relatively undeformed gabbronorite. Sulphides are associated with a quartz–magnetite–amphibole skarn	McAgney, M. S., & others, 1987, 1989 Hoatson, D.M., & others (Bull 242)
SHERLOCK BAY (72 km east of Karratha)	1×1½	<0.5	Steeply-dipping pipe-like body(?)	Peridotite, gabbro, Ni–chromite–cobalt–Ni–Cu sulphide ore	Ni, Cu, Co, PGE 0.7% Ni	Serpentinised peridotite with minor pyroxenite, gabbro, and norite. Ni–Cu sulphide mineralisation also occurs in overlying gossan	Miller, I.–J.A. Smith, M.K., 1975 Marston, R.J., 1984

REGIONAL SETTING
SCALE 1:100 000

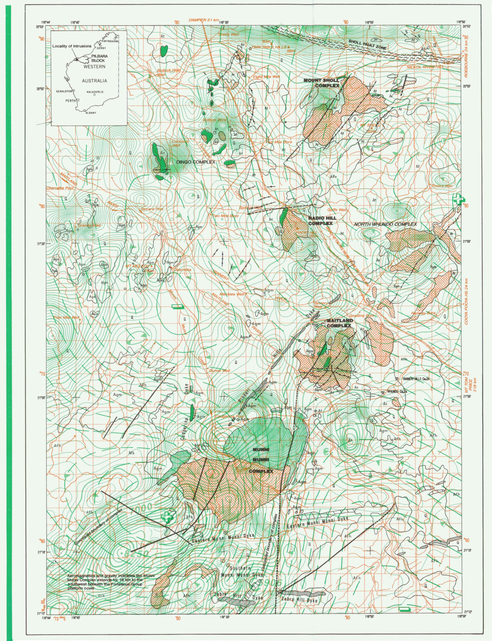
Locality of Introduction
PILBARA CRATON
WESTERN AUSTRALIA
KIMBERLEY
NULLAGINE
MARBLE BAR
MOUNT SHOLL COMPLEX
DINGO COMPLEX
RADIO HILL COMPLEX
MAITLAND COMPLEX
MUNNI MUNNI COMPLEX
MOUNT WELCOME
MOUNT ANDOVER
KARRATHA
ROEBOURNE
DAMPIER
WICKHAM
PORT HEDLAND
Geological units in area enclosed by dashed line are shown in detail on the Munni Munni Complex map
Locality of Mount Sholl Complex
Locality of Dingo Complex
Locality of Radio Hill Complex
Locality of Maitland Complex
Locality of Munni Munni Complex
Locality of Mount Welcome Complex
Locality of Mount Andover Complex
Locality of Balla Balla Complex
Locality of Sherlock Bay Complex
Locality of Gidley Granophyre
Locality of Radio Hill
Locality of Mount Sholl
Locality of Dingo
Locality of Maitland
Locality of Munni Munni
Locality of Andover
Locality of Balla Balla
Locality of Sherlock Bay
Locality of Gidley Granophyre
Locality of Mount Welcome
Locality of Mount